

Lecture Notes in Civil Engineering

Amit Kumar Verma ·

Edy Tonnizam Mohamad ·

Ramesh Murlidhar Bhatawdekar ·

Avtar Krishen Raina · Manoj Khandelwal ·

Danial Armaghani · Kripamoy Sarkar *Editors*

Proceedings of Geotechnical Challenges in Mining, Tunneling and Underground Infrastructures

ICGMTU, 20 December 2021

 Springer

Lecture Notes in Civil Engineering

Volume 228

Series Editors

Marco di Prisco, Politecnico di Milano, Milano, Italy

Sheng-Hong Chen, School of Water Resources and Hydropower Engineering,
Wuhan University, Wuhan, China

Ioannis Vayas, Institute of Steel Structures, National Technical University of
Athens, Athens, Greece

Sanjay Kumar Shukla, School of Engineering, Edith Cowan University, Joondalup,
WA, Australia

Anuj Sharma, Iowa State University, Ames, IA, USA

Nagesh Kumar, Department of Civil Engineering, Indian Institute of Science
Bangalore, Bengaluru, Karnataka, India

Chien Ming Wang, School of Civil Engineering, The University of Queensland,
Brisbane, QLD, Australia

Lecture Notes in Civil Engineering (LNCE) publishes the latest developments in Civil Engineering - quickly, informally and in top quality. Though original research reported in proceedings and post-proceedings represents the core of LNCE, edited volumes of exceptionally high quality and interest may also be considered for publication. Volumes published in LNCE embrace all aspects and subfields of, as well as new challenges in, Civil Engineering. Topics in the series include:

- Construction and Structural Mechanics
- Building Materials
- Concrete, Steel and Timber Structures
- Geotechnical Engineering
- Earthquake Engineering
- Coastal Engineering
- Ocean and Offshore Engineering; Ships and Floating Structures
- Hydraulics, Hydrology and Water Resources Engineering
- Environmental Engineering and Sustainability
- Structural Health and Monitoring
- Surveying and Geographical Information Systems
- Indoor Environments
- Transportation and Traffic
- Risk Analysis
- Safety and Security

To submit a proposal or request further information, please contact the appropriate Springer Editor:

- Pierpaolo Riva at pierpaolo.riva@springer.com (Europe and Americas);
- Swati Meherishi at swati.meherishi@springer.com (Asia - except China, and Australia, New Zealand);
- Wayne Hu at wayne.hu@springer.com (China).

All books in the series now indexed by Scopus and EI Compendex database!

More information about this series at <https://link.springer.com/bookseries/15087>

Amit Kumar Verma · Edy Tonnizam Mohamad ·
Ramesh Murlidhar Bhatawdekar ·
Avtar Krishen Raina · Manoj Khandelwal ·
Danial Armaghani · Kripamoy Sarkar
Editors

Proceedings of Geotechnical Challenges in Mining, Tunneling and Underground Infrastructures

ICGMTU, 20 December 2021

 Springer

Editors

Amit Kumar Verma
Department of Mining Engineering
Indian Institute of Technology (BHU)
Varanasi, India

Ramesh Murlidhar Bhatawdekar
Innovative Consultancy
and Research Pte. Ltd.
Singapore, Republic of Singapore

Manoj Khandelwal
School of Engineering, Information
Technology and Physical Sciences
Federation University
Ballarat, VIC, Australia

Kripamoy Sarkar
Department of Geology
Indian Institute of Technology
(Indian School of Mines), Dhanbad
Dhanbad, India

Edy Tonnizam Mohamad
Geotropik Universiti Teknologi Malaysia
Johor Bahru, Malaysia

Avtar Krishen Raina
Central Institute of Mining
and Fuel Research
Nagpur, India

Danial Armaghani
Department of Civil Engineering
University of Malaya
Kuala Lumpur, Malaysia

ISSN 2366-2557

ISSN 2366-2565 (electronic)

Lecture Notes in Civil Engineering

ISBN 978-981-16-9769-2

ISBN 978-981-16-9770-8 (eBook)

<https://doi.org/10.1007/978-981-16-9770-8>

© The Editor(s) (if applicable) and The Author(s), under exclusive license
to Springer Nature Singapore Pte Ltd. 2022

This work is subject to copyright. All rights are solely and exclusively licensed by the Publisher, whether the whole or part of the material is concerned, specifically the rights of translation, reprinting, reuse of illustrations, recitation, broadcasting, reproduction on microfilms or in any other physical way, and transmission or information storage and retrieval, electronic adaptation, computer software, or by similar or dissimilar methodology now known or hereafter developed.

The use of general descriptive names, registered names, trademarks, service marks, etc. in this publication does not imply, even in the absence of a specific statement, that such names are exempt from the relevant protective laws and regulations and therefore free for general use.

The publisher, the authors and the editors are safe to assume that the advice and information in this book are believed to be true and accurate at the date of publication. Neither the publisher nor the authors or the editors give a warranty, expressed or implied, with respect to the material contained herein or for any errors or omissions that may have been made. The publisher remains neutral with regard to jurisdictional claims in published maps and institutional affiliations.

This Springer imprint is published by the registered company Springer Nature Singapore Pte Ltd.
The registered company address is: 152 Beach Road, #21-01/04 Gateway East, Singapore 189721,
Singapore

Preface

International Conference on Geotechnical challenges in Mining, Tunneling and Underground structures (ICGMTU2021) was conceived to devise a forum for interactions on various aspects of geoengineering. The conference was held online on December 20–21, 2021, has been organized jointly by ICGMTU2021 and aims to offer a platform for researchers, academicians and engineers in the field of mining, civil engineering, tunneling engineers and underground space technologists to share their experiences and research. The conference has been devised to address a host of issues in tunneling and mining projects. The conference included themes like underground mining and ground control, mining geotechnics, tunneling and case studies and underground structures and case studies. The conference received 60 submissions which were classified into different categories in accordance with the conference themes. The papers have been reviewed through a double peer-review system. As a result, a total of 58 papers have been finally selected for this book. It is our strong belief that this book of proceedings will provide the readers with an excellent exposure to the geotechnical issues faced by different types of underground and surface excavations.

The conference aims to build a forum for future interactions between the stakeholders in rock excavation engineering, geotechnical, civil and mining engineers with a focus on nurturing the young minds to pursue their research and interact with a host of experts available during the conference. We are hopeful that in the future the ICGMTU will assume a greater role in geo-technique with emphasis on international collaborations and learning through such interactions along with recognizing the contributions of high impact researchers.

We would like to express our sincere gratitude to Prof. T N Singh, Director, Indian Institute of Technology, Patna, for his guidance for organizing ICGMTU2021 and encouraging to publish the proceeding volume. We acknowledge the inspiration provided by Dr. H. S.Vankatesh National Institute of Rock Mechanics to their scientists for their valuable contribution. We also thank the staff of Geotropik and UTMSPACE of Universiti Teknologi Malaysia for supporting this conference.

ICGTMU2021 is organized by Federation University Australia, Geotropik, Universiti Teknologi Malaysia and Innovative Consultancy Research Pte Ltd (IC Research), Singapore, and co-organized by Hanoi University of Mining and Geology (HUMG), Universiti Tun Hussein Onn Malaysia (UTHM). We are thankful to all organizers and co-organizers for supporting this international conference and making the same grand success.

Finally, we would like to express our sincere thanks to Mr. M. Subramaniam, Director, IC Research, Singapore, for providing sponsorship and special thanks to Prof. Xuan-Nam Bui and Dr. Hoang Nguyen (HUMG). We would like to thank all the reviewers for reviewing all papers and thank all the authors for their valuable contributions.

Amit Kumar Verma
Edy Tonnizam Mohamad
Ramesh Murlidhar Bhatawdekar
Avtar Krishen Raina
Manoj Khandelwal
Danial Armaghani
Kripamoy Sarkar

Contents

Underground Mining and Ground Control

A Review of Soft Computing Techniques in Predicting Overbreak Induced by Tunnel Blasting	3
Biao He, Danial Jahed Armaghani, Ramesh Murlidhar Bhatawdekar, and Sai Hin Lai	
Review of Roof Skin Instability Challenges with Emphasis on South African Coal Mines	15
W. B. Motlhabane	
Communication Experiment of Wi-Fi Direct for Underground Mine Environment Visualization System	65
Hajime Ikeda, Youhei Kawamura, Oluwafemi Kolade, Daniyar Malgazhdar, Mahdi Saadat, Fumiaki Inagaki, Hisatoshi Toriya, and Frederick Thomas Cawood	
Critical Aspects of Longwall Top Coal Caving Method for Application in Indian Geomining Conditions	77
Nasina Balasubrahmanyam and Gnananandh Budi	
Ultimate Pit Limit Optimization by Computerized and Manual Methods for Dadiin Khar Tolgoi – 2 Coal Mine – A Case Study	97
Tuvshinzaya Purevdavaa and Manoj Khandelwal	
Appropriate Support Design for Incline Lip Opening and Drivages in Fragile Rock Mass Formation: An Empirical and Numerical Based Case Study	117
Avinash Paul, Niraj Kumar, Pramod Kumar, and Ashok Kumar Singh	
Prediction of Rockburst Using Supervised Machine Learning	133
Tharun Balaj Kishore and Manoj Khandelwal	

Challenge to Explain the Upward Surface Movement Above Abandoned Coal Mines	155
André Vervoort	
Challenges in Drill Equipment Selection vis-à-vis Underground Excavations – A Methodology	167
B. N. V. Siva Prasad, V. M. S. R. Murthy, and Sripad R. Naik	
Fracture Characterization Using Downhole Camera in Deep Boreholes at Southern Johor Bahru, Malaysia	183
Vynotdni Rathinasamy, Edy Tonnizam Mohamad, Ibrahim Komoo, Mariatul Kiftiah Ahmad Legiman, Nurul Amaniyah, Ramesh Murlidhar Bhatawdekar, Muhammad Nassir Bin Hanapi, and Eka Kusmawati Binti Suparmanto	
Tunneling and Case Studies	
Numerical Modelling of Shoring Systems: Case Study	201
Arunava Ray, Rajesh Rai, Ashok Jaiswal, Deepak Dagdi, and Ajit Kumar Jha	
Effect of Ground Vibration Due to Blasting Activity in Large Section Tunnel Close to Pantai Timur Highway LPT 1	217
Azita Yusooif, Edy Tonnizam Mohamad, and Mohd Saidini Misnan	
Assessment of Structural Damage Due to Blasting in Hydro Power Tunnel	229
G. C. Naveen, V. R. Sastry, and K. Ram Chandar	
Tunnel Excavation in Highly Stressed Weak Rockmass Condition	241
G. C. Naveen, B. N. V. Siva Prasad, R. Balachander, G. Gopinath, H. S. Venkatesh, and Sripad R. Naik	
Surge Shaft Instrumentation and Monitoring in Himalayan Hydroelectric Projects	259
K. Sudhakar, B. H. V. Sekar, and S. R. Naik	
Construction Approach of Longest Railway Tunnel of India	273
Syed Naseem Akhtar and Rajesh Sonkar	
Geoenvironmental Assessment of Soil Slopes Around Leh Manali Highway in Himachal Pradesh, India	297
Geshu Khare, Vipin Kumar, and Sahil Sardana	
Parametric Study of Influence of Groundwater and Joint Spacing on Stability of a High Overburden Tunnel	305
A. Srivastav, Ashutosh Kainthola, V. Dangwal, and T. N. Singh	

Stability Analysis of a Rectangular Tunnel in Granitic Rocks at a Depth of 205 m, Bhima Basin, Karnataka 317
 Binu Kumar, R. K. Bajpai, and T. N. Singh

Ground Improvement in Fractured Basaltic Terrain Along TBM Drives Near to Arabian Sea – A Case of Mumbai Metro, India 331
 Anshul Sindhvani, V. M. S. R Murthy, Aloke Kumar Dey, Afzal Hossain Khan, and Palwinder Singh

Drill and Blast Optimisation at an Underground Copper-Gold Mine... 343
 Alex Guegan-Brown, Larissa Koroznikova, and Manoj Khandelwal

Underground Structures and Cases Studies

Investigation for Influence of Pressure on Face Stability of Mega Tunnel 357
 Shilpa Kulkarni and M. S. Ranadive

Delineation of Water Seepage Flow Path in the Underground Metro Rail Tunnel Using Cross-Hole GPR Tomography: A Case Study 371
 B. Butchibabu, P. C. Jha, N. Sandeep, and Y. V. Sivaram

Challenges for Mechanized Tunnelling in Urban Areas in Hanoi Vietnam 383
 Dang Trung Thanh, Dong Van Manh, Tran Tuan Minh, and Pham Duc Tho

Estimation of Deformation Modulus of Rock Mass for an Underground Cavern Based on Back Analysis 393
 H. V. Sekar Bellapu, Rabindra Kumar Sinha, and S. R. Naik

Construction of Underground Pump House Cavern in Medium Stress Condition—A Case Study from India 405
 A. K. Naithani, L. G. Singh, Prasanna Jain, D. S. Rawat, and R. N. Suribabu

Safety and Stability Monitoring of Underground Structures - Role of Geotechnical Instruments 419
 K. Sudhakar, Rabindra Kumar Sinha, and S. R. Naik

Mining Geotechnics

Numerical Modelling of Mining Induced Seismicity in Deep Closed Mines: A Case Study 437
 Praveena Das Jennifer, P. Porchelvan, and Sripad R. Naik

Intelligent Techniques for Prediction of Drilling Rate for Percussive Drills in Topically Weathered Limestone 457
 Ramesh Murlidhar Bhatawdekar, Bishwajit Roy, Saksarid Changtham, Manoj Khandelwal, Danial Jahed Armaghani, Edy Tonnizam Mohamad, Pranjal Pathak, Subhrojit Mondal, Radhikesh Kumar, and M. F. Md Dan

Influence of Freeze-thaw Cycles on the Velocity of Elastic Waves in Saturated Rock Specimens	473
Sahil Sardana, Rabindra Kumar Sinha, Mamta Jaswal, A. K. Verma, and T. N. Singh	
Effect of Firing Pattern on Rock Fragmentation in Surface Mine Blast-A Case Study	481
Lalit Singh Chouhan, A. K. Raina, and V. M. S. R. Murthy	
Investigations into the Influence of Intact Rock and Machine Properties on Exploratory Coring Rate for Aiding Selection of Coring Machine	489
P. Alam, A. K. Raina, and V. M. S. R. Murthy	
Operators Skill Evaluation with Virtual Reality Technology	511
Job Steven James Nanadrekar, Manavalan Subramanian, Gaurav Jain, Vynotdni Rathinasamy, and Ramesh Murlidhar Bhatawdekar	
Excavation Assessment on Granitic Area at Ulu Kinta, Perak, Malaysia for an Earthwork Project	521
Eka Kusmawati Suparmanto and Edy Tonnizam Mohamad	
Tackling the Asian Sand Crisis—A Case Study in Applying GAIN™ Best Practices in Viet Nam’s Mekong Delta	537
Jim OBrien	
Impact of Enhanced Production from the Opencast Coal Mines on Ambient Particulate Emissions	551
Ravi Kiran Podicheti and Ram Chandar Karra	
A Comprehensive Review of Rockmass Classification Systems for Assessing Blastability	563
Ramesh Murlidhar Bhatawdekar, A. K. Raina, and Danial Jahed Armaghani	
Empirical and Numerical Evaluation of a Cut Slope Near Rishikesh, India	579
V. H. R. Pandey, Ashutosh Kainthola, and T. N. Singh	
Recent Developments in Machine Learning and Flyrock Prediction . . .	597
Ramesh Murlidhar Bhatawdekar, Ashutosh Kainthola, V. H. R. Pandey, Singh Trilok Nath, and Edy Tonnizam Mohamad	
Evaluation of Machine Learning Models for Ore Grade Estimation . . .	613
Gaurav Jain, Pranjali Pathak, Ramesh Murlidhar Bhatawdekar, Ashutosh Kainthola, and Abhishek Srivastav	
Robots in Mining	625
Job Steven James Nanadrekar, Manavalan Subramanian, Umng Aditya, Gaurav Jain, Vynotdni Rathinasamy, and Ramesh Murlidhar Bhatawdekar	

Utilizing a Bagging Model Based on Decision Trees and k-nearest Neighbors for Predicting Slope Stability in Open Pit Mines 633
 Hoang Nguyen, Nguyen Tam Tinh, and Dinh Tien

Extra Trees Ensemble: A Machine Learning Model for Predicting Blast-Induced Ground Vibration Based on the Bagging and Sibling of Random Forest Algorithm 643
 Xuan-Nam Bui, Hoang Nguyen, and Phonepaserth Soukhanouvong

Managing Slope Stability Hazards in Volcanically Active Environments 653
 Wayne H. Scott

Management Strategy for Indian Housing Development Waste 669
 Paramjeet Singh, Zainab Toyin Jagun, Dzurllkanian Daud, Ajit Bhoslay, Satish Kumar Palniappan, and Ramesh Murlidhar Bhatawdekar

Development of Architecture of Autonomous Hydraulic Rock Breaker for Limestone Mines 683
 Aryan Sinha, Sabari Giri Vasam, Job Steven J. Nandrekar, Umang Aditya, Manoj Khandelwal, Naresh Prasad, Ramesh Murlidhar Bhatawdekar, and Vynotdni Rathinasamy

Application of Slope Mass Rating and Kinematic Analysis Along Road Cut Slopes in the Himalayan Terrain 697
 Tariq Siddique, Mohammed Sazid, Manoj Khandelwal, Harsh Varshney, and Sayem Irshad

Analysis of Joint Parameters to Understand it’s Effect on Rock Blasting 709
 Rajesh Silwal, Suman Panthee, and Ashutosh Kainthola

Effect of Sand Bed Thickness on the Response of Concrete Block Pavement: A Numerical Investigation 721
 Subhashini Anandan, Vivi Anggraini, and Mavinakere Eshwaraiah Raghunandan

Effect of Petrographic Properties on the Strength Parameters of Indian Metamorphic Rocks 737
 A. K. Verma, Amit Jaiswal, and T. N. Singh

Appropriate Geotechnical Engineering Helps Improve Mineral Reserves 745
 Srikant Annavarapu

Design and Evaluation of Stability of Slope Geometry of an Iron Ore Mine - A Case Study 755
 A. Y. Bharath Kumar, Sultan Singh Meena, T. Amrith Renaldy, and A. Rajan Babu

Intelligent Technique for Prediction of Blast Fragmentation Due to the Blasting in Tropically Weathered Limestone 773
Ramesh Murlidhar Bhatawdekar, Deepak Kumar, Saksarid Changtham, Devanshu Pathak, Singh TrilokNath, and Edy Tonnizam Mohamad

Assessment Parameters of Rock Masses for Excavation in Relation to Moisture Content 785
Mariatul Kiftiah Ahmad Legiman, Edy Tonnizam Mohamad, Eka Kusmawati, Vynotdni Rathinasamy, Zuraini Zainal, Nurul Eilmy Zainuddin, and Zulkifli Ismail

Geotechnical Challenges in World Record Making Mine Rescue 797
Binay Kumar Samanta

Underground Mining and Ground Control

A Review of Soft Computing Techniques in Predicting Overbreak Induced by Tunnel Blasting



Biao He, Danial Jahed Armaghani, Ramesh Murlidhar Bhatawdekar, and Sai Hin Lai

Abstract Blasting is an economical and practical construction technique for excavating underground structures. However, there are some undesirable environmental issues caused by tunnel blasting. One of the detrimental effects induced by tunnel blasting is overbreak. To alleviate the influence of overbreak, some techniques like empirical, statistical, and numerical have been proposed to solve this problem. However, considering the limitations of the aforementioned methods in analyzing the relationship between the target tunneling overbreak and influential input parameters, soft computing (SC) and artificial intelligence (AI) techniques were developed and employed to evaluate the impact of each factor related to the formation of overbreak. The researchers still face difficulties in making an optimal choice of the best SC and AI techniques to solve complex problems related to overbreak. Hence, this review paper aims to present the state of the art about the application of SC/AI techniques for predicting tunnel overbreak and discuss the advantages and disadvantages of the used SC/AI techniques. First, the background and reasons for the formation of overbreak are introduced. Then, the mechanism of influential parameters governing the overbreak is explained. These parameters can be divided into three categories: controllable parameters such as tunnel blasting design parameters, uncontrollable

B. He (✉) · S. H. Lai

Department of Civil Engineering, Faculty of Engineering, University of Malaya,
50603 Kuala Lumpur, Malaysia
e-mail: s2005282@siswa.um.edu.my

S. H. Lai

e-mail: laish@um.edu.my

D. J. Armaghani

Department of Urban Planning, Engineering Networks and Systems, Institute of Architecture and Construction, South Ural State University, 76, Lenin Prospect, Chelyabinsk 454080, Russia
e-mail: danialarmaghani@susu.ru

R. M. Bhatawdekar

Centre of Tropical Geoenvironment (Geotropik), School of Civil Engineering, Faculty of Engineering, Universiti Teknologi Malaysia, 81310 Skudai, Johor, Malaysia
e-mail: rmbhatawdekar2@graduate.utm.my

parameters such as rock mass properties and geological characteristics, and semi-controllable parameters such as tunnel geometry and size. Then, the SC/AI techniques used for estimating overbreak are summarized, while these techniques include single and hybrid models. The details of these models for predicting overbreak are reviewed. Subsequently, performance assessments about the advantages and disadvantages of the used SC/AI algorithms have been described, respectively, to compare the accuracy level of these algorithms in estimating overbreak and then introducing the most powerful AI/SC techniques to be used in this area. Finally, a new perspective that uses physics-based machine learning techniques to estimate overbreak is proposed.

Keywords Tunnel blasting · Environmental issues of blasting · Overbreak · Soft computing · Physics-based machine learning models

1 Introduction

The main construction method of mountain tunnels is the drill-blasting method. It is a method of excavation by mechanical drilling and filling with explosives to carry out blasting operations [1]. The drill-blasting method has the following advantages: (1) it is highly adaptable and can be designed to meet the requirements of most tunnels due to the different geological conditions of the surrounding rock, (2) it does not need to rely on large mechanical pieces of equipment, and the required equipment resources are relatively small compared to other construction methods, (3) personnel organization and management when blasting is relatively simple, and blasting design parameters can be adjusted promptly according to the actual geological conditions of the surrounding rock [2]. The drill-blasting method has long been the dominant method in mountain tunneling and also is the most economical and practical method. However, there are inevitable drawbacks to this method. For instance, after the blasting operation, the excavation cross-section can have two major problems, which are called as overbreak and underbreak. The overbreak is defined as a surplus drilled section of the tunnel while the underbreak is defined as the remainder of the blast operation [3]. Simultaneously, these two areas are also known as construction damage zone, and all of them can be reduced by changing the blasting factors [4].

Overbreak has been an issue of concern and difficulty for many scholars, especially in the prediction and control of overbreak due to blasting. Research conducted by Chakraborty et al. [5] presented that a holistic index, i.e., Tunnel Blasting Index (TBI), integrated Rock Mass Factor (RF), Tunnel Configuration Factor (TF), and Blast Design Factor (BF) to characterize the overbreak. TBI is capable of evaluating the importance of each parameter so as to identify which parameter is the most influential. Daraei and Zare [6] used the strength factor to estimate the overbreak and the developed model is with an approximately up to 40% difference between the predictions and observations. Navarro et al. [7] put forward a drilling index from measure while drilling (MWD) parameters, which can predict the potential overbreak induced by tunnel blasting. To achieve this, blasting factors are considered as constant, and

the overbreak is mainly influenced by the rock mass characteristics. Then, the MWD parameters are utilized to assess the rock mass characteristics and simultaneously predict the overbreak successfully. Foderà et al. [8] proposed a method to differentiate the overbreak into two types. One is the technical overbreak, mainly related to drill-and-blast design and execution, and the other one is geological overbreak, typically influenced by rock-mass characteristics. According to their study, an empirical model was developed to estimate the total volume of specific overbreak. The proposed empirical model is based on two factors influencing the overbreak, which are the rock mass rating (RMR) index for the geological overbreak and the length of the blast holes for the technical overbreak. Finally, the validation of the model was verified in the corresponding engineering. Mohammadi and Azad [9] proposed a rock engineering system (RES) based model to predict the overbreak. In their study, a total of 14 causative factors in overbreak were selected to develop the model, and the results show that the proposed model is with good accuracy (coefficient of determination, $R^2 = 0.91$), which has a favorable ability in estimating overbreak. Similarly, this study concluded that the tunneling rock quality index, perimeter specific charge, and burden to spacing ratio play a large role in overbreak prediction.

Overbreak caused by blasting has several hazards, for example, excessive overbreak can increase the volume of rock to be discharged from the tunnel boring, thus increasing the volume of additional shotcrete used, which results in the increasing of construction costs and seriously slowing down the construction schedule. Besides, overbreak also reduces the stability of the surrounding rock, creates local stress concentrations, and gives rise to possible water seepage through unfilled voids at the lining extrados, which can affect the safety and stability of the tunnel in the long term [10–12]. In order to have a clear understanding of overbreak, thus, it is imperative to research to summarize the present studies on overbreak prediction. To achieve this, this study presents a comprehensive review to improve the understanding of the application of artificial intelligence (AI) techniques on predicting overbreak induced by tunnel blasting, which is so as to provide a new perspective for relevant researchers.

2 Overbreak Effective Parameters

Overbreak is an inevitable phenomenon when excavating the tunnel, and the causative factors have a great impact on overbreak. According to some relative literature, factors that cause overbreak in a tunnel can be classified into three categories, i.e., geological factors, blasting factors, and geometric properties of the tunnel [1, 4, 12, 13]. Among them, blasting factors and geometric properties of the tunnel are controllable factors while geological factors are uncontrollable. The following sections describe these three types of causative factors, respectively.

2.1 Geological Factors

Geological factors are uncontrollable or fixed parameters, which have a significant influence on the overbreak phenomenon. Geological factors may include weathering zone, rock mass strength, the initial status of rock mass such as joints, faults, bedding, fractures, dips, and water condition. Some research has been conducted to decipher the relationship between geological factors and overbreak. For example, some scholars believed that pre-existing joints and beddings in the rock mass have a significant influence on overbreak. Because the fractures in the rock mass play a dominant role in the nature of the blast-induced fracture pattern, they dramatically influence the overbreak compared with the mechanical properties of the rock. Chakraborty et al. [14] utilized the scaled blasting model tests and field observations to assess the effect of vertical joint orientation through the tunnel axis and rock mass on overbreak. During field observations of the inclines under sedimentary rocks, it was noted that a large number of overbreak occurred when the joint plane was oriented in proportion to the tunnel axis. When the joint slopes gently, more overbreaks are observed in the sidewalls than in the crown. On the other hand, when the joint shows a steep inclination, the crown suffers more damage than the sidewalls. The authors' comment on this phenomenon is that shock waves are likely to propagate in the lateral direction in the plane of the joint but are limited in the forward direction.

2.2 Blasting Pattern Parameters

Blasting factors are controllable parameters, which can be modified. Thus, overbreak can be managed by varying these parameters. The blasting factors may include the explosive type, powder factors, charge concentration, delay timing, perimeter blast hole pattern, drilling deviation, and blast hole length as well as its diameter, etc. All blasting factors will affect the overbreak in a complex relationship in just a few milliseconds [13]. In fact, in order to obtain a smooth fracture plane without any wall damage, correct implementation and proper design of drilling and blasting patterns are very crucial. Any deviation from the designed pattern can result in getting away or approaching the hole's ends and due to the explosive concentration increment or reduction cause to overbreak. According to the research conducted by [15], concerning the simultaneous and micro-sequential initiation systems, both of them have advantages and disadvantages. However, the field test results showed that the simultaneous initiation system was found to be superior in minimizing overbreak as the maximum radial crack length into the remaining rock mass of simultaneous initiation systems created a 1.3–9.0 times, which was less than that of the micro-sequential initiation system whose firing delay between contour holes is only 1 ms.

2.3 *Geometric Properties of the Tunnel*

Geometric properties, such as tunnel size and shape, are semi-controllable parameters that determine the amount of power factor and overbreak [4]. Moreover, there are inversely proportional correlations between average powder factors and tunnel area. In other words, tunnels with a small area have relatively high powder factors whereas large tunnels have low powder factors. Geometric properties have only recently been introduced in some of the research on the development of AI models. However, based on the results of relevant literature that focus on AI model development, geometric properties such as tunnel size are not significant parameters that can dominate the overbreak [16, 17].

3 **AI Models Used in Predicting Overbreak Induced by Tunnel Blasting**

A large number of scholars have made attempts at predicting overbreak induced by tunnel blasting. For example, Ibarra et al. [18] developed a predictive model by using multiple linear regression analysis and considered the perimeter powder factor and Q-system as input variables. However, the proposed model is not adaptable, which is due to the limited consideration of the blasting parameters. Similarly, Murthy et al. [19] also used statistical methods to propose a model for predicting overbreak. In this model, only the maximum charge per delay was used, which cannot generalize to the other cases. As previously mentioned, it can be seen that the statistical methods are limited in their capability to introduce a proper relationship as a predictive model. The main reason is that there are many uncertainties in the nature of overbreak, which engineers cannot overcome these difficulties only by using simple ways like statistical methods. Therefore, new methods should be developed to overcome this difficulty. Recently, there has been an increasing interest in applying AI techniques in the prediction of overbreak. Researchers who have worked on the issues of overbreak prediction are summarized in Table 1.

The first attempt for overbreak prediction using soft computing methods has been done by Jang and Topal [13]. They used artificial neural network (ANN) and linear and nonlinear multiple regression analysis, with 49 datasets collected from Bigye tunnel in South Korea, to estimate the corresponding overbreak. The input parameters of the predictive model include rock mass rating (RMR) value, unconfined strength of rock (UCS), rock quality designation (RQD), spacing of joints, the state of joints, and groundwater condition. Based on the results of their study, the ANN model outperforms the statistical models because of the high correlation coefficient (R^2) that is 0.945. This study took a big step for the research field of overbreak prediction, leading the way in the application of AI techniques in the field. Nevertheless, in their study, only geological factors are considered whereas the blasting parameters, which have a great influence on overbreak, are ignored. Similarly, Shaorui et al. [20]

Table 1 Relevant research in the field of using AI techniques in predicting overbreak caused by tunnel blasting

Authors	Methods	Input	No.	R-square	Most effective parameters	Least important parameters	Location
Jang and Topal [13]	ANN	UCS, RQD, Js, Ja, Jo, GW	49	0.945	/	/	Located in South Korea
Shaorui et al. [20]	WNN	TL, S, DO	/	/	/	/	Located in China
M. Mohammadi et al. [21]	FST	PF, SD, NC, CB, LS, JO, RMR	202	0.96	/	/	Located in Iran
Mottahedi et al. [16]	ANN, FL, ANFIS, SVM	SC, SD, CB, TA, RMR	267	ANN: 0.93 (test) FL: 0.96 (test) ANFIS: 0.97 (test) SVM: 0.87 (test)	SD, SC, RMR	CB, TA	Located in Iran and India
Mottahedi et al. [17]	ANFIS; ANFIS-PSO	TA; PF; SD; S; RMR	270	ANFIS: 0.847(train) 0.945(test); ANN-PSO: 0.946(train) 0.961(test)	SD, S	TA	Located in Iran and India
Jang et al. [22]	ANN	Ff, UCS, Fw, Fdd, Fde, Fdf	90	0.808 (train); 0.785 (test)	UCS, Fdf	Ff, Fw	Located in Japan
Koopialipoor et al. [23]	ANN, GA-ANN	ND, SD, B, S, PF, AL, RMR	406	ANN: 0.703 (train), 0.639 (test); GA-ANN: 0.903 (train), 0.881 (test)	RMR	ND	Located in Iran
Koopialipoor et al. [24]	ANN, ANN-ABC	RMR, AL, SC, HB, RB, PS, ERS, ND	255	ANN:0.921(train) 0.923(test); ANN-ABC: 0.943(train) 0.939(test)	/	/	Located in West of Iran

(continued)

Table 1 (continued)

Authors	Methods	Input	No.	R-square	Most effective parameters	Least important parameters	Location
Koopialipoor et al. [3]	ANN	RMR, AL, SC, HB, RB, PS, ERS, ND	255	0.921 (train) 0.923 (test)	/	/	Located in West of Iran

UCS: uniaxial compressive strength, RQD: rock quality designation, Js: joints spacing, Ja: joints state, Jo: spatial orientation of joints, GW: groundwater condition, TL: trace length, S: spacing, DO: discontinuous orientation, PF: powder factor, SD: specific drilling, NC: ratio of number of contour holes to the total number of holes, CB: ratio of the amount of charge in contour holes to the burden in contour, LS: ratio of the length of holes to the stemming, JO: joint orientation favorability, RMR: rock mass rating, SC: specific charge, TA: tunnel cross-section area, Ff: unsupported face condition, Fw: face weathering and alteration, Fdd: discontinuities—frequency, Fde: discontinuities—condition, Fdf: angle between discontinuities and tunnel contours, ND: number of delays, B: burden, AL: advance length, HB: the holes periphery burden, RB: the end row burden, PS: periphery spacing, ERS: end row spacing

used wavelet neural network (WNN) models that a feed-forward network based on wavelet analysis construction to predict overbreak at Hongfeng tunnel in China. In their study, input variables also only consist of the geological factors, including the orientation, trace length, and the spacing of the structural plane. The results show that there are 10~30% differences between the predictions and observations.

In terms of the selection of input parameters for predicting overbreak, one study conducted by M. Mohammadi et al. [21] was the first attempt to use blasting factors as input parameters. The selected inputs include blasting factors such as powder factor, specific drilling, the ratio of the number of contour holes to the total number of holes, the ratio of the amount of charge in contour holes to the burden in contour, and the ratio of the length of holes to the stemming, as well as geological factors such as joint orientation favorability and RMR. Then, fuzzy set theory and multiple linear regression were employed to estimate the overbreak. The R^2 of fuzzy set theory and multiple linear regression were 0.96 and 0.55 respectively, which indicated that the AI model has a great accuracy than the statistic model. Henceforth, blast factors have been gradually introduced into the development of AI models. For geometric properties of the tunnel, it was first introduced in the studies of [16]. In the mentioned study, geological factors like RMR, blasting factors like specific drilling, the ratio of the amount of charge in contour holes to the burden in contour and specific charge, and geometric properties of the tunnel such as tunnel cross-section area were considered as input parameters. And four AI models, i.e., ANN, fuzzy logic (FL), adaptive neuro-fuzzy inference system (ANFIS), support vector machine (SVM), were employed to predict overbreak. Based on the obtained results, it can be seen that ANFIS has a good accuracy compared with other AI models. In addition, the sensitivity analysis indicated that RMR, specific charge and specific drilling are the

most effective parameters, whereas the ratio of the amount of charge in contour holes to the burden in contour and tunnel cross-section area are the least important parameters.

Recently, several studies attempted to utilize heuristic algorithms, such as particle swarm optimization (PSO), genetic algorithm (GA), and artificial bee colony (ABC), to optimize the SC models so as to obtain the hybrid models with better accuracy. For example, Mottahedi et al. [17] used ANFIS and ANFIS-PSO to develop the predictive models. To construct the models, five input variables were used, including tunnel cross-section area, specific drilling, spacing, powder factor, and RMR. According to the values of R^2 and root mean square error (RMSE), the results indicated that the ANFIS-PSO model showed better performance than the ANFIS model in terms of overbreak prediction. Besides, this study also shows that tunnel cross-section is the least important parameter, which is accordant with the previous research by [16]. Koopialipoor et al. [23] used ANN and GA-ANN with 406 datasets to predict overbreak caused by blasting in the Gardaneh Rokh tunnel, Iran. To achieve this aim, RMR, spacing, burden, special drilling, number of delays, powder factor, and advance length were considered as inputs. Based on the values of R^2 , RMSE, and variance account for (VAF), it can be inferred that the hybrid models, i.e., GA-ANN, is with high-performance capacity in predicting overbreak. Koopialipoor et al. [24] developed a three-layer ANN model with high accuracy to predict overbreak and then used the ABC optimization algorithm to obtain the pattern minimizing the amount of overbreak induced by tunnel blasting. The results of R^2 also revealed that the ABC-ANN model is better than the ANN model in overbreak prediction.

As noted above, research in overbreak prediction has gradually been developed at the present phase. Certainly, the influence of geological and blasting factors cannot be ignored when doing the AI modeling for overbreak prediction, however, the influence of tunnel geometric properties has been concluded to be insignificant in the current study, but further research is still needed to be conducted to verify the conclusion. In addition, the development of hybrid models has confirmed that they have good performance in accuracy compared with the single models. Moreover, it should be noted that developing generalized models is of great importance, which is appropriate for predicting overbreak in different rock or formation conditions.

In recent years, a new AI technique termed physics-based machine learning (ML) has been proposed to consider not just accuracy but also its ability to provide physical connections with the practical phenomenon. For ML models, a major limitation is that the use of “black-box” is often agnostic to the underlying scientific principles driving the real-world phenomenon, thus resulting in serious false discoveries in scientific problems [25]. The drawbacks of black-box ML methods can be summarized as follows: (1) A black-box ML model can only be as good as the representative quality of the labeled data that it is fed with. It is easy to learn spurious relationships that look deceptively good on both training and test sets when the datasets are small but do not generalize well outside the available labeled data. (2) A black-box ML model lacks scientific consistency, without taking into account any physical laws. Even if a black-box ML model achieves somewhat more accurate performance but cannot adhere to meaningful understandings of the underlying physical processes,

it cannot be used as a basis for subsequent scientific developments [26, 27]. On the other hand, physics-based models are based on the physical laws that expound on a relationship between independent variables and dependent variables. Usually, the given relationship has been simplified, and similarly, there existing a large number of parameters that should be calibrated employing limited observed data, which leads to the limited use of these models [28]. Fortunately, with the development of physics-based ML methods, a new framework that combines the powerful ML models and physics-based models has gradually been developed by researchers. This new model not only enables accurate predictions of the targets but also maintains a strong link to the actual meaning of the problem. In addition, the method has no strict requirements for labeled data. In the current study of overbreak prediction, the used AI techniques are all based on ML methods, and there is not a clear relationship between input parameters and overbreak. Although many scholars used sensitivity analysis to evaluate the importance of each input, the conclusions obtained are based more on the association between the data itself rather than on the actual meaning between input parameters and overbreak. Therefore, it is necessary to research by utilizing physics-based ML methods to predict overbreak, and develop generalized models that are suitable for practical engineering.

4 Conclusions

A comprehensive review that was aimed at improving the understanding of the overbreak prediction in tunnel blasting has been presented. By reviewing mentioned works, it can be concluded as follows. On the one hand, concerning the application of AI techniques on overbreak prediction, one of the vital steps is the selection of the inputs. Inputs parameters affecting overbreak can be divided into three categories: controllable parameters such as tunnel blasting factors, uncontrollable parameters such as geological properties, and semi-controllable parameters such as tunnel size. Among them, the current study concluded that blasting factors and geological properties are crucial, but for tunnel size, further research is needed to determine its significance. On the other hand, although several single and hybrid ML models have good performance in accuracy for predicting overbreak. However, it is hard to identify the practical correlation between inputs and overbreak. Furthermore, the generalized models that are suitable for being applied in various stratigraphic environments have not been developed. Fortunately, the development of physics-based ML techniques can overcome the aforementioned difficulties, thus it is imperative to research to develop new models so as to predict overbreak more accurately and successfully.

References

1. Mandal SK, Singh MM (2009) Evaluating extent and causes of overbreak in tunnels. *Tunn Undergr Sp Technol* 24(1):22–36. <https://doi.org/10.1016/j.tust.2008.01.007>
2. Murthy VMSR, Dey K (2003) Predicting overbreak from blast vibration monitoring in a lake tap tunnel - a success story. *Fragblast* 7(3):149–166. <https://doi.org/10.1076/frag.7.3.149.16787>
3. Koopialipour M, Ghaleini EN, Haghighi M, Kanagarajan S, Maarefvand P, Mohamad ET (2019) Overbreak prediction and optimization in tunnel using neural network and bee colony techniques. *Eng Comput* 35(4):1191–1202. <https://doi.org/10.1007/s00366-018-0658-7>
4. Mohammadi H, Barati B, Chamzini AY (2018) Prediction of blast-induced overbreak based on geo-mechanical parameters, blasting factors and the area of tunnel face. *Geotech Geol Eng* 36(1):425–437. <https://doi.org/10.1007/s10706-017-0336-3>
5. Chakraborty AK et al (2004) Development of rational models for tunnel blast prediction based on a parametric study. *Geotech Geol Eng* 22(4):477–496. <https://doi.org/10.1023/B:GEGE.0000047042.90200.a8>
6. Daraei A, Zare S (2018) Prediction of overbreak depth in Ghalaje road tunnel using strength factor. *Int J Min Sci Technol* 28(4):679–684. <https://doi.org/10.1016/j.ijmst.2018.04.013>
7. Navarro J, Sanchidrián JA, Segarra P, Castedo R, Costamagna E, López LM (2018) Detection of potential overbreak zones in tunnel blasting from MWD data. *Tunn Undergr Sp Technol* 82(August):504–516. <https://doi.org/10.1016/j.tust.2018.08.060>
8. Foderà, G.M., Voza, A., Barovero, G., Tinti, F., Boldini, D.: Factors influencing overbreak volumes in drill-and-blast tunnel excavation. a statistical analysis applied to the case study of the brenner base tunnel – BBT. *Tunn Undergr Sp Technol* 105(May):103475 (2020). <https://doi.org/10.1016/j.tust.2020.103475>
9. Mohammadi H, Azad A (2020) Applying rock engineering systems approach for prediction of overbreak produced in tunnels driven in hard rock. *Geotech Geol Eng* 38(3):2447–2463. <https://doi.org/10.1007/s10706-019-01161-z>
10. Verma HK, Samadhiya NK, Singh M, Goel RK, Singh PK (2018) Blast induced rock mass damage around tunnels. *Tunn Undergr Sp Technol* 71:149–158. <https://doi.org/10.1016/j.tust.2017.08.019>
11. Kim Y, Moon HK (2013) Application of the guideline for overbreak control in granitic rock masses in Korean tunnels. *Tunn Undergr Sp Technol* 35:67–77. <https://doi.org/10.1016/j.tust.2012.11.008>
12. Singh SP, Xavier P (2005) Causes, impact and control of overbreak in underground excavations. *Tunn Undergr Sp Technol* 20(1):63–71. <https://doi.org/10.1016/j.tust.2004.05.004>
13. Jang H, Topal E (2013) Optimizing overbreak prediction based on geological parameters comparing multiple regression analysis and artificial neural network. *Tunn Undergr Sp Technol* 38:161–169. <https://doi.org/10.1016/j.tust.2013.06.003>
14. Chakraborty AK, Jethwa JL, Paithankar AG (1994) Assessing the effects of joint orientation and rock mass quality on fragmentation and overbreak in tunnel blasting. *Tunn Undergr Sp Technol* 9(4):471–482. [https://doi.org/10.1016/0886-7798\(94\)90106-6](https://doi.org/10.1016/0886-7798(94)90106-6)
15. Rustan AP (1998) Micro-sequential contour blasting—how does it influence the surrounding rock mass? *Eng Geol* 49(3–4):303–313. [https://doi.org/10.1016/S0013-7952\(97\)00062-8](https://doi.org/10.1016/S0013-7952(97)00062-8)
16. Mottahedi A, Sereshki F, Ataei M (2018) Development of overbreak prediction models in drill and blast tunneling using soft computing methods. *Eng Comput* 34(1):45–58. <https://doi.org/10.1007/s00366-017-0520-3>
17. Mottahedi A, Sereshki F, Ataei M (2018) Overbreak prediction in underground excavations using hybrid ANFIS-PSO model. *Tunn Undergr Sp Technol* 80(May):1–9. <https://doi.org/10.1016/j.tust.2018.05.023>
18. Maerz NH, Ibarra JA, Franklin JA (1996) Overbreak and underbreak in underground openings Part 1: measurement using the light sectioning method and digital image processing. *Geotech Geol Eng* 14(4):307–323
19. Murthy VMSR, Dey K, Raitani R (2003) Prediction of overbreak in underground tunnel blasting: a case study. *J Can Tunn Can* 109–115

20. Shaorui S, Jiaming L, Jihong W (2013) Predictions of overbreak blocks in tunnels based on the wavelet neural network method and the geological statistics theory. *Math Probl Eng* 2013:1–9. <https://doi.org/10.1155/2013/706491>
21. Mohammadi M, Hossaini MF, Mirzapour B, Hajiantilaki N (2015) Use of fuzzy set theory for minimizing overbreak in underground blasting operations - a case study of Alborz Tunnel, Iran. *Int J Min Sci Technol* 25(3):439–445. <https://doi.org/10.1016/j.ijmst.2015.03.018>
22. Jang H, Kawamura Y, Shinji U (2019) An empirical approach of overbreak resistance factor for tunnel blasting. *Tunn Undergr Sp Technol* 92:103060. <https://doi.org/10.1016/j.tust.2019.103060>
23. Koopialipour M, Armaghani DJ, Haghghi M, Ghaleini EN (2019) A neuro-genetic predictive model to approximate overbreak induced by drilling and blasting operation in tunnels. *Bull Eng Geol Environ* 78(2):981–990. <https://doi.org/10.1007/s10064-017-1116-2>
24. Koopialipour M, Ghaleini EN, Tootoonchi H, Armaghani DJ, Haghghi M, Hedayat A (2019) Developing a new intelligent technique to predict overbreak in tunnels using an artificial bee colony-based ANN. *Environ Earth Sci* 78(5):8163. <https://doi.org/10.1007/s12665-019-8163-x>
25. Karpatne A et al (2017) Theory-guided data science: a new paradigm for scientific discovery from data. *IEEE Trans Knowl Data Eng* 29(10):2318–2331. <https://doi.org/10.1109/TKDE.2017.2720168>
26. Karpatne A, Watkins W, Read J, Kumar V (2017) Physics-guided neural networks (PGNN): an application in lake temperature modeling. <http://arxiv.org/abs/1710.11431>
27. Jia X et al (2021) Physics-guided machine learning for scientific discovery: an application in simulating lake temperature profiles. *ACM/IMS Trans Data Sci* 2(3):1–26. <https://doi.org/10.1145/3447814>
28. Han WEJ, Zhang L (2020) Integrating machine learning with physics-based modeling, pp 1–23. <http://arxiv.org/abs/2006.02619>

Review of Roof Skin Instability Challenges with Emphasis on South African Coal Mines



W. B. Motlhabane

Abstract South African underground coal mines continue to be challenged by roof skin instability problems. Falls of ground between installed bolts, roof skin delamination and dislodging of weathered roof skin material between the bolts are characteristic of ‘friable’ roof. Roof skin can be described as roof surface material not extending to more than 10 to 15 cm into the roof. Typical incidents associated with roof-skin falls are body scratches, limb amputation and even fatal occurrences. South African underground coal miners’ perceptions of roof-skin instability and approaches to deal with it, are rather informal and somewhat not standardised.

For most of South African underground coal mines, installation of Osro straps is usually the first step in mitigating against roof skin problems. Osro straps provide partial areal roof coverage. Two main products are known to be used in South African underground coal mines, plastic nets and welded wire mesh. These products are used sparingly at highly prioritised areas where roof-skin problems cannot be overlooked. However, one underground mine in the Vaal basin is known to have adopted total areal coverage (welded-mesh) approach as a result of serious friable roof problems. One other mine is known to be currently in the process of rehabilitating belt roads and travelling ways for hundreds of kilometres using plastic nets. The use of surface liner products is very rare. At the moment only one mine in the Secunda area is known to be using fibre-reinforced cement based liner called Tekcrete Fast M at selected high risk areas in the belt road. The author visited that mine and observed that the product adheres very well to the coal roof surface. The product however is also known to be very expensive and not intended for large scale use but for select high risk zones. Most prominent approach for majority of the underground coal mines in South Africa is physical roof barring. Several changes have been made to pinch bar to encourage effective barring. Some South African mines are known to train and issue every employee deployed underground with ‘barring certificate’. Whether there are any significant physical barring limitations is another separate issue yet to be dealt with.

W. B. Motlhabane (✉)

Department of Mining and Survey, University of Johannesburg, John Orr Building, 3rd Floor,
37 Nind Street, Johannesburg, South Africa
e-mail: basimanem@uj.ac.za

In general, responses to several issues and questions pertaining to roof-skin instability in South African coal mines are unclear and need investigation in order to enable the industry to wage a collective and harmonious combat against roof skin problems. Some pertinent issues and questions are:

- Justification and clear recognition of roof skin problems in South African coal mines.
- Are South African coal mines mitigating well against roof skin problems, and what are these mitigating efforts?
- Past or current paper pertaining to roof skin problems in South African underground coal mines.
- What are the perceived and encountered challenges in addressing this problem?
- Are there positive notable trends, forecasts, developments or milestones in regards to dealing with roof skin problems in South African coal mines?

This paper will attempt to investigate these issues, outline their status and exploit the opportunity to standardise the approach to deal with roof skin instability.

1 Introduction

Roof support in underground coal mines has seen significant development over the years, particularly roof bolts. Up until the mid-1990s the traditional support for underground coal mine roof were end-anchored thin roof bolts, normally 16–18 mm rebars. According to David Posta (personal communication, March 10, 2019), these installations did not consider the potential the influence of horizontal stress and there were numerous roof falls during that era. The types of roof falls associated with the era of end-anchored bolts were typically large collapses that could be as thick as bolt lengths or even beyond bolt length reach and roof skin failures. The introduction of thicker 20 mm roof bolts in the late 1990's, with high shear strength and full column resin significantly reduced roof fall incidents in South African underground coal mines, especially the large collapses. Roof skin collapses however remain unabated. Roof skin can be described as roof surface material not extending to more than 10 to 15 cm into the roof. Largely, the controls pertaining to roof skin instability in South African coal mines are not standardised. These controls vary from mine to mine and unlike primary support, their implementation are a prerogative of management. Mostly these controls include welded mesh, plastic nets, w-straps, osro straps and barring. Two main products are known to be used in South African underground coal mines, plastic nets and welded wire mesh. These products are used sparingly at highly prioritised areas where roof-skin risk problems cannot be overlooked. However, one underground mine in the Vaal basin is known to have adopted total areal coverage (welded-mesh) approach as a result of serious friable roof problems. One other mine is known to be currently in the process of rehabilitating belt roads and travelling ways for hundreds of kilometres using plastic nets. Thin spray-on liners are not common

in underground coal mines as they are in hard rock mines. At the moment only one mine in the Secunda area is known to be using some fibre-reinforced cement based liner called Tekcrete Fast M at selected high risk areas in the belt road. The product however is also known to be very expensive in the order of five to six times in rands per metre squared (R/m²) over welded mesh and plastic nets. This paper is concerned with determining the state of affairs in South African underground coal mines in regards to roof skin control and management as well as to include some recommendations.

1.1 Problem Definition and Overview

Recent statistics pertaining to roof skin failures from eight (8) underground coal mines in the Secunda area, Mpumalanga is shown in Fig. 1. No near misses were observed. The approach in these mines is to install roof screen at selected areas, mainly depending on physical roof barring. It is clear from Fig. 1 that these mines are seriously vulnerable to roof skin failure. These mines are the only ones in South Africa who classify skin failures as such and record their occurrences. Most mines record all falls of ground as purely ‘fall of ground’ with no detailed classification about the nature of the fall. Statistics in Fig. 1 recorded by these mines could be viewed as a fair representation of all South African mines with roof skin problems since the common roof skin for most South African coal seams is characterised by coal, sandstone, siltstones, mudstones and shales [5].

Statistics in Fig. 1 shows that there is a cause for concern in regards to the roof skin stability. However, there is no known study or paper that was specifically intended

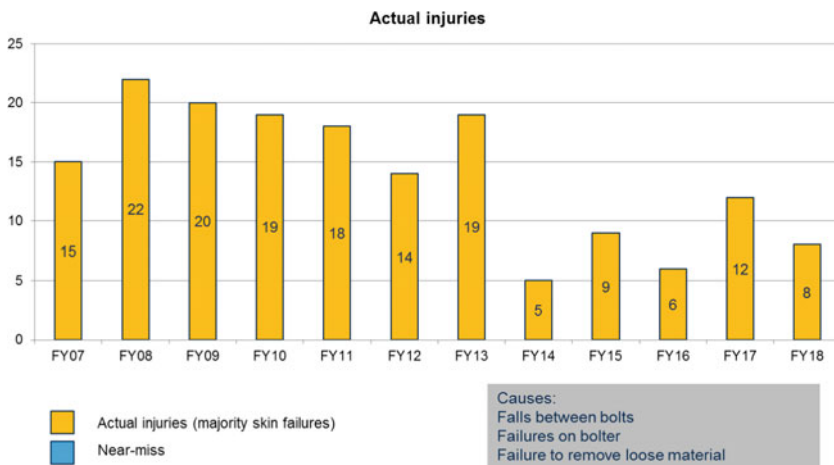


Fig. 1 Skin failure incidents statistics from eight (8) underground coal mines in Secunda area, Mpumalanga

to outline and address the problem of simple roof skin failures and management in South African underground coal mines. This paper is a result of that gap and will attempt to qualitatively assess the status of roof skin management in South African coal mines and draw up recommendations.

Common trend in South African underground coal mines is that the areal coverage support is installed on an ad hoc basis, at selected sites and as follow on support usually several days after the excavation is exposed. In some instances, it is a proactive measure instigated after observed roof skin failure. Very few excavations are pre-designed to include areal coverage support. Exceptions may include service excavations.

In order to enable the industry to wage a collective and harmonious combat against roof skin problems in underground coal mines, some pertinent issues and questions need be addressed. These include:

- Justification and clear recognition of roof skin problems in South African coal mines.
- Are South African coal mines mitigating well against roof skin problems, and what are these mitigating efforts?
- Past or current paper pertaining to roof skin problems in South African underground coal mines.
- What are the perceived and encountered challenges in addressing these problems?
- Are there positive notable trends, forecasts, developments or milestones in regards to dealing with roof skin problems in South African coal mines?

This paper aims to investigate these issues, outline their status and exploit the opportunity to standardize the approach to deal with roof skin instability as well as to provide other relevant recommendations in regards to these problems.

2 Review

2.1 Roof Skin Instability Problem

The author's observation in South African coal mines is that generally literature on the subject of rock falls and their cost to companies tend to be kept private because of its legal implications. There is very little material specific to the subject of rock falls incidents and accidents on the internet except for partial references in mining technical papers on other subjects. Reference to roof skin failures is found in the literature as far back as the late 1920s [1]. It is a problem as old as underground coal mining and persists to date. This type of roof failure has been termed skin or surface fall. These falls do not extend more than 10 to 15 cm into the roof. The support used to prevent these falls are called surface controls. Coal mines make use of various surface controls such as large roof bolt plates, steel straps, header boards, steel screen or weld mesh and plastic nets. Most of the literature available on the

subject is very old and it comes from the USA and Australian collieries. There are no updates in recent years.

In the USA, there was a dedicated effort to investigate this problem in the early 2000s. A study was conducted and statistics recorded in USA of the impacts of screening in lowering accidents and incidents associated with roof skin failure. The focus was to highlight the benefits of roof screen, especially the steel mesh and to dispel a view that it is an expensive and unprofitable exercise. Studies were conducted with actual mining panels (in 2 mines) where mesh was installed [21]. Their results showed that the panels or mines can still be profitable with good production rates even if they installed welded mesh. In addition, their statistics in Figures 2 and 3 also proved that there was steep decline in roof skin injuries from the time the mines began to install the mesh. The statistics presented were from 1991 before mesh installation, mesh was installed around 1994 and 1996 and the sudden drop in injury rates was sustained until 2001 when that specific study ceased.

Generally, the study pointed out that welded mesh is a likely solution to roof skin problem. In this study there is no quest to replace the mesh with anything potentially better, the study was solely weld mesh orientated. There is also cost savings when injuries are prevented or decreased. In 2000, NIOSH created a model to estimate

Fig. 2 Number of skin fall injuries per year at a northeastern U.S. mine before and after the implementation of screening [21]

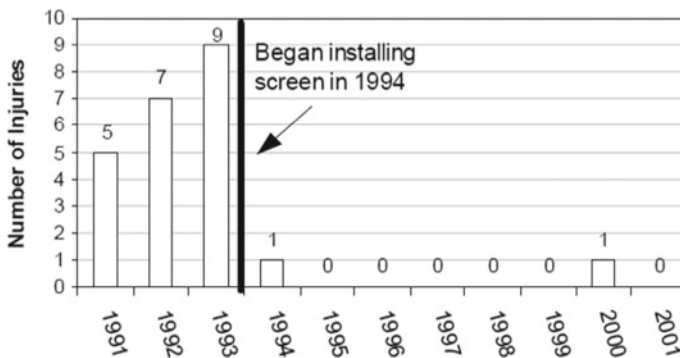
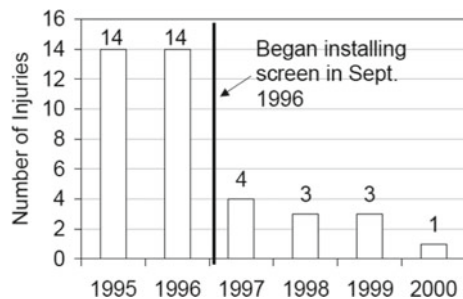


Fig. 3 Number of skin fall injuries per year at a central U.S. coal mine before and after the implementation of screening

“societal” costs for MSHA lost-time injuries. The average cost for this injury type (injuries from roof due to broken rock or coal) from 1997–1999 was \$9,937 per injury and it is expected that presently this cost has increased. This cost is specific for underground coal mines at the face area and does not include outby injuries from roof skin falls. The cost to the mine may be higher because this model does not take into account the cost of damaged equipment/materials, replacement, or retraining. There has not been any follow-up study on this specific interest ever since, to determine the current cost per injury. In South Africa chances of finding that information (let alone publishing it) is very remote due to legal implication, such information is not readily available and in the internet is not available at all.

Since the paper by Robertson et al. [21] in the USA, there has been only two (2) papers that are specifically related to roof skin instability topic. One was published in 2007 titled “Roof Screening for Underground Coal Mines: Recent Developments” [14]. A finding of this study was that Roof screen could potentially prevent numerous injuries arising from falls between the bolts. The ability of roof screen to cover all the gaps between permanent supports makes it by far the most effective method for preventing these relatively small rock falls. Modifications of screen material handling and dispensing procedures could make the installations swift and efficient and could significantly reduce the risk of a back or strain injury to roof bolter operators especially. Some of these modifications could include for example supplying roof screen to racks or rails fitted on bolters or at least leaning the screen against the rib instead of leaving it on the ground. Also well planned supply methods and best practice installation techniques can minimize the economic effects of roof screen installation on a mine’s overall mining cycle. They also determined that reducing the number of rock fall injuries at a mine will also have a very positive effect on the economics of a mine and it can improve the morale of the entire workforce. The other and the last publication on this issue was a peer reviewed journal published in 2011 titled “Current trends in Reducing Ground Fall Accidents in US Coal Mines” [12]. This paper acknowledges that there has been a reduction in equipment related fatalities but they allude to the fact that the same cannot be said of the other categories, especially falls between the bolts. They emphasise that available technologies such as roof screen could lower or nearly eliminate these incidents. They encourage mines to incline towards engaging these technologies.

In Australia the problem was so glaring that there was a paper initiative, which has since been stalled, looking specifically at this problem at one of its universities, University of Wollongong. University of Wollongong undertook a paper to replace welded mesh with spray-on polymer based liner. This idealised product would have to be:

- Cheap
- Easier to apply
- Good adhesive properties especially to coal material
- Sufficient shear, tensile and compressive strength to withstand shearing and dilation of the bearing coal strata

It is uncertain at the moment whether the paper will resume. However, stacked against this noble quest to replace the mesh is a *resistance inspired* view amongst miners worldwide that the regular welded mesh, which currently is still the most popular areal coverage product is expensive and tends to slow down the production rates. This view is very prevalent in South Africa.

In South Africa, roof skin instability in underground coal mines and its associated injuries on the workers, is an ‘elephant in the room’. There are no public debates at least on the subject even though the awareness is there. There is hardly any literature on the subject in South Africa. There is only one Phd paper in which roof skin instability is portrayed as a sideline issue. That study did not even recommend screening of any sort but rather the use of short bolts and no further discussions on that issue.

Available technologies such as roof screening could reduce injury and fatality rates if they were used more widely. Screen works best because it can cover almost the entire roof [12, 21]. Screen also offers a first line of defence for roof bolter operators by confining or deflecting small rocks that can come loose during drilling or bolt installation. Numerous studies have now shown that mines that use screen routinely have much lower rates of “struck by” rock fall injuries [12, 14].

2.2 Roof Skin Problems, South African Paper

2.2.1 Causes of Skin Falls

The three basic common causes of roof skin instabilities in coal mines are weak rock, horizontal stress and weathering. This paper is however not centred on causes of roof skin instability but rather the control or management thereof. Nevertheless, the causes are discussed here briefly. Van der Merwe et al. [24] undertook a study to determine the causes of skin failures in South African coal mines and the results are shown in Figs. 4, 5 and 6. The breakdown of the causes of roof skin deterioration and

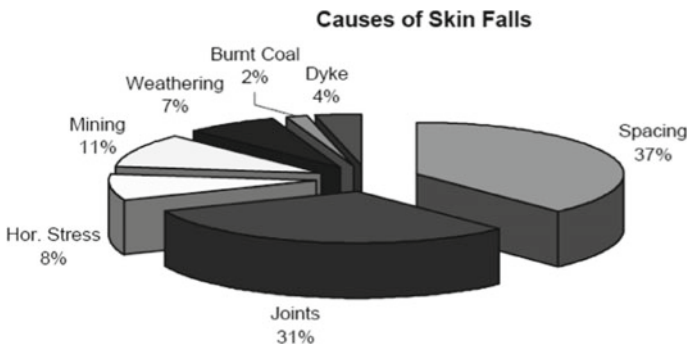
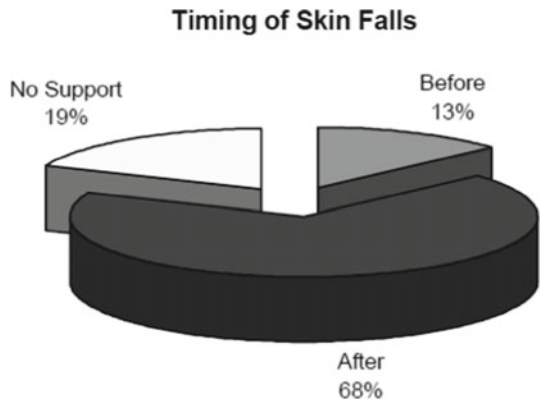


Fig. 4 Breakdown of the causes of skin falls, showing dominance of excessive bolt spacing and poor support of joints (after Van der Merwe et al. [24])



Fig. 5 Locations of roof skin falls (after Van der Merwe et al. [24])

Fig. 6 Timing of roof skin falls relative to timing of bolt installation (after Van der Merwe et al. [24])



failure are shown in Fig. 4 while the typical location and timing of roof skin failures are shown in Figs. 5 and 6, respectively.

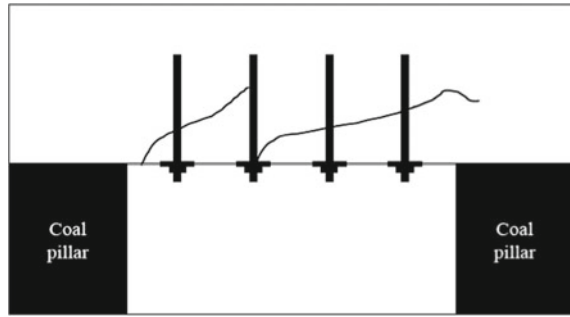
From Fig. 5 it can be seen that the intersection is more prone to roof skin failure. From Fig. 6, it can be observed that a large number of skin falls occur after bolt installation, between the bolts. The implication is that the bolts do not play a significant role in controlling roof skin failures.

2.2.2 Roof Skin Management

Fundamentally, areal support coverage is an essential component of effective support design [10]. Kuijpers [10] describes in detail weak skin in excavations and their remedial support actions in hard rock mines. He mentions that the role of areal coverage support in deep level mining excavations is to stabilise the skin of the excavation walls under various loading conditions. He further asserts that inadequate support coverage of fragmented excavation walls constitute the vast majority of rock fall accidents. Therefore, for this reason, he emphasises that areal support coverage is crucial for the effectiveness of support system where weak excavation skin exists. The author firmly affiliates with Kuijpers' views.

However, the use of roof screen in South African coal mines has not been standardised. It is most often installed on an adhoc basis and only when the roof skin

Fig. 7 Simple roof skin support (after Canbulat [4])



conditions are severe. Canbulat et al. [3] investigated six (6) South African underground coal mines to determine their roof rating system and support recommendations based on those ratings. Of all these mines only Arnot Colliery provided support recommendations for ‘poor roof’ which was W-straps with cable anchors and had no mention of roof skin management. All the other mines did not provide support recommendations for poor roof based on their respective ratings. Recommendations pertaining to roof skin control were not discussed in that investigation.

Canbulat [4] makes a brief mention of the design of roof bolt patterns to cater for simple roof skin control. He suggests the use of short light weight bolts to address simple skin failure (Fig. 7). The author is not aware of an instance where this method has been implemented in South Africa or elsewhere.

2.2.3 Roofskin Barring

Barring can be described as an activity of dislodging loose rock from the surface of an excavation. Barring itself is indeed another dangerous task in an attempt to make the roof safe. There is much emphasis on barring in South African coal mines. Commitment to barring overlooks the human physical strength requirements and assumes that everyone underground should and can bar down to make the roof safe. One South African coal mine in the Highveld region of Mpumalanga provides training for barring to everyone deployed underground and issues them with barring certificates. A paper by Boodoo et al. [2] for Mine Health and Safety Council (MHSC) found that 50% of the accidents that happen during barring is due to human deviations. They concede that human physical barring is not always possible and that mechanical barring without human exposure would be vital to prevent rock fall incidents. They produced Fig. 8 below to show rock fall fatal incidents that could have been prevented and the same can be said for drilling. In Fig. 8 conditions that should have been implemented to prevent these fatalities from occurring are represented in the vertical axis. Note:

- 24 fatalities that could have been prevented if mechanical barring was in place or implemented (i.e. remote barring).
- 37 fatalities that could have been prevented by areal coverage (i.e. nets)

94 preventable fog fatalities (2009 -may 2011)

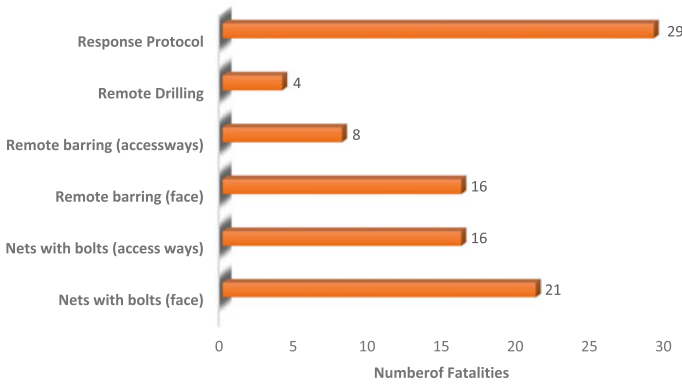


Fig. 8 Modes by which FOG fatalities may have been prevented—Note the instances where remote barring of the accessways or at the face could have been a solution

They also pointed out relevant legislation in regards to barring, related equipment, training and the execution of barring activities.

- i. *Section 10, 21, 22 and 23 of Chapter 2 (Health and Safety at Mines)* says that employers must provide health and safety training to enable employees to perform their work safely and without risk to their health. Manufacturers and Suppliers have a responsibility to design, repair or supply barring implements that allow mine employees to safely perform this duty. Every employee has a duty to take reasonable care for his or her own safety, as well as the safety of others. This applies to barring to the mine standard. Barring may at times be too challenging to carry out in a working place that may be considered dangerous. The individual must decide if it is safe to bar at all and if not, has the right to leave a dangerous working area.
- ii. *Section 14.1 (5) of Chapter 4 (Protection of Surface and the workings)* states that at every mine, if a working place becomes unsafe during a shift, the employer must ensure that all persons, other than those examining and making safe, are removed from such an unsafe area and are not permitted to return until it has been declared safe.

There is a need for improved worker safety training programmes, as a means to reduce accidents in South African mines, this is view being emphasised by all industry stakeholders and driven by legislation. Accident statistics highlight the need to address falls of ground as the primary safety hazard in underground mining operations.

In order to ensure that mine employees are adequately trained for the task of barring, (South African Qualifications Authority) SAQA’s registered unit standard 244,416 titled “Make safe a workplace by means of barring”. Specific outcomes and assessment criteria are detailed. Mines ensure that barring training is carried out as per

the unit standard, whilst also ensuring that mine specific requirements are covered. The training is intended to promote general skills, knowledge and understanding of how to make a workplace safe by barring.

This unit standard does not take into consideration physical strength requirements of barring personnel. Barring related accidents continue to indicate this shortcoming in regards to this standard.

Boodoo et al. [2] also found out that there is serious overall non-compliance by workers in regards to barring standards, in all mining commodities see Fig. 9, It is the author's view that physical demands of barring is potential the major contributor towards non-compliance even though there is no mention of it amongst other causes in Fig. 13. Note that coal mines are more complaint as compared to gold and platinum mines. The reason for superior coal mines compliance has been attributed to potentially lack of blast damage and thus having a less fractured roof than in gold or platinum. The coal mining sector is a completely different type of underground mining environment where the roof is higher and the pinch bar length is longer. Coal mining safety procedures are different to gold and platinum so the sounding and barring activities and equipment differs substantially from gold and platinum. Sounding and barring activities are perceived to be negligible when the roof conditions have been deemed good.

Overall compliance is shown in Fig. 9, platinum Fig. 10, gold in Fig. 11 and coal in Fig. 12.

Reasons for non-compliance are outlined in Fig. 11 below.

For coal specifically it was determined by this study that the reason for non-compliance are s follows:

- i. Sounding and barring was often completed diligently during visits. It is suggested that this was possibly due to visitor presence. The lack of evidence

Fig. 9 Overall percentage compliance to barring standards

ALL COMMODITIES OVERALL BARRING TO STANDARD

■ Compliance ■ Non-compliance

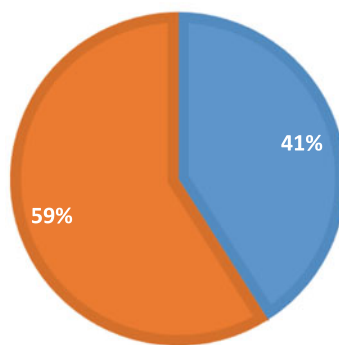


Fig. 10 Percentage compliance to barring standards—platinum observations

BARRING TO STANDARD

■ Compliance ■ Non-compliance

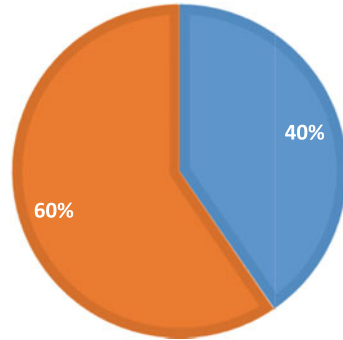
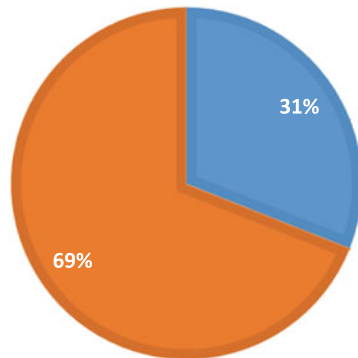


Fig. 11 Percentage compliance to barring standards—gold observations

BARRING TO STANDARD

■ Compliance ■ Non-compliance



of sounding marks on the roof in certain areas indicates that perhaps barring was not done as thoroughly during shifts prior to the visits. This would not be ascertainable for shifts post the application of stone dust.

- ii. Production pressures and the drive for first sump were indicated by many workers as the primary reasons for entry exam not being completed thoroughly on many occasions. First sump may be described as the first shear of coal by the continuously mining machines (CM) as attack bits are “sumped” into the face. Usually collieries have a specified time when the first sump or coal cutting should begin, and often this was noted to be 07 h30.
- iii. Personnel are left at machines they operate, as the team walks in sequence through the section doing entry examination. The remaining personnel and

Fig. 12 Percentage compliance to barring standards—coal observations

BARRING TO STANDARD

■ Compliance ■ Non-compliance

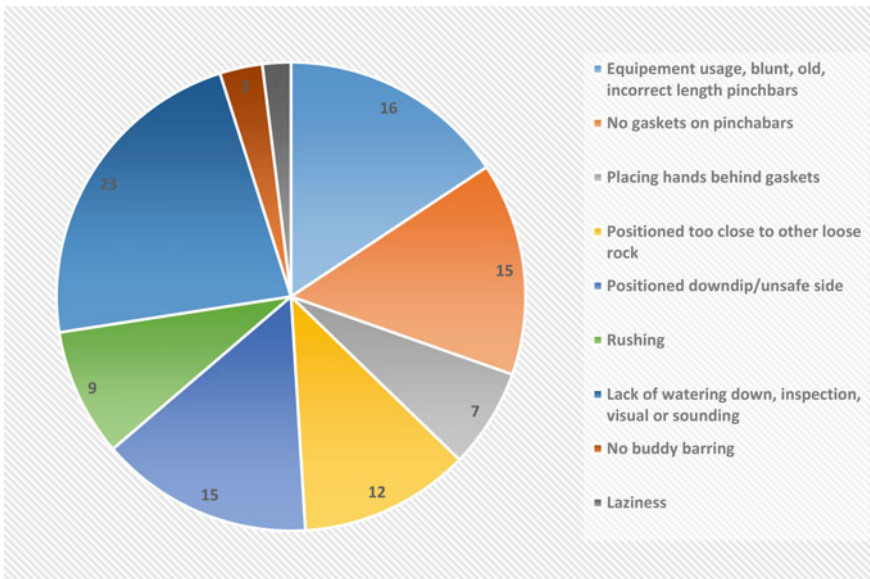
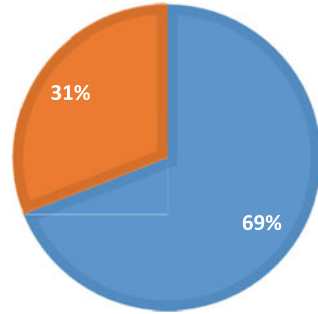


Fig. 13 Reasons for non-compliance

miner often continue making the entire section safe throughout the shift. Good crews across all the coal mining houses showed adherence to the process as miners and remaining personnel would complete making safe of the entire section at a steady pace.

- iv. Isolated cases showed that personnel seem to get complacent easily, due to the lack of barring accidents and do not complete the barring process adequately. One interviewee said “We just carry the sounding stick only as we hardly ever use a pinch bar. When we really need it, then we’ll fetch it.” This was

concerning as observers proceeded to do entry examination from the waiting place with only the sounding stick. They had to travel quite a distance to fetch the pinch bar when it was required.

- v. Rib sides/Stick sides are sometimes overlooked as focus is placed on the roof.
- vi. The length of pinch bars and sounding sticks posed a challenge to successful barring in excavations that were higher than planned. The higher areas may have been due to poor cutting, the occurrence of brows or falls of ground.
- vii. Fibreglass combination sticks and hollow steel pinch bars, which are lighter to carry, show consistent equipment modifications by suppliers to improve barring and sounding.
- viii. Fixed steel or hard plastic gaskets on the middle of pinch bars made the use of gaskets a non-issue as compared to gold and platinum mines. A fixed gasket was suggested but may not be applicable for hard rock stopping environments due to low excavation heights. In narrow stopping widths, the gasket on the pinch bar needs to be moved along the bar to accommodate the position that the bar is held however in high ends there is less variation in the position where the pinch bar is held. Hence, fixed gaskets are more effective in high ends. This is a practice that could possibly be used for 3 m long pinch bars or longer in hard rock development ends where rocks are potentially deflected off the pinch bar before it reaches the employee's hand.
- ix. Poor ground conditions are often experienced in areas of dyke and fault intersections, friable shale roof and areas with burnt coal. Geotechnical environment varies only slightly in the Highveld area between roof conditions for the different seams. This does not require changes in the barring process or focus. The coal roof in Kwa-Zulu Natal shows that personnel there may indeed bar for longer time periods than their Highveld counterparts to achieve safer roof conditions.

2.2.4 Pinchbar Modifications

A study by Otterman et al. [19] sponsored by South African Mine Health and Safety Council determined that barring equipment can be arduous and difficult to use. Hence it is expected that persons will find short cut in utilising these equipment. However, according to Otterman et al. [19] studies were conducted in Canada and it was found that conventional hand held equipment are arduous to use and that there is almost a guarantee that excavations requiring a lot of barring will not be rendered safe adequately. In light of this finding they set out to design a pinchbar that will minimise the physical effort demand from operators by:

- Reducing weight of equipment to reduce stress during percussion;
- Reducing effort of penetration and prying loose rock by using mechanical jaws

They reckon that equipment will reduce the exposure to fall of ground hazards, by improving barring quality through a reduction of stress and physical effort by the operator.

Fig. 14 Photo of lightweight pinch bar



2.2.4.1 Light Weight Pinchbar

In Fig. 14 a photo of a lightweight pinch bar is shown.

The inclusion of a “knock off” capability of the tips was investigated, which would have the advantage that only the tips would have to be taken for resharpening. This capability can be included in the design or as a different model. It was decided against this capability for the prototype development as this would add to the weight and cost of the pinch bar. The design of the prototype lightweight pinch bar included the following:

- Use of extruded fibreglass tube—38 mm.
- Use different steel tips 19 and 25 mm for different applications.
- Different lengths: 1.8 m.
- 2.0 m.
- 2.8 m.
- 3.5 m—for use in coalmines.

The connection of the steel bits into the fibreglass tube was made easier and cheaper. A low-density foam plug is pushed into the tube to the desired depth. The tube is placed upright and the steel bit is placed in the centre, resting on the foam plug. The area around the hexagonal tip is then filled with resin and chop strand. To strengthen the tube at the end to prevent it from splitting open a single layer of glass and resin is wound around the tube in the area of the tip. In Fig. 15 the layout of the

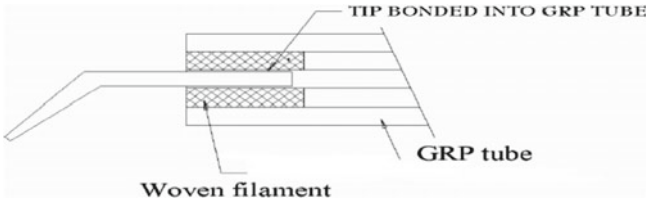


Fig. 15 Layout of connection between steel bit and fiberglass tube

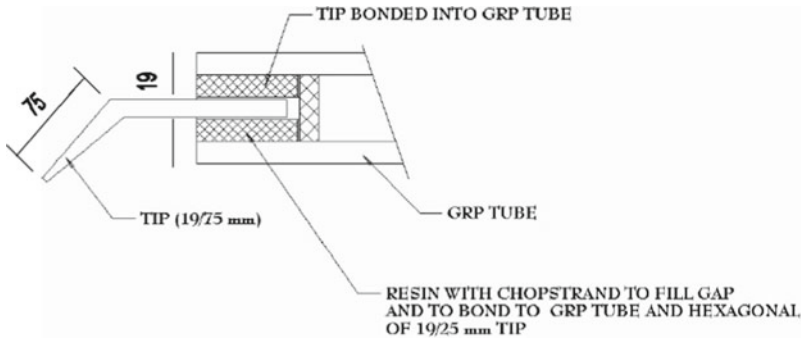


Fig. 16 Assembly drawing of lightweight pinch bar

connection between the steel bit and the fiberglass tube is shown. Figure 16 shows the assembly drawing of the lightweight pinch bar.

The following lengths and numbers of the prototype lightweight pinch bars were built for tests and underground evaluations:

- 1.5 m * 6
- 1.8 m * 3
- 2.0 m * 3
- 2.6 m * 4
- 3.0 m * 1
- 3.5 m * 5
- 4.0 m * 2
- 5.0 m * 5 On special request for a coalmine.

The prototype lightweight fibreglass pinch bars were comparatively tested with aluminium, 25 mm square steel tube and 19 and 25 mm solid hexagonal steel pinch bars. Table 1 shows a summary of the results of the comparative tests. From the table it can be seen that the lightweight pinch bars are significantly lighter than the steel pinch bars and compare favourably with the mass of aluminium pinch bars. In Fig. 17 the weight comparison of the pinch bars is shown. In Fig. 18 the deflection comparison of the pinch bars under a load of 25 kg at 2,6 m length is shown. Although

Table 1 Comparative test results of pinch bars

Pinch bar type	Unclamped length (m)	Clamped length (m)	Mass (kg)	Mass (kg) for 2,6 m length	Deflection (25 kg load @ clamped length) (mm)	Bending/Breaking load (kg)
Lightweight 25 mm tip	3.5	2.6	4	3.3	930	35
Aluminium	2.6	2.6	4.5	4.5	465	25+
25 mm hexagonal steel	2.9	2.6	13	11.7	275	80
25 mm square tube	2.6	2.6	4.5	4.5	940	30
Lightweight 19 mm tip	1.6	1.6	1.8	2.7	215	50+
19 mm Hexagonal steel	1.63	1.6	4.6	7.5	215	50

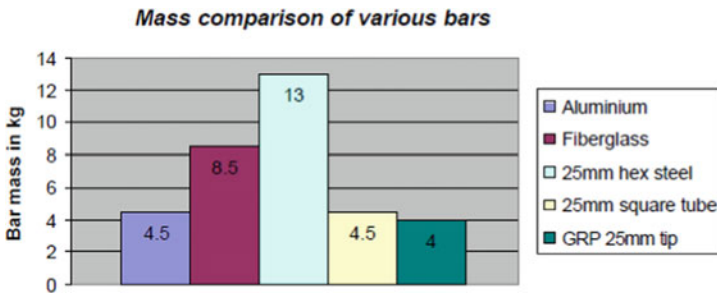


Fig. 17 Weight comparison of pinch bars

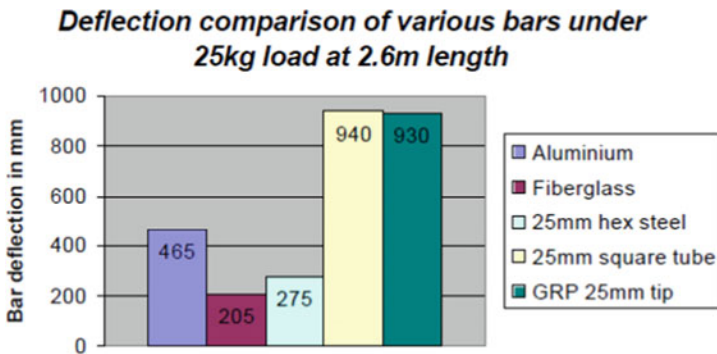


Fig. 18 Deflection comparison of pinch bars

the deflection of the lightweight pinch bars is higher than that of the solid steel pinch bars, it is less than that of the bar manufactured from square tubing.

The breaking load (the load at which permanent bar deformation occurs) of the lightweight pinch bar is also superior to that of the aluminium and square tube bars. Interestingly the 1.6 m lightweight pinch bar has similar deflection to that of the 19 mm solid steel hexagonal bar. This appears improbable when compared to the excessive bending of the longer 25 mm lightweight bar but the tests show that the bending of the lightweight bars increases exponentially the further one moves away from the end where the solid steel tip is infused into the tube.

2.2.4.2 Light Weight Pinchbar Underground Evaluations

The lightweight pinch bars were evaluated at Driefontein Gold Mine, Karee platinum mine and Bank colliery. In the gold and platinum mines the evaluation was done in the gully as well as in the stope areas. Figure 19 show light weight pinch bar in operation. A number of pinch bars were left with the mines for continued use and positive feedback has been received.

The following results and comments were obtained during the underground evaluations:

- Due to its relative lightweight, the work rate is much higher than with other pinch bars (especially steel).
- The lightweight makes it easier to maneuver.
- Sounding loose rock is very effective as the hollow tube acts as a sound box.
- A hand guard to protect the hands from falling or detached rocks is a necessity.
- Depending on the stoping width or height of roof different length pinch bars are required.
- Depending on the type of work 19 or 25 mm tips are required.
- In the specific coal mine the pinch bars longer than 4 m-length were too long.



Fig. 19 Lightweight pinch bar in operation in gold mine

- Contrary to the gold mines where a striking action is used to chisel off loose rock, the coalmines make use of a levering action. The barring technique has the operator insert the chisel end of the bar into the cracks between rock layers and lever the bottom layer loose. This highlighted the fact that the chisel tips used in the lightweight pinch bars are too short i.e. the chisel point does not protrude far enough into the crack to allow for sufficient levering off of the bottom rock layer.
- A different steel tip is required for the pinch bars in coalmines. It is recommended that a tip be used where the chisel tip point bends out at a 45° angle to the chisel shaft and where the chisel point protrudes at least 100 mm from the shaft, see Fig. 20.
- The durability of the pinch bars is good. Only one pinch bar was reported broken. This pinch bar was used in the coalmines and the evidence suggests that the glass fibers of the tube were mechanically damaged, i.e. the pinch bar got caught between two sharp edges. Figure 21 shows a photo of the damaged pinch bar.
- A number of requests were received to buy pinch bars.

Fig. 20 Recommended tip (25 mm) to be used for coalmine pinch bars

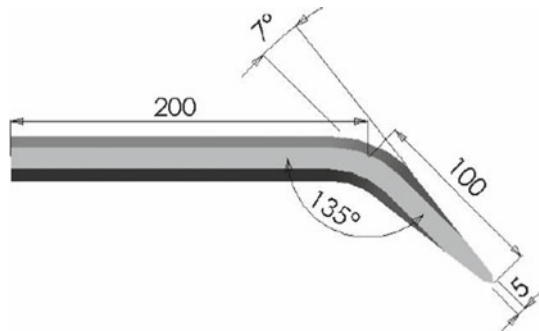


Fig. 21 Damaged pinch bar



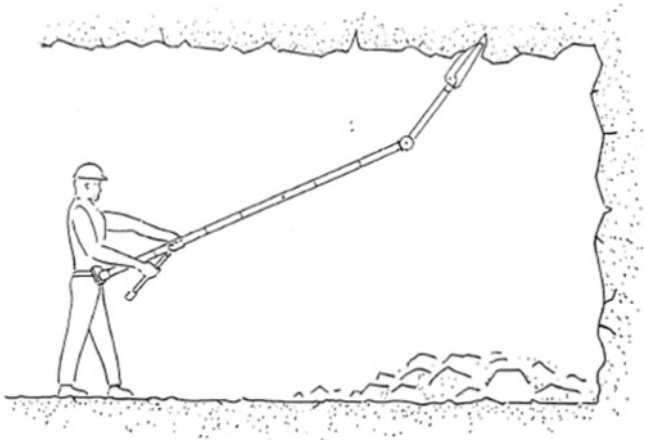


Fig. 22 Rock prying apparatus in use

2.2.5 Mechanical Jaws

The concept consists of a prying mechanism connected to a rod. The purpose of this tool is to reduce operator effort in prying rock loose. The rod is carried by the operator who manoeuvres the prying mechanism (hydraulically operated “jaw”) into a crack (see Fig. 22). The prying mechanism comprises a pair of jaws with sharp tips so that they can be inserted into a crack. The jaws are opened hydraulically to apply a prying action to the rock mass when the tip is inserted into a crack. A lever operated hydraulic pump placed at the base of the rod supplies the hydraulic fluid under pressure. The hydraulic reservoir forms part of the rod, making it a self-contained system. The rod is hinged at a position close to the operating end (jaws) to be able to direct the prying mechanism towards a crack. The direction of the prying mechanism is preset. A remotely operated slide hammer is positioned behind the prying mechanism to force the jaws into exposed cracks prior to the actuation of the prying mechanism.

The experimental development model (XDM) mechanical “jaws” was designed in detail and detail drawings of all the components were made. The design consists of the “jaws” that can exert a force of 5000 N (500 kg) and the hydraulic pump and a rod (tube) connecting the jaws to the pump. The hydraulic system is self-contained with a reservoir placed in the tube. A sliding hammer is placed behind the jaws to hammer the jaws into a chosen crack. Figure 23 shows the solid model and Fig. 24 the assembly drawing of the mechanical “jaws”.

2.2.5.1 Mechanical Jaws Underground Evaluations

The mechanical “jaws” prototype was evaluated at Driefontein Gold Mine and Bank colliery. Figure 25 shows photos of the underground evaluation.

The evaluation produced the following results and comments:

- The mechanical “jaws” can be successfully used to dislodge rocks.

Fig. 23 Solid model of XDM mechanical “jaws”

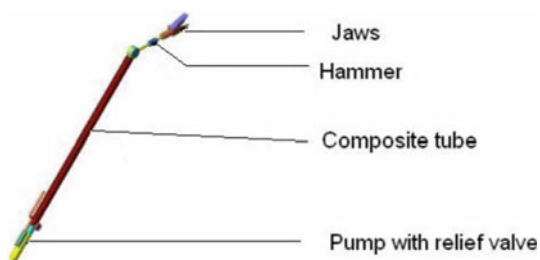


Fig. 24 Photo of the prototype mechanical “jaw” assembly



Fig. 25 Photos of mechanical “jaws” in underground operation

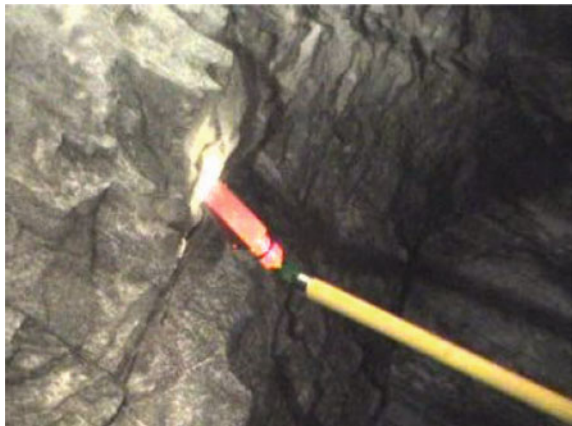
- In some overhead positions, where the length of the tube was too short to comfortably reach the crack, the mechanical “jaws” was difficult to handle (see Fig. 26).

Fig. 26 Photo showing the difficulty of operating in an overhead position



- Although the tool is relatively lightweight the weight of the “jaws” should be reduced so that it can be easily manoeuvred. This can be done by redesigning the “jaws”.
- Depending on the height of roof a different length tube is required. Different models for different jobs.
- The tips of the “jaws” are too wide and can only fit into and successfully work in cracks of 10 mm width or greater (see Fig. 27).
- The jaws need to open wider to dislodge most loose rocks.
- The spring-loaded hammer does not improve the insertion of the tips of the “jaws” into the crack. It is also in some positions difficult to press the “jaws” hard enough to load the hammer. It is recommended that the mechanical “jaws” be built without the hammer mechanism.
- Sounding loose rock can be done with the mechanical “jaws” as the hollow tube acts as a sound box.

Fig. 27 Photo showing difficulty of getting the “jaws” into the crack



- A hand guard to protect the hands from falling or dislodged rocks is a necessity.

2.2.6 Roof Skin Areal Coverage

In one South African colliery, the rock engineers recognise and acknowledge that the roof needs some form of areal coverage but the resistance from production mine management prevails. The strategy of rock engineers at this mine is now to make production management sign an agreement that absolves the rock engineers for not implementing areal coverage support. Given reasons for this resistance implicate costs and potential slow mining rates.

A symposium titled ‘Shotcrete for Africa’ was held in South Africa in 2009. All papers presented at this symposium were shy of addressing any of the coal mining areal coverage concerns.

The use of thin spray-on liners (TSL), usually sprayed on rock surface with a typical thickness of 4 mm has gained good reputation in terms of their areal support capabilities as established by the study conducted by Stacey et al. [23]. This assertion is rather true for hard rock mines but from the personal experience of the author this is not necessarily true for coal mines. They also mention from their study that there are no established support design methods for TSLs. The reason for this is that there are so many contributing parameters and that the mechanisms of these contributions are relatively unknown. In an attempt to remedy this lack of knowledge to some extent, analysis was carried out to investigate the influence of several parameters on the support capacity. These are:

- *Thickness of liner*
- *Stiffness of the liner*
- *Tensile strength of the liner*
- *Bond strength between liner and rock*
- *Penetration of liner material into a joint or fracture*
- *Rock surface irregularity.*

Stacey et al. [23] have determined from hard rock conditions other factors that could enhance the stability of roof skin and these factors are:

- *Promotion of block interlocking.*
- *Basket mechanism*
- *Extended faceplate:*

There has not been any dedicated paper work or trials in South Africa to align these principles with underground coal mines. The author’s perceived relevance and applicability of these factors in terms of underground coal mine conditions is summarised below:

Promotion of Block Interlocking. Promotion of block interlocking depends directly on penetration of liner and is commonly achieved by low viscosity liners. The nature of roof skin failure in a typical underground coal rockmass is characterised by delaminating strata and/or inherently weak roof. There are no particular key blocks in

which the unravelling of the roof could depend. There are no interlocking blocks that could be enhanced by the penetrating TSL/shotcrete. In fact TSL/shotcrete is unlikely to penetrate beyond the exposed surface into a plane (of detachment) on which failure will be initiated. Therefore, promotion of block interlocking is not readily applicable to roof skin failure types as experienced in underground coal mines.

Basket Mechanism. This is when surface support develops the form of a basket, which then contains the failed rock. Basket mechanism is a more common measure to combat roof skin failure in underground coal mine. Welded mesh and plastic nets are typical examples of this mechanism. A presentation on the use of plastic nets at mine in the Highveld region by Neal [15] is a typical example of basket mechanism as applied in a coal mine. The mine was plagued by roof delaminations, see Fig. 28. Initially the strategy was to address only hot spots but that did not work. From the assessment of the problem and inspired by the zero harm policy of the company, it was determined that elimination of the problem was impossible but separation was plausible. According to Neal [15] spray-on liners were not satisfactory and conventional mesh were difficult to maneuver in belt roads, potential handling risks. It was then decided to install plastic nets. It is an extensive project and ongoing to date (2020) since 2010 even though the completion target was only two (2) years. There has been stoppages as a result of contract management issues and nets installation teething issues that delayed the completion of the project. The following are the conditions under which these installations are being carried out:

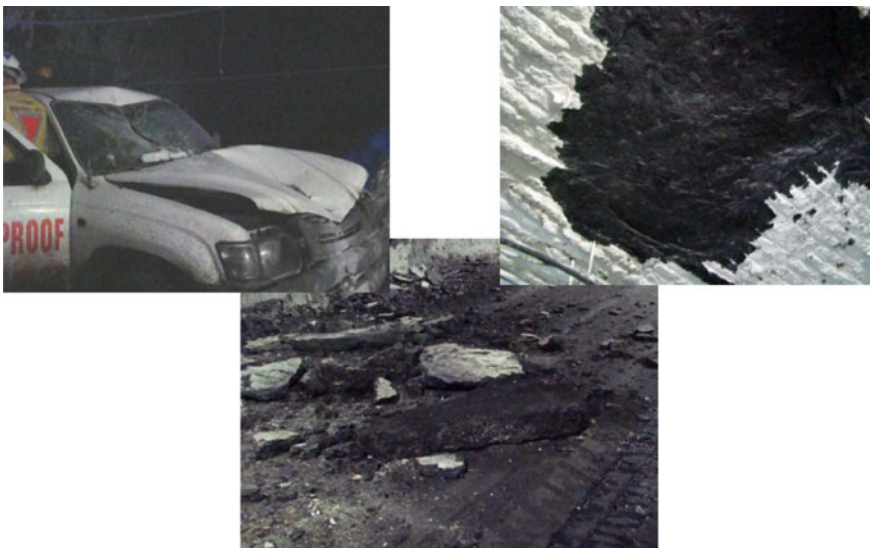


Fig. 28 Incidents that led to the implementation of plastic nets at a coal mine in the Emalahleni area

- The installation is covers ± 14 km of both the belt road and travelling road, including the sidewalls and span between travelling and belt roads.
- These travelling and belt roads are aged from 2 to 25 years

The nets were tested in a specially constructed for their capacity to arrest delaminating roof from various heights and the results are shown in Fig. 29.

It can be seen from the above results that the nets would successfully arrest more than 90% of the roof delaminations since the installation sag will not be more than 0.2 m, see Fig. 30.

Extended Faceplate. In this case surface support will extend the area of influence of rock bolt by some form of a bearing plates. This approach, like basket mechanism, has proven so far to be more relevant measures to combat roof skin failure in underground coal mine and has been applied before in underground coal mines, especially coupled

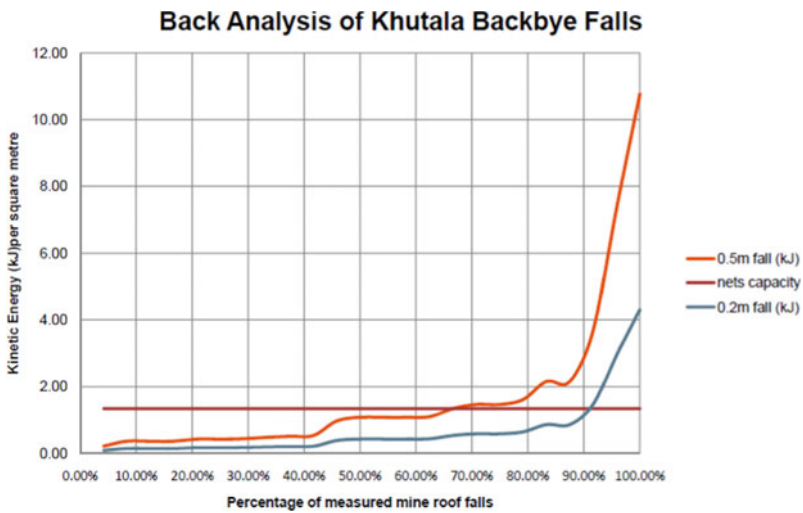


Fig. 29 Nets capacity testing results



Fig. 30 Installed roof nets at the mine

with the 'old' system of end-anchored bolts. Wooden face boards were coupled to the old thinner bolts to extend areal coverage. The use of those wooden face boards was a clear recognition and control measure for roof skin problems. However, when the new generation full-column 20 mm resin bolts were introduced, 'wooden face boards' that were usually coupled with old thinner bolts disappeared completely. The reasons for this disappearance are largely attributed to wood decay and water damage.

Underground coal mine roof is typically characterised by thin (1–15 cm) delamination. The failure of these laminations is progressive, starting from roof surface and migrating into the roof. These laminations are usually impenetrable except through visible joints or other discontinuities. Therefore, a surface liner would only coat the exposed surface. The aim of the liner should be to inhibit unravelling of the near-surface delamination, therefore the bond strength between liner and the roof surface and tensile strength of the liner are of prime importance in regards to roof skin control in underground coal mines.

Spearing and Hague [22] assert that support liners have reached their maturity in terms of their scope of application. However, there is no known coal mine in South Africa where liners have been applied or made a known significant contribution in regards to addressing roof skin failure as they have in hard rock mines.

However, recently in 2019, Minova (Pty) Ltd. has been trialling a certain product called Tekcrete™ Fast M in South African underground coal mines. Tekcrete™ Fast M is a specially designed, extremely rapid hardening, high performance gunite. Fibre reinforced, this product offers strengths over 55 MPa, and can be used in conventional, dry-process gunite equipment. It is ideal where immediate structural strength is required.

The product has been applied in select belt road sections at a mine in Secunda area. The belt road is old and has sections that are deteriorating and impacting the belt conveyor with falls of ground. The author visited this mine and observed that the product adheres very well to coal roof compared to his previous experience with a cement based spray-on liner. The product can actually be used as an areal coverage in underground coal mines. However, this product is fairly expensive in the order of five to six times rands per square metre (R/m²). Therefore, regular application like weld mesh cannot be achieved cost effectively. The product is intended for special case projects not for widespread usage across a mine. From a cost effectiveness point of view the product is not intended to replace the usual welded mesh or plastic nets.

Roof skin failures may not be overlooked in terms of their impact on the mine's productivity. Roof skin falls can prove very disruptive and costly for a mine. An ideal example of the disruptiveness of widespread friable roof instabilities in an underground coal mine is best illustrated by Hunter [8] at Sigma Colliery where the mine had to increase labour in back areas to assist with roof barring and support.

Sigma Colliery is, to date (2020), the only mine in South Africa with wire-mesh roof screen incorporated as primary support (Personal Communication with David Postma and a mine visit by the author's confirmed this). However, profitability of the mine as a result of this implementation has not been studied but roof skin incidents at the mine have since reduced dramatically to almost near non-existence. In order

to reduce falls of ground, appropriate support measures need to be in place and must be accompanied by change in mind set, culture and discipline [6].

2.3 Roof Skin Fall Risk Assessment

Majority of the time, roof skin instability can be seen or comprehended with a naked eye through underground observations by a trained or experienced personnel. The well-established Coal Mine Roof Rating (CMRR) and Impact Splitting can also be used as a guide when considering the need for areal coverage.

2.3.1 Coal Mine Roof Rating (CMRR)

Coal Mine Roof Rating (CMRR) can be used as a guide when considering the need for areal coverage [14]. In the 1990s, Coal Mine Roof Rating System (CMRR) was developed by NIOSH specifically for coal mining conditions in USA (Molinda and Mark 1994 cited by Prosser et al. [9]). It incorporated 5 parameters to classify a rock mass where strong bedding planes can have a significant influence:

- Unit rating for distinct rock intervals (cohesion and roughness)
- Intensity of discontinuities (spacing and persistence)
- Number of discontinuity sets
- Unconfined Compressive Strength or Point Load Index
- Moisture sensitivity.

Adjustments relating to strong beds, unit contacts and ground water are made to the CMRR value obtained from the summation of these individual parameter ratings. CMRR is arrived at by summing individual ratings and adjustments to obtain a final CMRR value on a 0–100 scale.

Mines with exceptionally low-strength roof (UCS <24 MPa, CMRR <40) are much more likely to experience roof falls than other mines [11]. If the CMRR of the roof is below 35, installing roof areal coverage could help control roof skin failures and maintain long term stability in the roof. This system is however not popular in South Africa and it does not play any role in the design of support system in South African mines.

2.3.2 Impact Split Test

Impact split test developed by Oldroyd and Buddery in 1992 is based on determining the susceptibility of roof material to delamination. It can therefore be used to judge if the roof will require areal coverage or not. An impact split test was developed whereby a constant impact is applied to every 20 mm of drill core by dropping a 1.5 kg chisel from a predetermined height according to core diameter. The higher the frequency of core unit splits, the weaker the material and the lower the roof and unit rating. Table 2 below is the summary of the impact results and Table 3 is the implication on support installation.

Table 2 Impact split test unit rating and coal classification systems

Unit rating	Rock class	Roof rating
<10	Very poor	<39
11–17	Poor	40–69
18–27	Moderate	70–99
28–32	Good	11–129
>32	Very good	>130

Table 3 Impact split test general guide for support and rock classification

Roof rating	Bord width (m)	Example of support
Very good	6.5	1.2 m × 16 mm, point anchor, 5 bolts per intersection only
Good	6.0	1.2 m × 16 mm, point anchor, 5 bolts intersection, 2 bolts per row, rows 2 m apart
Moderate	5.5	1.5 m × 16 mm, point anchor, 9 bolts per intersection, 3 bolts per row, rows 1.5 m apart
Poor	5.0	1.8 m × 20 mm, point anchor, 16 bolts per intersection, 4 bolts per row, rows 1.0 m apart, possibly with W-straps
Very poor	<5.0	Specialised support, e.g. combination of cable anchors, roof trusses, shotcrete, W-straps, etc.

It can be seen that Impact Split ratings from poor to very poor recommends that some form of areal coverage must be used. South African underground coal mines have adopted this system but is hardly ever used proactively to specifically determine requirements for areal coverage.

The process to assess roof fall risk and implement controls to manage these risks can be thought of as a series of steps as shown in Fig. 31 [9]. The first step is to recognize and rank defective roof conditions within active portions of the mine. By doing this, hazards are identified and some attempt can be made to rank these hazards from low to high. The next step uses a wide variety of risk analysis techniques to determine roof fall probability associated with specific conditions. Miner exposure, a key element in assessing risk, is next determined by estimating the amount of time miners are expected to occupy the different locations within the active underground workings. Combining the probability of roof falls with the estimation of miner exposure yields a suite of roof fall risk levels that is tied to changing roof conditions. Because risk can be ranked across the mine, risk management methods can be used to determine how to mitigate the risk [9].

2.4 Roof Screening Barriers in Coal Mines

The problem is that roof supports, like bolts or ATRS, are designed primarily to prevent large rock falls and major roof collapses. They do not protect miners from

Table 4 Summarised results of screening study

Considered factors	Mine A	Mine B	Mine C	Mine D
Roof skin condition	Weak claystone, weathering, clay veins, and potting	Clay shale roof, which is highly slicken sided and brittle	Weak roof, horizontal stress, and weathering	Not stated
Mining height	1.9 m	–	2–3 m	Not stated
Road width	5.5 m	5 m	5 m	Not stated
CMRR	22	19–33	22	Not stated
Screen size	4 × 1.5 m @ 8 gauge	4 × 1.5 m @ 8 gauge	4.5 × 1.5 m @ 8 gauge	Not stated
Number of miners installing roof screen	3—Two roof bolter operators and one bolter helper install roof screen	3—Two roof bolter operators and one bolter helper install roof screen	Two roof bolter operators load and handle roof screen, and operate a Fletcher CHDDR walk-thru bolter	Not stated
Roof bolter machine and type	J. H. Fletcher DDR, twin boom bolter with mast feed that enables angle bolting—Non walk-through bolter	J. H. Fletcher twin boom bolter with mast feed that enables angle bolting—Walk-through bolter	J. H. Fletcher CHDDR walk-thru bolter with a storage area at the rear of the machine for bolting supplies	J. H. Fletcher CHDDR walk-thru bolter equipped with material handling system (MHS) that has many features that reduce material handling and address ergonomic principles. There is a separate screen tray that minimizes the potential for screen damage and snagging on other supplies
Additional time due to screening/per 36 m of advance	52 min	12.6 min	39 min	25 min
Experience with screening	Recent implementation	5 years	7 years	Not stated

(continued)

Table 4 (continued)

Considered factors	Mine A	Mine B	Mine C	Mine D
<p>Other ergonomic problems due to material handling OR ergonomic barrier breakthroughs</p>	<p>The screen sometimes snagged on bolting materials or on other pieces of damaged screen. The damage occurred when the scoop moved the screen from place to place before loading it onto the bolter. The screen also got damaged when tramming around corners. Because of this damage, the operators had to jerk the sheets apart from each other, therefore subjecting themselves to injury. Also, the sheets were cumbersome to handle, and involved lifting, pulling, reaching, and twisting motions. The bolters had difficulty keeping the screen from sliding around on the ATRS. Twice during the study, the screen slid inby the ATRS making the sheets difficult to recover. This sliding made up a majority of the time spent on handling screen</p>	<p>Screen can get damaged when moved around by the scoop. The rib bolter must carry the screen along the side of the bolter, making it difficult to see his/her footing. The screen must be lifted from the ground to an overhead position, putting the person at risk of musculoskeletal injury. Adding to these problems, the walk-thru bolters is higher because of the elevated walkway</p>	<p>Because the sheets are quite long, sheets of screen can get damaged while making a turn. Damaged wires on sheets snag on other sheets. Sometimes the screen gets caught on the bolting materials stored underneath. This makes it difficult for operators to remove the sheets from each other or from the supplies. In addition, it is strenuous to lift and pull the screen to the front of the bolter. The operator must lift the screen overhead and then twists before the other bolter handles the sheet. The screen must be placed over the bolter canopies and on top of the ATRS</p>	<p>Strain/stress is reduced in handling screen because the operator can pull off the screen at a more comfortable level. The screen has less chance of becoming damaged because the bundles are handled less and do not get damaged when turning corners. Roof bolters do not have to struggle to retrieve bolting materials because the screen is on a separate tray. Fatigue is reduced because operators do not hand-load screen and supplies. The large sheets of screen would obviously cover the walkway when loaded onto the machine. This would not allow a clear exit from the machine boom in case of emergency. But by design, the tray has eight directions of movement and can be moved out of the way</p>

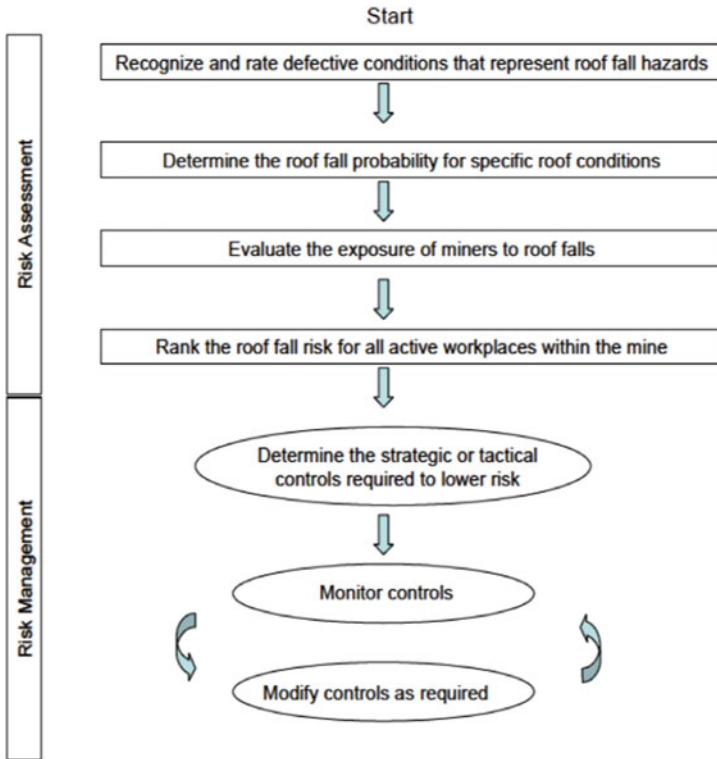


Fig. 31 Flow diagram depicting the generalized structure of Roof fall risk assessment activities and its relation to risk management activities [9]

smaller pieces of rock that fall from between or around the supports. Figure 32 shows two (2) roof skin failure accidents involving rocks that fell between roof bolts and injured continuous miners' (CM) operators in a Highveld coal mine during the time that author was employed at this mine. The author was also involved the Incident Cause Analysis Method (ICAMS) investigation which were conducted for both these incidents. The results of the ICAMS was that there was failure to either identify loose rocks in the roof or failure to bar down, or both. A recommendation was that CM operators need to be retrained on making safe procedures, especially roof barring. Lack of areal support was not considered as a contributing factor towards these roof skin failures. The author can also comprehend that South African underground coal miners' mindset is not yet ready for a noble idea of full cover areal support in order to eliminate roof skin failure accidents. Areal coverage was not even mentioned during the ICAM, instead there is a clear dependence on barring.

Unfortunately, many mines do not use roof screen because they think installing it would be awkward, time consuming and expensive. However, studies reported by NIOSH have shown that simple machine modifications, well-planned supply methods and best-practice installation techniques can minimize the effects of roof screen

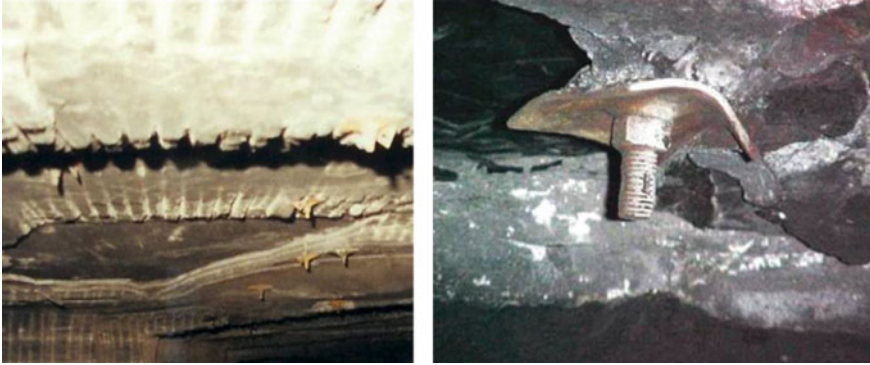


Fig. 32 Photographs of rock that fell from between roof bolts and seriously injured a mineworkers in a Highveld underground coal mine on different dates in 2012

installation on a mine's overall mining cycle ([14], cited by [12]) and this view is even relevant today. Moreover, at many mines, the savings in worker's compensation costs alone could cover much of the cost of roof screen (Moore et al. 2010, cited by [12]).

Safety culture is the most important attribute that has a huge potential to address roof skin falls. For example, over eight (8) years following the ratification in 1969 of Coal Mine Health and Safety Act in the USA, the rate of fall of ground fell to about 0.15, an unprecedented 75% reduction. Careful analysis indicated that this reduction was not primarily due to new technology, but rather to widespread application of technologies that were already available. In particular, much of the improvement can be attributed to the requirement that essentially all roof be supported according to a mandated roof control plan (Mark 2002, cited by [12]).

Nevertheless, skin failures continue to occur between the bolts even though there are not reported accurately as skin failure. For example, in April 6, 2017 an American coal miner was fatally injured by fall between the bolts.

Preliminary accident report on that incident reads:

"A section foreman was seriously injured by roof rock that fell in the No. 3 entry on the active working section. The rock fell from between roof bolts and was approximately 3 ft wide by 2 ft long by 3 to 4 in. thick. First aid was administered and the injured miner was transported to a medical center. Due to medical complications from the injuries he sustained, the victim died on April 6, 2017."

Final report overview reads:

"On February 23, 2017, at approximately 9:30 p.m., Dennis J. Fillinger, a 62-year-old section foreman, was seriously injured when a portion of loose, inadequately supported roof rock fell, crushing him against the mine floor. He was working on the active section at the time. Due to complications resulting from the injuries he received in the accident, Fillinger died on April 6, 2017. The accident occurred because examinations failed to identify loose, inadequately supported mine roof where miners are required to work and travel." [26]

A contrast between the preliminary and final report is that there is no mention of ‘*fall between the bolts*’ in the final report. Rather a new description was used ‘loose, inadequately supported roof’. Falls between the bolts are the type of falls that this paper is concerned with, skin delamination and rocks dislodging between the bolts. The preliminary report exposes that there is such a problem in the mine but the final report is not highlighting the problem as a roof skin incident as is the preliminary report. Coherent reporting should be encouraged.

Despite the apparent benefit of greater use of roof screen, many operators, for example, in the United States do not think of screening as an appropriate support, especially in cycle. There are a number of barriers which prevent its full acceptance, including material cost, slower bolting advance rate due to screen handling, and possible ergonomic risks to the operators. The concern is that the use of screen may increase the likelihood of musculoskeletal injuries such as strains and sprains. As much as 29.7% of all mining industry lost time days in the USA (1997–1999, excluding fatalities) are from sprain injuries of the back, knee, or shoulder. Also, 27% of all lost time days were from material handling injuries. Using the NIOSH cost model, the average cost of material handling injuries from 1997–1999 was \$22,284 per injury.

A concern is therefore that material handling injuries may increase due to increased materials and supplies associated with screen installations and sheets of screen can be cumbersome to handle. Overhead lifts and awkward positioning, along with lifting, pulling, and twisting movements, may have negative ergonomic consequences on operators.

2.5 Screening Impact on Mining Advance Rate

Advance rate due to screen handling and installation is discussed separately here because it is regarded as the single most technical barrier linked to a mine’s profitability. Robertson et al. (2005) conducted a study in four (4) American mines where roof screen was being installed. For these studies, only activities that delayed the bolting advance rates were considered as time to handle the screen. For example, a scoop operator delivering screen to a cut does not slow down bolting but the time taken by the roof bolt operators to load the screen onto the bolter and then dispense these sheets to an installation position does slow down bolting. The results of that study are summarised in Table 3.

Results show significant variation in the additional time necessary for screening. This reflects the experience and resources of the individual mine. A lower bolting advance rate is a barrier that can be improved with time and practice.

Time savings can be achieved when loading bolting supplies with the material handling system (MHS). A comparison was made of operators loading supplies in Mine C and Mine D. In Mine C, it takes 3 men approximately 13 min to hand-load a shift’s worth of supplies onto the bolter. In Mine D, it takes 2 men about 6 min to load the left and right material pods onto the bolter, including the removal of the

empty pods, based on accounts of bolter operators and mine personnel. Each pod contains a shift's worth of materials. Any supplies left on the empty pods are taken outside, removed by vendors, and credited to the mine's account.

2.6 Review of Work Done to Develop a Polymer Product to Replace Mesh

Installation of steel mesh can be onerous and time consuming especially when speed of installation has direct bearing on production. Many other products have been trialled to take its place. Ideally, the properties of these new products should be similar or better than those of the steel mesh. Thin Spray-on Liners (TSL) trialled in the mines according to the authors experience have had many problems including poor adhesion to the coal wall and more expensive than mesh. Therefore, they cannot at the moment compete with steel mesh. Currently, manually handled steel mesh is still the most widely used product to control friable strata in underground mines. Despite potential benefits for TSL, Mitra et al. [13] asserts that the original aim of using TSL as an alternative to mesh and shotcrete has not been achieved.

Work done at the University of Wollongong by Nemicik et al. [16] to develop a polymer that could potentially replace steel mesh, is contained in publications spanning from 2008 until 2011. Since 2011 there has not been any further work or update published in regards to this specific product.

In 2008, Nemicik et al. [16] established the desired material properties of polymeric skin that could potentially replace mesh. The ideal product should have the following attributes:

- should provide an effective skin confinement equal or superior to mesh;
- should require minimal human intervention in its installation;
- should remove personnel from immediate face area;
- should enable high development rates of underground roadways;
- should be safe to use;
- should be cost effective.

The product must have the following properties:

- able to spray-on without slumping;
- non-toxic emissions during application, initial set or curing;
- rapid initial set (seconds) and develop full strength over time (minutes to hours);
- good adhesion to coal and typical coal host rocks in a coal mining environment;
- not pH sensitive;
- semi-permeable to water and gases;
- high strength but flexible;
- able to arrest or retard flaking and spalling of roof and ribs;
- light coloured;
- anti-static;

– fire retardant.

In a search for a polymer product that could replace the mesh, Nemicik et al. [17] investigated or rather tested the polymer skin reinforcing capabilities. This is a significant step towards attaining the objective of replacing mesh with polymer product and this investigation is outlined here to some detail. Several numerical models were developed to test the roof response to displacement of fractures in the roof. The models were designed to simulate fracture behaviour with dilation and displacement parallel and perpendicular to the fractures. The numerical simulations were done with and without the polymer skin reinforcement. During the fracture movement two distinct displacement mechanisms occur:

- (i) fracture displacement along its length (shearing); and
- (ii) fracture dilation perpendicular to the fracture plane due to fracture irregularities.

The mechanism of fracture movement can be seen in Fig. 33 with combined fracture displacements parallel to the fracture plane and the influence of the fracture asperities on fracture dilation. Other fracture opening mechanisms are also common during strata bending or tension.

It can be seen in Fig. 33 that the mechanism incorporates fracture dilation and fracture shearing. The two processes were studied separately. Fracture dilation is in the order of few millimetres depending upon the roughness of the fracture surface as shown in Fig. 34, and shear is shown in Fig. 36. It must be pointed out that the fracture shearing and dilation are not separate events but occur at the same time. Several numerical models are said to have been used to compute the results for these tests. Figures 35 and 37 are the results of fracture dilation and shear, respectively.

In Fig. 12 above, the polymer skin was bonded to the rock surface and fracture dilation simulated. In response to the fracture dilation the polymer skin de-bonded in the immediate vicinity of the crack but the strong adhesion to the rock kept the polymer skin anchored a short distance from the crack opening. Opposing the fracture

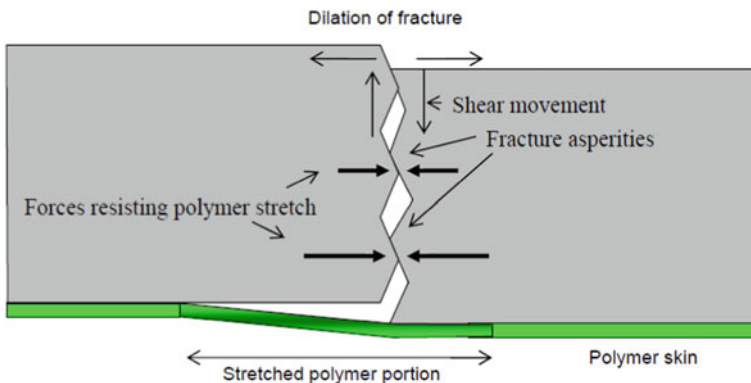


Fig. 33 Shearing and dilation mechanisms of fracture surface (after Nemicik et al. [17])

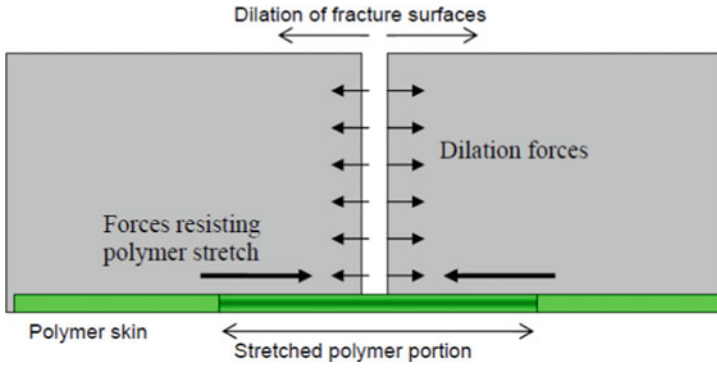


Fig. 34 Dilation mechanism parting the fracture surface (after Nemcik et al. [17])

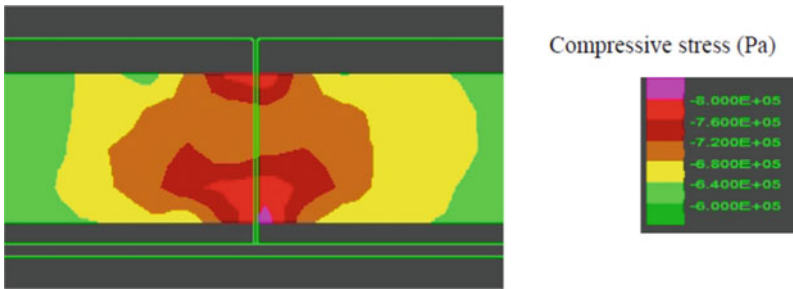


Fig. 35 Effect of fracture dilation on lateral stress across the fractured surface (after Nemcik et al. [17])

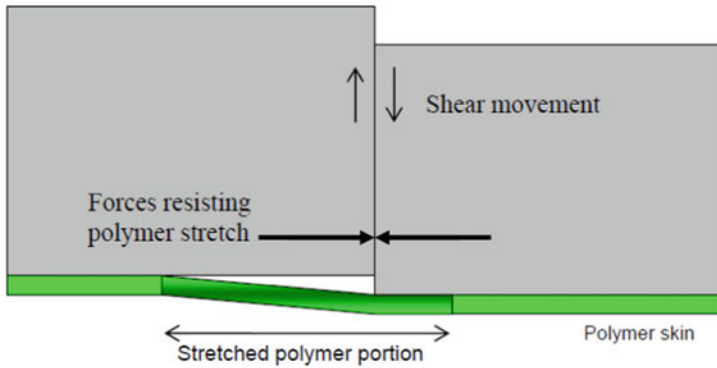


Fig. 36 Shearing mechanism along the fracture surface [17]

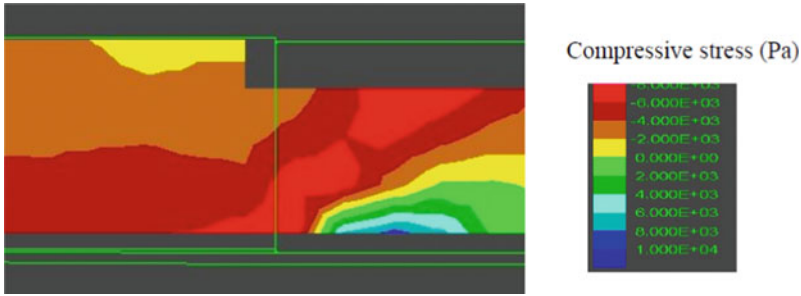


Fig. 37 Effect of fracture shearing on lateral stress across the fractured surface (after Nemcik et al. [17])

opening, the stretched polymer induced a compressive stress within the rock. The test results can be observed in Fig. 13.

The stress contours shown in Fig. 13 clearly show a significant compressive stress normal to the fracture that occurred in response to 2 mm of fracture dilation. The magnitudes of stress that develop within the lower roof is said to depend on:

- (i) fracture displacement,
- (ii) polymer bonding properties,
- (iii) polymer stiffness, and
- (iv) polymer thickness.

In the second model (Fig. 14), a completely smooth vertical fracture was gradually displaced and the polymer skin response observed. During the vertical shearing, strata movement parted the polymer skin away from the rock surface, de-bonding a short section of the polymer/rock interface. The polymer was thus forced to stretch across the fracture as the distance from the bonded anchorage on each side increased.

The reaction force of the skin polymer induced a small compressive stress within the rock across the fracture area, as shown by contours in Fig. 15. It is the fracture dilation that in this case produced greater stress across the fractured surface as compared to shear displacement.

2.7 Other Polymer Tests

2.7.1 Adhesion Test

Mitra et al. [13] conducted in situ adhesive tests of a certain liner in an underground mine in New South Wales (NSW). A liner was applied on the ribside in fractured and intact coal surfaces as in Fig. 38. Test apparatus used was distributed force a pull off system with a maximum force of 6.3 kN. Test dollies 28.2 mm were glued to the surface and test area covered with a coring bit to ensure that pull off is only restricted to the test area as in Fig. 39.

Test were done at different curing times and results are depicted below in Fig. 40.

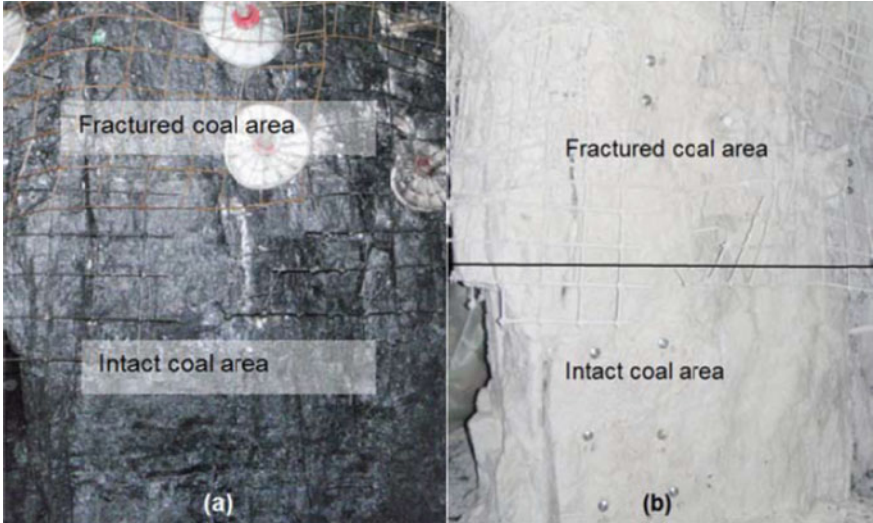


Fig. 38 In situ adhesion test area before and after TSL application (after Mitra et al. [13])



Fig. 39 In situ adhesion strength test showing overcoring on the left and dolly under test on the right

It can be observed that the strength increase with curing times. Other observations were that failure modes were that of coal internal substrate. Conclusions were that this particular TSL could be implemented for underground coal mining conditions. The tests were conducted parallel to the strata, recommendations were that further tests normal to strata should be conducted to test the adhesive strength in the dimension and that effect of long term curing should also be investigated.

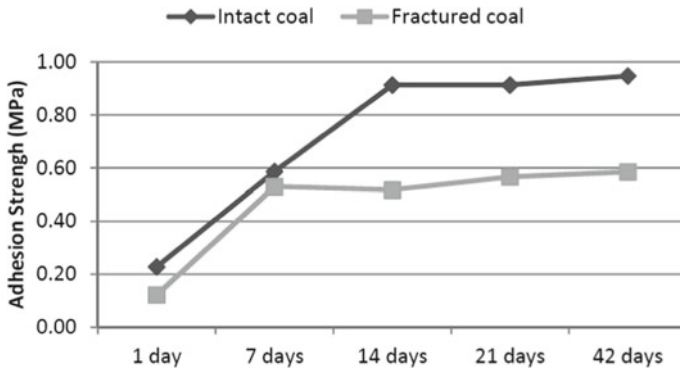


Fig. 40 Results of adhesion strength test at different curing times 9 after Mitra et al. [13]

2.7.2 Polymer vs Steel Mesh

Nemcik et al. [18] also conducted full scale tests to compare fibre re-inforced polymer with steel mesh. Specimen were prepared as in Figs. 41 and 42 respectively. Specimen were firmly secured and in-situ loading was simulated on the specimen.

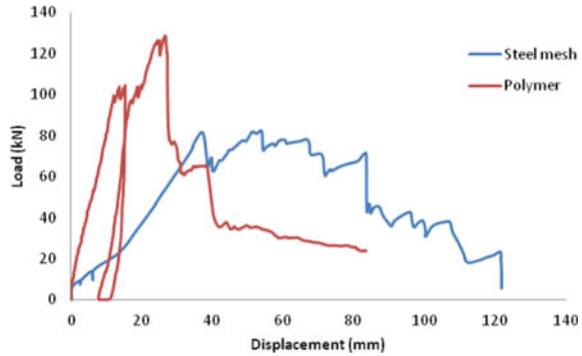
Fig. 41 Concrete sections on the top of the steel mesh (after Nemcik et al. [18])



Fig. 42 Fibre reinforced polymer liner (after Nemcik et al. [18])



Fig. 43 Load–displacement curves for bonded polymer liner and steel mesh (after Nemcik et al. [18])



It can be seen from Fig. 43 that the polymer liner provides higher support loads at lower displacements while it continues to support the strata at large displacements. The polymer liner provides greater confinement to the strata at lower displacements and when overloaded it is still able to provide significant support to the fractured strata as displacement increases. It is not practical to prevent the formation of mining induced fractures but it is possible to enhance the excavation surface condition by applying an effective support system at an early stage of mining. The nature of rock support is to preserve the rocks self-supporting ability by the use of the rock support material rather than holding the dead weight of the rock. Even if the plain polymer sheet is weaker than steel mesh, it is able to provide better load bearing capacity when bonded to the broken concrete slab than steel mesh in a similar situation. If the performance of the bonded polymer was replicated in the full scale test, the expected peak load would be around 70 kN (7 tonnes), 50% greater than standard roof mesh. It appears therefore from these tests that a liner is a much desirable support than mesh in as far as enhancing the competence of the rock mass structure.

2.8 Chapter Summary

Various paperers are in agreement about key issues related to roof skin problems. Areal coverage by means of welded mesh or nets could be very effective ways of reducing fall of ground accidents between the bolts [10, 12, 14, 15, 21]. Polymer liner could be the future of underground coal mining solution to deal with roof skin problems [13, 16–18]. Barring, despite being a noble idea and practice has physical and physiological limitations [2, 19].

In the USA paper around the topic of mitigating against roof skin has been inactive over nearly the last decade. Most of the recent work comes from Australia. One of the last investigation work in line with this topic was by Nemcik et al. [16, 17]. The work entails investigation of polymer-based alternative to steel mesh. They indicate that over 20 products are now available in the market and are mostly designed to provide secondary support in addition to mesh. The work also entails geotechnical

assessment of polymeric material as skin reinforcement in underground mines. In this work the strength and performance of a particular polymer product was tested.

The work performed by Nemcik et al. [17] when testing the capabilities of polymer product indicated that fracture dilation induced significant compressive forces across the fracture as compared to fracture shearing. The implications are that the polymer would need significant tensile strength and yield-ability to accommodate fracture dilation. In regards to fracture shearing, less compressive stresses are generated across the fracture but there is a tendency of the skin polymer to detach from the roof. Therefore, a good adhesive strength would be required for the polymer to perform well. Two findings stand out from this experiment, that the polymer would need high tensile and adhesive strength.

Other polymer characteristics such as the adhesion and direct comparison between welded mesh and polymer have been studied [13, 18] and results promise that polymer liner could be the future product to deal with roof skin problems.

In the US, publications in line with roof skin control and management also ceased for more than a decade now. Robertson et al. [21] produced graphically represented data from 1991 up to 2001 of all roof skin related injuries. A downward trend in the injuries began in the mid-1990s influenced by the installation of roof screen at the time. From the author's communication with the officer of the National Institute for Occupational Safety and Health (NIOSH) it emerged that no such data have been collated or presented or made available since 2001. In any case, as far as the roof screen (mesh) is concerned, Robertson et al. (2002) have demonstrated that it could reduce number of injuries associated with roof skin failures and from the work study they conducted at four (4) mines, it could improve productivity. Extensive paper has been done in order to improve the effectiveness of barring [2]. During this project two concepts, namely the lightweight pinch bar and the mechanical "jaws" were developed to the tested prototype stage. An experimental development model for each concept was first designed, built, and tested after which design reviews were held and prototypes built. The prototypes were tested in the laboratory after which the design was again modified. The prototypes were then evaluated underground in platinum, gold and coal mines. The underground evaluation revealed that the products could be further improved with certain minor modifications. Although the prototypes were successfully tested underground these tests revealed that the tools could still be improved. The underground evaluations showed that both the lightweight pinch bar and the mechanical "jaws" can be successfully used for making safe. The mechanical "jaws" needs modifications to ease penetration into cracks. Depending on the job or conditions the pinch bar and/or the mechanical "jaws" can be used. Different tools for different jobs. The lightweight pinchbar could be used to sound and penetrate a crack, and then to insert the jaws and pry the rock loose. This process will reduce operator effort and stress considerably, leading to better quality and safer barring in underground excavations.

Findings of that work can be summarised below:

- There is a need for a simple barring system to enable operators to stabilise the rock effectively and efficiently from a safe distance before work begins in an area.

The operator often is unable to work at a safe distance and is sometimes directly underneath unstable rock when attempting to “make safe”.

- Furthermore, current methods are physically demanding on the operator, which can lead to poor concentration, improper completion of tasks, and accidents.

The following changes to the prototype designs are recommended:

Lightweight pinch bar

- The pinch bars should be available with different size steel tips: 19 and 25 mm.
- Different length pinch bars should be available for different heights of roof.
- For the coalmines a different steel tip is required. It is recommended that a tip be used where the chisel tip point juts out at a 45° angle to the chisel shaft and where the chisel point protrudes at least 100 mm from the shaft to facilitate proper levering of the loose rock.

Mechanical Jaws

- The mechanical “jaws” should be available in different lengths.
- The tips of the “jaws” should be narrower to fit easier into cracks.
- In order to dislodge more rocks with one opening, the “jaws” should be able to open wider.
- Reduce the weight of the “jaws” by modifying its design.
- The hammer action on the tips does not help to insert the tips into cracks and can be done away with.

Dedicated paper is required in South African mines to address the problem of roof skin failure and management, besides barring. In South Africa, van der Merwe et al. [24] performed a fundamental work of identifying the causes of roof skin failures, their locations and their timing occurrence. However not much of this study was dedicated to managing these roof skin failures. Work done by Canbulat [4] for his thesis titled “Evaluation and Design of Optimum Support Systems in South African Collieries using the Probabilistic Design Approach” indicated that short bolts can be used to pin delaminating roof skin, a practice the author of this report has never seen before. In general for South African coal mines, roof skin management is not incorporated in support design. There is no established guideline for the use of roof screen. Injuries and incidents related to roof skin failure are mostly not captured or reported. Installation of roof screens are mostly adhoc and a prerogative of mine management. However, Fall of Ground Task Team formed since 2017 by Mineral Council South Africa intends to develop a guideline in regards to the use of roof screens to prevent roof skin failure injuries. South African underground coal mines seem to be leaning heavily on roof barring using a pinch bar, despite known physiological challenges associated with manual physical barring.

Around the world, indications are that there is a conscious and deliberate effort towards addressing a problem of areal coverage on the mines. Work undertaken at the University of Wollongong to develop a polymer product that cures in seconds and forms an instantaneous strata binder that surpasses the properties of steel mesh [16] is a forefront example of that effort. The outcomes or the progress of this work

cannot be established currently. Other ideas and products may be in the market and could be trialled.

3 South African Coal Mines' Current Approaches and Practices to Manage Roof Skin Problems

All South African coal mines have at least to some degree of roof skin instability problems that according to the author need to be resolved. Nevertheless, as mentioned before in the introduction, areal support in South African coal mines is installed on an ad-hoc basis at selected sites and as a follow-on support usually several days or months or even years after the excavation is exposed or after the primary support is installed. It is not a proactive measure. In most instances it is applied only after some roof skin failure incidents and other relevant motivations. Very few excavations are pre-designed to include areal coverage support. Exceptions may include service excavations.

Almost all South African coal mines have roof skin problems. However, there is a mine in the Standerton area (Mpumalanga) that has thick competent sandstone in the roof and roof skin stability is not a concern for this mine. The author is not aware of any other mine besides this one, which is known to have no roof skin problems. The problem is fairly countrywide.

3.1 Roof Skin Support Installation in South African Mines

Typically in South African coal mines only severe and unavoidable roof skin conditions are met with welded mesh and bolts. In regards to incorporating roof screen, especially wire-mesh in a primary support system, there are mixed reactions in regards to the approach. Some miners are reluctant to spend money and incorporate areal coverage as an essential standard support where roof skin problems are known to exist. There are three (3) key problematic issues or hindrances in regards to standardising areal coverage in South African coal mines where roof skin failure poses a risk. The author has named and critiqued them as follows:

- **Slow rate of installation and skill.** There is a concern that there will be loss of cutting time as Continuous Miner (CM) may have to wait for the bolter to finish installing support because of additional work of screen installation. However, Robertson et al. [21] proved in a practical study that this view is mythical. Slow rates of installation can be improved as the operators become more used to the system. Besides, installation of roof screen does not have to be done the same time as the primary support.
- **Cost.** Ferreira and Pirrido [7] point out that most mines view the areal coverage support products (wire mesh screens, nets, cementitious liners) as expensive. They

also point out that routine or cyclic use of these support items will put pressure on the miners in regards to potentially slow advance rates. The additional cost of roof screen support cannot compare with the monetary compensation due to injuries sustained by personnel and damage to property as a result of roof failure [20].

- **Culture.** Underground coal mining, especially in South Africa, has been carried on for many decades with an ‘almost acceptable’ risk of roof skin failure. The mitigation has always been physical barring. Dependence on physical barring has not impacted visibly on the problem as the statistics indicate and perhaps time has come to shun dependence on physical barring and vigorously explore potential alternatives.

Typical areal coverage support products in South African coal mines are plastic nets and wired-mesh. The author is not aware of any South African coal mine where cement liners or shotcrete has been or is being applied, except a Minova product called Tekcrete Fast M which is being applied at a Secunda mine in the belt road at selected high risk areas. Application of cement liners is common in hard rock mines.

In 2007, the author was involved in a brief shotcrete application experiment in a mine near Secunda area. Shotcrete was applied on pillar sidewalls and roof in an attempt to subdue scaling, spalling and roof skin failure. The section was particularly prone to roof skin failure and sidewall scaling. In a matter of few days all the shotcrete had scaled away from the pillar sides and from the roof, together with some coal material. Consequently, the appropriateness of cement liner as an areal support to combat roof skin failure in underground coal mine was not accepted and was never tried again. Tekcrete Fast M has since come along in 2019 and it displays superior characteristics compared to the liner the author trialled more than ten (10) years ago, in 2007.

Another mine near Emalahleni is currently installing hundreds of kilometres of plastic nets in old (back bye) areas to *arrest* roof skin delamination. The focus of installation is the traveling road and the belt roads. Roof skin delamination incidents were a frequent occurrences at this mine. Vehicles especially were frequently impacted while driving through these roads. Conveyor belts were often on break down because of being struck by roof falls. All these falls were thin delaminations and could at times be significantly wide, however thin. The strategy at the colliery is not to prevent roof delaminations but rather to arrest them with the nets. This method of roof skin control is also known as separation or basket mechanism.

Another colliery in the Vaal basin, Free State has incorporated welded mesh as part of primary roof support. That is a milestone development and it shows that total areal coverage in a mine is a real possibility.

The author is not aware of any other mine in the country where areal coverage support is incorporated into primary support and or installed mine wide.

The author was also involved with one coal mining company in the Highveld in trials to customise the roof bolters to install the mesh in a hands free fashion. The idea behind this was to incorporate a mesh reel in a roof bolter from where the mesh could be rolled flush against the roof and pinned with bolts. Experiments and trials in

regards to this approach have since ceased and seemingly capped. That idea should be revisited because if it materialised it could make the screen installation quicker and could lower opportunity cost of the continuous miner, meaning the continuous miner may not have to wait for support installation to complete before it could cut.

3.2 *Roof Barring*

Roof barring has always been the first and critical step to deal with delaminating roof. In former times when blasting was still the main mining system before the introduction of continuous miners, roof barring was done vigorously. There were dedicated crews just performing roof barring. Even then, roof skin delamination was still a problem but it was masked by major roof falls. Roof support system in South African mines was still in its earliest development. Roof bolts were thin and were end anchored. The phenomenon of horizontal stress and its impact was yet to be fully appreciated and catered for later with thicker roof bolts and full column resin. There was no clear distinction then between roof skin failure and just a roof fall. Mesh installation during those times was even rarer than present day. However, there has always been awareness of the need for total areal coverage and this can be attested to by the use of extended wooden headboards that were common in those days.

The introduction of continuous miners saw the disappearance of dedicated barring crews. Barring is now performed less frequently. It now forms part of working place entry examination. During the shift, roof barring is ever hardly performed. In most underground mines in South Africa, roof barring is not the responsibility of a specific personnel, every person underground is expected to perform roof barring if needs be. Whether or not it is a reasonable expectation that all persons exposed to underground environment should be able to bar down, needs further investigation.

There are several challenges pertaining to physical roof barring:

- *Physical strength requirement.* In order to effectively bar down one needs the physical strength, endurance and agility. This requirement is not favourable to some of the employees who are not endowed with such physical traits, even though they passed the medical fitness. It would be therefore unreasonable to expect such individuals to bar down. Even though attempts have been made to make the pinch bar lighter, no studies have been made to actually assess the impacts of that effort. From the experience of the author this modification to the pinch bar to reduce its weight has had no pronounced known benefit. It is still physically demanding. Most mines do not test the physical capacity of employees even though they are expected to bar the roof. One mining company in the Highveld has taken this issue further by introducing ‘barring test’ facility. All new underground general workers recruits have to pass this test in order to be signed on at the mine. In this test, a 3 m pinch bar is used to imitate barring at the average height roof height of 3 m. This exercise is performed for straight 20 min. Heart rate is taken before the commence of the exercise and after. The final heart rate may not exceed 150

beats/minute. If the heartrate exceeds this threshold, the candidate shall not pass medical fitness to work underground. This test is a step in the right direction in as far as justifying the expectation to bar down the unstable roof.

- *Extreme Mining Heights.* Mining heights in excess of around 3.5 m are particularly difficult to bar down safely. The pinch bar has to be longer and heavier and there is also a risk of personnel barring down inadvertently upon themselves. This condition inevitably leads to the roof remaining unbarred.
- *Scope of barring.* Normally there is vast amount of roof exposed per shift that requires inspection and barring. Typical shift staff in South African coal mines comprise of around 8 (eight) people who have other specific responsibilities besides barring. Barring as a responsibility to the crew becomes therefore a side issue and it is often ignored.

During several site inspections in underground coal mines, South African rock engineers often find that roof barring had not been performed or it was not effectively done. The reason could be attributed to the 3(three) main factors discussed above. It is for these reasons that dependence on roof barring should be investigated.

3.3 Roof Skin Failure Reporting and Database

There is a formal system for reporting falls of ground by way of South African Mines Reportable Accidents Statistical System (SAMRASS) forms. According to the law, the following uncontrolled rock or ground movement must be reported:

An extensive rock burst or fall of ground causing the following damage underground:

- i) At least 10 linear metres of working face has been severely damaged and choked and will require re-establishment and re-supporting, or be abandoned;
- ii) At least 25 m² of working area has been severely damaged and choked rendering support units ineffectual and will have to be re-established and re-supported or be abandoned;
- iii) At least 10 linear metres of gully has been restricted with rock clearly recently displaced from the hanging wall and gully sidewalls;
- iv) At least 10 linear metres continuous or 30 linear metres cumulative of access ways of tunnel or travelling way has been severely damaged and will require rehabilitation or be abandoned;
- v) At least 10 m² of roof or 5m³ of rock has been displaced from the roof of the mining cavity or excavation;
- vi) At least 10 m³ of rock has been freshly displaced from pillars or tunnel sidewall.

It is clear from the above that roof skin delamination type of falls are likely not to be captured in, hence there is no state database existing in regards to these falls. Where there is no database a problem of roof skin instability cannot be fully comprehended, appreciated and surely it is unlikely to receive the attention it deserves. Only one

mining company in the Secunda area has recognised roof skin incidents as worth capturing as shown in Fig. 1.

The Code of Practice guidelines also does not specifically address roof skin problems. Specific inclusion of roof skin control in the Code of Practice could potentially encourage mining companies to deliberate on the implementation of areal coverage support, thereby formulate standard approach and allocate a budget.

4 Conclusions

The main hindrance to the effective implementation of areal coverage support is the cost and anticipated slower mining rates. However dedicated and systematic planning or lack thereof seems to also play a role. The use of areal coverage in South African coal mines is not informed by any roof rating system or immediate roof testing such as Slake Durability. The installation of areal support is largely motivated by visual observations. This approach has a limitation in that signs of roof skin instability are not evident at the time of cutting. Therefore, areal support is hardly installed proactively and the installation becomes a high risk operation because the roof is already unstable at the time of installation.

In the USA, however, there is a systematic determination for the use of areal coverage stemming from Coal Mine Roof Rating (CMRR). It is recommended to enlist some form of areal coverage to values of CMRR below 35. CMRR is not very popular in South African coal mines. A consideration to adopt CMRR in South African mines as guideline for the use of areal support may be a worthwhile exercise to pursue.

Popular roof rating system in South African coal mines is the Impact Split test. Even though the Impact Split test does give an indication of the roof skin condition, proactive implementation of areal support stemming from poor ratings is hardly done. Full adoption of Impact Split test and its recommendations could significantly improve roof skin conditions but that is not the case. Impact Split tests seem to be performed in South African coal mines just for knowledge of the roof competency. Its recommendations are never adopted, especially for poor and very poor ratings.

South African coal mines uses a variety of basket mechanism products. Basket mechanism is when surface support develops in the form of a basket, which then contains the failed rock. Welded mesh installed with double-nutting is one example of such products. Plastic nets is another but most mines who trialled the nets have abandoned them due to their lack of stiffness and subsequent difficulty to control during installation. One mine in the Highveld is the only prominent installer of plastic nets in old travelling and belt roads. Spray-on products are not very common in underground coal mines in South African mines. Only recently in 2019 has Minova tested a cement-based liner in one of the mines in the Secunda area at selected sections of belt road. The preliminary results are encouraging. The product shows good adhesive properties to coal strata and no visible signs of weakening. The product is reportedly more expensive than the welded mesh and it therefore cannot be used on

relatively large scale. There are no other trials or applications of spray-on products at the moment in South African coal mines' roof to deal with the risk of skin failure. There has been dedicated attempts at the University of Wollongong to develop a spray-on polymer liner to replace the welded mesh but that project had since been stalled. Nemcik et al. [16] described the design requirements and ideal characteristics of such a product and ran a numerical simulation test on a sample. The author is not aware of reasons for halting this project. There are apparently other products in the market as evidenced by the product used by Mitra et al. [13] to test the adhesion of this product on a coal stratum.

The installation of areal coverage strategy is employed as a very last resort in South African underground coal mines. The preferable strategy is barring. Roof barring has limitations:

- Physical strength requirement
- Minimum height restrictions
- Scope of barring

Sasol mining however has taken a step in a right direction to test the capacity of personnel to bar down by introducing a barring test as part of on-boarding fitness test for new employees. This practice also serves to raise awareness of new employees of the real potential risk of roof skin failure and entrenches upon them a good culture of barring.

There is no geotechnical system to determine proactively, the requirement of areal coverage support in South African coal mines. This could assist with budget adjustments to include the cost areal coverage at the planning phase of mining. Most mines are caught off-guard because ad hoc installation of areal coverage support on observations and 'gutfeel' prerogative of mine management. In such instances most mines are thrown off budget and this is the reason why installation of areal support is perceived to be expensive. The unexpectedness of areal coverage support requirement is the main contributor towards subtle resistance to embrace it. Therefore, for these reasons:

- A well-papared risk rating model that can be used to assess the probability of damaging instability needs to be conducted.
- A model to cost the effect of skin failures (could be an industry-wide model) or a framework for constructing a mine-specific model needs to be papared.

Combining the above recommendations will enable the cost-benefit analysis of potential solutions to be done on a rational basis. In regards to barring, other mines could do well to follow the example of a mining company in Secunda area, to test the capacity of personnel to bar down before considering it as a given that every underground worker should bar down.

References

1. Bauer ER, Dolinar R (2000) Skin failure of roof and rib and support techniques in underground coal mines. In: Proceedings of new technology for coal mine roof support. Conference paper, NIOSH Publication No. 2000-151, pp 99–109
2. Boodoo A, Jermy CA, Kuppusamy V, Ramsaroop P (2016) Identify opportunities to improve the safety of barring-down practices. Mine health and Safety Council (MHSC) Paper Report No. 140202
3. Canbulat I, Dlokweni T (2002) Rating systems for coal mine roofs. SIMRAC Paper Report No. 2002-0528
4. Canbulat I (2008) Evaluation and design of optimum support systems in South African collieries using the probabilistic design approach. Ph.D. thesis. Submitted in partial fulfilment of the requirements for the degree Philosophy of Doctor in the Faculty of Engineering, Built Environment and Information Technology, University of Pretoria
5. Jeffrey LS (2005) Characterization of the coal resources of South Africa. In: South African Institute of Mining and Metallurgy, proceedings of conference on sustainability of coal, Johannesburg, South Africa, 7–9 September 2004
6. Ferreira PH (2012) A perspective on underground support technologies in Southern African platinum mines to reduce safety risks and enhance productivity. In: Proceedings of Southern African Institute of Mining and Metallurgy, fifth international platinum conference ‘a catalyst for change’, Sun City, South Africa, 17–21 September 2012
7. Ferreira PH, Piroddi A (2011) The application of GRP and thin sprayed liner support products in a typical block cave mining method to enhance safety and productivity. In: The Southern African Institute of Mining and Metallurgy 6th Southern African base metals conference. The Hans Merensky Hotel & Spa, Phalaborwa, North West Province, 18 July 2011–21 July 2011
8. Hunter F (2003) Roof support evolution at sigma colliery. Mine internal document
9. Iannacchione AT, Prosser LI, Esterhuizen GS, Bajpayee TS (2007) Methods for determining roof fall risk in underground mines. *Mining Eng* 59(11):47–53. NIOSHTIC2 Number: 20032865. Peer Reviewed Journal Article
10. Kuijpers JS (2008) Support coverage: an essential component in effective support design. The Southern African Institute of Mining and Metallurgy and South African National Institute of Rock Engineering. In: Stacey TR, Malan DF (eds.) 6th international symposium series S51, Ground Support in mining and civil engineering construction, pp 391–408
11. Mark C, Molinda G, Burke LM (2004) Preventing falls of ground in coal mines with exceptionally low-strength roof: two case studies. In: Proceedings of the 23rd international conference on ground control in mining, Morgantown, West Virginia University, 3–5 August 2004, NIOSHTIC No. 20025354
12. Mark C, Pappas DM, Barczak TM (2011) Current trends in reducing ground fall accidents in US coal mines. *Mining Eng* 63(1):60–65. NIOSHTIC2 Number: 20040109. Peer Reviewed Journal Article
13. Mitra R, Chalmers D, Saydam S, Li Z (2015) Investigation on adhesion strength of thin spray-on liners in an underground coal mine. In: Proceedings of the 2015 coal operators’ conference, University of Wollongong Mining Engineering, University of Wollongong, 11–13 February 2015, pp 191–197
14. Molinda GM, Compton CS, Gallagher S, Mark C, Wilson G (2007) Roof screening for underground coal mines: recent developments. In: The 26th international conference on ground control in mining, Lakeview Scanticon Resort & Conference Center, Morgantown, WV, USA, July 31–August 2 2007, pp 270–276
15. Neal D (2010) Mine safety nets in coal mines. A presentation made at SANIRE meeting in Emalahleni, Golfclub, 4 October 2010
16. Nemicik J, Spinks GM, Porter I, Baafi E, Lukey C (2008) Polymer-based alternative to steel mesh for coal mine strata reinforcement. In: Proceedings: coal operators’ conference, University of Wollongong & the Australasian Institute of Mining and Metallurgy (2008)

17. Nemcik J, Porter I, Baafi E, Lukey C (2009) Geotechnical assessment of polymeric materials as skin reinforcement in underground mines. In: Proceedings: coal operators' conference, University of Wollongong & the Australasian Institute of Mining and Metallurgy
18. Nemcik J, Porter I, Baafi E, Shan Z (2014) Full scale tests to compare the strength of polymer liners with high tensile steel mesh. In: Proceedings of the 2014 coal operators' conference, University of Wollongong Mining Engineering, Australasian Institute of Mining and Metallurgy and the Mine Managers Association of Australia, 12–14 February 2014, University of Wollongong, pp 193–201
19. Otterman RW, Burger NDL, Von Wielligh AJ, Handley MF (2003) Development of an effective pinch bar. SIMRAC Paper Report No. 020201
20. Pollard JP, Moore SM, Mark C (2012) Reduced workers' compensation costs with roof screening. *J Safety Health Environ* 7(2):23–29. NIOSHTIC2 Number. 20040106-. Peer Reviewed Journal Article
21. Robertson SB, Hinshaw GE (2002) Roof screening: Best practices and roof bolting machines. In: Proceedings of the 21st international conference on ground control in mining, Morgantown, West Virginia, 6–8 August 2002
22. Spearing AJS, Hague I (2003) The application of underground support liners reaches maturity. In: ISRM 2003:10th congress of the ISRM symposium series S33, technology roadmap for rock mechanics, Johannesburg, South Africa, 8–12 September 2003, vol 2, pp 1127–1132
23. Stacey TR, Mason DP, Fowkes N (2009) A review of mechanisms of shotcrete and thin spray-on liner support, and recent investigations. In: The Southern African Institute of Mining and Metallurgy, Symposium Series S55, Shotcrete for Africa, Misty Hills Conference Centre, Cradle of Humankind, Randburg, South Africa, 2–3 March 2009, pp 237–249
24. Van Der Merwe JN, Van Vuuren JJ, Butcher R, Canbulat I (2001) Causes of falls of roof in South African collieries, SIMRAC Project. Revised August 2001
25. Vorster B, Franklin D (2008) Immediate ground support after development or stope face exposure can prevent falls of ground. In: Proceedings of The Southern African Institute of mining and metallurgy conference, Narrow Reef Vein 2008, Randburg, South Africa, 5 September 2008
26. US Department of Labour, Mine Safety & Health Administration, Preliminary report of accident report (2017) Fatality #5 - 02/23/2017. <http://www.msha.gov/fatals/fabc.htm>

Communication Experiment of Wi-Fi Direct for Underground Mine Environment Visualization System



Hajime Ikeda, Youhei Kawamura, Oluwafemi Kolade, Daniyar Malgazhdar, Mahdi Saadat, Fumiaki Inagaki, Hisatoshi Toriya, and Frederick Thomas Cawood

Abstract One of the main problems in the modern metal mining sector is the depletion of near-surface deposits, the decline in grades. Available deposits near to surface are available and the focus of the industry is shift to deep underground deposits. However, with increase in mining depth risk of rock falls and rock bursts increases concurrently. In order to solve these problems, “smart mining” technology has been

H. Ikeda (✉) · D. Malgazhdar · M. Saadat · F. Inagaki · H. Toriya
Graduate School of International Resource Sciences, Akita University, Akita, Japan
e-mail: ikeda@gipc.akita-u.ac.jp

D. Malgazhdar
e-mail: m6021218@s.akita-u.ac.jp

M. Saadat
e-mail: mahdi.saadat1@gipc.akita-u.ac.jp

F. Inagaki
e-mail: fumiaki.inagaki@gipc.akita-u.ac.jp

H. Toriya
e-mail: toriya@gipc.akita-u.ac.jp

Y. Kawamura
Division of Sustainable Resources Engineering, Faculty of Engineering, Hokkaido University, Sapporo, Japan
e-mail: kawamura@eng.hokudai.ac.jp

North China Institute of Science and Technology, Hebei, China

O. Kolade
Sibanye-Stillwater Digital Mining Laboratory (DigiMine), Faculty of Engineering and the Built Environment, Wits Mining Institute (WMI), University of the Witwatersrand, Johannesburg, South Africa
e-mail: femikolade@outlook.com

School of Electrical and Information Engineering, University of the Witwatersrand, Johannesburg, South Africa

F. T. Cawood
Wits Mining Institute (WMI), University of the Witwatersrand, Johannesburg, South Africa
e-mail: frederick.cawood@wits.ac.za

introduced. “Smart mining” is an area that combines ICT and intelligent resource development. We have developed a communication system that plays a fundamental role in this field, and have conducted communication tests. Communication systems in underground mines are essential for better safety and productivity. In this research, wireless sensor networks (WSNs) have been proposed to record and transfer environmental and worker position data. This research proposes a communication system using “Wi-Fi Direct”, in which data loggers and mobile terminals (i.e., smartphones) transfer data between nodes. According to the technology, data is transmitted from a fixed underground base unit to a worker’s mobile terminal. Next, these datasets transferred to a data logger on surface once the worker gets close enough, the data transmitted wirelessly between surface and underground locations. To verify the feasibility of this system, the communication range, transfer speed, and received signal strength indicator (RSSI) in different environments were measured.

Keywords Underground communication · Wi-Fi direct · Visualization system

1 Introduction

Underground mines operate under the hazards of poor lighting, confined spaces, falling rocks, poor ventilation, high humidity, limited communication, and structural complexity. In this context, safety and productivity are the primary concerns of underground mining companies. To solve these problems, various monitoring methods have been proposed to make safer underground environment. The underground environment can be monitored by installing sensors in the mines to acquire measurements such as temperature, humidity, and gas concentration. Deep underground, rock stress is caused by load of ground itself and the effects of structural movement. When excavating an underground cavity, it is very important to know the rock stress (in-situ stress) and rock displacement (strain) to design and construct an efficient and safe mine [1, 2]. In recent years, numerical calculations using computers such as the Finite Element Method (FEM) have made great progress, but even with rigorous numerical calculations using FEM, there are still many factors that are difficult to estimate, such as support and loading conditions [3, 4]. To evaluate post-excavation stability and safety, it is necessary to monitor the changes of in-situ stress and strain around the tunnel over a long period of time after excavation, in addition to a temporary in-situ stress and strain measurement.

In this study, an in-situ rock stress monitoring system in an underground mine is taken as an example of visualizing the environment in an underground mine. An ad hoc wireless communication system for monitoring has been implemented and validated. This paper reviews several technological trends in underground mine security and technologies, using the modern sensor technologies and ICT (Internet Communication Technology), not limited to mining technologies. The feasibility and problems of these technologies will be discussed.

2 Related Work

2.1 *Measurement of Rock Mass Condition in an Underground Mine*

Two typical methods for measuring in-situ stress using drilling are the hydraulic fracturing method, in which the magnitude of the stress is measured directly by injecting a high-pressure fluid and causing tensile fracture, and the stress release method, in which the amount of strain when the drilling core is released from the stress, in-situ stress measured and determined by calculating the physical properties of the rock sample. The hydraulic fracturing method is considered undesirable for the long-term safety and stability of the area around the drift after excavation, because of possible damage of the rock mass in measured area. The disadvantages of the stress-release method contain difficulty of fixing the strain gauge to the measurement site and the elastic transverse number data of the surrounding rock required. In addition, both hydraulic fracturing method and stress release method are methods to obtain the in-situ stress and strain at the time of the measurement, and they cannot measure subsequent changes in-situ stress and strain. In underground mines, which constantly changing with the progress of mining, temporary in-situ stress/strain measurement methods are insufficient [5]. Therefore, the method of measuring differential stress after stress release is often selected for long-term monitoring around the mine after excavation [3]. In other words, a new measurement method that enables nondestructive and continuous differential measurement is required.

There are two ways to measure in-situ stress and displacement: the non-contact method, where a reference is set in space and the displacement of the non-measured object is measured from that point, and the contact method, where the sensor is directly attached to the object. The advantage of the contact method is it is easier to implement, except when the measured rock is so light that it is affected by the mass of the sensor, or when the temperature is so high that direct mounting of the sensor is not possible. The non-contact method can measure the displacement, but not stress.

2.2 *Wireless Communication Technology in Underground Mines*

Most monitoring systems use wired communications (e.g. Ethernet cables). As reviewed in Sect. 2.1, there are many measurement methods, but unless the data can be acquired by wireless communication, the information cannot be utilized. The use of wireless sensor networks (WSNs) for informatization in underground mines can prevent underground collapses and machine malfunctions, make mining equipment unmanned, aggregate information from various measuring instruments,

and create big data [6, 7]. WSNs can be configured as autonomous networks by not only automatically setting up a large number of nodes via wireless connections, but also by not requiring any technical infrastructure to build WSNs [8, 9]. Every node will transmit its own data and act as a router for nearby nodes [10]. Network supports a reliable monitoring and communication system that includes many nodes, as compared to wired communication, which is much more likely to fail due to cable damage [11, 12]. This allows WSNs to have flexible network configuration and management against failures. If one communication route fails to transmit data, WSNs allow other communication-enabled routes to maintain network functionality. WSNs can also diagnose, repair, and manage network failures without interrupting mining operations.

Among the WSNs, ad hoc communication using ZigBee and Wi-Fi set the standard; ZigBee has a large number of connectable terminals and multi-hop support, but the communication speed is slow [6, 13, 14]. On the other hand, in addition to the advantages of WSNs, ad hoc communication using Wi-Fi can directly establish a P2P connection between devices without access point and use the movement of the used equipment as a means of information transfer. However, P2P connections can cause communication problems when multiple devices are within communication range.

2.3 Monitoring in Underground Mines

The measurement section reviewed in Sect. 2.1 and the communication section reviewed in Sect. 2.2 are independent technological systems. In the future, field monitoring systems should be created by organically integrating these technologies. While this technology has become the norm in factories and machinery, where the infrastructure is relatively easy to maintain, its introduction in underground mines, where communication technology is still in its infancy, has lagged behind. Monitoring is divided into two categories: 1) Environmental monitoring, which includes detection of dust and smoke, measurement of toxic gas concentrations, temperature, humidity, and monitoring of stresses in rocks [15, 16]. 2) Operational monitoring, which includes detection of derailment of heavy equipment and automation of heavy equipment and ventilation systems [17]. The ability to monitor underground mine conditions remotely can also improve productivity and safety. Currently, mining companies are spending a lot of money on understanding the conditions inside underground mines, however effectiveness and cost of monitoring networks is considered as a big issue. As a result, some underground mining companies are often reluctant to set up a communication environment.

2.4 Visualizing in Mining

The visualization of underground mine information obtained as well as monitoring has been a matter of recent interest. Visualization is an effective way to improve productivity and safety in underground mines. Fire hazards in underground mines are one of the major hazards that occur in the mining industry. The simulation method of fire hazards in underground mines using Cellular Automata has been investigated and its visualization effect has been studied [18]. Mining loss rate and dilution rate are important indicators of mining technology and the management level of mining enterprises. 3D models of ore body units and mining areas are built, and Boolean calculations are performed between models to obtain the calculation parameters of loss and dilution, so that the dilution rate and loss rate of mining areas can be calculated more quickly and accurately [19]. The accurate understanding and visualization of the complex internal structure and stress distribution of rocks is very important to solve various problems in underground engineering printing and incorporating freezing stress techniques proved to be a promising method for quantifying and visualizing complex fracture structures and their impact on the 3D stress distribution in the subsurface rock mass, which can be used to validate numerical simulations [20].

3 Proposed Underground Mine Stress Monitoring System

3.1 WSNs used in Underground Mine Monitoring System

The use of wireless sensor networks for underground mine monitoring systems stabilizes operational functions by mitigating the problem of damaged communication lines in wired communications due to underground collapses and machine malfunctions [21]. Underground mining companies use WSNs for environmental monitoring (detection of dust and smoke, measurement of toxic gas concentrations, temperature, humidity, and monitoring of rock stress), worker location, and communication systems [15, 16]. Wi-Fi, Bluetooth, and ZigBee are examples of WSNs [6, 13, 14]. In a previous study, an environmental monitoring system using ZigBee was tested and operated in an underground mine in Western Australia with reliable results [6, 21].

The main applications of communication systems in underground mines are monitoring, communication, and location of miners and heavy equipment. Monitoring is divided into environmental monitoring and operational monitoring. What kind of information is useful for improving productivity and safety in an underground mine is described in Sect. 4, which discusses how much data needs to be transferred during a day.

Wired or wireless communication technologies are increasingly being used for communication systems in underground mines. Wired communication is characterized by the increased risk of wire breakage and the need to redeploy communication lines. WSNs, on the other hand, reduce the number of access points and allow P2P connections to the sensors themselves. There are differences in the number of connected terminals, communication speed, and communication distance, and it is necessary to select one according to the type and amount of data desired.

3.2 Proposed Stress Monitoring System in Underground Mines

The rock mass stress monitoring system proposed in this study can be divided into two parts: the sensing part, which is the differential measurement of in-situ stress and strain, and the data transfer part using ad hoc communication (Wi-Fi Direct). Figure 1 shows the system design of the in-situ stress monitoring system. As shown in Fig. 1, the proposed monitoring system consists of a sensor unit with ad-hoc communication capability drilled into the top of the tunnel. Figure 2 shows the sensor unit with ad hoc communication function and the mobile terminal used in the experiment. The sensor unit is a data logger with ad-hoc communication capability. The sensor unit in Fig. 3 has strain gage attached to the inside of each of the three surfaces and a 9-axis sensor (LSM9DS1) fixed inside. The dotted sensor unit was buried in a blank hole after stress release, and the difference of stress applied from the rock mass was determined from the value of strain gauges. To estimate how much stress is applied from which direction, it is necessary to detect the orientation of the sensor unit. By burying multiple sensor units in the underground space, it was attempted to continuously check the stress status of the entire underground mine.

As shown in Fig. 1, miners acquire measurement data from sensor units. Next, the measurement data can be passed on from other miners who enter the communication range or from other sensor units. Finally, one of the miners goes out of the underground mine to finish transmitting the measurement data to a mine site office on the

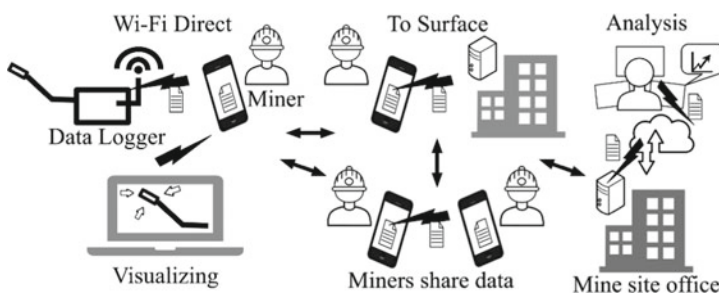
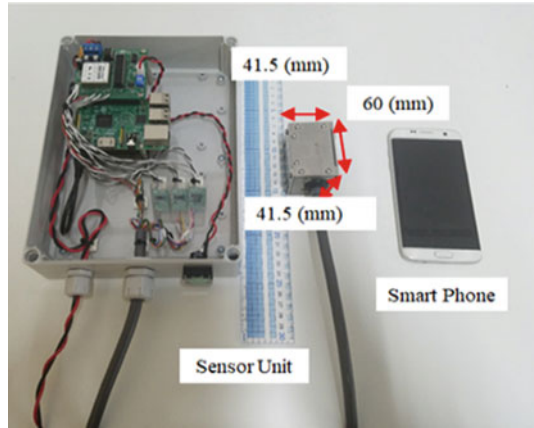


Fig. 1 The system design of the in-situ stress monitoring system

Fig. 2 The sensor unit with ad hoc communication function and the smartphone



surface that is equipped with infrastructure. The data sent to the mine site office can be analyzed and edited anywhere in the world via the cloud. The visualized data can be viewed in the underground mine.

4 Ad Hoc Wireless Communication (Data Transmission)

4.1 Evaluation Indices for Ad Hoc Wireless Communication Tests

Received Signal Strength Indication (RSSI), communication speed, and communication distance are used as indicators to evaluate communication performance. In addition, communication performance varies greatly depending on the surrounding conditions and wireless communication standards. The surrounding conditions should be considered, as this can cause communication errors.

When using wireless communication, it is important to ensure that the signal is stable. In a wireless LAN, the farther the distance, the weaker the signal strength. Therefore, the communication speed becomes slower. RSSI is a measure of the strength of the signal received by a wireless communication device. It is mainly used in wireless communications such as wireless LAN and Bluetooth for purposes such as controlling the transmission range. The reason for this is that if the output power is too strong, it will cover unnecessarily distant areas, resulting in wasted power and the risk of eavesdropping. The communication speed is the amount of data transferred per unit of time. When the RSSI exceeds -80 (dBm), stable wireless communication is established. The theoretical maximum communication speed is different from the actual measured communication speed. And RSSI and communication speed are attenuated by distance. Therefore, in a communication test between two points, it is necessary to measure RSSI and communication speed at each distance.

4.2 Overview of the Ad Hoc Wireless Communication Test

Wi-Fi Direct is used as an ad hoc communication method, which is different from Wi-Fi infrastructure in that it allows devices to communicate directly with each other without the need for routers or auxiliary wiring. Wi-Fi Direct is a communication standard that inherits the advantages of Wi-Fi Ad Hoc and improves on the problems of complicated settings and security. One of the most important features is that smartphones with direct Wi-Fi connectivity can be used as access points. To evaluate the performance of ad hoc communication in underground mines, it is necessary to evaluate it in terms of communication distance and speed, latency, and data stability. These values can be determined by measuring RSSI and communication speed (i.e., throughput). The communication range and speed were calculated from communication tests on both straight paths and angle path. The parent and child devices used were Raspberry Pi 3 computers modified to use the IEEE 802.11 a/ac/b/g/n standard with GW-300S KATANA modules. Specifically, the IEEE 802.11n standard was used for communication testing, and the output voltage of the module was maximized. A Sony IMX219PQ sensor was used as the sub-unit camera module. The resolution of this module was reduced to acquire and transmit image files with a size of 1 (MB). The smart phone (Android Operating System) used in this communication test is IEEE 802.11 a/ac/b/g/n multiple-input multiple-output (MIMO) capable. When the underground environmental data such as temperature, humidity and gas concentration are measured at the appropriate sampling frequency, the data volume is 2 MB/day. This amount of data can easily be transmitted by the communication system implemented in this project. In this paper, a communication system that transmits data from underground to above ground (or from above ground to underground) by means of bucket relay communication between mobile terminals and sensor units is proposed.

5 Communication Test Results

The communication test was conducted at the Osarizawa Mine in Akita Prefecture (Fig. 3). The communication standard of the equipment used in the experiment was

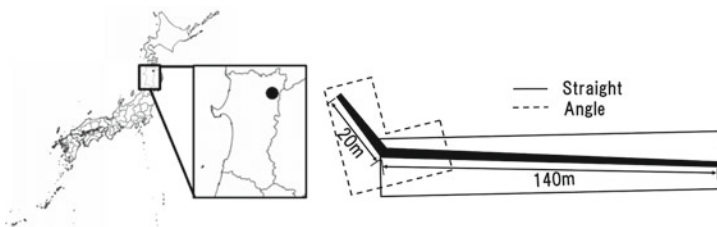


Fig. 3 Location of Osarizawa mine

modified from Wi-Fi Ad Hoc to Wi-Fi Direct, and the other experimental conditions were the same. The measurement results of RSSI for straight path and angled path in the Osarizawa mine are shown in Fig. 4. In this Fig. 4, the data with the lowest RSSI obtained from the communication test on the straight path is -76.8 (dBm) at 130 (m). After that, the RSSI never dropped below -80 (dBm) within a measurable distance of 140 (m). Furthermore, after applying logarithmic regression, a trend line with an R^2 of 0.75 was obtained. Thus, the trend line indicates a relatively poor goodness of fit of the data values. This discrepancy could be attributed to the nature of the underground mine where uneven rock walls affected the wave reflection. Therefore, the free-space propagation loss is not an appropriate estimate in this situation. In the case of the communication test at the bend, Fig. 4 shows that the RSSI was -88.6 (dBm) at 25 (m). After that it shows a further decrease with distance. Similarly, a logarithmic regression was performed on the median value and a trend line with an R^2 of 0.96 was obtained. Thus, the trend line was a good fit to the data obtained from this communication test. Using this trend line, the communication distance for the angled path can be concluded 20 (m). However, since the distance at which communication was possible was also short, the number of points at which it could be attempted was also small. Figure 5 shows the results of the communication speed. Figure 5 shows the results of the communication speed. As shown in Fig. 5, the speed in a straight path was 130 (Mbps) at 5 (m), but high-speed communication of 60~80 (Mbps) was observed when the RSSI was above -80 (dBm). As a result, it was decided to verify the success rate of transmission at speeds exceeding 7.5~10 (MB/s) or 60~80 (Mbps). The results of both communication tests are as follows.

Based on the overall results, it can be concluded that a parent unit should be installed at every 140 (m) at a turn or straight line. However, due to the space limitations of the experimental site, communication experiments at distances longer than 140 (m) could not be conducted, and the limits of the communication distance could not be determined. This configuration is suitable for building a stable Wi-Fi Ad Hoc network in an underground mining environment. Furthermore, it was found that communication rates of 7.5~10 (MB/s) or 60~80 (Mbps) are possible when RSSI is at least -80 (dBm) in almost all locations. It was also possible to communicate at

Fig. 4 The measurement results of RSSI

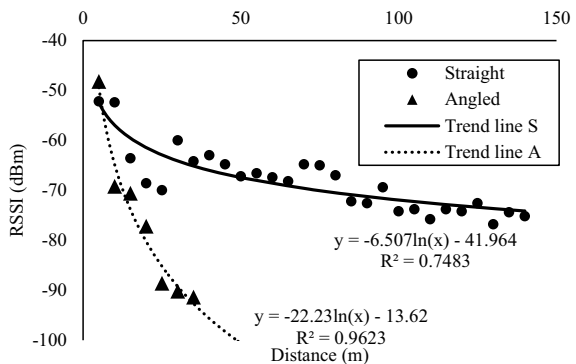
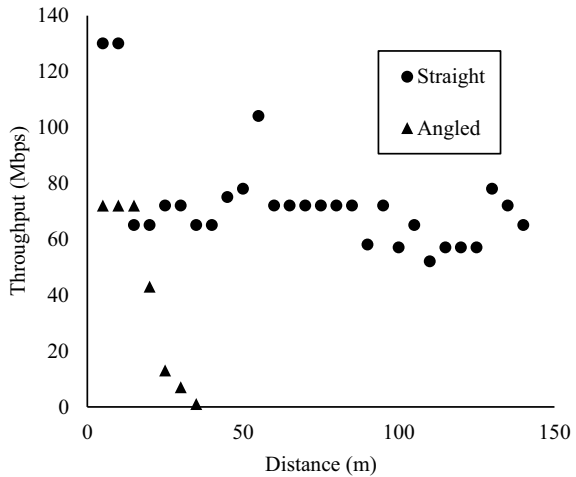


Fig. 5 The measurement results of communication speed



130 (Mbps) when it was above -60 (dBm). In other words, it is possible to estimate the approximate communication speed just by measuring the RSSI.

6 Conclusion

Sensor technology and ICT are tools to improve productivity and safety in underground mines. As an example, this study proposes an “in-situ rock stress monitoring system for underground mining using ad hoc communication and strain sensor cells”, and basic tests were carried out to verify the superiority of the technology. The functionality of the system was investigated by dividing it into three components: measurement of rock mass conditions in underground mines, wireless communication technology in underground mines, and monitoring in underground mines.

Problems of measuring rock mass stress and strain, underground working environment such as ventilation, temperature and humidity, and underground communication technology were summarized. Measurement of rock stress/strain and underground working environment such as ventilation, temperature and humidity were conducted.

The “In-situ rock stress monitoring system for underground mining by using ad-hoc communication and strain sensor cells” proposed in this study is to install a sensor unit with built-in strain gauges having multiple axes in a drill hole for rock mass support after stress release (after opening), like a bucket relay of data. It is a monitoring system that collects and consolidates observation data to an operation center on the surface via Wi-Fi Ad Hoc communication. This communication system does not require the installation of a Leakey Feeder or 4G/5G communication infrastructure. An advantage is that, there is no need to install Wi-Fi access points. The

mobile terminals owned by the miners will serve as relays for the data hops, enabling data collection without the need for special equipment or infrastructure.

In order to understand the performance of this communication system, three communication experiments were conducted at the Osarizawa mine, an experimental mine in South Africa, and an operational mine, and summarized the results. The results show that the combination of a sensor unit and ad hoc communication can be used to monitor a rock mass at a low cost. Rock mass monitoring system will enable quantitative understanding of medium- to long-term rock mass deformation, and expected to improve safety in the mine.

References

1. Khanzode VV, Maiti J, Ray PK (2011) A methodology for evaluation and monitoring of recurring hazards in underground coal mining. *Saf Sci* 49(8–9):1172–1179. <https://doi.org/10.1016/j.ssci.2011.03.009>
2. Saleh JH, Cummings AM (2011) Safety in the mining industry and the unfinished legacy of mining accidents: safety levers and defense-in-depth for addressing mining hazards. *Saf Sci* 49(6):764–777. <https://doi.org/10.1016/j.ssci.2011.02.017>
3. Funato A, Ito T (2017) A new method of diametrical core deformation analysis for in-situ stress measurements. *Int J Rock Mech Min Sci* 91:112–118. <https://doi.org/10.1016/j.ijrmms.2016.11.002>
4. He MC, Tao ZG, Zhang B (2009) Application of remote monitoring technology in landslides in the Luoshan mining area. *Min Sci Technol* 19(5):609–614. [https://doi.org/10.1016/S1674-5264\(09\)60113-7](https://doi.org/10.1016/S1674-5264(09)60113-7)
5. Zhang QB, He L, Zhu WS (2016) Displacement measurement techniques and numerical verification in 3D geomechanical model tests of an underground cavern group. *Tunn Undergr Sp Technol* 56:54–64. <https://doi.org/10.1016/J.TUST.2016.01.029>
6. Moridi MA, Sharifzadeh M, Kawamura Y, Jang HD (2018) Development of wireless sensor networks for underground communication and monitoring systems (the cases of underground mine environments). *Tunn Undergr Sp Technol* 73:127–138. <https://doi.org/10.1016/j.tust.2017.12.015>
7. Dohare YS, Maity T, Das PS, Paul PS (2015) Wireless communication and environment monitoring in underground coal mines – review. *IETE Tech Rev* 32(2):140–150. <https://doi.org/10.1080/02564602.2014.995142>
8. Minhas UI, Naqvi IH, Qaisar S, Ali K, Shahid S, Aslam MA (2018) A WSN for monitoring and event reporting in underground mine environments. *IEEE Syst J* 12(1):485–496. <https://doi.org/10.1109/JSYST.2016.2644109>
9. Bai C (2017) Application of WSN fire monitoring system in coal mining. *Int J Online Eng* 13(3):17–26. <https://doi.org/10.3991/ijoe.v13i03.6856>
10. Reddy NS, Saketh MS, Dhar S (2016) Review of sensor technology for mine safety monitoring systems: a holistic approach. In: 2016 IEEE 1st international conference control measurements instrumentation, no Cmi, pp 429–434. <https://doi.org/10.1109/CMI.2016.7413784>
11. Singh A, Singh UK, Kumar D (2018) IoT in mining for sensing, monitoring and prediction of underground mines roof support. In: Proceedings 4th IEEE international conference recent advanced information technology. RAIT 2018, pp 1–5. <https://doi.org/10.1109/RAIT.2018.8389041>
12. Srivastava S, Singh M, Gupta S (2019) Wireless sensor network: a survey. In: 2018 international conference automation computing engineering. ICACE 2018, vol 38, pp 159–163. <https://doi.org/10.1109/ICACE.2018.8687059>

13. Ikeda H, Kawamura Y, Tungol ZPL, Moridi MA, Jang H (2019) Implementation and verification of a Wi-Fi ad hoc communication system in an underground mine environment. *J Min Sci* 55(3):505–514. <https://doi.org/10.1134/S1062739119035843>
14. Ikeda H, Kawamura Y, Tungol ZPL, Ito Y, Jang H (2018) Development of underground space communication systems using Wi-Fi ad hoc for smart mining. *Geoinformatics* 29(1):3–11. https://doi.org/10.6010/geoinformatics.29.1_3
15. Ralston J, Reid D, Hargrave C, Hainsworth D (2014) Sensing for advancing mining automation capability: a review of underground automation technology development. *Int J Min Sci Technol* 24(3):305–310. <https://doi.org/10.1016/j.ijmst.2014.03.003>
16. Diao J, Zhang G, Hu H, Zou Z, Zhang B (2015) Design and application of electrical fire monitoring system in mining industry. *Int J Min Sci Technol* 25(2):305–310. <https://doi.org/10.1016/j.IJMST.2015.02.021>
17. Moridi MA et al (2015) Development of underground mine monitoring and communication system integrated ZigBee and GIS. *Int J Min Sci Technol* 25(5):811–818. <https://doi.org/10.1016/j.ijmst.2015.07.017>
18. Li C, Li J, Hu L, Hou D (2015) Visualization and simulation model of underground mine fire disaster based on cellular automata. *Appl Math Model* 39(15):4351–4364. <https://doi.org/10.1016/j.APM.2014.12.051>
19. Wang W, Huang S, Wu X, Ma Q (2011) Calculation and management for mining loss and dilution under 3D visualization technical condition. *J Softw Eng Appl* 04(05):329–334. <https://doi.org/10.4236/jsea.2011.45037>
20. Ju Y et al (2014) Visualization of the complex structure and stress field inside rock by means of 3D printing technology. *Chin Sci Bull* 59(36):5354–5365. <https://doi.org/10.1007/s11434-014-0579-9>
21. Moridi MA, Kawamura Y, Sharifzadeh M, Chanda EK, Jang H (2014) An investigation of underground monitoring and communication system based on radio waves attenuation using ZigBee. *Tunn Undergr Sp Technol* 43:362–369. <https://doi.org/10.1016/j.tust.2014.05.011>
22. Akyildiz IF, Sun Z, Vuran MC (2009) Signal propagation techniques for wireless underground communication networks. *Phys Commun* 2(3):167–183. <https://doi.org/10.1016/j.phycom.2009.03.004>
23. Akyildiz IF, Stuntebeck EP (2006) Wireless underground sensor networks: research challenges. *Ad Hoc Netw* 4(6):669–686. <https://doi.org/10.1016/j.adhoc.2006.04.003>
24. Saraswala PP (2013) A survey on routing protocols in ZigBee network. *Int J Eng Sci Innov Technol* 2(1):471–476
25. Chehri A, Fortier P, Tardif PM (2009) UWB-based sensor networks for localization in mining environments. *Ad Hoc Netw*. <https://doi.org/10.1016/j.adhoc.2008.08.007>

Critical Aspects of Longwall Top Coal Caving Method for Application in Indian Geomining Conditions



Nasina Balasubrahmanyam  and Gnananandh Budi

Abstract Although the future of coal mining lies belowground, the present status of Indian underground (UG) mining and, in particular, thick seam mining is not inspiring. Thick seams share about 40% of the proven Indian coal reserves. However, several consistent efforts were made, no method could sustain effective extraction, and it remained an ever-posing technical challenge to the Indian mining engineers. The longwall-based top coal caving methods (LTCC) are developed and excelled in China for their production, productivity, and conservation advantages over other thick seam mining methods. In this perspective, a study into the feasibility of the application of LTCC in Indian geo-mining conditions is taken up. The present paper reviews the LTCC mechanism, safety issues, and the global experiences for implementation in the Indian geo-mining conditions. This study contributes to evolving a bulk-producing underground mining method with conservation and safety in India.

Keywords Thick seam mining technologies · Longwall top coal caving · Risks · Indian geo-mining conditions

1 Introduction

In India, presently, thick seams up to a thickness of 4.5 m are effectively extracted from underground by only two methods, namely Bord and Pillar mining in conjunction with continuous miner and Single Pass Longwall mining (SPL) method. For the coal seams thicker than 4.5 m, these methods lead to poor conservation. Further, poor conservation is a potential source of the spontaneous heating/fire from the loss of coal in the goaf. Indian has a great history of thick seam underground mining. The experiences of multi-slice longwall mining (MSL) with inclined slicing and

N. Balasubrahmanyam (✉)

Directorate General of Mines Safety, Government of India, Hyderabad, India

e-mail: nasinabalasubrahmanyam@gmail.com

G. Budi

Indian Institute of Technology (Indian School of Mines), Dhanbad, India

horizontal slicing (both by caving and stowing), sub-level caving, hydraulic mining, blasting gallery method are significant. However, none of the methods sustain in the long run. The significant reason behind their unsuccess is productivity, strata control and fire.

During the past two decades, the longwall-based top coal caving methods (LTCC) have been developed and excelled in China for their mass production, productivity, and conservational advantages over the other thick seam mining methods. Subsequently, the methods are adopted successfully in Australia, Vietnam, Turkey, and Bangladesh. The present article reviews critical parameters that affect the LTCC feasibility for its application in Indian geomining conditions.

Mine planning, particularly deep underground coal mining by mechanized longwall mining, requires a thorough understanding of the geotechnical parameters of the coal measures strata. The understanding of geotechnical parameters is an invariable part of the integrated mine planning approach. Most of the failures of previous Indian longwalls were attributed to a lack of proper understanding of geology or adequate geological data.

Regular caving of overlying roof strata immediately after support advance influences the longwall production and safety. In case of longwall top, coal caving, the top coal shall fracture, fragment adequately, and cave down onto the rear conveyor immediately after advancing the power supports. Rocks in a mining area can fail in different ways, and it can have hazardous effects if in the form of roof and side falls or air blast in underground mine, bench slope in an opencast mine, etc.

The most distinguishing feature of LTCC over the SPL method is the design of the power support. Three different support systems evolved during the LTCC development. Initially, a single conveyor support system was designed in which the canopy is provided with a chute. The fractured top coal passes through the chute is directed onto the front armored flexible conveyor by gravity. The single conveyor support system with a chute was commonly practiced during the 1980s and late 1980s. One significant example of this system is DBT 320-24/32 support (Fig. 1).

Fig. 1 DBT 320-24/32 LTCC support (cited by Hepplewhite et al. 2002)

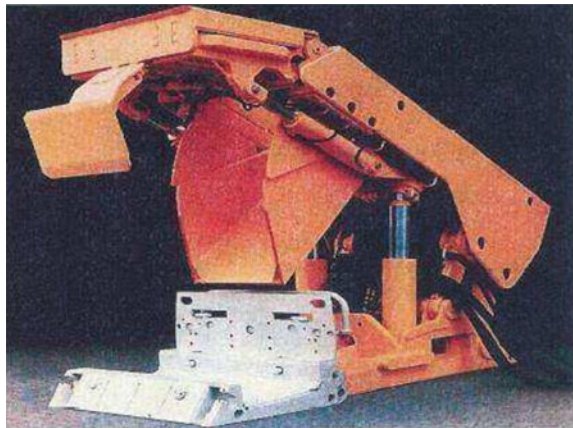
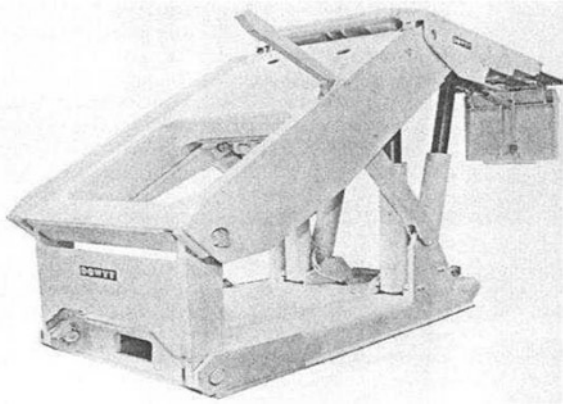


Fig. 2 The schematic view of the twin conveyors supports the system with a rear AFC located within support DT 4/400 LTCC (after Bewick 1983)



In this system, coal production was restricted because cutting and caving operations could not be activated in parallel. Besides, the transport of coal through the chute caused serious dust issues.

The second significant design is the twin conveyors support system with a rear AFC located within the support (Fig. 2), introduced in the 1990s. The second AFC was located in the supporting basement. A rear door is designed in the support system, and the fractured top coal is directed to the rear armored flexible conveyor through this door. Thus, the drawbacks of the single conveyor support system were overcome in this system with the twin conveyor system.

However, the following significant issues are encountered in this system:

- The caving window was small, could not accommodate large coal blocks, and left the top coal between two adjacent supports.
- The rear AFC was located within the support and resulted in a low clearance capacity.
- The support canopy was fixed and could not provide a positive compressive force against the top coal.

The breakthrough during the 1990s was the development of a twin conveyors system with a rear AFC located behind the support base (Fig. 4), which has the following merits over the previous two designs:

- no fine coal is jammed between flight bars as the rear AFC sits on the seam floor,
- swing up and down provision allowing sizeable top coal blocks to cave down, the swingable canopy also provides a compressive force against the top coal and results in better coal fracturing, and
- less dust generation due to the low height of the support.

The basic difference between SPL and LTCC mining methods are depicted in Figs. 3 and 4.

The chief advantages of LTCC over the Multi-Slice Longwall (MSL) method are (i) reduced production cost and time, (ii) less equipment, with one more AFC

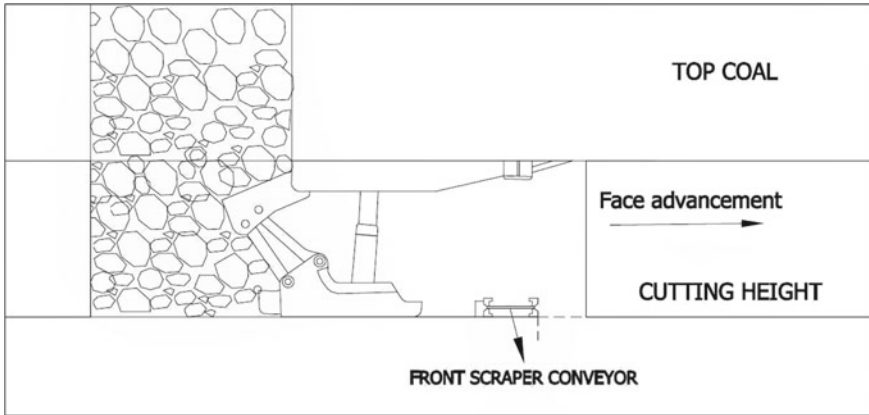


Fig. 3 Illustrative sketch of conventional Longwall method

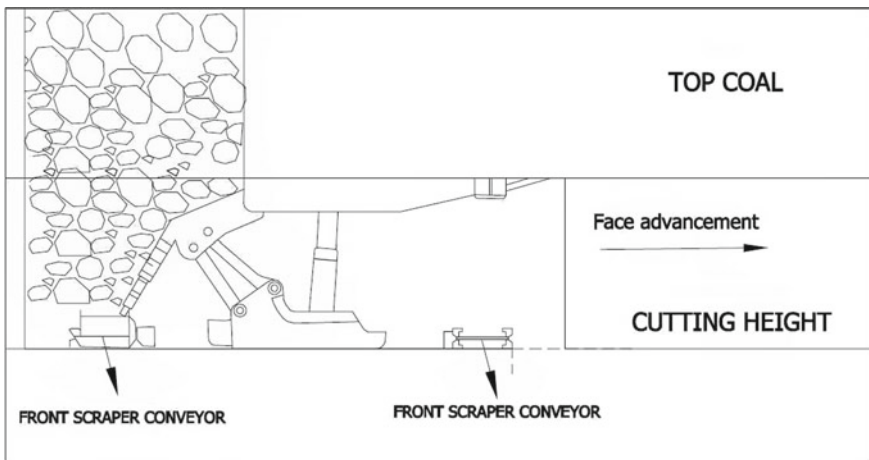


Fig. 4 Illustrative sketch of Longwall top coal caving method

behind powered supports are enough to obtain more coal, (iii) the reduced number of face transfers, and (iv) parallelization of both cutting and caving, which benefits production and productivity (Zhongming 2001; cited by Vakili 2009). Only one set of main headings are enough for LTCC development, whereas multiple gate roads are necessary for the Multi-Slice Longwall (MSL) method.

The main advantage of LTCC over High Reach Single Pass Longwall mining (HRSPL) is the operational cost to drive gate roads per tonne of longwall coal recovered during extraction is significantly reduced. The recovery of the coal reserves is high in the case of HRSPL when compared to the LTCC method. In High Reach Single Pass Longwall mining (HRSPL), the present maximum cutting height is 7 m (Wang 2011; [19]) and commonly extracts efficiently, seam below six thicknesses. Face

stability, handling of heavy and more oversized equipment, spontaneous heating, and gas emissions are the problems associated with increased height in HRSPL. Hence, LTCC with lower cutting height improves face stability and top coal removal and controls spontaneous combustion, enhancing overall safety compared with HRSPL.

The LTCC method is not feasible for every thick seam. Khanal et al. [12] recommended that the proposed area's comprehensive Geological reports database be studied thoroughly before planning for LTCC. The critical geomining conditions applicable to top caving mining (Hebblewhite and Cai 2004, Dao 2010) are presented here:

- (i) *Coal Seam Reserve Condition:* The stable coal seam reserve of thickness between 5–10 m, inclination 0–15°, Protodyaknov coefficient of coal, $f = 3$ (Uniaxial compressive Strength preferably 10–25 MPa). Discontinuities in coal seams have different effects on top coal caving. In the case of the soft and highly jointed coal seam, there is a possibility of risk of formation of roof cavity and pause the entire extraction system; on the other hand, stiff and less jointed top coal caves beyond the rear canopy in the goaf that too in the form of larger blocks affecting the LTCC production.
- (ii) *Nature of Roof and Floor:* An ideal condition for the LTCC is the immediate roof that caves down with the face advance. In contrast, in the case of overhanging goaf, there is every possibility of risk of air-blasts and further support failures. The immediate roof shall collapse down so that the filling height should be equal to the height of shearer cutting. The floor lithology should be strong.
- (iii) *Caving characteristics of top coal:* The top coal cavability and fragmentation depend on the peak front abutment pressures and horizontal stress component. The horizontal stress component is manifested in cutter roof failure and restricts the load transfer from upper strata to lower strata. However, the effect of the same will be nullified once the first top coal caving takes place.
- (iv) *Geological Structure:* The geological structure should preferably be without considerable coal seam fluctuation or folds or faults of big throw and free of igneous intrusions. There should not be any hard stone layers of more than 300 mm in thickness in top coal.
- (v) *Other significant parameters:*
 - i. The expected life of the mine for LTCC working,
 - ii. Longwall Face Reserve: Normally, the top caving face length is 150–350 m; the panel length is 1000–3000 m, panel reserve is preferably 1–20 million tons.
 - iii. Status of the financial health of the mine,
 - iv. database of comprehensive Geological reports of the mine area [12],
 - v. Mechanization Culture and machinery and equipment available at the mine for standard longwall extraction,
 - vi. Danger due to inundation: All the precautions against the danger of inundation shall be risk assessed standard code of safe operating procedures, and trigger response action plans shall be formulated.

- vii. The danger of spontaneous heating & fires: Besides accelerating the advancing speed of the longwall face to complete within the incubation period of the seam, all other standard measures, including correct ventilation by pressure-balancing, goaf inertisation by nitrogen flushing Etc., should be planned to prevent any risk of spontaneous heating and fires.

2 Geotechnical Principles of LTCC

The LTCC terminology includes “top coal,” “immediate roof,” and “main roof” strata which can be defined in the following manner (Peng 2008, Vakili 2009):

- i. The “Top coal” is the upper portion of a coal seam over the extraction horizon and below the immediate strong strata. The top coal is not mined by shearer but caves under gravity with the progress of panel behind powered supports on a rear armored chain conveyor.
- ii. The “Immediate roof” is the layer of band overlying the top coal. The Immediate roof may fail and cave either instantly or after the advance of powered support.
- iii. The main roof is the strata above the immediate roof but beneath the fractured Zone. The primary roof strata can fail; this main roof has an essential role in longwall working and power support capacity determination. Because the main roof does typically not cave and specific length overhangs, and it can still transmit the horizontal force. The mapping of these terms in the site is vital to analyse the face conditions.

Stress distribution in LTCC: As far as the bottom extraction part of the coal seam is concerned, the LTCC mechanism generally matches the conventional Longwall caving mechanism.

Xie et al. [5] studied the LTCC mechanism on a 7.5 m thick and nearly flat coal seam in China. Using numerical modeling techniques, the researcher studied the direction and magnitude of the major and minor horizontal principal stresses. It was observed that the peak front abutment pressure acts about 6 m ahead of the face.

The abutment pressures extend up to a distance of 40 m ahead of the face. In this case study, the horizontal stress was double the vertical stress. Yasitli and Unver [22] conducted FLAC3D numerical modeling studies of LTCC panel on Omerler underground mine, Turkey. The coal seam was about 8.0 m thick, inclined at a slope of 10°, and the depth was 240 m. The shearer cut the bottom 2.8 m of the coal seam, and the rest of the 5.2 m is recovered from the top coal caving. Under these conditions, it was observed that the peak front abutment pressure was acting at a distance of 7 m from the face, which finally reduced to a normal stress field after 70 m ahead. The effect of the shield and spatial shape of the drawing body was not considered in most studies.

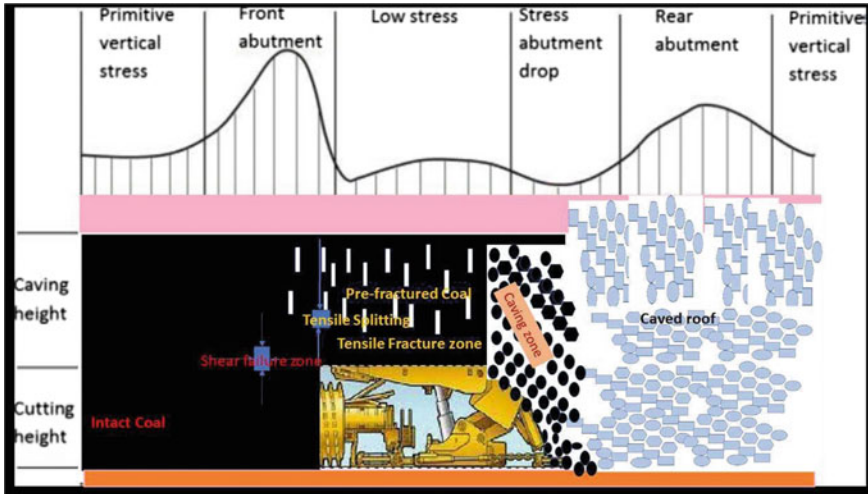


Fig. 5 Conceptual model of Longwall top coal caving

3 Top Coal Caving Mechanism

3.1 Top Coal Failure and Fracturing Process

The process of failure of top coal by its fracturing and development of cracks in the top coal is the most critical criteria in the success of the LTCC system. Zhongming et al. 1999 observed that the top coal fracturing is basically due to the abutment stresses and depends on the strength of the coal. The same was corroborated by other researchers (Humphries and Poulsen 2008). The shear failure and tensile cracking cause the failure and fracturing of the top coal. The cracking and fracturing process initiates when peak front abutment stresses are generated due to the extraction process. Under the influence of these stresses, the top coal undergoes horizontal dilation. Because it is the top coal is subjected to the vertical load without proper confinement in the horizontal direction (Fig. 5). The subsequent stage is caving the fractured top coal and falling along with the rear canopy onto the rear AFC by gravity.

Humphries and Poulsen 2008 observed that poor fracturing created formations with larger blocks from the top coal. The poor fracturing leads to poor recovery and creates practical problems of blockage of the conveyor. Excess fracturing leads to issues of support and strata management. The degree of fracturing can be estimated by simulation through numerical modeling techniques. Humphries et al. 2006, Humphries and Poulsen 2008, Wang et al. 2014 advocated that the top coal fracturing process can be divided into four phases/zones as shown in Fig. 6.

Zone-I is the deformation zone that is located ahead of the peak front abutment stress. In this Zone, coal deformation is primarily elastic.

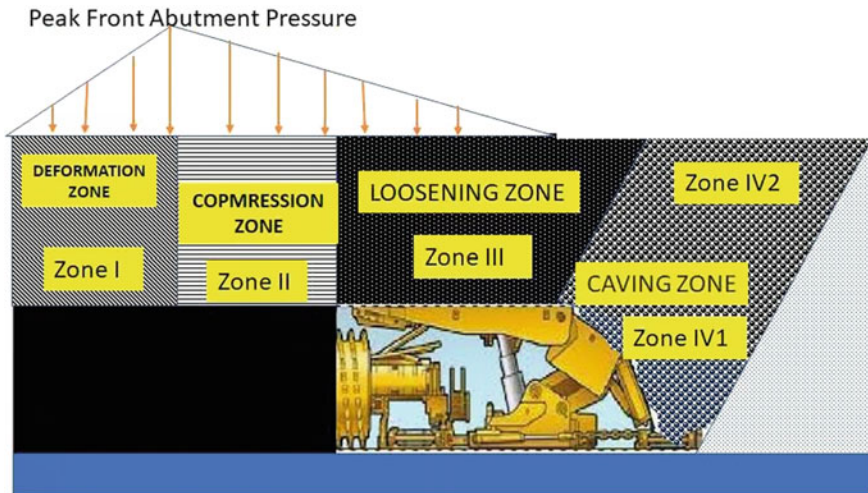


Fig. 6 The top coal fracturing process in four phases/zones (Humphries et al. 2006)

Zone-II is the compression fracturing zone which is located in between the face line and the peak front abutment stress. Zone -II is the high-stress concentrated Zone where fracturing and fragmentation of the top coal occurs. It is observed that this Zone extends up to a distance of 15 m from the face line. In this Zone, high vertical stress without or with the least horizontal confinements results in the top coal's horizontal dilation.

Zone-III is the loosening zone that is located precisely above the support canopy. As the face retreats, the cycles of loading and unloading repeatedly lead the top coal to break. In this Zone, vertical displacement is more significant than horizontal displacement, particularly in the upper top coal.

Zone-IV or Caving zone: This Zone is located at the rear of the canopy of the face supports. Coal in the bottom portion of this Zone is broken into small blocks and quickly drawn. The upper top coal is often compressed into an arch and is drawn by articulating the rear caving door or advancing the supports. Small blocks in the lower part of the Caving zone (i.e., Zone-IV1) are straightforwardly dealt with by a rear armored chain conveyor. However, the top part of the Zone (i.e., Zone-IV2) is collected into the rear armored chain conveyor by moving the articulated rear canopy (Humphries et al. 2006; Humphries and Poulsen 2008; Wang et al. 2014).

3.2 The Caving Process

As illustrated by Humphries et al. 2006, the top coal is fractured due to the vertical front abutment pressures. Further, it is loosened by the mining cycles. With the advancing of the support, the lower restraint to the top coal is removed. Hence, the

broken top coal falls directly onto the rear armored flexible conveyor. The top coal will cave on the rear side of the canopy at a certain angle above the supports called the caving angle. The caving angle is dependent on the strength of top coal. Hard coals are observed to cave comparatively at an angle of 40 to 70°, whereas soft coals have an angle of caving up to 100 to 110°, as shown in Fig. 7.

All the above concepts arrived due to observations of Chinese LTCC panels in the last two decades. The in-situ stress environment of the site, abutment stresses induced during extraction, the strength of the top coal, cavability of roof rocks were extensively studied in China. The studies were based on physical modeling as well as numerical modeling techniques.

The combined effect of the abutment stresses induced during extraction, cavability of roof rocks, and chock movement should exceed the top coal's strength. Under this condition, fresh fractures are induced, and the natural fractures of bedding planes and cleats further lose the entire top coal thickness and allow reasonable caving. However, the size of caving fragments of top coals dictates the recovery. Maximum recovery of top coal is achieved when the percentage of caved top coal fragments is conveniently evacuated by the rear conveyor and not lost in goaf. In a highly jointed rock mass such as coal measure rock, there is an assumption that the roof rock caving is mainly controlled by discontinuities (Vakili 2009; Dao 2010). Vakili (2009) advocated four concepts by which the caving is shown in Fig. 8.

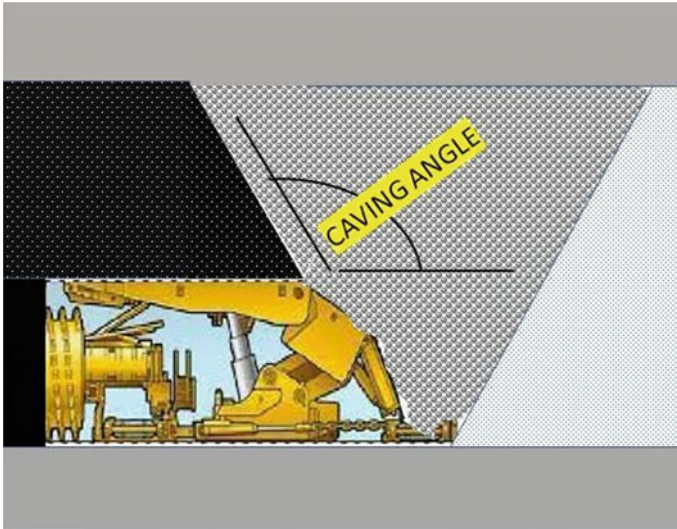


Fig. 7 Caving angle in LTCC (Humphries and Poulsen 2008)

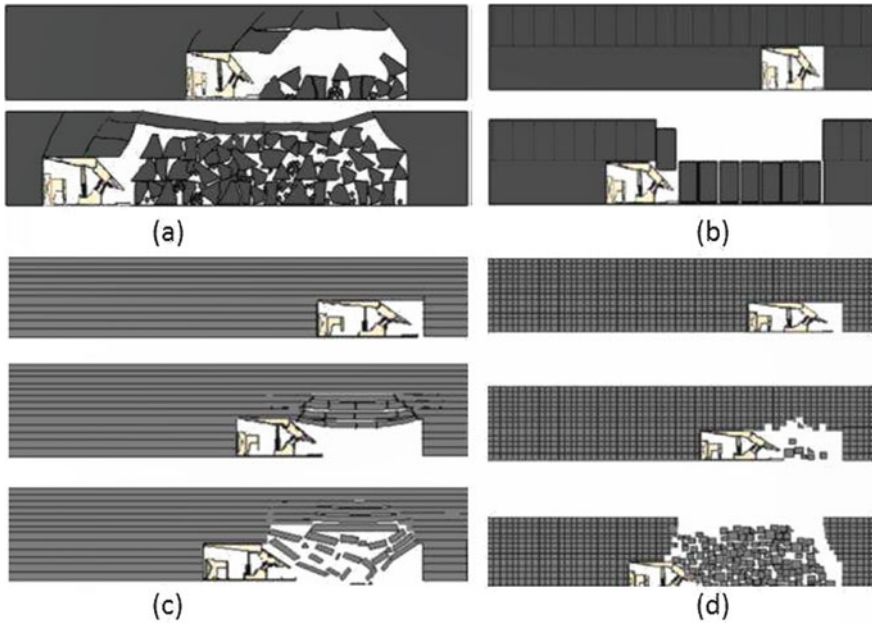


Fig. 8 Conceptual caving models. **a** Bulking factor model; **b** vertical discontinuities; **c** horizontal discontinuities; **d** combined horizontal-vertical discontinuities (after Vakili 2009)

4 Main Technical Issue of Top-Coal Caving

As per the experiences, coal of moderate strengths is suitable for LTCC.

4.1 *Hard-Top Coal Management*

In the LTCC method, a significant problem arises with the cavability and fragmentation of the top coal due to higher coal strengths. Coals that do not yield properly may even lead to the problems of air blast and spontaneous heating. Thus, the solution is softening the top coal. The obvious question is in what way the hard-top coal can be made soft. Methods like high-pressure water injection in coal seams and deep-hole blasting could not result from desired results. Chinese research on the subject resulted in three methods, namely, Pre-blasting, Hydraulic Fracturing, and vibration.

- i. Pre-blasting: At the Omerler underground mine in Turkey, though 1.5 m thick bottom part of the top coal was caved correctly, the top part problems arose with the rest 3.5 m top coal caving process. In another case, pre-blasting was necessitated at the Xinzhouyao Coal Mine in north China to improve maximum coal recovery [20]. Pre-blasting in 3.5 m of the coal seam was recommended

Fig. 9 Vibration system provided on the shield (Xie et al. 2006 cited by Alireza Jabinpour et al.)



to attain proper top coal caving. The case was analyzed through numerical modeling by FLAC3D software Itasca (Unver and Yasitli 2006, [22]).

- ii. Hydraulic Fracturing: Huang et al. 2015 reported that a standard and safe production was achieved by applying hydraulic fracturing with 20 MPa pressure. The study on this subject is ongoing.
- iii. Vibration Technology: The immediate lower part of top coal flows correctly, but the problem is with the middle and top parts of the top coal. The middle and top parts of the top coal form a stable arch with larger blocks and get locked, creating caving and flowing. It was stimulated by numerical modeling that these blocks can be unlocked by creating horizontal vibration forces, making the arch unstable. For this, a mechanism of producing low frequency and high-power vibrations is made on the top of shield support, as shown in Fig. 9. These vibrations reduce that top coal's cohesion and friction angle, thereby breaking the stable arch formation. With the aid of a vibration mechanism, in the Wang Zhuang mine, Lu'an Coal Industry Company, the recovery ratio of top coal was stated to be increased by 3%.

4.2 Inflammable Gas Emission and Outburst

The total methane emission in LTCC is higher than other methods due to its higher production from the entire thickness of the coal seam. Further, the cracked Zone in the roof rocks is higher, leading to gas migration from the adjacent seams. Jian Wu et al. 1999 classified the LTCC face into four parts, namely A, B, C, and D, based on the presence of inflammable gas and methane, as shown in Fig. 10.

In Zone A, the lowest methane concentrations can be observed at the face due to higher (about 70%) ventilating air quantity. All the methane emissions from the goaf and caving coal have to pass through Zone C. The air velocities are smaller in this Zone, so a high methane concentration is observed. As such, the methane concentrations in the Zone are observed in zones A and C. The rear side of the support is zone D, where higher methane concentrations are found. However, all the gas from this Zone flows into the face area.

The gas problems are dealt with in the following ways:

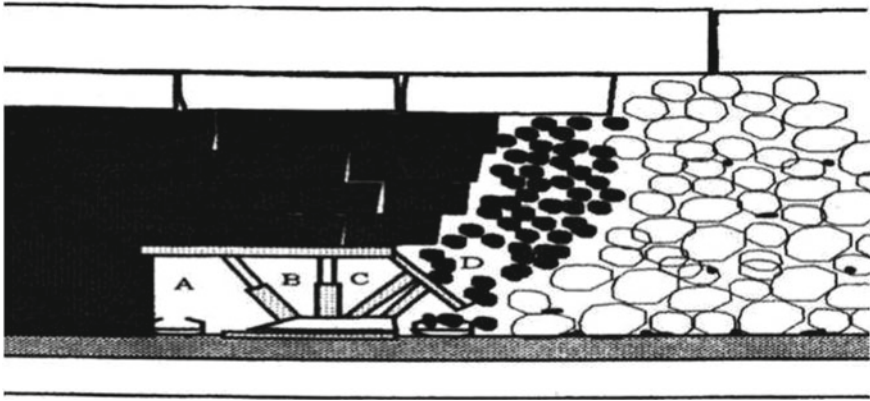
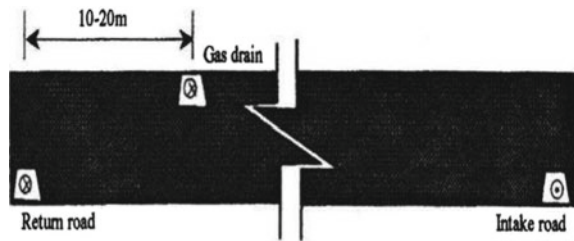


Fig. 10 Methane distribution in the face (after Wu et al. [8])

Fig. 11 E type ventilation system



- i. Gas Drainage: Methane drainage is an invariable precaution to prevent firedamp explosions. Methane drainage results in the reduction of original gassiness. Gas drainage can be done in four stages: pre-drainage, gas drainage during mining, and gob gas drainage.
- ii. Proper ventilation design: In China, the mines are primarily gassy. Since 1992, the E form of ventilation system (Fig. 11) has been effectively used. This system includes one additional heading to the U form. A heading called a gas drain is driven at the top of the coal seam. No person or equipment is deployed or allowed in this heading. The leakage air in goaf and above the power supports is drained from this heading.

4.3 Spontaneous Heating/Fire

Since a certain amount of caved top coal is invariably left in the goaf, the risk of spontaneous heating is omnipotent in LTCC. Jian Wu, Yueping Qin, and Minghua Zhai presented vide their paper on “Mining Safety of Longwall Top-coal Caving in China” during the 8th US Mine Ventilation Symposium, to be held on June 14–17,

1999, on the campus of the University of Missouri-Rolla stated that the experiences in the LTCC mines led to the following preventive measures:

- i. Fast rate of extraction: The goaf of the LTCC panel can be categorized into three zones of susceptibility for spontaneous heating/fire, namely, spontaneous combustion: cooling zone, oxidation, and asphyxia zone. The oxidation zone shall always be kept minimum. The rate of longwall face retreat shall be improved to keep the oxidation zone to the minimum; thereby, the risk of spontaneous heating/fire can be eliminated. Further, the extraction shall be completed within the incubation period.
- ii. Goaf area with Nitrogen gas leads to oxygen deprivation in the area. The Nitrogen gas is injected into the goaf area through pipeline arrangement.
- iii. Injection of mud slurry in the goaf is one of China's most commonly adopted methods to prevent spontaneous combustion.
- iv. Reinforcement the roof and sides of the gateroads to fill up the cracks and prevent air leakage into the sides.
- v. Pressure balancing: Maintaining the pressure difference between the LTCC face and goaf areas to keep their pressures minimum. This measure prevents entry of methane from goaf into the working area and air leakage into goaf.

4.4 Respirable Dust

Heavy dust concentrations in the LTCC workings is a significant issue, which causes the Coal Miner's Pneumoconiosis, a lung affecting disease. Dust issues are more prevalent among LTCC mines, and the major sources are:

- (i) intake roadways,
- (ii) coal discharge points at (a) the BSL to belt conveyor in the main gate, (b) crusher, and (c) front/rear AFC transfer point,
- (iii) coal caving, (iv) chock movement, (v) shearer drum cutting, and
- (iv) coal spalling ahead of the leading drum of the shearer.

An LTCC system needs stringent coal dust prevention measures. The following methods have been adopted for dust control [8] at LTCC faces:

- i. Replacement of high caving gate supports with the low caving gate supports.
- ii. Water-cloud dust control should be improved. Sprayers are positioned beneath the front canopy to contain the dust generated by the shearer drum. Sprinklers are fitted on the gob shield, which sprays automatically as the support or top-coal moves. Further, to improve the dust control effect, a wetting ingredient is sometimes dissolved in water. In China, preliminary injection inseam is commonly employed.
- iii. Wet collecting net system: Chen et al. [3] conducted research and developed a wet collecting net system. The curtain, which can encompass the full cross-section of the critical dust-prevention regions via flexible adjustments, shall

enclose the entire cross-section of the critical dust-prevention regions via flexible adjustments. According to them, this device had a dust removal efficiency of 69.6%.

4.5 Summary of Risks Associated With the LTCC Method

See Table 1.

Table 1 Different parameters of geo-mining conditions of the site pose different types of risks. The summary is furnished in Table

Geo-mining state of coal seam	Parameters	Critical risk	Associated hazard
Soft and weak roof/seam/floor	Soft coal (UCS < 10 Mpa) and weak roof/floor rock (UCS < 20 Mpa)	Roof and side falls, unpredicted large roof falls, heavy dust	Injury to the workforce, reduction in production, Coal dust explosions
Hard & strong roof/seam	Strong strength in coal (UCS > 25 Mpa) and roof rock (UCS > 80 Mpa)	Roof and side fall, poor top coal recovery, large overhanging goaf	Reduced output per man-shift, Injury to the workforce, damage to the machinery
Steeply dipping & Ultra-thick	Inclination > 25 deg, Thickness > 30 m	Roof and side fall, in the stability of face supports and machinery, poor top coal recovery	Injury to the workforce, damage to the machinery, reduced production time
Mildly dipping & Ultra-thick	Thickness > 15 m	Roof and side fall, unpredicted large roof falls, High concentrations of coal dust	Injury to the workforce, damage to the machinery, reduced production time
Soft & Marginally thick	Seam thickness ~4 m, soft coal	Roof and side fall, unpredicted caving, Unpredicted roof falls	Reduced output per man-shift and reduced top coal recovery
Gaseous	Inflammable gas content >6m ³ /t in-situ	Presence of high concentrations of inflammable gas	Firedamp explosions, Injury to the workforce, damage to the machinery, reduced production time
Proneness to spontaneous heating	Lesser incubation period	Spontaneous heating fire in goaf due to loss of unrecovered top coal	Injury to the workforce, damage to the machinery, reduced production time

5 Implementation of LTCC in China, Australia, Vietnam, and Turkey

LTCC Face No. 8603 of Yangquan coal mine was the first successful in achieving an output of 140,000 tonnes per month in 1990 with a recovery ratio at the working face of over 80% (Jian et al. 1999).

- 5.1. The LTCC method was first introduced in China in 1982 and then advanced swiftly over the next two decades. Currently, production from the LTCC method accounts for nearly 10% of China's underground production (Tien 1998).
- 5.2. After five years of applying the LTCC method to extract the 5.6–6.5 m thick coal seams with a gradient of 3–80 in Dontan mine, Yazhou coalfield, the maximum monthly output increased from 151,786 tonnes in 1994 to 501,068 tonnes in 1999, and annual productivity increased from 2,821 tonnes to 14,306 tonnes per man. The maximum annual production of a face has reached 5.1 million tonnes per year (Yingdi et al. 1999).
- 5.3. Now, the LTCC method is being extended to implement in more difficult geomining conditions like soft, weak roof/floor, hard and strong roof/coal seam, steep, ultra-thick, gaseous, seams prone to spontaneous heating.
 - i. LTCC is working with soft and weak roof/ seam/floor conditions in about eleven Nos. of mines in China, namely Lu'an Wuyang, Lu'an Tunliu, Datong Tongxin, Quandian, Yankuang Nantun, Pingzhuan Gushan, Luling, Xinji No. 1, Zhuxian, Xinyao, Shitanjing Wulan.
 - ii. At the same time, Hard and strong roof/seam conditions were also negotiated while working LTCC in about eleven Nos. of mines in China, namely Meiyukou, Xinzhouyao, Mahuangliang, Dafosi, Jinyuan Honghui No. 1, Taixi Baijigou.
 - iii. Steeply dipping & Ultra-thick seams are extracted in about eight mines in China, namely Luweihu, Liudaowan, Dahonggou, Jianguo, Wangjiashan, Yaojie, Adaohai, Huating.
 - iv. Soft & Marginally Thick seams are worked in three mines in China, namely Xishan Chengzhendi, Renlou, Huainan Mines, Pingdingshan No. 12, Handan Yunheling. Gassy seams at Lu'an Tunliu, Tingnan, Dafosi, Laohutai, Baijigou, Gengcun, and Qingqiu are also worked by LTCC.
 - v. Further, it is to note that eight mines having coal seams prone to spontaneous heating at Dayan No. 2, Ciyaopu No. 2, Qingshuiying, Daxing, Zhuxianzhuang, Qianqiu, Yimei, Changchun are worked successfully by this method.
- 5.4. After China, the LTCC method was subsequently successfully applied in Australia, Vietnam, Turkey. Feasibility studies were conducted in India by CSIRO, Australia.

Some of the important LTCC working mines are briefed in Table 2.

Table 2. Working parameters of some of the LTCC mines

Mine	Details of LTCC working
Austar Coal Mines, Newcastle Coalfield, Australia	The Greta Coal Seam. Maximum 6.5 m in thickness, and height of cutting of 2.9 m. Immediate rock and coal’s uniaxial compressive strengths are between 20 to 60 MPa and 15 to 20 MPa, respectively. Depth of cover ranging from 390 to 530 m
Xinglongzhuang Coal Mine, Yanzhou Mining Area, China	The No. 3 Coal Seam. The average thickness of about 8.6 m, and the height of cutting of 3.5 m. Immediate rock’s and coal’s compressive strengths are 57 and 25 MPa, respectively. Depth of cover ranging from 354.7 to 503.5 m
Yang Danh Coal Mine, VINACOMIN, Vietnam	The No. 8 Coal Seam. The average thickness of about 7.3 m. Height of cutting of 2.7 m., immediate rock’s and coal’s uniaxial compressive strengths are between 42.7 and 25 MPa (average), respectively Depth of cover of 250 m A notable characteristic is shale and siltstone of thickness from 2.85 to 15 m in was the immediate roof
Nam Mau Coal Mine, VINACOMIN, Vietnam	The No. 6 Coal Seam (Semi anthracite). The average thickness of about 6.7 m, and the height of cutting of 2.8 m Immediate rock’s and coal’s uniaxial compressive strengths are 45.6 and 25 MPa, respectively. The depth of the cover range is 150 m
Halam Coal Mine, VINACOMIN, Vietnam	The seam 11 (anthracite) with an average seam thickness varies from 2.7 to 14.66 m. The cutting height was 2.6 m. uniaxial compressive strengths of immediate rocks vary from 46.7 MPa (shale) to 57.0 MPa (siltstone). The coal strength ranges from 15 to 30 MPa. Depth of cover of about 300 m
Omerler underground mine, Turkey	The coal seam was about 8.0 m thick, inclined at a slope of 10°, and the depth was 240 m. The shearer cut the bottom 2.8 m of the coal seam, and the rest of the 5.2 m is recovered from the top coal caving. uniaxial compressive strengths of immediate rocks vary from 14.4 MPa (claystone)) to 16.1 MPa (Marl). Under these conditions, it was observed that the peak front abutment pressure was acting at a distance of 7 m from the face, which finally reduced to a normal stress field after 70 m ahead

6 Indian Geomining conditions Vis-a-Vis Global Experiences

Thick seams are nearly 40% of proven Indian coal reserves. Thickness varies from 4.5 to 15 m normally. The coals are stronger, with UCS ranging from 25–50 MPa. The thickness of some of the thick seams and their strength (UCS) is shown in Fig. 10 (Figs. 12 and 13).

The thickness of the top coal is a critical factor that may influence the caving performance of the top coal. Usually, thinner top coal will cave right behind the support. Therefore a better recovery rate is expected. With thicker top coal, caving at early stages may not be as good as for thinner top coal due to the delay in caving the upper layers of the top coal. However, as the face advance distance increases, the top coal caving performance will improve. In practice, however, the overall impact will be minimal if operational measures are taken to improve the top coal caving performance and recovery rate. Another effect of the thickness of the top coal is that with the same caving angle, as the top coal gets thicker, in some cases, the upper portion of top coal will cave to the floor at distances too far away to be reached from the longwall face (Dao). Hard coals are observed to cave comparatively at an

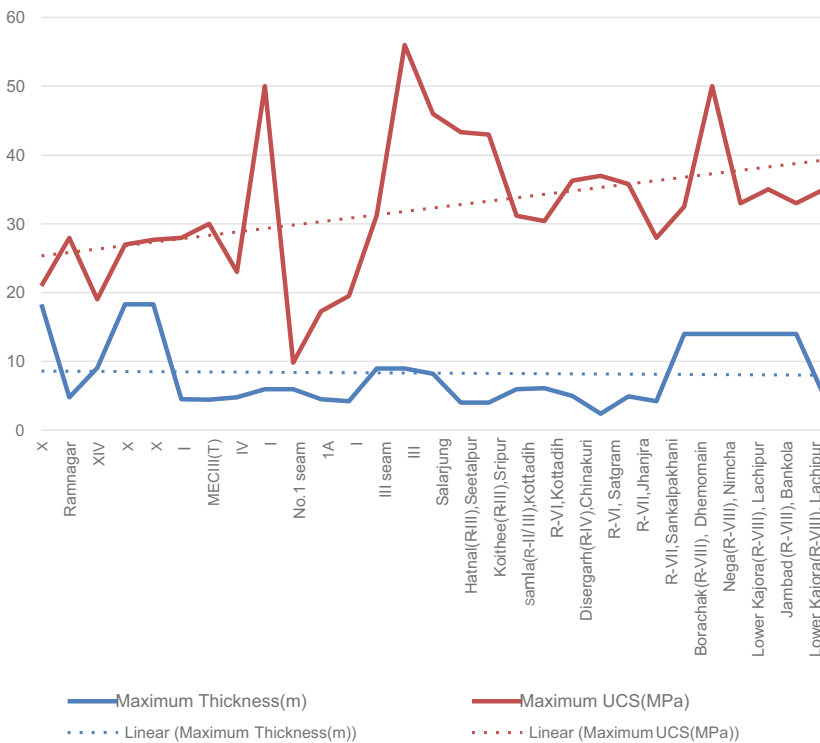


Fig. 12 Seam thickness and strength (UCS) of Indian thick coal seams (discluding GVCF)

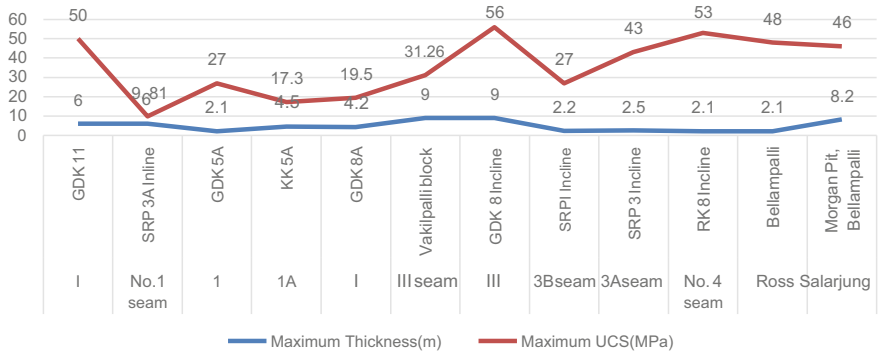


Fig. 13 Thickness and strength (UCS in MPa) of GVCF thick coal seams

angle of 40 to 70°, whereas soft coals have an angle of caving up to 100 to 110°. Hence, suitable parametric studies on the effect of cutting/caving thickness ratio, the strength of coal, and discontinuities are to be carried out to assess top coal caving feasibility.

The earlier failures of several prestigious Indian longwall projects are attributed to the strong massive main roof, which is a prevalent phenomenon in Indian geo-mining conditions. While planning for LTCC, appropriate support capacity and induced caving of main roofs shall be studied.

Most Indian coal mines are of degree I or II in gassiness as defined by the Coal Mines Regulations, 2017. Hence, the methodology for dealing with inflammable gases becomes an invariable part of the mining plan for LTCC.

The authors of this paper [2] have conducted studies on top coal caving feasibility for Indian geo-mining conditions. The study revealed the following: The discontinuities of top coal mass (value of the CMRI-ISM RMR) has a major direct relationship ($R^2 = 1$) on the FTCD followed by strength of coal (UCS) ($R^2 = 0.978$) and the top coal thickness ($R^2 = 0.988$). When the CMRI-ISM RMR, the coal (UCS) strength, and the top coal thickness are higher, the top coal caveability is poorer. However, as the working depth ($R^2 = 0.85$) and cutting height ($R^2 = 0.6$) increase, the FTCD decreases, and top coal caving improves.

The simulated FTCD values are used to develop an empirical equation,

$$FTCD (m) = -1.726 - 0.5039 EH + 1.498 TC + 0.0915 CMRI-ISM RMR + 0.09257 UCS - 0.007519H$$

by statistical analysis.

The FTCD index helps in the preliminary assessment of LTCC feasibility. The parameters of the FTCD index calculation involve the most commonly available data of the Indian coal mines and do not require any complex geotechnical investigations.

7 Discussion and Conclusion

The problems are many and varied, and no one technique can be of universal application. Importing technology proved elsewhere is a simple solution. However, it requires a comprehensive study of the method and effective analysis of the modifications to be incorporated to suit it for the site-specific geo-mining conditions.

This paper presents a brief and thorough review of all aspects of LTCC with global experiences. The review presents us with ample opportunity to examine the applicability of the LTCC method in India. The LTCC method has proven advantageous over the multi-slice longwall method and other thick seam underground mining methods, including High reach Single Pass Longwall mining (HRSP). The lower height of the face in LTCC facilitates comparatively low-cost equipment and offers better face conditions. Moreover, LTCC can be conveniently and economically deployed in thick seams with comparatively less human resources.

8 Recommendations

In the last 30 years, thick coal seam top coal caving has developed very quickly in China, improving efficiency with economics. Indian has extensive underground thick coal reserves of 5–12 m thick suitable for the application of LTCC. There is considerable experience from LTCC mining under various geo-mining conditions of China, Australia, and Vietnam. As per the International Cooperation Annual Report 2017-18 of the Ministry of Coal, Government of India, action for collaboration has been initiated by CIL with CSIRO in Longwall Top Coal Caving (LTCC). The recent decision of the Government of India for 100% foreign direct investment (FDI) in coal mining can be a booster for attracting highly mechanized underground mining methods like LTCC.

Acknowledgements The views expressed in this paper are those of the authors and not necessarily that of the Directorate General of Mines Safety and also express their sincere gratitude to all those who helped directly or indirectly in preparing this manuscript. The analysis and work reported in this paper form part of the Ph.D. work of the first author.

References

1. Jabinpour A, Bafghi AY, Gholamnejad J (2016) Vibration in longwall top coal caving method. *Int Acad J Sci Eng* 3(2):102–109. ISSN 2454-3896 102. www.iaiest.com
2. Balasubrahmanyam N, Budi G (2021) Techno-economic feasibility of the longwall top coal caving method based on the FTCD index: a parametric case study in India. *Energies* 14:6115. <https://doi.org/10.3390/en14196115>

3. Chen D, Nie W, Cai P, Liu Z (2018) The diffusion of dust in a fully-mechanized mining face with a mining height of 7 m and the application of wet dust-collecting nets. *J Clean Prod* 205:463–476
4. Si G, Jammikar S, Lazar J, Shi J-Q, Durucan S, Korre A, Zavšek S (2015) Monitoring and modeling of gas dynamics in multi-level longwall top coal caving of ultra-thick coal seams, part I: borehole measurements and a conceptual model for gas emission zones. *Int J Coal Geol*
5. Xie H, Chen Z, Wang J (1999) Three-dimensional numerical analysis of deformation and failure during top coal caving. *Int J Rock Mech Mining Sci* 36
6. Wang J, Zhang J, Song Z, Li Z (2015) Three-dimensional experimental study of loose top-coal drawing law for longwall top coal caving mining technology. *J Rock Mech Geotech Eng* 7:318–326
7. Wang J, Wang Z, Li Y (2020) Longwall top coal caving mechanisms in the fractured thick coal seam. *Int J Geomech* 20:06020017
8. Wu J, Qin Y, Zhai M (1999) Mining safety of longwall top-coal caving in China. In: *The 8th US mine ventilation symposium*
9. Wang J, Yu B, Kang H, Wang G, Mao D, Liang Y, Jiang P (2015) Key technologies and equipment for a fully mechanized top-coal caving operation with a large mining height at ultra-thick coal seams. *Int J Coal Sci Technol* (2015, Publication)
10. Wang J (2016) Demonstration project of safe and efficient mining operations in extra-thick coal seam. *Front Eng Manage* 3:264–274
11. Rakesh K, Kumar SA, Kumar MA, Rajendra S (2015) Underground mining of thick coal seams. *Int J Mining Sci Technol* 25:885–896
12. Khanal M, Adhikary D, Balusu R (2015) Prefeasibility study—geotechnical studies for introducing longwall top coal caving in Indian mines. *J Min Sci* 50:719–732
13. Khanal M, Adhikary D, Balusu R (2011) Evaluation of mine scale longwall top coal caving parameters using continuum analysis. *Min Sci Technol (China)* 21:787–796
14. Özfırat M, Şimşir F, Gonen A (2005) A brief comparison of longwall methods used at mining of thick coal seams. In: *Proceedings of the 19th international mining congress and fair of Turkey (IMCET)*, Izmir, Turkey
15. Ren T, Wang Z, Zhang J (2018) Improved dust management at a longwall top coal caving (LTCC) face – a CFD modeling approach. *Adv Powder Technol* 29:2368–2379
16. Tu S, Yuan Y, Yang Z, Ma X, Wu Q. Research situation and the prospect of fully mechanized mining technology in thick coal seams in China. In: *The 6th international conference on mining science & technology*
17. Klishin VI (2019) Innovative technologies for thick coal seam mining based on powered roof support with controlled coal discharge. In: *IOP conference series: earth and environmental science*
18. Wang J, Yu B, Kang H, Wang G, Mao D, Liang Y, Jiang P (2015) Key technologies and equipment for a fully mechanized top-coal caving operation with a large mining height at ultra-thick coal seams. *Int J Coal Sci Technol* 2(2):97–161
19. Wang J, Yang S, Li Y, Wei L, Liu H (2014) Caving mechanisms of loose top-coal in longwall top coal caving mining method. *Int J Rock Mech Mining Sci* 71:160–170
20. Xie H, Chen Z, Wang J (1999) Three-dimensional numerical analysis of deformation and failure during top coal caving. *Int J Rock Mech Min Sci* 36(5):651–658
21. Zhao Y, Xie Y, Guo J, Huo L (2008) The technical principle of top-coal caving with vibration and its practice. *Chinese J Rock Mech Eng* 27(1):187–192. *Yanshilixue Yu Gongcheng Xuebao*
22. Yasitli N, Unver B (2005) 3D numerical modeling of longwall mining with top-coal caving. *Int J Rock Mech Min Sci* 42(2):219–235
23. Yuan Y, Tu S, Zhang X, Li B (2015) Dynamic effect and control of key strata break of immediate roof in fully mechanized mining with large mining height. *Shock Vibr* 2015
24. Li Z, Xu J, Yu S, Ju J, Xu J (2018) Mechanism and prevention of a chock support failure in the longwall top-coal caving faces: a case study in Datong Coalfield, China. *Energies* 11
25. Zhang Z, Wang J, Wei W, Chen Y, Song Z (2018) Experimental and numerical investigation on coal drawing from the thick, steep seam with longwall top coal caving mining. *Arab J Geosci* 11:1–19

Ultimate Pit Limit Optimization by Computerized and Manual Methods for Dadiin Khar Tolgoi – 2 Coal Mine – A Case Study



Tuvshinzaya Purevdavaa and Manoj Khandelwal

Abstract Open-pit mine design and long-term planning are crucial parts of the mining industry. It contains the technical plan that must be followed from the beginning of mine development to mine closure. Every deposit can be mined entirely, however, many things need to be carefully considered before mining the whole deposit. An optimal pit outline is one of the most important parameters that affect both the economy and the safety of mining. Therefore, the purpose of this study is to determine the effectiveness of an optimal pit outline by using both software and hand methods based on cost and revenue. This study investigates Dadiin-Khar Tolgoi2's optimal pit outline and design to maximize the profit of using Surpac and Whittle software. The study compares the economic gain of both entirely extracted proved (B) and probable (C) reserve mines that were designed on the Surpac software and the hand technique of determining optimal pit outline. Whittle software computed that Pit Shell – 27 of Dadiin-Khar Tolgoi – 2 is the best pit outline regarding profit and safety. Besides, entirely mined Pit outline –B and Pit outline – C gives the loss in economics both –\$6 344 080 and \$171 304 160, respectively. On the other hand, the optimized pit (Pit Shell – 27) has offered the highest gain in finance, which is \$40,945,661. This economic profit shows that every mining should determine its optimal pit limit to maximize its economics.

1 Introduction

An open-pit mine design and long-term planning is a complex structure part of the mining industry, however, it is one of the most critical aspects of the mining project. It involves the plan that needs to carry through from early-stage mining to mine closure to maximize the economy's value. The primary purpose of running an open-pit mine is to obtain maximum ore recovery with the lowest possible cost to earn

T. Purevdavaa · M. Khandelwal (✉)

School of Engineering, Information Technology and Physical Sciences, Federation University
Australia, Ballarat, VIC 3350, Australia

e-mail: m.khandelwal@federation.edu.au; mkhandelwal1@gmail.com

maximum profit. In other words, the availability of extracting low-grade ore needs to be carefully considered to mine. Thus, it can lead to well-organized planning and design of the pit to achieve maximum profit. Open-pit mine design and long-term planning are complex components, however, it is an essential part of mining projects. Furthermore, it gives the technical plan that must be followed from the opening of mine to mine closure. Dimitrakopoulos (2007) makes the very valid point that an optimized mine design has a great deal of effect on the economic value of the mine time [4–6]. Indeed, mining engineers do carefully design an open pit to get the highest financial revenue. On the other hand, inverse, insufficient planned mine design might lead to a loss of profit, even bankruptcy.

This study's primary goal is to determine Dadiin Khar Tolgoi-2 optimal pit design, optimization, the starting point of the mining operation, and mineable ore reserve regarding optimal pit outline. There are a number of critical factors used to investigate the primary goal, such as the geological features of the deposit, cut-off grade, topography and mineral resource, reserve, etc. [1, 5–7]. This highlights that numerous research studies agreed with mentioned essential factors to determine the optimal open-pit design.

There are a number of studies that have focused on computer software to determine optimal pit design, such as Whittle, Minemax, Surpac, Vulcan, MineSight3D, and Datamine software because limiting pit outline is time-consuming and laborious [3, 6, 7]. Their study, however, was limited in its application as it relied on computer software solely. This study would have been more illustrative if it had broadened the methods evaluated and compared with hand methods or computer-assisted hand methods to determine optimal pit design and outline. While there has been much research on computer software, few researchers have taken hand methods or computer-assisted hand methods [2, 5]. This study compares and evaluates the results of Dadiin Khar Tolgoi – 2 mining's both computer software and hand methods or computer-assisted hand methods. For computer simulation, Surpac and Whittle software are used, whereas for hand methods or computer-assisted hand methods, a basic concept of Hustrulid's technique published in 2013 is used.

2 Case Study

This study approaches its aim in two different ways, i.e. software and hand methods. Moreover, these two different way starts from the same step, which is creating a block model [4, 7]. Figure 1 shows a summary flow chart of optimizing the pit and designing both methods.

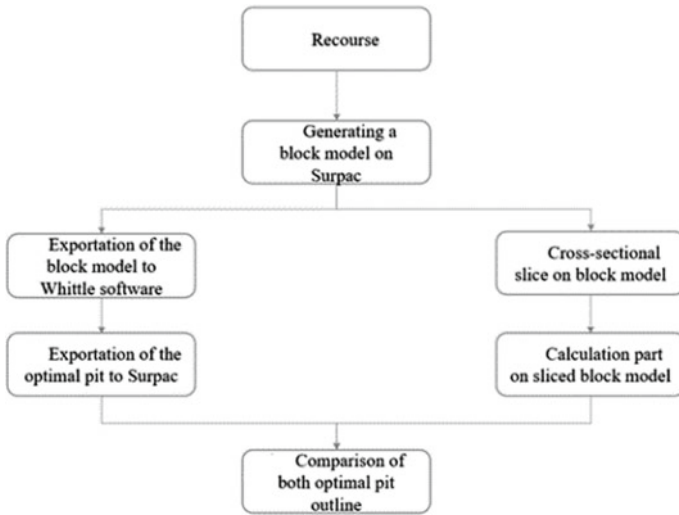


Fig. 1 The systematical approach to achieving the optimal pit design

2.1 Resource

The exploration data of the Dadiin-Khar Tolgoi-2 deposit was obtained and processed by the QMC group in Mongolia. Furthermore, this study has processed the borehole database using Surpac software. From the exploration data, the QMC group has estimated about 9 390 800 tonnes of coal with an average grade of 1.35 t/m³ that can be mined using the open-pit method (Fig. 2).

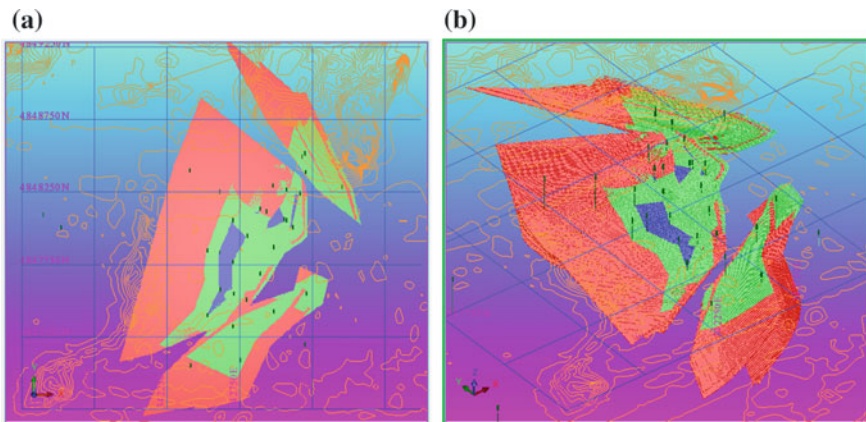


Fig. 2 Categorization of Dadiin Khar Tolgoi -2 coal deposit. Blue color and green color represent Proved **a** and Probable **b** ore reserve, respectively

2.2 Generating a block model on Surpac

Block model helps to determine ore shape, dimensions, and grade by generating a 3D model [4] as well as it contains all information about coal such as ash, calorie, sulphur even angle of dip of deposit. In addition, it is the base of any mining project as it includes every crucial information about the ore. The creation of the block model on Surpac consists of several essential steps that must be carefully done in Surpac to design a decent actual life project. Even the slightest mistake leads to error and miscalculation. The following steps show generating a block model on Surpac.

2.2.1 Loading and Creation of Borehole Database

Loading and creation of borehole database started from arranging drill hole data. Furthermore, organized drill hole data must be categorized into three different text files such as survey, collar, and assay. Tables 1, 2 and 3 show each text file. The survey, collar, and assay categories represent the depth of borehole data, coordination, and information of the borehole core, such as coal ash, calorie, and percentage of sulphur.

Table 1 illustrates the survey text file of borehole data. It consists of hole ID, depth, dip, and the azimuth of a borehole.

Table 2 shows the collar text file of borehole data. It is made of hole ID, coordination of hole, and depth.

Table 1 Part of the survey text file (Survey.txt)

HOLE_ID	Depth	Dip	Azimuth
HV0002	183	-90	0
HV0003	149.8	-90	0
HV0016	200	-90	0

Table 2 Part of the collar text file (Collar.txt)

HOLE_ID	Y	X	Z	max_depth
HV0002	4,848,000	341,505.7	753.97	183
HV0003	4,846,153	343,824.9	754.59	149.8
HV0016	4,847,082	342,745.5	754.18	200

Table 3 Part of the assay text file (Assay.txt) (full version - see appendix C)

HOLE_ID	Depth_from	Depth_to	Ash_d	Sulphur_d	Calore_d
HV0028	28.25	29.37	12.5	0.29	7024
HV0028	29.53	31.65	15.7	0.39	6747
HV0028	64.84	67.75	10.17	0.52	7083

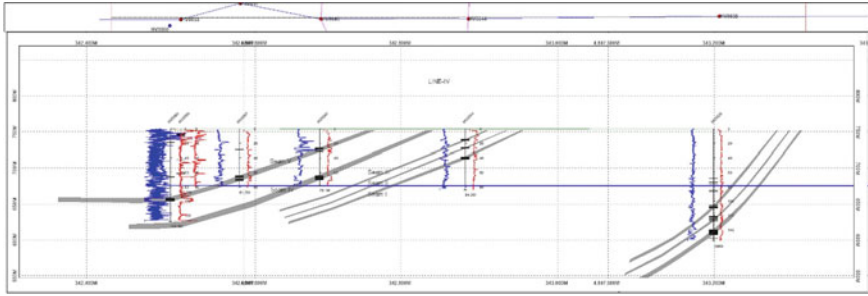


Fig. 3 Section of HV0050 to HV0038 boreholes showing Digitized Ore Zone

Table 3 represents the assay of borehole data. It consists of borehole id, depth regarding average components such as ash, sulphur, and calorie of coal.

2.2.2 Creation of Solid 3-D Model

After slicing a borehole into a plane regarding digitized geological ore zones, the same was drawn on Surpac software by a string. In addition, digitized geological ore one is computed and processed by a geologist. There are ten sections of slices drawn at 200–250 m intervals. Figures 3, 4 and 5 show some of the cross-sectional slices of borehole data done by a geologist. In addition, cross-sectional slices of coal deposit are used to make 2-D solid on software which is Surpac and Minex. Lastly, Surpac software connected those sliced digitized ore zones using a simple command to make a solid 3-D model. The 3-D model shows that there are five coal seams underneath of crest.

2.2.3 Creation of Empty Block Model

Using MINEX software, the coal seam’s ceiling and ground have been converted into Surpac software. The following steps are a very crucial part of determining an optimized open-pit depth.

- Determination of coal seam (1, 2, 3, 4, and 5)
- Determination of coal category (Probable (C) and Proved (B))
- Determination of categorized weight on coal.
- Using the techniques of Geostatistics, interpolated the value of a coalfield.

2.2.4 Filling the Empty Block Model with Attribute Values

Dadiin Khar Tolgoi –2 coal deposit consists of 5 seams, and it’s located between the West to the East angle of dip ranges 30–45°. Furthermore, it belongs to the class

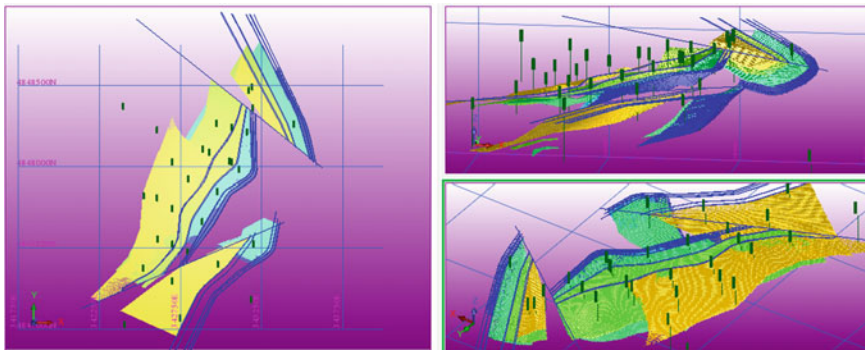


Fig. 4 3-D model of coal seams by Geovia SURPAC

Block Model Geometry						
Min Coordinates	Y	4846476.492	X	341437.932	Z	391.041
Max Coordinates	Y	4849466.492	X	344087.932	Z	778.541
User block Size	Y	10	X	10	Z	2.5
Min. block Size	Y	5	X	5	Z	1.25
Rotation	Bearing	0	Dip	0	Plunge	0

Fig. 5 Size of 3-D block model on Surpac

of steep ore reserves. The following attribute values are loaded into Surpac software to fill the empty block model with attributes such as interpolation of coal calorie, average sulphur, ash, ore reserve classification, seam numbers, etc. (Figs. 5 and 6).

2.3 Exportation of the Block Model to Whittle Software

The Dadiin-Khar Tolgoi-2 block model was exported into Whittle software for optimization of the pit. Tables 4 and 5 show the economic and technical parameters that determined the optimized pit (Table 4).

Whittle software is commonly used for the determination of open-pit depth and shells. It is using the market selling price of coal, the cost of mining, and processing. Moreover, it finds out revenue factor = 1,0, which gives the highest profit of pit shell. Coal price has been calculated as \$25/t, and the overall angle of slope is 38–42, which is based on rock mechanics of geological condition of Dadiin Khar Tolgoi – 2 mines (Table 5).

Pit outlines can differ from each other depending on their open-pit limit and economic factors.

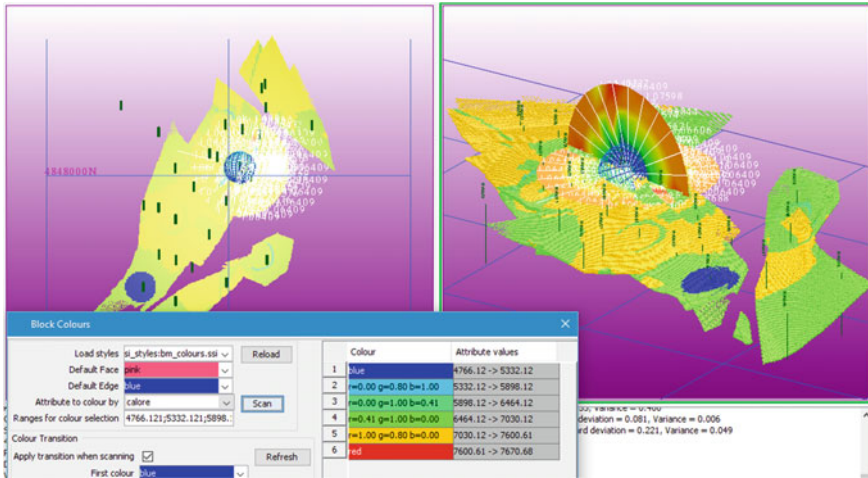


Fig. 6 Interpolation of coal calorie in the block model

Table 4 Economical parameters of Dadiin-Khar Tolgoi-2

Technical parameters	Amount	Unit
Extraction of waste cost	3	\$/m3
Coal price	25	\$/tn
Capital cost	8,987,131	\$
Mining recovery	100	%
Mining dilution	10	%
Processing cost	3.74	\$/tn
Revenue factor range	From 0.3 to 2	
Overall slope angle	37°	Degrees

Table 5 NPV of 86 pit shells

Final Pit	NPV			Coal Tonne	Waste Tonne	Mine life years	
	Best	Specified	Worst			Best	worst
25	22,037,823	18,763,766	18,763,766	3,671,743	35,661,800	6.7	6.7
26	22,315,864	18,823,179	18,823,179	3,785,316	37,117,025	6.8	6.8
27	25,009,788	17,102,871	17,102,871	5,820,381	64,513,755	9.9	9.7
28	25,067,934	17,080,953	17,080,953	5,871,286	65,209,887	9.9	9.7
29	25,155,434	16,873,819	16,873,819	5,961,555	66,487,175	10.0	9.9

Table 5 shows that pit shell – 27 has a lower amount of the whole production of coal. However, it gives the highest NPV of all pit limits. In conclusion, pit shell – 27 has been chosen as the best-optimized open-pit.

2.4 Exportation of the Optimal Pit to Surpac

Exportation from Whittle pit shell to Surpac software will be done by a straightforward command. However, it will be designed as a block model. A block model of whittle was redesigned to pit design using Surpac software.

2.5 Pit Design Using Surpac Software

This study has been completed to design three kinds of pit outlines using the same block model of mine to compare how efficient the determined pit outline is – 27. Pit outline – 1 pit design is mainly focused on extracting proved (B) reserve, whereas pit outline – 2 is focused on removing whole (B+C) ore reserve. The designing of the open-pit requires crucial parameters. Table 6 shows parameters applied to the pit design.

2.5.1 Pit Outline – 1

For this particular mine design, proved (B) ore reserve was the main aim of it. This mine design will extract all proved (B) reserves. In addition, it also contains some probable (C) ore (Fig. 7).

For this particular mine design, probable (C) ore reserve was the main of it. This design will extract all the up to down (B + C) ore reserves (Fig. 8).

Optimal pit outline – 27

This pit outline was achieved by the Lerch-Grossman algorithm employed by the Whittle software. It is challenging and time-consuming to design an optimized pit design using a shell that Whittle software gave (Fig. 9).

Table 6 Pit design parameters

Parameters	Unit	Value
Ramp and Haul road width	m	15
Ramp gradient	%	10
Bench height	m	10
Berm	m	3
Bench slope angle	%	55

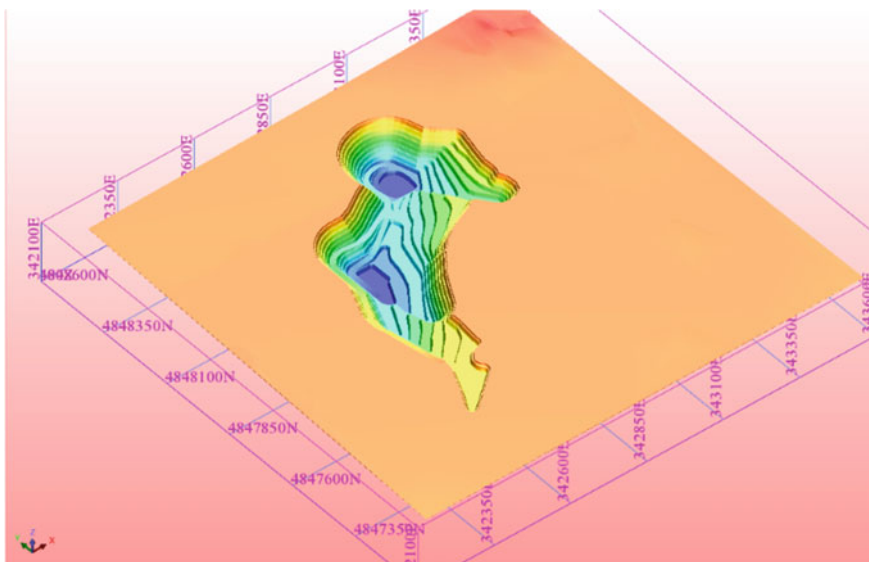


Fig. 7 Pit outline - 1

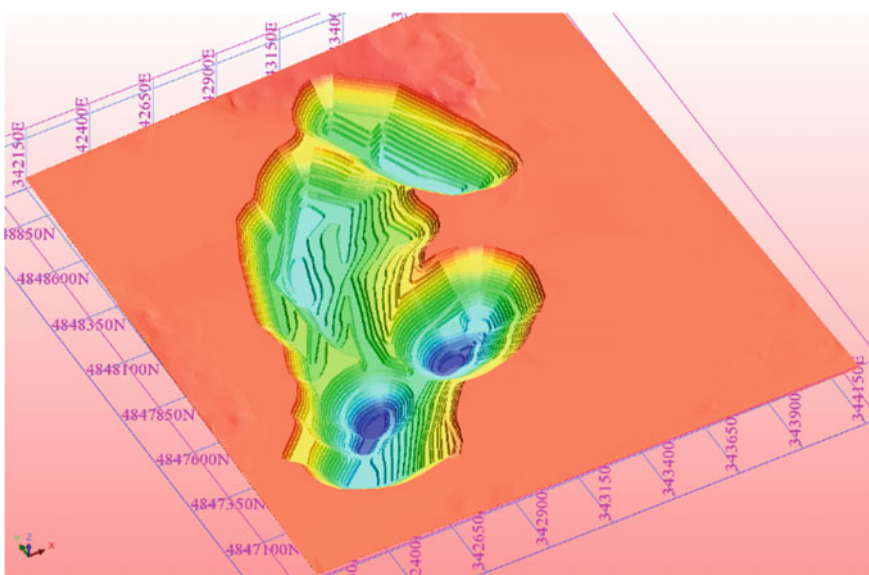


Fig. 8 Pit outline - 2

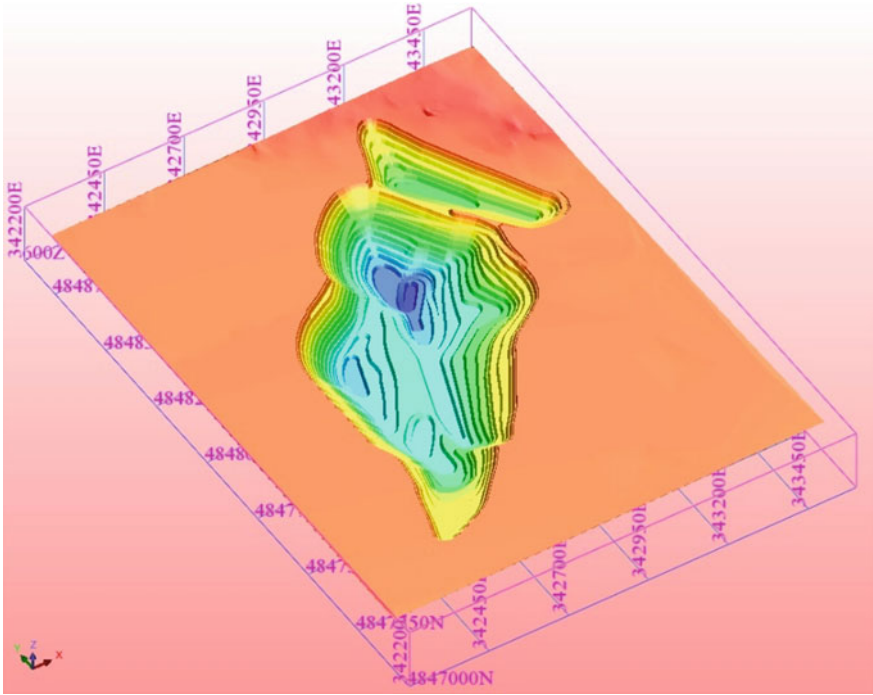


Fig. 9 Optimized ultimate pit – 27

2.6 Locating a Pit Limit by Using the Basic Concept of the Hand Method

The hand method technique can't be done in a short period in the whole mine. Thus, this study has chosen four primary cross-sectional slices that can represent the entire mine. Figure 10 demonstrates the location of the cross-sectional slices and borehole ID. In 2013, Hustrulid stated that there are a number of hand methods for determining pit limits by using simple calculations, however, hand methods are very laborious and time-consuming. It is impossible to determine the pit limit on any whole deposit because it requires enormous time to complete. Thus, Dadiin-Khar Tolgoi – 2 will analyze pit limits on cross-sectional slices of A–A', B–B', C–C', and D–D', where cross-sectional slice interval ranges from 200–250 m.

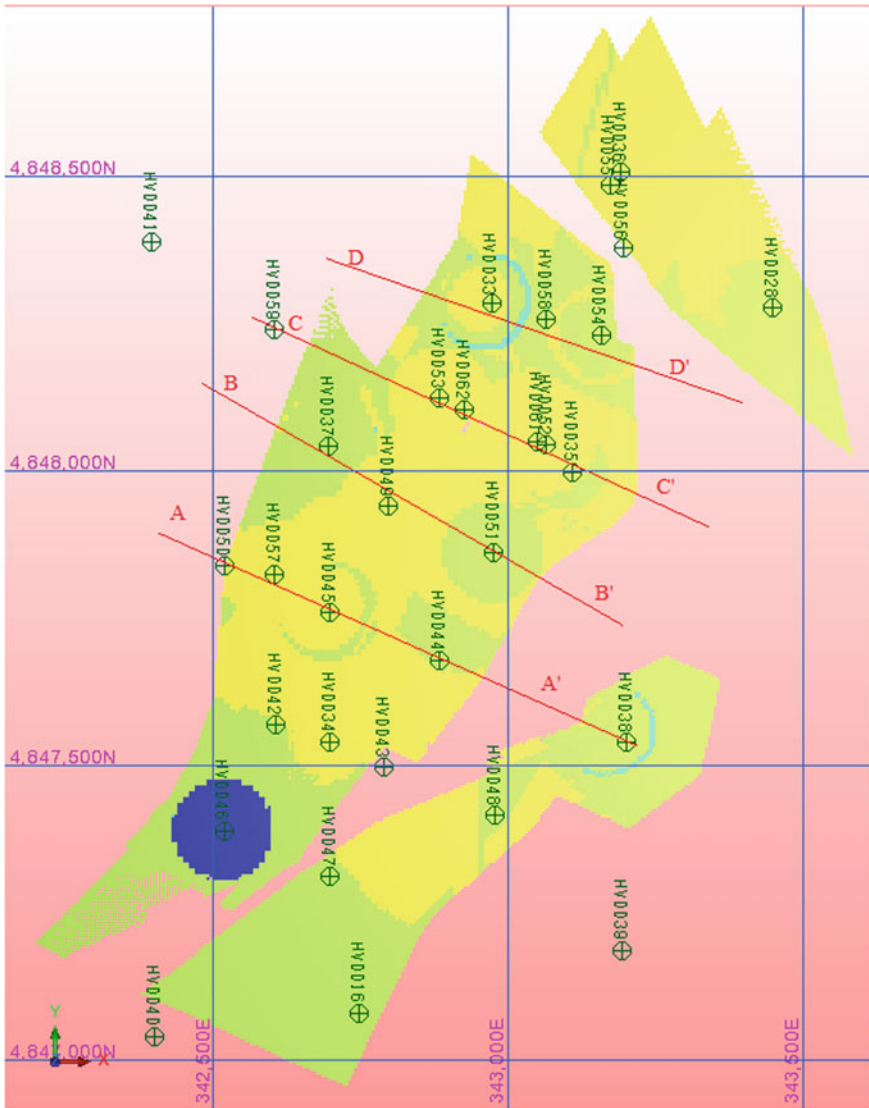


Fig. 10 Plan of the block model

2.7 Calculation Part on the Cross-Sectional Slices to Determine Optimal Pit Limit

The coal seams extend ranges surface from 755 to 610 m in depth. The following equation is used to determine the location of the final pit wall.

Table 7 Parameters used on the hand method technique

Parameter	Unit	Value
Overall slope angle	Degrees	38–42
Density of coal	Tonn/m ³	1.35
Density of waste	Tonn/m ³	2.72
Cost of processing coal	\$/ton	3.74
Cost of extracting coal	\$/ton	2
Cost of extracting waste	\$/m ³	3

$$NV = V_o \times P_o - V_w \times C_w$$

where:

V_o – Volume of waste

V_w – Volume of ore

C_w – Net value from selling one unit volume of ore (the money remaining after all expenses have been paid)

V_w – Cost for mining and disposing of the waste [4].

This basic concept of the hand method chooses the pit limit that gives the highest net value. Moreover, there are four kinds of comparison on pit limit depth that ranges from 80–140 m.

There are some crucial parameters to determine the net value of the ultimate pit limit, such as the cost of mining, stripping cost and coal price. Table 7 shows parameters applied to the pit design. Autocad software measures how much coal and waste locates between the pit limit using the simple code of “AREA.” Furthermore, this study assumes a thickness of 1 m hypothetically.

Pit limit on A–A’ cross-sectional slice (Fig. 11 and Table 8).

Pit limit on B–B’s cross-sectional slice (Fig. 12 and Table 9).

Pit limit on C–C’ cross-sectional slice (Fig. 13 and Table 10).

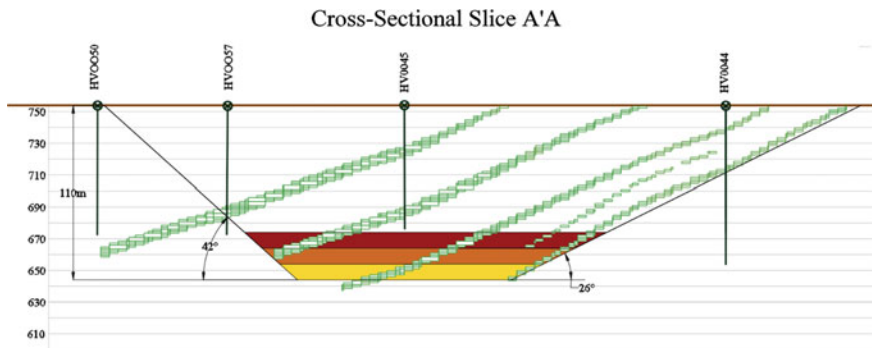


Fig. 11 Analysis of ultimate pit at cross-sectional slice A–A’

Table 8 Pit limit analysis

H (m)	Total coal, tonn	Waste, m3	ISR	Revenue, \$	Cost of process, \$	Cost of mining coal, \$	Cost of extracting waste, \$	Net Value, \$
110	5192.1	29,821	5.74	129,803	19,418	10,384	89,463	10,537
100	5036.85	28,446	5.65	125,921	18,838	10,074	85,338	11,672
90	4394.25	27,211	6.19	109,856	16,434	8789	81,633	3000
80	3244.05	25,768	7.94	81,101	12,133	6488	77,304	-14,824

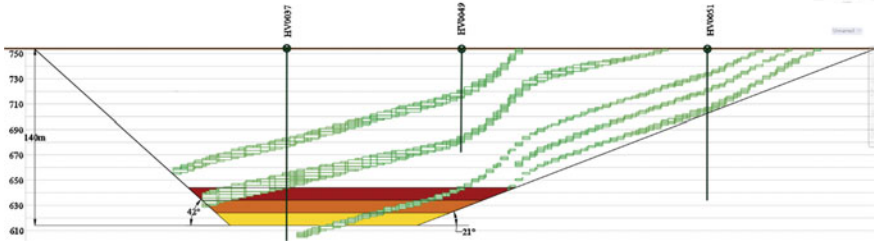


Fig. 12 Analysis of ultimate pit at cross-sectional slice B-B'

Table 9 Analysis of ultimate pit at cross-sectional slice B-B'

H (m)	Total coal, tonn	Waste, m3	ISR	Revenue, \$	Cost of process, \$	Cost of mining coal, \$	Cost of extracting waste, \$	Net value, \$
140	9069.3	50,353	5.55	226,733	33,919	18,139	151,059	23,616
130	8880.3	48,773	5.49	222,008	33,212	17,761	146,319	24,716
120	8438.85	47,118	5.58	210,971	31,561	16,878	141,354	21,178
110	7812.45	45,191	5.78	195,311	29,219	15,625	135,573	14,895
110	7088.85	42,884	6.05	177,221	26,512	14,178	128,652	7879

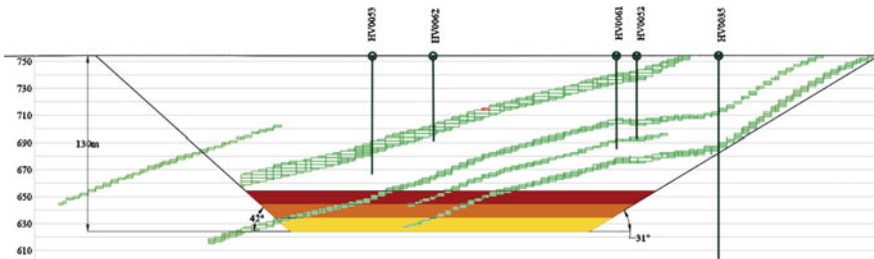


Fig. 13 Analysis of the ultimate pit at cross-sectional slice C-C'

Table 10 Analysis of ultimate pit at cross-sectional slice C–C’

H	Total coal, tonn	Waste, m3	ISR	Revenue, \$	Cost of process, \$	Cost of mining coal, \$	Cost of extracting waste, \$	Net Value, \$
140	7387.2	48,764	6.60	184,680	27,628	14,774	146,292	−4015
130	7387.2	46,681	6.32	184,680	27,628	14,774	140,043	2234
120	7258.95	44,437	6.12	181,474	27,148	14,518	133,311	6496
110	6924.15	42,098	6.08	173,104	25,896	13,848	126,294	7065
100	6512.4	39,466	6.06	162,810	24,356	13,025	118,398	7031

Pit limit on D–D’ cross-sectional slice (Fig. 14 and Table 11).

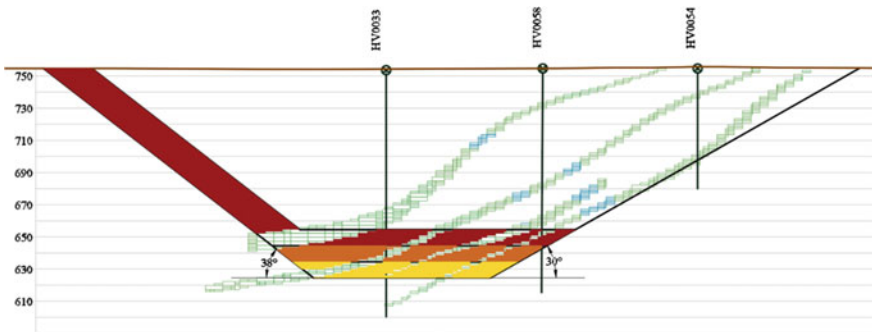


Fig. 14 Analysis of the ultimate pit at cross-sectional slice D–D’

Table 11 Analysis of ultimate pit at cross-sectional slice D–D’

H (m)	Overall coal, tonnage	Waste, m3	ISR	Revenue	Cost of process	Cost of mining coal	Cost of extracting waste	Net value, \$
130	5742.9	35,752	6.225426	143,572.5	21,478.45	11,485.8	107,256	3352.254
120	5413.5	34,840	6.435762	135,337.5	20,246.49	10,827	104,520	−255.99
110	5044.95	33,606	6.661315	126,123.8	18,868.11	10,089.9	100,818	−3652.26
100	3956.85	29,586	7.47716	98,921.25	14,798.62	7913.7	88,758	−12,549.1

3 Results and Discussion

3.1 Summary Results of Whittle Software

Exploration data of Dadiin-Khar Tolgoi – 2 deposit of mine has announced about 9 390 800 tonnes of coal with an average calorific value and a grade of 7000 J/m³ and 1.35 t/m³, respectively, that can be mined using the open-pit method. Table 12 shows the simplistic technical–economic result of both three mine designs. It indicates that Pit-Outline 2 has the highest revenue in selling coal, on the other hand, its overall cost has already outnumbered its income. Also, pit outline – 1 is not able to recover its cost (Table 12).

This simple table shows that optimized pit outline –27 has enormous profit compared with the other two pit outlines due to a high total of coal and low waste. However, this particular economic analysis is limited by operating costs excluding capital costs and general and administrative costs. Figures 15, 16, 17 and 18 compare open-pit designs and cross-sectional slices of A–A’, B–B’, C–C’, and D–D’ of pit outlines made by software.

Table 12 Analysis of economic comparison on pit designs (see Appendix O)

	Pit outline - 1 (B)	Pit outline – 2 (B + C)	Optimized pit outline -27
Total ore (t)	1,701,771.00	9,292,760	5,820,381
Total waste (m3)	13,040,063.00	116,760,906	23,718,292.28
Stripping ratio (m3/t)	7.66	12.56	4.08
Revenue for selling coal (\$)	42,544,275	232,319,000	145,509,525
Cost of processing (\$)	6,364,624	34,754,922	21,768,225
Cost of mining coal (\$)	3,403,542	18,585,520	11,640,762
Cost of extracting waste (\$)	39,120,189	350,282,718	71,154,877
Overall cost (\$)	48,888,355	403,623,160	104,563,864
Profit (\$)	–6,344,080	–171,304,160	40,945,661

3.2 Summary Results of Manual Method

The highest net value of the pit limit has been calculated in four different cross-sectional slices on Dadiin Khar Tolgoi –2 open-pit mine. For this particular sub-chapter, this study will compare optimized pit outline – 27 and the highest net value of pit outline that used the hand method. Moreover, economic analysis will be done on operating costs excluding capital, and general and administrative costs.

The cross-sectional slice A–A’ shows that the highest net value of the pit limit is at 100 m by using the hand method on the 2-D block model (Fig. 15).

The cross-sectional slice B–B’ shows that the highest net value of pit limit is at 130 m by using the hand method on the 2-D block model (Fig. 16).

The cross-sectional slice C–C’ shows that the highest net value of pit limit is at 110 m by using the hand method on the 2-D block model (Fig. 17).

The cross-sectional slice D–D’ shows that the highest net value of pit limit is at 130 m by using the hand method on the 2-D block model (Fig. 18 and Table 13).

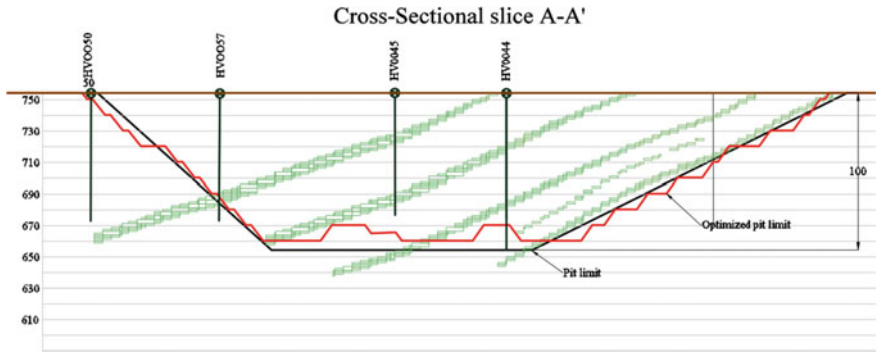


Fig. 15 The cross-sectional slice of both the optimized pit and the hand method technique pit limit - cross sectional slice A-A'

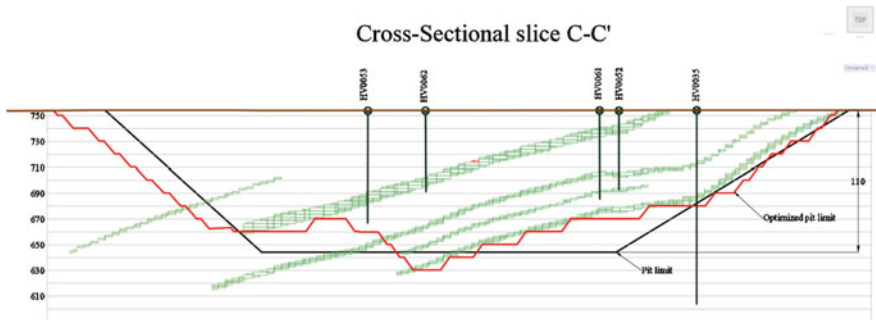


Fig. 16 The cross-sectional slice of both the optimized pit and the hand method technique pit limit - cross sectional slice C-C'

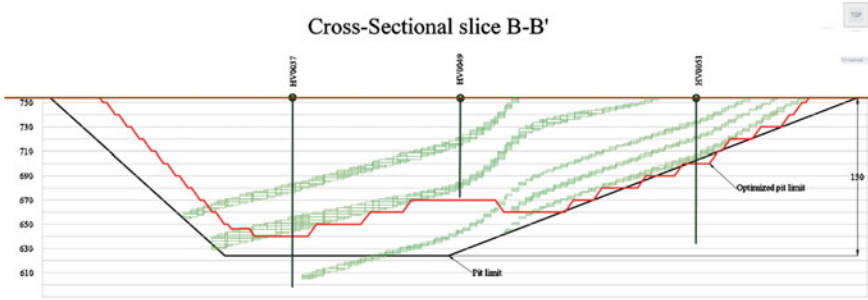


Fig. 17 The cross-sectional slice of both the optimized pit and the hand method technique pit limit - cross sectional slice B-B'

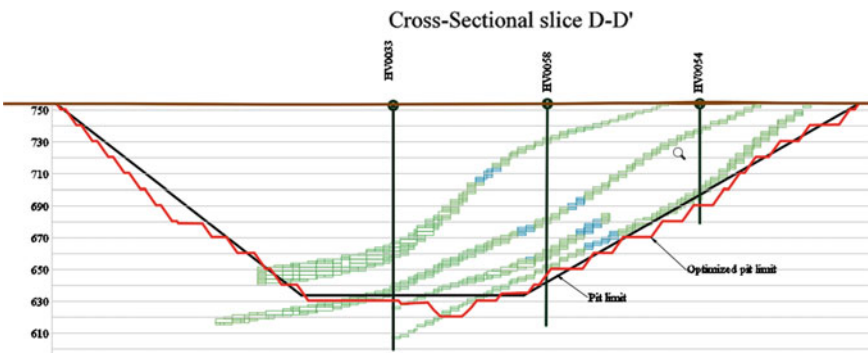


Fig. 18 The cross-sectional slice of both the optimized pit and the hand method technique pit limit - cross sectional slice D-D'

Table 13 shows economic analysis on both different processes and evaluates it.

4 Discussion

This study aims to determine the optimal pit outline of Dadiin Khar Tolgoi – 2 using the computation technique such as Whittle and Surpac software.

4.1 Analysis of Both Results

The determination of pit limit is an essential aspect of the mining industry, as well as it is time-consuming and laborious. Dadiin Khar Tolgoi – 2 coal mine computed the pit limit with the help of Whittle and Surpac software, which gives the highest net

Table 13 Comparison of economic analysis for both methods (full version – see Appendix P)

Cross-sectional slices	Total coal, tonn	Waste, m3	ISR	Revenue, \$	Cost of process, \$	Cost of mining coal, \$	Cost of extracting waste, \$	Net Value, \$
A-A'	Hand method pit outline	28,446	5.65	125,921	18,838	10,074	85,338	11,672
	Software pit outline	27,569	5.65	121,888	18,234	9751	82,706	11,197
B-B'	Hand method pit outline	48,773	5.49	222,008	33,212	17,761	146,319	24,716
	Software pit outline	35,337	4.47	197,771	29,587	15,822	106,011	46,352
C-C'	Hand method pit outline	42,098	6.08	173,104	25,896	13,848	126,294	7065
	Software pit outline	36,163	5.10	177,123	26,498	14,170	108,489	27,966
D-D'	Hand method pit outline	35,752	6.23	143,573	21,478	11,486	107,256	3352
	Software pit outline	34,684	5.70	152,042	22,745	12,163	104,053	13,080

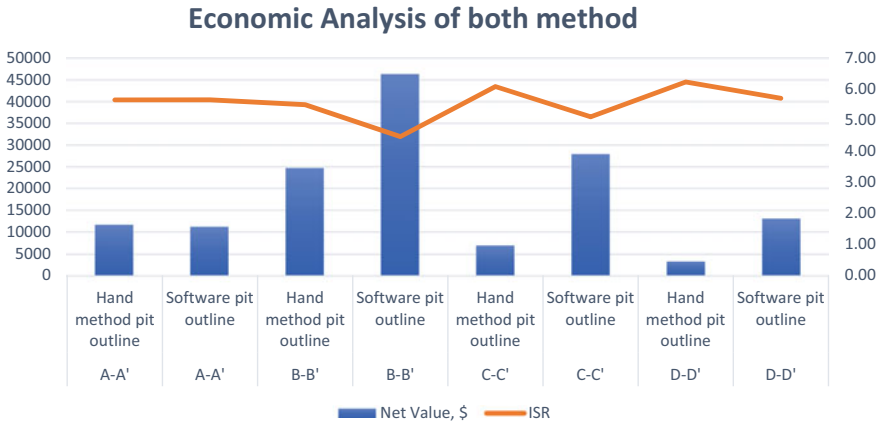


Fig. 19 Economic analysis of both methods

value compared with other versions. Economic analysis of blindly extracted pit limits 1 and 2 show that operating cost outnumbered the revenue. The pit limit analysis using the hand method technique has been done in the primary four cross-sectional slices, which represent the whole mine. Every cross-sectional 2-D block model is analyzed in different depths of the mine. The economic analysis gives the best net value depending on their depth and pit limit. Moreover, the highest net value of the pit has been chosen.

4.2 Analysis of Economics

The analysis of economics on both methods shows that the computation method is a higher net value than the hand method. However, A–A’ cross-sectional slice shows that the net value of this particular pit net value is slightly higher than the computation technique. Figure 19 shows the economic analysis of both methods.

Figure 19 also shows that the net value of the computation method is remarkably high compared with the hand method.

5 Conclusions

The determination of optimal open-pit design required the consideration of many parameters such as the deposit geology, borehole data, cut-off grade, the market price of a deposit, the cost of mining, the cost of processing, and the market price of ore. This study provided a simple method to determine the ultimate open pit outline by using Whittle. On the other hand, design and planning were completed

on blindly extracted ore reserve (B) and probable reserve (C) with the same pit design parameters. The profit of the ultimate pit outline is remarkably the highest, \$40,945,661, compared with any pit outline. However, it can be changed, if the market price of coal increases, our optimal pit outline will expand too. On the other hand, if the market price of coal goes down, the pit outline will shrink.

The hand technique of determining pit limit is time-consuming and very hard to apply to the whole mine. Thus, it has been designed on four primary cross-sectional slices of Dadiin Khar Tolgoi – 2 mine. It is not as effective as the software method, whereas it mainly focuses on the pit's depth. However, the analysis of the financial results shows that the design and plan are relatively close to optimized pit mine – 27.

Overall, it shows that the computation method Whittle, which applies the Lerch's-Grossman method, can be the best technique for the determination of the open-pit limit for Dadiin Khar Tolgoi –2 mine. It gives the opportunity of calculating the average grade of calorific value, ash, and sulphur with single command of Surpac software.

References

1. Akisa DM, Mireku-Gyimah D (2015) Application of surpac and whittle software in open pit optimisation and design. *Ghana Mining J* 15(1):35–43
2. Bakhtavar E, Shahriar K, Oraee K (2008) A model for determining optimal transition depth over from open-pit to underground mining. In: Paper presented at the proceedings of 5th international conference on mass mining, Luleå, Sweden.
3. Githiria J (2016) Cut-off grade optimisation to maximise the net present value using whittle 4X. *International Journal of Mining and Mineral Engineering* 7(4):313–327
4. Hustrulid WA, Kuchta M, Martin RK (2013) Open pit mine planning and design, two volume set & CD-ROM pack: CRC Press, Boca Raton
5. Kennedy BA (1990) *Surface mining*: SME
6. Kentwell D (2002) MineMAX Planner vs Whittle Four-X an open pit optimisation software evaluation and comparison. MineMax. <https://www.minemax.com/downloads/Minemax-Planner-vs-FourX.pdf>
7. Mariko I, Mireku-Gyimah D (2018) Open pit optimisation and design of tabakoto pit at anglogold ashanti sadiola mine using surpac and whittle software. *Ghana Mining J* 18(2):37–47

Appropriate Support Design for Incline Lip Opening and Drivages in Fragile Rock Mass Formation: An Empirical and Numerical Based Case Study



Avinash Paul, Niraj Kumar, Pramod Kumar, and Ashok Kumar Singh

Abstract The production of underground coal is directly related to the safety of the mine. When any fatality occurs, mostly due to roof fall and side fall, production of the mines gets affected. In India roof fall in underground mines still contributes a fair amount of percentage, i.e., in and around 40% towards the fatalities of the accident. Thus the roof fall in underground mines has to be minimized by the application of a rational and appropriate support system. The design of support for soft rock formation still drives a real concern for engineers as it requires lots of effort, hard work and experience. In this study, support design is given for the incline lip opening in fragile and soft rock geological formation. The study on the apt support for incline drivages has also been conducted. Rock load has been estimated applying CMRI rock mass classification, Bieniawski's Geomechanical System and numerical modeling. On comparing rock load obtained by CMRI rock mass classification has been observed on upper side. To ensure the safety and stability of incline drivages, CMRI rock mass classification has been considered to design a support system so as to maintain factor of safety above two.

Keywords Support design · Rock load · Incline · Roof fall · CMRI rock mass classification

1 Introduction

The presence of cracks, fissures, joints, faults, and slips always acts as a contributing factor that triggers the roof fall in underground mines and in drivages. The greater depth condition along with high stress also plays a key role to increase the vulnerability of the roof fall. [1]. Thus, the proper identification of the geological factors can help the site engineers to improve the ground condition with the application of adequate and appropriate safety measures to minimize the roof fall. Fatal accidents occurring in underground mines still need serious attention for geologists and

A. Paul (✉) · N. Kumar · P. Kumar · A. K. Singh
CSIR - Central Institute of Mining and Fuel Research, Dhanbad, Jharkhand 826015, India
e-mail: avinashpaul@cimfr.nic.in

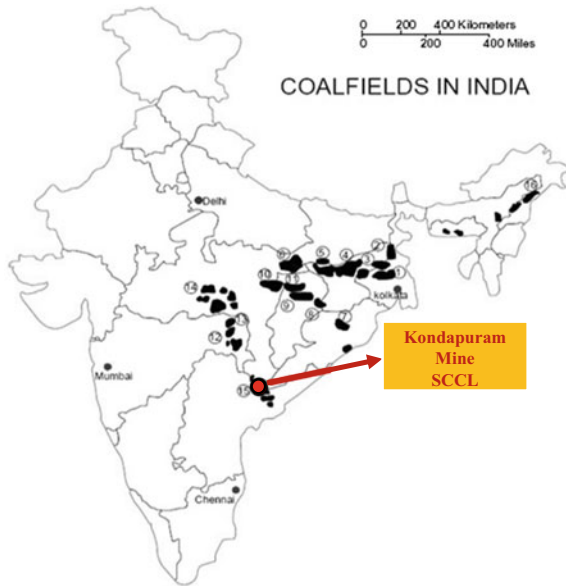
© The Author(s), under exclusive license to Springer Nature Singapore Pte Ltd. 2022
A. K. Verma et al. (eds.), *Proceedings of Geotechnical Challenges in Mining, Tunneling and Underground Infrastructures*, Lecture Notes in Civil Engineering 228,
https://doi.org/10.1007/978-981-16-9770-8_6

mining engineers. Around 40–45% of the fatalities in underground mines are due to roof fall and ground movement [2]. During the course of mining, redistribution of the induced stresses takes place and rock mass tries to converge towards the gallery drivages. If suitable support is provided at the time of redistribution of the stresses, it can restrict the occurrence of the ground movement as well as roof fall which is considered a crucial factor for serious fatalities [3–5]. Rock mass classification system plays an imperative role in the selection of a prominent support system. For the last several years, the rock mass classification system always holds a key place during the empirical support design approach for underground mines [6, 7]. Rock mass classification system also helps in the formation of the preliminary support design guidelines for underground mines [8–10]. Support system always acts as a canopy for mine workers and enhances the safety as it safeguards them and deployed machines from the adverse working condition related to the side and roof fall. Hence, by supporting mine workings without any time lag after excavation, the stability of the mine roof can be improved and also curtails the probable occurrence of roof fall [11–13]. Correct estimation of rock load also plays a vital role during the selection design of a safe and suitable support system [14–16]. In this study, the design of the support system is suggested in three stages. The sequential stages of support for the incline drivage beginning from the support design of the incline's lip opening followed by the design of support for fragile roof condition and finally the support design is given for incline drivage for fair roof condition. For the drivage in fair roof condition, the rock load is estimated by applying both empirical and numerical approaches and after detailed comparison and study, a safe design of support is suggested.

2 Area of Study

This study was conducted at Kondapuram mine of SCCL having two workable seams namely “Thick Seam Top Section” and “Thick Seam Bottom Section” as shown in Fig. 1. The thickness of the top section varies from 1.5 to 2.0 m and the minimum and maximum depth of cover was 22.25 and 231.8 m respectively. Similarly, the thickness of the bottom section varies from 2.5 to 4.8 m with a minimum and a maximum depth of 18.14 and 243.16 m respectively. Presently, the bottom seam is being accessed through punch entries created at the bottom of the high wall of the OC-II project. The bottom seam has been developed and the top seam would be connected by underground drift. The two inclines are driven along with one shaft from surface to coal seam for the convenience of ventilation and hauling man and material. The length of the incline from the surface up to weak rock formation was measured up to 121.68 m. After 121.68 m, the incline's roof strata was observed as moderately fair due to the presence of medium grained sandstone. The dimension of the incline was 6 m wide and 3.6 m in height with a maximum depth of cover of 13.9 m. The immediate roofs of inclines are mainly composed of fine, medium, and coarse grained sandstone in combination with shale and coal at few places. As the

Fig. 1 Investigated site for the study



average RQD estimated from the borehole is 74%, so it can be assumed that mine is free from major discontinuities with the appearance of random joints at the maximum places. The roof condition is mainly dry. The area of the study is concerned with the design of support for incline lip opening, incline drivage with poor and fair roof condition. The objectives of the study are:

- Support design of portal in extremely weak rock formation (up to 58.3 m from the surface).
- To support the lip opening and incline drivage for weak and fragile rock formation (from 58.3 to 121.68 m).
- Support design for drivage in moderately fair roof condition (from 121.68 m up to coal seam intersection).

3 Design of Support for Extremely Weak and Fragile Roof Condition

The support design is given for the portal of 58.38 m length and incline lip opening with drivage having length of 63.3 m. The roof of the drivage is extremely weak and fragile. The total length of this section from surface is 121.68 m. The same has been illustrated in following section.

3.1 Borehole Location and Physico-Mechanical Properties

The five core boreholes (BH-1 to BH-5) were drilled at different locations of varying depth. The available physico-mechanical properties of B.H no.04 & B.H no.05 are given in Table 1 which was considered for support design.

Table 1 Physico-mechanical properties of bore hole considered for support design [17]

Borehole BH - 04									
Depth		STRATA	A	B	C	D	E	F	G
From	To								
10.0	13.0	Sandstone, brown, Mcg, pebbly, M.S	1.94	5.03	69	0.23	13.50	46.85	0.20
13.0	16.0	SST, brown, Mg, M.S	1.96	5.26	79	0.25	14.77	47.03	0.24
16.0	17.0	SST, brick red, Fmg, Massive, M.S	2.12	–	107	0.30	–	47.53	0.36
17.0	19.0	SST, grayish white, Mcg, pebbly, M.S	2.05	7.17	93	0.27	18.71	47.28	0.30
19.5	21.3	SST, grayish white, Mcg, pebbly, M.S	2.16	9.89	145	0.37	27.44	48.21	0.53
31.0	33.0	SST, grayish white, Mg, pyritic, M.S	2.17	10.45	149	0.38	28.59	48.28	0.55
Borehole BH - 05									
10.0	10.5	SST, brown, Mcg, pebbly, clayey, M.S	2.09	6.22	73	0.23	15.44	46.92	0.21
10.5	11.0	SST, brown, Cg, pebbly, M.S	2.04	6.51	73	0.22	14.68	46.74	0.17
11.0	11.6	SST, brown, Cg, pebbly, M.S	2.09	–	73	0.23	–	46.92	0.21
15.0	15.3	SST, brown, Mcg, pebbly, M.S	2.13	–	108	0.30	–	47.55	0.37
16.0	17.0	SST, brown, Mcg, pebbly, M.S	2.11	9.85	93	0.27	21.93	47.28	0.30
17.0	18.0	SST, brown, Mcg, pebbly, M.S	2.12	10.67	112	0.31	25.05	47.62	0.38
18.0	18.6	SST, brown, Mcg, pebbly, M.S	2.21	12.65	129	0.34	29.27	47.92	0.46

Note A = Density (gm/cc), B = Tensile Strength (Kg/cm²), C = Compressive strength (Kg/cm²), D = Young modulus (Kg/cm²), E = Shear Strength (Kg/cm²), F = Impact strength index no., G = Protodya-konov strength

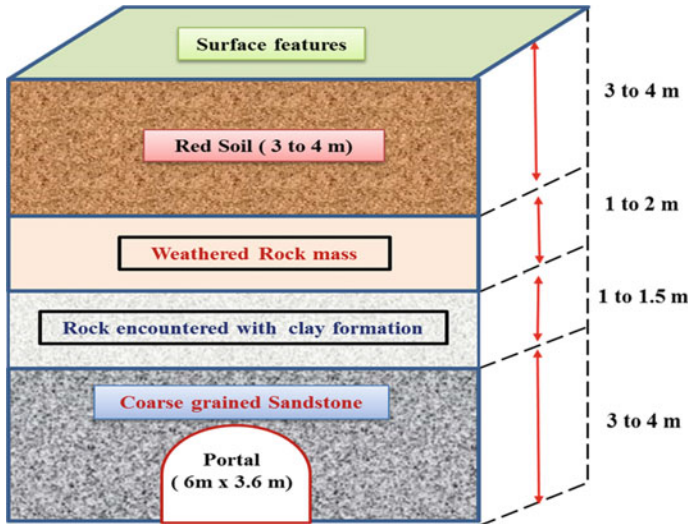


Fig. 2 Disposition of strata at the incline’s mouth

3.2 Support Design for Portal

The portal should be supported with RCC along roof & walls and PCC floor from surface up to 58.38 m. The thickness of RCC wall and PCC floor should be 300 mm and 200 mm thick respectively. Deep grooves should be designed on the underground floor so that during machine movement proper grip should be provided. In the vertical section of interaction plane, the strata succession comprises red soil, clayey rock, weathered rock and coarse grained sandstone while traversing downward (Fig. 2).

3.3 Support Design for Lip and Incline Drivage with Weak and Fragile Roof Condition

The support system mentioned for lip and incline drivage in weak and fragile roof condition of strata. Weak rock-mass present in and around the incline’s lip and thus special method of pre-support is required before actual opening. To ensure the safety of overlying surface features it is suggested to support the lip by fore-polling pre supporting method so that the roof strata gets reinforced and strengthened. Stage wise opening of the lip was also suggested initially up to the height of 2 m and then up to full height of 3.6 m. This precautionary measure has been suggested to safe guard the surface features else it may cause collapse of the lip opening endangering the life of the associated persons as well as surface features. Further, the rock reinforcement

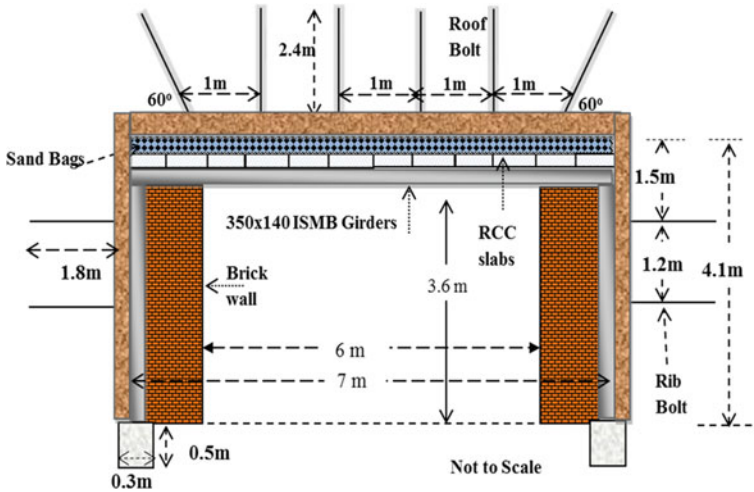


Fig. 3 Design of support for inclines lip and inclines drivages for weak and fragile roof condition

suggested for this section was with six numbers of resin grouted roof bolt, each 2.4 m long and 20/22 mm diameter should be installed at 1 m grid pattern (Fig. 3).

Two side bolts should be grouted at an angle of 60 degree to the horizontal whereas the rest four bolts should be vertical. Additional bolting and supporting with steel bolts, W straps and RCC slabs shall also be fixed wherever required. Two numbers of resin grouted roof bolt each side of incline drivage should be installed as a rib support. The bolt length should be 1.8 m and diameter 20/22 mm. Installation of goal-post support with ISMB 350 × 140MM of 7.0 m length along roof placed over two nos. of 4.0 m height side goal-posts at an interval of 1.0 M/ 0.6 m centre to centre with a sharp coat of anti-corrosive paint (including double lib girders). In case of encountering of any weak strata, the interval of goal-post support shall be reduced to 0.60 M c/c and RCC pre-cast slabs shall be installed accordingly. For each goalpost support erected- fabrication of steel plates of 6 Nos. of 0.40 m L × 0.30 m W × 12 mm thickness for fixing of Horizontal roof girders to the side goal-posts, including bottom plates on cement concrete bed of 0.50 thick. The 0.5 m wide brick wall with 0.5 m foundation in both side of tunnel of height 3.6 m is to be constructed after bolting and skin support system behind the brick wall. The water percolation property of brick should be checked before utilizing otherwise the water garland should be made during construction. On brick wall, the I-section steel girder of 7 m long, should be placed at an interval of 1.0 m. RCC slabs of size 0.30 × 0.1 × 1.0 m (pre-casted) should be placed skin to skin over to steel girder. A total 23 numbers of such slabs would be placed in full width of incline drivage. The gap should be packed with sand filled bags. in between the wire-net and RCC slabs. The support system is suggested for drivage from 58.38 to 121.68 m.

4 Design of Support of Drivage with Fair Roof Condition

Design of support for drivages in fair roof condition, rock load was determined by using both empirical and numerical approaches to check the variation keeping safety aspects in view. The empirical approaches used for determination of rock load are CMRI Geomechanical Classification System and Bieniawski’s Geomechanical Classification System respectively [18, 19]. For numerical simulation Flac 3D modeling was used to estimate the rock load with respect to rock load height.

4.1 Determination of Rock Load by CMRI Geomechanical Classification System

The immediate roof of incline drivage is composed of fine to medium grained sandstone. The inclines are encountered by random joints. The roof is dry. RMR for roof rocks of driven inclines for B/S and T/S seam workings was determined on the basis of borehole loggings using CMRI Geomechanical Classification System. Average value of compressive strength and slake durability is taken from the borehole’s physico-mechanical properties provided by mine management. The ratings of different parameters are as follows (Table 2).

Lower value of RQD was taken (74%) for roof top section and layer thickness was determined as 9.7 cm by using the relationship between RQD and frequency of bedding plane (λ).

$$RQD = 100(0.1 \lambda + 1)e^{-0.1\lambda} \tag{1}$$

Adjustment of RMR was done under two conditions:

- a) For adjustment, 10% reduction for solid blasting and
- b) 10% reduction for gallery width > 4.8 m.

Table 2 CMRI geomechanical classification system

Parameter	Sandstone	
	Description	Rating
(Layer thickness)	9.7 cm	15
Structural features	Random Joints (Indices-07)	15
Weatherability	80%	07
Compressive strength	135 kg/cm ²	03
Groundwater	dry	10
RMR	50	

Hence, Adjusted RMR = $50 \times 0.9 \times 0.9 = 40.5$, the roof is classified as III A, Fair Rock load was estimated for Incline roadways using following equations:

$$\text{Rock load (t/m}^2\text{)} = \text{B.D. [1.7 - 0.037.RMR + 0.0002.RMR}^2\text{]} \quad (2)$$

Where, B = Roadway width (m) and

D = Dry density (t/m³).

In the study area RMR = 40.5

Density of roof rocks, D = 2.1 t/m³, and

Width of drivage, B = 6.0 m.

Rock load for 6.0 m wide incline road ways = 6.67 t/m².

4.2 Determination of Rock Load by Bieniawski's Geomechanical Classification System

RMR of inclines drivage roof was also determined using Bieniawski's Geomechanical Classification System. Ratings of different parameters are as shown in Table 3. These ratings and tested values was used as input parameters for the numerical modeling studies and support design.

Rock load was estimated for Incline roadways using following equation:

$$\text{Rock load at incline/Tunnel roadways (t/m}^2\text{)} = \text{B.D. [(100-RMR)/100]} \quad (3)$$

where, B = Roadway width (m), and

D = Dry density (t/m³).

In the study area,

RMR = 59.

Density of roof rocks, D = 2.1 t/m³, and

Width of gallery, B = 6.0 m

Rock load for 6.0 m wide incline drivage = 5.16 t/m².

Table 3 Bieniawski's geomechanical classification system

Parameter	Sandstone	
	Value	Rating
Strength of intact rock (MPa)	13.5	02
RQD (%)	74	17
Spacing of joints	0.5 to 1 m	15
Condition of joints	Slightly rough surfaces, separation < 1 mm, hard wall rock	20
Groundwater	Dry	10
Joint Orientation (Adjustment)	Fair	(-5)
RMR	59	

4.3 Determination of Rock Load by Numerical Modeling

3D finite difference software (FLAC3D) developed by ITASCA group of USA was used for determination of rock load by numerical modeling. The different parameters required for the numerical modeling is illustrated below.

In-situ Stress. For the study, theoretical in-situ-stresses values suggested by Sheorey [20] was used as the real stress value owing to unavailability of actual field data. For determination of horizontal stresses a study was conducted under S&T funded project by Ministry of Coal and relationship was developed between horizontal in-situ stress and depth of cover for Indian geo-mining condition [21].

The vertical in-situ stress

$$S_v = \gamma H \text{ MPa} \quad (4)$$

Where, γ = unit rock pressure, 0.025 MPa/m and
H = hard rock cover below surface, m

The horizontal in-situ stress

$$S_H = S_h = 2.4 + 0.01 H \text{ MPa} \quad (5)$$

Where, S_H & S_h = major and minor horizontal in-situ stresses, MPa and
H = depth of cover, m

Rock Mass Strength and Safety Factor Evaluation. The rock mass strength was evaluated by applying an empirical criterion suggested by Sheorey (1997) [22] expressed as:

$$\sigma_1 = \sigma_{cm} \left(1 + \frac{\sigma_3}{\sigma_{tm}} \right)^{bm} \quad (6)$$

Evaluation of the safety factor for each element was done in the modeling process to assess stability of the openings. The safety factor is defined as.

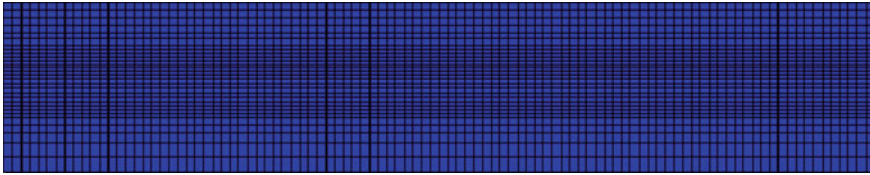
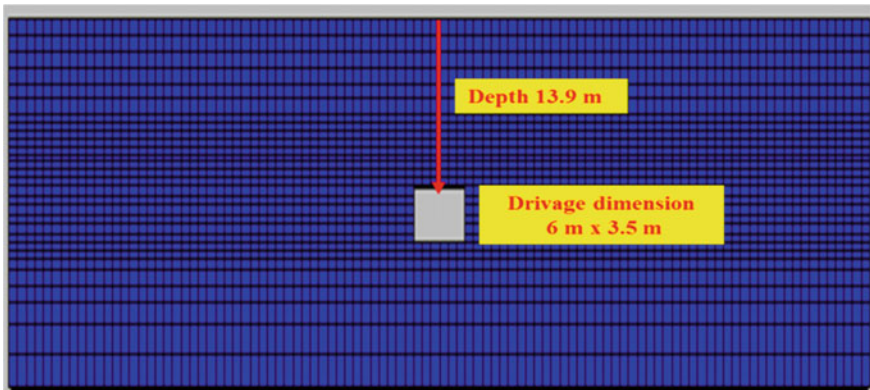
$$F = \frac{\sigma_1 - \sigma_{3i}}{\sigma_{1i} - \sigma_{3i}} \quad (7)$$

Where σ_{1i} and σ_{3i} are termed as major and minor induced stresses as the output result of numerical model.

Rock Properties Used for Modeling. The rock properties used for numerical modeling is detailed Table 4. The first three elastic constant parameters and density plays a key role for execution of the numerical model. On the other hand, the remaining three parameters are related to strength which is essential for evaluation of

Table 4 Properties used in the modeling

Rock type	Modulus of elasticity, GPa	Poisson's ratio	Rock density Kg/m ³	Intact compressive strength, MPa	b	RMR
Sandstone	4.0	0.25	2150	13.5	0.5	50

**Fig. 4** Virgin numerical model at depth of 13.9 m for 6.0 wide drivages**Fig. 5** Extracted numerical model at depth of 13.9 m for 6.0 wide drivages

the safety factors. Normally, unadjusted RMR value is considered in the numerical modeling as the adjustment factors are taken care by modeling itself.

Modeling Methodology. The data illustrated below are taken for preparation of the numerical model (Fig. 4.). Existing geo-mining condition was also considered while selection of the given parameters.

- i. Extraction height of drivage 3.6 m
- ii. Depth of cover: 13.9 m (approx.)
- iii. Width of the drivage 6.0 m

In modeling, drivages of 6.0 m × 3.6 m was excavated in stone (Fig. 5). Safety factors indicated by color contours at different heights was used to assess the stability of the immediate sandstone roof. The unstable zone height was considered from 0.5 to 1 by the safety factor color contours in the stone roof which needs to be supported.

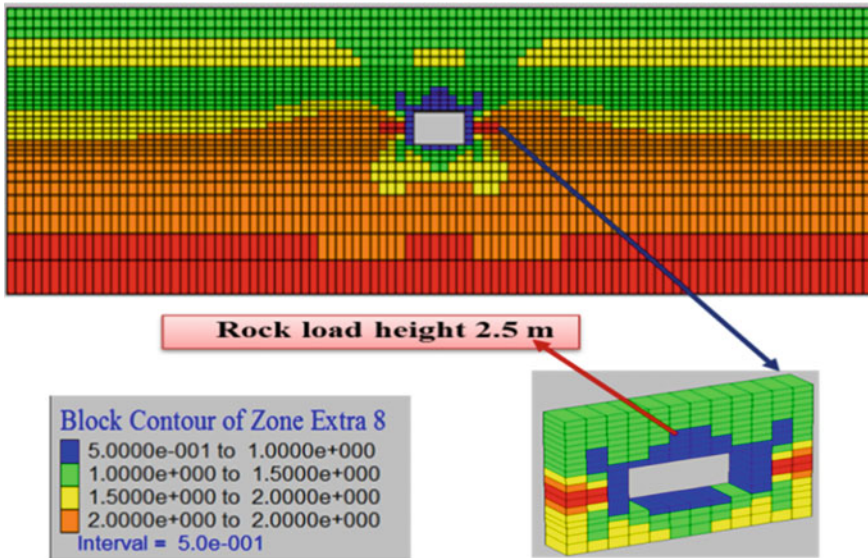


Fig. 6 Numerical model showing rock load height along with safety factor contours for 6 m wide drivages

Numerical Modeling Results. Failure height was determined for incline drivage with the help of numerical modeling (Fig. 6).

The incline drivage stability figures were shown with their respective rock load height in terms of safety factor contours of different colours. The height of extraction was 3.6 m. The failure height was anticipated up to 2.5 m above roof (safety factor contour ≥ 1) with the development of 6 m drivage width and with extraction height of 3.6 m. Rock load was determined from model after multiplying the rock load height with density of the rock which comes to 5.25 t/m^2 .

4.4 Comparison and Selection of Rock Loads for Drivages

Different values of rock load was obtained on its determination by different techniques as listed in Table 5. The rock load values varied from 5.16 to 6.67 t/m^2 and was observed that the maximum rock load value was obtained by CMRI Rock Mass Classification system as 6.67 t/m^2 .

The rock load values were compared with RMR for different methods shown in Fig. 7.

High rock load with less RMR and high RMR with less rock load was observed resulting in selection of suitable support density. High support density has to be followed for was rock load varying from 5.25 to 6.67 t/m^2 with RMR variation upto 40.5 in CMRI RMR. On the other hand, zone of low support density was delineated

Table 5 Comparison of rock load obtained by different approaches

S. No	Methods	Approaches	Rock load (t/m ²)	Remarks
1	Empirical method	CMRI rock mass classification system	6.67	Rock load determined by CMRI rock mass classification is considered for support design
2	Empirical method	Bieniawski's rock mass classification system	5.16	
3	Numerical method	Numerical simulation	5.25	

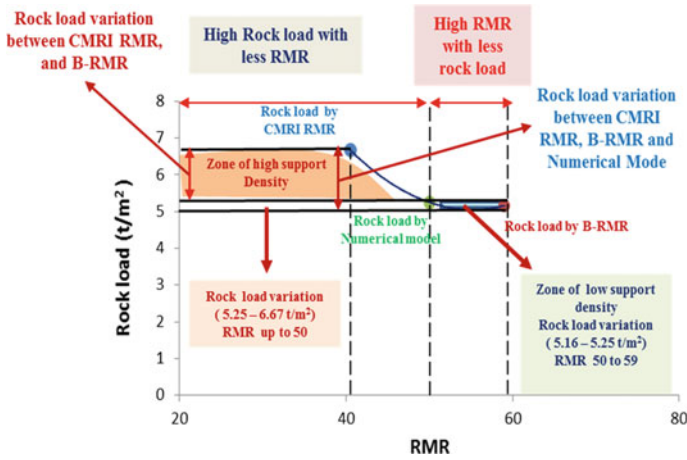


Fig. 7 Comparison of rock load obtained using different approaches

when the variation in rock load was seen from 5.16 to 5.25 t/m² when RMR scaling from 50 to 59. Thus for the same scale of RMR, CMRI RMR shows high rock load value with high support density compared to numerical modeling and Bieniawski's RMR. Selection of the support system on the basis of low support density sometimes leads to the under supporting condition and may cause serious roof failures. Thus, least RMR value with maximum rock load obtained by CMRI RMR rock mass classification system has been considered for design of support for incline driveage from safety perspective view point.

4.5 Design of Support for Drivages

In Kondapuram Mine, the geotechnical studies of the roof rocks revealed that CMRI RMR for inclines driveage comes to 40.5 categorized as Class III A and falls under fair

roof condition. The rock load was estimated for 6.0 m wide drivages using Eq. (2) as 6.67 t/m^2 . Six full column resin grouted roof bolts in a row at spacing of 1.0 m was suggested to support the drivages. The side bolts should be spaced at 0.5 m from both sides of the incline drivages (Fig. 8).

The bolting row should be also spaced at 1.0 m interval. The two side bolts should be inclined at an angle of 60° to arrest the cutter failure and the stresses develop at the corner edges (depicted from the numerical model); while the central bolts should be grouted vertically. The length of the bolt should be 2.4 m having dia of 20–22 mm, made of TMT ribbed bar. The support resistance for designed support system estimated as 12 t/m^2 with a safety factor of 1.8 calculated as follows:

$$\begin{aligned} \text{Support Resistance} &= \frac{\text{No. of roof bolt} \times \text{Anchorage strength (t)}}{\text{Width of gallery (m)} \times \text{Row spacing (m)}} \\ &= (6 \times 12/6 \times 1.0) = 12 \text{ t/m}^2 \end{aligned}$$

$$\text{Safety Factor} = \text{Support Resistance/Rock load}$$

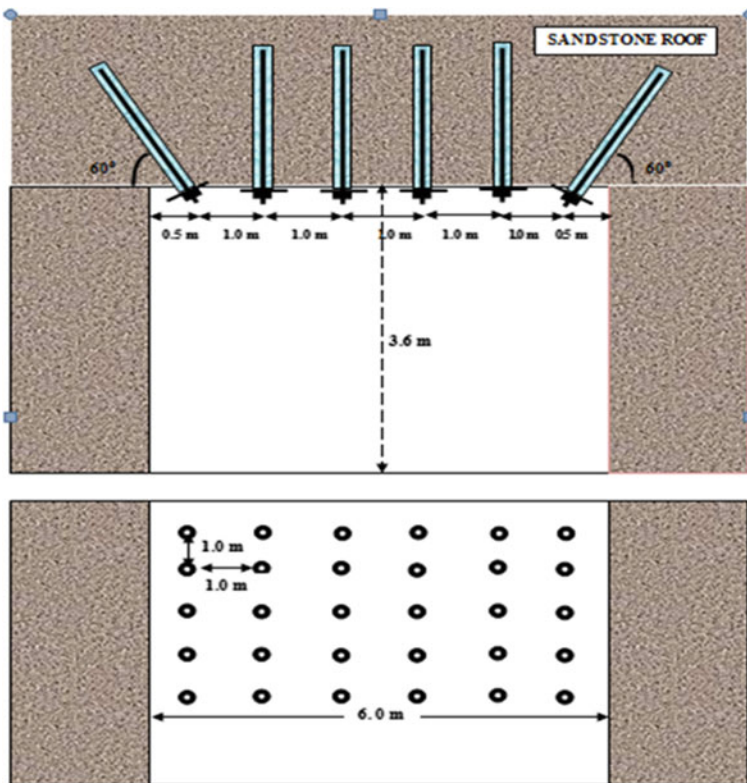


Fig. 8 Design of support system for drivages of Kondapuram Mines, SCCL

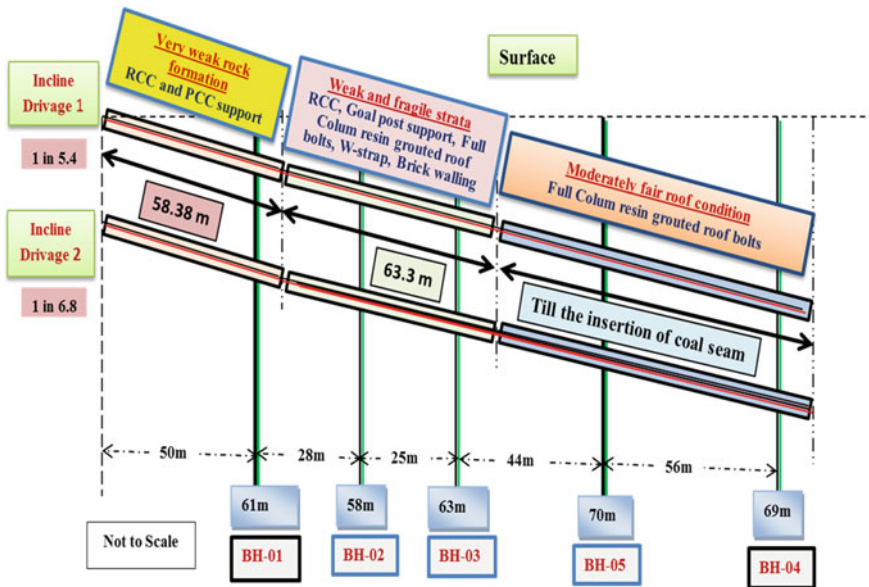


Fig. 9 Proposed support design along incline drivages under different rock mass condition

$$= 12.6.67 = 1.8$$

After detailed field study, based on different rock mass condition the proposed support design for incline drivages along longitudinal section shown in Fig. 9.

5 Conclusion

Any excavation in weak and fragile rock formation needs careful planning and experience. Before supporting such type of the rock mass it is necessary to have good knowledge of in and around strata by borehole lithology, geo-mining conditions, geo-technical investigations along with the application of the rock mass classification system. The portal should be supported with RCC along roof & walls and PCC floor for extremely weak rock formation. Support design was also suggested for incline’s lip and for the adjoining incline drivage from 58.38 to 121.68 m in weak and fragile rock formation. Before any excavation the incline lip opening should be initially supported with fore polling pre-support system in view to strengthen the overlain strata followed by resin grouted roof bolts, W-strap, RCC and goal post support along with brick walling. The same support system was suggested for the adjoining incline’s drivage. Finally, for moderately fair rock formation Rock Mass Rating (RMR) was determined applying two geo-mechanical classification system

namely CMRI Geomechanical Classification System and Bieniawski's Classification System. Rock Load was also determined by using numerical models to validate the rock load obtained from above classification systems. Although the rock load obtained by Bieniawski's Rock Mass Classification System and numerical approach was less compared to the rock load obtained by CMRI Geomechanical Classification System but to avoid the state of under supporting condition and as well as in the view of permanency of the surface features, later was considered for design of support for drivage. The support design given for 6.0 m inclines drivages should be supported with six full column resin grouted roof bolts. The suggested bolt length should be 2.4 m. The pretensioning should be given to the roof bolts using the bearing plates. The safety factor obtained from the designed support system was 1.8 and accordingly, safe support design has been formulated for incline drivage.

Acknowledgements The support and cooperation received by the mine management for conducting the research work in comprising site selection and rock sample collection is rightly acknowledged. Authors thank Director, CSIR - Central Institute of Mining and Fuel Research, Dhanbad, India for his guidance, support and permission.

References

1. Molinda GM (2003) Geologic hazards and roof stability in coal mines. Pittsburgh, PA: U.S. Department of Health and Human Services. Public Health Service, Centres for Disease Control and Prevention, National Institute for Occupational Safety and Health, DHHS (NIOSH) Publication No. 2003-152, IC 9466
2. Dash AK, Bhattacharjee RM, Ahmad A (2016) Case study of accidents related to fall from height in indian coal mining industry: an analysis. *Int Jr Sci Eng Res* 7:387-392
3. Ghosh CN, Ghose AK (1992) Estimation of critical convergence and rock load in coal mine roadways – an approach based on rock mass rating. *Geotech Geol Eng* 10:185-202
4. Paul A, Murthy VMSR, Singh AK (2014) Rock load Estimation in development galleries and junctions for underground coal mines: a CMRI –ISM rock mass rating approach. *J Mining*. <https://doi.org/10.1155/2014/618719>
5. Paul A, Murthy VMSR, Prakash A, Singh AK (2017) Performance investigation of rock mass classification systems for coal mine support design in indian mining conditions. *Int J Earth Sci Eng* 10(6):974-5904
6. Laubscher DH (1984) Design aspects and effectiveness of support systems in different mining conditions". *Trans. Inst. Min. Metall.* 1:70-81
7. Wickham GE, Tiedemann HR, Skinner EH (1972) Support determination based on geologic predictions. In: Lnae KS, Garfield LA (EDS) *Proceedings North American rapid excavation Tunnelling conference*. Soc. Min. Engrs, Am. Ins. Min. Metall. Petolm Engrs, Chicago, pp 43-64
8. Ventakeshwarlu V, Raju NM (1987) Support design for mine roadways - a geotechnical approach. In: *World mining congress 13th (Stockholm)*, pp 857-864
9. Ghose AK, Raju NM (1981) Characterization of rock mass vis-à-vis application of rock bolting – modelling on Indian coal measures. In: *Proceedings U.S symposium rock mechnaism, 22nd (Massachusetts Inst. Technol)*, pp 422-427
10. Carter TG (1992) Prediction and uncertainties in geological engineering and rock mass characterization assessments. In: *Proceedings of 4th international rock mechanics and rock engineering conference*, Trino, Paper vol 1

11. Bieniawski ZT (1973) Engineering classification of jointed rock mass. *Trans South Afr Civil Eng* 15:335–344
12. Bieniawski, Z.T. : Rock mass classification in rock engineering. In *Exploration for Rock Engineering*. In: Bieniawski ZT (ed) *Proceedings of the Symposium*, Cape Town, Balkema, vol 1, pp 97–106
13. Barton NR, Lien R, Lunde J (1974) Engineering classification of jointed rock mass for the design of tunnel support. *Rock Mech* 6(4):189–239
14. Paul A, Murthy VMSR, Prakash A, Singh AK (2020) Prediction of rock load emphasizing excavation damage of in-situ rock caused by blasting in coal mines. *Curr Sci* 118(1):123–132
15. Paul A, Murthy VMSR, Prakash A, Singh AK (2018) Estimation of rock load in development workings of underground coal mines – a modified (RMR_{dyn}) approach. *Curr Sci* 114(10):2167–2174
16. Paul A, Singh AP, John LP, Singh AK, Khandelwal M (2012) Validation of RMR-based support design using roof bolts by numerical modeling for underground coal mine of Monnet Ispat, Raigarh, India—a case study. *Arab J Geosci* 5:1435–1448
17. Kumar N, Paul A, Kumar DL, Ghosh CN (2018) Design of support for mine tunnel at low depth in weak rock mass :a case study. *TAEMM*, 177–184
18. CMRI (1987) *Geomechanical Classification of Roof Rocks vis-à-vis Roof Supports*. S & T Project Report
19. Venkateswarlu V, Ghose AK, Raju NM (1989) Rock-mass classification for design of roof supports—a statistical evaluation of parameters. *Mining Sci Technol* 8(2):97–107
20. Sheorey PR (2001) *Design of pillars in underground coal mining*, Course on Theory and practices of ground control on board and pillar mining. CMRI, Dhanbad, Jharkhand, India, pp 91–115
21. CMRI (2002) *In Situ Stress measurement in underground coal mines and its application to stability analysis*. S & T Report
22. Sheorey PR (1997) *Empirical Rock Failure Criteria*. A. A. Balkema, Rotterdam, pp 54–55

Prediction of Rockburst Using Supervised Machine Learning



Tharun Balaj Kishore and Manoj Khandelwal

Abstract The rockburst is one of the serious mining hazards, that cause injury, death, damage to mining equipment, and leads to financial problems in mining constructions. At the same time, mining is the major and essential resource of mineral commodities, that all mining locations uncover important for sustaining and enhancing their needs of dwelling. Moreover, mining contributes a significant portion of the GDP (Gross Domestic Production) growth of nations such as China, Australia, Russia, and the USA. These countries play major roles in exporting mineral commodities, which has been creating a huge demand to find out conventional methods for predicting the rockburst occurrence during mining. Moreover, determining rockburst occurrence using formulation or machine-based equipment has not been ideal in showcasing the result, due to changing geological parameters and the mining environment. In recent years, various soft computing and machine learning tools have been developed significantly, which help us to improve predicting models more accurate. In this research, original Rockburst data set have been collected in the last 20 years. Then standard empirical formulation method which is currently used in mining and supervised machine learning models has been used to predict rockburst occurrence. Finally, an interacting machine learning model developed in a way to predict the Rockburst occurrence result in three Indicators (high, medium and low Rockburst) are presented.

Keywords Supervised machine learning · Rockburst prediction · Random-forest classifier

T. B. Kishore · M. Khandelwal (✉)
School of Engineering, Information Technology and Physical Sciences, Federation University
Australia, Ballarat, VIC 3350, Australia
e-mail: m.khandelwal@federation.edu.au

© The Author(s), under exclusive license to Springer Nature Singapore Pte Ltd. 2022
A. K. Verma et al. (eds.), *Proceedings of Geotechnical Challenges in Mining, Tunneling and Underground Infrastructures*, Lecture Notes in Civil Engineering 228,
https://doi.org/10.1007/978-981-16-9770-8_7

1 Introduction

One of the major hazards the underground construction faces is a Rockburst, which is a sudden release of energy from the rock mass due to seismic events and unstable underground rock properties.

This phenomenon can reach such proportions that it makes rock volumes stand out with high energy. Due to the greatness of rockburst, there are several reports of its appearance in well-known underground works such as the Mont Blanc tunnel in France, the tunnel Gotthard in Switzerland, the Dai-Shimizu and Kanetsu tunnels in Japan and hydroelectric power as is the special case of Jinping II in China [3, 4, 6]. Regarding mining tunnels, this phenomenon is well known since several reports were reported. examples in South Africa and Canada [1].

Rockburst is a phenomenon whose deformation energy of the rock mass surrounding the tunnel is released abruptly. This sudden rupture occurs essentially in rocks with a high level of confinement as is the case of igneous and metamorphic rocks. If such rock masses are tested under uniaxial load conditions, it appears that when the peak resistance of the rock, certain rock fragments detach and are thrown to open the tunnel. As such, and following this reasoning, the failure surface is entirely related to the deformation extensional [5].

Regarding the rockburst initiation process, it is necessary to consider the triggering of a mechanism (trigger), as regards the existence of two disparate cases:

1. Rockburst remotely triggered - where the location of the remote seismic event (quake land or landslide) and excavation damage occur at different sites;
2. Self-initiated rockburst - where the site of the seismic event and excavation damage occur in practically identical places.

Regarding the first case, it is known that it occurs especially in situations that integrate regions with the active seismic zone as discussed by Kaiser [4]. How much to the second case, it is known that rockburst occurs in particular situations, more concretely when the stresses at the excavation boundary exceed the strength of the rock mass, which leads to the failure of the rock in an unstable and violent way. In the case of the stored energy of the massif resistance itself does not dissipate during the fracturing process, i.e. when the rigidity of the storage is softer than stiffness after peak rock breakage, rockburst occurs quickly and violently [5].

As predictable, the rock will break when the stress exceeds its strength or by itself or remotely triggered. The referred stresses occur due to the combination of some or all the following factors:

- Gravitational stress;
- Stress-induced by excavation;
- Dynamic forces due to mass vibrations (inertial forces during acceleration and slowdown);
- Increase in dynamic stresses due to the dynamic stress of the mass (caused by deformation waves).

Thus, the failure or even triggered is initiated when the above voltages exceed the capacity of supported and unsupported rock even if temporarily. For the definition of the potency of rockburst stress levels are used (or the stress ratio, i.e., $\sigma_{wall}/\sigma_c = \sigma_{max}/\sigma_c$) [5].

2 Theories of Rockburst

In recent years many theories have been put forward to explain rockburst. However, the main theories in common use among mining engineers are those of beam, dome and continuous elastic medium, rebound & dilatancy. Miller (1962) has outlined these theories as follows:

Beam Theory

This theory takes into consideration the particular physical nature of the ground namely stratification/lamination. As support by the reef or seam is removed from the hanging wall and footwall by mining, a series of beams form due to the failure of the intervening surface of different beds. Due to the effect of gravity, each beam in the hanging wall sags under its weight, the effective length of each successive seam decreasing as the distance into the hanging wall increases. In case a rockburst occurs in the abutments (just ahead of the Slope face), it will be considered to have been induced by the leverage action of the immediate beams.

Dome Theory

This theory was postulated by Evans (1940) who proposed the existence of a ‘Vousoir’ arch or beam over the mined-out area. When an excavation is made underground, the load of an unsupported portion of the roof is transferred onto the abutments. Subsequently, the ground tries to sag under its weight. The resulting redistribution of stress forms an arch with its base at the walls of the excavation and is hence called the dome of stress. The abutment supporting the dome remains on the sides of the excavation so that the size of the dome increases as the span of the excavation increases. The profile of this imaginary stress arch has the property of transmitting stresses along with this profile onto the abutments. So, in the limiting stage, the abutments fail under continuous loading resulting in a severe rockburst. The type of rockburst so taking place depends upon the behavioural pattern of the weight of the stressed zone, properties of rock etc., following the failure of abutments.

Continuous Elastic Medium Theory

This theory considers the rock as a continuous elastic medium and does not postulate the existence of beam or dome formations around the excavation. Using the classical theory of elasticity principles, it is possible to make a more rigorous quantitative assessment of stress around mine openings than can be made by either the beam or dome theories, which are essentially qualitative assessments. It is possible to determine the state of stress of a point in the rock by comparing this with the physical

characteristics of the rock to roughly determine whether failure will occur or not and in event of failure the energy liberated as failure occurs.

Rebound Theory

This theory is based upon two assumptions [8] (i) a medium is permeated with a continuous field of defects, and the quantification of them can be done by the defect density field, and (ii) in an advanced precursory stage, there is a flow process, over the whole region concerned, which accounts for the defect propagation (crack movement and grouping).”

3 Classification of Rockburst

Rockburst classification is based on different modes of failure initiation processes at the place of occurrence, based upon the geometry of mining is recommended as inherent and induced. The latter may be further classified based on the attributed originating cause into the following four sub-groups:

a) Slope bursts b) Pillar and remnant bursts c) Area rockburst d) Bursts in working shafts.

Slope Bursts

Slope bursts occur when a shear crack parallel to the face enters one of the walls. The wall rock is then able to expand freely into the Slope, heavily compressing those supports which previously had not taken stress. As a result, the face disrupts and fills the Slope with debris.

The second type of stope burst occurs when stresses around a level, (rise or winze) are so increased by the influence of an approaching Slope face that, at some point on the periphery, the rock fails. The stress ring is broken and the rock of the sides, back and bottom expand suddenly and violently into the excavation, causing a rockburst. Spalding [7] analysed the stress concentrations at the periphery of excavations and their decay, with the increase in distance from the excavations. The fractured rock adjacent to the excavation shifted the zone of peak stress concentration further into the solid rock. Furthermore, the larger the excavations the greater the extent of spread of the high-stress zone. Spalding visualised the existence of high-stress rings or zones around stoping areas.

Pillar and Remnant Bursts

Failures of remnants and premonitory as well as those of pillars by crushing are termed as ‘Pillar- burst’ or ‘Remnant burst’. If there is a series of pillars or remnants in an area, the bursting of one pillar is liable to trigger off a burst in an adjacent pillar or remnant.

After a pillar burst, it is found that all supports on every side of the pillar have been heavily squeezed. It is likely that total failure has occurred and that mining of the remainder of the pillar can be carried out comparatively safely.

Area Rockburst

In the case of an ore-shoot that has been Sloped out haphazardly, resulting in a large number of remnants and promontories and if the remaining ground is being gradually removed, then more and more stress will fall on those portions which are yet upslope. If one remnant fails suddenly, a great increase in stress will be thrown onto the remaining ground and the supports. This sudden extra stress is liable to cause the remaining remnants to burst, usually in fairly quick succession. The result is an area rockburst.

Bursts in Working Shaft

If a shaft lies within a stressed zone resulting from large scale stopping operations, the penetration of this stressed zone around a shaft will cause a burst, often resulting in great damage to the working shaft.

Inherent Burst

In the case of a burst of this nature, there is no neighbouring excavation and the bursting is due to the stresses set up about the excavation concerned. These bursts may be broadly divided into two categories (i) those due to violent arching, and (ii) those due to the influence of fissures or adjacent excavations on the stress redistribution.

Visually rocks at great depth are under a state of great compression and added to it is the locking up of potential energy released due to mining. As a consequence whenever a small scale local failure occurs, the neighbouring rocks aggravate the situation by trying to expand and release the stress resulting in a tremendous violent rockburst. All types of rockburst usually follow these general guidelines.

With the extensive investigations of the occurrence and effects of rockburst and experience in combating rockburst danger as well as the Geomechanical and Seismological analysis in GDR, Knoll (1990) suggested the following classification.

Type 1–Mining or Static rockburst, Type 2–Tectonic or Dynamic rockburst.

Type-1 is closely connected with face mining. Therefore its foci are located in the direct vicinity of mine openings. The cause of this type is the direct consequence of stress redistribution in connection with advancing faces which are highly loaded and reach almost the critical state. Blasting can then trigger the brittle fracture connected with the energy release. The foci of these fractures have been seismically located near active working faces. Further parameters include such as the geomechanical, geological and tectonic conditions of the mining.

Type-2 is only indirectly connected with mining activities. Its formation results from regional redistribution within the rock mass in the far-field environment of the stopping areas. Stress redistribution is due to mining activities in large working areas or whole mines. This type is triggered by high tectonic stress already in the virgin rock mass at great depths. The burst originates especially when geological faults

are oriented favourably to the tectonic stress field in the form of zones of weakness capable of brittle fracturing.

Shemyakin (1986) suggested rockburst classification based on (i) intensity and (ii) location. The rockburst based on the intensity is further classified into:

a) Bumps b) Shocks c) Microbursts d) True Bursts e) Spalling f) Intense Loosening.

The rockburst based on location are further classified into the following:

a) In solid pillars, b) In pillars cut through by workings, c) In pillars separated from the bed by workings, d) In marginal portions of a coal seam, e) In workings laid through a coal bed, f) In workings with the destruction of roof or floor of the seam, g) In workings through the rock.

The rockburst is comprised of intense dynamic events and has the following three features:

- i) The location of the focal zone
- ii) Interaction of a rockburst and tectonic structure (faults)
- iii) The energy released by the dynamic event

4 Machine Learning Techniques

Tom M. Mitchell affirms that machine learning is an area that studies how to build computer programs that improve their performance in some tasks thanks to experience. This is based on the ideas of various disciplines, such as artificial intelligence, statistics and probability, information theory, psychology and neurobiology, control theory and computational complexity. The same author states that to use the learning approach, a series of decisions must be considered, including the selection of the type of training, the objective function to be learned, its representation and the algorithm to learn that function from examples of training.

According to Mitchell, learning algorithms have proven useful in various application domains, such as in data mining in large databases that contain implicit regularities, which can be discovered in an automated way, in domains that are poorly understood and where humans do not possess the knowledge necessary to develop effective algorithms, and in domains where programs must dynamically adapt to respond to changing conditions in the environment.

For their part, Fang Lu and Qingyuan Bai mention that learning techniques are the predominant approach to categorizing texts. These authors define the techniques as a general inductive process that automatically builds a classifier, learning from a set of pre-classified documents.

Learning techniques are classified as supervised, unsupervised, and semi-supervised. In supervised, the goal is to learn the mapping of the correct responses to the input data provided to you; For this, a set of training data made up of pairs consisting of correct input and output patterns is used. In this way, the system learns the correct output mapping for each input pattern presented to it.

Yu Wanjun and Song Xiaoguang state that the supervised learning stages applied in the categorization of text are initially a set of already classified examples that are presented to the algorithm with which a classifier is built. Subsequently, unclassified examples are presented to the classifier for sorting. Finally, steps must be taken to evaluate the performance of the classifier.

Some examples of supervised machine learning techniques are decision trees, maximum entropy, naive Bayes, support vector machines, and so on.

In unsupervised learning techniques, human intervention is not required to produce a previously categorized data set to be presented to the learning algorithm. The goal of unsupervised learning is to find interesting patterns by considering the distribution and composition of the presented data. A total of 9 unsupervised learning techniques are clustering these techniques.

Semi-supervised learning techniques are a middle ground between supervised and unsupervised learning. In this type of learning, the data is divided into two parts: a group of classified data and another of unclassified data. This is called standard semi-supervised learning.

For Olivier Chapelle, Bernhard Schölkopf and Alexander Zien, semi-supervised learning is more useful when there is a greater amount of unclassified data than classified data. Especially when getting classifieds requires a lot of effort, takes a long time, or is very expensive; since, in addition, obtaining unclassified is generally less expensive. 10 Examples of semi-supervised learning techniques are the techniques of transductive support vector machines, expectation–maximization (EM), etc. Some applications of semi-supervised learning mentioned by the authors are speech recognition, web page classification and protein sequencing.

Hsinchun Chen and Michael Chau mention the main paradigms of machine learning, which are the probabilistic model, symbolic learning and rule induction, neural networks, evolution-based algorithms, analytical learning, and hybrid methods.

The probabilistic model is one of the oldest learning methods that are frequently used to classify different objects into previously defined classes based on a set of characteristics. Examples of this are the Bayesian model and the naive Bayes model.

Symbolic learning and rule induction can be classified according to the underlying learning strategy in routine learning (rote), by instructions, analogy, examples, and by discovery. Examples of techniques of this type are the decision tree algorithm ID3 and its variation in the algorithm. These present the result of the classification in the form of decision trees or a set of production rules.

Artificial neural networks mimic human neurons. Here knowledge is represented by symbolic descriptions; knowledge is learned and remembered by networks of artificial neurons interconnected by synapses with weights and logical threshold units (Lippmann; Rumelhart, Hinton, and McClelland). There are different models of neural networks; some examples are feedforward/backpropagation, Kohonen's self-organizing maps (SOM) and Hopfield's neural network model.

Evolutionary algorithms mimic the process of evolution in nature. Fogel identifies three categories of these: genetics, evolutionary strategies, and evolutionary

programming. 15 Genetic algorithms imitate the principles of genes and use mutation and crossover operators in the population to select the most adapted individuals and repeat this operation in several generations until the best individual is obtained. In evolutionary strategies, a population of real numbers is evolved that encodes the possible solutions of a numerical problem and the jump sizes; selection is implicit in evolutionary strategies. In evolutionary programming, a population of finite state machines is made to evolve, subjecting them to unit transformations.

Analytical learning represents knowledge as logical rules and makes reasoning about them to search for tests, which are compiled into more complex rules to solve problems with a small number of searches.

It should be noted that, in practice, these machine learning paradigms are often used by combining several techniques to take better advantage of the advantages that each one presents and also correct the weaknesses that they have if they were used individually. This is known as the hybrid method. In the next section, some considerations about text mining are presented.

Machine learning methods have often been applied for rockburst prediction since the work of Feng and Wang (1994) using ANN. For instance, Zhang et al. (2011) employed a Particle Swarm Optimization-BP Neural Network; [10] and Peng et al. (2014) proposed a rock burst classification based on SVM, Li and Liu (2015) employed the RF approach; Liu et al. (2013) employed cloud models with attribution weight; and Zhou et al. (2016b) employed stochastic gradient boosting for predicting rockburst damage in burst-prone mines. Others have employed fuzzy technologies ([9], Guo and Jiang (2009), Yu et al. (2009) and Adoko et al. (2013a)) to infer rock burst and its risks, and Bai et al. (2009) developed a Fisher discriminant analysis model (FDA) for rockburst prediction in deep rock engineering.

4.1 Merits of Using Machine Learning in Predicting Rockburst

The predictive methods discussed above have some limitations in relation to the prediction of the two challenges addressed in this research - rockburst and tunnel squeezing—, which makes it worthwhile to attempt new ways to tackle such problems. For instance, one shortcoming associated with the analytical and numerical methods discussed above is that, although they have been often shown to have “backward” predictive capabilities (ie, they can be fitted to reproduce the occurrence of an observed behaviour), their “forward” predictive capabilities have not yet been validated so well, due to the difficulty to assess or fit the model parameters at an early stage of the project, when enough good quality data or performance observations are not yet available. In addition, the complexity of the models involved makes their use often beyond the capabilities of many design offices [2]. Therefore, there is a need for better empirical models that can be used with the limited amount of data that is typically available at the early stages of one project.

Similarly, many of the methods discussed above have the limitation that they are deterministic, hence providing little information about the uncertainties associated with their predictions. In other words, they cannot be used in the context of risk analyses. Therefore, there is a need to develop new methods that probabilistically estimate the likely occurrence (or not) of the rockburst and squeezing problems discussed herein. And, similarly, those traditional methods for rockburst and squeezing predictions are meant to be employed under a ‘complete state of information, or when information about all the input parameters that ‘feed’ the model is available. Since that is often not the case when projects are at an early stage of development, there is a need to develop new methods that can still predict incomplete states of information, being able to update (and, hopefully, improve) such predictions as more information becomes available.

Empirical methods predictive capabilities significantly depend on the quality of the data employed for their development, so there is a need to develop even more extensive data sets of good quality case histories associated with the problems under analysis. In that sense, a significant effort has been made to further extend the existing databases (e.g., for squeezing prediction) and, to build new ones (e.g., for rockburst prediction), so that they can be employed for the analyses conducted herein and, in the future analyses is conducted by other researchers.

5 Methodology

The prediction of rockburst in this study has been separated into two methods, one is using the empirical formulation method, which is generally used to determine the rockburst occurrence manually and another method is the supervised machine learning technique, which comes under the soft computing technique.

In supervised machine learning, the details are observed based on attributes in data, according to that the best 05 most accurate machine learning algorithms were selected to perform prediction of the rockburst. These predictions will be based on training and testing data according to attributes to give the best result.

5.1 Data Sources

In this study, rockburst data sets were collected from the last 20 years from different journals and books which are authenticated as original data values (Table 1). Moreover, these data sets have been separated into two sets, where has 1st date set contains 50 data samples which can be only used to determine empirical models and 2nd data set contain 240 data samples with more detailed values of rockburst compared to the first data set. This 2nd data set is used in supervised machine learning to predict the rockburst.

Table 1 Statics of dataset -1

Basic statics of dataset -1				
	MTS (OR) $\sigma\theta$	UCS (OR) σC	uts (or) σt	wet
Max	108.4	306.58	22.6	10.57
Min	7.5	52	2.49	1.3
Total data	50	50	50	50
Mean	58.4326	157.1372	10.1074	5.541
Median	56.55	155	8.515	5.73
St. deviation	31.60153063	61.077827	5.528899514	2.177703574

The first Data set contain 4 parameters and result columns such as Maximum tangential stress, the uniaxial strength, Elastic energy index and tensile strength, then the output of the 1st dataset have been classified into two types ‘Yes’ mean rockburst occurrence have been taken place and ‘No’ showcase that rockburst has not taken place.

From the above table, the statics detail of dataset -1 can be seen, which is applied in empirical formulation to determine the accuracy of the method by comparing the result with dataset -1 and the Result derived from the empirical formulation. Fig. 1 shows the result of dataset-1, where 76% of dataset results are shown as rockburst occurred and 24% with no rockburst occurrence.

The second Data set contains an additional set of information compared to data set –1, such as Type of rock, Stress coefficient, Brittleness coefficient B1, Brittleness coefficient B2, and D_m . These data types have been used in several studies for long term rockburst predictions. The output column of dataset –2 has been simplified

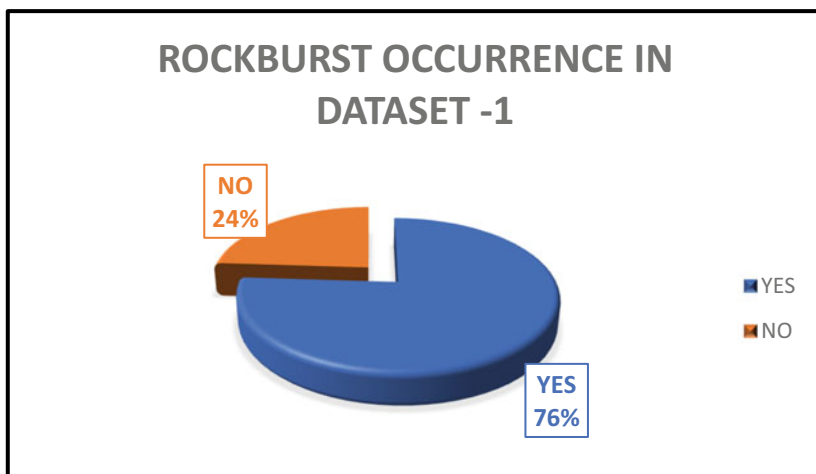


Fig. 1 Rockburst result in dataset-1

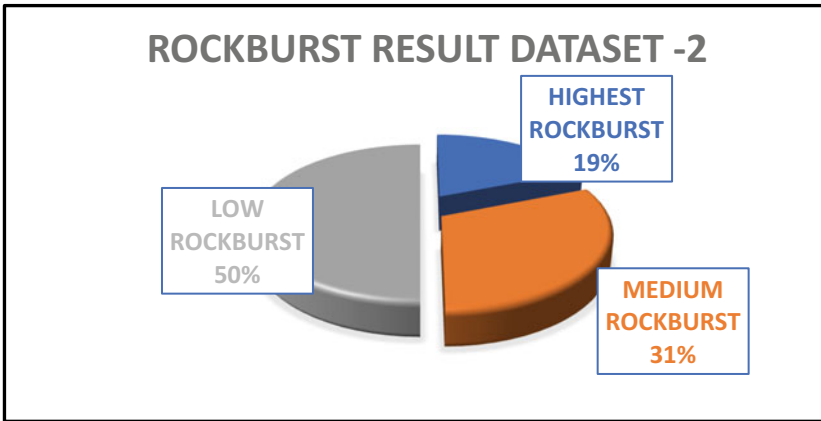


Fig. 2 Dataset –2 rockburst result piechart

into three types, such as Low Rockburst which define the rockburst intensity with very low to No rockburst, Medium Rockburst which has an intensity that partially or severely impacts the zone where the rockburst occurred, and Finally High Rockburst, which create more damages in rockburst zone.

In Fig. 2 it can be observed that rockburst results have been in order where Low rockburst contributes more data, followed up with medium rockburst with 31% and High rockburst with very little data of 19%.

Where dataset –2 will be divided into two parts before applying to supervised machine learning language, one for the training set and another set will be for evaluating the accuracy of supervised machine learning. Mostly, the Training set will be with more data set nearly 70% and evaluating set will be having near 30% of the data set. These training and testing sets are chosen in random order while dividing them.

5.2 Empirical Method

In this method Dataset -1 is used under three empirical criteria, each criterion has been classified into four groups such as ‘High, medium, Low and None’ Rockburst. But in this dataset -1 result column have classified into ‘Yes and No’ Rockburst which makes it difficult to compare the result and value the accuracy of the Empirical method according to the actual result, so to compensate for it high, medium and low from the empirical method can be taken equal to ‘Yes Rockburst’ in Dataset -1 and ‘None rockburst’ from empirical criterion will be taken equal to ‘No rockburst’ in dataset -1.

The three empirical criteria are Hoek criterions 1980, Rock brittleness criteria and finally using Elastic energy index criteria.

Empirical method	Equation	Classification criteria			
		None rockburst	Light rockburst	Moderate rockburst	Strong rockburst
Hoek criterion (1980)	$\sigma\theta/\sigma_c$	>0.5	0.34–0.42	0.42–0.56	<0.7
Brittleness criterion	σ_c/σ_t	<10	10 to 14	14 to 18	>18
Elastic energy index	EI	<2	2–3.5	3.5–5	>5

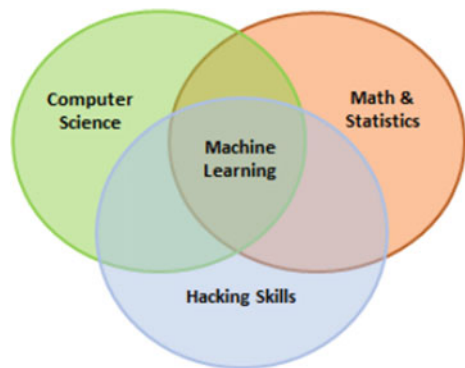
5.3 Supervised Machine Learning Model Building

Machine learning is the division of computer science that uses past experience to learn from information to make future decisions. Machine learning is at the connection of computer science, engineering, and statistics. The aim of machine learning is to generalize a detectable pattern (Fig. 3).

5.3.1 Steps Involved in Machine Learning Model:

1. Data Importing
2. Data preparation
3. Feature Engineering
4. Train algorithm and validation
5. Test algorithm and validation
6. Model building
7. Prediction
8. Deployment

Fig. 3 ML connection



1. Data Importing

The prerequisite for doing data-related operations in python is data cleaning, data exploration, and data visualization to perform all these activities, the data need to be imported into python. Python can support all kinds of files such as (.csv,.xlsl,.tsv,.html,.json, etc.).

2. Data Preparation

Data should be arranged in the way of a machine learning algorithm, while preparing the data it needs to be checked whether the data consists of an outlier, missing values, data format etc. This is to be done to achieve good accuracy for a model, to reduce this kind of issue we need to perform so machine learning treatment. Such as missing value treatment is performed to mutate the missing value and for outlier treatment, we need to mutate the mean and median.

3. Feature Engineering

Feature engineering is the most important division in machine learning. A detailed explanation of their sub-Division are presented.

Step -1: Imputation

Missing values is the major problem faced when data are prepared for modelling. One of the major reasons for missing values is human error, disruptions in the data flow, confidentiality concerns, etc. Effective problems done on machine learning models are due to missing values. Some of the operations which can be performed are:

Numerical Imputation: Numerical Imputations are generalized central tendency (Mean, Median) values to the appropriate feature to prevent the loss of data.

Categorical Imputation: For Categorical Features, the missing values can be replaced with a central tendency measure called Mode, which is a repetitive occurrence of the same instance throughout the feature.

Random Sample Imputation: This method is used to remove the missing value in the data (Figs. 4 and 5).

Imputing done at $\text{mean} + 3 * \text{std}$

Step -2: Handling Outliers

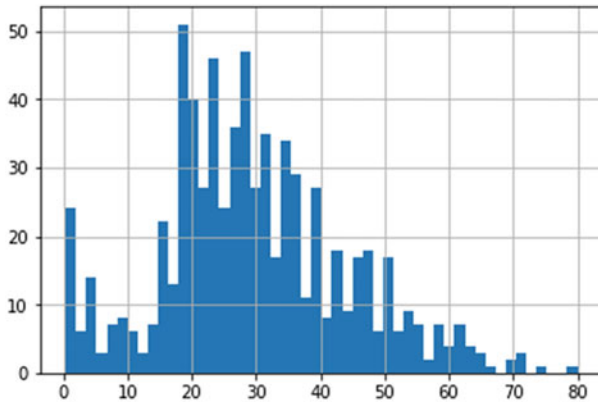
Outliers Through Standard Deviation

A value higher than the average, the instance (x) multiplied by standard deviation, will be considered an outlier.

Outliers Through Percentile

Percentiles are a range of data, which is an amount of data ranging from 0 to 100, the breakup criteria to access such information without the need of units assigned to data like dollars in our case. The top 5% is not the values between 96 and 100. Top 5% means values that are out of the 95th percentile of data (Fig. 6).

Out[48]: <matplotlib.axes._subplots.AxesSubplot at 0x28618d75f28>



```
In [53]: extreme=df.Age.mean()+3*df.Age.std()
```

Fig. 4 Machine learning Imputing Sample

Which Machine Learning Models Are Sensitive To Outliers?

- 1. Naive Bayes Classifier--- Not Sensitive To Outliers
- 2. SVM----- Not Sensitive To Outliers
- 3. Linear Regression----- Sensitive To Outliers
- 4. Logistic Regression----- Sensitive To Outliers
- 5. Decision Tree Regressor or Classifier---- Not Sensitive
- 6. Ensemble(RF,XGboost,GB)----- Not Sensitive
- 7. KNN----- Not Sensitive
- 8. Kmeans----- Sensitive
- 9. Hierarchical----- Sensitive
- 10. PCA----- Sensitive
- 11. Neural Networks----- Sensitive

Fig. 5 Sensitive Machine learning Outliers

Step -3: Binning

Binning is applicable for both numerical and categorical Features. The main purpose of binning is to make the model prevent itself from overfitting and more robust.it is more important in the performance of the model. When data is dropped by considering some outlier and missing value, data become more regularized when data is lost (Fig. 7).

Step -4: Log Transform

Log transformation is used in scientific transformations for feature engineering.

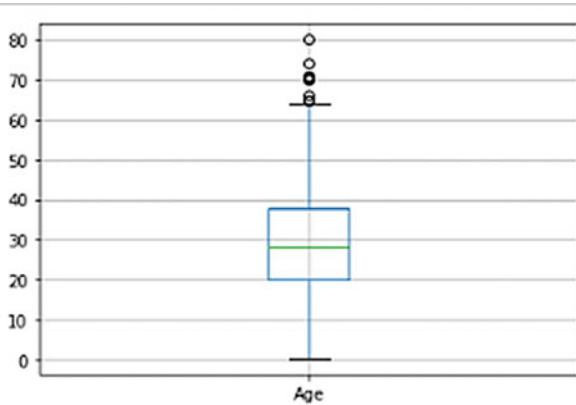


Fig. 6 Identifying outliers through a boxplot

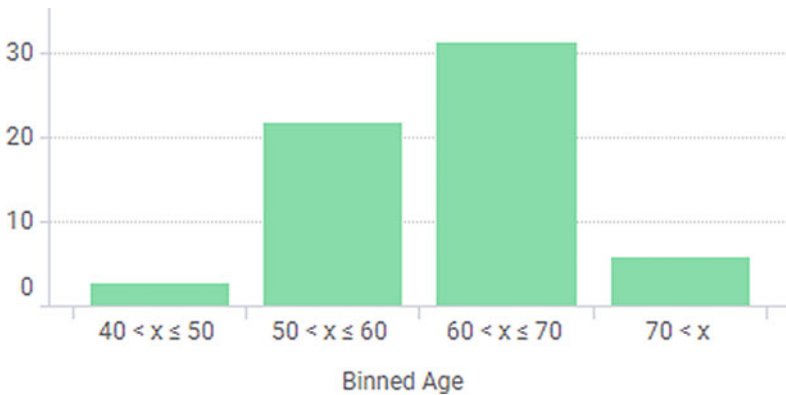


Fig. 7 Binning method

Handling Skewed data, the distribution becomes normal (devoid of outliers).

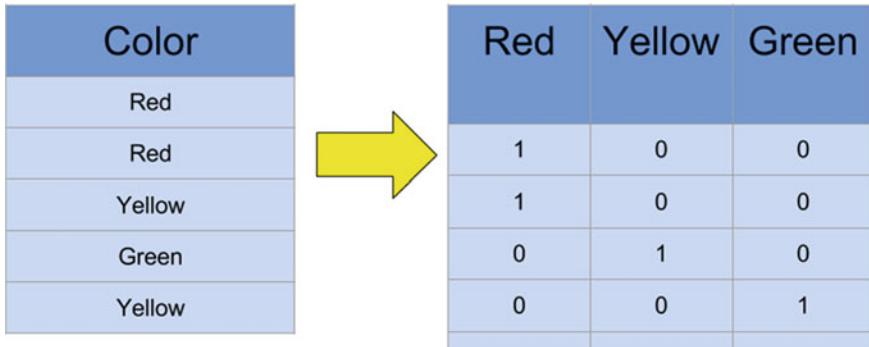
Decreased effect of outliers caused due to normalization of differences, also the model becomes more robust.

The value applied to log transformation must be positive, else will return an error.

Step -5: One-Hot Encoding

One-Hot Encoding is a feature encoding technique by instance wise, will convert each instance of a categorical column into multiple columns and assign 0 and 1. This binary represents the relationship between grouped and encoded features.

This technique allows for converting features into useful information instead of dropping it and losing information (Fig. 8).



Color
Red
Red
Yellow
Green
Yellow

Red	Yellow	Green
1	0	0
1	0	0
0	1	0
0	0	1

Fig. 8 One hot encoding methodology

Step -6: Grouping Method

a. Categorical Grouping

Performed by using a basic pivot table or grouping based on aggregate functions using lambda.

b. Numerical Grouping

Central Tendency is enough to function well in most cases.

Step -7: Scaling

The numerical features in the dataset do not have a certain range and they may differ from each other. For a dataset such as symmetric, scaling is required.

Normalization

Normalization applies an extreme scaling technique which makes the value fixed between only 1 and 0. Normalization does not affect the feature distribution of data and the standard deviation is also effectively reduced resulting in increased outliers. It is highly suggested that outliers should be taken care of before the process of Normalization.

Standardization

Standardization maintains equality among the standards in instances while taking into account standard deviation. For different standard deviations, results with slightly deviated range. Standardization was implemented majorly for the reduction of outliers (Figs. 9 and 10).

Standardizations are necessary to avoid skewness and increase scalability.

5. Train Algorithm and Validation

After Cleaning and feature engineering the dataset is divided into two parts. Training set and Testing set. The machine learning algorithm will train on the training set and

Fig. 9 Normalization formula

$$x_{i,j}^* = \frac{x_{i,j} - x_j^{min}}{x_j^{max} - x_j^{min}}$$

Fig. 10 Standardization formulae

$$z = \frac{x_i - \mu}{\sigma}$$

predict the new data instance with the help of validated results obtained from the testing set. Applicable hyperparameters are used to achieve peak model performance.

6. Test Algorithm and Validation

When a model has shown enough performance on train data, its performance will be checked against the unseen data. If the model still performs well, then the next step needs to proceed.

7. Model Building

Model Building is essential to make sure the algorithms understand every aspect of data before making the prediction. Models can be tuned, which is up to the output of our choice.

8. Prediction

Predictions are nothing but an outcome made out of the model building to compare the predicted result with the result in hand (test data), and then compare the model performance.

9. Automation

When the dataset is static and the desired output is achieved through our model preference then proceed with automation and rely on it to predict the new data based on historical predictions made.

5.3.2 Building Machine Learning Algorithm

In, this modelling rockburst data set -2 has been used which contains 230 data samples. Moreover, there are several algorithm methods to achieve this prediction model, but they are applied based on the combination of the attributes that suit and widely used algorithm to achieve the model.

Machine Learning Algorithms Used: -

1. Extra-Tree Classifier
2. Random-Forest Classifier
3. XGBoost Classifier
4. K-Neighbours Classifier
5. Decision Tree Classifier

6 Results of Empirical Method and Supervised ml

6.1 Empirical Results

The Below table shows the prediction part of the rockburst based on the Hoek criterion, Brittleness criterion and Elastic energy index, these results have been compared with the Actual result in dataset -1 one to provide the accuracy of the empirical method. From, the prediction of the rockburst it is clearly demonstrated that “HOEK CRITERION” give more accuracy in the prediction of rockburst compared to other methods (Tables 2 and 3).

6.2 Supervised Machine Learning Result

Data processing plays a major role in determining the results. So for data pre-processing, a Label Encoder from the sklearn metrics package, available in python has been used. The response variable is now labelled encoded for machine learning algorithms. Also dropping the unused columns in machine learning. Few of the columns from the dataset are dropped due to unwanted bias created during the time of modelling.

Only variables showing variance in predicting the response variable are chosen through repetitive feature engineering techniques such as Variable importance, Recursive Feature Elimination and Correlation among independent to dependent variables. Also, manual trial and error methods are used. The following columns are dropped through the final decision made by **Rock, B1, B2, and SCF**.

Before applying machine learning techniques the data sets need to be split into training and testing and the data types of each feature need to be checked. **Train Test Splitting** is essential in any machine learning technique to understand how well the model would behave on unseen data. The conventional ratio is **67% (Train) to 33% (Test)**, since training a model requires more data and testing is for our reference purposes to see if any changes need to be done for modelling.

Table 2 Analysis of empirical method

Empirical rockburst analysis data set -1								
NO	MTS (MPa)	UCS (MPa)	UTS (MPa)	EEI	Actual rockburst result	Hoek criterion (1980)	Brittleness criterion	Elastic energy index
1	89.56	190.3	17.13	3.97	Yes	Yes	Yes	Yes
2	89.56	170.28	12.07	5.76	Yes	Yes	Yes	Yes
3	89.56	187.17	19.17	7.27	Yes	Yes	No	Yes
4	56.1	131.99	9.44	7.44	Yes	Yes	Yes	Yes
5	54.2	133.99	9.09	7.08	Yes	Yes	Yes	Yes
6	70.3	128.52	8.73	6.43	Yes	Yes	Yes	Yes
7	48.75	180	8.3	5	Yes	No	Yes	Yes
8	62.5	175	7.25	5	Yes	Yes	Yes	Yes
9	75	180	8.3	5	Yes	Yes	Yes	Yes
10	57	180	8.3	5	Yes	Yes	Yes	Yes
11	89	236	8.3	5	Yes	Yes	Yes	Yes
12	50	130	6	5	Yes	Yes	Yes	Yes
13	108	140	8	5.5	Yes	Yes	Yes	Yes
14	18.8	178	5.7	7.4	No	No	Yes	Yes
15	11	115	5	5.7	No	No	Yes	Yes
16	55.4	176	7.3	9.3	Yes	Yes	Yes	Yes
17	30.9	82.56	6.5	3.2	Yes	Yes	Yes	Yes
18	89	128.6	13.2	4.9	Yes	Yes	No	Yes
19	12.3	237.1	17.66	6.9	No	No	Yes	Yes
20	55.6	256.5	18.9	9.1	Yes	No	Yes	Yes
21	91.3	225.6	17.2	7.3	Yes	Yes	Yes	Yes
22	61	171.5	22.6	7.5	Yes	Yes	No	Yes
23	34.15	54.2	12.1	3.17	Yes	Yes	No	Yes
24	108.4	138.4	7.7	1.9	Yes	Yes	Yes	No
25	69.8	198	22.4	4.68	Yes	Yes	No	Yes
26	105	171.3	22.6	7.27	Yes	Yes	No	Yes
27	105	237.16	17.66	6.38	Yes	Yes	Yes	Yes
28	105	304.21	20.9	10.57	Yes	Yes	Yes	Yes
29	25.49	54.2	2.49	3.17	Yes	Yes	Yes	Yes
30	72.07	147.09	10.98	6.53	Yes	Yes	Yes	Yes
31	21.8	160	5.2	2.22	No	No	Yes	Yes
32	20.9	160	5.2	2.22	No	No	Yes	Yes
33	12.1	160	5.2	2.22	No	No	Yes	Yes
34	75	170	11.3	9	Yes	Yes	Yes	Yes

(continued)

Table 2 (continued)

Empirical rockburst analysis data set -1								
NO	MTS (MPa)	UCS (MPa)	UTS (MPa)	EEI	Actual rockburst result	Hoek criterion (1980)	Brittleness criterion	Elastic energy index
35	43.4	123	6	5	Yes	Yes	Yes	Yes
36	62.6	165	9.4	9	Yes	Yes	Yes	Yes
37	30	88.7	3.7	6.6	Yes	Yes	Yes	Yes
38	105	128.61	13	5.76	Yes	Yes	No	Yes
39	105	304	9.12	5.76	Yes	Yes	Yes	Yes
40	105	306.58	13.9	6.38	Yes	Yes	Yes	Yes
41	7.5	52	3.7	1.3	No	No	Yes	No
42	24.93	99.7	4.8	3.8	No	No	Yes	Yes
43	14.96	99.7	4.8	3.8	No	No	Yes	Yes
44	34	150	5.4	7.8	No	No	Yes	Yes
45	60.7	111.5	7.86	6.16	Yes	Yes	Yes	Yes
46	54.2	134	9.09	7.08	Yes	Yes	Yes	Yes
47	70.3	129	8.73	6.43	Yes	Yes	Yes	Yes
48	35	133.4	9.3	2.9	Yes	No	Yes	Yes
49	38.2	53	3.9	1.6	NO	Yes	Yes	No
50	11.3	90	4.8	3.6	NO	No	Yes	Yes

Table 3 Accuracy of empirical method

Rockburst criterion	Rockburst prediction accuracy (%)
Hoek criterion	92
Brittleness criterion	68
Elastic energy index	78

Before admitting the data to train test split operation, a separate predictor and predicting variables need to be performed. Also, notice that a hyperparameter “Stratify” which makes sure that all the labels in the response variable in train and test sets are of equal proportion.

The Extra-Trees rule builds an Associate in a Nursing ensemble of an unpruned decision or regression trees per the classical top-down procedure. It’s a pair of main variations with totally different tree-based ensemble units of measurement that splits nodes by choosing cut-points completely indiscriminately which uses the entire learning sample (rather than a bootstrap replica) to grow the trees.

As such, their unit of measurement is three main hyperparameters to tune up the algorithm; they are the number of decision trees at intervals of the ensemble, the number of input choices to each approach selected and have confidence for each

split purpose, and conjointly the minimum vary of samples required throughout a node to form a replacement split purpose.

First performed, also provided with the highest accuracy out of all the other models is **Extra-Tree Classifier**. The test achieved an **accuracy of 96%** with an overall **precision of 96%**. Notice that **max_depth**, a hyper-parameter that explains the depth of each tree built inside the classifier, each unit describes each split.

Another ensembling technique achieved the desired accuracy. Random Forest Classifier, from **sklearn.metrics** package in python. The test achieved accuracy for this classifier is **92%** with an overall average **precision of 92%**.

Neighbour's Classifier and classical classification techniques are based on Euclidean distance between each data point. The test achieved an **accuracy is 84%** with an overall average **precision of 83%**.

Decision Tree Classifier and single tree built based on recursive binary splitting of each class in accordance with independent variables. The test achieved an **accuracy of 75%** with an overall average **precision of 72%**.

XG Boost classifier is a sequential tree building assembling supervised machine learning technique. The model in supervised learning generally refers to the mathematical structure in that the prediction is created from the input a customary example could also be a linear model, where the prediction is given as a linear combination of weighted input choices.

The prediction value can have fully completely different interpretations, betting on the task, i.e., regression or classification.

As an example, it is logistically transformed to urge the chance of positive class in logistic regression will even be used as a ranking score to rank the outputs.

XGBoost or eXtreme Gradient Boosting is a sequential ensemble technique unlike random forest (which builds trees parallel) the trees are built one after the other to learn from the weak learners.

The achieved accuracy on this model stands next to the extra tree classifier with an outstanding **accuracy of 95%** with an overall average **precision of 95%**.

7 Conclusions

The Empirical Method and Five supervised algorithms have been analyzed. These two sets of data are used separately whereas Data set -1 is used for the empirical method and data set -2 is used for machine language.

In this supervised algorithm, 6 attributes have been used to predict the rockburst results. Then, the final comparing the result shows that machine learning has much higher accuracy compared to the empirical method. most of the algorithms used in this study have reached an average accuracy of 88% which is very higher compared to the similar studies done by different researchers (Table 4).

Table 4 Result comparison

Empirical method prediction		Supervised machine learning method prediction	
Empirical method	Accuracy (%)	Python algorithm	Accuracy (%)
Hoek criterion	92	Extra – tree classifier	96
Brittleness criterion	68	XGB	95
Elastic energy index	78	Random forest	92
		KNN	84
		Decision tree	75
Average accuracy = 79.33		Average accuracy = 88.40	

References

1. Brady BHG, Brown ET (2004) Energy, mine stability, mine seismicity and rockbursts. Rock Mechanics for underground mining. Springer Netherlands, Dordrecht, pp 271–311
2. Dong L, Wesseloo J, Potvin Y, Li X (2016) Discrimination of mine seismic events and blasts using the fisher classifier, naive Bayesian classifier and logistic regression. Rock Mech Rock Eng 49(1):183–211
3. Hudson J (2009) Predicting Rockburst occurrence and development of Rockburst vulnerability index (RVI). In: The international consultation report for the key technology of safe and rapid construction for Jinping II hydropower station high overburden and long tunnels, 2 March 2009. Chinese Society for Rock Mechanics and Engineering, Jinping, pp 29–35
4. Kaiser PK (2009) Failure mechanisms and rock Support aspects. In: The international consultation report for the key technology of safe and rapid construction for Jinping II hydropower station high overburden and long tunnels, 31 March 0229. Chinese Society for Rock Mechanics and Engineering, Jinping, pp 62–71
5. Kaiser PK, Diederichs MS, Martin CD Sharp J, Steiner W (2000) Underground works in hard rock tunneling and mining. In: Geo eng proceedings of the international conference on geotechnical & geological engineering Melbourne. Technomic Publishing Company, You launched, pp 841–926
6. Sousa LR (1987) The Structural Project in Underground Works. National Laboratory of Civil Engineering, Lisbon
7. Spalding J (1983) Theory and practice of ground control. Trans Inst Min Met (Lon) 47
8. Teisseyre R (1980) Earthquake premonitory sequence - dislocation processes and fracturing. Boll Geoff Teer Appl 88:245–254
9. Zhao Z, Gross L (2017) Using supervised machine learning to distinguish microseismic from noise events. In: SEG technical program expanded abstracts 2017. Society of Exploration Geophysicists, pp 2918–2923
10. Zhou J, Li X, Shi X (2012) Long-term prediction model of rockburst in underground openings using heuristic algorithms and support vector machines. Saf Sci 50(4):629–644

Challenge to Explain the Upward Surface Movement Above Abandoned Coal Mines



André Vervoort 

Abstract After the closure of several coal fields in Europe at the end of the twentieth century, a new phenomenon in the field of strata or ground control was observed above abandoned underground coal mines, i.e., the upward movement or uplift of the surface. A detailed analysis of Interferometry with Synthetic Aperture Radar data showed the complexity of this phenomenon. So far, it was a challenge to try to explain and understand this phenomenon. One should be aware that surface subsidence above the total extraction method of longwall mining already is one of the most complex rock mechanical problems. However, this type of downward surface movement is nowadays relatively well understood. On the other hand, the phenomenon of uplift has only been observed during the last decades and it is even more complex than surface subsidence, as the impact of the flooding of the underground infrastructure and rock mass plays a role too. By a systematic analysis of all relevant parameters, a framework has been established, allowing the calculation of the uplift above abandoned coal mines. It has been shown that not only the expansion of the softer parts, i.e., the collapsed or goaf material, is important, but the change in pore pressure in the non-collapsed strata layers must be integrated too into the model. The framework developed results in a good correlation between measured and calculated data along linear transects.

Keywords Longwall · Ground control · Surface movement · Uplift · Modelling

1 Introduction

After the closure of several coal fields in Europe at the end of the twentieth century, a new phenomenon in the field of strata or ground control was observed above abandoned underground coal mines, i.e., the upward movement or uplift of the surface [1–8]. However, this phenomenon is not limited to Europe [9]. Past research clearly linked the phenomenon of uplift with the flooding of the underground infrastructure

A. Vervoort (✉)
KU Leuven, 3001 Leuven, Belgium
e-mail: andre.vervoort@kuleuven.be

© The Author(s), under exclusive license to Springer Nature Singapore Pte Ltd. 2022
A. K. Verma et al. (eds.), *Proceedings of Geotechnical Challenges in Mining, Tunneling and Underground Infrastructures*, Lecture Notes in Civil Engineering 228,
https://doi.org/10.1007/978-981-16-9770-8_8

155

after mine closure [4–7]. In comparison to the total amount of subsidence, initiated by the total extraction method of longwall mining, the total amount of uplift is approximately an order of magnitude smaller [10]. The uplift is not a simple rebound of past subsidence [2, 11]. Since its behavior also varies as a function of time, the phenomenon becomes even more complex to understand.

The Belgian Campine coal district is well suited to study this complex phenomenon and to try to understand the various mechanisms involved. The mined zone in this district is approximately a narrow band with a width of 5 to 10 km (north–south) and a total length of about 60 km (east–west). Hence, a two-dimensional approach can be applied, which simplifies the analysis. As the strata are dipping to the N – NNE, north–south transects are considered. The largest variation in uplift occurs along these north–south directions. Below a particular location, up to 10 or more different seams were mined over a period of several decades. The depth interval of mining is several hundred meters, starting from depths between –400 to –600 m. Immediately after the coal extraction, it is generally accepted that the amount of subsidence is linked to the total mining height in the vicinity of a particular location. For the uplift, this is not the case [2, 3, 11]. Of course, the uplift occurs above the mined area and in the immediate vicinity, but there is no one-on-one relation between the total amount of uplift and the total mining height. Most north–south transects are characterized by an inverse trough shape, but not completely symmetric.

2 Measurements of Uplift Based on Radar Interferometry Data

In Fig. 1, data acquired by radar interferometry or Interferometry with Synthetic Aperture Radar (InSAR) are presented for a north–south transect. The times series of the European C-band ERS1/2 and of the ENVISAT-ASAR satellites were used. Data were acquired for research through a European Space Agency (ESA) research proposal [1]. They cover the period from August 1992 through December 2000, and the period from December 2003 through October 2010, respectively. To illustrate the variation of uplift as a function of time, 3 different time periods are presented in Fig. 1.

The first time period (Fig. 1a) is only 2.5 years long and covers the beginning of the uplift phenomenon. The coal mine was abandoned in 1988, followed by a short period of residual subsidence. The second and third time periods are 5 years long (Fig. 1b and 1c). They both are situated at the end of each time series. On the various graphs, the limits of the mined zone within this north–south transect are indicated by blue dotted lines, respectively at a north–south distance of 0.0 and 5.25 km. The data acquisition selects automatically reflecting surfaces of 4 on 20 m, which can be followed over the entire time series, and which are characterized by trustworthy variations over time. In other words, reflectors undergoing unrealistic jumps are eliminated. Most of the selected reflecting surfaces represents roofs of houses and

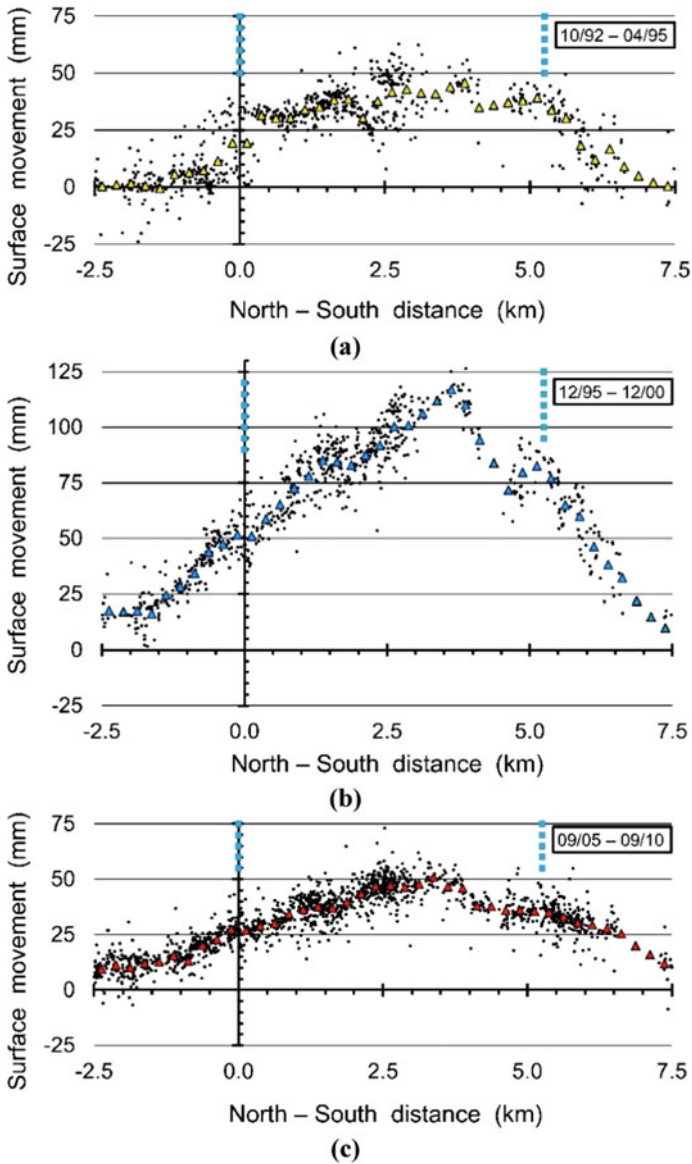


Fig. 1 Surface movements recorded by radar interferometry along a north-south transect during three different time periods: **a** 2.5-year period from October 1992 through April 1995; **b** 5-year period from December 1995 through December 2000; **c** 5-year period from September 2005 through September 2010. Individual reflectors are presented by black dots and averages over 250 m intervals are presented by colored triangles. Limits of the mined zone are indicated by blue dotted lines

buildings. In comparison to conventional levelling campaigns, the selected reflectors are not necessary along straight lines. Along a main road, bordered by houses or other buildings, one could observe variations along lines, but such roads are not necessarily orientated north–south. This means that if one wants to present data along a north–south transect (or, along any other direction), it is advisable to take all reflectors within a band width. For the data of Fig. 1, a width of 750 m is chosen. As mentioned above, the variation north–south is much larger in the Campine coal basin than the variation east–west. However, this east–west variation explains partly the spread of all the data points for a particular north–south distance. Other parameters that play a role are the different behavior of roads vs. buildings as reflecting surfaces, the type of building and its foundation, and the overall accuracy of the method. The accuracy of the average rate of movement over a long time period is normally assumed to be about 1 mm a year. A variation of ± 20 mm at a particular north–south distance of all reflectors within an east–west band width of 750 m is typical for the satellite data selected in the Campine coal basin. In addition to the individual data points, an average is estimated for 250 m long (north–south) intervals. In Fig. 1, these averages are presented by triangles.

For the sets of individual data points and of the averages, the following is observed:

- The uplift is from October 1992 onwards clearly visible above the mined zone.
- However, uplift also is observed in the proximity of the mined zone. The extent of the uplift seems to be larger to the north of the mined zone than to the south. There could be a link with the dip of the strata to the north. Both to the north and to the south, the extent of uplift is smallest during the first selected time period of 2.5 years.
- The average rate of movement varies over the three time periods selected. The maximum average rates per time period are 18.3, 23.4 and 10.2 mm/year, respectively. In other words, the rate is significantly smaller about two decades after mine closure.
- Overall, the shape corresponds to an inverse trough, but it is not symmetrical around the middle of the mined zone, i.e., 2.625 km. For the second time period selected, a very distinct maximum is observed at a north–south distance equal to 3.625 km. The other two time periods show plateaus of large average values with a length of 1 to 2 km.
- Above the mined zone, there could be a local minimum around 4.5 km. This is most clearly observed in the second time period selected (Fig. 1b).

These observations are typical for the Campine coal basin, although each transect is different.

3 Framework Helping to Understand and Calculate Uplift

Several researchers have attempted to model uplift [a.o., 12, 13]. This is done with varying degrees of success. It is always difficult to comment on other case studies

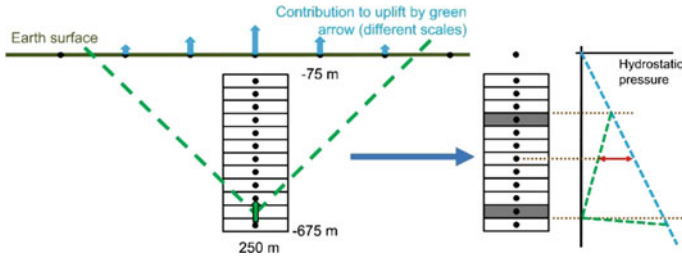


Fig. 2 Illustration of the principles for the proposed framework to model uplift above abandoned coal mines

since one does not know all details of them. Some of the approaches focus on the depletion of aquifers during mining and their recovery after closure, which certainly is a realistic scenario in some cases. Others focus on the mechanical expansion of the goaf material only when flooded. When studying subsidence, the focus is indeed on the collapse of the roof above longwall panels and the compaction afterwards of this goaf material. Subsidence is analyzed as a mechanical stress-deformation driven process. For a complex geometry of multi-seam mining, as observed in the Campine coal basin, the expansion of the goaf material only or the expansion of the soft material in the aquifers does not provide a good correlation between calculated uplift values and observed values (see further). The two main criteria to evaluate the soundness of the framework proposed will be (i) the order of magnitude of the uplift values and (ii) the shape of the uplift curve along north–south transects.

The proposed framework is an analytical approach, whereby the entire 2D north–south section is divided in elements with a height of 50 m and a north–south length of 250 m. In Fig. 2, an example is presented for one column of elements. In this case, the latter covers the depths between -75 and -675 m. Each element expands when the pore pressure is increased (see further). This expansion is assumed to take place at the center of each element (green arrow in Fig. 2, for the element at a central depth of -600 m). A transfer function based on the Boussinesq formula for a line load [14] is applied to translate the expansion of an underground element on the movement of the earth surface (see blue arrows). Here, an angle of influence of 45° is presented. The vertical stiffness of each element takes the real composition of each element into account, i.e., the thickness of the goaf volume of each longwall panel in an element and the thickness of the other non-collapsed strata within the element height of 50 m. By an increase in fluid pressure and considering the average vertical stiffness, the expansion of each element is estimated. The basic elastic equations are used that consider the impact of a change in effective stress on the vertical expansion [15]. For each node at the surface, the sum is made of the impact of all elements in the underground.

It is assumed that after the closure of the coal mine, the fluid or pore pressure evolves back to the original hydraulic gradient (see blue dotted line, right in Fig. 2). For the coal mine studied in this paper, the hydraulic gradient starts close to the surface. Due to the total extraction method by longwall mining, the entire coal strata

mass has drained. Based on measurements in other coal districts [16, 17], a variation as a function of depth is assumed, as explained for an example, whereby longwall panels have been mined in two elements, i.e., a first between -225 and -275 m, and a second between -575 and -625 m (These two elements are coloured grey in the graph at the right in Fig. 2). At the top of the first element, the original hydraulic gradient is already restored. The longwalls mined within the boundaries of this element have been mined a long time ago, and it is most likely that the entire area was sealed off. At the bottom of the second grey element (or in a more general situation, the deepest element with mining), the drainage is 100% and a fluid pressure of zero is assumed. Between the top and bottom elements with mining a linear decrease is applied (green dotted line). Below the bottom element with mining, it is assumed that the zone of influence corresponds to a height of 25 m. 25 m below the bottom element with mining the original hydraulic gradient has not changed during the mining phase. The total amount of fluid pressure increase after closure (red arrow in Fig. 2) is the pressure between the original (and final) blue dotted line and the green dotted line at mine closure.

In Fig. 2, the principles are presented for a single column of elements. The entire model is a repetition of this for all columns within the mined zone. A systematic study of different north–south transects in the Campine coal basin showed the best results, if one takes the possible flow along the strata dip into account. This is translated in considering a 1 km long zone to the north and to the south of the mined area. Within these two extensions, there also is a drop in pore pressure due to mining.

4 Calculations of Uplift Values

In Fig. 3, results are presented based on the framework explained in previous paragraph and for a basic set of input parameters. When studying subsidence and the strata behavior in the Campine coal basin, a ratio of 1 on 4 or 1 on 5 was mostly used for the mining height vs. the goaf thickness. A ratio of 1 on 4 is applied in the model presented. An average vertical stiffness ratio of 1 on 10 was assumed for the goaf vs. the rest of the coal strata layers. A value of 0.25 was taken for the Poisson's ratio of all material. In absolute terms, vertical stiffnesses of the goaf and of the rest of the strata of 0.2 and 2.0 GPa, respectively, result in realistic uplift values. By changing the stiffness value and keeping the same ratio, the total uplift can be changed easily without changing the shape along a north–south transect.

As indicated above, two main criteria are used to evaluate if the proposed framework and model input values result in a good fit between the calculated uplift values and the measured data, presented in Fig. 1.

First, the calculated maximum uplift value should be of the same order than the measurements. The maximum calculated value is 530 mm, and it is reached at a north–south distance of 3.375 km. The latter distance is more to the north than the middle of the mined zone (at 2.625 km). This is similar to the measurements. Around

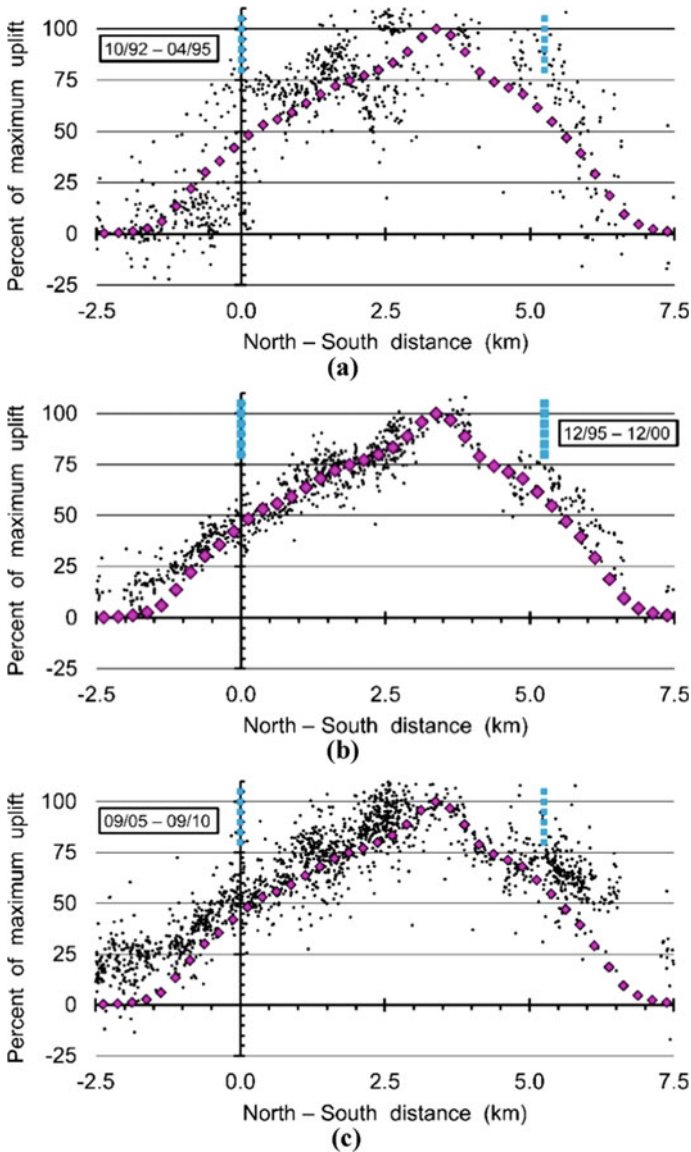


Fig. 3 Comparison between calculated uplift values (purple diamonds) and surface movements recorded by radar interferometry along a north-south transect (black dots). Both parameters are presented as a percentage of maximum uplift over 250-m intervals. Comparison is presented for three different time periods of observations: **a** 2.5-year period from October 1992 through April 1995; **b** 5-year period from December 1995 through December 2000; **c** 5-year period from September 2005 through September 2010

the maximum, individual uplift values of 300 to 450 mm were measured over a 20-year period. Since the upward movement is still taking place, more than 10 years after the last available measurement, the total uplift is not known yet. The latter is most likely to be about 1.5 times the measured value over 20 years (i.e., 1.5 times 300 to 450 mm, or 450 to 675 mm). These values are of the same order of magnitude than the calculated maximum value. By a small change in the absolute stiffness values, one can easily calibrate the calculated values to correspond to the measured value, once the latter would be known.

Second, the shape of the calculated values along the north–south transects should correspond well with the measured shapes. This is a much more difficult task than getting a good fit between the maximum measured and maximum calculated value. A correct comparison can only be done if the shapes are presented on a relative scale. In Fig. 3, the various graphs are presented as a percentage of the maximum value. For the calculated curve, this can be done easily, as the maximum calculated value is known, i.e., 530 mm at 3.375 km. For the three time periods presented in Fig. 1, the scaling is more difficult. In Fig. 3, the individual measurements are presented as a percentage of the maximum average value per period over the 250-m intervals. Therefore, some of the individual measurements presented correspond to values higher than 100%. Another difficulty encountered is that the three periods presented in Figs. 1 and 3 include the variation as a function of time of the uplift process, while the model so far only consider the complete recovery of the pore pressure and not how it evolves over time. The latter is still an unknown and some complex hydrogeological modelling is needed. However, without data to use for calibration it is a very difficult task. So, on the one hand, there is a single curve for the estimation and three slightly different shapes for the measurements.

A pure visual comparison indicates a good fit between the measured data and the calculated values. The best fit is probably for the time period in the middle, i.e., the 5-year period from December 1995 through December 2000 (Fig. 3b). Directly above the mined zone, there is nearly a perfect fit. Outside the mined zone, there is a small underestimation of the measured values. This could be further improved if one would assume that the zone of influence on the pore pressure by the mining is larger than 1 km to the north and to the south. However, a more detailed hydrogeological study should be first conducted to evaluate whether this is realistic or not. One should always be careful in just adapting the model to get a better result, if one has no data to support that decision. For the first time period, i.e., 2.5 years from October 1992 through April 1995, there is an underestimation of the measured data for nearly all positive distances (i.e., from the southern mining border to beyond the northern border). The scatter of the data points is also larger than for the second time period. The most likely explanation is that at the start of the uplift, the process of uplift is not fully active. This has been observed in other study areas of the Campine coal basin [3]. For the third time period, i.e., 5 years from September 2005 through September 2010, a small underestimation of the measured data is observed. This is probably linked to the spreading of the water flow outwards and the fact that the measured data are not showing a location with a clear maximum in the curve, in comparison to the model.

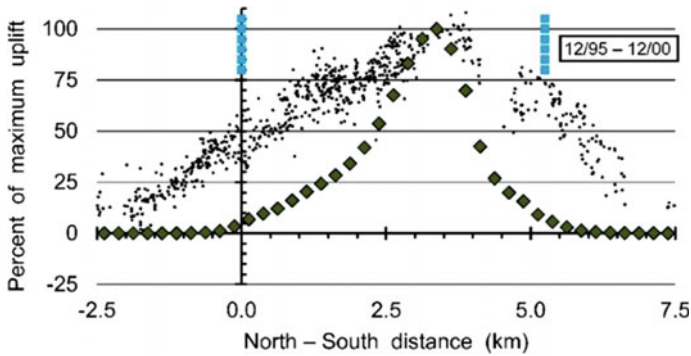


Fig. 4 Comparison between calculated uplift values (green diamonds), when considering the contribution of the goaf material only, and surface movements recorded by radar interferometry along a north-south transect (black dots; 5-year period from December 1995 through December 2000). Limits of the mined zone are indicated by blue dotted lines

The overall comparison between the measured and calculated values is more than satisfactory. Without doubt, the second time period is the most typical for the uplift phase. For this period a very good correlation is observed (Fig. 3b). This generates confidence in the framework presented in the previous paragraph.

Above, reference was made to attempts by other researchers to model uplift. Some of them focus clearly on the goaf volumes only and their expansion. If the same would be done for the case study of this paper, a curve is obtained, as presented in Fig. 4 (measurements correspond to second time period, Fig. 1b). Although the location of the maximum uplift is realistic, the rest of the shape is completely different. It results in a strong underestimation, both inside and outside the mined area. Changes in goaf stiffness or in goaf thickness do not change the shape of the calculated curve. Other researchers focus on the soft overburden and the depletion of aquifers within that zone. This could play a role in certain areas, but in the Campine coal basin it is not a significant factor. The impact of the expansion of one or more aquifers corresponds to approximately a constant uplift over the entire mined zone. Such a constant value would not improve the shape of the uplift curves, but it would make them more different from the basic inverse trough shapes observed. However, if a single seam is mined or the geometry of the mining is very regular, more simple models than presented in this paper could still provide a good correlation, even that not all processes are integrated in a model.

5 Conclusions

Although the phenomenon of uplift above abandoned and flooded underground coal mines is a very complex problem, a satisfactory framework has been established, allowing the calculation of the uplift. This framework helps also to understand the

process of uplift. From a geotechnical and hydrogeological point of view, it was a real challenge to establish this framework. This could only be done by a systematic analysis of all relevant and possible parameters, without imposing any prior assumptions. In this paper, the final result is only presented, but many scenarios were analyzed.

The two most crucial aspects that lead to a good correlation were: (i) the change in pore pressure, due to drainage, in the entire mined volume and in the surrounding rock mass must be considered, and (ii) not only the expansion of the goaf volume due to the fluid pressure being restored must be considered, but also the expansion of the rest of the strata layers, i.e., the non-collapsed strata layers. If both aspects are integrated in a model, satisfactory results are obtained, even for very complex mining geometries.

It could be seen as an anachronism that a pure analytical model is suggested and applied, when large computer power and many complex numerical modeling codes are available. However, a major advantage of an analytical model, even in combination with a rough discretization, is that one can analyze the impact of the various factors separately. This has greatly helped in understanding the process of uplift. Now, that the major aspects of the process of uplift are identified, a numerical model can be the next logical step to further improve the framework and the further understanding. As mentioned earlier, a better understanding of the water flow during the mining phase and after the closure of the mine is certainly a direction that has further to be explored. However, this task should not be underestimated, as natural faults and fractures, different strata with different permeability values, induced fractures, mine shafts and tunnels, etc. all play a role in the fluid flow. So far, it is assumed that the expansion or swelling of the rock is only due to a mechanical process. The physicochemical swelling capacity of the clay minerals is also part of the process of uplift. So far, the physicochemical swelling is assumed to be part of the mechanical expansion and is integrated in the calibration of the stiffness values.

In conclusion, although the proposed framework provides realistic uplift values and a good basic understanding of the uplift process, there should be no doubt that this framework is only an intermediate step in the challenge to establish a complete model of the uplift process.

References

1. Devleeschouwer X, Declercq PY, Flamion B, Brixko J, Timmermans A, Vanneste J (2008) Uplift revealed by radar interferometry around Liège (Belgium): A relation with rising mining groundwater. In: Proceedings of the symposium post mining, Nancy, France, pp 1–13
2. Vervoort A (2016) Surface movement above an underground coal longwall mine after closure. *Nat Hazards Earth Syst Sci* 16(9):2107–2121. <https://doi.org/10.5194/nhess-16-2107-2016>
3. Vervoort A, Declercq P-Y (2017) Surface movement above old coal longwalls after mine closure. *Int J Mining Sci Technol* 27(3):481–490. <https://doi.org/10.1016/j.ijmst.2017.03.007>
4. Samsonov S, d'Oreye N, Smets B (2013) Ground deformation associated with post-mining activity at the French–German border revealed by novel InSAR time series method. *Int J Appl Earth Obs Geoinf* 23:142–154. <https://doi.org/10.1016/j.jag.2012.12.008>

5. Baglikow V (2011) Damage-relevant effects of mine water recovery—conclusions from the Erkelenz hard coal district. *Markscheidewesen* 118(2):10–16
6. Bekendam RF, Pöttgens JJ (1995) Ground movements over the coal mines of southern Limburg, The Netherlands, and their relation to rising mine waters. In: Proceedings of the fifth international symposium on land subsidence, IAHS234, The Hague, The Netherlands, pp 3–12
7. Caro Cuenca M, Hooper AJ, Hanssen RF (2013) Surface deformation induced by water influx in the abandoned coal mines in Limburg. The Netherlands observed by satellite radar interferometry. *J Appl Geophys* 88:1–11. <https://doi.org/10.1016/j.jappgeo.2012.10.003>
8. Gee D, Bateson L, Sowter A, Grebby S, Novellino A, Cigna F, Marsh S, Banton C, Wyatt L (2017) Ground motion in areas of abandoned mining: application of the Intermittent SBAS (ISBAS) to the Northumberland and Durham Coalfield. UK. *Geosciences* 7(3):85. <https://doi.org/10.3390/geosciences7030085>
9. Yu Z, Huang G, Zhang C (2020) Monitoring and characterization of surface deformation after the closure of coal mines based on small baseline interferometric synthetic aperture radar. *Instrument Mesure Métrologie (IETA-J)* 19(2):141–150
10. Vervoort A (2021) Various phases in surface movements linked to deep coal longwall mining: from start-up till the period after closure. *Int J Coal Sci Technol* 8:412–426. <https://doi.org/10.1007/s40789-020-00325-0>
11. Vervoort A (2020) Long-term impact of coal mining on surface movement: residual subsidence versus uplift. *Mining Report Glückauf* 156(2):136–141
12. Herrero C, Muñoz A, Catalina JC, Hadj-Hassen F, Kuchenbecker R, Spreckels V, Juzwa J, Bennett S, Purvis M, Bigby D, Moore, D (2012) Prediction and monitoring of subsidence hazards above coal mines (Presidence). In: RFCS final report RFCR-CT-2007–00004, EUR 25057 EN, European Commission, Brussels, Belgium
13. Dudek M, Tajduś K, Misa R, Sroka A (2020) Predicting of land surface uplift caused by the flooding of underground coal mines – a case study. *Int J Rock Mech Mining Sci* 132: <https://doi.org/10.1016/j.ijrmms.2020.104377>
14. Fenner RT (1986) *Engineering elasticity, Application of numerical and analytical techniques*. Halsted Press, Chichester
15. Fjaer E, Holt RM, Raaen AM, Risnes R, Horsrud P (2008) *Petroleum related rock mechanics*, vol 53, 2nd edn. Elsevier Publishing Company, Amsterdam
16. David K, Timms WA, Barbour SL, Mitra R (2017) Tracking changes in the specific storage of overburden rock during longwall coal mining. *J Hydrol* 553:304–320. <https://doi.org/10.1016/j.jhydrol.2017.07.057>
17. Tammetta P (2013) Estimation of the height of complete groundwater drainage above mined longwall panels. *Groundwater (NGWA)* 51(5):723–734. (and comments by author on discussion, *Groundwater (NGWA)* 52(3):339–342)

Challenges in Drill Equipment Selection vis-à-vis Underground Excavations – A Methodology



B. N. V. Siva Prasad , V. M. S. R. Murthy , and Sripad R. Naik

Abstract Drilling forms an important component of a drill and blast cycle consuming a considerable time and resources of an excavation cycle and necessitates scientific selection and performance prediction. Drill penetration rate is influenced by many controllable and uncontrollable parameters such as intact rock, rock mass, bit, machine's design and operational parameters with varying degree of influence. Often, the predicted versus measured drilling rate has lot of variances thereby affecting drill economics, project time lines and feasibility. Wrong selection of drilling equipment can lead to an increase in development cycle time up to 30 to 40%. Therefore, in this study the challenges faced in selection of a right drill equipment and its associated influential factors are assessed. Selection methodology for a set of working ranges of underground drilling rigs is developed. Performance studies for mechanized drill jumbos operating in Indian and Bhutan underground hard rock environment are conducted. Performance studies for drill jumbos in underground hard rock mines over a period of one year indicated that the machine's availability is around 80% however its utilization is found to be only about 30% with 76% productivity on an average. The studies indicated that selection of drilling equipment affects tunnelling cycle greatly in civil excavations compared to mine development headings owing to larger scale and volume in former. However, there is a requirement of developing an all-inclusive drillability model which aids in selection of right drill equipment for obtaining a desired rate of drilling in a given geotechnical environment.

Keywords Rock drilling · Drill penetration rate · Equipment selection · Performance studies · Drill jumbo

B. N. V. S. Prasad (✉) · S. R. Naik
Numerical Modelling Department, National Institute of Rock Mechanics (NIRM),
Bengaluru 560070, India
e-mail: sivaprasadbnv@yahoo.in

V. M. S. R. Murthy
Department of Mining Engineering, Indian Institute of Technology (Indian School of Mines),
Dhanbad 826004, India

1 Introduction

Development of a nation requires uninterrupted supply of its available mineral resources and expansion of infrastructure [18, 25, 26]. Uneconomical stripping limits in surface or open pit mines, presence of higher-grade minerals at greater depths, scarcity of land for housing utilities, vehicular movements, growing population, requirement of undisturbed residential areas, need for urban development, placing water conducting systems and others necessitates planning of underground excavations. For a safe and economical mining scenario and a sustainable urban development, efficient underground space utilization becomes the need of the hour. The minerals existing worldwide are either being mined from surface or underground where drill and blast method is adopted for excavation in both soft and hard rock environment due to its ease of adaptability and efficiency. Underground or subsurface excavations in mining, tunnelling, caverns, civil engineering and infrastructure projects involve development of tunnels or underground space with openings of varied dimensions to cater the project’s requirements. Various types of underground excavations and their utility in various sectors are shown in Fig. 1.

Though blasting has been the most preferred means of rock removal/mineral exploitation, it is the most blamed activity since it creates environmental problems in the form of ground vibrations, air overpressure and flyrock [23]. Despite these problems, current underground mining scenario is inclining towards mechanized drilling and blasting (D&B) since it proves advantageous in many ways like controlled excavation profile, limited ground vibrations and better ground control, higher rates of advance, enhanced mine development rates besides maintaining a balance in overall economics of the project [18]. Proper adoption of D&B techniques can contribute significantly towards profitability and therefore optimization of these parameters is

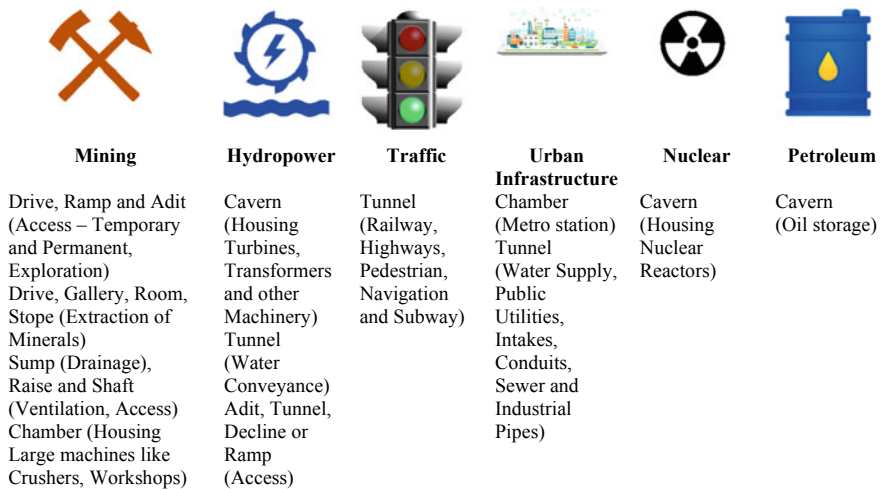


Fig. 1 Underground excavation in various sectors

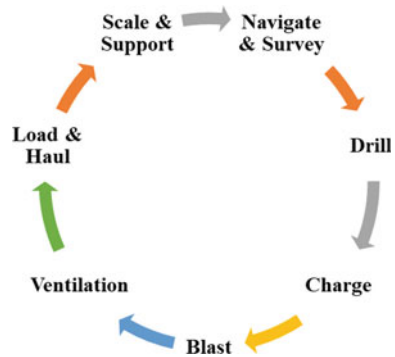
essential. This optimized parameter will be effective if a robust information model can be prepared based on the relevant practical data of the specific deposits [3] . Economics drive the selection of excavation methodology since a cost study of various aggregate quarries in Thailand indicated that D&B accounts for about 28% of total quarrying cost [4] which necessitates the review of existing drilling and blasting techniques.

Drilling is the foremost step in the drill and blast excavation cycle commonly measured by rock drillability or Drill Penetration Rate (DPR). Rock drillability or Drill Penetration Rate is defined as the rate of advancement of drill bit or the rock tool into the rock in a given time, measured in meter per minute, defining project’s progress and feasibility [24]. Rock drillability is influenced by various controllable and uncontrollable parameters altering the drill penetration rates to a great extent which includes the physico-mechanical properties [13]. Thus, selection of drill equipment for an encountered geo-environment becomes the most important parameter for deciding the progress of the project and its economic viability in totality. This paper aims to highlight the challenges faced in drill equipment selection and performance optimization.

2 Excavation Cycle

An underground excavation cycle comprises of various operations such as navigation and survey, drilling of blast holes, charging the drill holes with explosives, blasting and fragmentation, ventilation for removal of noxious gases from the blasted face, loading of blasted muck and hauling the same to the dumping point, scaling and supporting with rock reinforcement as shown in Fig. 2.

Fig. 2 Operations in an underground excavation cycle followed in mines and tunnels



3 Rock Drilling

Drilling is a process of cutting a cylindrical hole in the rock which can be useful for a variety of purposes such as charging and blasting, grouting, installation of rock reinforcement, drainage, oil and water wells, geothermal gradient studies and exploration. With the advancement of metallurgy post industrialization, there evolved different rock drilling systems as shown in Fig. 3. Though there exist several specialized drilling techniques, mechanical type of rock drilling is predominantly adopted in mining, civil, tunnelling, hydropower and infrastructure projects.

3.1 Limitations

Unlike engineered material, rock is discontinuous, inhomogeneous, anisotropic, and non-linearly elastic in nature which induces complexity when dealing with it [6]. Rock is an aggregate of minerals bound by the rock matrix with varied physico-mechanical properties and chemical composition. While the rock mass comprises of structural features or discontinuities like joints, folds, faults, foliations and fissures

Mechanical	<ul style="list-style-type: none"> • Percussion, Rotary, Rotary Percussion
Thermal	<ul style="list-style-type: none"> • Flame, Plasma, Hot Fluid, Freezing
Hydraulic	<ul style="list-style-type: none"> • Jet, Erosion, Cavitation
Sonic	<ul style="list-style-type: none"> • High Frequency Vibration
Chemical	<ul style="list-style-type: none"> • Microblast, Dissolution
Electrical	<ul style="list-style-type: none"> • Electric Arc, Magnetic Induction
Seismic	<ul style="list-style-type: none"> • Laser Ray
Nuclear	<ul style="list-style-type: none"> • Fusion, Fission

Fig. 3 Rock drilling techniques [10]

which introduces much more complexity in rock engineering. Drilling in rock is usually performed using an indenting tool with the help of a drilling machine that has parameters like percussion, feed, rotation, and flushing based on the method of drilling. Stress is built up under the indenting tool in bit-rock interaction process and the behaviour of rock under the impact generated stress, depends on the physico-mechanical properties of the rock and the method of drilling [14–16]. Broadly, the parameters influencing rock drillability can be classified into controllable (machine and operational) and uncontrollable parameters (rock mass, i.e., rock and discontinuities). Rock drill performance is usually measured by the advance rate of the drill bit or the penetration rate and the wear rate of rock tools [2, 17]. Rock mass parameters, RQD, lithology, joints dip, alteration, rock mass drillability index (RDi) and operational parameters were also used by researchers for performance prediction of excavation equipment in tunnel drives [1, 5, 7–9, 12, 20, 21]. A rock drillability characterization index (RDCi) was also proposed for DPR prediction [19].

High penetration rate at the face alone do not indicate a good drilling performance. Quite often the predicted penetration rate is affected by such uncontrollable parameters resulting in an unexpected rock drill performance. Owing to this, the project schedule is hampered and calls for precise prediction of drill penetration rate besides selection of appropriate drilling rig for a given geo-environment.

4 Drill Equipment Selection

A drill equipment is commonly used for making holes in the rock and by its size can be massive or light. A variety of drill equipment is available in market today providing a choice of features to meet the requirements of the project. The mine planners and the project schedulers own the responsibility to cautiously select the drill equipment since the development rates are dependent on the performance of this equipment besides having a direct financial implication on the project. Wrong selection of drilling equipment can lead to an increase in development cycle time up to 30 to 40% [11]. Therefore, in this study the challenges faced in selection of a right drill equipment and its associated influential factors were assessed.

4.1 *Components of a Drill Equipment*

A drill equipment primarily comprises of the following components [10]:

- Rockdrill or a drifter – In the process of rock drilling, the hammer or the rock drill generates the impact and/or rotation depending on the type of drilling method. The impact stress wave travels through the shank adaptor, coupler, drill rod and drill bit and is applied on to the rock being drilled.

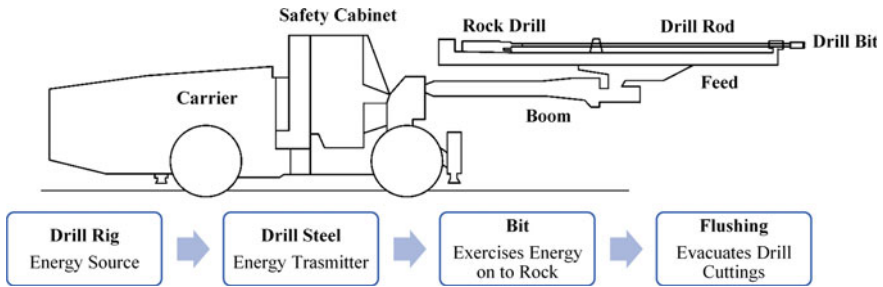


Fig. 4 Key components of a drilling rig

- Feed – Feed component of a drill rig ensures proper bit-rock contact for effective transfer of impact stress. Different types of advance systems in practice include use of airlegs, chain feed, screw feed, cable feed and hydraulic feed.
- Boom – For positioning the drill bit at the designed location.
- Translation system – For maneuvering the drill rig. It can either be towed or self-propelled with crawler, tire or a rail mount system.
- Energy Source – The energy source for maneuvering and drilling may be diesel, oil, electric or compressed air.
- Flushing arrangement – Drilling process generates detritus at the bottom of the drill hole which needs to be flushed out to generate fresh surface for drilling which otherwise shall result in regrinding the detritus and loss of energy. Flushing media currently being used are air, water or mist.
- Control system – It helps to control the drilling parameters and aids in collaring, anti-jamming, water monitoring, returning to start position after completion of drilling, control levels for operating percussion, rotation, feed and drill automation.

The key components of a drilling system are shown in Fig. 4.

4.2 Drilling Challenges and Developments

Depending on the location of drilling, the drill equipment can be used in surface or underground. Based on its utility, it can be either continuous such as development face drilling or occasional such as raise development. Depending on the investor's appreciation for the innovations in the field, the chosen equipment can house latest innovations or opt for a standard or proven technology. The safety, reliability and ease of use of the equipment is of paramount importance in today's "Safety first" industrial practices. Since rock drillability depends on controllable parameters such as machine and operational besides uncontrollable parameters such as rock and rock mass properties, there exists inherent complexity in prediction of drill penetration rates precisely. However, this section describes few of the things that needs to be

Project Conditions	Drilling Type	Rock Drill	Electrical System	Operator
Scale - Production and Development requirements	Rotary, Percussive, Down the Hole, Top Hammer	Type	Multi Voltage System	Safety cabinet
Complexity, Schedule	Power Source	Percussion power	Total Installed Power	Cab comfort
Excavation volume	Mechanical, Electrical, Hydraulic, Pneumatic	Impact Frequency	Air and Water Systems	Operation
Geology, Rock mass, Environment	Drilling Depth	Rotation speed and Torque	Flushing media - Air, water or mist	Working environment
Rock Properties – Hardness, Abrasiveness, Strength, Texture.	Shallow, Moderate, Large	Hole size	Booster pump – Power, Capacity	Ergonomics
Fragmentation size requirements	Diameter	Weight and Dimensions	Pressure – Inlet and Flushing	Exposure - Noise, Dust and Hazard
Compatibility with other equipment	Small, Medium, Large	Feed	Rock drill consumption – Oil, Air	Training & Skill
Costs - Ownership, operating and Maintenance	Drilling direction	Type, Force, Weight	Drill Accessories	Automation Features
Type of explosive products used	Horizontal, Vertical, Inclined, 360°	Lengths - Extension, Total, Hole and rod	Shank adaptor - Thread and Diameter	Measure while drilling
Utility	Equipment	Boom	Drill rod - Thread, diameter, length	Hole end correction
Surface, underground, deep water, outer space, geothermal, oil well	Number of holes to be drilled	Type, Number, weight	Drill bit - Thread, diameter, type, number of buttons, spherical, ballistic, semi ballistic or spike	Automatic boom movements
Operation Frequency	Total Drill length	Coverage, Extension	Drill accuracy	Auto navigation
Continuous, Occasional	Adaptability	Roll over angle	Drill deviations	Digital drilling
Features	Varied face dimensions (Cross sectional area)	Hydraulic System	Collaring, Alignment, Trajectory, Driller Inexperience	Auto feed drill plan system
Latest innovations, Standard / proven technology	Varied drill lengths and angles	Powerpack	Carrier	Performance Indicators
Mobility	Varied applications	Pumps - percussion, Feed, Rotation, Filtration	Type - Rail, crawler or wheel	Penetration Rate, Tool Wear Consumption
Autonomous (crawler), Truck mounted (trailer), rail	Safety, Reliability, Ease of Use, Versatility	Oil tank volume	Articulation angle, Ground clearance	Availability, Utilization, Productivity, OEE
Applications in Underground	Dimensions - Machine and Access Tunnels	Drilling Control System	Transmission, Translation system, Trimming speed	MTTA, MTTR, MTBF, PM, BD, HMR
Face drilling, Support holes, Grouting, Long / Blast holes	Maneuverability	Control system type, Mode, Automation	Gradeability, Tilt, Turning radius, Total weight	Cost per drilling meter

Fig. 5 Factors to be considered for selection of a drill equipment

considered for selection of a drill equipment. It is very challenging for selection of a suitable drill equipment for a given geo-environmental setup with a gamut of parameters involved as shown in Fig. 5, which can change with encountered rock or skill of operator.

Based on the type of encountered lithology and its associated hardness and mechanical properties, a decision on the suitability of drilling method can be made. There exist few prominent drilling types such as rotary, percussive, down the hole, top hammer, auger, core and pipe jacking. In rotary drilling, the rock yields due to the combined effect of pull-down pressure and the rotational forces usually adopted in soft rock conditions while in percussive drilling, the rock drill impacts the rock surface at drill hole bottom to create a chipping action and progressive cutting of the rock, adopted in hard rock environment. The most prominent and proven method of drilling is rotary-percussive which can drill in medium to very hard rock environments. It works on the principle of both rotary and percussive drilling techniques. The hammer generates the impact stress at a regular frequency and the rotation of the bit facilitates the impact on the fresh rock surface for each blow. Down the hole (DTH) and the Top-hole hammers uses the rotary-percussive drilling mechanism. DTH drills usually adopted in hard rocks and where the diameter and drill lengths are longer while the top hammer drills are used in shallow depth and small diameter drill holes owing to introduction of deviation component for longer holes by the latter. Depending on the availability and machine capacity, the power source can be either mechanical, electrical, hydraulic or pneumatic. The availability of the utilities such as compressed air, water and electric supply at the working front to connect to the drilling equipment needs to be checked. This becomes a challenge in case of

remote working areas in mines where the cable laying and extension of utility lines becomes way expensive.

The size of the drill machine depends on several factors such as the requirement of number of drill holes alternatively, total drill length i.e., development and production requirements, type of geology encountered in terms of rock hardness, type of explosive to be used, fragmentation size requirements matching with the bucket capacities of the loading equipment, operator and ownership costs.

Drill equipment selection shall also consider the depth of drill hole (shallow, moderate or large), diameter of drill hole (small, medium or large), direction of drilling (horizontal, vertical, inclined or all-round). Moreover, the area of cross section to be drilled demands sufficient number of booms, its parallel coverage and shall aid in selection of feed size, boom and its rotatability. Another challenge posed for selection of drill equipment size is the availability of access tunnel or drive dimensions. If the machine dimensions are larger than that of available tunnel dimension then the machine cannot be deployed till suitable arrangement for widening the access tunnel is made. The maneuverability of the machine is another challenge, especially at ramps with steep slopes. Every drill equipment is equipped with a translation arrangement that provides various tramping speeds and gradeability which needs to be checked prior to selection of the machine for a particular site.

Additional challenge for the drill equipment in action today is that it has to be adaptable for various dimensions, drill diameters and performing various operations by the same machine such as face drilling, scaling, support drilling and installation of support. These lay additional requirement on the drill rig for optimization of drill parameters during various operations. A constant parameter setup for different operation may result in damage of the drill accessories and tools. A drill rig's performance is primarily measured in terms of drill penetration rate and rock tool wear. A higher penetration rate is preferred for a maximized production or development rates however at the same time if the consumption of the drill bits or the rock tools increases the system's efficiency is deteriorated [22]. Thus, another challenge posed for drill equipment selection methodology is to optimize the penetration rate and tool wear. Overall, the performance of a drill rig can be deemed as directly proportional to the penetration and flushing rates, and indirectly proportional to the drilling cost per meter and the tool wear rate. A balance in these parameters needs to be maintained for selecting a drill equipment with optimized drill parameters.

Geological conditions pose the greatest challenge in selection of a drill equipment. All the estimated parameters derived from laboratory and field scale investigations might drastically change on encountering a structural discontinuity, a weathered zone, a fault zone, change in lithology, hydrothermal decomposition and hard rock intrusions. This challenge to some extent is being addressed by the Measure While Drilling (MWD) technology available today however such incorporation of technology increases the cost of the equipment which burdens small scale industries. The rock hardness and the fracturing indices are used to deduce the machine operational parameters in such cases. Usually, the machine parameters such as impact frequency, percussion, feed, rotation, flushing and damping pressures are to be selected rightly which otherwise shall damage the rock tools, shank adaptor and

lead to bit jamming and other drilling problems. Presence of discontinuities or the geological structural features in rock mass leads to drill hole deviations. Equipment's drill accuracy needs to be checked to avoid different drill pane and round bottom during face drilling. Generally, four types of deviations may be introduced into the drilling system (collaring, alignment, trajectory and due to driller inexperience). The costs and maintenance involved shall play an important role in maintaining the economic viability of the project. Frequent maintenance schedules shall result in hampering the work progress.

Last but not the least, the operator's issues are to be addressed prior to selection of any drill equipment. The environment in which the driller operates the equipment must be safe and free from noise, dust and avoidable hazards. Ergonomics also plays an important role in maintaining a peaceful working culture. The operator works under psychological stress for long working hours in a time pressure environment, standing for long durations under heat and cold stress, isolation and high hazard prone areas. Also, the same machine may perform differently when operated by two different operators with different skill levels. Drilling equipment used for underground excavations under varied operational conditions and their working ranges is listed in Table 1.

The equipment's selection and assessment of its performance is always a challenging task. Some of the key performance indicators of an equipment are the machine's availability, utilization, productivity, overall equipment effectiveness (OEE), mean time to repair (MTTR), respond and acknowledge (MTTA), mean time between failure (MTBF), periodic maintenance (PM), breakdown (BD), costs - running and maintenance, safety and hour meter reading (HMR). Based on extensive review of the available drilling equipment pertaining to underground drilling operations, a nomograph has been developed and the working ranges is presented in Fig. 6.

5 Field Investigations

For the current study, terrains such as Aravalli Hills and Bhutan Himalaya was selected to incorporate a wide variety of geological features that are encountered during drilling. Field studies were performed at developmental headings in underground Lead-Zinc mines from Zavar Group of Mines, Hindustan Zinc Limited (HZL), India and large caverns from Punatsangchhu-II Hydroelectric Project (PHEP-II), Bhutan. The locations of field investigations are shown in Fig. 7. The equipment used at the studied locations included single and double boom mechanized drill jumbos operating with varied drill hole diameters such as 45, 64 and 102 mm. During field investigations, various performance indicators of the drill equipment as mentioned in Fig. 5 such as drill penetration rate and tool consumption details were recorded along with various machine and rock mass parameters.

Table 1 Drilling equipment used for underground excavations under varied operational conditions [14]

Drill Rig Category	Develop ment	Low Profile	Rock Support	Tunnelling Jumbos	In the Hole (ITH) Long Hole	Secondary Breaking	Top Hammer Long Hole
Coverage, m ²	24-60	16.3-40	13.335- 49	49-217	NA	NA	NA
Hole length, m	3.44- 5.27	2.132-23	25-38	4.66-6.18	60.1-100	2.23-2.23	20-54.6
Percussion Power, kW	20-25	6.5-20	14-16	20-31	0-0	14-14	20-33
Max Percussion Pressure, bar	175-220	140-220	160-220	220-235	0-0	180-190	160-220
Impact Frequency, Hz	67-93	67-110	59-110	67-107	0-0	110-110	40-67
Rotation Pressure, bar	0-0	175-175	0-0	0-0	207-210	0-0	0-0
Max Rotation Speed, rpm	250-400	250-530	250-530	250-400	60-60	520-520	100-250
Rotation Torque, Nm	400-625	340-625	340-630	400-625	5730-5730	400-400	625-2330
Hole Size, mm	43-64	22-76	33-64	43-64	89-445	41-64	51-127
Reaming Hole size, mm	76-127	76-127	NA	76-127	445-762	NA	NA
Max Feed Force, kN	25-25	20-31	0-0	25-30	70-70	31-31	20-31
Boom Parallel coverage, m ²	24-54	11-36	0-0	44.5-166	0-0	30-30	0-0
Powerpack, kW	45-160	55-55	55-160	55-205	37-55	NA	45-160
Multi Voltage, V	380- 1000	380-575	380- 1000	380-1000	380-690	NA	380-690
Frequency, Hz	50-60	50-60	50-60	50-60	50-60	NA	50-60
Total installed power, kW	60-195	70-130	70-205	135-325	37-130	NA	60-135
Water pump capacity, l/min	33-185	30-100	13.6-100	12.7-400	27-30	10-16	33-375
Water Inlet Pressure, bar	2-7	2-7	1-2	2-10	4-7	2-7	2-7
Flushing pressure, bar	10-20	10-20	10-15	10-30	24-48	10-15	10-20
Sound pressure level, db(A)	69-124	98-124	69-80	69-128	0-0	80-80	69-127
Articulation, ±°	27-40	37-43	35-40	34-40	35-40	38-40	27-40
Ground Clearance, m	0.225- 0.42	0.3-0.3	0.32- 0.42	0.32-0.4	0.18-0.33	0.32-0.32	0.225- 0.42
Tramming Speed, km/hr	6-16	7-12	10-16	9-16	10-12	12-12	6.5-15
Tramming Speed, km/hr (1:7 Gradient)	4-6	4.3-5	5-12	3.5-6	5.5-7	5-5	3-6.5
Max Gradeability, °	15-15	15-15	15-15	11-15	15-20	15-15	15-15
Max Sidewise tilt, °	5-5	5-15	5-5	5-5	5-20	5-5	5-5
Min Drift Height, m	2.5-4.5	2-3	0-0	4-4	3.05-3.87	3-3	2.7-5.05
Min Drift Width, m	2.5-4.5	2.5-3.04	0-0	4-4	3.05-3.87	3-3	2.7-6.7
Turning width, m	2.6-3.87	3.11-4.95	3.9-4.61	3.5-11.86	3.076-4.15	3.6-3.9	2.51-4
Transport Height, m	1.9-3.42	1.38- 1.775	2.14- 3.32	2.35-4.14	2.51-2.939	2.14-2.14	1.5-3.25
Transport Width, m	1.4-2.5	2.25-2.26	2.02- 2.74	2.15-3.05	1.219- 2.345	1.98-2.02	1.99-2.75
Transport Length, m	9.605- 13.25	10.375- 13.21	11.37- 13.5	12.35-19.6	4.997- 10.87	9.68-10.9	6.85- 11.85
Total Weight, tons	9.1-27.5	13.6-20	15-30	22-51.5	8.165-30	15-16	8.9-26.5
Turning Radius, m	2.7-7.66	4.045- 8.245	5.91- 9.25	6.25-11.86	2.54-7.225	5.86-6.571	5.46-7.2

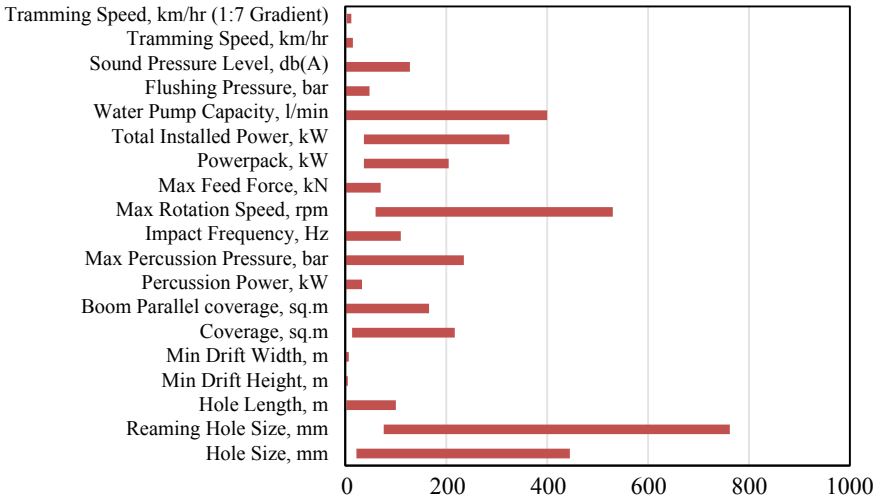


Fig. 6 Working ranges for various drill rigs available for underground operations



Fig. 7 Locations selected for field investigations

6 Results and Analysis

Performance studies conducted for various drill rigs operating in underground mines and tunnels gave an insight on the overall effectiveness of the equipment and system which further helps in assessing the progress of the project. Underground excavation's cycle time deemed as the final output was studied and compared for two different drill rigs operating in terrains from India and Bhutan hard rock environment and the details are presented in Table 2. The variation in cycle times is categorically analysed and presented for both sites in Fig. 8.

Various key performance indicators were assessed for a drill jumbo operating in an underground hard rock mine for a period of one year and the findings are presented

Table 2 Time study details for drill equipment operated in underground mine and tunnel

Parameters	HZL, India	PHEP-II, Bhutan
Excavation details	Face/Drive Development	Drive/Tunnel
Drill make and model	Sandvik DD321	Sandvik DT820
Coverage area, m ²	27.5 (5.5 × 5)	69.75 (9.3 × 7.5)
Number of drill holes	65	108
Number of reamer holes	4	1
Drill dia, mm	45	45
Reamer drill dia, mm	102	102
Drill length, m	4	2
Rock mass quality, Q	38	4.1
Rock type	Dolomite	Leucogranite
Excavation cycle		
Navigation and surveying, Hrs	0.5	0.5
Face drilling, Hrs	3	4.5
Charging and blasting, hr	2.25	3
Ventilation, Hrs	2	1
Loading and hauling, Hrs	5	2.5
Scaling, Hrs	3.25	2
Supporting, Hrs	4.25	2.5
Bottom cleaning, Hrs	1	1.25

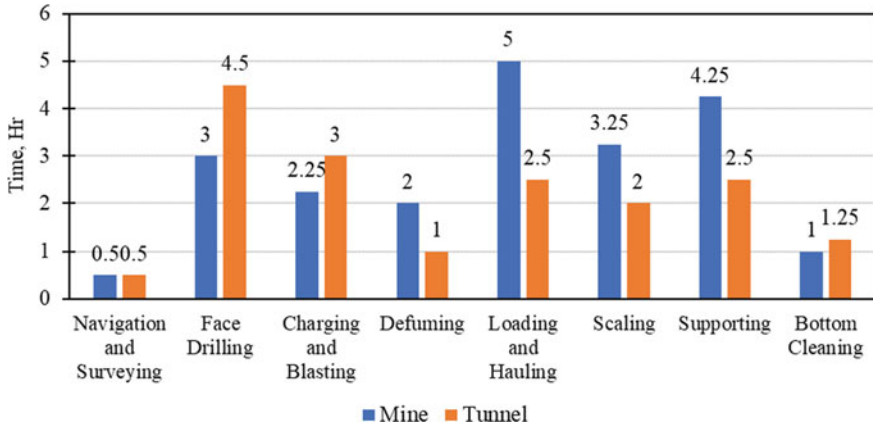


Fig. 8 Comparative study of excavation cycle time in underground mine and tunnel in hard rocks

in Fig. 9. Besides that, the net drill penetration rates for different drill equipment operating with varied drill diameters were studied and rock drillability studies were also performed at laboratory scale. Drilling Rate Index (DRI) values were determined from Siever’s J and Brittleness (S20) values and were compared to field penetration rates of various drill rigs operating with different drill diameters. The findings from which is shown in Fig. 10.

From Fig. 8, it is observed that loading and hauling took most of the excavation cycle time besides drilling, scaling and supporting in underground mine while face drilling is the most time-consuming operation in tunnelling. Inaccurate rock drilling can result in poor blasting, limiting the pull of the round, requirement of greater quantity of rock reinforcement, aggravated scaling and mucking requirements, additional backfilling quantities due to overbreak and the increase in difficulty in defining the

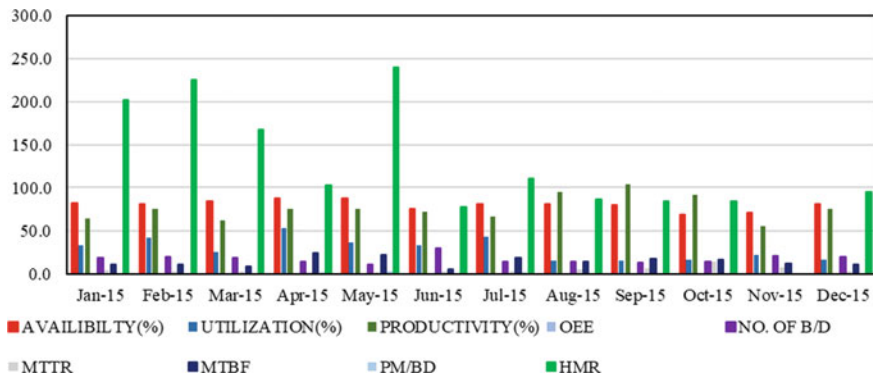


Fig. 9 Key performance indicators studied for a drill jumbo operating in an underground hard rock mine

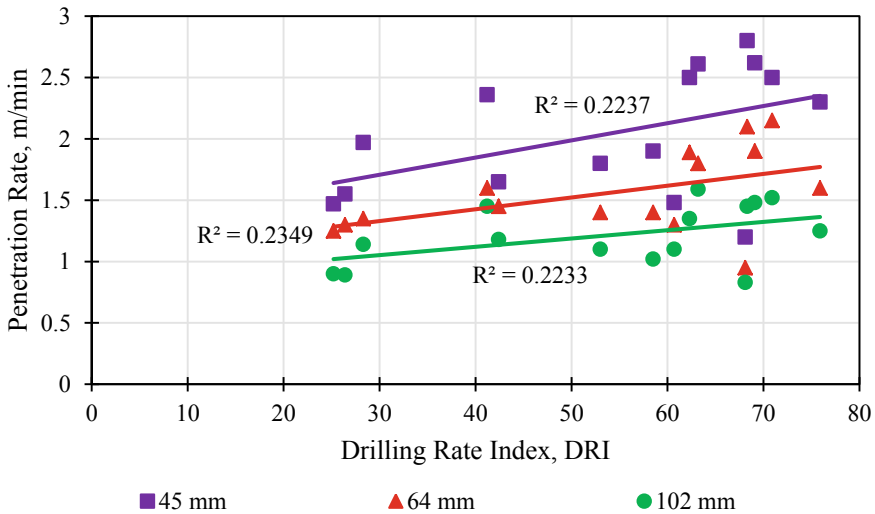


Fig. 10 Drill Penetration Rate studies for varied drill bit diameter and DRI values

quality of grouting and thus rock drilling process becomes the most crucial operation in the entire excavation cycle.

From Fig. 9, it is observed that against the total availability of the equipment, the utilization of the same was found to be very low. This is due to the reason of limited work fronts availability and working in a blind development heading with the equipment to wait for the next work front to be made available. This is the reason, though the utilization percentage of the drill equipment was low with respect to its availability but the productivity levels of the machine were found to be higher.

From Fig. 10, it is evident that increase in Drilling Rate Index (DRI) values indicated an increase in penetration rates signifying better performance of the drill rigs. Alongside, drilling with a larger drill bit resulted in reduction in drill penetration rates due to increase in the bit-rock contact area and reduction in effective drilling stresses. However, the coefficient of determination (R^2) values were low indicating a larger unexplained variance by the DRI. Thus, there is a requirement of development of an all-inclusive drillability model that can precisely predict drill penetration rates aiding in selection of right drill equipment for a given geo-environment.

7 Conclusions

Drill jumbos are being used extensively for the development of headings, drives, tunnels, ramps and other underground structures in mining, tunnelling, civil and infrastructure projects. Drilling plays an important role in optimizing the excavation cycle time. However there exists numerous factors especially rock and rock mass that

can alter the predicted rate of penetration vis-à-vis progress of the project drastically. Performance studies conducted for drill jumbos in underground hard rock mines over a period of one year indicated that the machine's availability is around 80% however its utilization is found to be only about 30% with 76% productivity on an average. The studies indicate that the drill planning and system in totality needs improvement with incorporation of the latest technologies. However, there exists certain limitations which needs due consideration. Due to the larger scale and volume of excavations in tunnelling or civil excavations than developmental headings in mining, the drilling equipment selection and its performance affects tunnelling cycle to a greater extent. However, there is a requirement of developing an all-inclusive drillability model which shall aid in selection of right drill equipment offering high drilling performance at lower operating costs besides obtaining a desired rate of drilling in a given geotechnical environment. Drillability models shall include the variability factor helping in realistic predictions aiding drill planning in mines and tunnel for faster tunnelling cycles.

Acknowledgements The authors are grateful to the Director, NIRM, Mine Management of Hindustan Zinc Limited, India and the Project Authorities of Punatsangchhu-II Hydroelectric Project, Bhutan for allowing the authors to perform the studies. The support extended by the officials of Rock Excavation Laboratory, Department of Mining Engineering, IIT (ISM) is duly acknowledged. This forms the part of PhD work being accomplished by the first author at IIT (ISM) Dhanbad.


References

1. Alireza C, Hasan KS, Shahriar K, Khademi Hamidi J (2012) An estimation of the penetration rate of rotary drills using the Specific Rock Mass Drillability index. *Int J Min Sci Technol* 22:187–193. <https://doi.org/10.1016/j.ijmst.2011.09.001>
2. Ataei M, KaKaie R, Ghavidel M, Saeidi O (2015) Drilling rate prediction of an open pit mine using the rock mass drillability index. *Int J Rock Mech Min Sci* 73:130–138. <https://doi.org/10.1016/j.ijrmms.2014.08.006>
3. Bhatawdekar RM, Edy MT, Danial JA (2019) Building information model for drilling and blasting for tropically weathered rock. *J Mines, Met Fuels* 67:494–500
4. Bhatawdekar RM, Mohamad ET, Singh TN, Armaghani DJ (2019) Drilling and blasting improvement in aggregate quarry at Thailand - a case study. *J Mines, Met Fuels* 67:357–362
5. Bilgin N, Yazici S, Eskikaya S (1996) A model to predict the performance of roadheaders and impact hammers in tunnel drivages. In: *ISRM international symposium - EUROCK 1996*, pp 715–720
6. Brady B, Brown E (2004) *Rock Mechanics for underground mining*. Third. Kluwer Academic Publishers
7. Franca LFP (2011) A bit-rock interaction model for rotary-percussive drilling. *Int J Rock Mech Min Sci* 48:827–835. <https://doi.org/10.1016/j.ijrmms.2011.05.007>
8. Hoseinie HS, Pourrahimian Y, Aghababaei H (2007) Analyzing and physical modeling of joints dipping effects on penetration rate of rotary drilling in open pit mines. In: *20th international mining congress and exhibition of Turkey, IMCET 2007*. pp 259–263
9. Hoseinie SH, Aghababaei H, Pourrahimian Y (2008) Development of a new classification system for assessing of rock mass drillability index (RD_i). *Int J Rock Mech Min Sci* 45:1–10. <https://doi.org/10.1016/j.ijrmms.2007.04.001>

10. Jimeno C, Jimeno E, Carcedo F (1995) Drilling and blasting of rocks, Balkema
11. Kumar S, Murthy V (2012) Drillability prediction and its assessment in coal measure rocks to aid rotary blasthole drill selection - some investigations. In: National seminar on mining equipment: new technologies, challenges & applications (MENTCA). pp 27–38
12. Oddsson B (1982) Rock quality designation and drilling rate correlated with lithology and degree of alteration in volcanic rocks from the 1979 Surtsey drill hole
13. Rathinasamy V, Mohamad ET, Komoo I, et al (2020) Influence of physico-mechanical properties of tuff on penetration rate – a case study in southern Johor Bahru, Malaysia. *J Mines Met Fuels* 68:136–143. <https://doi.org/10.18311/jmmf/2020/27644>
14. Sandvik Underground Drill Rigs And Bolters. <https://www.rocktechnology.sandvik/en/products/underground-drill-rigs-and-bolters/>, Accessed 3 Nov 2021
15. Sandvik Tamrock Corp. (1999) *Rock Excavation Handbook*
16. Siva Prasad BNV, Murthy VMSR (2018) Laboratory investigations into fracture propagation characteristics of rock material. In: AIP conference proceedings, pp 020009–1–7. <https://doi.org/10.1063/1.5030313>
17. Siva Prasad BNV, Murthy VMSR (2017) Influence of rock abrasivity and bit wear on drill penetration rate. In: *INDOROCK : 7th Indian rock conference*, pp 387–395
18. Siva Prasad BNV, Murthy VMSR, Pandey SK (2016) Investigations on rock drillability applied to underground mine development vis-à-vis drill selection. In: *Recent advances in rock engineering (RARE)*. Atlantis Press, pp 399–403. <https://doi.org/10.2991/rare-16.2016.62>
19. Taheri A, Qao Q, Chanda E (2016) Drilling penetration rate estimation using rock drillability characterization index. *J Inst Eng Ser D* 97:159–170. <https://doi.org/10.1007/s40033-015-0104-6>
20. Tanaino A (2005) Rock classification by drillability. Part I: analysis of the available classifications. *J Min Sci* 41:541–549
21. Tanaino AS, Lipin AA (2004) State and prospects of the percussive-rotary blasthole drilling in quarries. *J Min Sci* 40:188–198
22. Thuro K (1997) Drillability prediction: geological influences in hard rock drill and blast tunnelling. *Geol Rundschau* 86:426–438. <https://doi.org/10.1007/s005310050151>
23. Venkatesh HS, Balachander R, Gopinath G (2018) Drilling and blasting of tunnels in himalayan geology. *TAI J (A Half Yrly Tech J Indian Chapter TAI)* 2(7):21–28
24. Zare S, Bruland A (2013) Applications of NTNU/SINTEF drillability indices in hard rock tunneling. *Rock Mech Rock Eng* 46:179–187. <https://doi.org/10.1007/s00603-012-0253-y>
25. Siva Prasad BNV, Murthy Sripad, VMSR, Naik R Influence of static and dynamic rock properties on drillability prognosis for mining and tunnelling projects. *Indian Geotech J* <https://doi.org/10.1007/s40098-022-00608-0>
26. Siva Prasad BNV, Murthy Sripad VMSR, Naik R Drillability predictions in Aravalli and Himalayan rocks – A petro-physico-mechanical approach. *Curr Sci* 122(08):901–917. <https://doi.org/10.18520/cs/v122/i8/907-917>

Fracture Characterization Using Downhole Camera in Deep Boreholes at Southern Johor Bahru, Malaysia



Vynotdni Rathinasamy , Edy Tonnizam Mohamad, Ibrahim Komoo, Mariatul Kiftiah Ahmad Legiman, Nurul Amaniyah, Ramesh Murlidhar Bhatawdekar, Muhammad Nassir Bin Hanapi, and Eka Kusmawati Binti Suparmanto

Abstract Downhole camera is an effective tool to locate fractures and other geological features in boreholes although it does not quantify the characteristics of fracture directly. This study attempts to qualitatively characterize fractures in three deep boreholes, namely W1-W3 using downhole camera of R-CAM 1000 XLT as well as to investigate the geological features present at Southern Johor Bahru. The study area is underlain by Jurong Formation and Older Alluvium. Jurong Formation comprises of well cemented and consolidated volcanic-sedimentary rocks while Older Alluvium comprises of coarse, angular clayey sand with pebbles such as quartz, rhyolite, chert and argillite pebbles. The geological features encountered during the study are brecciated zone and veins such as quartz, calcite and pyrite. In addition, the fracture density in W2 (175/150 m) is found to be higher than W1 (79/165 m). Gently dipped ($<20^\circ$), single set of joints with tight to open aperture ($<0.1\text{--}4$ cm) are dominant in both wells. Major orientation of discontinuities is north-east ($0\text{--}90^\circ$) to south-west ($180\text{--}270^\circ$) which is subparallel to bedding plane and lineament orientations. Meanwhile, no major structure is observed in W3. Thus, the study shows the importance of downhole camera survey in locating and characterizing fractures in rock mass qualitatively.

Keywords Fracture characterization · Downhole camera survey · Deep boreholes

1 Introduction

Fractures in rock masses are given immense importance in the studies of rock engineering and mechanics especially for understanding the rock mass characteristics

V. Rathinasamy (✉) · M. K. A. Legiman · N. Amaniyah · M. N. B. Hanapi · E. K. B. Suparmanto
School of Civil Engineering, Faculty of Engineering, Universiti Teknologi Malaysia, UTM JB,
81310 Skudai, Malaysia
e-mail: vynotdni2@graduate.utm.my

E. T. Mohamad · I. Komoo · R. M. Bhatawdekar
Geotropik Centre, Block D03, School of Civil Engineering, Faculty of Engineering, Universiti
Teknologi Malaysia, UTM JB, 81310 Skudai, Malaysia

© The Author(s), under exclusive license to Springer Nature Singapore Pte Ltd. 2022
A. K. Verma et al. (eds.), *Proceedings of Geotechnical Challenges in Mining, Tunneling
and Underground Infrastructures*, Lecture Notes in Civil Engineering 228,
https://doi.org/10.1007/978-981-16-9770-8_10

183

and response to excavation, Excavation Damaged Zone (EDZ) analysis, numerical analysis, assessing of rock mass geometry and design of reinforcement [1]. The downhole camera system allows continuous, visualisation of borehole wall up to 360° in colour. Therefore, it aids in effectively detecting change in lithology and discontinuities found along the wells such as joints, fractures and other structures through the downhole camera survey with minimal data interpretation [2–5]. Several researchers have utilised this tool to characterise the fractures based on its type, aperture and dip angle [6–9]. Extensive literature on borehole camera technology shall be found in Chuan-ying and Law [10] and Han et al. [11].

As the downhole camera survey offers insightful visual analysis for various diagnostics of borehole, it has been utilized widely in Oil and Gas industry since the year 1980. However, the technology has advanced greatly in recent years and capable of capturing images with high quality and high frame-rate. It is certainly needed for computational analysis of structures and fluid flow throughout the borehole. Initially, the observed geological features especially fracture aperture, spacing and orientation were qualitatively evaluated through the downhole camera surveys. However, recent advancements in computer vision methods and image processing have enabled quantitative analysis [12] for intuitive conception of sophisticated information and precise interpretation. Some of the advancements of downhole camera system mentioned by Tymons and Moloney [13] are high frame video (30 frames/second) for rapid logging of clear images, adjustable LED lighting for every well condition, enhanced sensors and lens for high quality video and availability of sideward and downward facing cameras to set initial location or depth as well as for detailed observation. These advancements have enhanced the insight of complex borehole issues as well as decreased the operational time, risk and expense.

This downhole camera technology has been extensively utilized in geological investigations including petroleum [14–18], mining [19–21], glacier [22, 23], groundwater [24–28], geotechnical and environmental engineering [29–37]. In addition, it has also been utilized to monitor development of crack and evolution of fracture in underground excavations which directly assisted in developing characteristics of EDZ [37–39]. This study attempts to qualitatively characterize fractures in three deep boreholes, namely W1-W3 using downhole camera of R-CAM 1000 XLT as well as to investigate the geological features present at Southern Johor Bahru.

2 Study Area

Jurong Formation extends from part of Johor to Singapore. According to Burton [40], in Johor state, there are two members in Jurong Formation such as Bukit Resam Clastic Member and Gunung Pulai Volcanic Member. The Bukit Resam Clastic Member is considered to be Upper Triassic to Middle Jurassic age while the other member is considered to be Lower Triassic age. The discontinuity between these two members can be seen as Gunung Pulai volcanic rocks present as phenoclasts in Bukit Resam Clastic Member. Also, the existing chronological evidence shows

that emplacement of hornblende-bearing adamellite has occurred during the non-depositional period. The Bukit Resam Clastic Member is composed primarily of shale and immature sandstone with minor siltstone, conglomerate and volcanic layers. This deposition occurred in shallow water. On the other hand, the Gunung Pulai Volcanic Member is comprised dominantly of tuffs such as welded tuffs of rhyodacitic composition and containing hornblende. Lavas are present in minor. Although the tuffs are of sub-aerial origin, the subordinate intercalations of sedimentary rocks in this member hinted on partial deposition in water.


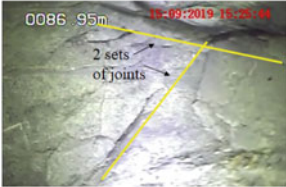



Meanwhile, Older Alluvium extends from part of Johor to part of Singapore as well. It was first documented by Scrivenor [41] as “high level alluvium”. It was further investigated by Alexander [42], Walker [43], Burton [40] and Dodd et al. [44] with various names. According to Woon and Yingxin [45], the Older Alluvium in Singapore is found to lie directly on quartzite sandstone and granite with thickness up to 200 m. The lithology is coarse, angular clayey sand with pebbles such as quartz, rhyolite, chert and argillite pebbles of diameter up to 4 cm. The fining upward sequence is observed. In addition, rare clastic dykes are seen at Bedok Quarry. The presence of thick clay with fine materials possibly indicates marine deposition.

3 Methodology

There are three deep boreholes, namely W1 (165 m), W2 (150 m) and W3 (170 m) in the study area which were developed through air-percussion rotary drilling. In this study, the underground survey was carried out using R-CAM 1000 XLT Downhole Camera System as in Fig. 1 up to the bottom of boreholes to determine geological features including fractures. According to Geopip Water Solutions Ltd. [46], this downhole camera system is absolutely portable, autonomous video monitoring system which could monitor boreholes up to diameter of 12 inch and depth of 300 m. The results were then, analysed manually.





Through the recorded video, important data namely discontinuities characteristics and geological features were collected. It must be noted that downhole camera does not directly quantify the characteristics of fractures such as orientation, dip angle and aperture unlike acoustic or optical televiewer (Williams et al. 2005). Hence, the fracture dip angle and aperture are measured qualitatively. The aperture was estimated based on difference in depth between beginning and end of fractures. Meanwhile, the approximate fracture orientation (dip direction and dip angle) was determined by slightly modifying technique suggested by Overby Jr. et al. [47]. Firstly, the known fracture orientation measured from the outcrop was identified. Then, a clear acrylic plastic sheet was marked with a cross and a series of increasing diameter ring. It was placed on monitor screen with center of circle at center of borehole. According to Overby Jr. et al. (1988), the cross will show the point on the wellbore where a fracture exactly normal to it will be found. Keeping the known orientation as reference, other fractures' orientations were fairly determined.

Table 1 Terminologies for rock type

Nature	Categories	Description
Type	Single set of joints	Single set of joint is visible as seen in W2 at depth of 28.55 m.
		
	Multiple sets of joints	Two or more sets of joints are visible as seen in W1 at depth of 86.95 m.
		
	Fractured vein	Fractured veins are filled by either quartz or calcite vein. Void is found along the vein as seen in W1 at 36.11 m.
		
Aperture size	Tight	No void is visible as seen in W1 at depth of 33.07 m. The approximate aperture size is less than 0.1 cm.
		
	Open	The size of void is in between 'tight' and 'major opening' as seen in W2 at depth of 107.13 m. The approximate aperture size is 0.1 – 4 cm.
		

(continued)

Table 1 (continued)

Major opening	The void is more than 30 % of monitor as seen in W2 at depth of 106.80 m. The approximate aperture size is more than 4 cm.	
Dip angle Gentle	The fracture is dipping less than 20° on monitor as seen in W1 at depth of 36 m. In most cases, it is almost horizontal.	
Moderate	The fracture is dipping in between 20° and 70° on monitor as seen in W1 at depth of 90.92 m.	
Steep	The fracture is dipping more than 70° on monitor as seen in W1 at depth of 99.36 m.	

3.1 Terminologies for Fracture Characterisation

In this study, several terminologies are used for fracture characterisation based on downhole camera survey. Table 1 shows terminologies for fracture characterisation in terms of fracture type, aperture size and dip angle. The fractures are categorized into single set of joints, multiple sets of joints and fractured veins. Next, the aperture is classified into tight, open and major opening based on the void of fracture as seen in the monitor. Meanwhile, the dip angle is measured as gentle, moderate and steep.

Fig. 1 Downhole Camera System of R-CAM 1000 XLT



4 Results and Discussion

The downhole camera helps in determining subsurface fractures and other geologic features clearly (Williams et al., 2005). Based on the survey carried out in all three deep boreholes, a few geologic features such as brecciated zone, veins (quartz, calcite and pyrite) and fracture system are determined. There are four brecciated zones in W1 at depths of 25–45, 65–70, 100–120 and 130–140 m.

Quartz veins are found at 80–110 and 120–165 m while calcite veins are found at 25–30, 35–45, 65–145 and 150–155 m in W1. Meanwhile, in W2, only two brecciated zones are found at depths of 45–50 and 60–65 m. Calcite veins are found throughout the W2 except at 70–75 m. Pyrite veins are found at 25–30, 35–40 and 58–68 m which indicates the hydrothermal alteration in the past. In addition, quartz veins are encountered at 70–130 and 140–150 m. No major geologic feature is found in W3. Figure 2(a)–(f) show geologic features found using the downhole camera.

During the survey, a total of seventy-nine fractures are observed in W1. This borehole is dominated by single set of joints with 82.28% which are mostly gently dipped ($<20^\circ$) with aperture of tight to open (<0.1 –4 cm) as in Fig. 3, 4 and 5. Then, multiple set of joints (7.59%) which are primarily gently dipped ($<20^\circ$) with tight (<0.1 cm) aperture are found. In addition, 10.13% of fractures encountered in this well are fractured vein with aperture of major opening (>4 cm) and mostly gently dipped ($<20^\circ$). Besides, there are twenty-three (23) fractures with major opening (>4 cm) in this well. The density of fractures at W1 is shown in Fig. 6(a). It is found that the density of fracture is less than five at most of the depths except at depths of 45, 110, 115, 150 and 165 m. The highest density of fractures is found at 155–160 m with 10 fractures per 5 m depth. The georose diagram is shown in Fig. 6(b). It shows that the major orientation of fractures is in northeast-east (45 – 90°) to southwest-west (225 – 270°). This orientation is similar to the orientation of bedding at this study area with strike/dip of $067/42^\circ$.

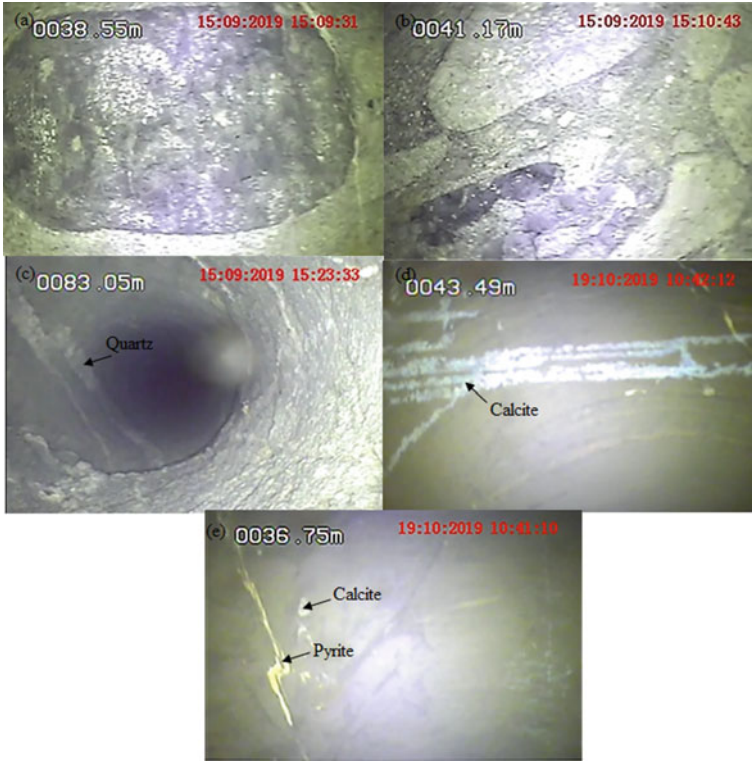


Fig. 2 Downhole camera images of geological features: **a** large size clastic material; **b** brecciated zone; **c** quartz vein; **d** calcite vein; **e** pyrite vein

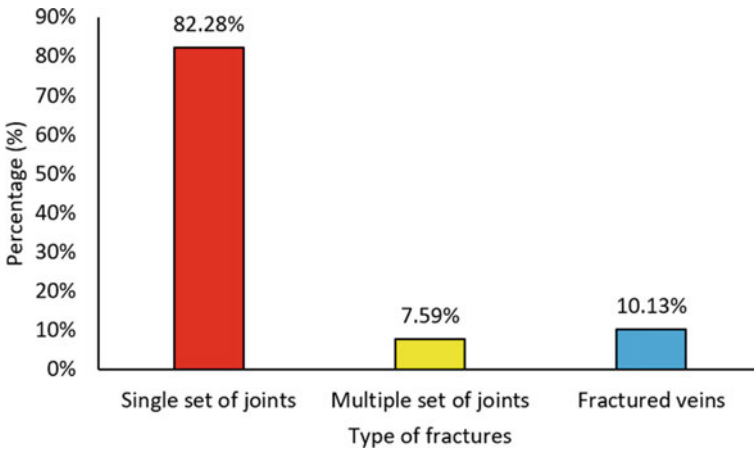


Fig. 3 Percentage of fracture type in W1

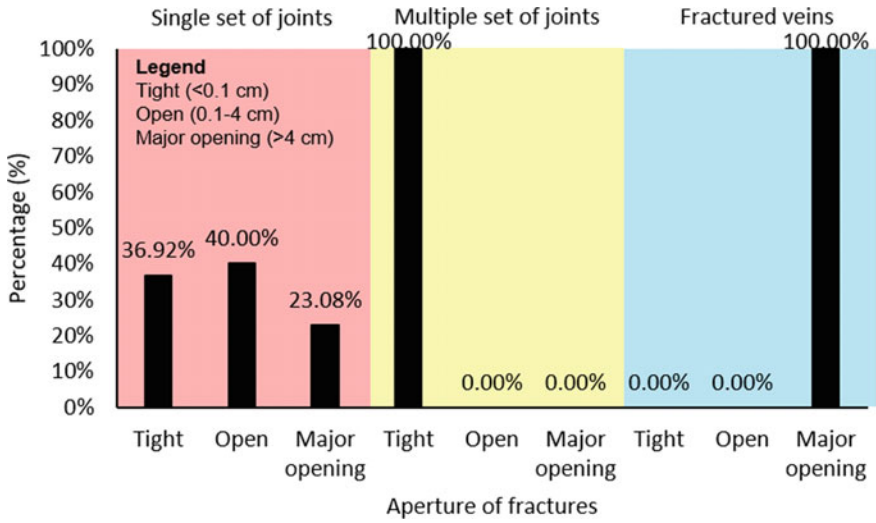


Fig. 4 Aperture classification for each fracture type in W1

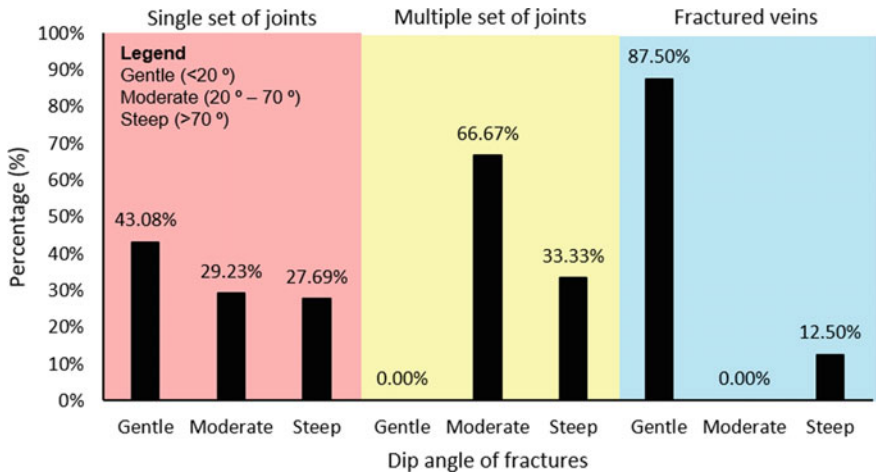


Fig. 5 Dip angle classification for each fracture type in W1

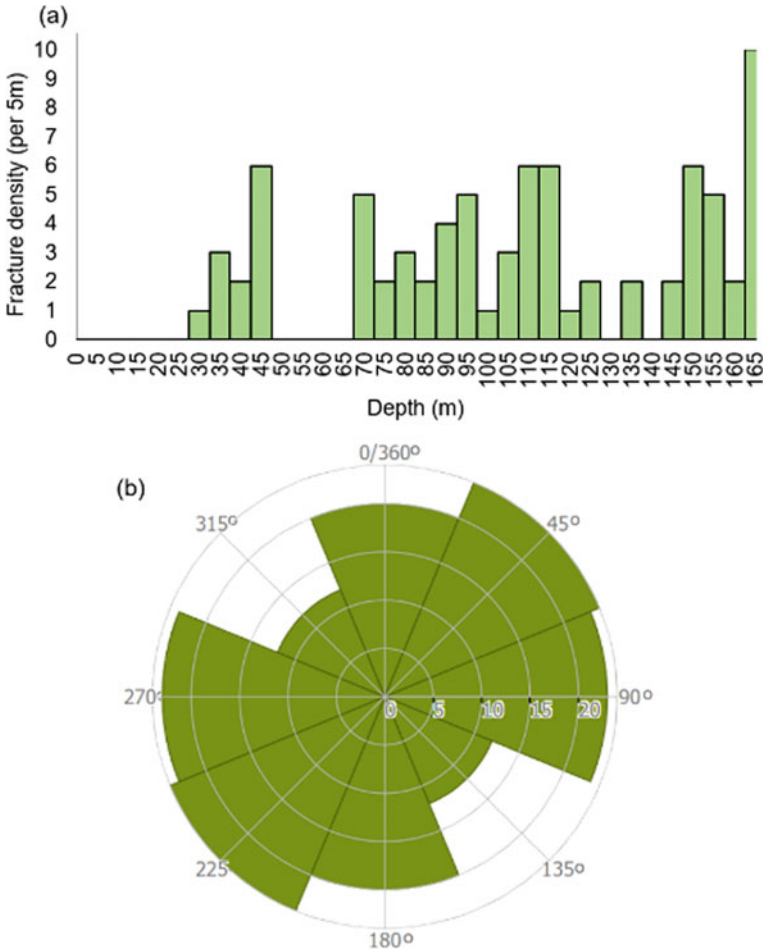


Fig. 6 Fractures at W1: **a** density; **b** georose

A total of hundred and ninety-five fractures are observed in W2. This well is dominated by single set of joints with 64.62% which are mostly gently dipped ($<20^\circ$) with tight aperture (<0.1 cm) as in Fig. 7, 8 and 9. Then, multiple set of joints with 32.82% which are primarily steeply dipped ($>70^\circ$) with tight aperture (<0.1 cm) are found. In addition, 2.56% of fractures encountered in W2 are fractured veins with aperture of major opening (>4 cm) and mostly gently dipped ($<20^\circ$). Besides, there

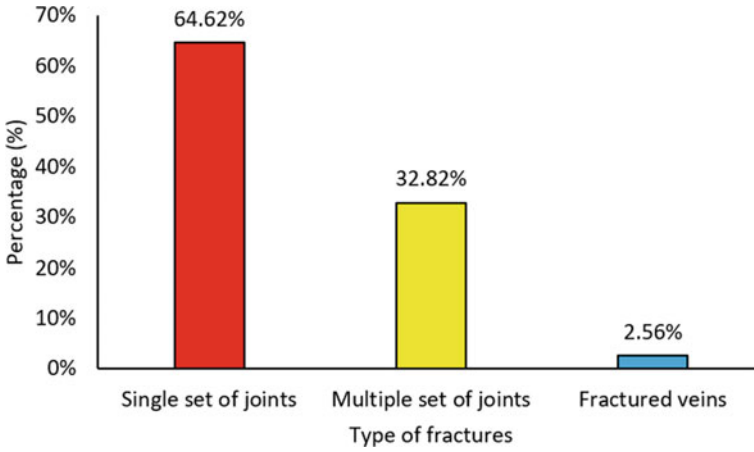


Fig. 7 Percentage of fracture type in W2

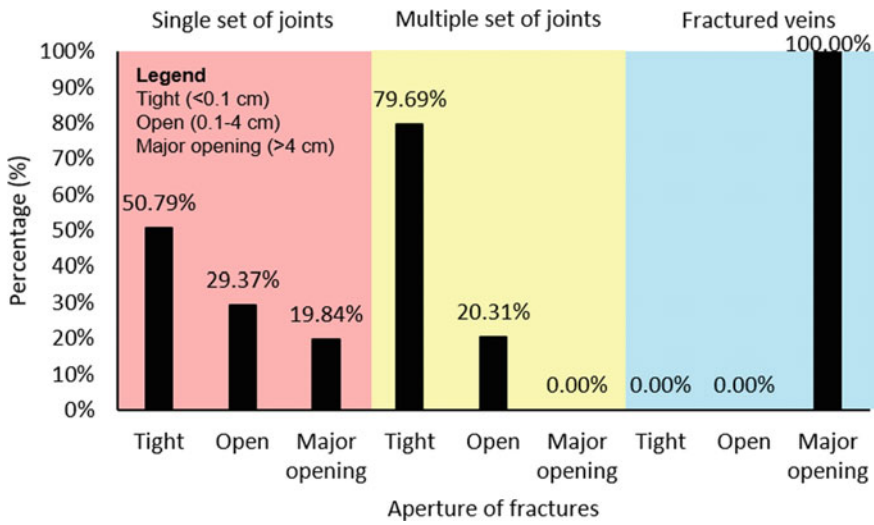


Fig. 8 Aperture classification for each fracture type in W2

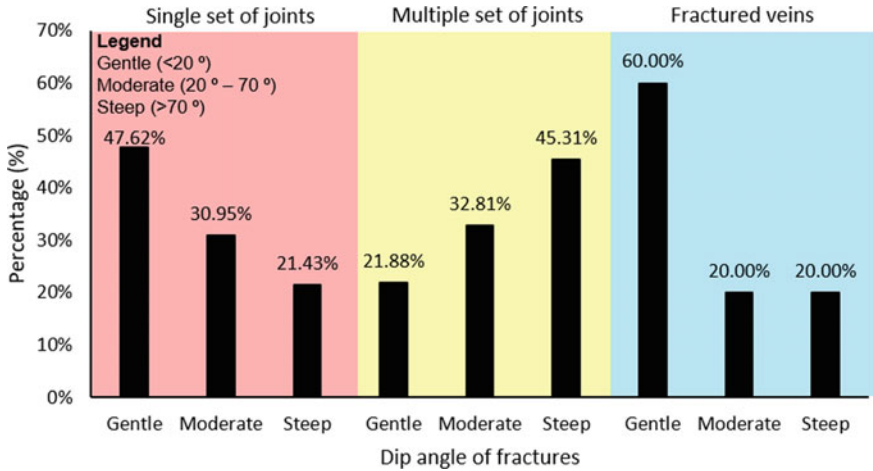


Fig. 9 Dip angle classification for each fracture type in W2

are thirty fractures with major opening in this well. The density of fractures along the depth of W2 is shown in Fig. 10(a). Unlike W1, in W2, the density of fractures is generally higher and shows the highest number of fractures at 50–55 m. The georose diagram is shown in Fig. 10(b). It shows that the major orientation is northeast to southwest (45–225°) which is similar to orientation of bedding in this region.

However, no major structure is observed in W3 which was drilled up to 170 m. It consists of older alluvium materials such as shale, quartz, chert, argillite and slate. borehole.

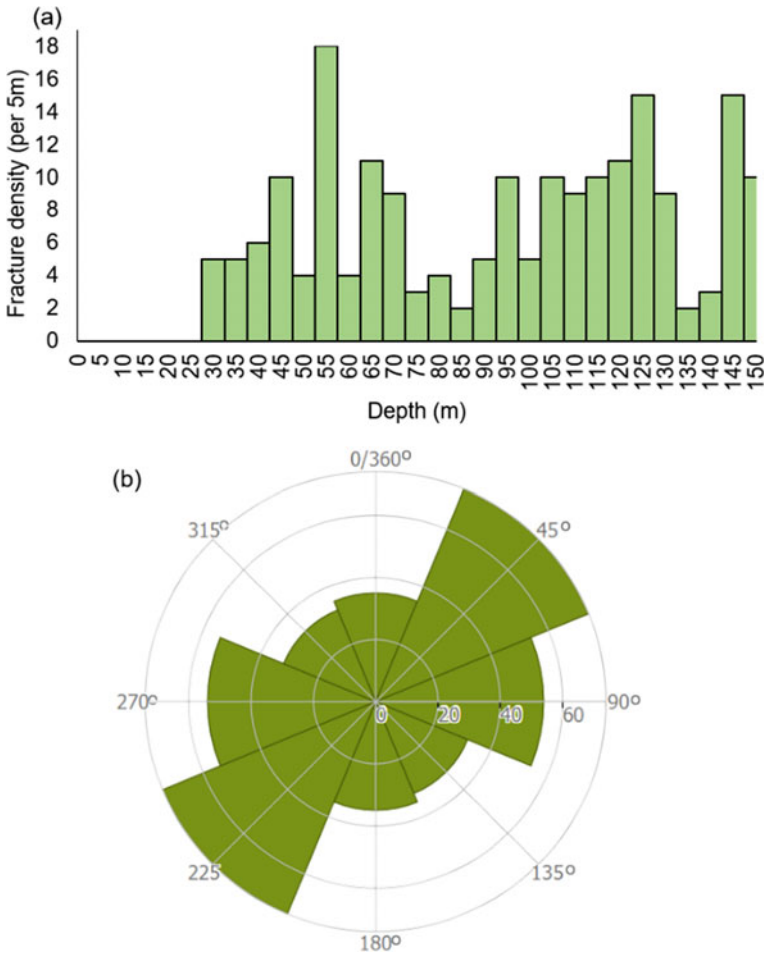


Fig. 10 Fractures at W2: a density; b georose

5 Discussion and Conclusion

According to Hansen et al. [48], in general, vertical and high angle fractures are most likely to be detected on outcrops than horizontal fractures and vice-versa in vertical boreholes. However, this study manages to determine many high angle and vertical fractures as well as horizontal fractures using the downhole camera. Also, the downhole camera survey shows that more fractures are present along W2 than W1. However, in W3, no major structure is found. This tool has greatly assisted in determining geological features and fracture characteristics as suggested by several researchers [4, 8]. Also, it must be noted that the geological features and fractures are clearly detectable along the boreholes. It is found that the major orientation

of discontinuities is north-east (0–90°) to south-west (180–270°). Although most of the fractures are subparallel to bedding and upriver orientation, several other fractures' orientations follow both regional and local tectonic activity in this study area. Therefore, this study vividly indicates the importance of role of downhole camera survey in detecting and characterizing fractures in rock mass.

References

1. Li SJ, Feng XT, Wang CY, Hudson JA (2013) ISRM suggested method for rock fractures observations using a borehole digital optical televiewer. *Rock Mech Rock Eng* 46(3):635–644
2. Paillet FL, Barton C, Luthi S, Rambow F, Zemanek JR (1990) Borehole imaging and its application in well logging-an overview. *Borehole imaging*. Society of Professional Well Log Analysts, Inc., Houston, Texas, pp 3–23
3. Pusch R (1998) Practical visualization of rock structure. *Eng Geol* 49(3–4):231–236
4. Williams LJ, Albertson PN, Tucker DD, Painter JA (2004) Methods and hydrogeologic data from test drilling and geophysical logging surveys in the Lawrenceville, Georgia, area, No. 2004–1366. U.S. Geological Survey, Georgia
5. Norbert S, Katarzyna G (2014) Evaluating selected lithological features using photographs taken with an introsopic camera in boreholes. *Int J Rock Mech Min Sci* 72:319–324
6. Kamewada S, Endo T, Kokubu H, Nishigaki Y (1989) The device and features of BIP system. In: The 21st symposium on rock mechanics proceedings, committee on rock mechanics. Japanese Society of Civil Engineers, pp 196–200
7. Wang CY, Law KT, Sheng Q, Ge XR (2002) Borehole camera technology and its application in the Three Gorges project. In: Proceedings of the 55th Canadian geotechnical and 3rd joint IAHC-CNC and CGS groundwater specialty conferences, Niagara Falls, Ontario, pp 601–608
8. Williams JH, Johnson CD (2004) Acoustic and optical borehole-wall imaging for fractured-rock aquifer studies. *J Appl Geophys* 55(1–2):151–159s
9. Williams LJ, Kath RL, Crawford TJ, Chapman MJ (2005) Influence of geologic setting on ground-water availability in the Lawrenceville area, Gwinnett County, Georgia. U. S. Geological Survey, Georgia
10. Chuan-ying WANG, Law KT (2005) Review of borehole camera technology. *Chin J Rock Mech Eng* 24(19):3440–3448
11. Han ZQ, Wang CY, Hu S (2015) Digital borehole camera technology and its applications in mining geology exploration. In: Proceedings of the 24th international mining congress and exhibition of Turkey, Antalya, Turkey, pp 14–17
12. Tymons T, Roberts G, Scott C (2019) From qualitative to quantitative—how visual data analytics has transformed downhole video diagnostic services. In: SPE Offshore Europe conference and exhibition. OnePetro
13. Tymons T, Moloney S (2016) Moving the oil and gas sector into the video age: vision assisted well interventions reduce cost and add value. In: Abu Dhabi International petroleum exhibition & conference. Abu Dhabi, UAE
14. Palmer ID, Sparks DP (1991) Measurement of induced fractures by downhole television camera in coalbeds of the Black Warrior basin. *J Petrol Technol* 43(3):270–275
15. Maddox SD ((1997)) Application of downhole video technology to multilateral well completions. In: SPE offshore Europe. OnePetro
16. Tague JR (1999) Downhole video optimizes scale removal program. *Int J Petrol Eng* 72(7):27–32
17. Nussbaum CV, Sathish Kumar B, Ariff Shazwan MN, Syed Mohd Shahril SA, Mohd Zulkiffi OB (2013) Strategic rigless approach in identifying and curing complex and multiple completion leaks in Malaysia. In: SPE/ICoTA coiled tubing & well intervention conference & exhibition. Society of Petroleum Engineers, Texas, USA

18. Yin-hua L, Xue-jie X, Yu-bin W, Wan-yong X, Kai L, Yuan L (2021) Application of down-hole camera technology in fault diagnosis of coalbed methane wells. *J Phys: Conf Ser* 1894(1):012046
19. Deltombe JL, Schepers R (2002) Combined processing of BHTV travel time and amplitude images. In: *Proceedings from the seventh international symposium on minerals and geotechnical logging*, Golden, Colorado, pp 1–13
20. Gochioco LM, Magill C, Marks F (2002) The borehole camera: an investigative geophysical tool applied to engineering, environmental and mining challenges. *Leading Edge (Soc Explor Geophys)* 21(5):474–477
21. Bar N, du Plessis P, Nicoll S, Welideniya S, Ryan C, McAllister P (2018) Risk management strategies for open pit mining through historic underground workings. In: *ISRM international symposium-10th asian rock mechanics symposium*. OnePetro
22. Engelhardt HF, Harrison WD, Kamb B (1978) Basal sliding and conditions at the glacier bed as revealed by bore-hole photography. *J Glaciol* 20(84):469–508
23. Tulaczyk S, Mikucki JA, Siegfried MR, Prisco JC, Barcheck CG, Beem LH, Behar A, Burnett J, Christner BC, Fisher AT, Fricker HA, Mankoff KD, Powell RD, Rack F, Sampson D, Scherer RP, Schwartz SY (2014) WISSARD at Subglacial Lake Whillans, West Antarctica: scientific operations and initial observations. *Ann Glaciol* 55(65):51–58
24. Somaratne N, Zulfic H, Ashman G, Vial H, Swaffer B, Frizenschaf J (2013) Groundwater risk assessment model (GRAM): groundwater risk assessment model for wellfield protection. *Water* 5(3):1419–1439
25. Chapman MJ, Huffman BA, McSwain KB (2015) Delineation of areas having elevated electrical conductivity, orientation and characterization of bedrock fractures, and occurrence of groundwater discharge to surface water at the US Environmental Protection Agency Barite Hill/Nevada Goldfields Superfund site near McCormick, South Carolina (No. 2015–5084). US Geological Survey
26. Post VE, Banks E, Brunke M (2018) Groundwater flow in the transition zone between freshwater and saltwater: a field-based study and analysis of measurement errors. *Hydrogeol J* 26(6):1821–1838
27. Khan M, Michael HA, Nath B, Huhmann B, Harvey CF, Mukherjee A, Chakraborty M, Choudhury I, Ullah MS, Ahmed KM, Goodbred SL, Schlosser P, Bostick BC, Mailloux BJ, Ellis T, van Geen A (2019) Arsenic-contaminated deep groundwater in the Bengal Basin: origin and implications for mitigation. In: *AGU Fall Meeting Abstracts*, vol 2019, pp GH21A-05
28. van Rooyen JM, Veltman S, Botha F, Matthee J (2021) Groundwater resource exploration & development - focus on groundwater to support surface water supply in the Lower Olifants River, South Africa. *J Afr Earth Sc* 180:104179
29. Lau JSO, Auger LF, Bisson JG (1987) Subsurface fracture surveys using a borehole television camera and acoustic televiewer. *Can Geotech J* 24:499–508
30. Uchita Y, Harada, T (1993) Behavior of discontinuous rock during large underground cavern excavation. In: *Proceedings of the international symposium on assessment and prevention of failure phenomena in rock engineering*, Istanbul, Turkey, pp 807–816
31. Miyakawa K, Tanaka K, Hirata Y, Kanauchi M (2000) Detection of hydraulic pathways in fractured rock masses and estimation of conductivity by a newly developed TV equipped flowmeter. *Eng Geol* 56(1–2):19–27
32. Schepers R, Rafat G, Gelbke C, Lehmann B (2001) Application of borehole logging, core imaging and tomography to geotechnical exploration. *Int J Rock Mech Min Sci* 38(6):867–876
33. Lahti M (2004) Digital borehole imaging of the boreholes KR24 upper part and PH1 at Olkiluoto, Working Report 2004–28. Posiva Oy, p 21
34. Cunningham KJ (2004) Application of ground-penetrating radar, digital optical borehole images, and cores for characterization of porosity hydraulic conductivity and paleokarst in the Biscayne aquifer, southeastern Florida, USA. *J Appl Geophys* 55:61–76
35. Cunningham KJ, Carlson JJ, Hurley NF (2004) New method for quantification of vuggy porosity from digital optical borehole images as applied to the karstic Pleistocene limestone of the Biscayne aquifer, southeastern Florida. *J Appl Geophys* 55(1–2):77–90

36. Roberson S, Hubbard B (2010) Application of borehole optical televiewing to investigating the 3-D structure of glaciers: implications for the formation of longitudinal debris ridges, midre Love'nbreen, Svalbard. *J Glaciol* 56(195):143–156
37. Li SJ, Feng X-T, Li ZH, Chen BR, Zhang CQ, Zhou H (2012) In situ monitoring of rockburst nucleation and evolution in the deeply buried tunnels of Jinping II hydropower station. *Eng Geol* 137–138:85–96
38. Yuji K (1983) Observation of crack development around an underground rock chamber by borehole television system. *Rock Mech Rock Eng* 16(2):133–142
39. Li SJ, Feng XT, Li ZH, Zhang CQ, Chen BR (2012) Evolution of fractures in the excavation damaged zone of a deeply buried tunnel during TBM construction. *Int J Rock Mech Min Sci* 55(10):125–138
40. Burton CK (1973) Geology and mineral resources Johor Bahru- Kulai area, South Johore. Geological Survey of Malaysia, Ipoh
41. Scrivenor JB (1924) The geology of Singapore Island: with a geological sketch-map. *J Malayan Branch Royal Asiatic Soc* 2(1(90)):1–8
42. Alexander FES (1950) Report on the availability of granite on Singapore and the surrounding islands. Government Printing Office, Singapore
43. Walker D (1956) Studies on the quaternary of the Malay Peninsula. Pt. I. Alluvial deposits of Perak and the relative levels of land and sea. *Federal Mus J*, 1–2
44. Dodd TJ, Gillespie MR, Leslie AG, Kearsey TI, Kendall RS, Bide TP, Dobbs MR, Millar IL, Lee MKW, Chiam K, Goay M (2019) Paleozoic to cenozoic sedimentary bedrock geology and lithostratigraphy of Singapore. *J Asian Earth Sci* 180:103878
45. Woon LK, Yingxin Z (2009) Geology of Singapore. Defence Science and Technology Agency, Singapore
46. Geoquip Water Solutions Ltd R-CAM 1000 XLT Downhole Camera System. <https://www.geoquipwatersolutions.com/r-cam-1000-xlt-downhole-camera-system.html>, Accessed 02 Oct 2021
47. Overby Jr WK, Yost LE, Yost AB (1988) Analysis of natural fractures observed by borehole video camera in a horizontal well. In: Proceedings of the SPE gas technology symposium, Dallas
48. Hansen BP, Stone JR, Lane JW (1999) Characteristics of fractures in crystalline bedrock determined by surface and borehole geophysical surveys, Eastern Surplus Superfund Site, Meddybemps, Maine (Vol XCIX). US Department of the Interior, US Geological Survey, Massachusetts

Tunneling and Case Studies

Numerical Modelling of Shoring Systems: Case Study



Arunava Ray, Rajesh Rai, Ashok Jaiswal, Deepak Dagdi,
and Ajit Kumar Jha

Abstract The present paper discussed different shoring systems for retaining Earth for shallow as well as deep excavations in soil. Numerical modelling technique has been used to simulate the different types of shoring systems. Three case studies have been taken for evaluating the shoring system for excavation at other conditions. The results of the numerical simulation in terms of Bending moment, shear forces, displacement, and axial forces have been analysed for these cases. Based on the analysis, the Solder piles (ISMB 450 mm) have been suggested for Project A with a depth of 19 m. Two/three anchors were suggested with a maximum load of 600 Kn with two loops of 15.2 mm strands & 9 m bond length. The RCC Contiguous Piles of 750 @ 850 mm spacing has been installed for Project B to the depth of 18.5 m. Anchors were designed with a maximum load of 578 kN with two loops of 15.2 mm strands. The micro pile is recommended for Project C based on the geotechnical condition of the area. Self-drilling Bolts (R32N (UL = 280 KN)) with 6 m length at 2.0 × 2.0 m c/c spacing has been installed on slope surface. Anchors were installed with a maximum load of 600 kN with two loops of 15.2 mm strands & 13 m bond lengths. The paper discusses the importance of installing anchors in the conjugation of shoring structures to increase the stability of the system.

Keywords Soldier piles · Ground anchors · Micro pile · Contiguous pile

1 Introduction

Authors Earth pressure is generated during the excavation in soil. Temporary or permanent shoring systems can be used to stabilise the excavation walls. The Earth pressure is exerted by soil on a shoring system depends on many factors. The factors

A. Ray · R. Rai (✉) · A. Jaiswal
Department of Mining Engineering, IIT (BHU) Varanasi, Varanasi 221005, India
e-mail: rajeshrai.min@iitbhu.ac.in

D. Dagdi · A. K. Jha
INDIGO InfraProjects, New Delhi 110049, India

© The Author(s), under exclusive license to Springer Nature Singapore Pte Ltd. 2022
A. K. Verma et al. (eds.), *Proceedings of Geotechnical Challenges in Mining, Tunneling and Underground Infrastructures*, Lecture Notes in Civil Engineering 228,
https://doi.org/10.1007/978-981-16-9770-8_11

201

are soil structure, its interaction with the retaining wall, method of backfill placement, the degree of compaction, backfill slope, type of backfill material and drainage provisions etc. These factors play a vital role in the design of shoring systems along with types of the shoring system. With the expansion of civilization and rapid urbanization, the need for deep excavations is felt strongly. It is essential when the surrounding area along the excavation is very less, and there is nearby any important structure present.

There are two types of earth pressure exerted on shoring system due to soil excavation, i.e. active pressure and passive pressure. Active pressure is a condition where soil exerts a force on the retaining systems whose members tend to move towards the excavation. Passive pressure, on the other hand, is a condition in which a retaining system exerts a force on the soil. Depending on the shoring system value of active and passive pressure can calculate using either of the Rankine, Coulomb, Log-spiral and Trial-wedge methods. For more accurate results, active pressure should be calculated using coulomb or Rankine Theory and passive pressure should be calculated based on log-spiral and trial wedge methods. The at-rest coefficients shall be used to calculate lateral earth pressure on non-yielding walls, which are restrained from any rotation and translation.

Retaining walls rely on their structural components for retaining Earth. There are various types of retaining structures used today as shoring systems for deep excavations. In the present paper, only three types of retaining structures have been discussed and numerically analyse, i.e. soldier piles, continuous piles and micropile.

1.1 Sheet Pile Walls

These walls are generally constructed of steel sections, rail sections or timber generally placed 2 to 3 m apart. Soldier piles are pushed into the ground through bore-holes (directly in case of soft soils), and the excavation progresses step by step. At each level, horizontal waling beams of timber, in-situ concrete or shotcrete is placed between the sections. These legging are subject to the type of soil and depth of excavation. In narrow excavations, struts are placed between the walls for lateral support [1–3]. These walls are preferred in narrow excavations but can also be applied in a deep and large excavation where water seepage is an issue.

1.2 Contiguous Pile

A retaining wall can be formed by closely spaced bored piles, perhaps for the establishment of a deep basement or a cut and cover tunnel. The piles may be erected so that they virtually touch each other (contiguous). A watertight environment can be achieved by grouting the gaps between the piles.

Alternatively (secant piles) every other pile may be constructed, with their centers less than two diameters apart. In-fill piles are then bored, cutting into the adjacent piles to form continuous structures. The first sets of piles may be cast with a lower grade of concrete. These may not be load-bearing and act as ‘seals’ between the main load-bearing piles. As the pile’s interlock, this form of construction leads to a more efficient form of structure. During the excavation of the soil, the piles will generally require propping before the permanent floor, and roof structure is completed [3].

1.3 Micropile

Micropiles are high-capacity, high-performance drilled deep foundation elements typically between 5–12 inches in diameter that can reach depths of 200 feet and attain working loads of over 200 tons. Micropiles are composed of high-strength steel casing, rebar and grout. Micropiles transfer the structural load to competent foundation soils through unsuitable soil layers. The loads are transferred from the foundation through the steel and grout of the micropile and shed to surrounding rock or soil via high values of friction. Micro-piles are piles moulded in situ to serve as deep foundations and highly tensioned stress along the shaft, composed of cement and sand mortar and comprehensively reinforced throughout its length. Micro-piles are employed in the highly compact or consistent ground or in the ground where bedrock or rocky formations are found, in which excavating may only take place with the use of rotating hydraulic drills [1, 2].

The present paper analyses three different shoring systems for retaining Earth in case of deep excavations in soil. Numerical modelling technique has been used to simulate the behavior of different types of shoring systems which include bending moment, shear stress, maximum displacement of the retaining system. The utility of using anchors in association with shoring systems has also been studied.

2 Case Study A: Design of Sheet Piling

The case study of sheet piling has been taken from Project A in Gurgaon. The upper strata of this area comprise the alluvium, made up predominantly of sandy silt and silty sand with gravel. These alluviums are underlain by harder formations of the system of rocks. Soldier piles and temporary ground anchors with waler beam and timber lagging have been considered as a temporary earth retaining system for the slope section of the Project A. The groundwater table is not present within the excavation depth of 18 m. The analysis has been done by finite element method considering geotechnical properties tabulated in Tables 1, 2 and 3. The section is shown in the figure with a maximum excavation depth of the pit is 16.3 m below EGL & 14.3 M adjacent to the pile wall. It is proposed to install soldier piles of 19.0 m (i.e. about 1.33 times of the excavation) before the excavation. Several models have

Table 1 Soil parameters used in the finite element modeling

No	Name	Depth [m]	ϕ_{ef} [°]	cef [kPa]	ρ [kN/m ³]	ν [-]	E [MPa]
1	Silty sand	5	30.00	2.00	17.20	0.28	7.50
2	Sandy silt	10	30.00	3.50	17.40	0.28	7.50
3	Sandy silt with gravel	14	30.00	5.00	17.80	0.28	9.00

Table 2 Anchor properties used in the finite element modelling

Tieback	Depth, m	length, 1 m	Bond length %	Slope [°]	Bond shear stiffness MN/m/m	Anchor spacing m
No 1	3.5	18	50	20	100	3.2
No 2	8.2	18	50	20	100	3.2
No 3	11.5	18	50	20	100	2.4

Table 3 Structural properties used in the finite element modelling

No	Name	Mod. of ele. MPa	Poisson's ratio -	Section length m	I M ⁴ /m	FArea m ² /m
1	Liner (AA')	200,000	0.296	19.0	3.040E-04	9.2E-03

been prepared and simulated by considering various permutation/combination of different size of a girder, anchors capacity and spacing. The load of the infrastructure on the ground adjacent to the proposed site has been assumed around 20 kN/m². Three layers of anchors at 3.5, 8.2 m and 11.5 from the surface have been installed in the subsequent stage of excavation at Project A. The inclination of anchors has been considered 200 from horizontal. The discretized view of excavation is shown in Fig. 1. The excavations and anchored have been carried out in stages.

2.1 Results and Discussions: Project A

The shoring system has been analysed with Phases2. The results obtained for bending moment, shear forces, and displacement are shown in figures. Figure 2 shows the plot of major principal stress in a subsequent stage during the excavation and installation of anchors. Figure 3 shows the results of different stages in terms of horizontal displacement due to excavation. Figure 4 and 5 show the bending moment and shear force on structure with depth from the surface, respectively. The maximum bending moment is 107.10 kNm in stage 7. The maximum axial forces on anchors are 571.34 kN in anchor no 3 at stage 7.

2.2 Case Study B: Design of Contiguous piling

The contiguous piling case study has taken from Project B in New Delhi. The maximum excavation depth of the pit is 13.0 m below EGL. The retaining system of RCC Contiguous piles has been considered for analysis purpose. Installation of vertical shoring system of RCC Contiguous piles and ground anchors is proposed to stabilise the ground behind the shoring wall. The analysis has been done the Finite Element Method using properties of soil (Table 4), properties of anchors (Table 5) and properties of the interface (Table 6).

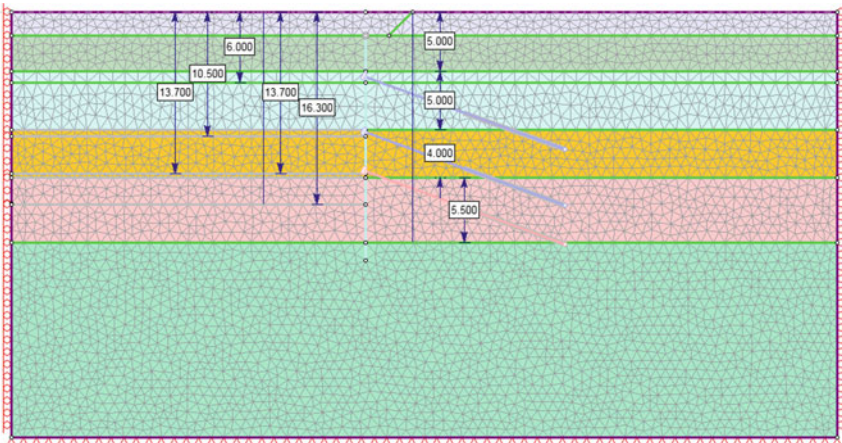


Fig. 1 A discretised model of excavation by the finite element method

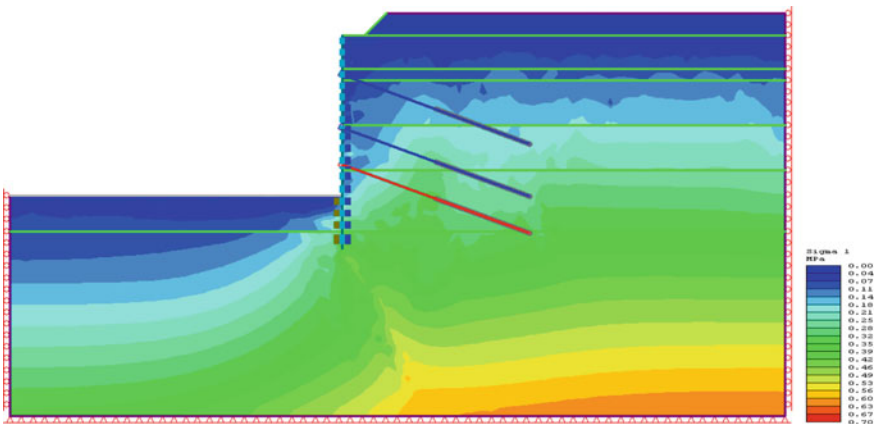


Fig. 2 Major principal Stress in final Stage

The simulation is carried out with the installation of RCC Piles (750 mm dia) of upto 18.5 m depth at a spacing of 850 mm c/c anchors in layers. Several models have been prepared and simulated by considering various permutation/combination of different size of piles, anchors capacity and spacing. The inclination of anchors has been considered 250 from horizontal. A surcharge of 60.00 KN/m² has been applied on the surface for construction works loading. The discretised view of excavation has been shown in Fig. 6 with anchored.

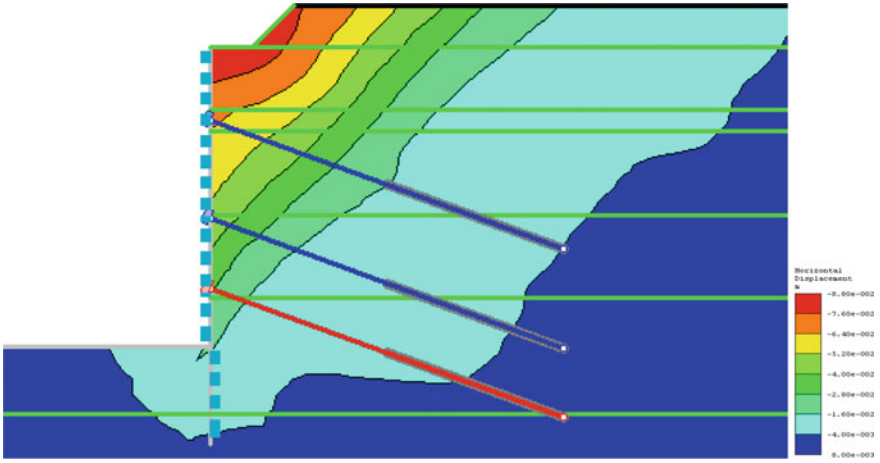


Fig. 3 Horizontal displacement in final stages

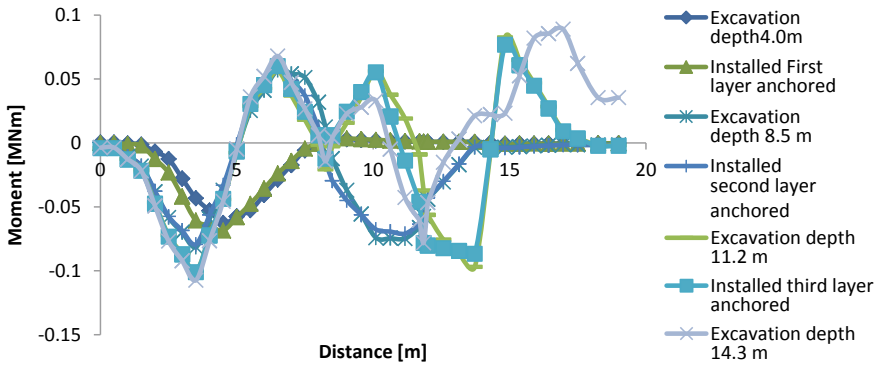


Fig. 4 Bending moments in structure element at various excavation stages

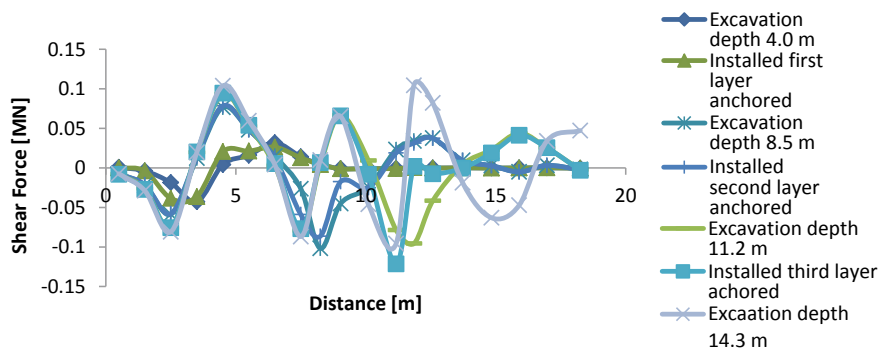


Fig. 5 Shear forces in structural element at various excavation stages

Table 4 Soil parameters used in the finite element modelling

No	Name	Depth [m]	ϕ_{ef} [°]	c_{ef} [kPa]	ν [-]	E [MPa]
1	Fill	2	5	2.00	0.28	8.0
2	Sandy silt	11	5	3.50	0.28	12.00
3	Sandy silt -2	18	5	5.00	0.28	12.00
4	Sandy Silt -3	20	5	5.00	0.28	12.00

Table 5 Anchor properties used in the finite element modelling

Tieback	Depth, m	length, l m	Bond length %	Slope [°]	Bond shear stiffness MN/m/m	Anchor spacing m
No 1	2.5	18	50	25	100	3.4
No 2	6.5	18	50	25	100	3.4
No 3	9.5	18	50	25	100	3.4

Table 6 Structural properties used in the finite element modelling

No	Name	Mod. of ele. MPa	Poisson's ratio -	Section length m	I M4/m	Area m2/m
1	Liner (AA')	28,284	0.20	19.0	0.013	0.37

2.3 Results and discussions: Project B

The earth retaining system has been analysed by the Finite element method. Various models have been simulated and result in terms of horizontal displacement and forces on anchors and structure are shown in figures. Figure 7 shows the plot of major principal stress in a subsequent stage during the excavation and installation of anchors. Figure 8 shows the results of different stages in terms of horizontal

displacement and bending moment due to excavation. Figure 9 and 10 show bending moment and shear force on Anchors. The maximum bending moment is 332.48 kNm. The maximum axial forces on anchors are 522 kN.

2.4 Case Study C: Design of Micropile

The current project was required steep/vertical shoring excavations up to -18.0 m for required multilevel structure construction. The analysis has been done by finite element method considering geotechnical properties for the project based on the field investigation & data available. The proposed excavation has been done in two stages. Therefore, two types of stabilising system are proposed and checked using the finite element method.

1.0 (Slope Stabilization – Grouted Bolts & Shotcrete): A combination of Self Drilled Rock (SDR) Bolts is proposed along with wire mesh & shotcrete to stabilise top 6–8 m height with a slope angle ranging from $55\text{--}75^\circ$.

2.0 (Micro Pile – Anchor System): A Combination of 168 Dia Grouted Steel Micro Piles is proposed along with tieback anchors & walers as shown in drawings.

The SDR Bolts at 2×2 m (H: V) with 6 m length & 100 mm thick wire mesh with shotcrete has been installed. Steel Micro piles (168 mm dia) of up to 12.0 m depth at a spacing of 1000 mm c/c has also been installed with anchors in layers stressed against walers.

Several models have been prepared and simulated by considering various permutation/combination of different size of pipes, anchors capacity and spacing. The inclination of anchors has been considered 250 from horizontal. A surcharge of

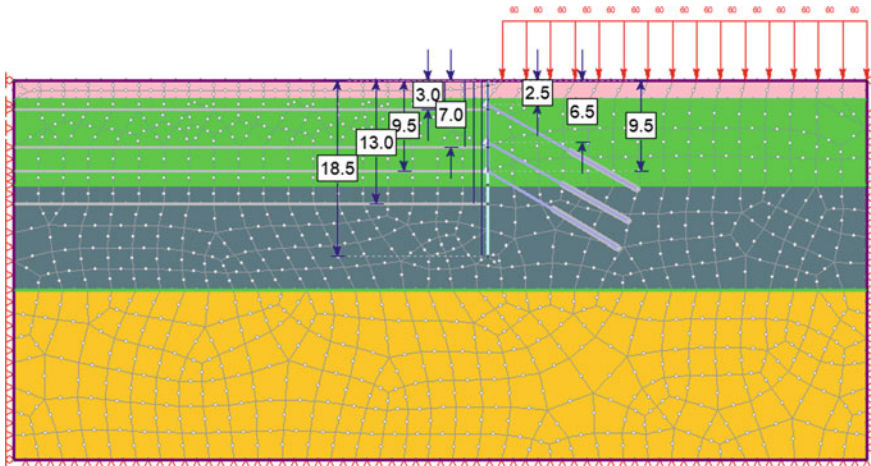


Fig. 6 A discretised model of excavation by the finite element method

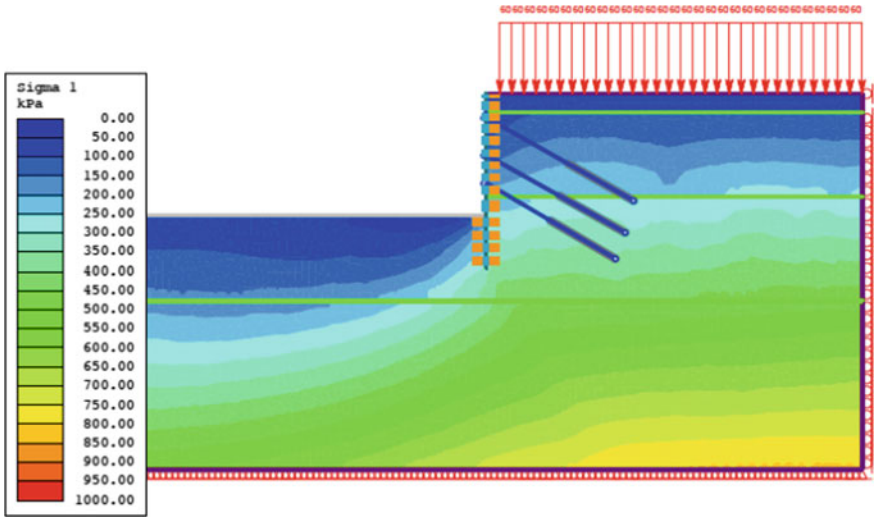


Fig. 7 Major principal stress due to excavation (final Stages)

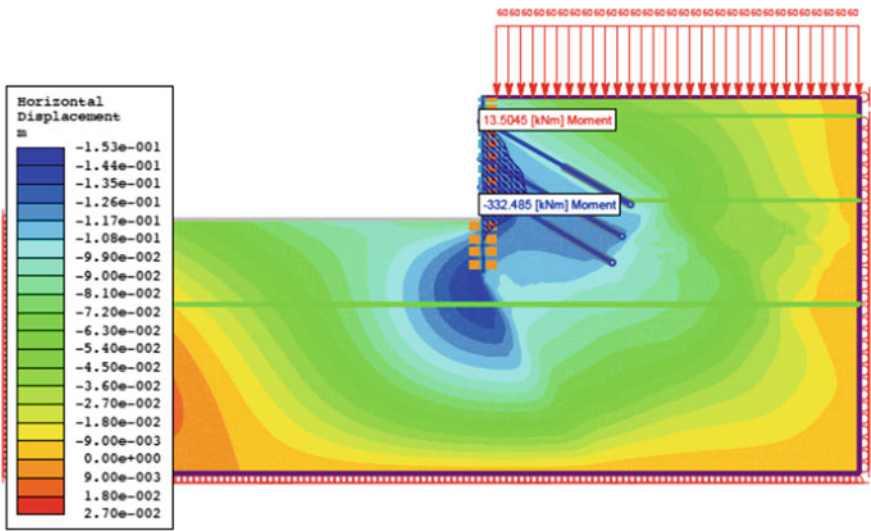


Fig. 8 Horizontal displacement & Bending Moments on Pile Wall (Various Stages)

20.00 KN/m² has been applied on the surface, i.e. 4.00 m with a length of 30.00 m from the excavation edge around. Elastic behaviour of bolt and grout material has been taken during simulation (Tables 7, 8 and Figs. 11, 12).

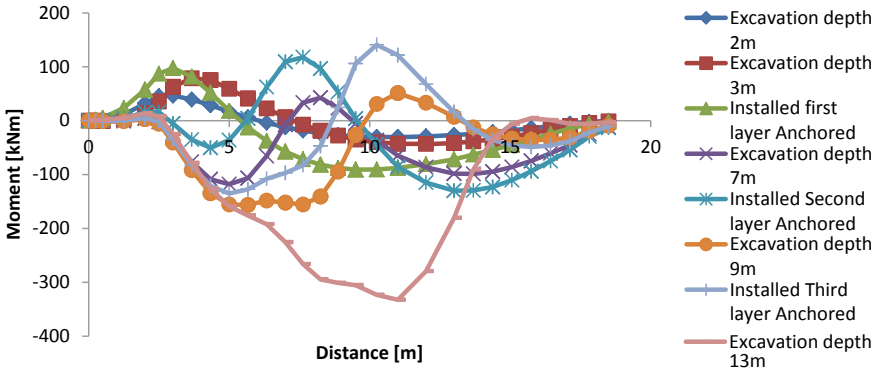


Fig. 9 Bending moments in structure element at various excavation stages

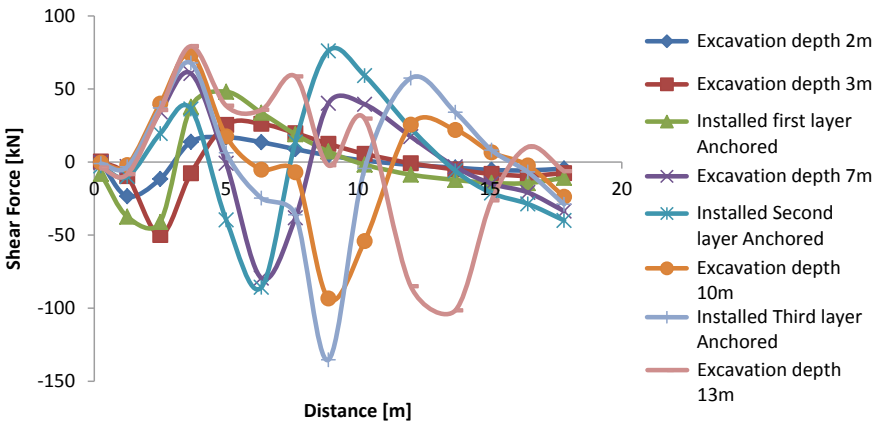


Fig. 10 Shear forces in the structure element at various excavation stages

Table 7 Physico-Mechanical Properties of soil

No	Name	Depth [m]	ϕ_{ef} kPa	c_{ef} kPa	ν []	E [MPa]
1	Soil	20	10	10	0.28	12

2.5 Results and Discussions: Project C

Various models have been simulated and result in terms of horizontal displacement and forces on anchored and structure are shown in figures. Figure 5 shows the plot of major principal stress in the subsequent stage during excavation and installation of anchors. The legend shows the value of stress in kPa. Figure 6 shows the results of different stages in terms of horizontal displacement and bending moment due to excavation. Figure 7 shows shear stress and axial force on the bolt with maximum

Table 8 Properties of liner

Linear	Linear 1	Linear 2
Linear type	Reinforced concrete	Reinforced concrete
Formulation	Timoshenko	Timoshenko
Reinforcement		
Type	Wire Mesh (dia = 4 mm)	Hollow section (PIPE): Pipe152STD
Spacing	0.1 m	1 m
Section depth	0.004 m	0.168 m
Area	1.26e-005m ²	0.00337 M ²
Moment of inertia	1.2566e-011 m ⁴	1.1e-005m ⁴
Young's modulus	2e + 007 kPa	2e + 008 kPa
Poisson ratio	0.25	0.2
Compressive Strength	400000 kPa	400000 kPa
Tensile Strength	400000 kPa	400000 kPa
Concrete		
Thickness	0.1 m	0.2 m
Young's modulus	3E + 006 kPa	3e + 007 kPa
Poisson ratio	0.2	0.2
Compressive strength	25000 kPa	25000 kPa
Tensile strength	3000 kPa	3000 kPa
Equivalent Young's modulus	3.16539e + 006kP	3.47969e + 007 kPa
Equivalent thickness	0.0995732 m	0.19979 m

value. The maximum bending moment is 106.325 kNm. The maximum axial force anchors are 596.16 kN in Anchor (Figs. 13, 14, 15, 16 and 17).

3 Discussion

Shoring is a type of retaining wall commonly used when installing the foundation of a building for supporting deep excavations. A shoring system such as piles and lagging or shotcrete will support the surrounding loads until the underground levels of the building are constructed. There are several different shoring types that construction professionals use. For the present study, the three types of retaining structures which include soldier piles, continuous piles and micropile have been discussed and numerically analyse. Major principal stress in subsequent stage during the excavation and installation of anchors shows maximum concentration near the excavated face for all

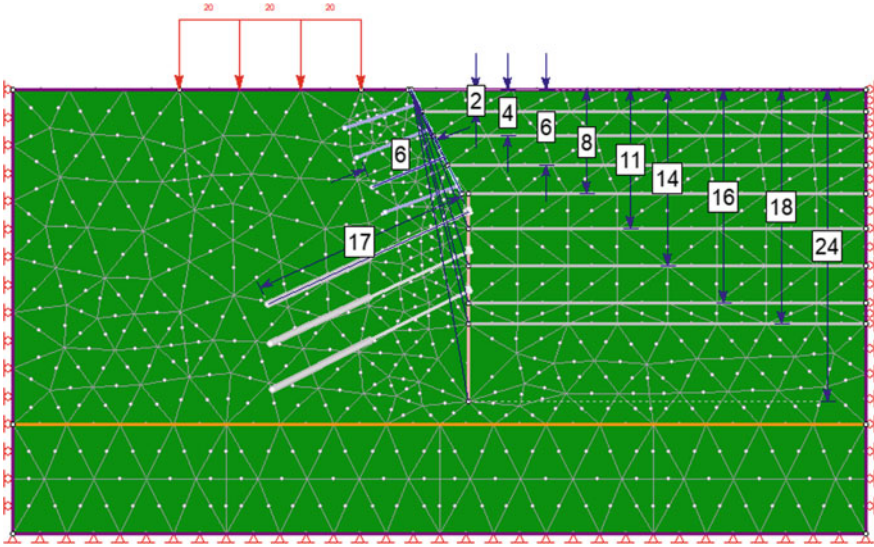


Fig. 11 Section at maximum Excavations depth (stage 1: No excavation)

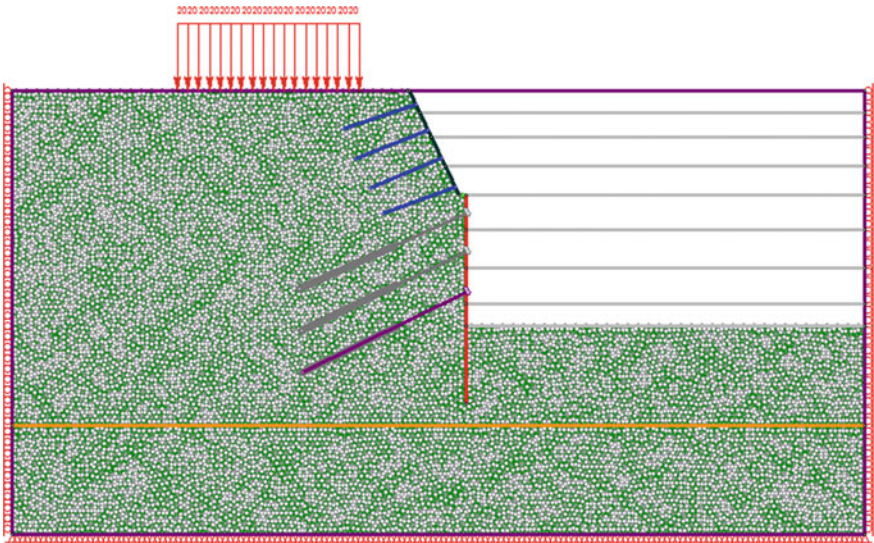


Fig. 12 Section at maximum Excavations depth (Excavation 18 m)

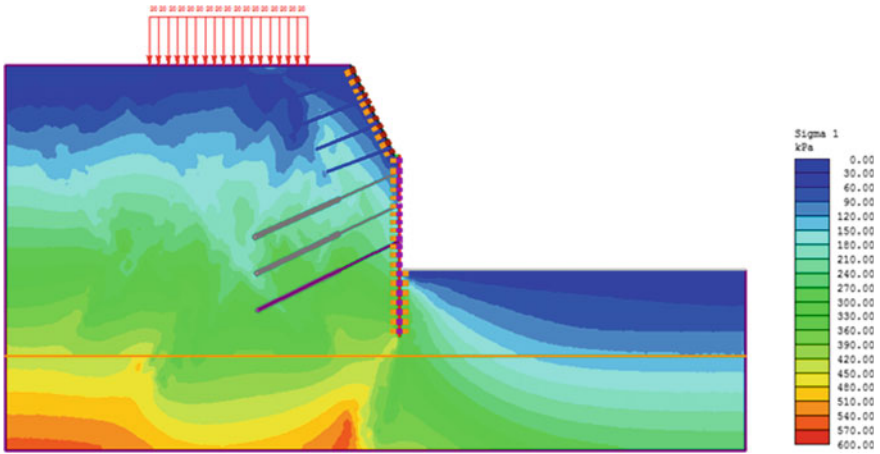


Fig. 13 Major principal stress to excavation (Zone A)

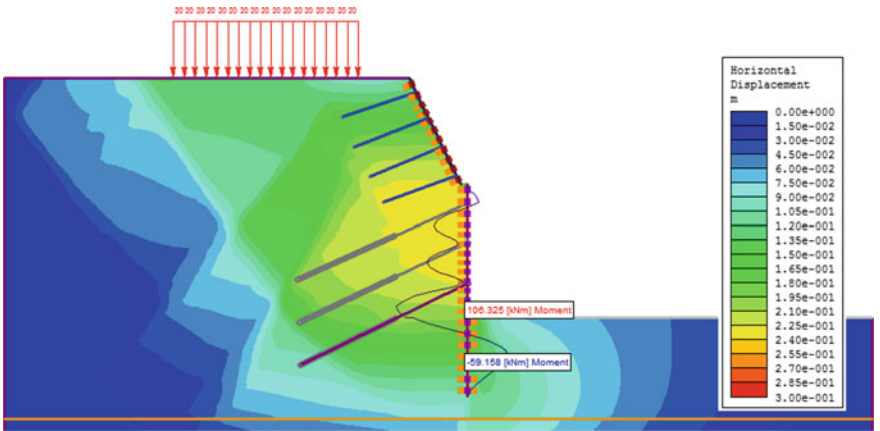


Fig. 14 Horizontal displacement due to excavation (Zone A) and various force on structure

the three case studies. The maximum bending moment on various retaining structures is increasing with increase in depth of excavation. Contiguous piling has been proposed for Case B where the depth of excavation is less compared to other two site still it has maximum bending moment occurring on the retaining wall. The maximum axial force occurring in the installed anchors is observed to be maximum for anchors installed at the lower portion of the retaining wall. The maximum horizontal displacement is observed to occur in the middle part of the retaining structure. The analysis indicates that the selection of any particular type of retaining structure will depend on the maximum bending moment and maximum shear force on the retaining wall. Also, the position of various support anchors is important to increase the utility of the installed shoring system. The anchor length increases with increase in the depth

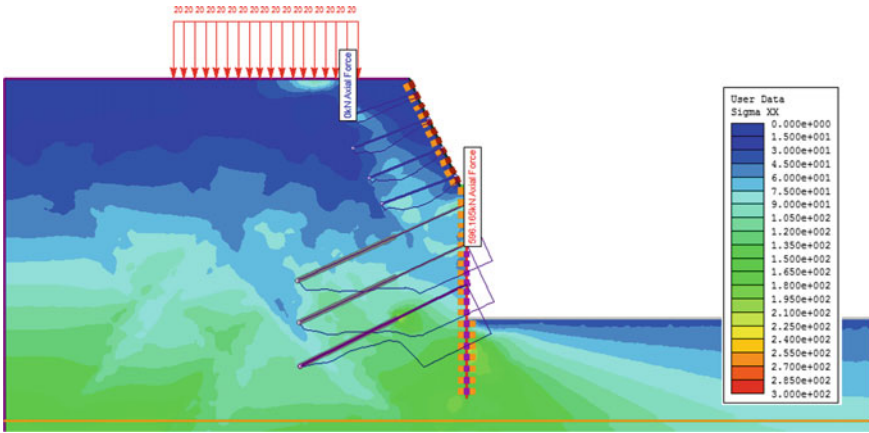


Fig. 15 Shear stress due to excavation (Zone A) and various force on bolts

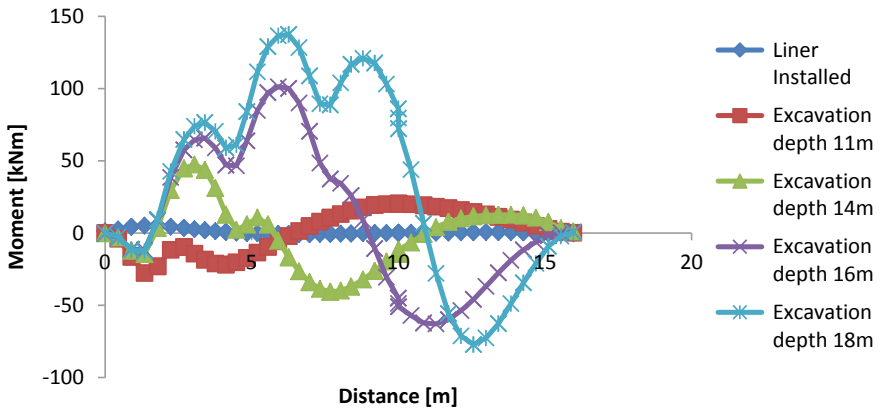


Fig. 16 Bending moments in structure element at various excavation stages

of placement of the anchors. Overall, the reliability of the shoring system depends on the combination of the retaining wall along with the supporting anchors. Before installing any retaining structure, numerical analysis must be performed to obtain the maximum bending moment and shear stress that will be acting on the retaining structure. Also, the support anchors must be placed in order to increase the stability of the shoring system.

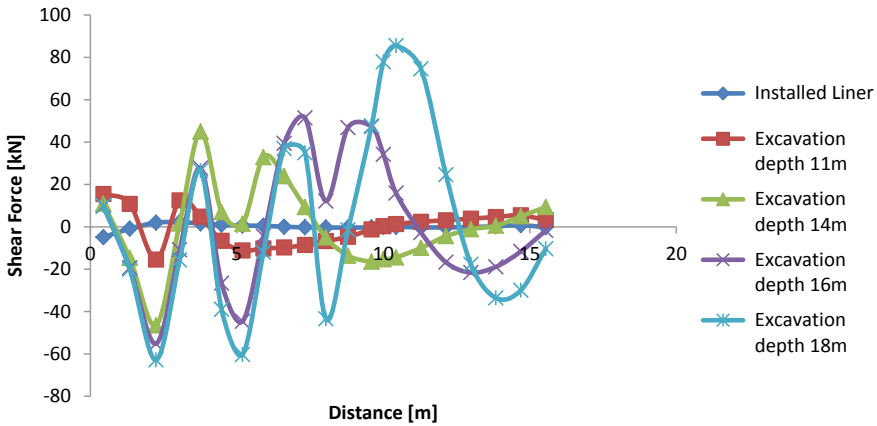


Fig. 17 Shear forces in structural element at various excavation stages

4 Conclusion

The design of shoring systems for deep excavation involves a systematic process of determination of earth pressures. The shoring system has been analysed by PHASE 2D based on the finite element method. Results obtained in terms of bending moment, shear forces, displacement and axial forces. The proposed shoring system is recommended for implementation at Project A, B and C are given below.

- The Solder piles (ISMB 450 mm) has been installed in Project A. The depth of soldier pile is 19 m, and excavation depth of the pit is 16.3 below EGL and 14.3 M adjacent to the pile wall. Soldier piles have been bored and inserted at 1.6 m (centre to centre) spacing. Anchors were designed with max. Load of 600 kN with 2 loops of 15.2 mm strands & 9 m bond length.
- The RCC Contiguous Piles of 750 @ 850 mm spacing has been installed for Project B up to the depth of 18.5 m. Tie back anchors shall be installed at shown levels with (centre to centre) spacing& capacities as shown in the drawings. Anchors were designed with max. load of 578 kN with 2 loops of 15.2 mm strands. Excavation should be carried out in steps of 1.5–2.0 m with shotcrete application between the piles.
- The micropile is recommended for Project C based on the geotechnical condition of the area. The Earth adjacent to shoring wall shall be excavated in steps not deeper than 2 m. First Layer Shotcrete to be applied for 25–40 mm thickness followed by wire mesh laying. The proposed shoring system is recommended for implementation at the current project site. Self-Drilling Bolts (R32N (UL = 280 KN)) with 6 m length at 2.0 × 2.0 m c/c spacing has been installed on slope surface. Micro Pile of 168 mm dia and 7 mm thick MS Pipe with fully Grouted has been installed at 1000 mm c/c. Anchors were installed with a maximum load of 600 kN with 2 loops of 15.2 mm strands & 13 m bond lengths.

References

1. Elsaied AE (2014) Performance of footing with single side micro-piles adjacent to slopes. *Alex Eng J* 53(4):903–910
2. Srivastava A, Kumar P, Babu GS (2016) Stability analyses of 18 m deep excavation using micro piles. IGC, Delhi
3. Cheng XS, Zheng G, Diao Y, Huang TM, Deng CH, Lei YW, Zhou HZ (2017) Study of the progressive collapse mechanism of excavations retained by cantilever contiguous piles. *Eng Fail Anal* 71:72–89

Effect of Ground Vibration Due to Blasting Activity in Large Section Tunnel Close to Pantai Timur Highway LPT 1



Azita Yusoo, Edy Tonnizam Mohamad, and Mohd Saidini Misnan

Abstract Tunnel blast activity for East Cost Railway Project is close to the Pantai Timur Highway at Kuantan, Pahang. Due to the constant rains and humid conditions in the tropical area, rock mass is subjected to severe weathering. This zone is characterized by a thick weathering profile, which necessitates careful caution during blasting. Weathered rock material has a complicated behaviors that is sometimes neglected, especially when dealing with development blasts. Type of rock which is granite was consider in this study. The rock mass character such as strength, geological structure, and discontinuities are affecting the blast design. This needs accurate data, particularly during the development stage, especially when dealing with weathered zones. Various research gaps of different rock mass classification system and safe blasting design are discussed. Field mapping and relevant laboratory, namely point load and compressive strength tests were carried out to establish the rock mass properties. Fifty rock samples were taken from the tunnel, Ch 336 + 996 to Ch 336 + 640. The average of I_{50} for Sample is 1.2 MPa and the UCS average is 26.51 MPa which is Grade V granite and excavated 56 m from the tunnel face. Rock Grade IV excavated 56 to 176 m and the average I_{50} and UCS is 1.77 and 30.05 MPa. Rock Grade III excavated 176 to 356 m, I_{50} average is 3.11 MPa and UCS average 60.42 MPa. Once the rock mass properties have been established, the effect of blast, i.e. fragmentation, flyrock, vibration and air blast were determined in order to find their relationship with the blast design adopted. Based on the result from the analysis, the blast design and method will be suggested to improve the safety and health of the workforce. In another case study, rock mass classification is suggested based on exploration data consisting of Q value from the tunnel face mapping, degree of

A. Yusoo (✉)

Department of Geotechnics and Transportation, School of Civil Engineering, Universiti Teknologi Malaysia (UTM), 81310 Skudai, Johor, Malaysia
e-mail: azitayusoo@gmail.com

E. T. Mohamad

Centre of Tropical Geoengeering (GEOTROPIK), Universiti Teknologi Malaysia, 81310 Skudai, Johor, Malaysia

M. S. Misnan

Faculty of Built Environment and Surveying, Universiti Teknologi Malaysia, 81310 Skudai, Johor, Malaysia

weathering, degree of hardness and fracture attitude. The three-bench method of blasting was introduced, and new blast design was adopted prior to make good the safety and health of the workforce during tunnel blasting activity.

Keywords Tunnel · Blast design · Rock mass classification · Fragmentation · Vibration · Q value · Safety and health

1 Introduction

In modern times, explosions have become a necessity for rock and other solid drilling, such as open-cutting, quarrying, tunneling, sinking and mining in general. In civil engineering, rock is removed to create structures such as tunnels, hydraulic channels or caverns, or deep excavation at the ground surface for road cuts, foundation or basements [1]. Blasting one of the process and method to break a solid rock by using explosive. Blasting is an accompanied develop a gas at a high temperature and under a tension sufficiently great to overcome the resistance of the enclosing body and which is thus shattered also the disintegrated. Before using the blasting method, rock was breaking and excavated by using hammer and chisel method, or by the ancient process of ‘fire-setting’ such as building a fire against the rock, which, on cooling, splits and flakes off. Water was often applied to the heated rock to hasten disintegration the loosened portion and being afterwards removed by pick or hammer and wedge.

Ground vibration is very important to consider due to avoid any incident and to protect the existing structure from any damage from blasting activity. The vibration is measure by using the instrumentation which is vibrometer. The results obtained from the instrument is numerical simulation can be compared with field experiments during all the blasting time period or in terms of magnitude values. The comparison of time results obtained with these two methods is usually used in the case of a sole explosion such as in metro due to terrorist act. A comparison of magnitude values can be used in the case of blasting shots with time delay such as explosions at a tunnel face during tunnel excavation by blasting method [2]. In Malaysia, the limitation of vibration allowable is 3 mm/sec for the historical building and it’s applied to all blasting activity in Malaysia. Refer to previous researcher, on how high vibration buildings can tolerate without damage was performed in the 50–70’s, especially in Sweden and in North America [3].

Ground vibration is affected by blast design parameter, the type of rock and mechanical properties of rock mass, type of explosive used, the geology condition of blasting pace and the distance of blasting area to the measurement structure. Vibration depends on two parameters, maximum charge used per delay as well as distance between blast face and monitoring point [4]. Refer to previous study, [5] In terms of the propagation law of blasting vibration, based on a large amount of monitoring data, studied the impact of different rock formations, different detonators, and explosives on the surface movement caused by blasting vibration near the underground. Beside

that, the blasting without control may occur the accident, flyrock and ground vibration are the source of the most injuries and damage in blasting works [4]. Refer to previous researcher, in smooth wall blasting, the final row of holes contains a lighter than normal charge, possibly a smaller burden and is ignited after the main charge is completed in order to limit the confinement of the holes and reduce damage back into the sidewalls [6].

2 Engineering Overview

The Malaysian government intends to link Kuala Lumpur and Port Klang to the east coast by building a strategic rail network, as part of its overall transportation plan. One of the major transportation projects planned for the East Coast Economic Region (ECER) is the Design and Construction of the East Coast Rail Link (ECRL). This railway will be designed for transport of cargoes and passengers between the east and west coasts of Malaysia. Gambang Tunnel has a north portal chainage of CH336 + 417 and a south portal chainage of CH337 + 025, with a total length of 608 m. The tunnel is a railway double track, and the area is 145 m². The engineering geological conditions for Gambang Tunnel is denuded hills and interdunal valleys, with large topographic relief in the hills. The location of Gambang Tunnel 1 shown in Fig. 1.

The tunnel was excavated through the granite. The Stratum lithology silty clay, yellowish gray and brownish red in color, hard plastic, with a thickness of approximately 0–2 m, interbedded with completely weathered sandstone; underlying Triassic (T) sandstone, grayish yellow and light brown in color, which is strongly to moderately weathered and among them is the highly weathered crushed sandstone with a

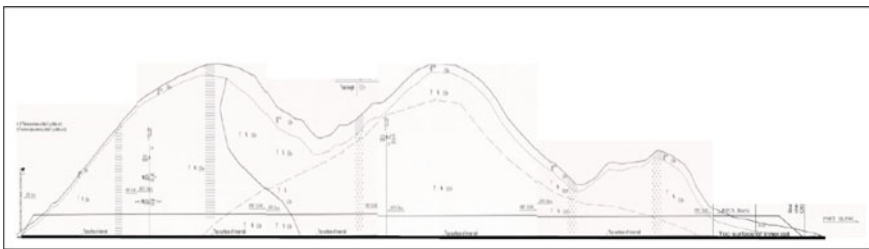


Fig. 1 Gambang tunnel 1

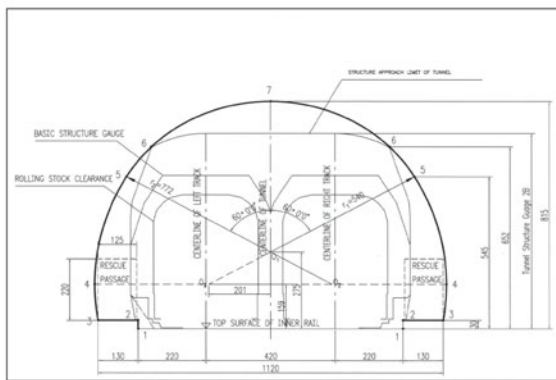
Table 1 Classification of surrounding rock

Start chainage	End chainage	Granite classification	Q-Value
336 + 417	336 + 540	V	0.04–0.10
336 + 540	336 + 640	IV	0.1–0.4
336 + 640	336 + 820	III	1.0–10
336 + 820	336 + 940	IV	0.1–0.4
336 + 940	337 + 025	V	<0.04

thickness of 2–50 m. The lower layer is moderately weathered rock. T granite, grayish white, moderately weathered silty clay, hard plastic; $c' = 27$ kPa, $\varphi' = 32.2^\circ$. Sandstone, highly weathered, point load strength: 1.21–3.47 Mpa; Sandstone, moderately weathered, saturated compressive strength: 29–45 Mpa. Average = 37 Mpa. Granite, highly weathered; Granite, moderately weathered, saturated compressive strength: 21–63 Mpa. Average = 36.8 Mpa. The classification of surrounding rock at Gambang Tunnel is presented in Table 1. The tunnel profile is shown in Fig. 2(a) and the tunnel section is shown in Fig. 2(b) below. The excavation of tunnel was started from south portal (Table 2).



(a)



(b)

Fig. 2 a Gambang Tunnel earth profile b Tunnel cross section

Table 2 ISRM (2007) suggestion for classification and description of rock masses

Term	Description	Class
Fresh (F)	No visible sign of matrix weathering; some rock discoloration may be present along main discontinuities	I
Slightly weathered rock (SW)	Discoloration of rock indicates beginning of rock matrix weathering and along discontinuities surfaces. All rock matrices can be discolored by weathering and can be slightly softer externally than in sound condition	II
Moderately weathered rock (MW)	Lower than half of rock matrix is decomposed or disintegrated to soil condition. Sound or discolored rock is present forming discontinuous zones or as corestones	III
Highly weathered rock (HW)	More than half of rock matrix is decomposed or disintegrated to soil condition. Sound or discolored rock is present forming discontinuous zones or as corestones	IV
Completely weathered rock (CW)	All rock matrices are decomposed or disintegrated to soil condition. Original structure of rock mass is commonly preserved	V
Residual soil (RS)	All rocks are transformed into soil. Geological structure of rock mass is destroyed. There is a great volume variation but no significant soil transport is present	VI

2.1 Sample Preparation

The PLT was conducted on 50 sample cores and the UCS was carried out on 50 rock cores obtained from Gambang Tunnel. For these samples, PLT and UCS are conducted at same chainage of excavation. The sample was collected within 10 to 360 m of excavation length. Preparation of samples was carried out according to ASTM D4543-08. Rock core were cut and polished to achieve desired dimensions and acceptable tolerances. Sample ends were polished to reduce the end friction effects in UCS.

2.2 Point Load Test

The point load test is an index test that classifies rocks based on their strength. Other intact rock properties with which the test correlates, such as uniaxial compressive and tensile strength, can be calculated using test. This index test involves subjecting a rock specimen to an increasing amount of focused stress until the material splits. Coaxial, truncated conical platens distribute the focused stress. To compute the point

load strength index and estimate the uniaxial compressive strength, the failure load is applied. The PLT is used as an efficient and applicable method to rock classification [7]. From the PLT result, the strength of rock is obtained. From the research, there is 50 sample of rock are taken and tested at ECRL laboratory. The point load strength index determined by PLT must be corrected to the standard equivalent diameter (D_e) of 50 mm. If the cores being tested have approximately 50 mm diameter, such correction is not needed. The suggested equation for PLI value I_s , by ASTM is as followed [7].

$$I_{s(50)} = (D_e/50)^{0.45} P_u / D_e^2 \quad (1)$$

where P_u and D_e are the failure load and the equivalent diameter which is the core diameter for immaterial test.

2.3 Uniaxial Compression Test

The Unconfined Compression Test is a laboratory test that determines a rock specimen's Unconfirmed Compressive Strength (UCS). The greatest axial compressive stress that a specimen may sustain under zero confining force is known as unconfirmed compressive strength (UCS) and the International Society of Rock Mechanics has standardized the UCS technique. The following simple equation may be used to compute the UCS value.

$$UCS = F/A \quad (2)$$

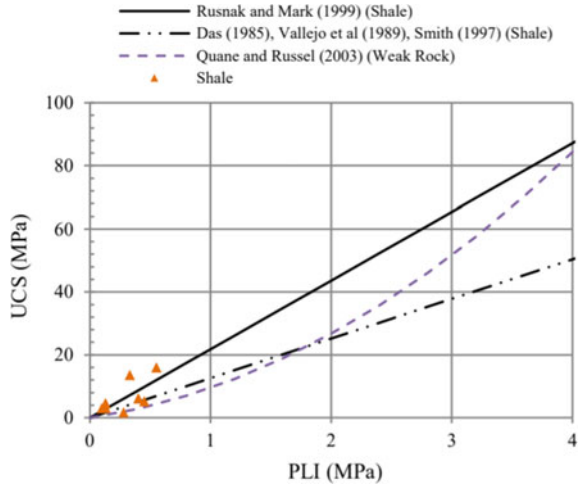
where F and A denote the maximum applied force and the cross - sectional area of the specimen, respectively. According to ASTM, if the length-to-diameter ratio is not on the order of two, USC should be rectified as follows:

$$UCS^* = \frac{UCS}{0.88 + \frac{(0.24d)}{h}} \quad (3)$$

where UCS^* is the corrected UCS for $h/d = 2$, h , d , and A are the height, diameter and cross - sectional area of the specimen, respectively.

Generally, the correlation between UCS and PLI for shale specimens is agreed well with the pervious correlation equations. In the case of marlstones, the results are almost agreed with the presented equation for sedimentary rocks, in particular for siltstone [7] (Fig. 3).

Fig. 3 Correlation between UCS and PLI for shale specimens [7]



2.4 Safety

Safety in blasting in blasting activity is very important to consider due to prevent any incident happened. The rock mass properties and blasting design also the blasting method applied were affect the safety performance. If the miner is unable to minimize the overbreak, there are a variety of safety issues, including decreased support capacity of support units spaced wider than planned, unravelling of the rock between supports needing frequent rehabilitation, extra energy imparted to loose rocks during a seismic event, and lowered support capacity owing to inadequate installation under challenging conditions. Factors such as flyrock and toxic fumes must be taken into account to insure the safety of persons and property from the results of a blast [8].

3 Results

3.1 ECRL Use Rock Test Result

Table 3 below shows rock is completely weathered rock which is class V for Gambang Tunnel use which includes I_s (MPa) and $I_{s(50)}$ (MPa) shows the sample of 15 rocks type V with estimate I_s (MPa) 1.18, $I_{s(50)}$ (MPa) 1.21 and estimate UCS with 22.25, average I_{50} (MPa) 1.21 and Average UCS 26.51. This shows UCS is in normal range for rock class V for the 15 samples of rocks. Average UCS it shows it slightly higher than point load test index. In term of point load index, MPa strength designation for rock class V shows is in high strength designation, I_{50} (MPa) 1.21 is in high strength designation and average I_{50} (MPa) 1.21 is also high strength designation.

Table 3 Point load test Index result and UCS at Ch336 + 996 to Ch 336 + 940

Rock classification	No	I _s (MPa)	I _{s(50)} (MPa)	Estimate UCS	Average I _s (50) (MPa)	Average UCS
V	1	1.38	1.39	30.51	1.21	26.51
	2	1.19	1.20	26.34		
	3	1.07	1.10	24.12		
	4	1.05	1.05	23.12		
	5	1.41	1.40	30.76		
	6	1.10	1.11	24.50		
	7	0.92	0.94	20.69		
	8	1.02	1.05	23.18		
	9	0.97	1.04	22.91		
	10	1.18	1.20	26.44		
	11	1.28	1.30	28.59		
	12	1.39	1.43	31.41		
	13	1.48	1.43	31.53		
	14	1.38	1.42	31.35		
	15	0.96	1.01	22.25		
Total	1.18	1.21	26.51	1.21	26.51	

Table 4 below shows rock classifications of class IV for Gambang Tunnel which is the material more than half of rock matrix is decomposed or disintegrated to soil condition. Sound or discolored rock is present forming discontinuous zones or as core stones and use which includes I_s (MPa) and I_{s(50)} shows the sample of 20 rocks type IV with estimate I_s 1.84 MPa, I_{s(50)} is 1.87 MPa and Estimate UCS with 41.10 MPa, average I_{s(50)} is 1.77 MPa and Average UCS 39.05 MPa. This shows UCS not in normal range for rock classification of IV for the 20 samples of rocks. Average UCS and estimate UCS shows it slightly higher than point load test of index. In term of point load index, MPa strength designation for rock classification of IV shows is in high strength designation, I_{s(50)} is 1.87 MPa is in high strength designation and average I_{s(50)} is 1.77 MPa is also high strength designation.

Table 5 below shows rock class III Moderately weathered rock (MW) for Gambang Tunnel use which includes I_s (MPa) and I_{s(50)} (MPa) shows the sample of 15 rocks class III with estimate I_s (MPa) 2.94, I_{s(50)} (MPa) 2.94 and Estimate UCS with 64.74, average I_{s(50)} (MPa) 3.11 and Average UCS 60.42. This shows UCS not in normal range for rock classification of III for the 15 samples of rocks. Average UCS and estimate UCS shows it slightly higher than point load test of index. In term of point load index, MPa strength designation for rock classification of III shows is in high strength designation, I_{s(50)} (MPa) 2.94 is in high strength designation and average I_{s(50)} (MPa) 3.11 is very high strength designation.

Table 4 Point load test Index result and UCS at Ch336 + 940 to Ch336 + 820

Rock classification	No	Is (MPa)	I _{s (50)} (MPa)	Estimate UCS	Average Is (50) (MPa)	Average UCS
IV	16	1.82	1.82	40.15	1.77	39.05
	17	1.73	1.78	39.06		
	18	2.02	1.95	43.00		
	19	1.70	1.74	38.29		
	20	1.95	1.90	41.69		
	21	1.41	1.45	31.84		
	22	1.35	1.39	30.60		
	23	1.61	1.63	35.86		
	24	1.64	1.60	35.19		
	25	1.78	1.84	40.46		
	26	1.83	1.89	41.68		
	27	2.07	2.07	45.64		
	28	2.13	2.16	47.55		
	29	1.94	1.98	43.46		
	30	1.31	1.33	29.20		
	31	1.70	1.74	38.37		
	32	1.63	1.69	37.24		
	33	1.88	1.92	42.29		
	34	1.82	1.85	40.64		
	35	1.64	1.76	38.79		
Total		1.84	1.87	41.10	1.77	39.05

3.2 Qvalue

Figure 4 below show the mapping result at Gambang Tunnel Ch336 + 971 to Ch336 + 941 conducted using Geological Radar Mapping. The Q_{value} from the tunnel face mapping 0.11. The stability of rock is poor, and groundwater slightly develop.

Figure 5 shown the mapping result at Ch336 + 867 to Ch336 + 837 conducted using Geological Radar Mapping. The Q_{value} from the tunnel face mapping 1.08. The stability of rock is fair and there is a risk of falling stone and collapsing from vault.

Figure 6 shown the mapping result at Ch336 + 821 to Ch336 + 791 conducted using Geological Radar Mapping. The Q_{value} from the tunnel face mapping 1.08. The stability of rock is fair and there is a risk of falling stone and collapsing from vault.

Table 5 Point load test Index result and UCS at Ch336 + 820to Ch336 + 640

Rock classification	No	Is (MPa)	I _s (50) (MPa)	Estimate UCS	Average I _s (50) (MPa)	Average UCS
III	36	3.13	3.10	68.15	3.11	60.42
	37	3.15	3.15	69.25		
	38	3.14	3.12	68.64		
	39	3.10	3.08	67.70		
	40	3.05	3.06	67.30		
	41	3.32	3.26	71.75		
	42	3.35	3.30	72.55		
	43	2.83	2.85	62.65		
	44	3.00	2.99	65.88		
	45	3.30	3.24	71.18		
	46	1.87	1.95	42.92		
	47	2.00	2.06	45.42		
	48	1.94	2.02	44.44		
	49	2.23	2.24	49.29		
	50	1.72	1.78	39.27		
Total		2.94	2.94	64.74	3.11	60.42

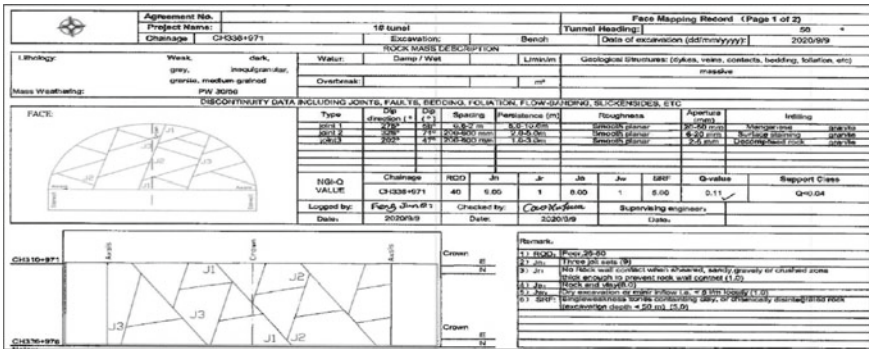


Fig. 4 Tunnel face mapping at Ch336 + 971 to Ch336 + 941, Qvalue 0.11

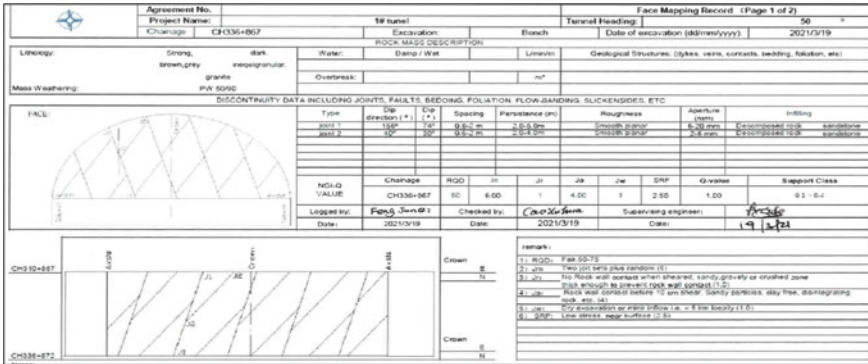


Fig. 5 Tunnel face mapping at Ch336 + 867 to Ch336 + 837, Q value 1.00

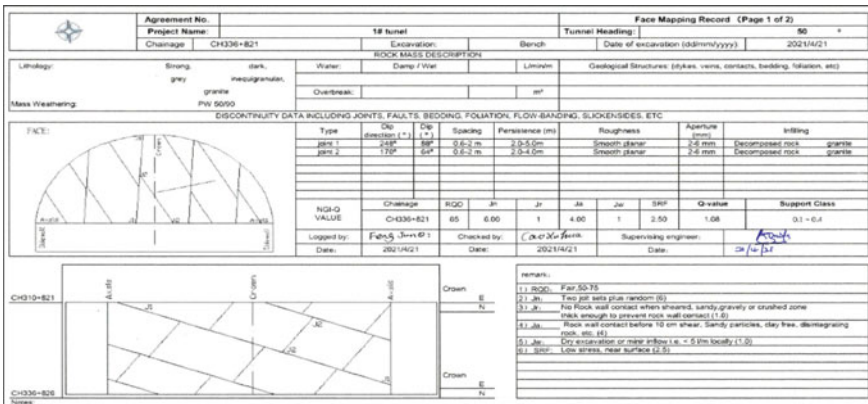


Fig. 6 Tunnel face mapping at Ch336 + 821 to Ch336 + 791, Q_{value} 1.08

4 Conclusion

As overall, rock is removed to create structures such as tunnels, hydraulic channels or caverns, or deep excavation at the ground surface for road cuts, foundation or basements. Blasting is an accompanied develop a gas at a high temperature and under a tension sufficiently great to overcome the resistance of the enclosing body and which is thus shattered also the disintegrated. Ground vibration is very important to consider due to avoid any incident happen during blasting activity. The tunnel is buried within 15 m of the tunnel entrance CH336 + 442–CH336 + 996 and the horizontal distance from the highway is 100–120 m. The blast cycle is within 3.0 to 4.5 m per blast. In term of point load index, MPa strength designation for rock classification for class V shows is in high strength designation, $I_s(50)$ (MPa) 1.21 is in high strength designation and average $I_s(50)$ (MPa) 1.21 is also high strength designation. For Ch336 + 940 to Ch336 + 820, rock class IV, In term of point load index, Mpa strength designation

for rock class IV shows is in high strength designation, $I_{s(50)}$ (MPa) 1.87 is in high strength designation and average $I_{s(50)}$ (MPa) 1.77 is also high strength designation. For Ch336 + 820 to Ch336 + 640, point load index, MPa strength designation for rock class III shows is in high strength designation, $I_{s(50)}$ (MPa) 2.94 is in high strength designation and average $I_{s(50)}$ (MPa) 3.11 is very high strength designation. Refer to the point load test index result and mapping result, Q value the three-bench method of blasting was introduced, and new blast design was adopted prior to make good the safety and health of the workforce during tunnel blasting activity.

References

1. Mohamad ET, Armaghani DJ, Noorani SA, Saad R, Abad SVANK (2012) Prediction of flyrock in boulder blasting by using artificial neural network. *Electron J Geotech Eng* 17:2585–2595
2. Dang VK, Dias D, Do NA, Vo TH (2018) Impact of blasting at tunnel face on an existing adjacent tunnel. *Int J GEOMATE* 15(47):22–31. <https://doi.org/10.21660/2018.47.04640>
3. Norén-Cosgriff KM, Ramstad N, Neby A, Madshus C (2020) Building damage due to vibration from rock blasting. *Soil Dyn Earthq Eng* 138:106331. <https://doi.org/10.1016/j.soildyn.2020.106331>
4. Armaghani DJ, Hajihassani M, Mohamad ET, Marto A, Noorani SA (2014) Blasting-induced flyrock and ground vibration prediction through an expert artificial neural network based on particle swarm optimization. *Arab J Geosci* 7(12):5383–5396. <https://doi.org/10.1007/s12517-013-1174-0>
5. Song Z, Mao J, Tian X, Zhang Y, Wang J (2019) “Optimization analysis of controlled blasting for passing through houses at close range in super-large section tunnels. *Shock Vib* 2019:1–16. <https://doi.org/10.1155/2019/1941436>
6. Sellers EJ (2011) Controlled blasting for enhanced safety in the underground environment. *J South Afr Inst Min Metall* 111(1):11–17
7. Alitalesh M, Mollaali M, Yazdani M (2016) Correlation between uniaxial strength and point load index of rocks. *Jpn Geotech Soc Special Publ* 2(12):504–507. <https://doi.org/10.3208/jgssp.IRN-08>
8. Bajpayee TS, Verakis HC, Lobb TE (2005) Blasting safety – revisiting site security, vol 2, pp 1–13

Assessment of Structural Damage Due to Blasting in Hydro Power Tunnel



G. C. Naveen, V. R. Sastry, and K. Ram Chandar

Abstract Excavation is a major activity in construction of mega underground hydropower project. Successful excavation of access and water conducting tunnels and caverns of different size and shapes by adopting highly economical and efficient method of excavation like drilling and blasting in extreme geological conditions makes the hydropower project a manmade marvel. The national codes which regulates the safety of structures while using explosives are successfully adopted where the tolerable limits for blast induced seismic waves are provided for different type of structures. This paper deals with impact of 9 m(W) and 8 m(H) tunnel blast induced seismic vibrations on the underground and surface concrete structures. The outcome of tunnel blasting with reference to peak particle velocity and related displacements gave a unique results where the seismic wave produced displacements up to 0.04 mm at large underground openings (250 m(L) × 18 m(W) × 59 m(H)) when compared to displacements of 0.016 mm in small openings of 9 m(W) × 8 m(H) with similar peak particle velocity levels of 20 mm/sec. These results subjected the structures which are located in the larger underground openings to lose their strength easily when compared to the structures located in small openings. Further, the structures located in the surface are more vulnerable to get damaged due to higher displacement recordings up to 0.123 mm. Experimental outcome was recorded for various blast design and results were further analyzed to optimize the blast parameters for successful control of blast induced vibration zone within 60 m. The relation between the structure locations where blast induced seismic wave propagates seems to play a key role in influencing on the structural damage, where less influence of peak particle velocity is observed.

Keywords Cracks · Displacement · Surface structure · Underground structure and Tunnel blast

G. C. Naveen · V. R. Sastry · K. R. Chandar (✉)
Department of Mining Engineering, NITK, Surathkal, Mangaluru, Karnataka 575 025, India
e-mail: krc@nitk.edu.in

© The Author(s), under exclusive license to Springer Nature Singapore Pte Ltd. 2022
A. K. Verma et al. (eds.), *Proceedings of Geotechnical Challenges in Mining, Tunneling and Underground Infrastructures*, Lecture Notes in Civil Engineering 228,
https://doi.org/10.1007/978-981-16-9770-8_13

229

1 Introduction

Excavation of rock is the vital operation in any mining and construction industry. Excavation in mining industry is to extract the valuable minerals or ores for economic development of the country. Whereas, excavation in civil industry is to make provision to accommodate roads, bridges, buildings, tunnels, underground multipurpose complex, dams, power houses, etc.,. Excavation of rock to build a mega underground hydropower project requires very high technical inputs in terms of pre investigation, under construction investigation and also post investigation. The rock is studied for geological variations, physico mechanical properties which determines the method of excavation. The various methods of rock excavation like mechanical cutting and blasting using chemical energy in the form of explosives is decided on the techno commercial viability, where drilling and blasting is always a priority for its adoptability friendly. The combination of unlimited drilling and explosive charging parameters which is again controlled by providing sufficient delays gives more flexibility in adoption in any circumstances [1]. Further, it is the cheapest method of excavation which provides maximum output in less time and is also economically viable when compared to other means of excavation methods. Lack of understanding risks and inadequate information associated with blasting may lead to over-conservative blast design assumptions, resulting unnecessary costs. Alternatively, underestimating blasting vibration risks can result in unexpected damages to buildings, complaints from the public and unforeseen delays. High magnitude blasting vibration effects the structure stability which reduces the life of the structure [2, 3]. There has been a continuous research to avoid blast induced damages by working on various blast design combinations. Rapid technical advances with upgradation of initiation system has resulted in immense flexibility in adoption of drilling and blasting in any sensitive areas [4, 5]. Since the structure responds varyingly to different levels of blast vibrations, selection of various drill blast combination is very effective in avoiding any structural damage. Proper management of risks associated with blasting requires fundamental understanding of vibration propagation in soil and rock and their interaction with structures.

When the explosive is detonated in the blast hole, radial cracks occur as the seismic wave propagates through the rock, the instantly expanding hot gases exert intense pressure on the blast hole walls which is high compared to the strength of the rock, leading to fracturing of the rock. Expanding gases continue to work on the rock, extending the cracks and moving the rock outward in the free face direction. Only 15% of the total energy generated by blasting is used as a working tool in the mechanism of rock fragmentation and displacement, other 80 to 85% of the explosive energy is converted to flyrock, air overpressure and seismic wave which gets transmitted in the surrounding rockmass in the form of ground vibrations [6]. This blast induced seismic wave which attenuates sharply with distance is associated with peak particle velocity, frequency, acceleration and displacement. All structures react to seismic load due to blast induced ground vibrations. Observations made as part of investigations into the effects of blasting in open pit coal mines on adjacent infrastructure by Dowding, C.

H found that the effect of blast induced ground vibration produced at a specific site is dependent on the proximity of structure to the blast location, on the geological conditions or site characteristics and on the attenuation of maximum acceleration [7]. To categorize the motion, the peak particle velocity, amplitude and its frequency and duration of blast induced vibrations should be known which can be captured by blasting seismograph. The predicted blast induced ground vibrations for varying blasting parameters can be used to demarcate the zones with potential high stress zone taking the considerations of predicted vibration levels. Ground vibrations from blasting normally have lower amplitudes and higher frequency range when compared to earthquake vibrations. This is mainly because of initial higher energies, short duration and also shortest propagation distance. Difference between construction blast and mining blast vibrations results were studied by R. Balachander et al. and found that construction blasts have comparatively larger amplitude with very high frequency [8]. The properties of the blast induced ground vibration wave is directly influenced by the elastic properties of the rock or other materials through which it travels i.e. the stiffness of the media plays a very important role in transmitting the blast induced ground vibrations. Propagation velocity can be up to 6000 m/sec for hard compact rock, whereas for soil it can be as low as 600 m/sec. When the strain wave reaches the rock/air interface, the wave is reflected back in tension and if the tension is greater than the tensile strength of the rock, spalling occurs.

2 Site Investigations

Due to modifications in existing plans with respect to achieve efficiency or to avoid hurdles, some of the underground excavations needs to be carried adjacent to the existing structures. These structures facilitate for project components, residence or commercial buildings, stock yard, etc.. To know the effect of underground blast induced seismic vibrations on the structures located in different underground openings and in surface, study was carried in underground mega hydropower project in Bhutan where shallow depth tunnel excavation was carried close to the existing openings like tunnels, caverns and to the surface. 9 m(W) × 8 m(H) of 290 m(L) D-shaped tunnel was excavated by adopting various drilling and blasting approach. The tunnel alignment is surrounded with small tunnels of 6 m(W) × 6 m(H), large tunnels of 9 m(W) × 8 m(H) and large underground openings (250 m(L) × 18 m(W) × 59 m(H)).

2.1 Concrete Structures

The study area was thoroughly studied for tunnel face advance, distance between the blasting face and tentative study structure location(block structure) and finally decided the structure location in such a way that as the tunnel excavation advanced,

the effect of blast induced seismic vibrations were captured in front, above and as well as behind the tunnel blasting face. The closest structure was built above the blasting face at a distance of 11 m and other two structures were built at a distance of 30 m in a tunnel and in cavern. Concrete shotcrete was sprayed in the surface at a radial distance of 50 m from the tunnel blasting face (Fig. 1 & 2 and Table 1).

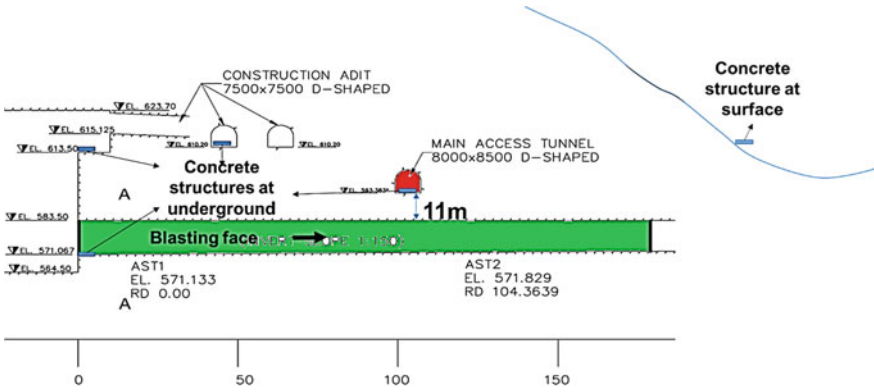


Fig. 1 Section showing location of concrete structure and blasting face



Fig. 2 Concrete structures built in underground tunnel, cavern and in surface

Table 1 Details of location of study structure and their minimum distance to blasting face

Structure	Location	Distance, m
Structure-I	D-shaped tunnel of 7.5 × 9.3 m	30
Structure-II	D-shaped opening of 8 × 8.5 m	11
Structure-III	Cavern	30
Structure-V	Surface	50
Structure-VI	Behind the blasting face	>30

2.2 Tunnel Blast Design

The D-shaped tunnel of 290 m length with height and width of 7.5 and 9.3 m respectively was excavated by adopting parallel hole cut/burn cut blasting pattern due to its improved pull and yield. The type of excavation like full face or pilot and widening blast, hole depth which varied from 2.5 to 3.5 m and charge distribution which varied from 180 to 300 kg per blast was decided on the geological conditions encountered in the tunnel alignment. As the orientation of joints and rockmass quality have huge effect on the results of tunnel blasting [9]. The rockmass was geologically studied for different joint orientations which resulted in prediction of three to four transversed joint sets with few minor shear seams. The rock type in the tunnel alignment is thinly foliated biotite gneiss with pegmatite and leucogranite intrusions. Minor bands of quartz were also found in the rockmass as shown in the Fig. 3. As per Bartons “Q” value, most of the rock mass in the study area was falling in Class-III to Class-V rockmass condition [10].

Once the blasting face was thoroughly studied, systematic excavation approach was derived. Wet drilling by L2D boomer was used to drill 45 mm diameter holes of 2.5 to 3.5 m depth and charged with 40 mm diameter, 390 of 300 mm long cartridge and initiated with half second full series non electric shock tube detonators where the maximum charge per delay varied from 12 to 64 kg (Fig. 4 and Table 2). Satisfactory blasting results was achieved by proper selection of explosive type and blast design parameters with an understanding of the rock mass characteristics [11]. During the course of excavation, each blast design was fine-tuned according to the site geological condition keeping the blast design similar. Rock Mass Quality by Barton and the results of studies carried by Ibarra, J.A et al. was considered while charging the contour holes which resulted in significant effect on the tunnel overbreak [12, 13]. Special care was taken to avoid over break in crown portion by adopting combination of line drilling and smooth perimeter holes blasting by carefully distributing the



Fig. 3 Varying geological condition encountered after every blast

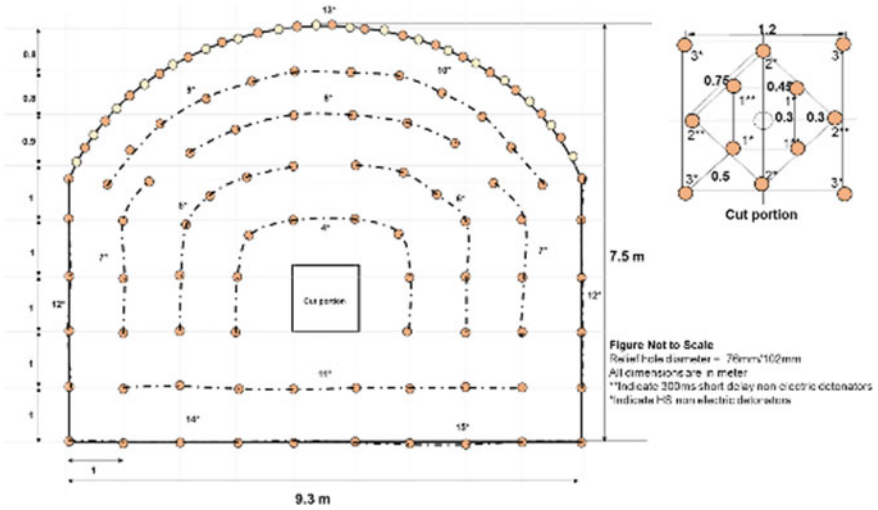


Fig. 4 Blast design adopted to excavate D-shaped tunnel

Table 2 Charging pattern and charge distribution adopted for parallel hole cut blast

Delay no	No. of holes	Charge per hole, kg	Charge per delay, kg
1	4	3.12	12.48
2	4	3.12	12.48
3	4	3.12	12.48
4	8	3.12	24.96
5	6	3.12	18.72
6	6	3.12	18.72
7	8	2.73	21.84
8	6	2.73	16.38
9	6	2.73	16.38
10	6	1.95	11.70
11	8	3.12	24.96
12	10	2.34	23.40
13	18	1.00	18.00
14	5	3.12	15.60
15	5	3.12	15.60
No of holes: 105		Total Charge: 263 kg	



Fig. 5 Monitoring of blast vibrations near the structure

charge in perimeter holes [14]. Initiation of charge in perimeter holes were delayed for 1 s to avoid any resistance for the movement of blasted rock, thereby the energy released does not disturb the surrounding intact rockmass.

2.3 Blast Induced Ground Vibration Monitoring

The dynamic load on the study structures due to blast induced seismic vibration were monitored by installing blasting seismograph which captured the particle velocity, frequency and related displacement. Seismic stress developed by the blast were monitored near the study structures by following the guidelines suggested for vibration monitoring by the International Society of Explosive Engineering (ISEE) and Director General Mines Safety (DGMS) as shown in Fig. 5 [15, 16]. All the recorded blast events were analyzed for varying wave characteristics using advanced module software. This analysis provided duration of the blast, particle velocity with respect to individual delay initiation, displacement with respect to particle velocity. Distance between the blasting site and monitoring location was radially calculated. The study structures were subjected to high intensity blast vibrations during their curing period up to seven days. In one of the event, blast was carried at a distance of 20 m from the study structure and the recorded peak particle velocity was 25.3 mm/s on the third day of casting and similarly, blast was carried at a distance of 11 m from the structure on sixth day of casting and the recorded peak particle velocity near the study structure was 190.7 mm/s (Table 3).

3 Discussion and Results

In this study, underground tunnel blasting with charge per delay varying from 2.5 to 64 kg was carried and the study structures built in underground and surface were studied for their integrity by subjecting them to high intensity vibration levels. The

Table 3 Maximum peak particle velocity recorded at different structure locations

Structure	Day of recording	Total charge, kg	Maximum charge per delay, kg	Distance, m	Peak particle velocity, mm/s
S-I	2	114.87	19.5	47	7.5
S-II	2	52.00	19.5	42.75	7.5
S-II	2	134.60	31.2	69	3.6
S-III	2	172	31.2	15	39.93
S-III	3	59.96	23.4	20	25.3
S-V	3	173	46.14	51	37.04
S II	6	217.6	28.5	11	190.7
S-I	7	51	11.5	18	31.84

vibrations which were recorded at study structures were analysed and correlated with the extent of damage observed in the study structures. Based on the data obtained, the graph of time versus recorded particle velocity for varying charge per delay is plotted in the Fig. 6. The particle velocity recorded for different charge varied very widely up to 20 times and the analysis indicated that, in most of the cases peak particle velocity produced by cut hole blast is relatively higher than 30% even the

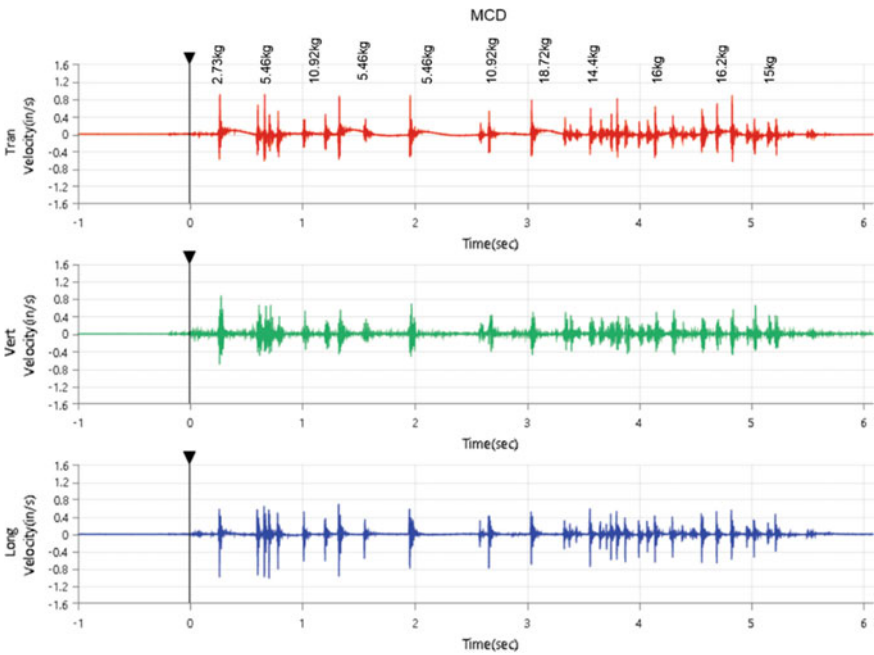


Fig. 6 Vibration generated for respective charge per delay

maximum charge per delay is comparatively more in production ring holes. It was also observed that the particle velocity is directly influenced by rockmass condition, where the particular series of explosive is detonated in hard rockmass, the intensity of blast induced ground vibration generated is high when compared to the same amount of explosive is detonated in fair rockmass condition.

From the results, further it was observed that the particle movement in vertical direction is relatively more in large underground span when compared to small underground openings. Therefore, it can be clearly understood that the structures located in large underground span are more prone to get damaged easily when compared to structures located in small underground openings. The study also revealed that when the seismic wave reaches the free surface, the effect of wave reflection converting compression seismic wave to tensile wave is observed in the form of high vertical displacements thus resulting additional stress on the structures located in the surface or bigger span (Table 4 and Fig. 7). Due to surface vertical movements, development of cracks in the concrete intersection areas and also in the shotcrete layer was observed as shown in the Fig. 8.

To check the anticipated internal cracks developed in the study structures, 54 mm diameter cores were collected before and after the blast. Even though the concrete block structures were subjected to high vibration levels, the data obtained by ultrasonic tests values indicated that there are no micro cracks developed in the test structures, whereas the P-wave velocity test results indicated that the compactness in the concrete was increased up to 7.7% depending on the age of the concrete (Fig. 9).

Table 4 Vibration and maximum displacement recorded at different study structure locations

Monitoring location	Particle velocity			Displacement		
	Long peak (mm/s)	Tran peak (mm/s)	Vert peak (mm/s)	Long displ. (mm)	Tran displ. (mm)	Vert displ. (mm)
Structure-I: Horizontal w.r.t blasting location	13.03	6.573	7.519	0.032	0.054	0.03
Structure-II: Above the blasting face in small openings (Tunnel)	9.033	11.64	10.98	0.026	0.022	0.016
Structure-III: Above the blasting face in large openings (Cavern)	25.66	31.84	36.93	0.042	0.071	0.044
Structure-V: In surface	14.98	15.29	37.04	0.066	0.056	0.123

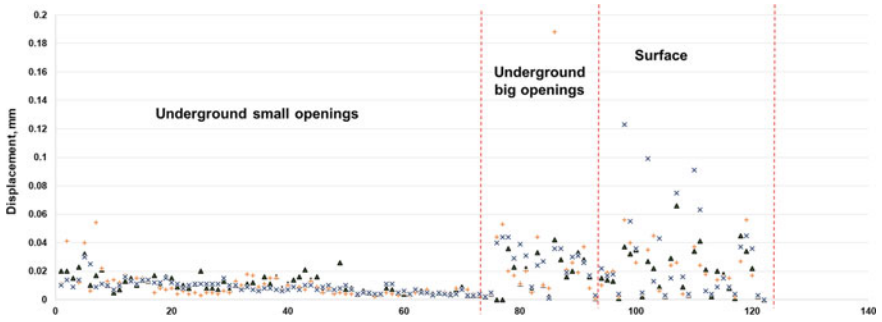


Fig. 7 Vertical displacement observed in underground and surface locations

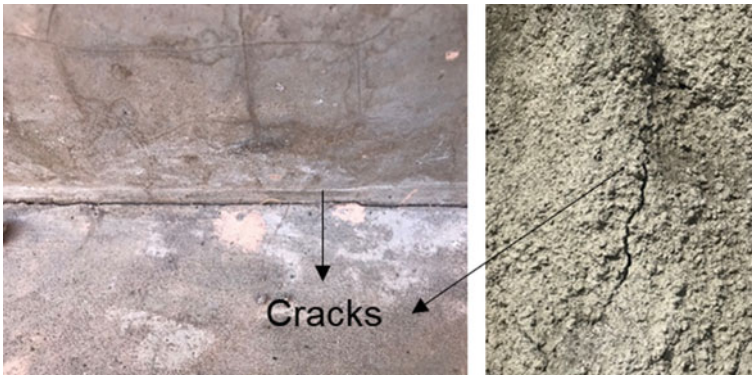


Fig. 8 Cracks observed in the concrete intersection areas and in surface shotcrete layer

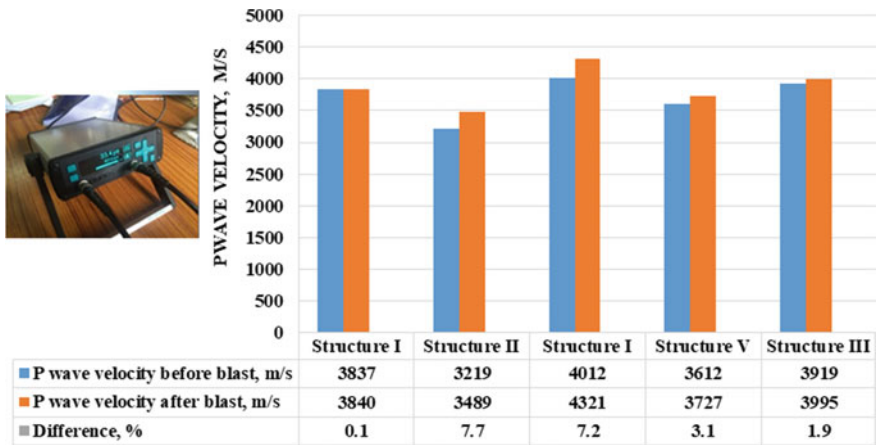


Fig. 9 Percentage difference in P-wave velocity values in the concrete during pre and post blast studies

4 Conclusions

Nature of damage to the structures due to underground blasting is complex due to involvement of large design parameters. Early detection of cause for development of cracks not only saves the life of men, but also saves considerable money in handling and maintenance of effected structure and also reduces the risk associated. Several structure design such as high strength steel, reinforced concrete have been adopted to control the damages. However, these methods induces high cost and also restrict the schedules. With the evidence of location of structures, a scope of avoiding damage based on the underground or surface span on which the structure is located has been analysed. According to the results and analysis, optimal type of structure can withstand the effect of the blast induced ground vibrations even they are subjected to high vibration levels.

The parameter such as span at which the structure is located was considered as a main parameter alternatively considering the displacement as output from underground tunnel blasting. From the study it can be concluded that,

- The maximum charge per delay has least influence on the generated ground vibration levels in tunnel excavation, where the maximum particle velocity is generated by detonation of cut holes as shown in the Fig. 6. The recorded peak particle velocity for varying maximum charge per delay varied up to 20times and the peak particle velocity produced by cut hole blast is 30% higher than the production holes. The main parameters which influenced the blast induced vibrations are initiation of cut hole explosive to create free face.
- The results of recorded displacement in all the three directions provided the relation between displacement and span width. The results of the study provided a clear cut message that the structure located in large underground cavern are more prone to get damaged when compared to the structures located in small underground openings. The analysis of the generated data showed that ground vertical movements in the surface is relatively high for underground blasts. The displacements recorded in the surface is 0.123 mm when compared to 0.044 mm in large underground caverns and 0.016 mm in small tunnels for the same maximum charge per delay.
- Based on the above study results, the location of structure is considered as one of the most contributing parameter in controlling the degree of damage to the structures. It was clearly observed that the contact zones between structure and rock/concrete are more prone to get damaged early before there is any damage in the structure and it can be stated that the deterioration of any structure due to underground blast induced ground vibrations is mainly dependent on structure location.

References

1. Wild HW (1976) Geology and blasting in open pits. *Erzmetall*
2. Siskind DE, Stagg MS, Koop JW, Dowding CH (1980) Structure response and damage produced by ground vibration from surface mine blasting. *Us Bureau of Mines*, 74
3. Siskind DE (1980) Structure response and damage produced by air blast from surface mining. *USBM RI 8485*
4. Kirkeby T (2011) Contor blasting tests with different drilling and charging plans. *Norwegian Public Road Administration, VD report 13*
5. Sastry VR, Teggi V, Ram Chandar K (2003) Influence of initiation systems on ground vibrations. *Min Eng J*, 8–18
6. Hagan TN (1977) Rock breakage by explosives. In: 6TH symposium on gas dynamics of explosives and relative systems, *Stockholm*
7. Dowding CH (1985) *Blast vibration monitoring and control*. Prentice Hall Inc., Englewood Cliffs
8. Balachander R, Gopinath G, Theresraj AI, Vamshidhar K, Venkatesh HS (2011) Report on Technical guidance for rock blasting and monitoring of ground vibration, air overpressure and fly rock during excavation at Underground stations from Chinnaswamy stadium to City railway station, BMRCL site, NIRM Project No. RB 10 06 C
9. Singh SP, Xavier P (2005) Causes, impact and control of over break in underground excavations. *Tunnel Undergr Space Technol* 20:63–71
10. Bieniawski ZT (1989) *Engineering rock mass classifications*. Wiley, Chichester
11. Adhikari GR, Rajan Babu A, Venkatesh HS, Theresraj AI (1994) Blast damage assessment for underground structures. In: *Proceedings of national symposium on emerging mining & ground control technologies*, BHU, Varanasi, 19–28 February 1994
12. Barton N, Loset F, Lien R, Lunde J (1980) Application of the Q-system in design decisions concerning dimensions and appropriate support for underground installations. In: *International Conference On Sub-Surface Space, Rock Store, Stockholm*. *Sub Surface Space*, vol 2, pp 553–561
13. Ibarra JA, Marez NH, Franklin JA (1996) Over break and under break in underground openings Part 2: causes and implications. *J Geotech Geol Eng* 14:325–340
14. Persso PA, Holmberg R, Lee J (1994) *Rock blasting and explosives engineering*. CRC Press Inc., Boca Raton, pp 259–264
15. Anon (1997) Damage of structures due to blast induced ground vibrations in the mining areas. *DGMS (Tech) (S&T) Circular No. 7 of 1997 dated 29.08.1997*
16. Anon (2001) *Method for Blast Vibration monitoring – Guidelines*. Indian Standard IS code 14881:2001

Tunnel Excavation in Highly Stressed Weak Rockmass Condition



G. C. Naveen, B. N. V. Siva Prasad, R. Balachander, G. Gopinath,
H. S. Venkatesh, and Sripad R. Naik

Abstract In any underground hydropower projects, there is mutual understanding between displacement recordings with the selection of excavation methods and support systems. The type of underground excavations mainly depends on rock mass geology, rock structure, hydrology and insitu stress regime. The extents of anticipated deformations and stresses arising due to alter in the equilibrium determines the type of support system required to maintain the stability of the excavated portion. This technical paper describes how instrumentation data aided in deciding the excavation techniques and supporting system while excavating horse-shoe shaped head race tunnel in fair to poor rock mass conditions under high induced stresses at Punatsangchhu-II Hydroelectric Project, Bhutan. The main focus was to excavate the stretch of 110 m (360.892 ft) in highly critical zone without any major deformations which could have resulted in collapse and hampered major activities. A good geological preinvestigation in combination with on-site investigations resulted in taking right decision to safely perform the excavation and support the tunnel. Displacement measurements with advanced monitoring setups provided continuous information about the condition of rock mass. Utilization of these instrumentation data in combination with geological studies, provided important information in selecting the excavation technique and reviewing the support system which resulted in successful excavation of 11 m (36.08 ft) large diameter horse-shoe shaped head race tunnel in weak rock mass condition.

Keywords Tunnel · Support · Excavation · Instrumentation · Weak rock mass · Hydroelectric project and self drilling anchors

G. C. Naveen (✉) · R. Balachander · G. Gopinath
Rock Blasting and Excavation Engineering Department, National Institute of Rock Mechanics,
Bengaluru, India
e-mail: rbeenirm@gmail.com

B. N. V. S. Prasad · S. R. Naik
Numerical Modelling Department, National Institute of Rock Mechanics, Bengaluru, India

H. S. Venkatesh
National Institute of Rock Mechanics, Bengaluru, India

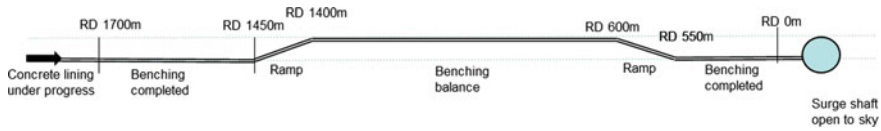


Fig. 1 Schematic diagram showing Head Race Tunnel operations

1 Introduction

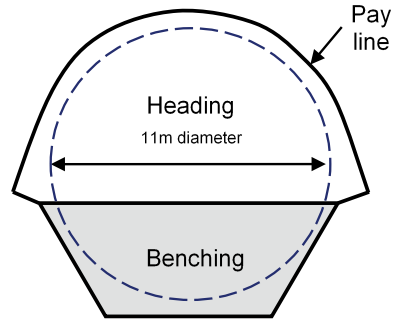
Tunnels are lifeline of any underground projects which acts as a service network during construction stage and some becomes main water conducting system during operation. Out of multiple tunnels of various sizes and shapes driven in hydropower projects, Head Race Tunnel is one of the major water conducting channel which connects desilting chamber from dam site to surge shaft in powerhouse complex. Horse shoe shaped Head Race Tunnel of 10.514 km (6.533 miles) long, 11 m (36.08 ft) diameter was excavated by drilling and blasting to connect the dam and powerhouse to harvest hydroelectric power from Punatsangchhu River in Bhutan by Punatsangchhu Hydroelectric Power Project Authority. The proposed estimated capacity of this underground hydroelectric project is 1020 MW ($170 \text{ MW} \times 6$). A schematic diagram showing Head Race Tunnel operations is shown in Fig. 1.

In any underground hydropower projects the selection of excavation technique and design of support system has to depend on response of rock mass through geotechnical instrumentation. This technical paper describes how displacement data was used in deciding the excavation method and support system while excavation of 11 m (36.08 ft) large diameter horse-shoe shaped Head Race Tunnel in poor rock mass condition. The authors were involved in technically guiding in selection of excavation methods to safely excavate the tunnel in fair to very poor rock mass conditions without any collapse. The authors were also involved in deciding on the excavation progress and redesigning support system while analysing the monitored displacements during the tunnel excavation. Use of such technical networks in designing and technically guiding with respect to on-site specifications enabled the authors to excavate a stable, less damaged Head Race Tunnel for the life of the project. The methodology adopted to drive the tunnel for a stretch of 110 m (360.892 ft) where the rock condition was very poor and highly stressed is described in this paper.

2 Background

Horse shoe shaped Head Race Tunnel of 10.514 km (6.533 miles) long, 11 m (36.08 ft) diameter was excavated by heading and benching method. The height of heading excavation was 6.5 m (21.32 ft) with excavated area of 83.894sqm (275.24 sqfeet) and 46.016 sqm (150.97 sqfeet) for benching. A typical cross section of Head Race Tunnel is shown in Fig. 2. Heading was completed through out the length of the

Fig. 2 Typical cross section of the Head Race Tunnel



tunnel by adopting parallel hole cut blast design in multiple faces, whereas benching was carried out in sections of 150 m (492.126 ft) each.

3 Geological Features

As highlighted by Nicholas Vlachopoulos, et al. [1], prior to determining the proper tunnelling technique and rock support method, a tunnel design engineer must make use of the information gathered from the site investigation, rock mass classification and rock characterization, the rock mass was studied for different geological features in the stretch from RD 764 m (0.47 miles) to RD 1120 m (0.69 miles). Geological features in the tunnel alignment changed drastically with every advancing face. The rock type in the alignment of tunnel is thinly foliated biotite gneiss with pegmatite and leucogranite intrusions. Minor bands of quartz were also found in the rock mass. In general, the rock mass comprising of three to four joint sets and major shear seams were observed. In the length of 356 m (0.22 miles), the rock mass in the stretch from RD 764 m (0.47 miles) to RD 866 m (0.53 miles) and RD 1050 m (0.65 miles) to RD 1120 m (0.69 miles) was classified as fair rock mass condition, from RD 866 m (0.53 miles) to RD 963 m (0.59 miles) was classified as poor rock mass condition and from RD 963 m (0.59 miles) to RD 1050 m (0.65 miles) the rock was falling in very poor rock mass condition as shown in the Fig. 3. Low dipping foliation joints present in the rock mass posed to slabbing in crown portion while erratic occurrence of intrusive bodies of variable dimension led to unpredictable behaviour of rock mass. The tunnel

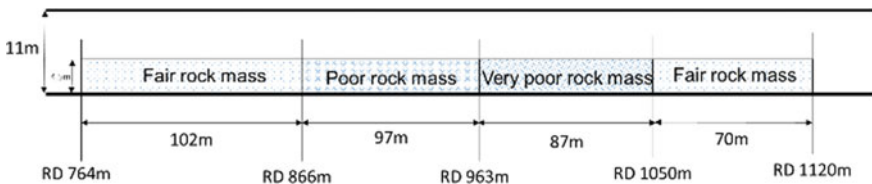


Fig. 3 Sections of varying rock mass condition from RD 764 m to RD 1120 m

alignment encountered fair to very poor rock mass conditions with limited stand up time in virtue of presence of low dipping foliation joints and adversely oriented discontinuities [2].

4 Heading Excavation and Support

From RD 764 m (0.47 miles) to RD 866 m (0.53 miles) and from RD 1050 m (0.65 miles) to RD 1120 m (0.69 miles) the rock mass condition was fair good to adopt full face blasting. For excavation of heading portion, parallel hole cut blast pattern was adopted due to its improved pull and yield [3]. Wet drilling by Atlas Capco's L2D boomer was used for drilling the holes. Even though the drill machine have capacity to drill upto 5 m (16.40 ft) hole depth, to maintain maximum chare per delay within the designed limts, hole depth was limited to 1.5 m (4.92 ft) to 4 m (13.0.12 ft) depending on the geological conditions. Even though the products like mechanised drilling and computer operated navigation systems have given the space to operate for better productivity and efficiency [4], due to site constraints semi mechanised drilling machines were used. 45 mm (1.77 in.) diameter drilled holes were charged with 40 mm (1.57 in.) diameter, 0.390 kg (0.85 pound) cartridged explosives. 2 to 4 relief holes of 102 mm (4 in.) diameter were drilled in cut portion depending on the site conditions as shown in the Fig. 4. Perimeter holes were drilled at a closer spacing of 30 cm (1 ft) and alternate holes were charged using 32 mm (1.23 in.) diameter, 0.2 kg (0.44 pound) cartridged explosive and initiated with half second full series non electric detonators. Upgradation of initiation system and proper delay timing has resulted in immense change in the output of blasting results, which even resulted in more flexibility to adopt drilling and blasting in any sensitive areas [5, 6].

Fig. 4 Blasting face with cut holes



During heading excavation, cavity upto a height of 10 m (32.8 ft) in crown portion was formed due to the presence of very weak rock mass and the area was highly stressed.

Before every advance, crown portion in poor rock mass condition was supported with 114 mm (4.48 in.) diameter, 12 m (39.37 ft) long, 6 mm (19.68 ft) thick perforated steel pipe/fore-poles in umbrella shape at close interval of 0.5 m (1.64 ft) over the final tunnel profile at an angle of 5° from horizontal to consolidate the surrounding rock mass. After installation of fore-poles, cement grouting was carried out through 114 mm (4.48 in.) diameter fore-poles at a maximum pressure of 5 kg/sq.cm (11 pounds/sq.cm). Each pile of 12 m long, provided support for about 8.2 m (26.9 ft) tunnel advance. As a primary support, 100 mm (3.93 in.) thick layer of SFRS was sprayed on the freshly exposed surface after every advance. Rock anchors of 25 mm (0.98 in.) diameter, 4.5 m (14.76 ft) long resin end anchored, fully cement grouted rock bolts were installed up to springing level in staggered pattern. Ribs of ISMB-300 was placed with a spacing of 0.4 m (1.31 ft) and channel section of ISMC-150 runners were installed joining at least 4 sets of ribs. M25 Concrete was back filled immediately after installing the ribs. Additional rock bolts were installed above the ribs in such a way that the installed rock bolt length is at least 5.5 m (18 ft) into the rock beyond actual excavated surface. Once the area behind the ribs was backfilled, the gaps between backfill concrete and excavated rock surface were fully grouted with cement by drilling 20 m (65.61 ft) deep holes. Each section was grouted in different angles and in different stages. Each section consumed about 300 kg (661.38 pound) to 400 kg (881.84 pound) of cement grout. It was also ensured that fissures around the anchors were also grouted.

4.1 Instrumentation to Monitor Rock Mass Response to Excavation

The rock mass has inherent discontinuities in it whose properties vary greatly from the host rock aiding in the development of potential failure zones during and after execution. The change in rock mass behaviour observed in such zones calls for safety controls to alarm the working personnel by installing geotechnical and geodetic instrumentation inside the rock mass to capture changes in its behaviour and promptly take up the remedial measures to prevent failures [7]. The key parameters which aids in assessing the rock mass behaviour is displacement, load, water pressure and vibration. Multi-point borehole extensometers are used to measure rock mass displacements at various depths depending on the anchors locations from the instrument head. To monitor rock mass displacements in the excavated portion of the tunnel, multipoint borehole extensometers with five anchors were installed inside the tunnel at crown and side walls of RD 998 m (0.62 miles) and RD1030 m (0.64 miles). A 3D view of Head Race Tunnel showing installed array of multi-point borehole extensometers anchors to monitor rock mass displacements is shown in Fig. 5. Anchors

Fig. 5 3D view of Head Race Tunnel showing installed array of multi point borehole extensometer anchors to monitor rock mass displacements

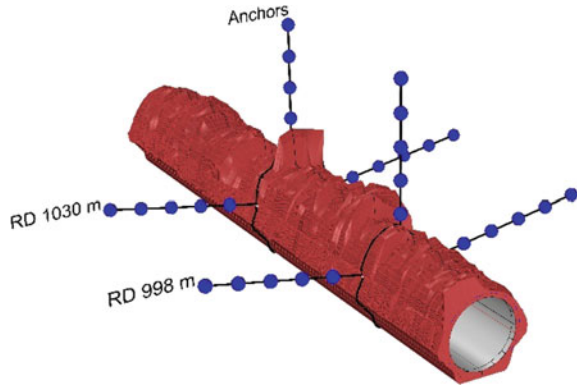


Table 1 Details of multi point borehole extensometer

Instrument	Multi-point borehole extensometer
Make	EncardioRite, India
Sensor	Vibrating Wire
Range	50 mm (1.96 in.) (± 25 mm(0.98 in.))
Accuracy	0.1% FSR
Over range	150% FSR
Anchor depths	5 m (16.40 ft), 10 m (32.80 ft), 15 m (49.21 ft), 20 m (65.61 ft) and 25 m (82.02 ft)
Bore hole diameter	102 mm (4.01 in.)

were installed at various depths, viz. 5 m (16.40 ft), 10 m (32.80 ft), 15 m (49.21 ft), 20 m (65.61 ft) and 25 m (82.02 ft) respectively which allowed the authors to monitor the rock mass displacements more than 2 times the diameter of the tunnel. Table 1 provides the details of the extensometers used for displacement measurements and Fig. 6 shows the installed extensometer at RD 1030 m (0.64 miles). By this instrumentation, the authors were confident to locate the exact stretch of potential displacements. These extensometers are connected to a data logger unit, where the data is acquired continuously and recorded for further analysis. Form the analysed data, it was possible to demarcate the inter-anchor zone displacements thereby indicating the contractional or dilational movement of rock mass between the positions of anchors with respect to time and site activities.

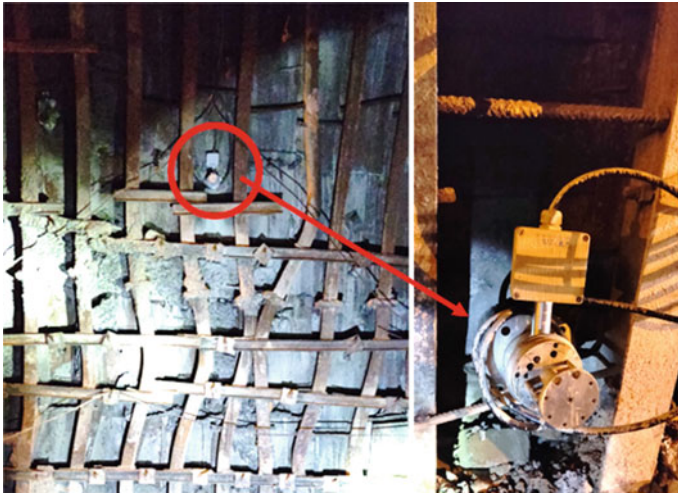


Fig. 6 Multi-point borehole extensometer installed at RD 1030 m (0.64 miles)

5 Bench Excavation

Once the instruments are installed and calibrated, bench excavation was started in stages by adopting multiple drift method as shown in the Fig. 7. The rock condition in the stretch from RD 866 m (0.53 miles) to RD 963 m (0.59 miles) was falling in Calss-IV condition and needed immediate support to avoid deformation. The major centre portion of about 4.5 m wide was blasted by adoting the blast design provided in the Fig. 8 leaving the rock ledge of 2 m on either side of the tunnel.

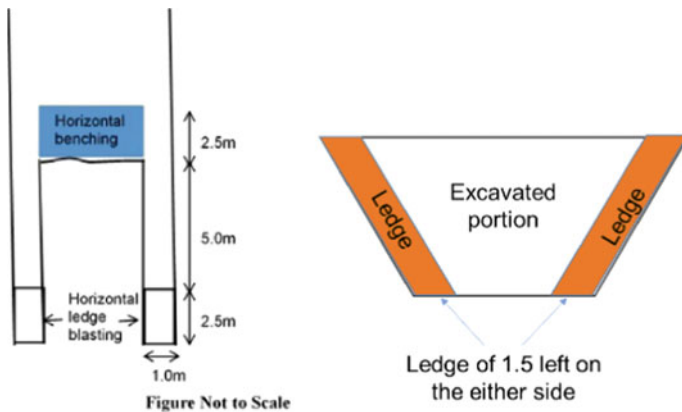


Fig. 7 Schematic diagram showing excavation in stages in Class-IV rock mass conditions

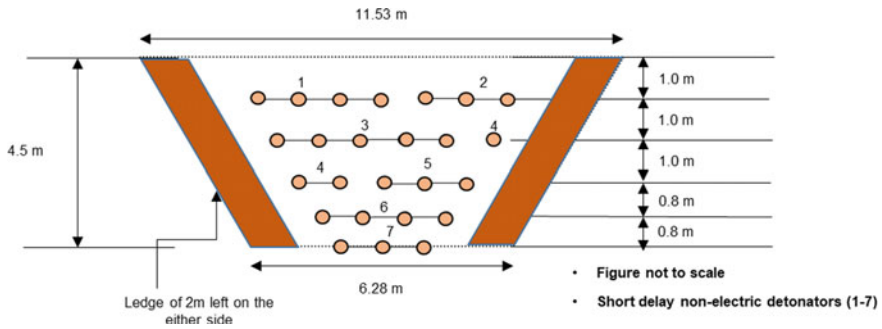


Fig. 8 Blast design adopted for excavation of bench in head race tunnel

The hole depth was restricted to 1.5 m (4.92 ft) and subsequently the charge per hole was reduced to limit the blast induced ground vibration on the surrounding rock mass. Horizontally drilled 45 mm (1.77 in.) diameter drilled holes were charged with 40 mm (1.57 in.) diameter, 0.390 kg (0.85 pound) cartridge explosives and initiated in combination with half second full series non electric detonators. There is huge effect of joint orientation and rock mass quality on the results of tunnel blasting [8, 9]. Line drilling was done with a spacing of 0.3 m (0.98 ft) along the final excavation line and alternate holes were charged with 32 mm (1.23 in.) diameter, 0.2 kg (0.44 pound) cartridge explosive depending on the site geological condition and was initiated at the last. The rock ledge of 1.5 m (4.92 ft) to 2 m (6.56 ft) left on the either side of the tunnel was removed by scaling/trimming using excavator and in some cases the ledge was trimmed with mild blasting (Fig. 9).



Fig. 9 Benching in stages

6 Monitoring of Rock Mass Response

The deformation characteristics of a tunnel excavated in poor rock mass can be monitored by proper measurement of crown settlement and horizontal displacements of side walls. While benching was under process by adopting controlled blasting technique, continuous monitoring was carried out to acquire instrumentation data over a period of three month until the excavation was complete and the tunnel was permanently supported (Fig. 10). Displacements of about 37.8 mm (1.48) was recorded at the spring level of left wall at RD 1030 m (0.64 miles) which showed inward tunnel displacement at the surface and between 5 m (16.40 ft) and 10 m (32.80 ft) depths. The summary of maximum displacements recorded during excavation of critical reach is provided in Table 2.

Graphical representation of inter-anchor displacements recorded by MPBX at different locations is shown in Figs. 11, 12, 13, 14, 15 and 16. Using the measured instrumentation data, contraction and dilation analysis was carried and the results of analysis is presented in Fig. 17 and Fig. 18 for RD 998 m (0.62 miles) and RD 1030 m (0.64 miles) respectively.

Tunnel squeezing is a common phenomenon in poor rock masses under high in situ stress regimes. Critical strain is defined as the strain level on the tunnel periphery beyond which instability and squeezing problems are likely to occur. From

Fig. 10 Acquiring of displacement data



Table 2 Summary of maximum displacements recorded during excavation in critical reach

RD, m	Location	Surface (0 m)	0 to 5 m	5 to 10 m	10 to 15 m	15 to 20 m	20 to 25 m
998	Right Wall	-6.6	-3.7	-2	-1.1	-0.2	-0.5
998	Crown	3.8	3.2	1.1	2.7	4.2	2.7
998	Left Wall	0.4	14.4	1.5	1.1	0.5	0
1030	Right Wall	10.4	6.5	3.3	6.5	4.7	1.7
1030	Crown	3.4	1.9	0.4	0.8	0.9	3.2
1030	Left Wall	37.8	7.6	27.1	15.4	17.6	2.6

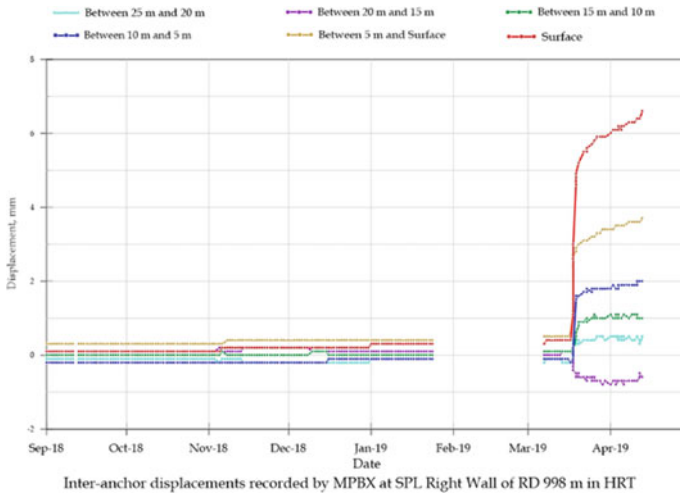


Fig. 11 Graphical representation of inter-anchor displacements recorded in right wall at RD 998 m

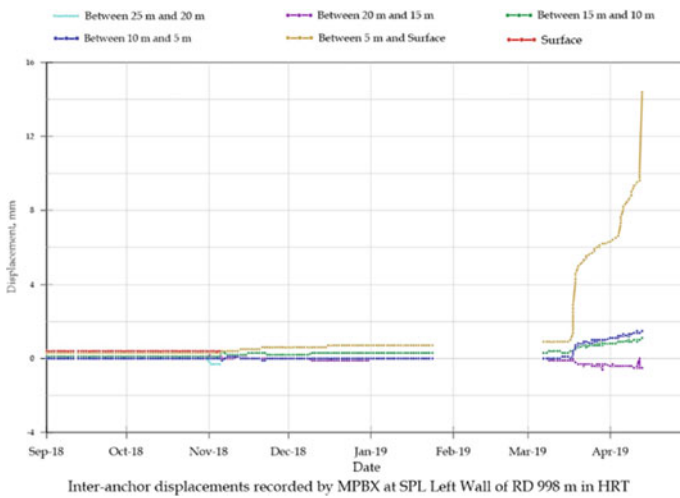


Fig. 12 Graphical representation of inter-anchor displacements recorded in left wall at RD 998 m

various literatures, the value of critical strain considered is 1% [10]. The critical strain parameter is an indicator which tolerates the degree of squeezing of the rock mass and needs to be quantified through instrumentation. These displacements have been accumulating over a period of time which resulted in twisting and misalignment of ribs into the final payline area as shown in the Fig. 19. These displacements were also correlated with the geological observations which indicated inward dipping of

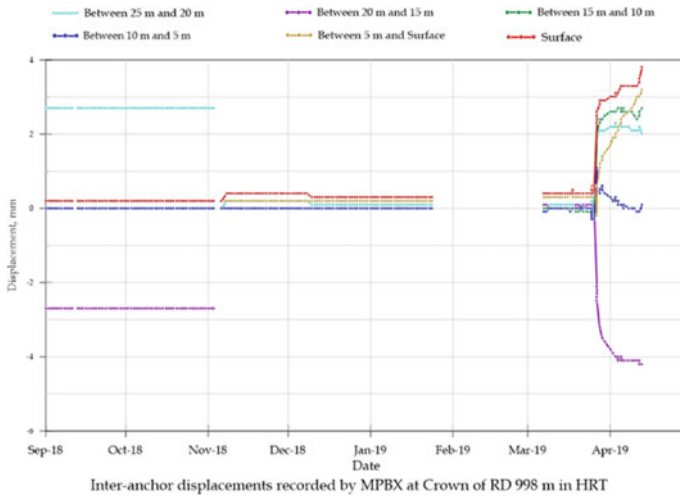


Fig. 13 Graphical representation of inter-anchor displacements recorded in crown at RD 998 m

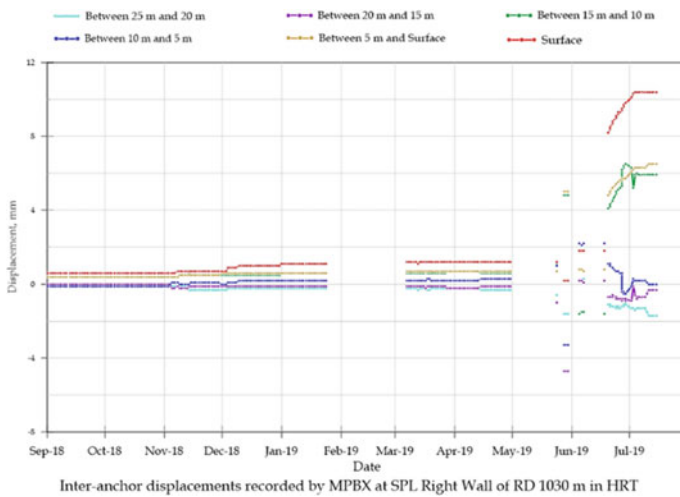


Fig. 14 Graphical representation of inter-anchor displacements recorded in right wall at RD 1030 m

prominent joint sets on left wall side which proved that the joint orientatiations were playing major role in deformations.

Based on the recorded displacements which were gradually increasing over time and the displacement data indicated deformations at alarming rate, the regular excavation technique and supporting system was reviewed. Benching excavation was immediately stopped and further additional support of the excavated portion from RD 990 m (0.61 miles) to RD 1050 m (0.65 miles) of the tunnel was started. Even

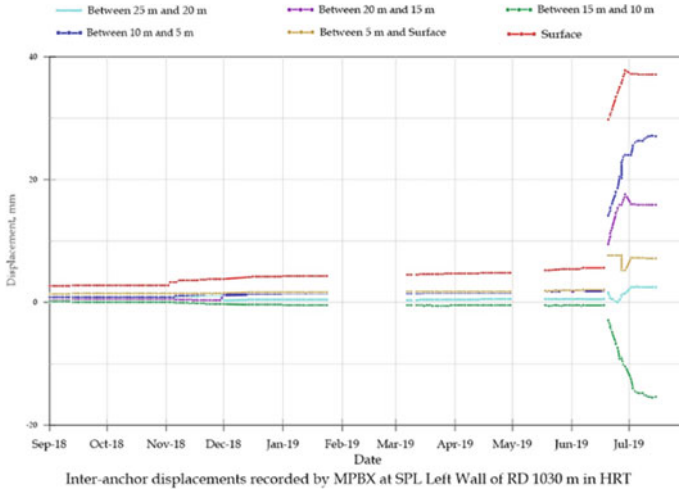


Fig. 15 Graphical representation of inter-anchor displacements recorded in left wall at RD 1030 m

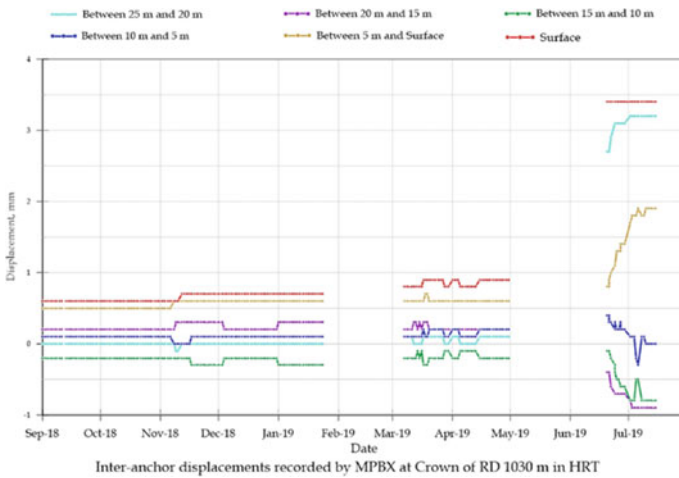


Fig. 16 Graphical representation of inter-anchor displacements recorded in crown at RD 1030 m

though the process is time consuming, to stabilize the weak rock mass and by considering the safety of men and material, additional support system was deemed essential which was effective in avoiding the collapse of the tunnel. Lot of forthcoming rock support was estimated, especially grouting, additional rock bolts in consultation with designers, site inspector, engineering geologist, and foreman to decide on the necessary rock support required along with the team leader. Due to difficulties faced during drilling and installation of rock bolts greater than 10 m (32.8 ft) long, self-drilling anchors comprise of a hollow threaded bar with an attached drill bit that can perform

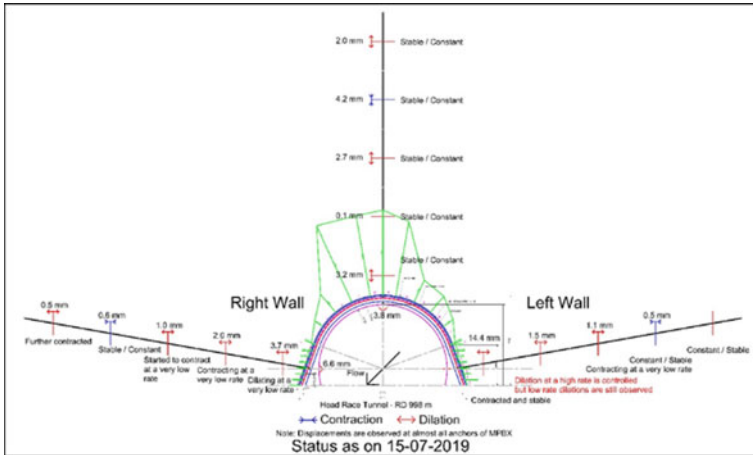


Fig. 17 Contraction and dilation recorded at RD 998 m (0.62 miles)

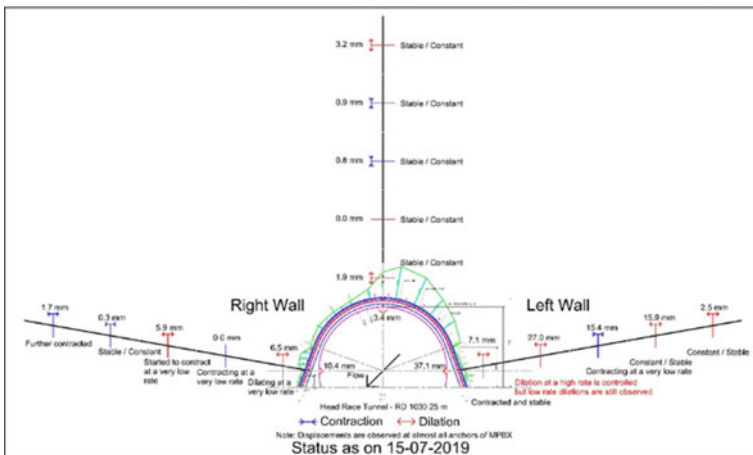


Fig. 18 Contraction and dilation recorded at RD 1030.25 m (0.64 miles)

drilling, anchoring and grouting in a single operation were used to stitch the weak rock mass. Self-drilled anchors of 76 mm (2.99 in.) diameter, 15 tons capacity were drilled to a depth of 20 m (65.61 ft) at an spacing of 3 m (9.84 ft) in staggered pattern. Grout was injected immediately after drilling which filled the hollow bar and completely covered the entire bolt. After installation, the anchored rods were tensioned to a load of 10 tons as shown in Fig. 20.

Optimized excavation method by decreasing the height and span of bench and modification of primary support can aid in better control over excavation process [11]. Since the rock mass condition was not suitable to adopt full face benching at one time and likelihood of further deformations resulted to workout the best suitable

Fig. 19 Twisted and misaligned ribs at RD 998 m (0.62 miles)



Fig. 20 Self drilling anchors installed in replacement of regular rock bolts

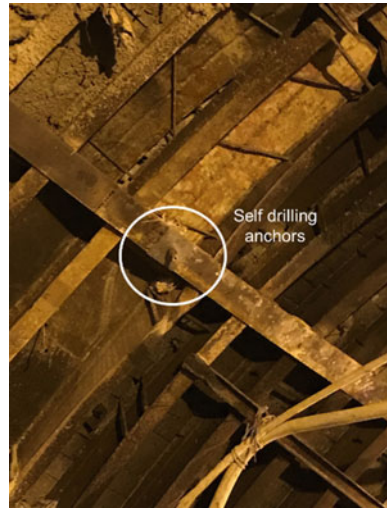
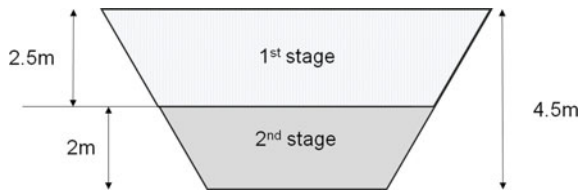


Fig. 21 Excavation sequence adopted while benching in very weak zone



excavation approach to deal with this particular stretch. Once the supporting system from crown to springing level was fully completed balance benching was excavated in stages as shown in the Fig. 21 which made provision for supporting the tunnel walls immediately after excavation which also enhanced further safety.

In the first stage, top 2.5 m (8.2 ft) bench was excavated and the freshly exposed rock surface was supported with primary support concurrently with advance. Combination of mechanical means and drilling and blasting was adopted by limiting the maximum charge per blast to 10 kg. Blast vibrations were continuously monitored (Fig. 22) behind the blast. 100 mm (3.93 in.) thick SFRS was applied at the freshly exposed side walls. Rock anchors of 25 mm (0.98 in.) diameter, 4.5 m (14.76 ft) long resin end anchored, fully cement grouted rock bolts were installed in staggered pattern (1.5 m (4.92 ft) \times 1 m (3.28 ft) spacing).

After every advance of first stage benching for about 15 m (49.21 ft) (Fig. 23), second stage excavation was carried and ribs of ISMB-250 was immediately extended up to invert level with a spacing of 0.5 m (1.31 ft). Horizontal strut of ISMB-250 were provided at the bottom connecting two legs as shown in the Fig. 24. Channel section of ISMC-150 runners were installed joining at least 4 sets of ribs. M25 Concrete was back filled immediately after installing the ribs. Ribs were anchored with 6 m (19.65

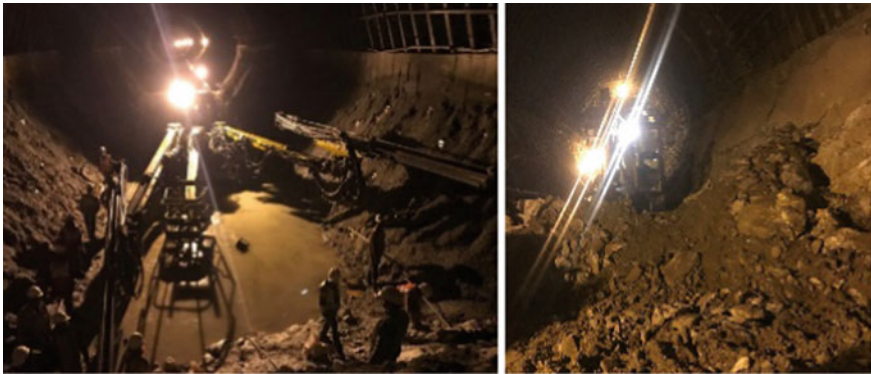


Fig. 22 Blasting limited to 10 kg per blast

Fig. 23 Stage wise benching in critical reach and extension of ribs from springing level





Fig. 24 Support extended to invert level along with horizontal struts

ft) long, 25 mm (0.98 in.) diameter resin end anchored, fully cement grouted rock anchors. Concrete was placed at the invert level filling the gap between the struts.

As the tunnel was completely supported with permanent support, the displacements were arrested. This confirmed the assumptions that most of the displacements have been already taken place while excavation and in practical terms the area was completely arrested for any further deformations. Finally with good geological preinvestigation in combination with site investigation inputs resulted in taking right decision to perform rock excavation and to supporting it (Fig. 25).



Fig. 25 Final lining of tunnel in critical zone

7 Conclusion

It was in special geological zone, where the rock condition was very poor and unforeseen results were expected due to its weakness. Decision on failure of one method was brought together to find the best solution to an unforeseen complex problem. Rock mass properties and on-site displacement data along with geometrical configuration is the key to success for any underground structure especially in poor rock mass condition. Displacements takes place immediately after any change in the equilibrium state by releasing the accumulated stress which is related to excavation progress. The geotechnical instrumentation data acquired during excavation progress is extremely useful to alert the project personnel in right time to timely review the excavation activity and support system.

An example of efficient and transparent communication between all the parties was made evident during execution. A good geological pre investigation data provided the information to decide on the excavation method to be adopted, whereas good site investigation provided the decision to be taken on permanent rock support system. Data from ground signatures indicating built up in stresses and displacement measurements based on geotechnical instrumentation data, the excavation methodology was changed from full fledge to moderate one. With the requirement of tunnel progress, unique support design was planned. This came with, extending the support up to invert level provided with horizontal studs. Introduction of self-drilling anchors allowed in reduction of drilling time, placement time and even provided with efficiency which also achieved immediate rock support. This example shows how efficient and benefit when in-situ developments are adopted in ongoing tunnelling projects.

Acknowledgements The authors are thankful to the authority of Punatsangchhu Hydroelectric Project, Bhutan for their support and cooperation extended during execution of this work. Our sincere thanks are due to National Institute of Rock Mechanics, India for according permission to publish this paper. Our thanks are extended to all field engineers and support design experts who were directly or indirectly associated while under taking this study.

References

1. Vlachopoulos N, Forbes B, Vazaios I (2019) Tunneling in weak rock. *Soft Rock Mech Eng*, 579–621
2. Barton N, Loset F, Lien F, Lunde J (1980) Application of the Q-system in design decisions concerning dimensions and appropriate support for underground installations. In: *International conference on Sub-surface Space, Rock Store, Stockholm*. *Sub Surface Space*, vol 2, pp 553–561
3. Murthy VMSR (2003) Prediction blasting induced rock damage in burn cuts using acceleration measurements. *Ind Min Eng J*
4. Mishra AK, Gupta RN (2013) Rapid excavation of tunnels using innovative drilling and blasting techniques. In: *10th international symposium on rock fragmentation by blasting, workshop on*

- tunneling in rock by drilling and blasting. *Fragblast10*, Vigyan Bhawan, New Delhi, 24–29 November 2012
5. Kirkeby T (2011) Contor blasting tests with different drilling and charging plans. Norwegian Public Road Administration, VD report 13
 6. Sastry VR, Teggi V, Ram Chandar K (2003) Influence of initiation systems on ground vibrations. *Min Eng J*, 8–18
 7. BNV SP, Naik SR (2018) Planning for geotechnical and geodetic instrumentation in underground caverns. In: International society for rock mechanics and rock engineering
 8. Chakraborty AK, Jethwa JL, Paithankar AG (1994) Effects of joint orientation and rockmass quality on tunnel blasting. *Eng Geol* 37:247–262
 9. Hagan TN (1995) The effect of rock properties on the design and results of tunnel blasts. *J Rock Mech Tunnel Eng* 1:25–39
 10. Singh M, Singh B, Choudhari J (2007) Critical strain and squeezing of rock mass in tunnels. *Tunnel Undergr Space Technol* 2(3):343–350
 11. Luo Y, Chen J, Chen Y, Diao P, Qiao X (2018) Longitudinal deformation profile of a tunnel in weak rock mass by using the back-analysis method. *Tunnel Undergr Space Technol* 71:478–493

Surge Shaft Instrumentation and Monitoring in Himalayan Hydroelectric Projects



K. Sudhakar, B. H. V. Sekar, and S. R. Naik

Abstract The main purpose of providing the surge shaft in hydropower projects is to absorb the water hammer. These shafts have larger diameter when compared to other type of shafts used in underground structures. Surge shafts also serve as a supply tank to the turbine when the water in the pipe is accelerating during increased load conditions and as storage tank when the water is decelerating during the reduced load conditions. The surge shafts may be of open to sky type or may be excavated under rock cover based on the topographical conditions.

Construction of these shafts are critical and expensive when weak geological conditions are encountered. Hence monitoring of these shafts using geotechnical instrumentation during construction will save construction time and cost. The general instrumentation that can be installed in shafts are to monitor displacements in rock around the opening using multipoint extensometers, convergence measurements with tape extensometers and total station, pore water pressure with piezometers, load on support elements using load cells. Based on the instrumentation data decisions can be taken for modification of support system, if required any. In this paper, two case studies related to the instrumentation monitoring of surge shafts in Himalayan region discussed. Numerical modelling studies were carried out using FLAC3D software for comparing the behaviour of the shafts with the instrumentation data.

Keywords Instrumentation · Displacements · Convergence and Pore water pressure

1 Introduction

Surge shafts/tanks are provided in water conducting system primarily to reduce the distance between the free water surface and turbine thereby reducing the water hammer effect on the penstock and protecting upstream tunnel from high pressure rises. The size (height and diameter) of the surge shaft depends on the net head,

K. Sudhakar (✉) · B. H. V. Sekar · S. R. Naik
National Institute of Rock Mechanics, Bengaluru, India
e-mail: kadiyala.sudhakar123@gmail.com

© The Author(s), under exclusive license to Springer Nature Singapore Pte Ltd. 2022
A. K. Verma et al. (eds.), *Proceedings of Geotechnical Challenges in Mining, Tunneling and Underground Infrastructures*, Lecture Notes in Civil Engineering 228,
https://doi.org/10.1007/978-981-16-9770-8_15

259

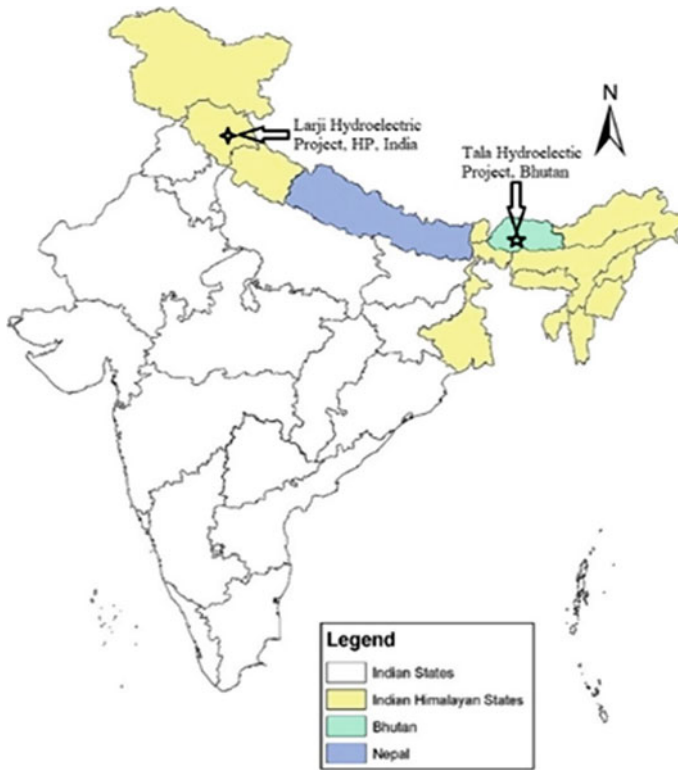


Fig. 1 Location of Tala and Larji HEP's

head loss, length and cross-sectional area of headrace tunnel, velocity of the flow in head race tunnel. Surge shaft excavation is carried out either by full sinking or pilot sinking followed by slashing. Two surge shafts of different sizes from two hydroelectric projects as shown in Fig. 1 are constructed in Himalayan region. During construction of the shafts, to measure the displacements around the opening, multi-point extensometers, convergence measurements by tape extensometers and total station, pore water pressure with piezometers, support system behaviour by way of anchor load-cell and rib load cells were installed and monitored.

1.1 Projects Details

Tala Hydroelectric Project (THP), Bhutan. The 1020 MW Tala Hydro Power Plant was constructed on river Wangchu in Chukha Dzongkagh of Western Bhutan immediately downstream of Chukha Hydroelectric Project. The project was commissioned in July 2006 and is generating power since then under Druk Green Power

Corporation Ltd (DGPCL). The project utilizes 861.5 m of head available from Chukha downstream to Tala Powerhouse.

The main components of the project are 92 m and 130 m long concrete gravity dam, three parallel desilting chambers (250 m (L) \times 13.9 m(W) \times 18.5 m(H), 23 km long and 6.8 m diameter modified horse shoe shape head race tunnel, 168 m deep restricted orifice type - 15 m/12 m diameter surge shaft, 1.1 km long and 4 m diameter dual circular pressure shafts, machine hall cavern (206.4 m \times 20.4 m \times 44.5 m) to accommodate 6 turbines of 175 MW each, transformer hall cavern (191 m \times 16 m \times 24.5 m) in 40 m downstream and 3.1 km long 7.75 m diameter tail race tunnel with other inter connected openings.

Larji Hydroelectric Project (LHP), India The 126 MW Larji Hydroelectric Project is situated on river Beas, about 40 km from Mandi in Mandi district of Himachal Pradesh. It is immediate upstream of Pandoh Dam of Beas-Sutlej Link Project and is located along the National Highway No. 21. The major components of the project are 26.5 m high concrete barrage, four parallel de-sanding chambers (177 m (L) \times 15 m(W) \times 28 m(H), 4.1 km long head race tunnel, 37 m diameter and 82 m deep surge tank, machine hall cavern (109 \times 20 \times 42 m) to accommodate 3 turbines of 42 MW each, transformer hall cavern (50 \times 15 \times 19 m) 40 m downstream and 260 m long tail race tunnel with other interconnected openings.

1.2 Geology at Project Sites

THP. The underground surge shaft and pressure shafts are aligned in lithounits of Thimphu and shumar formations. The contact between these formations crosses the pressure shafts between the EL1252m and EL1010m. Rocks above this thrust contact are mainly moderately jointed, highly folded, fresh variants of gneiss, muscovite/biotite schist, amphibolite and quartzite bands with heavy ingress of the water along the valleyward dipping joints. Fractured nature of rock mass and deep permeation poses problems during excavation and progress of widening of surge shaft. [3] Geological section along the surge shaft is shown in Fig. 2.

LHP. The project area includes Larji and Chail Formations, separated by Larji Thrust. The other geological features occurring in the area are: Aut Member (dolomite and limestone, with shale-slate partings, and algal (stromatolite) structures); and an N-S trending fold axis normal to the Beas gorge. [2]. The rock type encountered at surge shaft consists of Quartz-chlorite-mica schist. Cross section of Larji surge shaft is shown in Fig. 3.

Fig. 2 Geological section at Tala surge shaft

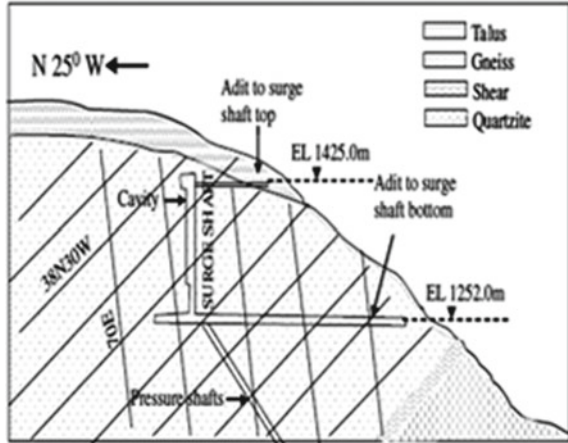
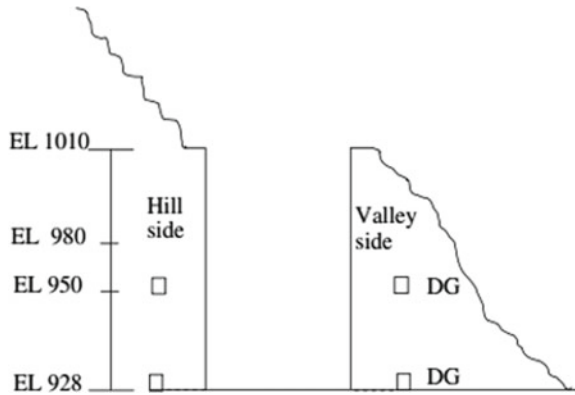


Fig. 3 Sectional view of Larji surge shaft



1.3 Support System in Surge Shafts

THP. The Support system consist of 50 mm thick SFRS as immediate support followed by 32 mm dia, 6 m long rock bolts in 1.5 m c/c staggered, steel ribs and concrete backfill as passive support system with 0.85 to 1.50 m thick RCC lining. [3]

LHP. The support system in the surge shaft consists of 32 mm diameter, 9 m long steel bolts, with the concrete lining. [2].

2 Instrumentation

THP. The rock mass deformations with Multi-Point Borehole Extensometers (MRMPBX) and load on support system (ribs) with the load cells has been monitored while excavation. Three MRMPBX were installed at 40.15, 78.5 and 122 m depth from surge shaft top. Load cell was installed on rib support at 59 m depth near the cavity formation and subsequent concrete back fill to study the effect of this on rib support while with the progress of excavation. Figure 4 shows the instrumentation layout at Tala surge shaft. MPBX was monitored till the completion of excavation [1] and the load cell monitoring was continued during operational period also.

LHP. The rock mass deformations with Multi Point Borehole Extensometers (MPBX) and load on support system (anchor bolts) with the load cells has been monitored while excavation. Installed three target point at EL1005 to monitor convergence/movement with reference point outside the shaft area, four piezometers at EL980, three remote extensometers at 40 m depth (EL970) and four anchor load cells at 65 m depth (EL945) from surge shaft top. Figure 5 shows the instrumentation layout at Larji hydroelectric project surge shaft. [2].

Fig. 4 Instrumentation at Tala Surge Shaft

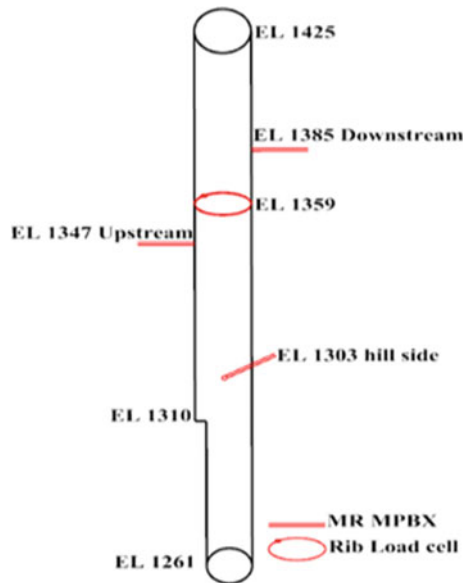
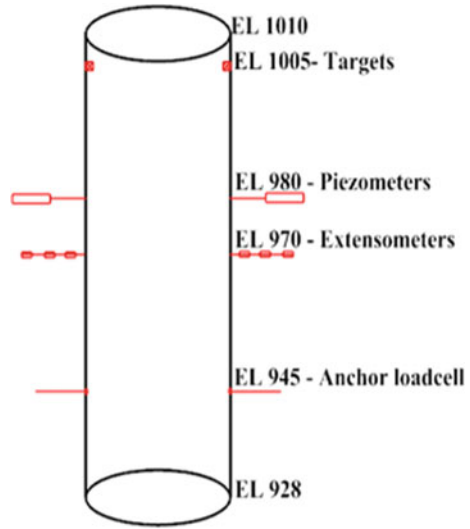


Fig. 5 Instrumentation at Larji Surge Shaft



3 Numerical Modelling of Surge Shafts

Numerical modelling studies were carried out for surge shafts located at Tala Hydroelectric project and Larji hydroelectric project using FLAC3D software. 3D view of the surge shafts at both the project locations are given in Fig. 6 & 7 respectively. 3D numerical modelling studies were carried out for predicting the displacements so as to compare with that of the measured values. The input parameters assumed for the analysis are given in Table 1. The predicted displacement from FLAC3D at EL 1385 m after complete excavation from the time of installation of the instrument at Tala surge shaft is about 2.5 mm whereas the measured displacement is 4 mm. The predicted displacement at EL 1005 m on downstream side for Larji HEP after complete excavation is about 53 mm. The displacements contours for surge shafts after complete excavation at Tala HEP & at Larji HEP are given in Fig. 8 & 9 respectively. However, comparison was not made for Larji surge shaft data due to the delay in installing of instruments with respect to the excavation sequence.

Fig. 6 3D numerical model of Tala Surge Shaft

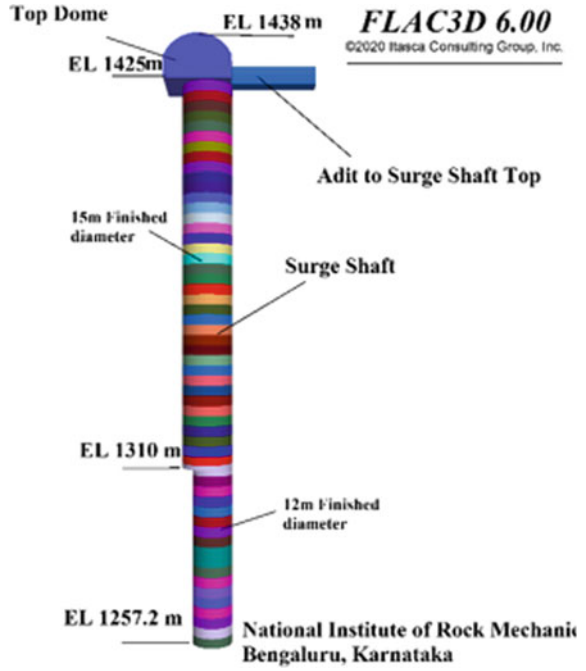


Fig. 7 3D numerical model of Larji Surge Shaft

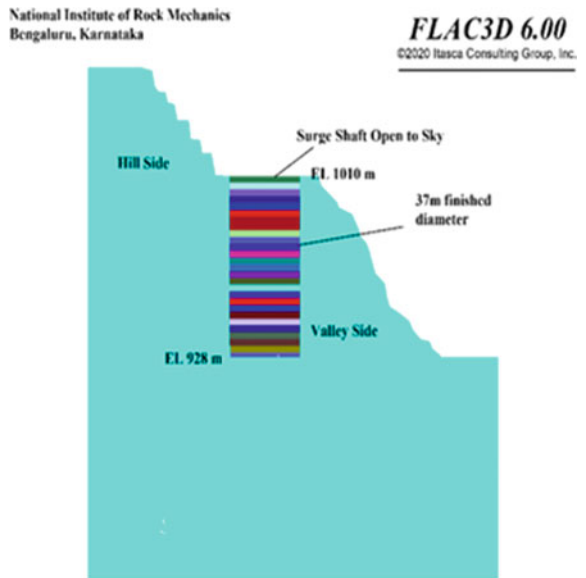


Table 1 Input Parameters considered for analysing the shafts in FLAC3D

Property	Tala surge shaft	Larji surge shaft
Density (kg/m3)	2650	2600
Elastic Modulus of rock mass (GPa)	3.971	6
Poisson's ratio	0.36	0.27
Cohesion (MPa)	1.32	1.2
Friction Angle (o)	29.9	40
Tensile strength (MPa)	0.2	0.2

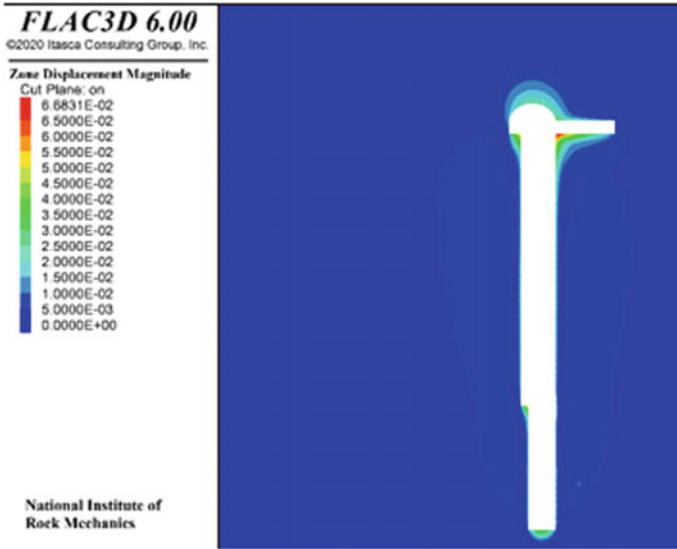


Fig. 8 Displacement Contours for surge shaft at Tala HEP

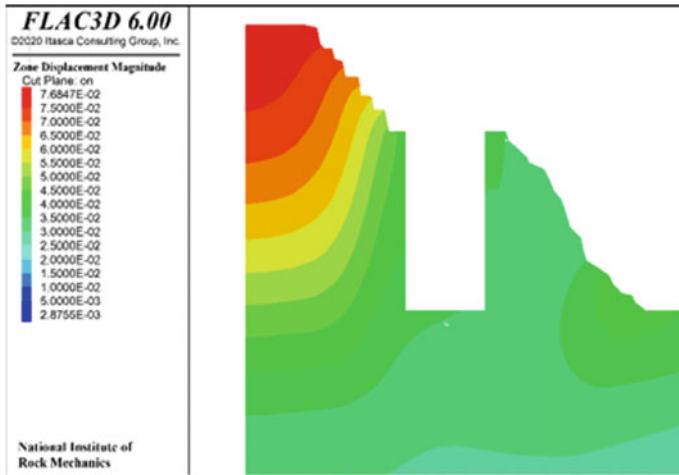


Fig. 9 Displacement Contours for surge shaft at Larji HEP

4 Results and Conclusions

Installation of instrumentation and monitoring was carried out in both projects during excavation stage and the results were presented. Figure 10 & 11 shows the MPBX

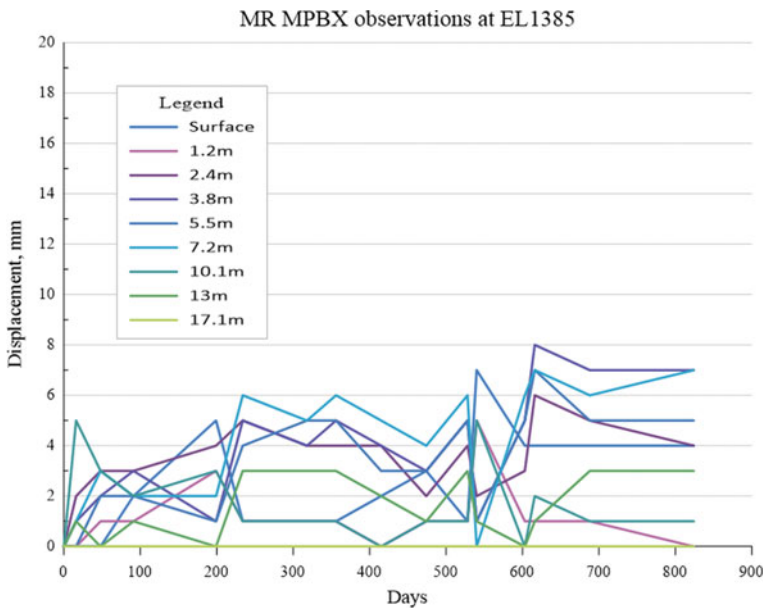


Fig. 10 MPBX at EL1385 at Tala surge shaft

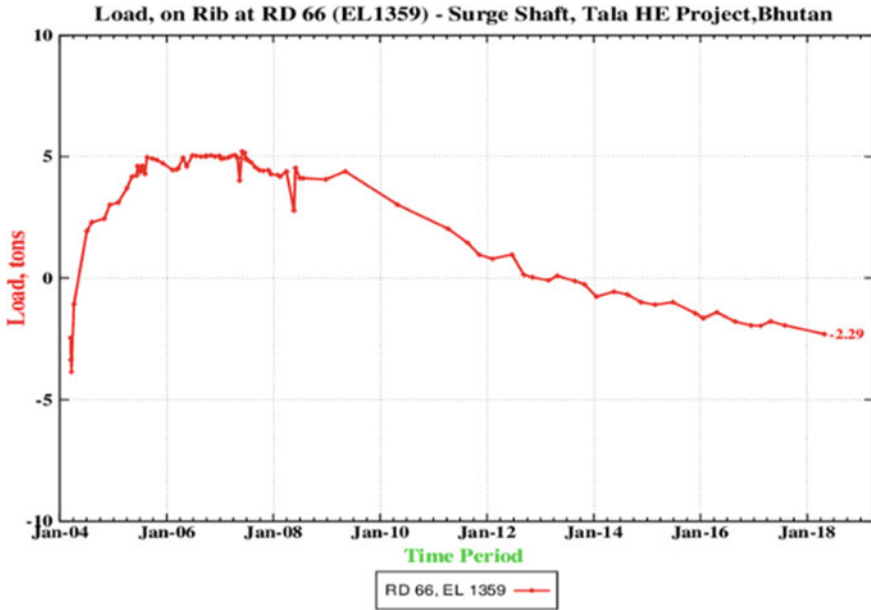


Fig. 11 Load cell at EL1366 at Tala surge shaft

and Load cell observations of Tala surge shaft. Figures 12, 13 and 14 shows the load cell observations, piezometer and target observations of Larji surge shaft.

4.1 Tala Hydro Project Surge Shaft

1. The MPBX at EL1385 measured surface displacement of 4 mm for the period of 824 days. The surface displacement at EL1347 of only 1 mm and at EL1303 only 2 mm was observed in 667 and 400 days.
2. The rib load cell at EL 1366 recorded maximum load of 7.65 tons in 1124 days and reduced to 0 after 5157 days from the date of installation. This may be due to lining transmits part of the internal water pressure to the surrounding rock which, to some extent, is balanced by the external rock pressure.
3. It was observed that there were insignificant movements during excavation and construction stage at Tala Hydroelectric Project.
4. 3D numerical modelling studies were carried out for Tala surge shaft for predicting the displacements to compare with that of the measured values. The predicted displacement from FLAC3D at EL 1385 m after complete excavation from the time of installation of the instrument at Tala surge shaft is about 2.5 mm whereas the measured displacement is 4 mm.

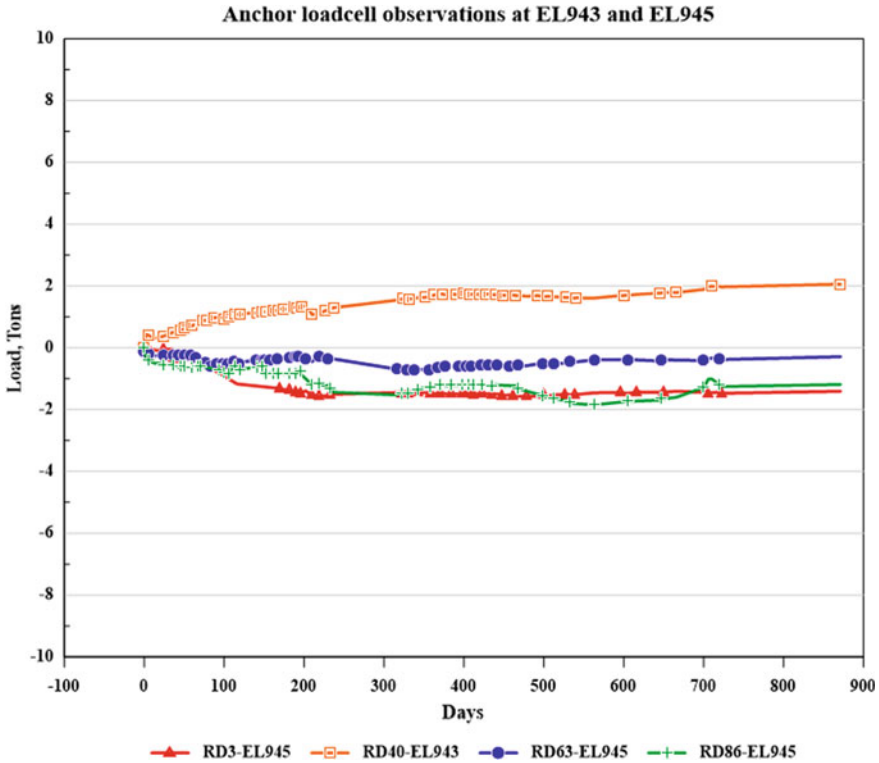


Fig. 12 Load cell at EL943 and EL945 at Larji surge shaft

4.2 Larji Hydroelectric Project Surge Shaft

1. In the piezometers installed at EL980, shows increase in the pore pressure from 5 to 30 kPa was when the lining work was in progress. These values were considered as high for this location. Accordingly, the project authorities were advised to make additional drainage holes to relieve the water pressure in that area.
2. In the load cells installed at EL943 and EL945. The maximum of load of 2.06 tons and stabilized at RD10, EL943 in 871 days. At other locations, the loads were reduced between 0.3 to 1.5 tons and there after shown stable observations.
3. In the Surge Shaft, excessive movements had taken place on the hill side leading to a bench failure while excavation is in progress. The major slide was predicted well in time using Total Station convergence points installed at EL1005. Here the movements recorded were more than 150 mm (vertical & horizontal), leading to the bench collapse. Thereafter, the movements in this area were insignificant.

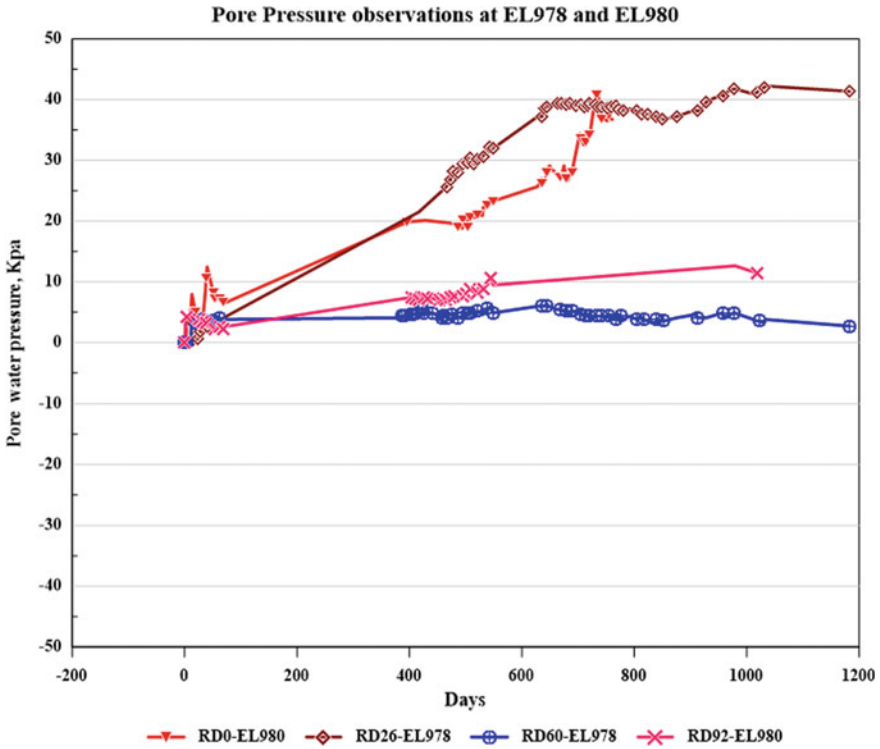


Fig. 13 Piezometer at EL978 and EL980 at Larji surge shaft

4. Based on the excessive movements recorded in the convergence points in the Surge Shaft, it was recommended to modify the blast pattern to minimize the damage to the excavation and the lining.
5. In the Surge Shaft slope, the fault plane is being monitored using convergence points for any potential slides in the future.
6. 3D numerical modelling studies were carried out for Larji surge shaft for predicting the displacements to compare with that of the measured values. The predicted displacement at EL 1005 m on downstream side for Larji HEP after complete excavation is about 53 mm. However, comparison was not made for Larji surge shaft data due to the delay in installing of instruments with respect to the excavation sequence.

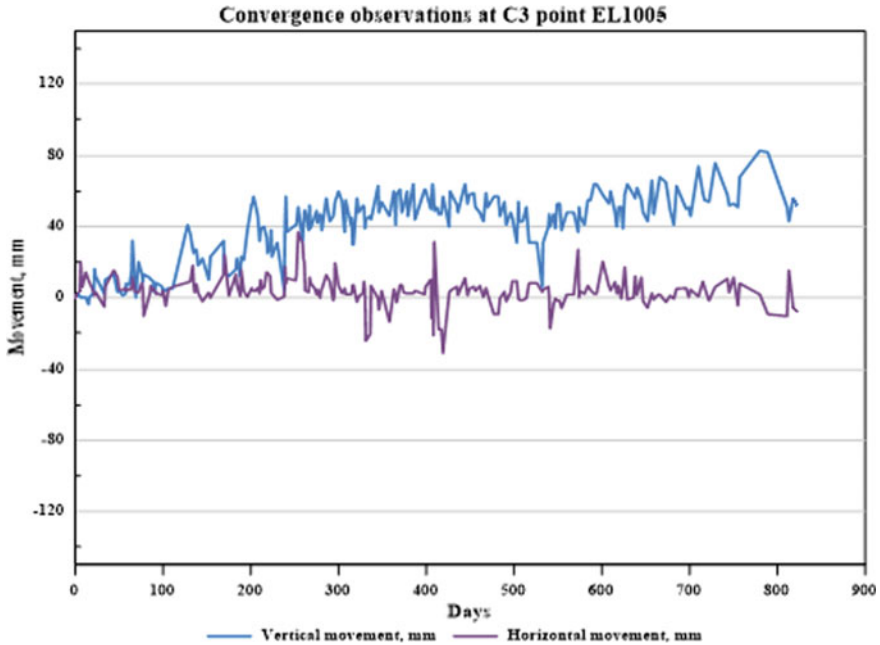


Fig. 14 Displacement observations at Larji surge shaft at EL1005

Acknowledgements Authors thank Director, NIRM for permission to conduct the studies at various project sites. The supports and facilities provided by the management of the hydroelectric projects are thankfully acknowledged.

References

1. Sripad et al (2006) Unpublished report of A study of Rock Behaviour at Powerhouse complex of Tala hydroelectric Project, Bhutan
2. Venkateswarlu V, et al (2007) Unpublished report of Investigations of Rock Deformations in the Underground Excavations at Larji Hydro Electric Project, HPSEB
3. Haride., Vidyarthi US, Jagota RK, Singh R (2007) quality assurance in construction of surge shaft of tala hydroelectric project. In: International workshop on experiences gained in design and construction of tala hydroelectric project Bhutan, New Delhi, 14–15 June 2007, pp 336–347
4. Mehta BK, Gupta RK, Agarwal GK, Rakesh T (2007) Design features of surge shaft and pressure shafts of tala H.E. project. In: International workshop on experiences gained in design and construction of tala hydroelectric project Bhutan, New Delhi, 14–15 June 2007, pp 336–347

Construction Approach of Longest Railway Tunnel of India



Syed Naseem Akhtar and Rajesh Sonkar

Abstract Infra work like tunnels, highways, metro and airport work is exponentially growing in India. One Highway Tunnel (T-80) is developed in Pir Panjal area between Jammu & Kashmir province of J&K(Union Territory) country India, constructed by IRCON in Udhampur-Baramulla-Srinagar-Rail Link Project. This Tunnel is 11 km long and is India's longest transportation Tunnel. The Tunnel has been constructed by New Austrian Tunneling Method (NATM). There were various challenges faced during tunneling in execution, blasting, geotechnical investigation, supports design etc. Collecting geotechnical data was a difficult task, which is backbone of any underground excavation works anyhow with instrumentation and good dedicated team of authors, detailed study was done and to know how the work done, this literature is written.

The purpose of this paper to present various steps and methods which have been followed for construction of Tunnel including selection of tunnel cross section, geology and geotechnical investigations, method of rock mass classification, instrumentation and monitoring etc. This NATM Method of Tunnel construction has been developed by Austrian Engineers based in underground experience gained over the years in Alps. The geological and topographical conditions in Alps and Himalayas mountains are mostly same. This tunnel has been completed within time schedule of its construction period. Construction of Udhampur-Srinagar- Baramulla Broad Gauge Railway Line was undertaken by Indian Railways Construction Organization (IRCON) to establish a dependable means of transportation in the state of Jammu & Kashmir and to connect it with rest of India., to have all-weather route to Kashmir valley. This railway line is passing through Pir Panjal mountain range of Himalayas to reach Kashmir valley and this job has been completed by constructing a railway Tunnel known as Pir-Panjal (T-80) Tunnel. This Pir-Panjal Tunnel is longest transportation Tunnel in India & second largest in Asia having mined length of about 11 km (10,960 km).

S. N. Akhtar
IRCON, New Delhi, India

R. Sonkar (✉)
NIT Raipur, Raipur, Chhatisgarh, India
e-mail: rajeshsonkariocl@gmail.com

Keywords NATM · Rock mass classification · Broad Gauge Railway Line

1 Introduction

Construction of Udhampur-Srinagar-Baramulla Broad Gauge Railway Line was undertaken by Indian Railways Construction Organization (IRCON) to establish a dependable means of transportation in the state of Jammu & Kashmir country India, and to connect it with rest of India. It has an all-weather route to Kashmir valley. This railway line has passed through Pir Panjal mountain range of Himalayas to reach Kashmir valley and this job was accomplished by constructing a railway Tunnel known as Pir-Panjal (T-80) Tunnel. This Pir-Panjal Tunnel is longest transportation Tunnel in India & second largest in Asia having mined length of about 11km (10960 km). South & North Portals of mined Tunnel were located at Chainages 152+600 & 163+560 respectively. This Tunnel across the Pir Panjal range is located between railway stations Banihal in the South & Qazigund in the North. It has extended by constructing 50 & 160 m of Cut & Cover Tunnels towards South & North respectively thereby making the total length of the Tunnel as 11170 m.

2 Tunnel Alignment

2.1 Horizontal Alignment

Except for a length of 42.3 m south of the North Portal, the tunnel is completely straight and runs almost parallel to North - South (1.9°) direction. From CH 163+517.667 the tunnel was in a transition curve of a left bend which extends over a length of 110 m to CH 163+627.667. The adjacent left curve has a radius of 567.516 m.

2.2 Vertical Alignment

The Tunnel has rising gradients of 1 in 100 up to 155+350 & 1 in 124.391 up to 159+101 followed by falling gradient of 1 in 300 with summit at 6.501 km from South Portal. The formation level at South Portal (Ch. 152+600) is 1713.634 m, at North Portal (Ch. 163+600) is 1756.694 m & at Summit (Ch. 159+101) is 1771.479 m.

3 Tunnel Cross Section

3.1 Standard Tunnel Cross Section

The main criteria considered for design of Standard Tunnel Cross Section are:

- The required dynamic clearance envelops of the rolling stock for the running track.
- The required minimum width for a maintenance/rescue vehicle.
- The requirement for a safe escape route for train passengers (walkway).
- The requirements for the electromechanical installations (ducts, pipes etc.).
- The requirements for the permanent drainage system.
- An area of 150 m minimum depth all around the tunnel arch is reserved for maintenance works.

The above requirements are met by providing a semicircular tunnel arch of inner radius 5150 mm (inner surface of inner lining) with the center point of the semi-circle located at a height of 1663 mm above the Rail Level. At the lower portions of the side walls, the inner radius is enlarged to 8150 mm. A 3.0 m wide road has been provided on the left side for maintenance/rescue vehicles.

3.2 Particular Tunnel Cross Sections

The following three types of Particular Cross Sections have been provided for special requirements:

- (i) Truck Turning Niches (for Turning of maintenance/rescue vehicles).
- (ii) Electrical Niches Type 1 (Medium Voltage Substations, UPS) at average internal of 1600 m.
- (iii) Electrical Niches Type 2 (Maintenance Substations) at every 250 m.

4 Water Proffing

This Tunnel has been constructed as a complete water proof tunnel. In order to achieve this, a water proof system has been provided between inner and outer lining of the tunnel. The water proofing system consists of an outer geotextile and an inner water proofing membrane (PVC). The geotextile is fixed locally to the shotcrete surface by means of plastic discs and nails and act as a protection for the water proofing membrane against the rough shotcrete surface and as a drainage layer. The water proofing membrane is the actual water barrier and is fixed to the plastic discs by means of thermal welding. The water proofing system is only installed in the tunnel roof and tunnel side walls.

5 Tunnel Drainage

The Pir Panjal Tunnel has a drainage system to collect the ground water inflow as well as other surface flows resulting e.g., from condensation, leakage and spilled water etc. The main components of the drainage system are as under:

- Main Collector drain/HDPE pipe under the road. Man holes are being provided at every 50 m.
- Perforated pipes of 200 mm in both the sides for collecting the underground water from the periphery of the tunnel. These pipes are connected with main Collector drain at interval of 50 m by lateral drainage pipes.
- Saucer drains of 150 mm on both the sides for surface inflows. These surface drains are connected with main Collector drain at interval of 50 m by lateral drainage pipes.

6 Geology and Geotechnical Investigations

In underground works geology and hydrogeology plays an important role during planning, design, and execution of works. Geology not only influence the cost of the project but it also affects the completion time, behavior of the structure and long-term maintenance practices.

Kashmir valley is situated between two arms of high and rugged mountain range of Himalaya namely Dhauladhar-Pir-Panjal range of middle Himalaya in S-W and Zaskar range of great Himalaya in the N-E. Himalaya being in nascent age, folding and faulting is common in the area and in addition the process of denudation is still continuing. This makes the geology of the area very complex and rapidly changing. Due to the steep slope, accessibility of all the locations on the Tunnel alignment is not possible which makes the situation more unpredictable.

Due to geological complexities involved, an elaborate geological and geotechnical investigation plan was prepared and carried out for Pir-Panjal tunnel. Investigations for the tunnel were planned in two different stages:

- (i) **Planning and Design Stage:** - These included investigations for alignment fixing, planning tunnel work, design and cost estimation.
- (ii) **Construction Stage:** - These included investigations during Excavation of tunnel for Design modification and prediction of approaching geology and hydrology situation etc.

6.1 Investigation During Planning and Design Stage

During planning stage following investigations were done:

- (i) **Geological Mapping:** - Geological Mapping (1:25,000) was performed by Geological Survey of India using Satellite images (1:12,500). This data was used for fixing the alignment with some bore holes to conform the data. After fixing the alignment, a detailed surface map of the area in the vicinity of the alignment (500 m on both sides of the center line) in 1: 1000 scale was generated. A detail drainage map and tectonic map of the area was also prepared.
- (ii) **Geophysical Survey:** - On the portal (across and parallel to the alignment) seismic reflection surveys were conducted. This survey helped in predicting the rock line and hydrology of the area.
- (iii) **Drilling:** - Total 14 nos. of bore holes were drilled in two different phases. The total length of drilling was about 4000 m. Almost all bore holes had crossed the tunnel formation level and maximum drilling length in a single hole was 640 m (BH B-3/80). Lab test were conducted on the samples recovered from the bore holes. Tests conducted in lab were Abrasively test, UCS, Triaxial, Brazilian test, petrography etc. Some field tests like point load test, permeability etc. were also conducted. All these data were used in detail design of the tunnel.

Rock units along the tunnel alignment mainly consists of

- Silicified Limestone/Limestone.
- Andesite/Basalt.
- Quartzite.
- Sandstone.
- Shale.
- Agglomerate Shale & tuff.

On the basis of above data following geological setting (Table 1) are defined along the tunnel alignment:

On the basis of above data, longitudinal section (Fig 1a) & Layout Plan (Fig 1b) of predicted geology were developed & confirmed with the help of bore holes.

6.2 Investigation During Construction Stage

During Construction Stage, face mapping on scale of 1:100 has been carried out for every blast. These mappings were used to update the geological model prepared earlier and suggest more accurate information regarding the geology ahead of the face. This prediction was also evaluated by the Probe holes drilled in the face. Probe holes drilling given information about the geology and hydrological conditions inside the tunnel face. All this data was used in design modification or correction as and when required.

Table 1 Geological setting along the tunnel alignment

Chainage	Geological description
152 + 600–153 + 240	Clayey silt and gravel - silt intercalation
153 + 240–156 + 400	Quartzites and shale's usually dipping to northeast with 30 to 40°. Steeper layers near fold cores and faults. Fold axis strike sub-horizontal northwest-southeast, dipping slightly towards southeast. Faulting usually rectangular to folding and schistose, parallel to folding and in some cases parallel to schistosity. The folding is brittle deformation. A strongly fractured zone with numerous changes of schistosity along a series of brittle folds results a repeated switching between northeast and southwest dipping between 154.250 and 154.700
156 + 400–157 + 300	Agglomeratic slates usually dipping to northeast with 30 to 40°. Steeper layers due to folding. Faults as before but with increase of structures parallel to schistosity. Repetition of tuff and conglomerate layers due to folding around agglomeratic shales
157 + 300–158 + 200	Panjaj Traps, dipping steeply towards southwest. In outcrops south of Panjal Range the dip direction is northeast with 40 to 50°. North of Panjal Range the dip direction is southwest again with 40 to 50°. The transition zone must be the Panjal Range itself. Faulting parallel to schistosity and as before
158 + 200–159 + 400	Quartzite's, shale's and thin limestone layers dip steeply to moderately into south-western direction. Faulting sub-parallel and parallel to schistosity, some rectangular faults and a few west-east bearing structures
159 + 400–162 + 500	Limestone section with a tectonic intercalation of a 500 m thick quartzite-sandstone sequence. Dipping steeply to moderately into south-western direction. Change of dipping (usually between 35 and 65°) due to large scaled folding. Predominance of parallel to schistosity and rectangular faults or fault zones
162 + 500–162 + 900	Quartzite's with minor shale, occasionally with small limestone and volcanic intersections, dipping to south-eastern direction
162 + 900–163 + 560	Clayey silt and gravel silt intercalation

7 Design Approach and Methodology

Pir-Panjaj tunnel design takes into consideration the effects of high overburden, rapidly changing geology, predicted hydrological conditions, safety aspects during construction and operation, and other railway specifications.

7.1 Tunnel System and Safety Approach

New railway tunnels in world use extensive safety measures. This includes safety of the structure and safety during operations. In long tunnel with high cover a twin tube solution is generally used.

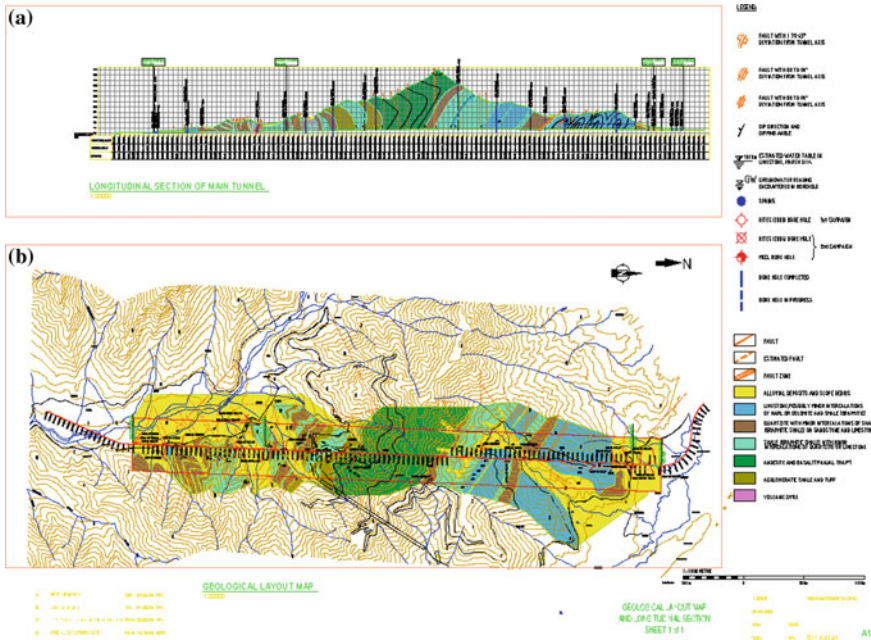


Fig. 1 a Longitudinal geological map b Geological layout plan

Pir-Panjal safety system was based on single tube concept. This includes single track broad gauge rail line and a 3.0 m wide rescue track. This 3.0 m wide road provides better flexibility in terms of the construction program, suitable for tunnel repair works and were used as rescue track.

7.2 Construction Approach

Pir-Panjal tunnel portals in north and south had a cover of around 10 to 16 m. This was considered sufficient to start the tunnel. As tunneling from both ends had to be done under soft ground conditions, hence both portals were constructed under pipe roof.

To complete the project within the stipulated time frame, high rate of progress was desired. This were achieved by means of New Austrian Tunneling Method (NATM). Creation of additional working faces would have definitely saved time.

TBM's are usually the first choice for long tunnels in the homogenous ground. The usage of TBM in the construction of Pir-Panjal tunnel had some reservations. Past experiences in Himalaya regarding TBM's were not encouraging. There was high risk of TBM getting stuck under squeezing ground conditions. TBM's in rapidly changing geology cannot work efficiently. Even then, if TBM's were decided to

be used, two machines would have to be specially designed for the project which would have taken around 12 months and big plants for fabrication of precast concrete segments had to be established. A more detailed geotechnical and geological survey would have been required which would have further increased the project completion time and cost.

NATM method of tunneling was most suitable for the project as it can quickly adjust to the changing geology, works better in soft, excavation sequences and support measures.

At both the Tunnel Portal Zones, Tunnel driving had proceeded through sections of soft ground conditions over several hundreds of meters. Tunnel Excavation in soft ground condition was become crucial for the overall construction time. This construction time were reduced by creating additional work faces and bypassing the soft ground locations at the Portal Zones by means of construction of Adits and Shafts. Therefore, suitable locations for Adit towards Southern side and for Shaft towards Northern side were identified (Fig 2).

Access Tunnel (Adit): The portal of the access tunnel near Tathar Village is about 100 m southwest of the NH-1A at about El 1811. Starting from the portal the alignment of the access tunnel was straight and falls at a gradient of 9.7% for a length of about 690 m. Following, the alignment makes a right turn and intersects the main tunnel at El 1741.3 having a total length of 772 m. At the curved section the gradient was 3%. A gradient of 10% has been used for standard tunnel trucks but required a well-maintained road surface.

Tunnel Shaft: In order to avoid a possible major delay in the main tunnel excavation from the north due to the approx. 600 m long soft ground tunnel section at the north

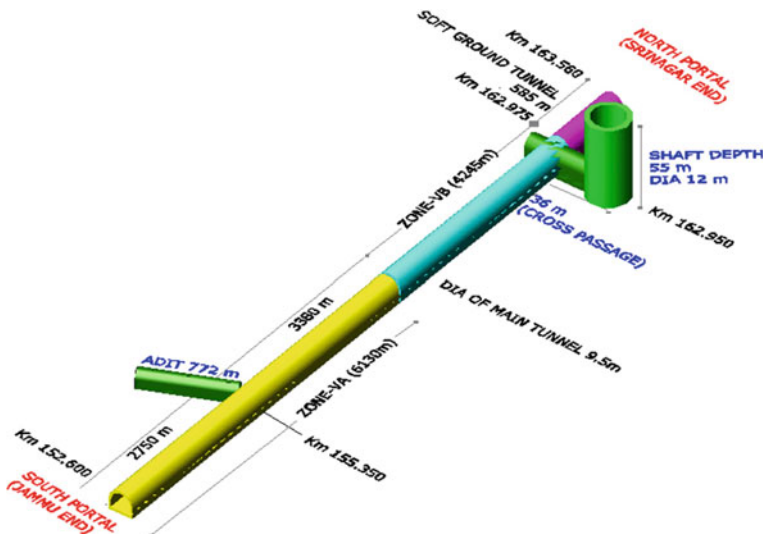


Fig. 2 Adit & Shaft arrangement

portal, an approx. 55 m deep, vertical, circular access shaft was constructed at CH 162+950 was constructed. This shaft was located near the end of the soft ground section close to the main tunnel alignment and was connected to the main tunnel with a cross passage. The access through the shaft enabled an early start of the main tunnel excavation in rock towards south. Consequently, the construction of the soft ground section in the north was no longer on the critical path for the overall construction program. The excavation diameter of the vertical shaft is 12 m. The excavation dimension of the Cross passage is about 11.3 m high and about 9.5 m wide.

7.3 Design Approach

Pir-Panjal tunnel was designed on NATM philosophy. As the name NATM implies, this method was developed by Austrian engineers and in its present form is the result of a long, continuous development with its beginning dating back some 40+ years. At that time there was also existing a so-called “Austrian Tunneling Method”, so the newly developed method was called “New Austrian Tunneling Method” or NATM.

The NATM is rather a concept or philosophy than a construction method. The NATM constitutes a concept, where the surrounding soil or rock mass of a tunnel is integrated into the overall support structure, the rock is activated to a load bearing ring around the tunnel. Old conventional tunneling methods considered the rock mass surrounding the tunnel only as a loading member.

In NATM the initial tunnel support consisting of shotcrete, reinforced by wire mesh or steel fibers, lattice girders and rock bolts, is installed in close contact with the rock surface which forms a composite structure. The composite system rock(soil)/supporting elements allows to control the deformations to achieve stress release and stress redistribution around the tunnel. It also limits the loss of natural rock/soil strength in order to maintain the carrying capacity of the rock arch around the tunnel.

During construction continuous geotechnical measurements and controls are carried out to monitor the stress re-arrangement process, to control stability and to optimize the supporting system, construction sequence and to verify the rock classification.

In Pir-Panjal tunnel inaccessibility of the locations restricted the geotechnical investigations. Hence tunnel design taken into account geotechnical uncertainties and has scope for adjustments to the local condition during construction. In NATM this was done by defining sufficient number of standard excavation classes and/or support classes based of the geotechnical information. Hence behavior of the tunnel during construction becomes foremost important. Pir-Panjal tunnel has a design life of 120 years.

7.4 Tunnel Support System

The Support System for the Pir Panjal Tunnel consists of following:

- i) Fore poles.
- ii) Primary lining i.e., Shotcrete layer with or without wire mesh/steel fibers.
- iii) Lattice Girders.
- iv) Rock Bolts.
- v) Secondary lining (PCC or RCC).

Determination of Rock Support System has been done in the following steps:

Step 1:- Determination of Rock Mass Type (RMT).

Step 2:- Determination of Rock mass Behavior Type (BT)

Step 3:- Determination of Excavation and Support

Step 4:- Determination of Excavation Classes

Step 1: -Determination of Rock Mass Type (RMT)

Rock Mass Type is defined as a geo-technically relevant rock mass volume, including discontinuities and tectonic structure. Different Rock Mass Types have different characteristic parameters that influence their Geo-mechanical behaviors. To determine Rock Mass type, key parameter has evaluated and defined. The key parameters primarily represent ground properties. The most important parameter groups for the Geo mechanical description of rock mass are:

- Intact rock properties
- Discontinuity properties
- Associated rock mass properties

The key parameters were selected, based on different rock types within the project area and the parameters relevant for an underground construction. The rock masses with similar combination of relevant parameters are distinguished to determine Rock Mass Type. Identical lithological types with significantly different discontinuity and intact rock properties have to be specified as different Rock Mass Types. For Pir Panjal Tunnel 12 different RMT (Rock Mass Types) were identified and prescribed as given Table 2. The parameters were obtained from engineering geological mapping and additional site and laboratory investigations.

Step 2: Determination of Rock mass Behavior Type (BT): The Rock Mass Behavior Type was defined as a rock mass with similar behavior with respect to the excavation, spatial and time dependent behavior and failure mode, without consideration of the sequence excavation and support. The rock mass behavior, as a reaction to the excavation, can be evaluated after assigning all relevant properties and influencing factors to each homogeneous section along the alignment. The excavated rock mass behavior resulting from the analyses was then categorized into Behavior Types which have to be assigned to one of the eleven general categories for the project as

Table 2 Different rock mass types at the pir panjal project

RMT	Lithology	Strength (Mpa)	Joint spacing(cm)	Joint properties	Weathering
1	Andesite, Basalt	50–100 to 100–250	60–200	Planar to undulating rough	Fresh to slightly weathered
2	Andesite, Basalt with minor shear zones	50–100	20–60	Planar to undulating rough	Slightly weathered
3	Quartzite, with minor intercalation of shale & conglomerates	50–100 to 100–250	20–60	Planar rough	Fresh to slightly weathered
4	Quartzite, with minor intercalation of shale &	25–50 to 50–100	6–20 to 20–60	Planar rough	Fresh to slightly weathered
5	Silicified Limestone with minor intercalation of shale and quartzite	50–100 to 100–250	20–60 to 60–200	Mainly undulating Smooth	Fresh to slightly weathered
6	Limestone with minor shale	25–50	6–20 to 20–60	Mainly undulating Smooth	Slightly weathered
7	Tuff (predominant), Agglomeratic shale	50–130	20–60	Planar rough to smooth	–
8	Agglomeratic shale (predominant), Tuff, occ. shear zones	80–160	20–60 to 60–200	Planar smooth	Fresh to slightly weathered
9	Shale with minor quartzite and sand stone	60–140	6–20 to 20–60	Planar rough to smooth	Fresh to slightly weathered
10	Quaternary sediments mainly silt-	Stiff-hard	–	–	–
11	Quaternary sediments, gravels and boulders in silty clay matrix	–	–	–	–
12	Crushed & faulted rock of any origin	–	–	–	–

Table 3 Different rock mass behaviour types (BT) for pir panjal tunnel

Behaviour Type (BT)	Description of potential failure modes/mechanisms during excavation of the unsupported rock mass
1 Stable	Stable rock mass with the potential of small local gravity induced falling or sliding of blocks
2 Discontinuity controlled block failure	Deep reaching, discontinuity controlled, gravity induced falling and sliding of blocks, occasional local shear failure
3 Shallow stress induced failure	Shallow stress induced brittle and shear failures in combination with discontinuity and gravity controlled failure of the rock mass
4 Deep seated stress induced failure	Deep seated stress induced brittle and shear failures in combination with large displacements
5 Rock burst	Sudden and violent failure of the rock mass, caused by highly stressed brittle rocks and the rapid release of accumulated strain energy
6 Buckling failure	Buckling of rocks with a narrowly spaced discontinuity set, frequently associated with shear failure
7 Shear failure under low confining pressure	Potential for excessive overbreak and progressive shear failure with the development chimney type failure, caused mainly by a deficiency of side pressure
8 Ravelling ground	Flow of cohesionless dry or moist, intensely fractured rocks or soil
9 Flowing ground	Flow of intensely fractured rocks or soil with high water content
10 Swelling	Time dependent volume increase of the rock mass caused by physical-chemical reaction of rock and water in combination with stress relief, leading to inward movement of the tunnel perimeter
11 Frequently changing behaviour	Rapid variations of stresses and deformations, caused by heterogeneous rock mass conditions or block-in-matrix rock situation of a tectonic mélange (brittle fault zone)

given in Table 3. Sub type has to be assigned, where one or more Behavior Type has been defined in one category.

Step 3:- Determination of the Excavation and Support

In the third step, different excavation and support measures were evaluated and acceptable methods were determined depending on the defined project specific Behavior Type. This includes the evaluation of the system behavior, which represents the interaction between the rock mass and construction measures. The parameters for the determination of system behaviors were:

- Rock Mass Behaviors Type
- Shape and size of underground opening, considering intermediate construction steps
- Spatial and time construction sequence
- Time dependent properties of the rock mass and support element, if relevant
- Support element, their place and time of installation.

Step 4: Determination of Excavation Classes

Finally, Excavation Classes or defined based on the evaluation of excavation and support measures. In Pir Panjal Tunnel after evaluation of RMT, BT, excavation method & support system Eight Different Types of Excavation/Support Classes were decided (Table 4) as under:

7.5 Construction Methodology

The construction methodology adopted in Pir Panjal tunnel could be broadly divided into six parts.

- i) Excavation of Heading along with the support installations (Fig. 3).
- ii) Excavation of Benching & Invert along with the support installations (Fig. 3).
- iii) Casting of Invert.
- iv) Casting of Kicker.
- v) Fixing of waterproofing membrane and geotextile.
- vi) Casting of Overt.

7.6 Tunnel Excavation

The total area of tunneling was excavated in 3 parts called Top Heading, Benching and Invert. The Invert Excavation was applicable only in Rock class – V & above. Based on the geological requirement, three excavation techniques were adopted in Pir Panjal Tunnel.

Table 4 Different rock mass classes and support system

Rock / Support Class	Rock Bolt (SDR/SN/Swellex)	Lattice Girder	Support				Round length
			Wire mesh		Shotcrete		
			1 st	2 nd	1 st	2 nd	
I	None or as per requirements				50mm in crown	> 3m	
II	Locally where Required SN or Swellex (L-3)		•		100mm	2.2 – 3m	
III	No. – 7 SN or Swellex L-4		•		150mm	1.5 – 2.2m	
IV	No. – 11 SN or Swellex L-4	•	•		200mm	1 – 1.5m	
V	No. – 8 SN or SDR L-4 with Fore pole and face bolt	•	•	•	• • 250mm	1 – 1.5m	
VI	No. – 21 SN or SDR L-4 with Fore pole and face bolt	•	•	•	• • 300mm	0.8 – 1m	
VII	No. – 6 SN or SDR L-4 with Fore pole and face bolt	•	•	•	• • 300mm	1 – 1.5m	
VIII	No. – 6 SN or SDR L-4 with Fore pole and face bolt	•	•	•	• • 300mm	1.6 – 2m	

Fig. 3 Excavation sequences

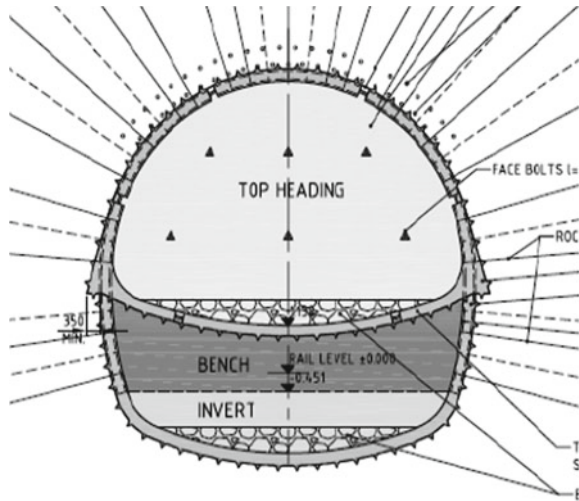


Fig. 4 Tunnel excavator

- a) Excavation by Tunnel Excavator.
- b) Excavation by Road header.
- c) Excavation by Drill & Blast method.

(a) Excavation by Tunnel Excavator:

This method was adopted in soft ground tunneling such as rock class VII & VIII. In this method tunnel face is excavated using a tunnel excavator SAMBOO STE 280 (Fig 4). It has a rotating boom arrangement which makes it very convenient to use in restrained excavation in sectors. This equipment was very useful for successful completion of tunneling in soft ground. The Mucking was carried out with the help of side tilting wheel loader of make Luigong and 20T Wagnor dumpers of make Atlas Copco.

(b) Excavation by Road header:

The road header (Fig 5) was used in north portal of the Pir Panjal Tunnel where the usage of road header was effective and the unconfined compressive strength of rock was less than 100 Mpa. The road header is equipped with a transversal cutting head (Picks) mounted on the end of a boom for excavation which is raised, lowered and slewed from side to side by hydraulic rams. The consumption of picks may vary from 0.025 to 0.3 per cum based on the varying UCS of rocks. The muck herein was accumulated in the apron in the equipment from where the same was loaded to the dumpers via the conveyor installed therein.

The maximum & effective usage of road header was not much possible in Pir Panjal Tunnel as the UCS of rocks was mostly higher than 100 Mpa which causes the reduction of road header performance and increase in consumption of Picks. The

Fig. 5 Road header

overall utilization of Road header in Pir Panjal Tunnel was approximately 9% of total Excavation.

(c) Excavation by Drill & Blast:

In hard rock strata where both of the above-mentioned excavation techniques were not much effective, the drill & blast method was adopted to expedite the excavation. The blast holes were drilled in the face as per the drill pattern (Fig 6) with a 2-boom hydraulic jumbo (L2C & L2D). Then the explosives are loaded in the drilled holes and blast was taken for breaking the face rock. The explosives used in Pir Panjal tunnel are power gel, Long delay detonators (LDD), Non electric detonators (NED), D-cord, 40 & 32 mm dia explosives for effective blasting.

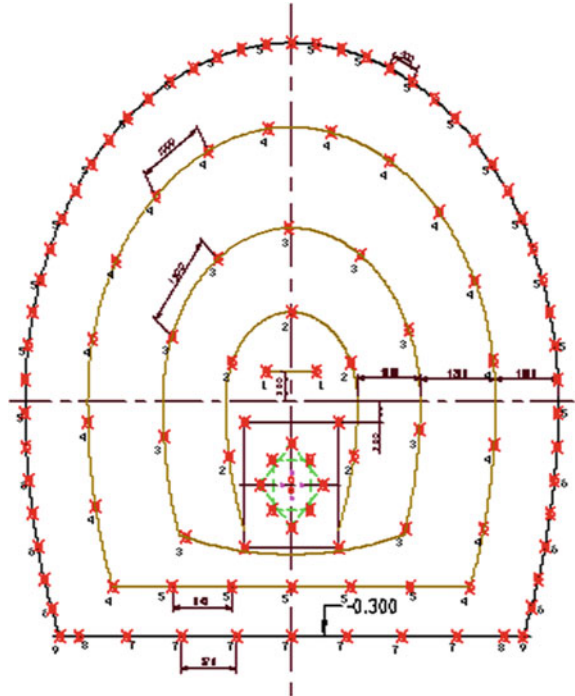
The NED was very useful in this project. The advantage of NED is safe working & the loading of NED can be done parallel to other activities. The mucking work is done with the help of side tilting wheel loader and the 20T wagons.

7.7 Support Installations

After every round of excavation, complete support system as per specific rock class requirement were installed for further advancement. The primary support measures adopted in Pir Panjal tunnel are

- a) Fore poles.
- b) Wire mesh.

Fig. 6 One particular drilling pattern



- c) Primary inner lining shotcrete.
- d) Lattice girder.
- e) Rock bolts.

(a) **Fore poles**

Fore poling was a pre-excitation support element required for tunnel excavation. The provision of Forepoling before excavation is shortening the free span of unsupported excavated surface. The Forepoling may be in the form of steel pipes or rods or self-drilling bolts based on the necessity & site conditions. In Pir Panjal tunnel (T-80), three types of fore poles were used:

- 1) MS Pipe of 40 mm dia.
- 2) SD bolts of 32 mm dia.
- 3) Rebars of 32 mm dia.

In some locations due to poor geological condition 76 mm dia pipe roofing was also used in heading & benching Portion.

(b) **Wire mesh**

The steel wire mesh of Fe 500 grade of size $150 \times 150 \times 6$ was used in Pir Panjal tunnel. The wire mesh is installed along the periphery of the excavated / shotcrete layer after completion of face sealing shotcrete. It was fixed tightly

along the excavated area with the help of steel hooks of 8 mm dia. The main purpose & function of wire mesh is to increase the shear strength and to reduce the shotcrete cracking due to creep and overstraining.

(c) **Primary lining (Shotcrete)**

The inner lining shotcrete with or without wire mesh was the primary support measure that was immediately applied to the excavated Profile. The thickness of shotcrete lining varies from 100 to 300 mm depending on the rock class requirement. The grade of shotcrete used in Pir Panjal tunnel is M25. For early setting of shotcrete, the alkali free accelerator (MEYCO SA -160, SIGUNIT L54 AF) is used. The type of shotcrete used in Pir Panjal tunnel was Wet shotcrete which is applied with the help of CIFA wet shotcrete machine with Robo Arm.

(d) **Lattice Girder**

Lattice Girder was a steel structure prefabricated and installed to impart triaxial strength to the primary shotcrete. It was manufactured with tor steel reinforcement of 25, 16 & 10 mm dia. It was a support element which enables the lateral loads to uniformly distribute across the cross-section. Two types of lattice girders were fabricated and used in Pir Panjal tunnel for primary supports. These were $95 \times 16 \times 25$ & $70 \times 16 \times 25$.

(e) **Rock bolts**

Depending upon the rock conditions, the rock bolts were installed both radially and in the faces with subsequent grouting to strengthen the strata. Various types & length of rock bolts are used in Pir Panjal Tunnel based on the required support system (Table 5). The rock bolts are fixed using 2 boom hydraulic Jumbo.

Tunnel Lining:

The permanent concrete lining work was carried out after completion of Excavation & primary support works. The lining work was carried out in parallel to other activities. The grade of concrete designed for tunnel lining is M30. The lining of main tunnel was being carried out in three stages (Fig 7) to a length of 12.5 m (called 1 Block) leaving construction joints behind which all were blocked by water stoppers.

(a) Casting of Invert portion

Table 5 Various types of rock bolts used in pir panjal tunnel

Sl. No.	Type of rock bolt	Length
1	Self-Drilling Rockbolts (SDR) of 32 mm dia	4, 6, 9, 12, 15 m with minimum yield strength of 200 to 230 KN
2	Soil Nail (SN) Rockbolts of 25 mm dia	3, 4, 6, 9 m with minimum yield strength of 200 KN
3	Swellex rockbolts	3, 4 m with minimum yield strength of 150 KN
4	Fiber glass Rockbolts	9 m

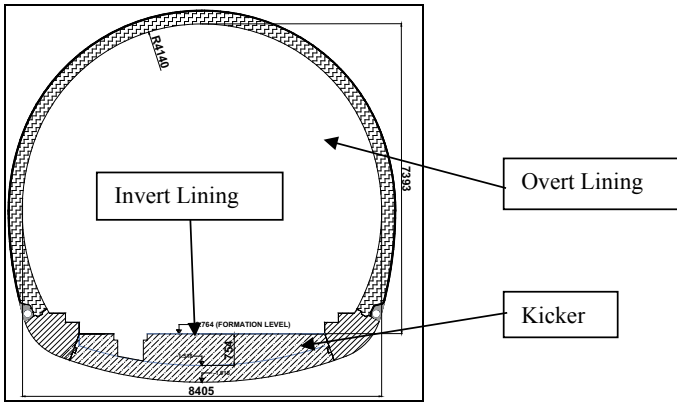


Fig. 7 Lined tunnel profile

- (b) Casting of kicker portion
- (c) Fixing of water Proofing Membrane.
- (d) Casting of Overt Lining.

8 Instrumentation and Monitoring

Systematic and frequent monitoring, observation and interpretation were important components of the NATM. The main function of instrumentation was to determine whether the observed system behaviour lies within the specified limits and to validate the appropriateness of excavation and support measures.

Another aspect of instrumentation is to predict and update geotechnical and geological models so to enable the designer to take appropriate corrective measures for further excavation and support systems.

8.1 Three-Dimensional (3D) Monitoring of Tunnel

Bireflex type of targets (Fig 9) are used for 3-D monitoring with measurements being done with help of Tunnel Profiler or Total Station. The targets were mounted on convergence bolts with an adapter in the final shotcrete layer and zero reading being taken just after the installation. 8–10 DMP points (Fig 8) from the previous monitoring section was used to setup the instrument. Initially daily reading of the section was taken with frequency was reduced with distance to face and decreasing rates of the displacements. These readings are than analyzed with the help of software EUPALINOS of GEODATA to observe any deformation in the tunnel which was produced in pictorial form.

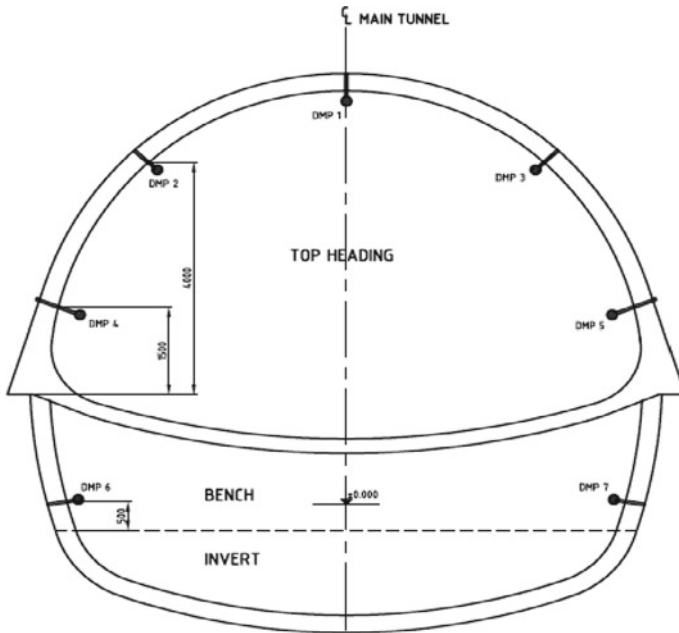


Fig. 8 Locations of bireflex targets

Fig. 9 Bireflex targets



8.2 Extensometers

Extensometers were used for determination of ground movements outside of the excavated structure. They allow an assessment of the development of strains in the surrounding ground and stabilization of movements around an excavation. In Pir

Panjajal Tunnel 3-fold extensometers (3, 6, 9 m) with anchors were used which were connected to the ground by grouting at predefined positions.

8.3 Rock Bolt Axial Force Meter “Measuring Anchor”

Measuring Anchors (Fig 10) were used to determine the load development along the anchor. Measuring anchors were installed together with rock bolt load cell and extensometers. Measuring anchor, also known as rock bolt extensometer, was a combination of rock bolt and extensometer and was used to determine the loading profile on rock bolts. It was used for evaluation of anchor system forces and their distribution within the anchor bolt and hence its safety and effectiveness. It serves as a complete anchor in system anchoring. With the obtained data, forces on anchor due to loosening effect of the rock and their distribution can be known. Thus the rate of utilization of anchoring may be determined and the length as well as the grid of the system anchors can be adjusted.

Fig. 10 Measuring anchors



Fig. 11 Strain meters



8.4 Strain Meters

The strain meters (Fig 11) are been installed to measure the strain in the lining. The strain gauges provided here is the resistance type strain gauge with the following specifications.

8.5 Pressure Cells

Shotcrete Pressure Cells (Fig 13) were used to monitor radial as well as tangential stresses in shotcrete and optimize its thickness. Cells were installed after excavating the tunnel but before applying the shotcrete. Radial cells (Fig 12) were placed at the interface between the excavated ground surface and the shotcrete lining. Tangential cells (Fig 12) were attached to the reinforcing cage or some other support so they will be embedded in the shotcrete lining. Once the cells are positioned, shotcreting takes place. After the shotcrete cures, cells are pressurized by crimping the cell's pressurization tube, which forces oil from the tube into the cell. The influx of oil causes the cell to inflate, forcing the sensitive side of the cell into contact with the surrounding shotcrete material.

Fig. 12 Radial and tangential pressure

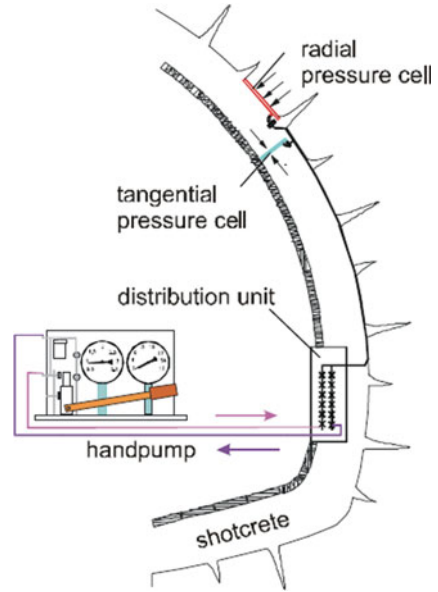
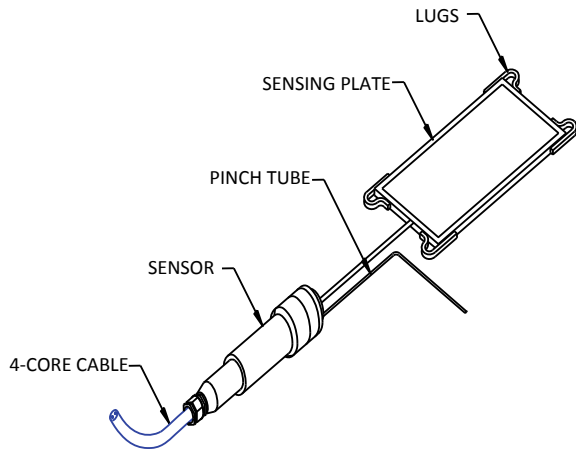


Fig. 13 Pressure cell



9 Conclusion

New Austrian Tunneling Method (NATM) has been proved to be very successful Tunneling Method in Himalayas where geological variations are very large and use of TBMs has not been very successful. This method provides flexibility in Design and construction based on behavior of different Types of Rock Masses as observed after excavation and results of instrumentation. This method is also economical in design as the inherent strength of surrounding Rock Mass is also taken into account.

Geological investigation, measurement, instrumentation, monitoring, data collection its analysis and interpretation is back bone of any tunneling operation. The data not only help in designing part, but in design of execution method and support system deployment. Further during execution regular geo monitoring, geo face mapping, 3D monitoring, deformation monitoring helps in redesigning the method and support system which in turn economizes project cost and early completion too.

References

1. Duggal VK, Pandey DK (2001) Design features of Jammu-Udhampur-Srinagar-Baramulla Rail Link Project
2. Kumar V (2008) Construction of India's largest underground railway project world tunnel Congress-India. In: World tunnel congress
3. NHPC Ltd Faridabad (1999) Final Geotechnical Report on Rail Tunnels (Udhampur - Katra Rail Link Project)
4. Tejal P, Udit J, Payal Z (2014) Rail link project a case study on Jammu-Udhampur-Srinagar-Baramulla. *Int J Curr Res Acad Rev* 2:167–172
5. Project IRCON: Tunnel T74R (2010) Detailed Design Consultancy, 3D Monitoring and Supervision of Tunnel T-74R (between km 125 and 134) in connection with construction of Dharam-Qazigund Section of Udhampur- Srinagar-Baramulla New BG Railway Line Project in Jammu and Kashmir State (India)

Geoenvironmental Assessment of Soil Slopes Around Leh Manali Highway in Himachal Pradesh, India



Geshu Khare, Vipin Kumar, and Sahil Sardana

Abstract The slope failure in the vicinity of the Atal tunnel in Himachal Pradesh is a serious concern which damages infrastructure and consequent traffic disruption along Leh Manali highway. It is the only link road connecting the Manali city to the Atul tunnel therefore, the stability assessment of road cut slopes along this stretch is the most important concern for safe transportation. The lack of earlier geotechnical and stability investigations motivates this study to focus on an integrated approach for the field investigation, geotechnical laboratory characterization and numerical modelling to understand the influence of various factors on slope instability. The mineralogical, geotechnical, and strength parameters that can affect the stability of existing slope have been determined in the laboratory for four soil slopes along this road. One of the slopes has a recurring failure in nature; therefore, a stability assessment was performed based on the limit equilibrium method and the result has been validated against the field observation. After that, a remedial measure has been proposed and validated through limit equilibrium analysis to achieve slope stabilization.

Keywords LEM · Field investigation · Geotechnical laboratory

1 Introduction

The stability of a slope is governed by numerous factors such as geomorphological features [1], freeze–thaw [2], rainfall/groundwater [3], seismic activities [4] and vegetation. The frequency of landslides in the Himalayan region has been increased due to the geodynamic behaviour of the slopes [5, 6]. Approximately 30% of the total losses due to landslides and related destruction has been contributed Himalayan region [7]. Due to rapid climatic change and an increase in the frequency and intensity of rainfall causing dislodging of the bulk of weathered material from its original location which has increased flows down the hills. The slopes in the Indian Himalayan region

G. Khare (✉) · V. Kumar · S. Sardana

Indian Institute of Technology (Indian School of Mines) Dhanbad, Dhanbad, Jharkhand
826004, India

e-mail: geshu.16dp000139@ese.ism.ac.in

© The Author(s), under exclusive license to Springer Nature Singapore Pte Ltd. 2022
A. K. Verma et al. (eds.), *Proceedings of Geotechnical Challenges in Mining, Tunneling and Underground Infrastructures*, Lecture Notes in Civil Engineering 228,
https://doi.org/10.1007/978-981-16-9770-8_17

297

are unstable and fall under the avalanche-prone area [8]. Which cause damages to infrastructures and also fatal accidents [9, 10]. Slope failures in the Himalayan region show interweaved relationship between tectonic and erosional processes that leads to the geomorphic denudation [11]. Climatic conditions have a crucial control on topographical development [12] and also accountable for various types of landslides in the Indian Himalayan Region [13–15].

This study focuses on an integrated approach to field investigation, geotechnical investigation and numerical modelling to understand the instability factors near Atal tunnel. Solang valley roadway is the only link between Manali city to the Atal tunnel that provides all-weather connectivity. This road has witnessed many slope failure events in history. In 2016, an earthquake act as a triggering event in the monsoon season that leads to slope failure along this roadway and large tension cracks where developed on the road. Absence of the previous study concerning geotechnical parameters and slope stability makes this study necessary for safe transportation and livelihood in this area.

2 Study Area

2.1 Location

The study area is located near south portal of Atal Tunnel in Himachal Pradesh, India, located above an altitude of 10,000 ft (3048 m). The south portal is about 24.3 km from Manali Atal tunnel is an alternative route to the Manali-Leh highway. Palchan is a tri-point for Manali, Solang Valley and Rohtang pass (Fig. 1).

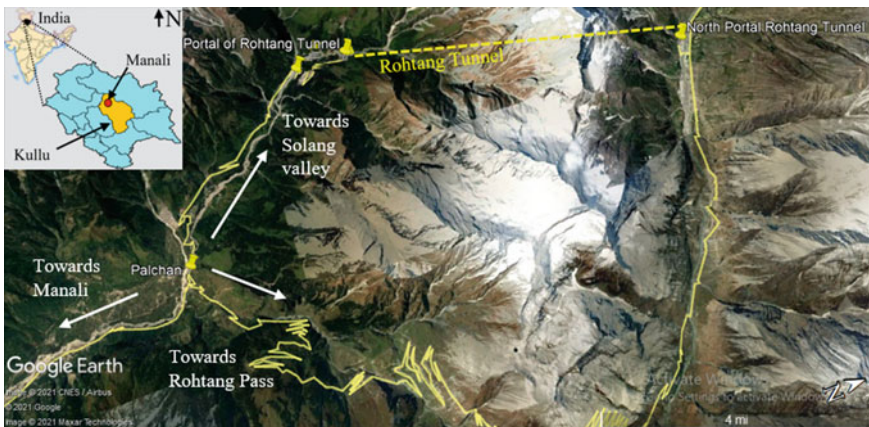


Fig. 1 Google Satellite image showing the location of studied slope near Atal tunnel

2.2 *Geology and Stratigraphy of the Area*

The study area comes under the northwest part of the Himalayas, with an elevation of 2600–3000 above MSL. The geological information reveals six major tectono-stratigraphic units around the Mandi-Rohtang area [16]. The studied area falls under two major stratigraphic units, namely Vaikrita Group and Jutogh Group. Atal tunnel project is located within the Vaikrita group of central crystalline Himalayas that have anticlinely folded structure that trends roughly along the axis of the Great Himalayan Range, extending from East to West. Tunnel mainly passes through the Salkhala Group, mainly comprised of Quartz-schist, from the South Portal.

3 Methodology

The present study focused on the experimental investigations and the stability analysis of the soil slope near the Atal tunnel. The soil samples were collected at a depth of about 1.0 to 1.5 m from the surface for the experimental investigation which includes mineralogical and geotechnical properties as per American Society for Testing Materials (ASTM) standards. Further, these values were used in the probabilistic and reliability analysis concerning slope stability.

4 Results and Discussion

A detailed field investigation has been carried out on the soil slope in the study area. The height and width of the slopes was approximately 30 and 110 m respectively. The roadway along these slopes has a width of 8 m. Further, the slope has a valley of more than 20 m in depth. Vegetation has been observed on the upper part of slope. Slopes in the studied area are observed to be vertical to sub-vertical. Figure 2 show the field photographs of the studied slope. A major failure has been observed on slope which damaged the roadway in September 2016, induced by an earthquake (Fig. 2b). Field investigation suggested that steep angles with overburden mass with significant erosion are responsible for slope sliding.

4.1 *Mineralogical Analysis*

The mineralogical and microscopic analysis has been performed using the X-Ray Diffraction (XRD) method and Scanning Electron Microscope (SEM). Minerals identified in the XRD analysis are quartz, albite, clinocllore (Mg rich chlorite) and

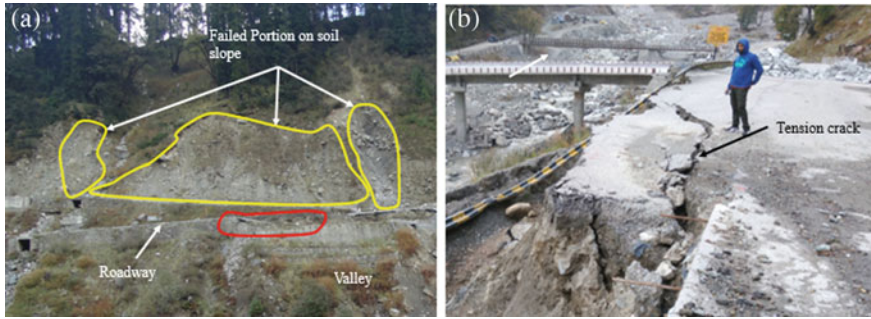


Fig. 2 Slope scenarios near Atal Tunnel, **a** failed section and **b** tension crack on roadway and valley side

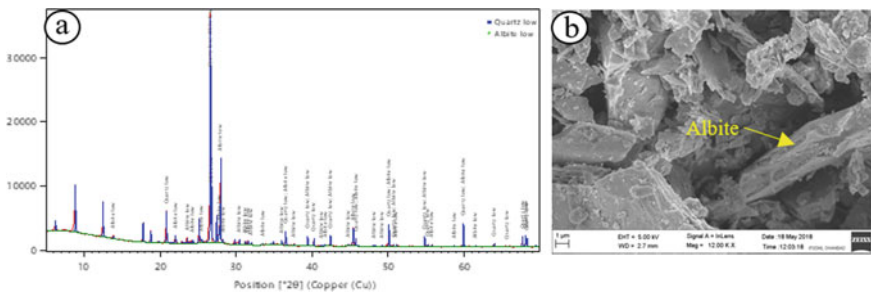


Fig. 3 **a** X-ray diffraction patterns and **b** SEM for the soil specimens

zeolite (Fig. 3a). SEM images showed weathering of the mineral particles. The micro-images (Fig. 3b) indicate the hexagonal nature of weathered quartz grain, weathered flakes of phyllosilicate minerals and triclinic habit of weathered albite respectively.

4.2 Geotechnical Characterization

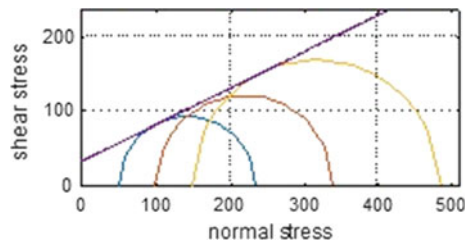
The following geotechnical properties, namely natural moisture content (NMC), specific gravity, grain size analysis, dry-density, liquid and plastic limit, UCS, cohesion and friction angle for four locations, have been determined in the laboratory in accordance with the ASTM and IS standards and their values are summarized in Table 1.

The lower moisture content shows lesser voids. The topsoil has a natural moisture content of about 8.1% with specific gravity of 2.66. Based on consistency limits, the topsoil shows low to intermediate plasticity with a plasticity index of 7.8 to 21.0%. Dry-density and optimum moisture content (OMC) have been determined using standard proctor compaction. Maximum dry density and OMC were obtained

Table 1 Geotechnical and strength properties estimated in the laboratory for the soil specimens

Property	Values	Unit
Natural moisture content	8.1	%
Specific gravity	2.66	–
Gravel	30.1	%
Sand	55.0	%
Silt	14.9	%
Liquid limit	37.7	%
Plastic index	19.8	–
Dry density	2.0	(g/cm ³)
UCS	73.56	KPa
Cohesion	33.4	KPa
Friction angle	26	degrees

Fig. 4 Mohr–Coulomb failure circles for studied slope based on the triaxial compression test



as 2.0 and approximately 12%, respectively. Generally, the values of NMC are less than OMC but in this study, NMC values are close to the OMC values as the sample was collected during the rainy season. In addition, unconfined compressive strength (UCS) and triaxial compressive tests were carried out on the soil specimens. Experimental results show that the UCS for the studied slope was about 73.56 kPa (Table 1). Cohesion and friction angle values have been estimated by plotting Mohr–Coulomb failure circles (Fig. 4) which show of shear strength parameters i.e. cohesion and friction angle are 33.4 kPa and 26°, respectively (Table 1).

4.3 Stability Assessment

In this study, the probabilistic and the deterministic analysis have been carried out to satisfy possible variations in the soil properties. Outcome of the stability analysis has been represented in terms of deterministic and probabilistic factor of safety (FoS), probability of failure (PF) and reliability index (RI). The RI is a probabilistic measure of safety and it can be mathematically represented as Eq. 1 for normally distributed safety factors. Value of RI should be higher than 3 for safety assurance. The RI of 0 indicates mean FoS = 1 and its negative value represents unsafe design i.e. mean

FoS < 1.

$$\beta = \frac{\mu - 1}{\sigma} \tag{1}$$

where, β : reliability index, μ :mean FoS, σ :standard deviation of FoS.

Stability analysis has been performed for pre-failure conditions using the Bishop method. Probabilistic analysis for pre-failure slope reveals FoS of 0.75, negative RI and 100% PF (Fig. 5a). Failure surfaces obtained in the analysis corroborates the failed surface observed during field investigations indicate a negative RI was expected in the analysis. Outcome of the analysis is tabulated in Table 2.

Major triggering factors for failed slope are rainfall, slope geometry and slope material properties. Installation of strata monitoring instruments over a failed surface is a quite difficult task. Therefore, a possible mitigative measure was suggested that includes reinforcement of slope using soil nails to stabilize the slope. Soil nails of 8 m length and 200 kN capacity were placed normal to the boundary of the model. Analysis of reinforced slope shows a mean FoS of 1.19, RI of 3.61 and 0.00% of PF (Fig. 5b).

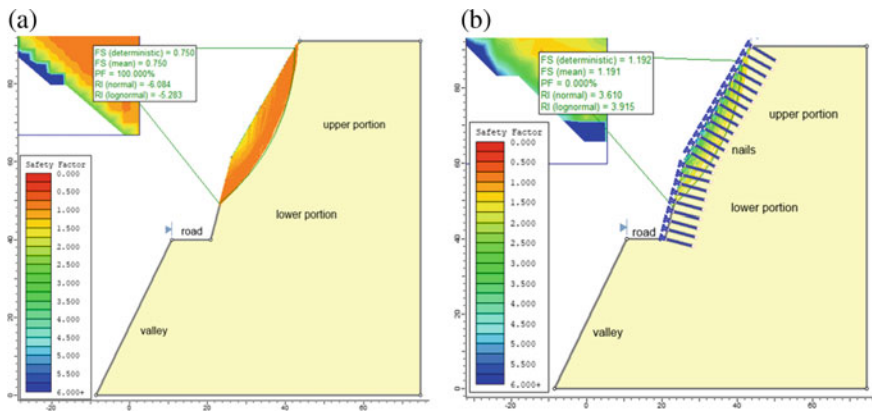


Fig. 5 Factor of Safety for a pre-failure slope b reinforced slope

Table 2 Outcome of the limit equilibrium analysis for studied slope

Slope	Factor of safety		Probability of failure (%)	Reliability index (normal)
	Deterministic	Probabilistic		
Pre-failure	0.75	0.75	100.00	-6.084
Reinforced	1.192	1.191	0.00	3.61

5 Conclusion

The study adopted an integrated approach of field investigation, laboratory investigation and slope stability assessment. Field investigation shows that the slope had a repetitive failure in the past few decades. XRD and SEM images have identified the minerals and the analysis reveals presence of weathered flakes of phyllosilicate, weathered quartz grain, and weathered albite. Some index properties such as NMC, specific gravity and grain size analysis were determined to classify soils. Probabilistic analysis shows an FoS less than 1, negative RI and a 100% probability of failure for slopes. Therefore, a mitigative measure of soil nail spacing of approximately 2.5 to 2.75 m is required to achieve the FoS of 1.2 and RI of 3 has been suggested that result in enhancement of FoS to 1.19, RI of 3.6.

References

1. Hoek E, Bray JW (1981) *Rock Slope Engineering*, 3rd edn. Institute of Mining and Metallurgy, London
2. Sardana S, Sinha RK, Verma AK, Singh TN (2021) Investigation into the freeze-thaw induced alteration in microstructure and deteriorative responses of physico-mechanical properties of himalayan rock. *Bull Eng Geol Environ*, 1–14
3. Jaswal M, Sinha RK, Sen P (2020) Delineation of phreatic surface in soil type slope—a comparative study using physical and numerical modeling. *J Min Sci* 56(3):494–504
4. Valagussa A, Frattini P, Crosta GB (2014) Earthquake-induced rockfall hazard zoning. *Eng Geol* 182:213–225
5. Verma AK, Sardana S, Sharma P, Dinpuia L, Singh TN (2019) Investigation of rockfall-prone road cut slope near Lengpui Airport, Mizoram, India. *J Rock Mech Geotech Eng* 11(1):146–158
6. Nikhil Kumar AK, Verma SS, Sarkar K, Singh TN (2018) Comparative analysis of limit equilibrium and numerical methods for prediction of a landslide. *Bull Eng Geol Environ* 77(2):595–608
7. Dahal RK, Hasegawa S, Yamanaka M, Dhakal S, Bhandary NP, Yatabe R (2009) Comparative analysis of contributing parameters for rainfall-triggered landslides in the Lesser Himalaya of Nepal. *Environ Geology* 58(3):567–586
8. Verma AK, Sardana S, Singh TN, Kumar N (2018) Rockfall analysis and optimized design of rockfall barrier along a strategic road near solang valley, Himachal Pradesh, India. *Ind Geotech J* 48(4):686–699
9. Sardana S, Verma AK, Singh A (2019) Laldinpuia: Comparative analysis of rockmass characterization techniques for the stability prediction of road cut slopes along NH-44A, Mizoram, India. *Bull Eng Geol Env* 78(8):5977–5989
10. Sardana S, Verma AK, Verma R, Singh TN (2019) Rock slope stability along road cut of Kulikawn to Saikhamakawn of Aizawl, Mizoram, India. *Nat Haz* 99(2):753–767
11. Bartarya SK, Valdiya KS (1989) Landslides and erosion in the catchment of the Gaula River, Kumaun Lesser Himalaya, India. *Mt Res Dev* 9(4):405–419
12. Bhargava ON, Srikantia SV (2014) Geology and age of metamorphism of the Jutogh and Vaikrita Thrust Sheets, Himachal Himalaya. *Himalayan Geol* 35(1):1–15
13. Verma AK, Sinha RK, Sardana S, Jaswal M, Singh TN (2021) Investigation into the rockfall hazard along Lengpui-Aizawl Highway, NH-44A, Mizoram, India. *Ind Geotech J* 51:1–14
14. Sardana S, Sharma P, Verma AK, Singh TN (2020) A case study on the rockfall assessment and stability analysis along Lengpui-Aizawl highway, Mizoram, India. *Arab J Geosci* 13(24):1–14

15. Sardana S, Verma AK (2017) Qualitative assessment of road cut slope in the northeast region of india - a case study. In: IndoRock 2017: seventh Indian rock conference, New Delhi, India, pp 284–289
16. Misra DK, Tewari VC (1988) Tectonics and Sedimentation of the rocks between Mandi and Rohtang, Beas Valley, Himachal Pradesh, India. August

Parametric Study of Influence of Groundwater and Joint Spacing on Stability of a High Overburden Tunnel



A. Srivastav, Ashutosh Kainthola, V. Dangwal, and T. N. Singh

Abstract In a complex terrane, excavation engineers have to take into account various problems and challenges. Himalaya is rugged with highly undulating topography, major discontinuous boundaries, extremely heterogenous lithology and complex subsurface water system, which makes the excavation process more troublesome in it. Groundwater decreases the strength of the rock mass through increase in pore-water pressure and decrease in effective stresses. The Present research is based on estimation of influence of groundwater and discontinuity spacing on tunnel stability through field deformation and numerical simulation. The study site is part of Rishikesh-Karnaprayag railway project in Uttarakhand Himalaya. The tunnel has the diameter of 7.8 m with the overburden depth of 200 m. Sandstone rocks surrounding the excavation boundary belong to Mandhali formation. Initially, numerical model was simulated using the properties of discontinuities exposed at the tunnel phase and the mean properties of Borehole log data nearest to the excavation site. Afterward, deformation is calibrated at different water pressure heads and various discontinuity spacings. The variation in deformation is significant with variation in groundwater pressure and discontinuity spacing and reveals the importance of these parameters during underground excavation and stability assessment.

Keywords Finite element analysis · Tunnel stability · Ground water influence

1 Introduction

During underground excavation in Himalaya, sometimes geologist and engineers are astonished by the unpredicted challenges and surprises due to complex tectonics and

A. Srivastav · A. Kainthola (✉)

Department of Geology, Banaras Hindu University, Varanasi 221005, UP, India

e-mail: ashutosh.geo@bhu.ac.in

V. Dangwal

RailVikas Nigam Limited, Rishikesh 249201, Uttarakhand Himalaya, India

T. N. Singh

Department of Earth Sciences, IIT Bombay, Mumbai 400076, MH, India

multiple deformation settings. In Himalaya, at regional scale several heterogeneities are common, however at local scale both types of conditions homogenous as well as inhomogeneous may exist. The tunnel stability and support installation depend upon rock mass conditions. The major parameters that make excavation process difficult and influence the rock mass conditions are lithology, overburden depth, ground water infiltration, weathering condition, scale of discontinuities and deformation present in the region.

Generally, the rock mass surrounding the tunnel is classified by empirical methods and primary support installed based on applied rock mass classification. The tunnel stability can be assessed through analytical methods and numerical modelling. The analytical methods are suitable for regular geometries instead of complex tunnel shapes [1]. The advantage with numerical methods is that they deal with complex geometries with ease and provide approximate solutions [2]. Discontinuities affect rock mass conditions mechanically [3]. Several researchers have included discontinuities during the numerical simulation [4–7]. The controlling factors in jointed rock mass are joint spacing, joint orientation relative to tunnel alignment, joint roughness and joint aperture [8]. The ground water influx is another parameter that affect tunnel stability strongly [9]. Several researchers have studied the ground water influence in tunnel stability [10, 11].

The present tunnel site is situated near Shivpuri, approximately 19 km from Rishikesh, Uttarakhand. The face conditions of chainage 22 + 300 are studied through numerical modelling with finite element method. The chainage is bearing the overburden pressure of 200 m depth. The mean material properties at different depths have been used from testing results of Borehole-29 (BH-29), conducted by Rail Vikas Nigam Limited (RVNL). In present research influence of groundwater and discontinuity spacing on tunnel deformation is studied keeping heterogeneities of Himalayan conditions in mind.

2 Study Area

Rishikesh-Karnaprayag railway project is 125.2 km long single tract railway line to be constructed under Rail Vikas Nigam Limited (RVNL) in Uttarakhand. Total 84% route length will be covered by 17 tunnels and 35 bridges (RVNL baseline report). The present studied tunnel is part of Rishikesh Karnaprayag project and is situated in Tehri Garhwal district, Uttarakhand, India.

Lithologically, the area is dominated by meta-sedimentary rocks of lesser Himalayan Succession and occurrence of sandstone, siltstone, limestone, shale, phyllites and slates are mainly present. These rocks are of Neoproterozoic to Paleozoic age. In Tehri Garhwal region, outcrops of Jaunsar group, Baliana group, Krol group and Tal group are present. Jaunsar group is comprised of Mandhali formation and Chandpur formation from older to younger respectively. Baliana group is formed by Blaini formation followed by Infra Krol formation. Stratigraphically, Baliana is followed by Krol group and it consists of rocks of Mahi formation, Jarashi formation

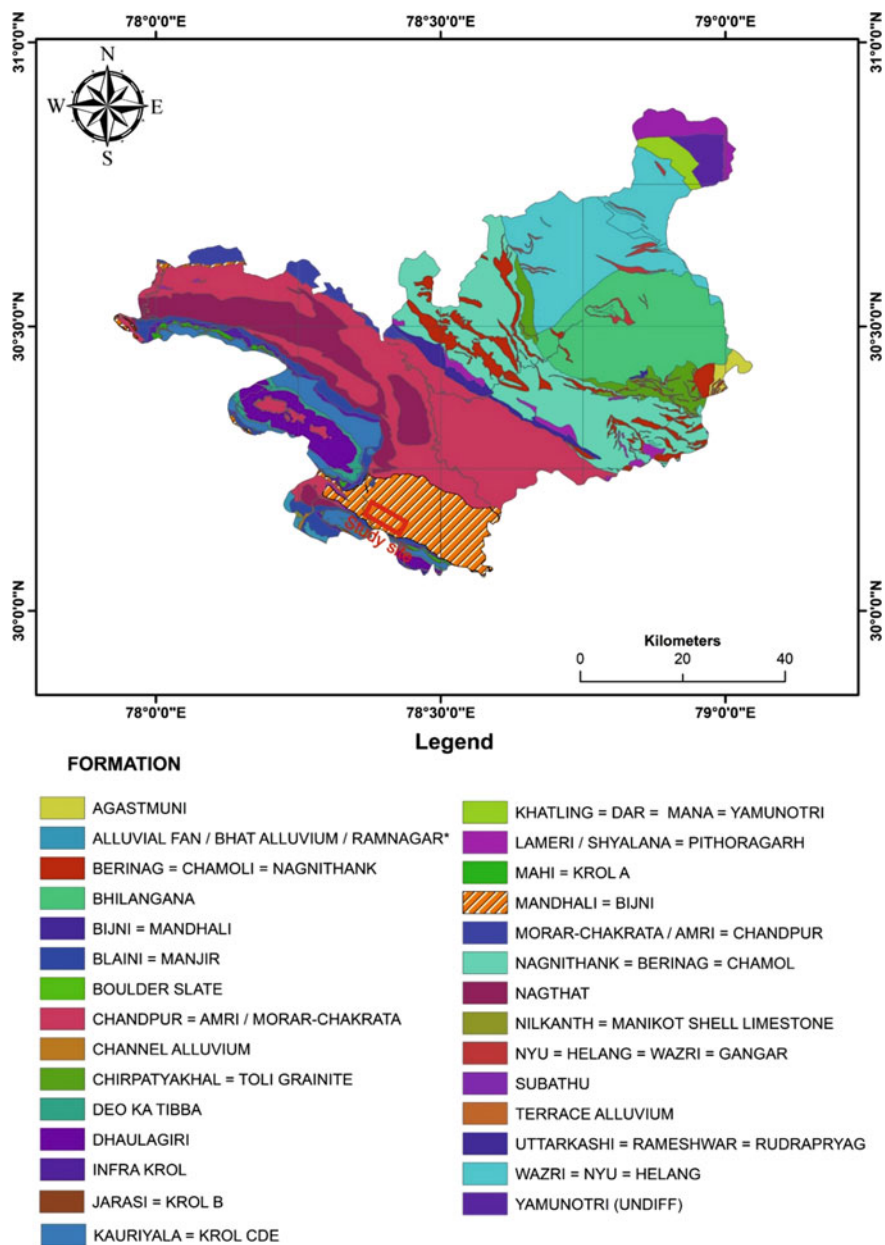


Fig. 1 Geological map of Tehri Garhwal district [12]

Table 1 Physical and elastic properties of rocks of BH-29 at different depths

Layer	Logged section depth (m)	Unit weight (KN/m ³)	Mean Poisson's ratio	Mean UCS (MPa)	Young's Modulus (MPa)
Sandstone top	24.5 to 62.2	26	0.15	40	1*10 ⁴
Sandstone middle	62.2 to 130	26.3	0.20	50	1.5*10 ⁴
Sandstone bottom	130 to 200	26.5	0.25	68	2.6*10 ⁴

and Kauriyala formation. Present study site consists of rocks of Mandhali formation of Jaunsar group. The rocks of purple sandstone, siltstone, grey phyllite and shale are exposed mainly in Mandhali formation.

The present study is based on stability assessment in T2 tunnel passing through rocks of purple sandstone of Mandhali formation. The characteristics of purple sandstones encountered during the excavation are that rocks are jointed, fresh and unweathered. Two parallel tunnels (one main tunnel and one escape tunnel) are being excavated simultaneously with respective diameters of 8.4 and 7 m (Fig. 1).

3 Methodology

3.1 Borehole Testing

The borehole testing has been conducted by Rail Vikas Nigam Limited in Package 2 of Rishikesh-Karnaprayag project near Adit 2. The strength properties of intact rock and rock mass, derived from borehole testing outcomes, are used in the numerical simulation. The tunnel is passing through overburden of 200 m near borehole-29 (BH-29). The overburden comprises of soil and sandstone rocks. The variation sandstone strength properties with depth is considered during modelling and simulation. Total three layers of sandstones has been considered based on mean properties of borehole testing at different depth ranges. The properties used in the numerical simulation from BH-29 are shown in the Table 1 (RVNL baseline report).

3.2 Numerical Simulation

Numerical simulation helps in visualization and analysis of engineering problems mathematically through computational software. Finite element method (FEM) is powerful and intuitive method to assess the tunnel stability condition and providing

both linear and non-linear solutions [13–15]. FEM discretizes the model as continuous body and solves the engineering problems using partial differential equations (PDE). FEM breaks the complex geometrical model into finite number of simple geometrical shapes and makes the calibration robust and easier. The tunnel stability has been assessed through 2-dimensional numerical model using RS² software of RocScience. During the modelling, 6 node triangular elements are used, for meshing. For solving the partial differential equations, Gaussian elimination method has been used in which matrix rows are reduced by elimination.

3.2.1 Boundary Conditions

The tunnels are mainly excavated in semi-infinite to infinite rock mass conditions. The boundary conditions are defined to separate the modelled rock mass from the rest [3]. Present model height is 255.5 m and width 139.4 m. The main tunnel has diameter of 8.4 m and escape tunnel has 7 m. Both tunnels are separated by 24 m distance. The side boundaries (width) and bottom boundary (depth) are kept 5–7 times of the tunnel diameter to reduce the influence of boundaries [16, 17]. The top surface is kept free restrained whereas side walls and bottom boundaries are applied fixed restrain in both X and Y directions. Tunnels in undulated topographical hilly conditions are under gravitational loading primarily [18]. Hence, only gravitational loading is applied. The stress field ratio (k) is considered 1 during the computation (Fig. 2).

3.2.2 Material Characteristics and Failure Criterion

Mohr–Coulomb failure criterion is applied in modelling soil material. The depth of soil material is upto 24.5 m. Mohr–Coulomb criterion is expressed in Eq. (1).

$$\tau = c + \sigma_n \tan \phi \tag{1}$$

where τ is shear strength (MPa), c is cohesion (MPa) and σ_n is normal stress. The properties of soil are derived from testing results of borehole soil samples (Table 2).

Poisson’s ratio of soil has been assumed 0.30 and Young’s Modulus has been obtained from Eq. (2) [19].

$$E = 291.759 - 0.723G - 0.815S - 1.673F + 0.115PL - 0.104 \ll +8.687\gamma - 90.256G_s \tag{2}$$

where G is % of gravel, S is % sand, F is % of fines, PL is plasticity limit, LL is liquid limit, γ is unit weight (KN/m³) and G_s is specific gravity. The values of G, S, F, PL, LL, γ and G_s are 10, 45, 45, 7, 22%, 20 (KN/m³) and 2.65 determined from the soil testing results of borehole data. Young’s modulus is calibrated 105 MPa from Eq. 2.

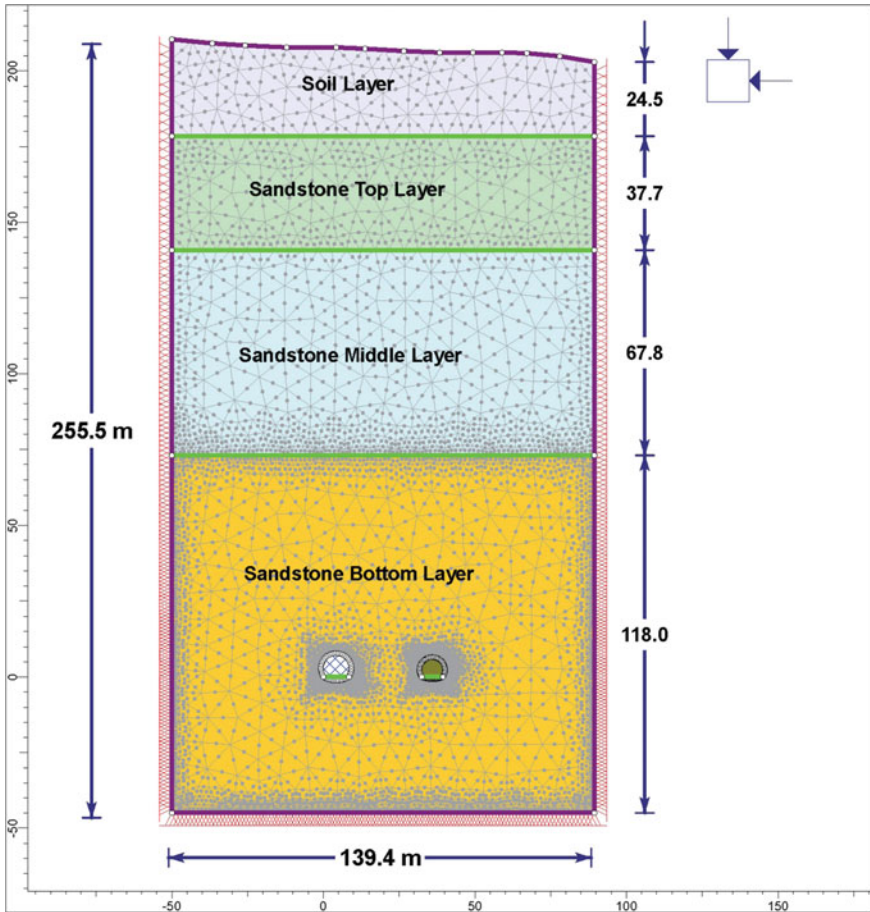


Fig. 2 Boundary conditions of numerical model [26]

Table 2 Properties of soil layer

Material type	Depth range (m)	Unit weight (KN/m ³)	Cohesion (KPa)		Friction angle (°)	
			Peak	Residual	Peak	Residual
Soil	0 to 24.5	20	10	5	30	24

Generalized Hoek–Brown failure criterion has been applied for the rock mass behaviour [20]. The failure criterion is expressed in Eq. (3).

$$\sigma'_1 = \sigma'_3 + \sigma'_{ci} \left(\frac{m_b * \sigma'_3}{\sigma'_{ci}} + s \right)^a \tag{3}$$

Table 3 Properties of rock mass

Material layer	GSI		m_b		s		a	
	Peak	Residual	Peak	Residual	Peak	Residual	Peak	Residual
Sandstone top	56	48	4.36	3.28	0.0075	0.0031	0.504	0.507
Sandstone middle	60	50	5.03	3.52	0.0117	0.0039	0.503	0.506
Sandstone bottom	63	52	5.60	3.78	0.0164	0.0048	0.502	0.505

where σ'_1 and σ'_3 are maximum and minimum effective stresses, σ'_{ci} is effective compressive strength. m_b is reduced material constant for the rock mass derived from intact material constant m_i . m_b is obtained from Eq. (4)

$$m_b = m_i e^{\frac{GSI-100}{28-14D}} \tag{4}$$

where, GSI is geological strength index, D is disturbance factor, its values vary between 0 to 1. s and a are rock mass constants calculated from the Eq. (5) and (6).

$$s = e^{\frac{GSI-100}{9-3D}} \tag{5}$$

$$a = \frac{1}{2} + \frac{1}{6} \left(e^{\frac{-GSI}{15}} + e^{\frac{-20}{3}} \right) \tag{6}$$

Properties of intact rock used in the numerical simulation are presented in Table 1. The rock mass properties applied during the simulation are shown in Table 3.

3.2.3 Joint Conditions

Two sets of primary joints ($41^\circ/074^\circ$ and $79^\circ/295^\circ$) are present at the chainage near BH-29. Tunnel alignment is in 135° . The apparent dips in section perpendicular to tunnel alignment are 23 and 61° . Discontinuities are defined by using Barton-Bandis joint slip criterion [21–25] (Table 4).

Table 4 Joint geometrical and mechanical properties of the chainage 22 + 300

Joint set	Joint spacing (m)	Length (m)	Persistence (m)	JCS (KPa)	JRC	Residual friction angle	Normal stiffness (KPa/m)	Shear stiffness (KPa/m)
J1	1	10	0.5	20,000	9	28	3.71×10^6	3.71×10^5
J2	1	10	0.5	20,000	9	28	3.71×10^6	3.71×10^5

3.2.4 Hydrological Conditions

The groundwater table is 26.5 m below the ground surface. The purple sandstone layer is aquifer and affecting the tunnel stability. Steady state method is used for groundwater analysis. The pore water unit weight is 9.81 KN/m³. The mean porosity of sandstone is 10%. The influence of ground water is assessed through finite element modelling at different groundwater depths. The ratio of hydrological conductivities k_2/k_1 is 1.

4 Result and Discussion

Initially, deformation is assessed with actual ground conditions with groundwater table at 26.5 m below the ground surface and joint spacings of 1 m. The maximum total displacement of 23 mm is determined through numerical simulation after excavation in the unlined tunnel condition. After that influence of joint spacing and pore water pressure is assessed at various range of joint spacings from 0.4 upto 3 m and water table depths from 26.5 to 200 m (Fig. 3).

Total 13 numerical models have been simulated at different water table depths with interval of 15 m each. After moving the water table down from actual conditions, the thickness of water column is reduced, with decrease in pore water pressure. The

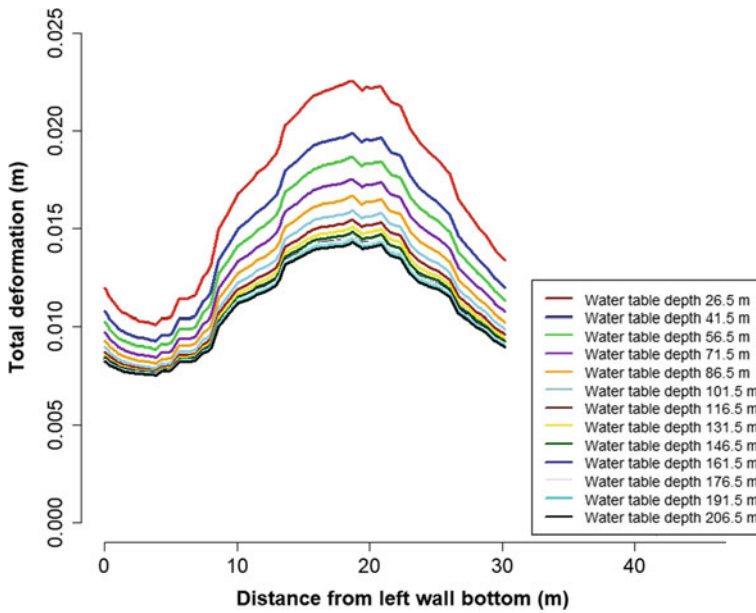


Fig. 3 Tunnel deformation at different water depths

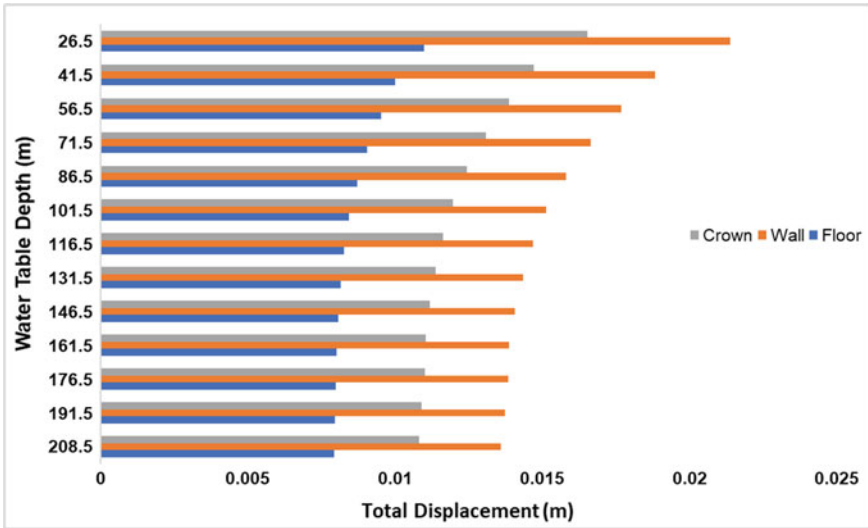


Fig. 4 Tunnel deformation with water depth at crown, wall and floor

numerical simulation has been done to numerically quantify the deformation with reduction in pore water pressure (Fig. 4).

The influence of declining water table is analyzed separately at crown, wall and floor. Initially, maximum total displacement is reduced at wall 11.9% followed by 11% reduction at crown and 9% at floor after declining the water from 26.5 to 41.5 m. After analyzing all the 13 models it has been observed that reduction in total deformation with decline in water table depth is not following linear path. The reduction in deformation was higher initially then lower with decline in water table depth. The variation of total displacement with water table depth is following given Power equations (Fig. 5).

$$Totaldisplacementatcrown = 0.032x^{-0.209}, R^2 = 0.9869 \tag{7}$$

$$Totaldisplacementatwall = 0.0434x^{-0.223} R^2 = 0.9868 \tag{8}$$

$$Totaldisplacementatfloor = 0.0182x - 0.162, R^2 = 0.9747 \tag{9}$$

where x is water table depth in m.

Different joint spacing models have been analyzed with discontinuity spacing from 0.4 to 3 m. Similar to water table declination, the total displacement is reducing non linearly with increase in joint spacing. Discontinuities reduce the strength of rock mass; hence displacement increases decrease in discontinuity spacing. X_j is joint spacing in m (Fig. 6).

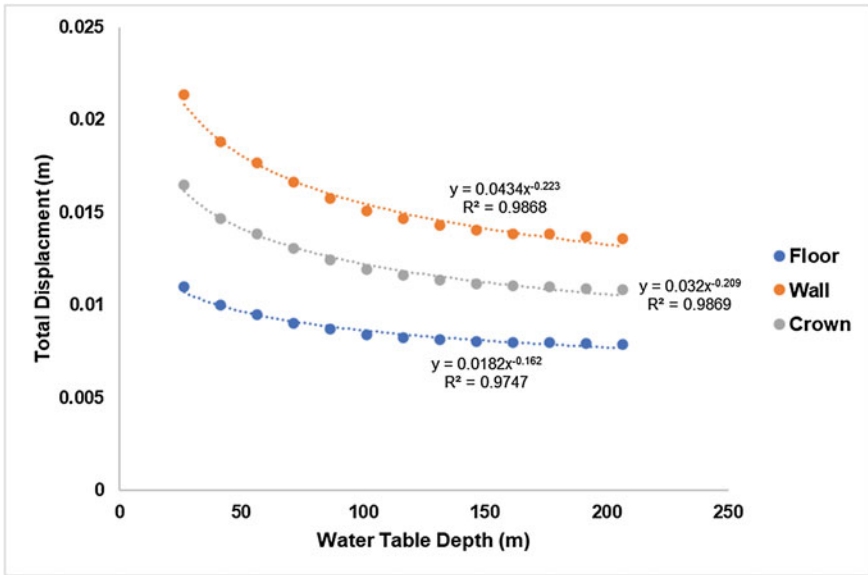


Fig. 5 Mean total displacement with water table depth at crown, wall and floor

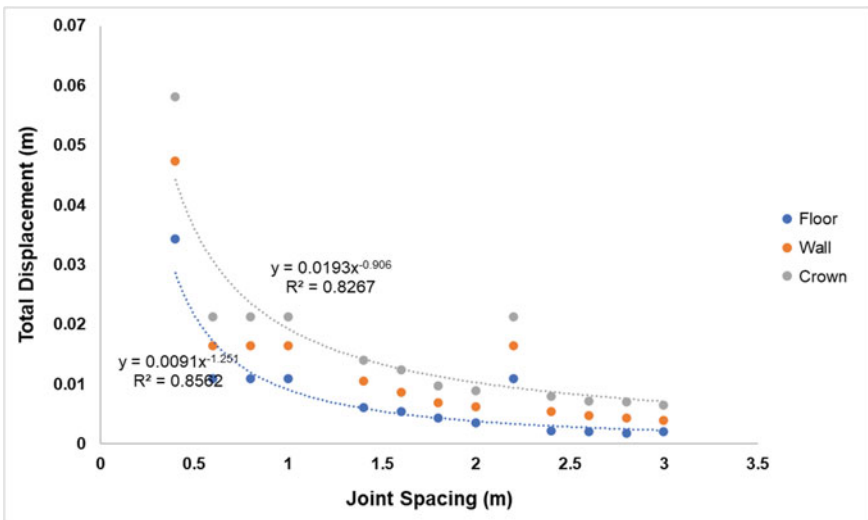


Fig. 6 Total displacement with joint spacing at crown, wall and floor

$$Total\ displacement\ at\ crown = 0.0193x_j^{-0.906}, R^2 = 0.826 \quad (10)$$

$$Total\ displacement\ at\ floor = 0.0091x_j^{-1.251}, R^2 = 0.8562 \quad (11)$$

5 Conclusion

Ground water influx and discontinuity spacing are significant parameters influencing tunnel stability. In present research, tunnel behaviour is observed with change in discontinuity spacing and ground water table depth. The maximum total displacement in unlined tunnel having water table at 26.5 m depth and 1 m joint spacing is 23 mm. Initially, a significant decline is observed with decline in water table or with decrease in discontinuity spacing from 1 m. The variation of both the parameters has been shown through Power equations from Eq. 7 to Eq. 11. These equations can be useful in assessing stability in similar conditions.

Acknowledgement The authors are grateful to Rocscience Inc. (Canada) for the analysis tool.

References

1. Sulem J, Panet M, Guenot A (1987) An analytical solution for time-dependent displacements in a circular tunnel. *Int J Rock Mech Min Sci Geomech Abstr* 24(3):155–164
2. Tani K, Itoh K, Takahashi M, Tanno H, Komuro T, Miyajima H (1994) Numerical study of free-piston shock tunnel performance. *Shock Waves* 3(4):313–319
3. Shen B, Barton N (1997) The disturbed zone around tunnels in jointed rock masses. *Int J Rock Mech Min Sci* 34(1):117–126
4. Hao XJ, Feng XT, Yang CX, Jiang Q, Li SJ (2016) Analysis of EDZ development of columnar jointed rock mass in the Baihetan diversion tunnel. *Rock Mech Rock Eng* 49(4):1289–1312
5. Do TN, Wu JH (2020) Simulation of the inclined jointed rock mass behaviors in a mountain tunnel excavation using DDA. *Comput Geotech* 117:103249
6. Das R, Singh TN (2021) Effect of rock bolt support mechanism on tunnel deformation in jointed rockmass: a numerical approach. *Undergr Space* 6(4):409–420
7. Broere W, Van Tol AF (2000) Influence of infiltration and groundwater flow on tunnel face stability. *Geotech Aspects Undergr Constr Soft Ground* 1:339–344
8. Tseng DJ, Tsai BR, Chang LC (2001) A case study on ground treatment for a rock tunnel with high groundwater ingress in Taiwan. *Tunn Undergr Space Technol* 16(3):175–183
9. Park KH, Owatsiriwong A, Lee JG (2008) Analytical solution for steady-state groundwater inflow into a drained circular tunnel in a semi-infinite aquifer: a revisit. *Tunn Undergr Space Technol* 23(2):206–209
10. Butscher C (2012) Steady-state groundwater inflow into a circular tunnel. *Tunn Undergr Space Technol* 32:158–167
11. Liu JQ, Chen WZ, Yuen KV, Zhou XS (2020) Groundwater-mud control and safety thickness of curtain grouting for the Junchang Tunnel: a case study. *Tunn Undergr Space Technol* 103:103429

12. <http://bhukosh.gsi.gov.in/Bhukosh/Public>
13. Matthies H, Strang G (1979) The solution of nonlinear finite element equations. *Int J Numer Meth Eng* 14(11):1613–1626
14. Kontoe S, Avgerinos V, Potts DM (2014) Numerical validation of analytical solutions and their use for equivalent-linear seismic analysis of circular tunnels. *Soil Dyn Earthq Eng* 66:206–219
15. Das R, Dhouchak R, Singh TN (2021) Analysis and prediction of brittle failure in rock blocks having a circular tunnel under uniaxial compression using acoustic Emission technique: laboratory testing and numerical simulation. *Int J Geo-Eng* 12(1):1–23
16. Su K, Zhang YJ, Chang ZH, Wu HG, Wang T, Zhou W (2019) Transverse extent of numerical model for deep buried tunnel excavation. *Tunn Undergr Space Technol* 84:373–380
17. Srivastav A, Pandey VHR, Kainthola A, Singh PK, Dangwal V, Singh TN (2021) Numerical analysis of a collapsed tunnel: a case study from NW Himalaya, India. *Ind Geotech J* 52:1–13
18. Zhang L (2013) Engineering properties of rocks. *J Chem Inf Model* 53:1689–1699
19. Sharma LK, Singh R, Umrao RK, Sharma KM, Singh TN (2017) Evaluating the modulus of elasticity of soil using soft computing system. *Eng Comput* 33(3):497–507
20. Hoek E, Carranza-Torres C, Corkum B (2002) Hoek-Brown failure criterion-2002 edition. *Proc NARMS-Tac* 1(1):267–273
21. Barton N (1973) Review of a new shear-strength criterion for rock joints. *Eng Geol* 7(4):287–332
22. Barton N (1976) The shear strength of rock and rock joints. *Int J Rock Mech Min Sci Geomech Abst* 13(9):255–279
23. Jia P, Tang CA (2008) Numerical study on failure mechanism of tunnel in jointed rock mass. *Tunn Undergr Space Technol* 23(5):500–507
24. Fan X, Kulatilake PHSW, Chen X (2015) Mechanical behavior of rock-like jointed blocks with multi-non-persistent joints under uniaxial loading: a particle mechanics approach. *Eng Geol* 190:17–32
25. Shin JH, Addenbrooke TI, Potts DM (2002) A numerical study of the effect of groundwater movement on long-term tunnel behaviour. *Geotechnique* 52(6):391–403
26. Rocscience Inc. 2021 RS² version 11–2D Finite element analysis, Toronto, Ontario, Canada. www.rocscience.com

Stability Analysis of a Rectangular Tunnel in Granitic Rocks at a Depth of 205 m, Bhima Basin, Karnataka



Binu Kumar, R. K. Bajpai, and T. N. Singh

Abstract The stability of underground excavation in hard rock at depth is significantly controlled by the direction and magnitude of the prevailing in-situ stress field and existing fracture patterns within the rock mass due to anomalous stress concentration and wedge formation. In this paper stress concentration and displacement around a rectangular tunnel of 4×3 m size and 20 m length excavated in granitic rocks at a depth of 205 m in the vicinity of a reverse fault has been analyzed using Phase-II FEM Code. The study area forms a part of Bhima basin in the district of Yadgir in Karnataka. The important rock types exposed in the area include proterozoic limestone in contact with basement granites. A total of 56 rock samples obtained from the rock mass around the excavation were tested for various rock mechanical parameters for their use as input in the numerical analysis. A total of 40 rock fractures measured in the rock mass around the excavation reveal the presence of two major joint sets strike direction $N55^\circ E$ & $N330^\circ W$ with dips of 90° & 45° respectively. The analysis using Hook and Brown failure criteria for the rectangular tunnel in fracture free granites shows a maximum 21.85 MPa tensile stresses at corner with maximum 0.3 mm vertical displacement at crown and 0.4 mm horizontal displacement at side wall. The stability index at corners thus reduces to 1.83 which in case of side walls is of the order of 4.32. The same rock mass with two joint sets reveal increase in vertical displacement (0.7 mm) in crown and sidewalls. The same excavation in reverse fault zone set up shows extremely unstable structure with Stability Index of <1 . However, in-situ measurements of displacements match with case of normal stress field and no indication of high stress field typical of reverse fault set up is noticed.

Keywords Underground excavation · In-situ stress · FEM · Rock mechanics

B. Kumar (✉) · R. K. Bajpai
Homi Bhabha National Institute, Mumbai 400094, India
e-mail: binu@barc.gov.in

T. N. Singh
IIT Patna, Patna 801106, India

1 Introduction

The structural stability of excavation at depth in hard rocks i.e., granite is significantly influenced by the direction and magnitude of the prevailing in-situ stress field and existing fracture patterns within the rock mass. The instability in such excavations is mainly triggered by accumulation of anomalous stress concentration in certain zones around the periphery resulting in reduced stability index (S.I.). In addition, presence of fracture/ joint planes also facilitates enhanced displacement and wedge formation which further reduce the stability index [1]. Excavations in such rock mass locally disrupt the stress field created by the combination of overburden stresses and in-situ geological stresses. This results in new set of stresses and associated displacements in the rock mass surrounding the excavation. Such modifications in turn decide the stability of the excavation geometry and also form the basis of support design for various applications like transportation tunnel, oil and gas storage, underground nuclear power plants, power house, etc. Knowledge of the magnitude and direction of these in-situ and induced stresses coupled with fracture network is thus an essential component of underground excavation design [2–4]. Though, the existing stress field and fractures cannot be altered, it is always possible to minimize their impact on the stability of the excavation by selecting an optimum shape, direction and geometry of the excavation.

In this paper, stress concentration and displacements around a rectangular tunnel of 4×3 m size having 20 m length excavated in granitic rocks at a depth of 205 m in the vicinity of a possible reverse fault have been analyzed using Finite Element (FE) Phase-II Code [5]. A total of 56 rock samples obtained from the depth range of 201.05 m to 211.45 m around the excavation by drilling of coring boreholes from the surface were tested for various rock mechanical parameters for their use as input in the analysis. A total of 40 rock fractures were also measured in the rock mass around the excavation revealing presence of two major joint sets strike direction $N55^\circ E$ & $N330^\circ W$ with dips of 90° & 45° respectively. The results of the finite element modeling were validated by excavating a 20 m long rectangular geometry tunnel at 205 m depth through controlled drill and blast method.

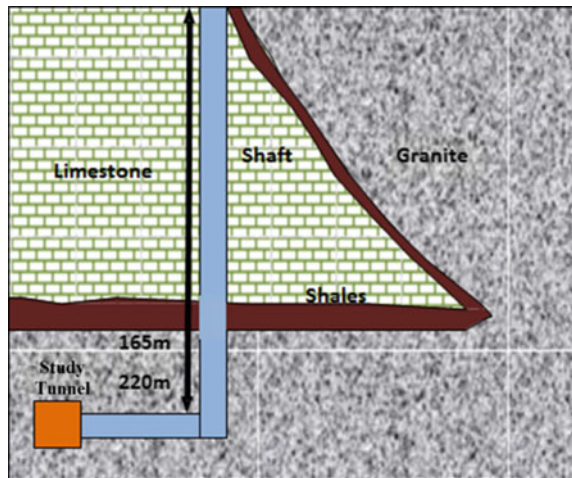
2 General Geology

The area lies between latitude $16^{\circ}20'-17^{\circ}35'N$ and longitude $76^{\circ}15'-77^{\circ}44'E$ on north western fringe of eastern part of Dharwar Craton. The area exposes of limestone (upto 155 m) of Bhima Basin resting on granite basement with a faulted contact as shown in Fig. 1. The excavation is located in the footwall side of the fault at 205 m depth. It is observed that the rock mass at 205 m depth are pink porphyritic granite grading into equigranular granite. These granites are characterized by very high RQD and less fracture. The geological succession of the area is shown in Fig. 2.

A total of 56 rock core samples obtained from excavation at site were tested and analyzed to obtain various rock mechanical properties for their use as input in the analysis. A prominent reverse fault trending NE-SW with SE dips varying from 50 to 80° , marks the contact between granite and limestone. The reverse faulting has resulted in ductile deformation in the granite axis evident by alternate bands of felsic and mafic components with flowage.

The inter-granular slips and ductile flow have caused overall reduction in strength of the rocks. However there is not much significant reduction in other rock mass parameters like RQD and RMR. The granites in the vicinity of tunnel display multiple joint sets. The prominent trends include NS, NE-SW, NW-SE and E-W with varying dips (Fig. 3). The cross section view of the rectangular tunnel excavation is shown in Fig. 4.

Fig. 1 Schematic geological cross section across the study area











Thickness		Lithological details	Engineering geological features	Field Photos
From (m)	To (m)			
0.00	09.00	Soil zone		
9.00	23.50	Limestone with wide aperture (1-5mm or more) fracture sub vertical to moderately dipping, highly weathered, yellow colored staining	Bedding fissility is very tight <1mm aperture but these wide aperture fractures are main groundwater conduits	
23.50	63.00	Grey limestone with less tendency to break along beddings	RQD is almost 100%/almost negligible fracturing	
63.00	102.00	Grey colored limestone with tendency to break along closely spaced beddings	RQD is low due to very poor cohesion and stiffness along bedding plane	
102.00	145.00	Grey limestone with less tendency to break along beddings	RQD is 70-100%, rock is competent perpendicular to the bedding but very poor cohesion along bedding	
145.00	153.00	Ferruginous shale	Very soft weathered, weak rock	
153.00	165.00	Grey shale	Relatively strong with better core recovery	
165.00	185.00	Weathered pink granites with fractures	RQD is 100%, but weak and weathered, sub vertical to moderately inclined fractures	
185.00	300.00	Hard pink granites with less fractures	Very high RQD, less fractures, clean fractures	

Fig. 2 Geological succession of the area

Fig. 3 Rose diagram of major fracture directions

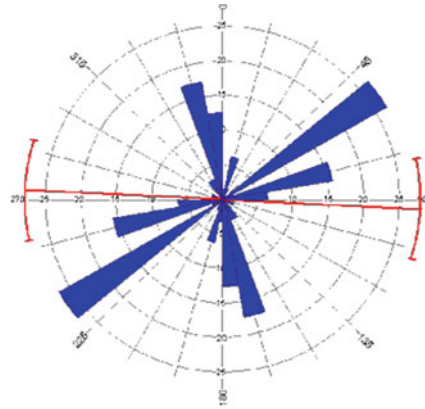


Fig. 4 Actual rectangular excavated tunnel



3 Rock Mass Quality and Mechanical Property

The rockmass at 205 m depth has been characterized by means of five coring boreholes drilled over an area of about 100×200 m up to a depth of 350 m. All the rock core samples were subjected to detail geological investigations to extract depth wise data like Schmidt hammer strength, fractures, their inclinations, alteration, ground-water conditions etc. Using these, a number of rock mass parameters [6] like RQD, RMR, Q, etc. were estimated.

The rock mass at 201–211 m depth have average RQD in the range of 80–90%. A typical case of rock mass quality in a borehole is shown in the Table 1. These values together with other parameters like UCS, Joints detail etc. render RMR value of 68–70 for these rockmass. A typical core length wise fracture details are shown in the Table 2.

Table 1 A typical RQD data of 201–211 m depth in a core sample

Sr. no.	From (m)	To (m)	Run length (m)	RQD (%)	Rock mass quality
1.	201.05	203.10	2.05	87.80	Good
2.	203.10	205.50	2.40	97.50	Excellent
3.	205.50	207.40	1.90	100.00	Excellent
4.	207.40	208.90	1.50	83.33	Good
5.	208.90	211.45	2.55	60.39	Fair
6.	211.45	214.45	3.00	99.00	Excellent

Table 2 A typical fracture data recorded from 201–211 m depth in a core

Sr. no.	From (m)	To (m)	0–15 ⁰	16–30 ⁰	31–45 ⁰	46–60 ⁰	61–75 ⁰	76–90 ⁰	Total
1.	201.05	203.10	2	2	2	1	1	–	8
2.	203.10	205.50	2	1	4	–	–	–	7
3.	205.50	207.40	3	1	3	–	–	–	7
4.	207.40	208.90	4	4	2	–	–	–	10
5.	208.90	211.45	2	2	5	–	–	–	9
6.	211.45	214.45	3	4	3	9	1	–	20

Then after, granite samples collected from the depth range of 180–210 m and were tested as per ISRM standard [7, 8] in laboratory for evaluation of various mechanical strength parameters as listed in Table 3.

Due to the impact of faulting and shearing in the site, laboratory based testing of granites obtained from both the hanging and footwall side of the fault plane has yielded relatively lower values of UCS (50–100 MPa) as compared with intact granite UCS of 150 MPa. Furthermore, due to unavailability of field test data for state and

Table 3 Rock mechanical properties

Sr. no	Parameter	Values
1	Density	2700 kg/m ³
2	UCS	80 MPa
3	Young modulus	6300 MPa
4	Internal friction angle	44°
5	Cohesion	10 MPa
6	Poisson ratio	0.15
7	mb	9.168
8	a	0.515
9	mi	32
10	D	0
11	s	0.02046

magnitude of in-situ stress, estimates have been made based on geological structure and other empirical relations [8, 9, 10]. In view of the above three possible stress field cases have been considered in the analysis. In the first case the vertical stress due to the overburden on the tunnel has been estimated as 5.53 MPa using depth and rock density data. In the second case, reverse fault stress model has been considered as the excavation site lies in the vicinity of a kilometer scale reverse fault. Stress estimation using empirical equations gives horizontal principal stress of the order of 20 MPa at right angle to the direction of fault trace [10]. The third case is essentially similar to second case, however, two sets of joints have been added in the model. Hook and Brown failure criteria [8, 11] has been considered in the analysis.

4 Numerical Analysis

In the FE analysis using code Phase-II, a rectangular excavation of 4×3 m size is considered in the granitic rock mass as shown in Fig. 5. The graded mesh with 3 noded triangles and a grade factor of 0.1 has been considered in all cases. The mesh density has been increased around the tunnel periphery for better results. Restrain boundary conditions is applied on the external boundary of the model.

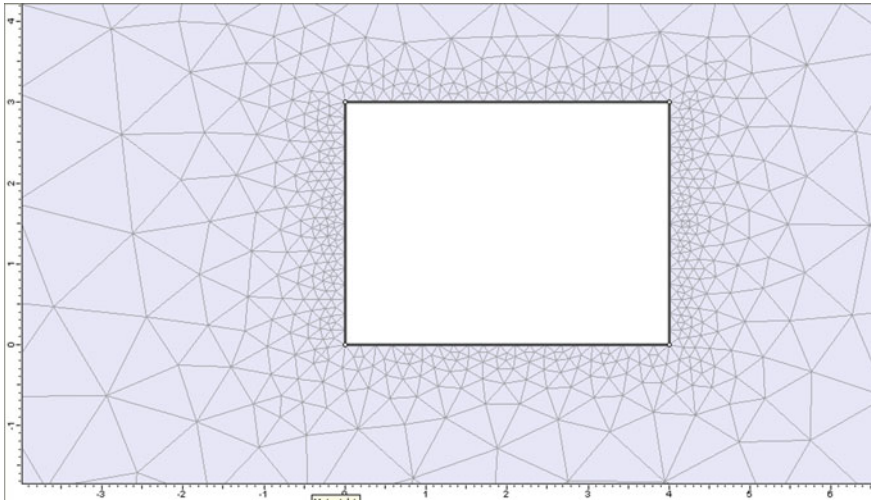


Fig. 5 Finite element mesh around rectangular excavation of 4×3 m

4.1 CASE I: Intact Rock with Overburden Load

In this case, the overburden stress loading is considered in the form of gravity with $K = 1.5$. A large number of parameters like σ_1 , σ_2 , σ_3 , horizontal and vertical displacement, mean stress, total displacement, factor of safety etc. have been evaluated and analyzed. The maximum tensile stress value of 21.85 MPa (Fig. 6) has been observed at the corner location in the excavation. The maximum tensile stresses observed in the floor and roof are of the order of 8.55 to 9.50 MPa. It is inferred that stress trajectories are parallel to surface of excavation along the floor, crown and walls. However they tend to attain high angle in corner locations. Stability Index i.e. $S.I. = \sigma_m$ (uniaxial compressive strength of rock mass/ σ_t (the tangential stress) of the roof region and corner are 4.32 and 1.83 respectively, which indicates stable excavation [9, 12, 13]. Though, corner area has 21.85 MPa tensile stresses and S.I. is of 1.83 which indicates slight loosening but no rock burst or spalling is observed.

The maximum vertical and horizontal displacement in the order of 0.30 and 0.42 mm respectively have been estimated (Fig. 7).

The displacements are well within the design limits for such excavations. The crown thus does not show any break up (Fig. 8).

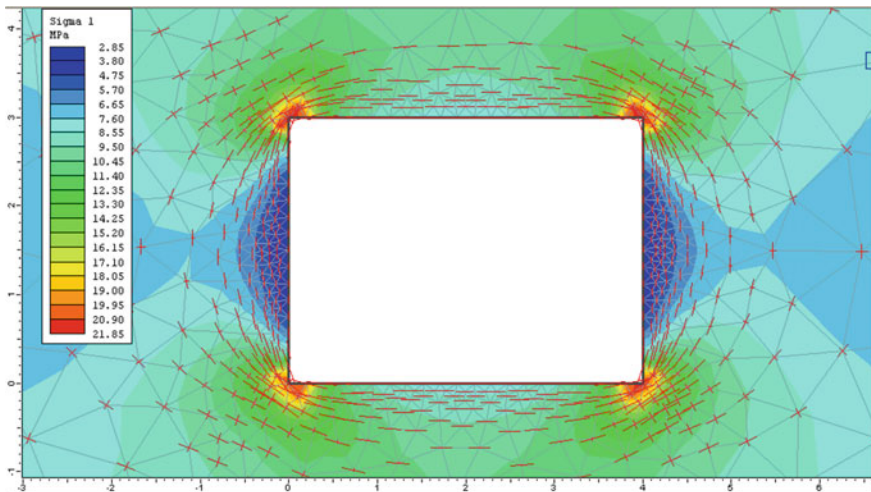


Fig. 6 Distribution of σ_1 and stress trajectory around the excavation

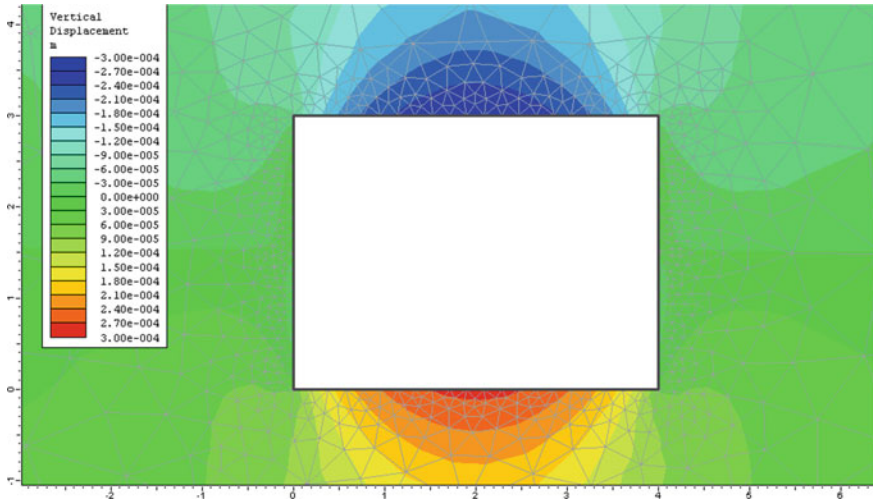


Fig. 7 Distribution of vertical displacements around the excavation



Fig. 8 Roof of the excavation at 206 m

4.2 CASE II: Intact Rock and Tectonic (Horizontal) Stress

Based on site geological conditions, conservative estimates have been made and σ_1 , σ_2 & σ_3 are assigned as 20, 5 and 10 MPa respectively. This stress load eventually leads to a K value of 4.

Maximum σ_1 concentration appears at the corner of the tunnels and is of the order of 47.50 MPa (Fig. 9). The tensile stress concentration in the crown and floor are also significantly high ranging in order from 20 to 30 MPa. Hence, such very

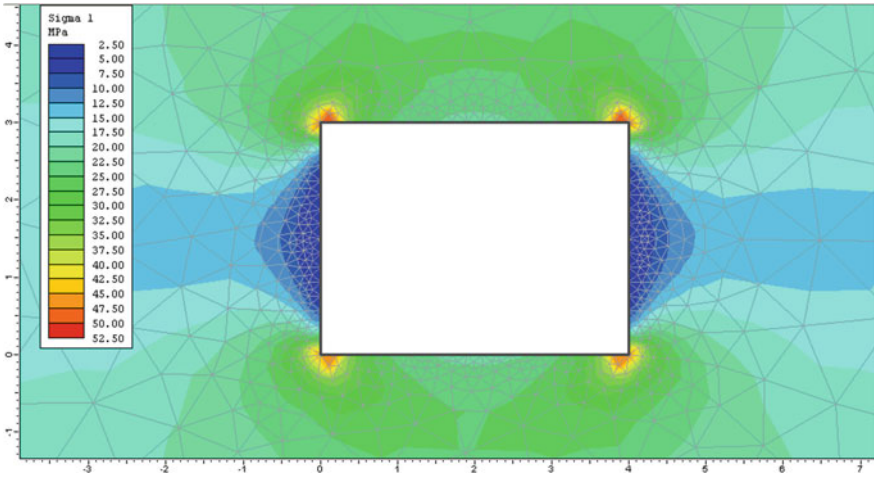


Fig. 9 Distribution of σ_1 and stress trajectory around the excavation

high stress concentration with lower UCS may results in very low S.I. (<1) resulting in heavy rock burst at corner area. However, at field, no such phenomenon have been observed during the excavation, it points towards nonexistence of high residual stresses as normally noticed in reverse fault area. Thus the fault in the region can be considered dormant. And as a result case one discussed earlier can be considered as representative of the area and results from that can be used for design purpose.

4.3 Case III: With Two Fracture Joint Sets

The excavation has also been analyzed for two joint sets having dips of 90 and 45° respectively representing the actual fracture joint sets in the depth range of excavation (Fig. 10). The excavation walls coincide with vertical fracture as measured in the

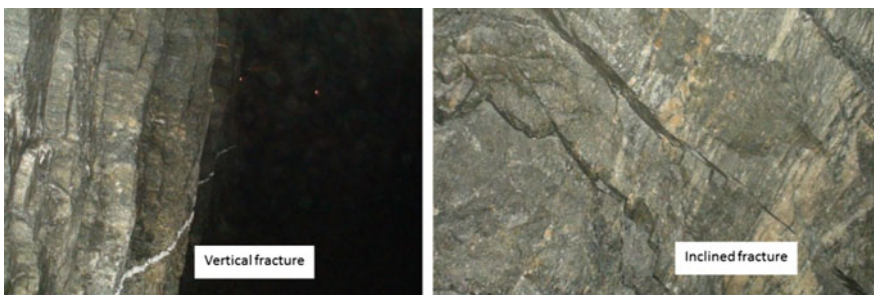


Fig. 10 Vertical and inclined fracture in rock mass

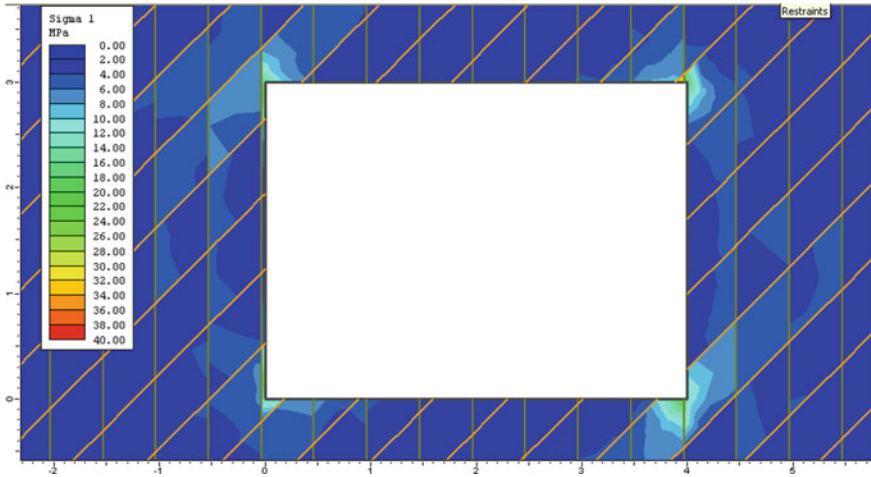


Fig. 11 Concentration of σ_1 along excavation periphery with two joint sets

Table 4 Maximum responses (Stress, displacement and stability index) in analysis

Sr. no	Parameters	Case I	Case II	Case III
0	Principle stress (MPa)	21.85	47.50	39.89
0	Vertical displacement (m)	0.31	0.50	0.80
0	Vertical displacement (m)	0.42	0.90	0.75
0	Stability index (SI)	4.32	0.99	1.20

field. Both sets have been assigned spacing of 0.5 m based on average spacing of these joints recorded in the field.

The distribution of σ_1 do not show as high concentration at corner as were noticed in case without fractures (Fig. 11). The maximum stress of 39.89 MPa has been recorded.

Table 4 summaries the maximum response obtained in the FE analysis. The amounts of displacement both vertical as well as horizontal are also higher (0.6 to 0.7 mm) in crown, floor and side walls (Fig. 12).

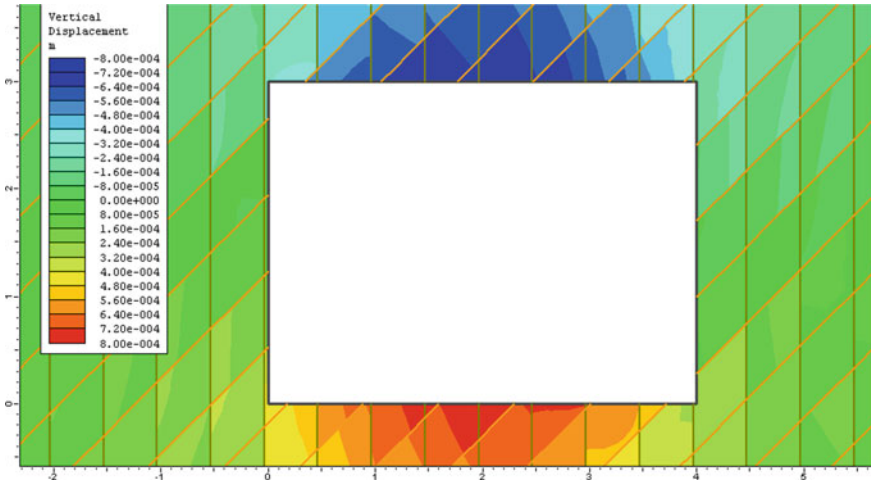


Fig. 12 Vertical displacement along the excavation periphery with two joint sets

5 Results and Conclusions

The stability analysis using Hook and Brown failure criteria for the rectangular tunnel in fracture free granites under overburden loads show maximum 21.85 MPa tensile stresses at corners with maximum 0.3 mm of vertical displacement at crown and 0.4 mm horizontal displacement at side wall in case I. The overall Stability Index in roof and sidewall area is >4 indicating very stable excavation. Only in corner area slightly unstable region develop with S.I. of 1.83. In the case of reverse fault stress regime without any fracture with high horizontal stresses ($K = 4$), maximum σ_1 concentration appears at the corner of the excavation and is of the order of 47.50 MPa. The stress concentration in the crown and floor are also significantly high ranging in order from 20 to 30 MPa. Under these stresses which results in S.I. < 1 , rock bursts are expected in corner regions. However such phenomenon has not been observed in the rectangular tunnel excavated at depth of 200 m. The analysis thus reveals the absence of tectonic stresses in the area. In the case III, wherein two joint sets representing joints measured in field were added in the analysis, higher displacement in the order of 0.6–0.7 mm are recorded. The peak stress concentration at corners is 39.89 MPa in the case with joints with high S.I. > 1 . However, average stress concentration is approximately 20 MPa with S.I. > 2 . These results indicate requirements of roof bolting to stabilize rock wedges formed by joint intersection to avoid gravity driven rock fall. The results thus indicate the presence of case I stress condition in the depth range of 180–210 m and further reveal highly stable excavation. The same has been validated through excavation of rectangular tunnel.

References

1. Bieniawski ZT (1967) Mechanism of brittle fracture of rock, parts I, II and III. *Int J Rock Mech Min Sci Geomech Abstr* 4(4):395–430
2. Bajpai RK (2012) Status Report on Geo-scientific Investigations at Underground Research Laboratory site, Vol2, No BARC/NRG/TDD/RES/URL/2012/Tech/2, pp 1–87
3. Arjang B (1998) Canadian crustal stresses and their application in mine design. In: Singhal (ed) *Mine planning and equipment selection*. Balkema, Rotterdam
4. Brown ET, Hoek E (1978) Trends in relationships between measured rock in situ stresses and depth. *Int J Rock Mech Min Sci Geomech Abstr* 15:211–215
5. Rocscience Inc (2008) Phase II – Two-dimensional finite element stability analysis code
6. Hoek E, Brown ET (1980) *Underground Excavations in Rock*. Institute of Mining and Metallurgy, London
7. Hoek E (1994) Strength of rock and rock masses. *ISRM New J.* 2(2)
8. Hoek E, Brown ET (1997) Practical estimates of rock mass strength. *Int J Rock Mech Mining Sci* 34(8):1165–1186
9. Sheorey PR (1994) A theory for in situ stresses in isotropic and transversely isotropic rock. *Int J Rock Mech Min Sci Geomech Abstr* 31(1):23–24
10. Sand CO (2006) Significance of In situ stress in stability analysis of underground nuclear waste disposal repository, *Tunnels & Underground Space*. *J Korean Soc Rock Mech* 17(1):26–31
11. Hoek E (1977) Structurally controlled instability in underground excavations. In: *American Rock Mechanics Association 18th U.S. Symposium on Rock Mechanics (USRMS)*, 22–24 June 1977, Golden ARMA-77-0362
12. Palmstrøm A (1995) *Characterizing Rock Burst and Squeezing By Rock Mass Index Design and Construction of Underground Structures*, New Delhi
13. Palmstrøm Arild (1996) Characterizing rock masses by the rmi for use in practical rock engineering, part 2: some practical applications of the rock mass index (RMI). *Tunnel Undergr Space Technol* 11(3):287–303. [https://doi.org/10.1016/0886-7798\(96\)00028-4](https://doi.org/10.1016/0886-7798(96)00028-4)

Ground Improvement in Fractured Basaltic Terrain Along TBM Drives Near to Arabian Sea – A Case of Mumbai Metro, India



Anshul Sindhvani, V. M. S. R Murthy, Alope Kumar Dey, Afzal Hossain Khan, and Palwinder Singh

Abstract Underground metro projects in Mumbai city has witnessed huge surge in the construction since last few years and large number of shielded tunnel boring machines were deployed for completing the project within scheduled time. TBM productivity largely depends on subsurface conditions and therefore, a prior understanding of the geological conditions is a crucial activity before start of tunnel excavation.

The colaba – vidhan bhavan tunnel stretch of Mumbai metro line-3 planned to be excavated using single shield TBM as it yields minimal surface intervention however the major challenge lies on its close proximity to sea. This paper presents a case study of tunnel section where the alignment was passed mere 15–20 m off the coast of Arabian Sea. It was attempted to infer the ground well before actual TBM drive and adopted suitable ground improvement technique to mitigate and minimize the risk of pressurized flow of water flooding the tunnel.

Keywords Metro · TBM · Fractured rock mass · Grouting · Geotechnical investigations

A. Sindhvani (✉)
IIT (ISM) Dhanbad, Dhanbad, India
e-mail: anshul.18dp000365@me.iitism.ac.in

V. M. S. R. Murthy
Mining department, IIT (ISM) Dhanbad, Dhanbad, India
e-mail: vmsrmurthy@iitism.ac.in

A. K. Dey · A. H. Khan · P. Singh
L&T Construction, Mumbai, India
e-mail: alokedey@lntecc.com

A. H. Khan
e-mail: ahkhn@lntecc.com

P. Singh
e-mail: palwnder@lntecc.com

1 Introduction

In order to improve the overall traffic and to provide sustainable transport system in the city of Mumbai, MML3 is the first fully underground metro project implemented by Mumbai Metro Rail Corporation (MMRC). Mumbai city is highly congested and therefore, underground metro projects for greater connectivity is the only solution in near future. Line-3 alignment is running from north to south of Mumbai, connecting with domestic and international airports.

Use of shielded tunnel boring machines (TBM's) in urban environment gained popularity in recent years and is considered as the most preferred method of tunnel construction in India and around the world as it offers fast, safe, and high speed tunnelling. Study area covers UGC-01 project which is in south of Mumbai and scope includes the design and construction of four underground stations at Cuffe Parade, Vidhan Bhavan, Churchgate and Hutatma Chowk and associated TBM and NATM tunnels (Fig. 1).

Geotechnical investigations had revealed anomalous zones near to sea and anticipated to encounter challenging ground conditions including fractured basalts, pressurized water flow during TBM excavation. Seismic refraction and electrical resistivity tests were done to cross verify the anomalies predicted during earlier investigations and it was strategized to implement ground improvement works which includes consolidation grouting on grey areas well before arrival of TBM.

The sea face of TBM drive was cordoned off by a line of grout curtain consisting of cement and bentonite. Closer spacing of grout holes had received moderate grout intake and acted as a barrier to the pressurized flow into the tunnel. Estimated and actual ground conditions were in close agreement as confirmed through periodic face



Fig. 1 Mumbai Metro Line-3 UGC-01 Plan

inspection during excavation. Curtain grout wall near the coast lead to successful TBM driving, however, one location where grouting was not feasible from surface due to presence of slums lead to huge water ingress. Single shield rock crossover TBM used for this project, capable of operating in both EPB / Rock mode.

2 Geology of Study Area

Geologically, Mumbai is part of deccan volcanic traps that was formed by tremendous volcanic activity and developed a formation called deccan traps covering 80% of the surface area of Maharashtra state. Deccan traps are one of the largest volcanic outburst feature on Earth and are formed from the deposition of subaerial lava flows of fissure eruptions [1] and consists of various lithologies including amygdaloidal, compacted, porphyritic and vesicular basalts, volcanic breccia, intertrappean beds of shale with tuff bands, dykes and red boles. Deccan traps consists of multiple layers of lava flows separated by the intertrappean beds of shale with tuff bands which shows geological breaks in the tectonic activities [2].

Mumbai Metropolitan Region (MMR) forms a part of great volcanic activity known as deccan traps. Lava flows of Mumbai region represents a much younger phase of deccan traps volcanic eruption and Mumbai island formation belongs to the Salsette subgroup [3]. Basaltic terrain of Mumbai is considered to be the youngest basalt of Eocene age [4]. Mumbai presents complex lithological combination showing large heterogeneity as it is located in the great volcanic formation building up the Deccan plateau.

Basalt flows are broadly horizontal over most of the area and it is only at places including Mumbai, Panvel where the flows are disturbed from their original horizontality and indicates gentle dips. Though faults are rare in deccan province, there are places where vertical or steeply inclined fractures along which movement has taken place. Continuous water seeping along the western coast is a common activity and it brings decompositions of basaltic rock mass.

Site geology of study area mainly composed of geological units mentioned below in order of disposition from the top ground surface:

- Filled up material + Silty/clayey sand
- Weathered Basalt (G-V/IV) + Bed Rock Basalt (G-III/II/I)

2.1 Geotechnical Investigations

A total of 4 boreholes were drilled before the start of TBM excavation and investigations revealed the overburden ranging from 4–7 m thick consisting of filled up material and silty / clayey sand with underlying basaltic traps of varying degree of fracturation (Fig. 2). One of the borehole drilled away from coast indicated deep weathering of basalt and open joints with high permeability recorded during in-situ

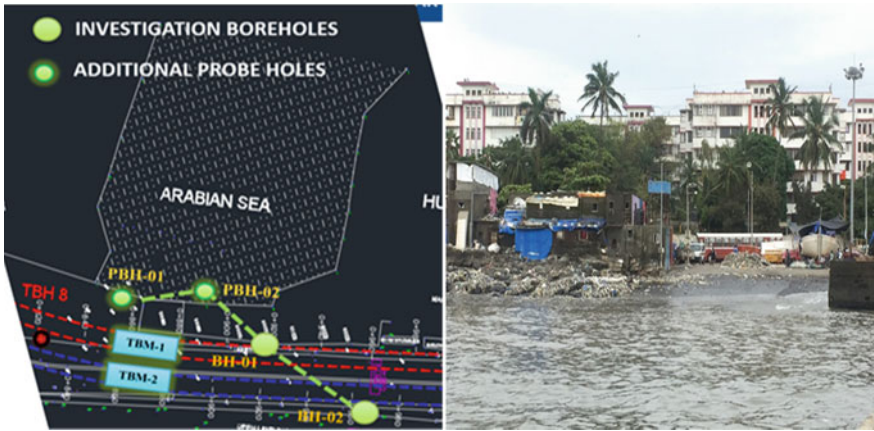


Fig. 2 Borehole layout (left) and study area location side view from coast (right)

testing. Groundwater table is encountered near to road level along the entire length of tunnel alignment due to proximity of sea.

2.2 Geophysical Investigations

Geophysical investigations were carried out additionally in order to delineate the extent of fractured zone and mitigate the risks of high water ingress flooding the tunnel during TBM excavation due to high degree of fracturation. Borehole investigations results coupled with geophysical investigation findings for detailed understanding of ground conditions. Also, Geophysical investigations will help in developing the subsurface model of the area for finding out the requirements of ground treatment.

Electrical resistivity and seismic refraction tests were conducted in vicinity of sea section and data acquired along two parallel lines of approx. 150 m in length for both tests and processed sections are included in Fig. 3–5. Electrical resistivity of ground clearly indicative of a low resistivity layer (Fig. 3) along entire section except at one location in the center. A 3D section prepared for electrical resistivity reveals that

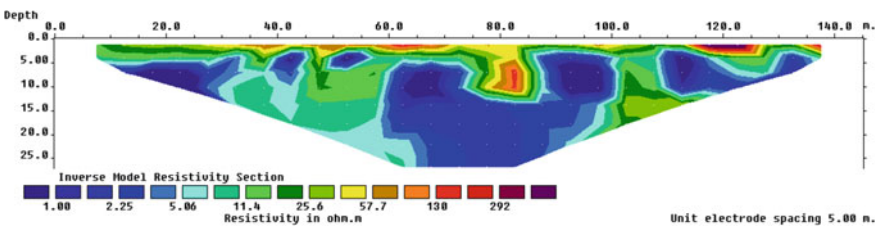


Fig. 3 Electrical resistivity section – 2d profile

the presence of low resistivity layer is limited nearest to sea and higher resistivity is noticed as moving away from the sea (Fig. 4).

Seismic refraction tests revealed presence of low velocity layer up to the tunnel center (Fig. 5) and the observations are in line with the electrical resistivity findings. High permeability which was witnessed during Insitu testing, combining with low resistivity and low velocity gives a clear indication of low strength material, high degree of fracturation and presence of open joints within the basaltic rock mass towards the sea.

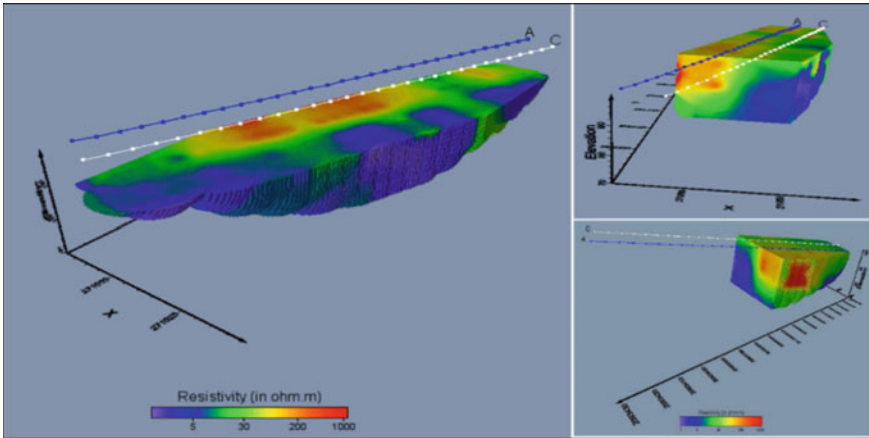


Fig. 4 Electrical resistivity section – 3d profile

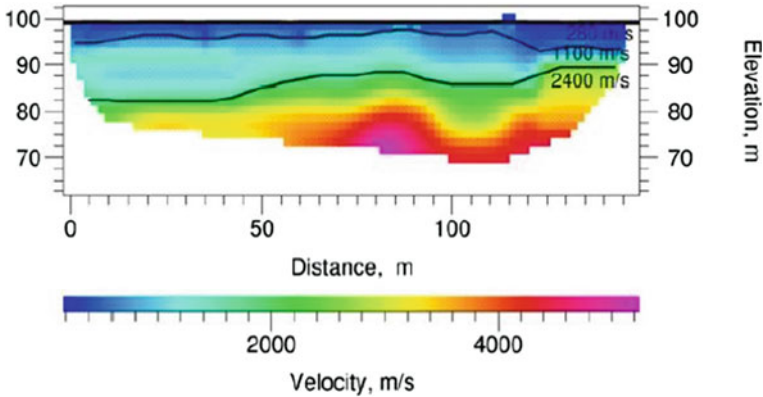


Fig. 5 Seismic refraction test – Velocity 2D profile

3 Ground Improvement

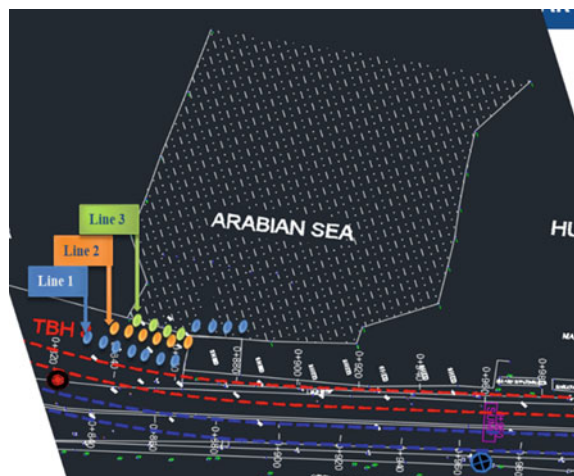
Detailed interpretation of investigation findings revealed that there is a greater possibility of encountering weathered and fractured basaltic terrain with high water ingress during the TBM excavation of the west bound tunnel and therefore, arises need of ground improvement in the anomaly zone near to sea. The objective of ground improvement is to create an impervious grouted wall towards sea to avoid any pressurized water inflow during mining.

Considering the presence of sub vertical joints in basaltic terrain as observed during the excavation of launching shaft in vicinity, it was also planned to do the ground treatment in overburden soil cover in addition to consolidation grouting in fractured basalts. TAM grouting method was proposed as the purpose is to permeate the grout in fractured strata in such a way that the strata becomes devoid of any fractures. A total of 60–65 m length is covered along the alignment for ground improvement considering the site feasibility as beyond specific chainage along the alignment, slums are located above tunnel and grouting was not feasible. A total of 3 rows/lines (Fig. 6) were proposed as primary, secondary and tertiary row of grout holes. The details of these different rows are mentioned below:

- Line 1 - Primary row of grout holes: 3–5 m spacing, 23 m depth.
- Line 2 - Secondary row of grout holes: 3–5 m spacing, 23 m depth.
- Line 3 - Tertiary row of grout holes: 2 m spacing for soil overburden, 6–8 m depth.

TAM (Tube-a-Manchette) grouting method procedure (Fig. 7) includes the drilling of grout holes at specified locations followed by the insertion of perforated pipes with short sections of rubber sleeve on outer part of the pipe that act as a one way valve for grout. Subsequent to drilling of holes, the gap between the excavation portion and tam pipe is filled with sheath grout of cement-bentonite mix and after setting of

Fig. 6 Grouting Layout



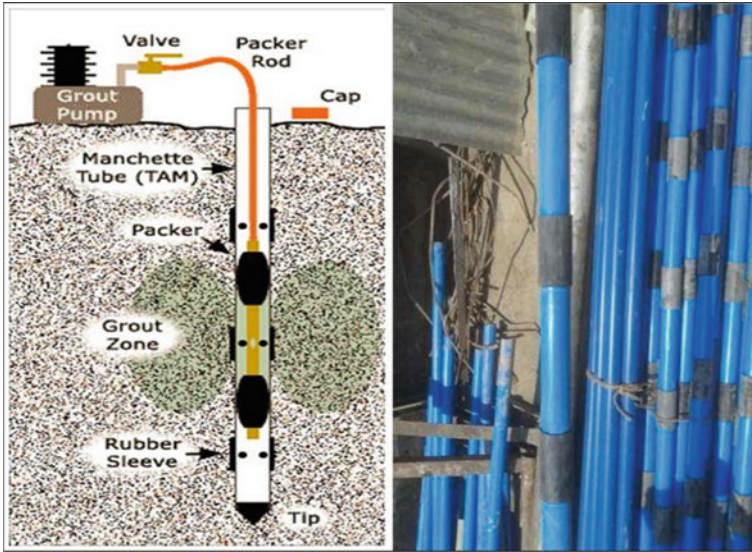


Fig. 7 TAM grouting layout (<https://www.huininkinfrastructure.com/grouting/tam>)

sheath grout, start of grouting in holes by OPC cement grout (Fig. 8) and continue grouting in stages at different pressures from bottom to top. Primary holes are being grouted first followed by secondary and tertiary grout holes.

Grout consumption was upto 25–30 bags per hole during grouting in line 1 and around 50% reduction in grout intake noticed in line-2 with comparison to line-1 and intakes are further reduced at high pressures. Refusal / minimal intake in



Fig. 8 Drilling of holes (Left) and Grouting of holes (Right)

the secondary holes of line-2 indicates consolidation of fractured rock mass and establishment of grout curtain wall along the sea coast. Grouting in line-3 taken up to consolidate the overburden soil cover however due to backfilled area, faced lot of difficulties during drilling in boulders and retaining the holes post drilling completion.

4 Summary of Observations Before TBM Excavation

High inflows of water during TBM excavation can be safely managed in basaltic terrain as the chances of stability issues are minimal due to shielded TBM but fractured rock mass with water ingress can significantly reduce TBM advance rates. A list of observations prepared before the start of TBM excavation which includes:

- Fracturation is observed only in one borehole near to sea section and rest all the boreholes indicates good quality rock mass.
- Loss of water consistently observed in the same borehole during Insitu testing.
- During drilling of holes for grouting, pressurized muddy water was coming out of holes like a fountain (Fig. 9).
- Moderate intake of grout in first 60 m zone ensured reduced possibility of any water ingress during TBM excavation.
- Cumulative of 450–500 m drilling carried out for grouting purpose along 60–65 m length coverage with full proof grouted holes ensured curtain grout wall along the coast.

Fig. 9 Pressurized muddy water during drilling of grout holes



- Big dewatering pumps to be arranged and grouting provision from inside the TBM to be kept ready to ensure the pre-excavation grouting if envisaged during face inspection.

5 Summary of Observations During TBM Excavation

Ground conditions encountered during TBM excavation are continuously monitored through either inspection of rock chips falling on screw conveyor or through face inspection during cutterhead intervention. A list of observations prepared during TBM excavation includes:

- Moderate water inflow with slightly to moderately weathered basaltic rock mass witnessed in the zone where grouting was carried out.
- Huge water inflow with highly to completely weathered basaltic rock mass encountered for about 15–20 m length where TBM progress drastically reduced as the TBM operational parameters were adjusted to avoid any ground loss and passed the zone without causing any ground settlement on slums located on surface.
- Water ingress managed well owing to high dewatering capacity inside the tunnel.
- Continuous face mapping ensured close monitoring of ground strata and accurate feedback to TBM crew for adjusting the parameters best suited for existing ground conditions.

Encountered ground conditions near to sea divided into three different categories mentioned below and included in Fig. 10 and 11.

- Unweathered to slightly weathered basalt with moderate water ingress.
- Moderately weathered basalt with high water ingress.
- Highly to completely weathered basalt with huge water ingress.

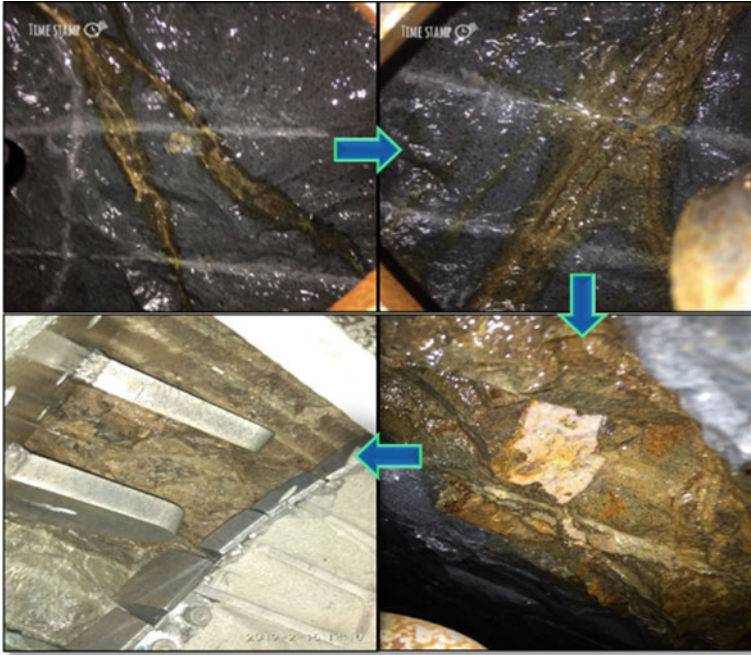


Fig. 10 Encountered ground conditions during face inspection

Fig. 11 Encountered rock chips during muck inspection



6 Conclusion

Majority of the urban tunnelling projects comes with challenges that needs to be either avoided or overcome by adopting suitable risk mitigation measures as mostly the tunnel is planned either below heavy traffic roads or below buildings or slums. One of the primary concerns in urban tunnelling planned near to sea is high water inflows flooding the tunnel.

However, in this case of basaltic terrain, any instability or settling ground is not of a much concern but to avoid significant reduction in TBM productivity and high-water inflow flooding the entire tunnel, it becomes important to be attended. Though risk mitigation in such cases should always be done through an extensive ground improvement scheme however TBM's ability to handle such high-water ingress is equally important and to be taken into consideration during selection of TBM. Ground improvement using TAM grouting carried out to minimize the water ingress and TBM was driven carefully considering this type of ground in advance and successfully negotiated difficult fractured ground conditions.

Predicting ground conditions in urban tunneling is one of the critical activity and needs high attention as it is useful in planning, design and successful excavation of any TBM. Though costs allocations for geotechnical investigations are always an aspect of concern but if planned and investigated properly, TBM excavation can be well managed and projects can be completed within stipulated cost under framed time schedule without inviting any contractual disputes.

Involvement of experienced geologist capable of analysing ground conditions coupled with operational parameters of TBM to provide detailed inputs related to ground risks and mitigation measures during tunnelling are factors of significance for delivering the projects successfully.

Acknowledgements This case study forms a part of main author's research being carried out at IIT (ISM), Dhanbad under the guidance of Dr. VMSR Murthy. Authors are thankful to the management of Mumbai Metro Rail Corporation (MMRC) and L&T STEC JV for allowing the author to continue the research.

References

1. Rao LR (1936) The deccan traps. Proc Indian Acad Sci Sect B 4:208–223
2. Rai SN, Thiagarajan S (2015) Groundwater prospecting in deccan traps covered tawarja basin using electrical resistivity tomography. J Ind Geophys Union 19(3):256–269
3. Sethna SF (1999) Geology of Mumbai and surrounding areas and its position in the Deccan volcanic stratigraphy, India. J Geol Soc India 53:359–365
4. Subbarao KV, Hooper PR (1988) Reconnaissance map of the Deccan Basalt Group in the Western Ghats, India. In: Subbarao KV (ed) Deccan Flood Basalts Geological Society of India, Memories, no 10, p 393

Drill and Blast Optimisation at an Underground Copper-Gold Mine



Alex Guegan-Brown, Larissa Koroznikova, and Manoj Khandelwal

Abstract The process of utilising drill and blast techniques is used to improve mining performance. Drill and blast techniques have been proven to be more efficient and cost-effective compared to conventional mechanical rock breakage with machines. The degree of efficiency of the drill and blast process varies from mine to mine. These influencing factors result in drill and blast patterns that cannot be directly transposed from site to site meaning specific plans need to be developed. When creating new blast plans, unless they are created flawlessly the first-time revision or optimisation is necessary to ensure they are as efficient and effective as possible. The drill and blast patterns can be optimised to reduce the overbreak. A site specifically the current development is mining in both a weaker fragmented shale as well as moving down into a more competent granite. The optimisation will be considered for both types of ground but will have a stronger focus moving into the granite as the mine is approaching the first ore drives which are within the granite rock mass.

1 Background

The underground Copper–Gold Mine is located in South Australia. The mine is the Gawler Craton, which is known as an Archaean to the Mesoproterozoic crystalline basement. It was formed anywhere from 1450 to 3400 Ma years ago and covers around 440,000 square kilometres [1]. The mine is of iron oxide-copper-gold (IOCG) ore deposit. The ore body is cylindrical and extends around 1500 m below the surface and spans approximately 300 m in diameter, overlying the deposit is 470 m of Start Shelf sediment overburden. To extract the ore a sublevel cave/block cave mining method has been planned due to the nature of the ground ability to naturally fracture and subsid to where it will be extracted from the draw points. In the current stage of the mine development, the overbreak has been too high in the shale ground and

A. Guegan-Brown · L. Koroznikova · M. Khandelwal (✉)
School of Engineering, Information Technology and Physical Sciences, Federation University
Australia, Ballarat, VIC 3350, Australia
e-mail: m.khandelwal@federation.edu.au; mkhandelwal1@gmail.com

© The Author(s), under exclusive license to Springer Nature Singapore Pte Ltd. 2022
A. K. Verma et al. (eds.), *Proceedings of Geotechnical Challenges in Mining, Tunneling
and Underground Infrastructures*, Lecture Notes in Civil Engineering 228,
https://doi.org/10.1007/978-981-16-9770-8_21

the outcome has been identified to reduce it to less than 15% moving forward into the granite lower in the mine. Moving into the ore body it is expected to see an improvement in the competency of the rock due to the transition into a hematite rich granite giving it a higher density, therefore there should be a reduction in overbreak.

Overbreak, a result of the drill and blast procedure, is inevitable due to uncontrollable factors such as geotechnical and rock properties as supported by [3–6]. Any extracted material that is outside the planned profile is considered to be over broken and puts the risk on both workers and equipment [4]. As observed in the mine, a large amount of material was dislodged during scaling.

Blasting parameters causing excess ground vibrations have a large impact on the severity of overbreak. When PPV is reduced, it directly relates to the amount of energy released during the blast [7]. Factors that have been explored commonly in drill and blast systems include how the face is charged, for example, the notion of decoupling [3]. Decoupling is the practice of leaving the blast hole partially empty, so the explosive does not occupy the entire diameter. The purpose of this is that as there is a medium between the explosive and surrounding rock, the blast energy transferred to the rock is reduced due to having travelled through the medium. The opposite is a coupled hole, where the explosive occupies the entire diameter of the hole. If decoupling the perimeter holes is the answer to the overbreak issue, why isn't it utilised more often? The decoupling notion is possible with pumped bulk emulsion which could make it a potential factor for the excessive overbreak at the mine [3].

The opportunity to optimise the drill pattern is due to the ability of the Sandvik DD422i jumbo to communicate with a computer on the surface. Initially, a drill pattern can be created by using an engineering previous knowledge in the process of underground drill and blast and basing the pattern of similar size headings already active in that mine. Once the plan has been created it is uploaded to the drill rig where it is stored on the system. Once the rig has drilled a face the DD422i can collect, collate and condense data to produce information that is then able to be analysed. The key advantage of this system is the ability to analyse the data remotely from a computer located on the surface.

This process of data transfer between the drill rig and a computer located on the surface allows the chance to optimise the drill plans by viewing the outcome and making changes following the results of the blast. Linked directly to the jumbo is the program called Isure, developed for use with Sandvik machines such as the DD422i boring jumbo. Isure is utilised to create drill plans and process the data from the drill rig to display viewable information such as total drill metres, penetration rates and three-dimensional images. The two-dimensional image displays the planned drill holes superimposed against the actual drill holes carried out at the face. The three-dimensional image shows a computer-generated surface recorded from where the jumbo collared the holes.

2 Data Collection

To identify the current overbreak value, three cuts were made with the DD422i jumbo used to compare the drill pattern used against a slice of the drive from Deswik. The cross-sectional area can be compared to identify the overbreak.

2.1 Planned Drill Pattern for 4580 ACC-200

The section between the chainage values of 11.5 and 20.5 m doesn't contain any turnouts or stripping. Due to these characteristics, it is suitable to use this section as a control measure as there were no modified drill patterns used during the drill and blast process (Fig. 1b). Three-dimensional modelling is utilised using Isure to view a theoretical scale image of the drill pattern that will look once drilled (Fig. 1a).

The layout consists of the chosen drill pattern for three cuts. Fig. 2a presents the planned profile against the resultant profile for each cut. The blue dots are indicating the planned holes and the red dots are the holes after drilling, each cut has a round length of 4.6 m. Fig. 2b illustrates the planned profile design superimposed against the resultant drive profile showing evidence of both over break and under the break.

A key feature of the Isure program is the three-dimensional imagines (Fig. 3). These images illustrate the face upon drilling and how it should look after firing. Additionally, it highlights protrusions in the face, concaving or convex.

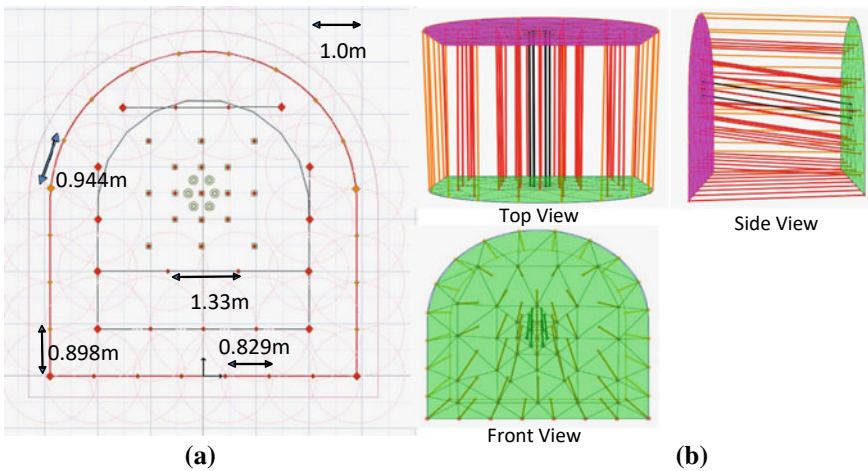


Fig. 1 (a) The drill pattern that was uploaded to the DD422i jumbo (T_5.8 × 6.2_1in25down), the theoretical drill pattern that should have been used. (b) Three-dimensional modelling (top, side and front view). The green surface represents the face profile surface area and the purple represent the bottom profile surface area

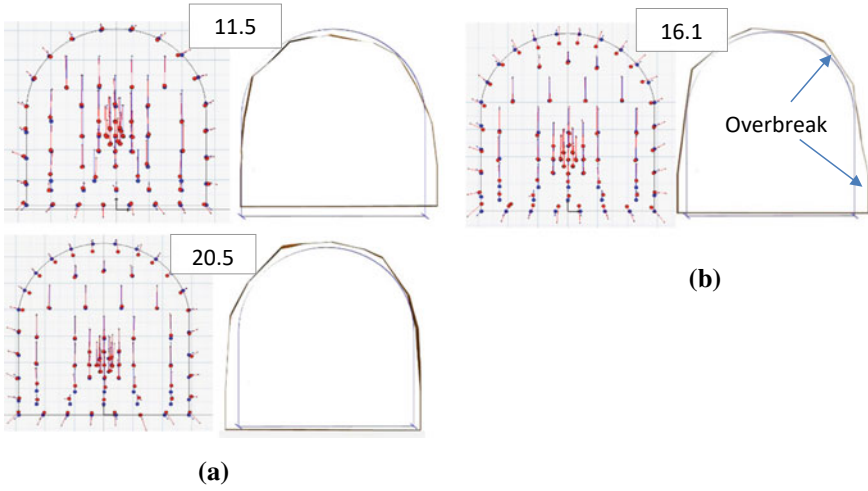


Fig. 2 Chainage 11.5, 16.1 and 20.5 m slice from Deswik (a); chainage drilled pattern (b)

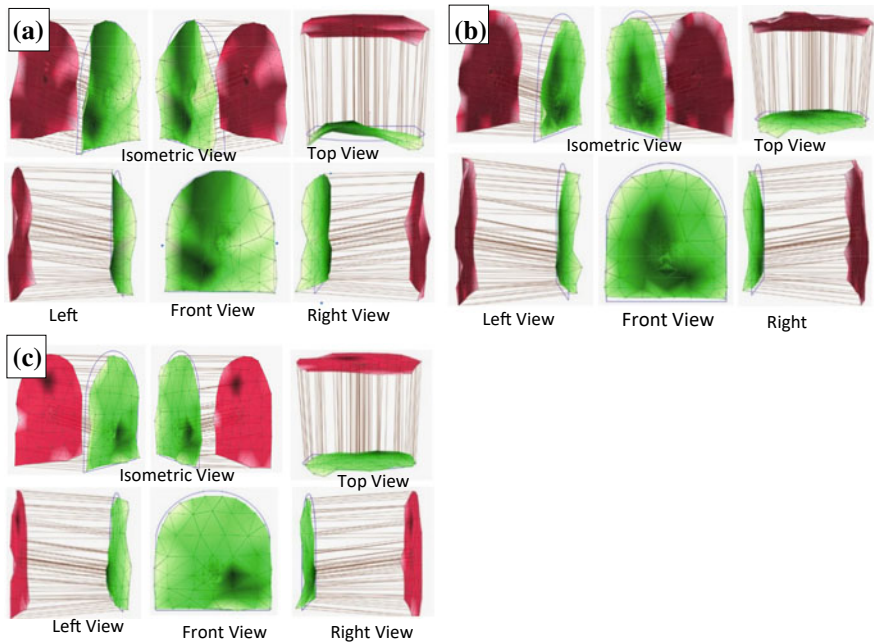


Fig. 3 Three-dimensional images: cut 1, (a) chainage 11.5 m; (b) cut 2, chainage 16.1 m; c cut 3, chainage 20.5 m. The green and red surfaces are the faces and bottom profile surfaces areas respectively

2.2 4580-ESD-001 New 51 mm drill plan—G_5.0 × 5.0_51bit Chainage: 37.3 m

The first trial was conducted at the chainage 37.3 m (Fig. 4). The major difference with this trial was the implementation of the 51 mm drill bits.

The drill plan results in the formation of large fragmentation (Fig. 5), which is undesirable because can have several implications relating to loading, hauling and processing.

Collars are defined as the drill hole on the initial face surface when boring a cut. The collars remain in the shoulder/back on the right-hand side, this was due to not having a sufficient number of perimeter holes. Although the results indicated a lack of perimeter holes and it can also be seen there are a few exposed half barrels.

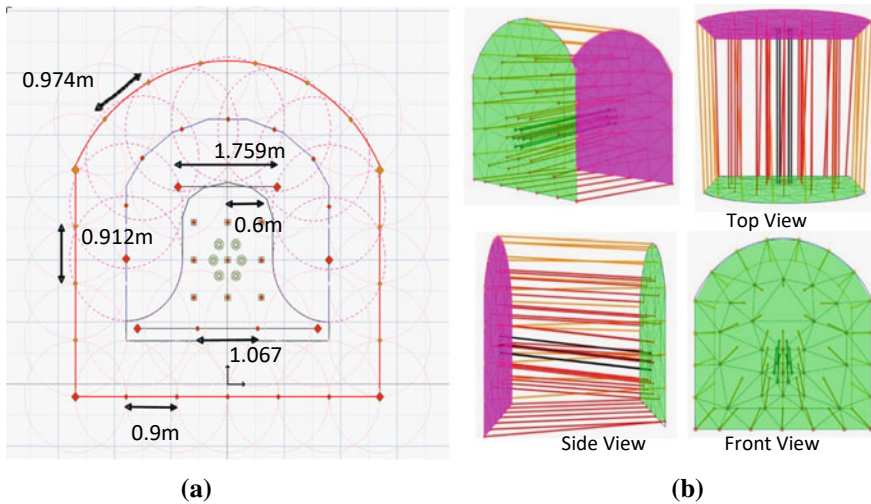


Fig. 4 (a) First adjustment and reduction in drill holes 51 mm drill trial. (b) Three-dimensional modelling (top, side and front views), 37.3 m drill plan



Fig. 5 ESD 001 first trial (4580-ESD-001 new 51 mm drill plan—G_5.0 × 5.0_51 bit, chainage 37.3 m)

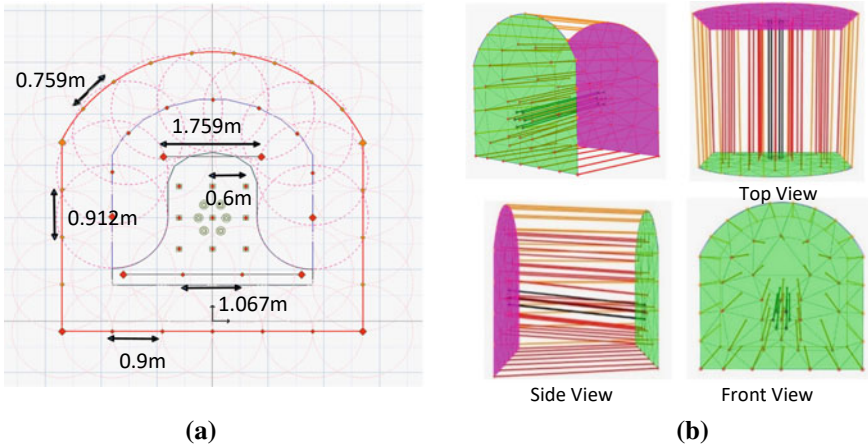


Fig. 6 (a) ESD 001 second trial (revised drill pattern, 51 mm bit, chainage 42.8 m) (b) Three-dimensional modelling (top, side and front views), 42.8 m

Half barrels indicate that the force from the perimeter hole explosion is directed in the intended direction. An ideal blast would leave half barrels around the entirety of the perimeter, shaping it to the desired profile. The version 2 design—G_5.0 × 5.0_51 bit_v2 was created as the second trial (Fig. 6a).

Adjustments were made due to the left shoulder/back having the collars present after blasting. To combat this the spacing of the perimeter holes was changed to 0.8 m, this allowed for the addition of two extra holes. The back holes were identified as wall contour perimeter holes not roof contour perimeter holes. Figure 6 gives the properties that this drill pattern has with explosive mass and drill parameters.

The inspection of the second trial (4580 ESD 001) displayed that the addition of perimeter holes mitigated substantial collars left in the face profile surface (Fig. 7). There were two shallow collars, one in the shotcrete and one in the left-hand shoulder, it would be possible to scale it out. Good fragmentation displayed led to the suggestion to reduce the number of centre blast holes as the average rock size is still quite small and powdery/dirt. Potential credibility was seen by the positive outcome of the overall



Fig. 7 ESD 001 second trial

profile seen on the bottom profile surface at the rear of the cut. This indicated that the adjustment in perimeter holes was a success and can stay the same during the next blast.

The main goal of the third trial in the 4580 ESD 001 was to reduce the number of blast holes in the centre of the drill design. The perimeter hole adjustment was successful in the second trial and it was decided to leave that as it was. As seen in the drill design, a complete row above the burn was removed and the spacing between the easer holes above the burn was increased (Fig. 8).

The inspection after the blast using the third version of this drill pattern proved to have a positive outcome. There were no oversized rocks, indicating good fragmentation. Figure 9 demonstrates that there were not any butts on the bottom profile face and no sign of collars remaining on the face profile surface. An even throw of material was produced during this blast and there was enough explosive to ‘heave’ and displace the material.

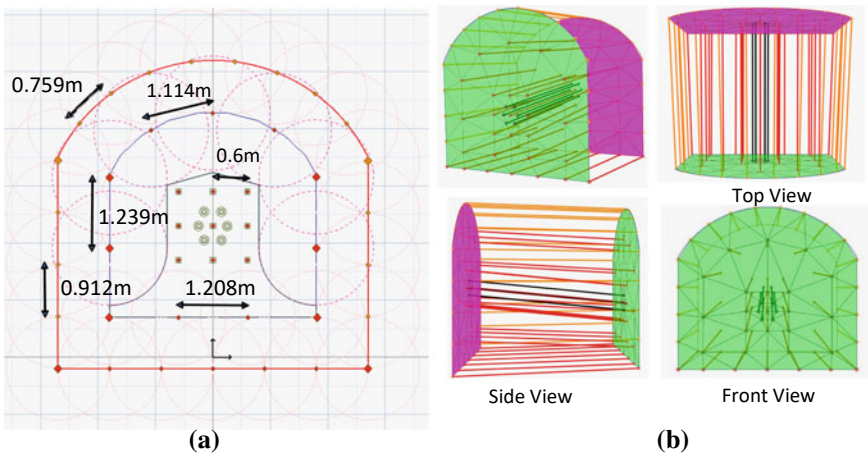


Fig. 8 (a) ESD 001 third trial (4580 ESD 001 47.7 m). (b) Three-dimensional modelling (top, side and front views), 47.7 m

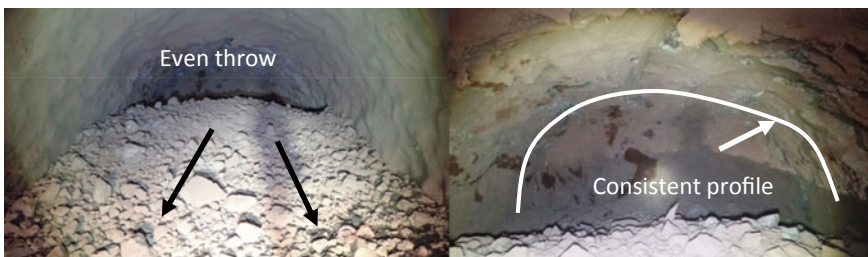


Fig. 9 ESD 001 third trial

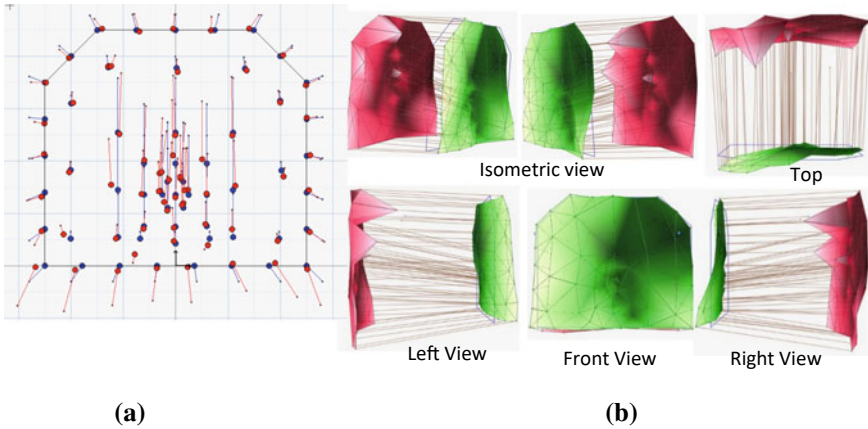


Fig. 10 (a) 4580 SMP001 Second trial—planned versus drilled. (b) Three-dimensional view, Drill plan E_5.0 \times 4.5_1in6down_V2

The inspection after the blast using the third version of this drill pattern proved to have a positive outcome (Fig. 9). Oversized rocks were not indicating good fragmentation. From what was visible there were not any butts on the bottom profile face and no sign of collars remaining in the face profile surface. It was good to see an even throw of material during this blast and to see there was enough explosive to ‘heave’ and displace the material.

2.3 Drill Plan E_5.0 \times 4.5_1in6down_V2

Operator feedback suggested the burn to be higher as it was hard to drill the burn with the long booms and the angle of the burn-in conjunction with the angle of the cut. It was suggested that the burn be moved 0.5 m higher to accommodate the boom movements and make it a lot easier (Fig. 10).

It is seen that there is a large protrusion in the bottom profile surface, this is not what was eventuated in the blast results as seen in the inspection photos but is to do with the automatic data extrapolation in the jumbos computer system regarding the stub holes.

An inspection of the blast result was carried out after re-entries were complete (Fig. 11). For this heading the opportunity arose to carry out inspections after the blast and after it was bogged out.

The new drill plan for 4555 ACC-001 is T_5.8 \times 6.2_1in6down_v2 (Fig. 12). The drill pattern profile names have been changed from displaying the dimensions first to having the allocated profile letter followed by the dimensions.

The first trial reducing drill holes in the T profile resulted in an increase in spacing in the perimeter holes including the backs, walls and lifters (Fig. 13). The burn

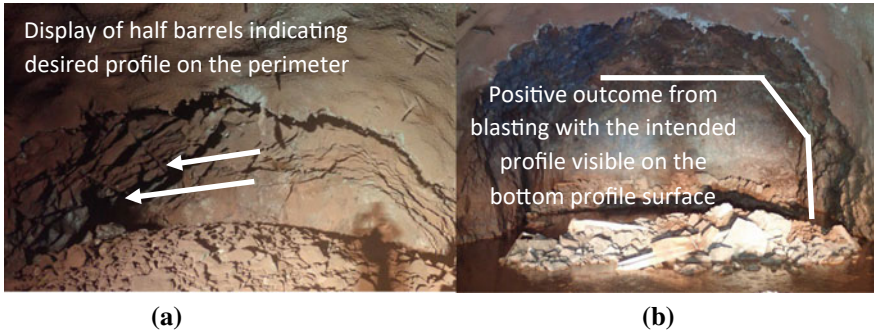


Fig. 11 (a) 4580 SMP 001 first trail, after blasting. (b) 4580 SMP 001 first trial, after bogging

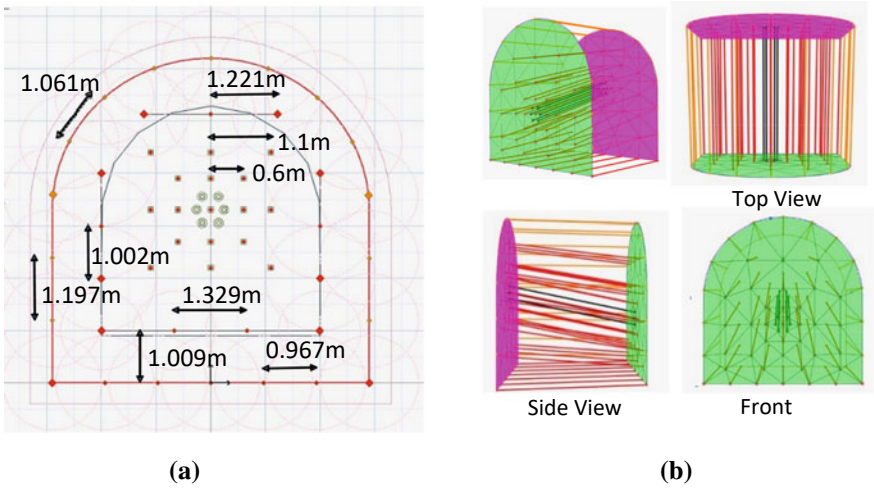


Fig. 12 (a) 4555 ACC 001 first trial, Chainage: 42.6 m. (b) Three-dimensional modelling, 4555 ACC 001 first trial, Chainage: 42.6 m

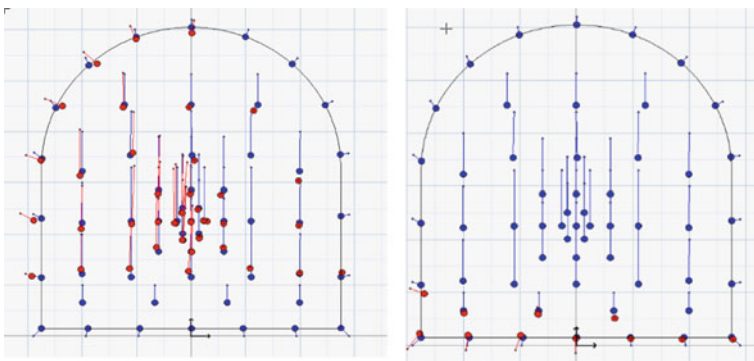


Fig. 13 4555 ACC 001 first trial—planned versus drilled



Fig. 14 4555 ACC 001 first trial

was expanded by 100 mm in both the inner and outer box. A row of knee easer holes was removed and subsequently the general spacing in the field lines increased. The heading was bogged before an inspection was possible. From boggler operator feedback the fragmentation was a good consistent size (Fig. 14).

3 Discussion

The initial intention of the drill and blast optimisation was to compare the effect of pattern alteration with the outcome of overbreak. The majority of trials had limited space in which they were conducted. This limit in space reduced the potential comparison between drill patterns as a minimum of 3 consecutive cuts are required to validate the results. Although certain headings were able to achieve 3 consecutive cuts, this was the maximum reached and therefore restricting any further comparison.

A main contributing factor that affects the data recorded was the change in geological conditions, this was present because of the difference in distance between the trials. Within the mine, there are numerous changes in geological conditions as both the depth and lateral position change and the rock behaves differently when it is under different in situ stresses and contains different characteristics. Different characteristics and rock parameters influence the results of a blast pattern. From this, it is not possible to compare the already revised patterns in each heading against one another.

Beneficial information that can be analysed is the costings that have been calculated from information collected regarding UJ003. The common perception that a reduction in only a few holes is not beneficial has been seen to be held across numerous operators, in the enlightenment of the above figures based on averages calculated from the last five-eight months small revisions can be seen to affect the financial outcome greatly.

Singular drill holes have multiple aspects that create cost reduction if mitigated in the design stage. Alongside the obvious reduction in drill metres, each hole contains

a specific amount of emulsion, a detonator and a booster. Costing has been calculated to correlate the consumable cost per metre drill and percussion hour cost per metre on average over the last five-eight months.

The outcomes and learnings discovered from using various plans have a major benefit on the rest of the project when the opportunity arises to have consecutive cuts within similar drives and geological conditions. Each heading that was investigated produced different results which contain specific aspects that in conjunction with each other will create a better understanding further down the track in future trials.

4 Conclusions

The cross-sectional slices computed from Deswik demonstrated the overall over break value for the trials in the 4580 XCD 326 has an average of 7.91%. For the 48 mm comparison, this average value surpasses the expectations of what was thought was going to be achieved.

It is noted that the calculated overbreak value over the entirety of the cross-sectional slices is within an acceptable limit it was found that the laser within the 4580 XCD 326 was out of alignment by 0.4 at 80 m down the drive. Having these trials conducted from 36 to 60 m this misalignment would have severely impacted their results giving higher over break values than what was eventuated. Although this error is not documented within the deswik program as it was found to be an issue after the survey picks up was completed it is a factor that needs to be considered when comparing the results between the 48 mm design and the above 51 mm design as it would skew the notion that the 51 mm design was not as effective as it was. Given the error was found over an 80-m length there is no quantitative data that can be subtracted from the overbake value to give a conclusive result to define the figures found between 36 and 60 m.

From a couple of months of trials, it can be seen that with the implementation of progressive adjustments, optimisation can be achieved over numerous headings throughout the underground mining process. Although the results that have been presented display a benefit and improvement of what was originally being implemented in the ore drives at the mine, but there is still room to further improve these designs. A project of such will always continue to be adjusted due to the ability of the geological conditions to change quite quickly given the rapid development rate. Moving forward it will be seen that UJ003 will continue to bore cuts using the 51 mm drill bits as the above research suggests that there has been a significant cost saving while resulting in an acceptable overbreak value.

References

1. Gawler Craton (2019). http://www.energymining.sa.gov.au/minerals/geoscience/geology/gawler_craton. Accessed 31 Oct 2019

2. Carrapateena Copper-Gold Project - Mining Technology | Mining News and Views Updated Daily (2019). <https://www.mining-technology.com/projects/carrapateena-copper-gold-project/>. Accessed 31 Oct 2019
3. Dowling M, Domotor R, Miller D (2014) Improving excavation efficiency at the ST Helena tunnel using best practice drill and blast techniques
4. Mottahedi A, Sereshki F, Ataei M (2017) Development of overbreak prediction models in drill and blast tunnelling using soft computing methods. *Eng Comput* 34(1):45–58. <https://doi.org/10.1007/s00366-017-0520-3>
5. Kim Y, Moon H (2013) Application of the guideline for overbreak control in granitic rock masses in Korean tunnels. *Tunnel Undergr Space Technol* 35:67–77. <https://doi.org/10.1016/j.tust.2012.11.008>
6. Singh S, Xavier P (2005) Causes, impact and control of overbreak in underground excavations. *Tunn Undergr Space Technol* 20(1):63–71. <https://doi.org/10.1016/j.tust.2004.05.004>
7. Sambuelli L (2008) Theoretical derivation of a peak particle velocity-distance law for the prediction of vibrations from blasting. *Rock Mech Rock Eng* 42(3):547–556. <https://doi.org/10.1007/s00603-008-0014-0>
8. Selection of Blasting Limits for Quarries and Civil Construction Projects (2018). https://www.oricaminingservices.com/uploads/uploads/200281_%20Selection%20of%20Blasting%20Limits%20for%20Quarries%20and%20Civil%20and%20Construction%20Project. Accessed June 2019

Underground Structures and Cases Studies

Investigation for Influence of Pressure on Face Stability of Mega Tunnel



Shilpa Kulkarni and M. S. Ranadive

Abstract Urbanization in Developing countries raise the demand of smart and efficient infrastructure facility. Due to faster growth rate, urban area meets many challenges like traffic congestion and thereby increased travel time. To cope with these, effective utilization of underground spaces is a need of time. Mega tunnel plays an important role to satisfy this need, as it is large diameter tunnel whose diameter is greater than 10 m. Mega Tunnel may facilitate with multi operating transport to prove its benefit for society. Tunnel excavation using Tunnel Boring Machine (TBM), is frequently performed to avoid surface traffic disturbance and to minimize construction time during project execution period. Face Stability of such type of tunnels has been emerging topic for researchers, as this issue get more critical with the increase in tunnel diameter. This increment of Critical cover to Diameter (C/D) ratio leads to increase in indirect construction cost. This paper focuses on the investigation of adequate pressures to be applied on Mega Tunnel to ascertain the ground induced settlement at various C/D ratios. Three-dimensional finite element analysis was performed by using Midas Gtx Nx software with different C/D ratios and pressure parameters for soft soil. Parametric study had been done on 15 m diameter tunnel. The conclusions were drawn based on 95 analytical models with five different cases. This study concluded that adequate application of pressure minimizes the C/D ratio to stabilize the face of Mega Tunnel, which can be proven to minimize the construction cost in practical use.

Keywords Finite element analysis · Mega tunnel · TBM · Face stability · Parametric study

S. Kulkarni (✉)
College of Engineering, Pune, India
e-mail: shilpakul10@gmail.com

M. S. Ranadive
Department of Civil Engineering, College of Engineering, Pune, India
e-mail: msr.civil@coep.ac.in

1 Introduction

Developing countries needs a sustainable infrastructure solution to satisfy the urge of efficient transport system. Due to growing population in urban areas, metropolitan city needs systematic planning approach to use underground space effectively. Mega Tunnel delivers the smart infrastructure idea to satisfy this need.

Tunnelling using EPBM is often being performed in urban area due to availability of soft strata, ground water table and considering the safety of the structure above the ground. Assessment of face stability of the tunnel structure is foremost important concern considering construction safety and ground control. The large diameter tunnel more than 10 m diameter is referred as Mega Tunnel. Z.X. Zhang [23], proposed study and concluded that the larger the tunnel diameter more challenging the face stability. Peng Zhang [9], suggested the face pressure as an important parameter in assessment of face stability. Guilhem Mollon [4], proposes the study to prevent tunnel face collapse by determining the minimal pressure. Numerous research [12, 30], were presented to prove the good agreement of analytical and experimental method with numerical method using Midas Gtx. Nx in face stability assessment of tunnel. Claudia Gonzalez [15], concludes face component is essential component for EPB machine and the face pressure needs to maintain within certain limit. Shilpa Kulkarni and M.S. Ranadive [31], concluded earth pressure or overburden as critical factor in assessment of face stability of Mega Tunnel in soft soil and adequate application of pressure can minimizes the Cover to Diameter ratio for face stability of Mega Tunnel.

Hence, it is important to investigate the adequate percentile range of numerous pressures to applied on EPBM for assessment of face stability. This research study proposes the range of face pressure, Jack thrust, earth pressure, water pressure on face stability of tunnel by investigating the vertical displacement of key node i.e., the crown and invert of Mega Tunnel. Midas Gtx. Nx. is used for modelling and analysis.

2 Literature Review

Ahmed S.N. Algha, David Chapman [30], determined collapse pressure with analysis by 3D finite element analysis using Midas Gtx. Nx. in homogeneous and layered ground and concluded face pressure is a more affected parameter on tunnel face stability. V.B. Maji, A. Adugna [18], concludes face pressure as a critical parameter in EPB tunnelling which leads to collapse the tunnel face with variation.

Caludia Gonzalez, Marcos arroyo, [15], figured face pressure should remained in limit to avoid collapse or blow-out the tunnel face. Qiuqing Pan and Daniel Dias [17], summarize that elevation of water table elevation exerts a significant unfavorable impact on face stability. As per Guilhem Mollon, et al. [6], determination of minimal pressure and ground deformation to prevent collapse of tunnel face was very important for determination of tunnel face stability issue. The C/D ratio has more importance in failure mechanism. Guilhem Mollon, et al. [6], suggests, the soil mass verging, the tunnel face can collapse into the tunnel if the applied face pressure drops below a critical value. It also states that, if $C > D$, collapse mechanism never offshoot. [7] studied the face instability of shield tunnel in sand by proposing experimental model at various C/D ratio. Soil arching during failure was monitored. [14], gives various critical pressure parameter to be considered for EPB TBM, while tunnel advancing and its effect on structural stability. It also gives required calculation models for various pressures like thrust pressure and grout pressure. Peng Zeng et al. [11], concludes that the face pressure is an important parameter to avoid face collapse. This also confirmed that the reliability of tunnel face stability increases significantly as face support increases or tunnel diameter decreases. [21] concluded that the face stability had become more challenging issue with increment in the tunnel diameter. [24] analyzed the face stability by numerical method at higher tunnel depth and suggest more pressure needed to support excavation face in soil. [26] describes the combined effect of surcharge load, self-weight and internal supporting pressure and studies stability number for the circular tunnel in cohesive soil.

3 Data Collection

Data was collected for various geotechnical parameter required to tunnel modeling for soft computing analysis as shown in Table 1.

Required pressures such as Face pressure, Jack thrust, skin resistance friction and the pressure due to gap between shield and segment were found out and validated. Validated pressures were used for further analysis.

Table 1 Geotechnical parameter [31]

No.	Design parameter	Soil	Segment	Steel	Grout
1	Modulus of elasticity (E) (kN/m ²)	1.3e ⁶	2.1e ⁷	2.5e ⁸	1e ⁷
2	Poisson's ratio	0.3	0.3	0.2
3	Unit weight (kN/m ³)	19	24 (saturated)	78	22.5
4	Cohesion (kN/m ²)	15
5	Friction angle	30
6	K ₀	0.5	1

4 Research Methodology

Standard research methodology was adopted to analyze the Mega Tunnel. The geotechnical parameters were collected from literature study. The required pressures for application on TBM were found out by Numerical modelling in Midas Gtx-Nx and based on empirical formulas considering 2% volume loss. These pressures were validated [31]. For observing effect of pressure, it was varied in certain range by keeping C/D ratio constant as 3.5. Diameter of tunnel was considered as 15 m. 3D numerical modelling was adopted using Finite Element Analysis. Observations were done to draw the conclusion and pressure application range was suggested.

5 Data Analysis

[31] presented the study for face stability of Mega Tunnel analyzing it for various C/D ratio, ranging from 1 to 13 at different interval. The applied pressures were validated. This validated set of pressure was analyzed at various range by modelling. The range was decided as 60, 80, 100, 120 and 140% of validated face pressure and jack thrust. Earth pressure and water pressure were validated with the proportion to tunnel diameter, as from 2 to 6D for earth pressure and from 0.6D to 4D for water pressure.

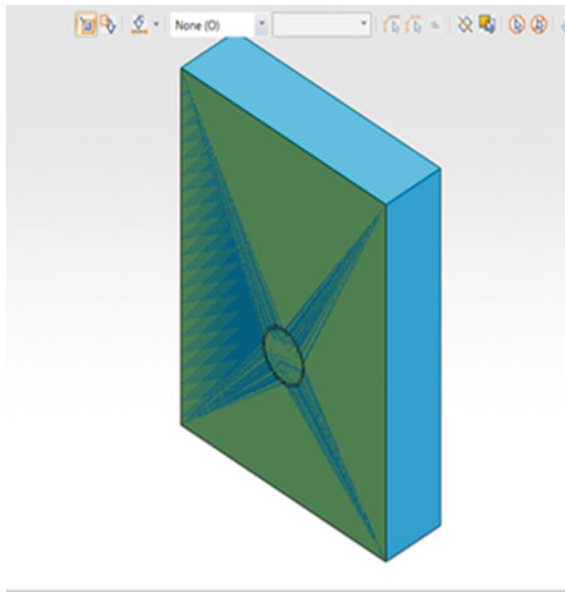


Fig. 1 Modelling of mega tunnel

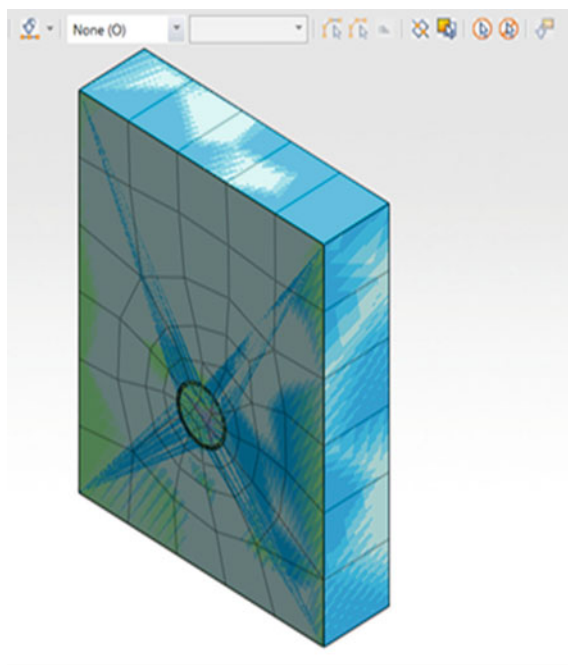


Fig. 2 3D meshing of model

Mohr's Coulomb Model was used while analysis. Auto constraint for boundary condition and construction stages was given. Parametric study had been done at the crown and the invert of Mega Tunnel. Vertical displacement was observed at every node and maximum displacement was considered for observation. Displacement of both vertical walls not taken into consideration as it was found negligible [31] please refer (Figs. 1, 2, 3 and 4).

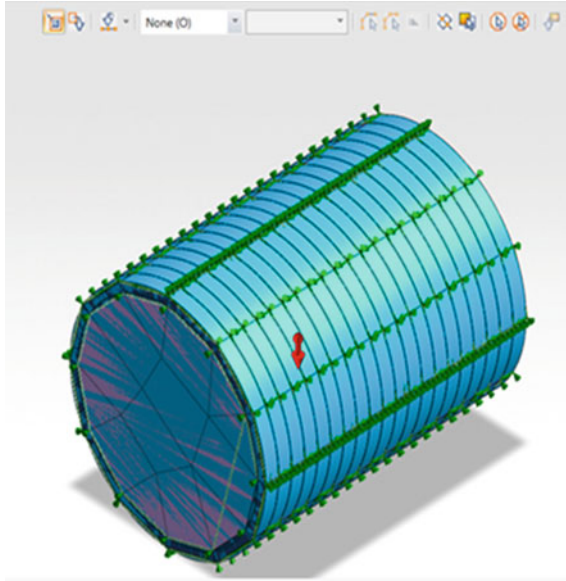


Fig. 3 Application of pressures

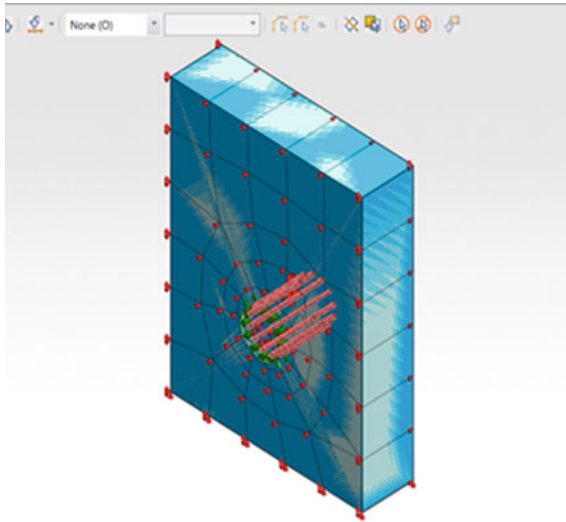


Fig. 4 Boundary constraint

6 Observations

6.1 Effect of Face Pressure

For observing effect of face pressure, the pressure set 1 applied was as shown in Table 2. Sign convention used as [\leftarrow (-ve), \rightarrow (+ve), \uparrow (-ve), \downarrow (+ve)].

Face pressure varies from 60 to 140% at every 20% interval, to observing the effect.

It was observed that application of low amount of pressure leads to collapse of ground in front of tunnel face as soon as TBM start drilling operation, this lesser amount of pressure leads to displace the ground strata in initial stages. Hence observing more displaced ground due to 60% face pressure application. 80 and 120% of face pressure application shows displacement to nearer 100% and validated face pressure. At 140% the displacement is more as compared to 80 to 120% value, but it

Table 2 Pressure set 1

Sr. no.	Pressure type	Amount of pressure (MPa)
1	Face pressure	Variable (60 to 140%)
2	Jack thrust	-75,670
3	Pressure due to contraction over the body of shield TBM	2120
4	Pressure due to gap between shield and segment	5510

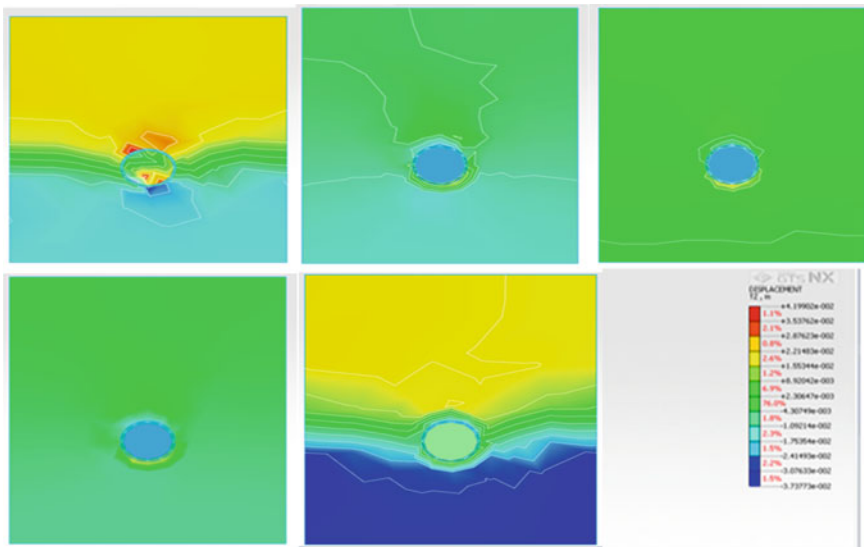


Fig. 5 Ground behavior under face pressure ranging from 60 to 140%

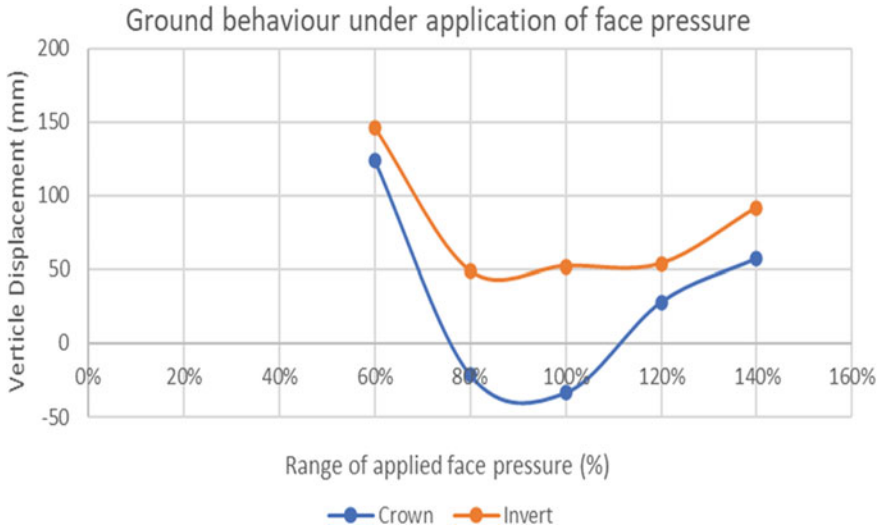


Fig. 6 Ground behavior under face pressure ranging 60 to 140%

was not impacted as 60% value. Refer Fig. 6 for graphical representation of ground behavior (Fig. 5).

Effect of Jack Thrust

For observing effect of Jack thrust, the pressure set 2 was applied as shown in Table 3.

It was observed that low amount of jack thrust is unable to move forward, hence it effect on excavating capacity of drill in forward direction, observing minimum displacement of the crown and the invert. Excess amount of jack thrust beyond critical limit shows the maximum displacement of crown in upward direction and invert in downward direction. Hence it was observed the critical amount of jack thrust is $\pm 10\%$ of the validated value. Figure 7, shows the observed ground behavior under the influence of Jack thrust.

Table 3 Pressure set 2

Sr. no.	Pressure type	Amount of pressure (MPa)
1	Face pressure	232.5
2	Jack thrust	Variable (60 to 140%)
3	Pressure due to contraction over the body of shield TBM	2120
4	Pressure due to gap between shield and segment	5510

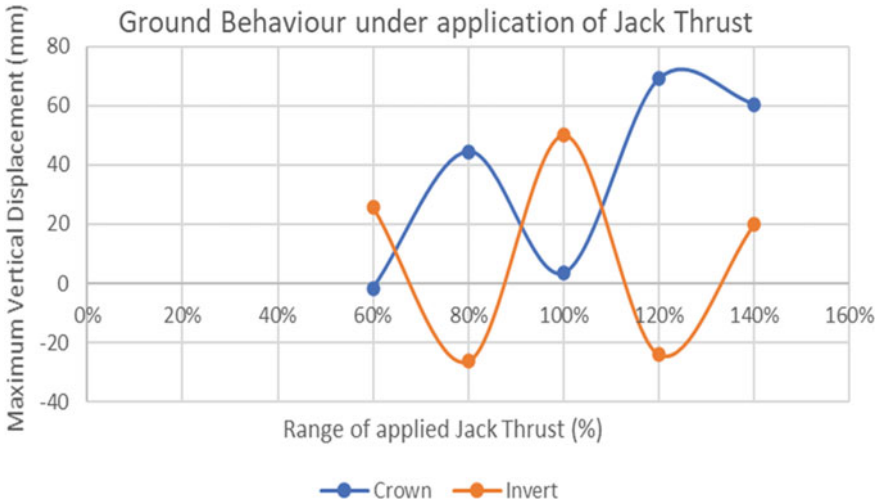


Fig. 7 Ground behavior under Jack Thrust ranging from 60 to 140%

6.2 Effect of Earth Pressure

For observing effect of earth pressure models were analyzed at various cover to diameter (C/D) ratio from C/D = 2, 3, 4, 5 and 6. Table 4, shows the applied pressure set 3, for analyze the effect of earth pressure. The displacement of crown and the invert as shown by graph. It was observed that earth pressure was the critical parameter affecting face stability of Mega Tunnel. The face can be stable from 3 to 6D, observed nearly equal ground settlement at C/D = 3, 5, and 6. After C/D = 4, Behavior of ground settlement of the crown and invert was opposite to each other. Figure 8, shows the behavior of the ground under earth pressure.

Table 4 Pressure set 3

Sr. no.	Pressure type	Amount of pressure (MPa)
1	Face pressure	232.5
2	Jack thrust	-75,670
3	Pressure due to contraction over the body of shield TBM	2120
4	Pressure due to gap between shield and segment	5510

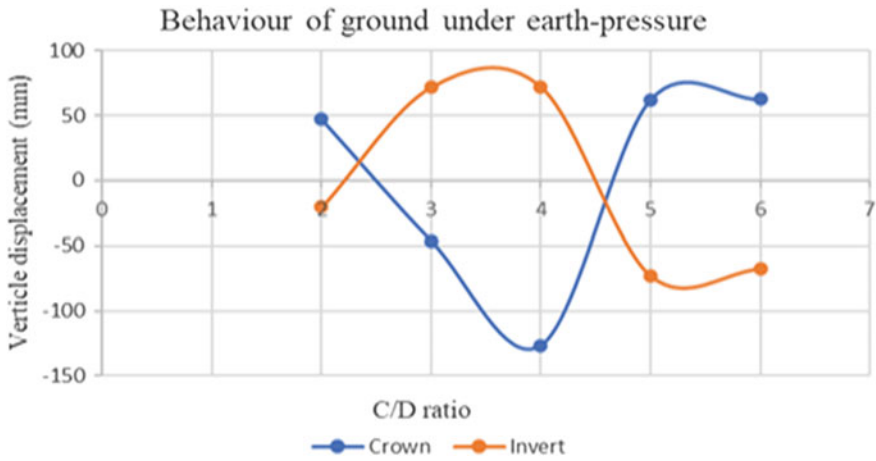


Fig. 8 Behavior of ground under earth pressure

6.3 Effect of Water Pressure

Pressure parameter given in Table 4 was used for analysis to observe effect of water pressure. It was observed that presence of water table critically affected on displacement of the crown due to uplift pressure of the Mega tunnel. The displacement of the invert shows stabilized behavior as compared to crown. It is significantly more when it exceeds twice of the tunnel diameter. Figure 9 shows, the ground behavior under the water pressure.

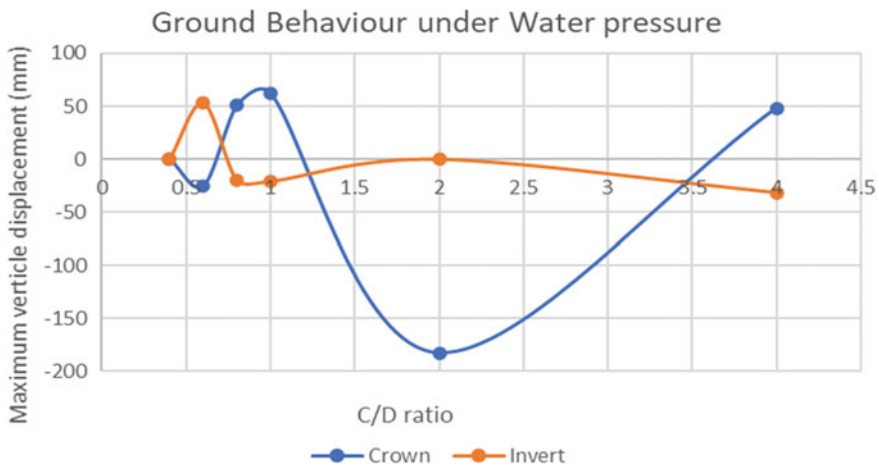


Fig. 9 Behavior of ground under water pressure

7 Discussion and Suggestion

From three-dimensional analysis performed on 15 m diameter Mega Tunnel, it was observed that the application of pressure is an important parameter to analyze the face stability. As the previous research suggests the importance of geological formation and the available ground strata are more concerning with the face stability. This research also judging the severity of application of face pressure and found its validity. Hence, the critical range of face pressure application is $\pm 20\%$ of the numerically founded value.

In case of jack thrust, it was observed it is equally affected pressure on face stability as that of face pressure value. It may fluctuate in a range of $\pm 10\%$. The jack thrust should calculate curiously considering weight and diameter of the TBM.

Earth pressure significantly affect more after increased in the C/D ratio; hence optimum C/D ratio can be considered while deciding the face stability of Mega Tunnel. [31] suggest that the earth pressure is the critical parameter in assessment of face stability of Mega tunnel rather than water pressure, but this research suggest that the water pressure being a critical factor if it exceeds the range beyond equal to its diameter.

8 Conclusion

Mega tunnel is a large diameter tunnel which exceeds 10 m diameter. The face stability of the tunnel depends upon two factors i.e., geotechnical parameter and the pressure application on TBM while excavation. This study concludes that right amount of pressure application assists to stabilize the tunnel face at shallow depth. Face pressure, Jack thrust was significant factor and right investigation of it proves beneficial in face stability assessment.

The range of variation for face pressure is acceptable in $\pm 20\%$ of numerically or analytically calculated value. Jack thrust is equally important parameter and plays crucial role in stabilizing the tunnel face. Hence, it can be calculated carefully. The weight and the diameter of the TBM have remarkable impact on tunnel face stability. The critical range of jack thrust application can be $\pm 10\%$. Water pressure can be a crucial parameter for face stability when it exceeds the proportion equal to diameter of the tunnel.

Hence, this research concludes that the three-dimensional finite element analysis is an appropriate tool to investigate the effect of pressure on face stability of Mega Tunnel. This acceptable limit of pressure optimizes the C/D ratio at 3.5 for structural stability and offers financial profitability in construction of Mega Tunnel.

References

1. Broere W (1998) Face stability calculation for a slurry shield in heterogeneous soft soil, tunnels and metropolises, pp 215–218
2. Kawadas MJ (2005) Monitoring ground deformation in tunnelling: current practices in transportation tunnels. *Eng Geol* 79:93–113
3. Kim S-H, et al (2006) Evaluation of shield tunnel face stability in soft ground. In: International symposium on underground excavation and tunneling
4. Mollon G, Dias D, Soubra A-H (2010) Face stability analysis of circular tunnels driven by a pressurized shield. *J Geotech Geoenviron Eng*. [https://doi.org/10.1061/\(ASCE\)GT.1943-5606.0000194](https://doi.org/10.1061/(ASCE)GT.1943-5606.0000194)
5. Kirsch A (2010) Experimental investigation of the face stability of shallow tunnel in sand. Springer
6. Mollon G, Phoon KK, Dias D, Soubra A-H (2011) Validation of a new 2D failure mechanism for the stability analysis of a pressurized tunnel face in spatially varying sand. *J Eng Mech*. [https://doi.org/10.1061/\(ASCE\)EM.1943-7889.0000196](https://doi.org/10.1061/(ASCE)EM.1943-7889.0000196)
7. Chen R et al (2013) Experimental study on face instability of shield tunnel in sand. *Tunn Undergr Space Technol* 33:12–21
8. Senent S, Mollon G et al (2013) Tunnel face stability in heavily fractured rock masses that follows the Hoek-Brown failure criterion. *Int J Rock Mech Mining Sci* 60:440–451
9. Zeng P, Senent S, Jimenez R (2014) Reliability analysis of circular tunnel face stability obeying Hoek-Brown failure criterion considering different distribution types and correlation structures (ASCE). [https://doi.org/10.1061/\(ASCE\)CP.1943-5487.0000464](https://doi.org/10.1061/(ASCE)CP.1943-5487.0000464).
10. Elarabi H, Mustafa A (2014) Comparison of Numerical and Analytical method of analysis of tunnel. In: Conference paper
11. Zeng P, et al (2014) Reliability analysis of circular tunnel face stability obeying Hoek-Brown failure criterion considering different distribution types and correlation structure ASCE
12. Ibrahim E, Soubra AH et al (2015) Three – dimensional face stability analysis of pressurized tunnel driven in multilayered purely frictional medium. *Tunn Undergr Space Technol* 49:18–34
13. Vu MN et al (2015) The impact of shallow cover on stability when tunnelling in soft soils. *Tunn Undergr Space Technol Incorpor Trenchless Technol* 50:507–515
14. Souza TG, et al (2015) TBM pressure models-observations, theory and practice. In: Geotechnical synergy in Buenos Aires
15. Gonzalez C, Arroyo M (2016) Thrust and torque component on mixed face EPB drives. *Tunn Undergr Space Technol* 57:47–54
16. Khezri N, Mohamad H, et al (2016) Stability assessment of tunnel face in a layered soil using upper bound theorem of limit analysis. *Geomech Eng*
17. Pan Q, Dias D (2016) The effect of pore water pressure on tunnel face stability. *Int J Numer Anal Meth Geomech* 40:2123–2136
18. Maje VB, Adugna A (2016) Numerical modelling of tunnelling induced ground deformation and its control. *Int J Mining Geo-Eng* 50:183–188
19. Zhang ZX, Liu C (2016) Three dimensional FEA on ground responses during twin tunnel construction using the URUP method. *Tunn Undergr Space Technol* 58:133–146
20. Mollon G, Dias D et al (2017) Range of the safe retaining pressures of a pressurized tunnel face by probabilistic approach. *J Geotech Geoenviron Eng* 139:1954–1967
21. Shiau J et al (2017) Stability charts for unsupported plane strain tunnel heading in homogeneous undrained clay. *Int J GEOMATE* 14:19–26
22. Pan Q, Dias D (2017) Three-dimensional face stability of tunnel in weak rock masses subjected to seepage forces. *Tunn Undergr Space Technol* 71:555–566. Incorporating to Trenchless technology
23. Zhang ZX, Liu C, Huang X (2017) Numerical analysis of volume loss caused by tunnel face stability in soft soil. *Environ Earth Sci* 76:1–19
24. Dias D (2018) Three-dimensional face stability analysis of circular tunnels by numerical simulation, ASCE

25. Wang J et al (2019) Face stability analysis of EPB shield tunnels in dry granular soils considering dynamic excavation process. *J Geotech Eng* 145:04019092
26. Hernandez YZ et al (2019) Three-dimensional analysis of excavation face stability of shallow tunnels. *Tunn Undergr Space Technol* 92:103062
27. Liu C, Peng Z et al (2020) Influence of TBM advance on adjacent tunnel during URUP tunneling: a case study and numerical investigation. *Appl Sci* 10:3746
28. Shiau J, Al-Asadi F (2020) Three-dimensional analysis of circular tunnel heading using Broms and Bennermark's original stability number. *Int J Geomech* 20(7):06020015
29. Neuner M et al (2020) On discrepancies between time – dependent nonlinear 3D and 2D finite element simulation of deep tunnel advance: a numerical study on Brenner Base tunnel. *Comput Geotech* 119:103355.c
30. Algha Ahmed S.N., Chapman David (2019) Numerical modelling of tunnel face stability in homogeneous and layered soft soil. *Tunn Undergr Space Technol* 94:103096
31. Kulkarni S, Ranadive M.S. (2021) Finite element analysis for parametric study of mega tunnel. In: International conference on advances in construction technology and management

Delineation of Water Seepage Flow Path in the Underground Metro Rail Tunnel Using Cross-Hole GPR Tomography: A Case Study



B. Butchibabu, P. C. Jha, N. Sandeep, and Y. V. Sivaram

Abstract Construction of infrastructure development projects in urbanized environment suffers with obstructions like lack of surface free space, underground utilities, traffic and shallow drainage system. These obstructions hamper the work progress as well as major factor for project delay and cost overruns. Obtain timely solution to these obstructions helpful in meeting the deadlines and reduce the inconvenience to the public. One such case was discussed here, where Mumbai Metro Rail Corporation Limited (MMRCL) proposed to construct a 33.5 km long underground metro rail tunnel between Colaba and SEEPZ. TBM was deployed to make 5.8 m dia tunnel at a depth of 18 m. After 265 m of tunnel excavation, water seepage was encountered with a high discharge flow rate of 60,000–80,000 L/h at Marol Naka station box area. To plug this flow path, Identification of source location or the direction of flow path is the prime concern. Surface investigations to identify this flow path were not possible, due to heavy traffic, shallow underground utilities and congested area. Ground Penetrating Radar (GPR) investigations through boreholes were proposed to delineate the probable water seepage flow path. Five bore holes were drilled over the station box area up to a depth of 25 m. Five sets of tomography investigations were carried out to map the high/low attenuation zones based on the radar wave attenuation characteristics of the subsurface medium. The Frequency Domain Attenuation Tomography (FDAT) analysis was done to characterize the attenuation pattern of observed radar wave signal in the dry as well as in the saturated medium. 3-D subsurface image was generated based on attenuation characteristics to demarcate the probable water seepage flow path in the study area.

Keywords Ground Penetrating Radar · Cross-hole tomography · Water seepage · Attenuation · Underground metro tunnel

B. Butchibabu (✉) · P. C. Jha · N. Sandeep · Y. V. Sivaram
National Institute of Rock Mechanics, Banashankari 2nd Stage, Bangalore 560070, India
e-mail: bbabugeo@gmail.com

© The Author(s), under exclusive license to Springer Nature Singapore Pte Ltd. 2022
A. K. Verma et al. (eds.), *Proceedings of Geotechnical Challenges in Mining, Tunneling and Underground Infrastructures*, Lecture Notes in Civil Engineering 228,
https://doi.org/10.1007/978-981-16-9770-8_23

371

1 Introduction

The rapid urbanization concurrently keep pace to meet the demand of urban passengers to facilitate with transportation infrastructure. The urban passengers suffers with lack of transportation infrastructure according to the needs of public demand constrain the development of urban regions. One effective way to solve the urban traffic problem is to develop metro rail network system, they have capabilities like high passenger carrying capacity, speed, convenience, comfort, and relatively low energy consumption. Construction of metro networks can help to mitigate traffic problems and promote the rapid development of urban economy. The construction of this metro networks are either on the elevated corridors or through underground tunnels and combination of both. Elevated corridors constructed by erecting series of piers along the proposed metro line, whereas construction of underground tunnels made either drilling blasting technique or deployment of Tunnel Boring Machines (TBM) or Soil Boring Machines (SBM). The construction of underground tunnels suffers with lack of detailed information in urban environment such as subsurface strata conditions, detailed geology along proposed metro line, ground water levels etc. Obtaining detailed information along the proposed metro line is extremely difficult because lack of surface free space to carryout investigations, close habitations, road traffic, utilities etc. These limitations in construction of underground tunnels face some surprises such as water seepage into the tunnel, encountering of large boulders, loosening of surrounding strata, roof fall at places, weak strata and lowering of groundwater table etc. Timely plugging of these incidents reduces further deterioration of strata condition as well as helps the tunneling progress.

Geophysical methods are rapid, high-resolution tools to identify/map the possible troublesome zones through surface investigations or borehole probing. Among all geophysical techniques electrical and electromagnetic methods are undoubtedly leading ones in exploration and management of groundwater related issues [1, 2]. Two well-known techniques especially for water seepage detection are of Ground Penetrating Radar (GPR) and Electrical Resistivity Tomography (ERT) [3]. Surface investigations restrict to conduct ERT at urban areas, then GPR is only the alternative.

GPR is relatively newer technique in exploration geophysics based on the characteristics of electromagnetic (EM) waves. This technique works on the principle of propagation and reflections of EM waves and forms a continues image based on the EM impedance of the target. The GPR system records the travel time, frequencies, amplitude, phase and they used for further processing as well as interpretation. GPR has been widely used in various fields and successfully solved complex problems such as pavement evaluation, underground utility detection, civil engineering applications [4–8]. This technique successfully applied for stratigraphy mapping [9, 10]; bedrock fracture detection [11]; archeological investigations [12, 13]; railway monitoring, assessment of tunnels, reinforcement bars [14]. The most common applications in underground metro tunnels are estimation of thickness of grouting layer [15]; assessment of barrier effect [16]; potential damage [17, 18]. GPR is a powerful technique

for detection of water content zones, water piping leaks, leakage pathways etc. [19–23]. The GPR studies reported above are based on the surface investigations, whereas the urban environment restrict the surface investigations due to lack of sufficient free space, continues traffic, underground utilities and less depth of investigation. Alternatively borehole investigations were preferable to achieve desired depth as well as resolution [24–26]. In addition GPR image will generate based on the amplitude of the reflections forms a hyperbola (arch) shape and these reflections may not form hyperbolas, if the contrast between medium and target is minimum. In this situation, studying frequency dependent attenuation characteristics may provide possible water seepage flow paths [27–29].

In the present study we have carried out five sets of cross-hole GPR tomography surveys in a zig-zag manner over the underground metro tunnel to map the probable flow path of water seepage. Attenuation characteristics were analyzed using Frequency Domain Attenuation Tomography (FDAT) to identify the probable water seepage flow path on the crown of underground metro tunnel.

2 Study Area and Problem

Mumbai Metro Rail Corporation Limited (MMRCL) is constructing 33.5 km long underground metro line in Mumbai named as Line-03 also called as Aqua Line between Colaba and SEEPZ via Bandra (Fig. 1). This metro line will connect Cuffe Parade business district in the extreme south of the city to SEEPZ in the north-central with 26 underground and one at-grade station. Once completed, this would be the city's first fully underground metro line. The construction of the Colaba-Bandra-Seepz metro tunneling work is divided into seven packages for the construction feasibility. The present study area is in the package-07 of Mumbai metro line-03 (MML-03) starting from Chhatrapati Shivaji International Airport (CSIA) to SEEPZ station via Marol Naka and MIDC stations. TBM-1 was deployed towards Mid Shaft to CSIA (up-line tunnel) for the 1261 m length with a finished diameter of 5.8 m at 16–18 m deep from the ground level. After 265 m tunneling, water seepage was encountered underneath the Mumbai metro line-01 (MML-01) elevated corridor near Marol Naka metro station on the Andheri-Kurla road. High water pressure was encountered in the up-line tunnel of MML-03 and this was badly affected the tunneling progress. The water discharge rate was recorded as 60,000–80,000 L/h and the water pressure reached up to 4.5 bar at the TBM chamber during tunnel liner installation. Under this situation, detection of water source or water seepage flow path is the prime concern around the Marol Naka underground station box area.



Fig. 1 Map showing proposed underground Mumbai metro rail network (MML-03). The study area (Marol Naka metro station) was marked with rectangular box on the metro network map

3 Geology of the Study Area

Geologically Mumbai is made up of Basaltic lava flows which are dipping towards west about 10° – 20° [30]. These lava flows have been identified as seven distinct sporadic episodes from upper Cretaceous to lower Eocene (60 to 50 million years). Basalt, volcanic breccias, Rhyolite, Trachytes, shales are the main rocks exposed at various locations in Mumbai. The intertrappean sedimentary rocks like shale's are long period of quiescence in volcanic activity. The thickness of overburden soil in the city ranging from 1.0 to 14.0 m predominantly with marine clay, boulders and

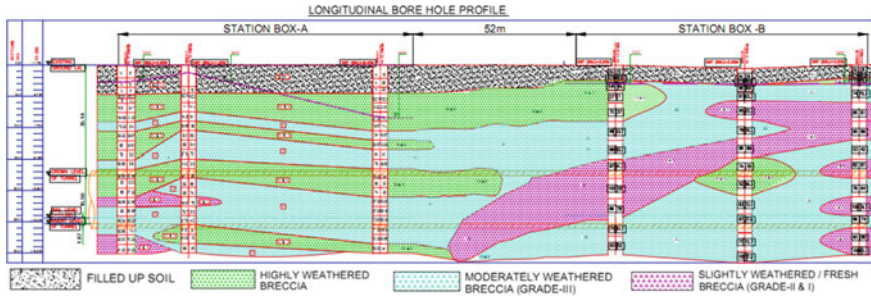


Fig. 2 Geological cross section of the proposed Marol Naka underground metro station has been prepared based on the 10-borehole data

filled-up material. The groundwater level is close to the ground level. The subsurface geological cross section at Marol Naka metro station boxes is plotted based on the 10 borehole data (Fig. 2). It consists of geological soil/rocks units: Fill from ground level to 2.0 m deep, followed by clay/residual soil layer between 2.0 to 6.0 m deep, Breccia GIV from 6.0 to 13.50 m deep, Breccia GIII from 13.50–30 m deep. In addition to the geological units, patches of weak rock was identified at different depths from the borehole data which are Breccia GIV from 6.0 to 10.50 m deep, Breccia GIII from 10.50–12.0 m deep, Breccia GIV from 12.0 to 13.50 m deep, Breccia GIII from 13.50–16.50 m deep, Breccia GIV from 16.50 to 21.0 m deep and Breccia GIII: from 21.0 m deep. The borehole data suggesting that the rock grade increasing with depth (grade V to grade I) and consists of alternating bands of geological units and weak rocks.

4 Data Acquisition and Analysis

Due to the space limitations and heavy traffic, the proposed underground Marol Naka station has been divided into two parts i.e. station box-A and station box-B for construction feasibility. The total length of station is around 270 m. Both station box-A and station box-B of the Marol Naka station, both up/down-line tunnels and locations of boreholes drilled for present investigation are marked on the site plan (Fig. 3). The portion between the two boxes is having the existing elevated metro line-01 (MML-01) and the footings of the metro line-01 piers are on the Andheri-Kurla road. This Andheri-Kurla road is always busy with heavy traffic because it connects to the Mumbai International airport. There are several underground utilities, power & network cables pass through this road. The present borehole geophysical investigation was proposed to carried out on the Andheri-Kurla road. Three boreholes (B1, B2 and B3) were proposed to drill on the western side of up-line tunnel (two boreholes (B1 and B3) on either side of Andheri-Kurla road and one borehole (B2) on the median (Fig. 3). One borehole (B4) was proposed in between up/down-lines

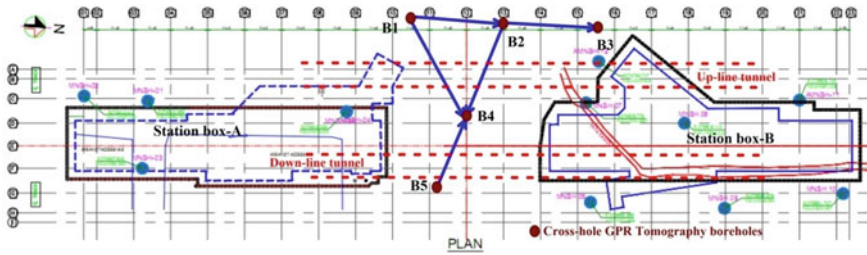


Fig. 3 Station box-A and Station box-B of the proposed underground Marol Naka station. Cross-hole GPR tomography borehole locations (B1 to B5) along with the direction of the survey conducted was marked on the site plan. Both up-line and down-line tunnels were marked with red dashed lines

Table 1 Borehole pairs used for cross-hole GPR tomography survey

Sl. no.	Tx-Rx borehole pairs for cross-hole GPR survey	Borehole separation (m)	Tomogram depth (m)
1	B1-B2	28.50	23
2	B2-B3	30.20	23
3	B2-B4	25.91	22
4	B4-B5	20.42	22
5	B1-B4	30.04	22

on the median of Andheri-Kurla road. The fifth borehole (B5) was proposed to drill on the eastern side of down-line tunnel and this borehole is in-line with the boreholes B2 and B4 along the central divider portion of Andheri-Kurla road. The details of the borehole pairs across which the cross-hole GPR survey was carried out are given in Table 1.

In the present investigation a Step Frequency GPR (SFGPR) of 1–3000 MHz frequency band was used for cross-hole GPR data acquisition (NGI Norway make). SFGPR is the second generation GPR that overcomes the limitations of the impulse radars [31]. In this the Network Analyser serves as the control unit. Transmitter (Tx) and receiver (Rx) antennas are identical pairs of passive elements connected to the network analyzer. Borehole antennas with central frequency of 200 MHz were used to acquire cross-hole GPR tomography data. During survey, the computer takes control of the functions of the network analyzer and serves as system controller. While in GPR data acquisition the transmitter antenna was kept at the bottom most point (23 m deep) in the transmitter hole and receiver antenna was kept at same depth level of in the receiver hole. For each Tx position, the Rx antenna was moved along the receiver borehole from borehole bottom most point to surface with an interval of 1 m. By placing different positions of Tx and Rx antennas a cross-hole GPR data set is obtained which characterizes the subsurface. In this fashion cross-hole GPR tomography survey was carried out using step frequency GPR between five pairs of boreholes (B1-B2, B2-B3, B2-B4, B5-B4 and B1-B4, Fig. 3).

Data processing was done using tailor-made software's (Asysist and Kong Tomo). In the case of cross-hole GPR survey, data processing and analysis was done to understand the radar wave velocity (travel time) and/or attenuation variations in the intervening medium. The velocity tomogram generated by extracting the maximum amplitude value for each of recorded trace (for each Tx-Rx position) in the collected data file. These extracted amplitude values were normalized with respect to the amplitude max. These normalized amplitudes were then converted into dB values and plotted to obtain the 2D image of the radar wave velocity between the pair of boreholes. If there is no variation in the velocity tomogram then switch over to attenuation tomogram using conventional SIRT algorithm, it may enhances the results. If both options were failed to produce reliable results, then there a new processing technique called FDAT [32] to carry out the analysis. In this FDAT a representative frequency should be chosen, which is most sensitive (having maximum amplitude variation over the data array) in the entire data set. The amplitude values at this frequency in various data files of the tomographic array constitute the input file, which is then, inverted using conventional SIRT algorithm. This exercise is repeated for different representative frequencies, and at last a resonant frequency is chosen for representing the attenuation tomogram. In the present case 100 MHz was selected as resonant frequency for FDAT analysis, the attenuation variation at this frequency is prominent in the entire acquired data.

5 Results and Discussions

In the present study cross-hole GPR tomography was carried out between five pairs, they are B1-B2, B2-B3, B2-B4, B5-B4 and B1-B4 to map the water seepage flow path. This investigation is to estimate the radar wave attenuation (loss of energy between transmitted and received signal) to understand the subsurface response in existence of water and dry conditions. The radar wave attenuation was determined using FDAT for all the data sets at a selected resonant frequency of 100 MHz and the obtained attenuation values was normalized with the max attenuation value to demarcate the probable water seepage zone. The normalized radar wave attenuation was varying from 0 to 4 dB/m for the rocks of volcanic breccia and basaltic rocks exist in Marol Naka metro station area. 2-D Tomogram was generated for each cross-hole pair up to the depth of 23 m (Fig. 4). The tomogram corresponding to B1-B2 (Fig. 4a) showing normalized attenuation of less than 2.5 dB/m (moderate attenuation), this normalized attenuation may infer the presence of moisture and wetness in the ground. There are few low normalized attenuation of less than 2 dB/m (high attenuation) pockets were mapped between B1 and B2 boreholes (Fig. 4a). These pockets may indicate the broken fragments of poor quality breccia with water saturation. The remaining three tomograms B2-B3 (Fig. 4b), B2-B4 (Fig. 4c) and B5-B4 (Fig. 4d) showing a normalized attenuation more than 3 dB/m (low attenuation) which indicates high density dry basaltic rocks producing this low attenuation. This intern infers that there is no wetness or moisture exist towards station box-B. The

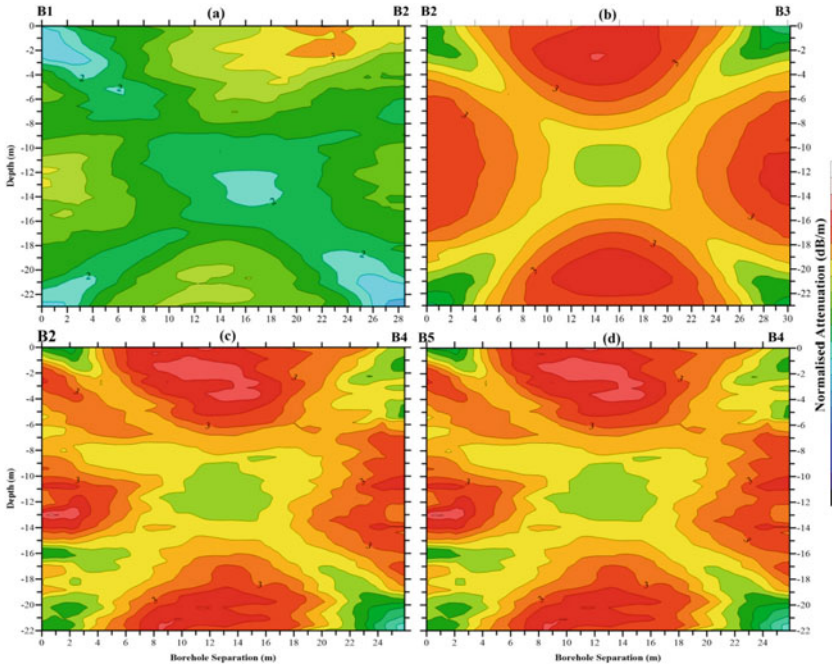


Fig. 4 Normalized attenuation Tomograms were generated based on FDAT analysis using a representative frequency of 100 MHz **a** Attenuation tomogram between B1 and B2 boreholes **b** Attenuation tomogram between B2 and B3 boreholes **c** Attenuation tomogram between B2 and B4 boreholes **d** Attenuation tomogram between B5 and B4 boreholes

presence of high grades (GIII to GI) of basalt as well as breccia might be the reason for not found the water ingress in the down-line tunnel (Fig. 4d).

The GPR tomogram corresponding to B1-B4 showing normalized attenuation in the range of 0.8 to 3.6 dB/m up to the depth of 22 m (Fig. 5). Though the tomogram shows the normalized attenuation up to 3.6 dB/m (low attenuation) but the dominant portion of this section has the normalized attenuation less than 2.5 dB/m (moderate attenuation). This indicates that the radar wave attenuation is more in this tomogram area, this intern infers that there is a presence of moisture content or water saturation till the borehole depth. There is a linear feature extending diagonally from the top of B1 borehole to bottom of B4 borehole with a normalized attenuation less than 2 dB/m (high attenuation). Radar wave attenuation is highest along this linear feature if we compare with entire study area. This could be the probable suspected zone producing high attenuation and might consist of weak breccia of low grade (GIV or GIII) as well as water saturated. This linear feature might be the probable flow path of water seepage into the up-line tunnel. This flow path zone was demarcated with two parallel dashed lines in red color between the boreholes B1 and B4 (Fig. 5). The high water head of 60,000–80,000 L/h might have caused erosion of poor quality breccia along the flow path. This might be the reason for stretching in the central

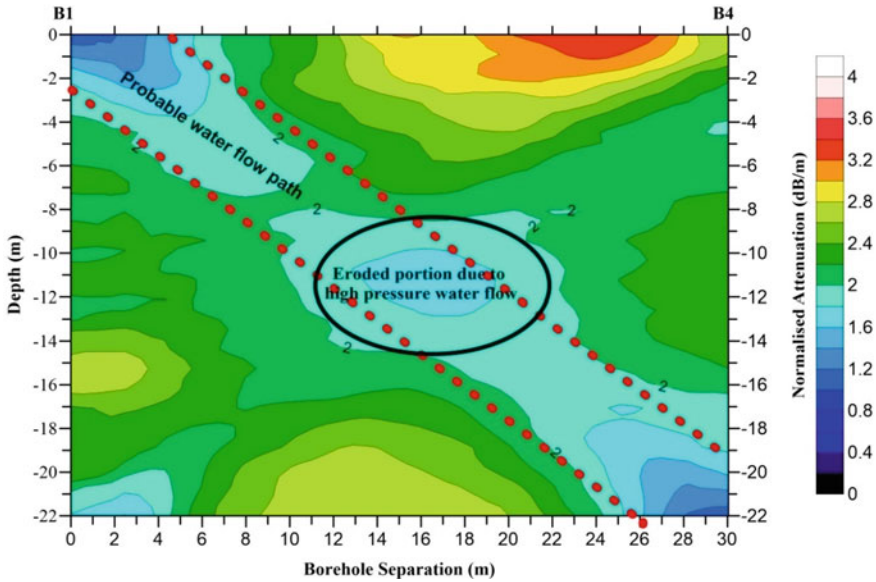


Fig. 5 Normalized attenuation tomogram generated for the borehole pair B1 and B4 based on FDAT analysis using a representative frequency of 100 MHz. Probable water seepage flow path was marked with dashed lines and the eroded portion was marked with circle

portion of tomogram marked with a black colored circle (Fig. 5). The GPR attenuation (representative frequency of 100 MHz) results infer the area of influence with water saturation and seepage is between the boreholes B1 and B4. The results also specify the probable source is in and around the B1 borehole because the high attenuation zones starts at the top of B1 borehole and reaching bottom of B4 borehole diagonally.

5.1 3-D Subsurface Attenuation Image

Cross-hole GPR tomography data was acquired between five pairs (B1-B2, B2-B3, B2-B4, B5-B4 and B1-B4) and the data was analyzed using FDAT with a representative frequency of 100 MHz. All these FDAT analyzed data were merged to generate a 3-D subsurface attenuation image. For this exercise, Easting of all the data was taken into X-axis and Northing is in Y-axis, Reduced level (RL) is in Z-axis and the attenuation was chosen as variable parameter. The resulting 3-D subsurface attenuation image of the mapped portion around Marol Naka underground metro station is shown in Fig. 6. The locations of five boreholes were shown (Fig. 6) and the viewing direction of this 3-D image is from M1-M5 side to towards M3 side (Fig. 6).

This 3-D image (Fig. 6) shows radar wave attenuation in the range of 1.2 to 4.5 dB/m in the entire study area. Except the area between B1-B4, the attenuation

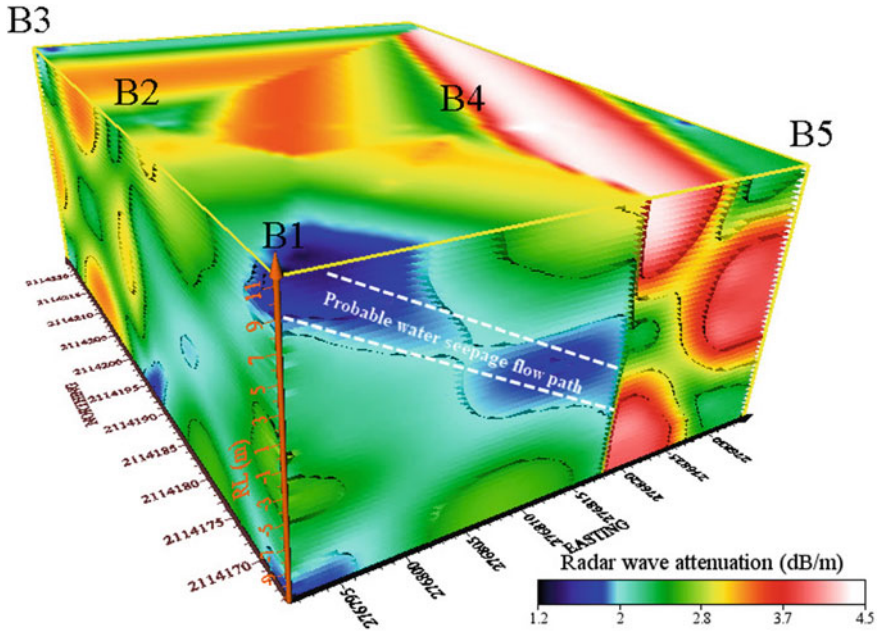


Fig. 6 3-D subsurface attenuation image was generated based on the FDAT data around the mapped portion of Marol Naka station area and probable water seepage flow path was marked on the 3-D image

values were high in the entire area indicating the high density basaltic rock (dry in nature). High attenuation zone (less than 2 dB/m) in blue color in the 3-D attenuation image indicates the presence of water and poor grade breccias. This zone, demarcated with white dashed lines, might be the probable water seepage flow path which we were intending to map in the present investigation. This 3-D tomogram enhanced the visualization of seepage flow path in the study area.

6 Conclusions

Step Frequency Ground Penetrating Radar (SFGPR) technique was successfully delineated the probable flow path of water seepage in Marol Naka underground metro station, Mumbai. Frequency Domain Attenuation Tomography (FDAT) analysis was the key to success in processing cross-hole GPR data. Out of five pairs of tomography investigations, the water seepage flow path and erosion zones were demarcated in one pair i.e. between B1-B4. The attenuation contrast between dry and water saturated rocks (basalt/breccias) were clearly distinguished using cross-hole SFGPR studies. 3-D subsurface attenuation image enhanced the visualization of probable water seepage

flow path in the study area. GPR technique was successful in solving the underground metro construction problems especially in urban environment.

Acknowledgements We are thankful to Mumbai Metro Rail Corporation Limited (MMRCL) and L&T-STEEL JV (Civil Contractor package 07) for providing us a chance to serve for the development of Mumbai. We extend our gratitude to the Director, National Institute of Rock Mechanics (NIRM) for taking up this investigation and granting permission to publish this work.

References

1. Goldman M, Kafri U (2006) Hydrogeophysical applications in coastal aquifers. In: Vereecken H, Binley A, Cassiani G, Revil A, Titov K (eds) Applied hydrogeophysics, pp 233–254
2. Attwa M, Günther T, Grinat M, Binot F (2011) Evaluation of DC, FDEM and IP resistivity methods for imaging perched saltwater and a shallow channel within coastal tidal flat sediments. *J Appl Geophys* 75:656–670
3. Afshar A, Abedi M, Norouzi G-H, Riahi M-A (2015) Geophysical investigation of underground water content zones using electrical resistivity tomography and ground penetrating radar: a case study in Hesarak-Karaj, Iran. *Eng Geol* 196:183–193
4. Davis JL, Rossiter JR, Meshner D, Dawley C (1994) Quantitative measurement of pavement structures using radar. In: *GPR 1994, Proceedings of the fifth international conference on ground penetrating radar*, Kitchner, Ontario, vol 1 of 3, pp 319–334
5. Dai S, Yan Q (2014) Pavement evaluation using ground penetrating radar. In: *Pavement materials, structures, and performance*, pp 222–230
6. Metwally M (2015) Application of GPR technique for subsurface utility mapping: a case study from urban area of Holy Mecca, Saudi Arabia. *Measurement* 60:139–145
7. Sagnard F, Norgéot C, Derobert X, Baltazart V, Merliot E, Derckx F, Lebental B (2016) Utility detection and positioning on the urban site Sense-City using Ground-Penetrating Radar systems. *Measurement* 88:318–330
8. Grandjean G, Gourry JC, Bitri A (2000) Evaluation of GPR techniques for civil-engineering applications: study on a test site. *J Appl Geophys* 45(3):141–156
9. Harari Z (1996) Ground-penetrating radar (GPR) for imaging stratigraphic features and groundwater in sand dunes. *J Appl Geophys* 36(1):43–52
10. Jol HM, Bristow CS (2003) GPR in sediments: advice on data collection, basic processing and interpretation, a good practice guide. *Geol Soc Lond* 211:9–28. Special publication
11. Hawkins AJ, Becker MW, Tsoflias GP (2017) Evaluation of inert tracers in a bedrock fracture using ground penetrating radar and thermal sensors. *Geothermics* 67:86–94
12. Moakhar OM (2008) Magnetic and ground penetrating Radar methods to detect shallow ancient underground cavities at Ghasr-e-Shirin town in the southwest of Iran. *J Earth Space Phys* 34:1–11
13. Negri S, Leucci G, Mazzone F (2008) High resolution 3D ERT to help GPR data interpretation for researching archaeological items in geologically complex surface. *J Appl Geophys* 65:111–120
14. Xiang L, Zhou H, Shu Z (2013) GPR evaluation of the Damaoshan highway tunnel: a case study. *NDT E Int* 59:68–76
15. Yu QM, Zhou HL, Wang YH, Duan RX (2016) Quality monitoring of metro grouting behind segment using ground penetrating radar. *Constr Build Mater* 110:189–200
16. Font-Capo J, Pujades E, Vázquez-Suñé E, Carrera J, Velasco V, Montfort D (2015) Assessment of the barrier effect caused by underground constructions on porous aquifers with low hydraulic gradient: a case study of the metro construction in Barcelona, Spain. *Eng Geol* 196:238–250

17. Karlovsek J, Scheuermann A, Willimas DJ (2012) Investigation of voids and cavities in bored tunnels using GPR. In: 2012 14th international conference on ground penetrating radar (GPR). IEEE, pp 496–501
18. Baek J, Yoon JS, Lee CM, Choi Y (2018) A case study on detection of subsurface cavities of urban roads using ground-coupled GPR. In: 2018 17th international conference on ground penetrating radar (GPR). IEEE, pp 1–4
19. Eyuboglu S, Mahdi H, Al-Shukri H, Rock L (2003) Detection of water leaks using ground penetrating radar. In: Proceedings of the third international conference on applied geophysics, Orlando-FL, pp 8–12
20. Pujari PR, Soni A, Padmakar C, Mahore P, Sanam R, Labhasetwar P (2014) Ground penetrating radar (GPR) study to detect seepage pathways in the Ajanta Caves in India. *Bull Eng Geol Environ* 73(1):61–75
21. Atallah N, Shakoor A, Watts CF (2015) Investigating the potential and mechanism of soil piping causing water-level drops in Mountain Lake, Giles County, Virginia. *Eng Geol* 195:282–291
22. Amran TST, Ismail MP, Ahmad MR, Amin MSM, Sani S, Masenwat NA, Ismail MA, Hamid SHA (2017) Detection of underground water distribution piping system and leakages using ground penetrating radar (GPR). In: AIP conference proceedings, vol. 1799, no 1. AIP Publishing LLC, p 030004
23. Di-Prima S, Winiarski T, Angulo-Jaramillo R, Stewart RD, Castellini M, Abou Najm MR, Ventrella D, Pirastru M, Giadrossich F, Capello G, Biddoccu M (2020) Detecting infiltrated water and preferential flow pathways through time-lapse ground-penetrating radar surveys. *Sci Total Environ* 726:138511
24. Lane JW Jr, Day-Lewis FD, Joesten PK (2007) Monitoring engineered remediation with borehole radar. *Lead Edge* 26(8):1032–1035
25. Chen G, Zhu J, Qiang M, Gong W (2018) Three-dimensional site characterization with borehole data—a case study of Suzhou area. *Eng Geol* 234:65–82
26. Liu S, Wang X, Fu L, Wei B (2018) Application of borehole radar for dam leakage detection. In: 2018 17th international conference on ground penetrating radar (GPR). IEEE, pp 1–4
27. Jha PC, Balasubramaniam VR, Sandeep N, Gupta RN, Sivaram YV (2002) Evaluating stability of excavations by borehole GPR profiling: a case study. In: ISRM regional symposium-advancing rock mechanics frontiers to meet the challenges of 21st century, New Delhi, pp VI (pp 26–34)
28. Neto PX, de Medeiros WE (2006) A practical approach to correct attenuation effects in GPR data. *J Appl Geophys* 59(2):140–151
29. Bradford JH (2007) Frequency-dependent attenuation analysis of ground-penetrating radar data. *Geophysics* 72(3):J7–J16
30. Sethna S (1999) Geology of Mumbai and surrounding areas and its position in the Deccan volcanic stratigraphy, India
31. Kong FN, By TL (1995) Performance of a GPR system which uses step frequency signals. *J Appl Geophys* 33(1–3):15–26
32. Jha PC, Balasubramaniam VR, Sandeep N, Sivaram YV (2004) Frequency domain attenuation tomography (FDAT) (a new approach in defect mapping using GPR). In: Proceedings of the tenth international conference on grounds penetrating radar, GPR 2004, vol 1. IEEE, pp 253–256

Challenges for Mechanized Tunnelling in Urban Areas in Hanoi Vietnam



Dang Trung Thanh, Dong Van Manh, Tran Tuan Minh, and Pham Duc Tho

Abstract Vietnam there is Hanoi capital with more than 10 million inhabitants, but still have no underground railway. Therefore, traffic jams have been a huge problem in Hanoi recent years. It happens daily trapping hundred thousand of vehicles, wasting time and billions of dollars, causing problems in all aspects of the society. The design and construction of metros is a necessity resulting from increasing population and is growing enormously. According to the decision No. 519/QĐ-TTg dated March 31, 2016 of the prime minister, the urban railway network will comprise 12+ urban railway lines with total length is approximate 455 km in Hanoi. There are a lot of challenges facing the metro development as Hanoi is building such systems for the first time. Previously, the metro systems have not been built in Vietnam. Therefore, there is a lack of required skills for development and implementation. Due to challenges occurring during the design and construction of the metro system in Hanoi. Hence, the first metro line started working officially began in 2010 and the target completion date was for 2022 but at this time the whole construction process of four underground stations is stopped and could not finish the work on time. The issues mentioned within the paper will be shown that there are plenty of challenges ahead for tunnelling in urban areas in Vietnam, especially in Hanoi capital. The authors hope within the paper will be offered you an interesting overview of the challenges of underground railway design and construction in Hanoi, Vietnam.

Keywords Mechanized tunnelling · Urban areas · Challenges · Hanoi capital

D. T. Thanh (✉) · T. T. Minh · P. D. Tho
Hanoi University of Mining and Geology, No. 18 Vien Street, Duc Thang Ward, Bac Tu Liem District, Hanoi, Vietnam
e-mail: dangtrungthanh@humg.edu.vn

D. V. Manh
FECON Corporation, Hanoi, Vietnam

© The Author(s), under exclusive license to Springer Nature Singapore Pte Ltd. 2022
A. K. Verma et al. (eds.), *Proceedings of Geotechnical Challenges in Mining, Tunneling and Underground Infrastructures*, Lecture Notes in Civil Engineering 228,
https://doi.org/10.1007/978-981-16-9770-8_24

383

1 Introduction

Vietnam is currently experiencing one of the most intensive urban transitions in the world. Hanoi is megacity with more than 10 million and urban population doubled over the last thirty years [3]. Therefore, traffic jams have been a huge problem in Hanoi capital recent years. There are a lot of solutions in order to reduce the issues e.g. viaducts, traffic tunnels construction in the city intersections, but short-term answers could not prevent traffic congestion worsening traffic in the [1] city. For a long-term vision, the the megacity planning benefits with underground railways or metro systems for a modern city are inescapable. The objective of the paper deals with various challenges of underground railway construction in Hanoi, Vietnam, such as the recommendations about the technical solutions, mechanised shield tunnelling technology, to associated specialised civil engineering measures, the difficulty due to geology, ground water conditions, faced with issues of resettlement or instability of buildings around the construction site in Hanoi, Vietnam. The authors hope in this way to offer you an interesting overview about challenges activity in underground railway construction in Vietnam using tunnel boring machine. Because the figures mentioned within the paper show that there are plenty of challenges ahead for an internationally oriented tunneller.

2 General Description of the Projects

2.1 General Description

According to the Hanoi Transportation Master Plan till 2020, total length of Hanoi Pilot Light Metro Line (HPLML) is 21.5 km from Nhon to Hoang Mai. The first phase of this line is from Nhon to Hanoi Railway Station, with 8.5 km elevated section and 4.0 km underground section. This line has 12 stations as presented in the following Fig. 1 (8 elevated stations and 4 underground stations).

2.2 Geology Conditions Along the Alignment

The geological units encountered along the tunnel alignment are briefly described herein (from surface to depth) [9]:

- Backfill materials;
- Fine-grained materials:
 - Lean clay with lenses of silt or clayey silt located at a depth minor than 25 m from surface (GU1_s1 if $N_{spt} < 10$ and GU1_s2 if $N_{spt} > 10$);

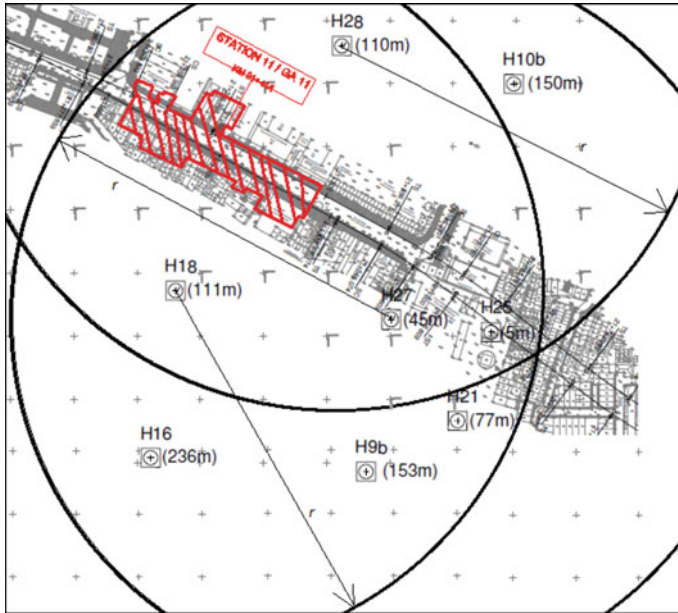


Fig. 2 Drinking water interest area in station 11 [7]

3 Identified Risks Related to Geotechnical and Groundwater

Based on the data is briefly described in Sect. 2. The main constraints and issues linked to the geotechnical and hydrogeological local context that shall be considered in four underground stations design are the following:

- The entire alignment of HPLML will run within clayey to sandy soils, under the piezometric load of Holocene or Pleistocene aquifers depending on the depth of the tunnel. At some points these aquifers could be connected, forming a unique hydro-geological system. Therefore, safety side when computing the required EPB pressure for the TBM advance, the groundwater levels will be measured, monitored and additional geotechnical investigations plan;
- Other challenges when excavating in soil conditions the risk of sinkholes and excessive settlements at surface. In order to limit “*geological unexpected conditions*” additional investigations should be carried out, improving the general knowledge of the sub-soil conditions;
- The water levels for four Stations are above the depth of excavation. Thus, a pumping system would be necessary to evacuate the water from the excavation;
- Water tightness construction details and execution procedures will be of paramount importance;

- Due to tunnelling will affect the main aquifer from which water is extracted for city consumption, it is fundamental to use environmental-friendly additives. The piezometers net should be used also to check the quality of the groundwater;
- The cutting tools wear that it is strictly related to the abrasivity of the materials to be excavated. According to geotechnical baseline report [9] the soil located along the alignment of HPLML can be classified as “*very abrasive*”. Therefore, it is necessary to check the cutting head to ensure the ability to remove soil and ensure the excavation rate;

When excavating in clays, clogging problems that may hinder TBM advance are often encountered due to the stickiness of the clay to metal. A quick check to estimate the clogging potential of the clayey units along the alignment has been made using the criterion proposed by Thewes [2] which is based on empirical data from slurry machine tunnel projects. In the Fig. 3 is reproduced the estimation of the stickiness potential of the cohesive materials present along the Hanoi metro project alignment. Based on the analysis results in Table 1, 69% of the samples have no clogging potential, 2% have low potential, 22% medium potential and only 7% have a high potential of clogging.

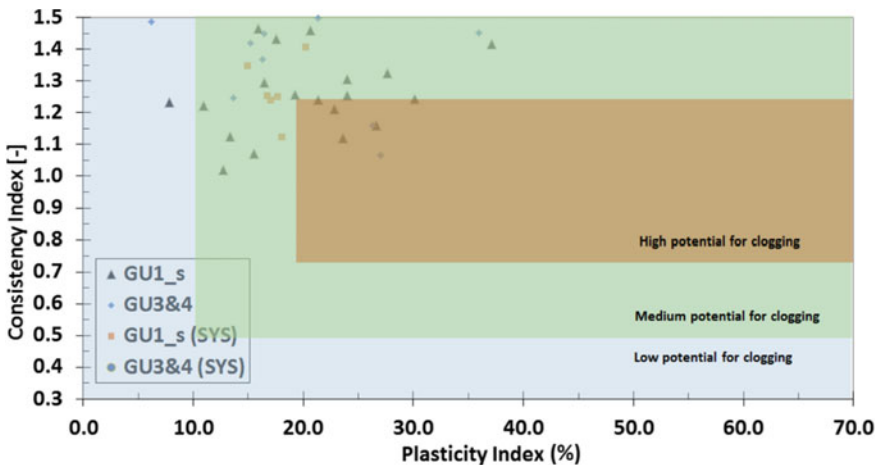


Fig. 3 Clogging potential for clayey units along underground alignment [9]

Table 1 Clogging potential

Clogging potential	Number of samples	Percentage (%)
High potential	7	7
Medium potential	24	22
Low potential	2	2
No potential	74	69

4 Neighbouring Buildings

According to the available information, there are critical buildings close to four underground stations. A building is considered “critical” when its foundation potentially interfering with the tunnel alignment or the station location. Within the construction design, a more detailed assessment of buildings sensitive to settlements, vibrations, etc. will have to be done to single out those buildings requiring mitigation measures. However, there are buildings near to the diaphragm walls which are tall and/or have a deep foundation. Their characteristics are summarized in the table below:

As a typical example of risks during construction is at the S11 station, there was a case where the apartment building was not within the scope of site clearance, but the construction process caused a crack to occur, potentially causing unsafety, so the construction had to be stopped. In addition, there are works above the tunnel that will affect when the tunneling machine works, so it is necessary to have a policy for temporary migration. Based on main buildings close to the underground alignment is described in Table 2. The authors propose solutions related to the impact of neighbouring buildings on the structure of four underground stations:

- The tunnel will be executed in a very dense urban environment, thus special attention will be paid in limiting the effects of the excavation to the buildings and structures at surface level. The main challenges during excavation process in urban and densely populated area is that effects of the excavation should not be perceived at ground surface, avoiding, minimizing damages or settlements to buildings and structures located at surface. The selection of the TBM features will be focused to have minimum volume loss (lower than 0.5%, preferably);
- The existing buildings near to the underground alignment are quite new, in relatively good conditions and some of them have many stories. The interaction between the existing buildings and the retaining structure of the station must be considered through the transfer of lateral load on the diaphragm walls, according to the method described in the stations’ Design Criteria;
- The effect of the station excavation on the existing buildings must be considered both in terms of induced deformations, settlement, and of potential vibrations.
- A settlement analysis and risk assessment must be performed for the buildings around the station, based on the computed deformation of the diaphragm walls, and using semiempirical methods;
- During construction, vibrations will be limited according to the prescriptions of DIN 4150-3, (version 1999) [10];
- A monitoring system must be designed for buildings for controlling total and differential settlement, deformation and vibrations;
- The proper selection of the TBMs and the adequate definition of the procedures and method statements will be the most important aspect to ensure safe tunnelling conditions;
- Currently, four underground stations are stopping construction because of could not land clearance of neighbouring buildings. The authors propose to create all favorable conditions to be able to land clearance as quickly as possible in order to

Table 2 Main buildings close to the underground alignment [5–8]

No building	Side	Number of floors	Foundation		Use
			Type	Depth from ground (m)	
<i>Close to Station 9</i>					
0112	Track 1	5	Raft	0–15	No information
0113	Track 1	No information	Pressed or driven piles	15–20	Tenement house
0114	Track 1	5	Raft	0–5	No information
0115	Track 1	5	Bamboo piles	0–5	No information
0116	Track 1	6	Bamboo piles	0–5	No information
0118	Track 1	5	Raft	0–5	No information
<i>Close to Station 10</i>					
0007	Track 1	5	Pressed or driven piles	10–15	–
0457	Track 2	–	Pressed or driven piles	15–20	Under construction
0568	Track 1	7	Pressed or driven piles	16	Residential
0012	Track 1	5	Pressed or driven piles	10–15	Commercial
0059b	Track 2	–	Bored piles	>25	Under construction
0060a	Track 2	5	Pressed or driven piles	>25	–
0060b	Track 2	5	Pressed or driven piles	>25	–
0060c	Track 2	5	Pressed or driven piles	>25	–
0060d	Track 2	5	Pressed or driven piles	10–15	–
0063	Track 2	5	Pressed or driven piles	20–25	Commercial
0064	Track 2	5	Pressed or driven piles	20–25	Commercial
<i>Close to Station 11</i>					
0022b	Track 2	7	Pressed or driven piles	10–15	Beside station
<i>Close to Station 12</i>					
2309	Track 2	3	–	–	Collective Quater
0043	Track 2	>6	Bored piles	>25	No information

(continued)

Table 2 (continued)

No building	Side	Number of floors	Foundation		Use
			Type	Depth from ground (m)	
0047	Track 1	>6	Bored piles	>25	No information
0044	Track 2	5	Raft	5–10	Vietnam Development Bank
–	Track 1	2	–	–	Viettin Bank
0051a+ 0051b	Track 2	5	Pressed or driven piles	10–15	Dai Duong Bank
2354	Track 2	3	–	–	Heart Hospital

the contractor has the construction site to continue, avoiding interruptions, causing high construction costs and affecting the environment.

5 Identified Risks Related to the Resettlement

In order to construct metro line alignment Nhon–Hanoi Station, the project needs to acquire some land along several segments of the line and around Nhon Depot. According to the resettlement plan, the project will acquire total nearly 185,900 m² of land acquisition which belongs to affected households and organizations. Consequently, many houses, buildings and public facilities will be affected either partly or fully in terms of structure displacement or business and in come lost.

From July 2021 up to now, all four underground stations have stopped construction due to ground clearance problems but there is no mechanism or solution to solve the issues. A typical example, at S9 underground station, there are currently 2 households who do not comply with the decision on land acquisition or the land user lives outside of Vietnam.

6 Conclusions

The urban metro network in Hanoi will comprise 12+ urban railway lines with total length is approximate 455 km in Hanoi. Hence, there is a need for better understanding of the problems during construction time of the first phase of line from Nhon to Hanoi Railway Station in order to increase the efficiency of tunnel boring machines. In this paper, several challenges for mechanized tunnelling in Hanoi Vietnam are described. In view of these objectives, according to the specific geology, groundwater conditions along the alignment are identified. Subsequently, the recommendations for the design and the construction of the four stations are proposed. The recommendations during

the construction of four underground stations in the condition that there are many neighbouring buildings around are proposed as well.

Some issues are missing within the paper. Therefore, in the very near future studies, the topic can be explained more detail about the entire challenges of the disturbances during the construction time at metro systems in Vietnam e.g. Hanoi Capital and Ho Chi Minh city.

References

1. Labbé D (2021) Urban transition in Hanoi: huge challenges ahead. Yusof Ishak Institute, Singapore. ISBN 9789814951364
2. Thewes M, Burger W (2004) Clogging risks for TBM drives in clay. *Tunn Tunn Int* 36(6):28–31
3. Thewes M (2014) Huge potential for metro construction. *Geomechanik und Tunnelbau* 7(3). <https://doi.org/10.1002/geot.201490021>
4. HGU-IMP-TRE-WAG-L10-00002-B-3A (2017) Report on additional geotechnical investigation
5. PIC-TEC-TRE-WSU-S09-05103-E-1A: Site specific geological, hydrogeological and geotechnical report - Kim Ma Station (Station 09)
6. PIC-TEC-TRE-WSU-S10-05104-E-1A: Site specific geological, hydrogeological and geotechnical report - Cat Linh Station (Station 10)
7. PIC-TEC-TRE-WSU-S11-05105-E-1A: Site specific geological, hydrogeological and geotechnical report - Van Mieu (Station 11)
8. PIC-TEC-TRE-WSU-S12-05106-E-1A: Site specific geological, hydrogeological and geotechnical report - Hanoi Railway Station (Station 12)
9. HGU-TEC-TDR-WAG-L10-41002-E-3B: Geotechnical baseline report (geotechnical interpretative report)
10. DIN 4150-3:1999 structural vibration - effects of vibration on structures (foreign standard)

Estimation of Deformation Modulus of Rock Mass for an Underground Cavern Based on Back Analysis



H. V. Sekar Bellapu, Rabindra Kumar Sinha, and S. R. Naik

Abstract The deformation modulus or modulus of deformation of rock mass is one of the important engineering parameter in the design of underground structures especially large caverns for housing turbines in case of hydroelectric projects. The deformation modulus may be estimated indirectly based on the empirical relations available in the literature or may be measured in the field based on the in-situ testing. The commonly performed in-situ tests in the field for measuring the deformation modulus of rock mass are Plate jacking test, Plate loading test and Goodman jack test. The measured in-situ deformation modulus of rock mass by each method varies because of the different techniques and test procedures involved in calculating it. Hence, because of these wide variation in values choosing the correct value of deformation modulus to be considered in the design of underground excavations becomes a challenge.

The displacements predicted based on the in-situ deformation modulus as input parameter in the 3D numerical modelling may not match with that of the measured displacements in the field during excavation of the caverns. An attempt has been made in this paper for arriving at the actual value of the deformation modulus based on the back analysis of the instrumentation data especially the displacements for an underground cavern using 3D numerical modelling studies by FLAC3D software.

Keywords Deformation modulus · In-situ tests · Numerical modelling

1 Introduction

Sardar Sarovar Project is one of the largest multipurpose (irrigation and hydroelectric) water resource project on Narmada River near Navagam, Gujarat. There are two

H. V. Sekar Bellapu (✉) · R. K. Sinha
Indian Institute of Technology (Indian School of Mines), Dhanbad, India
e-mail: hema.17dp000199@me.iitism.ac.in

S. R. Naik
National Institute of Rock Mechanics, Bengaluru, India

power houses viz. Riverbed underground Powerhouse and Canal Head Powerhouse with an installed capacity of 1200 and 250 MW respectively.

The geology at the cavern location consists of Basalt, Dolerites and Shear zones. In-situ plate bearing tests were carried out for determining the modulus of deformation for Basalt and Dolerites and found to be 1.3 and 2.2 GPa. Several authors have carried out the analysis of the underground powerhouse cavern by considering different values of deformation modulus. Varadarajan et al. [13] carried out elastic finite element (FEM) analysis of powerhouse cavern by considering young's modulus as 55 GPa for rock mass and 10 GPa for shear zone area. Sheorey et al. [17] has used 3-dimensional (3D) finite element program 'BMINES' for analysing the underground powerhouse cavern. The analysis was carried out by assuming a constant value of modulus of deformation as 18 GPa and Poisson's ratio as 0.2 for the entire rock mass. However, the presence of shear zones has not been considered in the analysis. Dasgupta et al. [1] has carried out 3DEC analysis of the powerhouse cavern by considering the modulus of deformation as 7 GPa for the rock mass and 1 GPa for the shear zone. The Poisson's ratio was considered as 0.2 for both the rock mass and shear zone. Samadhiya et al. [11] analysed powerhouse cavern using FEM based 'ASARM' software and considered the modulus of deformation as 23 and 19 GPa for Basalt and Dolerites. In the present paper FLAC3D continuum analysis has been considered for estimating the deformation modulus for the rock types of Basalt and Dolerite by calibrating the model with the available instrumentation data.

2 Layout of the Powerhouse Cavern

The underground powerhouse cavern is aligned N 10° E (i.e., parallel to the main dam) and is located 30 to 65 m below the ground surface. The underground powerhouse cavern is 210 m long, 23 m wide and 57.6 m height (measured from crown to draft tube pit) and is located at 67.5 m from the toe of the dam. The cavern houses six Francis type turbine units with each unit rated at 200 MW. The units are operated with head varying from 77.5 to 117.8 m. There are six intakes comprising of inclined steel lined pressure shafts of each having 7.61 m internal diameter. Topographically, the area above the powerhouse cavern is gently rising to a flat hillock. Presently the powerhouse cavern is under operation. The chainage (Ch.) of the powerhouse cavern starts at 1470 m and ends at Ch. 1680 m.

3 Geology

The powerhouse area consists of lava flows of Basalt, separated by hard agglomerate, and intruded by Dolerite dykes [9]. An agglomerate band having a length of 40 and 2–3 m width is also present about 1 m above the crown of the cavern [14]. There are also several shear zones present in the powerhouse area. Three major shear zones were

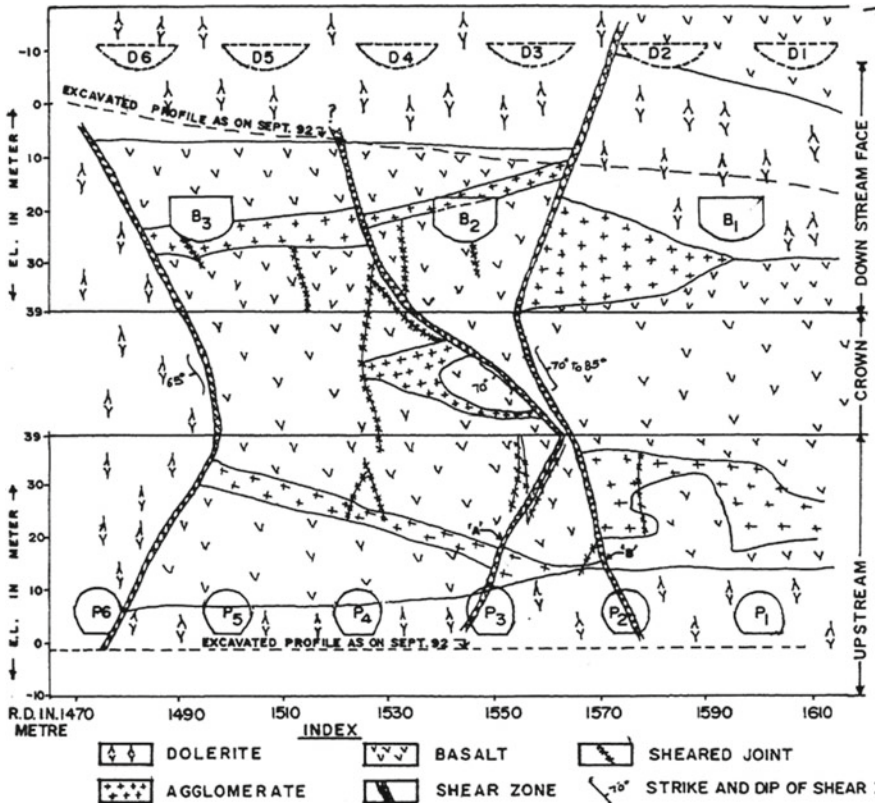


Fig. 1 3D geological log showing the location of the shear zones [8]

identified in the powerhouse area. The thickness of the shear zones encountered is 1–2 m. 3D geological log of the cavern showing the location of the shear zones is shown in Fig. 1. The rock mass encountered in the powerhouse area can be broadly divided in to three litho units namely Basalt, Dolerite and Shear zone for the purpose of geological classification. Basalt rock encountered at cavern belongs to Good quality (RMR = 63, Q = 9.2 to 14.4), Dolerite rock belongs to Good quality rock (RMR = 72, Q = 14.2–18.5) and Shear zone belongs to Poor quality (RMR = 23, Q = 0.33). Geological L-section of the powerhouse cavern is shown in Fig. 2.

4 Geomechanical Properties

Initially a 3 m wide, 3.5 m high and 300 m long exploratory drift was excavated along the long axis at crown level of the powerhouse cavern i.e., at EL 45 m and also three cross drifts were also excavated at 60 m intervals for assessing the geological

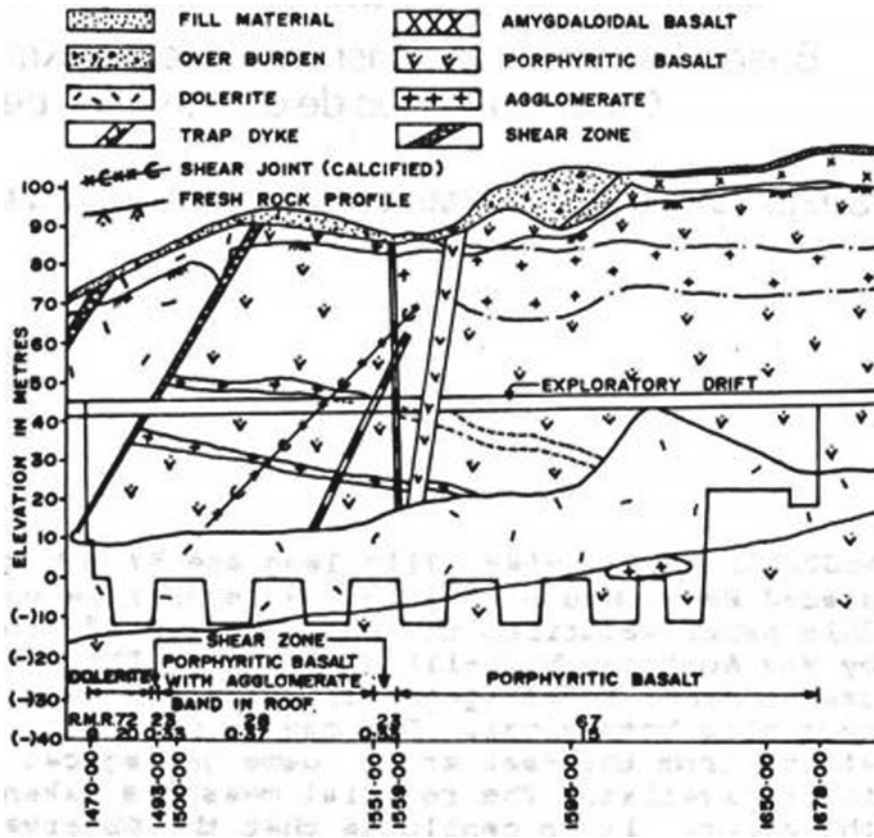


Fig. 2 Geological L-section of powerhouse cavern [12]

conditions of the cavern. Laboratory tests were carried out on core samples for determining the specific gravity, uniaxial compressive strength (UCS), tensile strength for Basalt and Dolerite rocks. The test results are given in Table 1. The geomechanical characteristics of the shear zone was evaluated by conducting large box shear tests on five disturbed samples and the results are given in Table 2 [9].

Table 1 Geomechanical properties of intact rocks [9]

Property	Basalt	Dolerite
Specific gravity	2.85	2.95
UCS (MPa)	115	77.6
Tensile strength (MPa)	11.5	7.7

Table 2 Geomechanical properties of shear zone [9]

Property	Shear zone
Density (kg/m ³)	1680
Cohesion (MPa)	0
Angle of internal friction (°)	36–39

5 In-Situ Testing

Hydro-fracture tests were carried out for determining the in-situ stresses around the powerhouse cavern by National Geophysical Research Institute (NGRI). The major in-situ stress is approximately 2.5 times the vertical stress and is parallel to the long axis of the cavern. The intermediate principal stress is perpendicular to the cavern axis and is approximately 1.25 times the vertical stress. The minor in-situ stress is vertical and is equal to the depth below the surface times the unit weight of the rock (Prakash et al. [16]). Plate bearing tests were carried out for determining the modulus of deformation. The modulus of deformation for Basalt ranged between 1.2–1.4 GPa and for Dolerite is 2.2 Gpa [6].

6 3-Dimensional Numerical Modelling

Three-dimensional continuum analysis was carried out for the study using FLAC3D software. FLAC3D utilizes an explicit finite volume formulation that captures the complex behaviors of models. The 3D model considered for the analysis is shown in Fig. 3. The surface topography was idealized based on the L-Section of the powerhouse cavern. The three shear zones which were identified and shown in Fig. 1 were also considered in the 3D model. L-section of the upstream wall of powerhouse cavern is shown in Fig. 4.

6.1 Excavation Sequence

The exploratory drift was initially enlarged to the full width of 23 m in a length of 5 m from Ch. 1493 to 1498 m for a depth of 18 m which is about 1/3rd of the total height of the cavern. The drift was further widened in a similar way from Ch. 1475 to 1493 m and from Ch. 1498 to 1540 m i.e., a total of 65 m was widened to full width for a height of 18 m for monitoring the shear zone and agglomerate band by installing instruments like Multi point bore hole extensometers (MPBX), load cells (20 tons capacity) and pressure cells. The enlargement work was completed in Apr.' 1985. The excavation works again started in Dec. 1987 and by Dec. 1990 the cavern was excavated to full length of 210 m up to EL 20 m. Multi drift excavation sequence was adopted for the excavation of the powerhouse cavern [12]. The excavation sequence

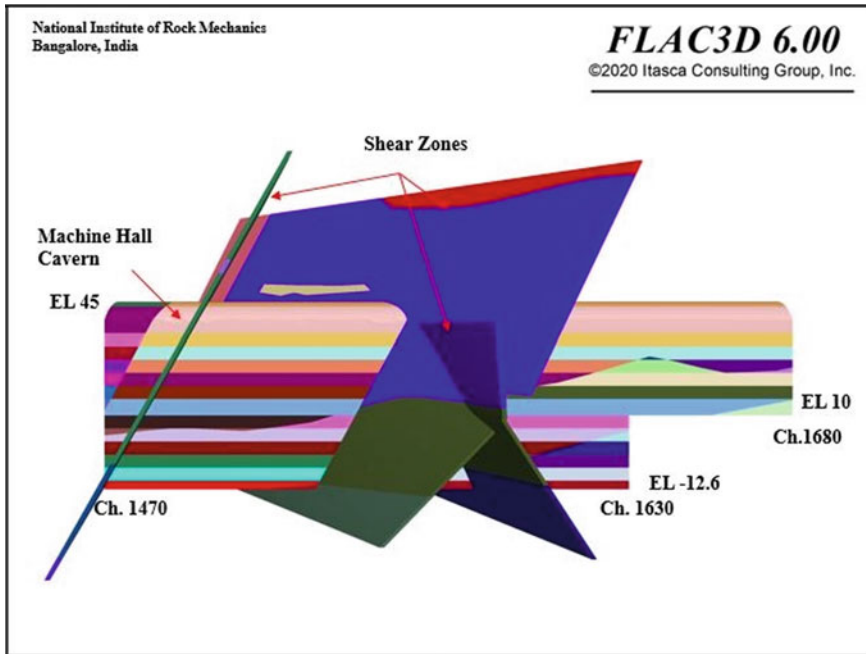


Fig. 3. 3D view of cavern in FLAC3D

considered based on the Multi drift method in the present model is shown in Fig. 5. Bench height of 4 m is simulated in the present study for the excavation of the machine hall cavern.

6.2 Support System

The support system was provided in the cavern based on the empirical approach. The NGI's Tunnelling Quality Index (Q) and CSIR Geomechanics classification (RMR) systems were adopted for arriving at the support system. The support system in roof consisted of 25 mm diameter, 6 m long high yield strength expansion shell type groutable rock bolts with a spacing of 1.75 m and pre-tensioned to 14 tons. The support system in wall consisted of 25 mm diameter, 6 & 7.5 m long with a spacing of 1.52 m. In shear zone areas rock bolts of 10.5 m are provided in roof with a spacing of 0.87 m. Two layers of shotcrete of thickness 38 mm with welded wire mesh is also provided [9].

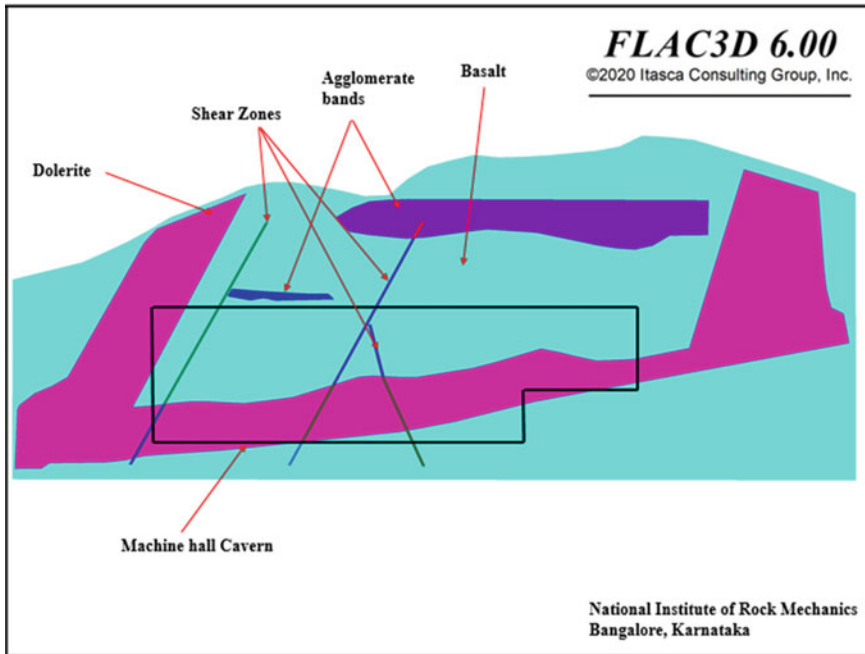


Fig. 4 L-Section of upstream wall of powerhouse cavern showing lithology

6.3 Material Properties

In order to arrive at the measured displacement values in the model, several model runs were done by varying the deformation modulus of the Basalt and Dolerite while the modulus of the shear zone was kept constant. The model with the closest match with the measured values was chosen for further analysis. The derived values of deformation modulus is given in Table 3. In addition to the deformation modulus other parameters which are considered as input for the present analysis was given in Table 3. As no testing data is available regarding to agglomerate band, Basalt material properties are assigned to the agglomerate band in the numerical model. The other rock mass parameters were estimated by using Roclab (Rocscience [10]) software by considering GSI, UCS and modulus ratio as input parameters for arriving at cohesion and friction angle. Two models were considered for analysis namely Model 1 with in-situ deformation modulus values for Basalt as 1.3 GPa, Dolerite as 2.2 GPa and Model 2 calibrated with deformation modulus values for Basalt as 6 GPa & Dolerite as 7 GPa. The other parameters were kept same for both the models.

Fig. 5 Excavation sequence simulated in numerical model

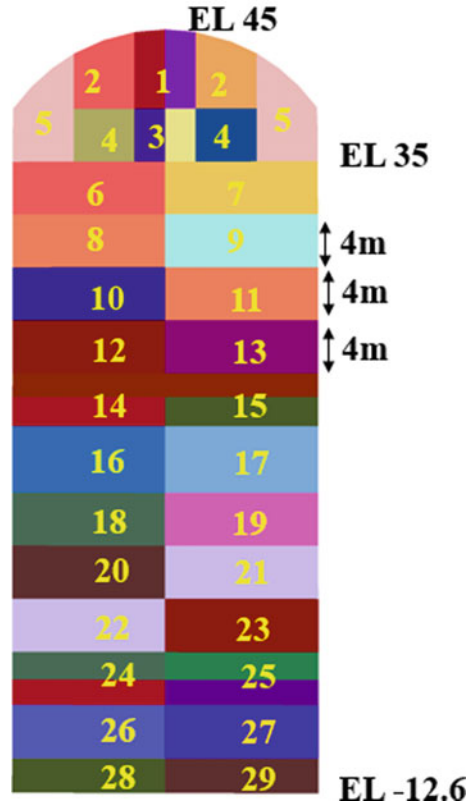


Table 3 Material properties considered in the analysis

Property	Basalt	Dolerite	Shear zone
Density (kg/m ³)	2600	2600	1650
Deformation modulus (GPa) for Model 1	1.3	2.2	0.5
Deformation modulus (GPa) for Model 2 (Derived)	6	7	0.5
Poisson's ratio	0.2	0.2	0.2
Cohesion (MPa)	1.11	1.44	0.01
Angle of internal friction (°)	65.7	61.6	36

7 Instrumentation and Comparison of Results

Instrumentation was carried out in the powerhouse cavern by way of installing the MPBX, load cells and pressure cells especially between the Ch. 1493 to Ch. 1498 m to monitor the displacement in the shear zone areas. The observed values of displacement in the field given by different authors are taken as reference for calibrating

Table 4 Comparison between predicted displacements for Model 1 & Model 2 with that of observed values of displacements

S. no.	Excavation		Location of Instruments	Predicted displacement based on Model 1 (mm)	Predicted displacement based on Model 2 (mm)	Observed displacement (mm)
	From EL (m)	To EL (m)				
1	45	27	Crown (between ch. 1493–1498 m)	14	3.2	2.1–3.5#
2	45	27	walls (between ch. 1493–1498 m)	20	5	0.64#
3	45	6	Crown—near shear zone	18	4.8	10*
4	45	6	Crown—away from shear zone	14.5	3.1	6*
5	45	6	U/s wall—near shear zone	43	12	10–15*
6	45	6	U/s wall—away from Shear Zone	33	6.2	5*
7	45	6	D/s wall—near shear zone*	43	11.3	10–15*
8	45	6	D/s wall—away from shear zone*	28	6.7	5*

#Ramaswamy et al. [9], *Samadhiya et al. [11]

the model are given in Table 4. The analysis of the results (displacements) for two models, i.e., Model 1 based on the in-situ deformation modulus (for Basalt = 1.3 GPa and Dolerite = 2.2 GPa) and Model 2 with the calibrated value of deformation modulus (for Basalt = 6 GPa and Dolerite = 7 GPa) that matched with the observed displacements in field are given in Table 4. Displacement contour plots for the two models at Ch. 1495 m when the depth of excavation was at EL 27 m and at EL 6 m are given in Figs. 6 and 7. The predicted values of displacement based on Model 1 are very high when in-situ values of deformation modulus are used as input parameters in the model whereas for Model 2 the values of predicted displacements matched closely with that of the actual observed values.

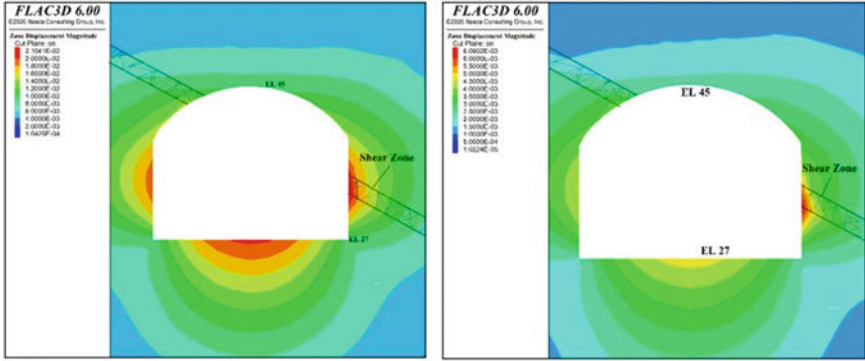


Fig. 6 Displacement contours at RD 1495 for Model 1 & Model 2 when excavation is at EL 27 m

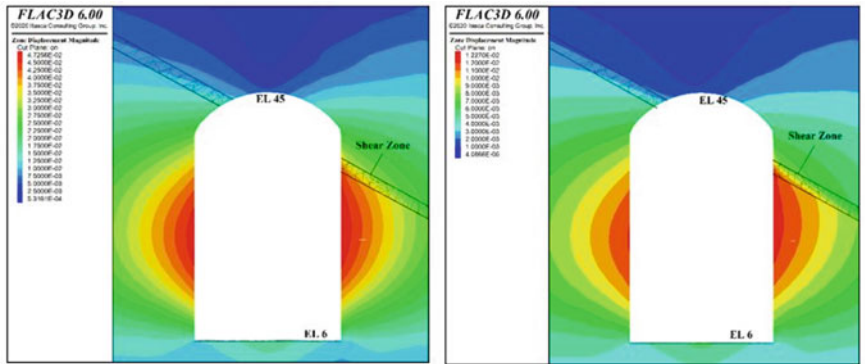


Fig. 7 Displacement contours at RD 1495 for Model 1 & Model 2 when excavation is at EL 6 m

8 Conclusions

Based on the 3D numerical modelling studies carried out using FLAC3D the following conclusions can be drawn.

1. The predicted values of displacement for Model 1 with the actual in-situ values of deformation modulus for Basalt as 1.3 GPa and for Dolerite as 2.2 GPa are almost 3 times more than that of the observed values.
2. The predicted values of displacement for Model 2 with deformation modulus for Basalt as 6 GPa and for Dolerite as 7 GPa shows close agreement with that of the observed values.
3. The displacements predicted by Dasgupta et al. [1] by using Distinct Element Code (with deformation modulus for rock mass as 7 GPa and for shear zone as 1 GPa) and by Samadhiya et al. [11] by using FEM based software ASARM (with the deformation modulus for Basalt as 23 GPa and Dolerite & shear zone

as 19 GPa) matched well at most of the locations with that of the observed displacement values. Although the deformation modulus values varied a lot the predicted values of displacements matched with that of the observed values at most of the locations this may be due to the use of different numerical tools and their formulations used in their analysis.

4. From the numerical modelling studies carried out using FLAC3D it can be noted that the in-situ values of deformation modulus are 3–4 times less than that of the back calculated value of deformation modulus based on observed displacement values. The in-situ deformation modulus value may always cannot correctly represent the true value in most of the cases.

Acknowledgements The authors are grateful to the Director, NIRM and the Project Authorities of Sardar Sarovar Narmada Nigam Limited. This forms the part of the doctoral research work being carried out by the first author at IIT (ISM), Dhanbad. The views expressed in this paper are those of the authors and not necessarily of the organisation to which they belong.

References

1. Dasgupta B, Dham R, Lorig LJ (1995) Three dimensional discontinuum analysis of the underground power house for Sardar Sarovar Project. In: Fujii T, Rotterdam Ed, Balkema AA (eds) Proceedings of the 8th international congress on rock mechanics, Tokyo, Japan, Vol. II, pp 551–554
2. Dasgupta B (2000) Numerical modeling of large underground caverns for hydro power projects. Trends Rock Mech 50–64
3. Goel RK, Jethwa JL, Dube AK (1998) Experiences of the support designs in the two large underground openings in India. In: Proceedings: fourth international conference on case histories in geotechnical engineering, St. Louis, Missouri, pp 789–792
4. Hoek E, Carranza-Torres CT, Corkum B (2002) Hoek-Brown failure criterion – 2002 edition. In: Proceedings. North American rock mechanics society meeting in Toronto in July 2002
5. Hoek E, Diederichs MS (2006) Empirical estimation of rock mass modulus. Int J Rock Mech Mining Sci 43:203–215
6. Prakash I, Sangneria JS (1993) Geotechnical problems of the underground excavation in the Deccan Basalts of Sardar Sarovar (Narmada) project, Gujarat, India. In: Proceedings: third international conference on case histories in geotechnical engineering, St. Louis, Missouri, pp 889–894
7. Prakash I, Desai N (2004) Rock mass evaluation of the Sardar Sarovar (Narmada) Dam and underground powerhouse, India. In: International conference on case histories in geotechnical engineering. Paper no 2.26
8. Prakash I (2013) Application of observational method in the successful construction of underground structures, Sardar Sarovar (Narmada) project, Gujarat, India. In: Proceedings: seventh international conference on case histories in geotechnical engineering, St. Louis, Missouri, pp 1–8
9. Ramaswamy N, Shah BJ, Shah KN (1988) Sardar Sarovar (Narmada) project: geotechnical investigations for Power House Cavern. In: International symposium on tunneling for water resources and power projects, New Delhi, pp 59–64
10. Rocscience Ltd. (2013) ROCLAB Software for Calculating Hoek–Brown Rock Mass Strength, Toronto, Ontario. www.rocscience.com

11. Samadhiya NK, Viladkar MN, Singh B (2004) Three-dimensional analysis of a powerhouse cavern in an anisotropic rock mass. *Int J Rock Mech Min Sci* 41(3):2B33-1-6
12. Subba Rao T, Subhranian KR, Dham R, Kumar M (1991) Special design features of Power House Cavern of Sardar Sarovar project. In: *Proceedings of the 7th international congress on rock mech.*, Aachen, Deutchland, pp 1207–1211
13. Varadarajan A, Sharma KG (1984) Analysis of power house cavern by finite element method. Indian Institute of Technology, New Delhi
14. Verman M, Jethwa J, Singh B (1992) Monitoring of a large underground power house cavity. In: *7th international congress on rock mechanics*, Aachen, Germany, pp 1233–1236
15. Verman M (2009) Interpretation of tunnel instrumentation data. *Indian Geotechnical Congress*, pp 996–1000
16. Prakash I, Srikarni C (1998) Geotechnical investigations of Sardar Sarovar (Narmada) project, India. In: *Proceedings: Eighth International Congress International Association for Engineering Geology and the Environment*, Vancouver, Canada, pp 377–384
17. Sheorey PR, Banerjee G, Biswas AK, Prasad M, Jethwa JL, Goel RK, Verman M, Dhar, BB (1993) Three Dimensional Finite Element Stress Analysis of Sardar Sarovar Powerhouse Cavern, CMRI Report, May, p 22

Construction of Underground Pump House Cavern in Medium Stress Condition—A Case Study from India



A. K. Naithani, L. G. Singh, Prasanna Jain, D. S. Rawat, and R. N. Suribabu

Abstract Underground pump house cavern for the lifting of 2.0 TMC water per day is being constructed in the Telangana State of India. Concurrently with the excavation of the pump house, 3D engineering geological mapping was carried out of the heading portion for rock mass classification and recommendation of support. The direction of the longest axis of the pump house was finalized based on the in situ hydrofrac testing inside the borehole. Classification of rock mass was done following the Tunnel Quality Index ‘Q’ method. Ground condition was non-squeezing; accordingly, Q-values were used for the estimation of roof support and walls support pressure. Based on NMT technology and site geological conditions, rock support arrangements were recommended for structural stability of crown and walls. Using the integrated approach, the capacity of the support system is determined to appraise the efficacy of the planned support system.

Keywords Engineering geology · Underground pump house cavern · Support system · Rock bolt · Drainage hole

1 Introduction

Palamuru Rangareddy Lift Irrigation Scheme (PRLIS) is being constructed to cater the needs of irrigation in the drought prone upland areas of southern districts of Telangana State, India by drawing and lifting 120 thousand million cubic feet (TMC) of water from foreshore of Srisailem reservoir through tunnels and gravity canals, and also provide drinking water facility to enroute villages/towns and industrial uses. This scheme is being constructed, having the five stages of lifts (I, II, III, IV and V) from Srisailem reservoir (FRL +269.735 m) to K.P. Lakshmidivipalli reservoir (FRL +670 m) through approach channel of total length of 63.875 and 47.866 km

A. K. Naithani (✉) · L. G. Singh · P. Jain · D. S. Rawat
National Institute of Rock Mechanics, Bengaluru, India
e-mail: anaithania@gmail.com

R. N. Suribabu
Megha Engineering and Infrastructures Ltd., Hyderabad, India

© The Author(s), under exclusive license to Springer Nature Singapore Pte Ltd. 2022
A. K. Verma et al. (eds.), *Proceedings of Geotechnical Challenges in Mining, Tunneling and Underground Infrastructures*, Lecture Notes in Civil Engineering 228,
https://doi.org/10.1007/978-981-16-9770-8_26

Table 1 Summary of input data

1.	Length of pump house	402.50 m	8.	Ground levels	507.74 m
2.	Excavated width of cavern (B)	26.00 m	9.	Rise of arc	8.00 m
3.	Height of pump house	59.50 m	10.	Length of the arch	32.13
4.	Height of pump house walls	51.50 m	11.	Bottom floor level	375.00 m
5.	Crown level	434.50 m	12.	Dewatering pit level	369.00 m
6.	Spring level	426.50 m	13.	Service bay level	408.00 m
7.	Height of overburden above crown (H)	73.25 (average)	14.	Static head	121.00 m

tunnels and the water will be lifted to a total height of 400 m. This paper is pertaining to the excavation of underground pump house cavern (402.50 m long \times 59.50 m high \times 26.00 m wide) of PRLIS lift-III in a medium stress condition (Table 1). The capacity of support system was determined to evaluate the efficacy of the proposed support system. In the pump house cavern, 145 MW capacity each 9 numbers of pumps will be installed and discharge capacity of each pump will be 75 Cumecs. The static head will be 121.00 m.

Rock mass characterization was done based on 3D geologic mapping of the heading portion and in-situ stress measurement. For the orientation of the long axis of the pump house cavern, hydrofrac test inside the NX borehole was carried out by National Institute of Rock Mechanics. 130 m deep vertical borehole was drilled from the surface for the measurement of in situ stresses. Magnitudes of the principal stresses as well as the direction of maximum horizontal principal stress were determined. The calculated vertical stress (σ_v) for a rock cover of 60 m is 1.58 MPa and measured maximum (σ_H) and minimum (σ_h) horizontal principal stresses are 2.541 ± 0.3105 and 1.694 ± 0.207 respectively. After detailed analysis it was concluded that the K-value indicates a medium stress magnitude and the maximum horizontal principal stress direction N50°, which was recommended for the orientation of the long axis of the cavity to reduce ground control problems [1]. For pump house cavern sufficient lateral rock cover is available, and the vertical cover is more than 73 m. On basis of NMT Q-system chart and site geological characteristics, support system is recommended and its efficacy is assessed.

2 Geological Setting

Concurrently with the excavation of heading portion, 3D engineering geological mapping on 1:100 scale was carried out (Fig. 1). Heading portion was excavated using pilot and side slashing because size of the cavern is very large (Fig. 2). Regionally this area is a part of Eastern Block of Dharwar Craton of Peninsular

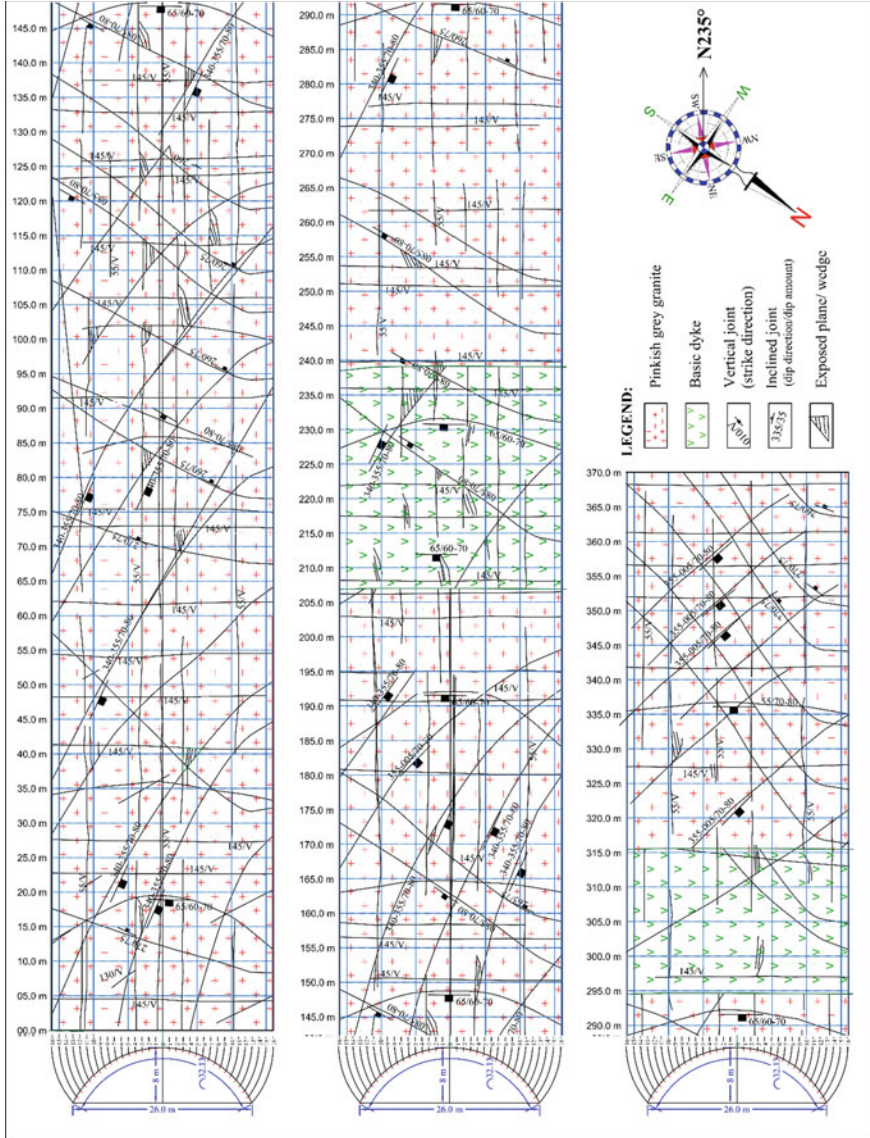


Fig. 1 3D geological map of the heading portion

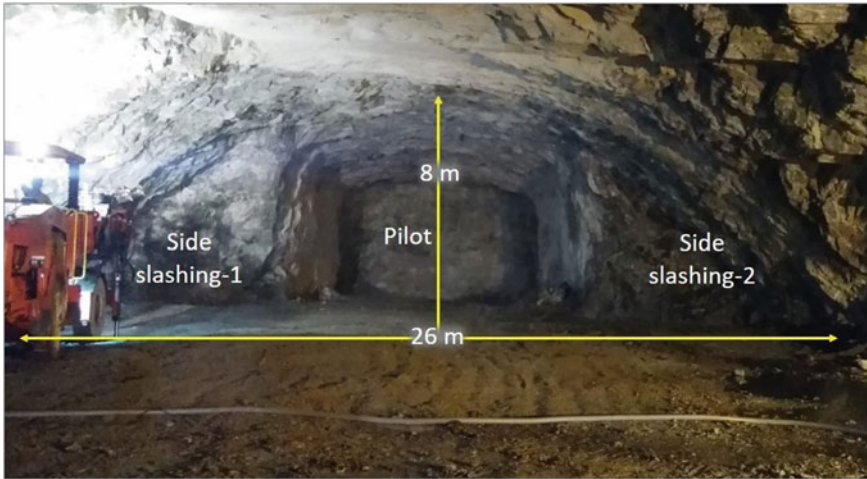


Fig. 2 Excavation of heading portion through pilot and side slashing

Shield, Indian Sub-continent [12]. The formation mainly comprised of Archaean granites and gneisses. These terrains are traversed by several mafic dyke, quartz-pegmatite-aplite veins trending in different directions, age ranging from Archaean to Upper Proterozoic [5, 12, 14]. Granites-younger granite of this variety occur as discrete plutons and intruded within the Peninsular Gneiss and greenstones [13]. The pump house complex is mostly occupied by granites/granitic gneiss and traversed by mafic dykes. Granites/granitic gneiss are coarse grained, hard, jointed in nature and shows phenocryst of alkali feldspar and quartz. Main minerals composition are alkali feldspars, quartz, mica and amphiboles. Mafic dykes are generally fine grained, hard, jointed and sheared along the contact of granite/granitic gneiss. Plagioclase and clinopyroxene (augite/titanaugite) are the main minerals compositions. Three to four prominent joints set are developed and along the joint plane clay coating was also recorded (Table 2). Joints are moderately close to widely spaced in nature. Moderately weathered to fairly fresh and hard dolerite dyke trending in N165° direction was mapped between chainage 210 and 250 m. It was extrapolated that same rock type will be exposed during the benching up to pump house invert level.

3 Rock Mass Classification and Estimation of Support Pressure

The rock mass was classified on the basis of six parameters (Eq. 1) of tunnelling quality index (Q) [2-4]. Where RQD is Rock Quality Designation (degree of jointing), J_n is Number of joint sets, J_r is Joint roughness number, J_a is Joint alteration number, J_w is Joint water reduction factor and SRF is Stress Reduction Factor

Table 2 Joint sets recorded in granite and dolerite dykes

Joint sets	Azimuth/Dip amount	Spacing (cm)	Strike length (m)	Roughness	Aperture (mm)	Infilling	Ground Water
J1	310–320/5–15	40–100	>20	Slightly rough-smooth, planar	Tight to 3	Fresh/clay	Dry
J2	140/5–15	50–100	>20	Slightly rough-smooth, planar	Tight to 3	Fresh/clay	Dry
J3	235/V	30–50	>20	Slightly rough-smooth, planar	Tight to 3	Fresh/clay	Dry
J4	140/V	30–60	>10	Smooth, planar	Tight to 20	Clay	Dry
J5	340/65	100–200	>20	Slightly rough, planar	Tight to 2	Fresh/clay coated	Dry
J6	260/V	30–60	>10	Smooth, planar	Tight	None	Dry
J7	050–065/60	40–150	>20	Smooth, planar	Tight to 3	Fresh/clay	Dry
J8	350/V	70–100	>10	Smooth, planar	Tight to 2	Fresh/clay coated	Dry
J9	130–140/70	20–70	>10	Smooth, planar	Tight	None	Dry

$$Q = \frac{RQD}{J_n} + \frac{J_r}{J_a} + \frac{J_w}{SRF} \tag{1}$$

The individual parameters are determined during 3D geological mapping and for crown and walls, discontinuities per 5 m length were measured at five-five locations and average values are taken for the calculation of ‘Q’ (Table 3). The ultimate support pressure of crown and walls is related with the rock mass quality (Q). For the estimation of ground squeezing condition, minimum Q-value was used for the analysis. The Q-values are varying from 3.30 to 8.30, and it comes under poor to fair rock mass category.

Roof support and wall support pressure was estimated as per Eqs. 2 and 3 [2, 3]. Where P_{roof} is permanent/ultimate roof support pressure in kg/cm², P_{wall} is ultimate wall support pressure in kg/cm², J_r is joint roughness number, Q is rock mass quality, Q_w is wall quality/factor equal to 2.5Q for intermediate qualities (0.1 < Q < 10) in case of medium stress.

$$P_{roof} = \frac{2.0}{J_r} Q^{-1/3} \tag{2}$$

$$P_{Wall} = \frac{2.0}{J_r} Q_w^{-1/3} \tag{3}$$

Table 3 Q-values recorded from the heading portion of the pump house

Chainage	Rock type	RQD (%)	J _n	J _r	J _a	J _w	SRF	Q value	Rock class
0–10	Medium to coarse grained grey/pink granite	70	9 × 2 = 18	1	1	1	1	3.89	Poor
10–30	Medium to coarse grained grey/pink granite	70	9	1	1	1	1	7.78	Fair
30–90	Medium to coarse grained grey/pink granite	75	9	1	1	1	1	8.33	Fair
90–120	Medium to coarse grained grey/pink granite	70	9	1	1	1	1	7.78	Fair
120–150	Medium to coarse grained grey/pink granite	75	9	1	1	1	1	8.33	Fair
150–190	Medium to coarse grained grey/pink granite	70	9	1	1	1	1	7.78	Fair
190–208	Medium to coarse grained grey/pink granite	60	9	1	1	1	1	6.67	Fair
208–240	Dolerite Dike	40	9	1.5	2	1	1	3.33	Poor
240–260	Medium to coarse grained grey/pink granite	60	9	1.5	2	1	1	5.00	Fair
260–295	Medium to coarse grained grey/pink granite	60	9	1	1	1	1	6.67	Fair
295–315	Dolerite Dike	40	9	1.5	2	1	1	3.33	Poor
315–330	Medium to coarse grained grey/pink granite	75	9	1	1	1	1	8.33	Fair
330–350	Medium to coarse grained grey/pink granite	70	9	1	1	1	1	7.78	Fair
350–360	Medium to coarse grained grey/pink granite	75	9	1	1	1	1	8.33	Fair
360–370	Medium to coarse grained grey/pink granite	70	9	1	1	1	1	7.78	Fair

For the estimation of non-squeezing ground condition, Eq. 4 suggested by Singh et al. [15] based on 'Q' data and overburden (H) was used. For this minimum Q-value is used and above pump house cavern, cover is 73.25 m hence ground condition is non-squeezing. The required support pressure for crown is varying between 7.800 to 10.628 t/m² and for walls 5.747 to 7.831 t/m² (Table 4). The average support pressure for crown is 9.876 t/m² and for walls 7.276 t/m².

$$H < 350Q^{1/3}$$

$$73.25 < 350 \times 3.3^{1/3} = 521 \quad (4)$$

4 Rock Support and Estimation of Support System Capacity

As per design, the underground pump house is having an excavated width of 26.00 m and length 402.50 m. The bottom level of pump house is kept at EL 375.00 m and crown level is kept at EL 434.50 m. Pump house with 500 mm thick concrete lined in the lower portion is proposed. Reinforcement support pattern which includes rock bolt, steel fibre reinforced shotcrete (SFRS), grouting and drainage hole using Norwegian Method of Tunnelling (NMT) Q-system was used for the pump house cavern (Table 5, Fig. 3). Excavation Support Ratio (ESR) of underground pump house is applied to 1.0 as given in the ESR updated classification standard of NMT Q-system [11].

As per the integrated approach given by Singh et al. [16], Singh and Goel [17] and IS: 15,026 [6], capacity of support system is determined. For the construction of large underground caverns, this approach was used by the Authors [7–10]. As per this approach, the total support pressure ($u + p_{\text{roof/wall}}$) will be equal to the sum of capacities of support system (Eq. 5).

$$u + p_{\text{roof}} = p_{\text{sc}} + p_{\text{bolt}} + p_{\text{gt}} \quad (5)$$

Where u = seepage water pressure = 0.0 t/m², p_{roof} = roof support pressure (between 7.800 and 10.628 t/m²), p_{wall} = wall support pressure (between 5.747 and 7.831 t/m²), p_{sc} = capacity of SFRS (t/m²), p_{bolt} = capacity of rock bolts (t/m²), p_{gt} = capacity of grouted rock arch/rock column (t/m²).

It is presumed that the SFRS is closely in contact with the rock mass surface and having the propensity to fail by shearing. The capacity of steel fibre reinforced shotcrete as determined (Eq. 6) for roof and walls is 9.763 and 4.929 t/m² respectively.

$$p_{fsc} = \frac{2q_{fsc}xt_{fsc}}{BF_{fsc}} \quad (6)$$

Table 4 Support pressure for the roof and walls of pump house cavern

Chainage (m)	Q value for roof	Q value for wall	Joint roughness number for crown & wall	Joint alteration number for crown & wall	Ultimate roof support pressure		Ultimate wall support pressure		J_r/J_a	Friction angle ϕ_j = $\tan^{-1}(J_r/J_a)$
					(kg/cm ²)	MPa	(kg/cm ²)	MPa		
0.0–10	3.89	9.73	1.0	1.0	1.272	0.125	0.937	0.092	1.00	45
10–30	7.78	19.45	1.0	1.0	1.009	0.099	0.744	0.073	1.00	45
30–90	8.33	20.83	1.0	1.0	0.987	0.097	0.727	0.071	1.00	45
90–120	7.78	19.45	1.0	1.0	1.009	0.099	0.744	0.073	1.00	45
120–150	8.33	20.83	1.0	1.0	0.987	0.097	0.727	0.071	1.00	45
150–190	7.78	19.45	1.0	1.0	1.009	0.099	0.744	0.073	1.00	45
190–208	6.67	16.68	1.0	1.0	1.062	0.104	0.783	0.077	1.00	45
208–240	3.33	8.33	1.5	2.0	0.893	0.088	0.658	0.065	0.75	37
240–260	5.00	12.50	1.5	2.0	0.780	0.076	0.575	0.056	0.75	37
260–295	6.67	16.68	1.0	1.0	1.062	0.104	0.783	0.077	1.00	45
295–315	3.33	8.33	1.5	2.0	0.893	0.088	0.658	0.065	0.75	37
315–330	8.33	20.83	1.0	1.0	0.987	0.097	0.727	0.071	1.00	45
330–350	7.78	19.45	1.0	1.0	1.009	0.099	0.744	0.073	1.00	45
350–360	8.33	20.83	1.0	1.0	0.987	0.097	0.727	0.071	1.00	45
360–370	7.78	19.45	1.0	1.0	1.009	0.099	0.744	0.073	1.00	45

Table 5 Systematic rock support arrangement

Structure	Rock bolt	Shotcrete	Grouting	Drainage arrangement
Crown	8 m long, 25 mm diameter fully cement grouted rock bolts (Fe ≥ 500) at 1500 mm c/c (staggered)	150 mm thick steel fibre reinforced shotcrete in three layers	Consolidation grouting using 32–45 mm dia hole at 6 m c/c spacing up to 8.5 m deep is recommended	9.0 m long 45 mm diameter drain hole @ 6000 mm c/c
Side walls	8 m long, 25 mm diameter fully cement grouted rock bolts (Fe ≥ 500) at 2000 mm c/c (staggered)	150 mm thick steel fibre reinforced shotcrete in three layers	Consolidation grouting up to EL 401 m using 32–45 mm dia hole at 6 m c/c spacing up to 8.5 m deep is recommended	9.0 m long 45 mm diameter drain hole @ 6000 mm c/c up to EL. 401 m (motor top level)

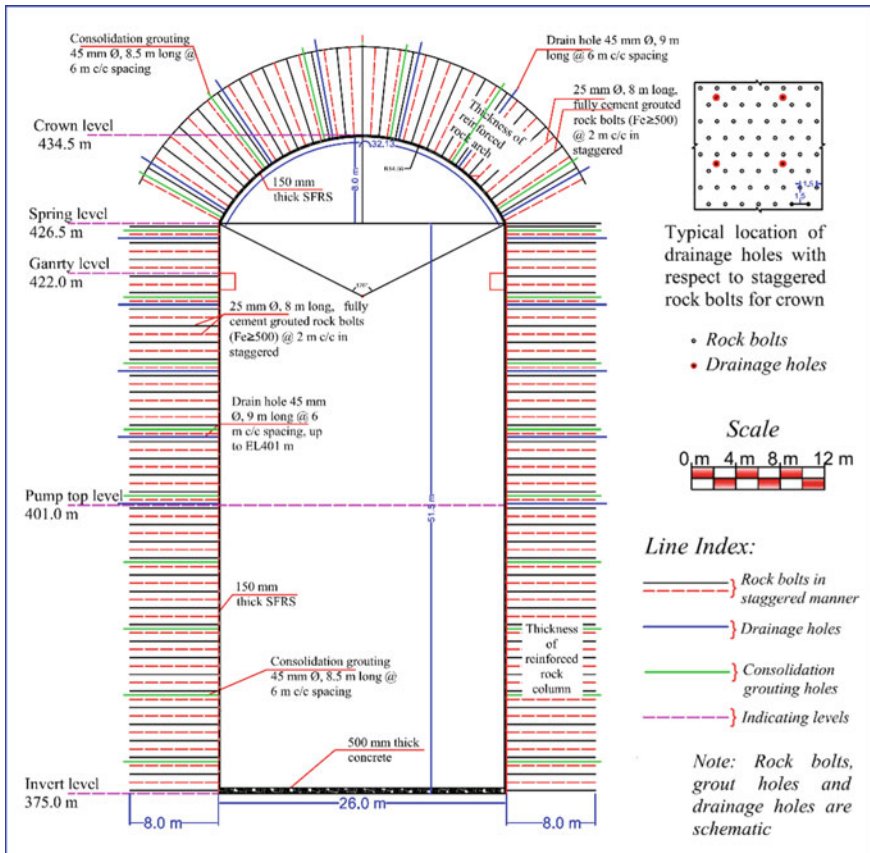


Fig. 3 Support system of pump house cavern

Where p_{sc} = support capacity of SFRS lining (t/m^2), q_{fsc} = shear strength of SFRS ($550 t/m^2$), t_{fsc} = thickness of SFRS, B = size of opening, F_{fsc} = mobilization factor for shotcrete (0.6 ± 0.05 —higher for cavern).

The capacity of rock bolt is estimated (Eq. 7) and the minimum capacity for roof and walls calculated is 3.417, and 0.714 t/m^2 respectively.

$$p_{bolt} = \frac{2q_{crm} \times l' \sin\theta}{BF_s} \tag{7}$$

where p_{bolt} = capacity of rock bolt (t/m^2), q_{crm} = UCS of reinforced rock mass, l' = thickness of reinforced rock arch/rock column, $\theta = 58$; $\sin\theta = 0.852$, B = size of opening F_s = mobilization factor for rock bolts.

UCS of reinforced rock mass is calculated (Eqs. 8 and 9) which was between 34.438 and 49.847 t/m^2 for roof and 19.372 to 28.040 t/m^2 for walls.

$$q_{crm} = \left[\frac{P_{bolt}}{S_{bolt}^2} - u \right] \times \left[\frac{(1 + \sin\phi_j)}{1 - \sin\phi_j} \right] \tag{8}$$

$$\tan\phi_j = \frac{J_r}{J_a} \tag{9}$$

Where: q_{crm} = minimum uniaxial compressive strength of reinforced rock mass, P_{bolt} = capacity of bolt or tension in bolt (tones), S_{bolt} = spacing of bolt (1.5 m for roof and 2.0 m for walls), u = seepage pressure in the rock mass ($0.00 t/m^2$), J_r = Joint roughness number, J_a = Joint alteration number.

Effective thickness of reinforced rock arch is calculated (Eqs. 10 and 11) which is 7.025 and 4.900 m for crown and walls respectively.

$$l'_{arch} = l - \frac{FAL}{2} - \frac{S_{bolt}}{4} + S_{rock} \tag{10}$$

$$l'_{column} = l - \frac{FAL}{2} - \frac{S_{bolt}}{4} + S_{rock} - d \tag{11}$$

Where l' = Effective thickness of reinforced rock arch/rock column, l = length of bolt, FAL = fixed anchor length (2.5 m), S_{bolt} = spacing of bolt, S_{rock} = average spacing of joints (0.650 m), d = depth of damaged rock due to blasting in walls (av. 2.0 m).

Back analysis of Barton et al. [2] support systems case studies were carried out by Singh et al. [16] and they proposed mobilization factors for rock anchor anchor and rock bolt. In this study for rock bolt, mobilization factors (F_s) are calculated from Eqs. 12 and 13. For roof F_s values are between 3.898 and 4.640 while for walls values are from 4.339 to 5.163.

$$F_s = 9.5 \times p_{roof}^{-0.35} \text{ (for rock anchor \& full column grouted rock bolt)} \quad (12)$$

$$F_s = 9.5 \times p_{Wall}^{-0.35} \text{ (for rock anchor \& full column grouted rock bolt)} \quad (13)$$

Where F_s = mobilization factor for rock bolt, p_{roof} = roof support pressure.

Grouted rock arch/rock column capacity is calculated (Eq. 14) and the maximum grouted arch/rock column capacity for roof and surge pool walls calculated is 8.361 and 2.113 t/m² respectively.

$$p_{gt} = \frac{2q_{gt}x l_{gt}}{BF_{gt}} \quad (14)$$

Where p_{gt} = support capacity of grouted arch (t/m²), q_{gt} = UCS of grouted rock mass (34.438 & 49.847 t/m² for roof and 19.372 & 28.040 t/m² for walls) l_{gt} = thickness of grouted arch/rock column (8.50 m for roof and walls), B = size of opening, F_s = mobilization factor for grouted arch/rock column.

Mobilization factor (F_{gt}) for grouted arch and rock column is calculated (Eqs. 15 and 16), for roof F_{gt} values are between 3.898 and 4.640, and for walls from 4.339 to 5.163. For roof and walls of pump house cavern, total capacity of support system at different chainages is given in Table 6.

$$F_{gt} = 9.50 \times p_{roof}^{-0.35} \quad (15)$$

$$F_{gt} = 9.50 \times p_{wall}^{-0.35} \quad (16)$$

Table 6 Capacity of support system for roof and walls

Chainage (m)	Ultimate support pressure (t/m ²)		Capacity of SFRS (t/m ²)		Capacity of rock bolt (t/m ²)		Capacity of grouting (t/m ²)		Total support capacity of support system (t/m ²)	
	For roof	For walls	For roof	For walls	For roof	For walls	For roof	For walls	For roof	For walls
	0.0–10	12.746	9.381	9.763	4.929	5.888	1.230	8.361	2.133	24.012
10–30	10.095	7.443	9.763	4.929	5.425	1.134	7.705	1.967	22.893	8.030
30–90	9.891	7.239	9.763	4.929	5.387	1.123	7.651	1.948	22.801	8.000
90–120	10.095	7.443	9.763	4.929	5.425	1.134	7.705	1.967	22.893	8.030
120–150	9.891	7.239	9.763	4.929	5.387	1.123	7.651	1.948	22.801	8.000
150–190	10.095	7.443	9.763	4.929	5.425	1.134	7.705	1.967	22.893	8.030
190–208	10.605	7.851	9.763	4.929	5.521	1.155	7.840	2.004	23.124	8.088
208–240	8.973	6.628	9.763	4.929	3.598	0.752	5.109	1.305	18.470	6.986
240–260	7.749	5.710	9.763	4.929	3.417	0.714	4.853	1.238	18.033	6.881
260–295	10.605	7.851	9.763	4.929	5.521	1.155	7.840	2.004	23.124	8.088
295–315	8.973	6.628	9.763	4.929	3.598	0.752	5.109	1.305	18.470	6.986
315–330	9.891	7.239	9.763	4.929	5.387	1.123	7.651	1.948	22.801	8.000
330–350	10.095	7.443	9.763	4.929	5.425	1.134	7.705	1.967	22.893	8.030
350–360	9.891	7.239	9.763	4.929	5.387	1.123	7.651	1.948	22.801	8.000
360–370	10.095	7.443	9.763	4.929	5.425	1.134	7.705	1.967	22.893	8.030

5 Conclusions

Because of the big size of the cavern, excavation was done by pilot and side slashing. For a large cavern, preference should be given for this type of the excavation methodology. By doing this, geological predictions will be easy and one can avoid unforeseen things also. In situ stress measurements are conducted which are very essential for rock mass characterization and to know about the cavern behavior during the excavation. Empirical approach is used for the recommendation of support design and its capacity is also conducted. For the walls support capacity is less, so it is recommended to increase the support for walls. It is strongly recommended that it should be validated by designer or through modelling and finally an observation approach is recommended.

Acknowledgements This paper is a part of sponsored project by M/s MEIL, so we sincerely thank the management of MEIL for the same. Authors are thankful to Dr. H.S. Venkatesh, Director NIRM for the permission to send the manuscript for publication, encouragement and technical guidance.

References

1. Anon (2017) Report on determination of in situ stress parameters at the proposed underground surge pool of Palamuru Rangareddy lift irrigation scheme lift-III-pumping station. Unpubl. NIRM report no. GE1704C, 22p
2. Barton N, Lien R, Lunde J (1974) Engineering classification of rock masses for the design of tunnel support. *Rock Mech* 6(4):189–236
3. Grimstad E, Barton N (1993) Updating of the Q-system for NMT. In: Proceedings of the international symposium on sprayed concrete, Fagernes, Oslo, pp 46–66
4. Grimstad E, Kankes K, Bhasin R, Magnussen A, Kaynia A (2002) Rock mass quality Q used in designing reinforced ribs of sprayed concrete and energy absorption. In: Proceedings: international symposium on sprayed concrete, Davos, pp 134–142
5. GSI (1995) Geological Quadrangle maps of GSI: No. 57E (2004) and 56L. Published by Geological Survey of India
6. IS 15026 (2002) Tunnelling methods in rock masses – guidelines, Bureau of Indian Standards, New Delhi, 26p
7. Naithani AK (2017) Geotechnical investigations and support design of underground pump house cavern – a case study from lift irrigation project. *Int J Geotech Geol Eng* 35(5):2445–2453
8. Naithani AK, Singh LG, Prasanna J (2017) Rock mass characterization and support design for underground additional surge pool cavern – a case study, India. *Geomaterials* 7:64–82
9. Naithani AK, Rawat DS, Jain P, Singh LG, Srisailam M, Venkatramaiah V (2019) Rock mass characterization and support system for underground pump house cavern – a case study, India. In: Proceedings 14th international conference on underground construction Prague 2019, paper no. S4-OP7, pp 1–9
10. Naithani AK, Prasanna Jain, Rawat DS, Singh LG (2020) Rock mass characterization for the underground surge pool cavern – a case study. *India J Geol Soc India* 96:265–271
11. NGI (2013) Using the Q-system – rock mass classification and support design. NGI Publication, Norway, p 54p
12. Ramam PK, Murty VN (2012) *Geology of Andhra Pradesh*. Geological Society of India, 244p
13. Reddy GT, Rao VN (1991) Study of granitic rocks in Gadwal Makhtal area, Mahbubnagar District, Andhra Pradesh. *Rec Geol Surv India* 124(5):256–258

14. Sharma R, Murthy CVVS, Mishra VP, Nagaraju Gouda HC, Singh RK (2008) Study of structural pattern through aeromagnetic data for mineral prospecting and Kimberlite clan rocks in an area around Mahbubnagar, A.P. *J Geol Soc India* 72:175–189
15. Singh B, Jethwa JL, Dube AK, Singh B (1992) Correlation between observed support pressure and rock mass quality. *Tunn Undergr Space Technol* 7(1):59–74
16. Singh B, Viladkar MN, Samadhiya NK (1995) A semi-empirical method of the design of support systems in underground openings. *Tunn Undergr Space Technol* 3:375–383
17. Singh B, Goel RK (2011) *Engineering rock mass classification*. Elsevier Inc. Publ., U.K. 364p

Safety and Stability Monitoring of Underground Structures - Role of Geotechnical Instruments



K. Sudhakar, Rabindra Kumar Sinha, and S. R. Naik

Abstract Construction of large underground caverns and tunnels are playing vital role in development of the nations around the globe, in various sectors like mining, hydropower, irrigation, transportation, water supply, oil storage, sports, nuclear and defense sectors. The limited space availability and environmental concerns are some of the reasons in opting for underground structures. Successful construction of these in even, at highly varied geological areas is possible with implementation of innovated construction methods along with monitoring techniques. The use of geotechnical instruments is playing major role in monitoring and assessing the stability of the structures during excavation. The changes in deformations and loads while excavation can be measured, and this guides the stakeholders in decision making during critical stages of construction. Like in other fields, during past few decades geotechnical instruments are also transformed from simple mechanical systems to sophisticated real-time monitoring systems. The monitoring data will be used for calibration of the numerical models prepared to understand the response of the ground to excavation stages. It will also help in assessing the performance and behaviour of the ageing structures, with long-term monitoring. Improved construction control and safety monitoring can be achieved with comprehensive instrumentation and field measurements. In this paper, how the stability of some of the underground structures are evaluated based on the actual instrumentation data during construction and post construction period is explained. The recent developments in instruments and its application, and selection of instruments based on the ground conditions, benefits achieved during construction in some of the underground structures is also explained.

Keywords Caverns · Geotechnical instruments · Technology and stability monitoring

K. Sudhakar (✉) · R. K. Sinha
Indian Institute of Technology (Indian School of Mines), Dhanbad, India
e-mail: kadiyala.17dp000198@me.iitism.ac.in

S. R. Naik
National Institute of Rock Mechanics, Bengaluru, India

© The Author(s), under exclusive license to Springer Nature Singapore Pte Ltd. 2022
A. K. Verma et al. (eds.), *Proceedings of Geotechnical Challenges in Mining, Tunneling and Underground Infrastructures*, Lecture Notes in Civil Engineering 228,
https://doi.org/10.1007/978-981-16-9770-8_27

1 Introduction

Large caverns and long tunnels were constructed worldwide in mining and civil infrastructure projects for nation development. Similarly in India and Bhutan, many large caverns were constructed in hydro sector in last thirty years and some are under construction.

Geotechnical Instruments provide vital information under observational approach method like NATM and NMT. It plays major role in monitoring and assessing the surrounding rock mass and behaviour of the rock support during excavation. The measured data are used for calibration of the numerical models prepared to understand the response of the ground to various excavation stages. It also helps in assessing the performance and behaviour of the aging structures, with long-term monitoring. Improved construction control and safety monitoring can be achieved with comprehensive instrumentation and field measurements. The success of instrumentation depends on selection of suitable instruments, timely installation and monitoring, analysis of the data and timely implementation of the results.

Adoption of systematic implementation of ground monitoring procedures during construction and operational periods, leads to successful completion of the projects safely and economically. Careful selection of instruments and its ranges is important always [1]. It can be achieved with proper study of instrumentation data available at caverns and tunnels constructed at varied geological and geotechnical ground conditions from Himalayan region to peninsular region.

2 Developments in Instruments and Applications

Sensor is the basic part in monitoring system for different parameters to be measured. Sensors were developed in chronological order with Mechanical, Pneumatic, Electrical, Optical, and most recent as Digital Sensors. The sensors made with Linear variable differential transformer (LVDT), Vibrating Wire, Accelerometer, Micro-electromechanical system (MEMS) and Fiber Optic technology are used in geotechnical instruments.

Fiber Optic Solutions. Recently optical fibers usage increased in structural health monitoring systems. The technology is being innovatively used for monitoring change in strain and temperature using single optical fibre cable over large lengths. The main components of the system are sensor comprising of a specially graded cable, an interrogator unit, a computer, and appropriate software. The main feature in this technology is fast in installation, intrinsic safety and simple in setup. It can provide the accuracy in micron and uninterrupted monitoring in all-weather conditions [5].

Automatic and Real Time Monitoring System. Automatic data acquisition system offers on-line management of a network of several hundred instruments, collection of large quantity of data, checking of design hypothesis, operating support during the

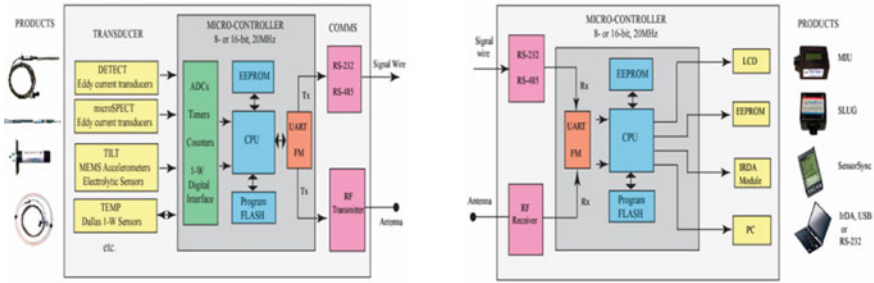


Fig. 1 Digital sensor architecture with transmitter and receiver unit

tunnel construction and data analysis and evaluation of tunnel safety. Well-planned Real Time Monitoring system will provide information of hazardous conditions before the catastrophic failure of the structures.

Autonomous Sensors. These are basically, a sensor with data logger and cellular network connectivity. Useful to monitor the isolated problems spread over large area in civil engineering structures like bridges, metro networks also for slope stability problems on open cast and land slide prone areas. Like tilt sensors, strain gauges, piezometers and crack meters can be used as autonomous sensors by interfacing to data logger with data transmission facility.

Digital Sensors and Wireless Data Transmission. Digital sensors transform continuous signals from analog transducers, into discrete digital output signal encoded as 1 and 0 s. Digital sensor consists of programmable microcontroller unit (MCU) with an 8 or 16-bit core, memory, timers and counters and ADC (Analog to Digital Converter)’s packaged into a single integrated circuit (IC). The main benefits associated are: (i) to transform an esoteric transducer output into real world units that can be immediately and routinely interpreted, and (ii) to convert a weak signal from the transducer into a robust signal that lends itself to transmission in the harsh mining environment. The reasons for the Digital sensors are better due to improved accuracy, improved reliability, improved accessibility to the data, simpler data management and storage and reduced cost. Figure 1 shows the digital sensor architecture with transmitter and receiver unit [9].

3 Instrumentation and Monitoring

Instrumentation and monitoring provide realistic behaviour of surrounding rock mass during preconstruction, construction, and post construction stages. A well-planned monitoring program can be divided in to developing stage and execution stage.

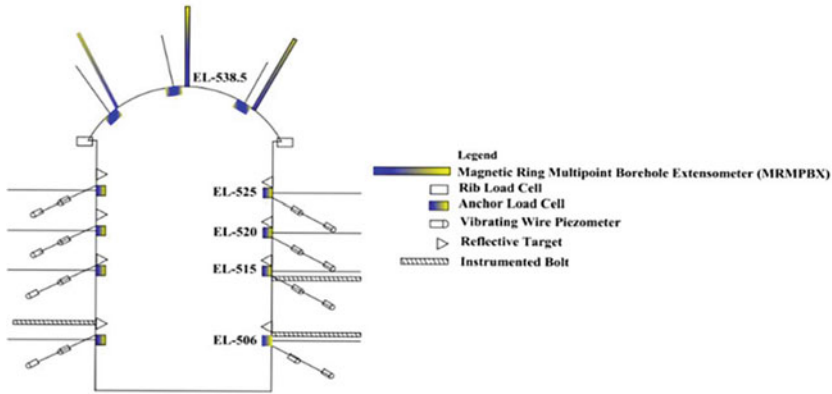


Fig. 2 General layout of instrumentation section for an underground cavern

Determination of the purpose of the instrumentation, selection of parameters to be monitored, definition of factors influencing the measurements, budget preparation, selection of instrument locations, preparation of instrument specification and procurement, planning for installation and maintenance comes under developing stage. Procurement and installation, maintenance of instruments and readouts, data collection, data analysis and interpretation and corrective instrument implementation comes under execution stage.

The general and essential group of instruments consists of MPBX, loadcells and optical targets, piezometers, and instrumented bolts. The parameters like deformation, convergence, load on support, pore water pressure is measured with these instruments. Figure 2 shows the instrumentation layout for large underground cavern. The instrumentation sections and layouts provided during design stage are to be reviewed based on the numerical modelling studies and as per the actual geological conditions at the site. Table 1 summarises the instrumentation for the conditions to monitor surface movements and sub-surface movements, loads and stresses [1].

3.1 Short-Term Critical Monitoring (Monitoring During Construction)

The frequency of the readings should be related to the construction activity and to the rate at which the readings are changing. It is to be noted that, too many readings overload the processing interpretation capacity, whereas too few causes missing of important events, and prevent timely actions required. Several sets of readings are required to establish the base readings. When the construction commences and approaches the instrumented location, readings should be taken frequently that is once a week, once a day, once a shift or even more frequently in relation to the construction

activity. The frequency of observations can be decreased when the readings are stabilised and remain constant.

3.2 Broad-Scale Long Term Monitoring (Monitoring During Operational Periods)

In view of the importance of the underground structures it is required to continue the monitoring after construction, i.e. in operational and maintenance periods also. It can be achieved through continuation of monitoring of the working instruments and to ease out the monitoring process, they may be connected to a data acquisition system, where monitoring frequency can be set and the manpower requirement can be greatly reduced. In some of the projects in India and Bhutan, the large caverns are monitored during the operation period with varying degree of automation.

3.3 Instrumentation for Underground Caverns

As various utilities are housed inside the cavern for very long period of time, it is important to ensure the stability of the cavern. The behaviour of the cavern can be studied by monitoring the rock mass behaviour surrounding the cavern. Important parameters to monitor are deformation of the surface of the cavern, deformation inside the rock mass at different horizon, stress changes in the rock mass, pore water pressure in the rock mass etc. In addition, the behaviour of the supports provided inside the cavern also need to be monitored. This can be achieved with proper planning and implementation of a good instrumentation during construction and operational stage. The instrumentation carried out during construction at some of the underground caverns are shown in Table 2.

4 Case Studies on Cavern Monitoring

4.1 Underground Powerhouse Cavern at Sardar Sarovar Project

The riverbed powerhouse (211 m long, 23 m wide and 57 m high) located about 150 m downstream of the dam is parallel to the power blocks (55 to 60) of non-overflow section. The powerhouse is located at a shallow depth below a sloping ground surface. The rock cover varies between 45–60 m along the length of the powerhouse. The cavern is being excavated in lava flows of Amygdaloidal Basalt and Porphyritic Basalt intruded by near vertical Dolerite dykes and near horizontal

Table 2 Monitoring systems in some of the underground projects

Sl. No.	Underground caverns	Purpose/application	Parameter and instruments
1	Powerhouse cavern at Tala HEP	Power generation	Load on rock bolts - Anchor load cells Load on ribs - Rib loadcells Deformation - Bore hole extensometers Convergence - Total station targets Stress on rock bolts - Instrumented bolt Pore water pressure - Piezometers
2	Desilting chambers at Tala HEP	Silt removal up to 0.2 mm	Load on rock bolts - Anchor load cells Load on ribs - Rib loadcells Deformation - Bore hole extensometers Convergence - Total station targets Pore water pressure - Piezometers
3	Powerhouse cavern - NJ HEP	Power generation	Deformation - Bore hole extensometers Convergence - Total station targets (Operational period)
4	Desilting chambers at Teesta-III	Silt removal up to 0.2 mm	Load on rock bolts - Anchor load cells Deformation - Bore hole extensometers
5	Storage cavern in Western India	Crude oil storage	Convergence - Optical targets Displacement - Extensometers
6	Powerhouse cavern at Teesta-V	Power generation	Load on rock bolts - Anchor load cells Deformation - Bore hole extensometers
7	Powerhouse cavern at	Power generation	Deformation - Extensometers Convergence - Tape extensometers

Dolerite sills [2]. Agglomerate bands of varying thickness are also present. In Phase-I extensive instrumentation was carried out during construction stage in view of the stability issues during the construction of the cavern and later based on further studies, it was decided to monitor the cavern by installing the instruments at critical chainages and crown area of the cavern keeping long term monitoring perspective. Accordingly, NIRM installed MPBX (Magnetic type) in walls and bus galleries (in

2000), Targets on crane columns (in 2006) and MPBX (Magnetic type) at surface of the cavern (in 2011).

MPBX at Surface of the Powerhouse Cavern. Mechanical extensometers were installed at the surface of the underground riverbed powerhouse of Sardar Sarovar Project to monitor the effect of agglomerate band encountered between EL 47 and 48.5 m during construction. It highlighted the need for longer rock bolts to strengthen the crown area of the cavern [6]. Figure 3 shows the monitoring of the MPBX (mechanical type) installed at Ch1508, EL93 during construction. Figure 4 shows the results of MPBX (magnetic type) at Ch1558, EL94.18 during operational period.

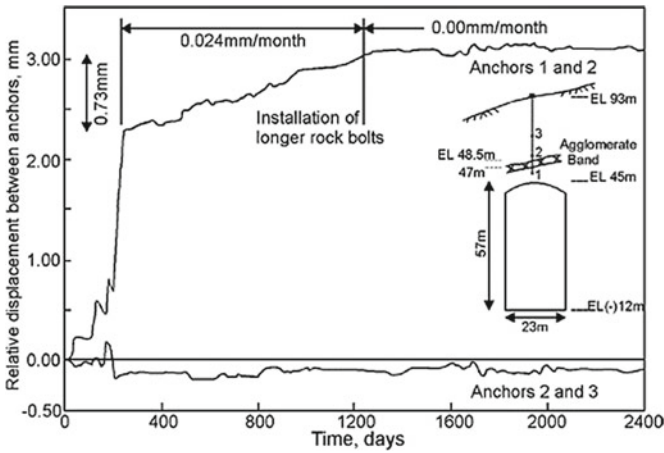


Fig. 3 MPBX at Surface of PHC at SSP [6]

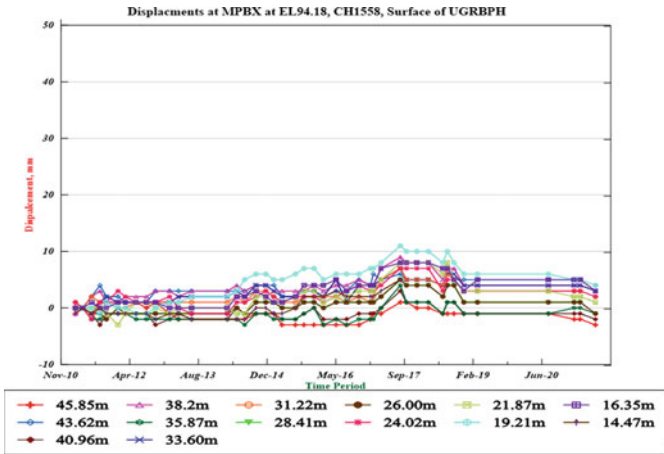


Fig. 4 MPBX at Surface of PHC at SSP [8]

MRMPBX and Targets Installed inside the Machine Hall. Magnetic Ring Multi Point Borehole Extensometers (MRMPBX) were installed for measuring the displacements at various depths and reflective target points for measuring the surface movements and individual wall convergence with a fixed reference point. Figures 5, 6, 7 and 8 show the MPBX observations at Ch1580 EL17.5 m and total station target observations between the chainage from 1494 to 1607 m [8].

Analysis of the instrumentation data indicate that there were no abnormal displacements during operational stages. Cumulative surface movement of 10 and 30 mm were measured at Ch 1580, EL17.5 m in both sides. The individual wall deformation measured at targets at EL33 were less than 5 mm over last 15 years (rate 0.0005 mm), shows stability of the cavern. Table 3 shows the summary of the MPBX observations at critical locations inside the powerhouse.

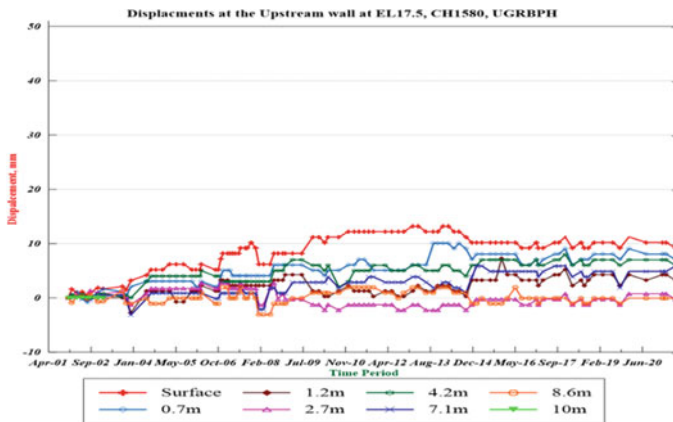


Fig. 5 MPBX-UCH1580, EL17.5 in SS PH cavern

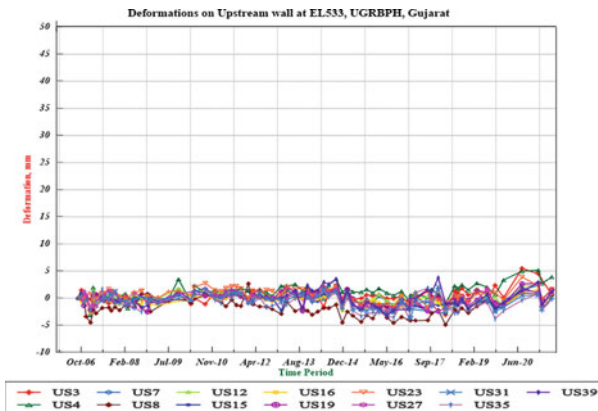


Fig. 6 Targets-US, EL33 in SS PH cavern

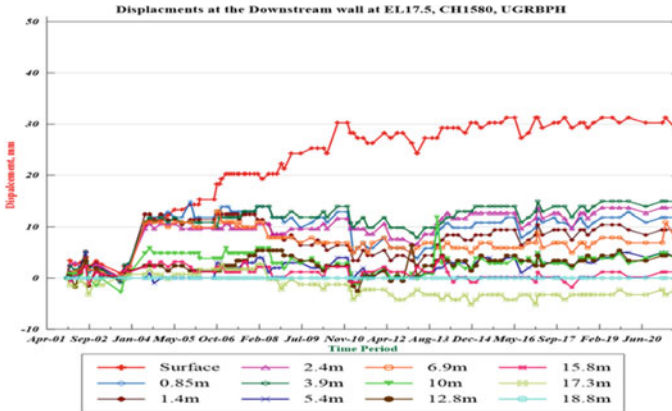
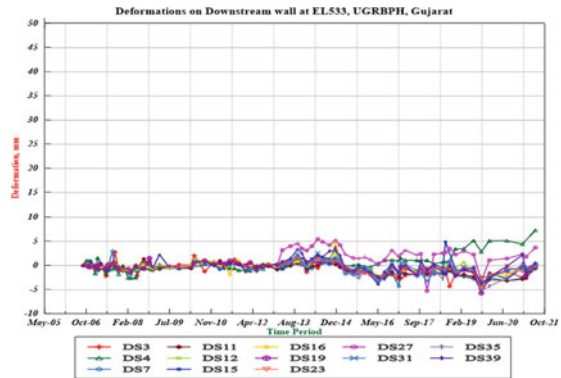


Fig. 7 MPBX-DCH1580, EL17.5 in SS PH cavern

Fig. 8 Targets-DS, EL33 in SS PH cavern



4.2 Tala Hydroelectric Project, Bhutan

Extensive instrumentation was carried out during the construction of the project to know the behaviour of the rock mass and support system performance. It was evident that it was very useful while construction of caverns and tunnels [4]. The rock formation in Tala project area comprises of gneiss and schists of Thimphu formation and phyllites, phyllitic quartzites and basic intrusive belonging to Shumar formation. The contact between these formations is marked by regional tectonic feature known as Main Central Thrust (MCT) in the Himalayan tectonics. Powerhouse complex is situated in a hillock with overburden ranging from 400–500 m. In Machine Hall (206 m long, 20.4 m wide and 45.5 m high), the rock mass mainly consists of jointed, foliated, and folded phyllites, Phyllitic quartzite, quartzite bands [7].

Table 3 Summary of MPBX observations in SS powerhouse cavern

Locations	Depth, where max displacement occurred	Cumulative displacements, mm	Days	Period of monitoring	Rate of displacements, mm
BG1MH	7.10 m	22.27	7831	Feb 2000–Jul 2021	0.002
BG2MH	8.42 m	24.86	7833	Feb 2000–Jul 2021	0.003
BG1DT1	3.31 m	26.29	7833	Feb 2000–Jul 2021	0.003
BG2DT3	12.96 m	24.09	7833	Feb 2000–Jul 2021	0.003
BG3DT5	1.35 m	12.17	7674	Feb 2000–Jul 2021	0.001
DCH 1515, EL0	Surface	14.24	6999	May 2002–Jul 2021	0.002
DCH1580, EL17.5	Surface	29.22	7161	Dec 2001–Jul 2021	0.004
UCH 1552, EL0	Surface	31.37	7832	Feb 2000–Jul 2021	0.004
UCH1580, EL17.5	Surface	9.21	7161	Dec 2001–Jul 2021	0.001

Tala Head Race Tunnel and Desilting Chamber. Timely information from the instruments has helped in strengthening the supports and stabilizing the excavations and help in evaluating the support designs. At Tala head race tunnel section where the rock cover varied between 600–660 m, and rock type is thinly foliated quartz- biotite schist, biotite schist, occasional quartzite bands, magnetic ring multi-point extensometers (MRMPBX) were installed for measurements of deformation (15 m long with 4–5 intermediate anchors). MPBX observation shows the movements in deeper horizons as shown in Fig. 10, which resulted in surface movement, cracks on shotcrete layer and bed separation near rock bolt interface. The immediate counter measures like installation of additional rock bolts stabilized the area before commencement of the concrete lining [3]. At Desilting chambers, critical unstable areas were observed in chamber 3. The additional supporting measures in roof and walls were taken before going for excavation at the hopper portion and trench part. To ascertain the stability above the cavern area, Convergence (relative movement between walls) between the walls at EL1336 and 1333 was measured. Figures 9 and 10 show the data plots of MPBX at HRT section and wall convergences at Desilting Chamber 3 [3].

Machine Hall Cavern of Tala PHC. The anchor load cells were installed on 12 m long fully grouted Dywidag high tensile rock bolts. Load cells were installed at the

Fig. 9 MPBX -MCUS RD1514 Tala HRT

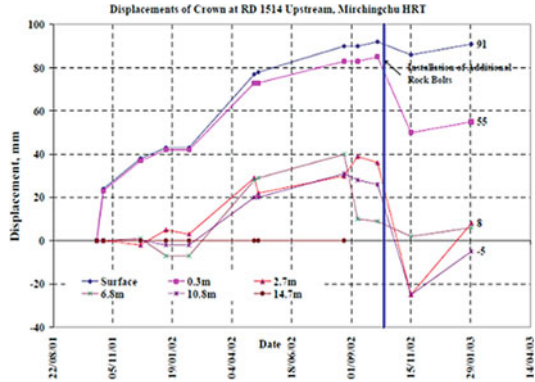
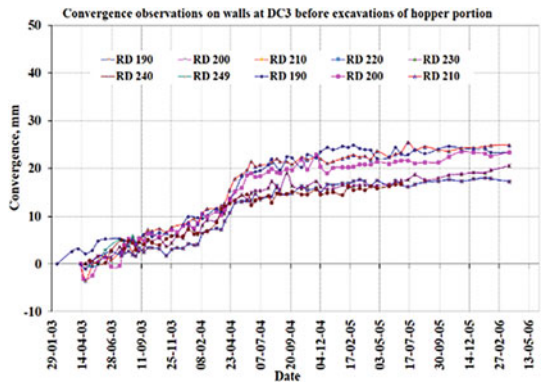


Fig. 10 Convergence observations at desilting chamber 3



time of installation of the rock bolt. The designed pre-tension up to 30tons was given to the rock bolt in few sections at higher elevations. Later, the pre-tension load was reduced to 10–12 tons. Resin capsules were used for first 4 m of the rock bolt and remaining hole was filled with cement grout. Thus, monitoring of the load cell started from the time of installation of rock bolt, which was the main supporting element for the side walls. The load cells were installed at EL 529.75 m, EL 525 m, EL 520 m, EL 515 m and EL 506 m. Figures 11 and 12 show the data plots of loadcell observations at elevation 525 and 515 [Sripad et al. 2018].

The wall convergence of machine hall cavern was measured using reflective targets with total station. Total Station Leica TDA 5005 with an angular accuracy of 0.5’ was used for this purpose. Although reflective targets were installed at EL 525, 520, 515 and 506 m, during operational stage, targets at EL 525 and EL 520 are available for monitoring. Additional targets were installed in 2008 at EL 525 and EL 520 at RD’s 31, 47, 75, 95, 120, 160 and 180 m during the operational period. (Sripad et al. 2018) Fig. 13 and 14 shows the data plots of loadcell observations at elevation 525 and 515 [3]. The convergence rate is at 0.7 mm/day immediately after the excavation

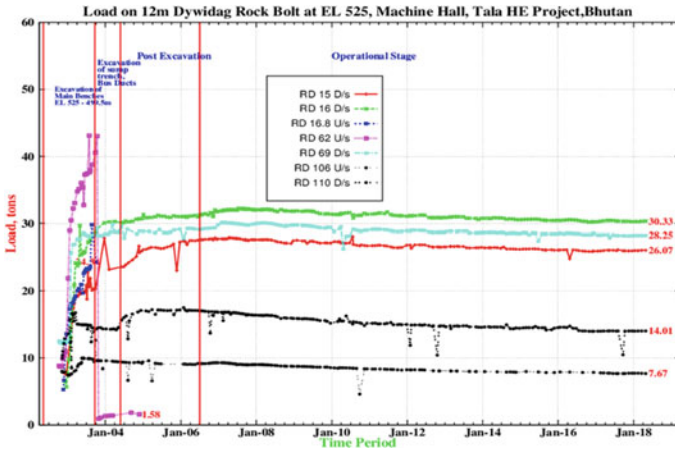


Fig. 11 Load cell observations at EL525

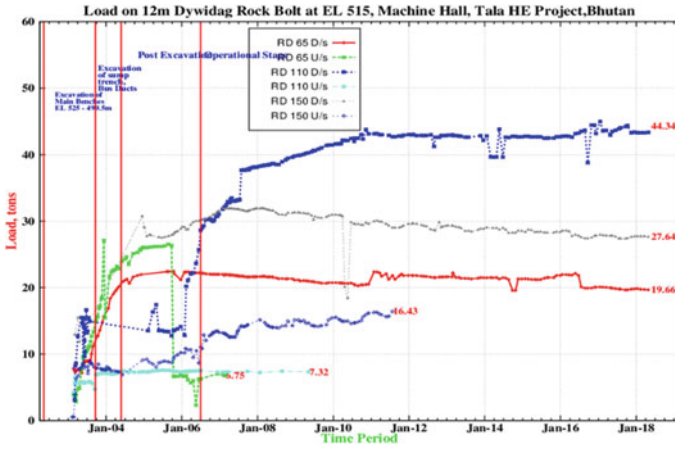


Fig. 12 Load cell observations at EL515

and has come down to 0.2 mm/day after 2 years and after 14 years, it is reduced to 0.001 mm/day [7].

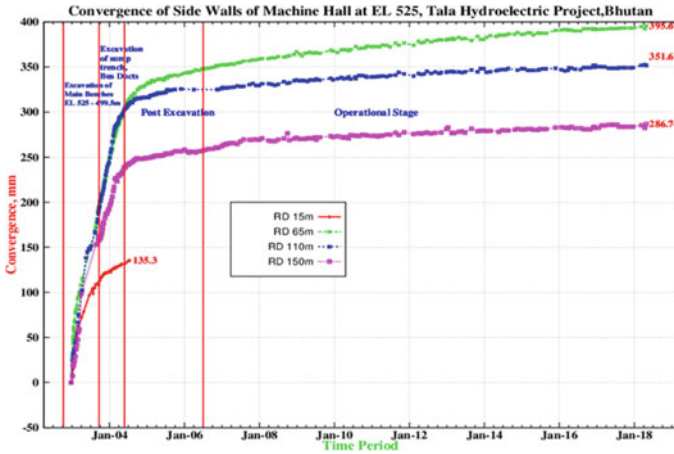


Fig. 13 Convergence observations at EL525

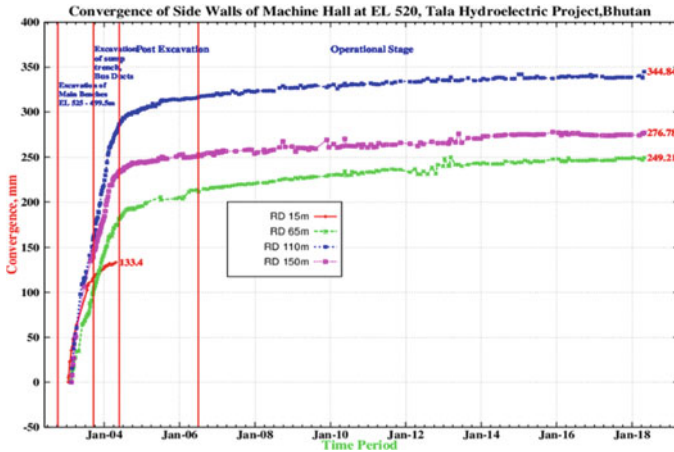


Fig. 14 Convergence observations at EL520

5 Conclusions

Regular instrumentation and monitoring during the construction of large caverns have been very beneficial as shown by the case studies discussed in this paper. In all the above cases, the monitoring of the instruments is continuing during operational stage also for more than 10–15 years and have been assuring the stability of the caverns. Instrumentation is a tool and an integral part of the underground structures for stability evaluation and support system performance. The monitoring programme taken up at various underground caverns have revealed that variation in stresses and deformation occurs during construction stage and continue for very long time.

Sometimes rock mass around the caverns undergoes time dependent deformations, that must be monitored to ascertain stability of caverns. Technology developments in hardware and analysis software enhances instrumentation usages in critical and unapproachable areas.

Acknowledgements Authors thank Director, NIRM for permission to conduct the studies at various project sites. The supports and facilities provided by the management of the hydroelectric projects are thankfully acknowledged. This forms the part of the doctoral research work being carried out by the first author at IIT (ISM), Dhanbad. The views expressed in this paper are those of the authors and not necessarily of the organisation to which they belong.

References

1. Dunicliff J (1993) Geotechnical Instrumentation for monitoring Field Performance. Wiley Inc., New York
2. Dasgupta B, Dham R, Lorig LJ (1995) Three dimensional discontinuum analysis of underground powerhouse for sardar sarovar project. In: Proceedings in 8th ISRM Congress, September 1995, Tokyo, Japan
3. Sripad P et al (2006) A study of rock behaviour at head race tunnel tala hydroelectric project, Bhutan
4. Sripad P, Sudhakar K, Nair R (2011) Instrumentation—a key to stability analysis of large caverns in hydroelectric projects. In: International Conference on Underground Space Technology, 17–19 January 2011, Bangalore, India
5. Gujral A (2019) Instrumentation for underground excavations – the future. ISRM (India) J 8(2). ISSN: 2277-1328
6. Goel RK (2019) Role of instrumentation in underground excavations. ISRM(India) J 8(2). ISSN: 2277-1328
7. Sudhakar K, Naik SR (2019) ISRM2019, Long-term stability monitoring of underground cavern using geotechnical instrumentation—a case study. In: Proceedings in Earth and Geosciences on Rock Mechanics for Natural Resources and Infrastructure Development, vol 6, pp 1340–1341. ISSN: 2639-7749
8. Sudhakar K et al (2021) NIRM 2021, Unpublished Report on Deformation Monitoring of Underground Powerhouse Cavern of Sardar Sarovar Project, Kevadia (Gujarat)
9. Product brochures from Geotechnical Instrument Manufactures

Mining Geotechnics

Numerical Modelling of Mining Induced Seismicity in Deep Closed Mines: A Case Study



Praveena Das Jennifer, P. Porchelvan, and Sripad R. Naik

Abstract Mining Induced Seismicity may be defined as a type of dynamic disaster experienced in both stages of mining and post mining. As the mining depth increases, the induced seismicity becomes a major concern causing unforeseen damage to equipments and major fatalities within the mine. During post mining, the scenario becomes even more difficult to understand the effects of induced seismicity taking into consideration the high uncertainties involved like no access, complex geology, inundation and failure of supports within the mine. To understand the dynamic behavior of induced seismicity, numerical modelling tools can be used in addition to seismic methods available.

The study presents an approach to analyze the effect of mining induced seismicity on a closed deep underground Kolar Gold Fields mine combining both numerical modelling and results of seismic analysis. A total of 40 mining induced events were recorded during the monitoring period. The seismic monitoring studies show considerable seismic activity in the vulnerable areas as identified by the model studies but of low magnitudes were detected within safe limits. The Finite Element approach is used for the analysis. The model studies in the closed Kolar Gold Fields mine show the vulnerable zones of seismicity to be concentrated at a depth of 900 to 1500 m from the surface and the maximum peak ground accelerations observed at the surface was 0.10 to 0.30 g.

The application of integrated approach of combining both seismic and numerical modelling has proved to be efficient in quick assessment of stability of the underground closed mine and its effects on the surface structures. Numerical model tools can help in assessment of an existing condition with all the prevalent geo-mechanical data as inputs in the model.

Keywords Mining induced seismicity · Numerical modelling · Integrated approach · Finite element · Seismic stations network · Post mining

P. Das Jennifer (✉) · S. R. Naik
National Institute of Rock Mechanics, Bengaluru, Karnataka, India
e-mail: pravi.jenniferdas@gmail.com

P. Porchelvan
School of Civil Engineering, VIT University, Vellore, Tamil Nadu, India

1 Introduction

Mining Induced seismicity is experienced both during active mine working and post mining on closure of the mine. The stress redistribution is a continuous process which begins from the day of excavation in the mine and continues even after the closure of deep mines. These events of stress redistributions lead to requirement of continuous assessment of stability of the deep underground mine. The instability within the mine creates apprehensions related to unforeseen damage to equipments, major fatalities within the underground mine and stability of surface structures. The risk factor further increases when the closed deep mine involves presence of large mine voids, failed support system, inundated water and instable rockmass condition. Closed mines in Korea, Sweden, South Africa and Kolar Gold Fields of India have shown post closure mining induced seismicity. Various techniques and approaches are available to assess the seismic vulnerability of risk prone areas [14]. The approaches so chosen for assessment of seismic risk depends on various parameters and is usually site specific. Evaluation of mining induced seismicity with regard to mined-out stopes partially or fully inundated is a complex condition to be evaluated by empirical methods.

Numerical methods consider the relevant parameters required for assessment of mining-induced seismicity and to study its effects on surface structures. An underground mine presents complex geometry. To understand the overall behaviour of the mine, simulation of a model depicting the existing geology, geo-mechanical stress condition, non-linear behaviour of the rockmass with mined out spaces and current water level, the finite element method (FEM) approach with implicit dynamic integration is found to be more appropriate. In case of FEM, modelling of complex geometries and irregular shapes for finite elements are possible. The boundary conditions can be easily incorporated for basic and complex analysis.

In fault slip modelling analysis, the seismic moment is one of the major parameters. The shear movements are indicators of damage caused by fault movements or stress redistribution being induced. Based on the analysis, the fault-slip can be classified as seismic and aseismic. The classification helps in identification of aseismic/local events [11]. Considering the safety of surface structures, an attempt is made to understand and make a quick assessment of the stability of deep underground gold mine using an integrated approach. The approach involves an actual onsite short-term seismic monitoring study combined with numerical model analysis of the closed mine. The concept of integrating seismic data and numerical modeling analysis helps in solving rock mass stability problems, extent of damage estimation and understanding violent failure of rock mass [5].

2 Location Details

The area of monitoring chosen is part of the Archean complex of Southern India and falls in the Kolar Schist belt of the Archean greenstone belt of Karnataka. The

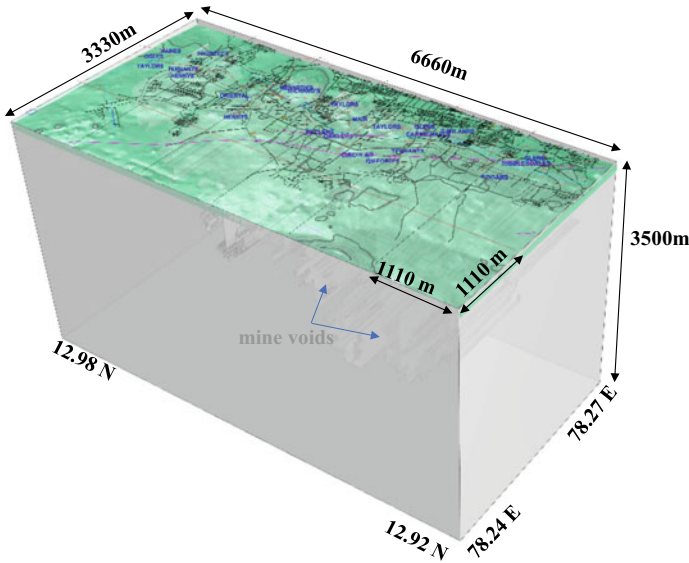


Fig. 1 3D view of entire mining area of Kolar Gold Fields, India

Kolar Gold Fields (KGF) mines area is at the southern tip of the schist belt and consists of two system of rock formations, the Dharwar schist (Hornblende Schist), metamorphosed from basic igneous rocks, and the peninsular gneiss series, formed by the granite intrusion from beneath. The Kolar Gold Fields mine lies on the Kolar schist belt spreading over an area of 8 km long in the North-South direction and about 4 km in width along the East-West direction. The Kolar Gold Fields mine was one of the deepest gold mines with a mining depth of 3.2 km [9, 10].

The mining area lies between 12.92 N–12.98 N and 78.24 E–78.27 E, at an altitude of 900 m above the mean sea level (MSL) as shown in Fig. 1. The gold mines have three major mines in the mining region, the Nundydroog Mine in the north, Champion Reef Mine in central and Mysore Mine in the south. The three major geological fault systems identified in this mining region are, the prominent Mysore North Fault (MNF), striking NW-SE right through the centre of the region and the other two identified faults are minor faults running sub parallel to MNF, Tennant Fault and Gifford Fault [3, 10].

3 Onsite Mining-Induced Seismicity Studies

The Kolar Gold Fields mine has experienced more than 10,000 seismic events since 1957. Since the complete closure of mines in the year 2001, there has been occurrence of seismic events of magnitude inducing notable surface events like subsidence, sink

holes and cracks in buildings in the surface structures [7]. Though there has been a decline in the number of events, the occurrence of events has brought apprehensions related to safety and stability of the mining area. The need for assessment and identification of seismically vulnerable areas arose.

3.1 Study Area and Sensor Details

A small-scale surface seismic monitoring system involving five-station network with triaxial geophones was installed. The mining area considered for the study was 6 (North to South) × 3 (West to East) × 3 km (in Depth). Based on a preliminary noise survey and monitoring the area, the locations of the five sensors were identified. On identification of five locations, sites were prepared for installation of sensors at the respective seismic stations. The installed triaxial geophones were portable and well-integrated (4.5 to 315 Hz) with advanced digitization, storage and communication technology. The layout of the geophones covered the entire mining area, two on either side (eastern and western) of the Mysore North Fault, one in the central mining area and the other two in the northern and southern area [12]. The layout of sensor installation is shown in Fig. 2.

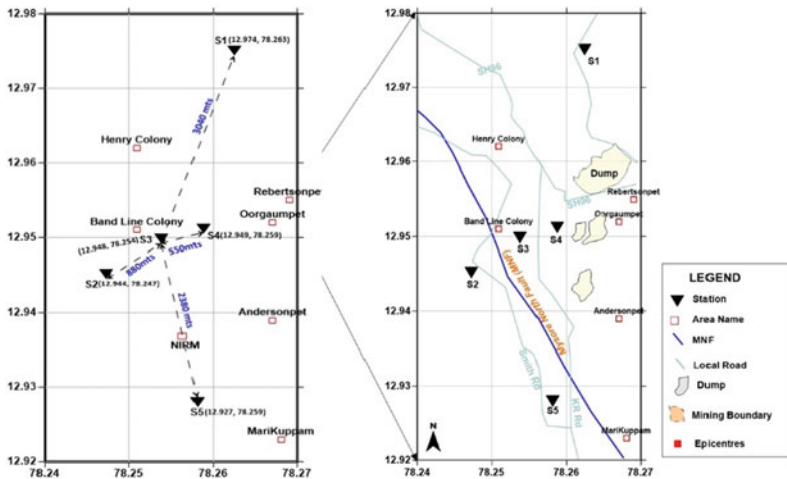


Fig. 2 Layout of installed seismic sensors within the mined-out areas [12]

3.2 Methodology

The data recorded on the geophones were processed and analyzed using SEISAN and 3D Insite-Geo software tool. The P-wave and S-wave velocity used was 5500 and 3500 ms⁻¹ taken from previous studies carried out at the mining area. The processing of the seismic data, identifying and segregation of seismic events from possible cultural noises, computation of source parameters (magnitude, seismic moment, depth, source radius), analysis of the events was carried out. The other parameters like seismic energy, stress drop, apparent stress ratio, the Peak Ground Acceleration (PGA) and Peak Ground Velocity (PGV) were deduced and used in the identification and delineation of seismically vulnerable areas.

3.3 Results and Analysis

Short-term monitoring of seismic events and recording the events picked up by the network of five surface sensors was carried out from May 2017 to May 2018. Out of the total recorded 72 seismic events, 40 events were filtered out as subsurface seismic events. These 40 events were analyzed and seismic source parameters were obtained to assess the seismic risk scenario existing in the closed mining area of Kolar Gold Fields. The 3D view of identified seismic events in the mining region is shown in Fig. 3.

Based on the source parameters using the site-specific relations, the ground motion parameters Peak Ground Acceleration (PGA) and Peak Ground Velocity (PGV) were derived. The site-specific attenuation relations were calibrated for small and shallow level seismic events. The maximum and minimum PGV was 0.540 and 0.004 cm/s. Low PGV values are associated with low magnitude values. The PGA of the recorded events varied from 0.001 to 0.059 g. The PGA and PGV values observed in the mining area is shown in the Fig. 4.

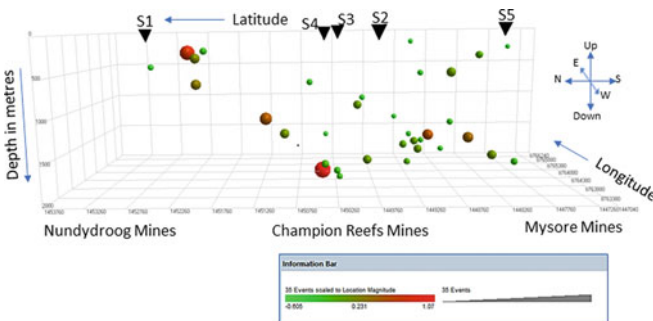


Fig. 3 3D view of seismic events in the study area [12]

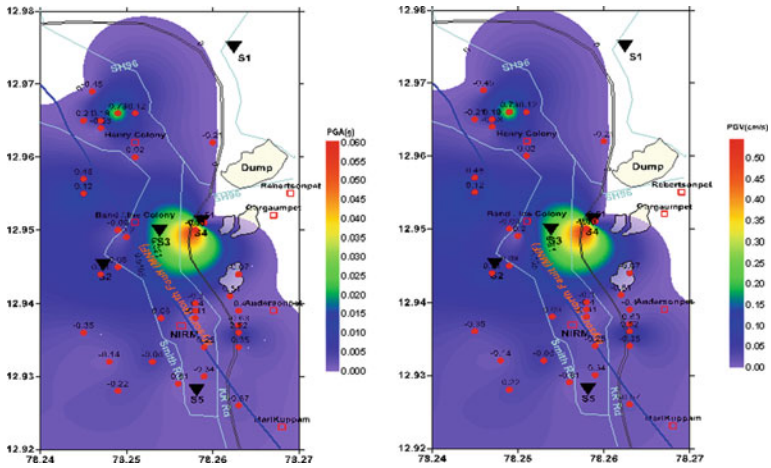


Fig. 4 PGA (left) and PGV (right) observed in the mining area [12]

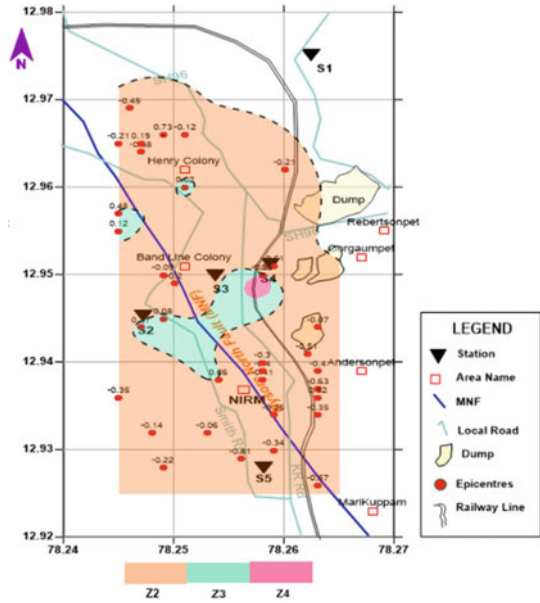
Table 1 Seismic vulnerability index

Magnitude → Depth ↓	-2 → -1	-1 → 0	0 → 1	1 → 2	2 → 3
0-500 m	Z1	Z2	Z3	Z4	Z5

A seismic vulnerability index map was prepared with identified five zone types (Z1, Z2, Z3, Z4 and Z5) based on magnitude and depth. The indexing is shown in Table 1 and accordingly represented over the entire mining area in the Fig. 5.

It is observed that 90% of the mining area falls under Z2 where the hazard is very low – low due to the weak energy of the events and very low PGV and PGA values. No physical damages to structures were reported due to this event. For the measured range of frequencies (5–80 Hz) of the seismic events in this depth range, the ground motion values are in safe limits.

Fig. 5 Seismic vulnerability map of the closed mine [12]



4 Numerical Modelling Studies

4.1 Study Area

The complete mining area of 6 (N-S) \times 3 (W-E) \times 3.5 km (D) comprises of shafts and 1400 km of tunnel work with 70% stoped out area, it becomes extremely difficult to model the entire stretch considering all the geological, geotechnical, and hydrological parameters. In this study two sections from the mining area were identified based on inhabited regions, recent seismic activities, areas close to major fault and type of surface structures. The two sections identified for numerical analysis is shown in Fig. 6.

Section 1 identified is 1 (N-S) \times 2 (E-W) \times 3.5 km (D) section of the deepest Champion Reef mine. The area covers the 3.2 km deepest (113 level) mined out section, Mysore North fault along with the Tennant’s fault and the railway line with Champion railway station. Section 2 identified is 1.11 (N-S) \times 2.22 (E-W) \times 3.5 km (D) section with Henry colony, Henry’s shaft and Mysore North fault traversing through the section. Both the sections are identified with previous and recent seismic activity.

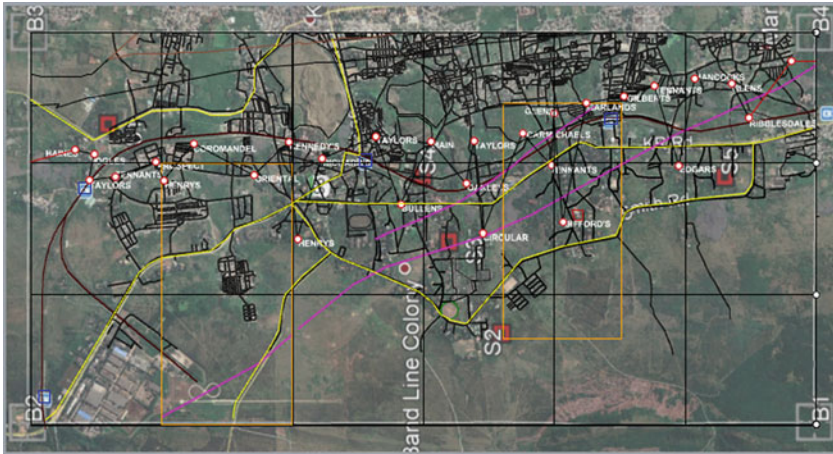


Fig. 6 Identified locations: Sect. 1 and Sect. 2 in the mining area

4.2 3D Model

Section 1: The area between Carmichael’s shaft and beyond Garland’s shaft lying between 12.935 N–12.944 N and 78.246 E–78.264 E with stoped out workings (mine voids). **Section 2:** The area between Henry’s shaft and beyond Oriental shaft lying between 12.96 N–12.97 N and 78.24 E–78.26 E with stoped out workings (mine voids).

3D Finite Element tool is used for the analysis. The 3D model of Sect. 1 and Sect. 2 showing the geology, faults (Mysore North Fault and Tennant’s Fault) and the mine voids is shown in Fig. 7. The geological details are from geological plan of Kolar Gold Fields mine from Survey Dept. 1956.

4.3 Material Properties

The rock materials are modelled as continuum using Generalized Hoek Brown Constitutive behaviour to analyse the stability of the model under different seismic loads. This material considers the stress decrease process as per jointed rock mass. The non-linear Generalized Hoek-Brown criterion [6] for rock masses is taken as input data for the analyses required for design of underground hard rock excavations.

The physico-mechanical material properties used as basic inputs are unit weight, elastic modulus, uniaxial compressive strength and triaxial properties. The properties are laboratory tested values of Kolar Gold Fields mine location obtained from Geological Survey of India (GSI) report (Panduranga et al., 2009). Based on laboratory test results, the GSI and intact rock parameter were decided referring to Hoek and Brown, [13] (Latest Edition for guidelines for GSI calculation). Table 2 shows

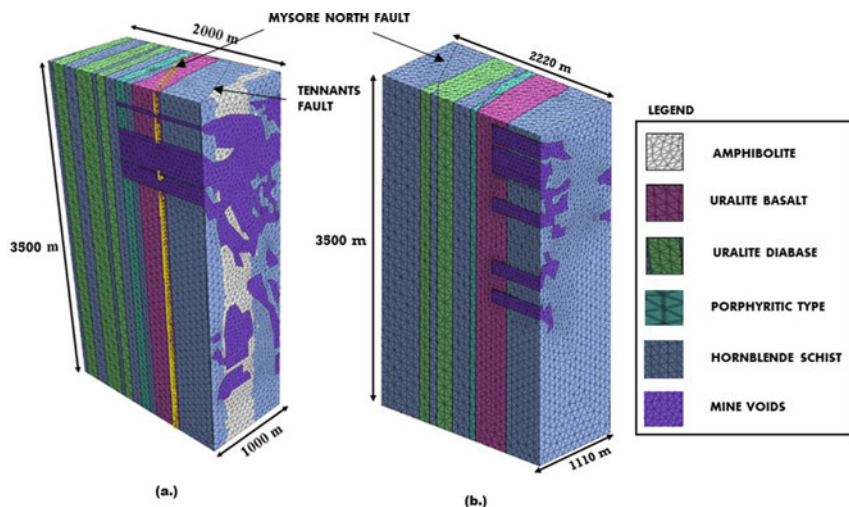


Fig. 7 3D model of (a.) Sect. 1 (b.) Sect. 2 identified for analysis

Table 2 Physico-mechanical properties of materials defined in the model

Material properties	Elastic modulus $\times 10^7$ (kN/m ²)	Unit weight (kN/m ³)	GSI	Intact rock parameter	mb	s	a	Uniaxial Comp. strength (kN/m ²)
Uralite Diabase	8.54	28.63	40	7	0.1968	0.0001	0.5114	87,377
Porphyritic type	6.82	26.68	45	30	1.1359	0.0002	0.5081	166,713
Uralite Basalt	9.36	29.61	40	17	0.4780	0.0001	0.5114	294,200
Hornblende Schist	8.26	29.62	30	4	0.0620	0.0000	0.5223	152,199

the elastic and non-linear properties defined in the model. Damping ratio of 0.05 and disturbance factor of 0.8 has been taken in the model analysis.

4.4 Methodology

An Artificial Earthquake Generation approach [1] is used in the study to generate the seismic load. This method uses the power spectral density of design spectrum as expected maximum response. The parameters of the seismic event with highest magnitude, to have experienced over the mining area is used to simulate a real

earthquake with parameters equivalent to that of the identified seismic event. A subsequent iterative process is run to match the target spectrum. The design spectrum of the Kolar Gold Fields area is considered according to IS 1893 (2002).

The response spectrum is converted to acceleration time history. The minimum, intermediate and maximum accelerations of 0.06, 0.10 and 0.22 g are being considered based on the previous ground motion studies [8]. The damping constants and stiffness of the viscous springs are calculated as per Lysmer & Kuhlmeyer, [2] and modulus of subgrade reaction approaches, respectively.

Considering the stopes are filled with water to a level of 500 m from the surface. To study the hydrodynamic fluid-rock interaction, water is modelled as a continuum linear material with Poisson's ratio equal to 0.49. The section comprises of two faults that are traversing through the modelled area. To establish the fault behaviour, interfaces are assigned at the fault location. Viscous boundary is modelled at the boundaries of the model to absorb all the waves (no reflected waves) generated due to the seismic load.

Material damping plays an important role in the energy dissipation in case of earthquakes. Hence Rayleigh damping approach is used in the model. Eigenvalue analysis is run preceding to the nonlinear time history analysis to compute the mass participation and frequencies (f_1 & f_2) of the model. It is observed that 73% of the mass is active and the first two predominant frequencies of the model are 1.4786 & 1.5987 cycles/sec. These frequencies are used to estimate the Rayleigh damping coefficients alpha (mass proportional coefficient) and beta (stiffness proportional coefficient) in the seismic analysis.

4.5 Results and Analysis

All the data are taken as inputs, a parametric seismic non-linear time history analyses is run for Peak Ground Accelerations of 0.06 (Case-1), 0.10 (Case-2) and 0.22 g (Case-3) being applied as ground acceleration at the lowest level of the model, at 3.5 km from the ground surface. In all the three cases, the initial stress in the rock is calculated using K0 condition and seismic analysis is carried out for both Sect. 1 and Sect. 2. A seismic activity in an abandoned mine affects not only the stability of stopes but also the super structures above the surface. The model was helpful in demarcating the vulnerable zones in close proximity to the surface.

Section 1: The vulnerable zones have been identified at 1000 to 1500 m from the ground surface. It is observed that the vulnerable zones are spread over a radius of 1000 to 1500 m from the point of high shear stress concentration and nearing almost plastic state as shown in Fig. 8. The plastic state presents the yielding of rockmass at these zones.

Section 2: The vulnerable zones have been identified at 900 to 1500 m from the ground surface. It is observed that the vulnerable zones are spread over the ground surface from the point of high shear stress concentration and nearing plastic state as

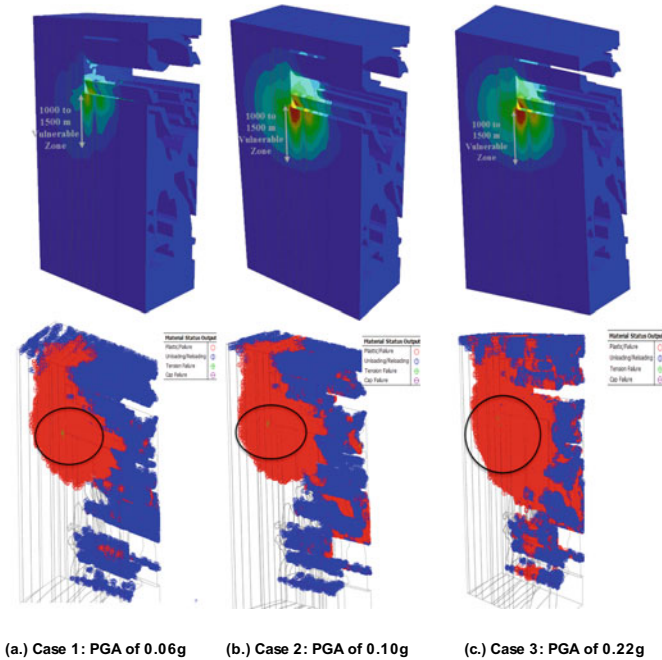


Fig. 8 Spatial distribution of shear stress and plastic zone for all cases- Sect. 1

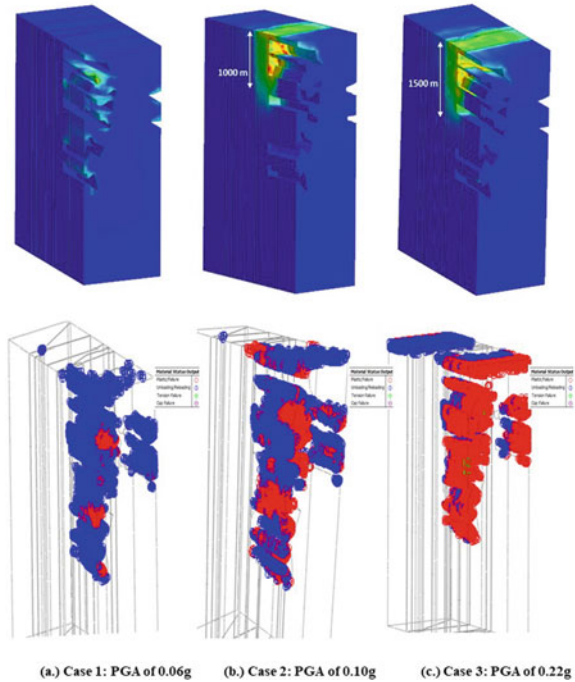
shown in Fig. 9. The plastic state presents the yielding of rockmass and the yielding has been predominant noticed in case 3 with PGA of 0.22 g.

The input parameter of peak ground acceleration is varied from a minimum PGA value of 0.06 g to a maximum PGA value of 0.22 g. It has aided in the identification of vulnerable zones and the effect of such magnitudes that can bring about on the surface. It is further observed, that as the input acceleration at the bottom is increased, the acceleration at the vulnerable zones also have increased indicating zones of high seismicity (rockburst/rockfall). The rockmass at these zones have failed.

The waves get amplified as it moves towards ground surface. The plastic failure zones are the vulnerable zones and the tensile stresses resulted in rockmass failure (rockburst). The ground motion spatial distribution can be analysed and used to understand the type of failure. Finite element numerical solution only allows continuum modelling and any sort of events such as rockbursts may result in the divergence in the solution. Hence the analysis got terminated for all the three cases when the rock at the vulnerable zone has failed.

The accelerations observed at the ground surface are not significantly amplified when compared with input acceleration till the violent failure of the rockmass as shown in Fig. 10 and Fig. 11. Since an instability like violent failure of rockmass presents a state of instability at the vulnerable zones and redistribution of stresses should be leading to further failure of stressed rock masses.

Fig. 9 Spatial distribution of shear stress and plastic zone for all cases- Sect. 2



The seismic activity at these vulnerable zones at their corresponding depths of occurrence in turn affect the overlying surface structures. The accelerations observed at the top ground surface for all the three cases at both the Sects. 1 and 2 is shown in Fig. 12. It can be inferred that as the acceleration is increased from 0.06 to 0.22 g there is a corresponding increase in ground acceleration at the surface from 0.06 to 0.30 g.

Section 1: It is observed as the seismic load 0.06 g is applied, the vulnerable zones at the surface are found to lie close to the prominent Mysore North fault and close to the railway line with varying intensity of 0.06 to 0.14 g. As the seismic load is increased from 0.06 to 0.1 g, the intensity of acceleration experienced at the surface increased up to 0.16 g at the vulnerable zones near the Mysore North fault. Finally on increasing the seismic load to 0.22 g, the vulnerable zones have increased radially with maximum intensity of 0.24 g.

Section 2: It is observed as the seismic load 0.06 g is applied, the vulnerable zones at the surface are identified at Henrys colony area and with increasing intensities towards the boundaries of the section. The intensity observed was 0.07 to 0.17 g. As the seismic load is increased from 0.06 to 0.1 g, the intensity of acceleration experienced at the boundary increased up to 0.11 g. Finally on increasing the seismic load to 0.22 g, the vulnerable zones have increased radially from the boundary with maximum intensity of 0.20 g.

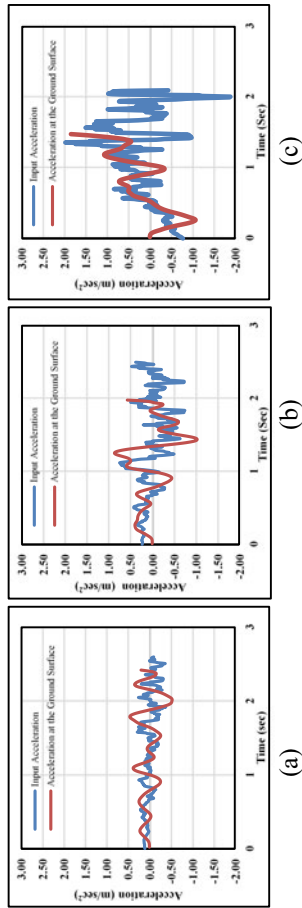


Fig. 10 Acceleration time history plot - at the ground surface for all three cases- Sect. 1

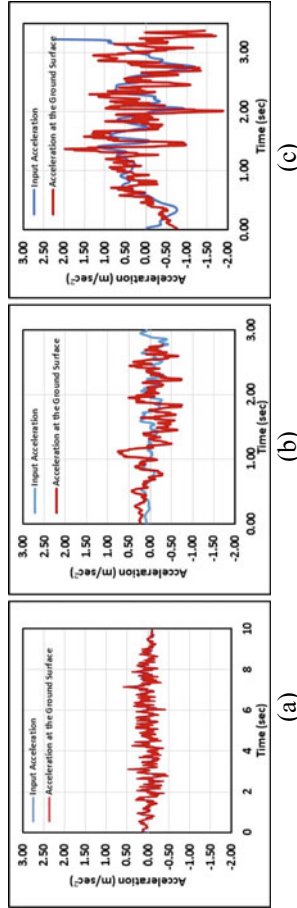


Fig. 11 Acceleration time history plot - at ground surface for all three cases- Sect. 2

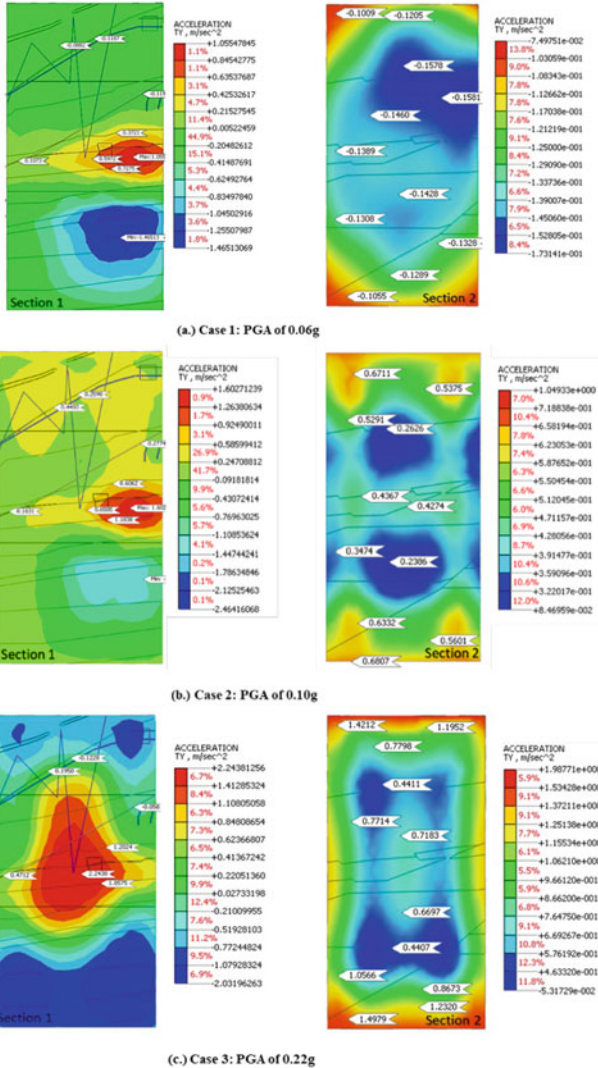


Fig. 12 Accelerations at the ground surface for all three cases in the two sections

5 Discussion

The Kolar Gold Fields mine has experienced more than 10,000 seismic events since 1957. Since the complete closure of mines in the year 2001, there has been occurrence of seismic events of magnitude The model developed has taken into consideration the fault system, the geology, the stoped out areas for the analysis. A seismic load was applied of a known intensity of earthquake equal to the maximum intensity

of rockburst experienced in the mine. The analysis conducted has been helpful in identification of vulnerable zones with their corresponding depth of occurrence.

The results of numerical model analysis can be compared with the seismic monitoring studies conducted at the identified closed mining area. It has been observed that the results from the model analysis comply well with the seismic zones identified. The following observations were made on comparing the results of both the analysis.

- a) The vulnerable zones and zones of seismicity are found to be concentrated upto a depth of 900 to 1500 m from the surface. Seismic studies show seismic events at the same locations along with their depth of occurrence.
- b) The vulnerable zones identified through short-term seismic study shows seismic events at the same locations but of lower magnitude in comparison to the intensity of vulnerable zones simulated by the numerical analysis. The model shows the intensity of ground accelerations that would be experienced at the surface on occurrence of a seismic event of such magnitudes.
- c) Post closure of mines, in 2005 rockburst events have occurred with maximum intensity of 0.22 g PGA recorded in the mining area till date [4, 8]. From the model studies, the maximum PGA observed at the surface varied from 0.1 to 0.3 g. The PGA from the seismic studies vary between 0.001 to 0.059 g of very low magnitudes.

The model simulations and seismic studies were validated with field observations being made from time to time, from the analysed data of recorded seismic events from the seismic monitoring systems installed previously. The observations made are as follows:

- The Champion Reef mine has experienced rockbursts at a depth of 300 to 1500 m and in some regions at a depth of 2100 to 3200 m.
- A total of around 1158 rockburst events were recorded for the period 2006–2012. The maximum acceleration ranged between 0.0006 to 0.10 g with duration of event ranging between 0.3 to 2.5 s (Srinivasan et al. 2013).
- The longitudinal section (north-south) of Kolar Gold Fields showing the spatial distribution of rockburst during mining at deeper levels is shown in Fig. 13. The spatial distribution of rockburst and the recent activity observed over the entire mining area is shown in Fig. 14. The events were found to concentrate along both sides of the prominent Mysore North fault.



Fig. 13 Longitudinal section of Kolar gold fields mine - spatial distribution of rockbursts



Fig. 14 Location of seismic activity in the mining area

6 Conclusions

The onsite short-term Seismic Monitoring studies and Numerical Model studies were carried out to identify the vulnerable areas in the closed mine and to study the ground motions at the surface due to these seismic events. Since mining region falls in zone 2 of seismological map of India, the tectonic stresses may not be the primary driving force of mine seismicity. Redistribution of lithostatic stresses could be one of the potential factors for the build-up of strain energy leading to the rockbursts in the mined-out area.

The seismic monitoring studies show considerable seismic activity in the vulnerable areas identified by the model studies but of low magnitudes within safe limits. This indicates that these zones are still active and needs to be monitored. The model studies in the closed Kolar Gold Fields mine show the vulnerable zones of seismicity

to be concentrated at a depth upto 900 to 1500 m from the surface and the maximum peak ground accelerations observed at the surface was found to be 0.10 to 0.30 g. The seismic study and the model developed in this study has aided in quick risk assessment of the current stability condition existing in the closed gold mine of Kolar Gold Fields and its effects on the surface structures.

Using the finite element approach, it was possible to study the seismic phenomenon and their effects on the surface structures. To further study the effects of seismic load on surface structures post rockmass failure in the underlying strata, the Discrete Element Method of comprehensive analysis is suggested.

Acknowledgements The authors are grateful to Dr. H S Venkatesh, Director NIRM for permitting to publish this paper in this Conference. The authors also express their thankfulness to Dr. V R Balasubramanian, Project Leader, Science and Technology research project work in the study area granted by Ministry of Mines, Govt of India.

References

1. Housner GW, Jennings PC (1964) Generation of artificial earthquakes. *J Eng Mech Div (Am Soc Civ Eng)* 90(February):113–1501964
2. Lysmer J, Kuhlemeyer RL (1969) Finite dynamic model for infinite media. *J Eng Mech Div ASCE* 95(4):859–877
3. Srinivasan C, Arora SK, Yaji RK (1997) Use of Mining and Seismological parameters as premonitors of rockburst. *Int J Rock Mech Min Sci* 34(6)
4. Srinivasan C, Benady S, Sivakumar C (2000) Fluid induced seismicity in Kolar mining region. In: *Proceedings of the Workshop on Dam Safety Including Instrumentation of Dams*, 15–17 November, Trivandrum
5. Mendecki AJ, Napier JAL, Ilchev A, Sellers E (2001) Fundamental aspects of the integration of seismic monitoring with numerical modelling. Report by ISS International Limited CSIR, Miningtek, GAP, p 603
6. Hoek EC, Carranza-Torres C, Corkum B (2002) Hoek-Brown criterion–2002 edition. In: Hammah RE et al (eds) *Proceedings of the 5th North American Rock Mechanics Symposium and the 17th Tunnelling Association of Canada: NARMS-TAC 2002*, Toronto, (1) Canada, vol 1, pp 267–273
7. Panduranga R, Dharuman R, Purusottaman D, Mishra AK (2009) A report on geotechnical evaluation of rockburst hazard in BGML area, Kolar Gold Fields, Kolar District, Karnataka (FS 2005–07)
8. Srinivasan C, Yesurathenam W, Gupta I (2010) Estimation of local magnitude of rockbursts using strong motion accelerograms in the mines of Kolar gold fields. *Acta Geophys* 58(2):300–316. ISSN (Online) 1895-7455, ISSN (Print) 1895-6572
9. Srinivasan C, Willy YA, Carter RM (2013) Characteristics of rockbursts in the flooded mines of Kolar gold field. In: *Proceedings of the 8th International Symposium on Rockbursts and Seismicity in Mines*, Moscow, Russia
10. Jennifer PD, Balasubramaniam VR, Goverdhan K, Ganapathy GP (2016) Overview of seismic monitoring and assessment of seismic hazard based on a decade of seismic events. In: *Proceedings of the International Conference on Recent Advances in Rock Engineering (RARE-2016)*, 16–18 November, Bengaluru, India, pp 238–245. <https://doi.org/10.2991/rare-16.2016.90>
11. Sainoki A, Mitri HS, Chinnasane D (2017) Characterization of aseismic fault-slip in a deep hard rock mine through numerical modelling: case study. *Rock Mech Rock Eng* 50:2709–2729

12. Balasubramanian VR, Jennifer PD, Goverdhan K (2018) Estimation of Seismic Hazard in and around the mined-out areas of Kolar Gold Fields, Karnataka (S&T Report No. ES1202) NIRM unpublished Report
13. Hoek E, Brown ET (2019) The hoek–brown failure criterion and GSI–2018 edition. *J Rock Mech Geotech Eng* 11(3):445–63
14. Jennifer PD, Porchelvan P (2021) An approach to assessment of post mining-induced seismic hazard in Kolar gold fields mines—a review. 69(3). <https://doi.org/10.18311/jmmf/2021/27784>

Intelligent Techniques for Prediction of Drilling Rate for Percussive Drills in Topically Weathered Limestone



Ramesh Murlidhar Bhatawdekar, Bishwajit Roy, Saksarid Changtham, Manoj Khandelwal, Danial Jahed Armaghani, Edy Tonnizam Mohamad, Pranjali Pathak, Subhrojit Mondal, Radhikesh Kumar, and M. F. Md Dan

Abstract Physico-mechanical properties of rocks have a direct correlation with the drilling rate of percussive drill. The prediction of drilling rate is important for the deployment of drills during the planning stage. In tropical climatic regions, limestone is classified as blocky, very blocky, blocky/ seamy and disintegrated based on the degree of weathering. Weathering of limestone takes place very rapidly in tropical (wet) climatic regions. Previous researchers have correlated different individual rock mass properties with rate of drilling. However, single property of limestone is not adequate to correlate with the drilling rate. In this study, sensitivity analysis of

R. M. Bhatawdekar · P. Pathak · S. Mondal (✉)
Department of Mining Engineering, Indian Institute of Technology, Kharagpur 721302, India
e-mail: subhrojit08@iitkgp.ac.in

R. M. Bhatawdekar
e-mail: rmbhatawdekar2@graduate.utm.my

P. Pathak
e-mail: pranjali9920@gmail.com

R. M. Bhatawdekar · E. T. Mohamad · M. F. Md Dan
Centre of Tropical Geoenvironment (GEOTROPIK), Faculty of Civil Engineering, University Technology Malaysia, 81310 UTM Skudai, Johor, Malaysia
e-mail: Edy@utm.my

M. F. Md Dan
e-mail: firdausd@uthm.edu.my

B. Roy
Department of Computer and Science Engineering, Bennett University, Greater Noida, Uttar Pradesh 201310, India
e-mail: Bishwajit.Roy@bennett.edu.in

S. Changtham
Siam City Concrete Company Limited, Bang Sue, Bangkok 10800, Thailand
e-mail: saksarid.changtham@siamcitycement.com

M. Khandelwal
School of Engineering, Information Technology and Physical Sciences, Federation University, Ballarat, Australia
e-mail: m.khandelwal@federation.edu.au

different properties of weathered limestone was carried out with respect to drilling rate. Rock density, rock quality designation (RQD), geological strength index (GSI), point load index (PLI) and Schmidt hammer rebound number (SHRN) were identified as crucial input parameters. 113 data sets were collected with the foregoing five input parameters and the output parameter as drilling rate of percussive drills. Data was analysed with multi variable regression analysis (MVRA) which showed R^2 value as 0.54. Artificial neural network (ANN) has been widely used for solving various engineering problems. On the other hand, optimization problems are solved by the Biogeography Based Optimization (BBO) model. Further this data was analysed with a hybrid intelligent model namely BBO- ANN. The R^2 values for training data set and testing data set 0.638 and 0.761 respectively.

Keywords Artificial neural network (ANN) · Black box optimisation (BBO) · Geological strength index (GSI) · Multivariable regression analysis (MVRA) · Point load index (PLI) · Rock quality designation (RQD) · Schmidt hammer rebound number (SHRN)

1 Introduction

Drilling is a primary important activity in any mines [1, 2]. Percussive drilling has been commonly used for hard rock strata [3–5]. Based on the performance of drilling and feedback from drilling, blast design can be carried out. Drilling efficiency is evaluated based on rate of penetration which is based on type of rock- sedimentary, metamorphic or igneous rock, strength of rock, density. Geological discontinuities, abrasiveness can have an adverse impact on rate of drilling [6]. Drilling performance is important for the prediction of blast performance as rock mass related factors have direct impact on blasting [7, 8]. The objective of blasting is to provide well fragmented rock. Blasting operation has direct impact on downstream operations such as rate of loading [9, 10], fill factor for dump trucks and crushing rate. Hence, prediction of drilling rate is important for understanding overall efficiency and effectiveness of mining operation [11, 12].

During exploration stage of any mineral, exploratory core drilling forms important part of identifying ore body. Physical properties of rock and geological structures are determined with geological mapping, geophysical logging and laboratory tests [13].

D. J. Armaghani

Department of Urban Planning, Engineering Networks and Systems, Institute of Architecture and Construction, South Ural State University, 76, Lenin Prospect, Chelyabinsk 454080, Russia
e-mail: danialarmaghani@susu.ru

R. Kumar

NIT, Patna 800005, India
e-mail: radhikesh12@gmail.com

M. F. Md Dan

Research Center for Soft Soil (RECESS), Faculty of Civil and Built Environment, University Tun Hussein Onn Malaysia, 86400 Batu Pahat, Johor, Malaysia

Due to high cost of exploratory drilling, it is done with wide spacing. Sometimes down the hole (DTH) and reverse circulation drills are used to identify additional information of rock. Production drilling provides certain additional information to cross check mineral extent. Geophysical logging provides physical properties of rock. However, geophysical logging or survey is time consuming and costly method. Hence, adequate data may not be available to determine physical properties. Also, if there are local geological discontinuities such as faults, folds, joints and bedding plane, it will not be economical to determine all physical properties of rock at every location. All discontinuities represent different intensity, orientation of fractures with variation of rock strength. All geological discontinuities may be local or regional level based on nature of the deposit. Researchers have identified indirect method of measurement while drilling (MWD) to classify different rock mass [13–17].

Types of Drilling Equipment: The drilling equipment can be classified as rotary percussive and rotary drilling. Rotary percussive is further divided into down the hole (DTH), top hammer (TH) and COPROD. Please see Fig. 1. All rotary percussive drills are suitable for uniaxial compressive strength (UCS) of 100 to 500 MPa. On the other hand, rotary cutting drills are suitable for drilling upto 100 MPa. Hole diameter TH drills, DTH Drills, rotary crushing and rotary cutting varies from 25 to 225, 87 to 225, 127 to 375 and 25 to 375 mm respectively. Various parameters are considered while selecting drill machines. COPROD drill is best in terms of penetration rate, overall production capacity, low fuel consumption, economic drill string life and difficult rock condition. DTH drills perform worst in penetration rate, production capacity fuel consumption. Top hammer drills are not suitable for difficult working condition, maintaining straightness of holes, greater depth and also drill string life is poor. DTH holes are best for going to greater depth and straightness of hole can be maintained. In DTH drilling, there is a fear that DTH hammer may be lost in difficult rock condition.

Percussive drilling in mining industry is well known for more than last 80 years. Various researchers have identified physical and mechanical properties which impact

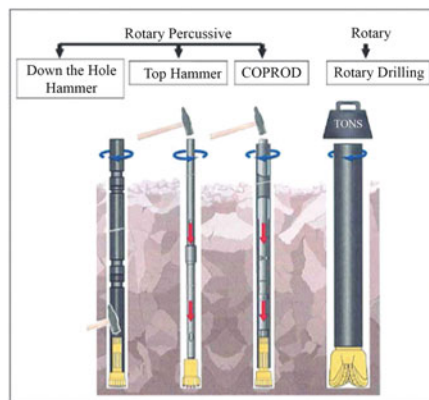


Fig. 1 Types of drilling used in mining industry

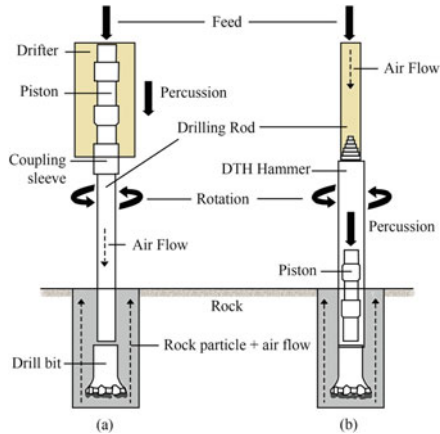


Fig. 2 Top hammer and DTH drilling process

rate of penetration in percussive drilling. Figure 2 shows method of top hammer (TH) drilling and down the hole (DTH) drilling. TH drilling method is used in civil and mining engineering projects mainly for blasting where drilling depth may vary from 10 to 20 m. Sometimes it may be extended upto 30 m depth. DTH dilling is used for mining as well as ground water purpose where depth of drilling may extend upto 400 m. Rocks are classified based on uniaxial compressive strength (UCS). Soft rock with UCS <20 MPA, medium hard rock with UCS between 20 to 50 MPA, hard rock with UCS between 50 to 120 MPA and very hard rock with UCS 120 to 200 MPA. Drilling rate is very high in soft rock and it drops down till hard rock. In very hard rock drilling rate drops down drastically. Various studies have been carried out on how the impact energy is transmitted from piston to drill bit and drill steel to rock for achieving desired efficiency in drilling [18, 19].

Drillability index for rotary drills is based on Compressive strength, Tensile strength, Point load index, Schmidt hammer rebound number, P- wave velocity, Elasticity, density, impact strength [20]. Scientists compared similarity of rebound of Schmidt hammer and DTH hammer piston and determined the relationship of quantum of rebound of the piston with the impact resistance index (K) [22]. There is a relationship established to predict bit wear based on rock abrasivity maximum feed rate and minimum specific energy [23, 24]. An investigation has been done on rate of penetration of top hammer with button bits and rock properties. Drilling rate is found to be based on Brazilian tensile strength, Compressive strength, Elasticity, density, impact strength, P- wave velocity, Point load index, Specific energy, Schmidt hammer rebound number [25]. On the other hand, rate of penetration can be correlated with Rock mass Drillability index, Compressive strength. Joint spacing, Joint filling, Joint dip, Rock texture, Mohs hardness [23, 24]. Models are also developed for estimation of Specific energy in DTH drilling [26]. Numerical model for drilling rate has been developed taking rock anisotropy and rock crack propagation as inputs [21]. [6] Models are also developed for drilling of rocks by finite element method based on energy transmission to rock. Scientists have predicted drilling rate based on

Specific energy, Compressive strength [27]. They have also predicted drillability by using machine learning algorithm, Artificial Neural Network (ANN) taking Impact strength index, Protodyakonov index, Shore hardness, Schmidt hammer rebound number and Rock wear factor as input parameters [22]. Liao et al., 2020 Intelligent methods have been used for prediction of rate of penetration based on Compressive strength, Revolutions per minute (RPM), thrust and flushing media.

Further various studies have been carried out on rate of penetration on different drill types [26, 27]. Specific energy consumption is important. Many researchers have studied rock mass classification systems for drillability [28–30].

2 Drill Performance

Any drill performance is measured with the following parameters.

1. Penetration Rate = Drill rod length/penetration time.
2. Drilling Rate = Hole depth (m)/(Penetration + rod change time).
3. Gross drilling rate = Total meterage/(a + b + c).

a = Penetration time,

b = Rod change time,

c = Shifting from one hole to another hole + minor repairs if any.

Performance of drilling Machine depends upon type of machine (TH/DTH), Operating pressure. Rod handling mechanism, hole diameter v/s design of drilling pattern including hole depth. Based on various studies it can be observed that drilling rate depends upon rock characteristics such as strength of rock (UCS, TS, PLI, SHRN), density, discontinuities, joint spacing, orientation, aperture.

Site Location of Limestone Mine: Construction aggregate is a backbone of construction of world class infrastructure in and around Bangkok in Thailand. Several limestone mines exist in the radius of 100 to 200 km from Bangkok. Selected limestone mine site supplies aggregates for construction purpose. There are also several limestone mines which are captive in nature supplying to manufacture cement. Limestone is sedimentary in nature. However, due to tropical climate, limestone is weathered and can be classified as fresh, slightly weathered, moderately weathered, highly weathered and completely weathered. Rock mass properties substantially vary from fresh to completely weathered limestone. Limestone has thickness of 100 m and six benches have been developed. Completely weathered limestone is found near the surface while fresh rock is found at depth. Completely weathered rock is soft in nature. Fresh rock is medium hard. Thus drilling and blasting efficiency drastically reduces from completely weathered rock to fresh limestone. Figure 3 shows drilling machine working at highly weathered limestone face.

Data Collection: Drilling is carried out at different locations from top bench to five benches below the surface. Limestone properties vary at each location. Various rock mass properties were considered based on various researchers. Measured output



Fig. 3 Drilling machine working at highly weathered limestone face

parameter consisted on ROP and five input parameters. Following method was adopted for collection of data sets of 113.

Density: Face samples from drilling face was collected and density was determined at laboratory.

RQD and GSI: Face where drilling was carried out was observed. RQD of the face was determined by scan line survey. GSI values are normally range of values. Mean value of GSI was used for the purpose of GSI as input parameter.

PLI: Samples were collected from drilling face. Representative sample was used to determine PLI from each face.

SHRN: At every drilling face, SHRN is determined.

ROP- Rate of penetration is determined for each hole separately. Hence, the values are cm/min (Table 1).

Table 1 Input and output data

	Density g/cc	RQD %	GSI	PLI MPa	SHRN Number	ROP cm/min
Min	1.91	10	15	0.1	2	12.4
Max	2.65	90	74	6.1	42	25.2
Mean	2.34	50.77	42.59	2.95	24.48	17.83
Standard deviation	0.20	22.52	16.00	2.04	12.56	2.70
Quartile1	2.22	34	30	0.95	13	15.6
Quartile3	2.49	72	55	4.725	34	19.4

3 Sensitivity Analysis

The sensitivity analysis of various parameters was performed in 1997. The results indicated that the relative influence of the various parameters on the neural network system was computed [31]. In order to apply this method, all of the data pairs were expressed in common L-space. The data pairs used to construct a data array L are defined as:

$$L = \{l_1, l_2, l_3 \dots, l_i, \dots, l_n\} \tag{1}$$

The elements l_i in the array L are a vector of length m as shown in Eq. 2:

$$l_i = \{l_{a1}, l_{a2}, l_{a3} \dots, l_{am}\} \tag{2}$$

Each pair can be trained to be a point in space where the coordinates are m - coordinates. The following equation explains the strength of the relation (r_{ab}) between the dataset L_a and L_b ,

$$r_{ab} = \frac{\sum_{k=1}^m x_{ak}x_{bk}}{\sqrt{\sum_{k=1}^m x_{ak}^2 \sum_{k=1}^m x_{bk}^2}} \tag{3}$$

4 What is Multivariate Regression?

Multivariate Regression falls in the category of supervised machine learning algorithm. It deals with multiple independent variables and a dependent variable. It gives a relationship between the feature (independent) variables and the target (dependent) variable which can then be used to predict the value of dependent variable for newer values of independent variables.

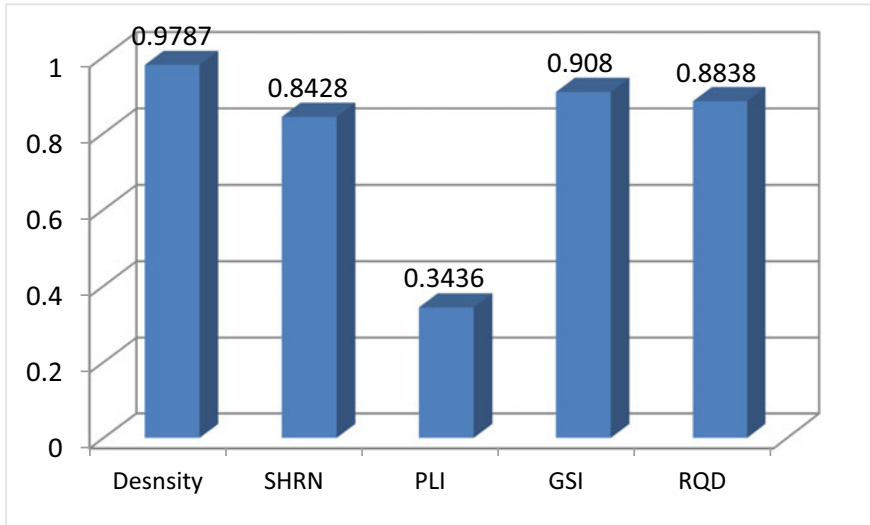


Fig. 4 Sensitivity analysis of input parameters

5 Mathematical Equation

A simple linear regression model fits a straight line between the dependent (y) and independent variable (x) i.e. $y = f(x)$. For multivariate regression, the generalized equation is,

$$y = b_0 + b_1.x_1 + b_2.x_2 + \dots + b_n.x_n$$

where n represents the number of independent variables, $\beta_0, \beta_1, \dots, \beta_n$ represents the coefficients for x_1, x_2, \dots, x_n independent variables respectively (Fig. 4).

6 Cost Function

In multivariate regression, the mean squared function is used as a cost function. It is equal to the sum of squared difference between the predicted value and the actual value divided by twice the number of training examples. Smaller the mean squared error, better is the model's performance.

It is given by the equation,

$$MSE = \frac{1}{2m} \sum (h_{\theta}(x)^{(i)} - y^i)^2.$$

7 Steps of Multivariate Regression Analysis

The key steps of Multivariate regression analysis are feature selection, normalizing of features, formulating the hypothesis and cost function, minimizing the cost function, obtaining hypothesis parameters, and testing the hypothesis function.

- **Feature selection**

The selection of features/variables is an important step in multivariate regression. All the relevant variables should be selected for better model performance.

- **Normalizing Features**

Normalizing features involves scaling of features. This maintains general distribution and ratios in data which helps in efficient analysis.

- **Formulating the hypothesis and cost function**

The hypothesis function is the relationship between the dependent and independent variables, The cost function calculates the mean deviation of predicted values from the actual values.

- **Minimizing the cost function**

An optimization algorithm such as Gradient descent is used to minimize the cost function.

- **Obtaining Hypothesis Parameters-**

Minimizing the cost function helps in obtaining the hypothesis parameters.

- **Test the hypothesis function-**

The hypothesis function can then be used to predict the value of dependent variable for newer values of independent variables.

8 Advantages of Multivariate Regression

Multivariate regression helps in understanding the relationships among the variables present in the dataset. It also helps in understanding the correlation between dependent and independent variables.

9 Disadvantages of Multivariate Regression

- It is complex and requires heavy mathematical calculations.
- Its output is not easy to interpret sometimes as it has loss and error output which are not identical.
- It works well only on larger datasets.

Multivariate regression comes into the picture when we have more than one independent variable and simple linear regression does not work. Real-world data involves

multiple variables or features and thus Multivariate regression analysis is required for better analysis.

10 BBO-ANN

In the year 2008, an algorithm called BBO (Biogeography Based Optimization) was evolved to solve global optimization problems [32]. It is based on migration of birds and animals between geographical locations. Since BBO is based on migration, which involves exploration as well as exploitation, it has been found to be a powerful technique. The biogeography phenomenon on which BBO is based are (a) arising of species (habitants), (b) movement of species from one location (habitat) to another and (c) extinction of species. This technique is becoming increasingly popular as an algorithm for resolving real-life optimization problems. The advantages of this technique is its stochastic distribution pattern, its efficiency of computation, flexibility and overall simplicity which does away with the need for objective function derivatives. This work would incorporate a review of 10 years of BBO research, summarized and organized for easy review and pointing out areas of research in future. Starting from the beginning and basics of BBO, various related algorithms and their modifications, hybrid-adaptations and their applications in math, science and engineering are discussed [33]. In this review, the network weights and biases of ANN are optimized by using BBO. In each habitat, the network weights and biases are proportional to the number of habitants or habitat features. The main process of BBO is that of migration, in which there is an I_m (immigration) and an E_m (emigration) going on at a specified rate. These migration operators determine the processes of BBO like exploration and exploitation. For example, based on the I_m (immigration) rate, the features of any specific habitat is modified by the BBO algorithm. Further, based on the respective E_m (emigration) rates, the BBO algorithm choses different habitats for one inhabitant migrating from one habitat to another. Thus, BBO is successfully deployed to convert local search and good governance to a global optimum. At first, the BBO algorithm develops a number of solutions based on habitat sizes, basically ANN generations, and with every run, the best fit of the habitat value is stored. This process is repeated until an acceptable level of fitness is reached or until the prescribed iteration number is reached. The fitness function of the BBO is represented by MSE (Mean-Square Error). Please see reference [34, 35] for a BBO Algorithm review in greater detail. The BBO has many parameters for initial setting, which would help improve the BBO-ANN model performance. Initially using a trial-and-error method, the BBO gave out values for the final parameters as follows:

(i) keep rate: 0.3, (ii) pMutation: 0.15, (iii) VarMin = 1, (iv) VarMax = 1, (v) Var Max = 50 (vi) Iteration = 100. Figure 5 shows the process flow chart of the proposed BBO-ANN.

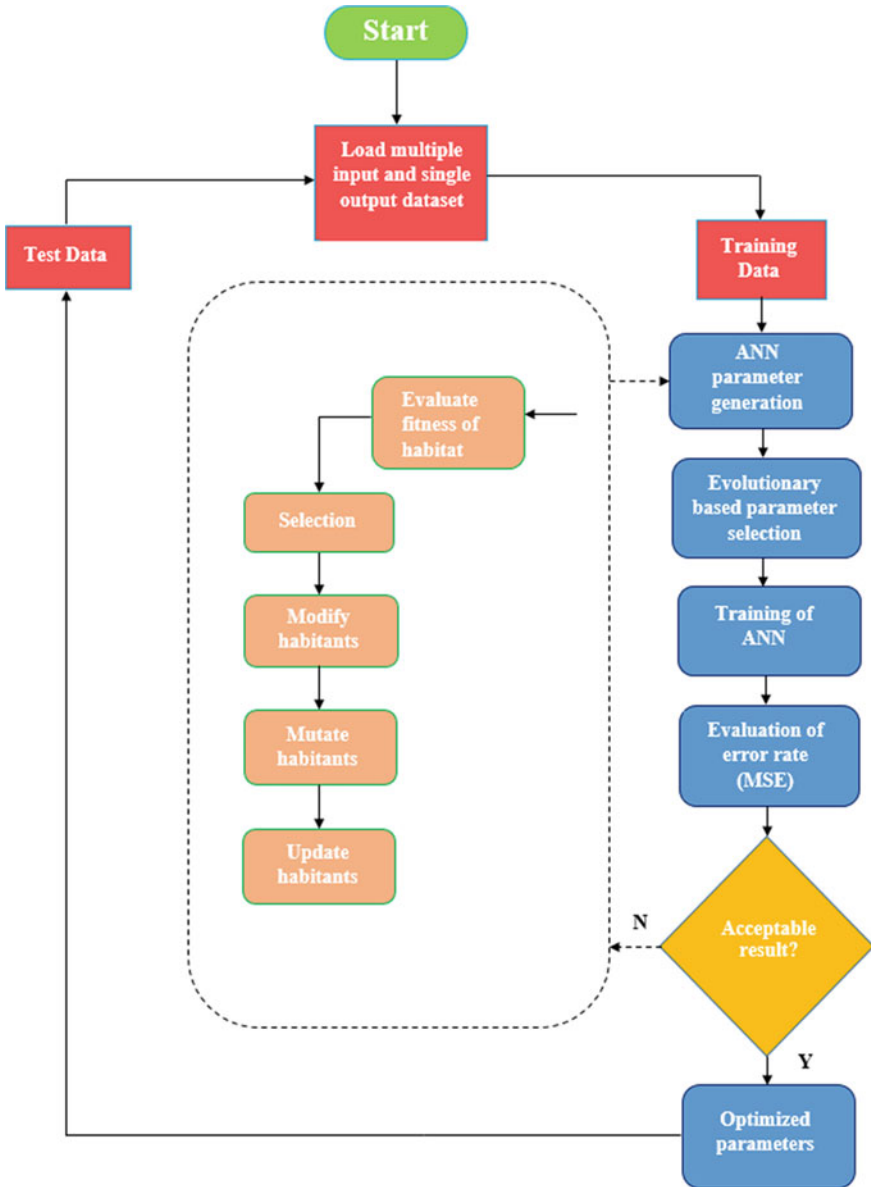


Fig. 5 Flow chart for BBO algorithm

It may be noted that in this study, different values for a number of different habitats were tested.

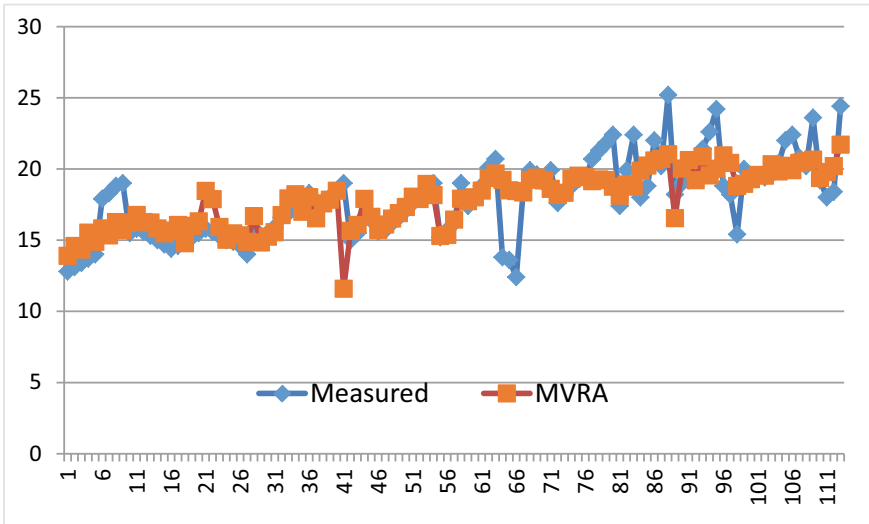


Fig. 6 Comparison of measured drilling rate v/s MVRA output

11 Discussion of Results

All input parameters (Density, SHRN, PLI, GSI and RQD) were processed using MVRA and BBO-ANN method and predicted output of drilling rate was compared with observed output (Density, SHRN, PLI, GSI and RQD). Figure 6 shows plot of measured drilling rate with MVRA output of all 113 data sets. Value R^2 with MVRA output showed 0.54. Further data set was divided into 88 data sets for training and 25 data sets for testing of data sets. Training data sets and testing data sets were processed with BBO-ANN model. Figure 7 shows comparison of measured drilling rate v/s output with BBO-ANN model for training data set. Figure 8 shows comparison of measured drilling rate v/s output with BBO-ANN model for testing data set.

Need for Future Research: In the past various research has been done based on various rock mass properties and comparing with ROP, drillability. Larger data base needs to be developed using different types of rock. Systematic way to select rock mass properties for each site needs to be developed and further research required for correlation with ROP.

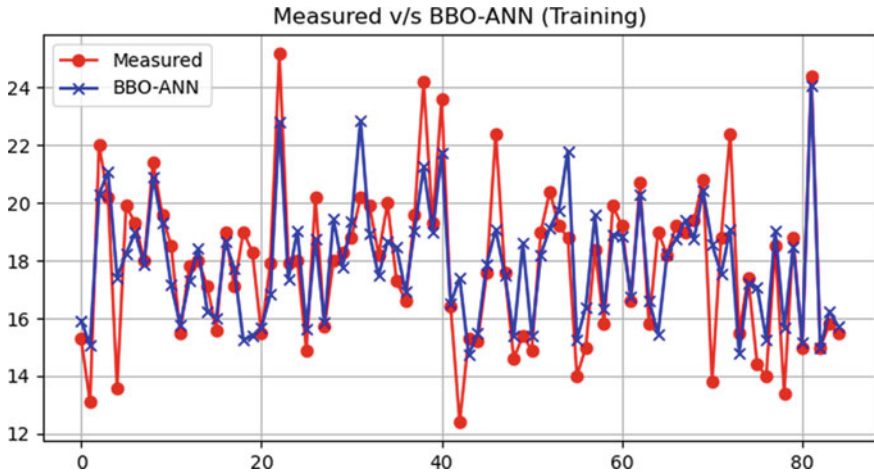


Fig. 7 Comparison of measured drilling rate v/s output with BBO-ANN model for training data set

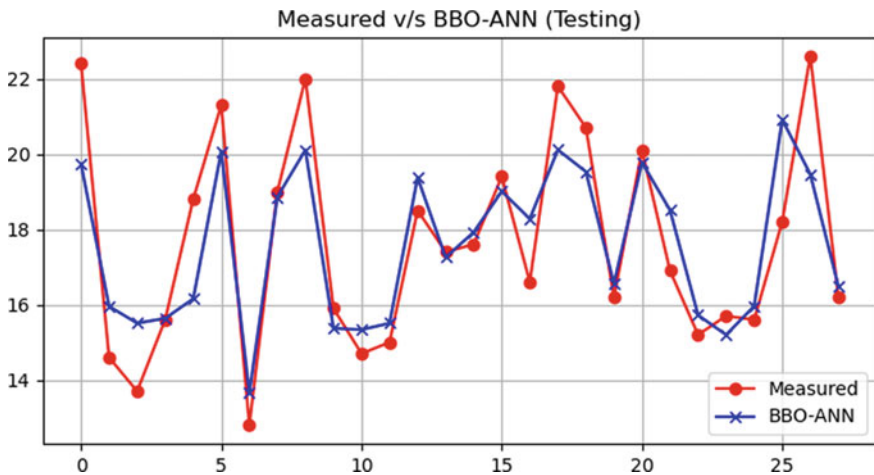


Fig. 8 Comparison of measured drilling rate v/s output with BBO-ANN model for testing data set

12 Conclusion

- (i) R^2 value with MVRA showed value of 0.54.
- (ii) R^2 value for training data set for BBO-ANN was 0.638 while R^2 value for testing data set for BBO-ANN was 0.761.
- (iii) BBO-ANN is the best model for this study.

References

1. Gokhale BV (2010) *Rotary Drilling and Blasting in Large Surface Mines*. CRC Press, Boca Raton
2. Abbaspour H, Drebenstedt C, Badroddin M, Maghaminik A (2018) Optimized design of drilling and blasting operations in open pit mines under technical and economic uncertainties by system dynamic modelling. *Int J Min Sci Technol* 28(6):839–848
3. Schunnesson H (1998) Rock characterisation using percussive drilling. *Int J Rock Mech Min Sci* 35(6):711–725
4. AyalaCarcedo F (2017) *Drilling and Blasting of Rocks*. Routledge, Milton Park
5. Cavanough GL, Kochanek M, Cunningham JB, Gipps ID (2008) A self-optimizing control system for hard rock percussive drilling. *IEEE/ASME Trans Mechatron* 13(2):153–157
6. Khodja M, Khodja-Saber M, Canselier JP, Cohaut N, Bergaya F (2010) *Drilling Fluid Technology: Performances and Environmental Considerations*. In: *Products and services; from R&D to final solutions*, pp 227–256. Sciyo Publications
7. Leighton J (1982) *Development of a correlation between rotary drill performance and controlled blasting powder factors*. University of British Columbia, Vancouver
8. Liu H, Yin KK (2001) Analysis and interpretation of monitored rotary blast hole drill data. *Int J Min Reclam Environ* 15(3):177–203
9. Beyglou A, Johansson D, Schunnesson H (2017) Target fragmentation for efficient loading and crushing—the Aitik case. *J South Afr Inst Min Metall* 117(11):1053–1062
10. Balamadeswaran P, Mishra AK, Singh DR, Sen P (2017) Effect of blast induced fragmentation on performance of hydraulic excavator: a case study. *NexGen Technol Min Fuel Ind (Volume I and II)*:333
11. Sinclair AJ, Blackwell GH (2006) *Applied Mineral Inventory Estimation*. Cambridge University Press, Cambridge
12. Haldar SK (2018) *Mineral Exploration: Principles and Applications*. Elsevier, Amsterdam
13. Khorzoughi MB, Hall R, Apel D (2018) Rock fracture density characterization using measurement while drilling (MWD) techniques. *Int J Min Sci Technol* 28(6):859–864
14. Tanguy DR, Zoeller WA (1981) *Applications of measurements while drilling*. Society of Petroleum Engineers. <https://doi.org/10.2118/10324-MS>
15. Hatherly P, Leung R, Scheduling S, Robinson D (2015) Drill monitoring results reveal geological conditions in blasthole drilling. *Int J Rock Mech Min Sci* 78:144–154
16. Ghosh R (2015) *Rock mass characterization using drill performance monitoring: problems, analysis challenges and limitations*. Lulea University of Technology, Lulea
17. Leung R, Scheduling S (2015) Automated coal seam detection using a modulated specific energy measure in a monitor-while-drilling context. *Int J Rock Mech Min Sci* 75:196–209
18. Hustrulid WA, Fairhurst C (1971) A theoretical and experimental study of the percussive drilling of rock, part I: theory of percussive drilling. *Int J Rock Mech Min Sci Geomech Abstr* 8(4):311–333
19. Hustrulid WA, Fairhurst C (1972) A theoretical and experimental study of the percussive drilling of rock, part IV: application of the model to actual percussive drilling. *Int J Rock Mech Min Sci* 9(3):431–442
20. Kahraman S, Balci C, Yazici S, Bilgin N (2000) Prediction of the penetration rate of rotary blast hole drilling using a new drillability index. *Int J Rock Mech Min Sci* 37:729–743
21. Li X, Rupert G, Summers DA, Santi P, Liu D (2000) Analysis of impact hammer rebound to estimate rock drillability. *Rock Mech Rock Eng* 33(1):1–13
22. Pflinninger RJ, Spaun G, Thuro K (2002) Prediction and classification tool wear in drill and blast tunneling. *Engineering geology for developing countries*. In: van Rooy JL, Jermy CA (eds) *Proceedings of 9th Congress of the International Association for Engineering Geology and the Environment*, 16–20 September. Durban, South Africa
23. Pflinninger RJ, Spaun G, Thuro K (2002) Predicting tool wear in drill and blast. *Tunnels Tunneling Int Mag* 1–5

24. Ersoy A (2003) Automatic drilling control based on minimum drilling specific energy using PDC and WC bits. *Min Technol* 112(2):86–96
25. Liao X, Khandelwal M, Yang H, Koopialipoor M, Murlidhar BR (2020) Effects of a proper feature selection on prediction and optimization of drilling rate using intelligent techniques. *Eng Comput* 36(2):499–510
26. Kahraman S, Bilgin N, Feridunoglu C (2003) Dominant rock properties affecting the penetration rate of percussive drills. *Int J Rock Mech Min Sci* 40:711–723
27. Izquierdo LE, Chiang LE (2004) A methodology for estimation of the specific rock energy index using corrected down-the-hole drill monitoring data. *Min Technol (Trans Inst Min Metall A)* 113:A225
28. Tanaino AS (2005) Rock classification by drillability. Part 1: analysis of the available classification. *J Min Sci* 41(6):541–549
29. Hoseinie SH, Aghababaei H, Pourrahimian Y (2008) Development of a new classification system for assessing of Rock mass Drillability index (RDi). *Int J Rock Mech Min Sci* 45:1–10
30. Hoseinie SH, Ataei M, Aghababaei H, Pourrahimian Y (2007) RDi-A new method for evaluating of rock mass drillability, In: *Proceedings of the 1st Canada-US Rock Mechanics Symposium, Vancouver, Canada*, pp 207–213
31. Yang Y, Zang O (1997) A hierarchical analysis for rock engineering using artificial neural networks. *Rock Mech Rock Eng* 30:207–222
32. Simon D (2009) Biogeography-based optimization. *IEEE Trans Evol Comput* 12(6):702–713
33. Ma H, Simon D, Siarry P, Yang Z, Fei M (2017) Biogeography-based optimization: a 10-year review. *IEEE Trans Emerg Top Comput Intell* 1(5):391–407
34. Haiping M, Simon D, Siarry P, Yang Z, Fei M (2017) Biogeography-based optimization: a 10-year review. *IEEE Trans Emerg Top Comput Intell* 1:391–40
35. Roy B, Singh MP (2019) An empirical-based rainfall-runoff modelling using optimization technique. *Int J River Basin Manag* 1–19

Influence of Freeze-thaw Cycles on the Velocity of Elastic Waves in Saturated Rock Specimens



Sahil Sardana, Rabindra Kumar Sinha, Mamta Jaswal, A. K. Verma, and T. N. Singh

Abstract The rock mass in the cold regions is affected by alternate cycles of snow-fall and normal weather. Water enters into the cracks in rocks during rainfall; subsequently, it freezes, leading to cracks enlargement due to the volumetric expansion of ice. This, in turn, weakens the rock structure leads to a reduction of the rock mass strength. Therefore, recurrent freeze-thaw cycles in hilly slopes result in instability in the rock slope. Several studies were carried out on the effect of freeze-thaw cycles on the various physical and mechanical properties of the rock. For most of the research, dry rock specimens were used to determine the physical and mechanical degradation of rock properties due to freeze-thaw cycles. However, limited research is available on saturated rock specimens. Therefore, in this paper, multiple freeze-thaw tests were performed on rock specimens in the laboratory and its effect on the velocity of elastic waves was observed. The results indicated a gain of about 13 to 34% in the velocity of elastic waves with respect to the repeated freeze-thaw cycle in the saturated rock specimens. This happens because the travel time taken by elastic waves is less for denser material than dry rock specimens.

Keywords Freeze-thaw · Elastic waves · Rock degradation

1 Introduction

Freeze-thaw mainly occurs in the region where temperature frequently fluctuates above and below the freezing point. In the freezing process, water inside the rocks turns into ice, and its volume expands by approximate 9%. It causes the expansion

S. Sardana (✉) · R. K. Sinha · M. Jaswal
Indian Institute of Technology (Indian School of Mines), Dhanbad, Jharkhand, India
e-mail: sahilsardana.ymca@gmail.com

A. K. Verma
Indian Institute of Technology (Banaras Hindu University), Varanasi, Uttar Pradesh, India

T. N. Singh
Indian Institute of Technology Bombay, Mumbai, Maharashtra, India

© The Author(s), under exclusive license to Springer Nature Singapore Pte Ltd. 2022
A. K. Verma et al. (eds.), *Proceedings of Geotechnical Challenges in Mining, Tunneling and Underground Infrastructures*, Lecture Notes in Civil Engineering 228,
https://doi.org/10.1007/978-981-16-9770-8_30

of pores, cracks and joints. During thawing, ice melts into water. Repeated freeze-thaw cycle can cause instability in the rock slopes due to the repeated volumetric expansion of water inside the cracks, pores and joints [1]. Winman [2] conducted freeze-thaw on four different rock types using two-temperature condition. After that, many researchers have reported degradation in physical and mechanical properties [3–5].

Elastic waves are classified into two types of waves; Primary or compressional wave (P-wave) and secondary or shear wave (S-wave). P-wave produces compressions and dilations while propagating through rock material. These are the fastest waves with a movement of a particle in the direction of wave propagation whereas, in the S-wave, the particle movement is the perpendicular to the direction of wave propagation [6]. P-wave and S-wave are known as an elastic wave as they deform the rock material elastically. The original shape and position of the rock re-gained after the wave passes through. The previous research reported that the sub-zero environment affects the velocity of P-wave (VP) and S-wave (VS). Ghobadi and Babazadeh [7] observed that the P-wave velocity for saturated rock specimen is higher than the dry rock specimen of the same rock material. King [8] reported an increase in velocity of P-wave and S-wave in the freezing bedrock. A similar result has been observed by Draebing and Krautblatter [9].

2 Specimen Description

The rock sample has been collected from the Solang Valley road, near Manali, Himachal Pradesh, India. The region comes under Indian Himalayan terrain. The one end of this road is connected to NH-3, Manali-Leh highway and the other end connects with the south portal of Rohtang tunnel which is the world's highest tunnel. A rock core of NX size has been prepared in the rock cutting lab (Fig. 1). A



Fig. 1 NX size specimens used in this study

total number of 18 specimens used in this study. The specimens have been divided into three groups namely A, B, and C representing 0, 10 and 20 freeze-thaw cycle respectively. Each group contains six specimens.

3 Experimental Procedure

Initially, specimens were submerged in the container filled with water prior to freezing. During the freezing, the container was placed in the freezer at $-20\text{ }^{\circ}\text{C}$ for approximate 12 h then the freeze specimens were taken out and placed in a water bath at $+30\text{ }^{\circ}\text{C}$ for thawing. Each freeze-thaw cycle requires a total 24 h i.e. 12 h of freezing and 12 h of thawing. The test was repeated for 20 freeze-thaw cycles. The velocity of P-wave and S-wave for saturated rock specimens were analyzed after the 0, 10, and 20 freeze-thaw cycles.

4 Results and Discussion

The influence of the freeze-thaw cycle on both P-wave and S-wave have been discussed below. All the rock specimens were saturated in the water for 48 h prior to the test.

4.1 Influence of Freeze-thaw on P-wave Velocity

The P-wave velocity of all the saturated rock specimens has been obtained with the help of a PUNDIT instrument and two transducers (Fig. 2). Both the transducers,

Fig. 2 P-wave PUNDIT instrument connected to a laptop and measuring the P-wave velocity of NX size specimens



have a frequency of 54 kHz and one of them act as a transmitter and another as a receiver. The P-wave velocity measurement has been carried out by the direct transmission method proposed by Kahraman [10]. It is the most sensitive methods as compared to other methods [11]. A gel has been used on the flat surfaces of the specimen to provide airtight contact between specimen and transducers. The velocity was calculated from the ratio of travel distance to travel time of the P-wave through the rock specimen as given in “Eq. (1)”.

$$V_P = \frac{d}{t_p} \tag{1}$$

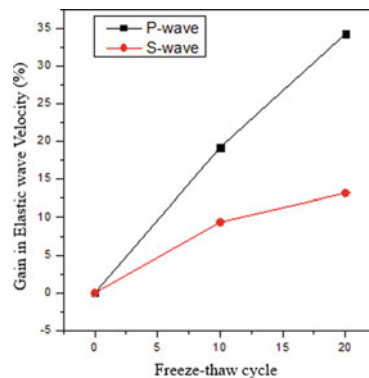
where V_P is the velocity of P-wave, d is the travel distance and t_p travel time taken by P-wave.

The P-wave velocities have been measured for group A, B and C before starting the freeze-thaw cycle. Average values of before and after the freeze-thaw cycle along with standard deviation (SD), coefficient of variation (CoV), and percentage of change from initial value are provided in Table 1. Average P-wave velocity for group A was measured 3631 m/s (i.e. before the freeze-thaw cycle). It has been increased from 3230 to 3850 m/s for group B (i.e. after 10 freeze-thaw cycles) and 3175 to 4262 m/s for group C (i.e. after 20 freeze-thaw cycles). Percentage change from initial value has also been calculated to account the effect of freeze-thaw on saturated rock specimens. The graph (Fig. 3) shows an increase in P-wave velocity has been observed with respect to the increase in a number of freeze-thaw cycles.

Table 1 P-wave velocities of saturated rock specimen after a different number of freeze-thaw cycle

Specimen group	Freeze-thaw cycle	Initial value	Final value	SD	CoV (%)	% Change
A	0	3631	3631	391	14	0
B	10	3230	3850	646	32.69	19.20
C	20	3175	4262	559	26.75	34.24

Fig. 3 Gain in velocities of P-wave and S-wave with respect to the number of freeze-thaw cycles



4.2 Influence of Freeze-thaw on S-wave Velocity

The S-wave velocity has been measured for saturated rock specimens with the use of sonic viewer 170 (Fig. 4) connected to the two transducers. Similarly to the PUNDIT instrument, these transducers act as a transmitter and receiver and have a frequency of 33 kHz. The saturated rock specimen has been placed between these two transducers. S-wave has been transmitting from one transducer through the specimen and received at another transducer. The velocity of S-wave has been measured by the ratio of travel distance to the travel time.

$$V_S = \frac{d}{t_s} \tag{2}$$

where V_S is the velocity of S-wave, d is the travel distance and t_s travel time taken by S-wave.

The S-wave velocities have been measured for all three groups (A, B and C) before starting the freeze-thaw cycle. Average values of before and after the freeze-thaw cycle along with standard deviation (SD), coefficient of variation (CoV), and percentage of change from initial value are provided in Table 2. For group A, the average S-wave velocity has been measured to 1.92 km/s. For group B, it has been found to be increased from 1.71 to 1.81 km/s. Similarly, in group C, it has been increased from 1.67 to 1.89 km/s. It has been observed that as the number of freeze-thaw cycle increases, the S-wave of the saturated rock specimen increases (Fig. 3).

Fig. 4 Sonic viewer 170 for measuring of S-wave velocity



Table 2 S-wave velocities of saturated rock specimen after a different number of freeze-thaw cycle

Specimen group	Freeze-thaw cycle	Initial value	Final value	SD	CoV (%)	% Change
A	0	1.92	1.92	0.42	25.70	0
B	10	1.71	1.87	0.32	23.56	9.36
C	20	1.67	1.89	0.27	15.38	13.17

5 Conclusion

The region where the temperature falls below zero degrees, freeze-thaw weathering occurs. The rock sample in this study was collected from the region where the slopes are covered under the snow for four to six months in a year. Repeated freeze-thaw cycles weakened the rock strength. The following conclusion can be drawn from this study:

- i. The P-wave velocity for saturated rock specimens has a tendency to increase with an increase in the number of freeze-thaw cycles. Approximate 34% rise has been observed in VP after 20 freeze-thaw cycles.
- ii. The S-wave velocity also indicates the same tendency as the P-wave variation shows. The gain of 13.17% has been observed in the VS with respect to repeated freeze-thaw cycle (after 20 freeze-thaw cycles).

The repeated freeze-thaw cycle causes volumetric expansion [12]. As the water freeze into ice, it expands about 9% of its volume which causes expansion of cracks and pores. Further, it has been observed that the time taken by the elastic waves through the saturated rock specimen were less as the travel medium become denser which leads to the increase in velocity of the elastic waves. However, it may be noted that the decrease in both P-wave and S-wave have been reported by many researchers for dry rock specimen.

Acknowledgements The authors would like to thank Rock Mechanics Laboratory, Mine Ventilation Laboratory and Rock Excavation Laboratory, IIT(ISM) Dhanbad, India for specimen preparation, to conduct freeze-thaw and elastic-wave testing on rock specimens.

References

1. Park J, Hyun CU, Park HD (2015) Changes in microstructure and physical properties of rocks caused by artificial freeze-thaw action. *Bull Eng Geol Env* 74(2):555–565
2. Wiman S (1963) A preliminary study of experimental frost weathering. *Geogr Ann* 45(2–3):113–121
3. Sardana S, Sinha RK, Verma AK, Singh TN (2022) Investigation into the freeze-thaw induced alteration in microstructure and deteriorative responses of physico-mechanical properties of Himalayan rock. *Bull Eng Geol Environ* 1–14
4. Sardana S, Sinha RK, Jaswal M, Verma AK, Singh TN (2020) Instability in Himalayan rock slope under recurrent freeze-thaw. In: EGU General Assembly Conference Abstracts, p 9058
5. Li J, Zhou K, Liu W, Zhang Y (2018) Analysis of the effect of freeze-thaw cycles on the degradation of mechanical parameters and slope stability. *Bull Eng Geol Env* 77(2):573–580
6. Jimeno CL, Jimeno EL, Carcedo FJA (1995) *Drilling and Blasting of Rocks*. Balkema, Rotterdam
7. Ghobadi MH, Babazadeh R (2015) Experimental studies on the effects of cyclic freezing-thawing, salt crystallization, and thermal shock on the physical and mechanical characteristics of selected sandstones. *Rock Mech Rock Eng* 48(3):1001–1016
8. King MS (1977) Acoustic velocities and electrical properties of frozen sandstones and shales. *Can J Earth Sci* 14(5):1004–1013

9. Draebing D, Krautblatter M (2012) P-wave velocity changes in freezing hard low-porosity rocks: a laboratory-based time-average model. *Cryosphere* 6(5):1163–1174
10. Kahraman S (2002) Estimating the direct P-wave velocity value of intact rock from indirect laboratory measurements. *Int J Rock Mech Min Sci* 39(1):101–104
11. Yavuz H, Altindag R, Sarac S, Ugur I, Sengun N (2006) Estimating the index properties of deteriorated carbonate rocks due to freeze-thaw and thermal shock weathering. *Int J Rock Mech Min Sci* 43(5):767–775
12. Matsuoka N, Murton J (2008) Frost weathering: recent advances and future directions. *Permafrost Periglac Process* 19(2):195–210

Effect of Firing Pattern on Rock Fragmentation in Surface Mine Blast-A Case Study



Lalit Singh Chouhan, A. K. Raina, and V. M. S. R. Murthy

Abstract Mine Mill Fragmentation System consists of several unit operations like drilling, blasting, excavation, loading and transportation, crushing etc. Blasting plays a vital role on cost of other unit operations in the system as fragmentation determines the down the line performance. A proper blast not only fulfills the material handling requirements, but also reduces the other unit operation costs viz. loading and hauling, crushing, wear and tear of loading and hauling machines and blast induced ground vibration and air overpressure. The core of the system thus is fragmentation and proper muck profile. A good blast fragmentation can be achieved by defining the blast design variables like burden, spacing, hole depth and stemming length through proper engineering. Away from engineering of the blast design variables optimum fragmentation can be achieved by selecting proper firing pattern. A case study is presented in this paper demonstrating that V-type firing pattern improves fragmentation and provides a reliable throw distance of the muck in comparison with other firing patterns.

Keywords Blasting · V-firing pattern · Fragmentation · Throw

1 Introduction

A continuous blast fragmentation analysis plays a vital role in the evolution of efficiency and productivity of quarry blast. If blast fragmentation is not of required

L. S. Chouhan (✉)

Mining Department, Kotputli Cement Work, UltraTech Cement Limited, Jaipur, India
e-mail: chouhan4569@gmail.com

A. K. Raina

CSIR-Central Institute of Mining and Fuel Research, Nagpur, India

V. M. S. R. Murthy

Department of Mining Engineering, Indian Institute of Technology (Indian School of Mines),
Dhanbad 826 004, India
e-mail: vmsrmurthy@iitism.ac.in

size, it can increase production cost and delay in quarry progress due to unnecessary secondary blasting which is a safety concern in blasting or require use of rock breakers to reduce the size of rock boulders which is costly. To reduce the production cost, blast design should be revisited to match the cost of the mine mill fragmentation system (MMFS). The drilling and blasting cost in open pit mine represent 15–20% of the total mining cost [1, 3, 6]. The cost of the blasting unit operation has inverse relationship with the cost of the loading, hauling and crushing. This calls for optimization of fragmentation in order to optimize the cost of MMFS.

However, away from increasing the cost of the blasting unit may not always be in favour of the system, if the same does not reduce the cost of the other unit operations. There are methods that can be used to improve the fragmentation like change in firing sequence. This paper focuses on the use of V-pattern of firing to improve the fragmentation with the help of inter-fragment collision process.

2 Blast Mechanism

It is known that explosive in a blast hole detonate rapidly and convert into gases of huge volume having high pressure and high temperature. This rapid change in volume from solid to gas generated a detonation pressure all around the blast hole. The pressure wave travels all around the blast hole and is transmitted through the rockmass. When this pressure wave (compressive wave) reaches to the free face, it returns back and resulting in tensile stresses. These continuous interceptions of waves working on the rock in opposite direction [5] result fragments the rock. Since, the tensile strength of the rock is nearly 10 times lower than the compressive strength of the rock [4], when the force applied by the tensile wave is higher than the tensile strength of the rock, the rock breaks.

3 Effect of Firing Patterns on Fragmentation

If a blast face having two free faces, then diagonal firing pattern (Fig. 1) provides two free faces for each blasthole and good fragmentation is achieved. However, if

Fig. 1 Diagonal firing pattern provides two free faces

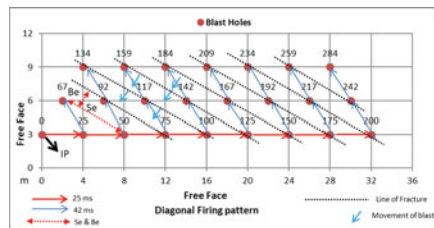
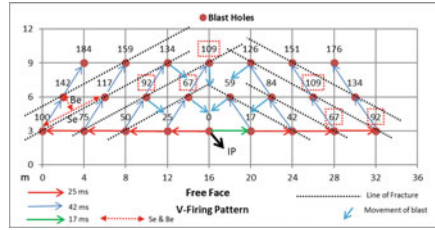


Fig. 2 V-type firing pattern gives better results with one free face



blast face is having only one free face, then V-firing pattern (Fig. 2) provide two free faces for each of the hole results good fragmentation achieved because in this type of firing pattern blast is initiated at the middle of the face and splits the blast into two parts which provide successive free faces for each row and holes [2].

In order to study the impact of V-type firing pattern, a study was conducted in a limestone mine where the rock is very strong and crystalline in nature.

4 Area of Study

The study was conducted in a limestone mine near Jaipur, India. The data pertaining to different aspects of the mine is compiled in Table 1. Blast data was generated from the mine using different firing patterns.

Table 1 Salient details of the test site

Sl. No.	Component	Value/description
1.	Geology	Precambrian Delhi Super Group
2.	Topography	Relief of about 75 m
3.	Lithology	Limestone etc.
4.	General strike direction	NE-SW
5.	Compressive strength of limestone	80 to 110 MPa
6.	Production	6 MTPA
7.	Explosive	ANFO density of explosive = 800 kg/m ³ Average velocity of the detonation of 3700 m/s
8.	Firing	Shock tube system and delay sequencing of 17, 25 and 42 ms
9.	Blast pattern	Staggered
10.	Loading operation	Shovel and backhoe
11.	Bench height	Up to 10 m
12.	Burden, spacing, stemming, drill diameter	2.75 to 3.0 m, 4.0 m, 2.50 to 3.50 m and 115 mm, respectively

The data thus generated was analysed further for impact of the firing patterns on the fragmentation.

5 Analysis of the Data Generated

Twenty-one full-scale blasts were conducted in the above limestone mine with monitoring of the blast design variables like burden, spacing and stemming, bench height, specific charge, and firing patterns. Summary of the data generated thus is presented in Table 2.

Here *L* – Line pattern, *D* - Diagonal Pattern and *V* – V-type pattern

The plot of three firing patterns viz. line, diagonal and V-pattern (Fig. 3) shows that there is strong influence of the firing pattern on the fragment size obtained. It

Table 2 Field data of blast variables monitored during the trials

Sl. no.	Burden (m)	Spacing (m)	Stemming (m)	Bench height (m)	Specific Charge (Kg/m ³)	Mean fragmentation size (K ₅₀)	Type of firing pattern	Throw (m)
1	2.86	3.95	3.5	9.84	0.45	0.48	L	35
2	2.89	3.88	3.5	8.85	0.41	0.47	L	36
3	2.84	3.98	3.5	9.09	0.41	0.46	L	35
4	2.8	4	3.38	9.82	0.43	0.46	L	38
5	2.82	3.83	3.04	9.15	0.49	0.45	L	40
6	3	4	2.77	9.5	0.38	0.44	L	45
7	2.89	4	3.45	9.85	0.41	0.4	L	35
8	3	4	3.13	8.88	0.44	0.38	D	25
9	2.85	4	3.35	8.85	0.47	0.31	D	25
10	2.77	4	3.29	8.55	0.45	0.36	D	25
11	2.85	3.91	2.95	7.3	0.43	0.35	D	22
12	3.02	3.94	3.31	8.11	0.45	0.29	D	30
13	2.95	4	2.5	9.85	0.45	0.28	D	30
14	2.91	3.99	2.93	6.14	0.43	0.28	D	28
15	2.87	4	2.5	8.55	0.43	0.26	V	14
16	2.84	3.5	2.5	8.63	0.56	0.26	V	15
17	2.72	3.5	2.5	9.79	0.6	0.24	V	15
18	2.7	3.93	2.5	9.56	0.52	0.22	V	16
19	2.78	3.89	2.5	9.66	0.47	0.19	V	15
20	2.77	3.92	2.5	9.54	0.5	0.19	V	12
21	2.75	3.88	2.5	9.91	0.53	0.21	V	16

Fig. 3 Mean fragmentation size (m) Vs firing patterns

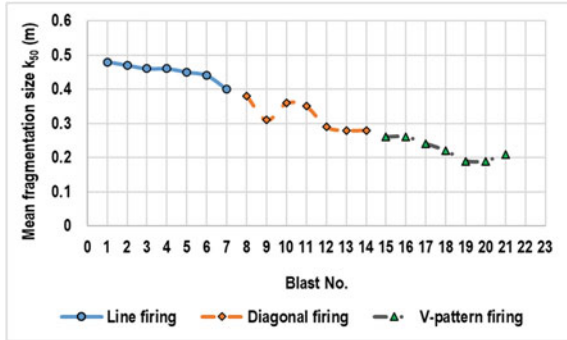
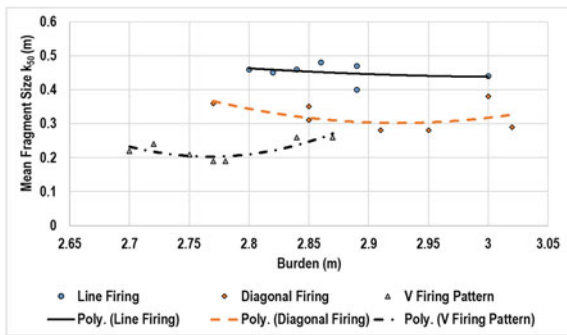


Fig. 4 Mean fragmentation size (m) Vs burden (various firing patterns)



is also evident that the fragmentation in case of line and diagonal patterns is coarse. However, the minimum fragment sizes are obtained in the V-type firing pattern.

Figure 4 revealed that with the increase in burden the relationships between mean fragment size of the blast and burden are quite undefined. In contrast, the V-type firing pattern shows a marked increase with increase in burden up to 2.85 m with asymptotic nature beyond that, and is logical in nature.

In addition to fragmentation, the throw of the broken rock was also evaluated. As can be seen from Fig. 5, the throw in case of diagonal firing is more than that observed in case of other patterns and varies over a wide range. The optimum throw of the muck is however obtained in case of V-type firing pattern.

One important observation is that the throw of the muck is similar in all blasts in case of V-type firing patterns. This points to the fact that the pattern is better suited to the mine in which trial blasts were conducted.

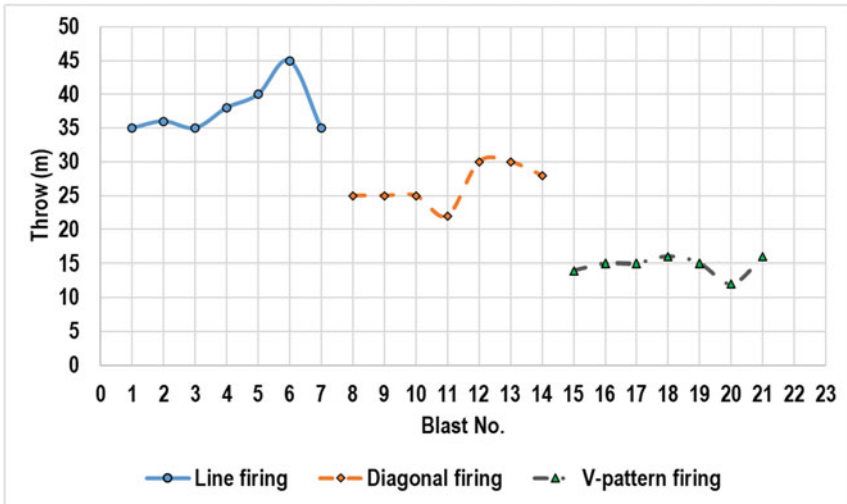


Fig. 5 Throw (m) Vs various firing patterns

6 Results and Discussion

There are many variations that can be deployed so far as firing pattern in blasting is considered. If 'V' pattern is said to further the process of breakage during the firing of the blast, it must satisfy some conditions enumerated below.

- The velocity of the fragments moving in opposite directions must be same so that the fragments meet during the flight in their trajectory path.
- The velocity of the fragments should be so that these carry sufficient force to further fragment the rock.
- The strength of the material should be such that the impact of the two fragments exceeds it and hence breaks it further.
- The alignment of the colliding particles should be in a particular direction so as to facilitate the collision breakage.
- It is important to mention that there are several doubts in the hypothesis which need to be answered.
 - One of the questions is whether the fragments achieve such velocities during the process and even if the same is achieved what is the mechanism of breakage?
 - Whether the breakage is in compression or in tension is still unanswered as in-flight collision is regarded as a compressional one. The forces available at the time of collision may not be sufficient to further fragment the rock.

7 Conclusions

- Initial results indicate that the mean fragment size and throw reduce significantly in V-Pattern.
- There is a complex relationship in burden, spacing, stemming and with the mean fragment size.
- The breakage due to in-flight collision is still not properly understood and needs to be explored further.
- A higher order analysis is required for developing rational models.

Acknowledgements The paper forms a part of the Ph.D. work of the first author. The authors are thankful to their respective employers for their permission to publish the findings. Help of several persons in conducting the study is duly acknowledged.

Conflict of Interest The authors declare that there is no conflict of interest to disclose.

References

1. Afeni TB (2009) Optimization of drilling and blasting operations in an open pit mine-the SOMAIR experience. *Min Sci Technol* 19(6):736–739. [https://doi.org/10.1016/S1674-5264\(09\)60134-4](https://doi.org/10.1016/S1674-5264(09)60134-4)
2. Chouhan LS, Raina AK (2015) Analysis of in-flight collision process during V-type firing pattern in surface blasting using simple physics. *J Inst Eng (India) Ser D* 96(2):85–91. <https://doi.org/10.1007/s40033-015-0076-6>
3. Da Gama CD, Jimeno CL (1993) Rock fragmentation control for blasting cost minimization and environmental impact abatement. *Rock Fragn Blasting* 273–280
4. Dey K, Sen P (2003) Concept of blastability-an update. *Indian Min Eng J* 42(8–9):24–31
5. Duvall WI, Atchison TC (1957) *Rock Breakage by Explosives*
6. Shim HJ, Ryu DW, Chung SK, Synn JH, Song JJ (2009) Optimized blasting design for large-scale quarrying based on a 3-D spatial distribution of rock factor. *Int J Rock Mech Min Sci* 46(2):326–332. <https://doi.org/10.1016/j.ijrmms.2008.07.006>

Investigations into the Influence of Intact Rock and Machine Properties on Exploratory Coring Rate for Aiding Selection of Coring Machine



P. Alam, A. K. Raina, and V. M. S. R. Murthy

Abstract A mineral project possesses important processing routes as it moves from discovery to technical and maintenance of the exploration and exploitation costs. The central thesis of studies in exploration is to increase the drilling optimization facilitating the selection of equipment and technology used to achieve highest drilling rate. A comprehensive survey of literature for prefeasibility stage of projects is presented to provide reliable and quantifiable options. The review classifies literature on exploratory coring rate into multiple classes and sub classes and identifies the nature of smart, connected systems offering new inter-operability in system of drilling processes. The research and development in this arena is resulting in focused on increasing the coring rate drilling efficiency without compromising safety and environment laws. A multi-disciplinary engineering approach in geophysics, sampling, weight on bit (WOB), machine selection, and flow rate (FR) on the rate of penetration (ROP) are the need of the hour to augment the ever increasing demand of mining industries.

Keywords Exploratory coring · Rate of penetration · Intact rock · Machine variables

1 Introduction

Multiple civil and mining applications are available in the field of mining for the purpose of mineral extraction using drilling, blasting cutting and mechanical excavations. India, over a period of centuries had coal, copper, zinc, lignite, lead gold,

P. Alam

Mineral Exploration Corporation Limited, Seminary Hills, Nagpur, Maharashtra 440 006, India

A. K. Raina (✉)

CSIR-Central Institute of Mining and Fuel Research, Nagpur Research Centre (Mining Technology), Telangkhedi Area, Civil Lines, Nagpur, Maharashtra 440 001, India
e-mail: rainaji@cimfr.nic.in

V. M. S. R. Murthy

Indian Institute of Technology (ISM), Dhanbad, Jharkhand 826 001, India

© The Author(s), under exclusive license to Springer Nature Singapore Pte Ltd. 2022
A. K. Verma et al. (eds.), *Proceedings of Geotechnical Challenges in Mining, Tunneling and Underground Infrastructures*, Lecture Notes in Civil Engineering 228,
https://doi.org/10.1007/978-981-16-9770-8_32

489

diamond and iron deposits and precious gemstones spread over a landmass of 3.2 million km [www¹]. The Geological Survey of India continued exploratory studies for mineral discoveries, post independence, in the period after 1947, contributing to India's infrastructural development. A scrutiny of the research over the period has revealed that India had detailed exploration in less than 10% of the total geological latent area. The 'Digboi Oil field' in Upper Assam (1867) was a major event in the history of exploration in India. This event triggered a new wave of enthusiasm for the search of oil and minerals, not limited to dense jungles and river-valleys, of the North-East viz Assam, but also in parts of pre-historic geological past and mineral potential of the country. Exploratory drilling is, thus, became an area of great interest and is up for a comprehensive discussion.

This brackets exploration in a unique position in so far as probable realization of geological location which promise oil/gas, precious metals and ultra-deep offshore sediments. Explorative investigation of sub-surface generates results by measuring at or near earth's surface, that are determined through the internal distribution of physical and chemical properties of the ores encountered. During exploration phase structural features such as fracture networks, restoration of core samples can give valuable data about identifying potential locations for drilling. Conventional exploratory core drilling methods were repeatedly challenged when exposed to extreme unsettling weather conditions. Over the years with the help of remote sensing applications, real time analysis, human machine interface, mobile & compact rigs, comparative differences in drilling were observed through strategic planning. From the earliest beginning of the contemporary times, development with drilling has been refined via four phases of industrialization [www.²]. From cable tool drilling we have arrived at integrated programme techniques today. Extending the same in the field of explorations in different lithologies with significant machine resources, several discoveries were encountered as explained in Fig. 1.

In the early stages, cabletool/ percussion drilling was the sole method available to drill a bore hole by delivery blows repeatedly to the rock using bits. Reverse circulation drilling, patented 30 years post introduction of cabletool drilling, was introduced exhibiting several innovations over the previous method. In the year of 1863, diamond core drill was invented leading to an expensive use of this technology. At the twilight of nineteenth century and beginning of the 20th, there were several incremental developments to original design and technology of the original technologies. Pioneering research came to place in response to a surge in exploration globally. This led to the creation of more cutting-edge equipments' which were utilized by core technology drilling companies to enhance their operations, further. The impact of core drilling to the exploration and merits and limitations of it to the integrity of mineral engineering thus need to be highlighted.

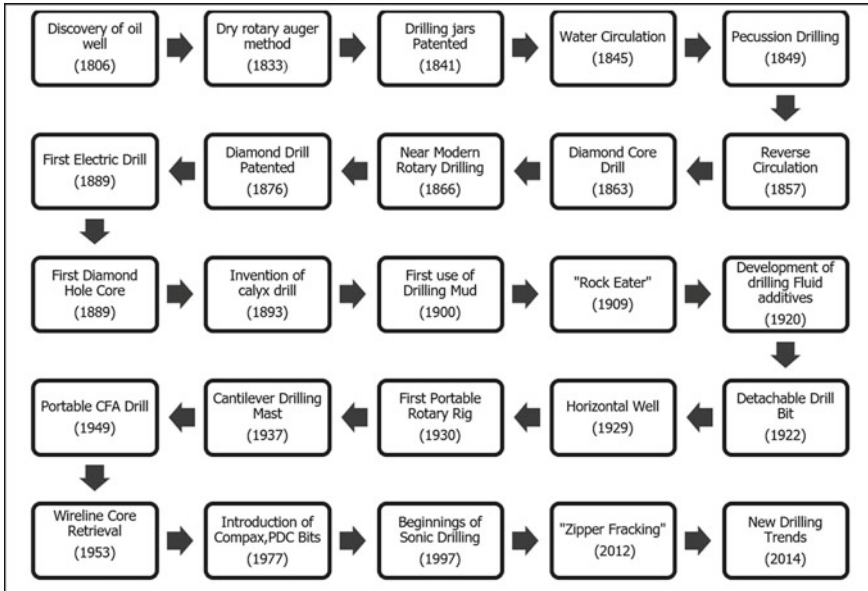


Fig. 1 Exploratory drilling timeline

2 Classification of Literature Review

Prominent literature on the enterprise core drilling can be grouped into four major categories as explained in this section (Fig. 2). It is evident from the published literature that researchers have detailed different aspects of drilling, ranging from geology, machine variables and operating conditions along with some future trends as described in detail in Fig. 2 below.

Physical and mechanical rock characteristics are of great importance in exploration, cutting-drilling and other rock working process. Their classifications are centered on different geology impacting the drilling rate. Yavuz et al. [68] suggested that the mechanical behaviour of the rock materials is significantly different under dynamic loading conditions. The literature review considers the technical issues associated with core drilling and methods for development and adaptation in drilling equipment and systems. The performance and efficiency of core drilling machines is of importance, not only in mineral exploration but in oil and gas, civil and geotechnical engineering as well. The rate of penetration, also known as ‘drillability’ is amongst the most critical parameters. It depends primarily on the formation hardness while also determining necessary value for the cost estimation and the project planning. Bilim [10] proposed that the prediction of penetration rate is very important in rock drilling. The purpose is to choose a suitable drill machine for drilling a particular rock and to find a suitable technology to achieve the best results while carrying out the drilling. Balci et al. [8] advised that the cutting tests would serve a basis

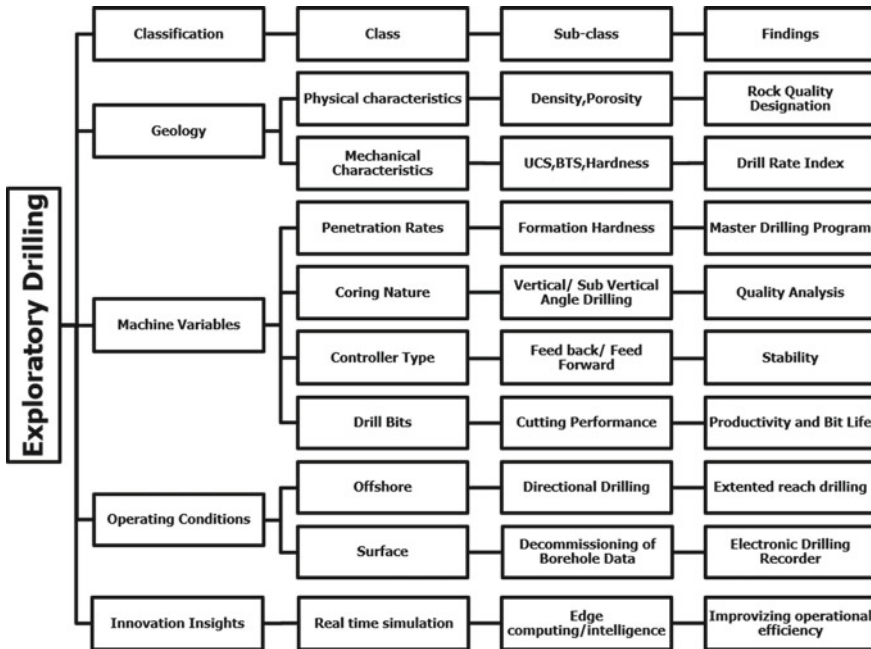


Fig. 2 Classification of exploratory drilling

to predict performance of mechanical miners to be used in hyperbaric conditions for which drill bit types are developed on cutting performance for high productivity. Modern analyses are ongoing for using of ultrasonic waves, high frequency electricity or thermal energy for breaking rock in situ. ASTM - American Society for Testing and Materials [5] recommended that RQD can be measured with a high level of accuracy with 3-D data. Further studies include geotechnical investigation, reliability and maintainability problems of machines and integrated automation technologies.

3 Influence of Geology on Drilling Operations

The early studied were focussed on the drillability of rocks and dependence of drilling rates on the mechanical and physical rock properties. The purpose of the proposed literature being to describe a few of the most significant researches, keeping in mind the historical perspectives, in order to provide an understanding of the shifting trends in several aspects and provide a brief review of the same.

Several authors have detailed the influence of physical, mechanical and mineralogical properties on rock penetration rate and drillability of the rock. Some of them are elemental rock characteristics that are conventionally studied in rock mechanics. , Specific energy and rate of penetration are some of the main experimental indexes

Table 1 Literature survey on drilling

Citations	A	B	C	D	E	F	G	H	I	J
Dickson et al. [18]	✓				✓	✓	✓	✓		
Simon (1956)					✓			✓		
Gstalder et al. [29]			✓				✓	✓		
Franklin [25]	✓			✓	✓	✓		✓		✓
Hustrulid et al. [35]		✓								
Tandanand and Unger [61]		✓			✓	✓	✓			✓
Onyia [48]	✓			✓	✓		✓			✓
Wang [65]				✓	✓	✓	✓	✓		✓
Ersoy and Waller [24]		✓			✓	✓	✓	✓		✓
Kahraman [35]					✓	✓				✓
Altundag [4]		✓			✓	✓				✓
Atici and Ersoy [8]		✓			✓	✓				✓
Rajesh Kumar et al. [49]					✓	✓				
Shreedharan et al. [56]				✓	✓				✓	
Ataei et al. [6]	✓		✓		✓	✓			✓	
Taheri et al. [58]				✓	✓				✓	✓
Krupa et al. [41]				✓	✓				✓	✓
Dwivedi et al. [20]	✓	✓		✓						✓
Kumar et al., [41]				✓	✓	✓				

A- Porosity, B- specific energy, C- drilling rate index, D- density, E- Compressive strength, F- tensile strength, G- Young’s modulus, H- hardness, I- P-wave velocity, J- Penetration Rate

indicating rock drillability. To put it concisely all the parameters mentioned have been investigated by various researchers in pursuit of improvement of penetration rate as have been compiled in Table 1.

Geological studies of the earth materials and mineral reserves provide data and information on structures and processes that have evolved over time by means of natural process. A common practice in the industry is to establish an index that can represent formation quality parameters by analysing the correlation between drilling parameters and rock-soil physical parameters from the perspective of mechanics and energy, obtained by a large amount of drilling of the rock and soil mass [51, 37, 32]. Since coring works at a microscopic level, researchers also use x-ray diffraction and accelerated mass spectrometry to determine the nature of minerals. Usually, appraisal seismic is completed by the natural resource’s agency, so as to supply initial information about the lithology and geology of the subterranean world. Seismic is the technique used by the geologists in the attempt of describing the rock layers and sediments along the Earth’s crust. From the literature survey, compressive strength, tensile strength, density and hardness have a profound implication on coring rates. Thus, such studies, provide greater insights into the properties such as lithology,

porosity, clay volume, grain size, water saturation, permeability and many other. All of these properties are essential for reservoir formation evaluation [42].

Density log contributes to direct/indirect measurement of penetration rates as it indicates electron density of formation. This method uses radioactive sources to generate gamma rays that collide with the electron in formation, thus losing energy. Detectors installed in the assembly measure the intensity of back scattered gamma rays, related to electron density of formation. The Electron density gives a measure of bulk density that varies with lithology, porosity, density and saturation of fluid in pores. Higher the gamma ray reflects greater the porosity of the rock. The petro-physical evaluation of log and core data provides main properties such as lithology, porosity, clay volume, grain size, water saturation, permeability and many others, which are essential for the evaluation of the reservoir formation [52, 48, 53].

It is noted that drilling technique relies upon distinctive geology. Using suitable method(s), a system of most logical cataloging can be employed based on form of rocks and possible problems can be identified as specified on mode of energy application and hence leading to identification of the proper penetration method as mentioned in Table 2.

Entire activities regarding drilling in such locations have primary involvement of geological studies, well logging and laboratory services. Drilling activities at mine sites are multiform and are used for two main functions, exploration which aims to obtain very minute data about the formations below ground surface and the production to facilitate the ore extraction. In essence, a favourable combination

Table 2 Influence of geology on drilling

Drilling method selection		Percussion drilling	Hand auger	Jetting	Sludging	Rotary percussion	Rotary drilling with flush
Gravel	Unconsolidated formations	✓!	×	×	×	✓!	×
Sand		✓!	✓	✓	✓	✓!	✓
Silt		✓!	✓	✓	✓	✓!	✓
Clay		✓slow	✓	!	✓	✓slow	✓
Sand with pebbles		✓!	×	×	×	✓!	×
Shale	Low to medium strength formations	✓	×	×		✓	✓slow
Sandstone		✓	×	×	×	✓	✓
Limestone		✓slow	×	×	×	✓	✓slow
Igneous	Medium to high strength	✓slow	×	×	×	✓	×
Metamorphic		✓v. slow	×	×	×	✓	×

✓ - Suitable drilling method, ✓! - Danger of Hole collapsing, ! - Possible problems, × - Inappropriate method

Table 3 Differentiation between conventional drilling and side wall drilling

Sl No	Conventional coring	Side wall coring
1	Complete rod string and core barrel has to be removed for core recovery	Recovery is not enough as drilling progressed in some of ecologic zones
2	Rigs out large samples	Rigs out small samples
3	Higher quality and uniform description of formations < 60 feet	Sidewall cores are an excellent cost-effective way to increase knowledge of formations
4	For Heterogeneous rocks and complex lithologies	More useful in paleontological works, deep ocean etc.

of mineral resource planning is to be generated. This can be divided into 4 main sub-systems depending on proposed exploratory locations.

4 Core Logging

Drill core logging, by geologists, commonly includes a qualitative description of the lithology, mineralogy and ore textures. Not only is it a time and fiscal resource consuming method, it relies heavily on the individual knowledge and experience of a geologist [12]. As is known to us, a cylindrical section of rock or fragments, taken as a sample of naturally occurring substance, extracted from the formation and brought to the surface using special hollow steel tube is called drill core. All drill hole data gathering during the process of extraction of the core from the rock and the studies conducted on the core immediately after its extraction is called logging. Direct measurements on core samples furnish data on geological and engineering data that aids in the understanding of the presence, quantity and distribution of formation and ultimately aids the selection of core drilling processes to maximise their profitable recovery. With recent technological advances in drill core scanning and industrial devices (e.g., Hy-Logger and SisuROCK) provides full automated fast identification of mineral phases to generate mineral maps at macro scale. This information gives the opportunity to quantify this textural information for comparison and classification purposes [55].

The purpose of core log is to visualize the cores, giving a better understanding of the general geology of the site. For a special geoscientific investigation soil prolific system do a fairly good job describing the rock character. Coring rate is an important aspect of core recovery, determining the rate of penetration (ROP) and depth of the deposit essential for geotechnical classifications of the rocks encountered.. Rate of core drilling is dependent on many different parameters such as uniaxial compressive strength (UCS), tensile strength (TS), quartz content, apparent porosity, P-wave velocity etc. as described by different authors and are compiled by Taheri et al. [58]. Among various methods available for coring a comparison between traditional and modern practices is established in Table 3.

Table 4 Field identification of the unconfined compressive strength

Description	UCS (MPa)	Formation types	Field identification
Very high strength	>200	Marble, Granite, Gneiss	Specimen can be peeled by geological hammer
High strength	100–200	Quartzite, Basalt, Limestone	Specimen requires many blows of geological hammer to fracture it
Medium strength	50–100	Sandstone, Shale, Limestone, Dolomite	Cannot be scraped or peeled with a pocket knife, specimen can be fractured with firm blow of geological hammer
Low strength	25–50	Coal, Siltstone, Sands	Can be peeled by a pocket knife with difficulty, shallow indentations made by firm blow with point of geological hammer
Ultra-soft strength	<25	Unconsolidated sand, Chalk, Salt, Clay stone	Crumbles under firm blows with point of geological hammer, can be peeled by a pocket knife

5 Understanding Compressive Strength and Drillability

UCS is a fundamental mechanical property for stability assessments in underground unprepared rock cores. Thuro [63] stated that UCS is the most frequently used rock properties with Young's modulus and the tensile strength. As a derived rock property, the ratio of unconfined compressive strength and tensile strength often is designated as toughness (or brittleness) of a rock material. Many authors tend to take one or more of those properties as main parameters of drillability [54, 66, 30, 11, 46]. A quantitative focus on the strength behaviour in rock mass engineering is achieved directly in laboratory experiments or by indirect estimation methods such as point load strength index test, Schmidt hammer test etc. The laboratory tests are expensive, time consuming and require standard cores samples of high-quality with regular geometry. UCS in comparison with other parameters has better capability to describe the rock's behaviour during the penetration of drill tool into rock [8]. Indirect estimation of UCS can be done with field identification according to Table 4.

Howarth et al. [32] found a relationship between compressive strength and penetration rate of rotary drilling machine and percussive drilling machine. Kahraman et al. [36] has reported various links between percussive drill rate and different rock properties. Together with the description of geological properties drilling types can be specified with some attributes listed below. It is to be noted that only unconfined

Table 5 Geological classification for drilling methods

Drilling type	Soil type	Comments
Rotary drilling	Soft Rock	Depths up to 5000 m, possibility of inclined or horizontal drilling
Down-the-hole drilling	Hard and cracked rock	Depth up to 4000 m
Top hammer drilling	Consolidated land	Small diameter (150 mm max.), Shallow Depth, Able to do inclined drilling
Auger drilling	Clay, clayey sand, gravel	Depth of few dozen meters
Core drilling	All soil types	Drilling for soil analysis, Able to do inclined drilling
Percussion drilling	Hard rock, Sandstone, Limestone, Shale	Depth up to 100 m
Pipe jacking	Clay, clayey sand, Gravel	Installation of horizontal or vertical pipes

compressive strength cannot always be used as index for strength of rock material. Classification of different drilling methods is mentioned in Table 5.

6 Analysis of Machine Variables

A large number of equipment are available for the purpose of rock drilling. However, choice of drill machine depends upon rock properties, nature of drilling and specific production requirement. Earlier hard rocks were broken by means of driving wedges through cracks, sledge hammering or foliating the rock by heating it with a fire built against it and then quenching with water. However, drilling has significantly evolved over time. From a practical and productive viewpoint, two factors are kept in mind for drilling machines, drilling the rock as fast as possible and keeping the wear minimum. Both of these inputs influence the machine performance. Rapid drilling impacts specific energy and bit performances which are functions of weight on bit (WOB) and revolutions per minute (RPM) of the drill bit.

The principal methods of rock drilling used in the mines, constructions etc. are mechanical and driven by either impact or simple rotation. Fig. 3 explains the development in drilling machines over the years. Now-a-days drill machine navigation systems are deployed with GPS to provide data related to production, positioning and machine health during each borehole drill and is sent to the operating machines on the site from the planning office [22]. The data of actual drill position is also sent to the planning cell for further computing and ROP optimization as is required for drilling in various formations (Fig. 4).

The mining industry made a significant progress on long-term mine planning during previous few decades [43]. Drilling instructions are taken into consideration on account of challenges faced during prior works and as such new contingency plans

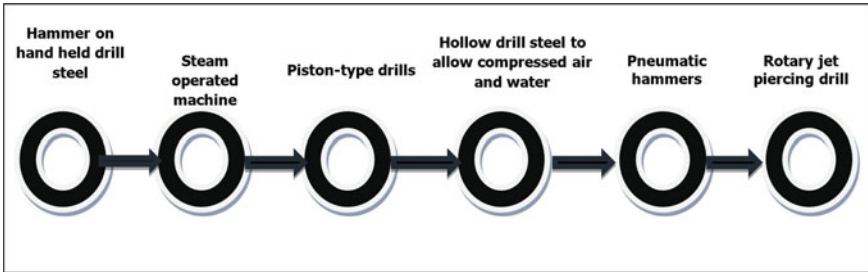


Fig. 3 Developments in drilling machine

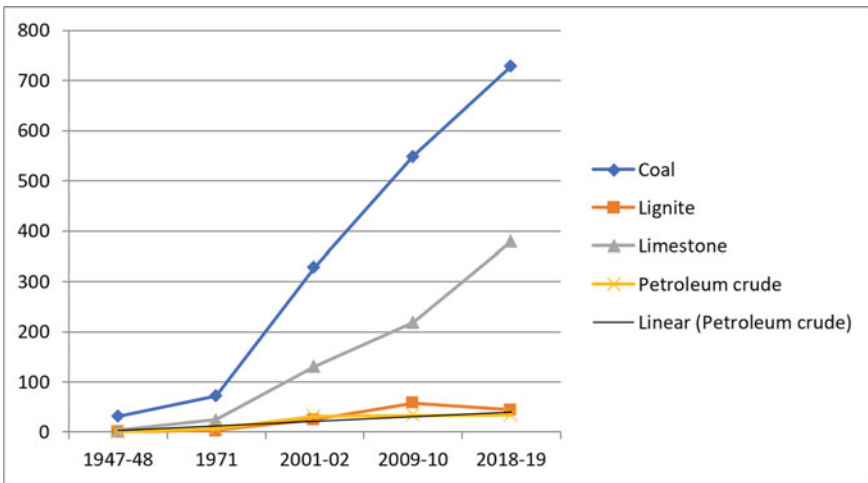
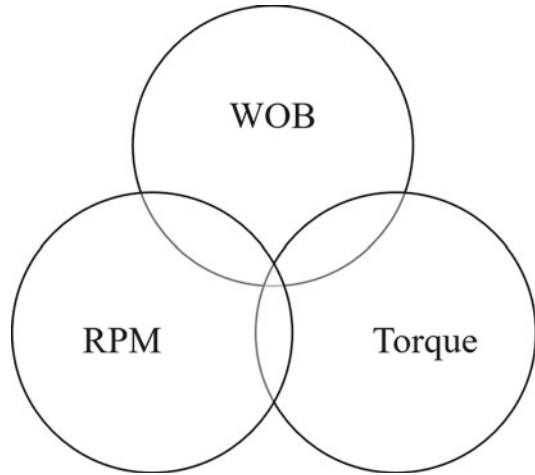


Fig. 4 Increased production due to machine advancements (Indian Bureau of Mines)

are prepared for anticipated challenges [28]. It may not be out of context to mention that there has been a remarkable growth in the production sphere of mining sectors, even for minerals which used to extract using conventional methods. The next step is to develop tactical plans by addressing specific activities in mining cycle.

Maurer [45] noted that ROP has a linear relationship with RPM under perfect hole cleaning conditions. As the drill string rotational speed increases, the bit impacts the rock more often and generates more cuttings that must be cleaned out of the hole. Gandelman [26] established that excessive RPM leads to vibrations. The energy dissipated through vibrations is wasted, decreasing ROP and inducing bit wear. Under human supervision the information of the machine parameters can be put to use in controlling drilling vibrations. The outburst of strokes may result in loss of energy, reduced life cycle of machine equipment, reduction in ROP and increased operation cost (Fig. 5).

Fig. 5 Technical parameters of machine variables



Teale [61] defines specific energy as “the energy required to excavate a unit volume of rock”. The specific energy (S.E.) of drilling may be defined as the quantity of energy from a source expended through the bit to drill volume of rock. It is a variable of the drilling process that is dependent on all the main drilling parameters: weight on bit, rotational speed, penetration rate and strength of rock. For example, the specific energy in a soft formation will differ from that in a hard one. Elbeblawi et al. [21] suggested S.E. is inversely proportional to ROP in all their tested rocks and in order to achieve a low S.E., it is obviously advantageous to have as high a penetration rate as much as possible.

7 Drill Bits

Drill bits have been extensively used in drilling engineering; therefore, it’s purposeful to capture the repercussion of drilling problems (e.g., drilling abrasive laborious rock, drilling dysfunctions) on the bit and to enhance future bit choice. As drill bits are non-repairable items; the aim of the work is to give a brief overview to the development in drill bits of various types presently used in the prospective ways in excavation. The bit cost is considered the most expensive part of a drilling operation, accounting for approximately 21% of the total operating costs [59]. Ghosh et al. [27] and Karpuz [38] used ROP as an indicator of drill bit replacement time, whereas Bilgin et al. (9) used the rock conditions as the indicator. Ford [24] insisted that it is essential to have an extremely hard cutter material backed by an intermediate hardness material and then attached to the steel drill body. This results in a self-sharpening feature which reduces frictional heating, thereby reducing wear and prolonging bit life. Summary of performance features and technical achievements of bits are shown in the Table 6. Ugurlu and Kumral [64] suggested that increasing the operating time of drill bits

Table 6 Mineral exploration drill bits

Performance features	Roller cone		Fixed cutters		Diamond impregnated
	Milled Tooth Bits (MT)	Tungsten Carbide Insert (TCI)	Polycrystalline Diamond Compact (PDC)	Diamond	
Global utilization	10%	15%	70%	29%	3%
Application	Soft and sticky, hard formations	Soft and sticky, hard formations	Hard formations, Direction wells, long wells, Shale formation	hard formations, Direction wells, long wells	Hard and abrasive formations
Rate of Penetration	High in soft formations	High in soft formations	High in sand, Shale, Clay and siltstone	High in sand, Shale, Clay and siltstone	High in sand, Shale, Clay and siltstone
Cost	Low	Low	Medium to High	High	High
Wearing/Damage Risk	Medium to High	Medium to High	Low to Medium	Low to Medium	Low to Medium

by 8% can make a considerable impact on the total replacement cost of a drilling operation.

Bit performance are determined by the amount of drilling by a bit (length), cost per unit length of hole drilled, cutting element used and rate of drilling. It is a function of numerous variables such as WOB (weight on bit), RPM (revolutions per minute), and hydraulic efficiency. Commissioning of cutter used is based on formation to be drilled. Soft formation needs long, thin, widely spread teeth to prevent bit balling. Moderately hard formations have shorter, wider teeth for withstanding heavier loads, wide spread to allow cleaning. Spread of cutters is less important in hard formations due to low ROP and small cutting sizes constraint. Cutter elements are screened with tungsten carbide to increase its wear resistance.

The rock cutting process generates a great amount of heat at the bit, the bits need to be cooled or it will overheat and wear out quickly. The primary application of drilling fluid is to assist in transporting cuttings, maintaining borehole pressure, providing support to the drilled formations and chemically stabilizing the hole [13, 44]. The circulating fluid will cool the bit and lubricate the cutting tools. Drilling fluid transports drilled material to the ground surface. Nevertheless, drilling fluid(s) also serve as coolants and lubricant to provide protection to drill string from mechanical and physio-chemical problem. The reduction of mud level in the wellbore reduces the potential to meet all these requirements, which may result in mild inconvenience or a serious threat [39]. It also provides a means to minimize damage to the formation and ensure safety. The rock cuttings produced by the drill bits are continuously removed from the bit face to increase drilling efficiency. The carrying capacity reckons on annular velocity, density and viscosity of mud (Fig. 6).

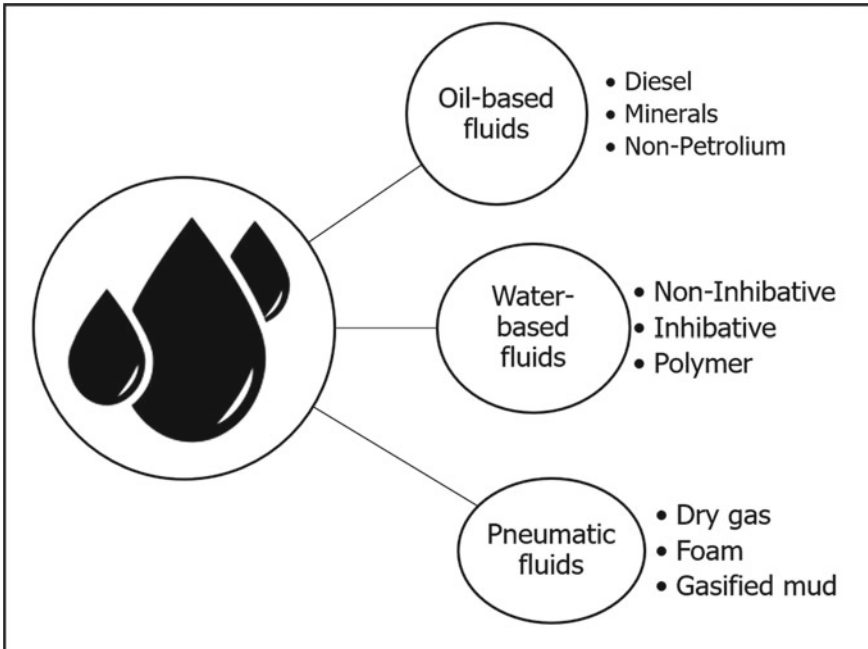


Fig. 6 Types of drilling fluids

Additionally, survey tools can predict fluid detection characteristics for achieving better results. Nevertheless, if these detection methods are analyzed in a combined manner along with the end effects the drilling will be more precise, advanced and provide statistically correct results in the drilling programs.

8 General Requirement for Exploratory Core Drilling Process

An economic mineral discovery is extremely difficult, time consuming, and costly in terms of physical and scientific efforts. The efforts of mineral exploration can be maximized by using some steps of exploration strategy.

- a) Land approximations for the prospective areas with potential for discoveries can be identified and preparation of drill site and drilling measures are reviewed from available information.
- b) Geologist ramp the process of accessing existing maps, historical data and geophysics studies.
- c) After an official resource estimate more data is fetched through drilling, 3D models and metallurgical tests.

- d) At this stage potential outcome of the project is studied in-depth to help make a production design, commercial production can be started by constructing a mine.
- e) Power system are to be installed for lightening, the diesel engines of the machines which runs on high-speed diesel are the most significant requirement for circulation system.
- f) According to the nature of drilling borehole assembly is to be established.
- g) Water transported from nearby pit installation would be used for engine cooling, equipment/string washing, sanitation, fire-fighting storage and drinking for the workers.
- h) Sample should be carefully taken out without being damaged.
- i) Testing facilities can be available at the site for speedy inspection of sample.
- j) The drill cuttings and fragments of rock, sand and silt is accountable for solid waste, these should properly collect dried and dispose of as per guidelines of authorized policy.

9 Relation of Operational Drilling Parameters on ROP

Rate of penetration (ROP) is one of the most important aspects in drilling optimization and has several data driven significant role in reducing drilling expenditure. Table 7 is provided to aid in establishing the optimal definitions of the controllable parameters in the drilling system.

10 Field Investigation Overview (Case Study)

The Total geology exposed over an area of 14,700 sq km in central India. It is situated between two tectonic trends of NE-SW Satpura range and NW-SW of Godavari Basin. It was further subdivided into lithological characteristics, floral content and coal bearing strata. The study was conducted in the Barakar Formation which resides under the Lower Gondwana Sequence dominantly exposed in Pench-Kanhan Region nearby Nagpur Maharashtra India. The Barakar formation consists of basalt, sandstone, shale, grits, coal seams and conglomerate. The core was extracted by KDR 1000 core drilling machine.

Table 7 Controllable drilling parameters

Parameters	A measure of	Effect on ROP
Depth	Vertical stress	Physio-mechanical properties are easily influence of many formations by drilling operation in depth
Weight on bit (WOB)	Axial thrust for rock crushing	As the WOB increases to a critical value, the ROP increases. If it exceeds the critical value the ROP will be reduce as bottom of the borehole may no longer be efficiently washed
Flow rate		Increase in flow rate leads to better removal of cuttings, thereby enhancing ROP
Rotary speed	Sheer cutting force	There is increase in ROP till the critical value of increasing rotary speed. However, after critical point ROP decreases due to reduction in well stability and washout
Drilling fluid density	Drilling fluid column pressure in the well	A reduction in drilling fluid weight results in fragmentation of bottom hole rock under the effect of formation fluid pressure, thereby increasing ROP
Porosity Log	Rock compaction	The higher the porosity of the rock, easier rock can be penetrated
Density Log	Mineralogy and rock compaction	Tendency of formation to be muddy is influenced by its mineralogy
Coring Rate	–	Analysis must be versed in many scientific and engineering sub-disciplines
Pump pressure	–	An increase in pump pressure results in enhanced bit nozzle force and hence better removal of cuttings, thereby increasing ROP

11 Exploratory Data Analysis

The influence of rock and machine properties on drilling at vertical and sub vertical angles was attempted in this study [69]. The geological and machine performance data of two boreholes drilled in a complex coal bearing strata was collected and analyzed to develop a model for penetration rate.

The data showed the high influence of depth of coring on the drilling performance; this resulted in conflicting situations while correlating rock properties and other machine variables with the coring performance.

There is a significant impact of drill depth of the coring, UCS and tensile strength on the penetration rate, it presented various issue with the influence of other major variables and encountered to develop logical model development.

12 Technological Trends

Since most outcropping deposits already have been discovered and mature mining camps have started to dry out, the discovery of new mineral deposits in the last 15 years has become increasingly expensive and risky [17]. Along with predicting the presence of metals in rocks, physical properties combined with machine learning have the potential to classify lithologies, characterize hydrothermal alteration, and estimate exploration vectors and geotechnical information in the drill core. Caté et al. [14] suggested that the combination of these predictions will significantly improve the work of logging geologists, the quality of geologic interpretations, and the decisions made during a drilling campaign and during the exploitation of a mine. Huges [33] predicted Implementing IoT has the potential to increase operational drilling efficiency by 5% and cut upstream operating expenditure by 20–30%, both significant values in a multibillion-dollar industry.

Automation and digitalization focus on integrating both sensors/instrumentation and algorithms to improve the way raw data is extracted, analysed, and turned into useful information, which can then be used to optimize drilling operations [15, 19, 52, 62, 67]. The recent trends in automation are designed to reduce human related cost errors, innovations such as big data analytics, Internet of Things (IoT) can extract the most useful information, structure it, and make judgements based upon it (Fig. 7).

Autonomy and digital advancement tools are unavoidable; they are therefore expected in the present circumstances in mining companies. Soares and Gray [57]

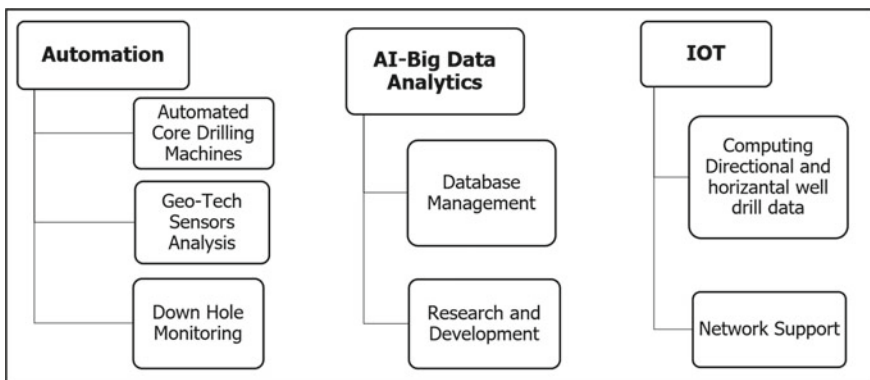


Fig. 7 Automation and future approach in drilling

demonstrated that machine learning ROP models predict drilling speed more accurately than analytical models with the same surface data generally utilized by the latter. Chalioris et al. [16] provided significant information mentioning that mechanical behaviour, chemical characterization, and structure of rock has significant impact on rock engineering. With increasing discoveries in surface mining, exploration of fossil fuels, quarrying in highly challenging locations, drilling operations are synonymously expected to be complicated, scientists and engineers must be forehanded with the contemporary state-of-the-art, innovative, environmentally friendly, and safe drilling methods must be developed (Fig. 8).

Coring rate can be significantly increased by improving following challenges and operations shown in the Table 8.

Coring rate is a key component in formulating innovative design for the deep-rock mechanism which can be valuable source of information. The analysis of the existing coring system is to be studied for better understanding of the structure and stress distribution of rocks underground and designed a new coring system (Fig. 9).

The efforts of the International Association of Drilling Contractors (IADC) are focused to promote industrialize machine control and for developing linkages to key stakeholders in mining industry. Such efforts have strengthened communication and ensured cooperation in providing guidelines for future technology standardization

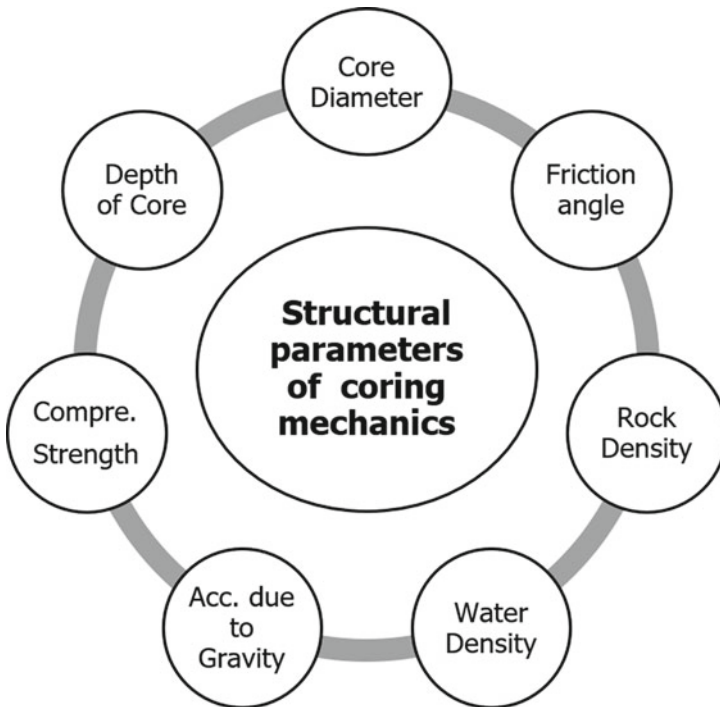


Fig. 8 Mechanical analysis of coring rate

Table 8 Challenges to improve coring rate

Sl. No.	Experimental parameters
1	New Powerful Automated Coring Machine
2	More Torque and Horspower at the drill bits to utilize higher power and operate in harsh coring environments
3	High-powered surface systems and high-strength wire line cables
4	Cutting and handling advancements for soft and hard formations
5	Modern combination of rotary coring and formation sampling to obtain formation pressures, fluid samples, and cores on a single run
6	Advance down hole monitoring of the coring operation, which includes the drilling functions like torque, bit force, penetration rate, and depth of the core drilling, along with tool orientation

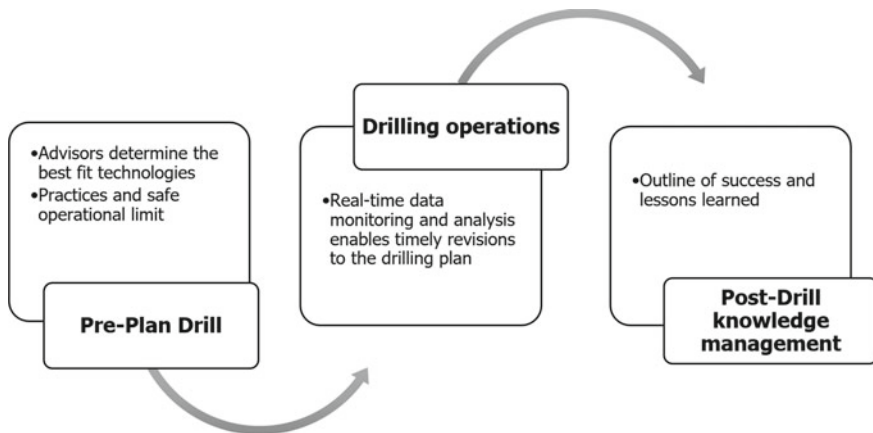


Fig. 9 Drilling advisory

of drilling-system automation. Automation should be only applied to the functions that the system can perform better or more reliably than people, to lighten workload, allowing the available services to be focused on managing those decisions that cannot be entrusted on machines.

13 Conclusions

Industries over the world have developed various drilling and coring techniques for almost any rock type or environment imaginable. However, exploratory drilling plays a vital task in scientific drilling, but even these practices offer many options and might confuse a scientist at first. There are significant references in the published domain that address various issues pertaining to the influence on exploratory coring

rate. Comprehensive studies of references are classified as: geology, machine variables, operating conditions, innovation insights. Much progress is to be done in improving constructive discussions of real time core drilling programs in Indian subcontinent as high quality results are only achieved by implementing professional organisations with input from industry, service providers and the government. With the practice of good quality, unbiased data from drill sites maximum value of current and future exploration efforts can be economically capitalized.

References

1. <https://www.brookings.edu/research/indias-mineral-exploration-legacy/>
2. www.nationaldriller.com/drilling-history
3. <https://www.slideshare.net/MTaHerHamdani/7-drill-bits>
4. Altındağ, R. (2003). Estimation of penetration rate in percussive drilling by means of coarseness index and mean particle size. *Rock Mech Rock Eng* 36(4):323–332. <https://doi.org/10.1007/S00603-003-0002-3>
5. ASTM–American Society for Testing and Materials (2008) Standard Test Method for Determining Rock Quality Designation (RQD) of Rock Core. ASTM International, West Conshohocken, PA, 5 January 2003
6. Ataei M, KaKaie R, Ghavidel M, Saeidi O (2015) Drilling rate prediction of an open pit mine using the rock mass drillability index. *Int J Rock Mech Min Sci* 73:130–138. <https://doi.org/10.1016/j.ijrmmms.2014.08.006>
7. Atici U, Ersoy A (2008) Evaluation of destruction specific energy of fly ash and slag admixed concrete interlocking paving blocks (CIPB). *Constr Build Mater* 22(7):1507–1514. <https://doi.org/10.1016/j.conbuildmat.2007.03.028>
8. Balci C, Copur H, Bilgin N, Ozdemir L, Jones GR (2020) Cuttability and drillability studies towards predicting performance of mechanical miners excavating in hyperbaric conditions of deep seafloor mining. *Int J Rock Mech Min Sci* 130:104338. <https://doi.org/10.1016/j.ijrmmms.2020.104338>
9. Bilgin N, Copur H, Balci C (2013) *Mechanical Excavation in Mining and Civil Industries*. CRC Press
10. Bilim N (2011) Determination of drillability of some natural stones and their association with rock properties. *Acad J Org* 6(2):382–387. <https://doi.org/10.5897/SRE10.878>
11. Blindheim O (1979) Drillability predictions in hard rock tunnelling. <https://pascal-francis.inist.fr/vibad/index.php?action=getRecordDetail&idt=PASCALGEODEBRGM8020217081>
12. Bonnici N, Hunt JA., Walters SG, Berry R, Collett D (September 2008) Relating textural attributes to mineral processing: Developing a more effective approach for the Cadia East Cu–Au porphyry deposit. In: *Proceedings of the Ninth International Congress for Applied Mineralogy Conference (ICAM)*, pp. 4–5
13. Byrom TG (2014) *Casing and Liners for Drilling and Completion: Design and Application*. Elsevier
14. Caté A, Perozzi L, Gloaguen E, Blouin M (2017) Machine learning as a tool for geologists. *Lead Edge* 36(3):215–219. <https://doi.org/10.1190/tle36030215.1>
15. Cayeux E, Daireaux B, Dvergsnes EW, Florence F (2014) Toward drilling automation: On the necessity of using sensors that relate to physical models. *SPE Drill Complet* 29(2):236–255. <https://doi.org/10.2118/163440-PA>
16. Chalioris CE, Papadopoulos NA, Angeli GM, Karayannis CG, Liolios AA, Providakis CP (2015) Damage evaluation in shear-critical reinforced concrete beam using piezoelectric transducers as smart aggregates. *Open Eng* 5(1):373–384. <https://doi.org/10.1515/ENG-2015-0046/HTML>

17. Schodde R (November 2011) Recent trends in gold discovery. In: NewGenGold Conference, Perth, vol. 2. pp. 1–19
18. Dickson R, Blair R, Hart H, Sharp J (1955) Drilling results and favorability criteria in bull canyon, Montrose and san Miguel Counties, Colorado. PART I. <https://www.osti.gov/biblio/4360419>
19. Dunlop J et al (2011) Increased rate of penetration through automation. In: SPE/IADC Drilling Conference, Proceedings, vol 1, pp 442–452. <https://doi.org/10.2118/139897-ms>
20. Dwivedi RD, Goel RK, Singh M, Viladkar MN, Singh PK (2018) Prediction of ground behaviour for rock tunnelling. *Rock Mech Rock Eng* 52(4):1165–1177. <https://doi.org/10.1007/S00603-018-1673-0>
21. Elbeblawi M, Sayed M, ... G. B. -J. J. of, & 2012, undefined (2012) Effect of operating parameters and formation properties on penetration rate in some sandstone rocks using diamond core bit. *J Ekb Eng* 40(2):581–594. https://journals.ekb.eg/article_113132.html
22. Erkayaoglu M (2019) Use of geospatial queries for optimum drilling and blasting practices in surface mining. In: Widzyk-Capehart E, Hekmat A, Singhal R (eds) Proceedings of the 27th International Symposium on Mine Planning and Equipment Selection–MPES 2018, pp 57–67. Springer, Cham. https://doi.org/10.1007/978-3-319-99220-4_5
23. Ersoy A, Waller MD (1995) Textural characterisation of rocks. *Eng Geol* 39(3–4):123–136. [https://doi.org/10.1016/0013-7952\(95\)00005-Z](https://doi.org/10.1016/0013-7952(95)00005-Z)
24. Ford L (1982) Mine roof drill bits that save money. <https://www.osti.gov/biblio/5381988>
25. Franklin JA (1970) Classification of rock according to its mechanical properties (Doctoral dissertation, University of London). <https://spiral.imperial.ac.uk/bitstream/10044/1/16391/2/Franklin-JA-1970-PhD-Thesis.pdf>
26. Gandelman RA (2012) Prediction of ROP and Real Time Optimization of Operational Parameters While Drilling Offshore Oil-Wells (Doctoral dissertation, MS thesis, Universidade Federal do Rio de Janeiro, Rio de Janeiro, Brazil)
27. Ghosh R, Schunnesson H, Kumar U (2016) Evaluation of operating life length of rotary tricone bits using measurement while drilling data. *Int J Rock Mech Min Sci* 100(83):41–48
28. Gooneratne CP et al (2020) Drilling in the fourth industrial revolution-vision and challenges. *IEEE Eng Manag Rev* 48(4):144–159. <https://doi.org/10.1109/EMR.2020.2999420>
29. Gstalder S, Raynal J (1966) Measurement of some mechanical properties of rocks and their relationship to rock drillability. *J Pet Technol* 18(08):991–996
30. Habenicht H, GEHRING K (1976) Rock characteristics and mechanical tunnelling. *Berg-und Huettenmaennische Monatshefte* 121(12)
31. He M, Li N, Zhang Z, Yao X, Chen Y, Zhu C (2019) An empirical method for determining the mechanical properties of jointed rock mass using drilling energy. *Int J Rock Mech Min Sci* 116:64–74. <https://doi.org/10.1016/J.IJRMMS.2019.03.010>
32. Howarth DF, Adamson WR, Berndt JR (1986) Correlation of model tunnel boring and drilling machine performances with rock properties. *Int J Rock Mech Min Sci Geomech Abstr* 23(2):171–175. [https://doi.org/10.1016/0148-9062\(86\)90344-X](https://doi.org/10.1016/0148-9062(86)90344-X)
33. Huges B (2016) International Rotary Rig Count. https://scholar.google.com/scholar?hl=en&as_sdt=0%2C5&q=Huges%2C+B.%2C+2016.+International+Rotary+Rig+Count.&btnG=. Accessed 29 July 2021
34. Hustrulid WA, Fairhurst C (1972) A theoretical and experimental study of the percussive drilling of rock part III—experimental verification of the mathematical theory. *Int J Rock Mech Min Sci Geomech Abstr* 9(3):417–418. Pergamo
35. Kahraman S (2002) Correlation of TBM and drilling machine performances with rock brittleness. *Eng Geol* 65(4):269–283. [https://doi.org/10.1016/S0013-7952\(01\)00137-5](https://doi.org/10.1016/S0013-7952(01)00137-5)
36. Kahraman SAIR, Bilgin N, Feridunoglu C (2003) Dominant rock properties affecting the penetration rate of percussive drills. *International J Rock Mech Min Sci* 40(5):711–723. [https://doi.org/10.1016/S1365-1609\(03\)00063-7](https://doi.org/10.1016/S1365-1609(03)00063-7)
37. Kalantari S, Hashemolhosseini H, Baghbaban A (2018) Estimating rock strength parameters using drilling data. *Int J Rock Mech Min Sci* 104:45–52. <https://doi.org/10.1016/J.IJRMMS.2018.02.013>

38. Karpuz C (2018) Energy efficiency of drilling operations. *Green Energy Technol* (9783319541983) 71–86. https://doi.org/10.1007/978-3-319-54199-0_5
39. Krishna S, Ridha S, Vasant P, Ilyas SU, Sophian A (2020) Conventional and intelligent models for detection and prediction of fluid loss events during drilling operations: a comprehensive review. *J Petrol Sci Eng* 195:107818. <https://doi.org/10.1016/J.PETROL.2020.107818>
40. Krúpa V, Kruláková M, Lazarová E, Labaš M, Feriančíková K, Ivaničová L (2018) Measurement, modeling and prediction of penetration depth in rotary drilling of rocks. *Measurement* 117:165–175. <https://doi.org/10.1016/J.MEASUREMENT.2017.12.007>
41. Kumar CV, Vardhan H, Murthy CSN, Karmakar NC (2019) Estimating rock properties using sound signal dominant frequencies during diamond core drilling operations. *J Rock Mech Geotech Eng* 11(4):850–859. <https://doi.org/10.1016/J.JRMGE.2019.01.001>
42. Kumar D, Sing KK (2017) Experimental analysis of delamination, thrust force and surface roughness on drilling of glass fibre reinforced polymer composites material using different drills. *Mater Today Proc* 4(8):7618–7627. <https://doi.org/10.1016/J.MATPR.2017.07.095>
43. Kumral M (2012) Production planning of mines: optimisation of block sequencing and destination. *Int J Min Reclam Environ* 26(2):93–103. <https://doi.org/10.1080/17480930.2011.644474>
44. Lavrov AV, Erasov VS, Nochovnaya NA, Kotova EA (2017) Ensemble of secondary cracks near the fatigue fracture surface of a titanium alloy VT23M specimen. *Russ Metall (Metally)* 2017(4):330–333. <https://doi.org/10.1134/S0036029517040127>
45. Maurer WC (1962) The perfect-cleaning theory of rotary drilling. *J Petrol Technol* 14(11):1270–1274. <https://doi.org/10.2118/408-PA>
46. Movinkel T, tunnelling, O. J.-T. &, & 1986, undefined. (n.d.) Geological parameters for hard rock tunnelling. Pascal-Francis.Inist.Fr. <https://pascal-francis.inist.fr/vibad/index.php?action=getRecordDetail&idt=8723688>. Accessed 13 Aug 2021
47. Mukerji T, Avseth P, Mavko G, Takahashi I, González EF (2012) Statistical rock physics: combining rock physics, information theory, and geostatistics to reduce uncertainty in seismic reservoir characterization. *20(3):313–319*. <https://doi.org/10.1190/1.1438938>
48. Onyia E & 1988 (n.d.) Relationships between formation strength, drilling strength, and electric log properties. *Onepetro.Org*. <https://onepetro.org/SPEATCE/proceedings-abstract/88SPE/All-88SPE/SPE-18166-MS/72440>. Accessed 2 Aug 2021
49. Rajesh Kumar B, Vardhan H, Govindaraj M (2011) Prediction of uniaxial compressive strength, tensile strength and porosity of sedimentary rocks using sound level produced during rotary drilling. *Rock Mech Rock Eng* 44(5):613–620. <https://doi.org/10.1007/S00603-011-0160-7>
50. Richard T, Dagrain F, Poyol E, Detournay E (2012) Rock strength determination from scratch tests. *Eng Geol* 147–148:91–100. <https://doi.org/10.1016/J.ENGCEO.2012.07.011>
51. Rider MH (1986) The geological interpretation of well logs, p 175
52. Sadlier A, Laing M, Shields J (2012) Data aggregation and drilling automation: connecting the interoperability bridge between acquisition, monitoring, evaluation, and control. In: *SPE/IADC Drilling Conference, Proceedings, vol 2*, pp 936–945. <https://doi.org/10.2118/151412-ms>
53. Sarasty JJ, Stewart RR (2003) Analysis of well-log data from the White Rose oilfield, offshore Newfoundland. *CREWES Res Rep* 15:1–16
54. Schimazek J, Knatz H (1970) Der Einfluß des Gesteinsaufbaus auf die Schnittgeschwindigkeit und den Meißelverschleiß von Streckenvortriebsmaschinen. *Glückauf* 106(6):274–278
55. Schodlok MC et al (2016) HyLogger-3, a visible to shortwave and thermal infrared reflectance spectrometer system for drill core logging: functional description. *Aust J Earth Sci* 63(8):929–940. <https://doi.org/10.1080/08120099.2016.1231133>
56. Shreedharan S, Hegde C, Sharma S, Vardhan H (2014) Acoustic fingerprinting for rock identification during drilling. *Int J Min Miner Eng* 5(2):89–105. <https://doi.org/10.1504/IJMM.2014.060193>
57. Soares C, Gray K (2019) Real-time predictive capabilities of analytical and machine learning rate of penetration (ROP) models. *J Petrol Sci Eng* 172:934–959. <https://doi.org/10.1016/J.PETROL.2018.08.083>

58. Taheri A, Qao Q, Chanda E (2016) Drilling penetration rate estimation using rock drillability characterization index. *J Inst Eng (India): Ser D* 97(2):159–170. <https://doi.org/10.1007/S4033-015-0104-6>
59. Tail M, Yacout S, Balazinski M (2010) Replacement time of a cutting tool subject to variable speed. *Proc Inst Mech Eng Part B J Eng Manuf* 224(3):373–383. <https://doi.org/10.1243/09544054JEM1693>
60. Tandanand S, Unger, HF (1975) Drillability determination: a drillability index for percussion drills (vol. 8073). US Department of the Interior, Bureau of Mines
61. Teale R (1965) The concept of specific energy in rock drilling. *Int J Rock Mech Min Sci* 2(1):57–73. [https://doi.org/10.1016/0148-9062\(65\)90022-7](https://doi.org/10.1016/0148-9062(65)90022-7)
62. Thorogood J, Aldred W, Florence F, Iversen F (2010) Drilling automation: technologies, terminology, and parallels with other industries. *SPE Drill Complet* 25(4):419–425. <https://doi.org/10.2118/119884-PA>
63. Thuro K (1997) Drillability prediction: geological influences in hard rock drill and blast tunnelling. *Geologische Rundschau* 86(2):426–438. <https://doi.org/10.1007/S005310050151>
64. Ugurlu OF, Kumral M (2019) Optimization of drill bit replacement time in open-cast coal mines. *Int J Coal Sci Technol* 6(3):399–407. <https://doi.org/10.1007/S40789-019-0254-5>
65. Wang, Z. W. (1995) The mechanics of diamond core drilling of rocks (Doctoral dissertation, University of Alaska Fairbanks)
66. Wanner H (1975) On the influence of geological conditions at the application of tunnel boring machines. *Bull Int Assoc Eng Geol–Bulletin de l'Association Internationale de Géologie de l'Ingénieur* 12(1):21–28. <https://doi.org/10.1007/BF02635424>
67. Wilson A (2015) Drilling-systems-automation roadmap: the means to accelerate adoption. *J Petrol Technol* 67(09):137–138. <https://doi.org/10.2118/0915-0137-JPT>
68. Yavuz H, Demirdag S, Caran S (2010) Thermal effect on the physical properties of carbonate rocks. *Int J Rock Mech Min Sci* 47(1):94–103. <https://doi.org/10.1016/J.IJRMMS.2009.09.014>
69. Alam P, Raina AK, Murthy VMSR (2022) Investigations on the influence of rock and machine characteristics on coring rates in vertical and mildly inclined exploration drilling in complex coal bearing rock formation. *Geomech Geophys Geo-energy Geo-resour* 8:13. <https://doi.org/10.1007/s40948-021-00319-5>

Operators Skill Evaluation with Virtual Reality Technology



Job Steven James Nanadrekar, Manavalan Subramanian, Gaurav Jain, Vynotdni Rathinasamy, and Ramesh Murlidhar Bhatawdekar

Abstract Mining application requires specialized education for operators in their explicit field to advance focussed awareness and accurate skills to do their jobs excellently. The objective of teaching is to empower all operatives to achieve their job in a method that is acceptable to the company and the staff. The study does not include all procedures and forms in place yet, but it embraces a system comparable to the one used in our Air Force sometime before. Also, the study relies on On Job Training (OJT) model training for the operators on a particular machine or process type. A training card for each process/machine type have been made up as well. The specific tasks related to the machine/process that the operator will be doing has been listed. The card is given to the operator and the operator is paired up with a more skilled operator from that machine. Also, listing the specific functions of the machine/process typically required different products to be processed through that sometimes have their own unique things about them. There are several older, more experienced operators to train and evaluate freshers. Therefore, the intends to analyse the various factors contributing to the human efficiency of Dumper Operators in Quarries, effectively creating an Operator Skills Matrix (OSM). The main objective is to create a blueprint for automated modelling of the operator efficiencies and to generate required data. Operator Skills Matrix could be effective in building an

J. S. J. Nanadrekar · G. Jain (✉)
Indian Institute of Technology Kharagpur, Kharagpur 721302, India
e-mail: gaurav.jain@iitkgp.ac.in

J. S. J. Nanadrekar
e-mail: jobsteven@iitkgp.ac.in

M. Subramanian
Dangote Cement Plc Ltd., Egbe, Kogi, Nigeria
e-mail: manavalan.subramanian@gmail.com

V. Rathinasamy · R. M. Bhatawdekar
Geotropik Centre, School of Civil Engineering, Faculty of Engineering, Universiti Teknologi Malaysia, UTM, Block D03, 81310 Johor Bahru, Malaysia
e-mail: vynotdni@utm.my

R. M. Bhatawdekar
e-mail: rmbhatawdekar2@graduate.utm.my

© The Author(s), under exclusive license to Springer Nature Singapore Pte Ltd. 2022
A. K. Verma et al. (eds.), *Proceedings of Geotechnical Challenges in Mining, Tunneling and Underground Infrastructures*, Lecture Notes in Civil Engineering 228,
https://doi.org/10.1007/978-981-16-9770-8_33

assessment metric. Operator Skill Index (OSI) centred on which the complete work of any operator would be standardized. Once such a benchmark is created, person in-charge can take sufficient methods to re-train whoever lacks skill. Operators are very important to improve safety and productivity which reduces the cost of mining. Thus, latest technique available is Virtual Reality Training (VR).

Keywords Virtual training (VR) · Mining · Downhole camera survey · Operator skill

1 Introduction

The main objective is to evaluate each operator and apply on-field performance. The operator's efficiency mainly depends on many field factors, but a phenomenal contributor is an operator. Thus, to enhance overall operational improvement and to reduce the cost of the whole operation, we will focus and study operators' efficiency mapping with virtual reality (VR) and transferring it to field application. VR training has become a progressively vital tool for education and teaching, set aside our teaching to beyond an eLearning course or classroom. It's anticipated around 50 million people are using VR training programs. VR is used in corporate training in several ways.

Audio–Video based training is appropriate and successful. It should describe events or circumstances that students will recognize and be acquainted with but are likely to occur on the job. Audio–Video based training is generally interactive, asking learners to think about various potential replies or explanations. Benefits of Audio–Video based training over traditional is quoted by Benjamin Franklin as “Tell me, and I forget. Teach me, and I may remember. Involve me, and I learn” [1]. The ancient “chalk and talk” system of training, where discussions get transmitted, imparted technique not adequately educated learner and not assure any enrichment on anyone's role performance and deciding talents.

In the age-old training system, the companies spent a lot of funds on training, but the result wasn't encouraging hence latest technology such as Audio-visual or VR system becomes essential. However, Audio–Video-based training is in the best of everybody's interests.

- a. Going ahead with constructive feedback: The learners are faced with real operations hence they fear of failing Audio–Video-based training programs due to the relaxed environment for them. This type of training makes students to take required decision quickly and be excellent staffs in the company as they knew to solve any problem that arises while on the job.
- b. Learn more in less time: To develop fresh staff companies very well know and spend on each staff to develop them business specific. Each organization wishes to develop its employees self-motivated and empowered which is of course by virtual Audio–Video based training. These systems are expected to have a definite impact and change them into self-confident staff who are sufficiently skilled to bring desired progress to the company.

- c. Situations trigger inherent behaviour: Younger/new staff should be developed to bring out their enormous power otherwise may lead to unforeseen outcomes. Well organized virtual scenario stimulates queries, ‘is it right?’ ‘What next?’ ‘The end result of all this?’ etc. These all help them to stay quiet and guess the highly rational and achievable solution.
- d. Encourage critical thinking through stories: There is a saying “you won’t know until you try”. Explaining events with a perspective story improves the awareness of a specific situation and executes the best decision. Influencing learners to acquaint with collaborative scenario stories in their own way.
- e. Improves knowledge preservation: Going through transparencies and trying to visualize real scenarios can get in terms of exposure, like some clips. Bringing learners on a passionate journey, where they closely recognize what action is right and how it impacts the journey next, helps them retain the learning taught substantially.
- f. High return of investment (ROI): Consumes significant resources of a company because of recurring training planning to educate trainees. The massive costs spent now require targeted results. Moreover, employees are likely to stick longer with a company where they see growing investments made towards their development.

The technical skills required for this purpose are as following:

- a. Problem resolving.
- b. Conclusion making.
- c. Intensity.
- d. Attention to fact.
- e. Collaboration.
- f. Able to follow guidelines and production programs.
- g. Talented to act swiftly when a challenge occurs.

2 Multitasking Talents

Multitasking talents are essential because they generate an economical work environment. The advantages of multitasking are enumerated below [2]:

- a. Time saving: It saves time by making a person to do multiple tasks simultaneously. For an example, the staff may key in client’s note while talking to them over phone call. Within short period, he could complete two tasks instead of doing each one separately and saving time on the same.
- b. Cost-effective: Employers prefer to recruit multitasking employees with excellent talents as they could perform more tasks simultaneously and save cost of hiring another employee. Demonstrating how good a person could multitask depicts him as an invaluable employee.

- c. Enhancement of efficiency: Multitasking surges efficiency as more tasks are achieved in a short period. People's productivity is especially higher during the day.
- d. Decreases postponement: Multitasking reassures people that they accomplished the task assigned because they do multi-job at a given time. This increases productivity with the inspiration of people to make working on their own to accelerate work thus productivity.

Multitasking comprises many services that one should develop to be more creative and experienced. Below are general skills needed for multitasking [3]:

- a. Organization
- b. Ranking
- c. Planning
- d. Delegation

Organization: Knowing exactly what task to do and when to do results in excellent multitasking. Organization incorporates management of daily, weekly and monthly work planning which aids in achieving milestones. Also, workspace must be kept tidy always to easily locate documents, notes and paperwork. Besides, organizing computer files and system are equally important for quick search and access of documents.

Ranking: It is the skill to evaluate the workload and arrange them in terms of importance to manage time. The priority of task shall be assigned depending on individual preference. For an example, one shall complete the easiest task first and spend the rest of time to finish challenging, bigger tasks. Also, one can start with the most time-consuming task and then continue with simpler, less crucial tasks. Thus, ranking is a crucial ability for effective multitasking.

Scheduling: Scheduling is planning and ensuring to meet the target or milestone on time. One must be capable of understanding complicated situations and break down the tasks into practicable phases and time limit. Planning daily tasks including preplanning for unwanted additional tasks, lets a person to decide on which task to multitask to complete as per schedule.

Delegation: Delegation is when a person ask assistance from others to carry out tasks and stay on schedule. Usually, people give smaller tasks to team members and focus on those with a greater importance by themselves. Thus, delegation is related to prioritization and scheduling. A person needs to know what sufficient workload is to manage time and when to delegate for an excellent multitasking.

3 Onboarding

In today's context, the Human Resources team applies the techniques of Onboarding referring to newly hired employee's introduction in an organization. Onboarding is

an important part of helping new employees to understand their new position and role obligations [4]. It’s also known as integrating them faultlessly with the rest of the company. New staffs “integration program” takes about weeks to a year but “effective integration” lasts to few months.

4 Simulations

The definition of a simulation is a model or representative example of something of real. When computer program is created, it is intended to fly of a plane, an example of simulation. However, it can be used in various fields including fishery to dynamically simulate fish population (salmon as in Fig. 2). The aim of a simulation is to give light on the inherent mechanisms which control the behaviour of a system. In general, simulation shall be utilized to predict future behaviour of a system and decide on actions or plans to overcome the problems as per predicted future behaviour (Fig. 1).

We are aware of no defined metric to measure the “grade”* of a HEMM Operator.

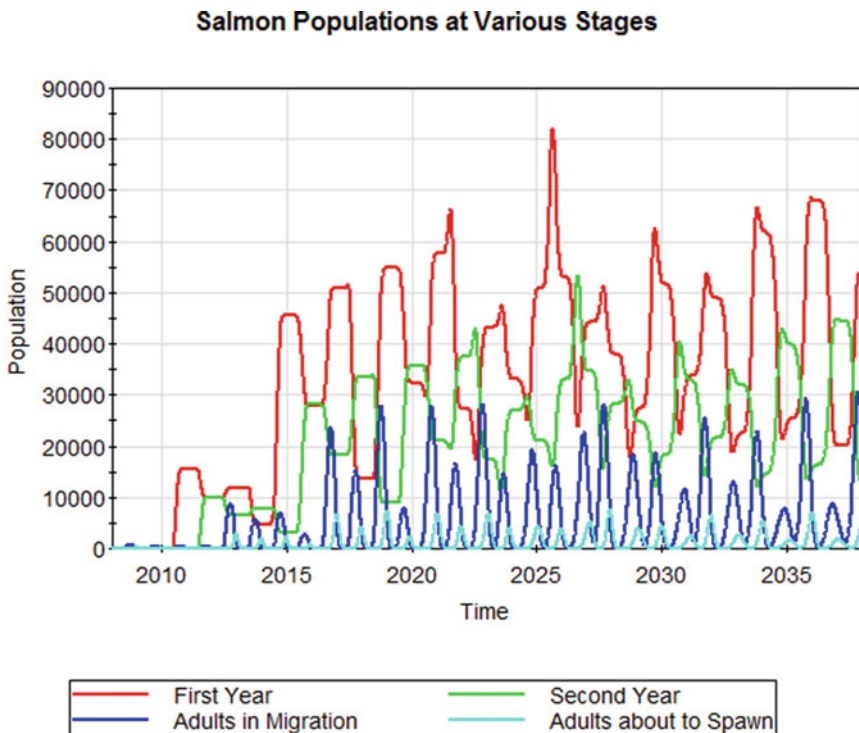


Fig. 1 Example of salmon population simulation [5]



Fig. 2 Use of VR in gaming

- a. HEMM operator's efficiency for any machine is the most vital factor contributing to the overall efficiency of the cycle-time. Each cycle time except loading, waiting and tripping depends on most common factor is operators' efficiency. Hence, we can conclude that the operator's efficiency directly or indirectly influences as much as 80% of the cycle time. It needs to be proven by data, measuring the operator's efficiency very challenging task. Based on which operators can be upskilled o and retrained on his lacking skill.
- b. How can we evaluate the "grade" of a HEMM operator?
- c. What should we do once we measure this "grade"?

Factors affecting the efficiency of operator is influenced by:

- a. Site and system factors: mine planning/design, mine scheduling, quantitative decision making.
- b. Machinery factors: Fuel efficiency, design efficiency.
- c. Human factors: Operations management, operator's skills.

The simulators to train and grade operatorives shall be classified into traditional and VR simulators.

- a. Traditional Simulators: Limited to aviation and space industry, training under a controlled environment, CapEx: INR 1 million to 10 million, versatility, OpEX: INR 1000 to 1500 per hour, monitoring, take up a huge facility, no risk on equipment damage and require periodic maintenance as well as quality checks.
- b. VR Simulators: Exhibit all the benefits of traditional simulators, wide variety of training scenarios can be replicated and repeated, give a 3-sense immersive sensory stimulation, are much cheaper than traditional simulators, can be used

for mass training in controlled environments and have a very low maintenance as well as operating cost.

5 Recent Development of VR for Quarry Operators Training

The models are currently trained by companies are hazard avoidance, cable move management, brake management, situational awareness, gear management, correct loading technique, operator productivity, fuel efficiency, brake management, tire preservation, engine management, site safety procedures, transmission management, minimizing unscheduled maintenance and situational awareness.

VR training can be superimposed for field operatives application leading to operators gradation and skill mapping. The differences between AR and VR are required devices and the experience itself. The AR utilizes a real-world setting. Meanwhile, the VR is entirely virtual [6, 7]. Besides, VR needs a headset equipment, but AR shall be accessed with a smartphone. While, AR improvises both the real and virtual world, the VR improvises fictional reality only.

VR shall be used as a learning lab [8]. Permit staffs to utilise virtual locations to create revolutionary new solutions to problems or appropriately upgrades to existing services or products. Anyone may utilize VR to enhance the advantages of scenario-based learning. The real-world decision-making and critical thinking abilities shall be improvised as well [9].

5.1 Advantages of VR

The advantages of VR are as following:

a. Experience as the finest teacher

Impressive VR experiences are illusions during which users may experience being in another world (place illusion) where the events taking place are real (acceptability illusion). Some people even assume themselves as a virtual body called avatar (personification illusion). In VR, the power lies in its capability to deceive the brain into believing that the unnatural events and environment are real [10]. Also, users experience things in context, in person while using VR. Circumstantial and ecological issues in VR seem to have a substantial optimistic effect on knowledge-construction activity and during the newly obtained capacities are employed.

b. Mental benefits

Although the content and instructional approach are more significant than the medium, VR-based training shall enhance learning attitudes. Aptly conceived VR reproductions appear to encourage learners to exercise more which directly increases perception on reality.

Symbolised reasoning philosophies propose that physical signals and communications in a virtual environment may advance mental processing due to high-level connection between human brain speed and visual processes. Besides, the emotions are found to have a major impact in solving hitches and making decisions particularly in bad conditions [11].

c. Gamification can improve motivation

Gamification as in Fig. 2 provides opportunities in VR to improvise learning and increase motivation of trainees. Engagement of trainees shall be increased by integrating training simulations with game-like aspects such as timed activities, rating and rewards while competing against each other in VR environment [12].

d. Cost-effectiveness and scalability

Having original simulator could be expensive with restricted ability whereas training in VR does not need actual presence on location. Thus, it prevents unnecessary costs of travelling while providing more viable moving strategies. VR training can be provided to all staffs, and they may safely practice as much as they want or feel prepared and confident. Besides, trainees could learn safely in VR regardless of making countless mistakes which may have expose them to unsafe or even awful events in the real world [13].

Example: Real simulants for training to nuclear power plant cost millions of rupees and further slot is not available often fully ordered. Whereas virtual imitation of the similar environment costs only a portion and execution of any modifications is rather simpler. It must be noted that 90% of employees at Fortum nuclear plant in Loviisa have undergone training in the world's first completely dynamic and interactive VR nuclear plant control room [14].

e. Real-time feedback and comprehensive analysis

One crucial aspect in education is assessing the learners' results. The build-in of most of VR systems provides accurate information about trainees' actions during the practice [15]. Therefore, the employee and trainees could obtain complete real-time feedback and instructions for future references. The crucial matter is to review trainee's performance and activities in a realistic environment with unparalleled accuracy and save information for future references.

f. Safe alternative: Controlled exposure to stressful environments

It is possible to expose trainees to real life emotional state in VR by offering a high level of spiritual presence. This enables them to learn to control their emotions during real life situation. In short, skills needed during dangerous environments shall be learned effectively using VR through realistic scenarios while real training would be expensive, unsafe or even not possible in actual life [16].

6 Conclusion

In short, a deeper understanding is required. We have traversed various topics with illustrations of VR education and the advantage of technological advantages [17, 18].

Though there is different between conventional (reality) vs virtuality training but, it is expected to give best result on account of participants feeling it as real images. Also, trainees familiarize with misapprehension as if it is real and correct themselves of any errors.

Moreover, VR technology is very cost effective and time saving. Gamification offers plenty opportunities to visualise as reality and quickly learn needed skills for the role. The head-mounted instrument enables users to experience being immersed in a simulated task environment instead of real life. VR learning is enthusiastic and committed to memory of our own encounters [19].

Theoretical classroom learning followed by practical experience and necessitated a new form of enlightening subject matter. Researchers point out that the “realistic environs” and “basic interaction” system factors are primary design needs for instructive VR applications.

Still there are no well-established best practices relevant to VR training as it is still in forming stage. Yet, presently available best practices shall be obtained from the current VR applications for the best learning outcomes.

The utilization of VR has a wider and more insightful effect on the users compared to conventional media which results in ethical complexities related to social dynamics, behavioural, physiological and cognitive effects [20].

Application of VR in the workforce teaching needs a profound awareness of all the aspects of technology and related human factors, but the rewards are quite high. The prediction signifies motivation and good learning with reduced cost and time, enough reasons to believe that VR teaching may become the only choice in future.

References

1. Sharma GV, Freeman AM (2014) Mentoring: why it matters even after training. *J Am Coll Cardiol* 64(18):1964–1965
2. Indeed Multitasking Skills: Definition and Examples. <https://www.indeed.com/career-advice/career-development/time-management-skills>. Accessed 10 Oct 2021
3. Indeed Time Management Skills: Definition and Examples. <https://www.indeed.com/career-advice/career-development/multi-tasking-skills>. Accessed 10 Oct 2021
4. Bauer TN (2010) Maximizing success. SHRM foundation’s effective practice guidelines series. SHRM Foundation, United States
5. GoldSim Simulation Primer. <https://www.goldsim.com/Web/Introduction/>. Accessed 10 Oct 2021
6. Tulane University What’s the Difference Between AR and VR. <https://sopa.tulane.edu/blog/whats-difference-between-ar-and-vr>. Accessed 10 Oct 2021
7. Farshid M, Paschen J, Eriksson T, Kietzmann J (2018) Go boldly!: explore augmented reality (AR), virtual reality (VR), and mixed reality (MR) for business. *Bus Horiz* 61(5):657–663
8. Fransson G (2020) Practice-based research and Virtual Realities (VR) in a Digital Learning Lab. Innovative school and learning environments in Germany and Finland. Research and findings of comparative approaches: Ideas of good and next practice. Waxmann Verlag., Munster, pp 208–209
9. Ali SA (2016) Virtual reality and Simulation (Doctoral dissertation). Suez Canal University, Egypt

10. Chalmers DJ (2017) The virtual and the real. *Disputatio Int J. Philos* 9(46)
11. Riva G, Mantovani F, Capideville CS, Preziosa A, Morganti F, Villani D, Gaggioli A, Botella C, Alcañiz M (2007) Affective interactions using virtual reality: the link between presence and emotions. *Cyberpsychol Behav* 10(1):45–56
12. Kapp KM (2012) *The gamification of learning and instruction: game-based methods and strategies for training and education*. Wiley, New York
13. Gunn T (2021) *The impact of virtual reality training on the clinical skill and confidence of medical radiation science students (Doctoral dissertation)*. Queensland University of Technology, Australia
14. Miettinen J (2008) Nuclear power plant simulators: goals and evolution. In: *Proceedings of seminar on transfer of competence, knowledge and experience gained through CSNI activities in the field of thermal-hydraulics (THICKET)*, Pisa, Italy
15. Geijtenbeek T, Steenbrink F, Otten B, Even-Zohar O (2011) D-flow: immersive virtual reality and real-time feedback for rehabilitation. In: *Proceedings of the 10th international conference on virtual reality continuum and its applications in industry*, pp 201–208
16. Cha M, Han S, Lee J, Choi B (2012) A virtual reality based fire training simulator integrated with fire dynamics data. *Fire Saf J* 50:12–24
17. Blascovich J, Bailenson J (2011) *Infinite reality*. HarperCollins, New York
18. Bennet R (2019) *Virtual re-embodied cognition (Doctoral dissertation)*. Israel Institute of Technology, Israel
19. Makransky G, Borre-Gude S, Mayer R (2019) Motivational and cognitive benefits of training in immersive virtual reality. *J Comput Assist Learn* 35(6):691–707
20. Kenwright B (2019) Virtual reality: ethical challenges and dangers. *IEEE Technol Soc Mag* 37(4):20–25

Excavation Assessment on Granitic Area at Ulu Kinta, Perak, Malaysia for an Earthwork Project



Eka Kusmawati Suparmanto and Edy Tonnizam Mohamad

Abstract Surface excavation work in tropically weathered rocks is challenging due to many uncertainties such as rock mass and material properties, environment, selection of best excavation method, machine characteristics, cost and production rate. The weathering profile of rock mass in the tropical region can be variable, unpredictable, and dominant in controlling rock behavior. Issues in confirmation on hard mass and rock mass in the surface excavation are discussed in this paper mainly in terms of definition and its relation to Jabatan Kerja Raya (JKR) Standard Specification Sect. 2:Earthwork, as essential references for practitioners related to surface excavation. It is crucial to ensure a reliable assessment on the most critical factors to reduce costs and unnecessary time delays. The study area is Ulu Kinta, Perak which is underlaid by granitic. This site was selected for this study because of the ongoing earthworks and exposure to rock outcrops. This study involved two geophysical methods, namely the 2D-Resistivity Method and Seismic velocity. Geophysical methods are beneficial for determining bedrock, type, and estimation of the volume of rock to be excavated for the areas, especially in the early stages of earthwork. The condition of the site consists of various grades where Grade I and Grade II granite was found at a depth of 33 m from the ground surface. Based on the correlation between borehole and seismic refraction, the overburden layer is dominated by low velocity values (<800 m/s) that correspond to low N values. This study also investigated the effect of moisture content on various grades of weathered granites, focusing on strength. It was found that moisture significantly affects weaker materials such as Grade IV and V was than stronger materials (Grade I and II). The trial excavation is carried out based on one type of excavator (EX 300); thus, confirmation can only be made to determine the hard mass for this area. The drilling method correlated well with the borehole result and proposed an alternative method in determining the hard

E. K. Suparmanto (✉)

Department of Geotechnics and Transportation, School of Civil Engineering, Universiti Teknologi Malaysia (UTM), 81310 Skudai, Johor, Malaysia
e-mail: ekakusmawati310@gmail.com

E. T. Mohamad

Centre of Tropical Geoenvironment (GEOTROPIK), Universiti Teknologi Malaysia, 81310 Skudai, Johor, Malaysia

and rock mass. Rock mass properties should be considered in the assessment, play a significant role in influenced excavatability and avoid problems that arise during excavation work.

Keywords Granite · Surface excavation · Drilling method · Geophysical methods · Trial excavation · Hard mass · Rock mass

1 Introduction

Reliable excavation assessment may significantly help the entire excavation process, incorporating the choice and improvement of the required methods or equipment. Unfortunately, this issue causes confusion among the contractor and clients on the best method to excavate. Furthermore, the lack of detailed information on the rock mass, such as weathering states, rock mass, and material properties, can significantly impact the project's feasibility. Therefore, comprehensive and systematic geological, geotechnical and geophysical information is crucial to help practitioners assess the relevant and significant parameters to consider in designing a method to use when facing this issue.

Ibrahim Komoo (1995) reported, among the primary difficulties in describing weathering descriptions is the weathering profile in Malaysia. It is formed due to highly intensive chemical weathering processes and then creates weathering processes for various rock lithologies (bedded and non bedded) very clearly. Weathering was observed to occur up to 100 m below the earth's surface. This view is supported by Khalil Abad et al. [1], who produced a combination of weather zones in granite profiles in the tropical region through field scale observations and geological studies. He proposed a typical mass weathering profile of tropically weathered granite rocks in the tropics, implemented in southern Malaysia. He found that the proposed weathering profile is a maximum thickness of 66 m. Excavation work in igneous origin is usually associated with the occurrence of boulders in a tropical region. Several researchers have studied rock weathering on granite boulders [2–4]. However, the relationship between the size, shape and distance of the rock from the base rock in the highly to a completely weathered rock where it formed is rarely studied and understood well. Md Dan et al. [5] conducted this study for the tropical region in Malaysia. Geological and geotechnical parameters are alternative methods used in civil engineering, essential in evaluating rock masses and determining suitable excavation methods. Therefore, by implementing the geophysical methods with conventional methods, site investigation problems maybe can be minimized. The cost and variation order (V.O) faced by the government on earthwork is bound to be the highest compared to other V.O, which has caused many losses to the government and delays in many projects.

1.1 Issues on Confirmation of Hard Mass and Rock Mass

The heterogeneity of rock mass causes great challenges and difficulties in performing surface excavation work. The condition of weak rocks (moderately (Grade III) to completely weathered (Grade V)) state often causing a different interpretation of the evaluation of the method of excavation to be made in tropical regions [6, 7]. This dispute involves contractors and clients due to cost and time factors between ripping and blasting methods [8]. Although many researchers have studied tropically weathered rock, there are still some loopholes for a dispute in quantifying changes in rock engineering properties due to weathering and its excavation method. Trial excavation is a direct method used to determine the easiness of excavation using types of machinery at the site studies.

Based on the Jabatan Kerja Raya (JKR) earthwork specifications published in 2013 (SPJ 2013 JKR), rock mass is stated as any hard material which can be excavated using an excavator with a minimum weight of 44 tonnes and net horsepower rating of 321 brake horsepower. While a production rate is not exceeding 50 m³/hour. Problems that are often encountered when dealing with construction sites consisting of weathering rocks in the tropics. Several issues are often associated with the specifications, such as difficulty obtaining a 44-tonne excavator machine, which is limited in the market. Besides that, choosing the appropriate method to decide the best excavation method for weathered rock in a tropical region is complex. Furthermore, this issue causing difficulty for engineer and practitioners on site in determining the material in the category of hard mass or rock mass type under the criteria in the existing specifications. Therefore, there is an urgent need for a more effective and reliable determination method to solve the problems on the site.

According to Standard Specification for Road Works published by the Public Work Department of Malaysia (PWD) in year 2020, hard mass is defined as the material that can loosen with an Excavator (Series 400) with a minimum weight of 41.4 tonnes which a net horsepower rating of 321 brake horsepower (BHP). While production rate not exceeding 50 m³/hour. Suppose the contractor is unable to provide the specified machine. In that case, he may suggest a similar machine for trial excavation purposes with an equivalent machine production rate calculated in Table 1 and Table 2. The calculation for the equal production rate is based on the method introduced by [9]. The actual production of the equipment is derived according to the various type of analysis, namely long-range, ratio and variance analysis.

When the direct method cannot confirm hard mass and rock mass classification based on the trial excavation method, the indirect method carried out a point load test on excavated material. Therefore, a minimum of ten (10) irregular samples from the excavated material resulting from trial excavation as indirect method (i) above shall be tested. The interpretation of the results is shown in Table 3.

The issue of hard mass or 'rock-soil' characteristics needs to be given due attention because it can lead to disaster and cause failure if not understood and dealing with properly, even for strong rocks such as granite.

Table 1 Equivalent production rate of hard mass based on type of excavators

Excavator series	Weight (Tonnes)	Engine horsepower (HP)	Factor compared with 41.4 tonnes (excavator series 400)	Equivalent production rate for hard mass (m ³ /hr)
150	15.4	99	0.33	16.5
200	21.2	170	0.58	29.0
250	27	188	0.63	31.5
300	31	242	0.67	33.5
350	36	271	0.75	37.5
400	41.4	321	1.0	50.0

Table 2 Equivalent production rate of rock mass based on types of track-type tractors with ripping equipment (Bulldozer Ripper)

Dozer	Flywheel power (kW)	Operating weight (Tonne)	Factor compared with 37 tonnes (Bulldozer Ripper)	Equivalent production rate for rock mass (m ³ /hr)
D6,D7	200 – 240	20 – 25	0.54	11.0
D8	303	37	1.0	20.0
D9	405	48	1.3	26.0

Table 3 Category of excavation based on corrected point load test index ($I_{s(50)}$)

Type of excavation	Corrected point load test index $I_{s(50)}$
Common excavation	Not applicable (no solid sample can be tested)
Hard mass	80% of the samples obtain result < 2 MPa
Rock mass	80% of the samples obtain result \geq 2 MPa

2 Site Location

2.1 Geology of the Site Area

The eastern part of Kinta Valley is bordered by the Granitic Main Range, which forms the backbone of Peninsular Malaysia, which runs north–south for more than 400 km. Meanwhile, the western part is bordered by Kledang Range. These ranges formed a reverse-V shape in topography. Figure 1 shows the location of the study area bordered by Main Granite Range and Kledang Range. The average age for the granite is 230–207 Ma. Generally, karstic limestone outcrops meet in the eastern part of the Kinta Valley. In the Kinta Valley and nearby areas, massive rock bodies

profiling methods. This method is implemented by first determining the weathering zones available on the site. The profile is selected based on the weathering change in the vertical section, and this change can be gradually changing. The profile was made by sketching each change in weathering levels and other geological features of the rock based on overall observations on site. Samples for each weathering level will be collected to provide a representative sampling to determine the rock material properties later [11].

3.2 Geophysical Investigation -Resistivity Method

Borehole drilling is widely used as a site investigation method to obtain soil stratification and soil type but only at discrete locations. Bacic et al. [12] pointed that the traditional borehole method guarantees more reliable geotechnical parameters, relying on human factors conducting the test in addition to time and financial aspects. Therefore, some concerns about geophysics may be among the suitable alternatives to address this emerging issue. Olona et al. [13] believes that geophysical methods have an advantage over the limitations of traditional methods, which give an inadequate characterization of heterogeneous soil and rock conditions in the area. Geophysical methods obtain spatial sampling and geotechnical parameters in the study area better. Besides, an alternative method of giving more detailed and precise information such as bedrock depth, cavities, dissolution features in carbonate rocks and boulders with a low cost and effective method [14–16]. The seismic refraction can generate information on stratigraphy and geomaterials features in two-dimensional (2D) [17]. He proved that the seismic method has a good correlation with borehole and promises more benefits.

3.3 Geophysical Investigation -Seismic Refraction Method

The main components of seismic refraction equipment are a source, detector and record. A seismic signal was recorded using ABEM Terraloc MK-6 Seismograph powered by a 12 V external battery. A 12 -pound sledge hammer generated the energy source and the 24 channel 28 Hz vertical geophone used as the detector. Geophysical investigation using seismic and resistivity results is shown below. Two (2) seismic lines of 115 m and four (4) resistivity lines of 200 m were carried out at the excavation area.

3.4 Drilling Method

Drilling is one of the common and accurate methods used, especially during earthworks, to obtain the properties of rock masses and geological exploration. The penetration rate is the most crucial parameter in rock mass characterization and drilling performance optimization. However, some parameters related to drilling need to be considered, such as power consumption and bit wear [18]. The penetration rate is the depth of penetration achieved during the drilling operation, expressed in (m/min). It is a parameter that gives the level of performance and efficiency of drilling. Therefore it is essential to maximize the rate of penetration [19]. Scoble et al. [20] conducted a study on drill monitoring. They found a correlation between drill performance parameters and changes in intact rock strength and other parameters. The parameters can be determined through empirical equations related to penetration rate, thrust on a bit, rotary speed, rotary torque and hole area. They also pointed out that laboratory tests can minimize the site's cost, time, and effort if MWD information obtains during drilling. Adebayo and Mukoya [21] reported a drilling machine problem of inappropriate parameters in rock formations, causing increased drilling costs due to the long time to make a blast-hole. A broadly similar point has also recently been made by [22]. He developed a model on rock mass strength estimation based on drilling information. It is beneficial for determining UCS and RQD values, especially for weak rocks, where specimens are relatively difficult to obtain.

3.5 Material Strength

A total of 50 rock samples were taken from the excavated material during the trial excavation method at the site. These samples were tested using a point load tester apparatus to obtain point load strength values for various types of rock weathering in this area. The dimensions of the rock samples were measured using a measuring tape and recorded using this test form. A load is applied to the rock sample until it fails and the load recorded. The test is performed by assessing the strength in a rock sample, whereby assessing the resistance load of the sample strength placed between two loading cones or bits that can adjust to grip. Point load index is useful in determining the strength properties of rock materials, but have a limitations.

3.6 Trial Excavation and Direct Assessment

The trial excavation was performed using machinery to obtain the production rate for the excavation work. Excavation performance was assessed to establish a relationship between geological and geophysical parameters. Each zone's production rates (Q) were recorded as a cubic meter per hour (m^3/h), dividing the volume by the excavation

Table 4 Specification of Komatsu PC 300–6 hydraulic excavator

Specification	Value
Engine power	134.3 kW
Operating weight	29,000 kg
Max travel speed	5.5 km/h
Track gauge	2590 mm
Reference bucket capacity	1.8 m ³

time. Observations and measurements made during the trial excavation measure and record several parameters such as ripping time, maneuvering time, ripping length, ripping width, and ripping depth [23]. Assessments of trial excavation and information such as the number of a bucket, bucket capacity and time of excavation were recorded and measured for different lithological and weathering grades, also used by Liang et al. [24]. The excavator operational specifications and properties were identified from the manufacturer (i.e., engine power, operating weight, maximum travel speed, track gauge and reference bucket capacity). The practical excavation rate (Q) is obtained for each excavator, which has various properties. The excavation operation was carried out by Komatsu PC300-6 hydraulic excavator. The properties and operational specifications of the selected excavator presented in Table 4.

4 Laboratory Works

4.1 Moisture Content

Samples collected from various lithological zones and weathering conditions were brought to the laboratory to test moisture content. The results of this test will establish a relationship between rock properties and excavatability. Two methods were conducted to achieve the desired level of moisture content in a test sample. First, a sample from each weathering grade was tested in initial/dry condition, 10, 30 and 60 min immersion. Second, the time was selected from dry to 60 min because the weathering grade IV and V samples were easily destroyed.

5 Results and Discussion

5.1 Field Mapping

Rock outcrops were studied to identify different rock mass and material characteristics for each weathering zone. The rock mass and material characteristics are joint

directions, joint orientation, joint number, spacing, moisture content and other conditions recorded for each weathering zone. The size and shape of boulders and relevant data will be recorded and analyzed to obtain significant parameters for rock excavation for the granitic area. Figure 2 shows an overview of the studied site. Five panels were classified from slightly weathered to completely weathered granite. The outcrop is 200 m in length and 15 m in height. Geological mapping, including identifying weathering zones, studying geological features, and measuring joint characteristics.

Table 5 tabulates the description of the studied panels. Five panels were classified based on the type of rock and the weathering state. It was found that at least two (2) joint sets characterized the rock mass with joint spacing varies from 0.01–2.0 m. The average joint spacing varies from 0.06 to 0.42 m (completely to slightly weathered zone). Alavi Nezhad et al. [25] reported a typical weathering of granite profile in the tropical region was established. The weathering zone has been divided into



Fig. 2 The overview of the studied site

Table 5 Description of studied panels at Ulu Kinta

Panel	Weathering zone	Joint set	Joint SPACING (m)	Average joint spacing (m)
1	II	2 joint sets: 070/80 265/05	J1 – 0.5–0.8 m J2 – 1.0–1.5 m	0.42
2	III	3 joint sets: 263/70 090/60 274/10	J1 – 0.3–2 m J2 – 0.2–1.5 m J3 – 0.3–1 m	0.28
3	III	3 joint sets: 260/62 070/68 302/70	J1 – 0.3–2 m J2 – 0.2–2 m J3 – 0.1–1 m	0.26
4	IV	3 joint sets: 235/60 089/16 269/12	J1 – 1.1–1.4 m J2 – 0.05–0.6 m J3 – 0.01–0.8 m	0.15
5	V	3 joint sets: 050/60 240/10 239/02	J1 – 0.05–0.3 m J2 – 0.08–0.2 m J3 – 0.1–0.3 m	0.06

subcategories to simplify rock mass structure and can be completed with or without boulders. He also reported that the mean joint trace length decreases as the weathering grade increases, which may be due to the rock undergoing disintegration and decomposition.

5.2 Seismic Refraction Result

Figure 3 shows a seismic line of S3. From the image, we can conclude that there are five zones. First zone is lower than 800 m/s (0–15 m); Second zone between 800–1200 m/s (15–22.5 m); Third zone is in between 1200–2400 m/s (22.5–27.5); Fourth zone is in between 2400–3200 m/s (27.5–33 m); Fifth zone is in more than 3200 m/s (>33 m). The first and second zone with seismic velocity values of less than 1200 m/s is residual soil, confirmed during the excavation test.

Figure 4 shows a seismic line of S6. From the image, there are five zones. First zone is lower than 800 m/s (0–10 m); Second zone is in between 800–1200 m/s (0–12 m); Third zone is in between 1200–2400 m/s (12–30 m); Fourth zone is in between 2400–3200 m/s (30–35 m); Fifth zone is in more than 3200 m/s (>35 m).

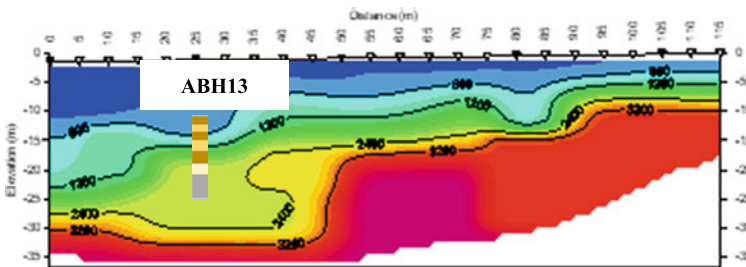


Fig. 3 Seismic line of S3

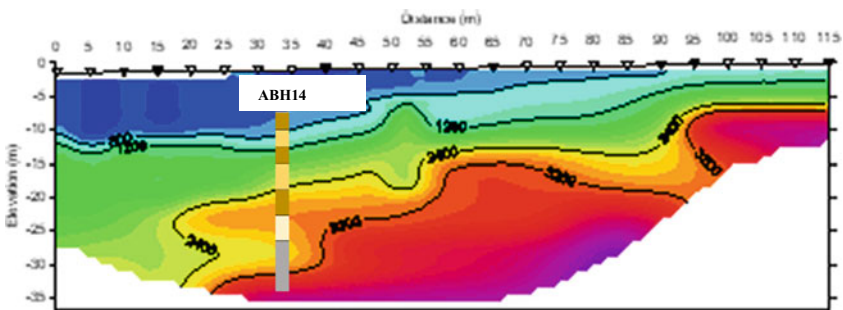


Fig. 4 Seismic line of S6

The first and second zones are residual soil. The excavation test found that the fourth and fifth zones are Grade I and II granitic rock.

In summary, the resistivity profiles obtained from the survey have a range of values between 1000–7,500 Ωm . In this study, three (3) types of significant resistivity values were found and were divided into three fields, as shown in Table 6. While Table 7 shows, a seismic value was divided into five ranges. It can be concluded that the ground conditions in this area show various levels of granite weathering. However, Grade I and Grade II fresh rock is estimated to be found at depths exceeding 33 m from the ground surface around high topographic areas. This finding matched the borehole profile where the granite was identified at 15–30 m depth. The results of the resistivity image study for Grade I and II showed a good correlation with the granite depth found in the borehole. This agrees with a statement made by Md Dan et al. [2], who made a study of boulders occurrence in tropical granite rocks. Grade I and II boulders are usually found at 1 to 30 m depth. However, fresh granite in the form of boulders is sometimes misinterpreted as bedrock in the borehole profile.

The borehole result in ABH13 (Fig. 5) shows that the site is underlain by soil type sandy SILT, and sandy CLAY to medium dense soil profile refers to soil properties based on SPT. The SPT reached 50 at depth 19.5 m, shown that a hard layer is found. However, this is not considered a bedrock. The soil profile in borehole ABH 14 is slightly similar to ABH 13, consisting of sandy SILT and sandy CLAY and a hard layer found at a depth of 28.0 m. The SPT values generally increase until each $N = 50$ at depth 28.0 m. From the observations in bore log ABH 13, the RQD values are 60, 65, and 67%, classified as fair rock quality. On the other side, RQD values in ABH 14 show a range of 55 to 63%, which the rock quality is also in the ranking as fair.

Table 6 Summary of resistivity value of weathered material for the study area

Depth (m)	Resistivity value (Ωm)	Material	Grade
0–15	1000–2200	Completely Weathered Rock – residual soil	V–VI
15–30 m	<1000	Moderately Weathered Rock – Highly Weathered Rock	III–VI
>30	2200–7500	Fresh Rock – Slightly Weathered Rock	I–II

Table 7 Summary of seismic value of weathered material for the study area

Depth (m)	Seismic value (m/s)	Material	Grade
0–15	800	Residual Soil	VI
15–22.5	800–1200	Residual Soil	VI
22.5–27.5	1200–2400	Moderately Weathered Rock – Highly Weathered Rock	III–VI
27.5–33	2400–3200	Slightly Weathered Rock	II
>33	3200	Fresh Rock	I

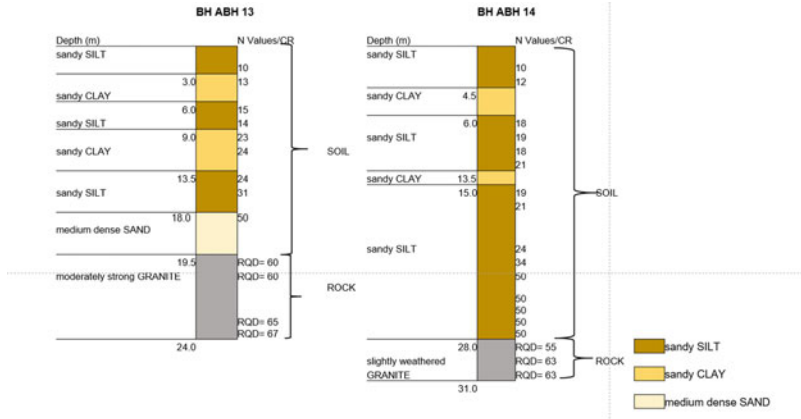


Fig. 5 Detail of borehole ABH 13 and ABH 14

The integration of analysis for resistivity and N value provides a more reliable and accurate subsurface relationship. These findings are similar to the conclusions of the study conducted by Mohamad, Alel et al. [26]. Correlation between geophysics and boreholes provides many advantages in terms of site investigation quality, reduces the risk of soil variation, provides more reliable results, and saves cost and time [15]. [27] Ismail et al. reported that this correlation can also determine the machines involved in excavation work to predict rock rippability. This statement was agreed by a researcher who also made a correlation between geophysics and site investigation.

From Tables 8 and 9 overall parameters comparing with core logs for BH1 and BH2, it is concluded that bit pounded and penetrates rocks read for measures parameter; feeding pressure and rotation pressure at above 2 MPa. However, for soils, the machine’s feeding pressure and rotation pressure reading was below 2 MPa. While for the calculated parameter, the Furukawa Top Hammer Hydraulic Crawler HCR1200-DS bit penetrates rocks at a penetration rate calculated below 2.15 m/min for the calculated parameter. As for soils, the penetration rate estimates above 2.15 m/min as it is penetrated faster than in rocks.

Tables 8 and 9 showed that the range for UCS (24.0–38.0 N/mm²) is low compared to the average value for granite in the tropical region. This condition is due to the high level of weathering in this area and causes mineral composition changes and rock color. High weathering causes the bonds of mineral structures to become weaker, further decreasing the UCS of these rocks. Both boreholes (BH1 and BH2) showed as UCS increases, decreasing penetration rate. The results of this test show the same results obtained by the researchers [28]; rocks with low UCS give higher penetration rate values. On the other hand, there are correlations between rock mass properties such as weathering grade and uniaxial compression strength (UCS) on the penetration rate. The penetration rate increases with increasing weathering grade, and in contrast, the penetration rate decreases linearly with increasing UCS. These findings are similar to the study conducted by Rathinasamy et al. [29].

Table 8 Correlation between all parameters for BH1

RL	Depth	BH1 Lithology	RQD (%)	SP T	Max Load kN	UCS (N/mm ²)	Percussive Pressure (MPa)	Feed Pressure (MPa)	Normalize Rotation Pressure (MPa)	Flushing Pressure (MPa)	Penetration Rate (m/min)
161	0 - 0.5	Sand, Soil		50			15	1	2	0.3	2.5
160.5	0.5 - 1.0						15	1	2	0.3	2.4
160	1.0 - 1.5						15	1	1	0.3	2.61
159.5	1.5 - 2.0						15	2	2	0.3	2.73
159	2.0 - 2.5						Moderately Weathered Granite	46	-	50	24
158.5	2.5 - 3.0	15	3	3	0.3	1.88					
158	3.0 - 3.5	15	3	3	0.3	1.5					
157.5	3.5 - 4.0	Slightly Weathered Granite	74	-	75	36	15	4	3	0.3	1.25
157	4.0 - 4.5						15	4.5	3	0.3	1.25
156.5	4.5 - 5.0						15	5	3	0.3	1.22
156	5.0 - 5.5	Fresh Granite	77	-	65	31	15	5	3	0.3	1.2
155.5	5.5 - 6.0						15	5	3	0.3	1.18
155	6.0 - 6.5						15	5	3	0.3	1.13
154.5	6.5 - 7.0	Fresh Granite	83	-	75	36	15	5	3	0.3	1.15
154	7.0 - 7.5						15	5	3	0.3	1.03
153.5	7.5 - 8.0						15	5	3	0.3	0.92

Table 9 Correlation between all parameters for BH2

RL	Depth	BH2 Lithology	RQD (%)	Max Load kN	UCS (N/mm ²)	Percussive Pressure (MPa)	Feed Pressure (MPa)	Normalize Rotation Pressure (MPa)	Flushing Pressure (MPa)	Penetration Rate (m/min)
155	0 - 0.5	Slightly Weathered Granite	49	55	26	15	5	3	0.3	2.00
154.5	0.5 - 1.0			120	57	15	5	3	0.3	1.88
154	1.0 - 1.5			75	36	15	5	3	0.3	1.33
153.5	1.5 - 2.0	Fresh Granite	93	110	52	15	5	3	0.3	0.77
153	2.0 - 2.5			80	38	15	5	3	0.3	0.61
152.5	2.5 - 3.0			80	38	15	5	3	0.3	0.61
152	3.0 - 3.5	Fresh Granite	90	50	24	15	5	3	0.3	0.65
151.5	3.5 - 4.0			80	34	15	5	4	0.3	0.75
151	4.0 - 4.5			70	33	15	5	4	0.3	0.76
150.5	4.5 - 5.0	Fresh Granite	91	95	45	15	5	3	0.3	0.74
150	5.0 - 5.5			70	33	15	5	3	0.3	0.75
149.5	5.5 - 6.0			80	38	15	5	3	0.3	0.69

In this case, this method is proposed because the contractor cannot provide the machine/equipment specified in the PWD Specification 2013 (in the determination of hard mass and rock mass) during the excavation work at the site. Therefore, this method is to be used as an alternative method to counter these issues. However, this method is not applicable and is used as a precedent for determining the rock for

the area. Therefore, it suggested that geophysical tests such as seismic refraction and resistivity could be applied as an accurate method in determining the initial estimation of rock quantity.

6 Conclusion

1. Although the drilling method has not been described as a method for confirmation of hard mass and rock mass, it is believed to quickly provide geological and geomechanical information (i.e., rock mass characterization) and at a minimal cost. However, an improvement is needed, namely the prediction of RQD in situ rock mass properties. Therefore, an early penetration rate prediction is necessary for cost estimation and planning of engineering design projects.
2. The hard layer is determined through the borehole method with the first SPT value $N = 50$ in the borehole data. However, this layer does not indicate that it is rock. However, seismic methods cannot provide rock mass quality based on the RQD value of the borehole.
3. Rock mass excavation is greatly influenced by factors such as the joint sets number and direction of discontinuities; currently, a more straightforward graphical method Pettifer and Fookes (1994) is more suitable for determining the excavatability of rocks. This graph considers only two parameters, namely point load strength and discontinuities spacing. Therefore, the material and mass properties can be as acceptable in the assessment.
4. The trial excavation is carried out based on one type of excavator only; confirmation can only be made to determine the hard mass for this area. Therefore, a further inspection using various types of excavators should be considered. In this case, the indirect method using the Point load test has confirmed that the rocks for this area are rock mass. The same goes for the use of dozers to determine rock mass.

References

1. Khalil Abad SV, Mohamad ET, Komoo I, Kalatehjari R (2015) A typical weathering profile of granitic rock in Johor, Malaysia based on joint characterization. Arab J Geosci 8(4). <https://doi.org/10.1007/s12517-014-1345-7>
2. Md Dan MF, Mohamad ET, Komoo I (2016) Characteristics of boulders formed in tropical weathered granite: a review. Jurnal Teknologi 9635. <https://doi.org/10.11113/jt.v78.9635>
3. Alavi Nezhad Khalil Abad SV, Mohamad ET, Komoo I, Kalatehjari R (2014) A typical weathering profile of granitic rock in Johor, Malaysia based on joint characterization. Arab J Geosci. <https://doi.org/10.1007/s12517-014-1345-7>
4. Vann JD, Olaiz AH, S Morgan, and C. Zapata, (2019) A practical approach to a reliability-based stability evaluation of precariously balanced granite boulders. In: US Rock Mechanics/Geomechanics Symposium

5. Md Dan MF, Mohamad ET, Tan SNMA, Komoo I (2015) Physical field characterization of boulders in tropical weathering profile—a case study in Ulu Tiram, Johor Malaysia. *J Teknol* 76(2):59–65. <https://doi.org/10.11113/jt.v76.5434>
6. Mohd Amin MF (1995) Classification of excavated material based on simple laboratory testings. *Geol Soc Malaysia* 179–190
7. Mohamad ET, Kassim KA, Komoo I (2005) An overview of existing rock excavability assessment techniques. *Jurnal Kejuruteraan Awam* 17(2):46–59
8. Tawaf MK, For M, Amin M, Asmani D, Yusof M, Nizam S (2018) Sandstone rippability assessment based on specific energy relationship with tensile strength and surface hardness. *J Adv Res Appl Sci Eng Technol* 1(1):25–33. issn: 2462-1943
9. Rafsanjani HN, Gholipour Y, Ranjbar HH (2009) An assessment of nominal and actual hourly production of the construction equipment based on several earth-fill dam projects in Iran. *Open Civ Eng J* 3(1):74–82. <https://doi.org/10.2174/1874149500903010074>
10. Meng CC, Sautter B, Pubellier M, Menier D, Sum CW, Kadir A (2014) Geological features of the kinta valley. *A J Eng Sci Soc* 10(2):2–14. https://www.researchgate.net/publication/283622669_Geological_features_of_the_kinta_valley
11. Gokceoglu C, Zorlu K, Ceryan S, Nefeslioglu HA (2009) A comparative study on indirect determination of degree of weathering of granites from some physical and strength parameters by two soft computing techniques. *Mater Charact* 60(11):1317–1327. <https://doi.org/10.1016/j.matchar.2009.06.006>
12. Bačić M, Librić L, Kačunić DJ, Kovačević MS (2020) The usefulness of seismic surveys for geotechnical engineering in karst: some practical examples. *Geosci* 10(10):1–17. <https://doi.org/10.3390/geosciences10100406>
13. Olona J, Pulgar JA, Fernández-Viejo G, López-Fernández C, González-Cortina JM (2010) Weathering variations in a granitic massif and related geotechnical properties through seismic and electrical resistivity methods. *Near Surf Geophys* 8:585–599. <https://doi.org/10.3997/1873-0604.2010043>
14. Saad R, Mohamad ET (2016) Geophysics applications in engineering and environmental issues. *J Teknol* 78(8):67–72
15. Azrief Azahar M, Farhan Zakiran Mahadi N, Rusli QN, Narendranathan N, Lee EC (2019) Use of geophysics for site investigations and earthworks assessments. *IOP Conf Ser Mater Sci Eng* 512(1). <https://doi.org/10.1088/1757-899X/512/1/012007>
16. Mehidi Y, Nouioua I, Kahoul I (2019) Geotechnical parameters acquisition using geophysical data by using seismic refraction method—a case study. In: *Proceedings of the 1st International Congress on Advances in Geotechnical Engineering and Construction Management*, vol I, pp 424–429
17. Hazreek M et al (2013) Mapping of geotechnical data using seismic refraction studies. *Casp J Appl Sci Res* 2:1–9
18. Sazidy MS, Rideout DG, Butt SD, Arvani F (2010) Modeling percussive drilling performance using simulated visco-elasto-plastic rock medium
19. Mensa-Wilmot G, Harjadi Y, Langdon S, Gagneaux J (2010) Drilling efficiency and rate of penetration—definitions, influencing factors, relationships and value. In: *SPE/IADC Drilling Conference Proceedings*, vol 1, pp 578–590. <https://doi.org/10.2118/128288-ms>
20. Scoble MJ, Peck J, Hendricks C (1989) Correlation between rotary drill performance parameters and borehole geophysical logging. *Min Sci Technol* 8(3):301–312. [https://doi.org/10.1016/S0167-9031\(89\)90448-9](https://doi.org/10.1016/S0167-9031(89)90448-9)
21. Adebayo B, Mukoya JGM (2019) Rock properties and machine parameters evaluation at Rössing Uranium Mine for optimum drill performance. *J South Afr Inst Min Metall* 119(5):459–464. <https://doi.org/10.17159/2411-9717/17/155/2019>
22. Basarir H, Karpuz C (2016) Preliminary estimation of rock mass strength using diamond bit drilling operational parameters. *Int J Min Reclam Environ* 30(2):145–164. <https://doi.org/10.1080/17480930.2015.1025561>
23. Basarir H, Karpuz H (2004) Development of a direct rippability assessment method

24. Liang M, Tonnizam E, Ibrahim M, Ma KC (2015) An excavability classification system for surface excavation in sedimentary rocks. *Bull Eng Geol Environ* 76(1):241–251. <https://doi.org/10.1007/s10064-015-0807-9>
25. Khalil Abad SV, Mohamad ET, Komoo I (2014) Dominant weathering profiles of granite in southern Peninsular Malaysia. *Eng Geol* 183:208–215. <https://doi.org/10.1016/j.enggeo.2014.10.019>
26. Mohamad ET, Alel MNA, Masdi NF (2015) Correlation between seismic refraction and bore-hole data for sursurface evaluation. *J Teknol* 76:2(August):9–15. <https://doi.org/10.11113/jt.v78.9285>
27. Ismail MAM, Kumar NS, Abidin MHZ, Madun A (2018) Rippability assessment of weathered sedimentary rock mass using seismic refraction methods. *J Phys Conf Ser* 995(1). <https://doi.org/10.1088/1742-6596/995/1/012105>
28. Hassan NF, Jimoh OA, Shehu SA, Hareyani Z (2019) The effect of mineralogical composition on strength and drillability of granitic rocks in Hulu Langat, Selangor Malaysia. *Geotech Geol Eng* 37(6):5499–5505. <https://doi.org/10.1007/s10706-019-00995-x>
29. Rathinasamy V, Mohamad ET, Komoo I, Bin Hanapi MN, Bhatwadekar RM (2020) Influence of physico-mechanical properties of tuff on penetration rate—a case study in Southern Johor Bahru, Malaysia. *J Mines Met Fuels* 68(4):136–143

Tackling the Asian Sand Crisis—A Case Study in Applying GAIN™ Best Practices in Viet Nam’s Mekong Delta



Jim OBrien

Abstract In early 2021, the author was requested by WWF Viet Nam to suggest solutions to the over-extraction of sand in the Mekong Delta. The study drew on the extensive experiences of the Global Aggregates Information Network (GAIN™), which had recently focused on challenges of river sand extraction globally. Relevant case studies from China, India, Malaysia, Colombia, Mexico, USA, Canada, New Zealand, UK, Netherlands, Myanmar and Japan provided key insights, these leading to a set of key recommendations proposed for implementation in Viet Nam. These recommendations ranged from suggested amendments to Viet Nam legislation, to designation of a strongly-empowered single regional authority to implement a rigorous permitting regime, using internationally-proven technical extraction guidelines, backed up by certification of professional operators, comprehensive compliance monitoring and strongly increased royalties, penalties and deterrents. International experiences also indicated the desirability of a project-specific champion to successfully implement these changes, which could also be greatly assisted by a professional national aggregates association and/or a construction industry association. Recommendations were also made on encouraging alternatives to river sand, such as manufactured sand and use of recycled and secondary materials, which can reduce the river sand demand to within its annual sedimentation budget. Commercial incentives to promote this shift can be achieved by using legislation to substantially reduce demand and increase the extraction costs of river sand. This “carrot and stick” approach can lead to a more sustainable extraction and construction industry in the Mekong Delta, as well as benefitting its fishermen, farmers, ecosystems and the wider community.

Keywords Aggregate · Global Aggregates Information Network (GAIN) · River sand · Manufactured sand (M sand) · Recycled materials · Secondary materials

Convenor, Global Aggregates Information Network (GAIN™), (www.GAIN.ie)

J. OBrien (✉)
Dublin, Ireland
e-mail: jim@jimobriencsr.com

© The Author(s), under exclusive license to Springer Nature Singapore Pte Ltd. 2022
A. K. Verma et al. (eds.), *Proceedings of Geotechnical Challenges in Mining, Tunneling and Underground Infrastructures*, Lecture Notes in Civil Engineering 228,
https://doi.org/10.1007/978-981-16-9770-8_35

537

1 Background on the Mekong Delta

Mekong River flows through six countries namely China, Myanmar, Lao PDR, Thailand, Cambodia and Viet Nam. The river's basin is home to about 70 million people of which 60 million live in Lower Mekong Basin (LMB) while 10 million live in Upper Mekong Basin (UMB).

The Mekong River is the tenth longest river in the world. It originates from the Tibetan plateau and flows through a narrow, deep gorge roughly parallel to the Salween and Yangtze Rivers. This area is popularly known as 'Three Rivers Area'. The Mekong River continues through Myanmar, Lao PDR, Thailand and Cambodia before finally draining into the sea in Viet Nam while creating a large delta.

The Vietnamese Mekong Delta (VMD) covers an area of approximately 40,500 km² in 13 provinces and is home to some 18 million people. Further 9 million people reside in the adjacent greater Ho Chi Minh City (HCMC).

While the region is undergoing rapid economic growth, the livelihood and food security of the majority of people living in Mekong's River Basin population is explicitly linked to the Mekong River (Fig. 1).

Mekong river is characterized as a nutrient-rich sediment river. This is because of the river's flood pulse character as at any given period, particularly post-monsoon, large volumes of water are flowing through the system along with sediments.

The fine materials are carried through the system to the sea as they are suspended in water. Depending on the flow velocity and discharge of the river, slightly coarser material ends up on flood plains and riverbanks where it serves as natural fertilizer and food for fisheries. Finally, large particles such as sand and gravel may take decades or longer to be transported and are often temporarily stored in the river channel, in sandbanks or on riverbanks thus contributing to the river geomorphology and bank stability.

The construction of hydropower dams (Fig. 2 overleaf) and extraction of sediments (Fig. 3 overleaf) for a booming construction sector have reportedly reduced sediment transport to the Mekong Delta by about 77% between 1992 (160 mt/year) and 2014 (75 mt/year), which by extrapolation may now be less than 50 mt/year.

These figures are for suspended sediment, mostly silt and clays, and are thus marginally relevant to sand mining. The statistic for sand alone is believed to be of the order of 20–30 mt/year pre-1990 and only 3–5 mt/year today. Sand demand now greatly exceeds natural supply, and strong measures are urgently needed to alleviate further deterioration of the Delta itself and of local farming, rice production, fishing and biodiversity. It is also reported that the available sand is becoming finer, making it less attractive for use in concrete, probably also requiring higher cement content.

Over-exploitation and its impacts have been analyzed and described in several publications in recent years as listed in references 1 to 14. These studies report both specifically on the sand deficits in the Mekong Delta [1, 4, 8, 11, 15], as well as the negative impacts on ecosystems, biodiversity, agricultural productivity, navigation and local communities [2, 3, 5, 8, 9, 14]. Within Viet Nam, public and press awareness



Fig. 1 Map of the Mekong river basin



Fig. 2 Dams on the Mekong river

of unsustainable river sand mining practices are rising sharply, arguably providing a social foundation for legislative and enforcement change.

Such impacts are by no means limited to the Mekong Delta. For example, Koehnken et al. [12] carried out a Quick Scoping Review of 505 international publications (75% from the previous 5 years) on the impacts of riverine sand mining on freshwater ecosystems worldwide, identifying 107 different impacts. These were broadly divided between changes to the channel morphology, alterations to the composition and movement of sediment, changes to larger scale river features, alterations to the flow regime, and impacts on water quality.

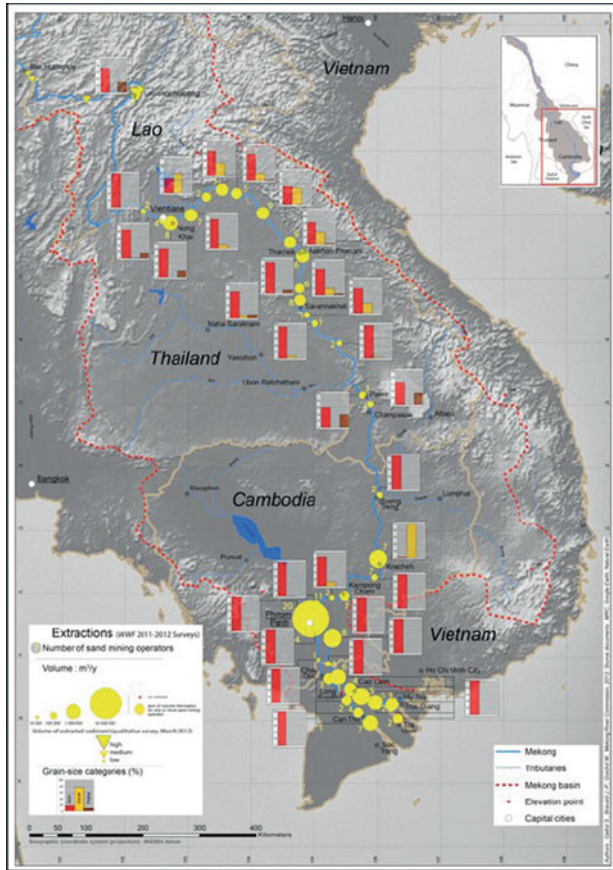


Fig. 3 Sand mining locations along the river

2 Sustainable Mining Initiative in the VMD

This **IKI Sustainable Sand Mining Initiative** in October/November 2020 reflects a highly-laudable and well-focused consultation process with the 13 Mekong Delta regions, comprising the 12 provinces - Long An, Dong Thap, Tien Giang, An Giang, Ben Tre, Vinh Long, Tra Vinh, Hau Giang, Kien Giang, Soc Trang, Bac Lieu, and Ca Mau, along with the centrally-run city of Can Tho. This is to be in cooperation with the Line Ministry MARD. Its purpose was to pool and share knowledge on all aspects of extraction of sand and potential substitutes within the Delta Region.

It was found that practices varied widely between provinces, and that it was very difficult (despite the open cooperation of all involved) to ascertain the extent of deposits of the various materials, of the actual quantities extracted and of their respective markets and end-uses; also the extent of environmental damage as landslides varied by region (Fig. 4).



Fig. 4 Alternative sources to river sand in the VND provinces

The provisional alternatives identified to river sand included:

- Manufactured sand is produced in small quantities in Kien Giang and An Giang provinces.
- Sea sand (marine sand/aggregates dredging) from Ben Tre, Kien Giang and Tra Vinh provinces, where in the latter two it is being used for sea encroachment projects.
- Coal slag (or fly-ash) from the former Duyen Hai 1 coal-fired power station.
- Basaltic soil is no longer viable because of transport costs and as it does not meet the requirements for highway development.

The main applications for both natural and manufactured sand were identified to be in construction, while the other materials could be used only for “leveling” purposes. There was little real information on sedimentation quantities, which were clearly insufficient to satisfy burgeoning construction demand.

However, recycled aggregates were not mentioned, an omission which could be incentivized by a requirement for engineered landfills, a landfill tax and a strong permitting regime such as outlined in the EU Directive on Waste Landfilling 1999 and the International Solid Waste association 3rd Edition Landfill Operational Guidelines 2019.

The Report also documented widely varying practices in licensing and monitoring, which had the effect of facilitating illegal activity, which thrived on inconsistent application between adjacent provinces. In one province, there was a pilot program of remote monitoring by cameras and GPS (based on Decree 23/2020). It found that river and coastal erosion was occurring in 12 of the 13 provinces, despite the good intentions of the regulatory instruments.

Their Report recommends a Delta-wide sedimentation study, closer investigation of alternative supplies (particularly of manufactured sand), improved extraction techniques and more public awareness campaigns. It identifies the need for more support from central government, particularly from the Ministry of Natural Resources and Environment.

3 Lessons Learnt from the Case Studies

Sand mining practices were studied in China, India, Malaysia, Colombia, Mexico, USA, Canada, New Zealand, Canada, UK, Netherlands, Myanmar and Japan. These twelve case studies demonstrate that:

- River extraction remains an important source of aggregates in many countries, though uncontrolled over-exploitation can cause severe damage to river infrastructure & environment.
- River extraction can be carried out in full harmony with nature within annual sediment deposition rates (once reserves have been given time to replenish), and furthermore can provide flood control and can foster biodiversity (as particularly demonstrated in the biodiversity-positive case studies from New Zealand, UK and Netherlands).
- However, unfortunately, due to the enticement of burgeoning construction demands and lax and inconsistent permitting, monitoring and enforcement controls and low extraction costs, river extraction in some countries has become illegal and irresponsible.
- There are learnings from both successes and pitfalls of the case studies which demonstrate that, with determination of all parties involved, river extraction can be well-controlled and that illegal extraction can be phased out.
- More sustainable solutions for construction can be developed by reducing river sand supply and simultaneously creating economic incentives for moving to alternative materials.

Three alternative methods to replace river sand are discussed in the following paragraphs.

1) **Manufactured Sand (“M-Sand”)**

Hard rock quarries are primarily designed to produce crushed stone aggregates, often also producing fines that often remain unsold. These quarries are usually semi-permanent, multi-decade operations, with large capacity and at a fixed location, facilitating regulation and enforcement (Fig. 5).

As in this case, by adding fine crushing equipment to a hard rock quarry at incremental low investment, manufactured sand may be produced by further crushing by-product materials, to produce high-quality sand. This fine-crushing may be achieved by using Vertical Shaft Impactors (VSIs), as shown here, or using grinding roller technology.



Fig. 5 Illustrates a manufactured sand plant in the United Arab Emirates, which product is shipped globally

Studies have shown that the best end product for various purposes can be achieved with high-velocity impact crushing; a vertical shaft impactor yields the soundness and shape of the material and produces a quality that is very close to natural sand. The better the grain shape of the end product, the better its performance in concrete, asphalt and base mixtures. Air classifiers are used to remove the needed amount of fine particles and dust, or alternatively, wet classification may be used.

The advantages of manufactured over natural sand include the ability to produce with exactly the right shape and gradation, When used in concrete, there may be saving in cement usage through achieving concrete of optimum quality, strength and structural integrity. Although not without environmental impacts, it can present substantial potential sustainability benefits vs illegally extracted river sand. Some manufactured sand is already produced in Kien Giang and An Giang provinces.

If river-based sand prices surge (due to interdiction and/or regulation, as in India), there can be strong financial incentives to invest in manufactured sand equipment with the result it can be more cost effective than natural sand, subject to a robust regulatory and enforcement regime. Manufactured sand is free of silt and clay particles, and has denser particle packing than natural sand. It also offers higher flexural strength, better abrasion resistance, higher unit weight and lower permeability. After initial familiarization, contractors prefer manufactured over natural sand, allowing them to produce higher grade concretes at lower costs, especially due to reduced cement demand for a specific concrete performance.

For example, ready mixed concrete producers in Yangon, Myanmar, prefer to use manufactured sand to that supplied by barge from riverbed mining in the Irrawaddy for any high specification structural concrete or for demanding international contractors, despite higher prices for manufactured sand.

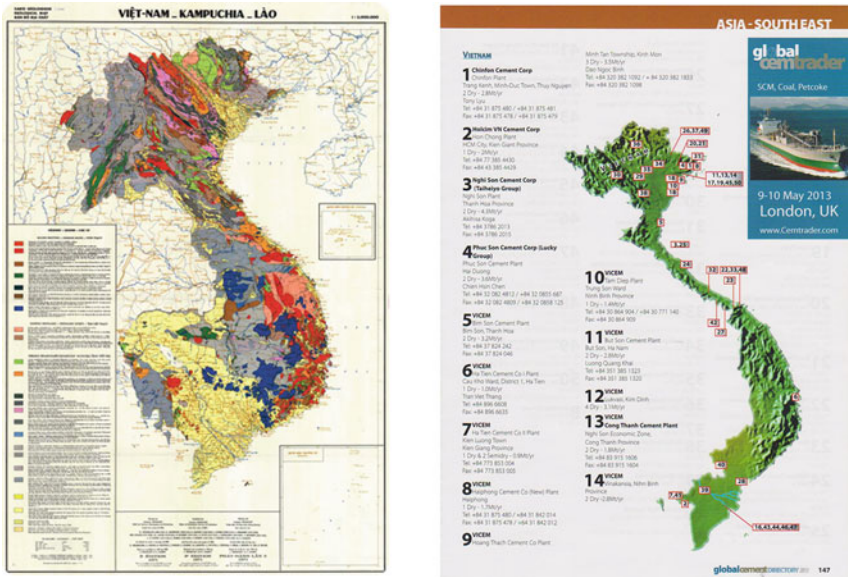


Fig. 6 In searching for a suitable hard-rock source for producing manufactured sands, the geological map (at left) shows that the Delta region, as expected, is covered principally by alluvial deposits

On the other hand, the Global Cement Directory map (at right) shows cement plants located in the Mekong Region, implying hard-rock resources potentially suitable for the production of manufactured sands (Fig. 6).

An industry source has confirmed that some hard-rock deposits exist within the VMD region and are capable of development; however, licensing conditions need to be stricter with longer permit durations (>30 years) to justify the capital investment in opening new larger-scale quarries.

An outstanding example of moving from natural to manufactured sand is in Hyderabad, the capital city of the State of Telangana, India’s technology industry hub, where rapid growth puts great pressure on regional infrastructure development. The city had long been struggling to get river sand, but governmental policies banned the use of river sand, citing that the depletion of the natural resource and the ill-effects of dredging and indiscriminate quarrying of river beds posed a great threat to the environment. There is now a rapid transition taking place from natural sand to manufactured sand, a win-win situation for all concerned.

The hard-rock quarry operators, encouraged by the authorities, have rapidly invested in this new business, and the construction industry is welcoming the higher quality, lower price, better reputation and performance of manufactured sand. Because of this rapid investment by the quarry operators, and consequent better supply of sand, the high “black-market” prices created by illegal operators have now disappeared, to the benefit of all concerned. In the VMD region, there are not many

Fig. 7 A large crushing and screening plant for recycling of construction and demolition materials in the Netherlands



hard rock quarries, although in An Giang and Kien Giang province- crushed sand production is available.

2) Recycled Aggregates

Recycled Aggregates (RCAs) are typically crushed concrete (or asphalt pavement) derived from sorted construction and demolition waste that is then reused in other building projects (Fig. 7).

This activity is an important source of aggregates in economies with high landfill taxation or bans and is of increasing importance worldwide. RCAs can be used for roadbase, fill, graded aggregates and as a (partial) component in both structural and non-structural concrete and in asphalt. Recycled fines may also be used to replace natural/river sand.

RCAs reduce both primary mineral extraction and landfilling and can (depending on location of the recycling unit) be a means to reduce costs of construction while also boosting “green” label points. For example, the US LEED® certification system recognizes recycled concrete in its point system.

As an example, Construction and Demolition (C&D) waste is the largest waste stream in the EU, often representing around one third of total arisings. Orders of magnitude of C&D waste in 2009 were 510 mt in the EU, 325 mt in the USA and 77 mt in Japan. The EU Waste Framework Directive 2008/98/EC established a target of 70% of C&D Waste to be recycled by 2020. However, with the exception of a few Member States, only about 60% of C&D total waste is typically being recycled. Some EU Member States have already developed and implemented a framework which leads to a recycling rate of up to 90% of available waste, equivalent to 25% substitution for primary aggregates.

3) Low Grade Materials for Land Raising

Use of low grade, but inert materials (for example, coal mine overburden, coal washings, steel slag) can be used for land raising applications, provided there are no impacts due to leaching (for example of heavy metal trace contents). However, some of these may better be beneficiated by cement producers, and may thereby attract a greater commercial value. Coal slag (or fly-ash) would arguably better be used by the local cement producers as alternative materials to clinker.

In 2019, a new Viet Nam standard called TCVN 12,660:2019 on ash from coal-fired power plants was published: This standard sets out the technical, construction and acceptance requirements for its use in construction of highway embankments. The standard identified certain risks which might limit the ability to apply this resource in the VMD and limited its use to the construction of embankments, but not in areas prone to flooding or at groundwater level.

Sea sand, if not washed, is generally less suitable for use in structural concrete because of reinforcing steel corrosion and efflorescence concerns; also near-shore extraction of sea sand may only exacerbate coastal erosion (as seems to be the case in Kien Giang and Tra Vinh in the VMD). It may be that additional consideration could be given to extraction of marine sand or aggregates several kilometers offshore (as in the UK case study), if suitable marine resources exist at modest depths, though that would require specialist dredging vessels and rigorous controls.

In Europe, the chloride limit is placed on the concrete producers, and the supplier of sea sand or marine aggregates has to declare a maximum chloride value which will not be exceeded. For use in reinforced concrete, the sand has to be washed in clean (non-saline) water, while seawater washing is acceptable for producing unreinforced concrete. The National Standard TCVN 9205:2012 [22] for crushed sand in concrete and mortar, sets limits for acid-soluble chloride content of <0.01% by weight when used in pre-stressed concrete and <0.05% when used in reinforced concrete and other concretes and mortars, though either may be exceeded if the total chloride ion content in 1 m³ of concrete is <0.6 kg. Other international research confirms acceptability of use of washed sea sand in concretes under controlled circumstances.

4 Some Observations Relating to the Mekong Delta

While banning river-based sand and gravel extraction (or tightly restricting it with extraction being limited to within annual regeneration) are desirable ultimate goals, the unintended consequences of imposing policies in isolation can include supply shortages affecting economic development and delaying construction programs, rising “black market” prices for sand and even potential for criminalization of extraction (described by UNEP as the “sand mafias”).

The solutions for addressing the impacts of river-based sand and gravel extraction should therefore ideally consider the wider implications for overall sustainable development, putting in place practical solutions which can assure a managed transition to the ultimate goal with a portfolio of measures which fulfil overall national sustainable development objectives, balancing environmental, social and economic outcomes. For the Mekong Delta, specific lessons can be learnt to adopt policies which can satisfy the various interest groups in the economic landscape.

Experiences from GAIN member show that, to be successful, there has to be very strong action by the relevant authorities, not just in regulation, but also in implementation and monitoring. GAIN experiences from other jurisdictions show that it is necessary not only to specifically permit river/delta extraction areas and

quantities, but to also introduce GPS tracking of operating vessels and of all delivery trucks, to ensure compliance. It is also highly desirable that the concrete industry suppliers and construction contractors cooperate through purchasing of aggregates certified to be responsibly-sourced.

Equally, responsible suppliers need to be encouraged to develop new hard-rock quarries in southern Viet Nam and cost-effective sustainable logistics routes from hard rock quarries in central and northern Viet Nam which should supply the necessary aggregates volumes for a rapidly-developing economy; there is also a real new and exciting opportunity for them to start producing manufactured sand. Viet Nam has the advantage of being a coastal country, while the VMD has a wide system of rivers and channels which would allow the economic delivery of aggregates and manufactured sand by barge or ship to all parts of the country from central or northern Viet Nam where more hard-rock deposits exist.

5 Recommendations and Conclusion

- Promote the production of high quality **manufactured sand** from hard-rock quarries (if not within the VMD, in central or northern Viet Nam) a measure that is being deployed with significant success in case study several regions. Indications are that there are some hard-rock resources within the VMD, but the licensing/permitting regime hitherto does not sufficiently encourage development.
- Promote the sorting and **recycling of construction and demolition waste** to produce both concreting aggregates as well as lower-grade leveling fill, with the potential additional benefits in reduced landfilling and aggregates transport. Also promote optimal beneficiation of low grade, but inert wastes for land raising applications.
- Suggested introduction of a **responsible sourcing certification** scheme for construction aggregates and land raising materials. These would have to accompany any supply of such materials, failure by construction project developers to be able to produce certificates for materials used could be punishable by fines.
- Royalties, fines and the proceeds of auctions could be paid to the regulatory authority to **internalize the externalities of sand mining** and be hypothecated for use in Lower Mekong Delta protection activities (including funding of: (1) the personnel and operating costs of the authority, (2) monitoring and enforcement activities, (3) the costs of the LMD Sand Project, Leader (see later), as well as (4) financial incentives to communities who actively work against illegal extraction – maybe as some form of monitoring grant per km for communities on each side of the rivers). Crucially, these additional costs would also aim deliberately to drive up the price of river sand (thereby making alternatives more economically attractive).

References

1. Jordan C et al (2019) Sand mining in the Mekong delta revisited—current scales of local sediment deficits, *Christian*. <https://doi.org/10.1038/s41598-019-53804-z>
2. Minderhout PSJ et al (2019) Mekong delta much lower than previously assumed in sea-level rise impact assessments. <https://doi.org/10.1038/s41467-019-11602-1>
3. Koehnken L (2018) Impacts of sand mining on ecosystem structure, process and biodiversity in rivers. In: WWF, 2018
4. Piman T, Shrestha M (2017) Case Study on sediment in the Mekong River Basin: current state and future trends. UNESCO/SEI Project Report 2017-03
5. Muller P et al (2017) Societal and institutional interrelations of aggregates mining in Viet Nam. In: International Conference on Resource Extraction, Hanoi. <https://www.researchgate.net/publication/332018866>
6. Schiappacasse P et al (2020) Construction aggregates and environmental policy integration in a one-party state: the case of Hoa Binh, Viet Nam. *Sustainability*. <https://doi.org/10.3390/su12176890>
7. Schiappacasse P et al (2019) Towards responsible aggregates mining in Viet Nam, *Resources*. <https://doi.org/10.3390/resources8030138>
8. Bravard J-P et al (2019) Geography of sand and gravel mining in the lower Mekong river. <https://doi.org/10.4000/echogeo.13659>
9. The Mekong Delta: an unsettling portrait of coastal collapse, *Financial Times*. <https://www.ft.com/content/31bf27a4-1c0e-11ea-9186-7348c2f183af>. Accessed 5 Jan 2020
10. Schiappacasse P et al (2019) The economic impacts of construction aggregates mining on regional development, the case of the Hoa Binh Region of Vietnam. University of Dresden
11. Khoi NN (2014) Mineral resources potential of Viet Nam and current state of mining activity. Hanoi University
12. Koehnken L et al (2019) Impacts of riverine sand mining on freshwater ecosystems: a review of the scientific evidence and guidelines for future research. WILEY
13. Van Tuan N et al (2018) Current status of construction and demolition waste management in Viet Nam: challenges and opportunities. *Int J GEOMATE* 15(52):23–29
14. Tong TK et al (2013) Recycling construction demolition waste in the world and in Viet Nam. In: National Symposium for Recent Trends in Civil Engineering, 26th April 2013
15. Vietnam is running out of sand amid construction boom: *Global Construction Review*, 27 October 2017

Impact of Enhanced Production from the Opencast Coal Mines on Ambient Particulate Emissions



Ravi Kiran Podicheti and Ram Chandar Karra

Abstract Coal still continues to be the major source of energy needs. It is estimated that power sector alone would require about 900 Mt of coal by the year 2025. Such large quantity requires more surface mines causing the load on environment. Among the various environmental factors, air pollution is one of the most important parameters to be considered and the estimation of emissions from a mine at various stages of its operations is vital which helps in taking preventive measures against pollution. Given the significance of mining as a source of particulates, accurate characterization of emissions is important for the development of appropriate emission estimation techniques for use in modeling predictions and for regulatory decisions. Estimation of emissions in the ambient air quality with regard to enhanced production needs to be established regionally. Keeping this in view, two opencast coal mines in South India are selected to evaluate the emissions of PM_{10} and $PM_{2.5}$ in the ambient air due to increased coal production and overburden removal. Emissions for these two mines have been studied from the year 2012 to 2019. It was observed that the PM_{10} values ranged from 152 to 229 $\mu\text{g}/\text{m}^3$ in the core zone and 71 to 98.2 $\mu\text{g}/\text{m}^3$ in the buffer zone. Similarly, $PM_{2.5}$ values ranged from 49.4 to 80.9 $\mu\text{g}/\text{m}^3$ in the core zone and 25.3 to 55.3 $\mu\text{g}/\text{m}^3$ in the buffer zone. Particulate emissions have increased proportionately with respect to the quantity of coal produced and overburden removed.

Keywords Ambient air · Air pollution · Overburden · Coal production

1 Introduction

Air pollution is one of the most important parameters to be considered in case of opencast mining and the estimation of emissions from a mine at various stages of its operations is vital which helps in taking preventive measures against pollution.

R. K. Podicheti · R. C. Karra (✉)
Department of Mining Engineering, National Institute of Technology Karnataka, Surathkal,
Mangalore 575025, India
e-mail: krc@nitk.edu.in

© The Author(s), under exclusive license to Springer Nature Singapore Pte Ltd. 2022
A. K. Verma et al. (eds.), *Proceedings of Geotechnical Challenges in Mining, Tunneling and Underground Infrastructures*, Lecture Notes in Civil Engineering 228,
https://doi.org/10.1007/978-981-16-9770-8_36

551

The quantity of emissions will follow the life cycle of mining operations and accordingly pollution levels may increase to a certain period up to peak production then stabilizes and later decreases by the end of the mine life. Obviously, the particulate emissions from an opencast coal mine will increase with increase in production.

Opencast mining operations have been identified as a major source of particulate pollution [1]. The major sources of air pollution in coal mining area include drilling, blasting, loading and unloading of coal and overburden, movement of heavy earth moving machinery on haul roads, dragline operations, crushing of coal in feeder breakers, presence of fire, exposed pit faces, wind erosion and exhaust of heavy earth moving machinery [2]. Particulate Matter (PM) is usually divided and denoted by its aerodynamic diameter and the most widely monitored particles are PM_{10} and $PM_{2.5}$, which refer to particles with aerodynamic diameter less than or equal to 10 and 2.5 μm respectively [3].

Coal mines and related mining activities result in the production of atmospheric particulate matter that is associated with human health effects [4]. Particulate matter such as PM_{10} has emerged concern today in the field of atmospheric pollution research for its adverse impact on human and the social environment [5, 6]. Apart from the mining activities, other multiple sources play a significant role in atmospheric particulate emission in the area. Again, a composite emission abatement including most of the sources will be required to obtain the desired air quality [7].

Prediction of air pollution is possible with the development of empirical formulae so that effective mitigation measures can be designed at planning stage itself [8].

However, even where the emission estimation methods are applied in mines in the country for which they were developed, the uncertainties can be large. National Pollutant Inventory emission estimation methods commonly adopted in Australia have been criticized for inaccuracy and for providing inconsistent data for major sources of emissions. Development of region-specific estimation techniques for PM_{10} and $PM_{2.5}$ from open-cut coal mines is necessary to allow accurate prediction of PM emissions to make decisions [9, 10].

The dispersion equations developed within the pit boundary provide a reasonable accurate estimate of PM_{10} dispersion within the near field of the deep OC coal mines [11, 12]. Some studies were conducted to estimate the particulate matter level inside the mine and understanding its dispersion as they travel from source to the surface. An empirical relationship between PM concentration and depth of the mine was also proposed [13]. The emission factors being implemented are required to adapt to the local conditions of each mine [14]. The same empirical formulae for determination of emission rates cannot be considered for all Indian mines [15].

In view of the this, estimation of emissions in the ambient air quality with regard to changing parameters like enhanced production needs to be established regionally. In order to assess the same, a systematic research study is taken up.

Table 1 Directions and distances of villages from respective mine boundaries

S. No	Mine name	Village name	Direction	Distance from the source (m)
1	Mine A	AA	South	500
		AB	North	500
		AC	East	600
		AD	West	800
2	Mine B	BA	South	800
		BB	West	1250
		BC	North	1000
		BD	East	600

2 Field Investigations

Two opencast coal mines located in South India have been considered for evaluating the impact of enhanced production on ambient particulate emissions and the data of PM_{10} and $PM_{2.5}$ has been collected and analyzed from the year 2012 to 2019. Both these mines are being operated with shovel dumper combination. Two monitoring stations are selected in the core zone (Mine boundary) i.e., one at the coal handling plant and the other at the workshop. Similarly, 4 stations in the buffer zone (within 10 km from the mine boundary) near the villages are selected covering all the four directions of the project boundary so that the dust generated in all the directions can be monitored. The distance from source to the villages of these two mines A and B are given in Table 1.

The PM_{10} and $PM_{2.5}$ monitors have been placed at a height of 3.0 m above the ground level and at least 2.0 m apart while monitoring for negating the effects of wind-blown ground dust. The monitors were placed at open space free from any obstruction including trees and vegetation which otherwise act as a sink of pollutants resulting in lower levels in results. Monitoring has been carried out as per the Central Pollution Control Board and Ministry of Environment, Forest & Climate Change guidelines. The monitoring was done fortnightly for a duration of 24 h of sampling.

3 Materials and Methods

Ministry of Environment, Forest and Climate Change (MoEF&CC) has stipulated environmental standards for coal mines vide GSR-742 (E), dt. 25.09.2000 for the monitoring stations within the core zone i.e., in the Project area. National Ambient Air Quality Standards vide G.S.R. 826 (E) dated 16th November 2009 was made in exercise of the powers conferred by Sect. 6 and Sect. 25 of the Environment (Protection) Act, 1986. These standards are applicable for stations monitored in the

buffer zone i.e., within 10 km radius of the mine boundary. PM_{10} and $PM_{2.5}$ have been monitored using Respirable and Fine dust samplers respectively.

The Respirable Dust Sampler uses proven Orifice Plate based Flow Metering System. The pressure drop across the orifice is measured by a manometer in which the scale is calibrated in units of flow rate (m^3/min). Dust concentration is measured within acceptable range of $\pm 10\%$. The Respirable Dust Standard set by the Central Pollution Control Board recommends a 10-micron cut-off size for respirable dust measurements. The cyclone of the Respirable Dust Sampler has been designed to provide a cut-off at 10-microns for particulates commonly found in the urban environment.

The ambient Fine Dust Sampler is being used for dust of 2.5 microns which uses wins Impactor principle. Ambient air is drawn at a constant volumetric flow rate of 16.7 L per minute through a specially designed sampling inlet which separates particles larger than 10μ and allows smaller particles to enter an internal particle size separator where suspended particulate matter in the $PM_{2.5}$ size range is collected on a Polytetrafluoroethylene (PTFE) filter over the specified sampling period of 24 h. Each filter is weighed before and after sample collection to determine the net mass of $PM_{2.5}$ collected on filter paper. The mass concentration of $PM_{2.5}$ particles in ambient air is computed by dividing the total mass of collected particles by the total volume of sampled air and is expressed in $\mu g/m^3$. Dust monitoring in the core and buffer zones are shown in Fig. 1 and Fig. 2 respectively.

As per the standards for coal mines notification no. GSR 742(E), Dt. 25th September 2000 stipulated by the Ministry of Environment, Forest and Climate



Fig. 1 PM_{10} and $PM_{2.5}$ instruments placed near CHP and Workshop in the core zone



Fig. 2 PM_{10} and $PM_{2.5}$ instruments placed in the nearby villages of the buffer zone

Change, New Delhi, PM₁₀ concentration in ambient air shall not exceed 250 µg/m³ in the core zone. Similarly, according to the National ambient air quality standards as stipulated by the Central Pollution Control Board, vide its notification no. B-29016/20/90/PCI-L, Dt. 18th November 2009, the PM₁₀ and PM_{2.5} values shall not exceed 100 and 60 µg/m³ respectively in the buffer zone.

4 Results and Discussion

The coal production and overburden removal of Mine A from the year 2012 to 2019 and the corresponding annual average values of PM₁₀ and PM_{2.5} monitored in the core zone at coal handling plant and workshop are given in Table 2. The coal production ranged from 2.26 million tonnes per annum (Mtpa) to a maximum of 3.61 Mtpa. The overburden removal ranged from 10.74 to 28.89 Mm³ per annum. The PM₁₀ values ranged from 152 µg/m³ to a maximum of 214.5 µg/m³ at coal handling plant and 119 to 170.2 µg/m³ at workshop whereas the PM_{2.5} ranged from 61.2 to 80.9 µg/m³ at coal handling plant and 49.4 to 70.5 µg/m³ at workshop.

It was found that as the production increases the particulate matter was found to increase. Figure 3 and Fig. 4 shows the PM₁₀ and PM_{2.5} values against coal and overburden removal in the core zone. The PM₁₀ and PM_{2.5} concentrations at both the locations i.e., CHP and Workshop show an increasing trend ranging from 119 to 214.5 µg/m³ and 49.4 to 80.9 µg/m³ respectively up to the year 2015–16, declined in the subsequent year and again increased from the year 2017–18 ranging from 124.0 to 180.8 µg/m³ and 64.0 to 80.3 µg/m³ which is in proportion to the production.

Similarly, coal production and overburden removal of Mine A from the year 2012 to 2019 and the corresponding annual average values of PM₁₀ and PM_{2.5} monitored in the buffer zone in 4 villages are given in Table 3. The PM₁₀ values ranged from

Table 2 Coal and OB removal Vs PM emissions in the Core zone of Mine A

Year	Coal Production in Mt	OB removal in Mm ³	Core zone (figs. in µg/m ³)			
			Coal handling plant		Workshop	
			PM ₁₀	PM _{2.5}	PM ₁₀	PM _{2.5}
2012–13	2.26	10.74	152.0	61.6	119.0	52.5
2013–14	2.97	19.49	173.0	61.2	127.0	49.4
2014–15	2.71	27.58	212.0	77.2	130.0	58.2
2015–16	3.37	26.89	214.5	80.9	130.2	62.2
2016–17	3.13	20.23	180.0	71.0	124.0	64.0
2017–18	3.61	28.89	180.1	79.5	166.4	70.5
2018–19	2.91	28.14	180.8	80.3	162.0	66.7
2019–20	2.60	28.36	174.5	73.2	170.2	70.4

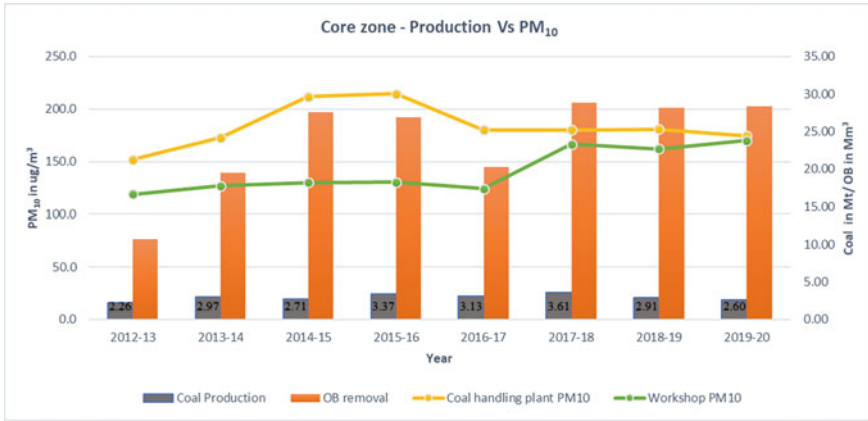


Fig. 3 Coal and OB production Vs PM₁₀ emissions in the core zone of Mine-A

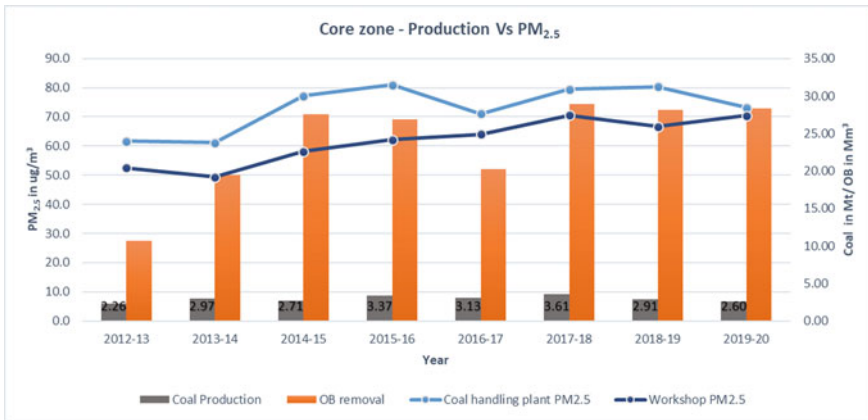


Fig. 4 Coal and OB production Vs PM_{2.5} emissions in the core zone of Mine-A

Table 3 Coal and OB removal Vs PM emissions in the Buffer zone of Mine A

Year	Coal Production in Mt	OB removal in Mm ³	Buffer zone (figs. in µg/m ³)							
			Village AA		Village AB		Village AC		Village AD	
			PM ₁₀	PM _{2.5}	PM ₁₀	PM _{2.5}	PM ₁₀	PM _{2.5}	PM ₁₀	PM _{2.5}
2012-13	2.26	10.74	64.0	39.5	66.0	39.7	73.0	39.8	69.0	38.9
2013-14	2.97	19.49	78.0	41.7	80.0	41.6	81.0	43.0	75.0	37.9
2014-15	2.71	27.58	79.0	43.8	93.0	55.3	87.0	52.1	76.0	40.8
2015-16	3.37	26.89	89.6	52.7	88.3	52.1	87.9	52.8	80.2	48.1
2016-17	3.13	20.23	71.0	46.0	70.0	49.0	70.0	47.0	69.0	45.0
2017-18	3.61	28.89	71.7	46.2	71.9	45.6	63.8	42.0	53.4	35.7
2018-19	2.91	28.14	66.2	46.3	64.4	44.0	65.8	45.5	45.7	27.7
2019-20	2.60	28.36	58.9	39.1	52.5	33.3	54.1	33.7	44.4	25.3

a minimum of $44.4 \mu\text{g}/\text{m}^3$ to a maximum of $93 \mu\text{g}/\text{m}^3$ and $\text{PM}_{2.5}$ ranged from $25.3 \mu\text{g}/\text{m}^3$ to a maximum of $55.3 \mu\text{g}/\text{m}^3$.

Figure 5 and Fig. 6 shows PM_{10} and $\text{PM}_{2.5}$ against coal and overburden removal in the buffer zone of Mine A.

It is evident from the Figs. 5 and 6 that PM_{10} and $\text{PM}_{2.5}$ concentrations increased up to the year 2014–15 and show a decreasing trend later on, even though there is an increase in production, which may be due to reclamation activities taken up, other pollution control measures carried out and movement of mining operations away from the vicinity of the villages.

The coal production and overburden removal of Mine B from the year 2012 to 2019 and the corresponding annual average values of PM_{10} and $\text{PM}_{2.5}$ monitored in the core zone at coal handling plant and workshop are given in Table 4. The PM_{10}

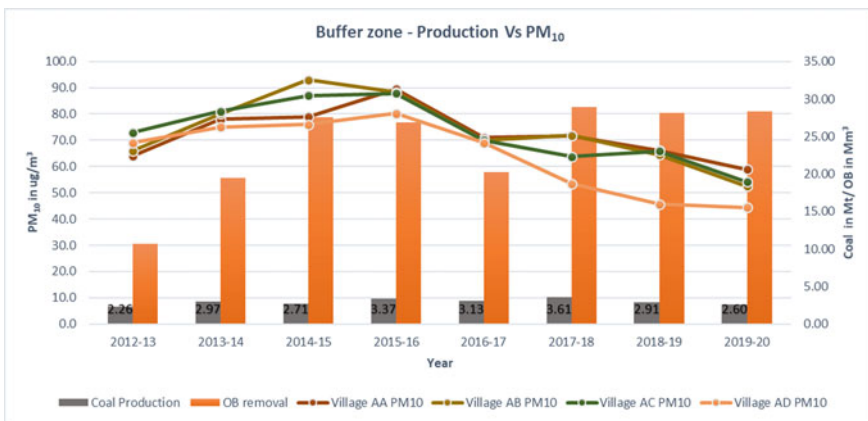


Fig. 5 Coal and OB production Vs PM_{10} emissions in the buffer zone

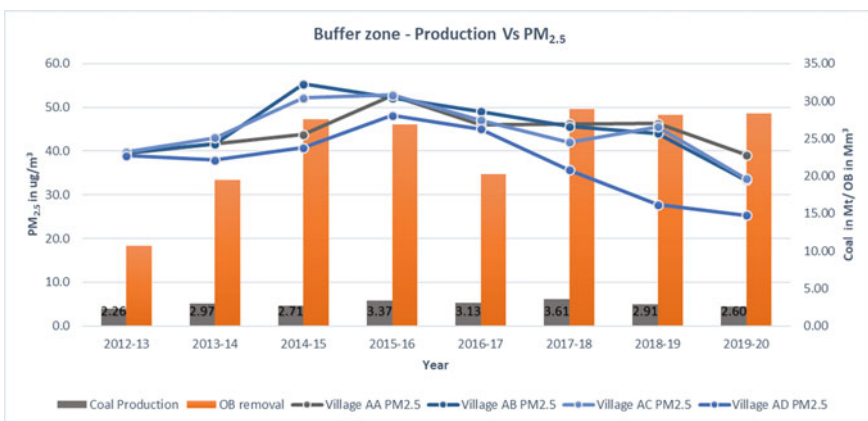


Fig. 6 Coal and OB production Vs $\text{PM}_{2.5}$ emissions in the buffer zone

Table 4 Coal and OB removal Vs PM emissions in the Core zone of Mine B

Year	Coal production in Mt	OB removal in Mt	Core zone (figs. in $\mu\text{g}/\text{m}^3$)			
			Coal handling plant		Workshop	
			PM_{10}	$PM_{2.5}$	PM_{10}	$PM_{2.5}$
2012–13	2.51	9.20	170.7	67.6	141.9	64.7
2013–14	1.45	11.35	209.0	64.4	210.0	63.8
2014–15	2.54	17.45	226.0	67.5	224.0	67.3
2015–16	2.71	18.78	192.5	61.2	192.7	59.1
2016–17	2.04	20.49	222.6	62.5	221.1	61.6
2017–18	2.58	33.89	220.9	60.5	240.0	66.3
2018–19	2.98	31.12	229.0	68.8	214.7	63.8
2019–20	2.97	24.73	212.3	53.8	201.3	51.2

values ranged from 170.7 $\mu\text{g}/\text{m}^3$ to a maximum of 229.0 $\mu\text{g}/\text{m}^3$ at coal handling plant and 141.9 to 240.0 $\mu\text{g}/\text{m}^3$ at workshop. The $PM_{2.5}$ ranged from 53.8 to 68.8 $\mu\text{g}/\text{m}^3$ at coal handling plant and 51.2 to 67.3 $\mu\text{g}/\text{m}^3$ at workshop.

Figure 7 and Fig. 8 shows the plot of PM_{10} and $PM_{2.5}$ against the coal and overburden removal in the core zone of Mine B. Here also, the values of PM_{10} and $PM_{2.5}$ increased from 141.9 $\mu\text{g}/\text{m}^3$ to a maximum of 240.0 $\mu\text{g}/\text{m}^3$ and 51.1 to 67.3 $\mu\text{g}/\text{m}^3$ respectively with respect to quantum of production in OB (from 9.20 to 33.89 Mt) and coal (from 1.45 to 2.98 Mt) respectively.

Similarly, coal production and overburden removal of Mine B from the year 2012 to 2019 and the corresponding annual average values of PM_{10} and $PM_{2.5}$ monitored in the 4 villages of buffer zone are given in Table 5. The PM_{10} values ranged from a minimum of 64.3 $\mu\text{g}/\text{m}^3$ to a maximum of 98.2 $\mu\text{g}/\text{m}^3$ and $PM_{2.5}$ values ranged from 32.9 $\mu\text{g}/\text{m}^3$ to a maximum of 54.0 $\mu\text{g}/\text{m}^3$.

Figure 9 and Fig. 10 shows the plot of PM_{10} and $PM_{2.5}$ against the coal and overburden removal in the buffer zone of Mine B.

Table 5 Coal and OB removal Vs PM emissions in the Buffer zone of Mine B

Year	Coal production in Mt	OB removal in Mt	Buffer zone (figs. in $\mu\text{g}/\text{m}^3$)							
			Village BA		Village BB		Village BC		Village BD	
			PM_{10}	$PM_{2.5}$	PM_{10}	$PM_{2.5}$	PM_{10}	$PM_{2.5}$	PM_{10}	$PM_{2.5}$
2012–13	2.51	9.20	93.3	52.6	74.3	43.7	82.0	47.4	72.1	45.7
2013–14	1.45	11.35	98.0	45.9	87.0	38.8	84.0	37.6	78.0	35.1
2014–15	2.54	17.45	98.2	50.6	85.0	44.1	89.0	45.9	83.0	41.0
2015–16	2.71	18.78	78.4	42.7	77.3	40.7	78.8	42.0	71.6	37.7
2016–17	2.04	20.49	94.5	54.0	82.4	47.4	89.1	51.6	85.6	48.5
2017–18	2.58	33.89	89.0	48.1	77.6	41.6	86.8	46.0	79.1	41.9
2018–19	2.98	31.12	93.5	48.0	71.3	39.2	85.6	45.7	79.3	40.6
2019–20	2.97	24.73	80.3	41.7	64.3	32.9	76.9	40.3	73.5	37.1

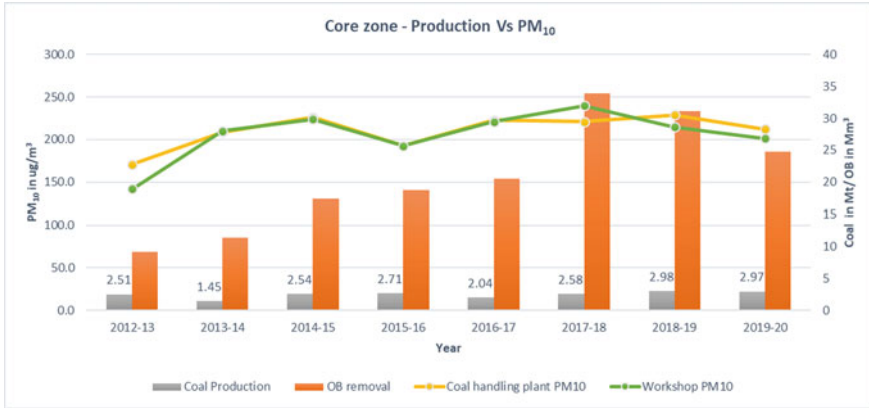


Fig. 7 Coal and OB production Vs PM₁₀ emissions in the core zone of Mine-B

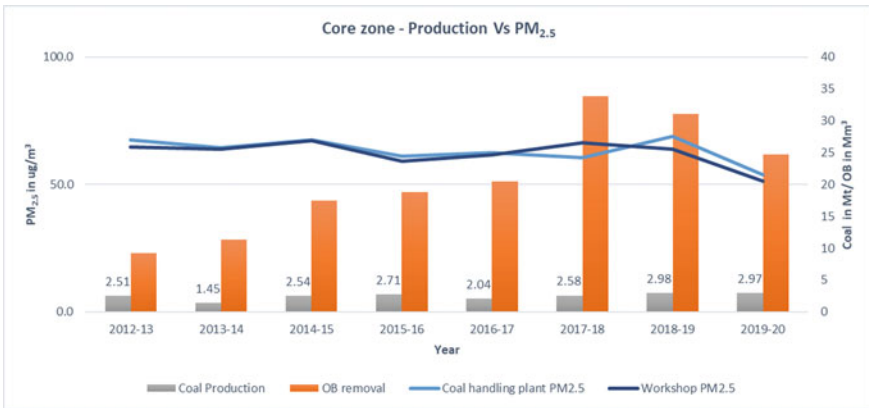


Fig. 8 Coal and OB production Vs PM_{2.5} emissions in the core zone of Mine-B

As observed from the Figs. 9 and 10, PM values in the core and buffer zone shows no significance when compared with the variation in quantum of production (OB and Coal). This may be again due to reclamation activities carried out and other environmental control measures adopted.

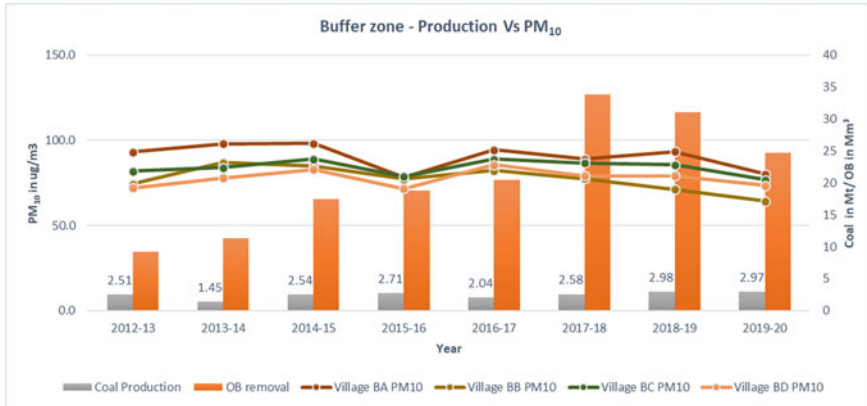


Fig. 9 Coal and OB production Vs PM₁₀ emissions in the buffer zone

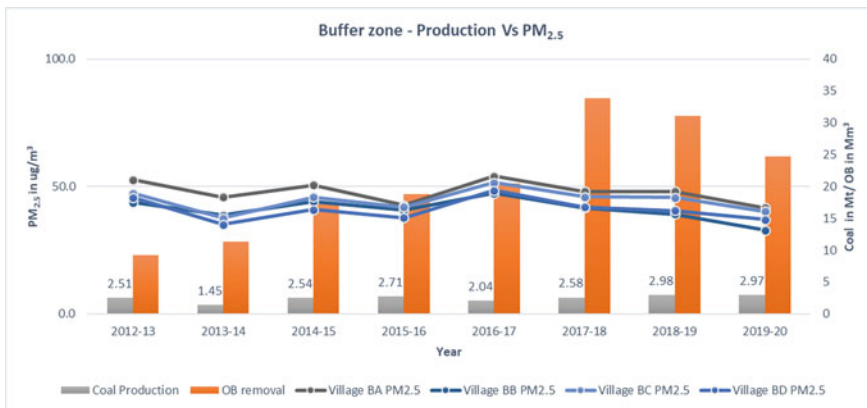


Fig. 10 Coal and OB production Vs PM_{2.5} emissions in the buffer zone

5 Conclusions

It is observed that the PM₁₀ and PM_{2.5} values in the core zone are increasing proportionately with respect to over burden removal in Mine A as well as in Mine B. However, these values in the buffer zone decreased and or dependent neither on overburden removal quantities nor coal production in of Mine A, but maintained a steady value over the years in case of Mine B. This may be due to coal transportation through trucks, local emissions and other meteorological factors which is resulting in change of the PM values.

In view of this, it may be concluded that the PM₁₀ and PM_{2.5} values are increasing with respect to over burden production in the core zone and show no significant impact in the buffer zone. Hence, steps need to be taken in the core zone with increase in

over burden production for effective mitigation of particulate matter emissions. In addition, avoiding transportation by trucks and adopting rail mode of coal transport or laying belt conveyors up to rail dispatch point will further help in reducing the particulate emissions in buffer zone.

References

1. Ghose MK, Majee SR (2000) Assessment of the impact on the air environment due to opencast coal mining—an Indian case study. *Atmos Environ* 34:2791–2796
2. Chaulya SK (2004) Air quality status of an open pit mining area in India. *Environ Monit Assess* 105:369–389
3. Hendryx M, Islam MS, Dong GH, Paul G (2020) Air pollution emissions 2008–2018 from Australian coal mining: implications for public and occupational health. *Environ Res Public Health* 17:1570
4. Mandal K et al (2012) Characterization of different road dusts in opencast coal mining areas of India. *Environ Monit Assess* 184:3427–3441
5. Ghose MK, Majee SR (2007) Characteristics of hazardous airborne dust around an Indian surface coal mining area. *Environ Monit Assess* 130:17–25
6. Gautam S et al (2012) Opencast mines: a subject to major concern for human health. *Geol Min* 2(2):25–31
7. Roy D et al (2020) Emission inventory of PM₁₀ in Dhanbad/Jharia coalfield (JCF), India: an intricate coal mining sector. *Environ Dev Sustain* 23(3):3048–3061
8. Chaulya SK et al (2003) Validation of two air quality models for Indian mining conditions. *Environ Monit Assess* 82(1):23–43
9. Richardson C et al (2017) Characterization of particulate emissions from Australian open-cut coal mines: toward improved emission estimates. *Air Waste Manag Assoc* 68(6):598–607
10. Cooper N, Green D, Meissner KJ (2017) The Australian National Pollutant Inventory fails to fulfill its legislated goals. *Environ Res Public Health* 14(5):478
11. Silvester SA et al (2009) A computational study of particulate emissions from an open pit quarry under neutral atmospheric conditions. *Atmos Environ* 43:6415–6424
12. Sumanth Ch, And Khare M: Particle Dispersion Within a Deep Open Cast Coal Mine, Air Quality-Models and Applications. <http://www.intechopen.com/books/air-quality-models-and-applications/particle-dispersion-within-a-deepopen-cast-coal-mine>. Accessed 14 July 2021
13. Gautam S, Patra AK (2015) Dispersion of particulate matter generated at higher depths in opencast mines. *Environ Technol Innov* 3:11–27
14. Huertas JI et al (2012) Standardized emissions inventory methodology for open pit mining areas. *Environ Sci Pollut Res* 19:2784–2794
15. Chakraborty MK et al (2002) Determination of the emission rate from various opencast mining operations. *Environ Modell Softw* 17:467–480

A Comprehensive Review of Rockmass Classification Systems for Assessing Blastability



Ramesh Murlidhar Bhatawdekar, A. K. Raina,
and Danial Jahed Armaghani

Abstract Rock mass classifications are in vogue for quite some time now. Lot of work has been done on the subject for engineering design of underground structures and their support, ground control, slope stability, foundation and rippability for excavations of varied nature. The essence of such classification systems is that most of them include information about the strength of the rock and its quality, joint conditions and joint filling. While some classifications are purely focused on defining the quality of rock and its continuity, others are of holistic nature. Such classifications have also been used to develop correlation between the rock class with cohesion and angle of friction. However, the use of such classifications for determining the blastability of the rockmass are very scant in nature. This paper attempts to mine the literature for cases where such classifications have been used to define the blastability of the rockmass. An attempt is made to critically analyze such use and define a course for future definition of blastability in relevant terms and determine whether such classification can be used as an aid to replace the existing rock factor in blasting with an eye on prediction of blast fragmentation and related outcomes of blasting.

Keywords Rock mass classifications · Slope stability · Blastability · Ground control

R. M. Bhatawdekar

Geotopik, Department of Civil Engineering, Universiti Teknologi Malaysia, Skudai,
Johor Bahru 81310, Johor, Malaysia
e-mail: rmbhatawdekar2@graduate.utm.my

A. K. Raina (✉)

CSIR-Central Institute of Mining and Fuel Research, 17/C, Telangkhedi Complex, Civil Lines,
Nagpur 440 001, India
e-mail: rainaji@cimfr.nic.in

D. Jahed Armaghani

Department of Urban Planning, Engineering Networks and Systems, Institute of Architecture and
Construction, South Ural State University, Chelyabinsk 454080, Russia

1 Introduction

Rockmass represents the rock including the flaws like joints, slips and micro-faults in its natural condition and is distinct from intact rock that is devoid of such defects. Both intact rock and rockmass can however be considered to be of inhomogeneous nature and more likely to be anisotropic owing to the formational characteristics, structure and composition. This is the primary reason for the contrast of their geomechanical characteristics. There have been attempts to relate the laboratory properties of intact rock samples to that of the in-situ conditions or rockmass, but keeping in view the independent nature of joints, such comparisons do not work to the full engineering advantage. In conformity with the general physical law, no rock can be stronger than the strength of the discontinuities. In line with the above, there have been several successful attempts to classify the rock using rating-based systems but were primarily designed for assessing the stability of the rockmass and estimation of support required for different excavations (Fig. 1) falling under the category of ground control. Such classifications have been used to devise support and even relate with other properties like cohesion and internal friction of the rockmass.

This paper tries discuss the most accepted rockmass classifications in brief, and to log the instances where such classifications have been attempted for use in blasting.

2 Rockmass Classification Systems

A brief explanation of the rockmass classification system is attempted over here. Although there are several classifications and indexes used for different types of excavations, some of the classification systems like rock quality designation (RQD), rockmass rating (RMR), rock quality index (Q) and geological strength index (GSI) have received wide attention and are currently in use for support system evaluation. A summary of the classification along with main features and uses are provided in Fig. 1.

Deere and Miller [14] introduced the Rock Quality Designation or RQD%. RQD is as a component of the RMR and Q rock mass classifications has been used widely in geomechanical problems. However, the studies of a significant number of researchers found that RQD suffers from several shortcomings and resulted in severe errors in calculation of RMR and Q [34]. However, with accurate measurements, it can be used for estimation of block size and hence may be useful in defining blastability. There have been attempts to correlate RQD with Terzaghi's rock load factors and to rock bolt requirements in tunnels. However, most of the works pertain to calculation of RQD for the purpose of RMR and Q. Some instances for its use in blasting are also traceable and will be discussed in relevant section. Rehman et al. [36] presented an excellent presentation of development, updates uses and critical review of RMR and Q system.

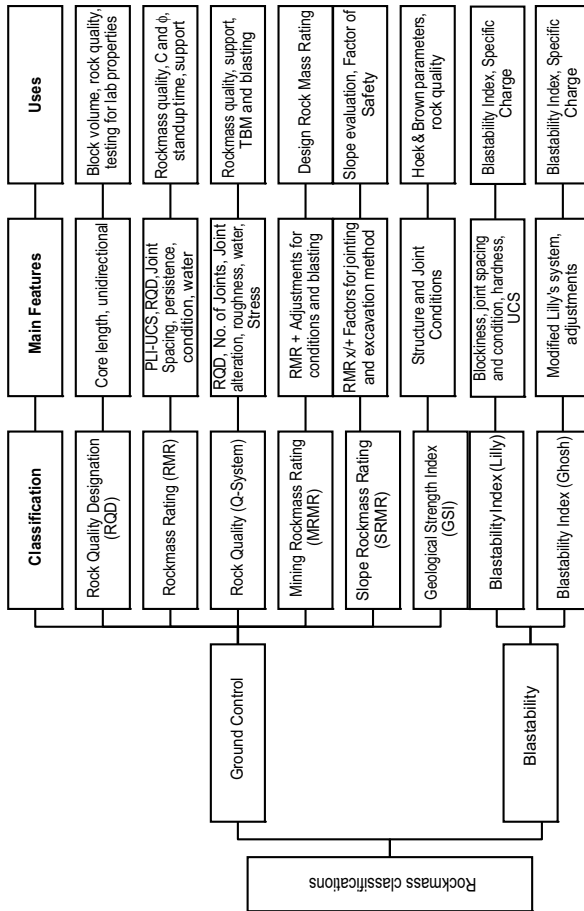


Fig. 1 Rockmass classification systems in vogue for ground control and blastability

Table 1 Rock classification based on RMR values

RMR	Rock quality
0–20	Very poor
21–40	Poor
41–60	Fair
61–80	Good
81–100	Very good

Rock Mass Rating (*RMR*) system or the geomechanics classification was devised by Bieniawski [7, 8] based on six parameters viz. UCS, RQD, spacing and orientation of condition of discontinuities and ground water condition. All these parameters are assigned rating through field and laboratory measurements and finally all the ratings are added. Based on the value attained, the rock is classified for geomechanical purpose as given in Table 1.

There are instances where corrections for different types of excavations have been made to find the final RMR. A modified RMR is the coal RMR defined by Paul Committee of DGMS India. RMR has been used extensively for rockmass classification, determination of the standup time and calculations of cohesion and friction angle.

Block caving operations in the USA were classified on Cummings et al. [43] and Kendorski et al. [44] have also modified Bieniawski's RMR classification to produce the *MBR* (modified basic *RMR*) system for mining. It involves the use of different ratings for the original parameters used to determine the value of *RMR* and the subsequent adjustment of the resulting *MBR* value to allow for blast damage, induced stresses, structural features, distance from the cave front and size of the caving block. However, the effect of weathering, blasting and induced stresses affect blasting needs to be evaluated for tunnel support or block caving support and blasting.

Mining Rock Mass Rating system for mining is described by [21, 25]. This MRMR system takes the basic RMR values on the basis of [7]. Mining RMR (MRMR) classification system has been used since 1974.

MRMR was modified to incorporate certain key parameters which are common in mining environment such as weathering, effect due to blasting and induced stresses. Mining personnel globally accept MRMR as the same is a comprehensive and versatile system. For numerous mining operations MRMR is applied as a planning tool after refinement and modification during last 40 years. There is further scope for improvement in MRMR by using empirical tables and charts.

Another widely used rockmass classification method was proposed by Barton et al. [5] and is called the Tunnelling Quality Index (*Q*) for the determination of rock mass characteristics and tunnel support requirements as defined below.

$$Q = \frac{RQD}{J_n} \times \frac{J_r}{J_a} \times \frac{J_w}{SRF}$$

where *RQD* is the Rock Quality Designation; J_n is the joint set number; J_r is the joint roughness number; J_a is the joint alteration number; J_w is the joint water reduction factor; *SRF* is the stress reduction factor (generally taken as 1).

There is impact due to water and stress reduction in tunnel support system. In case of blasting, effect of presence of water can be nullified by selecting appropriate strength and water-resistant explosives. Q system does not consider following aspects which are important in case of blasting:

(i) Type of rock – sedimentary, igneous, metamorphic (ii) degree of weathering (iii) density of rock (iv) variation in type of discontinuity e.g., fault/ fold (v) blast design parameters. The method was modified several times by its author and the latest developments include the correlation with dynamic properties of the rockmass and extension of the Q to tunnel boring machine penetration rate determination called as Q_{TBM} [6].

The geological strength index (GSI) was developed [19] to acquire reliable data of rockmass properties as inputs for numerical analysis for designing tunnels, slopes or foundations in rocks. The classification system is unique as it allows visual selection of the structural features and blockiness of the rock for workout of the GSI that can be useful in defining rockmass strength and its deformability. GSI is specifically designed to characterize rocks that are difficult to classify in field for engineering purpose. Several questions on the classification raised by different researchers size of the rock mass to be considered, its anisotropy, the influence of great depth, the presence of ground water, the aperture and the infilling of discontinuities and the properties of weathered rock masses and soft rocks and its applicability have also been answered by the authors [28].

Wickham et al. [42] developed Rock Structure Rating (RSR) classification system where $RSR = A + B + C$ with parameter A for geology, parameter B for geometry and parameter C for effect of ground water inflow and joint condition for all rocks.

Table 2 illustrates in details of authors, classification criteria for each rock mass classification system developed and common parameters which can be considered and research gap for the present study.

3 Rockmass and blastability

Blasting involves breakage of rockmass and its displacement with the help of explosive energy. Blasting is core to the mining in present times. The objectives of blasting in any mine are determined by the desired throughput for the machinery that operates in the mines. A simple scheme of such objectives is presented in Fig. 2.

A critical review of the design objectives given in Fig. 2 provides that fragmentation and muck profile are two most important outputs that demand optimization. The fragment size not only effects the production but the value of the ore. There are lot of references that advocate the necessity of fragmentation and its assessment. The degree of fragmentation affects the productivity [27, 35, 39] is well understood.

Table 2 Purpose of application development of each rock mass classification system

Application/Author	Classification criteria	Remarks
Tunnel design, Ritter [45]	An empirical approach to tunnel design for support requirement based on case history	Over the years various rock mass classification have been developed and careful application for other engineering problems
Support for tunnel, Terzaghi [46], Intact rock	Contains neither joints nor hair cracks. Roof may fall after several hours or days after blasting. Spalling/popping condition	Rock mass is uniform and extremely difficult to blast
Support for tunnel, Terzaghi [46], stratified rock	Individual strata with little or no resistance against separation along the boundaries between the strata Spalling condition common	Rock mass is individual strata and can be blasted as stratified thickness of rock mass, Very difficult to blast
Support for tunnel, Terzaghi [46], moderately jointed rock mass	Joints and hair cracks present. Intimately interlocked due to development of vertical joints. Spalling and popping condition common	Blasting will result in blocks due to vertical weakness planes. Difficult to blast
Support for tunnel, Terzaghi [46], Blocky and seamy rock	Chemically intact or almost intact rock fragments which are entirely separated from each other and imperfectly interlocked	Due to natural fragmentation of rock mass, easy to blast
Support for tunnel, Terzaghi [46], Crushed rock	Chemically intact rock has the character of crusher run. If most or all of the fragments are as small as fine sand grains and no recommendation has taken place, crushed rock below water table exhibit the properties of a water bearing sand	As rock mass is crushed, very easy to blast
Support for tunnel, Terzaghi [46], Squeezing rock	Slowly advances into the tunnel without perceptible volume increase. A prerequisite for squeeze is a high percentage of microscopic and sub-microscopic particle of micaceous minerals or clay minerals with a low swelling capacity	As rock particles are microscopic and submicroscopic, blasting may not be required
Support for tunnel, Terzaghi [46], Swelling rock	Rock advances into the the tunnel chiefly on account of expansion. E.g clay minerals	Rock consist of clay minerals and blasting is not necessary

(continued)

Table 2 (continued)

Application/Author	Classification criteria	Remarks
Safe tunnelling method, Pacher [47]	Support span determination through pilot tunnel approach. Forms part of the general tunnelling approach known as the new Austrian tunnelling method (NATTM)	Blasting is breaking of rock and thus rock properties are opposite to tunnel support required for forces acting against gravity
RQD, Deere et al. [14, 15]	Rock Quality designation RQD is defined as the percentage of intact core piece longer than 100 mm (4 inches) in the total length of core	Useful parameter for correlating with blastability of rock for initial exploration data. Does not consider orientation of joints. RQD is as a component of the RMR and Q rock mass classification system
Tunnel bolt requirements, Deere [14]; Merritt [50]	Correlation of RQD to Terzaghi's rock load factor	Tunnel bolts are required to keep rock mass intact against failure against gravity
Palmström [51]	RQD may be estimated from the number of discontinuities per unit volume $RQD = 115 - 3.3 J_v$ Where J_v is the sum of the number of joints per unit length for all joints per unit length for all joints (discontinuity) sets known as the volumetric joint count	This system consists of joints spacing which is also important in case of blasting. This classification does not consider joint orientation with respect to face which can have impact on blasting
Wickham et al. [52]	Parameter A Geology a. Rock type origin (igneous, metamorphic, sedimentary) b. Rock hardness (hard, medium, soft, decomposed) c. Geologic structure (massive, slightly faulted/folded, moderately faulted/folded, intensely faulted/folded) Parameter B a. Average joint spacing b. Strike perpendicular to axis c. Strike parallel to axis d. Dip prominent joints	Geology parameter affects blastability of rock. Rock type will have different impact based on origin. Rock hardness indicates extremely difficult to very easy for hard to soft rock Geological structure will affect blastability of rock Joint spacing and dip of prominent joints have an impact on blasting. Instead of axis of tunnel, comparable with quarry face for blasting

(continued)

Table 2 (continued)

Application/Author	Classification criteria	Remarks
Bieniawski [7, 8]	<p>Geomechanics Classification or the Rock Mass Rating (RMR) system where score out of 100 is given</p> <p>The following six parameters are used to classify a rock mass using the RMR system:</p> <ol style="list-style-type: none"> 1. Uniaxial compressive strength of rock material 2. Rock Quality Designation (RQD) 3. Spacing of discontinuities 4. Condition of discontinuities 5. Groundwater conditions 6. Orientation of discontinuities 	<p>RMR is one of the parameter for comparing blasting. The system does not give weightage for following factors from blasting point of view:</p> <ol style="list-style-type: none"> i) Type of rock – sedimentary, igneous, metamorphic ii) Degree of weathering iii) Density of rock iv) Variation in type of discontinuity. Eg: fault/fold is not considered v) Blast design parameters <p>Ground water condition has little impact on surface mining blasting in most of the cases. The effect is generally compensated with type of explosive being used</p>
Laubscher [53, 54] Laubscher and Taylor [55] Cummings et al. [43] and Kendorski et al. [44]	<p>Modified Rock Mass Rating System (MRMR) adjusts it to account for in situ and induced stresses, stress changes and the effects of blasting and weathering</p> <p>This system developed for block caving for underground mines</p>	<p>How the effect of weathering, blasting and induced stresses affect blasting needs to be evaluated for tunnel support or block caving support and blasting</p>
Barton et al. [5]	<p>Norwegian Geotechnical Institute proposed a Tunnelling Quality Index (Q) and uses</p> <p>J_n - the joint set number</p> <p>J_r - the joint roughness number</p> <p>J_a - the joint alteration number</p> <p>J_w - the joint water reduction factor</p> <p>SRF is the stress reduction factor</p>	<p>There is impact due to water and stress reduction in tunnel support system. In case of blasting, effect of presence of water can be nullified by selecting appropriate strength and water resistance explosives. Q system does not consider following aspects which are important in case of blasting:</p> <ol style="list-style-type: none"> i) Type of rock – sedimentary, igneous, metamorphic ii) Degree of weathering iii) Density of rock iv) Variation in type of discontinuity eg: fault/ fold is not considered v) Blast design parameters

(continued)

Table 2 (continued)

Application/Author	Classification criteria	Remarks
Bieniawski's RMR [7, 8] and Barton et al.'s Q [5]	Both methods incorporate geological, geometric and design/engineering parameters in arriving at a quantitative value of their rock mass quality. The similarities between RMR and Q stem from the use of identical, or very similar, parameters in calculating the final rock mass quality rating	RMR uses compressive strength directly while Q only considers strength as it relates to in situ stress in competent rock. Thus, RMR is more appropriate for using with blastability of rock mass

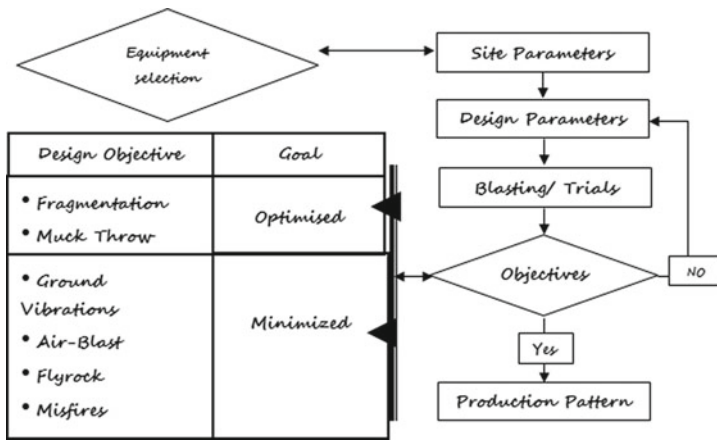


Fig. 2 The objectives of blasting operations & evolution of production pattern

The two most important factors that play a major role in determining the blast output are the drill diameter and burden. While drill diameter is constant for a mine for all practical purposes, burden is defined by the rock properties and the drill diameter used. All other blast design variables entering into the interaction are correlated to these. One of the important factors that determines the burden is the rockmass [3]. Accordingly, some thumb rules based on critical and breakage burden concept were introduced as factor ranging from 25 to 40 for estimating burden [22]. There have been attempts to introduce a rock factor for prediction of burden using Kuznetsov equation [13] that include modulus as a parameter in the original equation. The fragmentation distributions are mostly expressed in the models provided by Rosin–Rammler or Schuhmann Distribution model. A comprehensive review of such models [32] discusses their development in detail.

Various fragmentation prediction equations used worldwide, are generally known by the names of those who developed them. The most commonly used models are

of Langefors and Kihlstrom, Kuznetsov equation, Cunningham equation, SweDeFo Model, also known as SWEBREC function (Finn [33]). The various important parameters considered in those models are rock heterogeneity, explosives relative weight strength, specific charge, charge distribution, stemming to burden ratio and drilling accuracy. Most of these models were developed based on either laboratory studies or model studies. A detailed description of blastability including various models introduced over time and blastability index [26] has been provided by Dey and Sen [16].

The most popular and oldest predictive model is the one provided by Kuznetsov [24] as shown below:

$$k_{50} = A(V/Q)^{0.8}Q^{1/6}, cm$$

where, *A* is Rock factor, 7, for medium rocks, 10, for hard and highly fissured rocks, 13, for hard and weakly fissured rocks; *V* is the volume of rock broken per blast hole, m³, and *Q* is the mass of TNT containing the energy equivalent of the explosives charge in a blast hole, kg.

There have been several attempts to characterized the rock factor ‘A’ in the above equation by different researchers [4, 11, 37, 40]. The concept of blastability index [26] provided below, has been used by host of authors to characterize the rock factor.

Rock mass description (RMD) 1. Powdery / Friable 2. Blocky 3. Totally Massive	Rating 10 20 50	Joint Plane Orientation (JPS) 1. Horizontal 2. Dip out of face 3. Strike normal to face 4. Dip into face	Rating 10 20 30 40
Joint Plane Spacing (JPS) 1. Close (<0.1m) 2. Intermediate (0.1 to 1.0m) 3. Wide (>1.0 m)	Rating 10 20 50	1. Specific Gravity Influence (SGI) SGI = 25 * SG-50 SG – Specific gravity, T/M ³	
Hardness [Mohr’s scale]	1 to 10	Blastability Index, BI = 0.5*(RMD+JPS+JPO+SGI+H)	

The Specific Charge (q) and Energy Factors (Ef) can be worked out from the blastability index (BI) as given in following equations.

$$q = 0.004 \times BI, (Kg - ANFO/T);$$

$$Ef = 0.015 \times BI, (MJ/T)$$

As per Chakraborty et al. [48], the mean fragment size of a blast can be predicted by the following relation.

$$k_{50} = 0.07(l_s)^{0.54}(A/q)^{0.172} \quad , m$$

where, l_s is stemming column length, m ; q is specific charge, kg/m^3 , and A is Rock factor wherein, $A = 1$, when RQD is 40-50, = 3, for RQD of 50-60, =15, for RQD of 60-70, = 22, for RQD of 70-80.

The uniformity of fragmentation as designated by ‘ n ’, can be predicted by [13] equation given below:

$$n = (2.2 - 14 B/d)\{(1 + S/B)/2\}^{0.5}(1 - W/B)(l_{ch}/l_b)$$

where, B is burden, m ; d is hole diameter, mm ; S is spacing, m ; W is the standard deviation in drilling accuracy, m ; l_{ch} is charge length, m ; l_b is bench height, m .

More recently, Ouchterlony [33] devised a distribution model for blast fragmentation that takes care of the problem of the maximum size and fines simultaneously. A comprehensive review of the fragmentation models is provided by Ouchterlony and Sanchidrian [49].

However, the attempts to use rockmass classification systems for assessing the blastability of rockmass are very perfunctory in nature and are logged below in chronological order.

Keeping all blast design variables constant [17] evaluated the effect of rockmass in terms of RQD, in situ block size, RMR and Q. The authors however could use very limited blasts in similar rockmass and hence the outcome was more consistent with the blast design variations and confirmed accepted principles of rock breakage. [1] used rockmass quality (Q) for correlating the overbreak in underground excavations and large chambers. The authors concluded that the overbreak could not be properly defined with the help of Q. Studies were conducted in field to determine the role of block size, strength, jointing, ground water and weathering of rocks and RMR on controlled blasting [41]. The author discussed the role of RMR in HCF and peak particle velocity from blasting.

Lee et al. [10] defined a rock constant and devised formula (see Eq. below) for calculating the burden and charge configurations for tunnel blasting as given below.

$$c = 5.73 \times 10^{-3} RMR + 0.057$$

$$1^{st} \text{ quadrangle} \quad : B = 1.5\phi \frac{0.35}{c}$$

$$\text{Linear Charge concentration} \quad : l = 240 \frac{d \cdot \phi \cdot c}{S_{ANFO}}$$

$$2^{nd} \text{ and } 3^{rd} \text{ quadrangle} \quad : B_n = 1.02\sqrt{A'_{n-1}}$$

$$4^{th} \text{ quadrangle and over} \quad : A_n = 2 \cdot a_{n-1}$$

where ϕ is the diameter of the empty drill hole (in meters), a is the distance between a blasthole and center of the cut section (in meters), d is the diameter of blastholes (in meters), l is the linear charge

Rezaei et al. [37] used ANN to model the burden in blasting based on geomechanical properties of rockmass like blastability index (BI), RQD, density, UCS etc. They concluded that BI and RQD were the most sensitive variables while defining burden in blasting. A new classification for widely spaced jointed rocks called the blast quality index [9] explores the possibilities of use of GSI for the purpose of blasting explained with few case studies. Inanloo [20] devised a modified Kuznetsov model [24] for prediction of mean fragment size from blasting while using in situ block size and blast design variables like burden and spacing to burden ration. The authors reported that the model improved the accuracy by 11%.

Sayevand et al. [38] defined the 80% fragment size passing (k_{80}) in blasting while using some blast design variables along with RMR and employing imperialistic competitive algorithm. The authors concluded that RMR was one of the major influencing factors in defining the k_{80} of the blast. In order to control the wall overbreak and to design wall control blasting, a methodology was proposed that correlated GSI, RMR with BI [40]. They presented some case studies and decision making based on engineering for blast designs.

A neurogenetic method for characterizing the overbreak was used in tunnel blasting by Koopialipoor et al. [23]. In addition to the general blast design variables, the authors used RMR to define the output and sensitivity of the variables. RMR was found to have the maximum sensitivity in the analysis for defining the overbreak. The finding is very important as these establish the use the RMR in blast predictions. Geometric properties of discontinuities RMR and Q were used for prediction of fragmentation distribution during blasting [29]. However, no specific relationships were presented by the authors between the RMR, Q and mean fragment size.

Gao et al. [18] used RMR and other blast design variables to predict air overpressure in mines while using group method of data handling and genetic algorithm. The authors reported an R^2 of 0.988 in the predictions. Such correlations however, leave little space for uncertainties. Murlidhar et al. [31] reviewed the use of intelligent techniques in predicting environmental impacts of blasting. The use of RQD, RMR and other classifications in blast predictions have been documented in detail.

Rock Quality Designation (RQD) index, Uniaxial Compressive Strength (UCS), tunnel cross-section area, maximum depth of blast hole, and blast hole coupling were used for devising blast desing in tunnel blasting [2] using support vector machine algorithm. The authors reported very good correlation between RQD and specific charge and least error in its prediction with use of SVM.

Bieniawski's RMR and Barton's Q Both methods incorporate geological, geometric and design/engineering parameters in arriving at a quantitative value of their rock mass quality. The similarities between RMR and Q stem from the use of identical, or very similar, parameters in calculating the final rock mass quality rating. RMR uses compressive strength directly while Q only considers strength as it relates to in situ stress in competent rock. Thus, RMR is more appropriate for using with blastability of rock mass. Both schemes deal with the geology and geometry of the rock mass, but in slightly different ways. Thus, weightage to be considered in determination of blastability of rock mass with respect to RMR and Q system. Both

Table 3 The differences in application, factor use and blastability of various rockmass classification systems

Type of system	Main factors considered	Main differences with blastability
Tunnel support	<ul style="list-style-type: none"> • Falling of rock mass due to gravitational forces • Ground water has an impact 	<ul style="list-style-type: none"> • Instantaneous gaseous explosives energy breaking rock mass in all directions
Slope stability	<ul style="list-style-type: none"> • To maintain slope against gravitational forces • Ground water has an impact 	<ul style="list-style-type: none"> • Water effect can be nullified with strength of explosives/water resistance explosives
Excavability	<ul style="list-style-type: none"> • Mechanical breaking with excavator 	<ul style="list-style-type: none"> • Joint spacing, orientation has an impact on fragmentation
Rippability	<ul style="list-style-type: none"> • Mechanical breaking with dozer 	
Foundation	<ul style="list-style-type: none"> • Load bearing pressure of structure 	<ul style="list-style-type: none"> • Rock breaking resistance

consider groundwater and impact is met with type of explosives. Both include some component of rock material strength which is important for blastability of rock mass.

Issue with the rating-based systems is that these are discrete in nature and hence result in clustering at certain places which ultimately leads to a poor experimental method. Both RMR and Q schemes deal with the geology and geometry of the rock mass, but in slightly different ways.

Thus, weightage to be considered in determination of blastability of rock mass with respect to RMR and Q system. Both consider groundwater and impact is met with type of explosives. Both include some component of rock material strength which is important for blastability of rock mass. The approach of rockmass classification systems may be quantitative, analytical, observational, numerical and applied engineering design with purposes varying over wide range as defined in Table 3, that enumerates the differences in different such systems.

4 Conclusions

A review of rockmass classifications for ground support has been presented with a view of their utility in predicting blastability. A detailed research review of the citations found in the public domain relating the two have been compiled and presented here. A comparative analysis of the classifications has been presented and their applicability in blasting along with their shortcoming and further scope is presented. The paper is intended to infuse a fresh impetus to conduct research on the applicability, the refinement and better representation of the classification systems used for ground support for blasting purpose. These can well be modified to suite the requirements of fragmentation, throw and control of unwanted effects of blasting along with the possibilities of defining the rock factor for blast design.

Acknowledgements The authors are thankful to Director CSIR-CIMFR for his permission to publish the paper.

References

1. Adhikari GR, Rajan Babu A, Balachander R, Gupta RN (1999) On the application of rock mass quality for blasting in large underground chambers. *Tunn Undergr Space Technol* 14(3):367–375. [https://doi.org/10.1016/S0886-7798\(99\)00052-8](https://doi.org/10.1016/S0886-7798(99)00052-8)
2. Alipour A, Mokhtarian-Asl M, Asadizadeh M (2021) Support vector machines for the estimation of specific chargin tunnel blasting. *Period Polytech Civ Eng* 65(3). <https://doi.org/10.3311/PPci.17790>
3. Ash RL (1990) Design of blasting rounds. In: *Surface Mining*
4. Bameri A., Seifabad MC, Hoseinie SH (2021) Uncertainty consideration in rock mass blastability assessment in open pit mines using Monte Carlo simulation. *Eurasian Min* 35(1). <https://doi.org/10.17580/em.2021.01.07>
5. Barton N, Lien R, Lunde J (1974) Engineering classification of rock masses for the design of tunnel support. *Rock Mech Felsmechanik Mécanique Des Roches* 6(4):189–236. <https://doi.org/10.1007/BF01239496>
6. Barton NR (2018) TBM tunnelling under difficult conditions: too massive, too faulted, too wet, too deep. In: *1st International Conference on Advances in Rock Mechanics, TuniRock 2018*
7. Bieniawski ZT (1989) *Engineering Rock Mass Classifications: A Complete Manual for Engineers and Geologists in Mining, Civil, and Petroleum Engineering.*
8. Bieniawski ZT (2009) The rock mass rating (RMR) system (Geomechanics Classification) in engineering practice. In: *Rock Classification Systems for Engineering Purpose.*<https://doi.org/10.1520/stp48461s>
9. Chatziangelou M, Chararas B (2016) A geological classification of rock mass quality and blast ability for widely spaced formations. *J Geol Resour Eng* 4(4). <https://doi.org/10.17265/2328-2193/2016.04.002>
10. Lee CI, Jong YH, Jeon S, Choi YK, Kim HS (2005) The computerized design program for tunnel blasting. In: *Proc. of the 31th Annual Conference on Explosives & Blasting Technology, Orlando, USA, vol. 1, pp. 159–168*
11. Chung SH, Katsabanis PD (2000) Fragmentation prediction using improved engineering formulae. *Fragblast* 4(3–4). <https://doi.org/10.1076/frag.4.3.198.7392>
12. Cording EJ, Deere DU (1975) Rock tunnel supports and field measurements. *Int J Rock Mech Min Sci Geomech Abstr* 12(7). [https://doi.org/10.1016/0148-9062\(75\)90447-7](https://doi.org/10.1016/0148-9062(75)90447-7)
13. Cunningham CVB (1983) The Kuz-Ram model for prediction of fragmentation from blasting. In: *Proceedings of the 1st International Symposium on Rock Fragmentation by Blasting*, pp 439–453
14. Deere DU, Miller R (1966) Engineering classification and index properties for intact rock. Technical report, Air Force Weapons Laboratory, vol 1, pp 65–116
15. Deere DU, Deere DW (1989) Rock quality designation (RQD) after twenty years. US army corps of engineers report GL-89-1. In: *Department of the Army–US Army Corps of Engineers, vol 53, issue 9.* <http://www.dtic.mil/cgi-bin/GetTRDoc?AD=ADA207597>
16. Dey K, Sen P (2003) Concept of blastability-an update. *Indian Min Eng J* 42(8):24–31
17. Doucet C, Cameron A, Lizotte Y (1996) Effects of rock mass characteristics on fragmentation in controlled blasting experiments in small development headings. In: *Proceedings of the Annual Conference on Explosives and Blasting Technique*, p 2
18. Gao W, Alqahtani AS, Mubarakali A, Mavaluru D, Khalafi S (2020) Developing an innovative soft computing scheme for prediction of air overpressure resulting from mine blasting using GMDH optimized by GA. *Eng Comput* 36(2). <https://doi.org/10.1007/s00366-019-00720-5>
19. Hoek E (2007) *Practical rock engineering.* *Environ Eng Geosci* 40–58
20. Inanloo Arabi Shad H, Sereshki F, Ataei M, Karamoozian M (2018) Investigation of rock blast fragmentation based on specific explosive energy and in-situ block size. *Int J Min Geo-Eng* 52(1):2–7
21. Jakubec J, Laubscher DH (2000) The MRMR rock mass rating classification system in mining practice. *Australas Inst Min Metall Publ Ser* 7:413–421

22. Konya CJ, Walter EJ (1991) Rock blasting and overbreak control (No. FHWA-HI-92- 001; NHI-13211). In: Security (Issue 132)
23. Koopialipoor M, Jahed Armaghani D, Haghghi M, Ghaleini EN (2019) A neurogenetic predictive model to approximate overbreak induced by drilling and blasting operation in tunnels. *Bull Eng Geol Env* 78(2):981–990. <https://doi.org/10.1007/s10064-017-1116-2>
24. Kuznetsov VM (1973) The mean diameter of the fragments formed by blasting rock. *Sov Min Sci*. <https://doi.org/10.1007/BF02506177>
25. Laubscher DH, Jakubec J (2001) The MRMR rock mass classification for jointed rock masses. In: Hustrulid WA, Bullock RL (eds) *Underground Mining Methods: Engineering Fundamentals and International Case Studies*, Society of Mining Metallurgy and Exploration, SMME, pp 475–481
26. Lilly PA (1986) An empirical method of assessing rock mass blastability. In: *Proceeding AusIMM/IE*, pp 89–92. [https://doi.org/10.1016/0148-9062\(87\)92504-6](https://doi.org/10.1016/0148-9062(87)92504-6)
27. Mackenzie A (1966) Cost of explosives—do you evaluate it properly? *Min Congr J* 52(5):32–41
28. Marinos V, Marinos P, Hoek E (2005) The geological strength index: applications and limitations. *Bull Eng Geol Environ* 64(1). <https://doi.org/10.1007/s10064-004-0270-5>
29. Mariz JLV, et al (2020) Analysis of influence of structural geology and geomechanical in the blasting rocks prediction, pp 311–323. <https://doi.org/10.5151/2594-357x-33774>
30. Merritt AH (1975) Geologic predictions for underground excavations. *Int J Rock Mech Min Sci Geomech Abstr* 12(7). [https://doi.org/10.1016/0148-9062\(75\)90451-9](https://doi.org/10.1016/0148-9062(75)90451-9)
31. Murlidhar BR, Armaghani DJ, Mohamad ET (2020) Intelligence prediction of some selected environmental issues of blasting: a review. *Open Constr Build Technol J* 14(1):298–308. <https://doi.org/10.2174/1874836802014010298>
32. Ouchterlony F, Sanchidrián JA (2019) A review of development of better prediction equations for blast fragmentation. *J Rock Mech Geotech Eng* 11(5):1094–1109. <https://doi.org/10.1016/j.jrmge.2019.03.001>
33. Ouchterlony F (2005) The Swebrec© function: linking fragmentation by blasting and crushing. *Inst Min Metall Trans Sect A Min Technol* 114(1). <https://doi.org/10.1179/037178405X44539>
34. Pells PJ, Bieniawski ZT, Hencher SR, Pells SE (2017) Rock quality designation (RQD): time to rest in peace. *Can Geotech J* 54(6). <https://doi.org/10.1139/cgj-2016-0012>
35. Persson PA, Holmberg R, Lee J (1994) Rock blasting and explosives engineering. <https://doi.org/10.5860/choice.31-5469>
36. Rehman H, Ali W, Naji AM, Kim JJ, Abdullah RA, Yoo HK (2018) Review of rock-mass rating and tunneling quality index systems for tunnel design: development, refinement, application and limitation. *Appl Sci (Switzerland)* 8(8). <https://doi.org/10.3390/app8081250>
37. Rezaei M, Monjezi M, Moghaddam SG, Farzaneh F (2012) Burden prediction in blasting operation using rock geomechanical properties. *Arab J Geosci* 5(5):1031–1037. <https://doi.org/10.1007/s12517-010-0269-0>
38. Sayevand K, Arab H, Golzar SB (2018) Development of imperialist competitive algorithm in predicting the particle size distribution after mine blasting. *Eng Comput* 34(2):329–338. <https://doi.org/10.1007/s00366-017-0543-9>
39. Scott A, Morrell S, Clark D (2002) Tracking and quantifying value from mine to mill improvement. *Australas Inst Min Metall Publ Ser* 8
40. Segaetsho G, Zvarivadza T (2019) Application of rock mass classification and Blastability Index for the improvement of wall control: a hardrock mining case study. *J South Afr Inst Min Metall* 119(1). <https://doi.org/10.17159/2411-9717/2019/v119n1a4>
41. Singh SP (2003) The influence of rock mass quality in controlled blasting. *Australas Inst Min Metall Publ Ser* 1:219–222
42. Wickham GE, Tiedemann HR, Skinner EH (1974) Ground support prediction model RSR concept
43. Cumming-Potvin D, Wesseloo J (2014) Assessing the state of the rock mass in operating block caving mines: a review. In: *Proceedings of the Third International Symposium on Block and Sublevel Caving*, pp. 118–127. Universidad de Chile, Santiago

44. Kendorski FS, Cummings RA, Bieniawski ZT, Skinner EH (April 1983) Rock mass classification for block caving mine drift support. In: 5th ISRM Congress. OnePetro
45. Ritter W (1879) Die statik der tunnelgewölbe. J. Springer
46. Terzaghi K (1946) Rock defects and loads on tunnel supports. In: Proctor RV, White TL (eds) Rock tunneling with steel supports, vol 1, pp. 17–99. Commercial Shearing and Stamping Company, Youngstown, OH
47. Pacher F (1974) Zur Sicherung grosser Tunnelvoreinschnitte. In: Felsmechanische Grundlagenforschung Standsicherheit von Böschungen und Hohlraumbauten in Fels/Basic Research in Rock Mechanics Stability of Rock Slopes and Underground Excavations, pp. 79–88. Springer, Vienna
48. Chakraborty AK, Raina AK, Ramulu M, Choudhury PB, Halder A, Sahu PB, Bandopadhyay C (2004) Parametric study to develop guidelines for blast fragmentation improvement in jointed and massive formations. *Engi Geol* 73(2004):105–116
49. Ouchterlony F, Sanchidrián JA (2019) A review of development of better prediction equations for blast fragmentation. *J Rock Mech Geotech Eng* 11(5):1094–1109. <https://doi.org/10.1016/j.jrmge.2019.03.001>
50. Merritt AH (1972) Geologic prediction for underground excavations. In: Lane KS, Garfield LA (eds) Proc. North American rapid excav. tunneling conf., Chicago, vol 1, pp.115-132. Soc Min Engrs, Am Inst Min Metall Petrolm Engrs, New York
51. Palmström A (2009) Combining the RMR, Q, and RMi classification systems. *Tun Undergr Space Technol* 24(4):491
52. Wickham GE, Tiedemann HR, Skinner EH (1972) Support determination based on geologic predictions, In: Lane KSaG, L A, (ed) North American Rapid Excavation and Tunneling Conference: Chicago, p. 43-64. Society of Mining Engineers of the American Institute of Mining, Metallurgical and Petroleum Engineers, New York
53. Laubscher DH (1990) A geomechanics classification system for the rating of rock mass in mine design. *J South Afr Inst Min Metall* 90(10):257–273
54. Laubscher DH (1977) Geomechanics classification of jointed rock masses: mining applications. *Inst Min Metall Trans Sect A; (United Kingdom)* 86
55. Laubscher DH, Taylor HW (1976) The importance of geomechanics classification of jointed rock masses in mining operations. In: Proceedings of the Symposium of Exploration for Rock Engineering, pp. 119–128. AA Balkema, Johannesburg

Empirical and Numerical Evaluation of a Cut Slope Near Rishikesh, India



V. H. R. Pandey, Ashutosh Kainthola, and T. N. Singh

Abstract The stability analysis of cut slopes along any transportation corridor is necessary to safeguard people's and societal interests. The present work presents assessment of a steep rock cut slope near Rishikesh, along a national highway in Uttarakhand, India. The work details empirical and numerical examination of the slope stretching approximately 20 m in length along the road. The field investigation has been undertaken to ascertain discontinuities conditions, their orientations, spacing between them, geological strength index as well as slope geometries. Three joint sets were recorded with spacing of 10–120, 5–45, 6–35 cm respectively, with slope angle of 75° and slope height equal to 65 m. Moreover, the rock samples were taken in laboratory to further discern required geotechnical parameters such as unconfined compressive strength, Young's modulus, and Poisson's ratio etc. The empirical and numerical techniques were applied to examine the slope's health. Q-slope and Slope Mass Rating were the employed empirical method. Besides, the finite element approach was adopted to assess the slope stability numerical. Finally, outcomes of all these scientific assessments were compared with each other and ground reality. The Q-slope values achieved was 1.58 for the concerned slope, while the SMR value was 37. Finite element simulation yielded a safety factor of 1.6 for the dry condition. Furthermore, kinematic analysis of slope shows the possibility of planar and wedge modes of failures. Keeping in view the attained results, the slope should be excavated at an angle of 69° , while also making provisions for drainage of rain water.

Keywords Q-slope · SMR · Finite element method · Kinematic analysis · Slope stability

V. H. R. Pandey · A. Kainthola (✉)
Department of Geology, Banaras Hindu University, Varanasi, India
e-mail: ashutosh.geo@bhu.ac.in

T. N. Singh
Department of Earth Sciences, IIT Bombay, Mumbai, India

© The Author(s), under exclusive license to Springer Nature Singapore Pte Ltd. 2022
A. K. Verma et al. (eds.), *Proceedings of Geotechnical Challenges in Mining, Tunneling and Underground Infrastructures*, Lecture Notes in Civil Engineering 228,
https://doi.org/10.1007/978-981-16-9770-8_38

579

1 Introduction

The population increase and fight for habitable space has led people to settle in perilous hilly terrains [1–3]. People also make their way towards hill stations, to refresh and recharge after exhaustion from daily urban life style [4, 5]. India offers plethora of natural, cultural and historical picturesque sites that soothes tired minds and engender mental health. Tourism brings livelihood for locals and boost nation's economy [3]. Therefore, to attract greater number of visitors across the world and cater the needs of inhabitants, government fosters the development of safer infrastructures such as highways, bridges, railways tracks and tunnels [6, 7]. Also, access to high hills is crucial for the national security of India [8–10]. In the recent decades, India has shown a tremendous growth in civil works and extended its transportation network in various parts of the country, including several hilly, coastal and forested regions. This implementation of roadways requires assessment of various risks, before and after constructions [11–13]. Eventually, a rigorous evaluation of geological and geotechnical parameters of slope masses are enforced, and accordingly, construction is being planned [14–16]. The main motive of these slope examinations is to avoid danger of slope failure, rockfall, and debris flow using well planned engineering techniques [17–19].

Workers adopts well-studied assessment methods to check the stability of slopes, according to prevailing geological- geotechnical conditions and need [20]. Transportation of smaller vehicles requires narrower pathways, whereas heavy vehicles demand wider and more stable ones. Hence, agencies plan construction according to work load and time duration, without exploitation of available resources [21, 22]. Engineering geologists and civil engineers work together to achieve fastest, safest, economic and eco-friendly transportation network [23–25]. Geotechnical properties like cohesion, angle of internal friction, Poisson's ratio, Young's modulus, geological strength index (GSI), and UCS etc., form an essential component of stability analysis [26]. Besides, structural discontinuities present in the rock mass affect the slope's health based on their orientation, persistence, spacing, aperture, roughness and alteration [27]. Moreover, slope geometry such as slope height, slope angle, and slope shape have a major say in it. Apart from all these controlling factors of slope failure, several triggering attributes such as rainfall, glacier melting, earthquakes, and ground vibrations (due to heavy vehicles movement, blasting, and other human activities) dominates the occurrence of failure events [3, 28]. Therefore, an advance knowledge of aforementioned attributes can be viable for humankind to deal with landslides and slope failures.

The present work illustrates empirical and numerical assessment of slope, stretching 20 m across the road. The road connects the Rishikesh and Badarinarth, which is a major transportation corridor, supporting tourism and pilgrimage in Garhwal Himalayan region. Through this way, thousands of people enter the valley and further north. People's safety is of major importance for the government agencies, so their employees always have eye on the associated risk and take appropriate actions. The concerned road runs parallel to the river Ganga, which is perennially

flowing. Often, toe erosion of road can become severe, mainly during rainy seasons when river flows in full capacity & high velocity. The area receives significant amount of rainfall in between months of June and September each year, and reports of slope failure and landslide rises across the region.

2 Geological Framework

The geological setup of the study area is quite complex, as it belongs to the Lesser Himalayan terrain (Fig. 1) [29]. The mighty Himalaya originated as a result of tectonic collision between Indian and Eurasian plates in the geologic history [30]. The Indian plate subducted below the Eurasian plate which resulted in a large-scale folding, faulting, fracturing along with several volcanic processes [31]. As one moves northward from the Gangetic plain will pass through Shiwaliks, Lesser Himalaya, Higher Himalaya, and Tethys Himalaya on crossing Main Frontal Thrust (MFT), Main Boundary Fault (MBT), Main Central Thrust (MCT), and Indus Tsang-Po suture zone (ITSZ) respectively [32]. Beside, many other small to medium scale faults can be located in the Himalayan region [33]. The tectonic movements are still at work, which are causing several other new structural disturbances in the area.

The peculiar research area belongs to the Garhwal Himalaya of the Lesser Himalayan region of Uttarakhand. The area suffers from intense rainfall activity, temperature fluctuation, seismicity, and wind action, which are continuously deteriorating the rockmass conditions [29]. Consequently, the hill slopes are susceptible to failure and can lead to a calamity. Stratigraphically, Garhwal Himalaya has been demarcated into Tejam, Ramgarh, Jaunsar, Mussoorie, Damtha, Sirmur, and Almora groups [34]. The study area consists of metasedimentary sequences of rocks

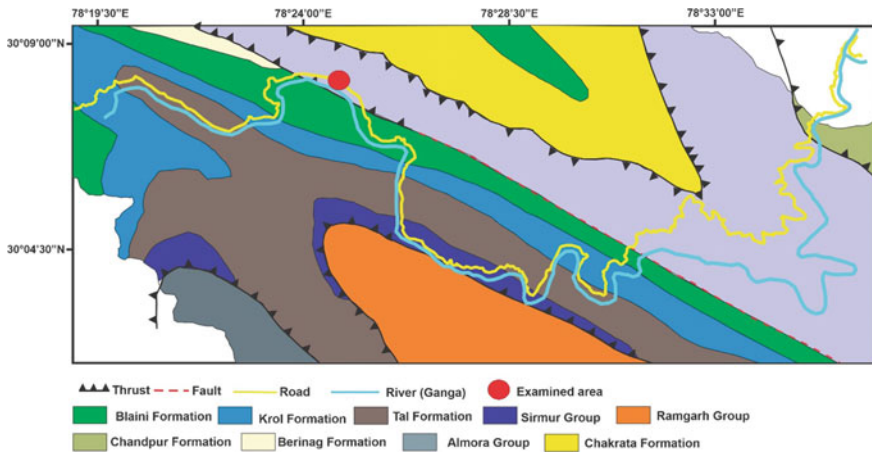


Fig. 1 Geological setup of the examined site (modified after Pradhan and Siddique [29])

belonging to Infra-Krol, Chakrata, Krol, Tal, Nagthat, and Blaini formations [35]. Therefore, shale, siltstone, limestone, sandstone, dolomite, and quartzite dominate the tectonically deformed lithology of the hilly terrains, which are ultimately cut by several perennial and rainfed streams. The studied rock cut-slope have proximity with MBT as well as the Ganga River flows parallel to it on the other side of the highway NH-52.

3 Methodology

The work was commenced with a scrupulous field investigation, followed by certain laboratory testing, afterwards empirical and numerical analysis were carried out. Moreover, based on the analysis results and field conditions the best possible slope scenario is pictured and assessed in the study. To begin the analysis part of the study, initially the kinematic assessment of slope and possible modes of structural instability were identified. The results of the kinematic analysis played a key role in further determination of Q-slope and SMR. Finally, a finite element analysis was carried out to ascertain the factor of safety of slope.

3.1 Kinematic Analysis

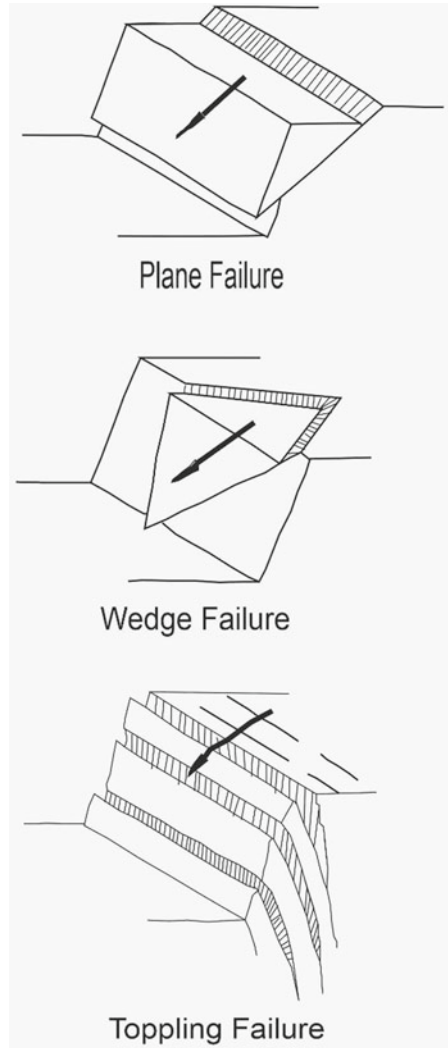
Kinematic analysis of slopes implies examining possible movements owing to rock-mass discontinuities relative to slope orientation, without involving forces [14]. Planar failure, wedge failure, and toppling failure are three modes of instability associated with relationship between geologic structures of bedrock and slope face (Fig. 2) [36]. Furthermore, the kinematic study of cut-slopes does not take cohesion into the consideration. However, the angle of internal friction associated with the joint planes finds application in the study [37].

Chances of plane failure becomes prominent when slope face and any joint plane has a nearly parallel (or within the limits of 20°) dip direction, and the joint should daylight on the slope face. Apart from this, joint should dip steeper than associated angle of internal friction along the joint plane. The conditions of plane failure can be demonstrated mathematically as in the Eqs. (1), if α , β , and γ are slope angle, joint dip, and angle of internal friction along the joint planes respectively [38].

$$\alpha > \beta > \gamma \quad (1)$$

Wedge failure is a play of two intersecting joints, if the line along their intersection plunges lower than the rock-slope angle and higher than the angle of internal friction. In this scenario a wedge of rockmass will slip outward from a rock slope, and can be a source of potential threat to nearby population or travelers depending on their volume. The wedge failure scenarios can be expressed using arithmetic Eqs. 2, if θ

Fig. 2 Modes of slope failure along discontinuities



is the plunge of line formed by intersecting joint planes [37]. Sometimes, it has been observed that wedge can slide along a single plane owing to its favorable conditions for sliding, in comparison to both the planes (or line of their intersection).

$$\alpha > \theta > \gamma \tag{2}$$

Toppling instability are enabled, if the discontinuities dip steeply into the slope face, as well their strikes are nearly parallel (within 30°). This instability scenario can be shown mathematically using Eq. 3 [38]. Workers have addressed two kinds of toppling failure, i.e., flexural toppling and direct toppling.

Table 1 Structural data associated with the rock-mass and slope

Discontinuities	Dip amount	Dip direction
Slope face	75°	240
J ₁	56°	226
J ₂	24°	305
J ₃	80°	120

$$(90 - \beta) + \gamma < \alpha \tag{3}$$

In the present work, three set of joints have been identified in the rockmass and a cut-slope for the development of Rishikesh-Badarinath highway was designed to make timely and safer transportation of goods and services in the region. Table 1 provides major structural set of the cut-slope, and Fig. 3 will illustrate rockmass conditions at the examined site.



Fig. 3 Rockmass conditions of the cut-slope in the study area

3.2 Q-Slope

The technique enhances the workers capability to examine rock cut-slope stability in real time [39]. Once the fresh rock conditions are exposed during excavation, Q-slope enables the engineer to decide the maximum slope angle without any engineered support [40]. The method is empirically derived from Q-system (applied in tunnels), owing to numerous pragmatic observations across the planet. One needs to ascertain six parameters to determine the Q-slope value (Eq. 4), namely, Rock Quality Designation (RQD), Joint set number (J_n), Joint roughness number (J_r), Joint alteration number (J_a), Geological and Environmental condition number (J_{wice}), and strength reduction factors SRF_{slope} [41]. Consequently, the maximum angle at which slope will be stable without implementation of any engineering solution can be enumerated as (Eq. 5) [42].

$$Q_{slope} = \left(\frac{RQD}{J_n} \right) * \left(\frac{J_r}{J_a} \right) * \left(\frac{J_{wice}}{SRF_{slope}} \right) \tag{4}$$

$$\beta_{20} * \log_{10}(Q_{slope}) + 65^\circ \tag{5}$$

RQD of the rockmass depends on the spacings between the available discontinuities, and is simple percentage of intact rock core lengths greater than 10 cm of the total core length (Eq. 6). Beside, another evaluation approach for RQD is to determine the spacing between each joint sets and deploy the Eqs. 7 and 8 [43].

$$RQD = \frac{\sum \text{Length of core pieces} > 0.1m}{\text{Total length of the core run}} * 100\% \tag{6}$$

$$J_v = \frac{1}{S_1} + \frac{1}{S_2} + \frac{1}{S_3} + \dots + \frac{1}{S_n} \tag{7}$$

$$RQD = 115 - 3.3J_v \tag{8}$$

J_n can be estimated by counting the number of joint sets and random joints and then examining the work of Bar and Barton [40]. Similarly, one will be able to decipher the values of J_r , J_a , J_{wice} , and SRF_{slope} with evidences from field setting and available literatures [39–42]. In case of “ J_r/J_a ” an orientation factor is worked out and depending on the kinematic assessment most critical joint set is identified with respect to slope orientation. Moreover, in case of wedge failure both the discontinuity planes are considered in evaluation of “ J_r/J_a ” along with a suitable and separate orientation factor for each of them. The orientation factor can be inferred from the previous works of Q-Slope [40, 44]. Furthermore, SRF_{slope} have three ways to be examined, therefore all the possible ones (SRF_a , SRF_b , and SRF_c) should be analyzed and the one with highest value should be assimilated in the work.

To discern the Q-slope value in the study area, all the six parameters were marked based on the field investigation, climatic condition prevailing at the site, and basic

Table 2 Q-slope attributes pertaining to the study area [40–42]

Parameters	Numeric values	Description
RQD	90–100	Excellent rockmass
J_n	9	Three joint sets are present
J_r	3	Rough or irregular, undulating
J_a	4	Sandy particles, clay free disintegrated rock
J_{wice}	0.5	Stable structure and competent rock lying in tropical storm condition
SRF_{slope}	$SRF_a = 2.5$; $SRF_b = 2.5$; $SRF_c = N/A$ (Maximum among these will be adopted in the study)	SRF_a : Slight loosening due to surface location, disturbance from blasting or excavation SRF_b : high stress-strength range SRF_c : not applicable as there are no major discontinuity plane

mathematical assessment, taking reference from available literature. Table 2 highlights all the numeric values of each attribute entrained in the determination of Q-slope belonging to the study area. Therefore, considering Table 2 and Eq. 4, one can evaluate Q-slope value. Eventually, maximum angle at which slope will be stable without implementing any engineering support can be deciphered through Eq. 5.

$$Q_{slope} = \left(\frac{95}{9}\right) * \left(\frac{3}{4}\right) * \left(\frac{0.5}{2.5}\right)$$

$$Q_{slope} = 1.58$$

$$\beta_{20} * \log_{10}(1.58) + 65^\circ$$

$$\beta = 68.97^\circ$$

3.3 Slope Mass Rating

Slope mass rating (SMR) is another method to assess the slope stability conditions, and an exquisite combination of rock mass rating (RMR_{basic}) and certain adjusting factors justifying the modes of failures associated in the cut slope [45, 46]. RMR_{basic} is a summation of certain rock mass parameters such as unconfined compressive strength (UCS), RQD, Joint Spacing, Discontinuity conditions and groundwater situation prevailing at the site (Eq. 9) [47–50]. Moreover, SMR can be enumerated using Eq. 10. The data pertaining to determination of SMR of the examined area can be

Table 3 Rock mass rating (basic) parameters of the study area [46–48]

Parameters	Description	Range of values
UCS	36 MPa	4
RQD	90–100%	20
Spacing	$S_1 = 200\text{--}600$ mm	10
Conditions of discontinuities	Slightly rough surface, Separation < 1 mm, highly weathered walls	20
Groundwater	Completely dry	15

Table 4 Adjustment ratings for joints in case of plane failure [46–49]

Cases	Range	Adjustment factors	Values
$ \alpha_j - \alpha_s = 240^\circ - 226^\circ = 14^\circ$	$20^\circ\text{--}10$	F_1	0.70
$\beta_j = 56^\circ$	$>45^\circ$	F_2	1.00
$(\beta_j - \beta_s) = (56^\circ - 75^\circ) = -19^\circ$	$<-10^\circ$	F_3	-60.00
Slope excavation method	Presplitting	F_4	10.00

where, α_j , α_s , β_j , and β_s are the joint dip direction, slope dip direction, joint dip and slope dip respectively

inferred from Tables 3 and 4.

$$RMR_{basic} = UCS + RQD + S + CD + GW \tag{9}$$

$$SMR = RMR_{basic} + [(F_1 F_2 F_3) + F_4] \tag{10}$$

Calculation of RMR_{basic} will be evaluated using above mentioned Eq. (9).

$$RMR_{basic} = 4 + 20 + 10 + 20 + 15$$

$$RMR_{basic} = 69$$

Hence, the rockmass falls under class number II and considered to be “good rock” [48]. Finally, we needed parameters such F_1 , F_2 , F_3 , and F_4 to estimate the SMR of the rockmass of the study area. So, one will have to establish the discontinuities to discern the probable modes of kinematic stability of the slope being examined.

Now, as per kinematic analysis planar and wedge modes of failures were identified. However, toppling failure is not possible for the given structural set of the rockmass and the slope. Therefore, one will have to enumerate the F_1 , F_2 , F_3 , and F_4 based on the planar failure features [45, 49]. The mathematical analysis presented below will form the base for the further estimation of concerned values.

So, using Eq. (10) SMR can be estimated based on determined RMR_{basic} and other adjusting factors as mentioned in Table 4.

$$SMR = 69 + [(0.70 * 1 * (-60)) + 10]$$

$$SMR = 37$$

3.4 Finite Element Analysis:

The pace of growth in last few decades is attributed to technical advancement in computing technology [51]. Every single sphere of the planet has seen an enormous change with advent of new methods of solving complex mathematical equations, that too with quite greater accuracy and precision in short span of time. The rapid development in new technologies defines several new chapters in various aspects of scientific era. Consequently, the geotechnical domain has witnessed enormous growth in later half of 20th century with introduction of numerical methods [52–54]. These numerical methods are much faster and efficient in deciphering the geomechanical responses than most of the established traditional methods [55]. Numerical simulations are devoid of several assumptions, and all the arithmetic operations are performed in numerous small elements which are connected with each other through nodes [56]. The number of elements and type of nodes adopted in model have significant impetus on time requirement and precision of the results [56, 57]. The physico-mechanical behavior of rockmass and soil material under constant static and dynamic loading can be enumerated with confidence in any underground opening or cut slopes [52]. The numerical techniques have, i.e., continuum, discontinuum, and hybrid modelling [29]. The continuum approach deals with uniform distribution pattern of physical and mechanical attributes throughout the structure [29, 54]. While, the discontinuum plays clear under varying engineering and geological properties within any geotechnical projects. Furthermore, hybrid models address where both the continuum and discontinuum conditions are assimilated together. Finite element, finite difference, and boundary element falls under the continuum numerical techniques [58]. In addition, discrete element method and discrete fracture network are reliable discontinuum numerical approaches meant to simulate heterogenous physico-mechanical engineering designs [59].

Considering the site conditions, following the field investigation and laboratory testing, geotechnical properties with respect to slope attributes were examined in finite element method (FEM). The present work performs slope stability assessment under the environment of RS² tool, a product of RocScience bundle. The FEM method will assess the safety factory of the rock cut-slope considering shearing stresses and shear strength of the material. Moreover, the failure zone develops at the points where shearing stresses dominates the shear strength of the material [52–56]. In the

present numerical assessment, shear strength reduction (SSR) technique is involved. In SSR technique the finite element, iteratively reduces the shearing strength of the material by dividing the cohesion and angle of internal friction with a numerical entity (factor), until the material fails to support the resulting stress acting on the slope (Eqs. 11 and 12) [58–64].

$$c' = \frac{c}{FoS} \tag{11}$$

$$\varphi = \arctan\left(\frac{\tan\varphi}{FoS}\right) \tag{12}$$

On observing the rockmass conditions and taking clues from the past literature, the present study adopts the Generalized Hoek–Brown (GHB) failure criteria for finite element calculations [55–57]. The GHB failure criteria governs the failure mechanisms of the rockmass in a pragmatic manner, developing slip surface either along discontinuities or within the intact rock, and sometimes through both at the same time (Eqs. 13 and 14) [29, 57, 60].

$$\sigma'_1 = \sigma'_3 + \sigma_{ci} \left(m_b \frac{\sigma'_3}{\sigma_{ci}} + s \right)^a \tag{13}$$

$$m_b = m_i * \exp\left[\frac{(GSI - 100)}{28} \right] \tag{14}$$

where, $\sigma'_1, \sigma'_3, \sigma_{ci}$, are the major effective principal stress, minor effective principal stress, uniaxial compressive strength of the intact rock respectively. Besides, m_i is the rock type dependent material constant. Moreover, s and a are based on disturbance factor (D) and GSI curve fitting parameters. Nonetheless, one can evaluate the values of s and a for good quality ($GSI > 25$) rocks using Eqs. (15 and 16) [29] and bad quality ($GSI < 25$) rocks using Eqs. (17 and 18). In the present rockmass determined GSI value is 45–55, which will be used here in finite element calculation, to satisfy the GHB failure criteria requirements.

$$s = \exp[(GSI - 100)/9] \tag{15}$$

$$a = 0.5 \tag{16}$$

$$s = 0 \tag{17}$$

$$a = 0.65 - GSI/200 \tag{18}$$

Therefore, the factor of safety of the rock cut-slope can be established in RS² program, employing FEM over SSR technique and GHB failure mechanism.

4 Results and Discussion

Slope stability examination kinematically discern that there are two possible modes of slope failure. The planar failure is possible along the J1 joint set, which can be a source of major destruction (Fig. 4a). Moreover, the risk of wedge failure is high along the line of intersection of joint sets J₁ and J₃, also a little chance of wedge failure along the line formed by intersection of J1 and J2 (Fig. 4b). Moreover, the study shows that the chances of toppling is quite negligible (Fig. 4c, d).

After the kinematically evaluating the slope sliding, the work further digs into few empirical techniques of slope stability examination. In this row, Q-slope and SMR techniques were analyzed in the study. Moreover, the relevant parameters required in ascertaining the results of these methods were carefully studied during field and laboratory investigations. Furthermore, the assessed parameters were marked numerically apropos to works of earlier researchers. In the present research, the value of Q-slope is 1.58, which means that a slope angle of approximately 69° will be ideally stable without any needed support structure. However, at present state rock cut-slope is standing at an angle of 75° without any support, which is little higher than the estimated value through Q-slope technique. The standing slope is slightly steeper than the calculated one, so a small instability may be rendered owing to extreme conditions like heavy rainfall or high magnitude earthquakes. As, the region is prone to higher duration of rainfall period, it will lead to development of pore water pressure in the fracture or other cracks within the rockmass. Consequently, stable slopes

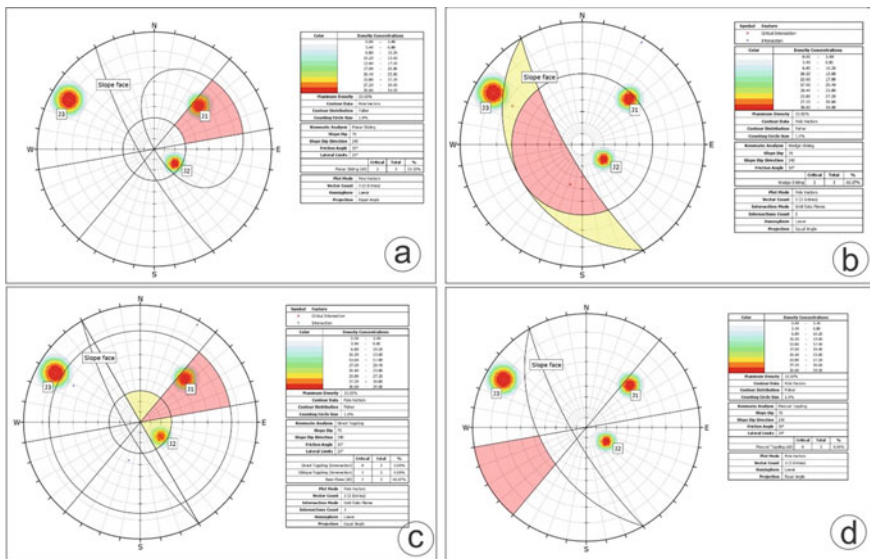


Fig. 4 Pictorial representation of kinematic analysis of the studies slope **a** planar sliding, **b** wedge sliding, **c** direct toppling, **d** flexural toppling

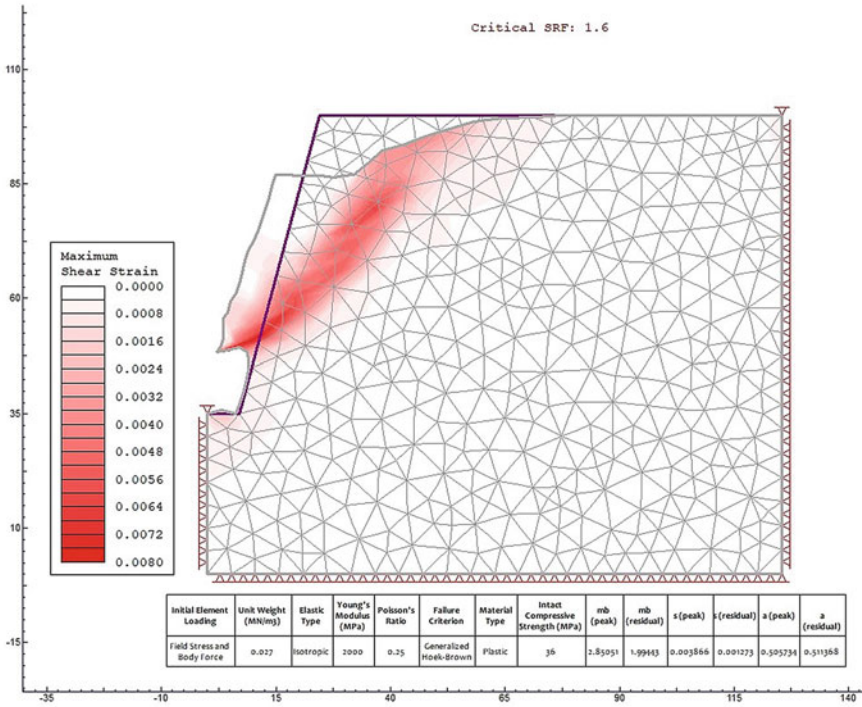


Fig. 5 Finite element analysis of studied rock cut-slope with safety factor and maximum shear stress distribution, moreover showing deformed boundary. Furthermore, scale is in meter with boundary condition suitable for numerical methods

will become precarious and may fails. Similarly, seismic events will exacerbate the shear strength of the intact and rockmass, and will render instability to the rock cut-slopes in the region. However, in hilly terrain of the Lesser Himalaya higher magnitude tremors are rare, so there are quite meagre chances of instability owing to earthquakes in the examined area. In the light of apropos discussion here, author will suggest the authorities to drainage holes in the slopes to avoid any casualty in the future.

The other empirical method employed in the present research, i.e., slope mass rating earns a numerical value of 37. Following, the RMR_{basic} examination in the process of SMR calculation provides an arithmetic number 69. The RMR_{basic} signifies that rockmass can be grouped into class II, a good rock quality based on the previous literatures. The SMR evaluation will need adjusting factors to be summed into the RMR_{basic} numerical value. Also, based on the kinematic study of slope stability, the most probable mode of failure was planar type. Hence, taking the outcomes of

kinematic analysis and other slope and discontinuities relationships the adjustment factors were enumerated in the study. Moreover, F_1 , F_2 , F_3 , and F_4 are 0.70, 1.00, –60.00, and 10 respectively. Additionally, the SMR value lies at the border of bad and normal quality rockmass, it can be concluded that slope stability will vary from being unstable to partially stable one. Therefore, support is necessary to make cut-slope safer for people.

On the other hand, the numerical stability assessment in finite element tool declares the slope to be stable with a quite higher safety factor. The slope was analyzed in the RS² program with shear strength reduction technique and under the condition of GHB failure criteria. To avoid the complexities the joint conditions were excluded in the FEM examination. The factor of safety for the examined rock cut-slope was 1.6 (Fig. 5).

Based on the techniques like Q-slope and finite element method the slope is stable and does not require any engineering support. However, the slope mass rating declares the slope to be precarious owing to which installation of supports becomes the necessity.

5 Conclusion

The present work is being performed to check the health of a rock cut-slope, which spread almost 20 m in length along the national highway-52. The study area is located in the Lesser Himalayan zone of the Garhwal region and quite close to MBT. The structural discontinuities developed in the geological past are the ramification of tectonic forces due to collision of Indian and Eurasian plates. These discontinuities are the planes of weakness associate in the rockmass, rendering precarious rock cut-slopes in the mountainous ranges. Moreover, the adverse climatic condition and regular seismicity in the valley are another factor affecting the slope health. Kinematic assessment resulted in the probability of plane failure; however, chances of wedge sliding cannot be neglected here.

The resulting Q-slope values signifies that slope will be stable at an angle of 69°, approximately 6° less than the actual one. According to workers, the slope should be stable without any heavy engineering support installation, however, looking at the other environmental factors drainage pipes needed. Furthermore, the SMR study declares the slope to be unstable, with a small value of 39. Therefore, on the basis of SMR cut-slope requires some engineering solution to deter any future fatalities the region and make the transportation route safer. In fact, change in the blasting method can increase or decrease the SMR value. Hence, the concerned authorities should choose a suitable excavation or blasting approach, that does not harm the strength of the rockmass any further. Additionally, factor of safety (1.6) resulted in the finite element examination is quite favorable in terms of safety of passengers of NH-52.

References

1. Ansari T, Kainthola A, Singh KH, Singh TN, Sazid M (2021) Geotechnical and micro-structural characteristics of phyllite derived soil; implications for slope stability, Lesser Himalaya, Uttarakhand, India. *Catena* 196:104906. <https://doi.org/10.1016/j.catena.2020.104906>
2. Bharati AK, Ray A, Khandelwal M, Rai R, Jaiswal A (2021) Stability evaluation of dump slope using artificial neural network and multiple regression. *Eng Comput* 9:1–9. <https://doi.org/10.1007/s00366-021-01358-y>
3. Kainthola A, Sharma V, Pandey VH, Jayal T, Singh M, Srivastav A, Singh PK, Champati Ray PK, Singh TN (2021) Hill slope stability examination along Lower Tons valley, Garhwal Himalayas, India. *Geom Nat Haz Risk* 12(1):900–921. <https://doi.org/10.1080/19475705.2021.1906758>
4. Ahour M, Hataf N, Azar E (2020) A mathematical model based on artificial neural networks to predict the stability of rock slopes using the generalized Hoek-Brown failure criterion. *Geotech Geol Eng* 38(1):587–604. <https://doi.org/10.1007/s10706-019-01049-y>
5. Daftariresheli A, Ataei M, Sereshki F (2011) Assessment of rock slope stability using the Fuzzy Slope Mass Rating (FSMR) system. *Appl Soft Comput* 11(8):4465–4473. <https://doi.org/10.1016/j.asoc.2011.08.032>
6. Kainthola A, Singh PK, Singh TN (2015) Stability investigation of road cut slope in basaltic rockmass, Mahabaleshwar, India. *Geosci Front* 6(6):837–845. <https://doi.org/10.1016/j.gsf.2014.03.002>
7. Kainthola A, Singh PK, Wasnik AB, Singh TN (2012) Distinct element modelling of Mahabaleshwar road cut hill slope. <http://www.scrip.org/journal/PaperInformation.aspx?PaperID=24023>
8. Khandelwal M, Rai R, Shrivastava BK (2015) Evaluation of dump slope stability of a coal mine using artificial neural network. *Geomech Geophys Geo-energy Geo-resources* 1(3):69–77. <https://doi.org/10.1007/s40948-015-0009-8>
9. Kundu J, Sarkar K, Jaboyedoff M, Singh TN (2019) GISMR: a computer application to perform kinematic analysis, slope mass rating and optimization of slope angle on a GIS platform with the aid of ArcGIS or QGIS. In: AGU fall meeting abstracts, December 2019, vol 2019, pp NH53A-05. <https://ui.adsabs.harvard.edu/#abs/2019AGUFMNH53A..05K/abstract>
10. Kundu J, Sarkar K, Singh AK (2019) EasySMR: a computer program to check kinematic feasibility and calculate Slope Mass Rating. In: Geophysical research abstracts, 1 January 2019, vol 21
11. Mahanta B, Singh HO, Singh PK, Kainthola A, Singh TN (2016) Stability analysis of potential failure zones along NH-305, India. *Nat Haz* 83(3):1341–1357. <https://doi.org/10.1007/s11069-016-2396-8>
12. Rai R, Khandelwal M, Jaiswal A (2012) Application of geogrids in waste dump stability: a numerical modeling approach. *Environ Earth Sci* 66(5):1459–1465. <https://doi.org/10.1007/s12665-011-1385-1>
13. Sardana S, Sharma P, Verma AK, Singh TN (2020) A case study on the rockfall assessment and stability analysis along Lengpui-Aizawl highway, Mizoram, India. *Arab J Geosci* 13(24):1–2. <https://doi.org/10.1007/s12517-020-06196-8>
14. RK U, Singh R, Ahmad M, TN S (2011) Stability analysis of cut slopes using continuous slope mass rating and kinematic analysis in Rudraprayag district, Uttarakhand. *Geomaterials*. <http://www.scrip.org/journal/PaperInformation.aspx?PaperID=8176>
15. Kainthola A, Verma D, Gupte SS, Singh TN (2011) A coal mine dump stability analysis—a case study. *Geomaterials* 1(01):1
16. Kainthola A, Verma D, Thareja R, Singh TN (2013) A review on numerical slope stability analysis. *Int J Sci Eng Technol Res (IJSETR)* 2(6):1315–1320
17. Kundu J, Sarkar K, Singh PK, Singh TN (2018) Deterministic and probabilistic stability analysis of soil slope—a case study. *J Geol Soc India* 91(4):418–424. <https://doi.org/10.1007/s12594-018-0874-1>

18. Kundu J, Sarkar K, Singh TN (2017) Static and dynamic analysis of rock slope—a case study. In: ISRM European rock mechanics symposium-EUROCK. OnePetro
19. Sarkar S, Pandit K, Dahiya N, Chandna P (2021) Quantified landslide hazard assessment based on finite element slope stability analysis for Uttarkashi-Gangnani Highway in Indian Himalayas. *Nat Haz* 106(3):1895–1914. <https://doi.org/10.1007/s11069-021-04518-x>
20. Tiwari VN, Pandey VHR, Kainthola A, Singh PK, Singh KH, Singh TN (2020) Assessment of Karmi Landslide Zone, Bageshwar, Uttarakhand, India. *J Geol Soc India* 96(4):385–393. <https://doi.org/10.1007/s12594-020-1567-0>
21. Rojat F, Labiouse V, Mestat P (2015) Improved analytical solutions for the response of underground excavations in rock masses satisfying the generalized Hoek-Brown failure criterion. *Int J Rock Mech Mining Sci* 79:193–204. <https://doi.org/10.1016/j.ijrmm.2015.08.002>
22. Ray A, Kumar V, Kumar A, Rai R, Khandelwal M, Singh TN (2020) Stability prediction of Himalayan residual soil slope using artificial neural network. *Nat Haz* 103(3):3523–3540. <https://doi.org/10.1007/s11069-020-04141-2>
23. Singh J, Verma AK, Banka H (2018) Application of biogeography based optimization to locate critical slip surface in slope stability evaluation. In: 2018 4th international conference on recent advances in information technology (RAIT). IEEE, pp 1–5. <https://doi.org/10.1109/RAIT.2018.8389070>
24. Singh AK, Kundu J, Sarkar K (2018) Stability analysis of a recurring soil slope failure along NH-5, Himachal Himalaya, India. *Nat Haz* 90(2):863–885. <https://doi.org/10.1007/s11069-017-3076-z>
25. Sharma P, Verma AK, Negi A, Jha MK, Gautam P (2018) Stability assessment of jointed rock slope with different crack infillings under various thermomechanical loadings. *Arab J Geosci* 11(15):1–6. <https://doi.org/10.1007/s12517-018-3772-3>
26. Verma D, Kainthola A, Gupte SS, Singh TN (2013) A finite element approach of stability analysis of internal dump slope in Wardha valley coal field, India, Maharashtra. *Am J Mining Metall* 1(1):1–6
27. Verma D, Thareja R, Kainthola A, Singh TN (2011) Evaluation of open pit mine slope stability analysis. *Int J Earth Sci Eng* 4(4):590–600
28. Wallace CS, Schaefer LN, Villeneuve MC (2021) Material properties and triggering mechanisms of an andesitic lava dome collapse at Shiveluch Volcano, Kamchatka, Russia, revealed using the finite element method. *Rock Mech Rock Eng* 1:1–8. <https://doi.org/10.1007/s00603-021-02513-z>
29. Pradhan SP, Siddique T (2020) Stability assessment of landslide-prone road cut rock slopes in Himalayan terrain: a finite element method based approach. *J Rock Mech Geotech Eng* 12(1):59–73. <https://doi.org/10.1016/j.jrmge.2018.12.018>
30. Yin A (2006) Cenozoic tectonic evolution of the Himalayan orogen as constrained by along-strike variation of structural geometry, exhumation history, and foreland sedimentation. *Earth-Sci Rev* 76(1–2):1–31. <https://doi.org/10.1016/j.earscirev.2005.05.004>
31. Kumar D, Thakur M, Dubey CS, Shukla DP (2017) Landslide susceptibility mapping & prediction using support vector machine for Mandakini River Basin, Garhwal Himalaya, India. *Geomorphology* 295:115–125. <https://doi.org/10.1016/j.geomorph.2017.06.013>
32. Srivastava P, Mitra G (1994) Thrust geometries and deep structure of the outer and lesser Himalaya, Kumaon and Garhwal (India): Implications for evolution of the Himalayan fold-and-thrust belt. *Tectonics* 13(1):89–109. <https://doi.org/10.1029/93TC01130>
33. Bose N, Mukherjee S (2019) Field documentation and genesis of the back-structures from the Garhwal Lesser Himalaya, Uttarakhand, India. *Geol Soc Lond Spec Publ* 481(1):111–125. <https://doi.org/10.1144/SP481-2018-81>
34. Valdiya KS (1980) Geology of Kumaun Lesser Himalaya. Wadia Institute of Himalayan Geology
35. Jiang G, Sohl LE, Christie-Blick N (2003) Neoproterozoic stratigraphic comparison of the Lesser Himalaya (India) and Yangtze block (south China): paleogeographic implications. *Geology* 31(10):917–920. <https://doi.org/10.1130/G19790.1>

36. Zavodni ZM, Broadbent CD (1978) Slope failure kinematics. In: 19th US symposium on rock mechanics (USRMS), 1 May 1978. OnePetro
37. Xiao S, Gao YT, Wu SC, Liu B, Tian QM (2018) Kinematic analysis of slope failure modes based on stereographic projection. In: Progress in civil, architectural and hydraulic engineering IV: proceedings of the 2015 4th international conference on civil, architectural and hydraulic engineering (ICCAHE 2015), Guangzhou, China, 20–21 June 2015. CRC Press, p 313
38. Admassu Y (2013) Shakoor A (2013) DIPANALYST: A computer program for quantitative kinematic analysis of rock slope failures. *Comput Geosci* 1(54):196–202. <https://doi.org/10.1016/j.cageo.2012.11.018>
39. Azarafza M, Nanehkaran YA, Rajabion L, Akgün H, Rahnamarad J, Derakhshani R, Raof A (2020) Application of the modified Q-slope classification system for sedimentary rock slope stability assessment in Iran. *Eng Geol* 264:105349. <https://doi.org/10.1016/j.enggeo.2019.105349>
40. Bar N, Barton N (2017) The Q-slope method for rock slope engineering. *Rock Mech Rock Eng* 50(12):3307–3322. <https://doi.org/10.1007/s00603-017-1305-0>
41. Bar N, Barton NR (2016) Empirical slope design for hard and soft rocks using Q-slope. In: 50th US rock mechanics/geomechanics symposium, 26 June 2016. OnePetro
42. Barton N, Bar N (2015) Introducing the Q-slope method and its intended use within civil and mining engineering projects. In: ISRM regional symposium-EUROCK. OnePetro
43. Palmstrom A (2005) Measurements of and correlations between block size and rock quality designation (RQD). *Tunn Undergr Space Technol* 20(4):362–377. <https://doi.org/10.1016/j.tust.2005.01.005>
44. Song Y, Xue H, Meng X (2019) Evaluation method of slope stability based on the Q slope system and BQ method. *Bull Eng Geol Environ* 78(7):4865–4873. <https://doi.org/10.1007/s10064-019-01459-5>
45. Zheng J, Zhao Y, Lü Q, Deng J, Pan X, Li Y (2016) A discussion on the adjustment parameters of the slope mass rating (SMR) system for rock slopes. *Eng Geol* 17(206):42–49. <https://doi.org/10.1016/j.enggeo.2016.03.007>
46. Tomas R, Cuenca A, Cano M, García-Barba J (2012) A graphical approach for slope mass rating (SMR). *Eng Geol* 124:67–76. <https://doi.org/10.1016/j.enggeo.2011.10.004>
47. Azarafza M, Akgün H, Asghari-Kaljahi E (2017) Assessment of rock slope stability by slope mass rating (SMR): a case study for the gas flare site in Assalouyeh, South of Iran. *Geomech Eng* 13(4):571–584. <https://doi.org/10.12989/gae.2017.13.4.571>
48. Riquelme AJ, Tomás R, Abellán A (2016) Characterization of rock slopes through slope mass rating using 3D point clouds. *Int J Rock Mech Mining Sci* 84:165–176. <https://doi.org/10.1016/j.ijrmmms.2015.12.008>
49. Romana M, Tomás R, Serón JB (2015) Slope Mass Rating (SMR) geomechanics classification: thirty years review. In: 13th ISRM international congress of rock mechanics, 10 May 2015. OnePetro
50. Romana MR (1993) A geomechanical classification for slopes: slope mass rating. In: Rock testing and site characterization. Pergamon, 1 January 1993
51. Chen GH, Zou JF, Zhang R (2021) Stability analysis of rock slopes using strength reduction adaptive finite element limit analysis. *Struct Eng Mech* 79(4):487–98. <https://doi.org/10.12989/sem.2021.79.4.487>
52. Chihi O, Saada Z (2020) Bearing capacity of strip footing on rock under inclined and eccentric load using the generalized Hoek-Brown criterion. *Eur J Environ Civil Eng* 4:1–5. <https://doi.org/10.1080/19648189.2020.1757513>
53. Dyson AP (2018) Tolooiyan A (2018) Optimisation of strength reduction finite element method codes for slope stability analysis. *Innov Infrastruct Sol* 3(1):1–2. <https://doi.org/10.1007/s41062-018-0148-1>
54. Dyson AP, Tolooiyan A (2019) Prediction and classification for finite element slope stability analysis by random field comparison. *Comput Geotech* 109:117–129. <https://doi.org/10.1016/j.compgeo.2019.01.026>

55. Hammah RE, Yacoub TE, Corkum BC, Curran JH (2005) The shear strength reduction method for the generalized Hoek-Brown criterion. In: Alaska Rocks 2005, the 40th US symposium on rock mechanics (USRMS). OnePetro
56. Kumar V, Burman A, Himanshu N, Gordan B (2021) Rock slope stability charts based on limit equilibrium method incorporating Generalized Hoek-Brown strength criterion for static and seismic conditions. *Environ Earth Sci* 80(6):1–20. <https://doi.org/10.1007/s12665-021-09498-6>
57. Lee YK, Pietruszczak S (2021) Limit equilibrium analysis incorporating the generalized Hoek-Brown criterion. *Rock Mech Rock Eng* 5:1–2. <https://doi.org/10.1007/s00603-021-02518-8>
58. Poklopová T, Pavelcová V, Šejnoha M (2021) Comparing the Hoek-Brown and Mohr-Coulomb failure criteria in FEM analysis. *Acta Polytechnica CTU Proc* 30:69–75. <https://doi.org/10.14311/APP.2021.30.0069>
59. Singh J, Banka H, Verma AK (2019) A BBO-based algorithm for slope stability analysis by locating critical failure surface. *Neural Comput Appl* 31(10):6401–6418. <https://doi.org/10.1007/s00521-018-3418-0>
60. Singh J, Banka H, Verma AK (2018) Analysis of slope stability and detection of critical failure surface using gravitational search algorithm. In: 2018 4th international conference on recent advances in information technology (RAIT), 15 March 2018. IEEE, pp 1–6. <https://doi.org/10.1109/RAIT.2018.8389049>
61. Yang Y, Xia Y, Zheng H, Liu Z (2021) Investigation of rock slope stability using a 3D nonlinear strength-reduction numerical manifold method. *Eng Geol* 292:106285. <https://doi.org/10.1016/j.enggeo.2021.106285>
62. You G, Al Mandalawi M, Soliman A, Dowling K, Dahlhaus P (2017) Finite element analysis of rock slope stability using shear strength reduction method. In: International congress and exhibition “sustainable civil infrastructures: innovative infrastructure geotechnology”, 2 July 2017. Springer, Cham, pp 227–235. https://doi.org/10.1007/978-3-319-61902-6_18
63. Zheng H, Liu DF, Li CG (2005) Slope stability analysis based on elasto-plastic finite element method. *Int J Numer Meth Eng* 64(14):1871–1888. <https://doi.org/10.1002/nme.1406>
64. Srivastav A, Pandey VH, Kainthola A, Singh PK, Dangwal V, Singh TN (2021) Numerical analysis of a collapsed tunnel: a case study from NW Himalaya, India. *Indian Geotech J* 1:1–3. <https://doi.org/10.1007/s40098-021-00567-y>

Recent Developments in Machine Learning and Flyrock Prediction



Ramesh Murlidhar Bhatawdekar, Ashutosh Kainthola, V. H. R. Pandey, Singh Trilok Nath, and Edy Tonnizam Mohamad

Abstract The blasting techniques are employed in mining and underground works to loosen the rock mass and ease the excavation. The blasting practices are economical and swifter in terms of their engineering application, however, they are of major environmental and safety concerns. The major issues related to blasting are flyrock, air over pressure, and ground vibrations etc. The rock fragments of rockmass are thrown outward after blasting, which can be threat to workers and machineries involved in the work, and sometimes nearby human settlements can be its victim. Therefore, an accurate prediction of the flyrock distance is the needed by mining practitioners. Earlier, experts have developed several empirical methods based on certain known parameters to assess flyrock distance. However, with time they become irrelevant and were easily replaced with advanced machine learning algorithm. The present study reviews some of these latest publications (2019–2021) examining flyrocks through artificial intelligent technique. The study incorporates types of machine learning models employed, input parameters used and number of datasets supporting the models. The input parameters were further classified according to rock-mass properties, blast design at site, and explosives responsible for blasting. Moreover, to compare the reliability of the model coefficient of correlation of the testing data of the all the documented model were evaluated. Rock density, rock mass rating and Shmidt hammer rebound number (SHRN) were found to be uncertain parameters.

R. M. Bhatawdekar

Department of Mining Engineering, Indian Institute of Technology, Kharagpur, Kharagpur 721302, India

R. M. Bhatawdekar · E. T. Mohamad

Centre of Tropical Geoengineering (GEOTROPIK), Faculty of Civil Engineering, Universiti Teknologi Malaysia, UTM, 81310 Skudai, Johor, Malaysia

A. Kainthola (✉) · V. H. R. Pandey

Geo-Engineering and ML Laboratory, Department of Geology, Institute of Science, Banaras Hindu University, Varanasi, India
e-mail: ashutosh.geo@bhu.ac.in

S. T. Nath

Department of Earth Science, Indian Institute of Technology, Bombay, Mumbai 400 076, India

Artificial Neural Network (ANN) and other hybrid models for prediction of flyrock were compared.

Keywords Machine learning · Optimization algorithms · Flyrock prediction · Blasting

1 Introduction

Blasting implies the fragmenting of rocks into smaller sizes. Chemical energy of the explosives is converted into mechanical energy, leading to fragmentation. Therefore, blastability can be defined as the characteristics of blast design, explosive features and legislative constraints, depending on the site particulars, and rockmass conditions [1–4]. Simply put, blastability indicates the ease of blasting a rockmass under a specific set of condition [5–8]. One of the major environmental and safety concerns with blasting in mining is flyrock distance. Flyrocks cause accidents and damage to equipment. Factors governing flyrock can either be controlled attributes viz., charge, burden and spacing or uncontrolled parameters, which is the fabric and strength of the rock mass. Mining engineers' control blasting setup based on their assessment of rock-mass parameters, geometrical analysis and prior experiences on similar site conditions [9–11]. Rock mass structure and parameters are crucial for ascertaining the blast design and blasting operations; hence, rock mass classification is routinely carried out in any mining or civil engineering project. Previously, researchers have correlated hole diameter with burden and spacing, eventually impacting the blast design [12]. The geotechnical engineers hold the major position to decide the blasting parameters and explosives prior to blasting on drilling locations. Moreover, initially the attributes like production capacity, loading equipment and bench height dominates the selection of drilling equipment [13]. Therefore, in order to understand and minimize flyrocks, it's imperative to assess the blasting mechanism and its correlation to flyrocks. Furthermore, myriad new approaches have been developed recently to estimate the flyrock distance based on contributing geotechnical and blasting parameters. The paper attempts to review these novel techniques in terms of viability and accuracy.

Blasting is the conversion of chemical energy into mechanical energy to fragment the rock mass. Geo-engineers and workers have found that explosive charge concentration per unit length is directly proportional to the hole diameter, consequently the extent of hole diameter directly affects the flyrock distance and ground vibrations [14, 15]. At certain blasting venues, different drill sizes can be viable to enhance the feasibility and production. Figure 1 provides details of blast design parameters for production blast such as burden (β), spacing (A), hole diameter ($\tau\delta$), stemming length ($\alpha\mu$), bench height ($\acute{u}\pi$), subdrilling (u) and hole depth (βo).

Burden (β) is the perpendicular distance between blasting face and hole. The relationship between hole diameter ($\tau\delta$) and burden proposed by many researchers and represented by Eq. (1).

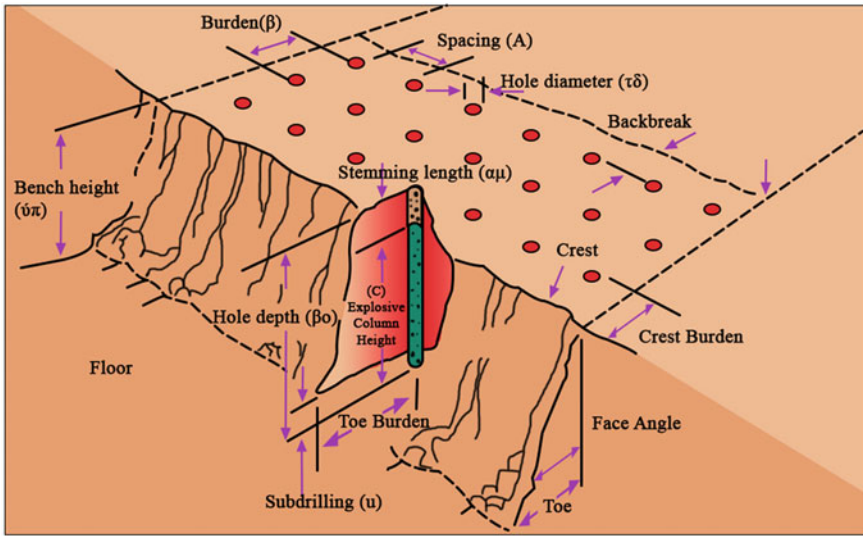


Fig. 1 Blast design and related terminology

$$\beta = C_1 * \tau \delta \tag{1}$$

where, C_1 is constant dependent upon inherent properties of rock mass and explosives. Table 1 highlights the range of C_1 values as proposed by several researchers.

Burden is also expressed in terms of bench height and can be expressed with following Eq. (2).

$$\beta = C_2 * \acute{\upsilon}\pi \tag{2}$$

where, C_2 is constant which varies from 0.25 to 0.50 for satisfactory blasts [20].

A vertical distance between toe and crest of bench literally means bench height ($\acute{\upsilon}\pi$), which is eventually determined considering the hole diameter and loading equipment. Longer bench heights render precariousness to design and favours rock-fall and flyrock. Since blasting occurs with conversion of explosives into gases, stemming technique avoids the chances of blown out shots, such as excessive flyrock and air over-pressure while blasting. Therefore, sufficient stemming lengths prevents

Table 1 Constants for drill hole diameter to burden

Name of researcher	Range of values for constant C_1
Jimeno et al. [16]	25 to 40
Hagan [17], Bhandari [18]	20 to 35
Dick et al. [19]	20 to 40

potential damage to workers, locals and avoids risk to environment [21, 22]. Hole depth in blasting setup can be evaluated as a summation of bench height and subgrade drilling length. To prevent toe formation subgrade drilling becomes essential, and it may vary from 10–20% of bench height. Scientific studies have revealed that the parameters like burden, hole diameter, spacing or bench height simultaneously control blasting operations, moreover, their ratios decide the blast performance [23, 24]. Spacing is related to burden and can vary from 1 to 1.8 times [12]. Many researchers utilize burden to spacing ratio for evaluation of blast performance. Bench height to burden is called stiffness ratio. Various workers have used stiffness ratio for the design of blast [25]. The same ratio is also utilized for prediction of blast fragmentation and flyrock [26].

Blasting phenomenon are associated with enormous energy, which are eventually released to loosen the rockmass and make excavation economical. However, only part of the released energy is involved in loosening the rock mass, and remaining ones create potential threat for the environment. Flyrock is also a result of the extra energy released in the process of blasting (Fig. 2). The flyrock causes severe problems to local inhabitants, and if suitable precautions are not adopted, they can turn into threat for civil workers and engineering machinery. Therefore, the accurate knowledge of flyrock becomes essential for agencies to reduce or mitigate their impact on population and property. In the same line, researchers and industries have worked together to mark critical factors responsible in assessment of flyrock (Fig. 3).

Moreover, a few potential parameters impacting the distance of flyrock at any blasting site had been categorised in the three main classes, namely, rock-mass of the area, blast design setup, and explosives involved. The rock density (RD) and rock mass rating (RMR) are assimilated in the present study to define the rock-mass. Burden (β), spacing (A), hole diameter ($\tau\delta$), stemming length ($\alpha\mu$), bench height ($\upsilon\pi$), subdrilling (u) and hole depth ($\beta\sigma$) are some of the attributes of blast design mentioned in the present work on flyrock. Besides, the values like Maximum Charge per Delay (C), Capacity of the explosive charge (W), Charge Length (CL), powder

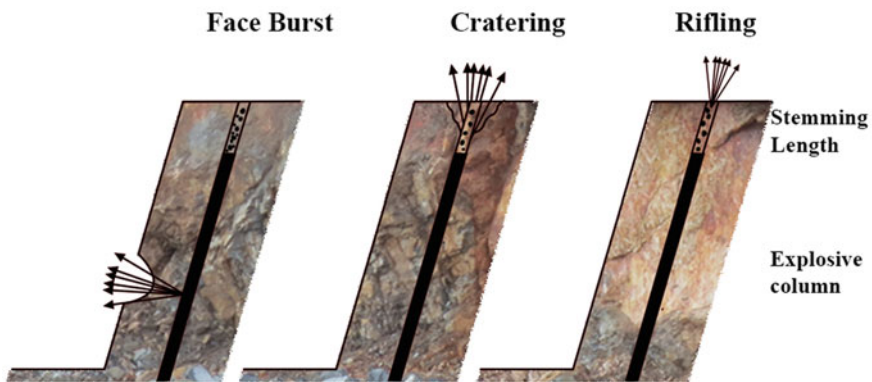


Fig. 2 Schematic diagram of flyrock (modified after Little [27])

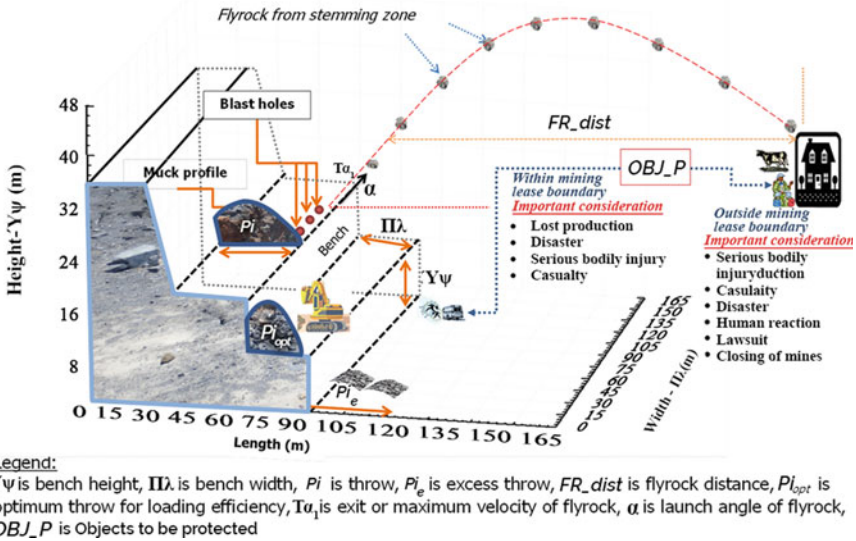


Fig. 3 Schematic diagram showing blasting site of granite quarry, throw, optimum throw, excess throw, flyrock

factor (PF), and amount of explosive used per blast (W_a) are the employed characteristics of explosive entrained in the present research. There is no prevalent engineering technique to simulate flyrock; however, based on the past events of flyrock, machine learning models can be a key player in discerning flyrock distances with greater accuracies [28–35]. Linear multivariate regression (LMR) and gene expression programming (GEP) methods were explored by Monjezi et al. [36] to simulate the flyrock prediction based on the certain blast design parameters and properties of explosives used. Ye et al. [37] examined the effectiveness of the techniques like genetic programming and random forest involving attributes like $\tau\delta$, $\alpha\mu$, β_0 , β/A , PF and C, moreover, coefficient of determination in the both the cases resulted approximately 0.90. Support vector regression, and Lasso and elastic-net generalized linear model (GLMNET) with parameters like β , A, $\alpha\mu$, and PF turned out to be valuable models in flyrock’s prediction [38]. Koopalipoor et al. [39] studied the role of imperialist competitive algorithm, genetic algorithm, and particle swarm optimization (PSO) over the artificial neural network (ANN) and compared their performance in flyrock prediction. A seventy-two dataset were incorporated β , A, $\alpha\mu$, and C as input to devise flyrock prediction models like, recurrent fuzzy neural network (RFNN) optimized with PSO, adaptive neuro-fuzzy inference system (ANFIS), and a non-linear regression model [40]. Zhou et al. [37]. investigated attributes like β , A, $\alpha\mu$, β_0 , C, and PF to examine an ANN model for flyrock prediction, earning coefficient of determination equal to 0.906. Armaghani et al. [42] modelled and compared three different machine learning techniques using 262 datasets implementing β/A , $\tau\delta$, $\alpha\mu$,

β_0 , C, and PF as means of input parameters and flyrock distance as output parameter. Correlation equations and the method used have been given in Tables 2 and 3.

2 Empirical Flyrock Estimation

The several workers in the past were curious to estimate the flyrock distances following the blasting events, and managed to establish the certain empirical relations based on their observations. This involves identification of factors influencing the flyrock distance, moreover collecting these data for further mathematical operations. Their scrupulous works (Table 2) earned significant results, and motivated several others to carry out research on flyrocks. Indeed, the results were founding stone for the present development in the blasting activities, that equipped the hands of agencies to minimize the flyrock distance. However, the complexities induced in these empirical relationships made the calculation of flyrock distance a tedious and time-consuming task. Furthermore, the present era of soft computing shows quite promising results in the last few decades in various other domains of scientific world. Therefore, the geotechnical engineers cannot keep themselves away from these modern developments for longer time and soon new discoveries replace the earlier ones.

3 Deep Learning Models for Flyrock

In the light of earlier mathematical works and advent of modern computational techniques people were excited to know whether machines can perform the human tasks. Scientists and engineers worked together to accomplish these tasks to bring the present shape of artificial intelligence (AI) and machine learning (ML). In the modern world, access to latest technologies made the availability of enormous data in very short span of time to the researcher. In the present study, one will gain insights of the some of key deep learning techniques used for the estimation of flyrock phenomenon.

The work discusses the application of techniques like Extreme Learning Machine (ELM), Outlier Robust ELM (ORLEM), Artificial Neural Network (ANN), Multiple Linear Regression (MLR), Artificial Neural Network with Particle Swarm Optimization (ANN-PSO), Artificial Neural Network coupled with Harmony Search (ANN-HS), Artificial Neural Network coupled with Advanced Dynamical Harmony Search (ANN-ADHS), Adaptive Neuro-Fuzzy Inference System in combination with Grasshopper Optimization Algorithm (ANFIS-GOA), Adaptive Neuro-Fuzzy Inference System in combination with Cultural Algorithm (ANFIS-CA), Imperialist Competitive Algorithm with ANN (ICA-ANN), Particle Swarm Optimization with ANN (PSO-ANN), Artificial Bee Colonization with ANN (ABC-ANN), Firefly Algorithm with ANN (FA-ANN), Genetic Algorithm with ANN (GA-ANN) (Table 3). These discussed works encapsulate several factors affecting the flyrock

Table 2 Empirical equations for prediction of flyrock

References	Equations	Descriptions
Lundborg et al. [43]	$L_{max} = 260(\tau\delta)^{2/3}$	L_{max} = maximum ejection distance (m); $\tau\delta$ = hole diameter (inch)
Olofsson [44]	$L_{max} = K\varphi.(\tau\delta)$	$K\varphi$ = factor of safety [45]; $\tau\delta$ = hole diameter (cm)
Richards and More [46]	$Faceburst L_{max} = \frac{k^2 \sqrt{m^{2.6}}}{g \beta}$ $Cratering L_{max} = \frac{k^2 \sqrt{m^{2.6}}}{g \alpha\mu}$ $Rifling L_{max} = \frac{k^2 \sqrt{m^{2.6}}}{g \beta} \sin 2\theta_0$	where, θ_0 = drill hole angle; L_{max} = maximum throw (m); β = burden (m); $\alpha\mu$ = stemming length (m); m = charge per meter (Kg/m); g = gravitational constant; k = site constant
Little [27]	$Faceburst L_{max} = \frac{k^2}{g}$ $Cratering L_{max} = \frac{k^2}{g}$ $Rifling L_{max} = \frac{k^2}{g}$	where, L_{max} = maximum throw (m); g = gravitational constant; k = site constant
Ghasemi et al. [47]	$F_d = 6946.547 [\beta^{-0.796} A^{0.783} (\alpha\mu)^{1.994} (\beta_0)^{1.649} d^{1.766} (PF/Q)^{-1.465}]$	$R^2 = 0.83$ F_d = flyrock distance (m); Q = mean charge per blast-hole (kg); PF = powder factor (t/kg)
Trivedi et al. [48]	$Flyrock = \frac{10^{5.1} q_1^{0.51} q^{0.14}}{\beta^{0.93} (\alpha\mu)^{0.64} \sigma_c^{0.75} RQD^{0.93}}$	$R^2 = 0.815$; q_1 = linear charge concentration; q = specific charge; σ_c = unconfined compressive strength; RQD = rock quality designation (%)
Armaghani et al. [49]	$Flyrock = 177.81 - (3.33 \times \beta_0) - (2.55 \times A) - (3.49 \times \beta) - (13.93 \times (\alpha\mu)) + (0.47 \times PF) + (1 \times MC) - (2.58 \times RMR)$	PF = powder factor, MC = Maximum Charge per Delay, RMR = Rock Mass Rating

Table 3 Prediction of fly-rock distance in blasting

References	Techniques	Input parameters			No. of datasets	R2
		Rockmass properties	Blasting setup	Explosives		
Lu et al. [50]	ELM	RD	β , A, $\alpha\mu$	PF	82	0.955
	ORELM					0.958
	ANN					0.912
	MLR					0.883
Hasanipanah et al. [51]	ANN	RD	β , A, $\alpha\mu$	PF	82	0.8319
	ANN-PSO					0.8328
	ANN-HS					0.8715
	ANN-ADHS					0.9299
Fattahi and Hasanipanah [52]	ANFIS-GOA	RD	β , A, $\alpha\mu$	PF	80	0.974
	ANFIS-CA					0.953
Li et al. [53]	ICA-ANN	RD, Rn	β/A , $\beta\sigma$, $\alpha\mu$	C, PF	113	0.9598
	PSO-ANN					0.9608
	ABC-ANN					0.9666
	FA-ANN					0.9719
	GA-ANN					0.9466
Wu et al. [54]	ICA-Linear	RMR	β , A, $\alpha\mu$	Weight charge	78	0.954
	ICA-Power					0.928
	ICA-Quadratic					0.952
	ANN					0.841

phenomenon in any blasting activity, like Burden (β), spacing (A), stemming length ($\alpha\mu$), hole depth ($\beta\sigma$), Powder Factor (PF), Rock Density (RD), Maximum Charge per delay (C), Rock mass rating (RMR) etc. The working principle behind these deep learning techniques have been detailed in the sections below.

3.1 ANN, ELM, ORLEM, MLR, ANN-PSO, ANN-HS, & ANN-ADHS

Artificial Neural Network (ANN) performs several complex operations using arrays of nodes in different layers based on past learning. The ANN model learns the way human brain does, moreover, the model performs better with rise in the number of training data. The most characteristic task of neural network is to perceive the inherent pattern in the data, and solve the complex problems with significant accuracies and swiftly. The structure of ANN has three layers, viz., input, hidden, and output layer;

the input and output layers have nodes equal to the number of input and output parameters assimilated in the study. Whereas, there is no defined number of nodes in the hidden layer, moreover, they can have further sub-layers to obtain best performing model. The best performing model can be engendered either on hit-and-trial basis or tuning through any optimization techniques.

Extreme Learning Machine (ELM) technique was devised to overcome the sluggish learning rate faced by conventional feedforward neural networks (FFNNs). The conventional FFNNs adopts gradient-based learning methods that are too slow, moreover, iterative tuning of each involved parameters is embodied making them further slow. The ELM adopts linear mapping to train the model, with tuning of the parameters numerically equal to the hidden layer nodes, therefore processing time and probability of overfitting is significantly reduced in these models. ELM improves learning speed, however have difficulty in dealing with outliers in data and may render inappropriate results. Therefore, the Outlier Robust Extreme Learning Machine (ORELM) method uses scanty data distribution pattern of outliers and applies the ℓ_1 —norm loss function to empower the ELM model capability.

Simple linear regression evaluates and expresses the dependency of one variable over another mathematically. However, there are times when a single parameter is not enough to sufficiently determine the relationship with another parameter, instead one needs to access several variables to find the best relationship numerically. This need is served in the establishing best relationship between multiple input and output parameters through multi-linear regression (MLR) analysis.

The optimization algorithms are involved in the machine learning models, to boost their performances by tuning their hyperparameters. The hyperparameters differ based on the type of machine learning technique involved in the research, moreover the selection of optimization algorithms depends on the direction of the work, speed and memory requirements. In PSO, the workability of any ANN model is enhanced by monitoring the collective direction of particles and tracking their earlier best performances of each particle and their neighbors [55, 56]. One can infer that this optimization algorithms evaluates the best personal and global performances of particles' swarm with successive iteration, eventually the best hyperparameters contribute the best model [39].

The service of harmony search (HS) algorithm is employed to optimize the network of ANN model, and determines the best performing model after a given number of iterations. The impetus behind the HS algorithm is the extemporization mechanism of musicians, implementing the best performing model with stochastic metaheuristic process [57]. The Adjusted Dynamical Harmony Search optimization techniques empowers the ANN to tune the best model structure supplanted with metaheuristic, and the algorithm is based on iterative learning as the enthused-music-search. The preferred harmony component is worked out using two key approaches in the ADHS, viz., harmony memory considering rate, and pitch adjusting rate. Both the approaches are magnified mathematically to update new variable in the harmony memory, after evaluation of maximum and minimum elements. Therefore, the ADHS, an advanced optimization technique augments the power of ANN in minimizing the error between the predicted outcomes of the model and original one [51].

3.2 ANFIS-GOA, ANFIS-CA, ICA-Linear, ICA-Power and ICA-Quadratic

Adoptive Neuro-Fuzzy Inference System (ANFIS) finds its application in enumeration of non-linear problems. The ANFIS benefits from fuzzy logic of human's qualitative reasoning (if-then rule) as well as neural learning approaches. In other words, the adoptive network is powered by neuro inference scheme, moreover neuro-fuzzy along with neural network render a sophisticated and robust machine learning technique by diminishing each other's drawbacks [58, 59]. However, again in search of best model structure certain optimization algorithms are needed according to the available datasets in different studies. Moreover, the grasshopper optimization algorithm (GOA) plays a vital role in tuning the hyperparameters of the ANFIS model, that promotes the viability of the model with significant rise in their robustness and accuracies. The motivation behind the GOA is the collective behavior of swarming grasshoppers, and is a type swarm intelligence working on the population-based optimization technique. In GOA, the researchers have established the mathematical relationship to determine the position of i^{th} grasshopper in the swarm as the summation of social interaction between them, the influence of wind advection and gravity on this [60].

The cultural algorithm (CA) boosts the ANFIS performing capabilities, as the method attains the inspiration from the evolution of human culture [61]. The algorithm sets to resolve non-linear problems and enables complex computation in search of best ANFIS structure. The algorithm simulates civic sense, reasoning and knowledge acquired in growth of human population with time by means of transfer of information from one generation to another [52].

ICA is acronym for Imperialist Competitive Algorithm, which is a powerful computing optimization technique inspired by socio-political evolution mechanism of colonies and imperialists [62]. History demonstrates the competition among several weaker and powerful kingdoms to gain the control on each other. The mightiest one is termed as imperialist, that governs number of colonies, and invade other countries to take control over them and expand their territories by competing with other rival imperialists. Finally, the strongest empire (colonies along with their imperialist) will hold control over the weaker ones. Atashpaz-Gargari and Lucas [63] coined the idea of ICA with the intention of identifying the dominating imperialist based on their economic, political, and military resources. The governing operations of ICA are to monitor three aspects, viz., assimilation policy, revolution, and competition [54]. The optimization power of ICA can be emplaced over several machine learning models to enhance their performance. Moreover, various multiple regression models (MRMs) benefit from the ICA to enhance their prediction results. In the same line ICA-Linear, ICA-Quadratic, and ICA-Power models can be developed on applying ICA optimization over linear, quadrating, and power MRMs respectively [64]. Similarly, neural network models like ANN can yield better outcomes and significantly reduce their cost/loss function on using optimizing capacity of ICA.

3.3 *ABC-ANN, FA-ANN, GA-ANN*

The acronym ABC stands for artificial bee colony optimization; the algorithm mimics the nectar collection traits of honey bees. Karaboga [65] introduced the technique to the scientific community, and highlighted its applicability in optimizing the prediction power of well-known machine learning tools. Group of bees organize themselves in three different groups to accomplish the nectar gathering task. The first set of bee group lookouts for the probable source of flower's nectar, and they randomly search for this. On locating a reasonable source, they communicate this information with other members once they return to hive. Afterwards, a few other members (second group) follow the scout bees for further exploitation of located nectar resource. Meanwhile, the third group of bees keep eyes on the hive, and exchange the relevant information with member bees. To transfer information related to the nectar collection bees perform waggle dance. The chain of data transfer will facilitate the selection of most appropriate nectar source and its exploration.

Firefly algorithm (FA) is a kind of metaheuristic algorithm that imitate attractiveness traits of fireflies among themselves. The attractiveness of fireflies relies on the brightness, means the intensity of light emitted by the individual firefly determines their attractiveness strength [66]. In other words, they hold proportional relationship. Moreover, the brighter one will attract the less-brighter one, despite of their sex as these are unisexual species. Furthermore, it has been noted that the objective of the fireflies determines their brightness level. However, the brightness also decreases with the mutual distance among two individual species. If in case any firefly is far away from their swarm, they will perform random movement. The fireflies rely on their bioluminescence behavior to talk, arrange food, and find mates [53]. This swarm-intelligence inspired by fireflies resulted in a valuable optimization algorithm, and aided in enumeration of complex mathematical operation with greater accuracies.

The Genetic algorithm (GA) engenders its working principles from Darwin's evolution theory of natural selection. The theory enunciates that the survival of any species depends in their capabilities to cope with different set of changing environmental and climatic conditions, as well as their instinct to adopt and response the changes. The theory further highlights the survival of fittest creature with dominant genes over the weaker ones. The GA simulates these in the arithmetic operations to assess the fittest organism, on examining the processes of selection, crossover, and mutation in the individual's population [67]. The advent of GA introduced the features of solving linear and non-linear lucidly in different scenarios and simulates real life challenges to boost the performances of known machine learning techniques.

The amalgamation of ANN with the optimization algorithms like ABC, FA, and GA resulted into models like ABC-ANN, FA-ANN, and GA-ANN respectively. Moreover, they improve the performance of the ANN models, after these techniques were employed in the existing ANN models.

4 Results and Discussion

The assessment of several ways of ascertaining the flyrock distance in advance can aid the mining engineers and planner to device the blasting setup. Proper design reduces the number of casualties and losses owing to flyrock associated to blasting. The detailed examination of previous literature suggests that machine learning models will be a swifter, economic, and intelligible tool for flyrock prediction, given that adequate number of datasets are available for training. Furthermore, these soft computing techniques offer better performance than empirical methods.

The present article examines several research works in between years 2019 to 2021 on machine learning based prediction of flyrock distance. Lu et al., developed a four deep learning models for flyrock estimation taking 82 datasets, and involved parameters like RD, β , A, $\alpha\mu$, and PF. The best result is shown by ORLEM earning a coefficient of determination value of 0.958 [50]. ELM is quite close to ORLEM with the R^2 of 0.955. Besides, two other models like ANN and MLR were developed from the same datasets and same parameters, however their outcomes were not as reliable as ORLEM and ELM.

Another work, taking similar parameters as in previous discussed work developed ANN, ANN-PSO, ANN-HS, and ANN-ADHS [51]. The work shows that implementation of PSO, HS, and ADHS certainly enhanced the capability of neural network model in flyrock prediction. Moreover, the greatest performance (in terms of R^2) was noticed in ANN-ADHS (0.9299) model, followed by ANN-HS (0.8715), ANN-PSO (0.8328), and ANN (0.8319).

In the work of Fattahi & Hasanipanah two ANFIS models blended with GOA and CA optimization algorithms are compiled and their outcomes were assessed with real outcomes [52]. In this work, the authors have taken 80 datasets to account these models based on attributes like RD, β , A, $\alpha\mu$, and PF. In terms of coefficient of determination, the ANFIS-GOA (0.974) beats the ANFIS-CA (0.953). In the year 2021, Li et al. [53] tried to access the effect of different optimization algorithms over ANN in flyrock prediction. Their work incorporated parameters namely, RD, Rn, β/A , $\beta\sigma$, $\alpha\mu$, C, and PF over 113 datasets. The research outcomes dictate the performance of models in terms of R^2 such as ICA-ANN (0.9598), PSO-ANN (0.9608), ABC-ANN (0.9666), FA-ANN (0.9719), and GA-ANN (0.9466). In the same line, Wu et al. [54] designed ICA-Linear, ICA-Power, ICA-Quadratic, and ANN taking RMR, β , A, $\alpha\mu$, and weight charge in the account. Seventy-Eight datasets were taken in the development of the model, and ICA-Linear have the best outcome and worst result were shown by ANN.

5 Conclusion

The present article details the mechanism of blasting and the associated catastrophic hazard of flyrock phenomenon. The fundamental attributes like spacing, burden,

hole depth, hole diameter, rock quality designation, rock density, stemming length, explosive characteristics etc., have major control on the flyrock distance. Therefore, a careful examination of these properties and a judicious planning can inhibit the risks related to blasting. A number of advanced deep learning computational models have been assessed and compared to ascertain viability of flyrock estimation model. Techniques developed between the year 2019–2021 have been considered in the present work, and their performance have been compared using a well-recognized statistical approach- coefficient of determination (R^2). Moreover, a few empirical equations governing the flyrock pattern owing to blasting have been accounted in the present work. The study finds that empirical methods lag behind the deep learning methods in precise estimation of flyrock distances in several aspects. The machine learning models namely, ANN, ELM, ORLEM, MLR, ANN-PSO, ANN-HS, ANN-ADHS, ANFIS-GOA, ANFIS-CA, ICA-Linear, ICA-Power, ICA-quadratic, ABC-ANN, FA-ANN, and GA-ANN models were addressed in detail. Beside, these models were evaluated in terms of number of datasets and type of input parameters involved in the structure of models.

References

1. Bhatawdekar RM, Edy TM, Singh TN, Armaghani DJ (2017) Tropical rock mass assessment system for blast ability purpose. In: International conference on recent trends in civil engineering and water resources engineering (RTCWRE-2017), Holy Mary institute of Technology and Science, Telangana 501301, India, 10th & 11th August 2017
2. Bhatawdekar RM, Edy TM, Singh TN, Armaghani DJ (2017) Rock mass classification for limestone in tropical climate for blasting. In: 15th national cement building (NCB) international seminar on cement, concrete and building materials, New Delhi, India, 5–9 December 2017
3. Boonbatr A, Walsri C, Bhatawdekar RM, Edy TM (2017) Cone and tower karst rock mass classification of Cambodia limestone for blasting. In: International conference on recent trends in civil engineering and water resources engineering (RTCWRE-2017), Holy Mary institute of Technology and Science, Telangana 501301, India, 10th & 11th August 2017
4. Bhatawdekar RM, Mohamad ET, Singh TN, Pathak P, Armaghani DJ (2021) Rock mass classification for the assessment of blastability in tropically weathered limestones. In: Proceedings of the international conference on innovations for sustainable and responsible mining. Springer, Cham, pp 13–44
5. Saksarid C, Bhatawdekar RM, Edy TM, Dan MF (2017) Geological strength index (GSI) and blastability index (BI) for limestone in Thailand. In: International conference on recent trends in civil engineering and water resources engineering (RTCWRE 2017), Holy Mary institute of Technology and Science, Telangana 501301, India, 10th & 11th August 2017
6. Bhatawdekar RM, Edy TM, Srikant A, Singh TN, Armaghani DJ (2018) Development of blastability index for Karst limestone. In: Proceedings of SME's annual conference held 25–28 February 2018, Minneapolis, Minnesota, USA
7. Bhatawdekar RM, Edy TM, Danial JA (2019) Building information model for drilling and blasting for tropically weathered rock. J Mines Met Fuels 494–500
8. Bhatawdekar RM, Edy TM, Armaghani DJ (2017d) Rock mass classification for karst limestone for karst limestone of Cambodia for blasting. In: International conference on deep excavation, energy resources and production (DEEP 2016), Indian Institute of Technology, Kharagpur 721302 India, 24–26 January 2017

9. Stojadinović S, Pantović R, Žikić M (2011) Prediction of flyrock trajectories for forensic applications using ballistic flight equations. *Int J Rock Mech Min Sci* 48(7):1086–1094
10. Kumar R, Choudhury D, Bhargava K (2016) Determination of blast-induced ground vibration equations for rocks using mechanical and geological properties. *J Rock Mech Geotech Eng* 8(3):341–349
11. Bhatawdekar RM, Wedage W, Silva G, Batagalla S, Madawala S, Edy TM (2020) Review of rock mass classification of tropically weathered limestone. *J Mines Metals Fuels* 68(3):91–96
12. Adhikari GR (1999) Studies on flyrock at limestone quarries. *Rock Mech Rock Eng* 32(4):291–301
13. Ayala Carcedo F (2017) *Drilling and blasting of rocks*. Routledge, London
14. Hasanipanah M, Monjezi M, Shahnazar A, Armaghani DJ, Farazmand A (2015) Feasibility of indirect determination of blast induced ground vibration based on support vector machine. *Measurement* 75:289–297
15. Armaghani DJ, Mahdiyar A, Hasanipanah M, Faradonbeh RS, Khandelwal M, Amnieh HB (2016) Risk assessment and prediction of flyrock distance by combined multiple regression analysis and Monte Carlo simulation of quarry blasting. *Rock Mech Rock Eng* 49(9):3631–3641
16. Jimeno CL, Jimeno EL, Carcedo FJ, De Ramiro YV (1995) *Drilling and blasting of rocks*
17. Hagan TN (1983) The influence of controllable blast parameters on fragmentation and mining costs. In: *Proceedings of the 1st international symposium on rock fragmentation by blasting*, vol 1, pp 31–32
18. Bhandari S (1997) *Engineering rock blasting operations*
19. Dick RA, Fletcher LR, D'Andrea DV (1983) *Explosives and blasting procedures manual*. US Department of the Interior, Bureau of Mines
20. Adhikari GA, Rajan B, Venkatesh HS, Theresraj AI (1994) Blast damage assessment for underground structures. In: *Proceedings of the national symposium on emerging mining and ground control technologies*, Varanasi, India, pp 247–55
21. Venkatesh HS, Bhatawdekar RM, Adhikari GR, Theresraj AI (1999) Assessment and mitigation of ground vibrations and flyrock at a limestone quarry. In: *Proceedings of the annual conference on explosives and blasting technique*, vol 2, pp 145–152
22. Cevizci H (1997) Ozkahraman HT (2012) The effect of blast hole stemming length to rockpile fragmentation at limestone quarries. *Int J Rock Mech Min Sci* 53:32–35
23. Sharma SK, Rai P (2017) Establishment of blasting design parameters influencing mean fragment size using state-of-art statistical tools and techniques. *Measurement* 96:34–51
24. Mehrdaneh A, Monjezi M, Sayadi AR (2018) Evaluation of effect of rock mass properties on fragmentation using robust techniques. *Eng Comput* 34(2):253–260
25. Monjezi M, Khoshalan HA, Varjani AY (2012) Prediction of flyrock and backbreak in open pit blasting operation: a neuro-genetic approach. *Arab J Geosci* 5(3):441–448
26. Faradonbeh RS, Armaghani DJ, Monjezi M (2016) Development of a new model for predicting flyrock distance in quarry blasting: a genetic programming technique. *Bull Eng Geol Env* 75(3):993–1006. <https://doi.org/10.1007/s10064-016-0872-8>
27. Little TN (2007) In: *EXPLO conference*, Wollongong, NSW, Australia, pp 35–43
28. Faradonbeh RS, Armaghani DJ, Monjezi M, Mohamad ET (2016) Genetic programming and gene expression programming for flyrock assessment due to mine blasting. *Int J Rock Mech Min Sci* 88:254–264
29. Nguyen H, Bui XN, Nguyen-Thoi T, Ragam P, Moayedi H (2019) Toward a state-of-the-art of fly-rock prediction technology in open-pit mines using EANNs model. *Appl Sci* 9(21):4554. <https://doi.org/10.3390/app9214554>
30. Rad HN, Bakhshayeshi I, Jusoh WA, Tahir MM, Foong LK (2020) Prediction of flyrock in mine blasting: a new computational intelligence approach. *Nat Resour Res* 29(2):609–623. <https://doi.org/10.1007/s11053-019-09464-x>
31. Murlidhar BR, Kumar D, Armaghani DJ, Mohamad ET, Roy B, Pham BT (2020) A novel intelligent ELM-BBO technique for predicting distance of mine blasting-induced flyrock. *Nat Resour Res* 29(6):4103–4120. <https://doi.org/10.1007/s11053-020-09676-6>

32. Guo H, Nguyen H, Bui XN, Armaghani DJ (2021) A new technique to predict fly-rock in bench blasting based on an ensemble of support vector regression and GLMNET. *Eng Comput* 37(1):421–435. <https://doi.org/10.1007/s00366-019-00833-x>
33. Dehghani H, Pourzafar M (2021) Prediction and minimization of blast-induced flyrock using gene expression programming and cuckoo optimization algorithm. *Environ Earth Sci* 80(1):1–7. <https://doi.org/10.1007/s12665-020-09300-z>
34. Nguyen H, Bui XN, Choi Y, Lee CW, Armaghani DJ (2021) A novel combination of whale optimization algorithm and support vector machine with different kernel functions for prediction of blasting-induced fly-rock in quarry mines. *Nat Resour Res* 30(1):191–207. <https://doi.org/10.1007/s11053-020-09710-7>
35. Fang Q, Yazdani Bejarbaneh B, Vatandoust M, Jahed Armaghani D, Ramesh Murlidhar B, Tonnizam Mohamad E (2021) Strength evaluation of granite block samples with different predictive models. *Eng Comput* 37(2):891–908
36. Monjezi M, Dehghani H, Shakeri J, Mehrdaneh A (2021) Optimization of prediction of flyrock using linear multivariate regression (LMR) and gene expression programming (GEP)—Topal Novin mine, Iran. *Arab J Geosci* 14(15):1–2. <https://doi.org/10.1007/s12517-021-07772-2>
37. Ye J, Koopialipoor M, Zhou J, Armaghani DJ, He X (2021) A novel combination of tree-based modeling and Monte Carlo simulation for assessing risk levels of flyrock induced by mine blasting. *Nat Resour Res* 30(1):225–243. <https://doi.org/10.1007/s11053-020-09730-3>
38. Guo H, Zhou J, Koopialipoor M, Armaghani DJ, Tahir MM (2021) Deep neural network and whale optimization algorithm to assess flyrock induced by blasting. *Eng Comput* 37(1):173–186. <https://doi.org/10.1007/s00366-019-00816-y>
39. Koopialipoor M, Fallah A, Armaghani DJ, Azizi A, Mohamad ET (2019) Three hybrid intelligent models in estimating flyrock distance resulting from blasting. *Eng Comput* 35(1):243–256. <https://doi.org/10.1007/s00366-018-0596-4>
40. Kalaivaani PT, Akila T, Tahir MM, Ahmed M, Surendar A (2020) A novel intelligent approach to simulate the blast-induced flyrock based on RFNN combined with PSO. *Eng Comput* 36(2):435–442. <https://doi.org/10.1007/s00366-019-00707-2>
41. Zhou J, Koopialipoor M, Murlidhar BR, Fatemi SA, Tahir MM, Jahed Armaghani D, Li C (2020) Use of intelligent methods to design effective pattern parameters of mine blasting to minimize flyrock distance. *Nat Resour Res* 29(2):625–639. <https://doi.org/10.1007/s11053-019-09519-z>
42. Armaghani DJ, Koopialipoor M, Bahri M, Hasanipanah M, Tahir MM (2020) A SVR-GWO technique to minimize flyrock distance resulting from blasting. *Bull Eng Geol Env* 79(8):4369–4385. <https://doi.org/10.1007/s10064-020-01834-7>
43. Lundborg N, Persson N, Ladegaard-Pedersen A, Holmberg R, Holmberg R (1975) Keeping the lid on flyrock in open pit blasting. *Eng Min J Sedish Detonic Res Found* 176:95–100
44. Olofsson SO (1990) Applied explosives technology for construction and mining. Applex, Sweden
45. Bajpayee TS, Rehak TR, Mowrey GL, Ingram DK (2002) A summary of fatal accidents due to flyrock and lack of blast area security in surface mining, 1989 to 1999
46. Richards AB, More AJ (2004) Flyrock control – by chance or design. In: Proceedings of the 30th annual conference on explosives and blasting technique, New Orleans, Louisiana, pp 1–13
47. Ghasemi E, Sari M, Ataei M (2012) Development of an empirical model for predicting the effects of controllable blasting parameters on flyrock distance in surface mines. *Int J Rock Mech Min Sci* 52:163–170
48. Trivedi R, Singh TN, Raina AK (2014) Prediction of blast-induced flyrock in Indian limestone mines using neural networks. *J Rock Mech Geotech Eng* 6(5):447–454
49. Armaghani DJ, Mohamad ET, Hajihassani M, Abad SA, Marto A, Moghaddam MR (2016) Evaluation and prediction of flyrock resulting from blasting operations using empirical and computational methods. *Eng Comput* 32(1):109–121
50. Lu X, Hasanipanah M, Brindhadevi K, Amnieh HB, Khalafi S (2020) ORELM: a novel machine learning approach for prediction of flyrock in mine blasting. *Nat Resour Res* 29(2):641–654. <https://doi.org/10.1007/s11053-019-09532-2>

51. Hasanipanah M, Keshtegar B, Thai DK, Troung NT (2020) An ANN-adaptive dynamical harmony search algorithm to approximate the flyrock resulting from blasting. *Eng Comput* 13:1–3. <https://doi.org/10.1007/s00366-020-01105-9>
52. Fattahi H, Hasanipanah M (2021) An integrated approach of ANFIS-grasshopper optimization algorithm to approximate flyrock distance in mine blasting. *Eng Comput* 2:1–3. <https://doi.org/10.1007/s00366-020-01231-4>
53. Li D, Koopialipoor M, Armaghani DJ (2021) A combination of fuzzy Delphi method and ANN-based models to investigate factors of Flyrock induced by mine blasting. *Nat Resour Res* 30(2):1905–1924. <https://doi.org/10.1007/s11053-020-09794-1>
54. Wu M, Cai Q, Shang T (2019) Assessing the suitability of imperialist competitive algorithm for the predicting aims: an engineering case. *Eng Comput* 35(2):627–636. <https://doi.org/10.1007/s00366-018-0621-7>
55. Kennedy J, Eberhart RC (1997) A discrete binary version of the Particle Swarm Optimization. In: 1997 IEEE international conference on systems, man, and cybernetics, vol 5. IEEE, pp 4104–4108
56. Murlidhar BR, Sinha RK, Mohamad ET, Sonkar R, Khorami M (2020) The effects of particle swarm optimisation and genetic algorithm on ANN results in predicting pile bearing capacity. *Int J Hydromechatron* 3(1):69–87
57. Kattan A, Abdullah R, Salam RA (2010) Harmony search based supervised training of artificial neural networks. In: 2010 international conference on intelligent systems, modelling and simulation. IEEE Press, New York, pp 105–110. <https://doi.org/10.1109/ISMS.2010.31>
58. Walia N, Singh H, Sharma A (2015) ANFIS: adaptive neuro-fuzzy inference system – a survey. *Int J Comput Appl* 123(13)
59. Singh R, Kainthola A, Singh TN (2012) Estimation of elastic constant of rocks using an ANFIS approach. *Appl Soft Comput* 12(1):40–45. <https://doi.org/10.1016/j.asoc.2011.09.010>
60. Meraihi Y, Gabis AB, Mirjalili S, Ramdane-Cherif A (2021) Grasshopper optimization algorithm: theory variants, and applications. *IEEE Access* 9:50001–50024. <https://doi.org/10.1109/ACCESS.2021.3067597>
61. Jin X, Reynolds RG (1999) Using knowledge-based evolutionary computation to solve nonlinear constraint optimization problems: a cultural algorithm approach. In: Proceedings of the 1999 congress on evolutionary computation-CEC 1999, vol 3, pp 1672–1678. <https://doi.org/10.1109/CEC.1999.785475>
62. Xing B, Gao WJ (2014) Imperialist competitive algorithm. In: Innovative computational intelligence: a rough guide to 134 clever algorithms. Springer, Cham, pp 203–209
63. Atashpaz-Gargari E, Lucas C (2007) Imperialist competitive algorithm: an algorithm for optimization inspired by imperialistic competition. In: IEEE congress on evolutionary computation (CEC 2007). IEEE Press, New York, pp 4661–4667
64. Tashayo B, Behzadafshar K, Soltani Tehrani M et al (2019) Feasibility of imperialist competitive algorithm to predict the surface settlement induced by tunnelling. *Eng Comput* 35:917–923 (2019). <https://doi.org/10.1007/s00366-018-0641-3>
65. Karaboga D (2005) An idea based on honey bee swarm for numerical optimization. Technical report-tr06, Computer Engineering Department, Engineering Faculty, Erciyes University
66. Yang XS, He X (2013) Firefly algorithm: recent advances and applications. *Int J Swarm Intell* 1(1):36–50
67. Mirjalili S (2019) Genetic algorithm. In: Evolutionary algorithms and neural networks. Springer, Cham, pp 43–55

Evaluation of Machine Learning Models for Ore Grade Estimation



Gaurav Jain, Pranjali Pathak, Ramesh Murlidhar Bhatawdekar,
Ashutosh Kainthola, and Abhishek Srivastav

Abstract Geostatistics has been widely used for qualitative estimation of ore deposits for many decades. However, ore quality does not vary uniformly in three dimensions which results in a poor quality estimation with the conventional geostatistical methods. Also, the time required for processing geostatistical data can be substantially high. On the other hand, with the advancement in computational processing power and development of advanced algorithms on artificial intelligence (AI) and machine learning (ML), the requirements of an accurate ore grade estimation in reasonable computation time can be fulfilled. In this paper, the applicability of various machine learning techniques like artificial neural network (ANN), extreme learning machine (ELM), gradient boosted decision trees (GBDT), random forests (RF), support vector regression (SVR) have been discussed for ore grade estimation of different mineral deposits like iron, gold and copper. This study also cross-examines the results of ordinary kriging (OK) and inverse distance weighted (IDW) techniques for qualitative estimation. Correspondingly, statistical parameters such as coefficient of determination (R^2) and root mean squared error (RMSE) have also been taken into account for a better understanding of the models. Nowadays, AI/ML techniques are extensively used in multiple fields worldwide, including the mining

G. Jain (✉) · P. Pathak · R. M. Bhatawdekar
Department of Mining Engineering, Indian Institute of Technology Kharagpur, Kharagpur
721302, West Bengal, India
e-mail: gaurav.jain@iitkgp.ac.in

R. M. Bhatawdekar
e-mail: rmbhatawdekar2@graduate.utm.my

R. M. Bhatawdekar
Geotropik, Department of Civil Engineering, Universiti Teknologi Malaysia, 81310 Skudai, Johor
Bahru, Johor, Malaysia

A. Kainthola · A. Srivastav
Geo-Engineering and ML Laboratory, Department of Geology, Institute of Science, Banaras
Hindu University, Varanasi, India
e-mail: ashutosh.geo@bhu.ac.in

A. Srivastav
e-mail: abhishek.srivastava15@bhu.ac.in

© The Author(s), under exclusive license to Springer Nature Singapore Pte Ltd. 2022
A. K. Verma et al. (eds.), *Proceedings of Geotechnical Challenges in Mining, Tunneling
and Underground Infrastructures*, Lecture Notes in Civil Engineering 228,
https://doi.org/10.1007/978-981-16-9770-8_40

sector, due to their fast and efficient prediction capability. The investigation of these models highlights the importance of accuracy in predicting the quality of the ore as the latter greatly impacts the economic feasibility of mineral deposits. This study forms a ground for developing new advanced intelligent approaches for improving the accuracy of ore grade estimation for mineral deposits.

Keywords Artificial neural network (ANN) · Gradient boosting (GB) · Machine learning (ML) · Ore grade estimation · Random forest (RF)

1 Introduction

Reserve estimation has always laid the foundations for the development of mineral ore deposits. The assessment of the reserves majorly relies on the ore grade estimation. These steps form the basic building blocks of mine planning. The imperfections of the evaluation resulting in under or overestimation of ore grades may cause serious economic and social challenges and a potential loss in the lifecycle of a mine starting from the exploration till the exploitation of a mining project. Thus, the necessity of accuracy surges very high for a feasible mine plan. The prime focus is to identify and develop the most reliable and versatile techniques. The selection of relevant methodology is held responsible for the prediction results. As we can understand that the prediction patterns may be varying nonlinearly and nonstationary due to the involvement of complex geological processes in the formation of ore deposits. Therefore, various geostatistic techniques have been taken into account that required a fair set of skills, knowledge and experience to be efficiently used by the researchers. Geostatistic techniques have dominated the field of qualitative estimation for a long time. Ordinary Kriging (OK) and Inverse Square Distance Weighing (ISDW) are the two most common methods involved in the task. But the applicability of these techniques have resulted unsatisfactorily in the ore grade estimation due to highly complex geologies and can not be considered as the best method.

With the rise of the new modern era of technology, the applicability of these techniques is regularly questioned. The limitations and prediction capabilities are given utmost value in the choice of methods. The advancement of technologies has entered numerous fields from mining to space and proved very satisfactory results. The emergence of soft computational techniques has gained a very high momentum due to a potential increase in the processing power of the systems. Nowadays, the concepts of Machine Learning and Artificial Intelligence are securing a very inspiring and dominant spot in every field. Therefore, many researchers have started investigating various machine learning methods like artificial neural networks (ANN), random forests (RF), support vector machines (SVM), extreme learning machines (ELM), gradient boosting machines (GBM), particle swarm optimisation (PSO), artificial bee colony (ABC) and many more to predict more accurately without the need of relying on pre-assumptions.

This pool of ample opportunities has attracted researchers for using data-driven methods. Among all these techniques, artificial neural networks have been extensively used worldwide over highly sparse and limited datasets. The literature also

reveals that the application of feedforward neural networks and backpropagation neural networks has highly influenced scientists for mineral grade estimation. Besides these benefits, the BPNN also brought several limitations of overfitting issues, rate of convergence and lack of reasoning power. Also, the requirement to train the model by selecting the number of neurons and proper tuning of the hyperparameters to obtain the optimum results required a lot of hit and trial approaches. Therefore, the emergence of extreme learning approaches tried to overcome the limitations of learning rate due to gradient-based learning algorithms. The advantage of mathematical convenience helped to design a single hidden layer neuron network that can randomly choose the weights and biases to obtain better results for qualitative prediction. Also, various natural events and processes inspired computer scientists to develop new algorithms based on these principles. In spite of the birth of new techniques, the implementation remained more or less the same. As the dataset is divided into two or three subgroups namely training, validation and testing datasets. Although sometimes validation is omitted due to several differences in principles of implementation. The dataset is mostly divided in the ratio of 80 and 20 for training and testing purposes. But may vary a little as per the behaviour of the dataset and the requirements of the model. In addition to this, statistical parameters like the coefficient of determination (R^2), coefficient of correlation (r) and root mean squared error (RMSE) has been the most popular aspects in prediction results. Further, with the development of new ones in the field, the experimentations kept on increasing with more increment inaccuracies.

Also, the limitations of the datasets were also paid more attention to as in the case of most of the mining exploitations, the prediction of mineral ore grade cannot be sufficiently fulfilled by the less dense distribution in the drill holes. Porphyry deposits have especially very challenging issues due to the very typical distribution of copper and uncertain variations. In most of the regions, these deposits have shown ore grades from low to medium values with the occurrence of minerals concentrated in randomly distributed patches. As a result, the selection of accurate predictors started involving conditions of heterogeneous distributions of samples and sparsity of data for learning purposes.

Various studies have shown that the ML models have obtained quite better results than the conventional methods for prediction like OK and ISDW. The literature also showed that every new ML method brings multiple additional benefits for more accurate ore grade estimation in certain circumstances but it still upholds some drawbacks. The selection of hyperparameters in these methods plays a critical role. There is no such fixed rule to determine them. These techniques can be made more reliable by hit and trial approaches. Also, these methods do not show a direct relationship between input and estimation that opens room for re-verification before completely relying on them. Thus, it highlights the importance of further investigation needed for the use of data-driven based learning algorithms.

In order to examine the applicability and limitations of the machine learning methods, we have cross-evaluated artificial neural networks, random forests, extreme learning machines, gradient boosting machines and many more with widely popular and traditional geostatistics methods like ordinary kriging and ISDW. The results

support the use of machine learning methods over conventional ones. The cross-evaluation of these techniques is summarized in the form of a table containing several columns as the name of authors, type of mineral deposit, techniques used, prediction results using some statistical parameters and a brief overall hypothesis to help in better understanding of the method. This study involves the assessment of iron, copper and gold mineral deposits.

This paper is divided into several sections such that the principles of various methodologies including geostatistical and machine learning methods are provided in Sect. 2. Section 3 shows the performance results of these techniques that are followed by the discussion and conclusion in subsequent Sects. 4 and 5.

2 Methods for Ore Grade Estimation

This section explains broad principles of ordinary kriging (OK), inverse distance weighting (IDW) as conventional methods and neural networks (NN), extreme learning machines (ELM), support vector regression (SVR) as machine learning methods for ore grade estimation.

2.1 Ordinary Kriging (OK) Method

Kriging is a well-known traditional geostatistical technique for ore grade estimation. It is an interpolation method that can deal with multidimensional input, ordinary kriging (OK) is the most common type of kriging, it takes into account the values of known sample points to predict the result at a given point. The result is estimated by a linear combination of a set of neighbourhood values, where the weights are assigned such that the variance of the predicted value is minimum. Lagrangian multipliers help to find the optimal weights under the constraint of normalisation. Ordinary kriging has an edge over other methods of interpolation that it makes use of empirical variogram to determine the weights, which further utilizes the spatial orientation of the sample.

2.2 Inverse-Distance Weighted (IDW) Method

The inverse-distance weighted (IDW) method is one of the most popular conventional geostatistical techniques being utilized for ore grade estimation. This method predicts the grade of the central block by taking advantage of neighbouring grades considering the inverse of the distance between the neighbour block and central block as weights. This implies that the blocks lying closer to the central block have a closer grade due to higher weight than the far ones. The dependency of the inverse weight can be increased by incrementing the value of the power n as suggested by Bartier and

Keller 1996.

$$G = \frac{\sum (G_i/l_i^n)}{\sum (1/l_i^n)} \quad (1)$$

where

G_i represents the known grade of a neighbour block of ore,
 l_i represents the linear distance between the estimation block and the corresponding neighbour block.

2.3 *Extreme Learning Machine (ELM)*

The earlier literature recognizes the influence of machine learning techniques for estimating the grade of mineral reserves over available geostatistical methods. The involvement of intricate structural and tectonic features along with heterogeneous geological attributes at the site of ore emplacement plays a critical role in mineral quality estimation. The artificial neural network (ANN) method is at the core of developed and applied machine learning techniques for the prediction of mineral quality with adequate accuracy. Generally, the ANN performs mapping of the mathematical relationship between inputs and outputs through the well-known back-propagation neural network (BPNN) approach. However, BPNN is not always infallible, moreover, these lag behind due to overfitting and slow convergence rate. Additionally, the techniques demand manual tuning of hyperparameters or look for known optimization algorithms to reach the best performing model structure. Therefore, to address these issues, researchers scrupulously studied several other machine learning models and compared their outcomes statistically. Eventually, they recognised the significance of extreme learning machines (ELM) in the estimation of mineral quality with greater accuracy and swiftly. The ELM technique presented by Huang et al. (2006) enumerates on the single hidden layer feed-forward neural network (SLFN) approach, with deciding power on randomly assigning weights and biases in the network to engender suitable prediction models. Apart from that ELM regulates the number of hidden nodes through gaussian probability. The ELM shows a great learning intent for any given datasets, and trains effectively to earn better results with the implementation of precise activation functions. The studies have shown a higher converging rate and better prediction performances in ELM, enabling their wider acceptability over other feed-forward networks. ELM will work out random input weights along with hidden biases to simplify as a linear system, furthermore enables the generation of output weights analytically in a SLFN through inverse mathematical operations. Besides, ELM is free from problems like local minima, overfitting, and improper learning rate rendering much faster-training speed than other traditional gradient-based machine learning models. Moreover, ELM is compatible with several activation functions whether differentiable or non-differentiable functions.

2.4 *Neural Network Model for Ore Grade Estimation*

Mining geologists have emphasized the study of a three-dimensional geological model to estimate ore grades relying on their geographical, tectonic, chemical alteration and lithology. Moreover, these factors hold a significant control to ascertain the chemical composition of mineral resources and reserves. The analysis of these factors to precisely determine the mineral grade analytically using a set of complex mathematical operations is quite cumbersome and takes enormous time. Whereas, the involvement of machine learning tools will ease the predictions of viability ore minerals with sufficient accuracy and swiftly. In the series of machine learning, artificial neural networks (ANNs) are inspired by bio-chemical learning and the information transfer mechanism of neurons in the human brain. The development of these ANN models can serve the purpose of ore grade prediction, with a network consisting of three main layers, viz., input, hidden, and output. The number of nodes (or neurons) in the input layer varies with the number of available parameters affecting the output, whereas, the neurons in output layers will be selected based on the requirement of the study. However, there is no defined rule for the number of nodes in the hidden layer. In fact, the hidden layer itself may have a number of sub-layers with a different number of respective nodes. There to evolve the best performing model with the least error and higher accuracy, one needs to tune hyperparameters of the ANN structure either manually or through optimization algorithms.

Kaplan and Topal [3] assessed the application of feed-forward neural network (FFNN) and k-nearest neighbour (k-NN) in ore grade estimation based on factors like geology and geography, ascribed through bore-hole made into deposits. As per the study, k-NN predicted the alteration and rock types of inaccessible sites, whereas FFNN models turn into a key player in predicting mineral grade (chemical composition). The FFNN models adopted in their work consists of 13 input nodes (parameters), two hidden layers with 64 nodes in each, and one output node (Fig. 1). The study selects the above structure as it renders the least error rate when compared with several other networks developed using the same datasets. These models were developed in an open-source Python environment supplanted by a deep learning application programming interface (API) known as Keras. Moreover, the model works on back-propagation learning algorithms to train the model and with each iteration minimizes the cost function. RMSProp optimizations technique aids the model to update the weights of nodes in each layer and enhances the performance of the developed neural network (Fig. 2). The k-fold cross-validation (with 5 as k-value) aids in selecting hyperparameters of a developed neural network, which comparted the training datasets into 5 different equal partitions (Fig. 3). For each partition, 80% of data were used in training the network, whereas the remaining caters for the need for validation. However, the study uses a trial and error method to decipher the number of epochs, optimizers, and learning rate for the developed model (Fig. 1).

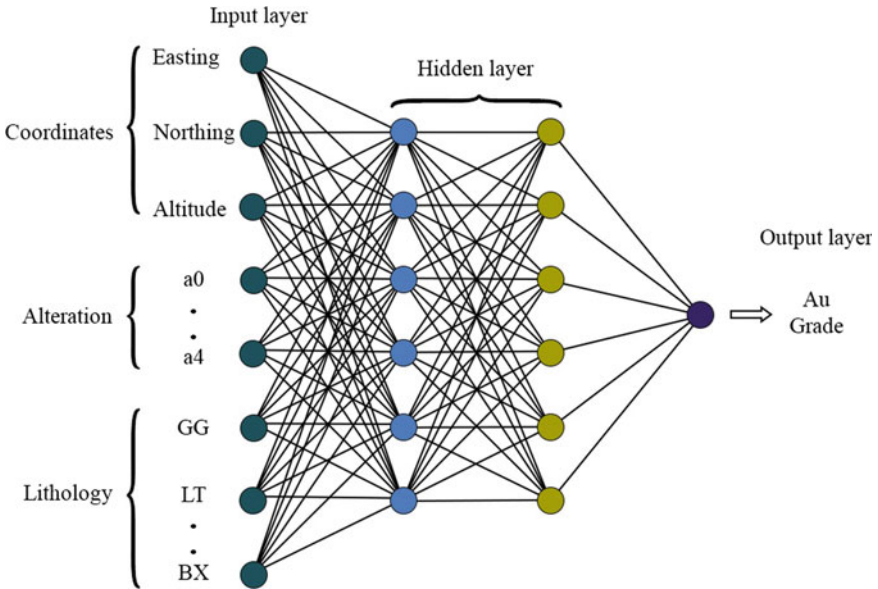


Fig. 1 Basic architecture of a NN model

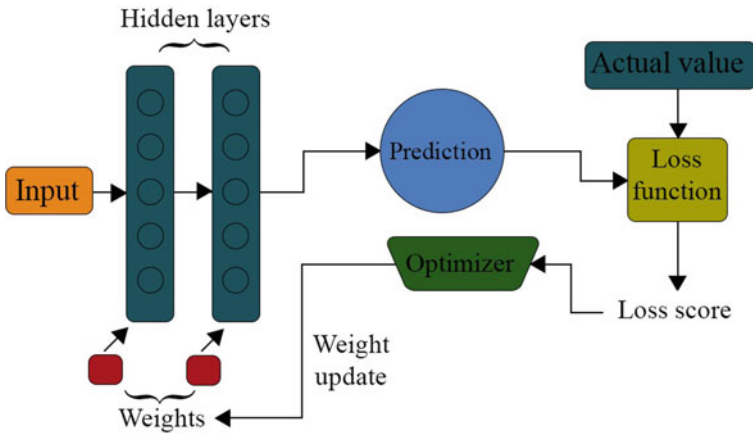


Fig. 2 Proposed architecture for NN model

2.5 Support Vector Machine Regression (SVR)

The first Support vector machine (SVM) technique was presented to the world in 1963, serving the role of binary classification. However, with time researchers evolve the technique that can cater for the functionality of regression models. Supervised

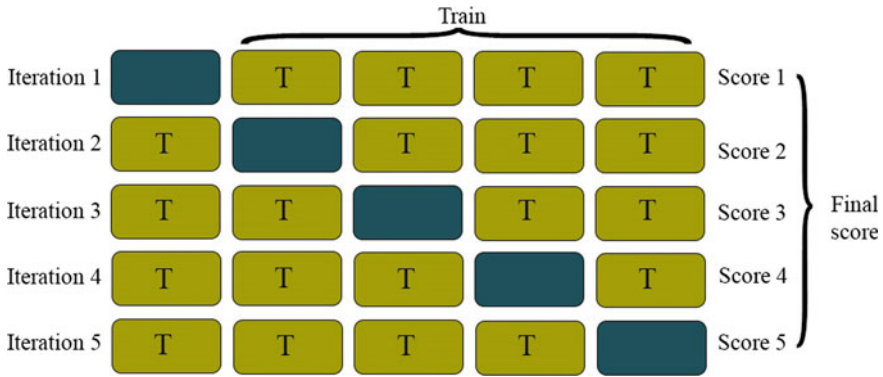


Fig. 3 Loss function relationship with optimiser function

learning is the basis of support vector regression (SVR) models, where distribution (like t-statistics) and quantity of datasets will determine the results. Moreover, developers divide all the data into two parts, one group called training datasets and the other is known as testing datasets. Researchers say to get better outcomes both groups should have the same distribution pattern. The SVR’s enforce its algorithms to find a function of maximum deviation “ τ ” pertaining to datasets being used in model development, simply the training datasets spread across $\pm \tau$ around a target value. In case, datasets are maligned by the error within them, the model will seek the addition of the error function ‘ ξ ’ to enhance the performance. Patel et al. [5] devised a SVR prediction model for estimating iron ore grade and implemented a radial basis kernel function (RBKF) in the model. The used RBKF can be expressed in terms of squared Euclidean distance ($\|x - x'\|^2$) between the two feature vectors and the spread of kernel function distribution (σ) using Eq. 1.

3 Tabular Evaluation

Name of Author (Ref.)	Type of mineral	Techniques	Results	Observation/Brief methodology
Clara Akalanya Abuntori et al. [1]	-	OK	$R^2 = 0.53$	This study is performed on a dataset of 3759 drill holes. Also, it has taken into account 5 ELM models for a better fit, out of which ELM-Sigmoid has outperformed the others
		BPNN	$R^2 = 0.28$	
		ELM-Sigmoid	$R^2 = 0.91$	
Umit Emrah Kaplan et al. [3]	Gold	XGBoost	$R^2 = 0.72$	This study proved XGBoost as the best model over OK and other gradient-based algorithms. However, only 29 drill holes were considered for investigation
		LightGBM	$R^2 = 0.65$	
		CatBoost	$R^2 = 0.67$	
		OK	$R^2 = 0.65$	

(continued)

(continued)

Name of Author (Ref.)	Type of mineral	Techniques	Results	Observation/Brief methodology
Mahdi Fathi et al. [12]	Iron	PSO-ELM	$R^2 = 0.83$	This study has utilised 9067 datasets and concluded lithological parameters as important to make better logical estimation at border boreholes
Reza Shamsi et al. [13]	Iron	IDW	$R^2 = 0.51$	This study adopted a hybrid algorithm IDW-ICA by utilising the ICA algorithm to modify the power, distance and coefficients of the IDW equation on a dataset of 32 boreholes
		OK	$R^2 = 0.67$	
		IDW-ICA	$R^2 = 0.94$	
Umit Emrah Kaplan et al. [4]	Gold	Real NN	$R^2 = 0.94$	123 drill holes dataset is taken into account to perform this study that resulted in the Real and Model NN models as far better than traditional NN
		Model NN	$R^2 = 0.52$	
		Traditional NN	$R^2 = 0.11$	
Bahram Jafrasteh et al. [2]	Copper	NN	MSE = 0.55	This study concluded GP as the best estimation method surpassing OK and other methods by considering 603 drill holes for the study
		RF	MSE = 0.43	
		GP	MSE = 0.35	
		OK	MSE = 0.45	
		IK	MSE = 0.40	
Ashok Kumar Patel et al. [5]	Iron	SVR	$R^2 = 0.94$	This research study adopted 53 sample images to predict ore grade by developing the SVR model using the optimised image feature subset
		ANN	$R^2 = 0.93$	
		GP	$R^2 = 0.88$	
Patel et al. [6]	Iron	GP	$R^2 = 0.95$	This study made use of 18 features (9-colors and 9-textures) being extracted from 26 sample images for ore grade estimation model development
		Tree	$R^2 = 0.94$	
		RBF	$R^2 = 0.89$	
B Manna et al. [8]	Copper	PCA-ANN	$R^2 = 0.88$	114 samples were used to develop the hybrid PCA-ANN model
Ashok Kumar Patel et al. [11]	Iron	SVR-RBF	$R^2 = 0.82$	This study utilised 88 image samples to extract 39 features then optimised them further to 4 using the GA technique to predict the ore grade
Neda Mahvash Mohammadi et al. [7]	Gold	PCA-Kmeans	$R^2 = 0.91$	256 samples were engaged in this study that helped in understanding the relationship between various elements of gold through PCA further their behaviour is investigated by Kmeans clustering
Yukui Zhang et al. [9]	Gold	IDW	RMSE = 3.48	This study incorporated the relevance vector machine (RVM) and weighted expected squared distance (WESD) into one regression model for better prediction of the ore grade.
		OK	RMSE = 3.89	
		ELM	RMSE = 2.70	
		WESD-RVM	RMSE = 2.25	
	Silver	IDW	RMSE = 21.01	This study uses statistical analysis to uncover mutual relationships between different elements of the deposit leading to a decrease in the estimation dependency on geographical position. The incomplete data is handled with high sparsity and accuracy by the proposed WESD-RVM model
		OK	RMSE = 29.60	
		ELM	RMSE = 13.92	
		WESD-RVM	RMSE = 11.47	
	Copper	IDW	RMSE = 3.07	
		OK	RMSE = 4.35	
		ELM	RMSE = 3.33	
		WESD-RVM	RMSE = 3.04	

(continued)

(continued)

Name of Author (Ref.)	Type of mineral	Techniques	Results	Observation/Brief methodology
Pejman Tahmasebi et al. [14]	–	ANN-GA	$R^2 = 0.99$	This study determines the parameters and topology for the ANN model by trial and error approach then applies GA on the obtained parameters to understand its effect on the results and thus evaluate model performance
Hamid Mahmoudabadi et al. [15]	Iron	OK	MSE = 0.235	Since the task of grade estimation is critical with fewer samples using neural networks or some other geostatistical methods due to the high sensitivity of initial weights. The proposed hybrid GA-LM model developed with 65 drill holes tries to resolve this issue
		GA	MSE = 0.17	
		GA-LM	MSE = 0.09	
B. Samanta et al. [16]	Gold	LMBP	$R^2 = 0.99$	This study aims to highlight the importance of global learning algorithms to avoid trapping in the local minima. However, the performance of both local and global learning algorithms in neural network modelling is nearly the same in the unimodal datasets but the superiority of the global method can be understood in multimodal problems
		NOVEL	$R^2 = 0.99$	
		SA	$R^2 = 0.99$	
	Bauxite	LMBP	$R^2 = 0.29$	
		NOVEL	$R^2 = 0.36$	
		SA	$R^2 = 0.28$	
	Iron	LMBP	$R^2 = 0.72$	
		NOVEL	$R^2 = 0.72$	
		SA	$R^2 = 0.76$	

OK—Ordinary Kriging, BPNN—Backpropagation Neural Network, ELM—Extreme Learning Machine, XGBoost—Extreme gradient boosting, LightGM—Light gradient boosting machine, Catboost—Categorical boosting, PSO—Particle Swarm Optimisation, IDW—Inverse Distance Weighted, ICA—Imperialist Competitive Algorithm, NN—Neural networks, RF—Random forest, GP—Gaussian process, IK—Indicator kriging, SVR—Support Vector Machine Regression, Tree—Decision Tree-Based Algorithm, ANN—Artificial Neural Network, RBF—Radial Basis Function, PCA—Principal component analysis, Kmeans—Clustering method, WESD—weighted expected squared distance, RVM—relevance vector machine, LM—Levenberg–Marquardt, GA—Genetic Algorithm, SA—Simulated Annealing, NOVEL—Trace-Based NOVEL Method, LMBP—Levenberg–Marquardt Back-propagation Algorithms

4 Discussion

The applications of machine learning techniques have proved very satisfactory results in the mining sector. Since, we know that the natural occurrence of every mineral varies along with different factors including geology, climate, air, water etc. Also, the existing methods of conventional geostatistic techniques always follow a defined approach for estimation that may neglect or reduce the influence of some exceptional parameters leading to faulty results. Therefore, the diverse nature of minerals necessitates the requirement of advanced and robust ore grade estimation methods to deal with the variance and provide fewer flaws for smooth planning and implementation of the mineral ore deposits. Thus, machine learning techniques confirm their presence by encountering diversification issues in minerals by a wide range of intelligent approaches. Many of these techniques are inspired by the natural actions and behaviour of the ecosystem. Also, their flexibility of combining to develop hybrid approaches opens the door for meeting complex and delicate aspects of the mineral.

The availability of these methods deal with many of the existing problems and shows green signals for future scope of research to fulfil the growing demands. However, the adaptability and versatility of any method need to be verified before the approval for extensive implementation. Therefore, this study helps to form a ground for the evaluation of these techniques.

5 Conclusion

This study aims to check the applicability of several AI/ML techniques for ore grade estimation of various minerals such as iron, copper and gold. The results of these methods can be compared with actual run-off-mine (ROM) quality for more justification, as this factor is often neglected. The implementation of conventional geostatistical techniques like OK and IDW have been discussed in Sect. 2. The major working principles of the neural networks (NN), extreme learning machines (ELM) and support vector regression (SVR) are briefly explained in this study. Also, there are various other algorithms like an imperialist competitive algorithm (ICA), random forests (RF), particle swarm optimisation (PSO), firefly algorithm (FA) etc., these algorithms differ widely in their principles and produce some very interesting results. Section 3 briefly elaborates the applicability of various ML methods adopted by the researchers. However, further extended research is required to apply multiple AI/ML models for different types of mineral deposits and to compare the outcomes with the actual quality of the mineral. Also, the assessment of probable and possible reserve estimates needs to be cross-checked with the proved reserves. The field of AI/ML technique is an emerging one and shall be very useful for the task of ore grade estimation among varying mineral occurrences in the next decade as the mineral industries will look for savings in exploration costs and will meet potentially to their requirements.

References

1. Abuntori CA, Al-Hassan S, Mireku-Gyimah D, Ziggah YY (2021) Evaluating the performance of extreme learning machine technique for ore grade estimation. *J Sustain Mining* 20(2). <https://doi.org/10.46873/2300-3960.1062>. Article 2
2. Jafrasteh B, Fathianpour N, Suárez A (2018) Comparison of machine learning methods for copper ore grade estimation. *Comput Geosci* 22:1371–1388. <https://doi.org/10.1007/s10596-018-9758-0>
3. Kaplan UE, Dagan Y, Topal E (2021) Mineral grade estimation using gradient boosting regression trees. *Int J Mining Reclam Environ*. <https://doi.org/10.1080/17480930.2021.1949863>
4. Kaplan UE, Topal E (2020) A new ore grade estimation using combine machine learning algorithms. *Minerals* 10:847. <https://doi.org/10.3390/min10100847>

5. Patel AK, Chatterjee S, Gorai AK (2018) Development of a machine vision system using the support vector machine regression (SVR) algorithm for the online prediction of iron ore grades. *Earth Sci Inform* 12:197–210. <https://doi.org/10.1007/s12145-018-0370-6>
6. Patel AK, Gorai AK, Chatterjee S (2016) Development of Machine vision-based system for iron ore grade prediction using Gaussian Process Regression (GPR). In: *Pattern recognition and information processing (PRIP 2016)*, Minsk, Belarus, pp 45–48
7. Mohammadi N, Hezarkhani A, Maghsoudi A (2017) Application of K-means and PCA approaches to estimation of gold grade in Khooni district (central Iran). *Acta Geochimica* 37. <https://doi.org/10.1007/s11631-017-0161-7>
8. Manna B, Samanta B, Chakravarty D, Dutta D, Chowdhury A, Santra A, Banerjee A (2018) IOP Conf Ser Earth Environ Sci 169:012108. <https://doi.org/10.1088/1755-1315/169/1/012108>
9. Zhang Y, Song S, You K, Zhang X, Wu C (2017) Relevance vector machines using weighted expected squared distance for ore grade estimation with incomplete data. *Int J Mach Learn Cybernet* 8. <https://doi.org/10.1007/s13042-016-0535-x>
10. Jafrasteh B, Fathianpour N (2017) A hybrid simultaneous perturbation artificial bee colony and back-propagation algorithm for training a local linear radial basis neural network on ore grade estimation. *Neurocomputing* 235:217–227. <https://doi.org/10.1016/j.neucom.2017.01.016>. ISSN 0925-2312
11. Patel AK, Chatterjee S, Gorai AK (2017) Development of online machine vision system using support vector regression (SVR) algorithm for grade prediction of iron ores. In: *2017 fifteenth IAPR international conference on machine vision applications (MVA)*, pp 149–152. <https://doi.org/10.23919/MVA.2017.7986823>
12. Fathi M, Alimoradi A, Hemati Ahooi H (2021) Optimizing extreme learning machine algorithm using particle swarm optimization to estimate iron ore grade. *J Mining Environ* 12(2):397–411. <https://doi.org/10.22044/jme.2021.10368.1984>
13. Shamsi R, Dehghani H, Jalali M et al (2021) Ore grade estimation using the imperialist competitive algorithm (ICA). *Arab J Geosci* 14:1409. <https://doi.org/10.1007/s12517-021-07808-7>
14. Tahmasebi P, Hezarkhani A (2010) Comparison of optimized neural network with fuzzy logic for ore grade estimation. *Austr J Basic Appl Sci* 4
15. Mahmoudabadi H, Izadi M, Menhaj M (2009) A hybrid method for grade estimation using genetic algorithm and neural networks. *Comput Geosci* 13:91–101. <https://doi.org/10.1007/s10596-008-9107-9>
16. Samanta B, Bandyopadhyay S, Ganguli R (2006) Comparative evaluation of neural network learning algorithms for ore grade estimation. *Math Geol* 38:175–197. <https://doi.org/10.1007/s11004-005-9010-z>
17. Patel AK, Chatterjee S, Gorai AK (2017) Development of machine vision-based ore classification model using support vector machine (SVM) algorithm. *Arab J Geosci* 10:107. <https://doi.org/10.1007/s12517-017-2909-0>
18. Huang GB, Zhu QY, Siew CK (2006) Extreme learning machine: theory and applications. *Neurocomputing* 70(1–3):489–501
19. Wang J, Lu S, Wang SH, Zhang YD (2021) A review on extreme learning machine. *Multimedia Tools Appl* 22:1–50

Robots in Mining



Job Steven James Nanadrekar, Manavalan Subramanian, Umng Aditya, Gaurav Jain, Vynotdni Rathinasamy, and Ramesh Murlidhar Bhatawdekar

Abstract Robots are being utilised for mining applications since 1976. However, since 2002, robots are widely into mining from conception to end product or even end-users. Lidar sensors connect robot with a real-time map making it travel safely but detects and avoids obstacles on its own. Autonomous Mobile Robots (AMR) are widely used to inspect abandoned mines for analysing real situations in highly hazardous conditions where man's entry is prohibited. The robot is a sub-domain of engineering that deals with the design, construction and operation. Robots' usage in mining applications becoming vital. Likewise use of robots and computers for their control, corporeal information processing vaguely. Nowadays robotics technology controlling every sphere of expression of work and back home. Robots have the capability to progressively change lives and work procedures best professionally, securely and quickly. Similarly in underground operation additionally Robots become important specifically anywhere, i.e., paucity of air circulation and ground care, flooded UG mines, transfer video feeds to ascertain situation, create system to connect with traveling robots, plotting of mines with drones, etc. Thus, robots are very widely

J. S. J. Nanadrekar · U. Aditya · G. Jain (✉)
Indian Institute of Technology Kharagpur, Kharagpur 721302, India
e-mail: gaurav.jain@iitkgp.ac.in

J. S. J. Nanadrekar
e-mail: jobsteven@iitkgp.ac.in

U. Aditya
e-mail: umangdt34@gmail.com

M. Subramanian
Dangote Cement Plc Ltd., Obajana, Kogi, Nigeria
e-mail: manavalan.subramanian@gmail.com

V. Rathinasamy · R. M. Bhatawdekar
Geotropik Centre, School of Civil Engineering, Faculty of Engineering, Universiti Teknologi Malaysia, UTM, Block D03, 81310 Johor Bahru, Malaysia
e-mail: Vynotdni@utm.my

R. M. Bhatawdekar
e-mail: rmbhatawdekar2@graduate.utm.my

and truly into entire mining field. Communication Technology has become identical with day-to-day human life thus mining business cannot be an exclusion. Mining industry also employing drones for exploration and surveying. Computerization of mining operators are rapidly replaced by robots.

Keywords Robot · Mining · Drones

1 Introduction

World mining survey indicates 28% lower productive now than 10 years back [1]. Decreasing mineral quality, rising costs, scarcity of skilled labour, low demand and strict controlling have been pushing mining industry to embrace robotic technology to enhance output and competence. Around several roles in the mining business procedures extend over a wider range of rules and regulation created but monotonous work not adding any value to the core business being still continued.

Automating with robot cut down repetitive and non-value adding tasks using software. More companies using robot process automation (RPA) and artificial intelligence (AI) platform facilitates robots to take decision leveraging intellectual processing and effortless system understanding. Most of mining work could be computerized using RPA to facilitate remote operation [2, 3]. Robots will do regular jobs like extracting, loading, verifying, or structuring records, estimating, etc. quicker with accuracy on a continuously, round the clock and improving overall efficiency of entire operation.

2 Robotic Process Automation (RPA) for Mining Industry

Computerisation is reshaping the job ecosystem for staff, specifically for greater staffs. Doing it properly would become an admirable job. Though mining is old fashioned, lot more mining companies are shifting their focus on renovation to automation with increasing perspective and proving digitization [4]. With more and more automation mining industry can achieve much superior operational proficiency to reap the higher profits of safety and cost reduction [5]. Besides, technology have increased skill of labour and taught workers to become more efficient than before. Robots are utilised to load and unload materials, storing, stacking, arc welding and machine assembly, dismantle as well as for movement of spare parts.

Digital transformation leading to operation of trucks, drills, trains and back-office activities as well as ordering and supply chain logistics. Global financial system crash during 2014 to 15 and rates of all products plunged by >30%, because of COVID-19 pandemic and make the mining industry too embrace best transformation for higher sustainability of economy [6]. Specifically, most of mining sector presently focuses to lower costs and enhance efficiency to take towards economisation of entire operation.

To accomplish all work process and machine operation continuously and automatically, robotic technology is deployed successfully. The objective of automation is to make plants and equipment's to automatically perform processes effectively and at a low/no mistake. Most of mining activities right from development to hauling are executed by robots in order to achieve very speedy growth. One robotic expert required to be added in our study team for mining automation with robotic application.

RPA for mining industry applying to achieve over all operational improvement especially safety and economising whole operation. The mining sector focusing to reduce cost and accelerate efficiency to bring down expenditures such as wages, energy, and materials as well as supplies. Each mining is moving towards automation, whether you believe it or not it will create some fresh jobs simultaneously. It will eliminate some irrelevant jobs, but it is inevitable to go for automation. However, automation will change many tasks and functions with more skill and result oriented. The mining industry have found crucial procedures and events had been brought in the scope of RPA vista for highest gain. Various regions computerisation exhibited incredible growth in competency and cycle time.

- Surveying, ore estimating of the same and reserve validation progressively in accordance with mine work evolves.
- Corporate back-office work such as purchase to payment i.e., annual requirement/annual payment and month end financial reporting.
- Continually receiving production report and reconciling the same received from different business units. Further manging consistently cost data and forecasting.
- Data processing for maintenance and managing assets along with workflow.
- Material evaluating from production systems with linkage of lab information integrations and workflows into material accounting.

Technology has greatly enhanced pace and proficiency of work [7]. Even fundamental work like notetaking and devising have become further pioneering with improved technique. The collaboration amongst employees and business has been massively affected by techniques over the years. RPA software manages parts requisition to purchase order and even to scheduling requirement schedule, managing finance and other core services. Application of RPA resulted cost saving about \$200 million a year in maintenance costs alone therefore imagine related to other area of operational gains. For intensive activities like transporting explosive and accessories or hazardous substances, material safety data sheets (MSDS) are a prerequisite one to alert whoever receives or uses the product. Also, maintenance of HR data of every employee with site specific information such as pay is needed as well. However, RPA application brought significant saving such as 30–80% less on manual work, 50–80% on mistakes, 25–50% on productivity and 20–50% on cycle time [8]. Therefore, the rational use and success of RPA will depend on over acceptance of entire society.

3 Energy Saving Automation Technologies

Diesel fired multi-function residential heat pump reduce energy consumption about 30% [9]. Over the years of research, robots have improved controls resulting lot of energy savings on account of various operational control. Change of field bus I/O systems to 110 V relays is another innovative recurrent energy saving. However, solar powered robots are into market to further decrease power consumption that will become highly cost effective.

Energy saving in electrical systems includes energy efficient MD, PF controllers, energy soft starters with variable speed drives, energy saver, electronic ballast, energy saving LED bulbs, occupancy sensors, energy efficient transformers and energy efficient lighting controls. Technological advances increase energy saving because of improved performance and low consumption for the quantity output or increased output.

4 Mining Robots Usage in Hazardous Site

Robot can autonomously orbit flooded locations. Robot can use cameras and sensors to identify different ore [10]. Robots can be utilised to enter into an abandoned mine to analyse and confirm mineral resources availability to take decision [3]. Minerals that weren't mineable before could be mineable because of demand and high return of investment (ROI). Based on robot inspection mines cannot be reopened but it can be used to discover and make reserve management and costing.

5 Mining Companies Are Accelerating Robotic Automation

Robotic automation going to redesign the mining work atmosphere for employees especially which requires many staff. Everyone aware mining is very old fashioned but, bigger mining companies are focusing on transformation with progressive posture. Mining operations make use of automation to study rock mass characterisation, predictive/preventive mining machinery maintenance, geological disturbance study and maintenance of engines, hydraulic pumps with sensors as well as forecasting anticipated failures to take corrective action which prevents major failure.

In general, robots do not do perfect job and never becomes tired while working continuously for 24 h a week. Yet, it does job much faster and quicker. Study indicates about 63% of machine maintenance is redundant, any company confidence in predictive maintenance technology, they reap the benefit of extended maintenance duration because the software predicts and confirms due date of next maintenance [11]. Technology offers solution to business office purchase, supply chain management with enhanced consistency of rate and standard.

Celonis software scrutinised business processes of the company to discover simplification method and speedup execution, emphasising the inadequacies and then examining and recommending methods to easily solve a problem. Because of automation, data in the year 1999 to 2009 indicated that no job has been lost based on job routine documentation. However, further study between 2010–2017 shows a small wage increase associated with little decline in employment.

5.1 *Application of Geospatial Technology*

Some of the exciting shifts in technology application in mining activity are spatial or geospatial technology, AI, automated drones and use of renewable energy. These technologies are described below.

- a. Raster data: It can be classified into two types such as continuous and discrete. Temperature and elevation dimensions are examples of continuous while population density is an example for discrete example. Thematic data, spectral data and pictures are another three types of raster datasets [12].
- b. Geographic Information Systems (GIS): It is a computer system which captures, stores, checks and displays information regarding locations on Earth's surface. In addition, it incorporates data of vegetation, water courses and various soil type. Numerous organizations utilise the system to communicate, execute analysis, share data and resolve complicated crises across the world [13].
- c. Artificial Intelligence (AI): Human intelligence simulation process by computer system is known as AI. Specific applications of AI include machine vision, expert systems, speech recognition and natural language processing [14–16].
- d. Automated drones: They can access extremely toxic, hard-to-reach locations to provide clearer insights for mine planning. Drones shall be utilized to locate hot spots in coal stockpiles, to assess feasible spontaneous combustion areas and enable personnel take pre-emptive measures. They can also assist in blast planning, haul-road surface mine operation and watershed management. Additionally, the business-grade drones are utilized for surveying, asset inspection, stockpile estimation, terrain mapping and surveillance as well as security of mining sites [17]. They support mining companies with an aerial perspective at a fraction of a cost and improve operational effectiveness. Drones self-directed and transmit precise footage directly which permits experts and operators take quick and effective decisions on its own. Therefore, drones can very well enter into any risky areas and advance safely.
- e. Application of renewable energy: Renewable energy technologies such as fossil fuel and solar power in mining and drilling operations very much put into usages. Off course, mining and drilling operations are mostly located in isolated areas, not connected with well-known electricity infrastructure [18].

6 Conclusion

Robotic mining is foreseeable and indispensable for exploration and all mining applications to overall economising mining operations. Begins from human resources' roles to finished product accomplishment to the end user. Robots are deployed to operate electric trucks, trains and even excavators for loading. Orapa mine of Botswana implemented extrapolative survey on experimental basis in their rock-crushing machine [19]. The software works in background to spy irregularities in machine performance and recognised serious matters ahead of a major event could happen. Later, it forecasted and saved millions of dollars in the project. On the other hand, Rio Tinto implemented RPA software to accomplish predictive and preventive maintenance such as preparing purchase requisition, scheduling, order placement and observing until material reaches at stores then consumption pattern [11]. This resulted in saving their iron ore business for almost \$200 million a year in maintenance only. Thus, robotic and information technology is profitable to change all domains of mining application and leading to saving and efficiency improvement. Some of the forthcoming consequence of robot and its' usage on mining business are fewer man mining, human in automated systems, amplified realism, nonstop mining, automatic drilling, robot loading and hauling, computerisation of charging and blasting, automation of ascending and strengthening as well as automation of broadcasting system. However, we have to wait and watch the accelerated changes of the advancement. For a successful RPA initiative, execution of automation based on transparent insights obtained from mining process is required [20].

References

1. Lala A, Moyo M, Rehbach S, Sellschop R (2016) Productivity in mining operations: reversing the downward trend. *AusIMM Bulletin*, Australia, pp 46–49
2. Nanda SK, Dash AK, Acharya S, Moharana A (2010) Application of robotics in mining industry: a critical review. *Indian Mining Eng J* 8:108–112
3. Noh JH, Shin SS, Park JH (2013) A study on the robot for mining of underground resources. *J Korean Soc Mar Eng* 37(4):399–403
4. Yang L, Birhane GE, Zhu J, Geng J (2021) Mining employees safety and the application of information technology in coal mining. *Front Public Health* 9
5. Ralston JC, Reid DC, Dunn MT, Hainsworth DW (2015) Longwall automation: delivering enabling technology to achieve safer and more productive underground mining. *Int J Mining Sci Technol* 25(6):865–876
6. Ibn-Mohammed T, Mustapha KB, Godsell J, Adamu Z, Babatunde KA, Akintade DD, Acquaye A, Fujii H, Ndiaye, MM, Yamoah FA, Koh SCL (2021) A critical analysis of the impacts of COVID-19 on the global economy and ecosystems and opportunities for circular economy strategies. *Resour Conserv Recycl* 164:105169
7. Flechsig C, Anslinger F, Lasch R (2021) Robotic Process Automation in purchasing and supply management: a multiple case study on potentials, barriers, and implementation. *J Purchas Supply Manage* 100718
8. Infosys Why Robotic Process Automation Makes Sense in the Mining Industry. <https://www.infosys.com/insights/ai-automation/robotic-process-automation.html>. Accessed 10 Oct 2021

9. Energy.Gov Multi-Function Fuel-Fired Heat Pump. <https://www.energy.gov/eere/buildings/downloads/multi-function-fuel-fired-heat-pump-0>. Accessed 10 Oct 2021
10. Huh S, Lee U, Shim H, Park JB, Noh JH (2011) Development of an unmanned coal mining robot and a tele-operation system. In: Proceedings of 11th international conference on control, automation and systems. IEEE, pp 31–35
11. Raconteur How automation can transform mining. <https://www.raconteur.net/sustainability/automation-mining-efficiency/>. Accessed 10 Oct 2021
12. ArcGIS What is raster data? <https://desktop.arcgis.com/en/arcmap/10.3/manage-data/raster-and-images/what-is-raster-data.htm>. Accessed 10 Oct 2021
13. Knowles AK (2008) GIS and History. Placing history: how maps, spatial data, and GIS are changing historical scholarship, pp 1–25
14. Chakraborti T, Isahagian V, Khalaf R, Khazaeni Y, Muthusamy V, Rizk Y, Unuvar M (2020) From robotic process automation to intelligent process automation. In: Proceedings of international conference on business process management. Springer, Cham, pp 215–228
15. Syed R, Suriadi S, Adams M, Bandara W, Leemans SJ, Ouyang C, ter Hofstede AHM, van de Weerd I, Wynn MT, Reijers HA (2020) Robotic process automation: contemporary themes and challenges. *Comput Ind* 115:103162
16. Lacity M, Willcocks L, Gozman D (2021) Influencing information systems practice: the action principles approach applied to robotic process and cognitive automation. *J Inf Technol* 0268396221990778
17. Shahmoradi J, Talebi E, Roghanchi P, Hassanalian M (2020) A comprehensive review of applications of drone technology in the mining industry. *Drones* 4(3):34
18. Paraszczak J, Fytas K (2012) Renewable energy sources—a promising opportunity for remote mine sites? In: Proceedings of the international conference on renewable energies and power quality, pp 28–30
19. Bot Nirvana Mine 4.0: How RPA and Robots are transforming mining in new ways. <https://botnirvana.org/how-automation-can-transform-mining/>. Accessed 10 Oct 2021
20. Geyer-Klingeberg J, Nakladal J, Baldauf F, Veit F (2018) Process mining and robotic process automation: a perfect match. In: *BPM (Dissertation/Demos/Industry)*, pp 124–131

Utilizing a Bagging Model Based on Decision Trees and k-nearest Neighbors for Predicting Slope Stability in Open Pit Mines



Hoang Nguyen, Nguyen Tam Tinh, and Dinh Tien

Abstract This paper aims at introducing a bagging model for predicting slope stability in open pit mines based on the combination of multiple k-nearest neighbors (k-NN) models based on the decision trees (DTs) algorithm. Accordingly, k-NN models were used as the base estimators for predicting the factor of safety (FOS). Subsequently, they were combined together using DTs algorithm, called DTs-k-NN model. To demonstrate the performance of the DTs-k-NN model, 495 samples of slopes with the FOS values were calculated and used based on the parameters of benches and geotechnics. The results indicated that the DTs-k-NN model worked very well in predicting slope stability model with MAE = 0.041, RMSE = 0.049, $R^2 = 0.954$, and VAF = 95.356 on the training dataset, MAE = 0.046, RMSE = 0.056, $R^2 = 0.941$, and VAF = 94.097 on the testing dataset. The obtained results were also compared with the single k-NN and DTs models and they showed that the performance of the bagging DTs-k-NN model is superior to the single k-NN and DTs models, and the k-NN model only achieved the performance with MAE = 0.047, RMSE = 0.058, $R^2 = 0.93$, and VAF = 93.461 on the training dataset, MAE = 0.050, RMSE = 0.061, $R^2 = 0.930$, and VAF = 92.712 on the testing dataset. The DTs model yielded the poorest performance with MAE = 0.064, RMSE = 0.081, $R^2 = 0.896$, and VAF = 87.281 on the training dataset, MAE = 0.064, RMSE = 0.082, $R^2 = 0.884$, and VAF = 87.118 on the testing dataset.

H. Nguyen (✉) · N. T. Tinh · D. Tien
Department of Surface Mining, Mining Faculty, Hanoi University of Mining and Geology,
18 Vien Street, Duc Thang Ward, Bac Tu Liem District, Hanoi 100000, Vietnam
e-mail: nguyenhoang@hmg.edu.vn

H. Nguyen
Innovations for Sustainable and Responsible Mining (ISRM) Research Group, Hanoi University
of Mining and Geology, 18 Vien Street, Duc Thang Ward, Bac Tu Liem District, Hanoi, Vietnam

N. T. Tinh
Vinacomim - Ta Phoi Copper Joint Stock Company, Lao Cai, Vietnam

D. Tien
Sin Quyen, Lao Cai - Vimico Copper Mining and Preparation - Branch of Vinacomim, Lao Cai,
Vietnam

Keywords Slope stability · Open pit mine · Bagging technique · Decision trees · k-nearest neighbors

1 Introduction

In open-pit mines, slope stability is a considerable concern due to the uncertainty characteristics of geotechnical parameters as well as the complex parameters of slopes. Whereas the steepest possible slope angle is the goal of engineers to achieve the lowest stripping ratio, the instability of slopes may be occurred with such slope angles. Therefore, selection of slope angle is a critical decision and it affects the safety and economic problems of the mining projects.

To select the slope angle properly, many geotechnical parameters are considered that have a relation to the stability of slopes, such as friction angle, bench height, cohesion, unit weight, to name a few. Based on these parameters, many researchers evaluated and predicted the stability of slopes [4, 5, 13, 15]. Indeed, most of previous studies focused on two approaches to predict slope stability: (i) Predict the safety of factor (FOS), (ii) Predict the status of slopes based on the field measurements and observations.

In recent years, geotechnical softwares have been introduced with the features of the FOS calculation and modelling the stability of slope with very high accuracy [1, 6, 17]. Nevertheless, the costs are high and cannot meet the requirements for slope stability assessment in a rapid way. Therefore, prediction of slope stability is considered a potential alternative solution for evaluating slope stability with a large area and big data.

For predicting slope stability, artificial intelligence (AI) is taken into account as robust technique with various neural networks and machine learning algorithms. It is worth noting that AI techniques are not only applied in slope stability prediction but also in different areas of real-life [2, 9–12, 16, 18–20, 22, 24–26]. Regrading slope stability, many AI models have been developed to predict slope stability. For instance, Feng et al. [7] applied the Naive Bayes (NB) to predict slope stability using 69 slope cases. The model was then validated using 13 new cases. The results were compared to an existing empirical model to prove the performance of the NB model in predicting slope stability. In another study, Qi and Tang [14] developed several integrated machine learning models based on the firefly algorithm and logistic regression, decision tree, random forest, gradient boosting machine, support vector machine, and multilayer perceptron neural network. The area under the ROC curve (AUC) was found with 0.967 for the firefly-support vector machine model in predicting slope stability. Zhou et al. [21] also applied the gradient boosting machine (XGBoost) model to predict circular mode failure. The AUC, classification accuracy rate and Cohen's kappa values of 0.900, 0.8654 and 0.7324, respectively for the prediction of slope stability in their study. Kardani et al. [8] also investigated the stability of slopes based on finite element analysis and field data and a hybrid stacking ensemble model. Accordingly, an artificial bee colony (ABC) algorithm, support

vector classifier (SVC), k-nearest neighbor (k-NN), decision tree (DT), XGBoost, random forest (RF), linear discriminant analysis (LDA), multilayer perceptron artificial neural network (MLPANN), logistic regression (LR), extremely randomized tree (ETs), and NB. The best stacking ensemble model was defined with AUC = 90.4% for predicting slope stability.

In this study, a bagging model based on DTs and k-NN (i.e., DTs-k-NN) was introduced as a new AI model for predicting slope stability in open pit mine based on finite element analysis. The standalone k-NN and DTs models were also developed for the same purpose and compare with the DTs-k-NN model.

2 Materials and Methodology

In this study, the finite element analysis method (FEM) was used to analyze the slope stability of an open pit mine in Vietnam. Accordingly, the slope height (H), slope angle (β), unit weights (γ), cohesion (C), and friction angle (φ) were used to simulate the slip surface of the slope, as illustrated in Fig. 1. Herein, various scenes of geotechnical parameters and slope parameters were analyzed with 495 cases. The dataset is summarized in Table 1.

For predicting slope stability, this study proposes a new methodology based on the bootstrap technique, k-NN, and DTs algorithms.

k-NN is known as a lazy machine learning algorithm. It does not learn anything from the historical dataset [3]. Instead, it remembers all the neighbors and calculates the distances to them. For a new dataset, k-NN analyzes the characteristics of the new dataset and check them with the memory to find the similar characteristics and make

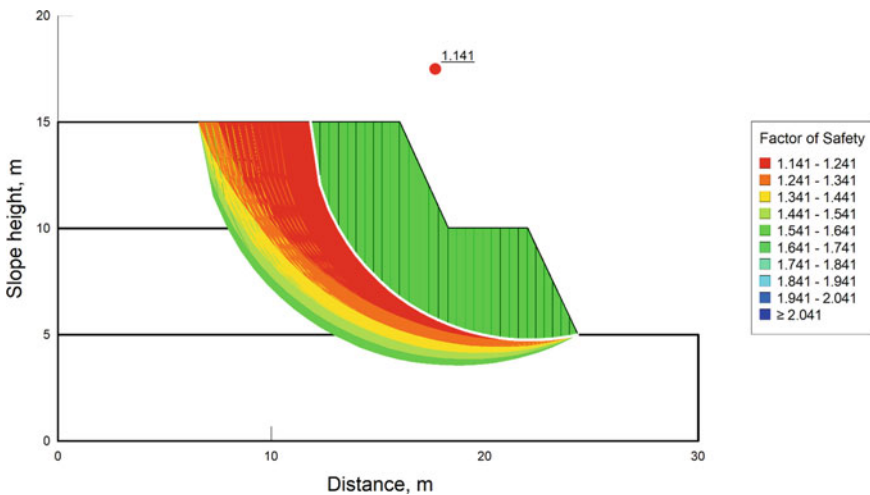


Fig. 1 Slope stability analysis based on the FEM

Table 1 Summary of the geotechnical parameters and FOS

H	β	γ	C	φ	FOS
Min.: 66.0	Min.: 30.60	Min.: 18.20	Min.: 51.21	Min.: 22.10	Min.: 0.858
1st Qu.: 121.0	1st Qu.: 34.60	1st Qu.: 23.20	1st Qu.: 70.87	1st Qu.: 27.80	1st Qu.: 1.085
Median: 131.0	Median: 38.00	Median: 24.69	Median: 101.92	Median: 29.60	Median: 1.269
Mean: 143.7	Mean: 38.76	Mean: 24.84	Mean: 93.74	Mean: 30.09	Mean: 1.276
3rd Qu.: 173.5	3rd Qu.: 42.80	3rd Qu.: 26.78	3rd Qu.: 109.72	3rd Qu.: 32.80	3rd Qu.: 1.437
Max.: 249.0	Max.: 50.20	Max.: 32.38	Max.: 153.35	Max.: 38.00	Max.: 1.798

a prediction based on the similar characteristics of the nearest neighbors. Therefore, k-NN is also preferred to as the non-parametric supervised machine learning model [23].

DTs is a supervised machine learning algorithm which is developed based on the structure of a tree. The main components of the DTs are root and leaf nodes. For developing the DTs model, various tasks, such as splitting, terminal node, pruning, sub-tree, parent and child node can be applied. The DTs implementation can be summarized in four steps, as follows:

- Step 1: Split the dataset into training and testing dataset. Then, the whole training set is considered as the root.
- Step 2: Feature values are preferred to be categorical. If the values are continuous then they are discretized prior to building the model.
- Step 3: Records are distributed recursively on the basis of attribute values.
- Step 4: Order to placing attributes as root or internal node of the tree is done by using some statistical approach.

For developing the DTs-k-NN model, the bootstrap technique is applied to split and resample the dataset into subsets. Subsequently, k-NN models are developed based on each subset. Finally, the DTs algorithm was used to combine the predictions from the developed k-NN models, called DTs-k-NN model. The framework of the DTs-k-NN model is proposed in Fig. 2.

3 Results and Discussion

To do this, the dataset was divided into two phases: 70% of the whole dataset was used for training the model, and the remaining 30% was used for testing the model's accuracy. Subsequently, the k-NN model was used as the base estimator with the

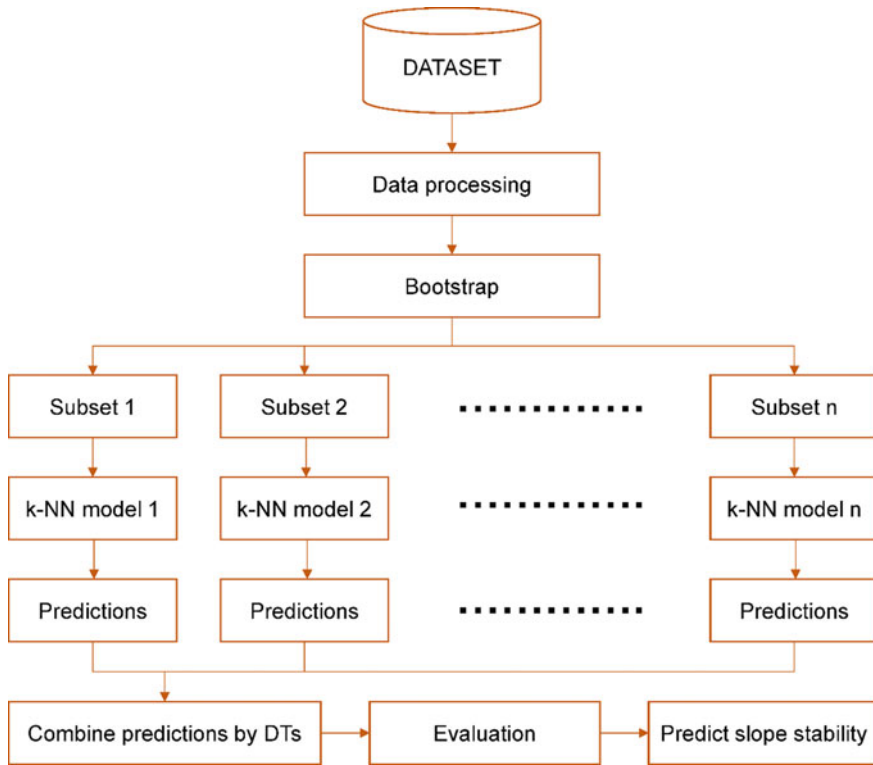


Fig. 2 Framework of the DTs-k-NN model for predicting slope stability

number of k was set in the range of 1 to 11. In other words, 10 k -NN models were developed to predict slope stability based on the training dataset. For evaluating the performance of the model, tenfold cross-validation technique was used. The performance of the k -NN model with different number of neighbors are shown in Fig. 3. Finally, the outcome predictions of the k -NN models were combined based on the DTs model. The obtained results of the DTs- k -NN model are shown in Fig. 4.

For the comparison purposes, the k -NN and DTs models were also developed based on the same datasets. The developed models were then evaluated through three performance indices, including mean absolute error (MAE), root-mean-squared error (RMSE), determination coefficient (R^2), and variance accounted for (VAF), as computed in Table 2.

As shown in Table 2, we can see that the proposed bagging model (i.e., DTs- k -NN) provided the most dominant model with MAE = 0.041, RMSE = 0.049, R^2 = 0.954, and VAF = 95.356 on the training dataset, MAE = 0.046, RMSE = 0.056, R^2 = 0.941, and VAF = 94.097 on the testing dataset. Meanwhile, the k -NN model only achieved the performance with MAE = 0.047, RMSE = 0.058, R^2 = 0.93, and VAF = 93.461 on the training dataset, MAE = 0.050, RMSE = 0.061, R^2 =

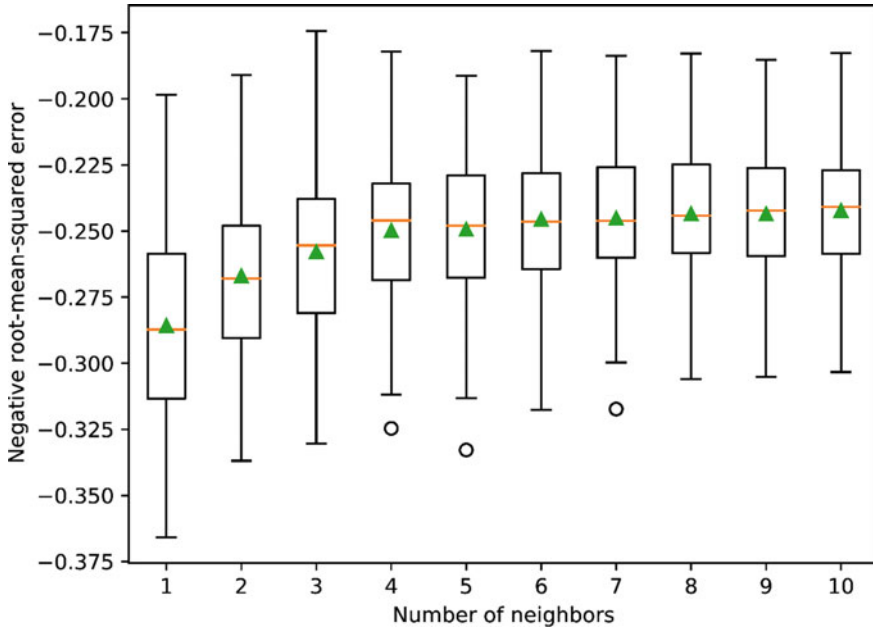


Fig. 3 Bagging k-NN number of neighbors versus the accuracy

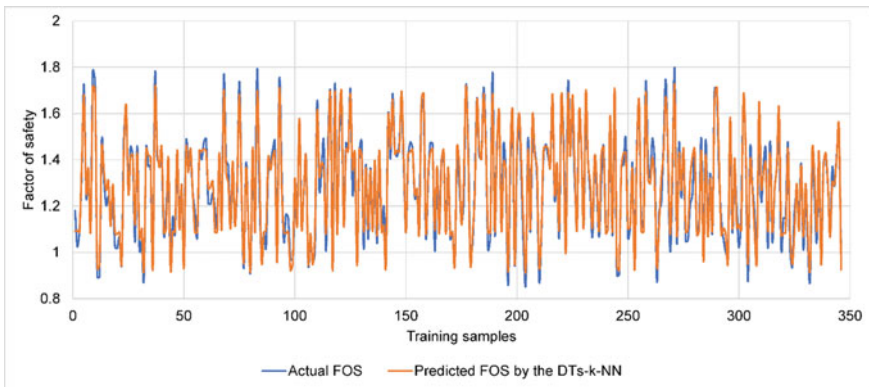


Fig. 4 Results of the DTs-k-NN model in predicting FOS on the training dataset

Table 2 Performance results of the developed models for predicting slope stability

Model	Training dataset				Testing dataset			
	MAE	RMSE	R ²	VAF	MAE	RMSE	R ²	VAF
DTs-k-NN	0.041	0.049	0.954	95.356	0.046	0.056	0.941	94.097
k-NN	0.047	0.058	0.937	93.461	0.050	0.061	0.930	92.712
DTs	0.064	0.081	0.896	87.281	0.064	0.082	0.884	87.118

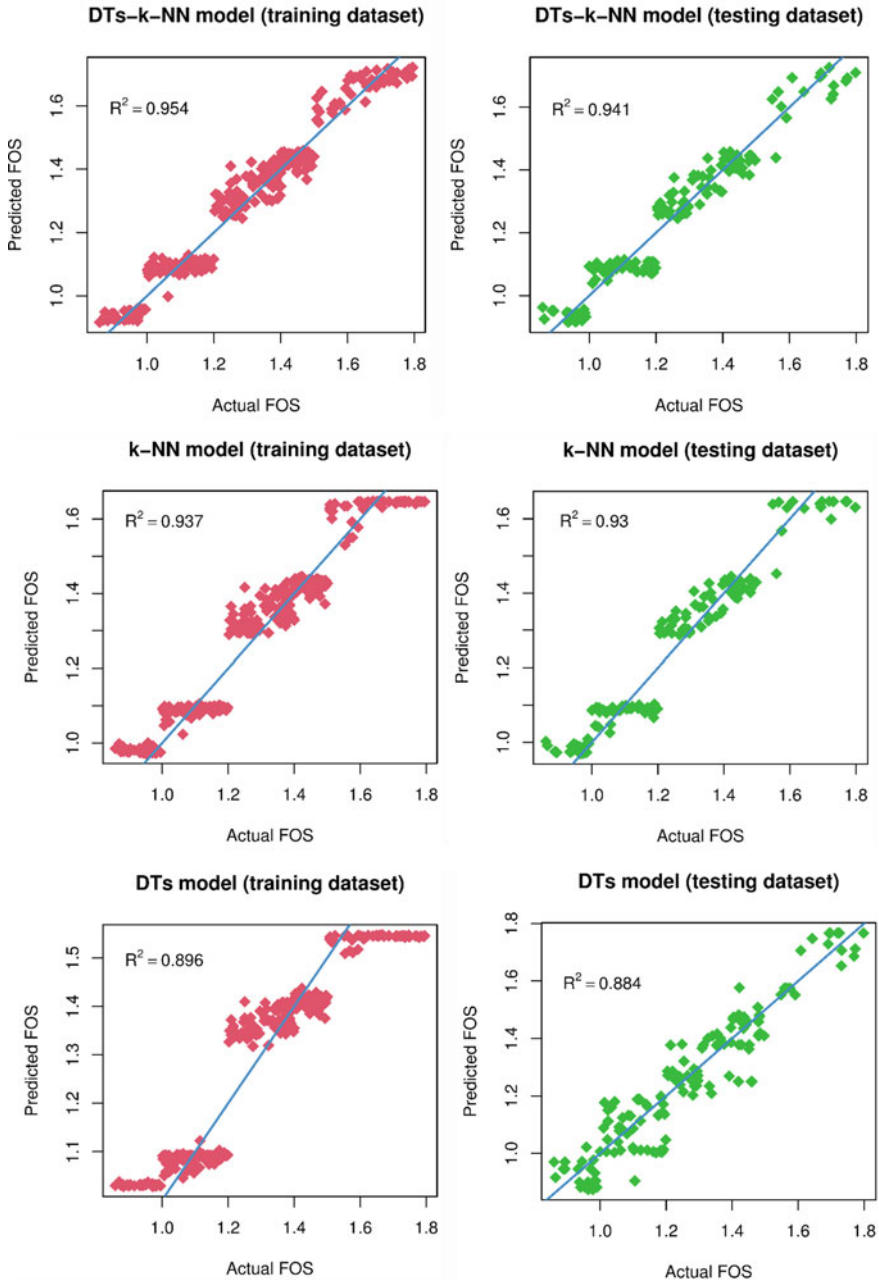


Fig. 5 Correlation between actual and predicted FOS

0.930, and $VAF = 92.712$ on the testing dataset. The DTs model yielded the poorest performance with $MAE = 0.064$, $RMSE = 0.081$, $R^2 = 0.896$, and $VAF = 87.281$ on the training dataset, $MAE = 0.064$, $RMSE = 0.082$, $R^2 = 0.884$, and $VAF = 87.118$ on the testing dataset. For further assessment of the proposed DTs-k-NN model, the correlations between actual and predicted FOS by the individual models were presented in Fig. 5.

As depicted in Fig. 5, it can be seen that the bagging DTs-k-NN model provided the best correlation with the highest convergence. In contrast, the k-NN and DTs models provided poorer correlations. Notably, the DTs model provided the lowest correlation between actual and predicted FOS with the lowest convergence. In other words, the proposed bagging DTs-k-NN model is the best model for predicting slope stability in this study.

4 Conclusion

Slope stability in open pit mine is a considerable concern and a challenge for engineers and researchers. Inaccurate evaluate or predict slope stability may lead serious damages in set of benches and slopes. In this study, a new AI model, namely bagging DTs-k-NN model, was introduced as a new approach to predict slope stability with the accuracy improved. The methodology is a generalize approach and we can develop other AI models based on this approach to predict slope stability in open pit mine. The obtained results indicated that the proposed DTs-k-NN model is a good model with high reliability, and its accuracy has been proved through the k-NN and DTs models.

Acknowledgments The authors would like to thank the Centre for Mining, Electro-Mechanical Research, Hanoi University of Mining and Geology, Hanoi, 100000, Vietnam for their kind support.

References

1. Arshad I, Babar MM, Javed N (2017) Numerical analysis of seepage and slope stability in an earthen dam by using geo-slope software. *PSM Biol Res* 2(1):13–20
2. Bac BH, Nguyen H, Thao NTT, Hanh VT, Duyen LT, Dung NT et al (2021) Estimating heavy metals absorption efficiency in an aqueous solution using nanotube-type halloysite from weathered pegmatites and a novel Harris hawks optimization-based multiple layers perceptron neural network. *Eng Comput*. <https://doi.org/10.1007/s00366-021-01459-8>
3. Bui X-N, Jaroonpattanapong P, Nguyen H, Tran Q-H, Long NQ (2019) A novel hybrid model for predicting blast-induced ground vibration based on k-nearest neighbors and particle swarm optimization. *Scientific reports*
4. Cho SE (2007) Effects of spatial variability of soil properties on slope stability. *Eng Geol* 92(3–4):97–109
5. Choobbasti A, Farrokhzad F, Barari A (2009) Prediction of slope stability using artificial neural network (case study: Noabad, Mazandaran, Iran). *Arab J Geosci* 2(4):311–319

6. Duncan JM, Wright SG, Brandon TL (2014) Soil strength and slope stability. Wiley, Hoboken
7. Feng X, Li S, Yuan C, Zeng P, Sun Y (2018) Prediction of slope stability using naive Bayes classifier. *KSCE J Civ Eng* 22(3):941–950
8. Kardani N, Zhou A, Nazem M, Shen S-L (2021) Improved prediction of slope stability using a hybrid stacking ensemble method based on finite element analysis and field data. *J Rock Mech Geotech Eng* 13(1):188–201
9. Nguyen H, Bui X-N (2021) A novel hunger games search optimization-based artificial neural network for predicting ground vibration intensity induced by mine blasting. *Nat Resour Res* 30(5):3865–3880. <https://doi.org/10.1007/s11053-021-09903-8>
10. Nguyen T, Hoang B, Nguyen G, Nguyen BM (2020) A new workload prediction model using extreme learning machine and enhanced tug of war optimization. *Procedia Comput Sci* 170:362–369. <https://doi.org/10.1016/j.procs.2020.03.063>
11. Nguyen T, Nguyen G, Nguyen BM (2020) EO-CNN: an enhanced CNN model trained by equilibrium optimization for traffic transportation prediction. *Procedia Comput Sci* 176:800–809. <https://doi.org/10.1016/j.procs.2020.09.075>
12. Nguyen T, Tran N, Nguyen BM, Nguyen G (2018) A resource usage prediction system using functional-link and genetic algorithm neural network for multivariate cloud metrics. In: 2018 IEEE 11th conference on service-oriented computing and applications (SOCA), 20–22 November 2018, pp 49–56. <https://doi.org/10.1109/SOCA.2018.00014>
13. Osman N, Barakbah S (2006) Parameters to predict slope stability—soil water and root profiles. *Ecol Eng* 28(1):90–95
14. Qi C, Tang X (2018) Slope stability prediction using integrated metaheuristic and machine learning approaches: a comparative study. *Comput Ind Eng* 118:112–122
15. Sakellariou M, Ferentinou M (2005) A study of slope stability prediction using neural networks. *Geotech Geol Eng* 23(4):419–445
16. Xie C, Nguyen H, Bui X-N, Nguyen V-T, Zhou J (2021) Predicting roof displacement of roadways in underground coal mines using adaptive neuro-fuzzy inference system optimized by various physics-based optimization algorithms. *J Rock Mech Geotech Eng*. <https://doi.org/10.1016/j.jrmge.2021.07.005>
17. Xie M, Esaki T, Qiu C, Wang C (2006) Geographical information system-based computational implementation and application of spatial three-dimensional slope stability analysis. *Comput Geotech* 33(4–5):260–274
18. Zhang H, Nguyen H, Bui X-N, Pradhan B, Mai N-L, Vu D-A (2021) Proposing two novel hybrid intelligence models for forecasting copper price based on extreme learning machine and meta-heuristic algorithms. *Resour Policy* 73:102195. <https://doi.org/10.1016/j.resourpol.2021.102195>
19. Zheng X, Nguyen H (2021) A novel artificial intelligent model for predicting water treatment efficiency of various biochar systems based on artificial neural network and queuing search algorithm. *Chemosphere* 132251. <https://doi.org/10.1016/j.chemosphere.2021.132251>
20. Zheng X, Nguyen H, Bui X-N (2021) Exploring the relation between production factors, ore grades, and life of mine for forecasting mining capital cost through a novel cascade forward neural network-based salp swarm optimization model. *Resour Policy* 74:102300. <https://doi.org/10.1016/j.resourpol.2021.102300>
21. Zhou J, Li E, Yang S, Wang M, Shi X, Yao S et al (2019) Slope stability prediction for circular mode failure using gradient boosting machine approach based on an updated database of case histories. *Saf Sci* 118:505–518
22. Vu DH, Nguyen HT (2021) Estimation of shale volume from well logging data using artificial neural network. *J Min Earth Sci* 62(3):46–52. [https://doi.org/10.46326/JMES.2021.62\(3\).06](https://doi.org/10.46326/JMES.2021.62(3).06)
23. Nguyen H (2020) Application of the k - nearest neighbors algorithm for predicting blast - induced ground vibration in open - pit coal mines: a case study. *J Min Earth Sci* 61(6):22–29. [https://doi.org/10.46326/JMES.2020.61\(6\).03](https://doi.org/10.46326/JMES.2020.61(6).03)
24. Pham NT, Bing P, Nguyen NV (2020) Study on the effect of some parameters of soil nails on the stability of vertical slopes. *J Min Earth Sc* 61(6):30–37. [https://doi.org/10.46326/JMES.2020.61\(6\).04](https://doi.org/10.46326/JMES.2020.61(6).04)

25. Le DN, Dang CV (2020) Application of fuzzy-logic to design fuzzy compensation controller for speed control system to reduce vibration of CBIII-250T drilling machine in mining industry. *J Min Earth Sci* 61(6):90–96. [https://doi.org/10.46326/JMES.2020.61\(6\).10](https://doi.org/10.46326/JMES.2020.61(6).10)
26. Tien NH, Hong ND, The VV, Thi ND, Tram Pham Van T (2021) Use of Artificial Neural Networks in predicting rate of penetration and optimization weight on bit for several wells in Nam Rong - Doi Moi field Vietnam. *J Min Earth Sci* 62(3a):37–47. [https://doi.org/10.46326/JMES.2021.62\(3a\).05](https://doi.org/10.46326/JMES.2021.62(3a).05)

Extra Trees Ensemble: A Machine Learning Model for Predicting Blast-Induced Ground Vibration Based on the Bagging and Sibling of Random Forest Algorithm



Xuan-Nam Bui, Hoang Nguyen, and Phonepaserth Soukhanouvong

Abstract In this paper, the extra trees ensemble (ETE) technique was introduced to predict blast-induced ground vibration in open pit mines. It was developed based on the extension of random forest (RF) algorithm to bagging and sibling the predictors. Accordingly, the ETE used a simple algorithm to construct the decision trees (DTs) models as the predictors. Next, it combines the constructed predictors to achieve as-good performance in predicting blast-induced ground vibration. Herein, more than 300 blasting events were implemented and their parameters, as well as the intensity of blast-induced ground vibration, were measured and collected for this study. The ETE model was then developed based on the collected dataset for predicting blast-induced ground vibration. In addition, the RF model was also applied to compare with the ETE model. The results showed that the ETE model is superior to the RF model in predicting blast-induced ground vibration. Its performance and accuracy are outstanding and should be used in practical engineering to control the adverse effects of blast-induced ground vibration in open pit mines.

Keywords Drilling and blasting · Ground vibration · Peak particle velocity · Open pit mine · Extra trees ensemble · Bagging technique · Random Forest

1 Introduction

In open pit mines, drilling-blasting is considered as the most effective method for rock fragmentation due to its advantages in low cost and high fragmentation efficiency

X.-N. Bui · H. Nguyen (✉) · P. Soukhanouvong
Department of Surface Mining, Mining Faculty, Hanoi University of Mining and Geology,
18 Vien Street, Duc Thang Ward, Bac Tu Liem District, Hanoi 100000, Vietnam
e-mail: nguyenhoang@humg.edu.vn

X.-N. Bui · H. Nguyen
Innovations for Sustainable and Responsible Mining (ISRMI) Research Group, Hanoi University
of Mining and Geology, 18 Vien Street, Duc Thang Ward, Bac Tu Liem District, Hanoi, Vietnam

P. Soukhanouvong
Department of Energy and Mines of Bolikhamxay, Pakkading, Lao PDR

© The Author(s), under exclusive license to Springer Nature Singapore Pte Ltd. 2022
A. K. Verma et al. (eds.), *Proceedings of Geotechnical Challenges in Mining, Tunneling
and Underground Infrastructures*, Lecture Notes in Civil Engineering 228,
https://doi.org/10.1007/978-981-16-9770-8_43

[7, 29, 34]. Nevertheless, its adverse effects, such as ground vibration, air blast, fly rock, and fumes, are significant and they can damage the surrounding environment [12, 36, 40]. Of those, blast-induced ground vibration, which is measured by peak particle velocity (PPV), is taken into account as the most dangerous effect.

To control the side effects on the surrounding environment induced by blast-induced ground vibration, many researchers studied how to estimate PPV before blasts? To answer this question, many empirical equations have been proposed [3, 15, 31, 41]. Nonetheless, they have been demonstrated with low efficiency and accuracy in other areas [10, 24, 44, 48].

To achieve better accuracy, artificial intelligence (AI) became the best solution for predicting PPV so far. It was not only applied in mine blasting but also in many other areas of the life [2, 37–39, 46, 47, 49]. Indeed, [4] applied the artificial neural network (ANN) and k-nearest neighbors (KNN) models and combine them together to predict PPV with a promising result. [42] also applied an ANN model to predict PPV in an iron ore mine of Iran with the determination coefficient (R^2) of 0.957. A similar approach with the application of ANN was also conducted by [35] for predicting PPV. [27] applied the classification and regression tree (CART) as a rule-based method to predict PPV with high accuracy. [6] considered a metaheuristic algorithm, i.e., imperialist competitive algorithm (ICA), for predicting PPV with the support of various forms of equations. Finally, the best ICA model was found with the quadric form. [45] also combined the particle swarm optimization (PSO) and extreme gradient boosting machine (XGBoost), named as PSO-XGBoost to predict PPV with high reliability was confirmed. In addition, many similar studies with various models were proposed to deal with this problem [20–23, 26, 28, 30, 32].

Although many AI models have been proposed to predict PPV, however, in this study, a new machine learning algorithm, namely extra trees ensemble (ETE), was introduced to predict PPV. It is worth noting that this algorithm has not been applied to predict PPV before, and its performance was evaluated and compared to the random forest (RF) model.

2 Extra Trees Ensemble

ETE is an ensemble machine learning model based on the supervised learning technique [33]. It is also preferred to as the extremely randomized trees model for both regression and classification problems [18]. ETE was developed as an extension version of the RF model with the aims to overcome the overfitting.

Similar to the RF algorithm, ETE uses a random subsets to train the base models, and finally, the predictions are combined as a data frame for the outcome predictions [25]. However, the ETE selects the best feature by randomly in splitting the node. Regarding the structure, ETE consists of a number of decision trees, and each tree composed of a root node, split nodes, and leaf nodes (Fig. 1). Given a dataset X , at the root node, the ETE splits the dataset into random subsets of features. Each subset is considered as a split/child node, and this procedure is repeated until reaching a leaf

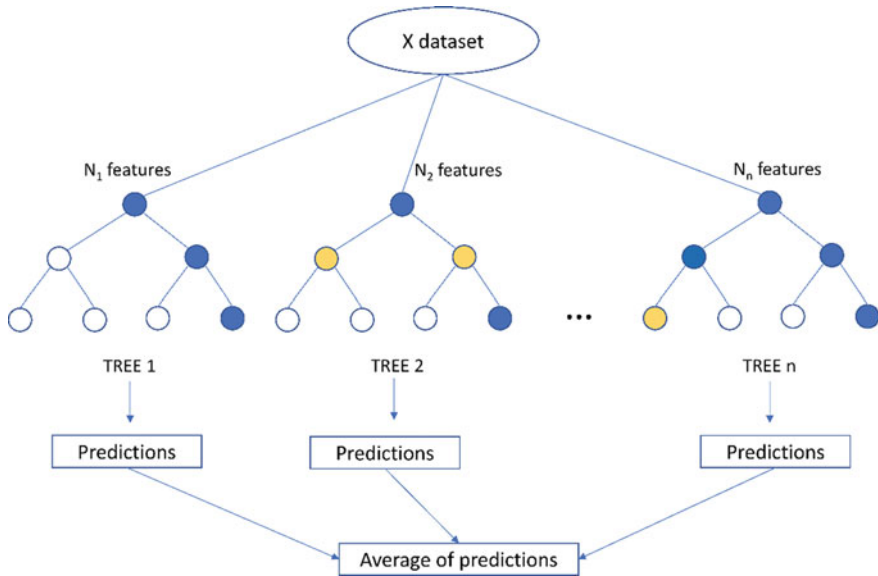


Fig. 1 ETE structure for regression problems

node. In each tree, the outcome predictions are calculated. Finally, they are combined from different trees and the average of predictions is taken into account as the official prediction of the model for regression problems. For classification problems, the majority voting of different classes is considered as the official predicted label.

In the ETE, three important parameters can be considered during developing the model, including the number of trees, number of features to select randomly, and minimum number of samples required for splitting. One of the robust advantages of the ETE is the ability to reduce bias and variance error based on the original training dataset and the selection of the cut-point and the explicit randomization of the subset of attributes [43]. In this study, the ETE algorithm was considered to predict PPV in mine blasting.

3 Dataset

To diagnose the performance of the ETE model in predicting PPV, a set of blasts in an open-pit copper mine in Vietnam was collected with a total of 300 blasting events. Ten independent variables were considered to predict PPV, including the diameter of borehole (D_{bh}), bench height (H), the length of borehole (L_{bh}), rock hardness (f), powder factor (PF), burden (B), spacing (S), stemming (ST), maximum explosive charged per delay (MEC), monitoring distance (D). The dataset is summarized in Table 1. In addition, the histogram of the variables are analyzed in Fig. 2. As depicted

Table 1 Summary of the blasting dataset used

D _{bh}	H	L _{bh}	f	PF	B
Min.:230.0	Min.:11.3	Min.:12.50	Min.:10.00	Min.:0.4060	Min.: 5.900
1st Qu.:230.0	1st Qu.:11.4	1st Qu.:12.90	1st Qu.:11.00	1st Qu.:0.5000	1st Qu.: 7.500
Median:230.0	Median:11.5	Median:13.00	Median:12.00	Median:0.5310	Median: 7.900
Mean:239.7	Mean:11.5	Mean:13.01	Mean:11.72	Mean:0.5215	Mean: 7.888
3rd Qu.:250.0	3rd Qu.:11.6	3rd Qu.:13.10	3rd Qu.:12.50	3rd Qu.:0.5550	3rd Qu.: 8.300
Max.:250.0	Max.:11.8	Max.:13.50	Max.:13.00	Max.:0.6140	Max.:10.300
S	ST	MEC	D	PPV	–
Min.:5.200	Min.:6.100	Min.:191.0	Min.:146.7	Min.: 7.10	
1st Qu.:6.900	1st Qu.:6.300	1st Qu.:288.8	1st Qu.:208.7	1st Qu.:10.60	
Median:7.300	Median:6.400	Median:319.0	Median:231.2	Median:11.60	
Mean:7.334	Mean:6.386	Mean:328.3	Mean:236.1	Mean:11.58	
3rd Qu.:7.800	3rd Qu.:6.500	3rd Qu.:362.2	3rd Qu.:255.4	3rd Qu.:12.60	
Max.:9.600	Max.:6.600	Max.:507.0	Max.:346.3	Max.:16.20	

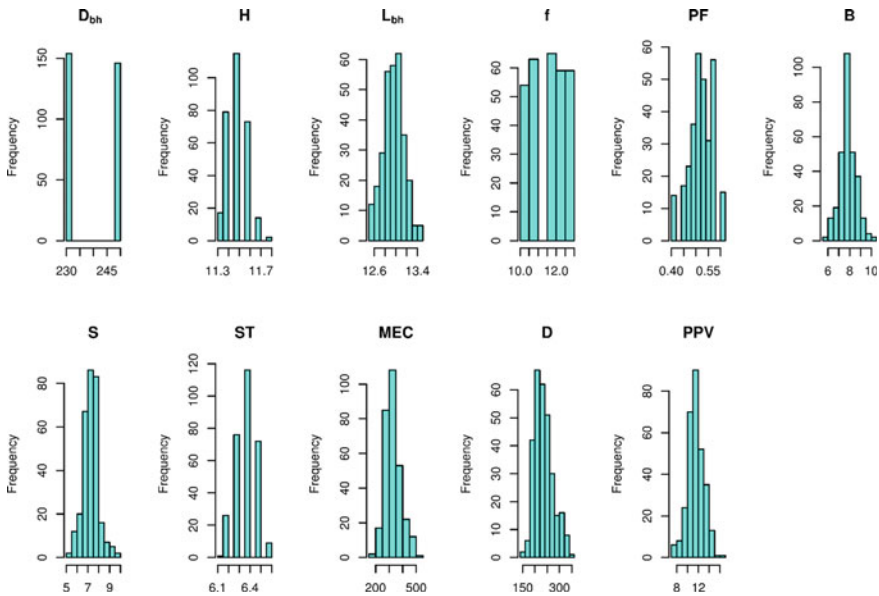


Fig. 2 Histogram of the blasting dataset

in Fig. 2, the frequency, the range of values, and the shapes of the variables were considered. Accordingly, most of the variables seem not to be normal datasets except the B variable. Therefore, data normalization is necessary to avoid overfitting of the models and improving the learning rate.

4 Results and Discussion

In this study, the ETE algorithm was introduced as the new approach to predict PPV. Due to the similar mechanisms compared to the RF algorithm; therefore, the ETE model was compared with the RF model in terms of PPV predictions. Prior to developing the models, the dataset was divided into two sections: 70% of the whole dataset was used for training the models, 30% of the dataset was used for testing the models. The standard scaling method was used to normalize the dataset in the range of 0 to 1.

For the development of the ETE model, the number of estimators (*n_estimators*), the maximum depth of the tree (*max_depth*), the minimum number of samples required to split an internal node (*min_samples_split*), the minimum number of samples required to be at a leaf node (*min_samples_leaf*), and the number of features (*max_features*) were used to control the accuracy of the ETE model. They were determined by a grid search technique through the RMSE objective function with 3 repeats and tenfold cross-validation.

Similar to the ETE model, the RF model was developed based on the same techniques with the same parameters were used to control the accuracy of the model. Finally, the best ETE and RF models were defined, and the testing dataset was used to evaluate the performance of these models, as shown in Table 2. Herein, MAE (mean absolute error), RMSE (root-mean-squared error), and R^2 (determination coefficient) were used as the metrics to evaluate the performance of the models.

Based on the results in Table 2, we can see that the ETE is more superior to the RF model in both training and testing datasets. Whereas the RF model only obtained an MAE of 0.240 and 0.303, RMSE of 0.350 and 0.573, R^2 of 0.933 and 0.905 on the training and testing phases, respectively, the ETE model obtained higher performance with an MAE of 0.190 and 0.232, RMSE of 0.248 and 0.424, R^2 of 0.966 and 0.948 on the training and testing phases, respectively.

As mentioned above, the main different between the ETE and RF models is the selection of the best feature by randomly in splitting the node. This stage helped the ETE model got better decision trees, as well as the outcome predictions from the generated decision trees. In addition, whereas the RF model used the bootstrap to train the decision trees, the ETE used the whole training dataset with the best feature to train the decision trees. Therefore, the ETE model is called as the extension version of the RF model, and its performance is much better than the RF model. Considering the convergence of the ETE model, the regression graph of the ETE model on the testing dataset was investigated and compared to the RF model, as shown in Fig. 3.

Table 2 Performance of the ETE and RF models for predicting PPV

Model	Train			Test		
	MAE	RMSE	R^2	MAE	RMSE	R^2
ETE	0.190	0.248	0.966	0.232	0.424	0.948
RF	0.240	0.350	0.933	0.303	0.573	0.905

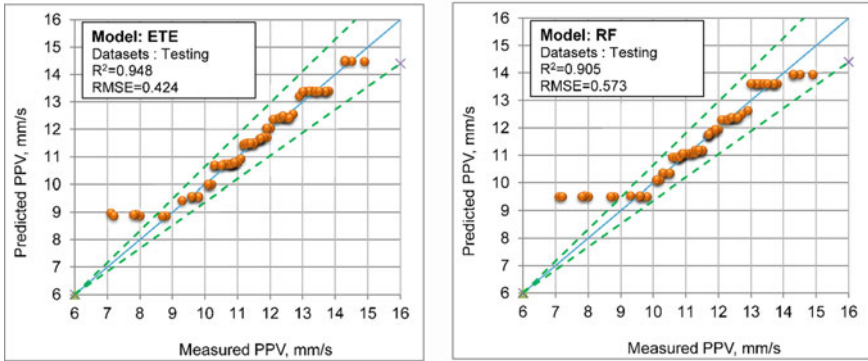


Fig. 3 Regression of the ETE and RF models on the testing dataset

The visualizations in Fig. 3 shows that the convergence of the ETE model is much better than the RF model, although the style of the plots seem to be similar. From an accuracy point of view, the ETE model provided higher accuracy than the RF model with more data points on and near the regression line, even though the data points are outside of the 80% confident level.

Similar to the RF model, the ETE model also composed of the feature importance analysis. This feature shows which variables are importance for the models in predicting PPV. In other words, it is used for feature selection or sensitivity analysis of the input variables. In this study, we diagnosed this feature of the ETE model and compared to the RF model to understand why the ETE model is better than the RF model in predicting PPV, as shown in Fig. 4.

It is of interest to see that whereas the ETE model appreciated four variables for predicting PPV, including f, PF, MEC, and D, the RF model appreciated only three

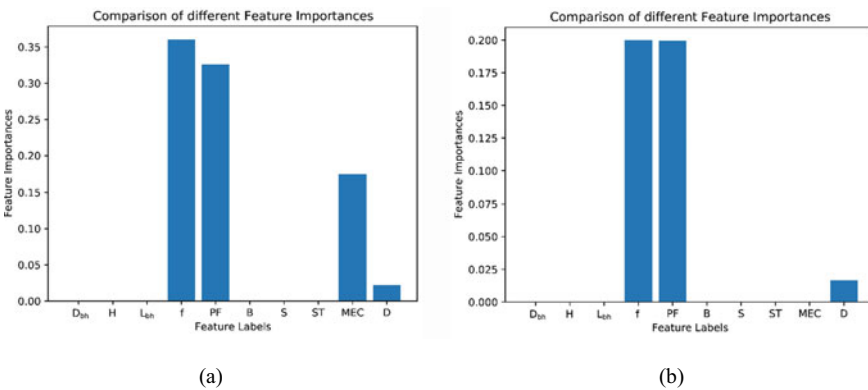


Fig. 4 Comparison of the feature importance of the ETE and RF models for predicting PPV **a** The feature importance analyses by the ETE model; **b** The feature importance analyses by the RF model

variables, including *f*, PF, and *D*. In other words, the RF model did not use the MEC variable in predicting PPV. Meanwhile, this variable was recommended by many previous researchers that have a significant effect on PPV [1, 4, 5, 8, 9, 11, 13, 14, 16, 17, 19, 21, 28–30]. Thus, the ETE model yielded better performance than the RF model in predicting PPV, and it is agreement with the previous discussion.

5 Conclusion

Blasting is an indispensable stage in open pit mines and it is the most effectiveness method so far. Although the efforts of researchers around the world have been adopted to predict PPV induced by mine blasting with promising results; however, the new techniques in this field are still necessary to improve the accuracy of the previous models. This study is, therefore, to introduce a new approach with the extension version of the RF model (i.e., ETE model) for predicting PPV with promising results. The accuracy of the ETE model was proved through the RF's performance and it obtained a better accuracy in predicting PPV. The convergence and feature importance of the ETE model was also considered and evaluated and they showed that the ETE model provided higher convergence than those of the RF model. Furthermore, the feature importance of the ETE model also better than the RF model when selected four parameters in developing the PPV predictive model (e.g., *f*, PF, MEC, and *D*). Meanwhile, the RF model selected only three parameters for this task, including *f*, PF, and *D*). As a conclusion, the ETE is a good model for predicting PPV induced by mine blasting, and it should be used in practical engineering. Advanced techniques/models based on the ETE model is also an interesting problem in future works in this field.

Acknowledgments This research is funded by Vietnam National Foundation for Science and Technology Development (NAFOSTED) under grant number 105.99-2019.309.

References

1. Abbaszadeh A, Ashoghi R (2018) Optimized developed artificial neural network-based models to predict the blast-induced ground vibration. *Innov Infrastruct Sol* 3:1–10
2. Ahmed AN, Van Lam T, Hung ND, Van Thieu N, Kisi O, El- A (2021) A comprehensive comparison of recent developed meta-heuristic algorithms for streamflow time series forecasting problem. *Appl Soft Comput* 105:107282. <https://doi.org/10.1016/j.asoc.2021.107282>
3. Ambraseys N, Hendron A (1968) Dynamic behavior of rock masses in rock mechanics in engineering practice (KG Stagg & OC Zienkiewicz, Eds.). John Wiley and Sons, New York, pp 203–207
4. Amiri M, Amnieh HB, Hasanipناه M, Khanli LM (2016) A new combination of artificial neural network and K-nearest neighbors models to predict blast-induced ground vibration and air-overpressure. *Eng Comput* 32(4):631–644

5. Armaghani DJ, Hajihassani M, Mohamad ET, Marto A, Noorani S (2014) Blasting-induced flyrock and ground vibration prediction through an expert artificial neural network based on particle swarm optimization. *Arab J Geosci* 7(12):5383–5396
6. Armaghani DJ, Hasanipanah M, Amnieh HB, Mohamad ET (2018) Feasibility of ICA in approximating ground vibration resulting from mine blasting. *Neural Comput Appl* 29(9):457–465
7. Armaghani DJ, Momeni E, Abad SVANK, Khandelwal M (2015) Feasibility of ANFIS model for prediction of ground vibrations resulting from quarry blasting. *Environ Earth Sci* 74(4):2845–2860
8. Arthur CK, Temeng VA, Ziggah YY (2019) Multivariate Adaptive Regression Splines (MARS) approach to blast-induced ground vibration prediction. *Int J Mining Reclam Environ* 34(3):198–222. <https://doi.org/10.1080/17480930.2019.1577940>
9. Bakhtavar E, Abdollahisharif J, Ahmadi M (2017) Reduction of the undesirable bench-blasting consequences with emphasis on ground vibration using a developed multi-objective stochastic programming. *Int J Mining Reclam Environ* 31(5):333–345
10. Bayat P, Monjezi M, Rezakhah M, Armaghani DJ (2020) Artificial neural network and firefly algorithm for estimation and minimization of ground vibration induced by blasting in a mine. *Nat Res Res* 29(6):4121
11. Bui XN, Choi Y, Atrushkevich V, Nguyen H, Tran QH, Long NQ, Hoang HT (2019) Prediction of blast-induced ground vibration intensity in open-pit mines using unmanned aerial vehicle and a novel intelligence system. *Nat Res Res* 29(2):771–790. <https://doi.org/10.1007/s11053-019-09573-7>
12. Bui X-N, Choi Y, Atrushkevich V, Nguyen H, Tran Q-H, Long NQ et al (2020) Prediction of blast-induced ground vibration intensity in open-pit mines using unmanned aerial vehicle and a novel intelligence system. *Nat Resour Res* 29(2):771–790. <https://doi.org/10.1007/s11053-019-09573-7>
13. Bui XN, Jaroonpattanapong P, Nguyen H, Tran QH, Long NQ (2019) A novel hybrid model for predicting blast-induced ground vibration based on k-nearest neighbors and particle swarm optimization. *Sci Rep* 9:1–14
14. Ding Z, Nguyen H, Bui X-N, Zhou J, Moayedi H (2019) Computational intelligence model for estimating intensity of blast-induced ground vibration in a mine based on imperialist competitive and extreme gradient boosting algorithms. *Nat Res Res* 29:751–769. <https://doi.org/10.1007/s11053-019-09548-8>
15. Duvall WI, Petkof B (1958) Spherical propagation of explosion-generated strain pulses in rock. US Department of the Interior, Bureau of Mines, vol 5481–5485
16. Fang Q, Nguyen H, Bui XN, Nguyen- T (2019) Prediction of blast-induced ground vibration in open-pit mines using a new technique based on imperialist competitive algorithm and M5 rules. *Nat Res Res* 29:791–806. <https://doi.org/10.1007/s11053-019-09577-3>
17. Faradonbeh RS, Monjezi M (2017) Prediction and minimization of blast-induced ground vibration using two robust meta-heuristic algorithms. *Eng Comput* 33(4):835–851
18. Geurts P, Ernst D, Wehenkel L (2006) Extremely randomized trees. *Mach Learn* 63(1):3–42
19. Hajihassani M, Armaghani DJ, Marto A, Mohamad ET (2015) Ground vibration prediction in quarry blasting through an artificial neural network optimized by imperialist competitive algorithm. *Bull Eng Geol Env* 74(3):873–886
20. Hasanipanah M, Monjezi M, Shahnazar A, Armaghani DJ, Farazmand A (2015) Feasibility of indirect determination of blast induced ground vibration based on support vector machine. *Measurement* 75:289–297
21. Hasanipanah M, Naderi R, Kashir J, Noorani SA, Qaleh AZA (2017) Prediction of blast-produced ground vibration using particle swarm optimization. *Engineering with Computers* 33(2):173–179
22. Hosseini SA, Tavana A, Abdolahi SM, Darvishmaslak S (2019) Prediction of blast-induced ground vibrations in quarry sites: a comparison of GP, RSM and MARS. *Soil Dyn Earthq Eng* 119:118–129. <https://doi.org/10.1016/j.soildyn.2019.01.011>

23. Huang J, Koopialipour M, Armaghani DJ (2020) A combination of fuzzy Delphi method and hybrid ANN-based systems to forecast ground vibration resulting from blasting. *Sci Rep* 10(1):19397. <https://doi.org/10.1038/s41598-020-76569-2>
24. Jahed D, Kumar D, Samui P, Hasanipanah M, Roy B (2020) A novel approach for forecasting of ground vibrations resulting from blasting: modified particle swarm optimization coupled extreme learning machine. *Eng Comput* 34:3221–3235. <https://doi.org/10.1007/s00366-020-00997-x>
25. John V, Liu Z, Guo C, Mita S, Kidono K (2015) Real-time lane estimation using deep features and extra trees regression. In: *Image and video technology*. Springer, Heidelberg, pp 721–733
26. Ke B, Nguyen H, Bui X-N, Costache R (2021) Estimation of ground vibration intensity induced by mine blasting using a state-of-the-art hybrid autoencoder neural network and support vector regression model. *Nat Resour Res*. <https://doi.org/10.1007/s11053-021-09890-w>
27. Khandelwal M, Armaghani DJ, Faradonbeh RS, Yellishetty M, Majid MZA, Monjezi M (2017) Classification and regression tree technique in estimating peak particle velocity caused by blasting. *Eng Comput* 33(1):45–53
28. Khandelwal M, Kumar DL, Yellishetty M (2011) Application of soft computing to predict blast-induced ground vibration. *Eng Comput* 27(2):117–125
29. Khandelwal M, Singh T (2006) Prediction of blast induced ground vibrations and frequency in opencast mine: a neural network approach. *J Sound Vib* 289(4):711–725
30. Kumar R, Choudhury D, Bhargava K (2016) Determination of blast-induced ground vibration equations for rocks using mechanical and geological properties. *J Rock Mech Geotech Eng* 8(3):341–349
31. Langefors U, Kihlstrom B (1963) *The Modern Techniques of Rock Blasting*. JohnWiley and Sons Inc., New York
32. Lawal AI, Kwon S, Hamed OS, Idris MA (2021) Blast-induced ground vibration prediction in granite quarries: an application of gene expression programming, ANFIS, and sine cosine algorithm optimized ANN. *Int J Min Sci Technol* 31(2):265–277
33. Maier O, Wilms M, von der Gablentz J, Krämer UM, Münte TF, Handels H (2015) Extra tree forests for sub-acute ischemic stroke lesion segmentation in MR sequences. *J Neurosci Methods* 240:89–100
34. Monjezi M, Ahmadi M, Sheikhan M, Bahrami A, Salimi A (2010) Predicting blast-induced ground vibration using various types of neural networks. *Soil Dyn Earthq Eng* 30(11):1233–1236
35. Monjezi M, Ghafurikalajahi M, Bahrami A (2011) Prediction of blast-induced ground vibration using artificial neural networks. *Tunn Undergr Space Technol* 26(1):46–50
36. Nguyen H, Bui X-N (2020) Soft computing models for predicting blast-induced air overpressure: a novel artificial intelligence approach. *Appl Soft Comput* 92:106292. <https://doi.org/10.1016/j.asoc.2020.106292>
37. Nguyen T, Hoang B, Nguyen G, Nguyen BM (2020) A new workload prediction model using extreme learning machine and enhanced tug of war optimization. *Procedia Comput Sci* 170:362–369
38. Nguyen T, Nguyen BM, Nguyen G (2019) Building resource auto-scaler with functional-link neural network and adaptive bacterial foraging optimization. In: *International Conference on Theory and Applications of Models of Computation*. Springer, Heidelberg, pp 501–517
39. Nguyen T, Nguyen G, Nguyen BM (2020) EO-CNN: an enhanced CNN model trained by equilibrium optimization for traffic transportation prediction. *Procedia Comput Sci* 176:800–809. <https://doi.org/10.1016/j.procs.2020.09.075>
40. Raina A, Murthy V (2016) Importance and sensitivity of variables defining throw and flyrock in surface blasting by artificial neural network method. *Current Sci* (00113891) 111(9):1524
41. Roy P (1993) Putting ground vibration predictions into practice. *Colliery Guard* 241(2):63–67
42. Saadat M, Khandelwal M, Monjezi M (2014) An ANN-based approach to predict blast-induced ground vibration of Gol-E-Gohar iron ore mine, Iran. *J Rock Mech Geotech Eng* 6(1):67–76
43. Saeed U, Jan SU, Lee Y-D, Koo I (2021) Fault diagnosis based on extremely randomized trees in wireless sensor networks. *Reliab Eng Syst Saf* 205:107284. <https://doi.org/10.1016/j.res.2020.107284>

44. Yu Z, Shi X, Zhou J, Gou Y, Huo X, Zhang J et al (2020) A new multikernel relevance vector machine based on the HPSOGWO algorithm for predicting and controlling blast-induced ground vibration. *Eng Comput* 28:1–16
45. Zhang X, Nguyen H, Bui X-N, Tran Q-H, Nguyen D-A, Bui DT et al (2020) Novel soft computing model for predicting blast-induced ground vibration in open-pit mines based on particle swarm optimization and XGBoost. *Nat Resour Res* 29(2):711–721
46. Nguyen Duong Hong HT, Nguyen Doan Thi VVT, Trung TPV (2021) Use of Artificial Neural Networks in predicting rate of penetration and optimization weight on bit for several wells in Nam Rong - Doi Moi field Vietnam. *J Min Earth Sci* 62(3a):37–47. [https://doi.org/10.46326/JMES.2021.62\(3a\).05](https://doi.org/10.46326/JMES.2021.62(3a).05)
47. Pham TK, Nguyen TD, Van Le C, Van Nguyen T (2020) Analyzing customer sentiments using K-means algorithm. *J Min Earth Sci* 61(5):145–150. <https://doi.org/10.46326/JMES.KTQTKD2020.19>
48. Nguyen H, Bui NX, Tran HQ, Le GHT (2020) A novel soft computing model for predicting blast - induced ground vibration in open - pit mines using gene expression programming. *J Min Earth Sci* 61(5):107–116. <https://doi.org/10.46326/JMES.KTLT2020.09>
49. Vu DH, Nguyen HT (2021) Estimation of shale volume from well logging data using Artificial Neural Network. *J Min Earth Sci* 62(3):46–52. [https://doi.org/10.46326/JMES.2021.62\(3\).06](https://doi.org/10.46326/JMES.2021.62(3).06)

Managing Slope Stability Hazards in Volcanically Active Environments



Wayne H. Scott

Abstract New Zealand is an island country of 5 million people in the south-western Pacific Ocean. It consists of two main landmasses - the North Island and the South Island. The country's varied topography and sharp mountain peaks, including the Southern Alps, owe much to tectonic uplift and volcanic eruptions. Slope stability is an issue for many parts of New Zealand. Steep slopes, tectonics and rainfall are the main causes of slope failure.

New Zealand has between 600–1,100 active quarries, most of them very small. Many operate intermittently based on seasonal or local demand and many lay dormant for periods up to 2 years. This is particularly relevant to hazards associated with slope stability, particularly in weathered rock at quarries in areas of high rainfall.

Slope failures can occur at mines and quarries in highly weathered faces, loosely consolidated excavated overburden faces, overburden dumps, product stockpiles, and tailings dam embankments. At sites where the risk of slope instability is high, it is critical that cracks, faces, tip heads and stockpiles are monitored for movement to ensure the protection of personnel, equipment and facilities.

If material does fail, the mine/quarry should have a pre-planned response to the movement. If a slope failure is imminent, personnel must immediately be pulled out of the hazardous area.

In New Zealand, the majority of mines and quarries are required to have Ground Control Management Plans (GCMP). The level of detail in these plans is determined through risk assessment of the slope stability hazards. It is important to consider the exposure time of personnel to potentially unstable walls, potential for short-term changes in ground conditions, the potential for long-term changes in ground conditions, and loose rock rill on berms that may affect the "catch" capability of falling rock.

Keywords Tectonic uplift · Volcanic eruptions · Ground Control Management Plans · Slope stability hazards

W. H. Scott (✉)

Aggregate & Quarry Association of New Zealand, Wellington, New Zealand

e-mail: wayne@aqa.org.nz

1 Introduction

New Zealand is an island country of 5 million people in the southwestern Pacific Ocean. It consists of two main landmasses—the North Island and the South Island, and more than 700 smaller islands, covering a total area of 268,021 square kilometres. New Zealand is approximately 2,000 kms (1,200 mi) east of Australia across the Tasman Sea and 1,000 kms (600 mi) south of the islands of New Caledonia, Fiji, and Tonga. The country's varied topography and sharp mountain peaks, including the Southern Alps, owe much to tectonic uplift and volcanic eruptions.

New Zealand has 12 active volcanos, all in and around the North Island [2]. The most active volcano, Whakaari/White Island erupted in December 2019 fatally wounding 22 people and injuring a further 25. Earthquakes also occur in New Zealand because we are located on the boundary of two of the world's major tectonic plates – the Pacific Plate and the Australian Plate. This is the Pacific Mobile Belt or "Ring of Fire" and the activity results from the structure of the Earth's crust. The crust is made up of a number of segments called plates, which move relative to one another in response to forces deep within the Earth. The plates may rub past one another, one may be forced down below another, or they may buckle at the edges as they meet head on. Wherever there is a plate boundary there is geological activity of a volcanic or tectonic nature.

Every year GNS Science detects over 15,000 earthquakes in New Zealand. About 100–150 of these quakes are large enough to be felt, the others we only know about because they are recorded by seismographs [3]. These plates are colliding with huge force, causing one to slowly grind over, under or alongside the other. As the brittle crust gives way under the pressure, a fault ruptures and an earthquake is unleashed. As violent and horrific as they can be, earthquakes have helped create New Zealand's varied landscape through complex processes of mountain building and erosion.

Volcanoes are also formed along the plate boundary. Volcanism has its origins deep within the Earth's interior. Vast convection cells in the upper mantle generate basaltic magma at mid-ocean ridges and drive cold basaltic oceanic crust away from the ridge crests and down into the mantle at subduction zones (Fig. 1).

2 Aggregate Geology [5]

Rock units are divided into three major classes based on their mode of formation.

Sedimentary rocks result from deposition and consolidation of particles mostly eroded from an adjacent land area. Different sources of material and depositional environments result in different types of sedimentary rock, such as sandstone, mudstone, and limestone. Most New Zealand sedimentary rocks are mudstone and

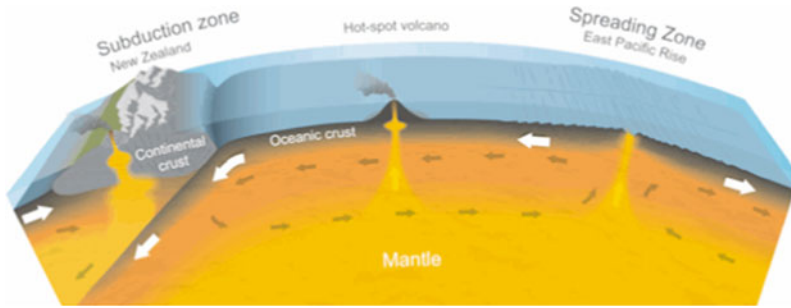


Fig. 1 Volcanos at a plate boundary [4]

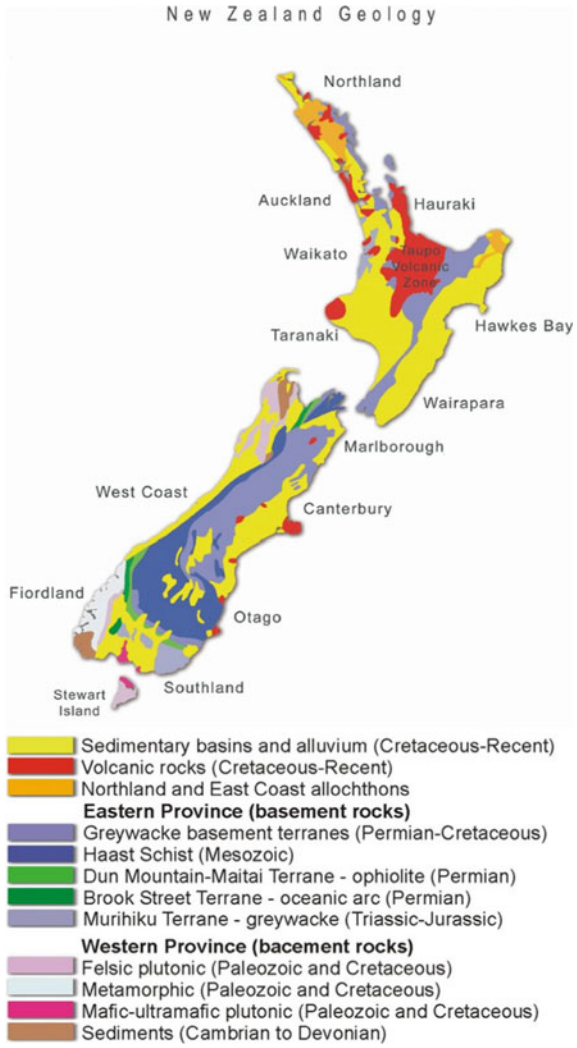
sandstone that were deposited beneath the sea. A sedimentary rock derived from ejected volcanic fragments (e.g., ash) is called tuff. Some sedimentary rocks, such as chert and certain limestones, are chemical precipitates.

Igneous rocks form when molten rock (magma) from deep within the Earth’s crust cools after being intruded into existing rocks or sediments, or after being extruded on to the surface. The rocks are classified as acid, intermediate or basic, according to the amount of silica they contain. Acid (silica-rich) igneous rocks are light in colour, whereas the basic (silica-poor) igneous rocks are darker. There is a secondary two-fold division of igneous rocks into: plutonic rocks which are intruded at depth, cool slowly, and are coarse grained (granite is an example of an acid plutonic rock, diorite is intermediate, and gabbro is basic); and volcanic rocks which are extruded on to the land surface, or beneath the sea, and cool quickly to form fine grained and sometimes glassy rocks. Acid volcanic rocks include rhyolite, ignimbrite and pumice, the last two being formed when the lava was particularly gaseous and explosive in nature. Common intermediate and basic lavas are andesite and basalt respectively.

Metamorphic rocks such as schist and gneiss, have been recrystallised under conditions of high temperature, pressure, or both. They vary depending on the nature of the parent rock (either sedimentary or igneous) and the intensity and type of metamorphism. Characteristic minerals form under certain conditions of temperature and pressure. For example, chlorite tends to crystallise in rocks metamorphosed at low to moderate temperatures and pressures, and biotite and garnet at somewhat higher temperatures and pressures. Gneiss forms at deep levels in the crust under conditions of high temperature and pressure.

New Zealand has a large supply of quality aggregates (endowment) but it is unevenly distributed geo-spatially or in quality (refer to Fig. 2), and not necessarily close to demand for infrastructure, housing etc. In addition, as urban centres have grown, environmental and cultural sensitivities have increased, aggregate resources have progressively over time become more difficult to access. According to [1], there

Fig. 2 Geological map of New Zealand (Source: Institute of Geological and Nuclear Sciences)



are four main sources of aggregates in New Zealand, out of which the first two are virgin hard rock quarry sources:

- Greywacke – makes up to 25% of the exposed rocks in New Zealand and supplies source rock for 75% of aggregates produced in the country. It is prominently found in the South Island although there are also significant resources in the North Island.

- Igneous rocks or volcanic rocks – a source rock for 25% of aggregates produced in the country. They are predominantly found in the North Island, especially in Northland, Bay of Plenty and Taranaki region.
- Gravels and conglomerates – sediments composed of pebble to boulder-sized rock fragments, sourced mainly from river or beach beds.
- Artificial aggregates – Slags produced mainly from iron and steel manufacturing (e.g. melter slag), fly ash and calcined bauxite.

3 New Zealand Quarry Industry

New Zealand is fortunate to have large areas of well-indurated (hard) rock and deposits of gravel throughout the country that can be utilised for aggregate to support infrastructure development. Over much of the country, this material is only weakly weathered and exposed at or near the surface, providing access to good-quality resources of rock. Both in situ hard rock and unconsolidated boulder, gravel, sand and clay deposits are quarried around the country, and a wide range of rock types are mined, including greywacke, sandstone, basalt, andesite and limestone, for a variety of purposes.

Aggregate resources in New Zealand can be largely grouped into two classes:

- **hard rock**, e.g. greywacke, sandstone, basalt and limestone; and
- **gravel**, e.g. unconsolidated deposits such as river gravels, sand and boulders.

These deposit types are distributed throughout New Zealand (Fig. 2), but quarries that extract them are typically located close to major cities and roads and clustered to meet demand. Hard rock quarries are usually located in areas of steeper terrain where un-weathered and indurated material can be accessed more easily from beneath unsuitable covering material, such as weathered overburden. Gravel quarries are typically located in river valleys and alluvial plains. Most gravel aggregate operations are limited in the depth they can extract material to by the local groundwater level, with only some exceptions where gravels are harvested from the active river channel.

New Zealand has between 600- 1,100 active quarries, most of them very small (see Fig. 3). Many operate intermittently based on seasonal or local demand and many lay dormant for periods up to 2 years. This is particularly relevant to hazards associated with slope stability, particularly in weathered rock at quarries in areas of high rainfall.

4 Slope Stability Hazards in New Zealand Quarries

“Experience shows that despite engineering solutions, natural processes ultimately determine whether a structure and the land it stands on fails or not. Determining the balance between allowing people to develop or use land and restricting their exposure

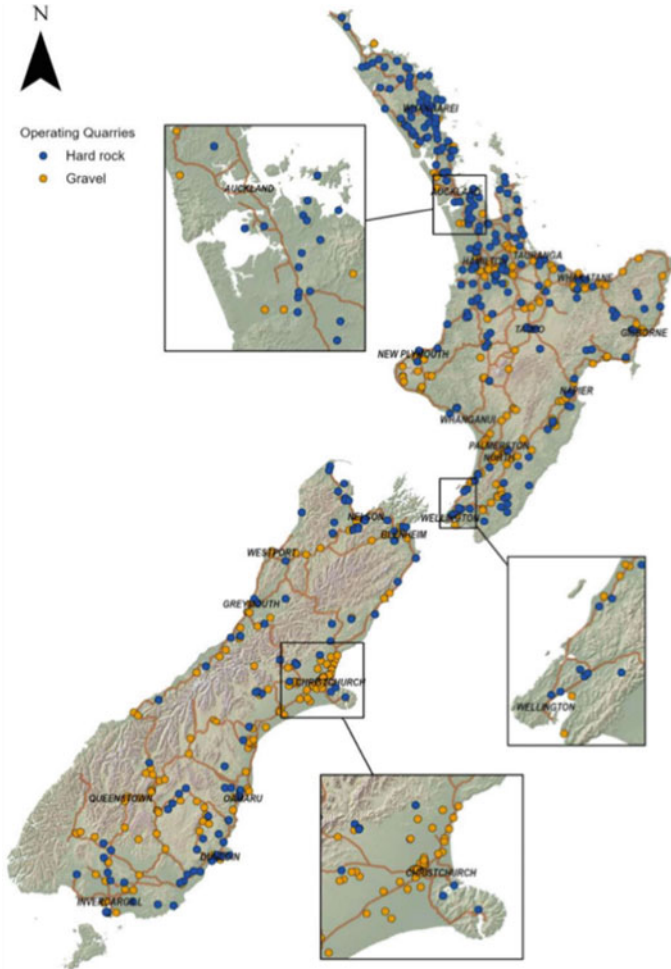


Fig. 3 New Zealand operating quarries reported by Inside Resources in 2020

to natural hazards in a sometimes rapidly changing landscape is complex” (CAENZ, 2007).

Slope stability is an issue for many parts of New Zealand. Steep slopes, tectonics and rainfall are the main causes of slope failure. However, the vulnerability of the land to slope failure can be increased by inappropriate use; thereby exposing people, property, and infrastructure to increased risk.

When quarry faces are exposed, relaxation of the rock occurs which may lead to loose material falling or rolling from the face.

The likelihood of rock falls and slope/batter instability increases when there is weak rock, bedding, joints, structures, blast damage, vehicle vibrations, crest loss, adverse weather (rainfall, wind) or inadequate design.

The following failures can occur in a mine or quarry:

- Planar failure
- Wedge failure
- Toppling failure
- Circular failure

4.1 Planar Failure

A planar failure occurs where a block moves downwards along a surface (Fig. 4).

An estimated two million tonnes of rock and rubble collapsed from the north wall of the Waihi mine in 2016. The high wall was being monitored at the time and no-one was in the pit (see Fig. 5). This site is also adjacent to the major fault line dissecting the North Island.

Fig. 4 Planar failure

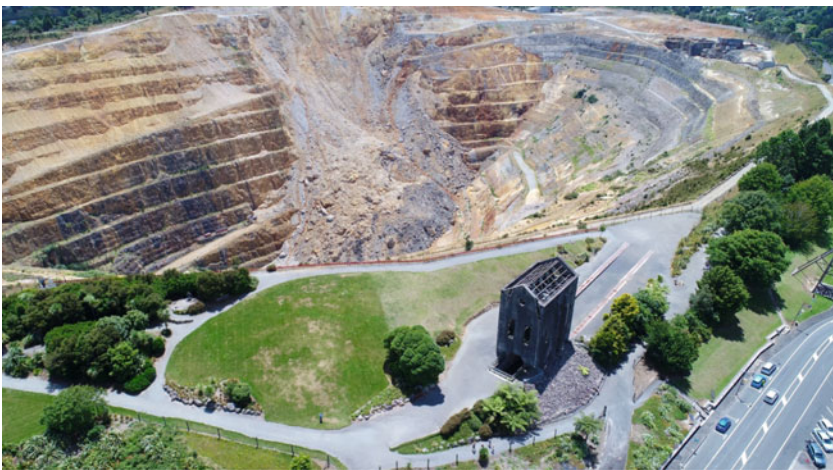
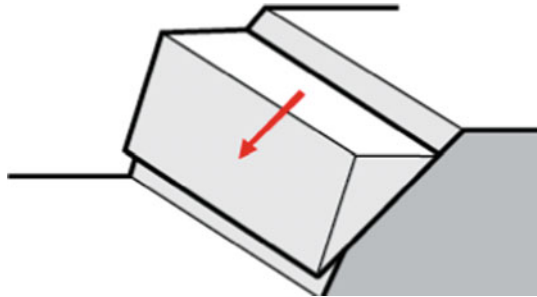
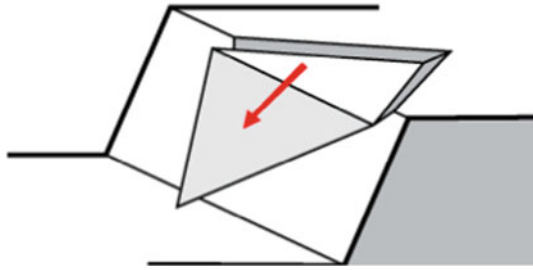
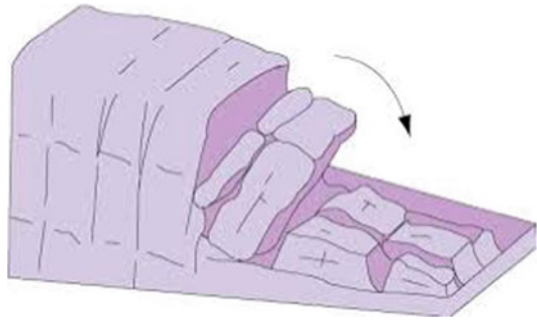


Fig. 5 Martha Mine planar failure 2016

Fig. 6 Wedge failure**Fig. 7** Toppling failure

4.2 *Wedge Failure*

A wedge forms when two intersecting surfaces (such as bedding, faults, joints) meet and the block moves downwards (Fig. 6).

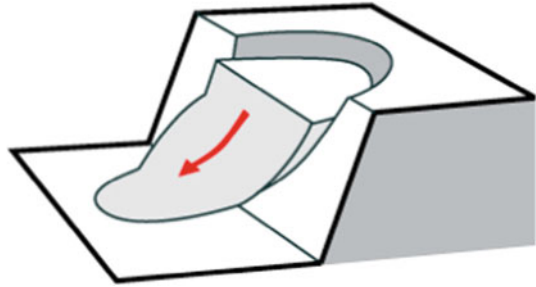
4.3 *Toppling Failure*

A toppling failure occurs as a result of vertical structures moving out and down due to lack of confinement (Fig. 7).

4.4 *Circular Failure*

A circular failure occurs when a mass of material moves in a downward direction leaving a circular shaped scour. It most often occurs in weak material when ground conditions become saturated. This is often referred to as slumping (Fig. 8).

Slope failures can occur at mines and quarries in highly weathered faces, loosely consolidated excavated overburden faces, overburden dumps, product stockpiles, and

Fig. 8 Circular failure

tailings dam embankments. There are a number of factors influencing the potential for failure including rock/soil mass strength, geological structures such as unconformities, the presence of weak planes, and the presence of water. Failures can also be initiated by vibration resulting from earthquakes.

A slope is not stable when driving forces (promoting downward movement of material e.g. gravity) overcome resisting forces (material shear strength) and the slope moves. These forces are impacted in New Zealand by the steep terrain, high rainfall and volcanic and seismic activity.

5 Monitoring for Slope Instability

At sites where the risk of slope instability is high, it is critical that cracks, faces, tip heads and stockpiles are monitored for movement to ensure the protection of personnel, equipment and facilities. Sites need to monitor any changes in the condition of benches and faces identifying such things as rocks on berms, roads and the floor, cracks in faces, crest loss and changes in water flow.

The formation of tension cracks at the top of a slope is an obvious sign of instability. Cracks form when slope material has moved toward the pit.

One of the most dangerous situations that can occur is an overhang.

Bulging material on a slope indicates creep or slow subsurface movement of the slope. Movement of trees at the crest of a slope can be an indicator of instability.

Fresh rubble at the toe or on the pit floor is an obvious indicator that instability has occurred. An effort must be made to determine which portion of the slope failed, and whether more material may fall.

Regular workplace inspections should be conducted and recorded so that potential "hot spots" of wall movement can be identified (refer Appendix 1 - Inspection checklist) [7]. The regularity of inspection will depend on the extent of movement, presence of rock falls etc. Inspections should be conducted after rainfall and earthquake events, and after prolonged periods of absence from the area.

There are a number of technologies available to monitor the stability of slopes, such as the global positioning system (GPS), the geographic information system (GIS), aerial photography, acoustic emissions and inclinometers. Each one of these

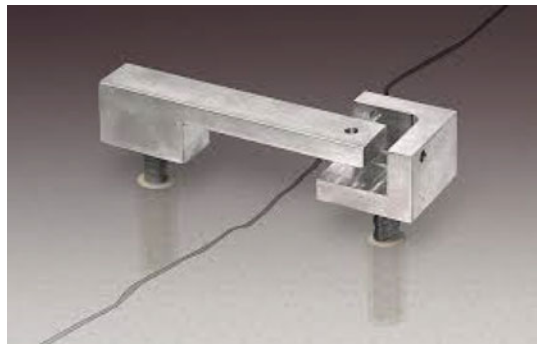
offers advantages against others, but at the same time also possesses different limitations.

Extensometers and crack meters are a useful means of measuring movement in cracks that appear on a bench. An extensometer is a device that is used to measure changes in the length of an object (refer Fig. 9). It is useful for stress–strain measurements and tensile tests. In its simplest form, a crack meter consists of pegs installed either side of the crack with the distance between the pegs measured at regular intervals to detect movement (refer Fig. 10).

Fig. 9 Extensometer



Fig. 10 Crack meter



6 Controls for Ground Failure

If material does fail, the mine/quarry should have a pre-planned response to the movement. If a slope failure is imminent, personnel must immediately be pulled out of the hazardous area.

Operating procedures should be in place to establish what level of movement will initiate evacuation, and how an evacuation would be communicated to workers.

Once a potential ground failure or slope instability has been identified, it is important to barricade off the area. Small scale rock falls may indicate larger scale ground instability. The following controls should be considered:

- Where practical, decrease bench heights and overall slope height and angle
- Increase catch bench width and height to as large as is practical
- Remove overhangs and other face hazards by blasting, scaling or cleaning faces. Ensure the use of appropriate type and size of equipment
- Place an adequate catch bund near the toe. This should be as large as possible to collect any falling material
- Create an adequate stand-off distance/exclusion zone near the toe
- Stabilise the toe by placing material against the face
- Establish procedures for safe entry to the pit following weather events or blasting

It is also important that there is adequate surface drainage away from the crest, safe blasting practices and blast damage minimisation, and operational procedures such as positioning the excavator cab way from the face when operating near a face.

6.1 Catch Bund

A catch bund is an important control to minimise exposure of workers to ground failure hazards and contain rock falls. The dimensions and position of the catch bund will depend on the size of the potential slope failure or rock fall. The area between the face and the bund wall should be sufficient in size to contain any rock fall.

6.2 Exclusion Zones

An exclusion zone is an effective way to separate workers from rock fall hazards. When determining an appropriate distance to position the exclusion zone from the face, consider loose rocks, cracks, water running from the face, back break from blasting, overhang, and factors such as earthquake risk, vehicle vibration, rainfall, and blasting.

The exclusion zone should be demarcated by bunding or some other form of delineation.

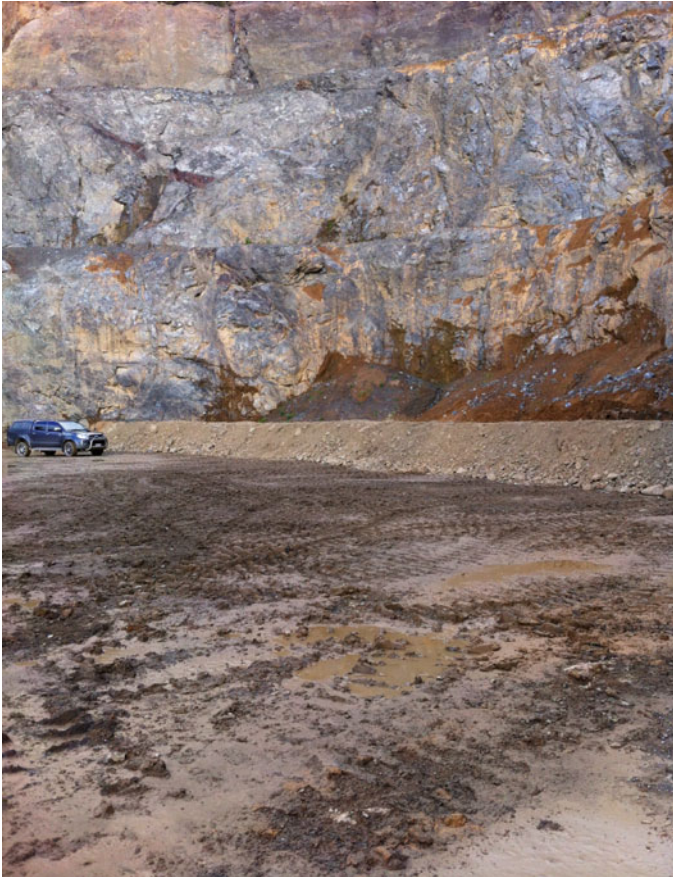


Fig. 11 Catch bund and exclusion zone at toe of slope

No work should be conducted, or vehicles parked, within exclusion zones (Fig. 11).

6.3 Design of Benches and Faces

Excavations, benches, and ponds should be properly designed, with:

- stable slope angles
- adequate benches
- bench widths at least half the face height, and not less than 3.5 m
- face heights suitable for the site conditions and excavation method
- faces that do not exceed the reach of the excavator

- faces scaled to control the risk of rock falls
- faces, at hard rock mines and quarries, and working benches in alluvial mines, that have not been undermined.

For mines, quarries and alluvials, an appraisal of the operation should also be done by a competent person to determine whether a geotechnical assessment is required. As a guide:

- For simple operations (e.g. shallow depth, soft material with faces less than 3.5 m, or competent rock with faces less than 15 m) the site should obtain a geotechnical appraisal by a competent person to determine that the face design is safe, adequate benching is in place, and confirm that a geotechnical assessment is not required.
- For complex operations (e.g. individual faces exceeding 15 m, overall excavation depth exceeding 30 m, fractured rock, disturbed geological structure) the site should obtain a geotechnical assessment by a competent person.

6.4 Ground Control Management Plans (GCMP)

In New Zealand, the majority of mines and quarries are required to have Ground Control Management Plans (GCMP). The level of detail in these plans is determined through risk assessment of the slope stability hazards however as a minimum the plan should address: [6]

- The geological structure and rock mass parameters
- Mine design and controls
- Ground monitoring systems
- Blasting considerations
- Surface or groundwater management
- Integration of the GCMP into the life-of-mine planning
- Risk management process
- Action plan for dealing with identified ground control issues
- Personnel role descriptions and responsibilities
- Training requirements for mine personnel with regards to ground awareness

It is important also to consider the exposure time of personnel to potentially unstable walls (e.g. when exploration drilling beneath pit walls), potential for short-term changes in ground conditions (e.g. earth tremors, rainfall, blasting), the potential for long-term changes in ground conditions (e.g. water seepage, weathering of the rock), and loose rock rill on berms that may affect the "catch" capability of falling rock.

When developing the GCMP, consideration should also be given to the size, shape and orientation of the excavation and geological controls (e.g. higher and steeper batters will require more significant berms to control/capture fallen ground),

the equipment and systems to be used for scaling or cleaning of batters and monitoring pit walls, the vertical and lateral distance between each mining area and the potentially unstable areas of the pit walls.

7 Conclusion

Working near faces can be hazardous due to rockfalls and slope failures. The best control for protecting people working near faces is a quarry/mine plan or design that has considered the site's particular geological and geotechnical characteristics. Planning for excavations requires a good understanding of ground conditions and identification of ways to avoid potential ground failure. As quarries and opencast mines develop over time, they usually get deeper and the overall slope angle becomes steeper which can increase the risk of rockfalls.

New Zealand's varied topography and sharp mountain peaks, including the Southern Alps, owe much to tectonic uplift and volcanic eruptions which add to the potential for slope instability and ground movement.

Regular inspections of faces, haul roads and working benches will identify small scale rockfalls and failures that may indicate larger scale ground instability.

It is important to recognise and manage potential rockfall hazards. All workers need to be able to recognise potential hazards and act accordingly. If in doubt about the stability of a face, barricade the area and seek technical assistance.

Appendix 1. Inspection checklist

Feature	Location	OK Y/N	Comment
Batters/Walls			
Constructed to design angle			
Face spalling or fretting			
Cracks/over hangs			
Toes maintained			
Water seepage			
Access ramp away from face			
Ramp bunded			
Blast damage			
Berms/Benches			
Design width achieved			
Crest loss			
Signs of instability			
Drainage adequate			
Pit surrounds			
Drainage away from pit			
Surface water ponding			
Windrows adequate			
Surface settlement or subsidence			
No environmental damage			
Road conditions			
Wide enough for vehicles			
Adequate passing areas			
Drainage adequate			
Roads in good condition			
Signage			
Access to site adequately sign posted			
Open pit hazard identified			
Exclusion zones			
Windrows/Catch bunds			
Catch berms installed			
Adequate height for rockfall			

Person Inspecting

Signature

Date

References

1. Black PM (2009) Geologic inventory of North Island aggregate resources: Influences on engineering materials properties. Mineral Wealth of North Island, Auckland. - NZTA TAR 19-03 National Supply and Demand for Aggregates in NZ, April 2021
2. Earthquake Commission GeoNet data 2021. <https://www.eqc.govt.nz/resilience-and-research/data-and-modelling/geonet/>
3. GNS Science NZ seismographic data. <https://www.gns.cri.nz/>
4. GNS Science Volcanic data. <https://www.gns.cri.nz/Home/Learning/Science-Topics/Volcanoes/Volcanoes-at-a-Plate-Boundary>
5. GNS Science Geology of New Zealand. <https://www.gns.cri.nz/Home/Our-Science/Land-and-Marine-Geoscience/Regional-Geology/The-Geology-of-New-Zealand>
6. Health and Safety at Opencast Mines, Alluvial Mines and Quarries Good Practice Guidelines November 2015. https://www.worksafe.govt.nz/search/SearchForm/?Search=good+practice+guideleins+mines+and+quarries&action_results=Go&Topic=&Industry=
7. MinEx – Extractives Health and Safety Council of New Zealand – Slope stability in opencast mines booklet. <https://www.minex.org.nz/regulations-and-guidelines/fact-sheets-booklets-and-cops/>

Management Strategy for Indian Housing Development Waste



Paramjeet Singh, Zainab Toyin Jagun, Dzurlkhanian Daud, Ajit Bhoslay, Satish Kumar Palniappan, and Ramesh Murlidhar Bhatawdekar

Abstract Housing development waste (HDW) comprises both construction and demolition waste. (define) HDW has been on the increase in India because raw materials and energy are consumed by India's housing development business due to the rise in population and the accompanying increase in the need for building/housing. Construction and demolition debris includes building material from debris and rubble from any civil structure being built or remodeled or repaired or torn down. Construction and demolition waste is among the most common types of waste generated in India. The Ministry of Environment, Forest, and Climate Change (MoEF&CC) notified the current India legislation on Waste Management Rules, 2016, on March 29th, 2016, to implement housing development and demolition waste prevention and recycling measures. However, there are insufficient tools to accelerate the development of waste recycling. As a result, it lacks resources that would allow Aggregates and Sand

P. Singh (✉)

Rise Eleven Delhi Waste Management Co., New Delhi, India
e-mail: pj.matharu@gmail.com

Z. T. Jagun · D. Daud

Department of Real Estate, Faculty of Built Environment and Surveying, Universiti Teknologi Malaysia, 81310 Skudai, Johor, Malaysia
e-mail: tjzainab@graduate.utm.my

D. Daud

e-mail: dzurll@utm.my

Z. T. Jagun

Department of Estate Management, College of Environmental Studies, Federal Polytechnic Offa, P.M.B 420, Offa, Kwara State, Nigeria

S. K. Palniappan · R. M. Bhatawdekar

Department of Mining Engineering, Indian Institute of Technology, Kharagpur, West Bengal 721302, India

A. Bhoslay

RMB Consultant, Thane 400610, India

R. M. Bhatawdekar

Department of Civil Engineering, Faculty of Engineering, 81310 Skudai, Johor Bahru, Malaysia

Manufacturing from Demolition Waste to grow more quickly and efficiently in the future. This study was conducted to determine the necessity of recycling factories that produce aggregates and sand from demolished concrete from housing development trash. Therefore, providing tools to accelerate the development of waste recycling.

Keywords Aggregates · Construction and demolition waste · Housing development · Recycling

1 Introduction

Housing is a fundamental human right as well as a requirement for earning a livelihood [32]. With India's population expected to reach 1.39 billion people (139 crores) in 2021, according to the most recent estimates from Unique Identification Aadhar India, which were updated in December 2020. Still, in the last 15 years, India has seen a significant increase in urbanization. An estimated 30 individuals move from rural to urban India per minute. In 2011, the urban population of India accounted for 30% of the country's total population [5]. This ratio is predicted to rise to 40% by 2030 when India's urban population would total 630 million people. Because of this rapid urbanization [21], cities and government agencies face challenges in housing development and construction waste management [15, 21]. There is an essential need for everyone to be able to exercise their right to Housing. [34], Housing in cities is currently short by roughly 10 million units, as reported. (M. S. [12] Due to rapid urbanization, construction and demolition operations have increased, resulting in massive amounts of waste. As a result of its significant environmental consequences and the efficiency of the building industry, the development of construction waste is widely regarded as one of the most pressing issues facing the industry. This brings about the development and redevelopment of the building [35].

1.1 *What is Construction and Demolition (C&D) Waste?*

Construction and Demolition waste means any waste generated during construction, demolition or re-modeling of any civil structure, such as buildings, bridges, flyovers, roads, drainage and laying of services etc. or associated activities for infrastructure provision such as, site preparation by way of digging, leveling, laying of pipelines, cables etc. Figure 1 shows construction and demolition waste/Almost 95% of waste of every construction activities can be recycled. Many countries is processing up to 90% recycling of C&D Waste, while other developed countries are trying to improve the processing efficiency. More than 50% waste generated worldwide is C&D that is generated from construction activities. Still people are dumping the C&D waste to low lying areas & MSW land fills and government is trying to educate them & imposing fine for illegal dumping of C&D waste. Figure 2 shows typical methodology adopted for demolition of C&D waste.



Fig. 1 Construction and demolition waste



Fig. 2 Typical disposition methods for C&D Waste

1.2 *Justification of Study*

While construction and demolition waste may seem like a waste products, they are valuable if used properly. Most of them can be repurposed as recyclable resources after sorting, shredding, and recycling; the materials used to create steel can also substitute sand in masonry and plastering mortars and make paving bricks, lattice bricks, and other building materials [24, 31]. In addition, wood, plastic, even doors and windows can be utilized as fuel for generators and heaters [20]. Despite several trash quantification methods available in the literature, waste generation measurement in India is grossly inadequate. The lack of common construction and demolition waste estimating approach and lack of awareness of construction and demolition waste processing by stakeholders such as generators, collectors, operators, regulators, and the general public can be related to these inadequacies [9]. Therefore, it is necessary to quantify the amount of construction and demolition waste generated and handled [12]. When it comes to tackling dwindling resources and accompanying pollution, recycling has been identified as a targeted strategy that reduces the demand for natural resources [30]. Recycling materials in the construction industry can assist in reducing the need for raw materials, which can lessen resource depletion and other environmental challenges in the long run [36]. It is, therefore, necessary to comprehend the significance and benefits of good management of construction and demolition waste and the difficulties and bottlenecks that must be overcome to develop effective implementation strategies. (Building Material and Technology Promotion Council, 2018).

The importance of increasing volumes of construction and demolition rubbish in urban areas is emphasized, as are substantial differences in origin, quality, and recycling and reuse options. Therefore, they were revised in the rules (Building Material and Technology Promotion Council, 2018). This development reflects a growing understanding of the importance of managing construction and demolition rubbish separately from municipal solid waste, which is reflected in the development. Furthermore, it encourages the use of construction materials and recycled construction and demolition waste items to develop affordable housing units by 2022 to address the country's severe housing crisis. Recycling regulations are in place, but the practice has yet to gain traction. Several factors contribute to this situation, including poor plant capacity and insufficient government oversight [33]. However, the waste generated at various building sites can be transformed into valuable material for general construction by construction and demolition waste recycling plants [31]. The Bureau of India Standard recognizes different construction operations as a suitable substitute for fresh materials. Recycling materials in the construction industry can assist in reducing the demand for raw materials, which can lessen resource depletion and other environmental challenges in the long run. If India had complied with the regulations proposed in 2016, all India's cities would have had this waste collection, transport, and recycling network.

The Swachh Bharat Mission has realized the importance of adequately managing construction and demolition trash in India. Swachh Survekshan 2021 ranking points for construction and demolition waste management have been raised to 100 points, with infrastructure for waste management and processing efficiency shared evenly. Instead of being disposed of in landfills, construction and demolition waste is now being recycled into building materials (recycled aggregate concrete, produced sand, etc.) [37]. This helps conserve natural resources while also reducing the amount of waste generated. In the absence of efficient implementation and enforcement of measures to reduce and regulate construction and demolition waste, the country's environment may be jeopardized. Because of limited landfill space and the increasing amount of demolition trash, mitigate and treat construction and demolition waste. Otherwise, there may be challenges with waste management and the hunt for landfill space in the future. It would create further issues for waste management programs that are also attempting to find innovative approaches to dealing with the expanding urban population and changes in the composition of municipal trash across the world. It is necessary to employ various strategies and technologies for waste reduction to reduce construction and demolition waste, such as design for deconstruction or the reuse of raw materials [27]. [6] stated that the use of recycled building and demolition waste products is technically viable and regulated. There are numerous beneficial application examples; nevertheless, it is still unclear how to effectively engage key stakeholders to maximize this opportunity in construction projects [4]. According to a previous study, the utilization of recycled construction and demolition waste materials in housing development has been met with some reluctance in the past [28]. This underscores the crucial need to assess key stakeholders' needs and encourage the recycling and reuse of construction waste. There are still significant hurdles to employing recovered construction and demolition debris in construction projects.

1.3 Government of India Initiation for C&D Waste

Indian Government introduced “**SWACHH BHARAT ABHIYAAN**” to create awareness for cleanliness & proper disposal of waste. The Swachh Bharat Mission has realized the importance of adequately managing construction and demolition trash in India. Swachh Survekshan 2021 ranking points for construction and demolition waste management have been raised to 100 points, with infrastructure for waste management and processing efficiency shared evenly.

C&D Waste Management Rules, 2016 have already been notified on 29-03-2016 by Ministry of Environment, Forest and Climate Change, Government of India clearly mentioned that all C&D Waste generated should be transported to C&D Waste Recycling Plants only. BIS had also revised the IS specification (IS383) to IS 383:2016 and specified that for lead bearing structures, **up to a maximum of 25% of coarse and fine Recycled Concrete Aggregate (RCA) can be mixed with PCC and up to 20% of course and fine RCA can be mixed with RCC.** For lighter, non load

bearing structure using lean concrete, the entire amount (100%) of coarse and fine aggregate of both RCA and Recycled Aggregate (RA) may be used.

Public Works Department (PWD), Govt. of NCT of Delhi has also issued an advisory to all Delhi Government departments to incorporate a clause in their tenders that mandates 2% to 10% use of recycled C&D waste products in Building and Road works respectively.

Instead of being disposed of in landfills, construction and demolition waste is now being recycled into building materials (recycled aggregate concrete, produced sand, etc.) [37]. This helps conserve natural resources while also reducing the amount of waste generated. In the absence of efficient implementation and enforcement of measures to reduce and regulate construction and demolition waste, the country's environment may be jeopardized. Because of limited landfill space and the increasing amount of demolition trash, mitigate and treat construction and demolition waste. Otherwise, there may be challenges with waste management and the hunt for landfill space in the future. It would create further issues for waste management programs that are also attempting to find innovative approaches to dealing with the expanding urban population and changes in the composition of municipal trash across the world. It is necessary to employ various strategies and technologies for waste reduction to reduce construction and demolition waste, such as design for deconstruction or the reuse of raw materials [27]. [6] stated that the use of recycled building and demolition waste products is technically viable and regulated. There are numerous beneficial application examples; nevertheless, it is still unclear how to effectively engage key stakeholders to maximize this opportunity in construction projects [4]. According to a previous study, the utilization of recycled construction and demolition waste materials in housing development has been met with some reluctance in the past [28]. This underscores the crucial need to assess key stakeholders' needs and encourage the recycling and reuse of construction waste. There are still significant hurdles to employing recovered construction and demolition debris in construction projects.

2 Related Works

On August 25, 2020, the non-profit Center for Science and Environment, based in Delhi, released a new report stating that India recycles only one per cent of its construction and demolition trash, which is an alarming figure. Furthermore, unsubstantiated estimates place the country's overall waste creation at a level three to five times greater than the official amount. According to a subsequent study, India only manages to recover and recycle 1 per cent of its construction and demolition waste. As a result, landfills and unattractive blights on our landscape will account for more than half of all waste generated. A construction and demolition waste management plan try to limit the amount of building and demolition debris that ends up in landfills by diverting it away from landfills while the project is in progress. [12], stated that as India's second-largest business, construction had experienced an explosive expansion in recent years. Despite the existence of several policies and guidelines,

improper construction waste management continues. Therefore, it is required that practical construction and demolition waste management is vital when demolition stakeholders are hired [14]. Even though each organization has a particular set of duties in construction projects, it is generally accepted that practical construction and demolition waste management involves the effective engagement and collaboration of the primary and other project stakeholders. [13, 22], stakeholders are critical in garbage management as India's housing development business consumes more raw materials and energy than any other economic activity [15] stated that Construction waste must be appropriately managed to reduce the environmental strain on India's environment and preserve the country's natural resources.

According to a recent assessment announced by the National Institutes of Health. Delhi-based non-profit Center for Science and Environment (CSE) on August 25, 2020, India recycles only 1% of its construction and demolition waste. It also recommends a workable strategy for better managing building and demolition trash in Indian cities. Only 13 cities had recycling facilities set up to recover material from construction and demolition waste by 2020. This is intolerable when demand for primary building resources such as minerals, stone, sand, iron ore, aluminium and lumber is growing unprecedented [18]. In addition to being recyclable and reusable, construction waste can be incorporated back into the construction process to replace organically obtained materials [8]. This needs a circular economy capable of repurposing construction and demolition waste as a helpful resource [1]. Although buildings and infrastructure can use less energy and have a less environmental impact if this is implemented, studies show construction debris like concrete, bricks, and metal was polluting Indian cities' waterways, green spaces, and public spaces[3, 23]. Furthermore, toxic dust particles from the waste were polluting the air when cities were required by the ongoing National Clean Air Program to cut particulate pollution by 20–30% by 2024. Despite removing legal barriers to employing recycled and demolition material in construction, the lamentable situation about construction and demolition trash persists.

According to the Bureau of Indian Standards, recycled concrete and processed construction and demolition waste can be used in place of regular concrete. India, in comparison, has a dismal track record. Before two years ago, municipal solid waste and construction and demolition waste were considered the same thing. As stated in the Municipal Solid Garbage (Management and Handling) Rules, 2000, construction and demolition waste shall be collected and disposed of separately according to State laws. "Only a small number of states had passed legislation at the time! However, in 2016, the Ministry of Environment, Forests and Climate Change separately notified the Construction and Demolition Waste Management Rules 2016. These 2016 Solid Waste Management Rules replaced the previous rules from 2000 recognized. Composting or bio methanation is less successful when construction and demolition waste is included in the mix, and the calorific value and combustibility of Municipal Solid Waste are also reduced [25]. A comparable degradation of recycled construction and demolition trash occurs when Municipal Solid Waste is present in the residue. While contractors and renovators are required to separate construction and demolition garbage, urban municipal governments enforce the Rules. Examples

include rules stating that between 10 and 20% of construction and demolition recycled products shall be used in all government construction projects, regardless of level (aggregates, kerbstones, paver blocks, tiles, and manufactured sand). Despite the National Green Tribunal's and other regulatory organizations' instructions, this hasn't happened. Furthermore, the 2016 Rules and Regulations for Construction and Demolition Waste require the usage of recovered materials.

However, building companies can save 12.3 million tonnes of raw material per year by using recycled materials such as demolition aggregates [19]. The construction sector can save 12.3 million tonnes of raw material annually [17], but we do not pay enough attention to the construction and demolition waste we produce, such as bricks, concrete, stones, hardcore subsoil, topsoil, lumber, glass, gypsum, ceramics, and even plastics. Aside from that, the massive amount of unprocessed Construction and Demolition waste poses significant challenges in some areas, notably in areas with a high concentration of residential, institutional, industrial, and commercial construction [9]. These materials are generated during the construction and demolition process. It's bad for the ecology and public health to ignore this garbage[16]). As reported by the World Resources Institute, practical construction and demolition waste management increased the life span of landfills, decreased the need for raw materials, decreased the costs of projects, created new business opportunities, and demonstrated the environmental commitment of project stakeholders [7]. On the other hand, state that The implementation of construction and demolition waste management has not yet met the expectations of project stakeholders, despite numerous attempts.

3 Proposed Solution

Furthermore, the 2016 Rules and Regulations for Construction and Demolition Waste require the usage of recovered materials. Cities must set up a system for collecting construction and demolition waste, charge for construction and demolition services, and separate waste into five different streams. Ranking points will be provided depending on the amount of waste processed and repurposed as part of the waste processing efficiency requirement. Swachh Bharat Mission and construction and demolition Waste Rules acknowledgement accordingly offered an opportunity. This research has examined the present construction and demolition problem and the technological and regulatory hurdles that stand in the way of putting the Rules into practice. Several techniques have been established to expedite Rule implementation and the acceptance of recycled materials in the market. "Ground-reality assessments in several cities support the findings.

Also the establishment of processing plant an example is the Rise Eleven Construction & Demolition Waste Processing Plant, located at Bakkarwala, Delhi, India that convert construction and demolition waste into RCA (Recycled Concrete Aggregate) –10/20/40 mm, RA (Recycled Aggregates) –10/20/40 mm, Stone Dust, Washed Sand, Plaster Sand, M. Sand, Brick Sub-Base (BSB) –>26<50 mm,

Screened Soil, Interlocking Pavers of various size, shape & color, Chequered Tiles of different design & colored, Tech Tiles, Kerb Stones of various size & shapes, Concrete Bricks & Blocks (Hollow & Solid), Other precast concrete products like –Drain/Manhole and covers, Boundary wall panels etc. the plant used are dry Processing Unit –greater than 60 TPH capacity, wet Processing Unit (Log Washer & Sand Washing Plant), Automatic Batching Plant for Ready Mix Concrete, Manufacturing unit for precast concrete products, Fully equipped Laboratory with all required equipment for testing of concrete and its constituent materials,

3.1 Infrastructure Required to Setup Plants for Production of Recycled Materials and Ready Mix Concrete (Dry Processing Unit –Greater than 60 TPH Capacity)

Following are the steps for setting up plant based on construction demolition waste.

- Wet Processing Unit (Log Washer & Sand Washing Plant)
- Automatic Batching Plant for Ready Mix Concrete
- Manufacturing unit for precast concrete products
- Fully equipped Laboratory with all required equipment for testing of concrete and its constituent materials
- Fleet of Excavators, Dumpers, Transit Mixers & Concrete Pumps

Photographs of integrated plant of Rise Eleven Delhi Waste Management Co., New Delhi, India are shown in the subsequent figures (Figs. 3, 4, 5 and 6).

Water Conservation – ‘Aqua Cycle Thickener’



Fig. 3 Front view of Water Conservation – Acqua cycle thicner

Wet Processing Unit



Fig. 4 Photograph of wet proccession unit at New Delhi, India



Fig. 5 M Sand Production Unit, New Delhi, India-



Fig. 6 Photograph showing Ready Mixed Concrete Unit

Table 1 Products offered by C&D plants

Recycled materials	Readymix concrete
<ul style="list-style-type: none"> • RCA (Recycled concrete aggregate) – 10/20 /40 mm 	<ul style="list-style-type: none"> • Concrete of all grades as per IS
<ul style="list-style-type: none"> • RA (Recycled aggregates) – 10/20/40 mm 	<ul style="list-style-type: none"> • Fiber-reinforced concrete (FRC)
<ul style="list-style-type: none"> • Stone dust 	<ul style="list-style-type: none"> • High-volume fly ash concrete (HVFAC)
<ul style="list-style-type: none"> • Washed sand 	<ul style="list-style-type: none"> • Self -compacting concrete (SCC)
<ul style="list-style-type: none"> • Plaster sand 	<ul style="list-style-type: none"> • Light weight concrete (LWC)
<ul style="list-style-type: none"> • M. sand 	<ul style="list-style-type: none"> • Temperature-controlled concrete (TCC)
<ul style="list-style-type: none"> • Brick sub-base (BSB) →>26 <50 mm 	<ul style="list-style-type: none"> • Stamped concrete
<ul style="list-style-type: none"> • Screened soil 	
<ul style="list-style-type: none"> • M Sand –super 	

Table 1 provides a list of products which C&D plant can produce.

4 Conclusion

A sizable percentage of the construction industry supports the redevelopment of Housing. Rather than new construction, rehabilitation, or maintenance, demolition of an old building or structure generates the most trash in the construction industry. Construction and demolition waste is generated during the construction, demolition, or remodelling of any civil structure, such as buildings, bridges, flyovers, roads, drainage, and service infrastructure. By way of a brief discussion and a review of the literature, this paper analyses the current condition of waste management in the construction and demolition industries, the types of stakeholders involved, the factors influencing the recycling and reuse of recycled construction and demolition waste products, and the factors influencing stakeholders’ decisions to use recycled construction and demolition waste products. As well as providing comments on how stakeholders’ viewpoints, actions, and behaviour influence the use of recycled construction and demolition waste products, the paper also emphasizes growing enablers and the significance of recycled construction and demolition waste products. also contributing to the body of knowledge is the study’s provision of insights into the current situation, which many stakeholders believe influences the need for recycled construction and demolition waste products, and it serves as a reference point for policymakers who wish to examine this strategy in the context of policy reform.

There are several benefits which are due to the installation of plant based on construction and demolition waste such as cost saving, job creation for local community and social responsibility to stop pollution, saving of landfill space, energy and greenhouse effect, availability of building material products nearby to the project site.

Acknowledgements Authors are thankful to the management of Rise Eleven Delhi Waste Management Company, New Delhi, India for providing photographs and other information for preparation of this paper.

References

1. Akanbi LA, Oyedele AO, Oyedele LO, Salami RO (2020) Deep learning model for Demolition Waste Prediction in a circular economy. *J Clean Prod* 274:122843
2. Allam Z, Jones DS (2018) Towards a circular economy: a case study of waste conversion into housing units in Cotonou, Benin. *Urban Sci* 2(4):118
3. Arya S, Kumar S (2020) E-waste in India at a glance: current trends, regulations, challenges and management strategies. *J Cleaner Prod* 271:122707
4. Caldera S, Ryley T, Zatyko, N. (2020). Developing a marketplace for construction and demolition waste based on a systematic quantitative literature review. In: Proceedings of the 1st Asia Pacific sustainable development of energy water and environment systems, Gold Coast, Australia, pp 6–9
5. Chaudhuri G, Clarke KC (2019) Modeling an Indian megalopolis—a case study on adapting SLEUTH urban growth model
6. Coelho A, De Brito J (2013) Economic viability analysis of a construction and demolition waste recycling plant in Portugal—part I: location, materials, technology and economic analysis. *J Clean Prod* 39:338–352
7. Dahlbo H, Bachér J, Lähäinen K, Jouttijärvi T, Suoheimo P, Mattila T, Saramäki K (2015) Construction and demolition waste management—a holistic evaluation of environmental performance. *J Clean Prod* 107:333–341
8. De Luca A, Chen L, Gharehbaghi K (2020) Sustainable utilization of recycled aggregates: robust construction and demolition waste reduction strategies. *Int J Build Pathol Adapt*
9. Faruqi MHZ, Siddiqui FZ (2020) A mini review of construction and demolition waste management in India. *Waste Manage Res* 38(7):708–716
10. Fields D (2017) Urban struggles with financialization. *Geogr Compass* 11(11):e12334
11. Hinojosa J, Meléndez E (2018) The housing crisis in Puerto Rico and the impact of Hurricane Maria: Centro de Estudios Puertorriqueños
12. Jain MS (2021) A mini review on generation, handling, and initiatives to tackle construction and demolition waste in India. *Environ Technol Innov* 22:101490
13. Jain S, Singhal S, Jain NK, Bhaskar K (2020) Construction and demolition waste recycling: Investigating the role of theory of planned behavior, institutional pressures and environmental consciousness. *J Clean Prod* 263:121405
14. Kim SY, Nguyen MV (2020) A performance evaluation framework for construction and demolition waste management: stakeholder perspectives. *Eng Constr Arch Manag*
15. Kolaventi SS, Tezeswi T, Siva Kumar M (2020) An assessment of construction waste management in india: a statistical approach. *Waste Manag Res* 38(4):444–459
16. Luangcharoenrat C, Intrachooto S, Peansupap V, Sutthinarakorn W (2019) Factors influencing construction waste generation in building construction: Thailand's perspective. *Sustainability* 11(13):3638

17. Marzouk M, Azab S (2014) Environmental and economic impact assessment of construction and demolition waste disposal using system dynamics. *Resour Conserv Recycl* 82:41–49
18. Michaux SP (2021) The Mining of Minerals and the Limits to Growth
19. Mistri A, Dhami N, Bhattacharyya SK, Barai SV, Mukherjee A, Biswas WK (2021) Environmental implications of the use of bio-cement treated recycled aggregate in concrete. *Resour Conserv Recycl* 167:105436
20. Nanda S, Berruti F (2021) Thermochemical conversion of plastic waste to fuels: a review. *Environ Chem Lett* 19(1):123–148
21. Nath B, Ni-Meister W, Choudhury R (2021) Impact of urbanization on land use and land cover change in Guwahati city, India and its implication on declining groundwater level. *Groundw Sustain Dev* 12:100500
22. Olanrewaju SD, Ogunmakinde OE (2020) Waste minimization strategies at the design phase: architects' response. *Waste Manag* 118:323–330
23. Pawar M, Gujjar S (2021) Waste Management Practices in Infrastructure Projects in India (2516–2314)
24. Pellegrino C, Faleschini F, Meyer C (2019). Recycled materials in concrete. In: *Developments in the Formulation and Reinforcement of Concrete*, pp 19–54
25. Prajapati KK, Yadav M, Singh RM, Parikh P, Pareek N, Vivekanand V (2021) An overview of municipal solid waste management in Jaipur city, India-Current status, challenges and recommendations. *Renew Sustain Energy Rev* 152:111703
26. Rai SM, Brown BD, Ruwanpura KN (2019) SDG 8: Decent work and economic growth—a gendered analysis. *World Dev* 113:368–380
27. Shoosharian S, Caldera S, Maqsood T, Ryley T (2020) Using recycled construction and demolition waste products: a review of stakeholders' perceptions, decisions, and motivations. *Recycling* 5(4):31
28. Silva R, De Brito J, Dhir R (2019) Use of recycled aggregates arising from construction and demolition waste in new construction applications. *J Clean Prod* 236:117629
29. Smith RE, Quale JD (2017) *Offsite architecture: Constructing the future*: Taylor & Francis
30. Smol M, Marcinek P, Duda J, Szoldrowska D (2020) Importance of sustainable mineral resource management in implementing the circular economy (CE) model and the european green deal strategy. *Resources* 9(5):55
31. Sormunen P, Kärki T (2019) Recycled construction and demolition waste as a possible source of materials for composite manufacturing. *J Build Eng* 24:100742
32. Stadler SL, Collins D (2021) Assessing Housing First programs from a right to housing perspective. *Housing Studies*
33. Turaga RMR, Bhaskar K, Sinha S, Hinchliffe D, Hemkhaus M, Arora R, Singhal P (2019) E-waste management in India: issues and strategies. *Vikalpa* 44(3):127–162
34. Vaid U (2021) Delivering the promise of 'better homes'?: assessing housing quality impacts of slum redevelopment in India. *Cities* 116:103253
35. Wilson D, Polter R (2020) Sustainable local economic development indicator framework: a tool for property building redevelopment projects. *Community Dev* 51(5):609–627
36. Xia B, Ding T, Xiao J (2020) Life cycle assessment of concrete structures with reuse and recycling strategies: a novel framework and case study. *Waste Manage* 105:268–278
37. Zanelli C, Marrocchino E, Guarini G, Toffano A, Vaccaro C, Dondi M (2021) Recycling construction and demolition residues in clay bricks. *Appl Sci* 11(19):8918

Development of Architecture of Autonomous Hydraulic Rock Breaker for Limestone Mines



Aryan Sinha, Sabari Giri Vasan, Job Steven J. Nandrekar, Umang Aditya, Manoj Khandelwal, Naresh Prasad, Ramesh Murlidhar Bhatawdekar, and Vynotdni Rathinasamy

Abstract Boulders which are generated during primary blasting are required to undergo secondary blasting prior to crusher operation. Hydraulic rock breaker is one of the techniques which is being utilized to break boulders instead of secondary blasting. This study aims to develop an architecture of AI model for rock breakers with autonomous remote operation. Firstly, several technical specifications of various rock breakers mounted on 30 T class hydraulic rock breakers were evaluated. Also, the factors affecting cost and operation were identified and discussed. Later, the autonomous rock breaker installed on the crusher hopper at a site in Australia was reviewed as global technological advancement. Based on the review, a five-stage architecture for developing autonomous hydraulic rock breaker was developed. The factors affecting the cost of hydraulic excavator and rock breaker can be classified into direct and indirect cost. The direct cost includes operational cost such as oil, replacement of chisel and bucket teeth and wages as well as maintenance cost. Meanwhile, the indirect cost is related to site issues such as locating boulder, boulders

A. Sinha · J. S. J. Nandrekar · U. Aditya · R. M. Bhatawdekar
Department of Mining Engineering, Indian Institute of Technology, Kharagpur, West Bengal
721302, India
e-mail: rmbhatawdekar2@graduate.utm.my

S. G. Vasan
Ultratech Cement, “B” Wing, 2nd floor, Ahura Centre Mahakali Caves Road, Andheri (East)
Mumbai 400 093, India
e-mail: sabari.vasan@adityabirla.com

R. M. Bhatawdekar · V. Rathinasamy (✉)
Geotropik, School of Civil Engineering, Faculty of Engineering, Universiti Teknologi Malaysia,
UTM JB, 81310 Johor Bahru, Malaysia
e-mail: vynotdni@utm.my

M. Khandelwal
School of Engineering, Information Technology and Physical Sciences, Federation University
Australia, Ballarat, Australia
e-mail: m.khandelwal@federation.edu.au

N. Prasad
RMB Consultant, Tikujiniwadi, Thane 400 610, India

jamming crusher, waiting dozer to push boulder, etc. Also, the factors influencing operation of hydraulic hammer shall be classified into very important (i.e. oil flow, chisel diameter), important (i.e. elasticity, impact rate) and desirable (i.e. hardness, chisel length). The five stages architecture for developing autonomous hydraulic rock breaker are development, data collection, data pre-processing, model deployment and model testing.

Keywords Hydraulic rock breaker · Limestone · Secondary blasting

1 Introduction

During primary blasting, certain quantity of boulders is generated based on type of rock, variation in strata, geological discontinuities, joint spacing and orientation, drill hole angle, blast design parameters, cavities, powder factor, maximum charge per delay, specific drilling [1–4]. Boulders generated during primary blasting cannot be sent to downstream crusher operation [5–8]. Hence, minimizing boulders generation and handling of boulders have been always challenging task for mines management [9–12]. In one of the limestone quarries, it is reported that in first bench there is more generation of boulders due to the geological conditions [13]. On the other hand, in tropically weathered limestone, maximum boulder generation is found in fresh/slightly weathered limestone and least boulder generation in completely weathered limestone [14, 15]. There is always risk of flyrock due to secondary blasting, geological conditions [16, 17]. Primary blasting has limitation for reducing spacing and burden [18, 19]. With increase in specific drilling, there is increase in drilling and blasting cost [20, 21]. With optimum spacing and burden, optimum fragmentation can be obtained at economical cost [2, 7, 22, 23]. Hence, boulders generated during primary blasting are broken with different methods such as drop ball method, pop shooting, secondary blasting, primary and secondary hydraulic rock breakers [24, 25]. Various researchers have developed computational techniques for optimization of blast fragmentation and minimizing secondary blasting [26–28].

This study was undertaken to review existing hydraulic rock breakers used in limestone mines and technological advancement of remote operation of rock breaker at crusher. Architecture for AI model for rock breakers with autonomous remote operation was proposed which would be beneficial for limestone mines in the near future.

2 Objective of the Study

The objective of the project was to develop an architecture of AI model for rock breakers. The project outlines the most important parameters affecting the autonomous operation and the output of rock breakers.

3 Methodology

The methodology involved study of existing hydraulic rock breakers used in limestone mines at different locations. Technical specifications of different rock breakers of mounted on 30 T class hydraulic rock breakers were compared. Factors affecting the cost of operation of hydraulic excavator and hydraulic rock breaker were compared. Factors affecting operation of rock breaker were divided into very important, important and desirable based on the feedback from the different limestone mines were compiled. One of the mine sites in Australia, autonomous rock breaker is installed on the crusher hopper which was reviewed as global technological advancement. Flow chart was developed as preliminary architecture for rock breaker mounted on 30 T class hydraulic excavator. Possible data sources for operation of rock breaker and hydraulic excavator were identified. Five stages architecture for developing autonomous hydraulic rock breaker was prepared.

Further recommendations were prepared so that this study can be taken up in the next level of research.

4 Hydraulic Rock Breaker

A rock breaker is a machine designed to manipulate large rocks, including reducing large rocks into smaller rocks. They are typically used in the mining industry to remove oversize rocks that are too large or too hard to be reduced in size by a crusher. Rock breakers consist of two major components, a hydraulic hammer and a boom (the arm). They are typically attached on backhoe excavators.

Study was undertaken to compare rock breakers mounted on 30 T Hydraulic excavators of Komatsu, Volvo, and Cateroillar make. Comparison of these models are tabulated in Table 1.

Table 1 Comparison of hydraulic rock breakers

Particulars	Komatsu L&T make	Volvo make	CAT make
1. Equipment model	PC300	EC300	330GC
2. Country of origin	India	India	India
3. Equipment weight	33,700 kg	30,400 kg	28,500 kg
4. Heavy duty bucket Suitable for Limestone excavation with horizontal lock pin system for bucket teeth	Fitted with 1.6 Cu.m Bucket	Fitted with 1.6 Cu.m, 1.8 Cu.m at different mines	1.8 Cu.m bucket
5. Engine Make, model and HP	Komatsu SAA6D114E-3 Net HP: 250 HP	Volvo D7 - 231 HP gross @ 1800 rpm	Cat C7.1 & 213 HP
6. Auto fire suppression system (AFSS)	Yes, provided at additional cost	Yes, provided at additional cost (Retrofit)	Yes, provided at additional cost (Retrofit)
7. Automatic Centralised Lubrication system (ACLS)	Yes, provided at additional cost	Yes, provided at additional cost (Retrofit)	Yes, provided at additional cost (Retrofit)
8. FOPS and AC Cabin	Yes, AC Cabin	FOG (Falling object guard) – Optional - at extra cost (Retrofit) Automatic Climate control AC as standard fitment	ROPS, standard sound suppression
9. Rear view camera	Yes, provided at additional cost	Yes, provided at additional cost (Retrofit)	Yes, provided at additional cost (Retrofit)
10. Audio Visual Alarm	Yes, provided	Yes, provided at additional cost	Yes, provided at additional cost (Retrofit) Travel Alarm is provided as standard fitment

(continued)

Table 1 (continued)

Particulars	Komatsu L&T make	Volvo make	CAT make
11. Safety feature - Battery cut off switch, High Engine Coolant temperature, Low engine lub oil pressure, low hydraulic oil level, High hydraulic oil temperature, Alarm for travel operation, operating lever mechanical locking provision, Swing lock provision, Diesel tank locking provision, 3 point contact safety belt, guards to prevent damage from stones for travel motor, hoses, engine/ travel mechanism, provision for limiting hydraulic cylinders	Battery Cut off provision in ignition switch available, 2 point contact safety Belt, Inbuild Swing parking brakes, Provision for limiting the hydraulic cylinder build. Alarm for Travel available, Diesel lock provision available, Travel motor mounted in enclosed compartment, Hoses are well protected, engine enclosed in compartment	Battery Cut-off switch, Travel Alarm & 3 point Seat belt: Yes provided at additional cost Track guiding guard, Centre section only High Engine Coolant temperature, Low engine lub oil pressure, low hydraulic oil level, High hydraulic oil temperature, operating lever mechanical locking provision, Swing lock provision, Diesel tank locking provision, provision for limiting cylinders: Yes	Yes 2 point seat Belt
12. Side rear view mirror both side & blind spot mirror	Side View Mirror Available, Blind Spot Mirror not provided	Yes	Yes, Mirror Provided, Blind Spot Mirror- Yes retrofitted
13. Full Track guard	Not provided	Not provided	Not provided
14. 500 h filter kit	Yes, Included	Yes, provided at additional cost	Yes, provided at additional cost (Retrofit) (through service dealer)
15. Adequate LED Lights	Yes, Included	Lights as per as per std. fitment available with Komatsu	Halogen lights - Standard fitment. LED lights – Yes provided at additional cost (Retrofit)
16. Suitable Ladder for operator and maintenance crew for climbing up/down from machine	Foot Step for operator and maintenance crew provided at appropriate places, Necessary handrails provided	Yes	Not provided. However, 3 point contact maintained for climbing up/down from the machine
17. Suitable width track grousers for limestone application	600 MM shoes will be provided, triple grouser	600 mm	600 mm. triple grouser shoes

(continued)

Table 1 (continued)

Particulars	Komatsu L&T make	Volvo make	CAT make
18. Vehicle health monitoring system with downloadable facility in pc/ laptop	Yes, Consite with detailed monitoring system included	Real time monitoring system available in Monitor inside cabin	MATRIS reports (download on laptop through cable) for real time operational, service scheduling, error functioning monitoring system can be downloaded by the service engineers and submitted. CareTrack (GSM based telematics) hardware is standard fitment along with 5 years free subscription of the GSM operator
19. Fire resistant hoses at hot zones	Heat resistant Hoses available	Heat resistant plePara>	Fire retardant hoses at hot zones supplied as standard fitment
20. Electric wires and sleeves are to be of fire resistance quality	Necessary BIS Standards are complied	Heat resistant	Fire retardant electric wires & sleeves supplied as standard fitment
21. Standard Tool Kit, 3 sets of Operator manual, shop manual & parts book. (Hard copy and Soft copy)	Standard Tool Kit, 1 copy of Operators manual will be provided	Std. Tool Kit, One set of Parts Book & O&M manual will be provided with machine at site	Std tool kit –1 set shall be provided O&M Manual - 1 set of hard + soft copy shall be provided Parts Manual –1 set of hard + soft copy shall be provided Shop Manual - Not provided
22. Training for Operator & Maintenance Crew	Will be provided	Yes. 3 days. Training can be arranged at site	Will be provided for 4–5 days during commissioning, and subsequent follow-up trainings shall be provided for 4–5 days. We have regular training programmes at Volvo Customer Centre at Bangalore, where we conduct training programs, and we have SIMULATOR facility as well for the same

(continued)

Table 1 (continued)

Particulars	Komatsu L&T make	Volvo make	CAT make
23. Unloading Tool	Crane to be provided by UTCL	To be provided by UTCL at site	Crane shall be provided by customer. Complete checklist for any other requirement shall be provided at the time of dispatch
24. Simulator training to be provided to operators at site as per DGMS norms	will be provided however transportation cost to be borne by UTCL	Not provided	Simulator Facility available at Bangalore. Training on chargeable basis
25. Cabin light to be maintained 50 lx	Sufficient Cabin Light provided	Fitment as per Komatsu spec available	Standard light would be provided. Not meeting specified Lux level
26. Complete Piping Kit only for Rock Breaker application	Yes provided	Yes provided	Yes provided

Factors affecting the cost of operation of hydraulic excavator and hydraulic rock breaker are shown in Table 2. This consists of direct cost (operating cost and maintenance cost). On the other hand, indirect cost is classified based on idle running of hydraulic excavator or rock breaker.

Questionnaire was framed into three categories such as rock characteristics, hydraulic hammer characteristics, face survey results and miscellaneous factors. Each factor was further classified as Very important, important and desirable. The factors affecting operation of hydraulic hammer are tabulated in Table 3. These factors are useful for developing architecture for autonomous hydraulic rock breaker.

Further study was taken on global technological advancement in the field of hydraulic rock breaker installed on the crusher hopper. Brief details of study are described in the next paragraph.

Table 2 Factors affecting cost for hydraulic excavator and hydraulic rock breaker

Particulars	Hydraulic excavator	Hydraulic rock breaker	Remarks
A)Direct cost			
1. Operating cost			
Diesel oil	Y		
Hydraulic oil	Y		
Engine Lub oil	Y		
Bucket teeth replacement	Y		
Chisel replacement		Y	
Operator wages	Y	Y	Skill of operator -most important
2. Maintenance cost			
Engine overhaul	Y		
Hydraulic pumps and motors overhaul	Y		
Undercarriage	Y		
Hammer overhaul		Y	
B) Indirect cost			
Boulders jamming at crusher	Y		Waiting for loading dump trucks
Sorting out boulders at face	Y		Routine activity during loading
Shifting between blasting face	Y		Relatively small time
Locating boulder to break		Y	Routine activity during breaking
Frequent shifting for breaking		Y	A lot of time idle time
Unable to break boulders		Y	Excess boulders piled
Waiting dozer to push boulders		Y	Shifting of broken boulders

5 Global Technological Advancement

Though a lot of research is going on, completely autonomous rock breakers have not been deployed. The most advanced remote rock breakers deployed is the tele robotic rock breaker, deployed in the iron ore mines of Perth, Australia as in Fig. 1 and 2. This is controlled by a person sitting 1000 kms away and uses a combination of direct visualization and virtual reality simulation [12].

Table 3 Factors affecting operation of hydraulic hammer

Intact Rock Characteristics	Hydraulic Hammer Characteristics	Survey results	Miscellaneous
Uniaxial Compressive Strength	Oil Flow	Bedding Plane	Size of boulder
Brittleness	Operating Pressure	Joints	Cutting Geometry
Elasticity	Chisel Diameter	Fractures	Operational factors
Tensile Strength	Impact Rate	Fault Zones	Type of Drill Bits
Hardness	Chisel Length	GSI	Cutting Mode
		Ground water conditions	

(Colour code: Very Important, Important, Desirable)



Fig. 1 System architecture showing components at the **a** remote West Angeles and **b** local locations at Perth, Australia [12]

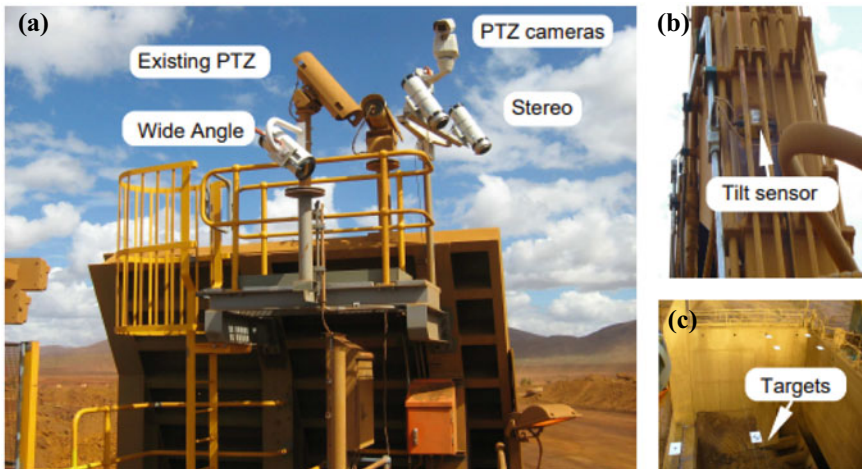


Fig. 2 Installed hardware: **a** cameras **b** tilt sensors and **c** calibration targets in ROM bin [12]

Data source, data requirement and data available data requirement operation of rock breaker can be divided into the following parts:

- Operation of excavators
- Operation of hydraulic hammers
- Operation of excavators can be modelled as autonomous vehicles. Autonomous vehicles work on the principle of Sense → Plan → Act. The operation principle can be seen in the flowchart shown in Fig. 3.

Data source for developing architecture for autonomous hydraulic rock breaker include face survey, machine specifications, sensors, laboratory tests and human inputs. The details of data source are shown in Fig. 4.

Further study was carried out and architecture in five stages was developed so that autonomous hydraulic rock breaker can be developed.

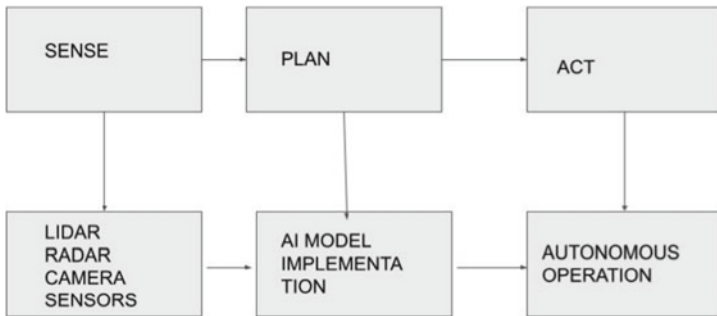
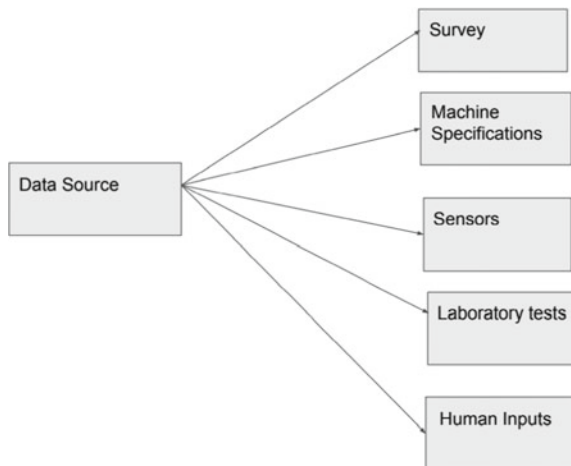


Fig. 3 Flow chart showing development of architecture for rock breaker mounted on 30 T class hydraulic excavator

Fig. 4 Data Source for developing architecture of autonomous hydraulic rock breaker



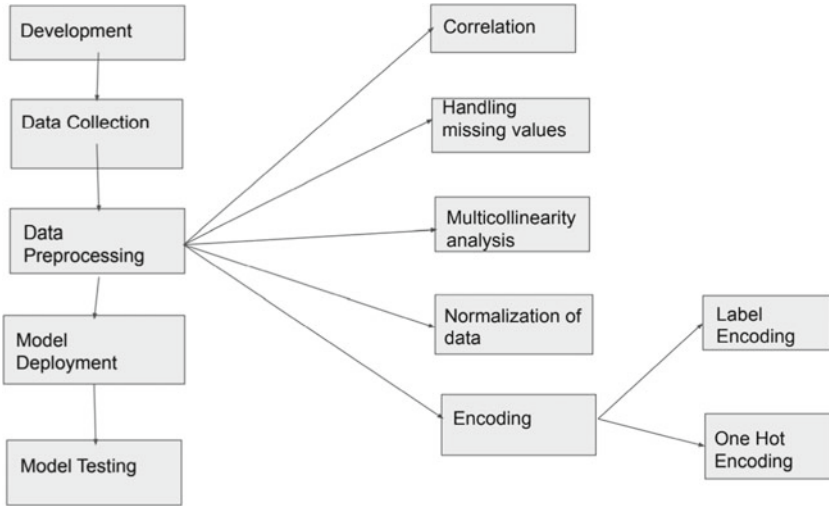


Fig. 5 Five stages architecture for developing autonomous hydraulic rock breaker

6 Recommendations and Conclusion

- It would be costly and time consuming to collect data for model development using conventional techniques. So, reinforcement learning can be used to collect data. Reinforcement learning is a technique where the AI model learns various patterns by itself while collecting data. Since the data collected is labelled, reinforcement learning can be applied easily without any extra cost. This results in better predictions with smaller datasets.
- Despite extensive research, completely autonomous rock breakers have not been deployed, due to a lot of hidden factors which are local (site dependent) and difficult to identify. So, a rock breaker developed only using conventional AI techniques may not perform better than an experienced operator.
- To overcome the above problem, a good solution would be simulation. The experienced operators can operate the rock breakers manually. The results can be compared with the results generated by simulation of AI models in computers.
- Another good solution would be automation of rock breakers in phases (or levels). The automation of rock breakers can be divided into 5 levels, with level 1 being completely manual, and level 5 being completely automated. At each level, more features can be added, which helps in automation of rock breakers.

Acknowledgements The authors are thankful to Mr. Ajit Ostwal, Senior Vice President Mining, Ultratech Cement, Mumbai for providing data/information and encouragement for preparing this paper. This paper is based on the report submitted by Aryan Sinha, Student of Mining Engineering from IIT Kharagpur.

References

1. McKee DJ, Chitombo GP, Morrell S (1995) The relationship between fragmentation in mining and comminution circuit throughput. *Miner Eng* 8(11):1265–1274
2. AyalaCarcedo F (2017) *Drilling and Blasting of Rocks*. Routledge, Milton Park
3. Bhandari S (September 1975) Burden and spacing relationships in the design of blasting patterns. In: *The 16th US Symposium on Rock Mechanics (USRMS)*. OnePetro
4. Monjezi M, Rezaei M, Varjani AY (2009) Prediction of rock fragmentation due to blasting in Gol-E-Gohar iron mine using fuzzy logic. *Int J Rock Mech Min Sci* 46(8):1273–1280
5. Kanchibotla SS, Valery W, Morrell S (November 1999) Modelling fines in blast fragmentation and its impact on crushing and grinding. In: *Explo 1999—A Conference on Rock Breaking*, The Australasian Institute of Mining and Metallurgy, Kalgoorlie, Australia, pp 137–144
6. Singh SP, Narendrula R (August 2009) Causes, implications and control of oversize during blasting. In: *Proceedings of the 9th International Symposium on Rock Fragmentation by Blasting*, pp. 311–317
7. Tosun A, Konak G (2015) Determination of specific charge minimizing total unit cost of open pit quarry blasting operations. *Arab J Geosci* 8(8):6409–6423
8. Beyglou AH (2012) Improvement of blast-induced fragmentation and crusher efficiency by means of optimized drilling and blasting in Aitik (Doctoral dissertation, Msc. Thesis of Civil Engineering, Department of Civil, Environmental and Natural Resources Engineering, Luleå University of Technology. The Lulea University of Technology)
9. Zhou H, Xie X, Feng Y (March 2018) Rock breaking methods to replace blasting. In: *IOP Conference Series: Materials Science and Engineering*, vol 322, no 2, p 022014. IOP Publishing
10. Bhosle S (2014) Overall increase in efficiency in raw meals
11. Duff E, Caris C, Bonchis A, Taylor K, Gunn C, Adcock M (2010) The development of a telerobotic rock breaker. In: Howard A, Iagnemma K, Kelly A (eds) *Field and Service Robotics*. Springer Tracts in Advanced Robotics, vol 62, pp 411–420. Springer, Berlin, Heidelberg. https://doi.org/10.1007/978-3-642-13408-1_37
12. Boeing A (2015) A remotely operated robotic rock-breaker with collision avoidance for the mining industry. *AusIMM Bull* (Jun 2015): 42–44
13. Venkatesh HS, Bhatawdekar RM, Adhikari GR, Theresraj AI (1999) Assessment and mitigation of ground vibrations and flyrock at a limestone quarry. In: *Proceedings of the Annual Conference on Explosives and Blasting Technique*, vol 2, pp 145–152. International Society of Explosives Engineers
14. Bhatawdekar RM, Edy TM, Danial AJ (2019) Building information model for drilling and blasting for tropically weathered rock. *J Mines Met Fuels* 494–500
15. Bhatawdekar RM, Tonnizam Mohamad E, Singh TN, Pathak P, Armaghani DJ (2021) Rock mass classification for the assessment of blastability in tropically weathered limestones. In: Bui XN, Lee C, Drebenstedt C (eds) *Proceedings of the International Conference on Innovations for Sustainable and Responsible Mining*. LNCE, vol 109, pp 13–44. Springer, Cham. https://doi.org/10.1007/978-3-030-60839-2_2
16. Mohamad ET, Murlidhar BR, Armaghani DJ, Saad R, Yi CS (2016) Effect of geological structure and blasting practice in fly rock accident at Johor, Malaysia. *Jurnal teknologi* 78(8–6)
17. Mohamad ET, Yi CS, Murlidhar BR, Saad R (2018) Effect of geological structure on flyrock prediction in construction blasting. *Geotech Geol Eng* 36(4):2217–2235
18. Ozdemir B, Kumral M (2019) A system-wide approach to minimize the operational cost of bench production in open-cast mining operations. *Int J Coal Sci Technol* 6(1):84–94
19. Kose H, Aksoy CO, Gönen A, Kun M, Malli T (2005) Economic evaluation of optimum bench height in quarries. *J South Afr Inst Min Metall* 105(2): 127–135
20. Roy MP, Paswan RK, Sarim MD, Kumar S, Jha R, Singh PK (2016) Rock fragmentation by blasting—a review. *J Mines Met Fuels* 64(9):424–431
21. Bhatawdekar RM, Mohamad ET, Singh TN, Armaghani DJ (2019) Drilling and blasting improvement in aggregate quarry at Thailand—a case study. *J Mines Met Fuels* 67:357–362

22. Bowa VM (2015) Optimization of blasting design parameters on open pit bench a case study of Nchanga open pits. *Int J Sci Technol Res* 4(9)
23. Afum BO, Temeng VA (2015) Reducing drill and blast cost through blast optimisation—a case study. *Ghana Min J* 15(2):50–57
24. Saliu MA (2008) Comparative analysis of hydraulic drop ball and secondary blasting technique for secondary breaking in aggregate quarries. A case study of associated granite industry, Igboora, Oyo State, Nigeria. *Int J Appl Eng Res* 3(11): 1557–1563
25. Anderson JT, Paplneau WN (1989) Extending Excavator Performance with Boom Mounted Attachments (No. 890976). SAE Technical Paper
26. Bhatawdekar RM, Danial JA, Edy TM (2018) A review of prediction of blast performance using computational techniques. *ISERME* 2018:37
27. Murlidhar BR, Armaghani DJ, Mohamad ET, Changthan S (2018) Rock fragmentation prediction through a new hybrid model based on imperial competitive algorithm and neural network. *Smart Construct Res* 2(3):1–12
28. Murlidhar BR, Armaghani DJ, Mohamad ET (2020) Intelligence prediction of some selected environmental issues of blasting: a review. *Open Construct Build Technol J* 14(1)

Application of Slope Mass Rating and Kinematic Analysis Along Road Cut Slopes in the Himalayan Terrain



Tariq Siddique, Mohammed Sazid, Manoj Khandelwal, Harsh Varshney, and Sayem Irshad

Abstract Hundreds of fatalities are being reported every year due to rampant slope failures along road-cut engineered slopes in the Himalayan region. Prevailing perilous conditions of cut slopes are mainly due to adverse geological attributes and ever-rising anthropogenic factors. To procure a landslide resilient design along roads in mountainous regions, a systematic geotechnical investigation is required. In this regard, the characterization of vulnerable slopes through empirical classification systems is of paramount importance for geotechnical appraisal. Eleven vulnerable road cut slopes along national highway-5 (NH-5), from Solan to Shimla have been studied herein. The present study incorporates the application of Slope Mass Rating (SMR) and its extensions, including Continuous Slope Mass Rating (CSMR) and Chinese Slope Mass Rating (ChSMR) to study various slopes. The outcomes of SMR and its extensions are used to classify cut slopes into different stability grades. In addition, prevailing structurally controlled failures have also been assessed by kinematic analysis. The majority of slopes are liable to undergo planar and wedge failures. The outcomes obtained by kinematic analysis, SMR and its extensions are used to propose adequate remedial measures.

Keywords Slope stability · Slope mass rating (SMR) · Continuous slope mass rating (CSMR) · Chinese slope mass rating (ChSMR) · Kinematic analysis

T. Siddique · H. Varshney · S. Irshad
Department of Geology, Aligarh Muslim University, Aligarh 202002, India

M. Sazid
Department of Mining Engineering, King Abdulaziz University, Jeddah, Saudi Arabia

M. Khandelwal (✉)
School of Engineering, Information Technology and Physical Sciences, Federation University
Australia, Ballarat, VIC 3350, Australia
e-mail: m.khandelwal@federation.edu.au; mkhandelwal1@gmail.com

1 Introduction

Himachal Pradesh is one of the most multi-hazard-prone states of India. According to Himachal Pradesh State Disaster Management Authority [4], the State faces various types of natural hazards including geological hazards, like earthquake and landslide hazards; hydrological hazards in the form of flash floods and glacial lake outburst floods; meteorological hazards including droughts, hailstorms and cloudbursts; and climatological hazards like cold waves, frosts and avalanche. These extreme events have severe impacts on agriculture, horticulture, human settlements, animals and humans. Besides these natural causes, the State also experiences various anthropogenic hazards such as forest fires, deforestation, transport-related accidents, stampedes, etc., that take many lives. Slope failures are one of the most common hazards along transportation routes in the hilly terrain of Himachal Pradesh. Every year, the State is affected by one or more significant landslides causing loss of life and damage to houses, agricultural fields, roads and infrastructure. In addition, rampant slope failures frequently cause blockage of roads and disrupt transportation and communication systems. Eight national highways pass through Himachal Pradesh with a total length of 1628 km, of which 993 km lie in a high-vulnerable zone, 516 km fall in the moderate risk zone and 10 km comes under the extremely vulnerable zone [33]. Most of the famous tourist hotspots in Himachal Pradesh are well connected by roads, but many of these roads have recurring landslides, which often cause lots of inconveniences. Unscientific land use and unplanned expansion of urban areas destabilize the slopes [1, 11, 21, 24, 26]. Such unplanned cut slopes may initially cause minor slides and occasional rockfall but may trigger a large-scale landslide when coupled with well-known triggers, like earthquakes and extreme rainfall. National highway-5 (NH-5) from Solan to Shimla has vulnerable road cut engineered slopes. The number of tourists visiting in and around Shimla district quadruples during the summer season, increasing massive inflow. To ensure the hassle-free and safe journey of tourists and residents, such transportation routes need a proper geotechnical appraisal on a routine basis. In the initial stages of such inspection, the use of rock mass classification systems is very effective. Among various classification methods in the literature, the SMR method is widely applicable under a diverse set of initial conditions [9, 19, 29, 32]. Large numbers of case records, including the application of SMR along with road cuts in the Himalayas, can be found in the literature [9, 11, 14, 20, 27, 30, 35]. The present study focuses on the characterization of the road cut engineered slopes along the NH-5, connecting Solan and Shimla of Himachal Pradesh, India. For much better characterization, continuous functions of CSMR are used to evaluate stability [10]. The impact of height and type of discontinuity is also assessed by employing Chinese SMR (ChSMR). These extended SMR methods enabled for much better characterization of the rock mass. Kinematic analysis of slopes is an integrated part of the SMR system, particularly for rock mass having multiple discontinuity sets. It enables to determine the favourability of different structurally controlled failures. Such case studies provide a way forward for geotechnical studies along Himalayan roads.

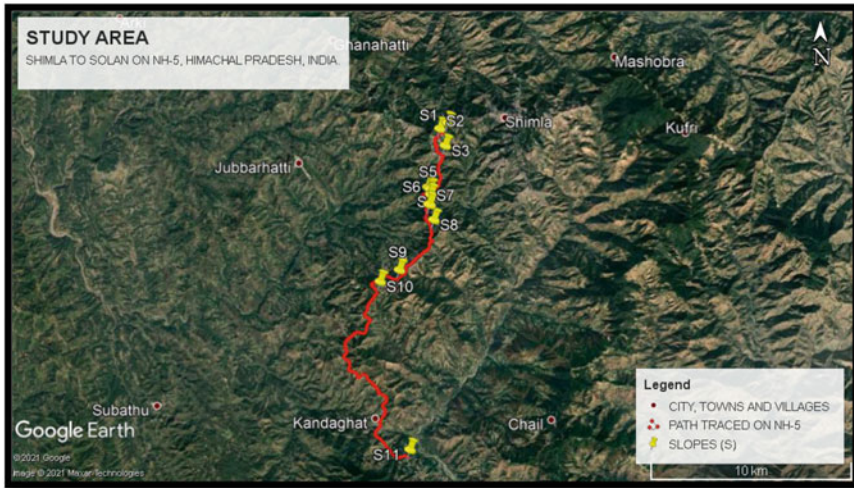


Fig. 1 Google Earth imagery depicting studied slopes along NH-5 from Solan to Shimla

2 Study Area

Shimla district covers 5131 square kilometers and is situated in the southern part of Himachal Pradesh. The elevation of Shimla ranges from 3000–6000 m with an average altitude of 2206 m. The average precipitation of the district is 1028 mm, which is capable enough to act as a triggering element for landslides along cut slopes. Studied vulnerable slopes along NH-5 are demarcated on the google earth imagery (Fig. 1). Several geological entities, including the Jutogh group, Jaunsar group, Sanjauli formation and Chhaosa formation are encountered while taking a traverse along NH-5, from Shimla to Solan [13]. Rock types including Mica-Schist, Quartzite, Phyllite and Limestone are found along studied cut slopes. These slopes are generally having 2–3 sets of discontinuities forming blocky and shattered rock mass.

3 Slope Stability Appraisal Along NH-5

Stability appraisal of road cut engineered slopes is a fundamental component of slope designing practices. In the initial field survey conducted along NH-5, eleven vulnerable zones were demarcated. During field surveys, occasional rockfall events were also noted in the studied section. Slopes are dissected by several sets of discontinuities forming shattered rock masses with small overhangs. Unscientific roadside planning is quite common along the route and several hairpin bends of the route are filled with debris to construct roadside shops. At some sites, minor tension cracks have been

developed, indicating failure liability of artificial dumps. Such inadequate planning along the route may be hazardous during heavy rainfall. Furthermore, a significant part of the studied route also lacks several geotechnical measures like retaining walls, gabion walls, wire mesh, and appropriate ditches. Engineered road cut slopes along NH-5 from Shimla to Solan need proper geotechnical evaluation. Globally accepted Slope mass rating and its extensions are being applied in the case study presented herein. Several parameters of SMR assessment were determined as per the standards mentioned below. SMR evaluation needs a basic Rock mass rating (RMR_{basic}), i.e. the sum of the first five ratings of Bieniawski's RMR or except parameter related to discontinuity orientation.

3.1 Rock Mass Rating (RMR)

The compressive strength of rock mass is a measure of the peak loading carrying capability of the rock mass [6]. In the case of jointed rock mass, compressive strength is substantially affected by the presence of discontinuities and physical properties of intact rock bridges [12]. The Schmidt hammer enables users to determine compressive strength in the field itself. It is an in-situ and non-destructive technique. In this study, the impact of discontinuities is also accounted well by using Schmidt hammer rebound values. Rebound values were determined during field surveys by following the guidelines of the International Society of Rock Mechanics [8]. Rebound values were used to determine UCS by using the empirical relationship (Eq. 1) suggested by [36] and accordingly, a rating is determined for the UCS parameter of RMR (Table 1). Large numbers of relationships among UCS and rebound values are being published under diverse sets of initial conditions [23]. In this study, similar lithological grounds and appreciable coefficient of determination are considered while selecting the said

Table 1 UCS, volumetric joint count, RQD and groundwater conditions of studied slopes

Site no	UCS (MPa)	Volumetric joint count (Jv)	RQD (%)	Groundwater conditions
S1	78	15.8	70.5	Damp
S2	61	6.2	94.6	Damp
S3	148	6.7	93.4	Dry
S4	5	12.5	78.7	Dry
S5	24	8.0	90	Damp
S6	7	13.1	77.2	Wet
S7	4	10.3	76.7	Damp
S8	14	18.5	63.7	Dry
S9	61	28.9	37.9	Wet
S10	60	6.5	93.7	Damp
S11	78	30.0	34.9	Damp

equation.

$$UCS = 0.0028 \times R^{2.584} \tag{1}$$

Here, R is Schmidt hammer rebound value.

The degree of fractures or discontinuities present in the rock mass directly or indirectly affects several other geotechnical factors controlling rock mass quality. It can be quantified by well-known parameters, i.e., rock quality designation (RQD). Since drill cores were not available, RQD was assessed by the volumetric joint count method [15, 16] and accordingly, ratings were assigned to studied slopes along NH-5 (Table 1).

The perpendicular distance between two discontinuities of a discontinuity set was also measured during the field survey to calculate mean discontinuity spacing. Several discontinuity conditions, including length of discontinuities, the roughness of joints, discontinuity opening, weathering conditions, and infilling material within discontinuities, were also assessed to assign ratings. Water deteriorates the inherent quality of rock mass and also shearing capability along the joint surface. All above-discussed properties related to discontinuities are determined by the standard procedure suggested by the International Society of Rock Mechanics [7]. Ratings of assessed parameters are added to determine the basic quality of rock mass (Table 2). In this study, [2] version of RMR is adopted and RMR_{basic} values of each site are used in the computation of SMR and its extensions. Discrete functions of original RMR give slightly different results from actual site conditions. Such differences occur when values lie near the border of the assigned class interval. To cope with this limitation, continuous functions are used in assigning ratings to the parameters of RMR.

Table 2 Ratings of parameters in RMR system

Parameters	Ratings of RMR parameters at studied slopes/sites											
	S1	S2	S3	S4	S5	S6	S7	S8	S9	S10	S11	
UCS	7	6	10.7	1.1	3.2	1.4	0.9	2.2	6	5.9	7	
RQD	14.5	19	18.8	16.1	18.2	15.8	15.7	13.3	8.3	18.8	7.7	
Discontinuity spacing	8.8	11.4	12.3	8.3	8.8	6.8	7.3	7.1	9.9	9.9	7.3	
Groundwater conditions	10	10	15	15	10	7	10	15	7	10	10	
Conditions of discontinuities	Persistence	2.1	3.2	1.1	2.4	0.9	0.9	1.1	0.9	0.4	0.4	0.9
	Aperture	0.7	6	0.5	0.9	1.5	1.5	0.2	6	0.9	1.5	0.4
	Roughness	3.3	1.5	0.9	3.6	1.5	1.5	1.5	5.1	2.1	0.9	3.3
	Infilling	5	5	5	5	5	5	5	5	1.8	5	5
	Weathering	5.7	5.2	5	4.6	5.6	4.3	5.2	5.5	5.3	5.5	5.1
RMR _{basic}	57	67	69	57	55	44	47	60	42	58	47	

3.2 Kinematic Analysis

Kinematics analysis is only a geometric evaluation of movement without considering its cause or mechanism involved in the failure. While carrying out slope stability studies by applying the slope mass rating method, kinematic analysis plays an important role in understanding the most prominent type of failure along with its causative discontinuity sets. In rock mass possessing discontinuities, shear failures are generally restricted along such weak surfaces. The relative orientation of existing discontinuities and slope face is used to assess structurally controlled failures [20, 25, 31]. The occurrence of such failures also relies on friction of joints, which was determined by the tilt test [28]. The orientation of slope face and dip direction & amount of discontinuities were measured by Brunton compass and the most prominent failure type was identified (Table 3). Geometric relationships among slope face and prevailing discontinuities were derived by plotting great circles of planes in Schmidt type stereonet. Shear failures in the form of planar sliding and wedges can be found in the studied section. One example from each mode is elaborated here. Daylight conditions are pronounced at Slope S5, which favours planar sliding due to discontinuity set J1 (Fig. 2). Failed blocks can also be seen in the field photograph of the site no. S4. At site no. S5, steep slope of dip amount 88° is inclined towards the southwest direction (212°) forming around 26° angle from dip direction of joint set J1. The amount of J1 is lying in between slope face and friction, thereby forming favourable conditions for planar sliding. Unlike planar, wedge failures are not controlled by a

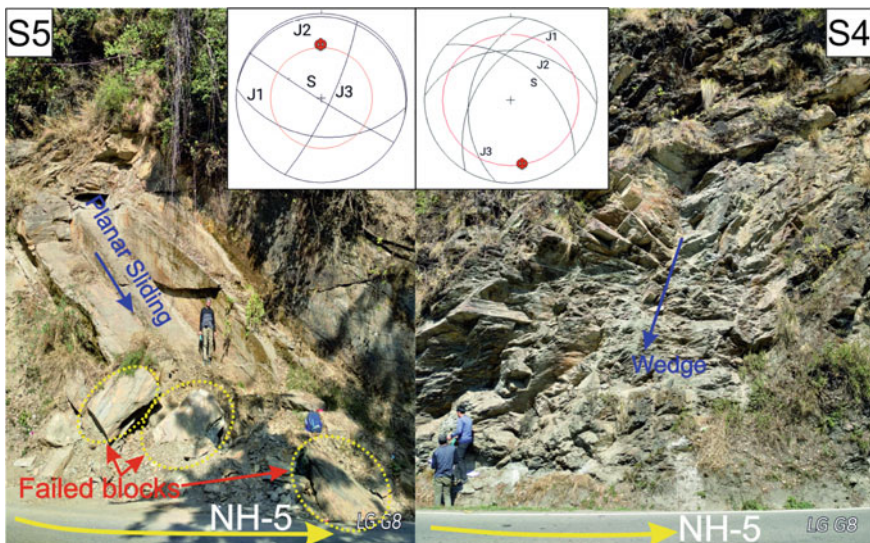


Fig. 2 Field photographs and corresponding stereoplots depicting planar and wedge failures at site nos. S5 and S4 respectively

Table 3 Orientation of discontinuities and slope along with probable structurally controlled failure

Site no	Orientation (Dip amount/Dip Direction) in degrees					Most prominent failure type & set causing failure
	Slope Face	J1	J2	J3	J4	
S1	47/322	28/245	56/020	n/a	n/a	Wedge due to J1 & J2
S2	72/065	88/131	46/232	64/056	n/a	Planar due to J3
S3	88/092	82/120	22/200	74/036	n/a	Wedge due to J1 & J3
S4	55/042	56/302	40/003	50/280	n/a	Wedge due to J1 & J2
S5	88/212	52/186	04/010	81/115	n/a	Planar due to J1
S6	88/340	61/112	88/110	60/005	n/a	Planar due to J3
S7	74/350	36/036	78/278	n/a	n/a	Wedge due to J1 & J2
S8	65/ 230	74/000	40/347	79/270	n/a	Wedge due to J1 & J2
S9	35/ 315	43/344	57/150	n/a	n/a	Planar due to J1
S10	50/056	48/044	49/302	69/195	n/a	Planar due to J1
S11	63/082	30/271	22/230	55/020	86/314	Wedge due to J3 & J4

single set of discontinuities; rather a particular intersection of two or more discontinuities favours wedge sliding conditions. Geometric relationship among prevailing discontinuities and slope face at site no. S4 favours wedge failure (Fig. 2). When the intersection of two discontinuity sets lies within a critical zone, i.e. the zone formed between a friction circle and a great circle of slope face. The probability of wedge sliding is maximum when an intersection point is formed in the middle portion of the crescent-shaped critical zone. Probability is reduced gradually when the intersection is near the periphery of the critical zone. Any intersection of discontinuities lying beyond the critical zone will not form wedge failure. In the studied section, site no. S4 is favourable for wedge sliding. Wedge failure is likely to occur at site no. S4, where the azimuth of the slope face is 042° and the intersection of discontinuity sets J1 and J2 is lying near the central portion of the critical zone formed between the great circle slope face and friction circle. The line formed by the intersection is plunging towards the azimuth of the slope face. The coupled effect of these conditions offers a significant probability of wedge failure occurring. Similarly, the most prominent mode of failure and contributing discontinuity (s) for all studied locations are determined by employing principles of kinematic analysis [5].

3.3 Slope Mass Rating (SMR) and its Extensions

Slope mass rating is a worldwide accepted classification and stability assessment of jointed rock mass [22, 28]. It was developed by Romana in 1985 [17] and later modified when applied to varying initial conditions of slope. It is based on the basic quality of rock mass evaluated in Bieniawski's RMR and some factors related to

Table 4 Results of discrete and continuous SMR system

Site No	RMR _b	Prominent failure	Function	F1	F2	F3	F4	SMR/CSMR	Class	Stability grade
S1	57	Wedge	D	0.70	0.15	-60	8	59	III	Partially stable
			C	0.74	0.21	-59.40	8	56	III	Partially stable
S2	67	Planar	D	0.85	1	-50	8	32	IV	Unstable
			C	0.87	0.97	-57.62	8	26	IV	Unstable
S3	69	Planar	D	0.15	1	-60	8	68	II	Stable
			C	0.27	0.98	-58.73	8	62	II	Stable
S4	57	Wedge	D	0.15	0.85	-60	8	57	III	Partially stable
			C	0.23	0.89	-58.64	8	53	III	Partially stable
S5	55	Planar	D	0.4	1	-60	10	41	III	Partially stable
			C	0.39	0.95	-59.47	10	43	III	Partially stable
S6	44	Planar	D	0.4	1	-60	8	28	IV	Unstable
			C	0.41	0.97	-59.32	8	29	IV	Unstable
S7	47	Wedge	D	0.7	0.7	-60	8	26	IV	Unstable
			C	0.8	0.68	-59.55	8	22	IV	Unstable
S8	60	Wedge	D	1	0.15	-60	10	61	II	Stable
			C	1	0.27	-59.58	10	54	II	Partially stable
S9	42	Planar	D	0.4	0.85	-6	15	55	III	Partially stable
			C	0.34	0.9	-2.38	15	56	III	Partially stable
S10	58	Planar	D	0.7	1	-50	8	31	IV	Unstable
			C	0.8	0.93	-51.14	8	28	IV	Unstable
S11	47	Wedge	D	0.15	1	-60	8	46	III	Partially stable
			C	0.23	0.95	-58.1	8	42	III	Partially stable

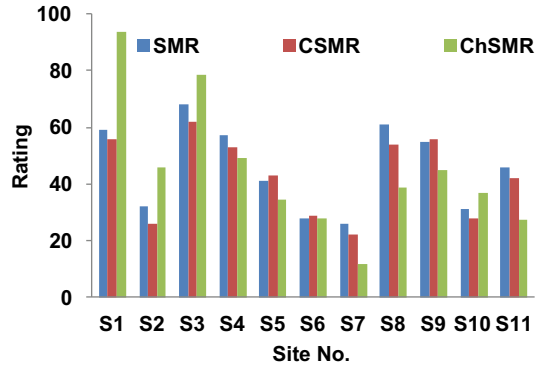
D: Discrete functions are used in SMR and C: Continuous functions are used in CSMR

Table 5 Results of ChSMR

Site no	Height (meters)	λ	F1	F2	F3	F4	ChSMR	Stability grade
S1	25	0.7	0.74	0.21	-59.40	8	93	Completely stable
S2	30	0.7	0.87	0.97	-57.62	8	46	Partially stable
S3	27	0.7	0.27	0.98	-58.73	8	78	Stable
S4	35	0.7	0.23	0.89	-58.64	8	49	Partially stable
S5	45	0.7	0.39	0.95	-59.47	10	35	Unstable
S6	26	0.7	0.41	0.97	-59.32	8	28	Unstable
S7	52	0.7	0.8	0.68	-59.55	8	12	Completely unstable
S8	60	0.7	1	0.27	-59.58	10	39	Unstable
S9	28	0.85	0.34	0.9	-2.38	15	45	Partially stable
S10	31	0.7	0.8	0.93	-51.14	8	37	Unstable
S11	47	0.7	0.23	0.95	-58.1	8	28	Unstable

the orientation of joints and excavation method [18]. The most vulnerable set of discontinuity favouring planar and wedge mode of failure was assessed by kinematic analysis of slopes. In this study, engineered cut slopes are categorized into different stability grades by applying extensions of the SMR system, including CSMR [34] and ChSMR [3]. The discrete nature of the original SMR system may mislead the results to some extent particularly when values are at or near the border of class intervals [28]. CSMR method is based on continuous functions of adjustment factors for discontinuity orientation, which is advantageous over a discrete SMR system [25]. SMR and CSMR are computed by using RMR_{basic} , kinematic analysis and orientation parameters (Table 4). It is noticeable that slope dimensions, particularly slope height are an important parameter in slope stability studies. The type of discontinuities also governs failure characteristics. Different types of discontinuities may not have a similar influence on the stability of slopes. SMR and CSMR methods neither account for slope height nor type of discontinuity. ChSMR method by [3] includes slope height and discontinuity factor (related to the type of discontinuity) in Romana's SMR. The combined role of continuous functions, slope height and type of discontinuity is assessed in this study by applying continuous functions of CSMR in ChSMR (Table 5). Outcomes of SMR and its extensions can also be compared with each other (Fig. 3). It is noticeable that most of the studied slopes have the least value by the ChSMR method. The results obtained by ChSMR may be considered as most reliable to classify the rock mass.

Fig. 3 Bar graph showing results of SMR, CSMR and ChSMR of studied slopes along NH-5



4 Conclusions

The majority of slopes along NH-5 are liable to undergo planar sliding and wedge failure. According to SMR and CSMR, most slopes fall under the unstable to a partially stable category, while some slopes are stable. The rating systems that take account of continuous functions and height, i.e., ChSMR are showing a diverse range of stability values ranging from 12 to 93 and the majority of the slopes fall from unstable to partially unstable category. Various stability measurements should be adopted to stabilize these road-cut engineered slopes. Such slopes must be treated with rock bolting, grouting and shotcrete. Cut slopes having blocky mass should have wire mesh to retain occasionally falling blocks. Such a quick assessment provided a brief insight into the slope instability issues of the studied section. Numerical simulation studies are suggested for a detailed appraisal of the underlying mechanism of slope failures along the highway.

References

1. Ansari T, Kainthola A, Singh KH, Singh TN, Sazid M (2021) Geotechnical and micro-structural characteristics of phyllite derived soil; implications for slope stability, Lesser Himalaya, Uttarakhand, India. *Catena* 196:104906. <https://doi.org/10.1016/j.catena.2020.104906>
2. Bieniawski ZT (1989) *Engineering rock mass classification*. Wiley, New York, p 251p
3. Chen Z (1995) Recent developments in slope stability analysis. In: *Proceedings of the 8th international congress of rock mechanics*, Tokyo, Japan.
4. Himachal Pradesh State Disaster Management Authority (HPSDMA 2017) *Himachal Pradesh State Disaster Management Plan 2017*, Shimla, Himachal Pradesh, India
5. Hoek E, Bray JW (1981) *Rock Slope Engineering*. In 3rd edition, The Institution of Mining and Metallurgy, London
6. Hoek E, Brown ET (1980) *Underground Excavations in Rock*. Institution of Mining and Metallurgy, London, London
7. ISRM (1978) Suggested methods for determining the uniaxial compressive strength and deformability of rock materials. *Int J Rock Mech Mining Sci Geomech Abstr* 16:135–140

8. ISRM (1981) ISRM Suggested methods for the quantitative description of discontinuities in rock masses. In: Brown ET editor. Rock characterization, testing and monitoring: ISRM suggested Methods. Pergamon, Oxford
9. Kumar M, Rana S, Pant PD, Patel RC (2017) Slope stability analysis of Balia Nala landslide, Kumaun Lesser Himalaya, Nainital, Uttarakhand, India. *J Rock Mech Geotech Eng* 9(2017):150–158
10. Kundu J, Sarkar K, Singh AK, Singh TN (2020) Continuous functions and a computer application for Rock Mass Rating. *Int J Rock Mech Min Sci* 129:104280
11. Kundu J, Sarkar K, Tripathy A, Singh TN (2017) Qualitative stability assessment of cut slopes along the National Highway-05 around Jhakri area, Himachal Pradesh, India. *J Earth Syst Sci* 126:112
12. Li J, Villaescusa E (2005) Determination of rock mass compressive strength using critical strain theory. In proceedings of Alaska Rocks 2005, The 40th U.S. Symposium on Rock Mechanics, Alaska
13. Mazumdar P, Mukhopadhyay A, Thorie A, Banerjee T, Rai SK (2021) Geochemistry of Neoproterozoic Chhaosa shales, Simla Group, Lesser Himalaya: Its implications on provenance and tectonics. *J Earth Syst Sci* 130:175
14. Neeraj PK, Sarkar S (2018) Stability assessment of cut slopes along Shivpuri – Kaudiyala road (NH-58), Uttarakhand Himalayas. In: Proceedings of Indian geotechnical conference, Bengaluru, India
15. Palmstrom A (1974) Characterization of jointing density and the quality of rock masses. Internal report, Berdal, Norway
16. Palmstrom A (1982) The volumetric joint count - a useful and simple measure of the degree of jointing. In: Proceedings of the 4th congress of international association of engineering geology, New Delhi, India: V.221–V.228
17. Romana M (1985) New adjustment ratings for application of Bieniawski classification to slopes. In: International symposium on the role of rock mechanics ISRM, Zacatecas, pp 49–53
18. Romana M (1993) A geomechanics classification for slopes: slope mass rating. In: Hudson J (ed) *Comprehensive rock engineering*, vol 3. Elsevier, Pergamon, pp 575–600
19. Romana M, Tomás R, Serón JB (2015) Slope Mass Rating (SMR) geomechanics classification: thirty years review. In: Proceedings of the 13th congress of international symposium on rock mechanics, Quebec, Canada, p 10
20. Sardana S, Verma AK, Singh A, Laldinpuia (2019) Comparative analysis of rockmass characterization techniques for the stability prediction of road cut slopes along NH-44A, Mizoram, India. *Bull Eng Geol Environ* 78: 5977–5989
21. Sarkar K, Sazid M, Khandelwal M, Singh TN (2009) Stability analysis of soil slope in Luhri area, Himachal Pradesh. *Mining Engineer's J* 10(6):21–27
22. Sarkar S, Kanungo DP, Kumar S (2012) Rock mass classification and slope stability assessment of road cut slopes in Garhwal Himalaya, India. *Geotech Geol Eng* 30:827–840
23. Sazid M (2018) Correlation of ultrasound velocity with physico-mechanical properties of Jodhpur sandstone. *Mater Test* 60(11):1093–1096. <https://doi.org/10.3139/120.111258>
24. Sazid M (2019) Analysis of rockfall hazards along NH-15: a case study of Al-Hada road. *Int J Geo-Eng* 10:1
25. Siddique T, Khan EA (2019) Stability appraisal of road cut slopes along a strategic transportation route in the Himalayas, Uttarakhand, India. *SN Appl Sci* 1:409
26. Siddique T, Pradhan SP (2018) Stability and sensitivity analysis of Himalayan road cut debris slopes: an investigation along NH-58, India. *Nat Haz* 93(2):577–600
27. Siddique T, Alam MM, Mondal MEA, Vishal V (2015) Slope Mass rating and kinematic analysis of slopes along national highway-58, near jonk, Rishikesh, India. *J Rock Mech Geotech Eng* 7(5):600–606
28. Siddique T, Mondal MEA, Pradhan SP, Salman M, Soheli M (2020) Geotechnical assessment of cut slopes in the landslide prone Himalayas: rock mass characterization and simulation approach. *Nat Hazards* 104:413–435

29. Siddique T, Pradhan SP, Vishal V, Mondal MEA, Singh TN (2017) Stability assessment of Himalayan road cut slopes along National Highway 58, India. *Environ Earth Sci* 76:759
30. Singh HO, Ansari TA, Singh TN, Singh KH (2020) Analytical and numerical stability analysis of road cut slopes in Garhwal Himalaya, India. *Geotech Geol Eng* 38:4811–4829
31. Singh J, Thakur M (2019) Landslide stability assessment along Panchkula-Morni road, Nahan salient, NW Himalaya, India. *J Earth Syst Sci* 128:148
32. Singh PK, Wasnik AB, Kainthola A, Sazid M, Singh TN (2013) The stability of road cut cliff face along SH-121: a case study. *Nat Hazards* 68(2):497–507. <https://doi.org/10.1007/s11069-013-0627-9>
33. Technical Advisory Response Unit (TARU 2015) Preparation of Hazard, Vulnerability & Risk Analysis atlas and report for the state of Himachal Pradesh. In *Landslide Hazard Risk Assessment Composite Final Draft Report*, New Delhi and Ahmedabad, India.
34. Tomás R, Delgado J, Serón JB (2007) Modification of slope mass rating (SMR) by continuous functions. *J Rock Mech Min Sci* 44:1062–1069
35. Umrao RK, Singh R, Ahmad M, Singh TN (2011) Stability analysis of cut slopes using continuous slope mass rating and kinematic analysis in Rudraprayag District, Uttarakhand. *Geomaterials* 03:79–87
36. Yagiz S (2009) Predicting uniaxial compressive strength, modulus of elasticity and index properties of rocks using the Schmidt hammer. *Bull Eng Geol Env* 68(1):55–63

Analysis of Joint Parameters to Understand it's Effect on Rock Blasting



Rajesh Silwal, Suman Panthee, and Ashutosh Kainthola

Abstract Rock mass consists of intact rock material and joints. Different joint parameters like orientation, spacing, persistence, aperture, infilling play important role in tunnel excavation. In drill and blast tunnel excavation, the propagation of blast shock wave differs from one rock mass to another rock mass based on their properties, because of which nature of rock fragmentation differs. All these directly affects the outcome of tunnel blasting. This study establishes the relationship between different joint parameters and excavation volume. In order to do so four different tunnel section of same tunnel alignment, with different joint properties were chosen and then collected data was processed to understand how different joint properties lead to different excavation volume within same tunnel. It was found that when the strike of the joint is parallel to the tunnel axis, the excavation volume obtained from blasting is comparatively higher than that when strike of joint is perpendicular to the tunnel axis, because when joints are parallel to the tunnel axis there is minimum reflection of blast wave from joint plane causing it to travel farther, increasing the fragmentation process. Shape analysis of blast fragments and natural rock block obtained from 3DEC was done in order to find the effect on fragmentation process. It was found that both blast fragments and natural rock block have similar percentage of different shape class proving fragmentation process during blasting of rock mass follows joint pattern, since they are the weak surface in rock mass.

Keywords Joint parameters · Blasting · Fragmentation · Natural block

R. Silwal · S. Panthee (✉)
Central Department of Geology, Tribhuvan University, Kathmandu, Nepal
e-mail: sumanpanthee@gmail.com

R. Silwal
e-mail: rajesh.silwal2@gmail.com

A. Kainthola
Department of Geology, Banaras Hindu University, Varanasi, India
e-mail: ashutosh.geo@bhu.ac.in

© The Author(s), under exclusive license to Springer Nature Singapore Pte Ltd. 2022
A. K. Verma et al. (eds.), *Proceedings of Geotechnical Challenges in Mining, Tunneling and Underground Infrastructures*, Lecture Notes in Civil Engineering 228,
https://doi.org/10.1007/978-981-16-9770-8_48

1 Introduction

Fragmentation due to blasting is influenced by the rock mass properties [1]. Properties like rock mass strength, joint conditions and pattern affects the propagation of shock wave generated by blasting [2, 3]. Joint planes restrict the shock wave travel, therefore, the orientation of joint planes, angle made by joint plane with blast hole dictate the nature of fragmentation [4]. Other than rock mass properties, the type and energy of the explosive also affects the result of blasting [5]. Design of the blasting pattern considering all these parameters is essential for controlled blasting in order to achieve the maximum possible excavation volume, without over break and under break [6].

Joint parameters like orientation, continuity, spacing, aperture, infilling material are localized for a tunnel excavation and dependent on the stress environment and geological conditions [7]. Likewise, blasting of rocks differs for each site and condition. Joint parameters affect the nature of blasting. There might be problem of over break and under break if similar kind of blasting pattern is sued for every tunnel. Therefore, the design of blasting pattern and the choice of the explosive should be based on the different factors, one of them is joint parameters [8].

Formation of natural rock block because of intersection of multiple joints is common in nature. These rock block decreases the rock mass strength also affecting the outcome of blasting. The fragmentation during blasting follows the joint plane producing the blast fragments similar in size and shape to that of natural rock block [9].

The study area lies along the Madhi river just below Tangting village located in Kaski district of Gandaki province, Nepal. The research work is done within the project site of super Madi Hydroelectric Project which is on construction phase. The latitude and longitude of the area is $28^{\circ}19'39''$ N to $28^{\circ}21'39''$ N and $84^{\circ}04'45''$ E to $84^{\circ}04'34''$ E.

2 Methodology

To understand the geological and engineering geological setup of the study area, engineering geological mapping was done. It was done by planning the study route with the help of topographic map and then visiting the route based on the route decided. For making engineering geological map different data such as attitude of the joints, foliation, geomorphological information, landslide information, soil and rock properties were collected.

For this research another important part includes the study of joint parameters inside the tunnel section and blasting parameters within same section of the tunnel. Joint parameters include joint orientation, spacing, aperture, persistence, infilling material whereas blasting parameters includes powder factor, blasting pattern, spacing and burden between blast hole, delay time etc. [10]. In order to collect these data, a data collection log sheet was prepared. After the blasting the fragments of rock charges out of tunnel face because of stress wave produced during explosion of emulsion inside the blast hole. These rock fragments are called muck

Fig. 1 Illustration of rock fragment with a, b and c axis

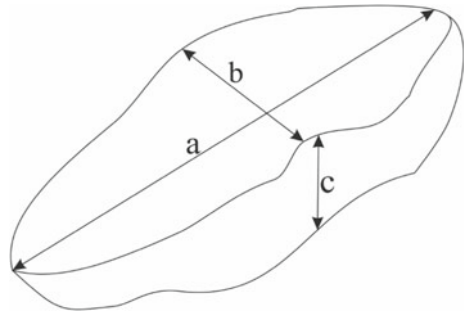
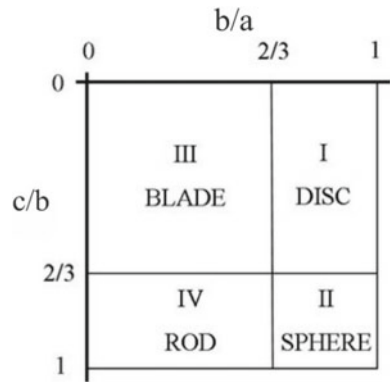


Fig. 2 Zingg [11] shape classification graph



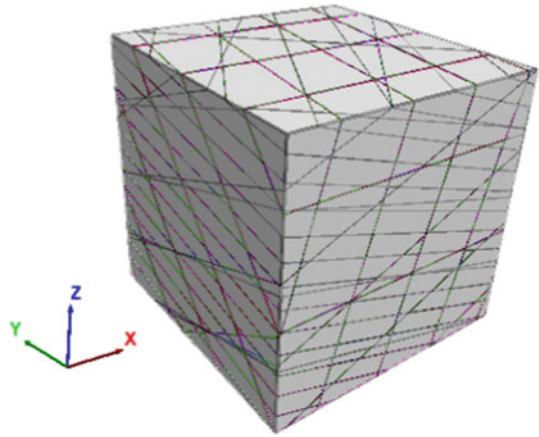
or blast fragments. The short axis (a), intermediate axis (b) and long axis (c) of these blast fragments were measured in the field using measuring tape (Fig. 1).

Data obtained from measuring the short, intermediate and long axis of the blast fragments were processed in the graph for the shape classification of rock fragments. Shape classification was done in order to compare the shape of blast fragments and shape of natural block formed by the intersection of joints. From this comparison we would know whether the joints affect the outcome of blasting or not. For the shape classification, Zingg [11] bi-variate graph was used which uses two shape indices b/a and c/b to define four shape classes: blade, disc, rod and sphere (Fig. 2).

2.1 Modelling of Natural Rock Block Using 3DEC

According to Block theory when three or more joint planes with different orientation intersect with each other there is formation of natural block of different shape and sizes [12–15]. To understand the shape and size of these natural block computer-based modelling was done using the software called 3DEC. From the software 3DEC, a natural block was created based on the data collected in the field. Data used to create the model were orientation of the joint plane, spacing of the joints and persistence of the joint. The rock bock of dimension $4 \times 4 \times 4$ m was created. The persistence of joint was kept 100% within the block to make the model simpler. 3DEC commands

Fig. 3 Intersection of joints within 3D block created using 3DEC



like polyBRICK, JSET were used to create the block (Fig. 3). After creating the block with different joints, the software generated different data like volume of each individual block, centroid of the individual block, XYZ axes of the block etc. The data obtain for the software was used to generate the shape classification graph for naturally occurred rock blocks.

3 Results

Joint parameters value might be similar within certain section of tunnel. So, there will be no variation in data collected and we cannot establish the relation in between two variables with the use of same data sets. In order to overcome this problem data were collected from different tunnel section having different tunnel axis and different joints data (Table 1). Tunnel axis is not same within whole length of tunnel in Super Madi hydropower project. Four different sections were chosen to collect the data (Fig. 4).

The axis of Sect. 1 of the tunnel alignment is 17° (Fig. 5). The attitude of the foliation plane within this section is 150/28. Major joint sets are 280/75, 22/53, 180/50. And the average spacing of the joint sets is 30–80 cm. Angle made by tunnel

Table 1 Different tunnel section with different axis

Tunnel section	Tunnel axis ($^\circ$)	Chainage (m)
Section 1	17	0–1350
Section 2	345	1350–1650
Section 3	29	1650–2770
Section 4	62	2770–4600

Fig. 4 Illustration of tunnel alignment with different tunnel sections

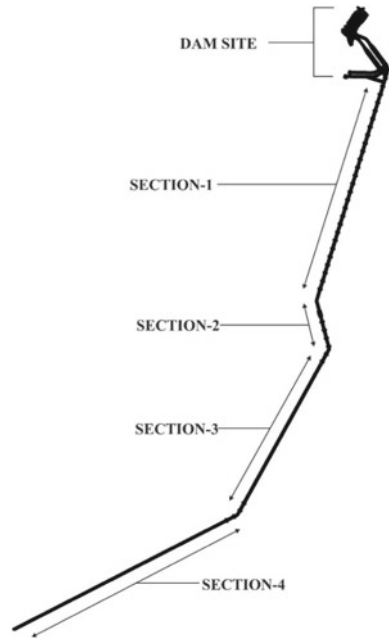
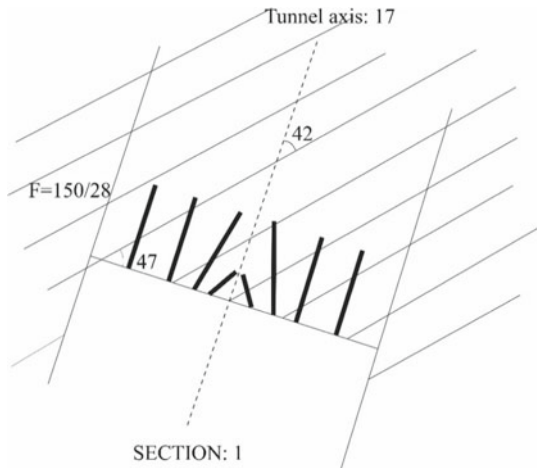


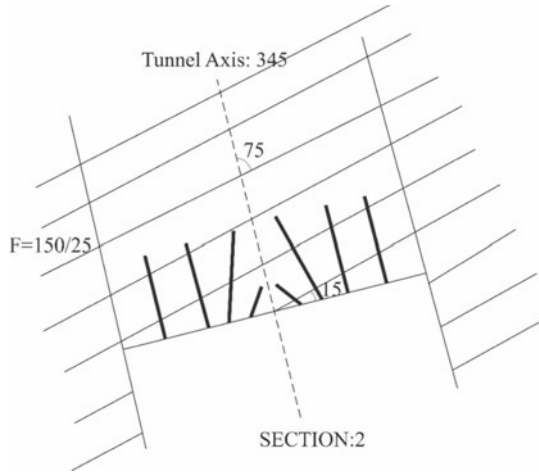
Fig. 5 Illustration of top view of tunnel Sect. 1



axis with the strike of foliation plane is 42 in this section. By using DIPS, the angle between blasthole and joint plane was calculated and found to be 18°.

The axis of Sect. 2 of the tunnel alignment is 345 (Fig. 6). The attitude of foliation plane within this section is 150/25. Major joint sets are 275/70, 030/50, 165/45. And the average spacing of joint sets is 25–80 cm. Angle made by tunnel axis with the

Fig. 6 Illustration of top view of tunnel Sect. 2



strike of foliation plane is 75°. Angle made by blast hole and foliation plane was calculated as 23°.

The axis of Sect. 3 of the tunnel alignment is 29° (Fig. 7). The attitude of foliation plane within this section is 80/70. Major joint sets are 185/55, 120/60, 310/30. And the average spacing of joint sets is 30–80 cm. Angle made by tunnel axis with the strike of foliation plane is 45°. Angle made by blast hole and foliation plane was calculated as 40° using DIPS.

The axis of Sect. 4 of the tunnel alignment is 62° (Fig. 8). The attitude of foliation plane within this section is 145/25. Major joint sets are 180/55, 120/60, 310/30. And the average spacing of joint sets is 30–80 cm. Angle made by tunnel axis with the

Fig. 7 Illustration of top view of tunnel Sect. 3

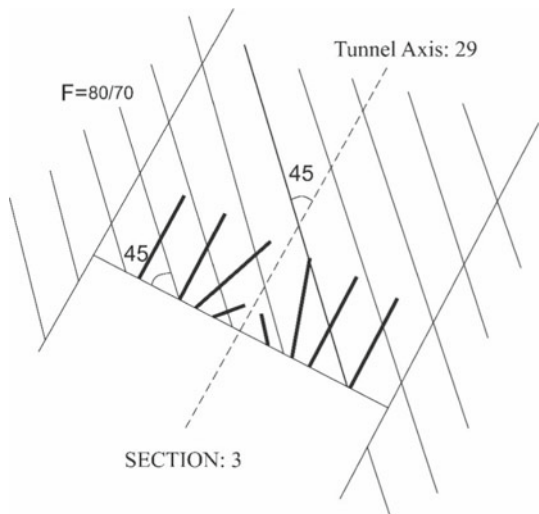
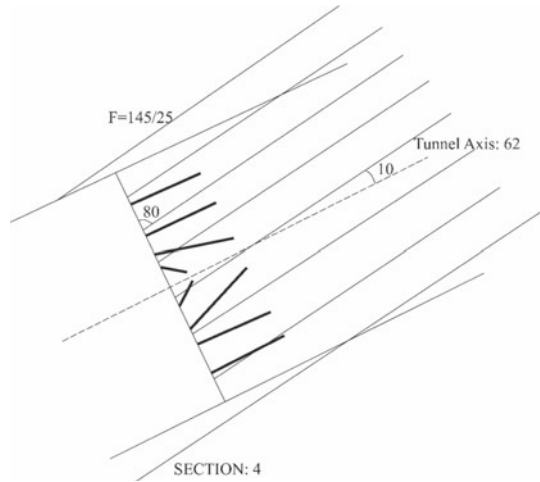


Fig. 8 Illustration of top view of tunnel Sect. 4



strike of foliation plane is 10°. Angle made by blast hole and foliation plane was calculated as 5 using DIPS.

3.1 Relationship Between Powder Factor and Q

From the graph (Fig. 9) a relation between PF and Q was established which is, $PF = 0.9637\ln(Q) + 4.4697$. With a R-squared value of 0.854 which shows that the strength of relationship between PF and Q is convenient.

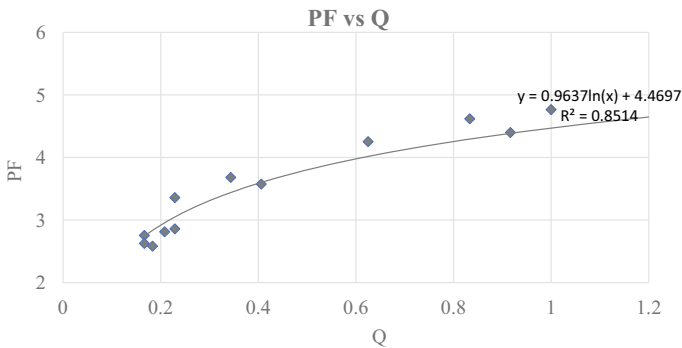


Fig. 9 Graph between powder factor and Q

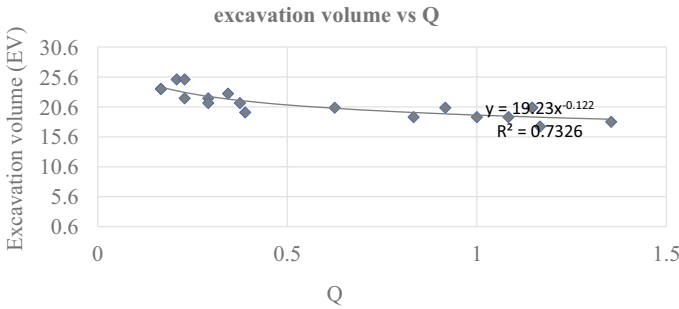


Fig. 10 Graph between excavation volume and Q

3.2 Relation Between Excavation Volume and Q

From the graph (Fig. 10) an empirical relation between EV (excavation volume) and Q was established as

$$EV = 19.23Q^{-0.122}$$

From the graph it is clear that as the Q value increases, the excavation volume decreases slightly.

3.3 Blast Fragments Shape Analysis

Data collected from the field were processed in Excel to do the shape analysis. Two different classification method were followed in order to find the percentage of different shape class. Figure 11 shows the Zingg shape classification graph [11, 16, 17], in which there are two axes. X axis represent the ratio of short axis to intermediate axis whereas Y axis represent the ratio of intermediate axis to long axis.

From the graph of Zingg shape classification was prepared listing the percentage of the different shape classes (Table 2). From the sampled rock fragments 22.4% were of oblate (disc) shape, 14.6% were of spheroid shape, 35.9% were of blade shape and 26.9% were of prolate (rod) shape.

3.4 Natural Block Shape Analysis

Natural block formed by the intersection of joints within the rock mass was modelled using the software 3DEC (Fig. 12). By using the software, we found the volume and centroid of each and every block within the model (Fig. 13). We also found the a, b

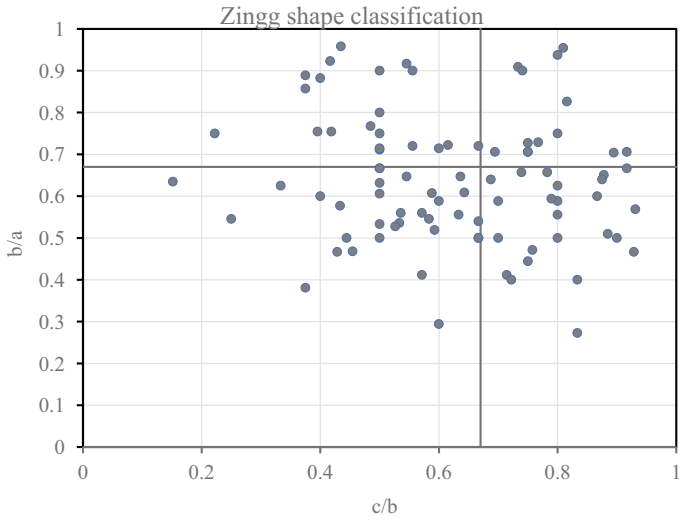


Fig. 11 Zingg shape classification graph for blast fragments

Table 2 Different shape class percentage obtained for Zingg shape classification

Class	Shape	Count	Percent
I	Oblate (disc)	20	22.4719
II	Spheroid	13	14.6067
III	Blade	32	35.9551
IV	Prolate (rod)	24	26.9663

Fig. 12 Intersection of different joints within a block

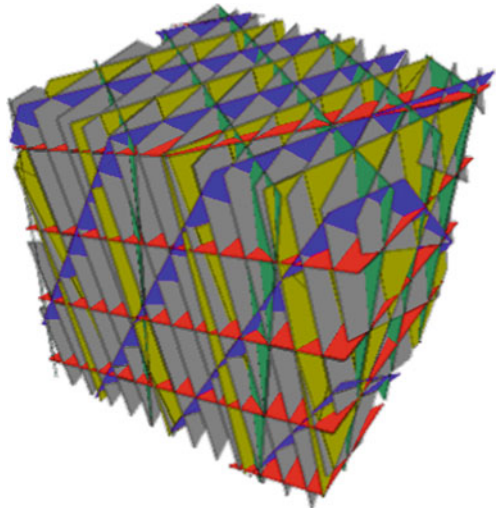
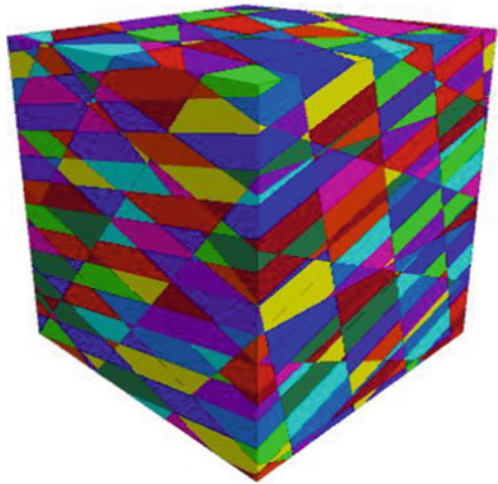


Fig. 13 Formation of in-situ natural block due to intersection of joints



and c axis of these block, which were used for the shape analysis (Fig. 14).

From the graph of Zingg shape classification Table 3 was prepared listing the percentage of the different shape classes. From the sampled rock fragments 23.52% were of oblate (disc) shape, 17.64% were of spheroid shape, 31.37% were of blade shape and 27.45% were of prolate (rod) shape.

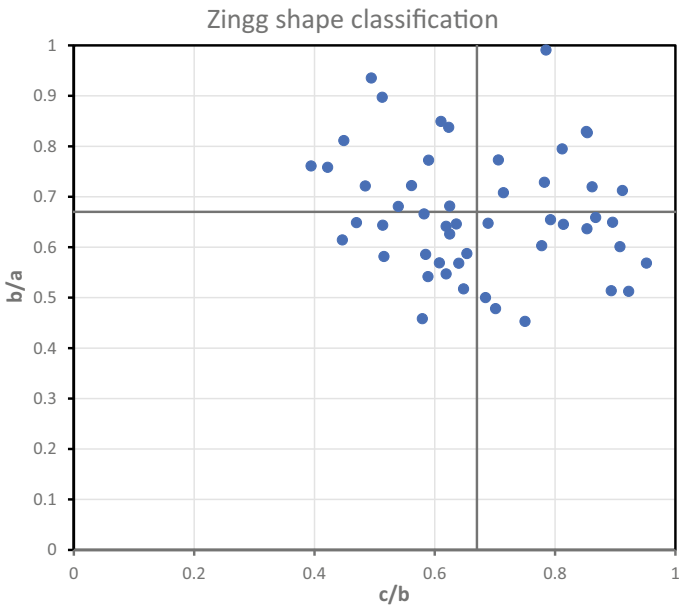


Fig. 14 Zingg shape classification graph for in-situ natural block

Table 3 Different shape class percentage obtained from Zingg shape classification of natural block

Shape	Count	Percent
Oblate (disc)	12	23.5294
Spheroid	9	17.6471
Blade	16	31.3725
Prolate (rod)	14	27.451

4 Discussion

The outcome of this research work includes understanding of outcome of blasting based on different joint parameters in different tunnel section, establishment of relation between PF and Q, Q and excavation volume (EV).

Previously, Chakraborty et al. [18] had studied the effect of rock mass quality and joint orientation on tunnel blasting in which they used the physical model for blasting in order to understand whether the propagation of shock wave is restrain by plane of weakness or not. From their research they found out that when joints are perpendicular to the tunnel axis wider crater was formed after blasting and when joints are parallel to the tunnel axis deeper crater was formed after blasting. Same concept was followed in this research but without using any kind of model, actual field data form four different tunnel section were used to find the similar result. This research work also includes that blasting results are not only affect by angle between joint and tunnel axis but also angle between blast hole and joint plane has significant role in blasting.

These shapes of natural block and blast fragments were compared to understand whether the joints responsible for formation of in-situ rock block have some effect on rock fragmentation. And, from the result of the block analysis, it is confirmed that joint pattern does affect the fragmentation of rock during blasting since for both natural block and blast fragments maximum percentage of shape class was bladed class.

5 Conclusion

From the study of analyzed and processed data form four different section of tunnel, it is concluded that, if the strike of joint is parallel to the tunnel axis, there is possibilities of obtaining maximum pull length after blasting.

Blast hole is near to 45°, the pull length will be high resulting high excavation volume.

Powder factor (PF) describes the relationship between the excavation volume and weight of explosive. From the relationship between powder factor (PF) and Q it was established that as the Q value increases the powder factor (PF) also increases.

Block shape analysis of both natural block and blast fragments were done from same tunnel section. And from this analysis it was found that shape class between blast fragments is almost similar to that of natural block which indicates that the fragmentation during tunnel blasting follows joint pattern, as joint planes are the weakest surface within the rock mass. Intersection of joints dominantly influence the formation of rock blocks of different shape and size, which indirectly affects the tunnel blasting result.

References

1. Grenon M, Hadjigeorgiou J, Liu Q (1998) Quantifying in-situ rock block size and resulting fragment size distributions due to blasting. *Int J Blasting Fragn* 2(2):205–218
2. Salum AH, Murthy VM (2019) Optimising blast pulls and controlling blast-induced excavation damage zone in tunnelling through varied rock classes. *Tunn Undergr Space Technol* 85:307–318
3. Wang ZL, Konietzky H (2009) Modelling of blast-induced fractures in jointed rock masses. *Eng Fract Mech* 76(12):1945–1955
4. Petrovic N, Toth I, Stranjik A (2010) Determination rock parameters for effective Blasting using GSI. In: Ivanov, A., Zivkovic, Z. (eds.) *Proceedings on 42nd International October Conference on Mining and Metallurgy*, University of Belgrade, Technical Faculty in Bor, pp 142–145
5. Hudaverdi T, Kuzu C, Fisne A (2012) Investigation of the blast fragmentation using the mean fragment size and fragmentation index. *Int J Rock Mech Min Sci* 56:136–145
6. Man K, Liu X, Wang J, Wang X (2018) Blasting energy analysis of the different cutting methods. *Shock Vib* 3:1–13
7. Bertuzzi R (2019) Revisiting rock classification to estimate rock mass properties. *J Rock Mech Geotech Eng* 11(3):494–510
8. Li M, Zhu Z, Liu R, Liu B, Zhou L, Dong Y (2018) Study of the effect of empty holes on propagating cracks under blasting loads. *Int J Rock Mech Min Sci* 103:186–194
9. Ge Y et al (2018) Automated measurements of discontinuity geometric properties from a 3D-point cloud based on a modified region growing algorithm. *Eng Geol* 242:44–54
10. Palmstrom A (2005) Measurements of and correlations between block size and rock quality designation (RQD). *Tunn Undergr Space Technol* 20:362–377
11. Zingg T (1935) *Contribution to gravel analysis* (doctoral dissertation, ETH Zurich).
12. Goodman RE (1995) Block theory and its applications. *Geotechnique* 45:383–423
13. Buyer A, Aichinger S, Schubert W (2020) Applying photogrammetry and semi-automated joint mapping for rock mass characterization. *Eng Geol* 264:105332
14. Yang D, Wang X, Wang Y, An H, Lei Z (2020) Experiment and analysis of wedge cutting angle on cutting effect. *Adv Civ Eng* 4:1–16
15. Innaurato N, Mancini R, Cardu M (1998) On the influence of rock mass quality on the quality of blasting work in tunnel driving. *Tunn Undergr Space Technol* 13(1):81–89
16. Janga H, Kawamura Y, Shinji U (2019) An empirical approach of overbreak resistance factor for tunnel blasting. *Tunn Undergr Space Technol* 92:103060
17. Yang R, Ding C, Yang L, Chen C (2018) Model experiment on dynamic behavior of jointed rock mass under blasting at high-stress conditions. *Tunn Undergr Space Technol* 74:145–152
18. Chakraborty AK, Jethwa JL, Paithankar AG (1994) Effects of joint orientation and rock mass quality on tunnel blasting. *Eng Geol* 37:247–262

Effect of Sand Bed Thickness on the Response of Concrete Block Pavement: A Numerical Investigation



Subhashini Anandan , Vivi Anggraini ,
and Mavinakere Eshwaraiah Raghunandan 

Abstract This paper presents an insight into the effect of increasing sand bed thickness on the response of the concrete block pavement (CBP) subjected to vehicular loads. CBP sections with sand bed thickness of 10, 20 and 70 mm were chosen in this study. Simulations were carried out using three sets of acceleration amplitudes from vehicular movement with frequency ranging from 0 to 100 Hz under steady state modal dynamic conditions. The finite element package ABAQUS was used for the simulations. Different soil constitutive models including the linear elastic model, Mohr–Coulomb model and cap plasticity model were used to model the material behavior of the soil layers underneath the paving block layer for every case. The results were obtained in terms of acceleration and displacement responses in the frequency domain. Sand bed thickness of 20 mm was found to be the optimal case as the increase or decrease in thickness from this median value resulting in relatively higher displacement values. CBP sections with 70 mm thick sand bed accounted for higher values of vertical deflection followed by CBP section with 10 mm thick sand bed. Considerable shift in the resonance frequency was also observed for the CBP section with 70 mm thick sand bed. Further simulations using Mohr–Coulomb and linear elastic model were found to overestimate the deflection values as compared to the cap plasticity model. The numerical predictions using cap plasticity model were in close proximity with the experimental results, thus concluding it as a stable constitutive model for such applications to this end.

Keywords Soil models · Dynamic analysis · Soil displacement · Acceleration · Resonance frequency

1 Introduction

Providing transportation and clear access to machinery to facilitate various mining related activities is pivotal to ensure smooth operation of the mines and mining

S. Anandan · V. Anggraini · M. E. Raghunandan (✉)
Monash University Malaysia, 47500 Bandar Sunway, Malaysia
e-mail: mavinakere.raghunandan@monash.edu

© The Author(s), under exclusive license to Springer Nature Singapore Pte Ltd. 2022
A. K. Verma et al. (eds.), *Proceedings of Geotechnical Challenges in Mining, Tunneling and Underground Infrastructures*, Lecture Notes in Civil Engineering 228,
https://doi.org/10.1007/978-981-16-9770-8_49

721

operation. Within the mine site, ground-transport is the most preferred transport mode. Ground vibrations caused by vehicular movement are studied in many research works [1]. But in most cases, the vibrations from the moving loads are amplified by the road unevenness itself. Especially in the case of concrete block pavements (CBP), the discontinuities on paving layer accounting for short wavelength irregularities, is an unavoidable feature of the pavement. This can lead to the further amplification of the vibrations induced by moving traffic. Especially under higher vehicular loads, larger amplitudes occur at resonant condition even though the resonant frequency is reduced [2]. Henceforth, accelerations levels and shear strains measured in the soil substructure of CBP were high as compared to regular asphalt pavements. Subsequent degradation in subgrade strength occurs which further leads to the deterioration in performance of both surface paving layer and underground utilities on a long run [3, 4]. Not limiting to that, the traffic vibration induced strain levels in soil are comparable to that of the shear strains caused in soil by acceleration base input motion of 0.5 g [5]. But most of the dynamic studies focus in the surface layer alone. Other than the surface discontinuity in CBP, the physical and dynamic properties of the soil layers in the substructure play a crucial role in altering the resonant frequency of the whole CBP system. Even certain studies reveal the dampening nature of fibre rubber composites which can possibly change the attenuation characteristics of soil [6, 7]. Further, many studies on soil layering have shown how the stiffness and thickness of the underlying or overlying layer alters the frequency response of the vibrating system [8, 9]. Among the soil layers underneath CBP, the sand bed layer is given key preference because of its properties to increase the interlocking efficiency and load dispersion capability of concrete block surface layer [10]. But there is no definite value defined for the sand bed thickness. Across the world, different design values are established for the compacted sand bed thickness ranging anywhere between 20 to 50 mm [11] based on the experimental studies with static loading on CBP. Additionally, these test results also reveal that, increasing or decreasing the sand bed thickness from its ideal design value can lead to pavement deflections [12]. But the underlying cause for this deflection phenomenon in a dynamic perspective should be explored in detail before deciding on the standard value of sand bed thickness. In order to investigate this, parametric studies will be required since various vehicular loads and speed are required to be considered along with several other factors. Using a numerical modelling platform will be both cost and time effective, as compared to experimental investigations especially in case of parametric studies. Further most of the existing works have used a linear elastic model for the soil mass owing to its simplicity. But non-linear models can serve for more detailed analysis particularly for the case of repeated traffic loads.

The main aim of this work is to study and analyze the dynamic response of CBP with varying sand bed thickness and material models under vehicular loading (vibrations) of different acceleration amplitudes. In order to achieve this, a series of finite element simulations were carried out using three constitutive soil models – Linear elastic, Mohr–Coulomb and Cap Plasticity, on three cases of concrete block pavements having varying sand bed thickness from 10 to 70 mm. The key objectives of the analysis include identification of the effect of sand bed thickness on the dynamic

response of the CBP system under vehicular load in terms of acceleration frequency response and displacement frequency response followed by cross comparison of the results from the constitutive models to evaluate the material model accuracy qualitatively. Further the characteristics of the input vehicular vibration such as the acceleration amplitude and frequency are varied to study the difference among the three cases of CBP in depth. The results are discussed in terms of peak vertical acceleration, vertical deflection at surface, equivalent damping ratios and resonant frequency values.

2 Case Description of Concrete Block Pavements

Three different CBP sections with superstructure made of square paving blocks followed by substructure comprising of sand bed layer of varying thickness, base course layers and subgrade are chosen for the study. CBP Sect. 1 is designed with a sand bed thickness of 20 mm followed by base layer of 300 mm in depth and subgrade of 1100 mm in depth. CBP Sects. 2 and 3 were having sand bed thickness of 20 and 70 mm respectively while the base course and subgrade layers remain unaltered. In all the three sections, soil substructure is non-homogeneous inhomogeneous. Since the analysis of the soil mass is intended to be carried out using different constitutive models such as linear elastic (LE), elastic – perfectly plastic Mohr–Coulomb model (MC) and modified Drucker Prager Cap model (DP), the material properties pertaining to each category is listed in the Table 1 below. The material properties for cap model were extracted through calibration in FE simulations, based on the experimental data obtained from previous studies [13]. Since Mohr–Coulomb parameters for the soil is unavailable, empirical Eqs. (1) and (2) from [14] were used as follows in order to convert Drucker Prager constants into Cohesion and friction angle values of soil.

Table 1 Material properties of the soil layers in concrete block pavement

Layer		Linear elastic model		Mohr–Coulomb model		Modified Drucker Prager model				
		Density (kN/m ³)	E (MPa)	μ	C (MPa)	φ (degree)	d (MPa)	β (degree)	R	α
Sand bed	18	350	0.3	0.01	39.6	1	45	5E-04	0.03	0.8
Base course	18	240	0.4	0.2062	39.6	0.8	45	5E-04	0.03	0.8
Subgrade	15	100	0.4	0.047	18.2	0.3	35	5E-04	0.03	0.8

E - Elasticity Modulus, μ - Poisson’s ratio, d - Cohesion; β - Friction angle; α - Transition surface radius, K - Flow stress ratio; R - Cap eccentricity

$$\tan \beta = \frac{6 - \sin \phi}{3 - \sin \phi} \tag{1}$$

$$d = \frac{18 C \cos \phi}{3 - \sin \phi} \tag{2}$$

where c and ϕ are the Cohesion and friction angle in Mohr–Coulomb model and β , d are the friction angle and cohesion in cap plasticity model.

3 Experimental Validation

Previously, experimental studies were conducted on CBP test section built in a test tank. The surface layer was subjected to sinusoidal vibrations of varying frequency under a surcharge load of 30 kN. The experimental test results of vertical stress and peak vertical acceleration (experimental analysis shall be discussed elsewhere) were used to validate the numerical finite element model. The comparison of experimental data with the numerical one is shown in Fig. 1a below. It can be observed that the simulation result values are little less than the experimental ones but the FE models were able to mimic the variation trend of experimental data to a good accuracy. The features of the validated CBP model is shown in Fig. 1b. On this validated model the proposed parametric studies were conducted by making changes in the soil profile in order to bring up the three different CBP sections under study.

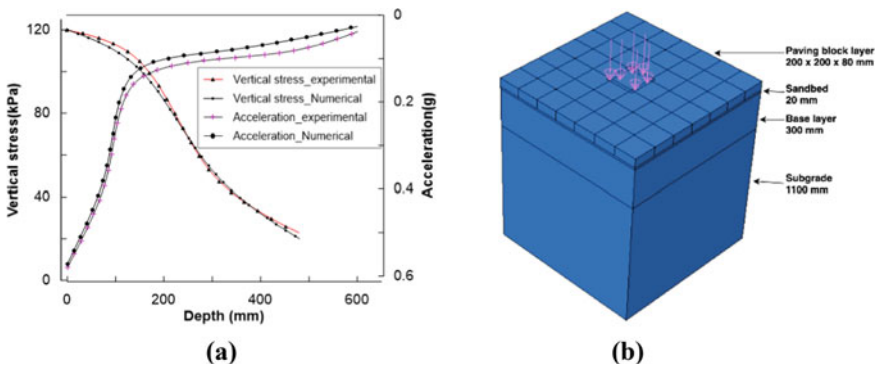


Fig. 1 a Variation of acceleration values and vertical stress with increasing depth at the loading area b Validated FE Model of CBP

4 Numerical Studies

The three-dimensional FE procedure is chosen for this study owing to the reduced cost and increased computational efficiency that can handle complex material properties and boundary conditions at ease. Effect of the increasing sand bed thickness in the pavement substructure on the wave propagation and resonance condition is investigated under vehicular vibrations of different amplitudes. Pure sinusoidal vibrations of amplitudes 0.6, 0.8 and 1 g as shown in Fig. 2a are chosen for the study. This is because the acceleration levels of imparted vibrations from a 2-axle vehicle was found in the range of 0.2 to 3 g in the case of concrete block pavements [3]. Higher values of 'g' correspond to higher energy associated with the waves produced by higher vehicular loads and vice versa. The loading area was determined based the single axle load of 41 kN and contact pressure of 0.6 MPa. The height and width of the model was chosen to be more than 3 to 4 times the width of the loading

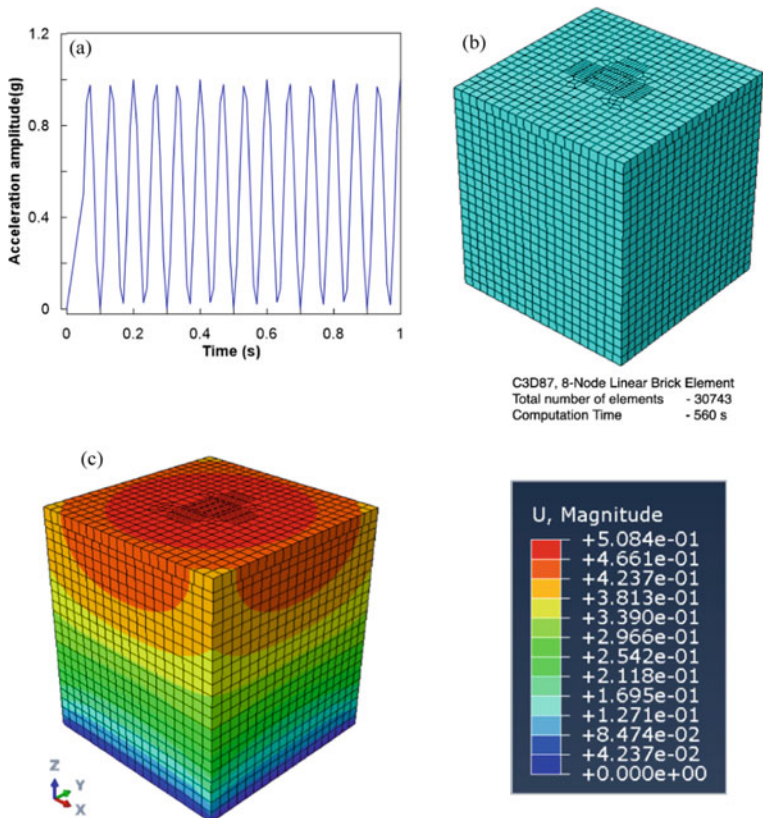


Fig. 2 a Sample of acceleration input of vehicular vibrations b Meshed CBP model c Deformed CBP Model (case 1-0.6 g)

area to avoid any boundary reflections that may occur. Thus, the model geometry of the CBP sections under analysis was $1400 \times 1400 \times 1500$ mm. The rigidity at the base is ensured by using encastre boundary condition at the bottom of the pavement model in order to constrain the movement in all directions and the interface between subgrade and base layer was addressed using a tie constraint, so as to save computation time. Load was applied at the center of the model. In any vibration analysis, time discretization is very important and hence analysis time increments were chosen in such a way to attain stable solution.

Proper evaluation of the soil strata is necessary in order to account for realistic and effective vibration response. Adapting a linear material model cannot account for the permanent deformations in the soil system. Hence non-linear models are mandatory. A non-linear model can be simple like a Mohr–Coulomb (MC) model or more advanced like the cap plasticity model and kinematic hardening model. MC model is a linear elastic-perfectly plastic model used to simulate soil behavior under monotonic loading conditions. This model requires only few basic parameters such as – cohesion and friction angle which typically represent the failure line. The yield function of the MC model in the deviatoric stress space is an irregular hexagonal cone [15] Hardening or softening behavior is not captured in MC model. The modified Drucker Prager or Cap plasticity model, is widely used in many geotechnical applications. Similar to MC model, the elastic material behavior is modelled using Hooke's law but the plastic material behavior is defined by cap yield surface and Drucker Prager failure surface. The equation of the cap yield surface is as follows.

$$F_c = \sqrt{(P - P_a)^2 + \left(\frac{Rt}{1 + \alpha - \frac{\alpha}{\cos \beta}}\right)^2} - R(d + P_a \tan \beta) = 0 \quad (3)$$

where, P_a is the evolution parameter accounting for the hardening or softening depending on volumetric plastic strain, R is the value of cap eccentricity signifying the cap shape and α is the transition surface radius that promotes a smooth transition between the Drucker Prager failure surface and cap yield surface. The variables β and d are basically the angle of friction and cohesion of soil. The cap surface hardens or softens depending on the volumetric plastic strain. DP model's yield function is a cylindrical cone which can overcome the sharp corner problems arising in MC model.

Since a comparison between the material models is proposed to be studied, every constitutive model is applied individually on the soil layers in the CBP sections under study thus leading to 9 models for every case of CBP section. While doing mesh discretization, small size elements were used in the loading area while coarse elements are used for the base course layers. This will ensure proper prediction of the results by improving the calculation efficiency. Mesh sensitivity analysis was carried out before proceeding with the job submission. The details of the mesh generated are shown in Fig. 2b. Subsequently Steady state dynamic Modal analysis was carried out in the frequency range of 0 to 100 Hz, under the assigned vehicular load of 0.6 MPa accompanied by sinusoidal vibrations. This frequency range is

chosen because, natural frequency values of the CBP model ranged up to 90 Hz in the first level of study (Modal analysis). Representative results of the vertical displacement obtained from the deformed model of CBP section is shown in Fig. 2c along with the displacement contour values.

In the current study three different vehicular amplitudes and three different material models are used on the CBP sections chosen. On the whole, 27 trials were performed to investigate the effect of 1) increasing thickness of sand bed 2) linearity or non-linearity of soil model 3) acceleration intensity of vehicular vibrations on the dynamic response of the concrete block pavement system. From the test results, the first ten modes of natural frequency, the resonant frequencies of the system along with the amplitudes and surface deflection of the pavement are studied.

5 Results and Discussions

The steady state dynamic analysis consists of two stages. The first stage is the modal analysis to find the natural frequency modes of the CBP sections. Second stage is the steady state modal analysis simulating the acceleration and peak displacement values swept over a range of chosen frequency thus giving the results in frequency domain.

5.1 Evaluation of Natural Frequency Modes and Finding Equivalent Damping Coefficient Values

To start with, modal analysis is carried out for all the CBP sections in order to find the natural frequency of the whole concrete block pavement and soil system. Since the resonant condition is expected to occur in the low frequency ranges, the first 10 modes of natural frequency alone are extracted for each case. The natural frequency of the system can vary depending on the material properties and hence analysis was repeated for linear elastic, Mohr–Coulomb and modified Drucker Prager constitutive models for every case of CBP section. In the case of CBP sections with 70 mm sand thickness, a 10% reduction in the density value of sand bed is made to account for the reduction in compaction efforts in field for sand bed thickness higher than 50 mm [9]. Based on the natural frequency values in the first two consecutive modes, equivalent damping constants α and β are obtained for every soil layer in all cases of CBP section under study using the following equations [16].

$$\alpha = \frac{2\omega_i\omega_j\varepsilon}{\omega_i+\omega_j}; \quad \beta = \frac{2\varepsilon}{\omega_i + \omega_j} \quad (4)$$

Table 2 Equivalent damping constants obtained for sand bed layers

Layer description	Linear elastic		Mohr–Coulomb		Cap plasticity model	
	α	β	α	β	α	β
10 mm sand bed	0.628	0.0067	0.628	0.0067	0.632	0.0063
20 mm sand bed	0.63	0.0065	0.63	0.0065	0.634	0.0062
70 mm sand bed	0.5039	0.00079	0.5039	0.00077	0.5042	0.00077

where, ω_i, ω_j are the natural frequency values from two consecutive modes and ε is the damping ratio of a single soil layer alone. The damping constants obtained for sand bed layer is detailed in Table 2.

Rayleigh damping is used in case of soil mass to account for proper attenuation behavior. Following this, employing the obtained damping constants, a series of steady state modal analysis is conducted in the frequency domain, for the input sinusoidal vehicular vibrations with amplitudes of 0.6, 0.8 and 1 g. The frequency range for the steady state analysis is determined based on the maximum frequency value obtained during modal analysis. Results of the simulations are discussed in following section.

5.2 *Vibration Response of Case Profile 1-CBP with 20 mm Thick Sand Bed*

A series of nine steady state vibration response simulations were run on case profile 1 to account for all three soil constitutive models and three different vibration amplitudes over the chosen frequency range. The peak acceleration values and vertical displacement values were obtained from the acceleration curves and displacement curves in the frequency domain.

Figure 3a to c shows the variation of mass scaled peak acceleration values with depth, measured at resonance frequency for the CBP sections with 20 mm sand bed thickness for various soil models. The acceleration values initially obtained from the simulations were high, because these values are calculated at nodes which don't have a mass. Hence a mass scaling factor of 10 was used based on the experimental test conducted over asphalt concrete pavements [4]. As can be observed, from all the three figures, the peak acceleration value increases with increase in the amplitude of incoming vibrations, with the lowest values at surface recorded for 0.6 g. Another common aspect to notice among the three soil models, is the sharp dip in the values of peak acceleration within the first 100 mm depth. Almost 68% of the amplitude of vibration waves is attenuated within the paving block surface layer and sand layer. Beyond 100 mm, the values of the peak acceleration were mostly in the range of 0.35 to 0.02 g irrespective of the increase in the amplitude of input vibrations. This signifies the dynamic effectiveness of the surface and sand bed layer as compared to the base course layers in dispersing the traffic loads and vibrations. For the CBP sections

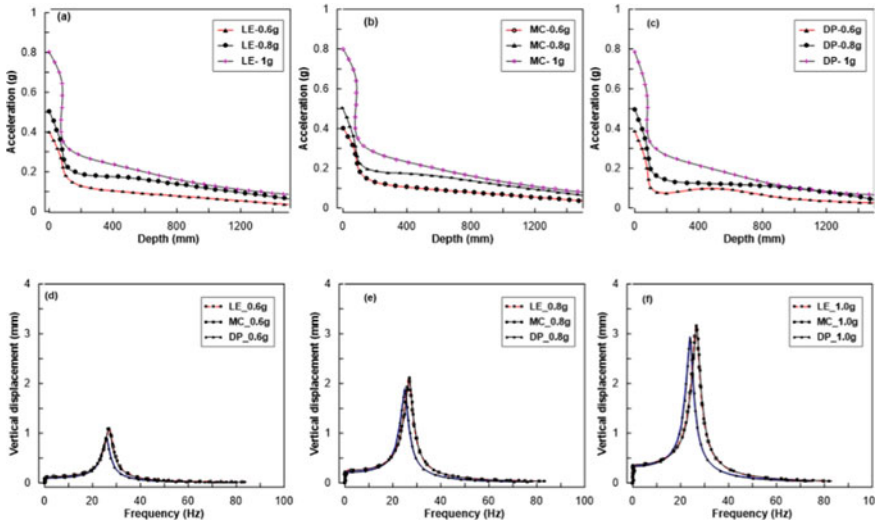


Fig. 3 Variation in acceleration values with increasing depth and amplitude of vibration for case 1 **a** Linear Elastic model (LE) **b** Mohr–Coulomb model (MC) **c** Modified Drucker Prager model (DP). Vertical displacement at pavement surface at various frequencies of loading for LE, MC and DP models at **d** 0.6 g **e** 0.8 g **f** 1 g

modelled using modified Drucker Prager model, there was a 3% decrease in the acceleration values recorded as compared to the Linear Elastic and Mohr–Coulomb models. The acceleration values recorded for linear elastic (LE) and Mohr–Coulomb (MC) cases however were almost similar. This is due to the stiffening effect under repeated cyclic vibrations caused by the plastic behavior of soil, being underestimated in the LE and MC models, thus leading to lower attenuation nature and slightly higher values of acceleration. This difference in acceleration values recorded among material models increased with increase in the amplitude of vibrations, thus revealing its significance on a long-term modelling of vehicular loads on CBP. Another aspect to notice is that, the acceleration values of the vibration didn't approach zero even at higher depths. This is attributed to the numerical problem arising from the bedrock simulation (fixed boundary constraint) where extremely small values of damping ratio are assumed in ABAQUS, thus leading to considerable values of acceleration (g). Similar behavior was observed with the acceleration response in a non - linear analysis of soil mass underlain by bedrocks [17].

Figures 3d to 3f, shows the variation of peak vertical displacement measured at the loading area on the surface of paving block with increasing amplitude and frequency of vehicular vibrations for various constitutive models. The graphs reveal significant peaks as well, thus delineating the resonance frequencies of the whole model in every case. From all three figures, it can be observed that the vertical displacement at surface increased with the increase in the amplitude of traffic vibration loads or all the material models chosen. The values of the vertical displacement recorded at

0.8 g, shown in Fig. 3e were found in good correlation with the experimental and numerical results observed from previous studies [12, 18] under the same vehicular load of 41 kN. It is also evident from figure, in which the linear elastic and Mohr–Coulomb models result in slightly higher values of vertical displacement as compared to modified Drucker Prager model. Even a prominent shift in resonance frequency was observed for the case of modified Drucker Prager model. This is because the increase in damping values arising from the plasticity of soil after yielding is not highly accounted for in the linear model and Mohr–Coulomb model. This is evident from the lower damping values observed in Table 2 measured for Mohr–Coulomb and linear elastic models as compared to the cap plasticity model for CBP section with 20 mm sand bed. Overall range of the resonance frequency for all 9 models studied for CBP sections with 20 mm thick sand bed was found in the range of 26.8 to 24 Hz.

5.3 Vibration Response of Case Profile 2-CBP with 10 mm Thick Sand Bed

Similar set of steady state vibration response analysis as mentioned in Sect. 5.1, were conducted on the case profile 2, to identify the effect of decreasing sand bed thickness on the dynamic response of the CBP system.

Figures 4a to 4c shows the variation of peak vertical acceleration with depth, recorded for the CBP sections with 10 mm sand bed. The acceleration values

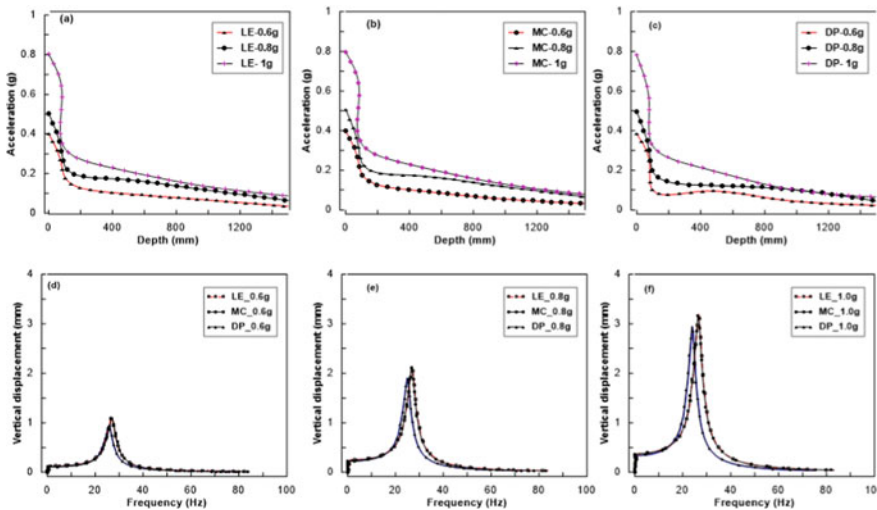


Fig. 4 Variation in acceleration values with increasing depth and amplitude of vibration for case 2 **a** Linear Elastic model (LE) **b** Mohr–Coulomb model (MC) **c** Modified Drucker Prager model (DP). Vertical displacement at pavement surface at various frequencies of loading for LE, MC and DP models at **d** 0.6 g **e** 0.8 g **f** 1 g

recorded were almost similar to that of the CBP section models with 20 mm sand bed recording only a 0.25% difference. And the decreasing trend of peak acceleration values with increasing depth was also similar to that of the previous case of CBP model, with major attenuation happening with the paving block layer and sand bed layer. Further among the various soil models, again overestimation of acceleration values was recorded for Mohr–Coulomb and linear elastic models. To this end, similar phenomenon of acceleration values not approaching zero at higher depths also remained unchanged. Figures 4d to 4f show the displacement frequency response obtained from the simulations employing linear elastic, Mohr–Coulomb and Modified Drucker Prager on the CBP section with 10 mm sand bed thickness at various vibration amplitudes. It can be observed that the variation trend of peak vertical displacement measured at loading surface remained similar to that of the previous case as well. But the displacement data recorded were on a higher side with values ranging up to 2.9 mm and there was a slight shift in resonant frequency observed among the various soil constitutive models. This can be attributed to the lower values of damping ratio found earlier as show in Table 2. The lower values of damping indirectly signify the reduced stiffness in the thin sand bed layer under vehicular vibrations. Even, it is evident from the experimental studies conducted earlier on CBP with sand bed thickness less than 20 mm [12, 18]. The lower values of sand bed thickness are known to cause pavement deflections during the laying operations itself and can prevent the interlocking phenomenon from happening.

5.4 Vibration Response of Case Profile 3-CBP with 70 mm Thick Sand Bed

Like the previous two cases as detailed in Sects. 5.2 and 5.3, steady state modal analysis was conducted on case profile 3 as well, to identify the effect of increasing sand bed thickness on the dynamic response of the CBP system.

Figures 5a to c shows the peak acceleration response measured across the depth of the CBP section. The decreasing trend and curves obtained were more like the previous two cases of CBP section. But the acceleration values recorded at the surface were lower for the current case of CBP section with 70 mm thick sand bed. The percentage decrease observed was around 8.8%. Not limiting to that, while comparing the material models, the acceleration values predicted by modified Drucker Prager model were less than that of the MC and LE models similar to the previous cases except that the difference in values were not high as 3% but only 0.25%. Figures 5d to f shows the variation in surface deflection recorded at the loading zone for different frequencies and amplitude of vibration obtained from a series of simulation with various constitutive models. From all three figures, it is well observed that the peak vertical displacement increased with increase in vibration amplitude. This kind of behavior is due to the stiffness degradation and the associated reduction in damping

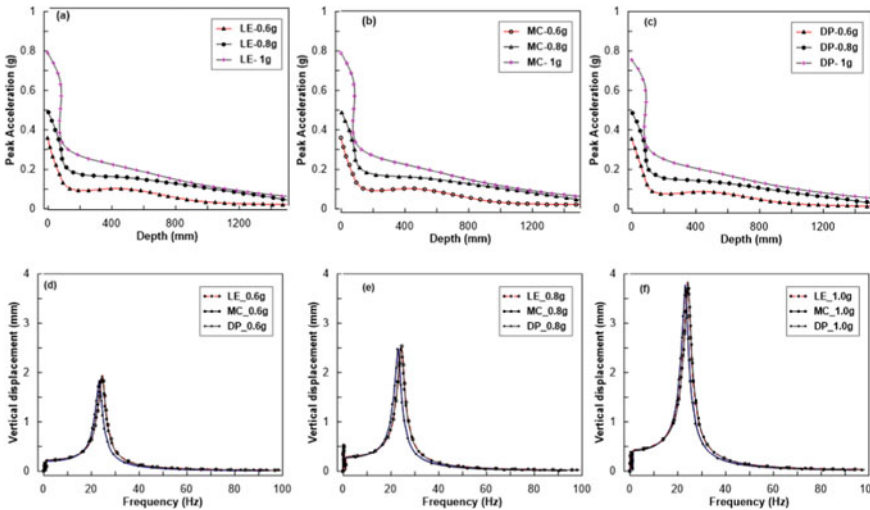


Fig. 5 Variation in acceleration values with increasing depth and amplitude of vibration for case 3 **a** Linear Elastic model (LE) **b** Mohr–Coulomb model (MC) **c** Modified Drucker Prager model (DP). Vertical displacement at pavement surface at various frequencies of loading for LE, MC and DP models at **d** 0.6 g **e** 0.8 g **f** 1 g

ratio caused by higher energy vibration as evident from Table 2. The peak deflection values measured at resonance frequency in Fig. 5e agrees well with the experimental and numerical results of surface deflection values obtained for Concrete block pavement with sand bed thickness greater than 70 mm [12]. High values of about 3.8 mm were recorded for CBP sections subjected to input vehicular motion amplitude of 1 g. But the resonance frequency values went down to as low as 22%. But the shift in the resonance frequency values due to the changes made in the material model were not so well defined in the curves, like the previous two cases though.

5.5 Comparative Study - Effect of Increasing Sand Bed Thickness on Pavement Dynamic Response

A comparative study is established among the three cases of CBP section discussed earlier, in order to find any detrimental response that might occur due to the variation in resonance frequency caused by altering the sand bed thickness. Since modified Drucker Prager model simulations of vertical displacements are close to experimental ones, the results of CBP sections under study pertaining to that of DP model are explained in depth in Fig. 6.

It is evident from Fig. 6a, that the vertical displacement values recorded for 70 mm thick sand bed (case3) are nearly twice that of the values observed for 10 mm (case2) and 20 mm thick sand bed (case1). Further, obvious shift in the resonance frequency

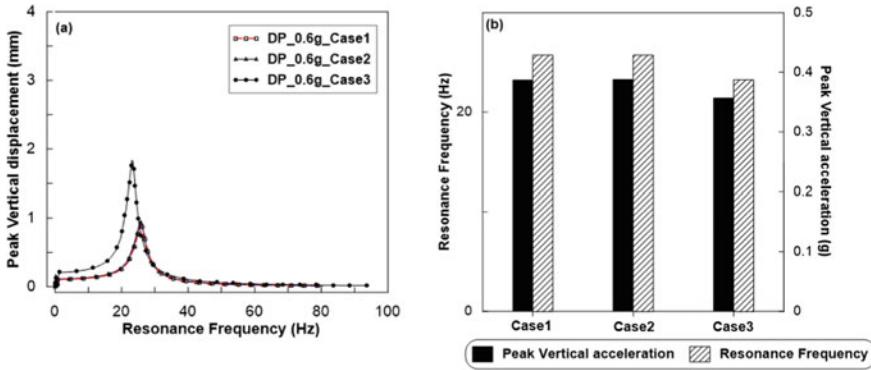


Fig. 6 a Vertical displacement at pavement surface for cases (1)–(3) at various frequencies of loading for DP model at 0.6 g **b** Variation in peak acceleration values at surface and resonance frequency for cases (1)–(3) DP model

is observed for case 3 CBP section with values nearing 22 Hz as compared to case 1 and case 2 values having resonant frequency values close to 25.7 Hz. The mechanism behind this behavior is explained as follows. Increasing sand bed thickness to 70 mm, caused the stiffness values of sand layer to go down, because for higher thickness of sand bed, the usual phenomenon of stiffness upgradation occurring in CBP surface layer and sand bed layer, during the first few cycles of loading doesn't happen fully. The energy of incoming vibrations is spent mostly at the surface layer itself leaving the sand bed to remain less stiff and loose. Whereas in the case of CBP sections with 20 mm sand bed, the energy of the incoming vibrations from the first few cycles, is sufficient to increase the interlocking and stiffness of both paving block layer and sand layer. Thus, the damping constant values obtained for 70 mm thick sand bed were lower as compared to 10 and 20 mm thick sand bed, leading to the shift in resonant frequency values. In the case of concrete block pavements, the dynamic load is mainly generated from the interaction between vehicle and surface unevenness. Henceforth the loading frequency (f) is dependent on the wavelength of roughness indicated by wavelength number and vehicle speed [19], as signified by the equation $f = \frac{v}{\lambda}$; where v is the vehicular load in m/s and λ is the wavelength number.

In case of CBP's, most of the real time loadings were having wavelength numbers in the range of 0.5 to 1 [3]. Hence, the frequency range of vehicular load for vehicles moving at speed of 40 kmph will be 22 to 11 Hz and subsequently increases with increasing value of speed. The highest speed recommended for CBP type pavements is 70 km/h [17]. By increasing the sand bed thickness to 70 mm, the resonance frequency was shifted to the operating frequency range of CBP pavements equal to 22 Hz. This ultimately led to the doubling up of vertical displacement values as observed in Fig. 6a which is unacceptable. But varying the sand bed thickness from a stable value of 20 to 10 mm, didn't affect much the peak acceleration values recorded at the surface as observed in Fig. 6b. But the peak acceleration values recorded for case 3 CBP section was lower than that of case 1 and case 2. This is due to effects of

calibration of Rayleigh damping which indirectly affects the computation results and underestimates the acceleration values at ground surface [17]. Even, the resonance frequency of the CBP section got reduced by only 0.3% but the vertical displacement values increased by at least 0.02 mm even for lower values of vibration amplitude imparted on CBP section modelled using modified Drucker Prager cap model. These values may look small but could get amplified on a long run after numerous vehicles passes. This has been proven via experimental studies on concrete block pavements, where surface deflection and vertical rotation of blocks were imminent if the bedding sand thickness goes below 20 mm. Overall, increasing sand bed thickness to 70 mm or decreasing it to 10 mm can induce unacceptable levels of surface deflection owing to the changes in the damping constants and shift in the resonance frequency to the operating frequency. Such vibration play an important role in safety and response of the adjacent infrastructure and their behavior [20, 21], which thereby signifying this preliminary study.

6 Conclusions

The current study has investigated the effect of variation in sand bed thickness on the dynamic response of the concrete block pavement through a series of steady state modal vibration analysis. Constitutive soil models and amplitude of input vibration are the variables used. The significant outcomes from this study include:

1. The resonant frequency decreases and approaches the range of operating frequency of vehicular loads for concrete block pavement section with sand bed thickness of 70 mm. This accounts for the higher surface deflection observed in the case of CBP sections with 70 mm thick sand bed
2. For the case of CBP section with 10 mm thick sand bed, even though the resonant frequency values didn't shift much, there was an increase in the surface deflection values observed due to the lower values of damping associated with the reduced stiffness in the sand bed layer
3. The equivalent damping constants of the CBP section was reduced by varying the thickness of sand bed to 10 and 70 mm. Stable values were observed for CBP sections with 20 mm thick sand bed
4. Modified Drucker Prager simulation results provided a closer approximation to the experimental values compared to Mohr–Coulomb (MC) and Linear Elastic (LE) models. MC and LE models were found to overestimate the results as changes in damping values associated with soil plasticity after yielding is less accounted for.

The main purpose of the study was to get an in-depth understanding of the changes in the CBP behavior under cyclic loads when the sand bed thickness doesn't match the design values as per standards. Efforts have been made to capture the inhomogeneity in the soil substructure of CBP to a certain extent by including two different soil layers beneath the sand bed and PB layer and a single geometry of model has been

used for study under a range of vehicular vibration frequencies. Even though the trends of variation observed in peak acceleration and peak vertical displacement responses are not significantly different, altering the sand bed properties based on their gradation along with changes in the joint sand friction coefficient and CBP laying patterns would have a definite influence on the magnitude of acceleration and displacement values observed. Further studies are required in this area by increasing the scale of model accompanied by complex real time boundary conditions and material models. Nevertheless, this study gives an insight into the dynamic reasoning behind the surface deflection of concrete block pavements with increasing sand bed thickness.

References

1. Lombaert G, Degrande G, Clouteau D (2000) Numerical modelling of free field traffic-induced vibrations. *Soil Dyn Earthq Eng* 19(7):473–488
2. Zakeri R et al (2021) Influence of rubber sheet on dynamic response of machine foundations. *Constr Build Mater* 274:121788
3. Lak MA, Degrande G, Lombaert G (2011) The effect of road unevenness on the dynamic vehicle response and ground-borne vibrations due to road traffic. *Soil Dyn Earthq Eng* 31(10):1357–1377
4. Ye Z, Lu Y, Wang L (2018) Investigating the pavement vibration response for roadway service condition evaluation. *Adv Civ Eng* 2018 Article ID 2714657: 14 p
5. Saleh Asheghabadi M, Cheng X (2020) Analysis of undrained seismic behavior of shallow tunnels in soft clay using nonlinear kinematic hardening model. *Appl Sci* 10(8): 2834
6. Anandan S et al (2020) Numerical and experimental investigation of oil palm shell reinforced rubber composites. *Polymers* 12(2):314
7. Loi SJ et al (2020) Compaction characteristics of kaolin reinforced with raw and rubberized oil palm shell. *Minerals* 10(10):863
8. Mott G, Wang J (2011) The effects of variable soil damping on soil-structure dynamics. *J Vib Control* 17(3):365–371
9. Raghunandan ME (2012) Effect of soil layering on the ground response parameters: a parametric study. *Nat Hazards* 63(2):1115–1128
10. Hassani A, Jamshidi A (2006) Modeling and structural design of a concrete block pavement system. In: 8th International Conference on Concrete Block Paving
11. Rada GR et al (1992) Structural design of interlocking concrete pavements in North America. In: Proceedings of the 4th Structural Design of Interlocking Concrete Pavement in North America, vol 1, pp 99–116
12. Panda BC, Ghosh AK (2002) Structural behavior of concrete block paving. I: sand in bed and joints. *J Transp Eng* 128(2): 123–129
13. Chiroux R et al (2005) Three-dimensional finite element analysis of soil interaction with a rigid wheel. *Appl Math Comput* 162(2):707–722
14. Moayed RZ, Tamassoki S, Izadi E (2012) Numerical modeling of direct shear tests on sandy clay. *World Acad Sci Eng Technol* 61:1093–1097
15. Robert D, Soga K, Britto A (2015) Soil constitutive models to simulate pipeline-soil interaction behaviour. In: International Conference on Geotechnical Engineering ICGE Colombo
16. Manual A.S.U.s. (2012) ABAQUS 6.14 ABAQUS/CAE User's Guide (2014). http://130.149.89.49:2080/v6.14/pdf_books/CAE.pdf
17. Karatzetzou A et al (2014) A comparative study of elastic and nonlinear soil response analysis. In: Conference: 2nd European Conference on Earthquake Engineering and Seismology, At Istanbul, Turkey. Aristotle University of Thessaloniki

18. Shafabakhsh G, Family A, Abad BPH (2014) Numerical analysis of concrete block pavements and comparison of its settlement with asphalt concrete pavements using finite element method. *Eng J* 18(4):39–51
19. Al-Qadi IL, Xie W, Elseifi MA (2008) Frequency determination from vehicular loading time pulse to predict appropriate complex modulus in MEPDG. *Asph Paving Technol Proc* 77:739
20. Loi DW, Raghunandan ME, Swamy V (2016) Seismicity of Peninsular Malaysia due to intraplate and far field sources. *Earthquakes Struct* 10(6):1391–1404
21. Loi DW, Raghunandan ME, Swamy V (2018) Revisiting seismic hazard assessment for peninsular Malaysia using deterministic and probabilistic approaches. *Nat Hazards Earth Syst Sci* 18(9):2387–2408

Effect of Petrographic Properties on the Strength Parameters of Indian Metamorphic Rocks



A. K. Verma, Amit Jaiswal, and T. N. Singh

Abstract The geotechnical properties of any rock are affected by its mineral composition, alteration, weathering, and micro structures of the rock. Limited experimental validation of the existing correlation between petrographical and physico-mechanical properties of rocks inhibits practical use of petrographical thin sections to determine the strength properties. In this study, the extensive analysis of thin sections shows that the quartz has a positive correlation with UCS in the rock samples while presence of K-feldspar, Plagioclase and Biotite shows negative correlation with UCS of different rock types.

Keywords Petrography · Metamorphic · Uniaxial compressive strength

1 Introduction

Geotechnical design of any rock structure requires physico-mechanical properties of rocks which in turn are mainly influenced by its mineral content [2, 6, 7, 11, 13, 15, 16]. The influence of mineralogy on the physical and mechanical properties of rocks has been examined from different perspectives by several authors such as [3, 5, 7, 9, 10, 14, 17].

This work focuses on the determination of rock geomechanical properties such as porosity, unit weight, UCS, Tangent modulus and poison's ratio based on quantitative microscopy. Physic mechanical laboratory tests were carried out as per ISRM specifications and petrographic parameters have been obtained from one polished thin section per sample using a polarizing microscope. Modal concentration was carried out to quantify the mineralogical data.

A. K. Verma (✉) · A. Jaiswal
Department of Mining Engineering, Indian Institute of Technology, BHU, Varanasi 221005, India
e-mail: akverma.min@iitbhu.ac.in

T. N. Singh
Department of Earth Sciences, Indian Institute of Technology Bombay, Mumbai, India

Table 1 The location and types of studies rock types

Geological study group	Rock type	Location
Chhotanagpur Granite Gneissic Complex (CGGC)	1. Mg-AL Granulite	Jharkhand
	2. Mafic granulite	
	3. Massive charnockite	
	4. Migmatitic Quartzofeldspathic gneiss	
East Singbhum	5. Porphyritic Granite	Jharkhand
	6. Granite gneiss	
South portal, Rohtang tunnel	7. Phyllitic quartzite	Himachal Pradesh
	8. Quartzitic phyllite	
	9. Migmatic gneiss	

3 Material and Methods

The experimental works include petrographical analysis and geomechanical investigation of rock samples. The collected rock types and prepared samples have been divided into nine groups for better analysis. The representative core specimens are shown in Fig. 2. Determination of modal percentage of mineralogical proportion in each thin section of all rock types have been carried out. Petrological microscope was used to determine mineralogical under both plane-polarized and cross-polarized luminescence. The correlations between UCS and mineralogical composition of rocks have been studied. The determination of mineralogical parameters has been put in one group and experiments related to the mechanical property such as UCS has been put into another group. At least three NX size samples have been prepared for each rock type to determine UCS.

The measured physico-mechanical properties have been correlated with the specific mineral percentage in the rocks. Statistical analysis has been carried out to obtain the best fit correlation coefficients for selected parameters. Extensive analysis

**Fig. 2** Representative cylindrical core samples of studied rock types

has been done to obtain the existing percentage of quartz, K-feldspar, plagioclase, and biotite minerals in each thin section of different rock types. For the calculation of existing different types of grain boundaries the field of observation was set such that it includes 100–150 grains per section.

4 Results and Discussion

The results of petrographic studies including average mineralogical composition are presented in Tables 2. Table 3 and Table 4 shows physico-mechanical properties of each rock group and there average value of UCS respectively.

Table 2 Average mineralogical composition of different metamorphic rocks

Sample groups	Quartz (%)	Plagioclase (%)	K-Feldspar (%)	Biotite (%)
1	52	32.65	13	2.18
2	43	34.65	14.2	2.1
3	39	35.48	14.9	2.04
4	31	42.76	11.1	1.93
5	28	45.43	11.8	1.89
6	26	47.32	17.2	1.83
7	24	50.12	17.6	1.61
8	21	54.23	18.4	1.56
9	19	60.43	19	1.43

Table 3 Average measured mechanical properties of different studied metamorphic rocks

Sample groups	Unit weight (KN/m ³)	Effective porosity (%)	Young's modulus (GPa)	Poisson's ratio
1	2.53	1.4	32.76	0.21
2	2.67	0.76	36.25	0.23
3	2.38	1.18	41.29	0.38
4	2.75	1.80	38.95	0.34
5	2.49	1.60	32.54	0.30
6	2.38	1.2	30.12	0.28
7	3.10	0.78	41.43	0.26
8	2.92	0.79	38.32	0.24
9	2.35	1.63	28.59	0.21

Table 4 Average uniaxial compressive strength of different studied metamorphic rocks

Sample groups	Average UCS (MPa)	Number of samples	Standard deviation	Rock type
1	70.76	12	12.5	CGGC: Mg-AL Granulite
2	83.45	14	18.4	CGGC: Mafic granulite
3	57.45	7	19.3	ES: Porphyritic Granite
4	65.34	12	9.4	ES: Granite gneiss
5	48.23	14	11.5	CGGC: Massive charnockite
6	43.67	15	14.3	CGGC: Migmatitic Quartzofeldspathic gneiss
7	101.52	19	15.2	SPRT: Quartzitic phyllite (QP)
8	95.32	15	13.5	SPRT: Phyllitic quartzite (PQ)
9	40.32	14	11.3	SPRT: Migmatic gneiss (MG)

CGGC: Chottanagpur Granite Gneiss Complex; ES: East Singhbhum; SPRT: South portal, Rohtang tunnel

4.1 *Physico-Mechanical Properties of Rocks*

Laboratory tests were performed on 122 rock specimens. Properties analysed were Unit weight (KN/m^3), Effective Porosity (%), Young's modulus (GPa), Poisson's Ratio and UCS of each specimen. Tested values have been given in Table 3 and Table 4.

Tests were carried out on core specimen which has NX diameter (54 mm) and having a length to diameter ratio of 2.5–3.0. The stress rate on the core specimens was controlled at approximately 0.5–1 MPa/s. Maximum load at failure was used to calculate the UCS of specimens. The average UCS value for 12 of samples of Mg-Al granulite, 14 samples of mafic granulite, 14 samples of massive Charnockite and 15 samples of Migmatitic Quartzofeldspathic gneiss of Chottanagpur Granite Gneiss complex where 70.76, 83.45, 48.23 and 43.67 MPa respectively. While the average UCS values of 7 sample of porphyritic granite and 12 samples of Granite gneiss of East Singhbhum are 57.45 and 65.34 MPa respectively. Also the average UCS value of 19 samples of Quartzitic phyllite (QP), 15 samples of Phyllitic quartzite (PQ) and 14 samples of Migmatic gneiss (MG) of south portal Rohtang tunnel are 101.52, 95.32 and 40.32 MPa respectively.

4.2 Influence of Mineralogical Composition on Rock Engineering Properties

Modal mineralogical composition for each rock type has been determined. Further, relative occurrence abundance of significant mineral constituent has been obtained from thin section by the counting 300 points for reliable information related to minerals [11]. Quartz is one of the most common mineral components in the selected rocks. The important feature of quartz is its resistance towards weathering.

In the present study, the positive correlation exists between modal concentration of quartz with UCS. Whereas, the negative correlation between modal concentration of K-feldspar, plagioclase and biotite with UCS has been observed (Fig. 3) and the corresponding coefficient of determinations have been given in Table 5. The results are in well accordance with the previous studies by [8, 11, 12, 15] where they also

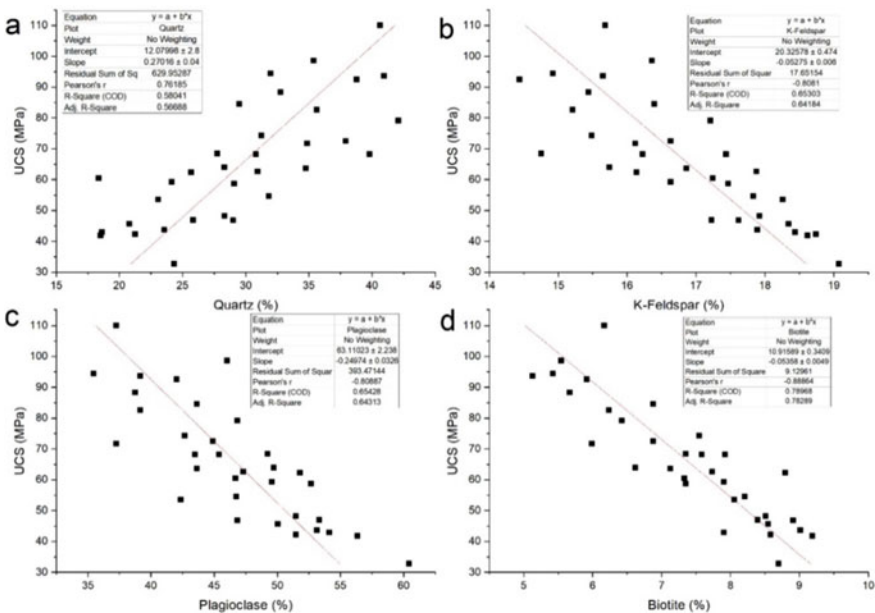


Fig. 3 Linear correlation of UCS value with different mineral percentage **a.** quartz ($R^2 = 0.58$) **b.** K-feldspar ($R^2 = 0.65$) **c.** plagioclase ($R^2 = 0.65$) **d.** biotite ($R^2 = 0.79$)

Table 5 Regression equations and coefficient of correlation, R^2 for the relations between UCS and modal composition of the rock

Sl. No.		R^2
1	UCS vs. Quartz	0.58
2	UCS vs. Biotite	0.79
3	UCS vs. K-Feldspar	0.68
4	UCS vs. Plagioclase	0.65

concluded that the higher quartz content results in high UCS. They have found direct correlation between the UCS and quartz content. But simultaneously, they have also noticed similar correlation with plagioclase which is in direct contrast to the present study.

5 Conclusions

The petrographical study of rock thin sections combined with geomechanical analysis of corresponding metamorphic rock samples shows considerable positive or negative correlation between petrographical features and strength properties of rocks. Presence of quartz has a positive correlation with UCS having coefficient of correlation R^2 value of 0.58 of the samples while presence of K-feldspar, plagioclase and biotite shows negative correlation with UCS of cylindrical specimens.

Conflict of Interest The authors wish to confirm that there are no conflicts of interest with this research article.

References

1. Acharyya SK (2003) A plate tectonic model for Proterozoic crustal evolution of central Indian tectonic zone. *Gondwana Geol Mag* 7:9–31
2. Akesson U, Stigh J, Lindqvist JE, Gorransson M (2003) The influence of foliation on the fragility of granitic rocks, image analysis and quantitative microscopy. *Eng Geol* 68:275–288. [https://doi.org/10.1011/S0013-7952\(02\)00233-8](https://doi.org/10.1011/S0013-7952(02)00233-8)
3. Baud P, Wong TF, Zhu W (2014) Effects of porosity and crack density on compressive strength of rocks. *Int J Rock Mech Min Sci* 67:202–211. <https://doi.org/10.1011/j.ijmms.2013.08.031>
4. Changkakoti A, Gray J, Morton RD, Sarkar SN (1987) The mosabani copper deposit, India—a preliminary study of nature and genesis of the ore fluids. *Econ Geol* 82:1119–1125. <https://doi.org/10.2113/gsecongeo.82.6.1119>
5. Howarth DF, Rowlands JC (1987) Quantitative assessment of rock texture and correlation with drillability and strength properties. *Rock Mech Rock Eng* 20:57–85. <https://doi.org/10.1007/BF01019511>
6. Hartley A (1974) A review of the geological factors influencing the mechanical properties of road surface aggregates. *Q J Eng Geol* 7:69–100. <https://doi.org/10.1144/GSL.QJEG.1974.007.01.05>
7. Irfan TY (1996) Mineralogy, fabric properties and classification of weathered granites in Hong Kong. *Q J Eng Geol Hydrogeol* 29(1):5–35
8. Khalil Ys, Arif M, Bangash HA, Sajid M, Muhammad N (2015) Petrographic and structural controls on geotechnical feasibility of dam sites: implications from investigation at Sher Dara area (Swabi), north-western Pakistan. *Arab J Geosci* 8:5067–5079. <https://doi.org/10.1007/s12517-014-1510-z>
9. Mendes FM, Aires-Barros L, Rodrigues FP, (1966) The use of modal analysis in the mechanical characterization of rock masses. In: *Proceedings of the 1st Congress of the International Society of Rock Mechanics*. Lisbon (Portugal), 25 September–1 October 1966, volume I, Theme 2:217–223

10. Prikryl R (2006) Assessment of rock geomechanical quality by quantitative rock fabric coefficients: limitations and possible source of misinterpretations. *Eng Geol* 87:149–112. <https://doi.org/10.1011/j.enggeo.2006.05.011>
11. Rigopoulos I, Tsikouras B, Pomonis P, Hatzipanagiotou K (2010) The influence of alteration on the engineering properties of dolerites: the examples from the Pindos and Vourinos ophiolites (northern Greece). *Int J Rock Mech Min Sci* 47:69–80. <https://doi.org/10.1011/j.ijrmms.2009.04.003>
12. Rigopoulos I, Tsikouras B, Pomonis P, Hatzipanagiotou K (2010) The influence of alteration on the engineering properties of dolerites: the examples from the Pindos and Vourinos ophiolites (northern Greece). *Int J Rock Mech Min Sci* 47:69–80. <https://doi.org/10.1011/j.ijrmms.2009.04.003>
13. Sajid M, Arif M, Shah MT (2014) Petrogenesis of granites from the Utlā area of Gadoon, north-west Pakistan: implications from petrography and geochemistry. *J Earth Sci* 25:445–459. <https://doi.org/10.1007/s12583-014-0435-5>
14. Sajid M, Coggan J, Arif M, Andersen J, Rollinson G (2011) Petrographic features as an effective indicator for the variation in strength of granites. *Eng Geol* 202:44–54. <https://doi.org/10.1011/j.enggeo.2011.01.001>
15. Shakoor A, Bonelli RE (1991) Relationship between petrographic characteristics, engineering index properties and mechanical properties of selected sandstone. *Bull Assoc Eng Geol* 28:55–71. <https://doi.org/10.2113/gseegeosci.xxviii.1.55>
16. Tamrakar SB, Mitachi T, Yasuo T (2007) Measurement of soil tensile strength and factors affecting its measurements. *Soils Found* 47(5):911–918. <https://doi.org/10.3208/sandf.47.911>
17. Tugrul A, Zarif IH (1999) Correlation of mineralogical and textural characteristics with engineering properties of selected granitic rocks from Turkey. *Eng Geol* 51(4):303–317. [https://doi.org/10.1011/S0013-7952\(98\)00071-4](https://doi.org/10.1011/S0013-7952(98)00071-4)
18. Zorlu K, Ulusay REŞAT, Ocakoglu F, Gokceoglu CANDAN, Sonmez H (2004) Predicting intact rock properties of selected sandstones using petrographic thin-section data. *Int J Rock Mech Min Sci* 41:93–98.

Appropriate Geotechnical Engineering Helps Improve Mineral Reserves



Srikant Annavarapu

Abstract Mineral resources are a valuable part of a country's economy, and the mineral industry relies on the skills of the industry professionals to extract the mineral resources safely and economically from the ground. The conversion of mineral resources to mineral reserves entails the development of a safe and economic mining plan for the extraction of the available resources. A major part of the mine planning and design exercise requires geotechnical engineering inputs which are based on preliminary information gathered during the exploration stage and during the development of design studies. The judicious use of available geotechnical engineering information for the design and planning of a surface or underground mining operation, and the generation of pertinent information helps in improving the conversion of mineral resources to mineral reserves. As the project progresses, the integration of additional key data points into the design process helps develop an updated information base for upgrading the mine design, thereby increasing the conversion of mineral resources to mineral reserves. The continuous improvement of the quality and quantity of information regarding the mineral resources and the estimated behaviour of the rock masses to excavation loading helps reduce the financial risk of the project. This keynote address covers the traditional geotechnical information generated during the evaluation of a mineral project and discusses the potential for improving the recovery of available mineral resource through the development of appropriate geotechnical databases, models and forecasting methods to help increase the conversion of mineral resources to mineral reserves.

Keywords Mineral resource · Mineral reserves · Geotechnical information

1 Introduction

The primary mandate of a minerals engineer is the safe and economic conversion of in-situ rock to saleable and valuable mineral. In this process, the mining geologist

S. Annavarapu (✉)

Master Geotech Services Pvt Ltd., Nagpur, India

e-mail: srikant@mgstucson.com

© The Author(s), under exclusive license to Springer Nature Singapore Pte Ltd. 2022
A. K. Verma et al. (eds.), *Proceedings of Geotechnical Challenges in Mining, Tunneling and Underground Infrastructures*, Lecture Notes in Civil Engineering 228,
https://doi.org/10.1007/978-981-16-9770-8_51

745

assesses the location of extractable resources, the mine design engineer designs the mining process to extract the mineral resources, and the mine operations engineer conducts safe operations to implement the processes designed by the mine design engineer, with necessary contingent steps to ensure safety and to improve productivity. The mineral processing engineer then takes the recovered raw material and enhances the mineral quality through various applicable processes of beneficiation. The entire process results in the conversion of mineral resources to mineral reserves and finally to saleable mineral.

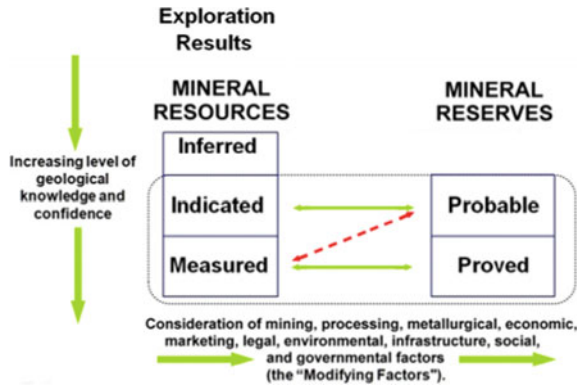
Mine design and mine operations processes are dependent on the available data on the behaviour of the rock masses in which the excavations are required to be made to extract the mineral from the ground. The process of mine design is optimised to recover the largest value of mineral from the ground at the lowest cost. While the design incorporates various items of operational expenses, the value of the mineral recovered is dependent on developing the largest stable excavations in the ground.

Geotechnical engineering is the management of the response of rock to mining and therefore plays an important role in design, planning and operations of a mine to ensure optimal extraction with the required level of safety. While mining companies cannot control the location, style and characteristics of an orebody, the behaviour of the rocks surrounding the orebody, or the natural stress environment, the response of the rock to mining activity can be managed through the design of the elements of the mine such as the slopes, excavations, pillars, the sequence of mining, and the timely application of required ground support. In most cases, the economic viability of a mining operation is heavily dependent on the effective management of the rock mass response to mining. For surface mining excavations, the steepest stable slopes are designed while for underground mines, the largest excavations with the smallest pillars are designed. These designs are based on the available geotechnical data and the estimation of rock mass behaviour to the stresses developed due to the excavations. Monitoring the designs during operations is an essential part of the iterative design and operation process to help make necessary adjustments to the excavations to continue safe operations. Such monitoring enables cost effective operation of the mine excavations, which results in increased recovery of mineral resource and addition to the mineral reserves.

2 Mineral Resources

As per the Committee for Mineral Reserves International Reporting Standards (CRIRSCO), mineral resources are defined as “a concentration or occurrence of solid material of economic interest in or on the Earth’s crust in such form, grade, quality and quantity that there are reasonable prospects for eventual economic extraction.” Fig. 1 shows the classification of Mineral Resources and Mineral Reserves as per CRIRSCO. The location, quantity, grade, continuity, and other geological characteristics of a Mineral Resource are known, estimated, or interpreted from specific geological evidence and knowledge, including sampling. A significant amount of

Fig. 1 Classification of mineral resources and mineral reserves (CRIRSCO)



effort and expense is incurred in the identification of a mineral resource with the expectation that the expense will be more than adequately be covered by the income from the sale of extracted minerals.

Mineral resources are defined through the analysis of drilling results from the area of expected mineralization. The extent of the drilling operations depends on the type of mineral and the complexity of the mineral deposit. The drilling results are normally used to create conceptual mineralization zones using standard techniques for the extrapolation of the results in areas of limited mineralogical knowledge and information and numerical modelling of the exploration results. Since drilling operations are expensive, especially at the beginning of an exploration project, efforts are made to optimise the drilling and rely on computational methods to estimate the presence and value of the mineral resource. These operations can be further optimised by adding value to the collected information in terms of some geotechnical data collected along with standard geological information. This increases the value derived from the drilling operations and provides early information for the design of potential mining methods and processes.

3 Mineral Reserves

CRIRSCO defines mineral reserves as “the economically mineable part of a Measured and/or Indicated Mineral Resource”. Mineral reserves must result in an estimated tonnage and grade which can be the basis of an economically viable project after taking account of all relevant Modifying Factors. The modifying factors include mining, metallurgical, economic, marketing, legal, environmental, social, and governmental factors affecting the cost of mining operations. The relationship between mineral resources and mineral reserves is shown above in Fig. 1.

The development of a mining schema at the scoping study stage and of a detailed mining plan at the feasibility stage requires several mine design parameters including the mining costs, mining recoveries and dilution. Gathering of required information

for the assessment of the modifying factors is key to the efficient and optimum conversion of mineral resources to mineral reserves. Typically, there is a value loss of 25–35% while converting from mineral resources to mineral reserves. This loss can significantly impact the economics of an operation and therefore it is imperative that steps be taken to minimise this conversion loss through suitable data collection and engineering.

4 Data Collection Protocols

The collection of basic geotechnical data is normally done after some indication of the presence of potential economic mineralization is established in an area. Core recovery and Rock Quality Designation (RQD) data is collected and recorded. The presence of major structural features such as faults, folds and intrusions are marked on the generated plans and sections.

Very often, however, the persons collected the geotechnical data are not completely aware of the protocols for the same. For example, while core recovery is an important element of geological data collection, RQD requires the drilling to be done without disturbing the intact quality of the rock. If the driller is tasked with quick achievement of the targeted meters of drilling, he will not pay attention to the drilling speed and/or the vibrations generated in the drilling process, which can result in breakage of the core during the drilling process and a consequential reduction in the RQD. Setting up the appropriate protocols and providing basic training of the exploration personnel will result in a higher quality of RQD data being collected at the protocols during the exploration process itself.

Most mineral exploration programs stop the drilling of an exploration drill hole just after the mineralized zone is crossed, except where multiple zones are expected. While adequate information is collected about the nature of the hangwall and of the mineralized zone, the information about the footwall is often scarce. In some cases, the drilling outside the mineralized zone is planned at a lower cost and no geotechnical information is available even from the hangwall side of the mineralized zone. The requirement and usage of geotechnical data at the different stages of the development of mining are shown in Fig. 2.

In the early stages of the project development lifecycle, financial resources are primarily allocated to determine the extent and value of the mineral resource. For companies with a long-term vision for their project, implementing a properly structured geotechnical data collection programme, concurrently with exploration drilling, will contribute to maximizing returns from their investment and reduce financial risk [3].

The inclusion of geotechnical data collection during the exploration stage may lead to an increase in the cost of exploration and this is untenable, especially in the case of greenfield exploration. The collection of some preliminary geotechnical data at the exploration stage helps generate the required data in advance of the mine design efforts, even at the scoping study stage, and helps plan the collection of geotechnical

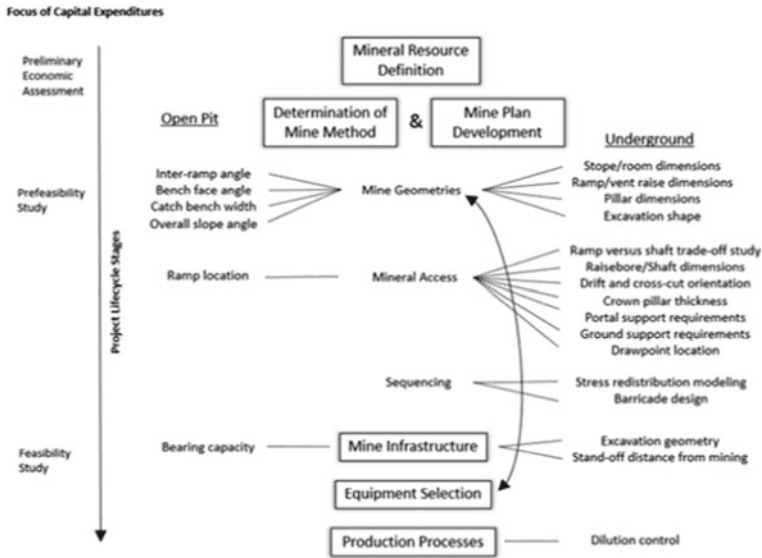


Fig. 2 Aspects of mining studies reliant on geotechnical data [3]

data during the scoping and pre-feasibility study stages. In addition, holes within the zone of interest should be kept available for potential use for down hole geophysical and geotechnical evaluation. Some drill holes may be kept aside for collection of hydrological information.

The requirement of geotechnical data during the design stages of a mining operation depends on the proposed nature of mining for the mineralized zone and is often based on the outcomes of the scoping study wherein some economically viable options are presented. The complexity of the mineralized zone and the potential mining methods will define the extent of the geotechnical data required for the analyses and design and will have to add to the data already collected during the exploration stage. The proper storage of drill core samples collected during the exploration stage will facilitate the generation of the required geotechnical data at different stages of the project.

5 Geotechnical Inputs for Mine Design

Geotechnical engineering forms an integral part of the design of surface and underground mine operations and is often considered in two parts – Data Collection and Data Analysis. The collection of geotechnical data includes an assessment of rock mass characterization, intact rock strengths, rock mass strengths and characteristics of discontinuities. The collected data is then sorted to created geotechnical domains

(zones of similar rock mass behaviour) and numerical models are developed to simulate the response to redistribution of stresses due to the creation of excavations. Depending on the size and complexity of the planned mine operation, deterministic or probabilistic models can be created to help design the excavations and support elements in the mine.

[2] reported that the response of rock (to mining, or any other disturbance) is essentially a function of four parameters:

- The strength of the rock mass including the effect of geological structures,
- Natural and/or imposed stresses in the rock,
- The geometry of the excavations, and the forces generated thereby,
- The effect if the ground support, if any, that is applied to the rock.

The function that relates these four parameters to the response is the model of behaviour of the rock, which can be empirical, physical, or mathematical. The efficient application of geotechnical engineering requires that each of the inputs be of similar accuracy, and that the sophistication of the model be matched to the given accuracy of the inputs and the required accuracy of the output. The iterative process of the application of geotechnical engineering in mine planning and operations is shown in Fig. 3.

Surface mine design and planning should release the largest value of the mineral deposit with the least quantity of waste movement and should be optimised to the point where the incremental stripping cost equals the value of the ore recovered. This optimization should be carried out on an incremental basis to maximize the economic

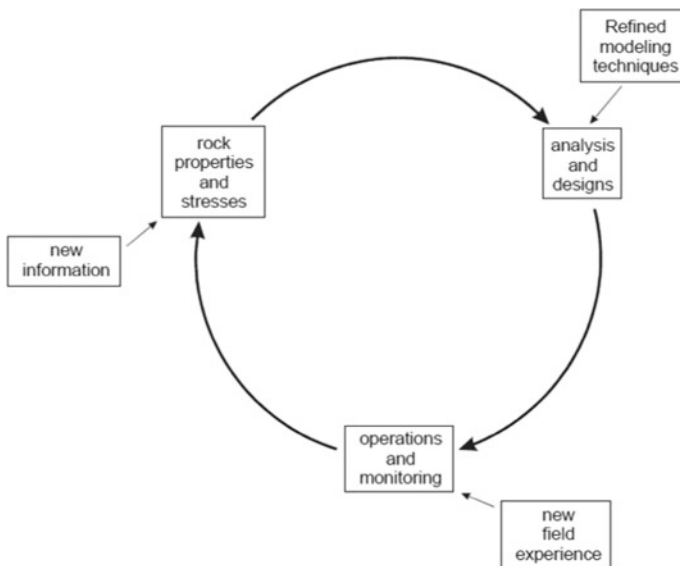


Fig. 3 Geotechnical engineering in mine planning and operations - an iterative process [2]

benefit over the life of the operation. In general, increasing the slope angle results in improvements in the stripping ratio and can significantly increase the value of the recovered ore [6] as shown in Fig. 4.

The design of underground mining operations requires the assessment of the largest excavations that can be created underground with the smallest intervening pillars, while ensuring stability of the excavations and pillars during the required life of the excavations. The resulting extraction ratio defines the recovery of mineral reserves from the available mineral resources. Figure 5 shows that the size of the pillars left to support the roof in the mineralized zone determines the extraction ratio and influences the value of mineral reserves. The design of the pillars is thus an important element of underground mine design and requires the development of a suitable information base of geotechnical data for the assessment of the appropriate dimensions.

The support for the mine excavations and/or the pillars is also a part of the design process, especially since this has an impact on the cost of mining and, consequently,

Fig. 4 Impact of changes in slope angle on ore recovery and stripping [6]

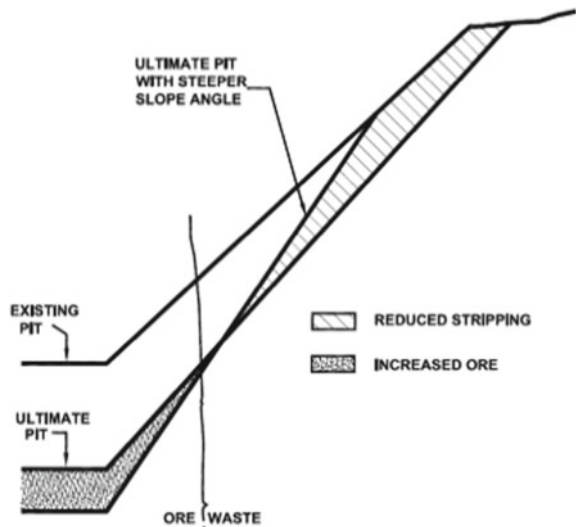
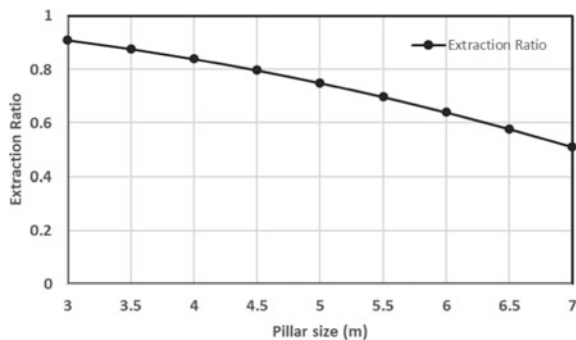


Fig. 5 Effect of pillar size on extraction ratio



the definition of mineral reserves. Different types of excavations in the underground mine have different time periods of use and the overall mining and ground support strategies for the stages of the excavation are thence designed to account for the requirements for all the different cases. Ground support design relies on the collection of adequate data for the classification of the rock mass and the assessment of the contingency amounts required to ensure that the excavation is reliably stable during the life of the excavation.

6 Stability Monitoring and Mine Operations

Field geotechnical observations help in the safe and efficient execution of excavation projects. Monitoring the stability of the excavations created by mining helps in the assessment of the ground support measures required to maintain the designed excavations or to modify the recovery of valuable mineral resources. The installation of instrumentation of different types provides vital information on ground response to the excavation and help in assessing the stability of the excavation and the adequacy of the ground support for the safety of the personnel exposed therein. The development and installation of a network of appropriate instruments covering the production areas generates information critical to safety and production. The timely and reliable collection and analysis of the data are of critical importance to the assessment of the stability of the excavations [1].

In surface mining, actions may be taken to increase the overall slope angle or to even “roll up the ramps” to add additional mineral reserves to a project [4]. These processes increase the level of exposure to risk due to rock mass instability changes and measures need to be taken to monitor the excavations while attempting to increase the conversion of mineral resources to mineral reserves. The use of remote monitoring tools such as slope stability radars to evaluate the stability of the excavations is relatively common, especially in high value projects (Fig. 6). Geotechnical reliability analysis and cost–benefit risk analysis in different forms are currently in use for open pit slope design in several mines around the world [6].

In underground mines, measures may be taken to recover mineral resources locked up in pillars (barrier pillars or shaft pillars) while retreating from the periphery of the deposit. The monitoring of stress changes and displacements within the working areas is crucial for the safety of personnel and mine assets during the recovery operations with the rate of change being a major indicator of stability/instability of critical areas of the mine. Developments in sensor technologies are making it possible to continuously monitor ground response to mining activity (Fig. 7).

Trigger Action Response Plans based on the data from geotechnical instruments monitoring the ground response can help reduce the response time to the ground reaction so that appropriate operating and/or geotechnical measures can be undertaken to address the changes in the ground conditions. These systems can also help improve the effectiveness of geotechnical personnel by ensuring that they are able to physically visit locations of greater geotechnical significance and provide appropriate

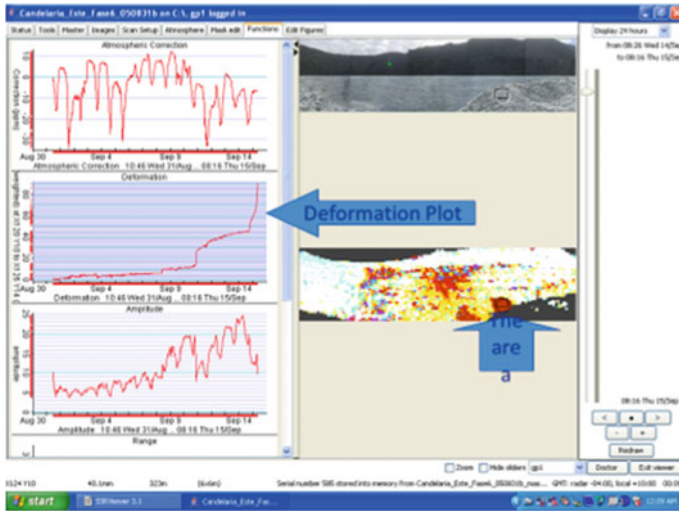


Fig. 6 Typical response from slope stability radar [5]



Fig. 7 Smart sensors for use in underground mines

technical advice to the Mine Operations groups. The analysis of the collected data can help the geotechnical engineers provide support to the Mine Design and Engineering groups to improve the effectiveness of the ground support and to optimize the cost of creating and maintaining underground excavations [1].

The ground response information can also be used to calibrate numerical models of the excavations and help improve the design process of the excavations and the deployed support systems. The observed performance can be used as a base and necessary modifications can be made to excavation and ground support practices so that future excavations in geotechnically similar conditions can be more appropriate.

7 Conclusions

The absence of adequate geotechnical data often leads to the use of gross assumptions in the mine planning and design process and increases the level of contingencies used in the development of operating cost estimates for the mining project. Unless the data is collected in time, this may delay projects for months to years and the financial implications of such a delay may be enormous. These delays may be of sufficient consequence to precipitate the termination of a project in a volatile and investor-cautious market.

Some of the possible impacts of the lack of appropriate geotechnical engineering include the isolation of deep ore due to unachievable pit slope angles in open pit mines, the inability to manage dilution within the sub-level stopes due to incorrect sublevel intervals or increased ground support costs in poor ground. Such situations result in lowering the value of the mining project and a consequent loss of valuable mineral reserves. The integration of geotechnical engineering data collection and analyses from an early stage of the project helps reduce the risk and increases the conversion of mineral resources to mineral reserves for the mining project.

References

1. Annavarapu S (2018) Managing the stability of underground excavations in modern mines. In: Managing Excavation Stability through Design, Analysis and Monitoring, MEAI, Nagpur, India
2. McCarthy PL, Lee MF, Bridges MC (1988) WASM Annual Conference, Kalgoorlie, Australia
3. Metcalfe J (2013) Timing your investment in geotechnical data collection can reduce financial risk. <https://amcconsultants.com/experience/timing-investment-geotechnical-data-collection-reduce-financial-risk>
4. Moss A, Diacehko S, Townsend P (2006) Interaction between the block cave and the pit slopes at Palabora mine. *J S Afr Inst Min Metall* 106:479–484
5. Rajmeny PK (2018) Prediction of slope failure in a moderately deep pit with weaker rock mass traversed with numerous geological discontinuities. In: Managing Excavation Stability through Design, Analysis and Monitoring, MEAI, Nagpur, India
6. Srikant A, Nicholas DE (2005) Incorporating reliability based geotechnical engineering into slope design. In: Advances in Mining Technology and Management, Kharagpur, India

Design and Evaluation of Stability of Slope Geometry of an Iron Ore Mine - A Case Study



A. Y. Bharath Kumar , Sultan Singh Meena , T. Amrith Renaldy ,
and A. Rajan Babu 

Abstract Extraction of valuable minerals like iron ore under complex strata conditions is a big challenge. Huge losses occur due to locked up ore left as a safety measure to maintain the stability of mine workings especially the bench slopes and ultimate pit slopes. In this paper a case study of an Iron Ore mine is presented which deals with the design of stable steep slopes and evaluation of slope stability. The study included collection of data on various geotechnical, mining and geological parameters. Wide ranges of soil samples were collected representing entire study area and lithology for which both physical and strength properties were determined in the laboratory. Design of slope geometry for the working benches and the Ultimate pit slope (UPS), was derived through numerical analysis using shear strength reduction (SSR) technique. Commercial software such Slide 6.0 software was used to design and assess the stability of the designed slope geometry. Physical and strength properties determined in the laboratory were used as input parameters for numerical analysis. The slope geometry for individual benches and ultimate pit slope angle was derived and optimized within the permissible safe factor of safety. Recommendations for reinforcement to create stable slopes and instrumentation for strata monitoring were suggested for safe operations.

Keywords Iron ore mining · Slope geometry · Stability evaluation

1 Introduction

Dharmapura Iron Ore Mine bearing M L No. 2543 situated in Ramagad Range, Dharmapura Village, Sandur Taluk, Bellary District, Karnataka over an extent of 10.00 Ha. This is a semi mechanized opencast mine. The lease located in the Sandur contains hematite ore in the Sandur schist belt has a lens-shaped deposit with a mean grade of 62% Fe and the hanging wall and foot wall comprises of shale/Phyllite. At present the pit is excavated up to a depth of 70 m from the hill top thus leaving

A. Y. B. Kumar (✉) · S. S. Meena · T. A. Renaldy · A. R. Babu
National Institute of Rock Mechanics, Bengaluru, Karnataka, India
e-mail: 044bharath@gmail.com

© The Author(s), under exclusive license to Springer Nature Singapore Pte Ltd. 2022
A. K. Verma et al. (eds.), *Proceedings of Geotechnical Challenges in Mining, Tunneling and Underground Infrastructures*, Lecture Notes in Civil Engineering 228,
https://doi.org/10.1007/978-981-16-9770-8_52

755

seven benches of each 8 m height. The advancement in the design and evaluation of stability of slope geometry of this has been discussed in this paper. The surface plan of the mine is shown in Fig. 1.

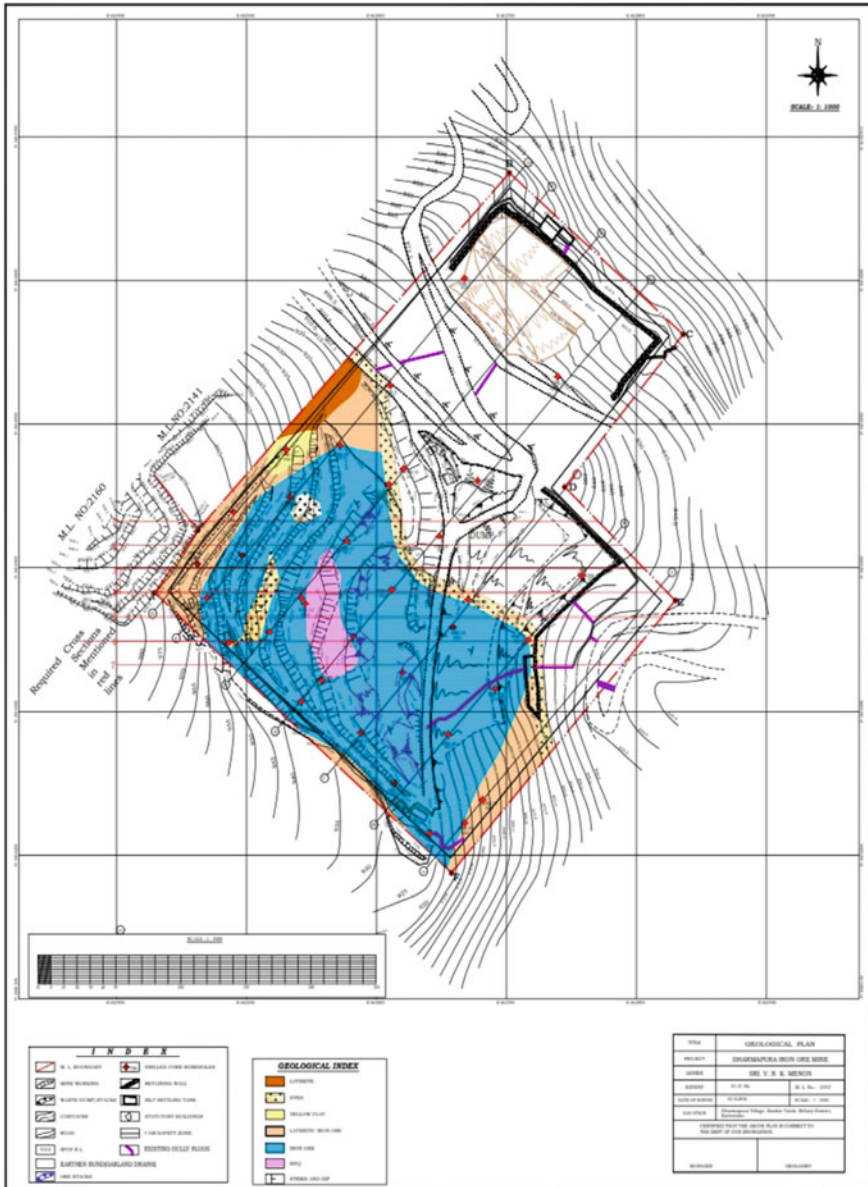


Fig. 1 Surface plan of the mine

The iron ore is a reef deposit occurring in a hilly terrain. Opencast mechanized method of mining with multiple benches is in practice. The average width of the ore body is 115 m and the reef is almost vertical. The width of the hill bottom is around 700 m at the ground level. The iron ore is excavated up to the depth of 122 m from the hill top leaving thirteen benches of each 8 m height. Modern technology using mechanized drilling & blasting, shovel dumper combinations, etc., are employed for the ore extraction and overburden removal.

2 Geology of the Area

The lease area is situated on the Ramghad hill range, running NW–SE. Maximum area is consisting of hill ranges and slopes. The high grounds are towards SW. The area slopes towards NE and SE. The maximum height is 973 m RL and minimum height is 810 m RL. The area belongs to famous Sandur schist belt which is part of Dharwar Precambrian supracrustal belts in Karnataka craton. This is the smallest of the three basins and covers an area of 960 sq.km. There is only one ore band running in the area. The strike of the ore body varies from N20°W - S20° to N60°E - S60°W and dips 40° to 70° due North-East. The different litho units present in the area are laterite, iron ore, banded hematite quartzite (BHQ) and shale. Shale is generally ferruginous in nature and is present at bottom level towards eastern part of the lease area. BHQ's are running in NW - SE direction and steeply dipping towards east at 60° to 70°. It is weathered on top and very hard below. The BHQ are having fractures and joints. Also, there is one small BHQ band towards eastern corner having almost E-W strike with steep northerly dip. The dolerite dyke is exposed in the central portion of the lease. The dyke trends NW – SE direction and dipping towards NE. The width of the dyke is almost 40 m.

2.1 Iron Ore Body

The ore body is oriented in 130°–310° and the strike length is more than 300 m with an average width of 115 m. The ore body is covered with a thin layer (1.5 to 5 m) of phyllitic rock. The ore is very hard in nature and grain size varies from medium to coarse grain. The streak of iron ore is reddish in colour.

3 Physico-Mechanical Properties

A number of samples of the material forming the benches were collected from different sections covering the entire area of the mine. As the material was soft,

Table 1 Values of cohesion and angle of friction [2]

Sl. No.	Lithology	Cohesion (kN/m ²)	Phi, deg
1	Dyke	32.94	37.32
2	Lateritic Iron Ore	38.62	51.48
3	Iron Ore	30.82	50.64
4	BHQ	44.97	49.43

it was treated like soil and soil testing procedures were adopted to determine its physico-mechanical properties.

3.1 Triaxial Testing

To determine the cohesion, friction angle and Hoek and Brown parameters of intact rock, triaxial compression test was carried out for the samples collected. The test was performed using Hoek Triaxial Cell and MTS compression testing machine. There are two methods of carrying out the triaxial compression test 1) Conventional method and 2) Multiple failure triaxial compression method (used here) (Table 1).

4 Slope Analysis

4.1 Analysis of Existing Bench Parameters

Slope stability analysis was carried out using limit equilibrium analysis by means of Slide 6.0 software. Limit equilibrium methods of slope stability analysis investigates the equilibrium of a soil mass tending to move down-slope under the influence of gravity. Two-dimensional (2-D) sections were analyzed and plane strain conditions are assumed. These methods assume that the shear strengths of the materials along the potential failure surface are governed by linear (Mohr–Coulomb) or nonlinear relationships between shear strength and the normal stress on the failure surface. Circular slip surface is assumed for the analysis. The main advantage for circular slip surface is that the direction of the normal force acting on the slip surface is directed towards the centre of the circle.

To safely exploit locked resources on the benches of a mine, it was intended to scientifically study and design safe and stable slopes for the benches and the overall pit slope. Accordingly, a few typical sections were selected initially to design slopes and study their stability. The study area is shown in Fig. 2 along with the selected sections starting from (Sect. 1, 2, 3, 4, 5, 6 and 7).

The factor of safety is defined as the ratio of the available shear resistance (the capacity) to that required for equilibrium (the demand). Limit equilibrium assumes



Fig. 2 Aerial view of the mine with sections taken for analysis

the factor of safety as the same along the entire slip surface. A value of factor of safety less than 1.0 indicates that the slope will be unstable. For the long-term stability of the slope the factor of safety is considered as 1.2.

Slide, a limit equilibrium program for two-dimensional slope stability analysis developed by Rocscience is used. Slide incorporates limit-equilibrium approach based on the method of slices. In this method, the soil mass above the assumed slip surface is divided into vertical slices for purposes of analysis. Bishop's simplified method was used for analysis of the slopes.

The analysis is carried out for the existing slope parameters of the mine and also for the modified slope parameters [1]. Factor of safety for the existing sections are shown in (Figs. 3, 4, 5, 6, 7, 8 and 9). The factor of safety for these sections are tabulated in Table 2.

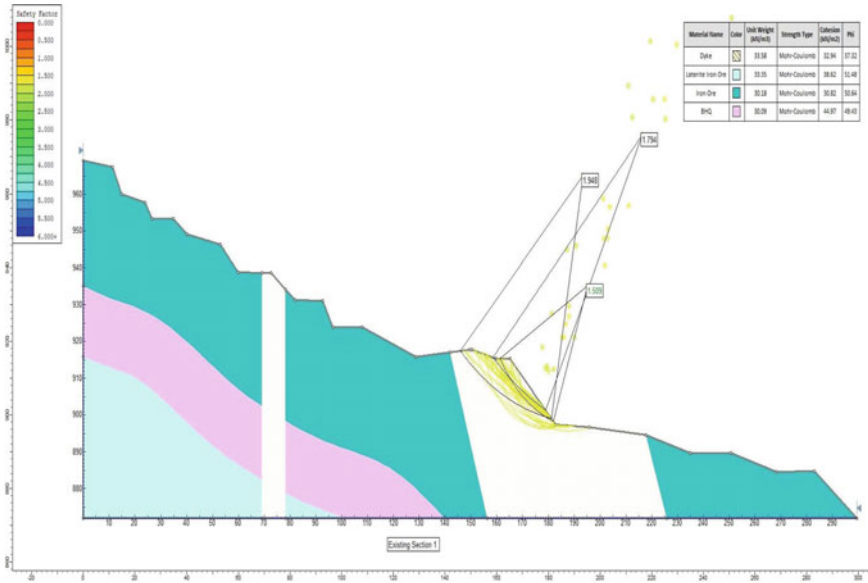


Fig. 3 FoS value of existing Sect. 3

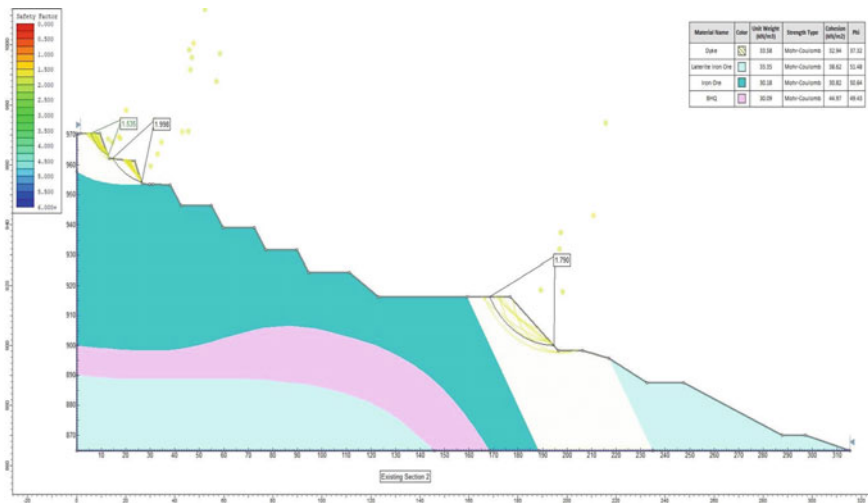


Fig. 4 FoS value of existing Sect. 2

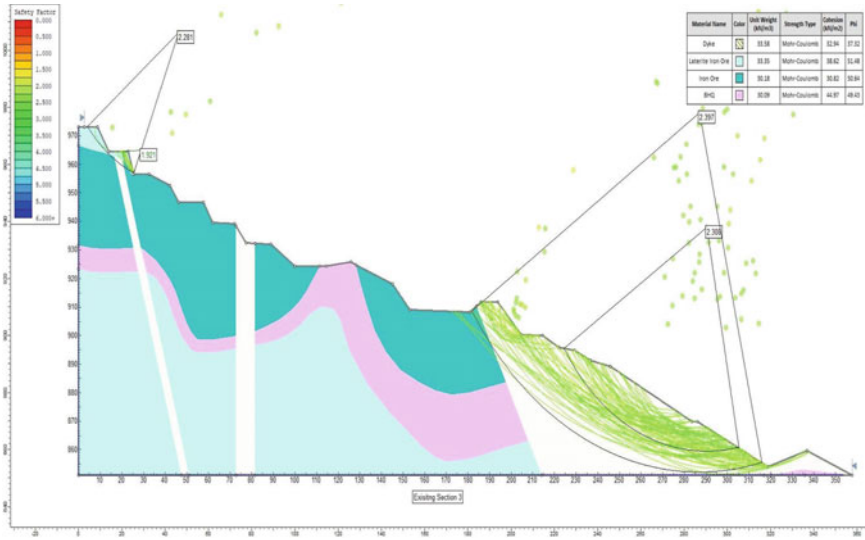


Fig. 5 FoS value of existing Sect. 3

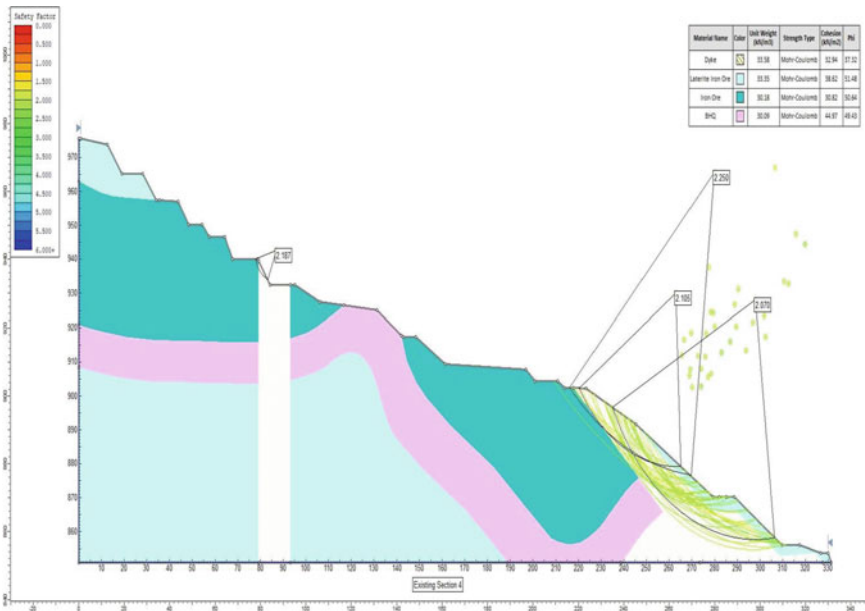


Fig. 6 FoS value of existing Sect. 4

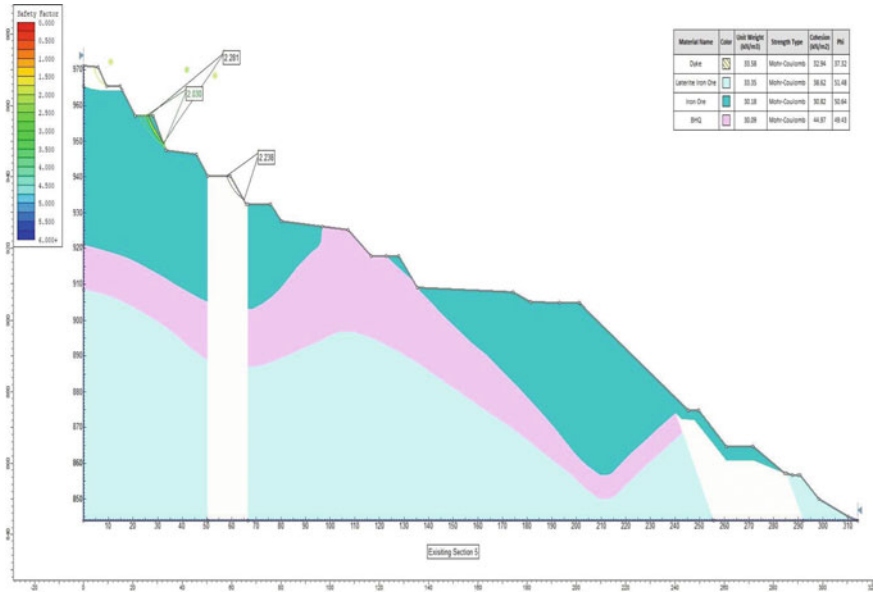


Fig. 7 FoS value of existing Sect. 5

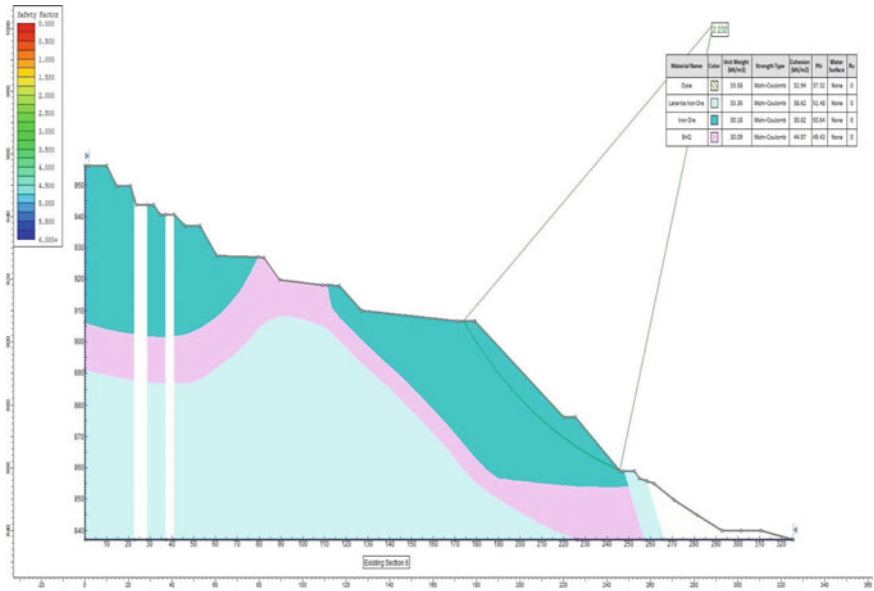


Fig. 8 FoS value of existing Sect. 6

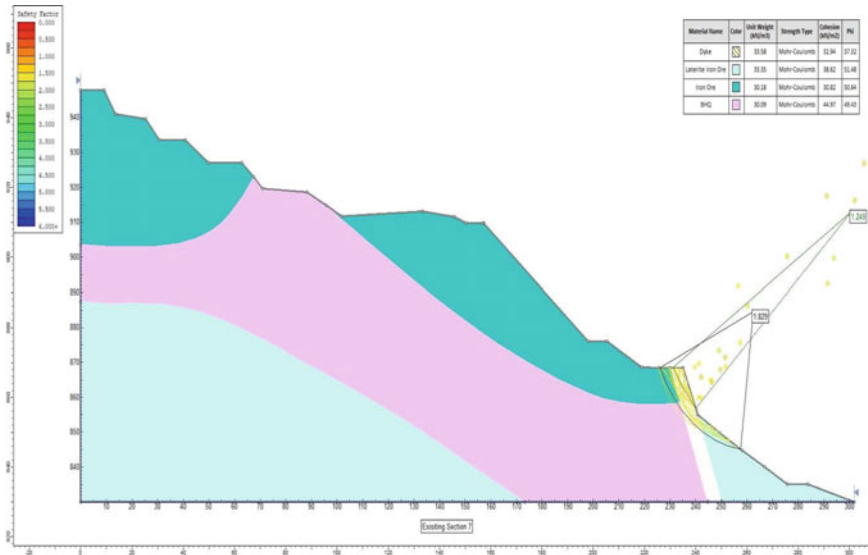


Fig. 9 FoS value of existing Sect. 7

Table 2 Summary of the FoS values of existing & modified sections

Section nos ^r	Factor of safety for existing sections	Factor of safety for modified sections
1	1.509	1.477
2	1.535	1.670
3	1.921	1.517
4	2.070	1.461
5	2.030	1.394
6	2.232	1.361
7	1.249	1.585

4.2 Analysis of Modified Bench Parameters

Using the limit equilibrium, analysis was carried out for the same sections incorporating corrections in the bench parameters. The width of the bench was 3 m for benches 1, 2, 4 & 5 and height of 8 m with an individual bench angle at 66° (Fig. 10). The analysis was carried out for all the cross sections and were redesigned for the new bench dimensions with safe distances from mine boundary (Figs. 11, 12, 13, 14, 15, 16 and 17).

The ultimate pit angle to be maintained is found to be 49° with the individual bench angle of 66°. The benches can be maintained safely with high degree of stability by providing proper drainage system.

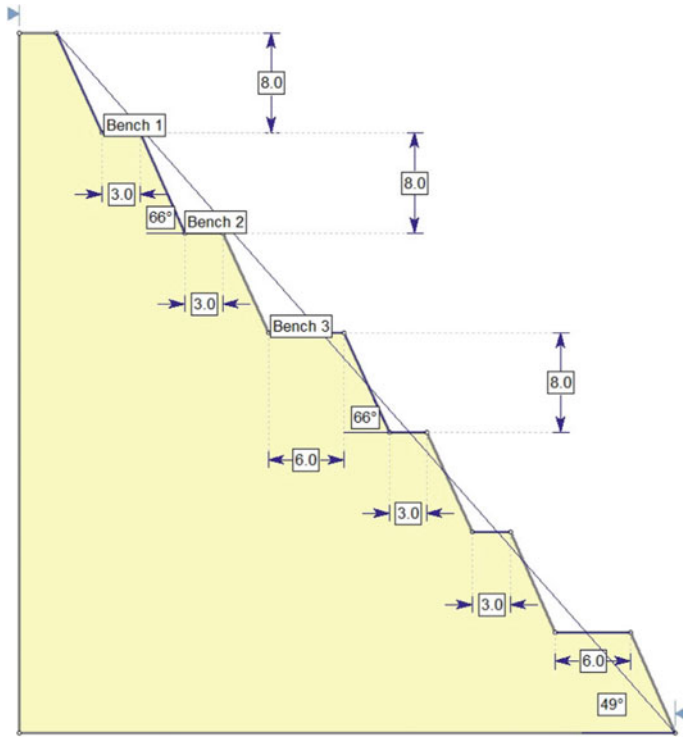


Fig. 10 New bench parameters

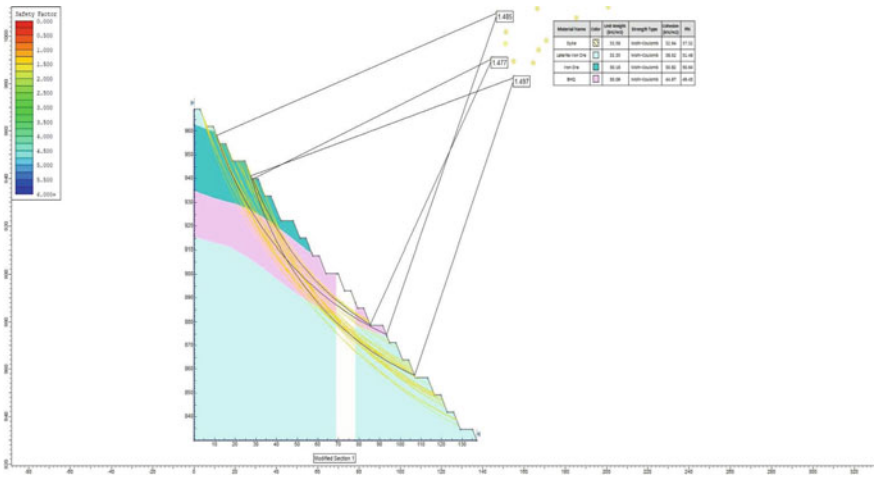


Fig. 11 FoS value of modified Sect. 1

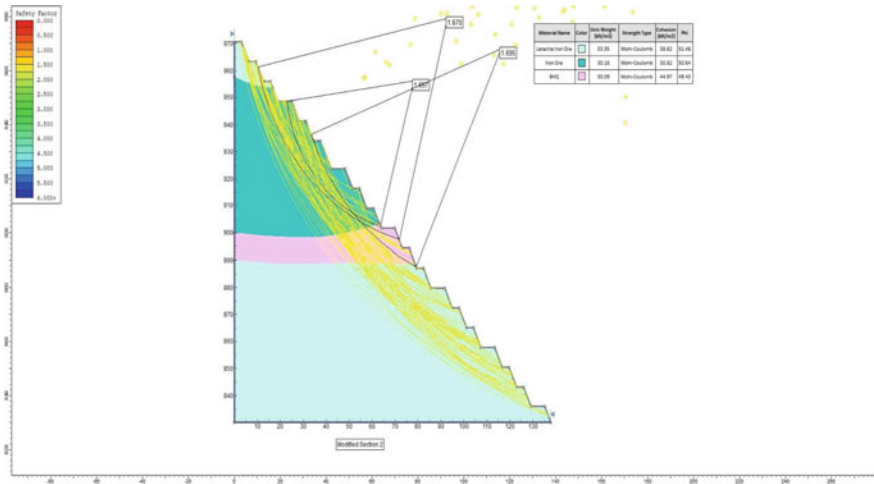


Fig. 12 FoS value of modified Sect. 2

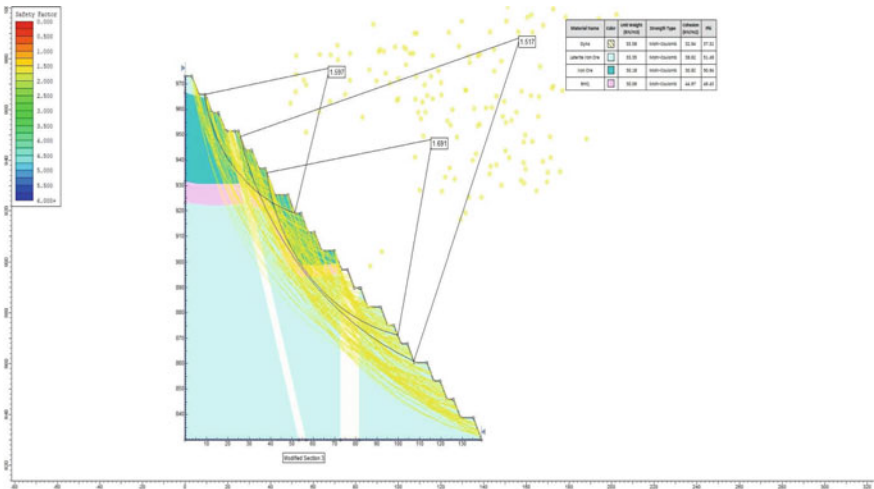


Fig. 13 FoS value of modified Sect. 3

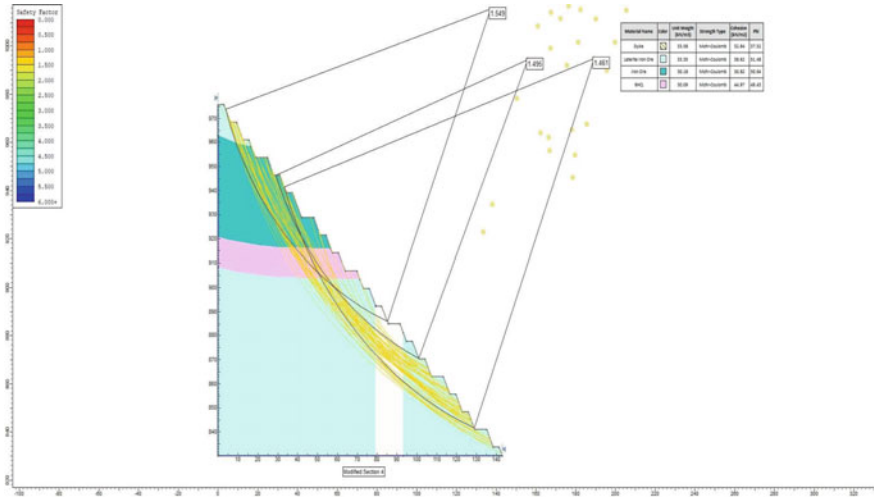


Fig. 14 FoS value of modified Sect. 4

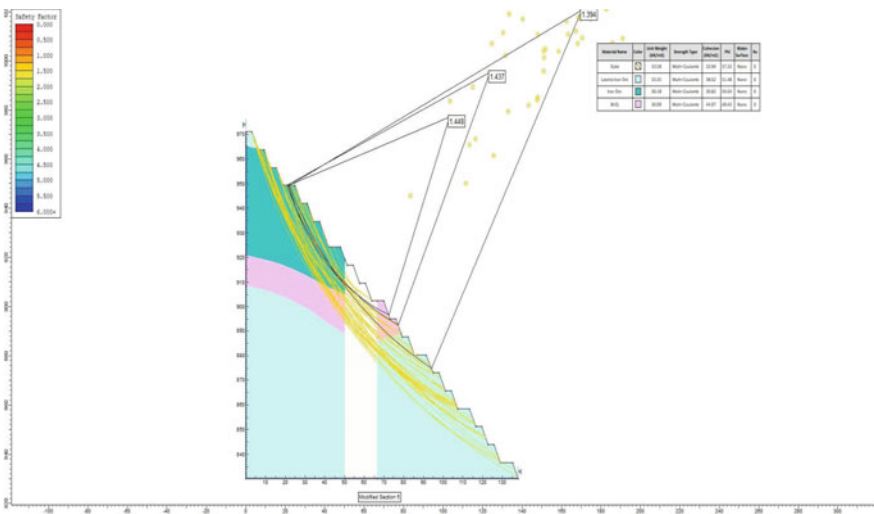


Fig. 15 FoS value of modified Sect. 5

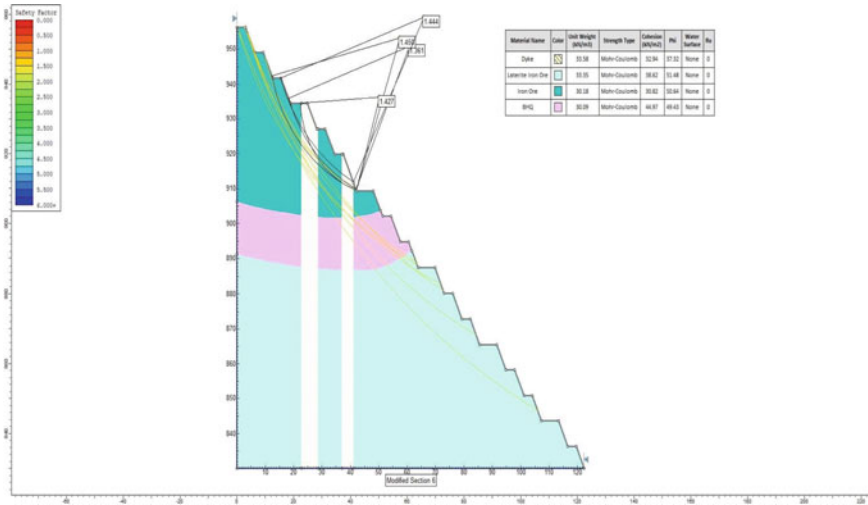


Fig. 16 FoS value of modified Sect. 6

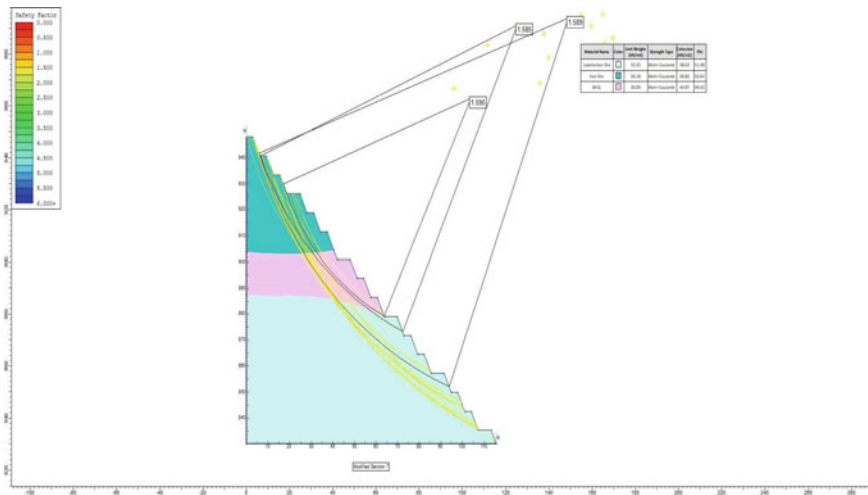


Fig. 17 FoS value of modified Sect. 7

4.3 Analysis of Existing Dumps

The slope analysis was carried out for the dumps at three sections in the mine, namely D-D', E-E', F-F'. The analysis was carried out for the existing cross sections and by increasing height of the dumps. The factor of safety determined are shown in the Figs. 18, 19 and 20. The derived FoS is given in Table 3.

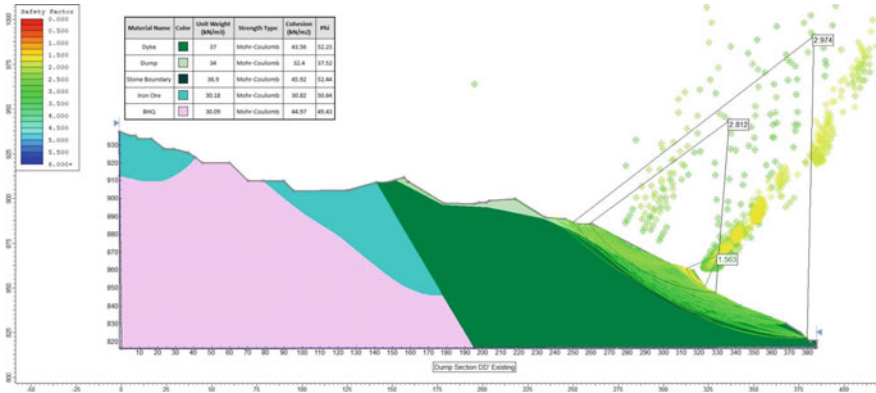


Fig. 18 Factor of safety of existing dump section D-D'

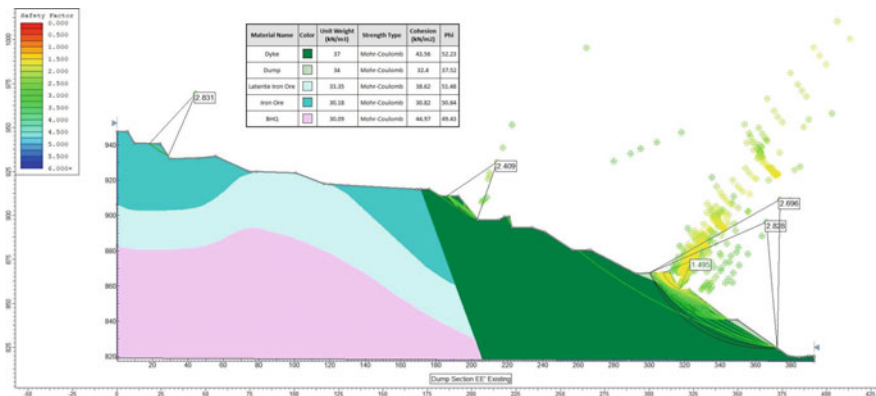


Fig. 19 Factor of safety of existing dump section E-E'

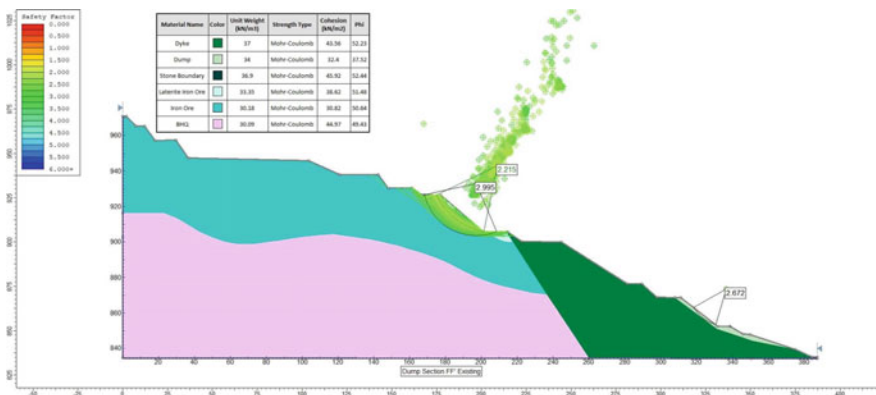


Fig. 20 Factor of safety of existing dump section F-F'

Table 3 Summary of the average FoS values for sections of existing the dump

Section nos'	Avg factor of safety
D-D'	2.45
E-E'	2.36
F-F'	2.63

4.4 Analysis of Modified Dumps

Using the limit equilibrium, analysis was carried out for the same sections with the corrections in the dump bench parameters. The modified dump sections DD', EE' & FF' were redesigned.

4.5 Modified Dump Section DD'

The section DD' is modified with the optimum bench design considering the mine boundary and the parameters used for analysis is shown in the Fig. 21. The modified dump parameter for section DD' involves a bench width of approximately 40 m height, width of 25 m, individual bench angle of 60° and overall slope angle of Dump section DD' as 40°. The overall slope FoS is 1.485, 1.748, 2.086, 1.004, 2.476 with the average FoS of 1.58.

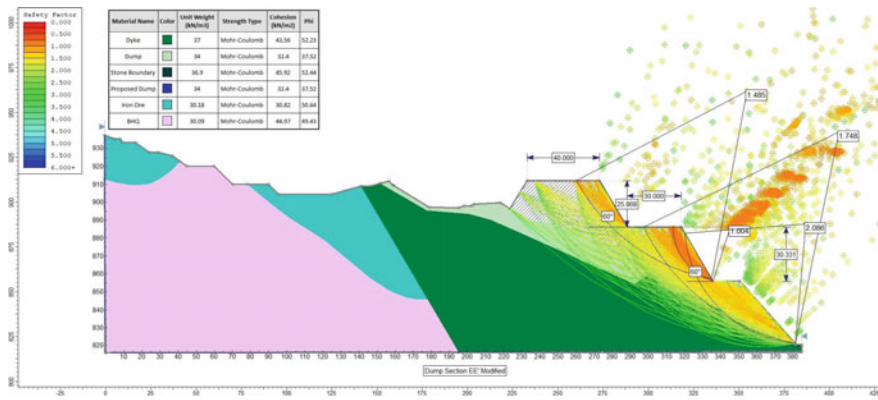


Fig. 21 Factor of safety of modified dump section D-D'

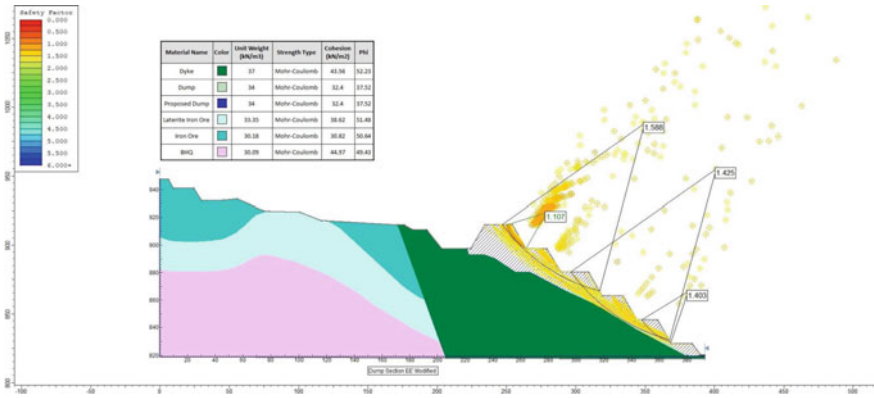


Fig. 22 Factor of safety of modified dump section E-E'

4.6 Modified Dump Section EE'

The section EE' is modified with the optimum bench design keeping the mine boundary into the consideration and the parameters used for analysis are shown in Fig. 22. The modified dump parameter for the section EE' is bench width of 15–17 m, height of 20 m, individual bench angle of 60° and overall slope angle of dump section EE' is 35° and the overall slope FoS is 1.588, 1.425, 1.403, 1.107 and the average FoS is 1.38.

4.7 Modified Dump Section FF'

The section FF' is modified with the optimum bench design considering the mine boundary and the parameters used for analysis is shown in the Fig. 23. The modified dump parameter for the section FF' has a bench width of 15 m, height of 17.3 m, individual bench angle of 60° and overall slope angle of dump section FF' is 37° with the overall slope FoS of 2.393, 2.413, 1.513, 1.346 with the average FoS of 1.91. The summary of values of FoS for the modified dump sections is given in Table 4.

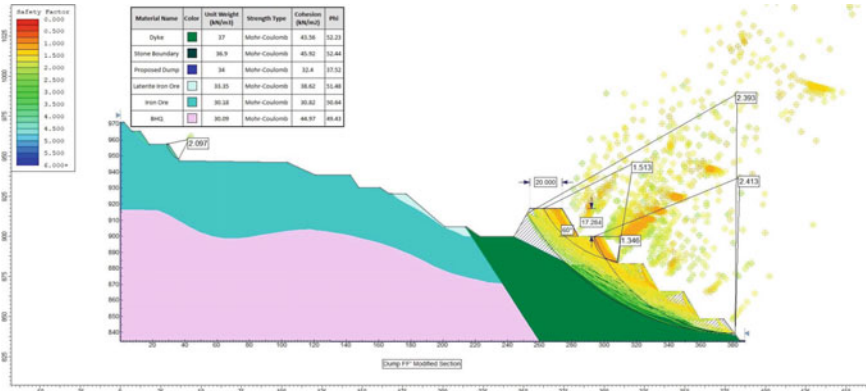


Fig. 23 Factor of safety of modified dump section F-F'

Table 4 Summary of the FoS values of modified sections of the dump

Section nos'	Avg. factor of safety for modified sections
DD'	1.58
EE'	1.38
FF'	1.91

5 Conclusions

The scientific investigations were carried out at the Dharmapura Iron Ore Mine by studying the geological and geotechnical parameters and through an indepth numerical analysis. The results of analysis yielded fairly good FoS for working benches and provided safe ultimate pit slope angles for the quarry pit and dumps thereby indicating stable slopes for all the sections studied.

- The FoS for the existing benches ranged between 1.249 to 2.232. The FoS for the modified benches varied between 1.361 to 1.670. The derived FoS are well within the permissible limit of 1.2 promising stable slopes.
- Based on the strength parameters and slope analysis, the benches were designed to be worked with top two benches having 3 m width and from the 3rd bench it is designed for 6 m width to be continued below by maintaining an individual bench height of 8 m.
- For stability purposes, the ultimate pit slope angle is found to be 48° with the individual bench angle of 66°.
- In case of dump, the ultimate dump slope angle is derived to be 37° to 40° with the individual bench angle being 60° for a width ranging between 20 to 40 m and the bench height varying between 15 to 25 m.

- The study helped to maximise the production by recovering a sizeable volume of locked up ore through the design of optimum bench parameters and stable pit slopes.

Acknowledgements We are thankful to the management of Dharmapura Iron Ore Mine and especially Shri VNK Menon for permitting to carry out the study. Thanks are due to Shri U Krishna Prasad and Shri Shivananda Reddy, Mine Manager. We extend our sincere thanks to the officers and staff for their cooperation during field study. We are extremely grateful to the Director, NIRM for his encouragement and permission for publishing this paper.

References

1. Bieniawski ZT (1984) Input parameters in mining. In: Balkema AA (ed) *Rock Mechanics Design in Mining and Tunneling*, 8 edn, Netherland, pp 55–92
2. NIRM report (2019)

Intelligent Technique for Prediction of Blast Fragmentation Due to the Blasting in Tropically Weathered Limestone



Ramesh Murlidhar Bhatawdekar, Deepak Kumar, Saksarid Changtham, Devanshu Pathak, Singh TrilokNath, and Edy Tonnizam Mohamad

Abstract In the rock blasting scenario, the success of fragmentation plays a major role. Prediction of blasted rock mass fragmentation has a significant role in the overall economics of opencast mines. Blast fragmentation has a direct impact on efficiency and cost of operation consisting of loading, transport and crushing. Tropical weathering has a direct impact on rock mass properties and strength of rock. Thus, challenging issues are created for blastability of tropically weathered limestone.

It is necessary to analyze the blast fragmentation and optimize the blasting parameters. Selected limestone mine for this study is in Thailand. Various rock mass properties such as GSI, RMR, and stemming length were studied to find out the correlation with rock fragmentation. Stiffness ratio, hole diameter to burden ratio, powder factor, maximum charge per delay, RQD, blastability index (BI), weathering index (WI) and mean block size were input parameters to analyse mean rock fragment size.

Total 105 data sets were collected. In this paper, a hybrid model with Artificial neural network (ANN), Particle swarm optimization (PSO) known as PSO-ANN was implemented to analyse the blast fragmentation. Multivariate regression Analysis (MVRA) was also performed. 83 datasets were trained and balance data sets were utilised for testing data. R^2 values for training with PSO-ANN and MVRA showed 0.818 and 0.657 respectively. R^2 values for testing with PSO-ANN and MVRA

R. M. Bhatawdekar · D. Pathak (✉)

Department of Mining Engineering, Indian Institute of Technology, Kharagpur, India

e-mail: pathakdevanshu9@gmail.com

R. M. Bhatawdekar · E. T. Mohamad

Geotropik, Department of Civil Engineering, Universiti Teknologi Malaysia, Johor Bahru, Malaysia

D. Kumar

Department of Civil Engineering, National Institute of Technology, Patna, India

S. Changtham

Siam City Concrete Company Limited, Bangkok, Thailand

S. TrilokNath

Earth Science Department, Indian Institute of Technology, Mumbai 400 076, India

showed 0.70 and 0.694 respectively. Thus the hybrid model PSO-ANN was found useful to predict fragmentation.

Keywords Artificial neural network (ANN) · Blastability index (BI) · Multivariate regression Analysis (MVRA) · Particle swarm optimization (PSO) · Weathering index (WI)

1 Introduction

The main objective of the rock blasting is to produce effective fragments of rock. Blasting operation management relies heavily on the size distribution of rock fragments and their classification [1, 2]. Fragmentation has an impact on all downstream processes, including loading, crushing, and hauling, and it can be used to reduce costs [2]. It is essential to have a fast and efficient method for measuring the degree of fragmentation in order to effectively manage and optimise the process.

A limestone mine in Thailand was selected for this study. Construction aggregates in Thailand are made mostly of basalt, limestone and granite [3, 4]. Limestone quarries that generate more than 200,000 cubic metres per month are referred to as large quarries, while those that produce less than that are referred to as small quarries. The majority of large quarries of Limestone are located in central Thailand. Limestone is primarily supplied by large limestone quarries for the manufacture of Cement. Limestone deposits consist of weathered limestone, massive limestone blocks and also moderately weathered limestone. The first layer of limestone deposit is the overburden which is 2–5 m thick. After that it contains highly weathered limestone which is 2–20 m thick. After the second layer, the deposit contains massive limestone blocks around 100 m thick.

The aggregate quarry having limestone is producing 2.5 MTPA. Typical large quarries utilize a 10 cm radius drill hole which carries a powder factor from 0.40 to 0.60 kg/ cubic meters [3]. Maximum charge per delay varies from 64.3 to 160 kg per delay for a distance of 150 m and 534.9 to 643.4 kg per delay for a distance of 300 m. For smaller quarries, the burden to spacing patterns of 1.5×1.8 m to 3.5×3.5 m patterns are used. For larger quarries, burden to spacing patterns from 5×6 m to 6×8 m are used. The objective of this study is to predict the blast fragmentation due to blasting through a hybrid model PSO-ANN [5, 6].

Blast fragmentation depends on many factors but the main factors which have a great influence on prediction of blast fragmentation are Rock Mass properties, Blast Design parameters and Explosives [7, 8].

The Rock mass properties have a significant impact on blast fragmentation prediction [7–10]. The frequency and direction of joints and fractures have a significant impact on the start and spread of blast damage in a rock mass. The RQD of the blasting face is one of the most significant parameters in estimating mean fragment size. Rock-quality designation (RQD) measures the percentage of the drill core whose length is 100 mm or more. RQD measures the quality of a rock mass. A rock mass

with an RQD of less than 70% is extremely susceptible to violence. If overbreak is to be reduced, lower RQD values require care in blast design [11].

Explosives are also an important factor that affects the blast fragmentation [7]. Explosive parameters like explosive types, their strength, density, Powder factor, and specific charge, etc. all have an effect on the degree of fragmentation. Several studies have shown that the powder factor as well as the total charge per delay are essential parameters to consider. Amount of explosive required to break the unit mass of rock is measured by the powder factor. As the powder factor is increased, the mean and maximum fragment sizes decrease. The maximum charge per delay in explosion correlates to the maximum energy released instantaneously, affecting the mean fragment size [14–17].

Third important factors are the Blast Design parameters [7, 8]. The blast fragmentation is affected by blast design parameters such as Burden, Spacing, Bench height, Hole diameter, Blastability index, stemming length, drilling pattern, stiffness ratio, and blasting sequence, etc. Stiffness ratio, (D/B) hole diameter to burden ratio and blastability index (BI) are some Blast design parameters used in this study to analyse mean rock fragment size. According to studies conducted by several Indian research institutes in the field of blast design, it is recommended that the minimum hole diameter should be one tenth of the bench height. It is also observed that the maximum boulder size likewise increases rapidly after the blast hole diameter reaches 125 mm. According to Konya and Walter, the stiffness ratio should be between 2 and 4 to produce an effective blast fragmentation (1990). According to research conducted in limestone quarries, it was found that higher boulders are formed mostly from the stemming section as the stemming length is positively correlated to the mean fragment size and also the optimum mean fragment size is obtained when the burden is 21 times the hole diameter [12, 13].

Numerous studies have revealed that the ratios of parameters such as hole diameter, burden, spacing, and bench height, contribute to blast performance, rather than a single parameter. Different burden to blasthole diameter ratio, bench height to burden, spacing to burden, and stemming length to burden ratios all play a role in predicting mean blast fragmentation size [14, 15].

2 Methodology

Limestone quarries in Thailand were investigated in this study and data was collected from these sites. At the quarry sites, blast design parameters were recorded. The maximum charge per delay, as well as the powder factor, were recorded from actual blasting data. In terms of weathering, Limestone deposits consist of highly weathered limestone, massive limestone blocks and also moderately weathered limestone. The first layer of limestone deposit is the overburden which is 2–5 m thick. After that it contains highly weathered limestone which is 2–20 m thick. After the second layer, the deposit contains massive limestone around 100 m thick.

Scan line survey technique was used at every quarry face to measure in situ block size (X_b) and RQD [18].

2.1 Blastability Index Lilly (1986)

Lilly(1986) developed an empirical method of blastability index based. The Blasting index is site-specific and is calculated using rock mass description, joint density, specific gravity, orientation and hardness. The Blastability Index (BI) is computed using the equation for various rock types:

$$BI = 0.5 \times (JPO + RMD + H + JPS + SGI)$$

Here, JPS represents joint plane spacing, RMD denotes rock mass description, JPO represents Joint Plane Orientation, H is mho’s scale of hardness and SGI is a specific gravity influence (Table 1).

Lilly has created a number of charts based on the powder factor and blastability index requirements for various rock masses. These charts are useful for carrying out initial trial blasts for estimating drilling requirements and powder factor requirements based on the blastability index. Each of the five parameters of the blastability index plays an important role in blasting performance. The structural nature of rock mass is important in blast design. Fractured rock mass requires a lower powder factor as compared to blocky rock mass. Closer joint spacing produces finer fragmentation as compared to wider joint spacing and requires lower energy. Joint plane orientation decides the movement direction of the blasted stockpile. Horizontal joints require shallow sub-drilling and lower powder factor. Higher density rock needs higher energy for breaking. Lilly had investigated the hardness of rock and was correlated with the compressive strength of rock. Hence, harder rock needs higher energy to break rock. Thus, the blastability index and powder factor for each site can be established [19].

Table 1 Blastability parameters with classification values. (Lilly 1986)

Parameter	Description			
RMD	Type of rock mass			
	10 = powdery, friable	20 = blocky	30 = totally massive	
JPS	Type of spacing			
	10 = close (<0.1 m)	20 = intermediate (0.1 to 1.0 m)	30 = wide (>1.0 m)	
JPO	Type of plane orientation			
	10 = horizontal	20 = dip out of face	30 = strike normal to face	40 = dip into face
SGI	25 × specific gravity of rock (t/m^3) – 50			
H	Mho scale of hardness (1–10)			

2.2 Weathering Index (WI)

Weathering index was calculated by collecting weathered limestone samples from each face. 10 samples were collected from each blasting site and Point load index (PLI), Porosity and water absorption were determined for samples collected. PLI is maximum for fresh limestone. Porosity and water absorption are maximum for completely weathered limestone. Ratio of each property was compared with the respective maximum value. The Weathering Index was determined based on the average of these three ratios.

Various Blast design parameters such as Hole diameter, Burden, Bench height, Powder factor and maximum charge per delay were recorded from individual blast data. After the blasting, Images were taken of the blasted muck pile by placing a ball of 1 m size at the blasted muckpile and the images were analysed with the help of Fragalyst Software to obtain the mean fragment size (X_{50}).

2.3 Data Collection

At each blasting face, the mean block size and RQD were measured and RQD varied from 50 to 90% with an average of 76%. 105 blasting data sets were collected from these quarry sites. For each dataset, Stiffness ratio (H/B), hole diameter to burden ratio (H/B), Powder Factor (PF), maximum charge per delay, RQD, blastability index (BI), weathering index (WI) and mean block size (XB) are used as input parameters to predict mean rock fragment size (Table 2).

A hybrid model of Particle Swarm optimization and Artificial Neural Network (PSO-ANN) was used as a model for the prediction.

Table 2 Summary of the data collected

Description	Symbol	Units	min	max	Avg	Q1	Q3
Stemming length	H/B	–	25	45	35	29.4	38.1
Hole diameter to burden ratio	D/B	–	1	4	2.5	2.0	3.2
Powder factor	PF	(kg/cu m)	0.061	0.49	0.30	0.20	0.40
Maximum charge per delay	C	kg	8	426	109	44.11	157.91
Rock quality designation	RQD	–	12	98	64	35	90
Blastability Index	BI	–	18.5	80.8	43.5	28.6	58.8
Weathering Index	WI	–	0.13	0.88	0.52	0.25	0.76
Mean block size	X_b	m	0.30	1.18	1.13	0.90	1.48
Mean fragment size	X_{50}	mm	102	531	257.4	198	305

B = Burden(m), D = Hole Diameter(mm), H = Bench Height(m).

2.4 Artificial Neural Network

In 1949, the first ANN training technique was proposed. Artificial neural networks (ANNs) are computer programmes inspired by the way the human brain processes information. ANNs learn by identifying patterns and connections in data and gathering information. A neural network contains several layers, each of which has its own job. As the model's complexity grows, the number of layers grows as well, which is why it's called a multi-layer perceptron.

Artificial Neural Network is made up of three layers: the input layer, the hidden layer (which grows in complexity as the complexity increases) and the output layer. The input layer receives the inputs and passes them on to the next layers, and in the end the output layer makes the final prediction. An activation function is used according to its need to activate the neuron during training. The weights are adjustable parameters, adjusted in such a way during backpropagation to minimize the loss. At the end, an output is generated with minimum loss.

The ANN is a tool which is being used in every field Medical, finance, engineering, etc. Neural Network is also being widely used in the Mining field. Various researchers have used a variety of statistics analysis tools, empirical equations, and artificial neural network methods to predict blast fragmentation, ground vibration, and airblast prior to blasting activities, etc. [17, 20, 21]. A large number of researchers have been studying the construction of simple, nonlinear mathematical solutions based on neuron optimization in hidden layers [20, 22]. Artificial neural network (ANN) is preferred over the other predictive techniques due to its ability to incorporate the numerous factors affecting the output. Although ANN is used to solve engineering issues quickly, it has a number of drawbacks, including a slower learning rate and a tendency to become stuck in a local minima.

2.5 Particle Swarm Optimization (Pso)

Particle swarm optimization (PSO) is an evolutionary optimization method based on the social behaviour of animals like birds and fish. It was introduced and developed by Eberhart, Kennedy [23]. The PSO uses less memory and offers faster information gain compared to other optimization algorithms. This approach employs a swarm of particles to determine the optimum location based on the best response, which includes the best personal and global locations. Through each iteration, particles' personal best and global best are found and updated. During the search, the optimal solution is discovered based on the experiences of all individuals in the swarm. A particle's velocity and position throughout its motion can be expressed as follows:

$$V_{new} = (W \times V) + A_1 \times (Pb - X) + A_2(G_b - X)$$

$$X_{new} = X + V_{new}$$

$$A_1 = L_1 \times rand_1$$

$$A_2 = L_2 \times rand_2$$

,Where $rand_1$ and $rand_2$ represent the random numbers between 0 and 1, P_b and G_b represent the personal best and the global best position of particle, L_1 and L_2 are learning factors, Particles current position and velocity are represented by X and V , Particle's new position and velocity are represented by X_{new} and V_{new} , and the inertial weight coefficient is represented by w .

2.6 Pso-Ann

ANN-based approaches have been shown in several studies to be reliable methods for predicting blast fragmentation. Most ANN training models, on the other hand, have substantial issues such as a slow learning rate and being stuck in their local minima. Particle swarm optimization (PSO) is an algorithm to optimize the performance of an ANN.

For example,(Rukhaiyar et al.2015)] used PSO to construct and optimise an ANN for seismic slope stability prediction. PSO was proposed as a strong technique for creating ANNs based on their findings, as PSO–ANN predictions are more accurate than ANN predictions. Another study used the PSO–ANN method to predict the maximum surface settlement caused by tunnelling at the Karaj subway station in Iran [26, 27]. In the end, the PSO–ANN model was found to be more accurate than the ANN model in simulating surface settlement [24–27].

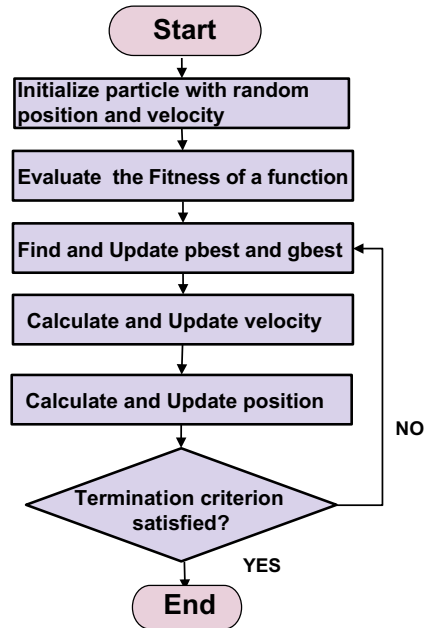
In this study, the PSO algorithm was used to improve the performance prediction of the ANN model in order to build a more accurate predictive model for blast fragmentation prediction. PSO is used as an optimization method to minimise a cost function by changing the weights and biases (Fig. 1).

3 Result and Discussion

Input factors played an important role in the prediction of blast fragment size. It was found that fragment size increased with the increase in the bench height. The blast fragment size was obtained to be positively correlated with stemming length.

More finer particles were produced when the maximum charge per delay was higher. The Weathering Index is a new index that is only appropriate for tropical weathered limestone and may not be useful for other limestone sites. Blastability index and Powder factor was found to be yielding porous fragments. Blastability index was negatively correlated to the mean fragment size and More finer particles were obtained with less RQD Values.

Fig. 1 The flow chart of ANN Optimized with PSO algorithm



Blast fragmentation depends on many factors but of those most appropriate features were selected, especially for the tropical climate. Blast design parameters such as Burden, Bench height, Hole diameter, Blastability index, Stemming length, etc.

Are used as input parameters in this study. Spacing and other blast design parameters were insignificant at this site.

A hybrid model of Particle Swarm optimization and Artificial Neural Network (PSO-ANN) was used for the prediction of blast fragment sizes. The hybrid model was found to be more accurate than other models in many studies. The R^2 value was used to evaluate the model. R^2 was achieved as 0.82 for the training data and 0.69 for the testing data of PSO-ANN. The predicted fragment size values by PSO-ANN models together with their observed values are shown in Fig. 2 and Fig. 3 below:

Figures: The predicted fragment size values by PSO-ANN model together with their observed values for training and testing data.

4 Conclusion

- The PSO-ANN model was found to be an appropriate model with reasonable accuracy.
- R^2 is achieved as 0.82 for training data and 0.69 for testing data on PSO-ANN, respectively.

Fig. 2 The predicted fragment size for training data by PSO-ANN model together with their observed values

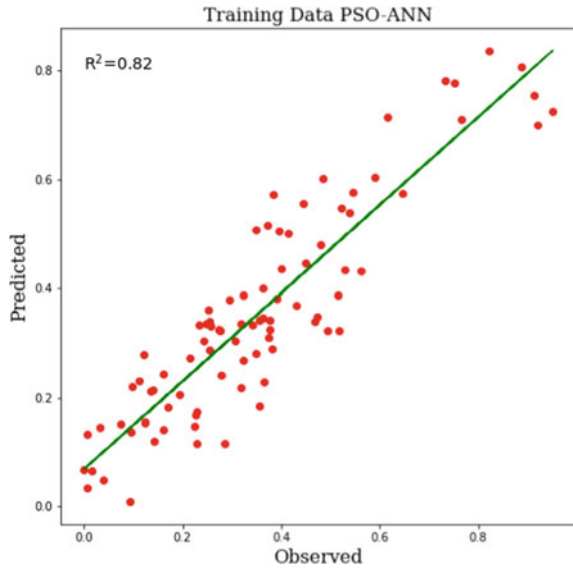
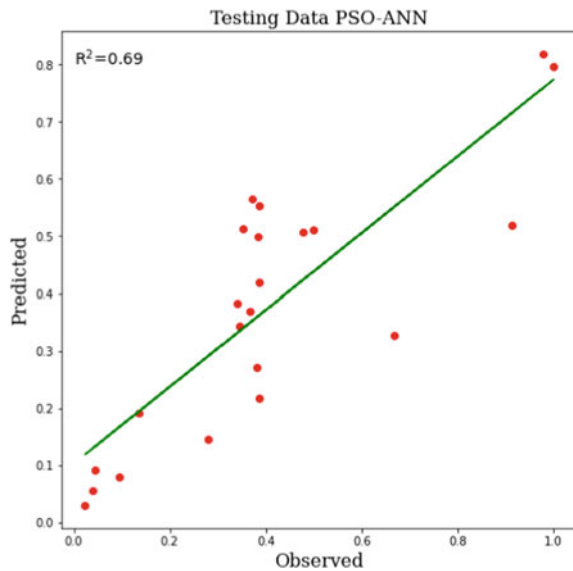


Fig. 3 The predicted fragment size for testing data by PSO-ANN model together with the observed values



- Input parameters consisting of mean block size (X_b), RQD, powder factor (PF), maximum charge per delay, (B/D) burden to hole diameter ratio, Bench height to burden ratio (H/B), Blastability index (BI) and Weathering index (WI) play significant role for predicting mean fragment size (X_{50}).
- This model is appropriate for this site; however, other sites will require different input values and modelling approaches.

- For each blasting site, the weathering index is calculated by collecting 3 face samples for each blast prior to blasting. RQD and blastability index is measured prior to the blast. RQD, BI and WI are uncontrollable parameters. On the other hand, balance parameters are controllable parameters. Once values of uncontrollable parameters are known prior to blast, controllable parameters are selected in such a manner to get desired fragmentation. This is a practical aspect of applying methodology for prediction and monitoring fragmentation.

References

1. Sereshki F, Hoseini SM, Ataei M (2016) Blast fragmentation analysis using image processing. *Int J Min Geo-Eng* 50(2):211–218
2. Kanchibotla S, Valery W, Morrell S (November 1999) Modelling fines in blast fragmentation and its impact on crushing and grinding. In: *Explo 1999—A conference on rock breaking*, The Australasian Institute of Mining and Metallurgy, Kalgoorlie, Australia, pp 137–144
3. Bhatawdekar RM, Mohamad ET, Singh TN (2017) Selection of Lidar technology for limestone quarries in Thailand. *J Mines Met Fuels* 65(7):393–399
4. Bhatawdekar RM, Mohamad ET, Singh TN, Armaghani DJ (2019) Drilling and blasting improvement in aggregate quarry at Thailand—a case study. *J Mines Met Fuels* 67:357–362
5. Hasanipanah M, Naderi R, Kashir J, Noorani SA, Qaleh AZA (2017) Prediction of blast-produced ground vibration using particle swarm optimization. *Eng Comput* 33(2):173–179
6. Trivedi R, Singh TN, Gupta N (2015) Prediction of blast-induced flyrock in opencast mines using ANN and ANFIS. *Geotech Geol Eng* 33(4):875–891
7. Thornton D, Kanchibotla SS, Brunton I (2002) Modelling the impact of rock mass and blast design variation on blast fragmentation. *Fragblast* 6(2):169–188
8. Akbari M, Lashkaripour G, Bafghi AY, Ghafoori M (2015) Blastability evaluation for rock mass fragmentation in Iran central iron ore mines. *Int J Min Sci Technol* 25(1):59–66
9. Hagan TN (1995) The effect of rock properties on the design and results of tunnel blasts. *J Rock Mech Tunn Technol* 1(1):25–39
10. Kılıçcedil AM, Yaşar E, Erdoğan Y, Ranjith PG (2009) Influence of rock mass properties on blasting efficiency. *Sci Res Essays* 4(11):1213–1224
11. Singh P, Narendrula R (2007) The influence of rock mass quality in controlled blasting. In: *Proceedings of the 26th International Conference on Ground Control in Mining*, pp 314–319
12. Prasad S, Choudhary BS, Mishra AK (August 2017) Effect of stemming to burden ratio and powder factor on blast induced rock fragmentation—a case study. In: *IOP Conference Series: Materials Science and Engineering*, vol 225, no 1, p 012191. IOP Publishing
13. Sharma A, Mishra AK, Choudhary BS, Meena R (2019) Impact of blast design parameters on rock fragmentation in building stone quarries. *Curr Sci* (00113891) 116(11): 1861–1867. Research paper
14. Hasanipanah M, Armaghani DJ, Monjezi M, Shams S (2016) Risk assessment and prediction of rock fragmentation produced by blasting operation: a rock engineering system. *Environ Earth Sci* 75(9):808
15. Kulatilake PHSW, Qiong W, Hudaverdi T, Kuzu C (2010) Mean particle size prediction in rock blast fragmentation using neural networks. *Eng Geol* 114(3–4):298–311
16. Hasanipanah M, Amnieh HB, Arab H, Zamzam MS (2018) Feasibility of PSO–ANFIS model to estimate rock fragmentation produced by mine blasting. *Neural Comput Appl* 30(4):1015–1024
17. Bahrami A, Monjezi M, Goshtasbi K, Ghazvinian A (2011) Prediction of rock fragmentation due to blasting using artificial neural networks. *Eng Comput* 27(2):177–181

18. Palmstrom A (2005) Measurements of and correlations between block size and rock quality designation (RQD). *Tunn Undergr Space Technol* 20(4):362–377
19. Lilly P (October 1986) An empirical method of assessing rock mass blastability. In: *Large Open Pit Mine Conference*, Newman, Australia, pp 89–92
20. Tiile RN (2016) Artificial neural network approach to predict blast-induced ground vibration, airblast and rock fragmentation. Missouri University of Science and Technology
21. Lawal AI, Idris MA (2020) An artificial neural network-based mathematical model for the prediction of blast-induced ground vibrations. *Int J Environ Stud* 77(2):318–334
22. Asl PF, Monjezi M, Hamidi JK, Armaghani DJ (2018) Optimization of flyrock and rock fragmentation in the Tajareh limestone mine using the metaheuristics method of firefly algorithm. *Eng Comput* 34(2):241–251
23. Kennedy J, Eberhart RC (1995) Particle swarm optimization. In: *Proceedings of IEEE International Conference on Neural Networks*, Perth, Australia, pp 1942–1948
24. Rukhaiyar S, Alam MN, Samadhiya NK (2018) A PSO-ANN hybrid model for predicting the factor of safety of slope. *Int J Geotech Eng* 12(6):556–566
25. Abdi MJ, Giveki D (2013) Automatic detection of erythemato-squamous diseases using PSO-SVM based on association rules. *Eng Appl Artif Intell* 26:603–60840
26. Hajihassani M, Armaghani DJ, Sohaei H, Mohamad ET, Marto A (2014) Prediction of airblast-overpressure induced by blasting using a hybrid artificial neural network and particle swarm optimization. *Appl Acoust* 80:57–67
27. Hasanipanah M, Noorian-Bidgoli M, Armaghani DJ, Khamesi H (2016) Feasibility of PSO-ANN model for predicting surface settlement caused by tunnelling. *Eng Comput* 32(4):705–715

Assessment Parameters of Rock Masses for Excavation in Relation to Moisture Content



Mariatul Kiftiah Ahmad Legiman, Edy Tonnizam Mohamad,
Eka Kusmawati, Vynotdni Rathinasamy, Zuraini Zainal,
Nurul Eilmy Zainuddin, and Zulkiffi Ismail

Abstract The influence of moisture content on weathered rock arise frequent issues to the excavation works. A systematic approach of field and laboratory assessments were structured with geological data collection and excavation trial at two sites which Bentong site consist of sandstone and shale while Ulu Kinta site is characterized by granite to propose suitable assessment parameters of rock mass for excavation in relation to moisture content. Field study includes geological mapping and discontinuity survey in order to characterize the weathering state. Thirty-six trial tests were carried out during sunny days and after rainy days. Fourteen trials on sandstone and shale respectively and eight for granite. From field study, joint spacing are 0.1–2 m with maximum of four joint sets. Block size shows decreasing trend ranges from 1–0.1 m³ is slightly weathered to completely weathered rock mass. The result showed that block size more than 0.6 m³ could not be excavated. When involves block size ranges from 0.15–0.5 m³, the productivity less than 15 m³/h for all type of rock for slightly weathered rock mass. In highly weathered, block size ranges from 0.1–0.8 m³, productivity increase between 10–45 m³/h. Block size ranges 0.1–0.8 m³ does not influenced much on the productivity of completely weathered resulting 25–50 m³/h. It was found that increment of moisture content help to increase the productivity when the block size measured less than 0.3 m³ for all types of rocks. The productivity increased by 20–50% when excavated after heavy rain on moderately and highly weathered sandstone and shale. This study prove that moisture content could affects

M. K. A. Legiman (✉) · E. Kusmawati · V. Rathinasamy
School of Civil Engineering, Universiti Teknologi Malaysia, 81310 Skudai, Johor, Malaysia
e-mail: kiftiah@graduate.utm.my

E. T. Mohamad
Centre of Tropical Geoengineering (GEOTROPIK), Universiti Teknologi Malaysia,
81310 Skudai, Johor, Malaysia

Z. Zainal · N. E. Zainuddin
Centre of Excellent for Engineering and Technology (CREaTE), Public Work Department,
78000 Melaka, Malaysia

Z. Ismail
Department of Geotechnical Engineering, Public Work Department, 50400 Kuala Lumpur,
Malaysia

the excavation performance significantly on highly weathered rock mass. The effects are minimal on slightly, moderately and completely weathered rock mass. The block size does not become important factor in controlling the excavation performance in the completely and slightly weathered rock.

Keywords Moisture content · Excavation assessment · Weathered rock mass

1 Introduction

The issues related to weathering process in tropical climate region such the functionality of moisture content's presence in reducing the rock strength reduction of rock material and mass should be taken into consideration as unique features. One of the issues in surface excavation works is related to mainly in the highly and completely weathered rock mass which make it difficult to predict the excavation performance. Thus, it is important to highlight the significant features in determining the differences of excavation in different weathering state.

Most of the existing excavation assessments were not developed specifically to handle the tropics issues. For example, the rock mass indicate that it underestimates the difficulty of excavation [1]. Mechanical properties of rock materials highly depends on the association between the particles and minerals present in it and cementations materials. Rock mass that has been undergo weathering process literally altered the rock materials. In addition, the comparison of geomechanical characteristics between each weathering state can be identified. Many cases have been reported to be very difficult to be excavated, however it becomes very easy to excavate after rain. This issue has caused confusion and arguments.

A major problem confronting geotechnical engineers in tropical climate is how to characterize the lithologies and the performance of the excavation. A reliable geotechnical characterization of the rock mass due to the influence of moisture should be established to enhance the excavation productivity. Properties and the parameter of machines are the major elements in affecting the mechanical excavation performance [2]. Geological properties that influenced the excavation works can be divided into two categories which are rock mass and material properties. As the mechanical excavation, geological properties of rock masses play significant role in determining the performance of machine [3]. Rock masses considered to be a function of number of measurable parameters, with respect to their geomechanical properties display in massive and actual form.

1.1 *Influence of Moisture Content*

There are many factors affecting the excavation process. These factors should be put in consideration to the process which are mass and material properties, cost and

production, environment and machineries included. Excavation performance mainly effected by the mass and material properties. Physical and mechanical properties of rock mass are very important in determining suitable excavation method [4]. The problem frequently arises when excavating hard material. Inhomogeneous rock mass has higher production rate as compared to homogenous rock mass [5]. Fundamentally, hard material is weathered rock that lies in highly or completely weathered rock mass which is in completely weathered form. There is misinterpretation of the weathering grade, physical material and discontinuity characteristic between soft rock and hard rock and it may cause to dispute among designer and builder subsequently result to project disaster [6].

JKR Excavation specification stated that hard material is classified when the material cannot be excavated using excavator with size of 44 tons and 321 BHP [7]. Engineering behaviour of weathered rock mass are often regulated by its relic structure retain from its geological past. This is a major distinction from a sedimented soil such as a sand or clay. Anisotropic strength from the relict discontinuities will describe the pattern of weathering throughout the mass [8]. Consequently, requirement to the accurate estimation for excavation performance is thus a detailed interpretation of site geology.

Generally, the evaluation of surface excavation can be divided into grading method, graphical method and approximation by seismic velocity. Excavation productivity depends on the parameters that influenced rock mass. In a general classification, geomechanical parameters of rock material and rock mass, parameters of excavation machine, and the specific type of application are the main influencing parameters in the performance of surface excavation [9, 10]. From the existing assessment, joints and material strength are the most discussed parameters in affecting excavation performance. In tropically climate condition, the issues on thick weathering profile have to take into consideration when focusing in excavation works. This is due to the influence of moisture in the strength of rock mass in minutes or years.

2 Study Area

Bentong site underlaid by Semantan Formation [11]. Based on paleontological evidence, the age was assigned as middle to upper Triassic. Depositional environment of Semantan Formation is deep marine due to the indication of sedimentary structure evidences. Six facies are recognized in Semantan Formation at Raub which are conglomerate, pebbly sandstone, thick-bedded sandstone, interbedded sandstone-shale, contorted sandstone-shale and shale-dominated heterolithics [12].

The eastern part of Kinta valley is bordered by the Granitic Main Range which also forms the 'backbone' of Peninsular Malaysia which runs in a north-south direction for more than 400 km. Meanwhile, the western part is bordered by Kledang Range. These ranges formed a reverse-V shape in topography. Figure 1 shows location of study area bordered by Main Granite Range and Kledang Range. The average age

where S_1 , S_2 and S_3 are joint spacing for each joint set and α , β and γ are the angle between the joint sets.

Moisture content of rock material were identified from laboratory work [19]. In this moisture content test, forty rock samples of each panel consist of slightly to completely weathered rock materials were weighted and placed in containers and dehydrated in an oven at a standard temperature of 110 ± 5 °C till a constant mass. Equation 1 are used to calculate the water content of the specimen.

$$\text{Moisture Content, } w = \frac{M_w}{M_D} \times 100 \quad (2)$$

where, W is water content, %, M_{cms} is mass of container and moist specimen, g, M_{cds} is mass of container and oven dry specimen, g, M_c is mass of container, g, M_w is mass of water water ($M_w = M_{cms} - M_{cds}$), g and M_s is mass of dry specimen ($M = M_{cds} - M_c$), g.

Trial excavation is monitored at the studied site in order to establish the correlation between moisture content and excavation performance using Komatsu EX300 excavator. Evaluation on ease of excavation and the average block size of rock material and measured during the monitored excavation test. Trial excavation were carried out during sunny day and after rain to determine the differences between the conditions. This method of evaluating ease of excavation was also adopted by [20]. The production rate is recorded for each panel to establish the moisture content and rock mass classification in relation to the excavation properties. The production rate obtained for eleven panels based on weathering grade consisting four panels in Sedenak site, three panels in Bentong site for sandstone and shale rock masses, and four panels in Ulu Kinta site for granitic rock masses.

4 Results and Discussion

In tropically climate region, the variation of moisture extremely affected the properties of rock masses and materials, in addition to the various state of weathering. The nature and formation of rock masses also lead to many confusions in the excavation performance faced by the practitioners. The data were analyzed and correlated to achieve the aim of the study that is establish the effect of moisture content to the excavation performance.

4.1 Geological Field Mapping and Site Observation

Bentong site comprise of mainly interbedded of shale and sandstone of Semantan Formation. Total length of studied outcrop is 150 m and the height of the outcrop

approximately 20 m. The shale layers with average thickness of 5 m dominated this area which interbedded with sandstone in average thickness of 1 m. Slightly weathered sandstone can be identified at site because the texture of intact surface rougher due to the bigger grain size and only breakable by geological hammer along discontinuities. Moderately weathered sandstone can break easily by geological hammer. In comparison, highly weathered sandstone can be identified at site because the texture of intact surface rougher than shale due to the bigger grain size. Discontinuity survey were carried out at the outcrops revealed that three major joint sets are presented which are J1 (062°/05°), J2 (245°/18°) and J3 (033°/87°) as in Table 1. The joints are slightly undulating planar and mostly covered of iron pan or clay. There is at least one joint or three maximum joints of each outcrop. The joint spacing ranges from few cm to 1.3 m.

Lithological zone for Ulu Kinta site were classified based on the characterization in accordance to [14] was tabulated Table 2. The length of the outcrop in Ulu Kinta site is 200 m and approximately 15 m in height. This site consists of slightly weathered to completely weathered granitic rock. Slightly weathered can be identified at site due to discoloration visible along the discontinuities. Some joints are weathered but the texture of parent rock still preserved. The color of medium grey to light grey remain unchanged. The rock material in slightly weathered granite is very strong. More than half of the rock mass is disintegrated and decomposed to soil for moderately weathered granite. The color of rock mass turned to light reddish. The surrounding rock material were decomposed but the original texture is preserved. The weathered rock material of highly weathered granite as completely discolored. The rock material was completely decomposed, but the rock mass still preserved. Highly weathered granite can be differentiating to moderately weathered granite by testing

Table 1 Geological field observation at Bentong site

Panel	Type	Weathering Grade	Joint Spacing	Orientation	Joint Set
B1	Sandstone	III	1.30	194/70	3
	Shale		1.00	130/50	3
B2	Sandstone	IV	0.60	161/85	3
	Shale		0.55	154/70	3
B3	Sandstone	V	0.45	060/70	3
	Shale		0.40	062/64	3

Table 2 Geological field observation at Ulu Kinta site

Panel	Type	Weathering Grade	Joint Spacing	Orientation	Joint Set
1	Granite	II	0.28	070/80	3
2		III	0.26	263/70	3
3		IV	0.15	260/62	3
4		V	0.06	050/60	3

the difficulty to be broke by hand. Completely weathered granite can be identified due to the completely decomposed of rock mass. The rock breaks easily by hand. Discontinuity survey were carried out at the outcrops revealed that three major joint sets are presented which are J1 (062°/05°), J2 (245°/18°) and J3 (033°/87°). The discontinuities of Ulu Kinta site are found in the form of joints and faults. The joint spacing ranges from few cm to 2 m.

4.2 Joint Spacing and Block Size

Block size are important in determining the behaviour of rock mass [14, 18, 21]. Table 3 shows block volume recorded for each weathering zone for all studied sites. It was found that block size continuously decreases from large volume to small volume along the weathering courses from slightly to completely weathered states, for sandstone, shale and granite, according to classification of block volume [21, 22]. This trend of joint spacings and weathering grades are similar to [22–24]. The block volume, however, decreases tremendously from slightly to moderately weathered state, where the degree of blockiness changes abruptly from massive to blocky between these two zones, for both sandstone and shale.

Table 3 Block volume for each weathering zone of studied sites

Site	Lithology	Weathering grade	Average joint spacing (m)			Average block size (m ³)
			This study	[23]	[24]	
Bentong	Sandstone	II	–	0.93	1.20	–
		III	1.30	0.89	0.75	0.90
		IV	0.60	0.63	0.55	0.60
		V	0.45	0.55	0.35	0.10
	Shale	II	–	0.93	1.20	–
		III	1.00	0.89	0.75	0.90
		IV	0.55	0.63	0.55	0.60
		V	0.40	0.55	0.35	0.10
Ulu Kinta	Granite	II	0.28	0.93	1.20	0.95
		III	0.26	0.89	0.55	0.90
		IV	0.15	0.63	0.35	0.60
		V	0.06	0.55	1.20	0.10

4.3 Excavation Production

The productivity and excavation period for each cycle were recorded during trial excavation to determine the actual production rate on Bentong and Ulu Kinta sites. The results of excavation production in various rock types and weathering rock states are presented in Fig. 2. The excavation production in slightly weathered to completely weathered sandstones during sunny day are 0, 10, 20 and 38 m³/h respectively. While, the production rate increased linearly to 12, 25 and 42 m³/h for moderately, highly and completely weathered after rain. For shale, the production in slightly weathered is 0 m³/h, moderately weathered is 20 m³/h, highly weathered is 30 m³/h and completely weathered is 48 m³/h. The excavation production for slightly and moderately weathered granite are 0 m³/h. Highly and completely weathered granite exhibit the production of 15 and 30 m³/h respectively.

The production of sandstone, shale and granite increased linearly as the increases of weathering state. The excavation production in sandstone and shale higher than granite due to the occurrence of bedding, folding and inhomogeneity of rocks are few distinctive differences compared to granite which is normally exist in massive mass. Shale has higher excavation production as compared to sandstone. Shale relatively lower mass strength as compared to sandstone. The excavation of sandstone is difficult due to the well-cemented grain particles as compared to shale. Shale has lamination structure in the bedding that provides spaces for water as weathering agent go through the grain materials. In addition, shale is the highest production rate due to the highest content of clay mineral in the rock material. The present of clay mineral will soften and loosening the structure the rock material affecting the reduction of rock strength [25]. Moreover, highly weathered rock mass exhibit higher excavation production compared to slightly weathered rock mass.

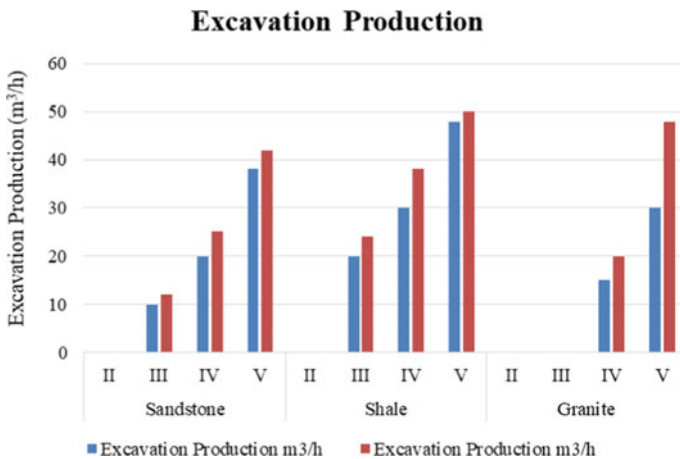


Fig. 2 Excavation production of sandstone, shale and granite from slightly weathered to completely weathered rock mass

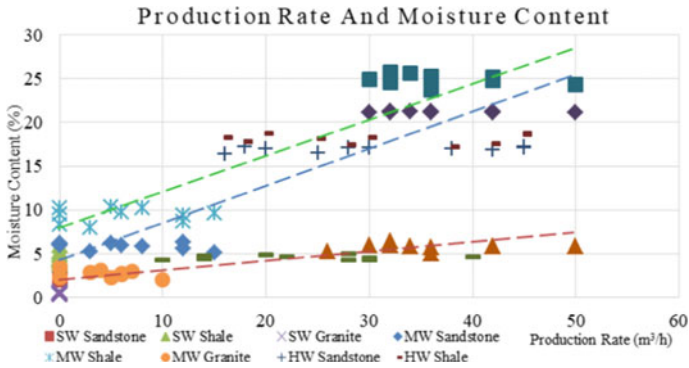


Fig. 3 Relationship of production rate and moisture content

4.4 Effect of Moisture on Excavation Production

Moisture content has been given little attention by previous researchers when assessing surface excavation performance due to the effect on the production of rock mass (Mammen et al., 2009). In this study, effect of moisture to the excavation performance were carefully studied. Variable moisture at testing sites were monitored and its excavatability were recorded. Twelve trial excavations were done in each studied site. The test results revealed that moisture content variation affects greatly rock masses that highly covered with sandstone. The relationship between moisture content and production rate are depicted in Fig. 3. From the figure, sandstone shows most correlated suggesting that moisture content in sandstone highly effecting the production rate. On the other hand, shale less correlated when moisture content effect the production rate due to high clay content. Granite shows least correlated with moisture content. This is due to the occurrence of granite boulders even in great weathered state.

5 Conclusion

It was also established at the studied site that in the moderately weathered zone, the presence of moisture is much lower than the highly weathered zone. The discontinuities parameter especially the block size governs greatly on its excavatability. This study prove that moisture content could affects the performance of excavation significantly on highly weathered rock mass. For completely weathered, slightly weathered and moderately weathered rock masses, the effects are minimal. The block size does not become important factor in the excavation performance in the completely to slightly weathered zone. A chart describing the relation between block size and moisture content for sandstone, shale and granite from slightly weathered

to completely weathered are presented to present the results graphically which could be useful guide when performing excavation work in this material.

The trial excavation reveal that all tested sites are classified as hard mass with the productivity of 25 to 45 m³/h. Completely weathered rock mass material shows the highest productivity 40 to 50 m³/h for sedimentary rock mass with the joint spacing ranges 0.01 to 0.35 m and block size ranges from 0.1 to 0.8 m³. While, productivity of completely weathered granite ranges 25 to 50 m³/h with joint spacing between 0.21 to 3.0 m and block size ranges from 0.1 to 0.8 m³. With the excavation productivity after rain increase 30%, it shows that moisture content does not significantly influence the productivity in sedimentary and granite rock mass.

Acknowledgements The authors wish to thank Universiti Teknologi Malaysia for providing facilities during the research work and Ministry of Higher Education for research grants of R.J130000.7309.4J338 and Q.J130000.2409.04G15.

References

1. Bewick RP (2021) The strength of massive to moderately jointed rock and its application to cave mining. *Rock Mech Rock Eng* 54(8):3629–3661
2. Fowell RJ (1993) The mechanics of rock cutting. In: Hudson JA (ed) *Comprehensive Rock Engineering*, Pergamon Press, Oxford, vol 4, no 155–176, pp 13–28
3. Singh RN, Denby B, Egretli I (January 1987) Development of a new rippability index for coal measures excavations. In: *The 28th US Symposium on Rock Mechanics (USRMS)*. American Rock Mechanics Association
4. Balasubramaniam A, Likitlersuang S, Surarak C (2016) Long-term behaviour prediction of the Bangkok MRT tunnels using simplified finite-element modelling. *Jpn Geotech Soc Spec Publ* 2(42):1507–1512
5. Hoek E, Brown ET (1980) Empirical strength criterion for rock masses. *J Geotech Eng Div* 106(9):1013–1035
6. Mohamed Z, Mohamad Noh N (2011) Geotechnical synthesis of 2D-Electrical resistivity tomography of geomaterial–laboratory model study. *Sci Res J* 8(1):1–16
7. JKR (1998) *Minit Mesyuarat Definition Rock, Unsuitable Material & Concrete Road Kerb*, Mac, Kuala Lumpur
8. Shirlaw JN, Tan TS, Wong KS (December 2005). Deep excavations in Singapore marine clay. In: *Geotechnical Aspects of Underground Construction in Soft Ground: Proceedings of the 5-th International Symposium*, Amsterdam, pp 13–28
9. Dey K, Ghosh AK (2008) Predicting cuttability with surface miners-a rockmass classification approach
10. Mohamad ET, Kassim KA, Komoo I (2005) To rip or to blast: an overview of existing excavation assessment. In: *Brunei International Conference on Engineering and Technology*, pp 27–36
11. Jaafar A (1976) The geology and mineral resources of the Karak and Temerloh area, Pahang. *Geological Survey of Malaysia Memoir*, no 15
12. Ismail HH, Madon M, Bakar ZAA (2007) Sedimentology of the Semantan formation (middle-upper Triassic) along the Karak-Kuantan highway, Central Pahang
13. Meng CC, Sautter B, Pubellier M, Menier D, Sum CW, Kadir A (2014) A geological features of the Kinta valley. *Platform* 10(2):2–14
14. ISRM (2007) The complete ISRM suggested methods for rock characterization, testing and monitoring: 1974–2006. In: Ulusay R, Hudson JA (eds) *Suggested methods prepared by*

- the commission on testing methods, International Society for Rock Mechanics, Compilation Arranged by the ISRM Turkish National Group, Kozan Ofset, Ankara, Turkey
15. Priest SD, Hudson JA (1976) Discontinuity spacings in rock. *Int J Rock Mech Min Sci Geomech Abstr* 13(5):135–148. Pergamon
 16. Priest SD (1993) The collection and analysis of discontinuity orientation data for engineering design, with examples. In: *Rock Testing and Site Characterization*, pp 167–192. Pergamon
 17. Priest SD (2004) Determination of discontinuity size distributions from scanline data. *Rock Mech Rock Eng* 37(5):347–368
 18. Palmstrom A (November 2000) On classification systems. In: *Proceedings of Workshop on Reliability of Classification Systems a Part of the International Conference GeoEng-2000*
 19. ASTM (2010) Standard Test Methods for Laboratory Determination of Water (Moisture) Content of Soil and Rock by Mass (D2216-10). ASTM International, West Conshohocken, PA. <https://doi.org/10.1520/D2216-10>, <https://www.astm.org/>
 20. Liang M, Mohamad ET, Khun MC, Alel MNA (2015) Estimating uniaxial compressive strength of tropically weathered sedimentary rock using indirect tests. *J Teknologi* 72(3):49–58
 21. Palmström A (February 1995) Characterizing rock burst and squeezing by the rock mass index. In: *International Conference in Design and Construction of Underground Structures*, vol. 10, no. 10
 22. Cai X, Zhou Z, Liu K, Du X, Zang H (2019) Water-weakening effects on the mechanical behavior of different rock types: phenomena and mechanisms. *Appl Sci* 9(20):4450
 23. Hack R, Price D (1997) Quantification of weathering. In: *Proceedings Engineering Geology and the Environment*, Athens, pp 145–150
 24. Tan SMA, Dan MM, Tonnizam ME, Saad R, Madun A, Hazreek ZAM (2018) Interpretation of 2D resistivity with engineering characterisation of subsurface exploration in Nusajaya Johor, Malaysia. *J Phys Conf Ser* 995(1):012078. IOP Publishing
 25. Brady BH, Brown ET (1993) *Rock Mechanics: For Underground Mining*. Springer Science & Business Media, Heidelberg. <https://doi.org/10.1007/978-1-4020-2116-9>

Geotechnical Challenges in World Record Making Mine Rescue



Binay Kumar Samanta

Abstract Mining is the most hazardous peacetime profession in the world and coal mining is more so for underground fire or explosions. Mining disasters are usually accidents with 5 or more fatalities and are mostly due to roof-fall, inundation, fire, explosions, etc. Underground methane emission maximizes in late monsoon, as percolating water drives out the occluded gas from pore-spaces. In this paper, the author briefly presents a case study of a mining inundation disaster of Nov'89 with the miraculous rescue of 65 employees, through a specially designed capsule, creating a world record, in which he played a key role. Out of four-pronged strategy planned- Dewatering working pits by submersible pumps; Rescue through punctured pit no.34; Driving incline from the rise outcrop, and Rescue through a borehole. Work was going on concurrently by different teams. Ultimately rescue through borehole by special capsule became the most expedient in 4 days from 13 to 16 November 1989. The capsule went on to win first prize in the International Trade Fair, in New Delhi in 1990 and the great saga was described in a feature article in Readers Digest in June 91 and in other languages. Geotechnical challenges were enormous, yet a record success was achieved. President's award was also given for the rescue.

Keywords Mine hazard · Dewatering · Borehole

1 Mine Disasters

Geotechnical challenges in mining, are numerous and need constant vigil and monitoring. According to available records with the National Institute of Occupational Safety & Health, from 1839 till 2010 around 726 mining disasters have taken place all over the world. Table 1 displays the ten worst mining disasters since 1899 in human history.

B. K. Samanta (✉)

Department of Mining Engineering, Indian Institute of Technology (Indian School of Mines),
Dhanbad 826004, India

e-mail: iitism.bks@outlook.com

Table 1 Worst mining disasters in human history

Ten Worst Mining Disasters In Human History
1. Benxihu Colliery, Liaoning, China, April 1942 (1,549 Deaths)- Gas and coal dust explosion
2. Courrieres Coal Mine, Courrieres, France, March 1906 (1,099 Deaths)- Gas and coal dust explosion
3. Laobaidong Colliery, Datong, China, May 1960 (682 Deaths)- Gas and coal dust explosion
4. Sumitomo Besshi Bronze Mine, Shikoku, Japan, 1899 (512 Deaths)- Landslide of debris
5. Hawks Nest Tunnel Silica Mine, West Virginia, USA, 1931 (476 Deaths)- Silicosis
6. Mitsui Miike Coal Mine, Fukuoka, Japan, November 1963 (458 Deaths)- Gas and coal dust explosion
7. Senghenydd Colliery, Cape, Wales, UK, October 14, 1913 (440 Deaths)- Gas and coal dust explosion
8. Coalbrook Colliery, Clydesdale, South Africa, January 1960 (435 Deaths)- Mine collapse
9. Wankie Coal Mine, Hwange, Zimbabwe, June 1972 (426 Deaths)- Blast Collapse
10. Chasnala Coal Mine, Dhanbad, India, December 1975 (372 Deaths)- Pit flooding

Accidents and disasters are continuing to happen around the world, with more demand for coal and minerals and increasing depths of mining. Table 2 shows major Indian coal mine disasters, generally termed as major accidents with casualties of more than 5 lives of the post independence period, till 2021. From the records of mine disasters in India, on 27/12/1975, Chasnala Colliery lost 375 employees from Inundation has the highest toll of lives. However, in India, fewer mine disasters have occurred after 2005, because of safety measures of internal safety organizations and the Directorate General of Mine Safety. Around the world, mine disasters are continuing to happen and are expected to reduce.

2 Mahabir Crisis

At Mahabir Colliery near Raniganj town, on November 13 of 1989 at 4.15 A.M. while workers were engaged in coal production, about 130 m below surface, a sudden inrush of water occurred and the Working Pits A and B were inundated up to 10 m above pit bottom landings, within an hour or so, allowing time for nearby employees to come out. Mahabir Colliery was one of the oldest mines of Raniganj coalfield and old Rly. Plan of 1889 showed subsidence areas. Un-organized mining in outcrops, even Damodar river bank might have started in the late eighteenth century. But proper underground mining could be around 1860 continuing and barriers between mines are uncertain.

There were 231 mine employees underground in Narankuri seam in the night shift of 12.11.89 and 150 of them managed to scramble out of the mine and 71 were trapped inside, as they could not avail of the cage winding facility. Despite inundation, fortunately, the surface to the underground telephone was working and information spread fast. Some salient points including technical decision making, scheduling, and quick implementation are narrated here.

Fortunately, the working district was in the rise-side of Narainkuri (R-VIII) seam and 65 mine employees survived, as more than 12 m of water had accumulated at working pit-bottom of Pit A-86.4 m deep, 3.6 m Φ and Pit-B-87 m deep and 4.8 m Φ . Electrical main pumping arrangements including motors, switchgear, and cables were drowned. Panic-stricken family members of the employees trapped, local

Table 2 Indian coal mine disasters

Sl. N	Dates of accident	Name of mines	Fatalities	Cause
1	12/07/1952	Dhemomain	12	Roof fall
2	05/08/1953	Majri	11	Inundation
3	14/03/1954	Damra	10	Explosion of fire damp
4	10/12/1954	NewtonChikli	63	Inundation
5	05/02/1955	Amlabad	52	Explosion of fire damp
6	26/09/1956	Burra Dhemmo	28	Inundation
7	19/02/1958	Chinakuri	175	Explosion of fire damp
8	20/02/1958	Central Bhowra	23	Inundation
9	05/01/1960	Damua	16	Inundation
10	28/05/1965	Dhori	268	Coal dust explosion
11	11/04/1968	West Chirmiri	14	Collapse of workings
12	18/03/1973	Jitpur	48	An explosion of firedamp
13	08/08/1975	Kessurgarh	11	Roof fall
14	18/11/1975	Silewara	10	Inundation
15	27/12/1975	Chasnala	375	Inundation
16	16/09/1976	Central Saunda	10	Inundation
17	04/10/1976	Sudamdih	43	Explosion of firedamp
18	22/01/1979	Baragolai	16	Ignition of firedamp
19	24/08/1981	Jagannath	10	Water-gas explosion
20	16/07/1982	Topa	16	Roof fall
21	14/09/1983	Hurriladiah	19	Inundation
22	13/11/1989	Mahabir	6	Inundation
23	25/01/1994	New Kenda	55	Fire/suffocation by gases
24	26/09/1995	Gaslitand	64	Inundation
25	06/07/1999	Prascole	6	Collapse of workings
26	24/06/2000	Kawadi	10	Failure of OC bench
27	02/02/2001	Bagdigi	29	Inundation
28	05/03/2001	DurgapurRayatwari	6	Collapse of partings
29	16/06/2003	GodavariKhani-7LEP	17	Inundation
30	16/10/2003	GDK-8A, Singareni	10	Roof fall
31	15/6/2005	Central Saunda	14	Inundation
32	29/12/2016	Lalmatia, Rajmahal	17	Loose earth crashing
33	13/12/2018	Illegal Meghalaya	17	Rathole coal mining
34	11/8/2021	Quartz Mine, Bhilwara	7	Collapse of ground

public, trade unions, media were frantic with criticism of the management. A Control Room was opened at the Colliery Office, guided by Area GM, Mr. R. C. Goyal, to Chairman, CIL, other subsidiaries, companies, and CMPDI. There was excellent teamwork, coordination, the leadership of ECL management, under Mr. J. N. Uppal, CMD, ECL.

A four-pronged strategy was evolved: -

- (i) Quick installation of submersible pumps through working pits for dewatering,
- (ii) Rescue of persons by temporary winding arrangements through Pit No.34,
- (iii) Excavating the outcrop area in the rising side, with diverted HEMM and
- (iv) Drilling of large diameter boreholes for food and final rescue.

3 History of Mining at Mahabir

In a total area of 611.63 Hectares, the number of shafts in Mahabir (R) Colliery was numerous and some had collapsed and some were abandoned and only A & B Pits were in use, at the time of the mishap. After the nationalization of coal mines in 1973, Mahabir (R) Colliery was formed with amalgamation of three collieries: -

- (i) Mahabir-448.83 Hect,
- (ii) Kajora selected-50.83 Hect, and
- (iii) Searsole-112.37 Hectares.

Three seams have been extensively worked, namely Searsole (R-IX), Nega (R-VIII), and Narainkuri (R-VII) seams, as they are outcropping in the leasehold of Mahabir (R) colliery, earlier called Raneegunge Colliery. At the time of the mishap, the colliery was working 3 districts, namely 33L-42 cross-cut development, 21L development, and NKM2 depillaring district. Mining in all the 3 panels was being done under the permission of Regulation 127, against the danger of underground inundation, of Coal Mines Regulations, 1957. Coal production per month during 89-90 up to Oct'89 ranged from 8,516 tonnes to 13,050 tonnes.

About 40 potholes had occurred over the leasehold area of the colliery. Due to the evacuation of water from the Searsole/ Nega seam, further collapse was apprehended, because of the mishap. Mahabir colliery had total manpower of 1472, with a mainly manual system of operation, with underground Bord & Pillar Method of mining by haulage and winder. The general gradient of coal seams is 1 in 25; in N 40 deg E direction and the seam section is shown in Fig. 3 (Fig. 1).

4 Rescue Possibilities

Dewatering had to be started through A & B pits by submersible pumps for restarting winding operations for the rescue of mine employees. The author posted then as Dy. CME was asked by TS to CMD to examine the mine plans since CMD, Directors

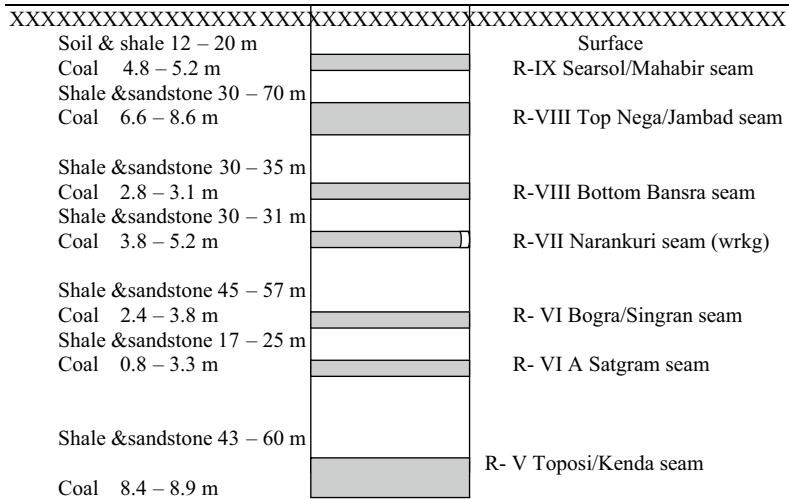


Fig. 1 Sequence of coal seams in mahabir

and other GMs had rushed to Mahabir in the morning. The following points were highlighted to TS to CMD, who called me and pit plans were examined in Sanctoria HQ, ECL and relayed to Mr.Uppal: -

- (i) Searsole and Nega seams above were waterlogged and the barriers shown in plans between the old mines could not be relied upon.
- (ii) Nega seam was outcropping in Damodar River, and the oldest coal mine of India, owned by M/S Carr, Tagore & Co, had worked in nearby region.
- (iii) Dewatering of the mine posed a great problem, as all main sump motors, transformers, switch gears and electrical cables got drowned and rendered useless.
- (iv) More than 100 million gallons of water, together with seepage from old workings and Damodar River made dewatering a formidable problem.

As per information relayed to the Headquarters, from top management camping at Mahabir Colliery, a three-pronged approach was decided upon and was being scheduled: -

- (1) Dewatering of the mine by the installation of submersible pumps through pits A & B, for which additional transformers, switchgear, winches, pulleys, submersible pumps, cables, pipes, etc. were being arranged, at top speed.
- (2) Rescue through abandoned Pit No. 34, which was to be fitted with a temporary head-frame, and a Crane with a Kibble, was being arranged for the purpose.
- (3) Rescue by driving an incline in the outcrop area of Narainkuri seam, for which Scraper, Dozer and Dumper were being arranged for removing the soil cover.

At this stage, the researcher had suggested to TS to CMD that he had read about Borehole rescue, somewhere in Germany. This suggestion was relayed to Mahabir

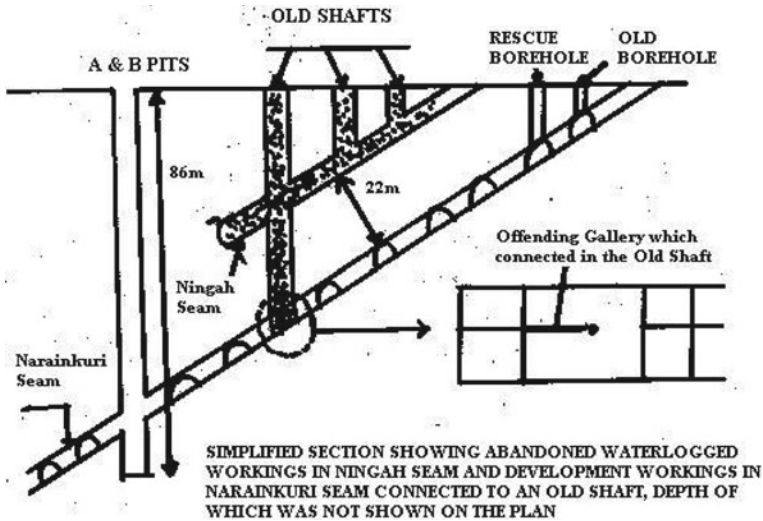


Fig. 2 Simplified section of workings

Colliery Control Room and the researcher was provided with a vehicle to arrange for Drill-rig for the borehole. Figure 2 shows a cross-section of the Mahabir mine disaster.

5 Mine Water Studies

A study of mine plans of Mahabir Colliery along with abandoned adjacent mines revealed there was a possibility of heavy water seepage through old quarries and underground breached barriers of extensively worked Nega seam, which could make dewatering a Herculean task. The pit water system investigated depended upon the interaction of 4 complex variables: -

- 1) Rain,
- 2) Surface water,
- 3) Water bearing strata, and
- 4) Mine induced flow or inrush.

Models predicting mine water inflow rates were computed from: -

- 1) Applicable for leaking artesian aquifers and the discharge rate depends upon, in size of panel- p ; $Q = 2p \cdot T_s \{w (ur/B)\}$, where, T_s - Transmissivity of main aquifers-seepage or flow-back or drawdown $\{ \}$ -connected to the rate of de-pillaring, etc.

- 2) Based on water table condition, the discharge rate is given by $Q = V \cdot S_y \cdot p \cdot b \cdot L$, where V -local velocity, S_y - effective area, b -aquifer thickness, L -width of the de-pillaring panel.
- 3) Expansion of cracks is assumed and discharge rate is given by $Q = Q_1 + Q_2$, where $Q_1 = S \cdot R \cdot h$ and S -co-efficient of storage, R -roof exposed per limit time, h -hydraulic head, and $Q_2 = 2p \cdot k \cdot h^2 / w(u)$, where k -horizontal permeability, $w(u)$ -the rate of de-pillaring.
- 4) Carslaw and Jaegers found heat flow and groundwater flow in porous media are quite similar and the Discharge rate is given by $Q = 4pTs/w(u,c)$ and is quite realistic.

The arguments and logic for the quickest rescue were mentally worked out and later a computer program in COBOL was coded and run to justify the decision. The computer used was Super-32 of ECIL, installed at ECL headquarters and its COBOL compiler was used. Afterward, for thesis purposes, the program was further coded and modified in Java.

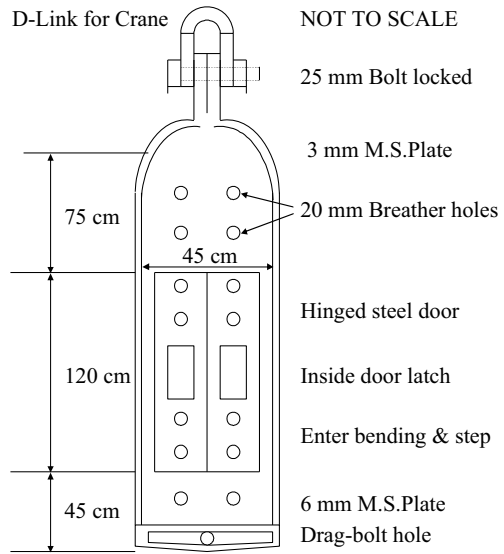
6 Crash Scheduling

At 11.30 A.M, on 13-11-89, the author was provided with a vehicle to contact Mineral Engineering Corporation, Dhanbad for diverting a large drilling rig, capable of drilling a 24" diameter borehole. On the way, CMRI was contacted about the crisis at Mahabir Colliery, around 1.30 PM. Then, the MEC camp office at Monidih was reached at around 3 PM and Dr. Dixit, Camp-in-charge, informed that although they have deep drilling rigs, large diameter drilling bits are not available with them but could be with Meghdoot Project, CMPDI - RI-II, Dhanbad. So, the author contacted the then RD RI-II, Mr. Lahiri, who informed that their only working large Φ drill LT-2500 was deployed at Rajmahal area of ECL, about 200 km away.

It was getting to be 5 PM, the author learned that an Engineer/Contractor, Mr. Bansal was engaged in drilling a borehole for food supply to survivors. He could build a large diameter drill bit for the rescue borehole. Then, the next urgent issue was man-riding capsule and the author contacted his former professor, Dr. M A Ramlu, former HOD(ME), and Actg. Director IIT, Kharagpur. He was at that time Chair Professor, Mining Machinery at ISM, Dhanbad, who had his doctorate from Germany, where earlier Rescue Capsule was deployed. After a discussion with him at Dhanbad, he brought out some approved design Rescue capsules, of German Rescue Station. Dr. Ramlu volunteered to come with the researcher since DGMS approval was required. Both of them returned by car and reached Mahabir Colliery at about 9 P.M on 13 November 1989.

At that time, the control room at Mahabir Colliery was full of all the top officials of CIL, DGMS, Trade Union leaders, and members of the Press. We broached the subject of capsule rescue, but the view of the top executives was non-committal and they were stressing more on quick dewatering by submersible pumps and the next

Fig. 3 Rescue capsule designed at mahabir



priority was rescuing through the abandoned pit No.34, below which puncture and flooding occurred.

Then, the researcher along with Dr. Ramlu decided to make an on-the-spot analysis of the crisis and went to the site of submersible pump installation in A and B pits. Two submersible pumps were already installed and work was going on at break-neck speed and yet there was no decrease in water level. Then, at the site of pit No.34, it was found that a temporary derrick was being installed for hanging kibble, and with the help of a crane; the trapped workers were being planned for rescue. There was a continuous roar of gushing water, audible from a great distance because of a downpour of a thick stream of water through 25 m, from Nega seam old goaves to a narrow opening above the Narainkuri seam and conditions were extremely difficult for rescue persons. Some German and Dutch mines had adopted this method of the rescue of trapped miners, through borehole by capsule, on small scale in the past. The record of such an experience was at Lengede. Ore Mine, near Brunswig, West Germany, where 11 men were rescued, after about 2 weeks, by this method.

After becoming sanguine that the capsule rescue would be the most expeditious, we again came to the control room and raised the topic of rescue capsule and we were directed to contact Mr. J N Uppal, CMD, ECL, who was in Survey Office studying plans. The researcher along with Dr. Ramlu, Mr. R.K.Sachdev, GM (Pandaveswar), Mr. Om Prakash, DDMS had approached Mr. Uppal and after prolonged discussions, he instructed the researcher to contact Mr. Chatterjee to make the capsule at Sodepur Workshop of ECL. Chief Engineer, ECL, Mr. Prasad, GM (Planning), Mr. P.N.Agarwal, D (T), ECL, CIL, and Mr. C.R.Das, TS to the Chairman, Mr. R.N.Misra, CMD (CMPDI), and many areas GMs were camping there. Mr. Bansal, Mining Engineer, and the drilling contractor was already engaged in widening an

existing borehole, for the supply of food, water, etc. to the survivors and he had volunteered to drill the rescue borehole fabricating the large bits.

As decided in Control Room, the author with Dr. Ramlu, reached Sodepur around 11 PM and explained the modified design of the Rescue Capsule to Mr. Gora Chatterjee Workshop began fabrication of the rescue capsule on 13.11.89 night itself. Mr. Lamba, Dy. Chief En.

7 Delay of Alternatives

As could be observed from the computer program run, that the most optimistic time for complete dewatering of the mine was nearly 1 month and borehole rescue could be completed in 2 days. Rescue through abandoned pit No.34 could also be done within 3 days, but for the safety problem of widening the opening in rock in gushing water from 25 m above. Entry through incline digging could be completed in 5 days if blasting in rock-bed was allowed.

The survey for the rescue borehole was done in the morning of 14.11.89 and by 9.30 A.M drilling for the borehole was started, with a CP-Screw Drill and connected with 200 mm bit. The progress of widening the boreholes was slow as larger drill bits were being constructed at the site. Reaming of the borehole was done in stages of 300 mm, 375 mm, 450 mm, and finally, 537 mm and was completed by 2 PM on 15.11.89.

Water inflow from Nega seam old goaves, was far more than anticipated, around 140–200 million gallons or 6.35–9.05 lakh cub.m of water had entered into the working seam. Even though 10 submersible pumps -5 each in A and B pits were completed by the afternoon of 14.11.89 and 6 pumps continually running, each of 38 L per second capacity and 180 m head, there was no noticeable decrease in water level of about 10 m above pit-bottom. Pumping had to be maximized by quick replacement of the pumps breaking down.

The Rescue Capsule frame had arrived from Sodepur in the afternoon of 14.11.89. Several suggestions of the researcher for the modification of the capsule were accepted. A flush hinged door with a latch in place of 3 belt straps, for quick opening and closing as 71 persons had to be rescued one by one. The bottom hook for tail rope was unnecessary, as the borehole was shallow, around 30 m and so round bottom was cut away and the flat bottom was made for easy resting on the seam floor. All modifications of the capsule as shown in Fig. 3 were completed by the morning of 15.11.89 and a Capstan winch was ready for trial.

Regular monitoring of the 71 survivors, through underground telephone, was being done and 65 employees could be traceable, even after a frantic search by the survivors. An existing borehole was widened for the supply of food, drinks, and water to the survivors. This borehole was started at 10.30 PM and connected at 3.30 AM on 14.11.89 and to extreme relief of trapped employees, food and water could be supplied to them after about 24 h of the disaster.

On 14.11.89 morning, a temporary head-frame was erected over Pit No.34, and a Crane was positioned for lowering Kibble (man riding bucket). A rescue-trained team was lowered by noon, but the impact of gushing water and up-cast air created turbulence to make any effective work impossible, like widening of the rock opening, at the bottom of the pit. So, old conveyor belting was hung to divert the force of water, and a steel-plate canopy, over the kibble, was made. 90% of the veteran mining engineers were sanguine that the rescue through #34 pit would be the most expedient. The Chairman, CIL, had meanwhile arranged with the Indian Navy and a busload of Scuba Divers arrived in the evening of 14.11.89.

Between 14 and 15th Nov'89, several attempts were made by several teams to go down Pit N.34 and widen the rock opening. Unfortunately, all the attempts were abortive, as either the belt conveyor swayed to one side of the pit and canopy bending down. DGMS did not permit Navy Scuba Divers to be lowered, as they were not trained in mine conditions.

The rise area incline digging was progressing well as long as soft soil cover was there, about 12 m with the help of HEMM like Dozer, Dumper, Shovel, Scraper, etc. By the morning of 15.11.89, hard rock was reached and drilling and blasting were required for making further progress. There were some village hutments nearby, whose occupants raised protests against blasting and a series of top-level meetings could not yield results and so further progress was stalled (Fig. 4).



Fig. 4 Video record of capsule rescue

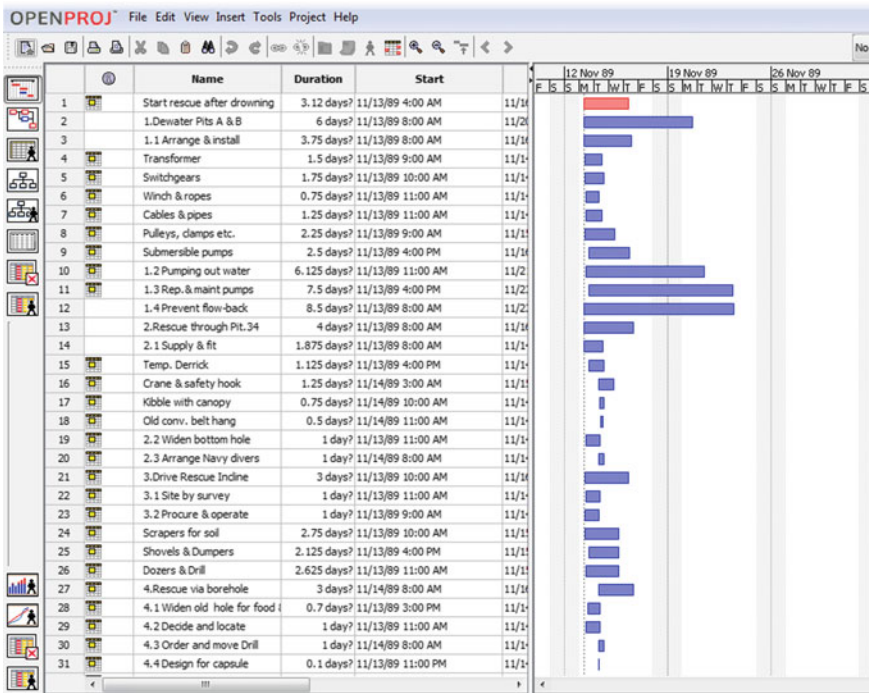
8 Record Success

By the afternoon of 15.11.89, it was abundantly clear that rescue through borehole with capsule was the most expedient. Although, widening of the rescue borehole to 537 mm was completed by 2 P.M on 15.11.89. The researcher was present when top-level discussions were taking place, between the Chairman, CIL, and DGMS, as to decide for the length of casing, up to rock-head (11 m) or full depth (30 m). It was decided to widen the boreholes up to the rock-head and the casing pipe would rest on the collar of the rock-head. The borehole was ultimately widened to 760 mm Φ up to a depth of 11.25 m and the casing pipe of 600 m Φ was anchored by 2.45 AM on 16.11.89. The survivors below were getting impatient, although regular food and drink were being sent to them through 150 mm boreholes. It was decided to start capsule rescue, instead of waiting till morning. A Capstan Hand-winch, 10 t capacity was anchored, a tripod derrick was centered over the hole, and some empty passes by the rescue capsule were made, before embarking on man rescue. This arrangement was approved and supervised by Mr. D. Saha, DMS (Mech), and engineers from ECL. Ambulances and first-aid were arranged for taking the rescued employees for checkups and treatment.

It was decided that a balanced rescue trained officer with strong nerves should go down the capsule first, signal the proper level of landing, examine the survivors, and send up the weakest first and continue in that order and the strongest was to be raised last. Mr. J S Gill, Adl.CME, Hdqrs., ECL, was chosen who went down the rescue capsule around 2.45 AM. Mr. Bhargava, Supdt. Rescue Station, Sitarampur, was rendering all possible assistance. Shaligram Singh was the first to be raised through the capsule, around 3 A.M, with much jubilation and fanfare, under the glare of international press and media, as well as public. Because of the extremely slow speed of manually operated capstan winch, only 14 men could come up by 5 A.M @ 10 min/trip.

Then, the winch was replaced with a Diesel Crane, 12 t Marshall Demag V-72 and jacked up in position and centered over the borehole, and rescue work resumed at a faster pace, about 3 min/trip. Thus, all 65 survivors were rescued; ending with Shri Anant Singh, Mining Sardar, and Shri Gill coming out last, before 9 A.M. on 16.11.89. The news was televised and flashed across the globe and a world record of borehole rescue, through capsule was created. The search for the remaining 6 employees was continued for another 2 days, by sending rescue teams and combing the entire dry area, without success. The researcher was the last person to ride in the capsule before the capsule was withdrawn. All other methods failed and in due course, all the 65 trapped mine employees were rescued on 16.11.89 by 7.45 A.M. within about 5 h and the epoch-making achievement is described. Disaster management scheduling, as accomplished, between 13/11/89 and 16/11/89, has been shown in Table 3.

Table 3 Disaster management schedule mahabir colliery-13/11/89 to 16/11/89



9 Conclusions

The rest of the 6 dead bodies, were later recovered, after dewatering of the mine and resumption of winding through pits A&B. First 2 bloated dead bodies were taken up on 11.12, the next 3 bodies on 18.12, and the last 1 body on 23.12.89 and the families could be consoled as heir last rites could be performed. The report of the Court of Enquiries by the Ministry of Labour is public and none could be held responsible. Important points worth recording for future prevention are: -

- The old mine plans can not be relied upon, as pit no. 34 was only shown up to Nega seam, but actually, it was driven up to about 2.5 m above Narainkuri seam, 25 m below.
- Advance boreholes, as per Regulations 127 up to 10 m in all directions must be followed.
- It is an outstanding example of planning and scheduling in disaster management, unparallel in the history of mining
- Despite the flooding of the mine, the underground telephone system was working, and the employees trapped in the rising district could communicate.
- The researcher’s contribution was acclaimed by not only the then CMD, ECL, by writing to the Chairman, CIL, but also by international journals like Reader’s

Digest, June'91 issue in English, Oct'91 issue in Hindi, January'92 issue in Dutch and in many other language editions.

- It has been mainly due to the immense concerted and coordinated efforts of many mining, electrical, mechanical engineers, personnel officers, etc.
- Led by Mr. J.N.Uppal, the then CMD, ECL in crash scheduling, monitoring, and operations, later supported by the then Chairman, CIL, Dr.M.P.Narayan for achieving this world-record-making feat.
- The designed capsule earned first prize in an Industrial Exhibition in New Delhi in 1990 and many papers carried lead stories on it.
- CIL imported a large diameter Boring Machine for the purpose and presently in the role Mine Rescue Station at Sitarampur, where the capsule is also kept for dealing with such eventualities in the future.
- The large Boring Machine procured by CIL is by M/S WIRTH, Type L4 A, mobile tires mounted, trailer, 11 m long, 2.5 m wide, could be extended to 16.4 m height, 30 t weight, diesel driven 175 kW or 239 HP. It could drill up to 1.5 m Φ with a full casing, with the rate of progress @ 4 m/h and up to a depth of about 240 m.
- President of India and many dignitaries sent congratulatory messages to CIL Chairman and CMD, ECL for the outstanding world record-making success for planning and scheduling expertise and required types of equipment from all over India.

In any disaster management, quick identification of possible solutions and parallel action on all options with different teams can help save loss of lives and property and ensure fast relief and rescue.

Acknowledgements The author is indebted to the Convener of ICGMTU-2021, Dr. Ramesh Bhatawdekar to present a paper at the conference. I express my Indebtedness to the then ECL authorities named in the paper to have entrusted me with the freedom to help decide on the best course of action possible. I am especially thankful to Mr. J. N. Uppal, the then CMD, ECL, who wrote to the Chairman, CIL, acknowledging my contribution. I am greatly indebted to Dr.M.A.Ramlu, who promptly accompanied me from ISM to the disaster site. The entire mining community almost participated in this world record-making rescue, in different spheres.

References

1. Enright C, Ferriter RL (2014) Mine rescue manual: a comprehensive guide for mine rescue team members. <https://books.google.com/?hl=en>
2. Hu Q, Wei Y, Enjie D (2019) State-of-the-art and trend of emergency rescue communication technologies for coal mine. <http://infocomm-journal.com/>
3. Wang L, Zhang R, Zhao Z, Zhang W (2006) Emergency rescue command and management information system for coal mine. J Liaoning 25:655–657. <http://en.cnki.com.cn/>
4. Meng L (2020) Research and development of coal mine disaster prevention and rescue drill platform based on VR virtual reality technology. J Phys Conf Ser. <http://iopscience.iop.org/>
5. Samanta BK (1999) Environment risk assessment & management plan of a coalfield. In: International symposium on clean coal initiatives, New Delhi, 22–24 January 1999

6. Sarkar BN, Samanta BK (1993) Mine mechanization with machine safety and system safety. In: XIII world congress on occupational safety and health, New Delhi
7. Samanta BK (1999) Disaster management scheduling with computer programming. In: Briefly presented in workshop on disaster management, ISM, Dhanbad, 1995, Rescue pamphlet of ECL, also presented in IIT, Kharagpur on 7th Jan 1998
8. Samanta BK (2004) Improved technologies for fire extinction, prevention, and control in coalmines. In: All India workshop on underground mine fire – prevention, control and their impact on coal production, 13–14th March 2004 at CMRI, Dhanbad chapter of IE(I)
9. Samanta BK (2003) Blasting efficiency and vibration damage control. In: National seminar on explosives and blasting, Institution of Engineers (India), 6–7 December 2003, DGMS, Dhanbad. <https://doi.org/10.13140/RG.2.2.223199.47529>
10. Samanta BK (2006) Disaster management in mining leading to a world record. In: Seminar on role of engineers in natural disaster mitigation and management - Engineers Day, 15th September 2006, IE(I), Dhanbad
11. Samanta BK (2008) Mine disaster management leading to a world record. In: 19th National convention of mining engineers & national seminar on disaster in mines, IE(I) Dhanbad Chapter with ISMU, Mining at GJT, ISMU, Dhanbad, 10–11 March 2008
12. Samanta BK (2011) Engineering preparedness for disaster mitigation. In: Seminar on 44th Engineers Day, 2011, Central Institute of Mining & Fuel Research, in collaboration with Institution of Engineers (India), Dhanbad Chapter, 15 September 2011
13. Wua Q, Xiea K, Chena Z (2012) A catastrophe model on the evaluation and classification of mine disaster rescue measures. *Syst Eng Procedia* 4:484–489
14. Wang H (2011) Coal mine disaster rescue life sign monitoring technology based on fbg and acceleration sensor. *Procedia Eng* 26:2294–2300
15. Watts T (2012) Challenges encountered by New Zealand mines rescue at the Pike River mine disaster. <http://ro.uow.edu.au/>
16. Wu Q, Guan E (2006) Preliminary study on water disaster emergency rescue counterplan in coal mine. *Mei T'an Hsueh Pao (J China Coal Soc)*. <http://osti.gov/>